

Bridge Engineering Handbook

SECOND EDITION

SUPERSTRUCTURE DESIGN

EDITED BY

Wai-Fah Chen and Lian Duan



CRC Press
Taylor & Francis Group

@Seismicisolation

Bridge Engineering Handbook
SECOND EDITION

**SUPERSTRUCTURE
DESIGN**

@Seismicisolation

Bridge Engineering Handbook, Second Edition

Bridge Engineering Handbook, Second Edition: Fundamentals

Bridge Engineering Handbook, Second Edition: Superstructure Design

Bridge Engineering Handbook, Second Edition: Substructure Design

Bridge Engineering Handbook, Second Edition: Seismic Design

Bridge Engineering Handbook, Second Edition: Construction and Maintenance

Bridge Engineering Handbook

SECOND EDITION

SUPERSTRUCTURE DESIGN

EDITED BY

Wai-Fah Chen and Lian Duan



CRC Press

Taylor & Francis Group

Boca Raton London New York

CRC Press is an imprint of the
Taylor & Francis Group, an **informa** business

@Seismicisolation

CRC Press
Taylor & Francis Group
6000 Broken Sound Parkway NW, Suite 300
Boca Raton, FL 33487-2742

© 2014 by Taylor & Francis Group, LLC
CRC Press is an imprint of Taylor & Francis Group, an Informa business

No claim to original U.S. Government works
Version Date: 20130923

International Standard Book Number-13: 978-1-4398-5229-3 (eBook - PDF)

This book contains information obtained from authentic and highly regarded sources. Reasonable efforts have been made to publish reliable data and information, but the author and publisher cannot assume responsibility for the validity of all materials or the consequences of their use. The authors and publishers have attempted to trace the copyright holders of all material reproduced in this publication and apologize to copyright holders if permission to publish in this form has not been obtained. If any copyright material has not been acknowledged please write and let us know so we may rectify in any future reprint.

Except as permitted under U.S. Copyright Law, no part of this book may be reprinted, reproduced, transmitted, or utilized in any form by any electronic, mechanical, or other means, now known or hereafter invented, including photocopying, microfilming, and recording, or in any information storage or retrieval system, without written permission from the publishers.

For permission to photocopy or use material electronically from this work, please access www.copyright.com (<http://www.copyright.com/>) or contact the Copyright Clearance Center, Inc. (CCC), 222 Rosewood Drive, Danvers, MA 01923, 978-750-8400. CCC is a not-for-profit organization that provides licenses and registration for a variety of users. For organizations that have been granted a photocopy license by the CCC, a separate system of payment has been arranged.

Trademark Notice: Product or corporate names may be trademarks or registered trademarks, and are used only for identification and explanation without intent to infringe.

Visit the Taylor & Francis Web site at
<http://www.taylorandfrancis.com>

and the CRC Press Web site at

<http://www.crcpress.com>

@Seismicisolation

Contents

Foreword	vii
Preface to the Second Edition	ix
Preface to the First Edition	xi
Editors.....	xiii
Contributors.....	xv

1 Precast–Pretensioned Concrete Girder Bridges	1
<i>Jim Ma and Say-Gunn Low</i>	
2 Cast-in-Place Posttensioned Prestressed Concrete Girder Bridges	51
<i>Lian Duan and Kang Chen</i>	
3 Segmental Concrete Bridges.....	91
<i>Teddy S. Theryo</i>	
4 Composite Steel I-Girder Bridges	171
<i>Lian Duan, Yusuf Saleh, and Steve Altman</i>	
5 Composite Steel Box Girder Bridges	217
<i>Kenneth Price and Tony Shkurti</i>	
6 Horizontally Curved Girder Bridges	259
<i>Eric V. Monzon, Ahmad M. Itani, and Mark L. Reno</i>	
7 Highway Truss Bridges	283
<i>John M. Kulicki</i>	
8 Arch Bridges	309
<i>Baochun Chen</i>	
9 Suspension Bridges	363
<i>Atsushi Okukawa, Shuichi Suzuki, and Ikuo Harazaki</i>	
10 Cable-Stayed Bridges	399
<i>Tina Vejrum and Lars Lundorf Nielsen</i>	
11 Extradosed Bridges	437
<i>Akio Kasuga</i>	

12	Stress Ribbon Pedestrian Bridges	463
	<i>Jiri Strasky</i>	
13	Movable Bridges.....	515
	<i>Michael J. Abrahams, Scott Snelling, and Mark VanDeRee</i>	
14	Floating Bridges.....	549
	<i>M. Myint Lwin</i>	
15	Concrete Decks	573
	<i>John Shen</i>	
16	Orthotropic Steel Decks	589
	<i>Alfred Mangus</i>	
17	Approach Slabs.....	647
	<i>Anand J. Puppala, Bhaskar C. S. Chittoori, and Sireesh Saride</i>	
18	Expansion Joints.....	677
	<i>Ralph J. Dornseife</i>	
19	Railings	705
	<i>Lijia Zhang</i>	

Foreword

Throughout the history of civilization bridges have been the icons of cities, regions, and countries. All bridges are useful for transportation, commerce, and war. Bridges are necessary for civilization to exist, and many bridges are beautiful. A few have become the symbols of the best, noblest, and most beautiful that mankind has achieved. The secrets of the design and construction of the ancient bridges have been lost, but how could one not marvel at the magnificence, for example, of the Roman viaducts?

The second edition of the *Bridge Engineering Handbook* expands and updates the previous edition by including the new developments of the first decade of the twenty-first century. Modern bridge engineering has its roots in the nineteenth century, when wrought iron, steel, and reinforced concrete began to compete with timber, stone, and brick bridges. By the beginning of World War II, the transportation infrastructure of Europe and North America was essentially complete, and it served to sustain civilization as we know it. The iconic bridge symbols of modern cities were in place: Golden Gate Bridge of San Francisco, Brooklyn Bridge, London Bridge, Eads Bridge of St. Louis, and the bridges of Paris, Lisbon, and the bridges on the Rhine and the Danube. Budapest, my birthplace, had seven beautiful bridges across the Danube. Bridge engineering had reached its golden age, and what more and better could be attained than that which was already achieved?

Then came World War II, and most bridges on the European continent were destroyed. All seven bridges of Budapest were blown apart by January 1945. Bridge engineers after the war were suddenly forced to start to rebuild with scant resources and with open minds. A renaissance of bridge engineering started in Europe, then spreading to America, Japan, China, and advancing to who knows where in the world, maybe Siberia, Africa? It just keeps going! The past 60 years of bridge engineering have brought us many new forms of bridge architecture (plate girder bridges, cable stayed bridges, segmental prestressed concrete bridges, composite bridges), and longer spans. Meanwhile enormous knowledge and experience have been amassed by the profession, and progress has benefitted greatly by the availability of the digital computer. The purpose of the *Bridge Engineering Handbook* is to bring much of this knowledge and experience to the bridge engineering community of the world. The contents encompass the whole spectrum of the life cycle of the bridge, from conception to demolition.

The editors have convinced 146 experts from many parts of the world to contribute their knowledge and to share the secrets of their successful and unsuccessful experiences. Despite all that is known, there are still failures: engineers are human, they make errors; nature is capricious, it brings unexpected surprises! But bridge engineers learn from failures, and even errors help to foster progress.

The *Bridge Engineering Handbook*, second edition consists of five books:

Fundamentals

Superstructure Design

Substructure Design

Seismic Design

Construction and Maintenance

Fundamentals, Superstructure Design, and Substructure Design present the many topics necessary for planning and designing modern bridges of all types, made of many kinds of materials and systems, and subject to the typical loads and environmental effects. *Seismic Design and Construction and Maintenance* recognize the importance that bridges in parts of the world where there is a chance of earthquake occurrences must survive such an event, and that they need inspection, maintenance, and possible repair throughout their intended life span. Seismic events require that a bridge sustain repeated dynamic load cycles without functional failure because it must be part of the postearthquake lifeline for the affected area. *Construction and Maintenance* touches on the many very important aspects of bridge management that become more and more important as the world's bridge inventory ages.

The editors of the *Bridge Engineering Handbook*, Second Edition are to be highly commended for undertaking this effort for the benefit of the world's bridge engineers. The enduring result will be a safer and more cost effective family of bridges and bridge systems. I thank them for their effort, and I also thank the 146 contributors.

Theodore V. Galambos, PE
Emeritus professor of structural engineering
University of Minnesota

Preface to the Second Edition

In the approximately 13 years since the original edition of the *Bridge Engineering Handbook* was published in 2000, we have received numerous letters, e-mails, and reviews from readers including educators and practitioners commenting on the handbook and suggesting how it could be improved. We have also built up a large file of ideas based on our own experiences. With the aid of all this information, we have completely revised and updated the handbook. In writing this Preface to the Second Edition, we assume readers have read the original Preface. Following its tradition, the second edition handbook stresses professional applications and practical solutions; describes the basic concepts and assumptions omitting the derivations of formulas and theories; emphasizes seismic design, rehabilitation, retrofit and maintenance; covers traditional and new, innovative practices; provides over 2500 tables, charts, and illustrations in ready-to-use format and an abundance of worked-out examples giving readers step-by-step design procedures. The most significant changes in this second edition are as follows:

- The handbook of 89 chapters is published in five books: *Fundamentals*, *Superstructure Design*, *Substructure Design*, *Seismic Design*, and *Construction and Maintenance*.
- *Fundamentals*, with 22 chapters, combines Section I, Fundamentals, and Section VI, Special Topics, of the original edition and covers the basic concepts, theory and special topics of bridge engineering. Seven new chapters are Finite Element Method, High-Speed Railway Bridges, Structural Performance Indicators for Bridges, Concrete Design, Steel Design, High Performance Steel, and Design and Damage Evaluation Methods for Reinforced Concrete Beams under Impact Loading. Three chapters including Conceptual Design, Bridge Aesthetics: Achieving Structural Art in Bridge Design, and Application of Fiber Reinforced Polymers in Bridges, are completely rewritten. Three special topic chapters, Weigh-In-Motion Measurement of Trucks on Bridges, Impact Effect of Moving Vehicles, and Active Control on Bridge Engineering, were deleted.
- *Superstructure Design*, with 19 chapters, provides information on how to design all types of bridges. Two new chapters are Extradosed Bridges and Stress Ribbon Pedestrian Bridges. The Prestressed Concrete Girder Bridges chapter is completely rewritten into two chapters: Precast–Prestensioned Concrete Girder Bridges and Cast-In-Place Posttensioned Prestressed Concrete Girder Bridges. The Bridge Decks and Approach Slabs chapter is completely rewritten into two chapters: Concrete Decks and Approach Slabs. Seven chapters, including Segmental Concrete Bridges, Composite Steel I-Girder Bridges, Composite Steel Box Girder Bridges, Arch Bridges, Cable-Stayed Bridges, Orthotropic Steel Decks, and Railings, are completely rewritten. The chapter Reinforced Concrete Girder Bridges was deleted because it is rarely used in modern time.
- *Substructure Design* has 11 chapters and addresses the various substructure components. A new chapter, Landslide Risk Assessment and Mitigation, is added. The Geotechnical Consideration chapter is completely rewritten and retitled as Ground Investigation. The Abutments and

Retaining Structures chapter is divided in two and updated as two chapters: Abutments and Earth Retaining Structures.

- *Seismic Design*, with 18 chapters, presents the latest in seismic bridge analysis and design. New chapters include Seismic Random Response Analysis, Displacement-Based Seismic Design of Bridges, Seismic Design of Thin-Walled Steel and CFT Piers, Seismic Design of Cable-Supported Bridges, and three chapters covering Seismic Design Practice in California, China, and Italy. Two chapters of Earthquake Damage to Bridges and Seismic Design of Concrete Bridges have been rewritten. Two chapters of Seismic Design Philosophies and Performance-Based Design Criteria, and Seismic Isolation and Supplemental Energy Dissipation, have also been completely rewritten and retitled as Seismic Bridge Design Specifications for the United States, and Seismic Isolation Design for Bridges, respectively. Two chapters covering Seismic Retrofit Practice and Seismic Retrofit Technology are combined into one chapter called Seismic Retrofit Technology.
- *Construction and Maintenance* has 19 chapters and focuses on the practical issues of bridge structures. Nine new chapters are Steel Bridge Fabrication, Cable-Supported Bridge Construction, Accelerated Bridge Construction, Bridge Management Using Pontis and Improved Concepts, Bridge Maintenance, Bridge Health Monitoring, Nondestructive Evaluation Methods for Bridge Elements, Life-Cycle Performance Analysis and Optimization, and Bridge Construction Methods. The Strengthening and Rehabilitation chapter is completely rewritten as two chapters: Rehabilitation and Strengthening of Highway Bridge Superstructures, and Rehabilitation and Strengthening of Orthotropic Steel Bridge Decks. The Maintenance Inspection and Rating chapter is completely rewritten as three chapters: Bridge Inspection, Steel Bridge Evaluation and Rating, and Concrete Bridge Evaluation and Rating.
- The section on Worldwide Practice in the original edition has been deleted, including the chapters on Design Practice in China, Europe, Japan, Russia, and the United States. An international team of bridge experts from 26 countries and areas in Africa, Asia, Europe, North America, and South America, has joined forces to produce the *Handbook of International Bridge Engineering, Second Edition*, the first comprehensive, and up-to-date resource book covering the state-of-the-practice in bridge engineering around the world. Each of the 26 country chapters presents that country's historical sketch; design specifications; and various types of bridges including girder, truss, arch, cable-stayed, suspension, and so on, in various types of materials—stone, timber, concrete, steel, advanced composite, and of varying purposes—highway, railway, and pedestrian. Ten benchmark highway composite girder designs, the highest bridges, the top 100 longest bridges, and the top 20 longest bridge spans for various bridge types are presented. More than 1650 beautiful bridge photos are provided to illustrate great achievements of engineering professions.

The 146 bridge experts contributing to these books have written chapters to cover the latest bridge engineering practices, as well as research and development from North America, Europe, and Pacific Rim countries. More than 80% of the contributors are practicing bridge engineers. In general, the handbook is aimed toward the needs of practicing engineers, but materials may be re-organized to accommodate several bridge courses at the undergraduate and graduate levels.

The authors acknowledge with thanks the comments, suggestions, and recommendations made during the development of the second edition of the handbook by Dr. Erik Yding Andersen, COWI A/S, Denmark; Michael J. Abrahams, Parsons Brinckerhoff, Inc.; Dr. Xiaohua Cheng, New Jersey Department of Transportation; Joyce E. Copelan, California Department of Transportation; Prof. Dan M. Frangopol, Lehigh University; Dr. John M. Kulicki, Modjeski and Masters; Dr. Amir M. Malek, California Department of Transportation; Teddy S. Theryo, Parsons Brinckerhoff, Inc.; Prof. Shouji Toma, Horrai-Gakuen University, Japan; Dr. Larry Wu, California Department of Transportation; Prof. Eiki Yamaguchi, Kyushu Institute of Technology, Japan; and Dr. Yi Edward Zhou, URS Corp.

We thank all the contributors for their contributions and also acknowledge Joseph Clements, acquiring editor; Jennifer Ahringer, project coordinator; and Joette Lynch, project editor, at Taylor & Francis/CRC Press.



Preface to the First Edition

The *Bridge Engineering Handbook* is a unique, comprehensive, and state-of-the-art reference work and resource book covering the major areas of bridge engineering with the theme “bridge to the twenty-first century.” It has been written with practicing bridge and structural engineers in mind. The ideal readers will be MS-level structural and bridge engineers with a need for a single reference source to keep abreast of new developments and the state-of-the-practice, as well as to review standard practices.

The areas of bridge engineering include planning, analysis and design, construction, maintenance, and rehabilitation. To provide engineers a well-organized, user-friendly, and easy-to-follow resource, the handbook is divided into seven sections. Section I, Fundamentals, presents conceptual design, aesthetics, planning, design philosophies, bridge loads, structural analysis, and modeling. Section II, Superstructure Design, reviews how to design various bridges made of concrete, steel, steel-concrete composites, and timbers; horizontally curved, truss, arch, cable-stayed, suspension, floating, movable, and railroad bridges; and expansion joints, deck systems, and approach slabs. Section III, Substructure Design, addresses the various substructure components: bearings, piers and columns, towers, abutments and retaining structures, geotechnical considerations, footings, and foundations. Section IV, Seismic Design, provides earthquake geotechnical and damage considerations, seismic analysis and design, seismic isolation and energy dissipation, soil-structure-foundation interactions, and seismic retrofit technology and practice. Section V, Construction and Maintenance, includes construction of steel and concrete bridges, substructures of major overwater bridges, construction inspections, maintenance inspection and rating, strengthening, and rehabilitation. Section VI, Special Topics, addresses in-depth treatments of some important topics and their recent developments in bridge engineering. Section VII, Worldwide Practice, provides the global picture of bridge engineering history and practice from China, Europe, Japan, and Russia to the U.S.

The handbook stresses professional applications and practical solutions. Emphasis has been placed on ready-to-use materials, and special attention is given to rehabilitation, retrofit, and maintenance. The handbook contains many formulas and tables that give immediate answers to questions arising from practical works. It describes the basic concepts and assumptions, omitting the derivations of formulas and theories, and covers both traditional and new, innovative practices. An overview of the structure, organization, and contents of the book can be seen by examining the table of contents presented at the beginning, while the individual table of contents preceding each chapter provides an in-depth view of a particular subject. References at the end of each chapter can be consulted for more detailed studies.

Many internationally known authors have written the chapters from different countries covering bridge engineering practices, research, and development in North America, Europe, and the Pacific Rim. This handbook may provide a glimpse of a rapidly growing trend in global economy in recent years toward international outsourcing of practice and competition in all dimensions of engineering.

In general, the handbook is aimed toward the needs of practicing engineers, but materials may be reorganized to accommodate undergraduate and graduate level bridge courses. The book may also be used as a survey of the practice of bridge engineering around the world.

The authors acknowledge with thanks the comments, suggestions, and recommendations during the development of the handbook by Fritz Leonhardt, Professor Emeritus, Stuttgart University, Germany; Shouji Toma, Professor, Horrai-Gakuen University, Japan; Gerard F. Fox, Consulting Engineer; Jackson L. Durkee, Consulting Engineer; Michael J. Abrahams, Senior Vice President, Parsons, Brinckerhoff, Quade & Douglas, Inc.; Ben C. Gerwick, Jr., Professor Emeritus, University of California at Berkeley; Gregory F. Fenves, Professor, University of California at Berkeley; John M. Kulicki, President and Chief Engineer, Modjeski and Masters; James Chai, Senior Materials and Research Engineer, California Department of Transportation; Jinrong Wang, Senior Bridge Engineer, URS Greiner; and David W. Liu, Principal, Imbsen & Associates, Inc.

We thank all the authors for their contributions and also acknowledge at CRC Press Nora Konopka, acquiring editor, and Carol Whitehead and Sylvia Wood, project editors.

Editors



Dr. Wai-Fah Chen is a research professor of civil engineering at the University of Hawaii. He was dean of the College of Engineering at the University of Hawaii from 1999 to 2007, and a George E. Goodwin Distinguished Professor of Civil Engineering and head of the Department of Structural Engineering at Purdue University from 1976 to 1999.

He earned his BS in civil engineering from the National Cheng-Kung University, Taiwan, in 1959, MS in structural engineering from Lehigh University in 1963, and PhD in solid mechanics from Brown University in 1966. He received the Distinguished Alumnus Award from the National Cheng-Kung University in 1988 and the Distinguished Engineering Alumnus Medal from Brown University in 1999.

Dr. Chen's research interests cover several areas, including constitutive modeling of engineering materials, soil and concrete plasticity, structural connections, and structural stability. He is the recipient of several national engineering awards, including the Raymond Reese Research Prize and the Shortridge Hardesty Award, both from the American Society of Civil Engineers, and the T. R. Higgins Lectureship Award in 1985 and the Lifetime Achievement Award, both from the American Institute of Steel Construction. In 1995, he was elected to the U.S. National Academy of Engineering. In 1997, he was awarded Honorary Membership by the American Society of Civil Engineers, and in 1998, he was elected to the Academia Sinica (National Academy of Science) in Taiwan.

A widely respected author, Dr. Chen has authored and coauthored more than 20 engineering books and 500 technical papers. His books include several classical works such as *Limit Analysis and Soil Plasticity* (Elsevier, 1975), the two-volume *Theory of Beam-Columns* (McGraw-Hill, 1976 and 1977), *Plasticity in Reinforced Concrete* (McGraw-Hill, 1982), and the two-volume *Constitutive Equations for Engineering Materials* (Elsevier, 1994). He currently serves on the editorial boards of more than 15 technical journals.

Dr. Chen is the editor-in-chief for the popular *Civil Engineering Handbook* (CRC Press, 1995 and 2003), the *Handbook of Structural Engineering* (CRC Press, 1997 and 2005), the *Earthquake Engineering Handbook* (CRC Press, 2003), the *Semi-Rigid Connections Handbook* (J. Ross Publishing, 2011), and the *Handbook of International Bridge Engineering* (CRC Press, 2014). He currently serves as the consulting editor for the *McGraw-Hill Yearbook of Science & Technology* for the field of civil and architectural engineering.

He was a longtime member of the executive committee of the Structural Stability Research Council and the specification committee of the American Institute of Steel Construction. He was a consultant for Exxon Production Research on offshore structures, for Skidmore, Owings, and Merrill in Chicago on tall steel buildings, and for the World Bank on the Chinese University Development Projects, among many others. Dr. Chen has taught at Lehigh University, Purdue University, and the University of Hawaii.



Dr. Lian Duan is a senior bridge engineer and structural steel committee chair with the California Department of Transportation (Caltrans). He worked at the North China Power Design Institute from 1975 to 1978 and taught at Taiyuan University of Technology, China, from 1981 to 1985.

He earned his diploma in civil engineering in 1975, MS in structural engineering in 1981 from Taiyuan University of Technology, China, and PhD in structural engineering from Purdue University in 1990.

Dr. Duan's research interests cover areas including inelastic behavior of reinforced concrete and steel structures, structural stability, seismic bridge analysis, and design. With more than 70 authored and coauthored papers, chapters, and reports, his research focuses on the development of unified interaction equations for steel beam-columns, flexural stiffness of reinforced concrete members, effective length factors of compression members, and design of bridge structures.

Dr. Duan has over 35 years experience in structural and bridge engineering. He was lead engineer for the development of Caltrans *Guide Specifications for Seismic Design of Steel Bridges*. He is a registered professional engineer in California. He served as a member for several National Highway Cooperative Research Program panels and was a Transportation Research Board Steel Committee member from 2000 to 2006.

He is the coeditor of the *Handbook of International Bridge Engineering*, (CRC Press, 2014). He received the prestigious 2001 Arthur M. Wellington Prize from the American Society of Civil Engineers for the paper, "Section Properties for Latticed Members of San Francisco-Oakland Bay Bridge," in the *Journal of Bridge Engineering*, May 2000. He received the Professional Achievement Award from Professional Engineers in California Government in 2007 and the Distinguished Engineering Achievement Award from the Engineers' Council in 2010.

Contributors

Michael J. Abrahams
Parsons Brinckerhoff
New York, New York

Steve Altman
California Department of
Transportation
Sacramento, California

Baochun Chen
Fuzhou University
Fuzhou, Fujian, China

Kang Chen
MGE Engineering, Inc.
Oakland, California

Bhaskar C. S. Chittoori
Boise State University
Boise, Idaho

Ralph J. Dornsite
Washington State Department
of Transportation
Olympia, Washington

Lian Duan
California Department of
Transportation
Sacramento, California

Ikuro Harazaki
Japan Bridge Engineering
Center
Tokyo, Japan

Ahmad M. Itani
University of Nevada
Reno, Nevada

Akio Kasuga
Sumitomo Mitsui Construction
Tokyo, Japan

John M. Kulicki
Modjeski and Masters, Inc.
Mechanicsburg, Pennsylvania

Say-Gunn Low
California Department of
Transportation
Sacramento, California

M. Myint Lwin
U.S. Department of
Transportation
Federal Highway
Administration
Washington, DC

Jim Ma
California Department of
Transportation
Sacramento, California

Alfred Mangus
Bridge Engineer
Sacramento, California

Eric V. Monzon
University of Nevada
Reno, Nevada

Lars Lundorf Nielsen
COWI A/S
Kongens Lyngby, Denmark

Atsushi Okukawa
Oriental Consultants Co., Ltd.
Tokyo, Japan

Kenneth Price
HNTB Corporation
Chicago, Illinois

Anand J. Puppala
The University of Texas at
Arlington
Arlington, Texas

Mark L. Reno
Quincy Engineering
Sacramento, California

Yusuf Saleh
California Department of
Transportation
Sacramento, California

Sireesh Saride
Indian Institute of
Technology
Hyderabad, India

John Shen
California Department of
Transportation
Sacramento, California

Tony Shkurti
HNTB Corporation
Chicago, Illinois

Scott Snelling
Parsons Brinckerhoff
New York, New York

Jiri Strasky
Strasky, Husty and Partners, Ltd.
Brno, Czech Republic

Shuichi Suzuki
Kensetsu-toso Kogyo Co., Ltd.
Tokyo, Japan

Teddy S. Theryo
Parsons Brinckerhoff
Tampa, Florida

Mark VanDeRee
Parsons Brinckerhoff
Tampa, Florida

Tina Vejrum
COWI A/S
Kongens Lyngby, Denmark

Lijia Zhang
California High-Speed Rail
Authority
Sacramento, California

1

Precast–Pretensioned Concrete Girder Bridges

Jim Ma
*California Department
of Transportation*

Say-Gunn Low
*California Department
of Transportation*

1.1	Introduction	1
1.2	Precast Concrete Girder Features	2
	Typical Sections • Typical Girder Span Ranges • Primary Characteristics of a Precast Girder • Prestressing Strand Profile	
1.3	Precast Girder Bridge Types.....	7
	Single-Span and Continuous Multi-Span Bridges • Posttensioned Spliced Precast Girder Bridges	
1.4	Design Considerations.....	12
	General • Materials • Loss of Prestress • Design Procedure	
	• Anchorage Zones • Camber and Deflection • Diaphragms and End Blocks • Lateral Stability • Seismic Considerations	
	• Spliced Girder Design	
1.5	Design Flow Chart.....	18
1.6	Design Example—Simple Span Precast–Pretensioned I-Girder Bridge.....	19
	Bridge Data • Design Requirements • Solutions	
	References.....	49

1.1 Introduction

Precast–pretensioned concrete girders, usually referred to as precast girders, are fabricated off-site (Figure 1.1), and then transported, erected, or launched into the project site. During the period of development of the United States’ Interstate highway system in the late 1950s and early 1960s, prestressed concrete became a practical solution in the design and construction of highway bridges. Most states in the United States adopted the precast–pretensioned concrete girder bridges as a preferred structure type because they facilitated off-site fabrication, leading to rapid construction techniques, and reducing on-site construction time. These bridges have served many state departments of transportation well for almost 50 years in the United States.

In recent years, the aging highway bridge infrastructure in the United States is being subjected to increasing traffic volumes and must be continuously rehabilitated while accommodating traffic flow. The traveling public is demanding that this rehabilitation and replacement be done more quickly to reduce congestion and improve safety. Bridge reconstruction is typically on the critical path because of the sequential, labor-intensive processes of completing the foundation, substructure, superstructure components, railings, and other accessories. The public demands for minimizing disruptions of traffic and short-time road closure become a main thrust for all state departments of transportation and their regional partners to accelerate project delivery. Because precast girders require little to no false-work, they are a preferred solution for jobs, where speed of construction, minimal traffic disruption,



FIGURE 1.1 Precast bathtub girder (with posttensioned ducts) in pretensioning bed.

and/or minimal environmental impact are required and temporary construction clearance needs to be maintained. It is expected that this trend will continue well into the future, particularly as new concrete materials such as self-consolidating concrete (SCC) and ultrahigh performance concrete (UHPC) become mainstream, thereby further enhancing the versatility of precast concrete structures.

Normally, the precast concrete girder bridge type is a very economical solution for any situation where large quantities of girders are required and details are repeatable. Precast concrete girder bridges become an optimum solution where bridge projects face constraints such as, but not limited to, the following:

- Falsework restrictions
- Limited construction time
- Limited vertical clearance
- Minimum traffic disruptions
- Environmental impact requirements
- Complex construction staging
- Utility relocation
- Preservation of existing roadway alignment
- Maintaining existing traffic
- Future deck replacement

This chapter discusses the precast–pretensioned concrete girder bridges and posttensioned spliced precast girder bridges. The cast-in-place posttensioned concrete girder bridges and segmental concrete bridge are presented in Chapters 2 and 3 respectively. Concrete design theory is addressed in Chapter 13 of *Bridge Engineering Handbook, Second Edition: Fundamentals*. For a more detailed discussion on prestressed concrete and precast–pretensioned girder bridges, references are made to textbooks by Lin and Burns (1981), Nawy (2009), Collins and Mitchell (1991), and PCI Bridge Design Manual (2011).

1.2 Precast Concrete Girder Features

Precast girders are prestressed to produce a tailored stress distribution along the member at the service level to help prevent flexural cracking. For member efficiency, the girders have precompressed tensile zones—regions such as the bottom face of the girder at midspan where compression is induced to

counteract tension due to expected gravity loads (e.g., self-weight, superimposed dead loads such as deck weight, barrier weight, overlay, and live loads). To achieve this, precast girders employ prestressing strands that are stressed before the concrete hardens. Pretensioning requires the use of a stressing bed, often several hundred feet long for efficient casting of a series of members in a long line using abutments, stressing stands, jacks, and hold downs/hold ups to produce the desired prestressing profile. The transfer of strand force to the pretensioned members by bond between concrete and prestressing steel is typically evident by the upward deflection (camber) of members when the strands are detensioned (cut or burned) at the member ends. Steam curing of members allows for a rapid turnover of forms (typically one-day cycle or less) and cost efficiency. Control in fabrication of precast girders also permits the use of quality materials and many benefits such as higher-strength materials and high modulus of elasticity, as well as reduced creep, shrinkage, and permeability.

1.2.1 Typical Sections

In the United States, the most commonly used precast girders are the standard AASHTO sections, as shown in Appendix B of PCI Bridge Design Manual (2011). A number of states have their own standard girder products. Local precast manufacturers should be consulted on girder form availability before design starts. Typical cross sections of precast girders used for common bridges are shown below:

- Precast I-Girder
- Precast Bulb-Tee Girder
- Precast Wide-Flanged Girder
- Precast Bath-Tub or U Girder
- Precast Solid and Voided Slab
- Precast Box Girder
- Precast Trapezoidal Girder
- Precast Double-Tee Girder
- Precast Deck Bulb-Tee Girder

Among these girders, the I-girder has been most commonly used in the United States for nearly 60 years. With bridge span lengths normally ranging from 50 to 125 ft, the I-girder typically uses a depth-to-span ratio of approximately 0.045–0.050 for simple spans. The depth-to-span ratio is approximately 0.005 less (i.e., 0.040–0.045) for multi-span structures made continuous for live load. This structure type has proven to be an excellent choice for rapid construction and widening of existing structures. With no requirement for ground-supported falsework, precast girder construction usually takes far less time than that taken for cast-in-place construction. Once the deck is poured, the structural section becomes composite, minimizing deflections.

The bulb-tee and bath-tub (or U-shape) girders are targeted for bridge spans up to 150 ft in length. The depth-to-span ratio is also in the range of 0.045–0.050 for simple spans and 0.040–0.045 for continuous structures. However, due to the weight limits of economic trucking, the length of bath-tub girders is limited to 120 ft.

The wide-flanged girder (Figure 1.2) was recently developed in several states in coordination with precasters to produce more efficient bottom and top flange areas that permit design for spans up to 200 ft, with a depth–span ratio of 0.045 (simple) and 0.004 (continuous). The larger bottom bulb accommodates nearly 40% more strands than the standard bulb-tee and, due to its shape, provides enhanced handling and erection stability even at longer spans. Greater economy is also anticipated due to larger girder spacing and reduction in girder lines. Sections have been developed for both pretensioning alone as well as combined pre- and posttensioned sections in some states. For longer span lengths, special permit requirements must be verified for hauling and consideration of trucking routes and erection.

Other girders that are less commonly used include girders with trapezoidal, double-tee, and rectangular cross sections as well as box girders. These are sometimes used for cost effectiveness and aesthetics, particularly for off-system bridges. Precast box girders are often used for railway systems and relatively short span lengths ranging from 40 to 100 ft.



FIGURE 1.2 California wide-flange girder.

TABLE 1.1 Girder Types and Applicable Span Length

Girder Type	Possible Span Length	Preferred Span Length
I-girder	50' to 125'	50' to 95'
Bulb-tee girder	80' to 150'	95' to 150'
Bath-tub girder	80' to 150'	80' to 100'
Wide-flange girder	100' to 200'	100' to 180'
Voided slab	20' to 70'	20' to 50'
Precast box girder	40' to 120'	40' to 100'
Precast delta girder	60' to 120'	60' to 100'
Precast double T girder	30' to 100'	30' to 60'

It should be noted that using bridge depth-to-span ratios to decide girder depth is approximate, but it is a reasonable starting point for initial design and cost estimates. Normally, girder spacing is approximately 1.5–2.0 times the bridge superstructure depth. When shallow girder depth is required, girder spacing may have to be reduced to satisfy all design criteria; however, this may result in increased cost.

1.2.2 Typical Girder Span Ranges

Each girder type has its own economical and practical span length range and span length limits. Table 1.1 lists the range of the span length of each girder type.

Local fabricators should be consulted and coordinated with for the form availability of all different girder shapes.

1.2.3 Primary Characteristics of a Precast Girder

For a precast girder, the following three basic stages of performance are addressed in design: transfer, service, and strength.

The stage of transfer refers to the time at which the prestressing force in the strands is transferred to the precast girder at the plant, typically by cutting or detensioning the strands after a minimum concrete strength has been verified. Because only the girder self-weight acts at this stage, the most critical stresses are often at the ends of the girder, midspan, or harping points (also known as drape points). Both tensile and compressive stresses are checked. Service refers to the stage at which the girder and slab self-weight act on the noncomposite girder, and additional dead loads (e.g., barrier and wearing surface) together with

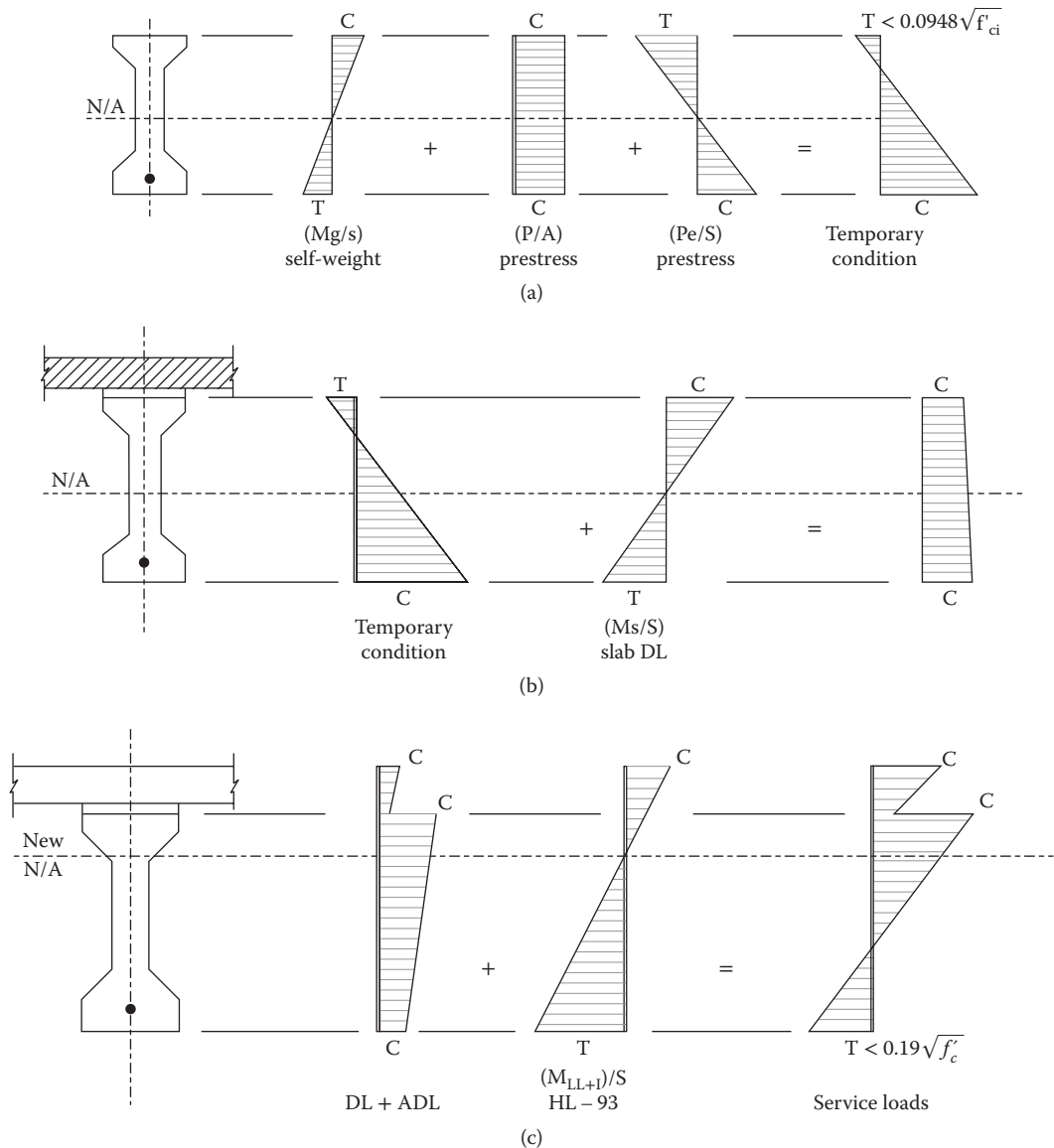


FIGURE 1.3 Concrete flexural stress distribution at section near midspan—at transfer, deck pour, and service. (a) At transfer (noncomposite section). (b) At deck pour (noncomposite section). (c) At service under dead and live loads (composite section).

the live load act on the composite girder. This stage is checked using the AASHTO LRFD Service I and III load combination. Flexural strength is provided to satisfy all factored loads. Figure 1.3 illustrates the different concrete flexural stress distributions at transfer, deck pour, and full service loading.

1.2.4 Prestressing Strand Profile

At the heart of the prestressed concrete design philosophy is the positioning of the prestressing strands within the precast girder: the center of gravity of the strands (cgs) is deliberately offset from the center of gravity of the concrete section (cgc) to maximize the eccentricity, which is defined as the distance

between the cgs and cgc at a section. This eccentricity produces a beneficial tailored flexural stress distribution along the length of the member to counteract the flexural tension expected from gravity loads. The largest eccentricity is provided at locations where tension is expected to be the greatest.

Efficient design of precast girders typically requires varying the strand eccentricity along the length of the member and/or limiting the strand force at transfer. Whether precast girders are used as a single span, made continuous with a cast-in-place deck for live load, or spliced together, they are fabricated, transported, and initially installed as simply-supported segments. For a simply-supported girder with straight strands, the large eccentricity between the cgs and the cgc section helps reduce tension and possible cracking at midspan at the service level. However, excessive flexural tensile stresses may develop at the top of the girder segments near the ends, where the flexural stresses due to self-weight are minimal. Excessive flexural compression stresses may similarly develop. The most critical location near the ends is at the transfer length, that is, the distance from the end of the girder at which the strand force is fully developed. For this temporary condition, AASHTO LRFD (2012) specifies the appropriate stresses' limit to mitigate cracking and compression failure.

To reduce the tensile and compressive stresses at the ends of girders, the designer normally considers two primary options: (1) harping (or draping) strands to reduce the strand eccentricity at the ends (Figures 1.4 and 1.5) or (2) debonding (or shielding) selected strands at the member ends to reduce the prestress force (Figure 1.6). Both are commonly used, often at the preference of the fabricator, who may be consulted when selecting these alternatives. In addition, sometimes transferring or transportation stresses may be controlled using temporary strands at girder tops that are shielded along the member length except at the ends. These strands can be cut at a later stage, such as erection, using a pocket that is formed at the girder top.

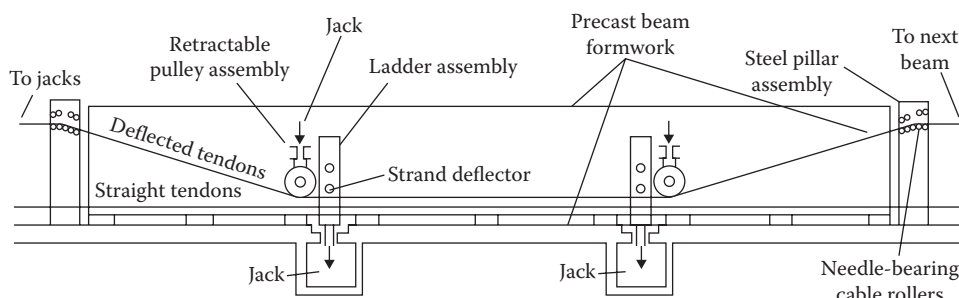


FIGURE 1.4 Typical draped strand profile.

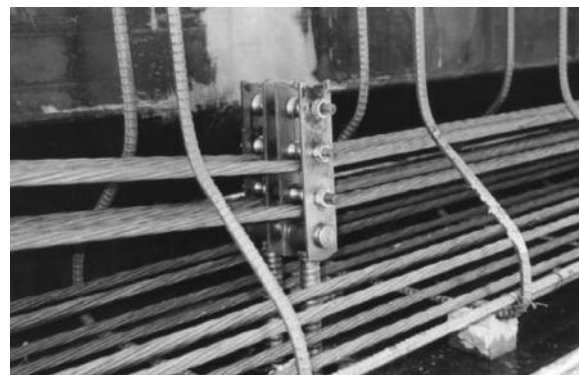


FIGURE 1.5 Hold-Down mechanism in stressing bed.

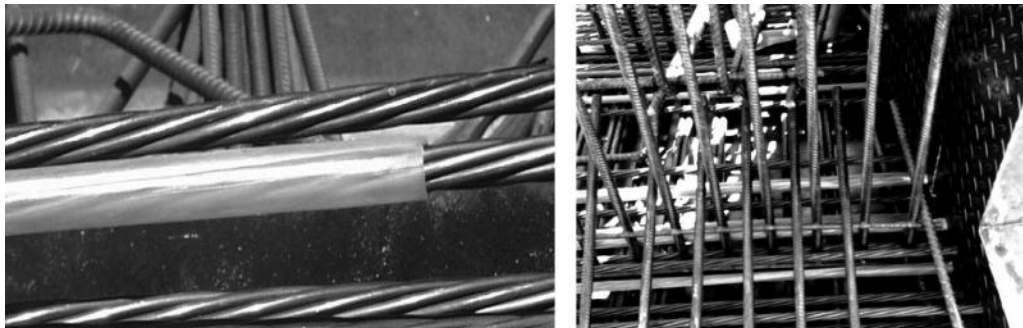


FIGURE 1.6 Debonding strand using plastic sheathing.

By harping the strands in a precast girder, the eccentricity can be varied in linear segments along the length of the girder by mechanically deflecting some of the stressed strands in the casting beds prior to casting and using hold-downs and hold-ups, as shown in Figures 1.4 and 1.5.

Although draping is limited to strands within the web, only a portion of the strands typically needs to be draped to achieve the required eccentricity at girder ends. Typically the drape points are located between approximately 0.30 L and 0.40 L. However, some fabricators may not have suitable equipment for all-drape profiles. In addition, the drape angle must be limited to ensure that jacking requirements and hold-down forces do not exceed the available capacity. One of the benefits of draped strands is to provide a vertical component to resist shear due to the drape angle at girder ends.

In order to maximize fabrication efficiency and lower tensile stresses near the ends of the girders, some manufacturers prefer to use straight strands with debonding some of the strands at the girder ends (eliminating the bonding between concrete and prestress steel) to satisfy stress limits at release. Figure 1.6 shows debonding of a strand by encasing the strand in a plastic sheathing. The debonding strand prevents the prestressing force from developing in the debonded region and causes the critical section for stresses to shift a transfer length away from the end of debonding. Debonded strands are symmetrically distributed about the vertical centerline of the girder, and debonded lengths of pairs of strands are equal. AASHTO LRFD (2012) limits the number of partially debonded strands to 25% of the total number of strands and the number of debonded strands in any horizontal row is limited to 40% of the strands in that row.

Temporary strands in the top flange of the girder may be used to help reduce the number of debonded strands in the bottom of the girder while maintaining concrete stresses within allowable limits at release. Temporary strands in the top flange of the girder may also be used to handle shipping stresses and enhance stability during shipping. Top temporary strands may be pretensioned and bonded for approximately 10 to 15 ft at girder ends and debonded along the middle portion of the girder. The temporary strands should be cut before the cast-in-place intermediate diaphragm or concrete deck is placed. A blockout at the top of the girder at midspan is required to allow cutting of top strands.

For some longer span bridges, the girder design may require addition of mild reinforcement to satisfy the strength limit state requirements. However, additional mild reinforcement may be difficult to place in some girders due to congestion. In such cases, the number of prestress strands may be increased to sufficiently enlarge its moment resistance. When the number of strands is increased for this reason, total prestressing force can remain unchanged for serviceability by reducing the jacking stress to less than a maximum limit of $0.75f_{pu}$.

1.3 Precast Girder Bridge Types

There are three main precast bridge types: precast–pretensioned girders, posttensioned spliced precast girders, and segmental precast girders. Table 1.2 summarizes the typical span lengths for these bridge types.

TABLE 1.2 Precast Bridge Types and Span Lengths

Bridge Type	Possible Span Length	Preferred Span Length
Precast–pretensioned girder	30' to 200'	30' to 180'
Posttensioned spliced precast girder	100' to 325'	120' to 250'
Segmental precast–pretensioned girder	200' to 450'	250' to 400'

The selection of these three bridge types is normally decided by the span length requirements. As shown in Table 1.2, a single precast–pretensioned girder could be designed and span from 30 to 200 ft. But the trucking length, crane capacity, and transporting routes may limit the girder length (and weight), which could be delivered. Therefore, a girder may need to be manufactured in two or more segments and shipped before being spliced together onsite to its full span length. Such splicing techniques can be applied by using posttensioning systems for both single-span and multiple-span bridges, which span up to 325 ft. Section 1.3.2 covers the aspects of the spliced girder bridges. For a span length of over 250 to 400 ft, segmental precast girder bridge may be considered. Chapter 3 of this handbook covers this type of bridge in more detail.

1.3.1 Single-Span and Continuous Multi-span Bridges

As the simplest application of precast girders, single-span bridges normally consist of single-element, simple-span girders. As shown in Figure 1.7, girders are set onto bearing pads at seat-type abutments. For precast girders bridges, abutments could be seat type or end diaphragm type.

Many design considerations for single-span bridges also apply to multi-span bridges because girders or girder segments exist as single-span elements for several stages including fabrication, transportation, erection, and deck pour. In addition, some multi-span bridges or portions thereof are constructed using expansion joints that create boundary conditions of a simply-supported, single-span bridge.

Most multi-span bridges are constructed with simple-span girders made continuous for live-load to increase efficiency and redundancy. This is accomplished by limiting expansion joints, designing deck reinforcement to serve as negative moment reinforcement at interior bents, and providing girder continuity at bents by using continuous cast-in-place deck and/or cast-in-place diaphragms.



FIGURE 1.7 Single-span I beam lowered onto abutments at bridge site.

For continuous multi-span bridges, intermediate supports are usually drop bent caps (Figure 1.8). Drop caps are commonly detailed to provide a nonintegral connection, without moment continuity to the substructure but with live-load moment continuity in the superstructure through negative moment reinforcement in the deck. Simple-span girders are placed on bearing pads at the top of drop caps. Girders at the top of drop caps are normally tied together with a cast-in-place diaphragm and dowels placed through the webs at the ends of the girders. Adequate seat width is required for drop caps to prevent unseating due to relative longitudinal displacement in a seismic event.

For continuous precast girder spans on bridges with drop bent caps or for posttensioned spliced girders joined at bent caps, bottom prestressing strands or reinforcing bars can be extended and conservatively designed to carry positive bending moments due to creep, shrinkage, temperature, and other restraint moments. Extended bottom strands or reinforcing bars can be hooked between the girders in the diaphragms at the bent caps to ensure adequate development. These strands and reinforcing bars can also be designed to resist earthquake-induced forces.

In addition, some bridges are detailed to provide an integral connection with full moment transfer between the superstructure and substructure using cast-in-place diaphragms, reinforcing bars between bent cap, diaphragm, and girders, and/or longitudinal posttensioning (Figure 1.9). An integral connection not only provides longitudinal continuity for live load but also longitudinal and transverse continuity for seismic and wind effects. Owing to moment continuity between the superstructure and



FIGURE 1.8 A typical drop cap for highway bridges.

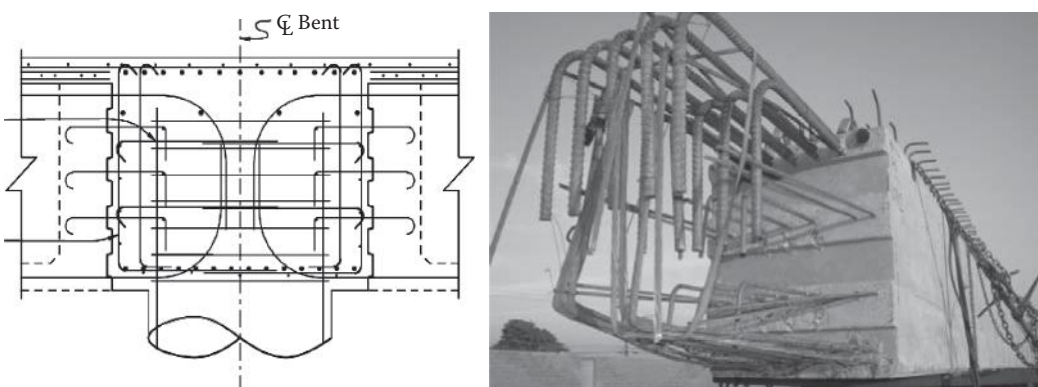


FIGURE 1.9 Integral bent cap connection.

substructure with integral connections, columns in multicolumn bents may be designed to be pinned at their base, thus reducing the foundation cost.

1.3.2 Posttensioned Spliced Precast Girder Bridges

Owing to limitations in transportation length and member weight as well as stressing bed size, a girder may need to be fabricated in two or more segments and shipped before being spliced together onsite to its full span length. Such splicing techniques can be applied to both single-span and multiple-span bridges. By using this approach, the designer has significant flexibility in selecting the span length, number and location of intermediate supports, segment lengths, and splice locations. Nowadays, posttensioning splicing is more commonly used for multi-span bridge construction; however, spliced girders have also been used successfully in the construction of several single-span bridges.

Splicing of girders is typically conducted onsite, either on the ground adjacent to or near the bridge location, or in place using temporary supports. Figure 1.10 shows two precast bathtub girder segments being placed on temporary supports in preparation for field splicing at midspan.

Full continuity should be developed between spliced girder segments. This is commonly achieved using continuous posttensioning tendons between segments and mechanical coupling of reinforcement that is extended from the ends of the girder segments within a cast-in-place closure pour.

Posttensioning spliced girders not only provide continuity but also enhance interface shear capacity across the splice joint (closure pour), which normally includes roughened surfaces or shear keys.

When splicing together multiple spans of precast girders, it is critical that the precast girder placement and posttensioning sequence are properly defined along with material properties. Figure 1.11 shows the construction sequence of a typical two-span spliced girder bridge. At each stage, concrete compressive strength and stiffness, creep and shrinkage of concrete, as well as tension force in the prestressing steel (and debonded length, if needed) must be checked. The designer must consider each stage as the design of an individual bridge with given constraints and properties defined by the previous stage.



FIGURE 1.10 Precast bathtub girder segments spliced near midspan using temporary supports at Harbor Blvd. OC in California.

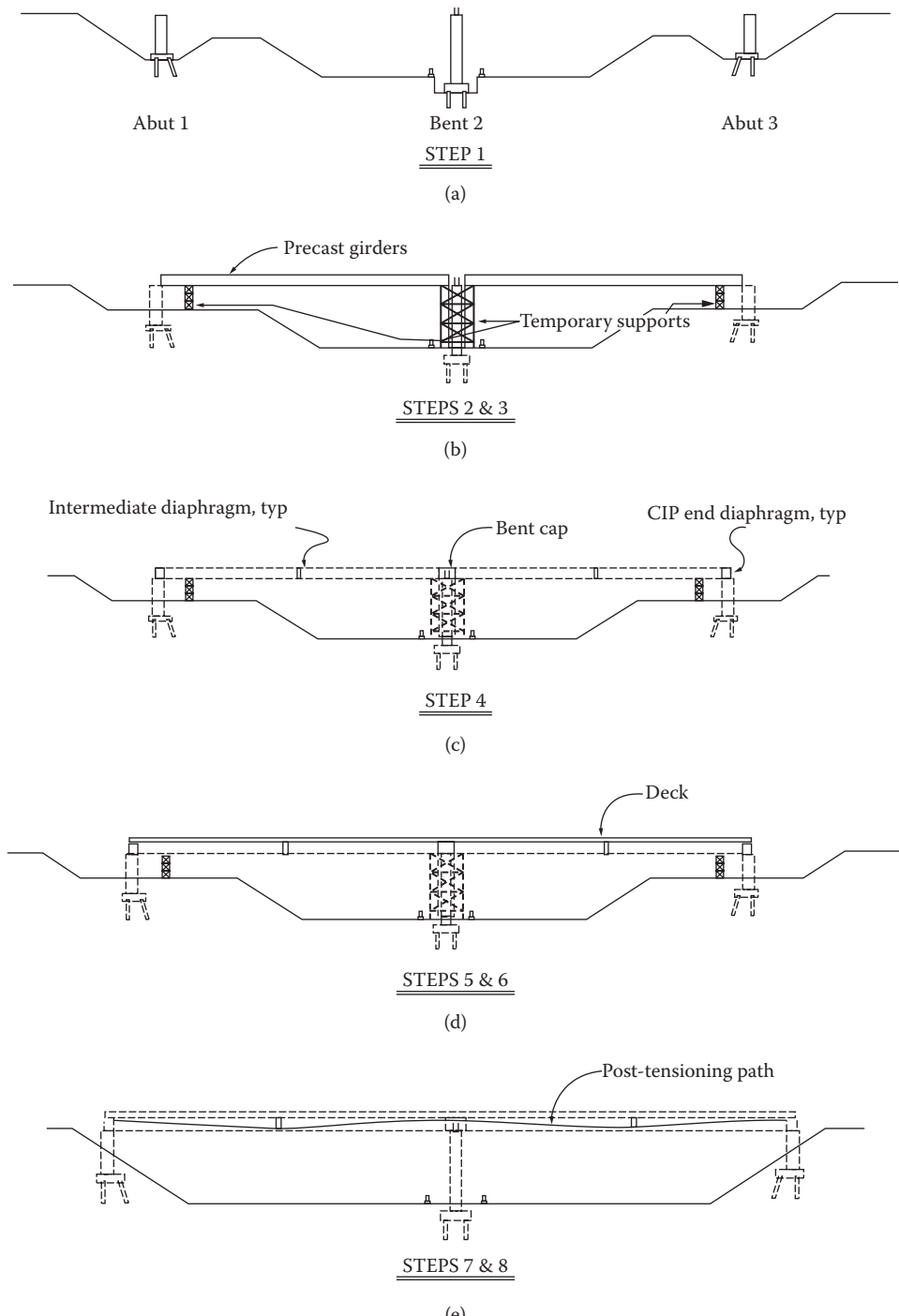


FIGURE 1.11 Posttensioned two-span spliced girder construction sequence. (a) Girder is cast at precasting plant while the substructures are constructed. (b) Erect temporary supports and set girder in place. (c) Construct cast-in-place end diaphragms, bent cap, and intermediate diaphragms. (d) Allow cast-in-place portions to reach minimum concrete strength, then place deck concrete. The temporary supports remain in place as a redundant support system. (e) Post-tension superstructure, remove temp supports, and complete construction of abutments.

The simplest multi-span precast spliced girder system includes consideration of a minimum of four stages or steps after fabrication and before service loads, as follows:

1. Transportation: The girder acts as a simply-supported beam, with supports defined by the locations used by the trucking company. Typically, the manufacturer or trucking company is responsible for loads, stability, and bracing during transportation of the girder.
2. Erection: The girder initially acts as a simply supported beam, with supports defined by the abutments, bents, or temporary falsework locations. A cast-in-place closure pour is placed after coupling of posttensioning tendons and reinforcing bar in splice joint. Optionally, a first stage of posttensioning may be applied before the deck pour instead of after-the-deck pour (not shown in Figure 1.11).
3. Deck Pour: The deck is poured but not set. Therefore, the girders carry girder self-weight and the wet deck weight noncompositely.
4. Posttensioning: The hardened deck and girder act compositely, and the girders are spliced together longitudinally using posttensioning. As the number of girders that are spliced and stages of post-tensioning increase, so does the complexity of design.

The advantages of the spliced girder bridges, which combine precast–pretensioned concrete girder and posttensioning technique, can be summarized as follows: (1) Construction with the use of precast elements reduces congestion, traffic delays, and total project cost. (2) Longer span lengths reduce the number of piers and minimize environmental impact. (3) Fewer joints in the superstructure improve structural performance, including seismic performance, reduce long-term maintenance costs, and increase bridge service life. (4) The use of posttensioning for continuity minimizes bridge superstructure depth, improving vertical clearance for traffic or railway. (5) The smaller amount of required falsework minimizes construction impact and improves safety for the traveling public and construction workers. (6) Increased girder spacing reduces the number of girder lines and total project cost.

1.4 Design Considerations

1.4.1 General

Precast girder design must address three basic stages of performance—transfer, service, and strength—as well as additional stages if posttensioning is introduced. Precast girder design, including section size, prestress force (number and size of strands), strand layout, and material properties, may be governed by any of these stages. Although design for flexure dominates the precast girder design process, other aspects must also be considered such as prestress losses, shear and interface shear strength, anchorage zones, deflection and camber, diaphragms, and seismic connections.

In general, the design of precast–pretensioned concrete girders includes the following: select girder section and materials, calculate loads, perform flexural design and determine prestressing force, perform shear design, check anchorage and horizontal shear transfer (shear friction), and estimate camber and deflection.

Either the precast manufacturer or the design engineer is responsible for design of the girder for handling, shipping, and erection. The engineer confirms that the girder is constructible and conforms to the required design criteria.

1.4.2 Materials

Concrete used in precast girders produced under plant-controlled conditions is typically of higher strength and quality than for cast-in-place concrete. Normally, the minimum concrete compressive strength at release, f'_{ci} , and minimum 28-day concrete compressive strength, f'_c , or precast girders is

4.0 ksi. In addition, the concrete compressive strength at release, f'_{ci} , may be selected to be as large as 7.0 ksi and f'_c as large as 10.0 ksi. However, designers should verify with local fabricators economical ranges of f'_{ci} on a project-specific basis, especially for f'_{ci} exceeding 7.0 ksi or f'_c exceeding 10 ksi. Minimum concrete compressive strengths may also be specified at girder erection and for posttensioning, when used.

In most precast girders, a relatively large value of f'_{ci} is used in design, which typically controls the overall concrete mix design. If an excessively large value of f'_{ci} is required in design to resist temporary tensile stresses at transfer in areas other than the precompressed tensile zone, such as the top flange at girder ends, then bonded reinforcement or prestress strands may be designed to resist the tensile force in the concrete, per AASHTO LRFD. This helps reduce the required f'_{ci} used in design.

The relatively large value of f'_{ci} used in design also results in a relatively large value of f'_c (e.g., often in excess of 7 ksi), which is normally larger than that required to satisfy the concrete compressive strength requirements at the serviceability and/or strength limit state. In cases where a larger f'_c is required to produce an economical design (e.g., girders of longer span, shallower depth, or wider spacing), a 56-day compressive strength may be specified to achieve the higher strength, rather than the normal 28-day strength.

Advantages of the concrete used in precast girders produced under plant-controlled conditions are wide ranging. Higher modulus of elasticity and lower creep, shrinkage, and permeability are by-products of the relatively higher compressive strength and steam curing process used for precast girders.

SCC is being more commonly used in precast plants. Although slightly more expensive than traditional concrete, it provides significant advantages such as elimination of consolidation, reduced manual labor, and smoother concrete surfaces, often combined with high strength and durability.

For economy, precast girders commonly use 0.6-in diameter, 270 ksi (Grade 270), low-relaxation strands. Use of 0.5-in diameter strands is less common because the 0.6-in diameter strands provide a significantly higher efficiency due to a 42% increase in capacity. The 3/8-in diameter strands are commonly used for stay-in-place, precast deck panels. Epoxy coated prestressing strands may be used in corrosive areas.

Deformed welded wire reinforcement (WWR), conforming to ASTM A497 based on a maximum tensile strength of 60 or 75 ksi, may be substituted for reinforcing bars for shear design within precast–pretensioned concrete members is permitted and commonly used as shear reinforcement in precast girder.

1.4.3 Loss of Prestress

Loss of prestress is defined as the difference between the initial stress in the strands and the effective prestress in the member. The loss of prestress includes both instantaneous losses and time-dependent losses.

For a pretensioned member, prestress losses due to elastic shortening, shrinkage, creep of concrete, and relaxation of steel must be considered. For a posttensioning spliced girder application, friction between the tendon and the duct and anchorage seating losses during the posttensioning operation must be considered in addition to the losses considered for a pretensioned member. Some of the important variables affecting loss of prestress are the concrete modulus of elasticity and creep and shrinkage properties. These variables can be somewhat unpredictable for a given concrete mixture and its placement procedure. These conditions are not fully controlled by the designer. Therefore, the estimation of losses should not be overly emphasized at the expense of other more important issues during the design process. Prediction of prestress losses may be determined by means of the approximate lump-sum estimate method, the refined itemized estimate method, or a detailed time-dependent analysis. The refined itemized estimate method should be used for the final design of a normal prestressed concrete member. For a posttensioned spliced concrete member with multistage construction and/or prestressing, the prestress losses should be computed by means of the time-dependent analysis method. The approximate lump-sum estimate method may be used for the preliminary design only.

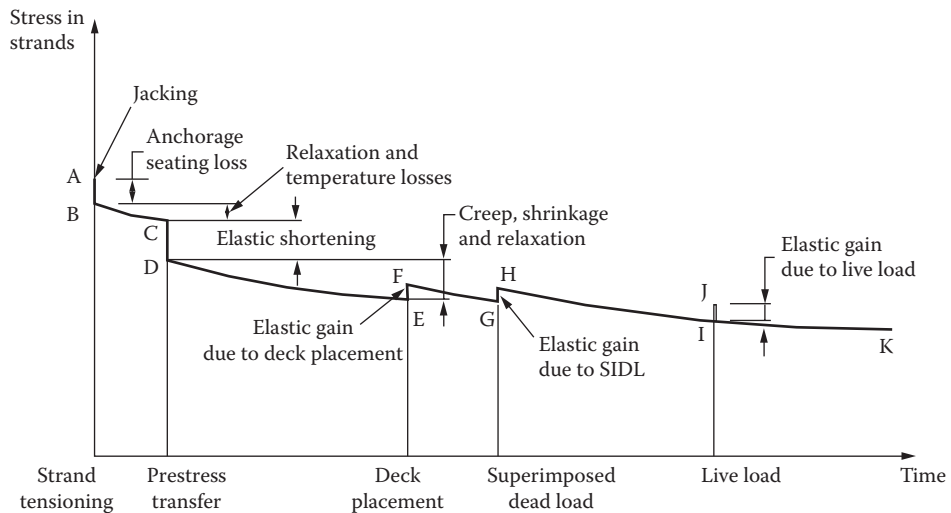


FIGURE 1.12 Strand stress versus time in pretensioned girder.

From the time prestressing strands are initially stressed, they undergo changes in stress that must be accounted for in the design. Figure 1.12 illustrates the change in strand stress over time for a typical pretensioned girder.

1.4.4 Design Procedure

Precast-prestressed concrete girders are usually designed at the service limit state to satisfy stress limits, and followed by checking of the girders at the strength limit state to provide adequate moment resistance. The midspan section of precast-prestressed concrete girders is usually subjected to positive moments and designed to be similar to a simply supported span for all permanent and transient loads for both single span and multi-span continuous girder bridges. In multi-span continuous bridges, the superstructure is generally designed for continuity under live load and superimposed dead loads at the bent locations. As a result, negative moment reinforcement is added in the deck over the bents to resist these loads. The member at the bent locations is treated as a conventional reinforced concrete section and designed to be fully continuous when determining both the negative and positive moments from loads applied after continuity has been established. A fatigue check of the strands is generally not required unless the girder is designed to crack under service loads. Fatigue of concrete in compression is unlikely to occur in actual practice.

For flexural design of precast girders, Figure 1.3 illustrates the change in flexural stress distribution near midspan for a typical precast girder at transfer, deck pour, and service level. In addition, the following practical aspects should also be noted in carrying out flexural design of precast girders: (1) The girder section size is typically based on the minimum depth-to-span ratio required for a given girder type. (2) The specified concrete compressive strengths (initial and 28-day) are commonly governed by the initial compressive strength, f'_c , required to limit stresses at transfer. (3) The total prestress force (number and size of strands) and strand layout are usually determined to satisfy the serviceability limit state but may have to be revised to satisfy flexural resistance at the strength limit state. (4) Girder design is based on the minimum overall depth when computing capacity of the section.

Shear design is typically performed using the sectional method or other methods as specified by AASHTO LRFD (2012). The sectional method is based on the modified compression field theory (MCFT), which provides a unified approach for shear design for both prestressed and reinforced concrete components (Collins and Mitchell, 1991). The MCFT is based on a variable angle truss model in which the

diagonal compression field angle varies continuously, rather than being fixed at 45° as assumed in prior codes. For prestressed girders, the compression field angle for design is typically in the range of 20° to 40°. To design a girder for shear, the factored shear should be determined on the basis of the applied loads at the section under consideration. The area and spacing of shear reinforcement must be determined at regular intervals along the span and at the critical section. For skew bridges, live load shear demand in the exterior girder of an obtuse angle is normally magnified in accordance with codes. Shear correction factor is not required for dead loads. Owing to the requirement of field bend for shear stirrups, the size of #5 stirrup reinforcement is preferred. Normally, the shear stirrup size should not be larger than #6.

Because shear design typically follows flexural design, certain benefits can be realized in shear design. For example, when harped strands are used, the vertical component of the harped strand force contributes to shear resistance. In addition, the higher-strength concrete specified for flexure enhances the V_c term for shear design. Because flexure-shear interaction must be checked per AASHTO LRFD, the longitudinal reinforcement based on flexural design must be checked after shear design to ensure that sufficient longitudinal reinforcement is provided to resist not only flexure but also the horizontal component of diagonal compression struts that generates a demand for longitudinal reinforcement. AASHTO LRFD includes an upper limit on nominal shear resistance, V_n , which is independent of transverse reinforcement, to prevent web crushing prior to yielding of transverse reinforcement.

Interface shear is designed on the basis of the shear friction provisions of design codes. For precast girder bridges, interface shear design is usually considered across the interface between dissimilar materials such as the top of the girder and the bottom of the deck slab, at the interface between girder ends and diaphragms at abutments or bents, or at spliced construction joints for spliced girders. A 0.25-in intentionally roughened surface or shear key at construction joints is provided to increase the friction factor and thus enhance the interface shear capacity.

1.4.5 Anchorage Zones

End splitting can occur along prestressing strands due to local bursting stresses in the pretensioned anchorage zone. To prevent failure, AASHTO LRFD requires the following vertical reinforcement to be provided within a distance $h/4$ from the end of the beam:

$$P_r = f_s A_s$$

where

A_s = area of vertical reinforcement (in^2)

f_s = stress in the mild tension reinforcement at nominal flexural resistance (ksi)

P_r = factored bearing resistance of anchorages (kip)

Per AASHTO LRFD, f_s should not exceed 20 ksi, and P_r should not be taken as less than 4% of the total prestressing force at transfer.

For spliced precast girders where posttensioning is directly applied to the girder end block, general zone reinforcement is required at the end block of the anchorage area based on AASHTO LRFD (2012).

1.4.6 Camber and Deflection

For precast girders, accurate predictions of deflections and camber of girders are difficult because the modulus of elasticity of concrete varies with the strength and age of the concrete and the effects of creep and shrinkage on deflections are difficult to estimate. Most of the time, the contractor is responsible for deflection and camber calculations and any required adjustments for deck concrete placement to satisfy minimum vertical clearance, deck profile grades, and cross slope requirements. Design provides nonfactored instantaneous values of deflection components due to deck weight and barrier rail weight. These deflection components are used to set screed grades in the field.

The design should be cognizant of girder deflections not only because of the magnitude of various dead loads and prestress force but also because of the timing of the application of such loads. This is especially important for bridge widening. If more accurate camber values are required during the design stage for unusual cases such as widening of a long span bridge, the assumed age of the girder may need to be specified.

A haunch is a layer of concrete placed between the top flange of the girder and bottom of the deck, used to ensure proper bearing between the precast girder and the deck. It accommodates construction tolerances such as unknown camber of the girder at time of erection. Adequate haunch depth is provided to allow the contractor to adjust screed grades to meet the designed profile grades. For long span girders or long span spliced girders, the deflection should be designed and checked to ensure that the bridge camber is upward under both short-term and long-term conditions. Because the camber values vary along the span length, the actual values of the haunch thickness vary along the span too. The minimum haunch thickness is defined as the difference (at the centerline of the girder) between the upward camber of the girder at erection and the downward deflection of the girder due to the weight of the deck and haunch. The minimum required haunch thickness should be calculated at both midspan and at supports to (1) accommodate variation in actual camber, (2) allow the contractor to adjust screed grades, (3) eliminate potential intrusion of the top flange of the girder into the cast-in-place deck, and (4) determine seat elevation at supports. Cross slope and flange width at the top flange of the girder should be considered in determining the minimum haunch thickness. The equation for determining the minimum haunch thickness is given in the design example of Section 1.6. Although the calculation of minimum haunch thickness is based on midspan, the need for minimum haunch thickness in construction applies firstly to the support locations, because this value is required to establish seat elevations for the bridge. Therefore, information of structure depth should show the following: (1) minimum structure depth at centerline of bearing at the supports, including girder depth, deck thickness, plus calculated haunch thickness, and (2) minimum structure depth at midspan, including girder depth, deck thickness, plus any minimum haunch thickness the designer may choose. The suggested minimum haunch at midspan can range from a half inch to one inch. For girders with large flange widths, such as wide-flange girders, large haunch could add up to significant quantities and weights of additional concrete. Therefore, selection of minimum haunch thickness at midspan should be practical.

1.4.7 Diaphragms and End Blocks

A multigirder bridge has diaphragms provided at abutments and bents. For certain span lengths, permanent intermediate diaphragms may be provided to stabilize the girders during construction.

Cast-in-place intermediate diaphragms normally are optional but they improve distribution of loads between girders and help stabilize the girders during construction. Girder lengths over 80 ft usually require one intermediate diaphragm, most efficiently located at midspan. Intermediate diaphragms should be used for high skewed bridges. For bridge skews of less than or equal to 20°, either normal or skewed intermediate diaphragms may be provided. For bridge skews greater than 20°, intermediate diaphragms normal to the girders are preferred as they can be staggered.

Owing to an increase in fabrication inefficiencies, girder weight, and overall cost, girder end blocks should only be used where it is essential.

1.4.8 Lateral Stability

Because precast girders tend to be rather long, slender members, they should be checked for lateral stability during all construction stages, including handling, transportation, and erection. Fabricators are normally responsible for all girder stability checks. However, the designer is encouraged to consider and verify lateral stability during design when nonstandard girders are selected.

Procedures for checking lateral stability were developed by Mast (1989 and 1993), and some commercial software incorporates this method. The designer should verify specific assumed supports

and stability parameters (e.g., support locations, impact, transport stiffness, super elevation, height of girder center of gravity and roll center above road, and transverse distance between centerline of girder and center of dual tire) with local fabricators, contractors, and other engineers, as appropriate.

1.4.9 Seismic Considerations

Seismic design is necessary in earthquake regions. Bridges of similar characteristics in different locations may behave different during an earthquake. Detailed seismic evaluation and correct seismic design of connections between precast girders, as well as connections between precast girders and the supporting substructure, are needed. The connection system must be designed to either protect the superstructure from force effects due to ground motions through fusing or plastic hinging, or transmit inertial forces through the load path into the ground. Ductile behavior is desirable in both the longitudinal and transverse directions for substructures. One of the common ways of meeting the seismic requirements is to achieve continuity and monolithic action between precast girders as well as the integral connection system between precast girders and the supporting substructure.

1.4.10 Spliced Girder Design

In addition to meeting requirements of design codes, general design considerations are as follows:

- Spliced girder design normally consists of design of precast–pretensioned girders and posttensioning spliced girders. Therefore, both pretensioning and posttensioning process shall be considered.
- Construction sequence and staging must be taken into account. Temporary supports and locations shall be considered and designed properly as these affect the girder section, span length, and pretensioning and posttensioning force. Temporary support locations and reactions for each stage of construction shall be noted.
- The service limit state must be addressed in design considering both temporary and final concrete stresses in girder segments at each stage of pretensioning and posttensioning as well as all applicable loads during construction. The strength limit state only needs to be considered for the final construction stage.
- Posttensioning may be applied to precast girders before and/or after placement of the deck concrete. When posttensioning is applied to the girders both prior to and after placement of the concrete deck, it is referred to as two-stage posttensioning. In general, one-stage posttensioning is relatively simple in design and construction and is mostly used with bridge span lengths less than approximately 120 to 140 ft. Normally, it is desirable to apply all of the posttensioning after the deck becomes a part of the composite deck-girder section. When the full posttensioning force is applied prior to deck placement, this allows for future deck replacement or can meet other project specific requirements. In this one-stage approach, the posttensioning force and girder compressive strength (f'_c) are usually higher than that required for posttensioning to the composite section or for two-stage posttensioning. When the bridge span length exceeds approximately 120 to 140 ft, two-stage posttensioning typically results in a more efficient bridge system. The first-stage posttensioning is designed to control concrete stresses throughout the continuous span for the loads applied before the second stage of posttensioning. The second-stage posttensioning force is usually designed for superimposed dead loads and live loads. Benefits of the two-stage posttensioning method include lower required pretensioning force, more efficient total posttensioning force for the structure, lower required f'_{ci} and f'_c for the precast girder, and better deflection control.
- Prestress losses due to the effects of pretensioning, posttensioning, and possible staged posttensioning shall be considered. Time-dependent losses associated with multiple stages shall be properly evaluated.

- Instantaneous deflections due to posttensioning at different stages should be noted. These deflection values will be used to set screed grades in the field.
- The posttensioning tendon profile shall be noted. Although a specific tendon placement pattern may not be provided in design, at least one workable tendon placement solution shall be developed at all locations along the span, including at anchorages.
- Wet closure joints between girder segments are usually used instead of match-cast joints. The width of a closure joint shall not be less than 24 in and shall allow for the splicing of posttensioning ducts and rebar. Web reinforcement, within the joint should be the larger of that provided in the adjacent girders. The face of the precast segments at closure joints must be intentionally roughened or cast with shear keys in place.

1.5 Design Flow Chart

A detailed precast–pretensioned concrete girder design flow chart is shown in Figure 1.13:

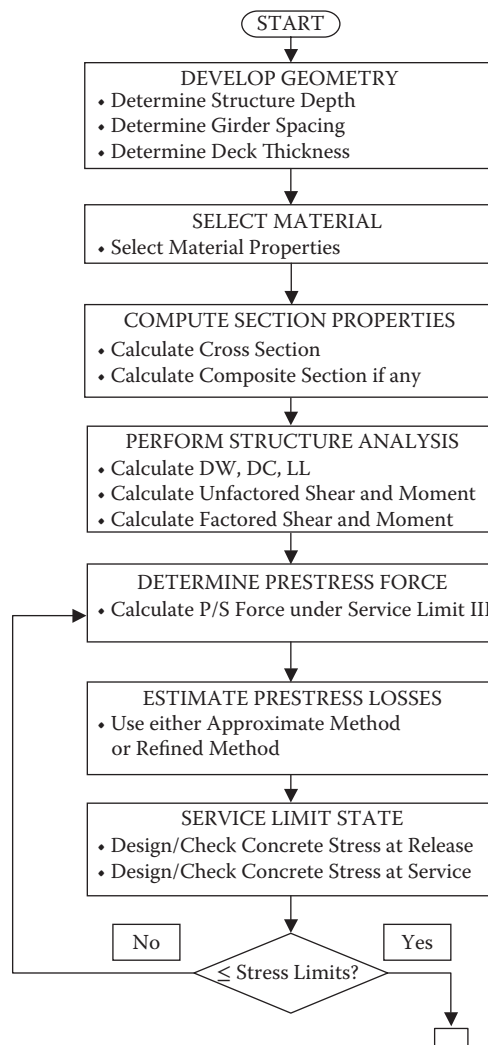


FIGURE 1.13 Precast–pretensioned concrete girder design flow chart

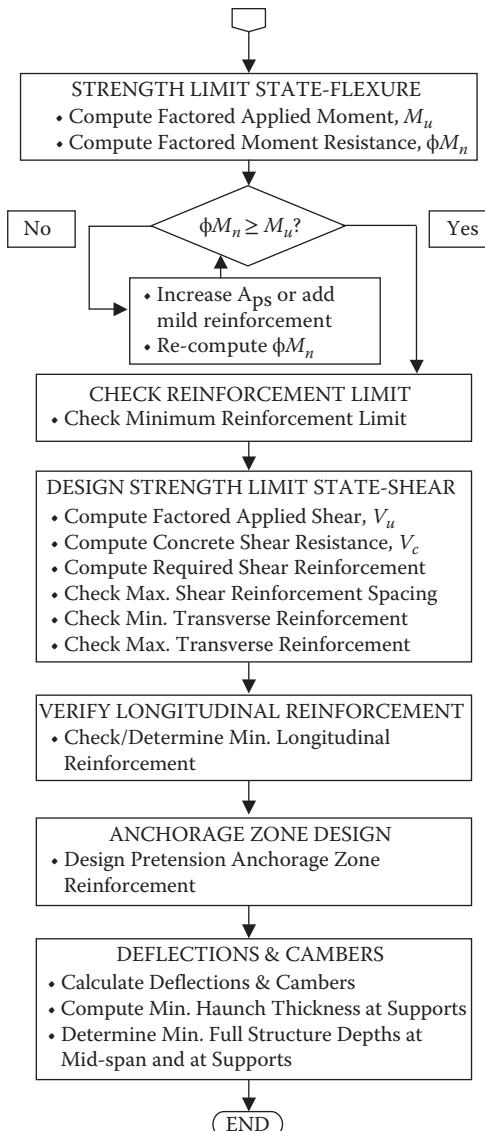


FIGURE 1.13 (Continued) Precast-pretensioned concrete girder design flow chart.

1.6 Design Example—Simple Span Precast-Pretensioned I-Girder Bridge

This example illustrates the typical procedure in designing a simple span precast-pretensioned concrete girder bridge in accordance with *AASHTO LRFD Bridge Design Specifications* (AASHTO 2012).

1.6.1 Bridge Data

The bridge has a span length of 85 ft (from centerline of support to centerline of support). Total deck width is 35 ft, including two 12 ft traffic lanes with two 4 ft shoulders and two 1.5 ft concrete barriers. Bridge elevation and plan views are shown in Figures 1.14 and 1.15, respectively. In Figure 1.15, the abbreviations BB and EB stand for “Begin Bridge” and “End Bridge” respectively.

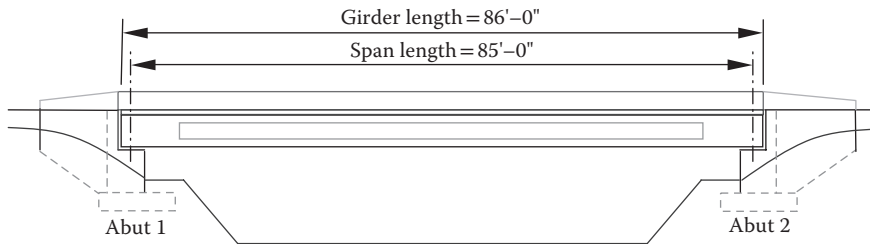


FIGURE 1.14 Bridge elevation.

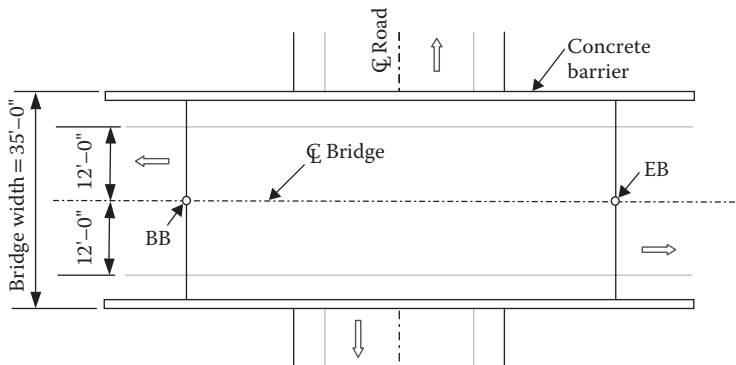


FIGURE 1.15 Bridge plan.

1.6.2 Design Requirements

A precast–pretensioned concrete I-girder bridge type is selected as the superstructure of the bridge. In this example, the following steps are performed for the design of an interior girder in accordance with the AASHTO LRFD Bridge Design Specifications (AASHTO 2012).

- Develop geometry.
- Select materials.
- Compute section properties.
- Perform structural analysis.
- Determine required prestressing force.
- Estimate prestress losses.
- Check concrete stresses for service limit state.
- Design for strength limit state—flexural.
- Design for strength limit state—shear.
- Check longitudinal reinforcement requirement.
- Design anchorage zone reinforcement.
- Calculate deflection and camber.

1.6.3 Solutions

1.6.3.1 Develop Geometry

For the constant depth superstructure of the precast–pretensioned I-beams, the structure depth-to-span ratio, D/L can be taken as 0.045, and the girder spacing-to-structure depth ratio of 1.5 is commonly used. It is also assumed that the prestressing steel is to be stressed to 75% of its strength with harped strands at $0.4L$ to control concrete stresses at the top of the girder at transfer stage.

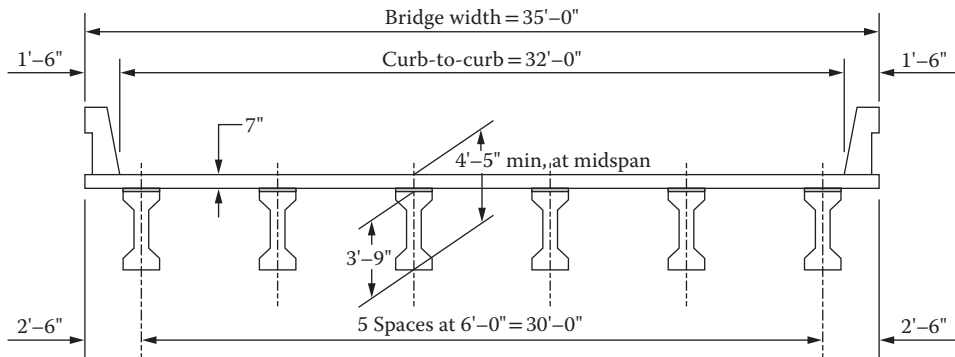


FIGURE 1.16 Typical cross section.

For this example, $L = 85.0$ ft, the desired structural depth $D = 0.045L = (0.45)(85.0) = 3.825$ ft = 45.9 in.

Assume that a 7-in concrete slab thickness is used for the bridge deck.

The desired precast girder height = 45.9 - 7.0. = 38.9 in.

Therefore, select the 3'9" AASHTO type III girders.

Assuming the minimum haunch thickness at midspan $t_h = 1.0$ in.

Total structure depth = 45.0 + 1.0 + 7.0 = 53.0 in > 0.045L = 45.9 in OK.

The girder spacing is determined as follows:

$$\text{Total bridge width} = 35.0 \text{ ft}$$

$$\text{Curb-to-curb} = 32.0 \text{ ft}$$

$$\text{Haunch width} = 16 \text{ in}$$

$$\text{Girder Spacing} = 1.5D = 1.5(53) = 79.5 \text{ in} = 6.63 \text{ ft}$$

Therefore, use girder spacing = 6.0 ft. A typical cross section of the bridge is shown in Figure 1.16.

1.6.3.2 Select Materials

Concrete unit weight, $w_c = 0.15$ kcf. Note that Table 3.5.1-1 of LRFD 2012 allows

$$w_c = 0.145 \text{ kcf} \quad \text{for } f'_c \leq 5.0 \text{ ksi}; \quad w_c = 0.140 + 0.001 f'_c \quad \text{for } 5.0 \text{ ksi} < f'_c \leq 15.0 \text{ ksi}$$

- (a) Concrete for cast-in-place deck slab

Concrete strength, $f'_c = 4.0$ ksi

$$\text{Modulus of elasticity, } E_c = 33,000 K_1 w_c^{1.5} \sqrt{f'_c} \quad (\text{AASHTO 5.4.2.4-1})$$

K_1 = correction for source aggregate = 1.0

$$E_c = 33,000(1.0)(0.15)^{1.5} \sqrt{(4.0)} = 3834 \text{ ksi}$$

- (b) Concrete for precast girder

Assume concrete strength at transfer, $f'_{ci} = 4.5$ ksi.

Modulus of elasticity, $E_{ci} = 4,067$ ksi.

Assume concrete strength at 28 days, $f'_c = 6.0$ ksi.

Modulus of elasticity, $E_c = 4,696$ ksi.

The concrete strength assumptions will be verified later in the example.

(c) Prestressing steel

Use 0.6 in diameter, seven-wire, low-relaxation.

Area of strand, $A_{ps} = 0.217 \text{ in}^2$ per strand.

Tensile strength, $f_{pu} = 270 \text{ ksi}$.

Yield strength, $f_{py} = 0.9 f_{pu} = 243 \text{ ksi}$.

$$\text{Modulus of elasticity, } E_p = 28,500 \text{ ksi}$$

(AASHTO 5.4.4.2)

The initial stress in prestressing steel before transfer, $f_{pbt} \leq 0.75 f_{pu}$

Therefore, use $f_{pbt} = 0.75 (270) = 202.5 \text{ ksi}$

(d) Reinforcing steel

Yield strength, $f_y = 60 \text{ ksi}$

$$\text{Modulus of elasticity, } E_s = 29,000 \text{ ksi}$$

(AASHTO 5.4.3.2)

1.6.3.3 Compute Section Properties

(a) Precast girder only

The shape and dimensions of a 3'9" AASHTO type III girder is illustrated in Figure 1.17.

Section properties of the girder are presented in Table 1.3.

Section modulus of precast girder for extreme bottom fiber of precast girder is as follows:

$$S_b = \frac{I}{y_b} = \frac{125,390}{20.3} = 6,177 \text{ in}^3$$

Section modulus of precast girder for extreme top fiber of precast girder is as follows:

$$S_t = \frac{I}{y_t} = \frac{125,390}{24.7} = 5,077 \text{ in}^3$$

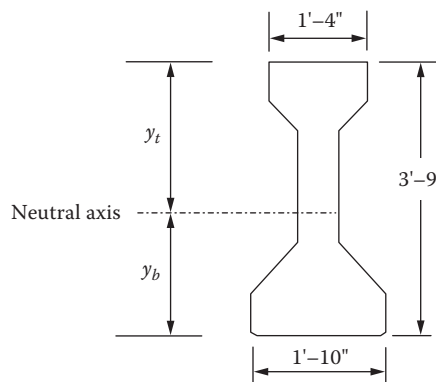


FIGURE 1.17 AASHTO type III girder.

TABLE 1.3 Section Properties—Girder Only

Area	560 in ²
y_t	24.7 in
y_b	20.3 in
Moment of inertia, I	125,390 in ⁴

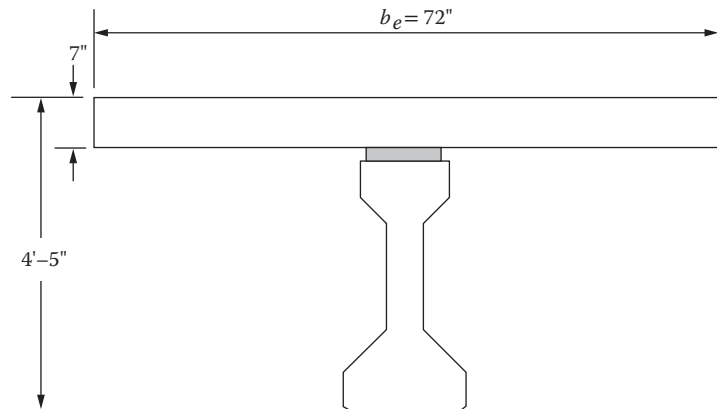


FIGURE 1.18 Effective flange width.

(b) Effective flange width

According to AASHTO Art. 4.6.2.6.1, for skew angles $\leq 75^\circ$, $L/S \geq 2.0$, and overhang $\leq 0.5S$, the effective flange width of a concrete deck slab for an interior girder can be taken as the tributary width, that is, girder spacing S . For this example, skew angles = 0 ($\leq 75^\circ$); $L/S = 85/6 = 14.2$ (> 2.0) and overhang width = 2.5' ($< 0.5S = 3.5'$). Therefore, the effective flange width $b_e = S = 72$ in (Figure 1.18).

(c) Composite section

The section properties of individual elements including girder, deck, and haunch are calculated in Figure 1.19.

In order to compute the section properties of composite section, it is necessary to transform the cast-in-place deck slab and haunch using a modular ratio, n_c , to account for the difference in concrete materials between precast girder and cast-in-place deck.

1.6.3.4 Perform Structural Analysis

(a) Calculate dead loads (DC and DW)

- Dead loads on noncomposite section.

$$\text{Precast girder, } w_g = \frac{560}{144}(0.15) = 0.583 \text{ klf}$$

$$\text{Deck slab, } w_s = \frac{(72)(7)}{144}(0.15) = 0.525 \text{ klf}$$

$$\text{Haunch, } w_h = \frac{16}{144}(0.15) = 0.017 \text{ klf}$$

- Dead loads on composite section.

According to AASHTO Art. 4.6.2.2.1, permanent dead loads (including concrete barriers and wearing surface) may be distributed uniformly among all girders provided all of the following conditions are met.

- Width of deck is constant.
- Number of girder is not less than 4. The example has $N_b = 6$.
- Beams are parallel and have approximately the same stiffness.

Section	Area, A_i (in ²)	y_i (in)	$A_i(y_i)$ (in ³)	$A(y_i - y_{cg})^2$	I_o (in ⁴)
Girder	560	20.3	11,368	87,500	125,390
Deck	411.6*	49.5	20,374	114,791	2,058
Haunch	13.1*	45.5	596	2,113	1
Total	985		32,338	204,404	127,449

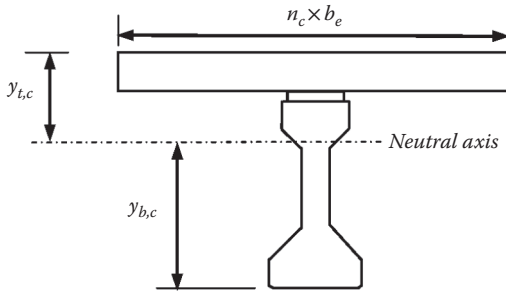
*multiplied by n_c

Deck $E_{cd} = 3,834$ ksi; Girder $E_{cg} = 4,696$ ksi; $n_c = E_{cd}/E_{cg} = 0.82$

$$y_c = \frac{32,338}{985} = 32.8 \text{ in}$$

$$y_{b,c} = y_c = 32.8 \text{ in}$$

$$y_{t,c} = 53.0 - 32.8 = 20.2 \text{ in}$$



$$I_c = 204,404 + 127,449 = 331,853 \text{ in}^4$$

$$S_{bc} = \frac{331,853}{32.8} = 10,117 \text{ in}^4$$

FIGURE 1.19 Section properties—composite section.

- Roadway part of the overhang, d_e , does not exceed 3.0 ft. The example has
 - $d_e = 3.0 - 1.5 = 1.5$ ft
 - bridge is on a tangent line and curvature in plan is zero.
 - cross-section is consistent with one of the cross-sections shown in AASHTO Table 4.6.2.2.1-1. Superstructure is type (k).

Therefore, all criteria are satisfied. However, for this example, the concrete barrier and wearing surface loads can be evenly distributed among the six girders based on dead load distribution factor (DLDF), which is determined as follows:

$$DLDF = \frac{\text{Tributary Width}}{\text{Overall Bridge Width}} = \frac{6}{35} = 0.171$$

$$\text{Barrier DC3} = \frac{444}{144}(0.15)(2)(0.171) = 0.159 \text{ klf}$$

$$\text{Future wearing surface } DW = (0.035)(32')(0.171) = 0.192 \text{ klf}$$

- (b) Calculate shear force and bending moment due to DC and DW

Many structural analysis software programs are available commercially and could be used to perform structural analysis. For a simply supported girder, unfactored moments and shears due to dead loads can be calculated by the following formulas and listed in Table 1.4:

$$M_x = \frac{wx(L-x)}{2}$$

$$V_x = w\left(\frac{L}{2} - x\right)$$

where

w = uniform dead load, k/ft

x = distance from left end of the girder

L = span length = 85 ft

- (c) Calculate shear force and bending moment due to live loads

The live load considered in this example is the AASHTO HL-93 load

- (i) *Live load distribution factor (for an interior girder)*

Live load shear forces and bending moments for an interior girder can be determined using the simplified distribution factor formulas specified in AASHTO Art. 4.6.2.2.2 and AASHTO Art. 4.6.2.2.3, if all of the conditions in AASHTO Art. 4.6.2.2 are met. It has been shown in the previous section that, for this example, these conditions are met. Therefore, the simplified distribution factor formulas are applicable.

Live load moment distribution factor

The live load distribution factor for moment in the interior girder, in lane, is computed as follows:

- (1) One design lane loaded

$$DFM = 0.060 + \left(\frac{S}{14} \right)^{0.4} \left(\frac{S}{L} \right)^{0.3} \left(\frac{K_g}{12L(t_s)^3} \right)^{0.1} \quad (\text{AASHTO Table 4.6.2.2.2b-1})$$

TABLE 1.4 Unfactored Shear Forces and Bending Moments

Location Dist/Span (x/L)	x (ft)	Girder Weight (DC1)		Slab+Haunch (DC2)		Barrier Weight (DC3)		AC Wearing Surface (DW)	
		V_x (kip)	M_x (kip-ft)	V_x (kip)	M_x (kip-ft)	V_x (kip)	M_x (kip-ft)	V_x (kip)	M_x (kip-ft)
0.00L	0.0	24.8	0.0	23.0	0.0	6.7	0.0	8.2	0.0
0.04L	3.4	22.8	80.9	21.2	75.1	6.2	22.0	7.5	26.6
0.10L	8.5	19.8	189.7	18.4	176.1	5.4	51.6	6.5	62.4
0.20L	17.0	14.9	337.2	13.8	313.1	4.0	91.7	4.9	111.0
0.30L	25.5	9.9	442.5	9.2	410.9	2.7	120.3	3.3	145.7
0.40L	34.0	5.0	505.8	4.6	469.6	1.3	137.5	1.6	166.5
0.50L	42.5	0.0	526.8	0.0	489.2	0.0	143.2	0.0	173.4
0.60L	51.0	-5.0	505.8	-4.6	469.6	-1.3	137.5	-1.6	166.5
0.70L	59.5	-9.9	442.5	-9.2	410.9	-2.7	120.3	-3.3	145.7
0.80L	68.0	-14.9	337.2	-13.8	313.1	-4.0	91.7	-4.9	111.0
0.90L	76.5	-19.8	189.7	-18.4	176.1	-5.4	51.6	-6.5	62.4
0.96L	81.6	-22.8	80.9	-21.2	75.1	-6.2	22.0	-7.5	26.6
1.00L	85.0	-24.8	0.0	-23.0	0.0	-6.7	0.0	-8.2	0.0

Provided the following ranges are met

- $3.5 \leq S \leq 16.0$

$S = \text{girder or web spacing} = 6 \text{ ft}$

- $4.5 \leq t_s \leq 12.0$

$t_s = \text{thickness of concrete slab} = 7.0 \text{ in}$

- $20 \leq L \leq 240$

$L = \text{span length} = 85 \text{ ft}$

- $N_b = \text{number of girders} \geq 4$

$N_b = 6$

- $10,000 \leq K_g \leq 7,000,000$

$K_g = 738,360 \text{ in}^4$ (see calc. below)

where

$$n = E_{\text{girder}}/E_{\text{slab}} = 1.22 \quad (\text{AASHTO 4.6.2.2.1-2})$$

$E_{\text{girder}} = \text{modulus of elasticity of girder} = 4,696 \text{ ksi}$

$E_{\text{slab}} = \text{modulus of elasticity of deck} = 3,834 \text{ ksi}$

$I = I_{\text{girder}} = 125,390 \text{ in}^4$

$A = A_{\text{girder}} = 560 \text{ in}^2$

$e_g = \text{distance between centers of gravity of girder and deck}$

$$= 49.50 - 20.30 = 29.20 \text{ in}$$

$$K_g = n(I + Ae_g^2) = 738,360 \text{ in}^4 \quad (\text{AASHTO 4.6.2.2.1-1})$$

$$DFM = 0.060 + \left(\frac{6.0}{14} \right)^{0.4} \left(\frac{6.0}{85.0} \right)^{0.3} \left(\frac{738,360}{12(85)(7)^3} \right)^{0.1} = 0.407 \text{ lanes/girder}$$

(2) Two or more design lanes loaded

$$DFM = 0.075 + \left(\frac{S}{9.5} \right)^{0.6} \left(\frac{S}{L} \right)^{0.2} \left(\frac{K_g}{12L(t_s)^3} \right)^{0.1} \quad (\text{AASHTO Table 4.6.2.2.2b-1})$$

$$DFM = 0.075 + \left(\frac{6.0}{9.5} \right)^{0.6} \left(\frac{6.0}{85.0} \right)^{0.2} \left(\frac{738,360}{12(85)(7)^3} \right)^{0.1} = 0.556 \text{ lanes/girder}$$

Therefore, for two or more lanes loaded controls, use $DFM = 0.556$ lanes/girder

Live load shear distribution factor

For one design lane loaded (AASHTO Table 4.6.2.2.3a-1)

$$DFV = 0.36 + \left(\frac{S}{25.0} \right) = 0.600 \text{ lanes/girder}$$

For two or more lanes loaded

$$DFV = 0.20 + \left(\frac{S}{12.0} \right) - \left(\frac{S}{35.0} \right)^{2.0} = 0.671 \text{ lanes/girder}$$

DFV is the larger of the one lane loaded and two or more lanes loaded.

Therefore, use $DFV = 0.671$ lanes/girder

Dynamic load allowance, IM

$$IM = 0.33 \text{ (Strength I limit state and service limit state)}$$

(AASHTO Table 3.6.2.1-1)

TABLE 1.5 Unfactored Live Load Moment and Shear Forces for Interior Girder

Location		Per Girder	
Dist/Span (x/L)	x (ft)	$M_{(LL+IM)}$ (kip·ft)	$V_{(LL+IM)}$ (kip)
0.00L	0.0	0	75.0
0.04L	3.7	219	70.8
0.10L	8.5	474	65.2
0.40L	34.0	1,213	37.8
0.50L	42.5	1,247	29.4
0.60L	51.0	1,213	-37.4
0.90L	76.5	474	-65.2
0.96L	81.3	219	-70.8
1.00L	85.0	0	-75.0

Span = 85 ft

Dynamic load allowance = 1.33

Number of lane = 2.667

Note: dynamic load allowance, IM, applies to truck load only.

Live load moment

The live load moment at tenth points can be obtained from any structural analysis programs. The analysis results are shown in Table 1.5.

In a simple span bridge, the maximum moment usually occurs at the midspan of the structure. With the 85 ft span length, the maximum HL-93 live load moment with impact equals 2240 k-ft for one design lane loaded.

For one interior girder,

$$M_{(LL+IM)HL93} = (0.55)(2,240) = 1,232 \text{ k-ft}$$

The HL-93 live load moment with impact at $0.4L$ equals 1199 k-ft.

(d) Load combinations

In an LRFD design, the total factored loads are taken as follows:

$$Q = \eta \sum \gamma_i Q_i \quad (\text{AASHTO 3.4.1-1})$$

where

η = a factor relating to ductility, redundancy, and operational importance (equal to 1.0 for this example)

γ_i = load factors

Q_i = specified loads

Check compressive stress in prestressed concrete components for Service I

$$\text{Service I: } Q = 1.00(DC + DW) + 1.00(LL + IM)_{HL-93} \quad (\text{AASHTO Table 3.4.1-1})$$

Check tensile stress in prestressed concrete components for Service III

$$\text{Service III: } Q = 1.00(DC + DW) + 0.80(LL + IM) \quad (\text{AASHTO Table 3.4.1-1})$$

Check resistances for Strength I

$$\text{Strength I: } Q = 1.25DC + 1.50DW + 1.75(LL + IM)_{HL-93} \quad (\text{AASHTO Table 3.4.1-1 \& -2})$$

1.6.3.5 Determine Required Prestressing Force

The preliminary prestressing force is usually determined on the basis of the service limit state service III load condition at midspan. The tensile stress limit for Service III is $0.19\sqrt{f'_c}$.

The center of gravity of the strands at midspan is assumed to be located at 5% of the girder depth from the bottom fiber.

$$5\% x(\text{girder height}) = 0.05(45) = 2.25 \text{ in. Try 3.0 in.}$$

$$\text{Eccentricity of prestressing steel at midspan } e_c = y_b - y_{bs} = 20.3 - 3.0 = 17.3 \text{ in.}$$

The stress at bottom of girder at the service limit state load combination is limited to as follows:

$$\begin{aligned} f_b &= \frac{(M_{DC1} + M_{DC2})}{S_b} + \left(\frac{M_{DC3} + M_{DW} + 0.8(M_{LL+IM}HL93)}{S_{bc}} \right) - \frac{P}{A} - \frac{Pe_c}{S_b} \\ &= \frac{(526.8 + 489.2)(12)}{6,177} + \frac{[143.2 + 173.4 + 0.8(1,247)](12)}{10,117} - \frac{P}{560} - \frac{P(17.3)}{6,177} \\ &= 3.535 - 0.00459P \end{aligned}$$

the stress at bottom of girder due to service Limit State III does not exceed the tensile stress limit

$$0.19\sqrt{f'_c} = 0.19\sqrt{6.0} = 0.465 \text{ ksi} \quad (\text{AASHTO Table 5.9.4.2.2-1})$$

$$f_b = 3.535 - 0.00459 P < 0.465 \text{ ksi}$$

Solving the above equation for P , the required minimum $P = 670$ kip.

Assume a 10% total prestress loss, then the required prestressing force at transfer (before any losses):

$$P_i = \frac{670}{0.90} = 745 \text{ kip}$$

$$\text{Area of prestressing strands required: } A_{ps} = \frac{745}{202.5} = 3.7 \text{ in}^2$$

Number of 0.6 in diameter strands required = $3.7/0.217 = 17.1$ strands.

Use 18 – 0.6" strands, $A_{ps} = 3.906 \text{ in}^2$

Providing 10 strands @2 in and 8 strands @4 in, which the centroid of strands is at 2.9 in from bottom of girder. To control the stress at transfer of prestressing force, harp two strands at middle web location to 36 in and two strands to 38 in at girder ends. The strand patterns at midspan and girder ends are shown in Figure 1.20.

Therefore, the eccentricity of prestressing force at midspan = $20.3 - 2.9 = 17.4$ in.

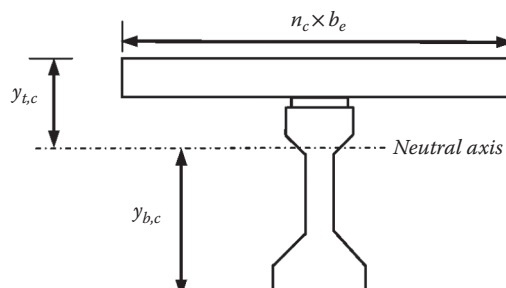


FIGURE 1.20 Strand pattern at midspan and at girder ends.

1.6.3.6 Estimate Prestress Losses

$$\text{Total prestress losses: } \Delta f_{pT} = \Delta f_{pES} + \Delta f_{pLT} \quad (\text{AASHTO 5.9.5.1-1})$$

where

Δf_{pES} = sum of all losses or gains due to elastic shortening or extension at the time of application of prestress and/or external loads (ksi)

Δf_{pLT} = losses due to long-term shrinkage and creep of concrete and relaxation of prestressing steel (ksi)

- (a) Instantaneous loss – elastic shortening

$$\text{Elastic shortening: } \Delta f_{pES} = \frac{E_p}{E_{ci}} f_{cgp} \quad (\text{AASHTO 5.9.5.2.3a-1})$$

The prestressing stress immediately after transfer (elastic shortening loss) may be assumed to be $0.9f_{pi} = 182.25$ ksi (assume 10% initial loss).

$$\begin{aligned} f_{cgp} &= \frac{P_i}{A} + \frac{(P_i e_c)^2}{I} - \frac{M_{DC1} e_c}{I} \\ &= \frac{712}{560} + \frac{(712)(17.4)^2}{125,390} - \frac{(526.8)(12)(17.4)}{125,390} \\ &= 1.271 + 1.719 - 0.877 = 2.113 \text{ ksi} \\ \Delta f_{pES} &= \frac{E_p}{E_{ci}} f_{cgp} = \frac{28,500}{4,067} (2.113) = 14.8 \text{ ksi} \end{aligned}$$

The prestressing stress immediately after transfer

$$f_{pi} = 0.75 f_{pu} - \Delta f_{pES} = 202.5 - 14.8 = 187.7 \text{ ksi.}$$

The calculated percent of prestressing loss due to elastic shortening is

$$(14.8/202.5) \times 100\%$$

= 7.3% < 10% assumed. Therefore, iteration is needed to calculate Δf_{pES} . A second iteration using $\Delta f_{pES} = 14.8$ ksi yields the following results:

$$f_{cgp} = 2.202 \text{ ksi}$$

$$\Delta f_{pES} = 15.4 \text{ ksi}$$

The initial prestressing stress (after elastic shortening loss) = $202.5 - 15.4 = 187.1$ ksi.

$$P_i = 187.1 (3.906) = 730 \text{ kips}$$

- (b) Long-term prestress losses – refined method

The prestress losses of the girder are determined using the refined method, as specified in Article 5.9.5.4 of the *AASHTO LRFD Bridge Design Specifications 2012 Edition*.

The long-term prestress losses in prestressing steel (due to creep and shrinkage of concrete, and relaxation of steel) are estimated according to the following:

$$\Delta f_{pLT} = (\Delta f_{pSR} + \Delta f_{pCR} + \Delta f_{pRI})_{id} + (\Delta f_{pSD} + \Delta f_{pCD} + \Delta f_{pR2} - \Delta f_{pSS})_{df} \quad (\text{AASHTO 5.9.5.4.1-1})$$

Δf_{pSR} = Prestress loss due to shrinkage of girder concrete between transfer and deck placement

Δf_{pCR} = Prestress loss due to creep of girder concrete between transfer and deck placement

Δf_{pri} = Prestress loss due to relaxation of prestressing strands between transfer and deck placement

Δf_{PSD} = Prestress loss due to shrinkage of girder concrete between deck placement and final time

Δf_{pCD} = Prestress loss due to creep of girder concrete between deck placement and final time

Δf_{PR2} = Prestress loss due to relaxation of prestressing strands between deck placement and final time

Δf_{pss} = Prestress gain due to shrinkage of deck

Concrete age at transfer: 1 day

Concrete age at deck placement: 90 days

Concrete age at final: 27,000 days

AASHTO LRFD recommends using transformed section properties for the refined method. The transformed section properties of girder at transfer and of composite section at final are calculated and shown in Figures 1.21 and 1.22, respectively.

Section	Area, A_i (in ²)	y_i (in)	$A_i(y_i)$ (in ³)	Y_{eg} in	$A(y_i - Y_{eg})^2 d$	I_o (in ⁴)
Girder	560	20.3	11,368	19.6	274	125,390
Strands	23.4*	2.89	67.7	19.6	6,544	
Total	583.4		11,436		6,818	125,390

Note: *Strand is transformed using $(n_i - 1)$

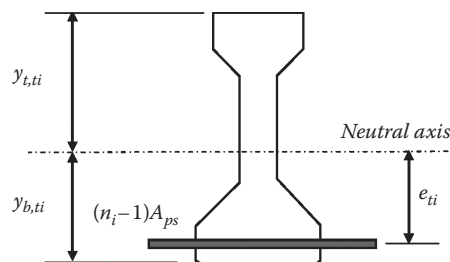
$$f'_{ci} = 4.5 \text{ ksi}; E_{ci} = 4,067 \text{ ksi}; n_i = E_{ps}/E_{ci} = 28,000/4,067 = 7$$

$$y_{ci} = \frac{11,436}{583.4} = 19.6 \text{ in}$$

$$y_{b,ti} = y_{ci} = 19.6 \text{ in}$$

$$y_{t,ti} = 25.4 \text{ in}$$

$$I_{ti} = 125,390 + 6,818 = 132,208 \text{ in}^4$$



$$S_{b,ti} = \frac{132,208}{19.6} = 6,745 \text{ in}^4$$

$$S_{t,ti} = \frac{132,208}{25.4} = 5,205 \text{ in}^4$$

$$e_{ti} = 19.6 - 2.89 = 16.7 \text{ in}$$

FIGURE 1.21 Transformed section properties—girder at transfer.

Section	Area, A_i (in ²)	y_i (in)	$A_i (y_i)$ (in ³)	Y_{cg} in	$A(y_i - Y_{cg})^2 d$	I_o (in ⁴)
Girder	560	20.3	11,368	19.7	195	125,390
Strands	19.8*	2.89	57.2	19.7	5,602	
Total	579.8		11,425		5,797	125,390

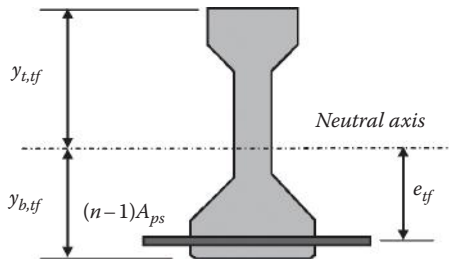
Note: *Strand is transformed using $(n - 1)$

$$f'_c = 6.0 \text{ ksi}; E_c = 4,696 \text{ ksi}; n = E_{ps}/E_{ci} = 28,000/4,696 = 6$$

$$\gamma_{cfg} = \frac{11,425}{579.8} = 19.7 \text{ in}$$

$$\gamma_{b,tf} = \gamma_{cg} = 19.7 \text{ in}$$

$$\gamma_{t,tf} = 25.3 \text{ in}$$



$$I_{tf} = 125,390 + 5,797 = 131,187 \text{ in}^4$$

$$S_{b,tf} = \frac{131,187}{19.7} = 6,656 \text{ in}^4$$

$$S_{t,tf} = \frac{131,187}{25.3} = 5,187 \text{ in}^4$$

$$e_{tf} = 19.7 - 2.89 = 16.8 \text{ in}$$

FIGURE 1.22 Transformed section properties—girder at final.

Prestress loss from transfer to time of deck placement

- (i) Deck shrinkage

$$\Delta f_{PSR} = (\varepsilon_{bid})(E_p)(K_{id}) \quad \text{AASHTO Eq. 5.9.5.4.2a-1}$$

$$\varepsilon_{bid} = (k_s)(k_{hs})(k_f)(k_{td})t_i^{-0.118}(0.48 \times 10^{-3}) \quad \text{AASHTO Eq. 5.4.2.3.3-1}$$

$$k_s = 1.45 - 0.13\left(\frac{V}{S}\right) \geq 1.0 \quad \text{AASHTO Eq. 5.4.2.3.2-2}$$

$$= 0.922 < 1.0 \quad \text{Use 1.0}$$

$$k_{hs} = 2.00 - 0.014H = 1.02 \quad \text{AASHTO Eq. 5.4.2.3.3-2}$$

$$k_f = \frac{5}{1+f'_{ci}} = 0.909 \quad \text{AASHTO Eq. 5.4.2.3.2-4}$$

$$k_{td} = \frac{t}{61 - 4f'_{ci} + t} = \frac{89}{61 - 4(4.5) + 89} = 0.674$$

T = maturity of concrete = $90 - 1 = 89$ days

$$\epsilon_{bid} = (1.0)(1.02)(0.909)(0.674)(0.48 \times 10^{-3}) = 0.30 \times 10^{-3}$$

$$K_{id} = \frac{1}{1 + \left(\frac{E_p}{E_{ci}} \right) \left(\frac{A_{ps}}{A_g} \right) \left(1 + \frac{A_g e_{pg}^2}{I_g} \right) \left[1 + 0.7 \Psi(t_f, t_i) \right]} \quad \text{AASHTO Eq. 5.9.5.4.2a-2}$$

$$e_{pg} = 20.3 - 2.9 = 17.4 \text{ in}$$

$$k_{hc} = 1.56 - 0.008H = 1.0$$

$$k_{td} = \frac{20,000 - 1}{61 - 4(4.5) + (20,000 - 1)} = 0.998$$

$$\begin{aligned} \Psi(t_f, t_i) &= 1.9(k_s)(k_{hc})(k_f)(k_{td})t_i^{-0.118} \\ &= 1.9(1.0)(1.0)(0.909)(0.998)(1.0) = 1.723 \end{aligned}$$

$$K_{id} = \frac{1}{1 + \left(\frac{28,000}{4,067} \right) \left(\frac{3.906}{560} \right) \left(1 + \frac{560(17.4)^2}{125,390} \right) \left[1 + 0.7(1.723) \right]} = 0.798$$

$$\Delta f_{pSR} = (0.30 \times 10^{-3})(28,500)(0.798) = 8.55 \text{ ksi}$$

Prestress loss due to creep of girder concrete between transfer and time of deck placement

$$\Delta f_{pCR} = \frac{E_p}{E_{ci}} f_{cgp} \Psi(t_d, t_i) K_{id} \quad \text{AASHTO Eq. 5.9.5.4.2b-1}$$

$$f_{cgp} = \frac{P_i}{A_{i,t}} + \frac{P_i(e_{i,t})^2}{I_{i,t}} - \frac{M_g e_{i,t}}{I_{i,t}}$$

$$P_i = 3.906(202.5) = 791 \text{ kips}$$

$$f_{cgp} = \frac{791}{583.4} + \frac{791(16.7)^2}{132,208} - \frac{(528.8 \times 12)(16.7)}{132,208} = 2.229 \text{ ksi}$$

$$\Psi(t_d, t_i) = 1.9(k_s)(k_{hc})(k_f)(k_{td})t_i^{-0.118}$$

$$k_{td} = \frac{89}{61 - 4(4.5) + 89} = 0.674$$

$$\Psi(t_d, t_i) = 1.9(1.0)(1.0)(0.909)(0.674)1.0^{-0.118} = 1.164$$

$$\Delta f_{pCR} = \frac{28,500}{4,067}(2.229)(0.674)(0.798) = 8.40 \text{ ksi}$$

 @SeismicIsolation

$$\Delta f_{pCR} = 1.2 \text{ ksi}$$

AASHTO Art. 5.9.5.4.2c

Prestress loss due to shrinkage of girder concrete between deck placement and final time

$$\Delta f_{pSD} = \epsilon_{bdj} E_p K_{df}$$

$$\epsilon_{bdj} = \epsilon_{bij} - \epsilon_{bid}$$

$$\begin{aligned}\epsilon_{bij} &= (k_s)(k_{hs})(k_f)(k_{tdf})(0.48 \times 10^{-3}) \\ &= (1.0)(1.02)(0.9090)(0.998)(0.48 \times 10^{-3}) = 0.444 \times 10^{-3}\end{aligned}$$

$$\begin{aligned}\epsilon_{bdj} &= (0.444 - 0.300) \times 10^{-3} \\ &= 0.144 \times 10^{-3}\end{aligned}$$

$$K_{df} = \frac{1}{1 + \left(\frac{E_p}{E_{ci}} \right) \left(\frac{A_{ps}}{A_c} \right) \left(1 + \frac{A_c e_{pc}^2}{I_c} \right) \left[1 + 0.7 \Psi(t_f, t_i) \right]}$$

e_{pc} = eccentricity of prestressing force from centroid of composite section

$$e_{pc} = 32.8 - 2.89 = 29.9 \text{ in}$$

$$\begin{aligned}K_{df} &= \frac{1}{1 + \left(\frac{28,500}{4,067} \right) \left(\frac{3.906}{985} \right) \left(1 + \frac{985(29.9)^2}{331,853} \right) \left[1 + 0.7(1.723) \right]} \\ &= 0.817\end{aligned}$$

$$\Delta f_{pSD} = (0.144 \times 10^{-3})(28,500)(0.817) = 3.35 \text{ ksi}$$

Prestress loss due to creep of concrete from deck placement to final.

$$\Delta f_{pCD} = \frac{E_p}{E_{ci}} f_{cgp} [\Psi(t_f, t_i) - \Psi(t_d, t_i)] K_{df} + \frac{E_p}{E_c} \Delta f_{cd} [\Psi(t_f, t_d)] K_{df}$$

Creep coefficient due to loading at deck placement to final,

$$\Psi(t_f, t_d) = 1.9(k_s)(k_{hc})(k_f)(k_{tdf})t_d^{-0.118}$$

Between deck placement and final,

$$k_{tdf} = \frac{t}{61 - 4(f'_{ci}) + t} = \frac{20,000 - 90}{61 - 4(4.5) + (20,000 - 90)} = 0.998$$

$$\Psi(t_f, t_d) = 1.9(1.0)(1.0)(0.909)(0.998)(90)^{-0.118} = 1.014$$

@Seismicisolation

Δf_{cd} = Changes in concrete stress between transfer and deck placement due to prestress loss, deck placement, deck weight, and superimposed dead loads.

$$\Delta f_{cd} = -(\Delta f_{pSR} + \Delta f_{pCR} + \Delta f_{pRI}) \frac{A_{ps}}{A_g} \left(1 + \frac{A_g e_{pg}^2}{I_g} \right)$$

$$- \left(\frac{M_{DC2} e_t}{I_{tf}} + \frac{(M_{DC3} + M_{DW}) e_{c,t}}{I_{c,t}} \right)$$

$$= -(8.55 + 8.40 + 1.20) \frac{3.906}{560} \left(1 + \frac{560(17.41)^2}{125,390} \right)$$

$$- \left(\frac{489.2 \times 12(16.8)}{131,187} + \frac{(143.2 + 173.4) \times 12(29.4)}{348,772} \right) = -1.370$$

$$\begin{aligned} \Delta f_{pCD} &= \frac{28,500}{4,067} (2.202)[1.732 - 1.164] 0.817 + \frac{28,500}{4,696} (-1.370)(1.014)(0.817) \\ &= 0.273 \text{ ksi} \end{aligned}$$

Relaxation of prestressing steel from deck placement to final time,

$$\Delta f_{pR2} = f_{pR1} = 1.2 \text{ ksi}$$

AASHTO Eq. 5.9.5.4.3c-1

Prestress gain due to shrinkage of deck concrete:

$$\Delta f_{pSS} = \frac{E_p}{E_c} \Delta f_{cdf} K_{df} \left(1 + 0.7 \Psi(t_f, t_d) \right)$$

AASHTO Eq. 5.9.5.4.3d-1

$$\Delta f_{cdf} = \frac{\epsilon_{ddf} A_d E_{cd}}{1 + 0.7 \Psi(t_f, t_d)} \left(\frac{1}{A_c} - \frac{e_{pc} e_d}{I_c} \right)$$

AASHTO Eq. 5.9.5.4.3d-2

ϵ_{ddf} = shrinkage strain of deck concrete between deck placement and final time

$$= 1.9 k_s k_{hs} k_f k_{td} 0.48 \times 10^{-3}$$

A_d = area of deck concrete = 72 (7.0) = 504 in²

E_{cd} = modulus of elasticity of deck concrete = 3,834 ksi

$\Psi(t_f, t_d)$ = creep coefficient of deck concrete at final time due to loading after deck placement

$$k_s = 1.45 - 0.13 \left(\frac{V}{S} \right)$$

$$= 1.45 - 0.13 \left(\frac{72(7)}{(72+7)^2} \right) = 1.04$$

@Seismicisolation

Assume that the initial concrete strength for deck is $0.75f'_c = 3.0$ ksi

$$k_f = \frac{5}{1 + f'_{ci}} = \frac{5}{1 + 3.0} = 1.25$$

$$k_{td} = \frac{t}{61 - 4f'_{ci} + t} = \frac{20,000 - 90}{61 - 4(3.0) + (20,000 - 90)} = 0.998$$

$$\begin{aligned}\epsilon_{ddf} &= k_s k_{hs} k_f k_{td} 0.48 \times 10^{-3} \\ &= 1.04(1.0)(1.25)(0.998)(0.48 \times 10^{-3}) = 0.623 \times 10^{-3}\end{aligned}$$

$$\begin{aligned}\Psi(t_f, t_d) &= 1.9 k_s k_{hc} k_f k_{td} t_i^{-0.118} \\ &= 1.9(1.04)(1.0)(1.25)(0.998)(1)^{-0.118} = 2.465\end{aligned}$$

e_d = eccentricity of deck with respect to the central gravity of composite section
 $= 53 - 7/2 - 32.8 = 16.7$ in

Creep of deck concrete,

$$\begin{aligned}\Delta f_{cd} &= \frac{\epsilon_{ddf} A_d E_{cd}}{1 + 0.7 \Psi(t_f, t_d)} \left(\frac{1}{A_c} - \frac{e_p e_d}{I_c} \right) \\ &= \frac{0.623 \times 10 - 3(504)(3,834)}{1 + 0.7(2.465)} \left(\frac{1}{985} - \frac{29.9(16.7)}{331,853} \right) = -0.217 \text{ ksi}\end{aligned}$$

A negative indicates a prestressing gain.

Prestress gain due to shrinkage of deck concrete,

$$\Delta f_{pss} = \frac{28,500}{4,696} (-0.217)(0.817)(1 + 0.7(2.465)) = -2.93 \text{ ksi}$$

Total time-dependent losses:

$$\begin{aligned}\Delta f_{pLT} &= (\Delta f_{pSR} + \Delta f_{pCR} + \Delta f_{pR1})_{id} + (\Delta f_{pSD} + \Delta f_{pCD} + \Delta f_{pR2} - \Delta f_{pSS})_{df} \\ &= (8.55 + 8.40 + 1.2) + (3.35 + 0.27 + 1.2 - 2.93) = 20.0 \text{ ksi}\end{aligned}$$

$$\Delta f_{pT} = \frac{20.0}{202.5} (100\%) = 10\%$$

f_{pe} = effective prestress = 202.5 ksi - 20.0 ksi = 182.5 ksi

Check prestressing stress limit at service limit state:

(AASHTO Table 5.9.3-1)

$$f_{pe} = 182.5 \text{ ksi} < 0.8 f_{py} = 0.8(243) = 194.4 \text{ ksi}$$

Therefore, the effective prestressing force after losses $P = 3.906(182.5) = 712.8$ kip

1.6.3.7 Check Concrete Stresses for Service Limit State

The AASHTO LRFD recommends the use of transformed gross concrete section combined with the new prestress loss estimations for service limit state design. When the transformed section properties are used, the elastic loss (or gain) at transfer, at deck placement, at superimposed load application, and live load application are not needed.

- (a) Check concrete stress limit at transfer condition
concrete stress limits
 Compressive stress limit:

$$\text{Stress limit} = 0.6 f'_{ci} = 2.700 \text{ ksi} \quad (\text{AASHTO 5.9.4.1.1})$$

Tensile stress limit:

- (i) In precompressed tensile zone without bonded reinforcement

$$\begin{aligned} \text{Stress limit} &= 0.0948 \sqrt{f'_{ci}} \leq 0.200 \text{ ksi} \\ \therefore 0.0948 \sqrt{4.5} &= 0.201 \text{ ksi} > 0.200 \text{ ksi} \quad (\text{AASHTO Table 5.9.4.1.2-1}) \end{aligned}$$

Therefore, stress limit = 0.200 ksi controls.

- (ii) In areas with bonded auxiliary reinforcement sufficient to resist the tensile force,

$$\text{stress limit} = 0.24 \sqrt{f'_{ci}} = 0.509 \text{ ksi}$$

Net-transformed section properties for interior girder at midspan

Net-transformed section properties for interior girder at midspan at transfer and at service are calculated in Figures 1.21 and 1.22, respectively. Figure 1.23 shows the transformed section properties at final (service) stage.

Check concrete stress at harped point

For pretensioned members with harped strands, the concrete stresses at the harped point location normally controls at the transfer stage. As time-dependent losses occur, the stresses at this location become less critical. The transformed section properties combined with the initial prestressing force should be used.

Harpd point location = $0.4 L = 0.4(85.0) = 34.0 \text{ ft}$

Total prestressing force at transfer, $P_i = (0.75)(270 \text{ ksi})(3.906 \text{ in}^2) = 791 \text{ kips}$

Eccentricity at $0.4L$, $e = 20.3 - 2.89 = 17.4 \text{ in}$

Calculate concrete stress at top of girder at transfer,

$$f_t = \frac{P_i}{A_{tr}} - \frac{P_i e}{S_{t,ti}} + \frac{M_{DC1}}{S_{t,ti}} = \frac{791}{583} - \frac{791(17.4)}{5,205} + \frac{505.8(12)}{5,205} = -0.122 \text{ ksi (tension)}$$

Since the stress is within the tensile limit (0.200 ksi), the stress limit is met.

Compressive stress at bottom of girder at transfer:

$$\begin{aligned} f_b &= \frac{P_i}{A_{tr}} + \frac{P_i e}{S_{b,ti}} - \frac{M_{DC1}}{S_{b,ti}} = \frac{791}{583} + \frac{791(17.4)}{6,745} - \frac{505.8(12)}{6,745} \\ &= 2.497 \text{ ksi (compression)} < 2.700 \text{ ksi.} \end{aligned}$$

Check concrete stress at midspan (at transfer)

The concrete stresses at midspan at transfer stage can be determined using the same procedure. The values for P_i , e , A_{tr} , $S_{b,ti}$, and $S_{t,ti}$ at midspan are the same as at $0.4L$. The bending moment at midspan $M_{DC1} = 526.8 \text{ kip-ft}$.

$f_{top} = -0.074 \text{ ksi (tensile)}$. The tensile stress limit (0.200 ksi) is met.

Section	Area, A_i (in ²)	y_i (in)	$A_i (y_i)$ (in ³)	$A(y_i - y_{cg})^2 d$	I_o (in ⁴)
Girder	560	20.3	11,368	79,836	125,390
Strands	19.8*	2.89	57.2	17,056	0
Deck	411**	49.5	20,357	122,514	1,679
Haunch	13.1	45.5	594	2,296	1
Total	1,004		32,376	221,702	127,070

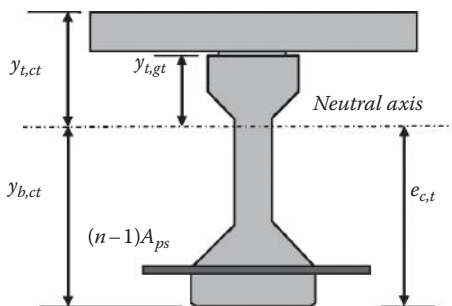
Note:

*Strand is transformed using $(n - 1) = 5$

**Deck is transformed using $n_c = 0.82$

$$y_{c,ct} = \frac{32,376}{1,004} = 32.2 \text{ in}$$

$$y_{b,ct} = y_{cg} = 32.2 \text{ in}$$



$$y_{t,gt} = 12.8 \text{ in}$$

$$I_{c,t} = 12,070 + 221,702 = 348,772 \text{ in}^4$$

$$S_{bc,t} = \frac{348,772}{32.2} = 10,818 \text{ in}^4$$

$$S_{lgc,t} = \frac{348,772}{12.8} = 27,333 \text{ in}^4; S_{tdc,t} = \left(\frac{1}{6.1}\right) \frac{348,772}{20.8} = 20,588 \text{ in}^4 e_{c,t} = 32.2 - 2.89 = 29.4 \text{ in}$$

FIGURE 1.23 Transformed section properties—composite at final.

$$f_{bot} = 2.459 \text{ ksi} < 2.700 \text{ ksi}$$

As shown in these calculations, the harped point location (0.4L) is the most critical section for concrete stresses at the transfer stage along the entire girder.

- (b) Check concrete stress at service condition

Concrete stress limit

Compressive stress limit

(AASHTO Table 5.9.4.2.1-1)

- Compression stress limit due to unfactored permanent loads (including girder, slab and haunch, barrier, and future wearing surface weights) and prestressing force combination: PS + Perm

$$\text{Precast girder} = 0.45 f'_c = 0.45(6.000) = 2.700 \text{ ksi}$$

$$\text{CIP deck} = 0.45 f'_{c,deck} = 0.45(4.000) = 1.800 \text{ ksi}$$

- Compression stress limit due to effective prestress, permanent, and transient loads (including all dead and live loads) combination PS + Perm + (LL+IM)_{HL-93}

$$\text{Precast girder} = 0.60 f'_c = 0.60(6.000) = 3.600 \text{ ksi}$$

$$\text{CIP deck} = 0.60 f'_{c,deck} = 0.60(4.000) = 2.400 \text{ ksi}$$

Tensile stress limit

For components with bonded prestressing tendons or reinforcement:

Load combination **service III** = [PS + perm + 0.8(LL+IM)_{HL-93}]:

$$\text{Precast girder} = 0.19 \sqrt{f'_c} = 0.19 \sqrt{6.0} = 0.465 \text{ ksi}$$

Check concrete stress at midspan (at service)

Top and/or bottom fibers of precast girder are checked for compressive stresses under the following load combinations:

- (i) Load combination **PS + perm**

Stress at top of precast girder:

$$f_{tg} = \frac{P_i}{A_{tr}} - \frac{P_i e_c}{S_{tgtf}} + \frac{(M_{DC1} + M_{DC2})}{S_{tgtf}} + \frac{(M_{DC3} + M_{DW})}{S_{tgtc}}$$

$$= \frac{712.8}{579.8} - \frac{712.8(16.8)}{5,187} + \frac{(526.8 + 489.2)(12)}{5,187} + \frac{(143.2 + 173.4)(12)}{27,333}$$

$$= 1.410 \text{ ksi (compression)} < 2.700 \text{ ksi}$$

Stress at bottom of precast girder:

$$f_b = \frac{P_f}{A_{tr}} + \frac{P_f e_c}{S_{b,tr}} - \frac{(M_{DC1} + M_{DC2})}{S_{b,tr}} - \frac{(M_{DC3} + M_{DW})}{S_{bc,tr}}$$

$$= \frac{712.8}{579.8} + \frac{712.8(16.8)}{6,656} - \frac{(526.8 + 489.2)(12)}{6,656} - \frac{(143.2 + 173.4)(12)}{10,818}$$

$$= 0.846 \text{ ksi (compression)} < 2.700 \text{ ksi}$$

Stress at top of CIP deck:

$$f_{td} = \frac{(M_{DC3} + M_{DW})}{S_{tdct}}$$

$$= \frac{(143.2 + 173.4)}{20,588}$$

$$= 0.185 \text{ ksi (compression)} < 1.800 \text{ ksi}$$

- (ii) Load combination **PS + perm + (LL+IM)_{HL-93}**

Compressive stress at top of precast girder:

$$f_{tg} = \frac{P_f}{A} - \frac{P e_c}{S_t} + \frac{(M_{DC1} + M_{DC2})}{S_{tff}} + \frac{(M_{DC3} + M_{DW})}{S_{tgc,t}} + \frac{(M_{(LL+IM)HL93})}{S_{tgc,t}}$$

$$= \frac{712.8}{579.8} - \frac{712.8(16.8)}{5,187} + \frac{(526.8 + 489.2)(12)}{5,187} + \frac{(143.2 + 173.4)(12)}{27,333} + \frac{1,247(12)}{27,333}$$

$$= 1.271 \text{ ksi (compression)} < 3,600 \text{ ksi}$$

Stress at top of CIP deck:

$$\begin{aligned} f_{td} &= \frac{(M_{DC3} + M_{DW})}{S_{tdct}} + \frac{(M_{LL})}{S_{tdct}} \\ &= \frac{(143.2 + 173.4)(12)}{20,588} + \frac{1,247(12)}{20,588} \\ &= 0.911 \text{ ksi (compression)} < 2.400 \text{ ksi} \end{aligned}$$

- (iii) Load combination **service III** = [PS + perm + 0.8(LL+IM)_{HL-93}]:
Check tensile stresses at bottom of precast girder under service III

$$\begin{aligned} f_b &= \frac{P_f}{A} + \frac{P_f e_c}{S_{bf}} - \frac{(M_{DC1} + M_{DC2})}{S_{bf}} - \frac{(M_{DC3} + M_{DW})}{S_{bcf}} - \frac{0.8(M_{(LL+IM)HL93})}{S_{bcf}} \\ &= \frac{712.8}{579.8} + \frac{712.8(16.8)}{6,656} - \frac{(526.8 + 489.2)(12)}{6,656} + \frac{(143.2 + 173.4)(12)}{10,818} + \frac{0.8(1,247)(12)}{10,818} \\ &= 0.795 \text{ ksi (compression)} \end{aligned}$$

Since the section is in compression, tensile stress limit is met. Therefore, OK.

1.6.3.8 Design for Strength Limit State—Flexural

- (a) Maximum factored moment, M_u

The maximum moment for a simple span structure occurs at the midspan.
Strength I:

$$M_u = 1.25 [M_{DC1} + M_{DC2} + M_{DC3}] + 1.5M_{DW} + 1.75[M_{(LL+IM)HL93}]$$

The critical design moment for an interior girder occurs at midspan.

$$\begin{aligned} M_u &= 1.25DC + 1.50DW + 1.75(LL + IM)_{HL-93} \\ &= 1.25[526.8 + 489.2 + 143.6] + 1.50[173.4] + 1.75[1,247] \\ &= 3,892 \text{ kip-ft} \end{aligned}$$

- (b) Average prestressing steel stress

For sections with bonded tendons and average stress in prestressing steel $> 0.5 f_{pu}$,

$$f_{ps} = f_{pu} \left(1 - k \frac{c}{d_p} \right) \quad (\text{AASHTO 5.7.3.1.1-1})$$

in which

$$k = 2 \left(1.04 - \frac{f_{py}}{f_{pu}} \right) = 2 \left(1.04 - \frac{243}{270} \right) = 0.28 \quad (\text{AASHTO 5.7.3.1.1-2})$$

For deck concrete, $f'_c = 4.0$ ksi

$$\beta_1 = 0.85 - 0.05(f'_c - 4.0) = 0.85 - 0.05(4.0 - 4.0) = 0.85 > 0.65 \quad (\text{AASHTO 5.7.2.2})$$

Use $\beta_1 = 0.85$

Assume that the compressive area is a rectangular section, and assume $c/d_x \geq 0.6$, thus $f_s = f_y$. (AASHTO 5.7.2.1). The distance from neutral axis to extreme compressive fiber is as follows:

$$c = \frac{A_{ps}f_{pu} + A_s f_s - A'_s f_s}{0.85 f'_c \beta_1 b + k A_{ps} \left(\frac{f_{pu}}{d_p} \right)} \quad (\text{AASHTO 5.7.3.1.1-4})$$

$$c = \frac{3.906(270) + 1.76(60) - 0}{0.85(4.0)(0.85)(72) + 0.28(3.906) \left(\frac{270}{50.1} \right)} = 5.42 \text{ in}$$

Depth of compression block: $a = \beta_1 c = 0.85(5.42) = 4.61 \text{ in}$

Since this is less than the slab thickness of 7.0 in., the assumption of rectangular compressive section is valid.

$c/d_x = 5.42/47 = 0.12 < 0.6$, therefore the assumption $f_s = f_y$ is also valid.

For tension controlled prestressed concrete, the flexure resistance factor $\phi = 1.0$ (AASHTO 5.5.4.2)

$$f_{ps} = f_{pu} \left(1 - k \frac{c}{d_p} \right) = (270) \left(1 - 0.28 \frac{5.42}{50.1} \right) = 261.8 \text{ ksi}$$

$f_{ps} = 261.8 \text{ ksi} > 0.5 f_{pu} = 0.5(270) = 135 \text{ ksi}$. Therefore, the equation is applicable. (AASHTO 5.7.3.1.1-1)

(c) Factored resistance moment

Assuming a tension-control section where the net tensile strain in the extreme tension steel is ≥ 0.005 when concrete strain $\epsilon_c = 0.003$ and using $\phi = 1.0$, we have:

$$\begin{aligned} \text{Factored resistance } \phi M_n &= \phi \left[A_{ps} f_{ps} \left(d_p - \frac{a}{2} \right) + A_s f_y \left(d_p - \frac{a}{2} \right) \right] \quad (\text{AASHTO 5.7.3.2.2-1}) \\ &= 1.0 \left[(3.906)(261.8) \left[50.1 - \frac{4.61}{2} \right] + (1.76)(60) \left[49.0 - \frac{4.61}{2} \right] \right] \\ &= 53,806 \text{ kip-in} \\ &= 4,483 \text{ kip-ft} > M_u = 3,892 \text{ kip-ft} \end{aligned}$$

Check the assumption that the section is tension-controlled, that is, $\epsilon_t > 0.005$. From Figure 1.24, the following is obtained:

$$\epsilon_t = 0.003 \left(\frac{d_t - c}{c} \right) = 0.003 \left(\frac{51 - 5.42}{5.42} \right) = 0.025 > 0.005 \quad \text{Therefore, } \phi = 1.0.$$

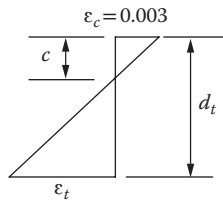


FIGURE 1.24 Strain diagram.

(d) Minimum reinforcement

The amount of prestressed tensile reinforcement at any section of a flexure member is adequate to develop a factored flexural resistance, AASHTO 5.7.3.3.2 requires that flexure resistance, M_r , equals the lesser of (i) 1.33 M_u and (ii) M_{cr} .

- (i) At midspan, factored moment M_u due to strength I = 3892 k-ft

$$1.33M_u = 5060 \text{ k-ft}$$

$$(ii) M_{cr} = \gamma_3 \left[\left(\gamma_1 f_r + \gamma_2 f_{cpe} \right) S_c - M_{dnc} \left(\frac{S_c}{S_{nc}} - 1 \right) \right] \quad (\text{AASHTO 5.7.3.3.2-1})$$

$$f_r = 0.24\sqrt{f'_c} = 0.24\sqrt{6.0} = 0.588 \text{ ksi} \quad (\text{AASHTO 5.4.2.6})$$

Compressive stress in concrete due to effective prestress forces only at extreme fiber of section where tensile stress is caused by externally applied loads is as follows:

$$f_{cpe} = \frac{P_f}{A_g} + \frac{Pe_c}{S_b} = \frac{712.8}{560} + \frac{712.8(17.4)}{6,177} = 3.281 \text{ ksi}$$

The total unfactored dead load moment acting on the noncomposite section is as follows:

$$M_{dnc} = M_{DC1} + M_{CD2} = 526.8 + 489.2 = 1,016 \text{ k-ft} = 12,192 \text{ k-in}$$

S_c = section modulus of the composite section for extreme fiber where tensile is caused by externally applied loads = $S_{bc} = 10,117 \text{ in}^3$

S_{nc} = section modulus of noncomposite section for extreme fiber where tensile is caused by externally applied loads = $6,177 \text{ in}^3$

γ_1 = flexural cracking variability factor = 1.6 for other than precast segmental structures

γ_2 = prestress variability factor = 1.1 for bonded tendons

γ_3 = ratio of specified minimum yield strength to specified tensile strength of reinforcement = 1.00 for prestressed concrete structures

$$\begin{aligned} M_{cr} &= 1.0 \left[(1.6(0.588) + 1.1(3.281))10,117 - 12,192 \left(\frac{10,117}{6,177} - 1 \right) \right] \\ &= 38,185 \text{ k-in} = 3,182 \text{ k-ft} \end{aligned}$$

Since $1.33 M_u (= 5,060 \text{ k-ft}) > M_{cr} (3,182 \text{ k-ft})$, M_{cr} requirement controls. Therefore, the nominal flexure strength (ϕM_n) provided must be greater than 3,128-ft.

$(\phi M_n) = 4,483 \text{ k-ft} > 3,128\text{-ft}$. Therefore, the minimum reinforcement requirement is satisfied.

Note that LRFD requires that the requirement for minimum reinforcement be checked at every section along the entire girder.

1.6.3.9 Design for Strength Limit State—Shear

In this example, only the shear design procedure for the critical section near the support is demonstrated. Other sections along the entire length of the girder can be designed following the same procedure.

For this example, the shear demand is controlled by the load combination strength I. The factored shear force and bending moment at the critical section are obtained from Table 1.4 (due to dead loads) and Table 1.5 (due to live loads) multiplied by appropriate load factors from AASHTO Table 3.4.1-1.

(a) *Critical section for shear design*

The critical section for shear design is located at d_v from the internal face of the support.

(AASHTO Art. 5.8.3.2). The effective depth for shear, d_e , is the largest of three values: (1) $d_e - a/2$, (2) 0.9 d_e and (3) 0.72 h . (AASHTO 5.8.2.9). d_e = effective depth from extreme compression fiber to centroid of tensile reinforcement = $H - y_{bs}$.

Several iterations may be needed to find the shear critical location. A distance from support needs to be assumed first to estimate the path of harped prestressing strands. Assume that the distance of 4.0 ft (about 90% of the structure depth) from the face of support is the critical location.

The mild reinforcement at the bottom of the girder is assumed to be 4-#6 bars as shown in Figure 1.25 and Table 1.6. The amount of mild steel required should be determined on the basis of the minimum longitudinal reinforcement requirement (AASHTO Eq. 5.8.3.5-1). The calculations are shown in Section 1.6.3.10.

Centroid of prestressing steel at harped point = 2.89 in from the bottom of the girder and at ends = 10.44 in

The height of prestressing steel at 4'0" from end of girder,

$$y_s = 10.44 - \frac{4.0}{34.0} (10.44 - 2.89) = 9.55 \text{ in}$$

$$y_{bs} = \frac{176.0}{19.34} = 9.10 \text{ in}$$

$$d_e = 53.0 - 9.10 = 43.9 \text{ in}$$

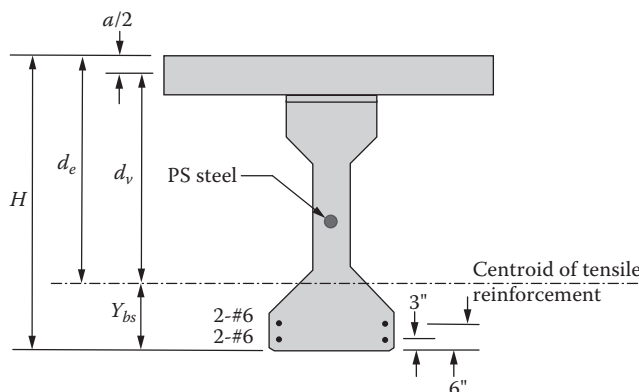


FIGURE 1.25 Definitions of y_s , d_e , and d_v

TABLE 1.6 Tensile Reinforcement at Critical Section

Layer	A_s (in ²)	y_i (in)	$(A_s)(y_i)$
1	$2 \cdot \#6 = 0.88$	3	2.64
2	$2 \cdot \#6 = 0.88$	6	5.28
3	$3.906 (270/60) = 17.58$	9.55	168.0
Total	19.34		176.0

Depth of compression block at 4'0", $a = 2.95$ in

$$\frac{a}{2} = \frac{2.95}{2} = 1.48 \text{ in}$$

$$d_v = \text{largest of } \left\{ \begin{array}{l} d_e - \frac{a}{2} = 43.0 - 1.48 = 42.4 \text{ in} \\ 0.9d_e = 0.9(43.9) = 39.5 \text{ in} \\ 0.72h = 0.72(53.0) = 38.2 \text{ in} \end{array} \right\} = 42.4 \text{ in}$$

Therefore, $d_v = 42.4$ in (3.5 ft) from the centerline of support, close to the initial assumption of 4.0 ft. Since the width of bearing has not been determined, it is conservative to assume that the support width equals zero.

- (b) Contribution of concrete to nominal shear resistance, V_c

Strain in flexural tension reinforcement ε_x

Figure 1.26 shows the critical section near the support. Strain in flexural reinforcement, ε_x is calculated by

$$\varepsilon_x = \frac{\left(\frac{|M_u|}{d_v} + 0.5N_u + |V_u - V_p| - A_{ps}f_{po} \right)}{E_s A_s + E_p A_{ps}} \quad (\text{AASHTO 5.8.3.4.2-4})$$

Factored forces at the critical section for strength I are $M_u = 667$ k-ft; $V_u = 197.5$ kips; $N_u = 0$; $V_p = P(\sin \omega)$

$$\omega = \sin^{-1} \left(\frac{10.44 - 2.89}{34.00 \times 12} \right) = 1.06^\circ$$

$$V_p = 712.8 (\sin 1.06^\circ) = 13.2 \text{ kip}$$

M_u should not be less than $|V_u - V_p|d$

$$M_u = 667 \text{ k-ft} > |V_u - V_p|d_v = |197.5 - 13.2|(42.4/12) = 651 \text{ k-ft}$$

f_{po} = a parameter taken as modulus of elasticity of prestressing tendons multiplied by the locked-in difference in strain between the prestressing tendons and the surrounding concrete. For the usual level of prestressing, a value of $0.7 f_{pu}$ is appropriate for the pretensioned member

$$f_{po} = 0.7 (270) = 189 \text{ ksi}$$

$$A_{ps} = 3.906 \text{ in}^2$$

$$E_s A_s = 29,000 \text{ ksi} (0.88 + 0.88) = 51,040 \text{ kips}$$

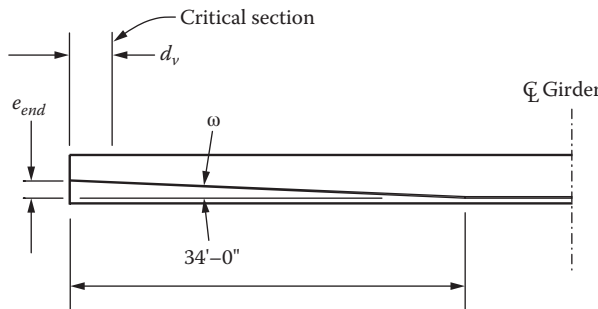


FIGURE 1.26 Girder elevation near support and the critical section for shear.

$$\varepsilon_s = \frac{\left(\frac{(667)(12)}{42.4} + 0.5(0) + |197.5 - 13.20| - 3.906(189) \right)}{51,040 + 28,500(3.906)} = \frac{-365}{162,361} = -0.00225$$

Since ε_s is a negative value, it should be taken as zero. Therefore, $\varepsilon_s = 0$

$$\beta = \frac{4.8}{1 + 750\varepsilon_s} = \frac{4.8}{1 + 750(0)} = 4.8 \quad (\text{AASHTO 5.8.3.4.2-1})$$

$$\theta = 29 + 3,500\varepsilon_s = 29 + (3,500)(0) = 29 \quad (\text{AASHTO 5.8.3.4.2-3})$$

Concrete contribution in shear resistance, V_c

$$\begin{aligned} V_c &= 0.0316\beta\sqrt{f'_c}b_v d_v \\ &= (0.0316)(4.8)\sqrt{6.0}(7.0)(42.4) = 110.3 \text{ kip} \end{aligned} \quad (\text{AASHTO 5.8.3.3-3})$$

Check cracking space,

$$s_{xe} = s_x \frac{1.38}{a_g + 0.63} \quad (\text{AASHTO 5.8.3.4.2-5})$$

where $12.0 \text{ in} \leq S_{xe} \leq 80.0 \text{ in}$

s_x is less than

- d_v
- Maximum distance between layers of longitudinal crack control reinforcement. For members with concentrated longitudinal reinforce, $s_x = d_v$

Therefore, $s_x = d_v = 42.4 \text{ in}$

a_g = maximum aggregate size, assume = 0.75 in

$$s_{xe} = 42.4 \frac{1.38}{0.75 + 0.63} = 42.4 \text{ in} < 80.0 \text{ in}$$

(c) Requirement for shear reinforcement

Check if $V_u \geq 0.5\phi(V_c + V_p)$

$$V_u = 197.5 \text{ kip} > 0.5\phi(V_c + V_p) = (0.5)(0.9)(110.3 + 13.2) = 55.6 \text{ kip}$$

Therefore, transverse shear reinforcement is needed at this section
Required area of transverse shear reinforcement

$$\frac{V_u}{\phi} \leq V_n = V_c + V_s + V_p \quad (\text{AASHTO 5.8.3.3-1})$$

$$V_s = \frac{V_u}{\phi} - V_c - V_p = \frac{197.5}{0.9} - 110.3 - 13.2 = 95.9 \text{ kip}$$

$$V_s = \frac{A_v f_y d_v (\cot \theta + \cot \alpha) \sin \alpha}{s} \quad (\text{AASHTO 5.8.3.3-4})$$

$$\frac{A_v}{s} = \frac{V_s}{f_y d_v (\cot \theta + \cot \alpha) \sin \alpha}$$

For this example, $\theta = 29^\circ$ and $\alpha = 90^\circ$ then we have

$$\frac{A_v}{s} = \frac{V_s}{f_y d_v (\cot \theta + \cot \alpha) \sin \alpha} = \frac{95.9}{(60)(42.4)(\cot 29^\circ + \cos 90^\circ) \sin 90^\circ} = 0.021 \frac{\text{in}^2}{\text{in}}$$

Try #4 (double legs), $A_v = 0.20$ (2 legs) = 0.40 in²

$$\text{Required } s = \frac{0.40}{0.021} = 19.1 \text{ in}$$

Providing #4 bar, double legs, at 12 in spacing, $A_v = 0.40 \frac{\text{in}^2}{\text{ft}}$

$$V_s = \frac{0.40(60)(42.4)(\cot 29^\circ)}{12} = 153.0 \text{ kip} > 95.9 \text{ kip}$$

(d) Check maximum spacing of shear reinforcement

Shear Stress, v_u

$$v_u = \frac{V_u - \phi V_p}{\phi b_v d_v} = \frac{197.5 - 0.9(13.2)}{(0.9)(7.0)(42.4)} = 0.695 \text{ ksi} \quad (\text{AASHTO 5.8.2.9-1})$$

$$v_u = 0.695 \text{ ksi} < 0.125 f'_c = 0.125(6) = 0.75 \text{ ksi}$$

Maximum spacing of shear reinforcement is as follows:

(AASHTO 5.8.2.7)

If $v_u < 0.125 f'_c$, maximum spacing, $s_{\max} = 0.8d_v \leq 24.0 \text{ in}$ (AASHTO 5.8.2.7-1)

For this case, $s_{\max} = 0.8d_v = (0.8)(42.4) = 33.9 \text{ in} > 24.0 \text{ in}$

Therefore, use $s_{\max} = 24.0 \text{ in}$

$s = 12 \text{ in} < s_{\max} = 24.0 \text{ in}$

(e) Minimum transverse reinforcement

Minimum transverse reinforcement

(AASHTO 5.8.2.5)

The area of transverse reinforcement provided satisfies the following:

$$A_v \geq \frac{0.0316\sqrt{f'_c}b_v s}{f_y} \quad (\text{AASHTO 5.8.2.5-1})$$

$$A_v = 0.4 \text{ in}^2 > \frac{0.0316\sqrt{f'_c}b_v s}{f_y} = \frac{0.0316\sqrt{6}(7.0)(12)}{60} = 0.11 \text{ in}^2$$

(f) Nominal shear resistance

To ensure that the web concrete will not crush prior to yielding of transverse reinforcement, nominal shear resistance shall be the lesser of Case (i) and (ii) shown below:

Case (i)

$$V_n = V_c + V_s + V_p = 110.3 + 153.0 + 13.2 = 276.5 \text{ kip} \quad (\text{AASHTO 5.8.3.3-1})$$

Case (ii)

$$V_n = 0.25 f'_c d_v d_v + V_p = (0.25)(6.0)(7.0)(42.4) + 13.2 = 458.4 \text{ kip} \quad (\text{AASHTO 5.8.3.3-2})$$

Therefore, nominal shear resistance is $V_n = 276.5$ kip

Using the above procedure, the transverse reinforcement at increments along the entire girder can be determined.

1.6.3.10 Check Longitudinal Reinforcement Requirement

The following calculations show the design of longitudinal reinforcement in the girder to meet the minimum longitudinal reinforcement criteria at midspan. As stated in AASHTO Article 5.8.3.5, the amount of longitudinal reinforcement (on flexural tension side) at all locations along the girder are proportioned to satisfy the following:

$$A_{ps}f_{ps} + A_s f_y \geq \frac{|M_u|}{d_v \phi_f} + 0.5 \frac{N_u}{\phi_c} + \left(\left| \frac{V_u}{\phi_v} - V_p \right| - 0.5 V_s \right) \cot \theta \quad (\text{AASHTO 5.8.3.5-1})$$

 A_s = area of nonprestressed tensile reinforcement

The following values at midspan were determined following the procedure described in the previous section.

 $M_u = 3,892$ k-ft; $V_u = 51.9$ kips; $V_s = 0$ kip; $V_p = 0$ kip; $N_u = 0$ kip; $d_v = 47.4$ in; $\theta = 34.2^\circ$; $f_{ps} = 261.8$ ksi.

$$\begin{aligned} & \frac{|M_u|}{d_v \phi_f} + 0.5 \frac{N_u}{\phi_c} + \left(\left| \frac{V_u}{\phi_v} - V_p \right| - 0.5 V_s \right) \cot \theta \\ &= \frac{|3,892 \times 12|}{(47.7)(1.0)} + (0.5) \frac{0}{1.0} + \left(\left| \frac{51.9}{0.9} - 0 \right| - (0.5)(0) \right) \cot 34.2^\circ \\ &= 1,063 \text{ kip} \end{aligned}$$

For longitudinal 4-#6 bars, its longitudinal force capacity is

$$A_{ps}f_{ps} + A_s f_y = 3.906(261.8) + 4(0.44)(60) = 1,128 \text{ kip} > 1,063 \text{ kip}$$

Therefore, the minimum reinforcement requirement is satisfied.

1.6.3.11 Design Anchorage Zone Reinforcement

The provision in AASHTO Art. 5.10.10 requires that the following vertical reinforcement be provided within the distance $h/4$ from the end of the girder.

$$P_r = f_s A_s \quad (\text{AASHTO 5.10.10.1-1})$$

f_s = stress in mild steel = 20 ksi

A_s = total of vertical reinforcement

$$P_r = 0.04 P_i = 0.04(0.75)(270)(3.906) = 31.6 \text{ kips}$$

$$\text{Requires } A_s = \frac{P_r}{f_s} = \frac{31.6}{20} = 1.58 \text{ in}$$

Using #5 bars with 2 vertical legs,

$$\text{Number of bars required} = \frac{1.58}{0.31(2)} = 2.5-\#5, \text{ double legs.}$$

Provide 3-#5 vertical bars (2 legs) within $h/4$ (14 in) from the end of the beam.

1.6.3.12 Calculate Deflection and Camber

Camber due to prestressing force and deflection due to self-weight of girder, slab, and haunch are calculated using the initial modulus of elasticity of concrete and section properties of the noncomposite girder.

Deflections due to concrete barrier and future wearing surface are calculated using gross composite section properties.

Instantaneous deflection due to prestressing force and girder weight is calculated at transfer. Long-term deflection of precast concrete girders could be computed as the instantaneous deflection multiplied by a factor.

At the time of stressing, the midspan of the girder will raise by an amount equal to $(\Delta_{pi} - \Delta DL_{gdr})$. Because the bottom fiber is more highly stressed than the top fiber, the girder will continue to rise with the passage of time (Naaman 2004). The total amount by which the girder will rise is dependent on its age at the time loading from the concrete slab. Different state transportation agencies use different multipliers to account for the long-term effects. Precast Prestressed Concrete Institute Bridge Design Manual multipliers (Martin 1977) are presented in Table 1.7.

To calculate deflection and camber at midspan and determine the minimum haunch thickness at supports, the following steps are required.

$P_i = 730 \text{ kip}$

$E_{ci} = 4,067 \text{ ksi}$

$I = 125,390 \text{ in}^4$

e_c = eccentricity of prestressing force at midspan = 17.4 in

e_e = eccentricity of prestressing force at endspan = 10.4 in

L_g = overall girder length = 86.0 ft

e' = difference between eccentricity of prestressing steel at midspan and at end
 $= 17.4 - 10.4 = 7.0 \text{ in}$

TABLE 1.7 PCI Multipliers

	Erection	Long-term
Prestressing force	1.80	2.20
Girder weight	1.85	2.40
Deck, haunch, diaphragms, noncomposite DL	—	2.30
Barrier, FWS, uniform composite loads	—	3.00

a = distance from end of girder to harped point = 34 ft

w_g = uniform girder weight = 0.583 klf

- (a) Camber due to prestressing force at midspan

$$\begin{aligned}\Delta_p &= \frac{P_i}{E_{ci}(I)} \left(\frac{e_c L^2}{8} - \frac{e' a^2}{6} \right) \\ &= \frac{730}{4,067 (125,390)} \left(\frac{17.4 [86 \times 12]^2}{8} - \frac{7.0 [34 \times 12]^2}{6} \right) = 3.04 \text{ in } \uparrow\end{aligned}$$

- (b) Deflection due to girder self-weight at midspan

$$\Delta_g = \frac{5w_g L^4}{384 E_{ci}(I)} = \frac{5 \left(\frac{0.583}{12} \right) (86 \times 12)^4}{384(4,067)(125,390)} = 1.41 \text{ in } \downarrow$$

- (c) Deflection due to weight of slab and haunch at midspan

$$\Delta_s = \frac{5w_s L^4}{384 E_{ci}(I)} = \frac{(5) \left(\frac{0.542}{12} \right) [(85)(12)]^4}{384(4,696)(125,390)} = 1.08 \text{ in } \downarrow$$

- (d) Deflection due to barrier weight at midspan

$$\Delta_b = \frac{5w_b L^4}{384 E_c(I_c)} = \frac{5 \left(\frac{0.159}{12} \right) [85 \times 12]^4}{384(4,696)(331,853)} = 0.14 \text{ in } \downarrow$$

- (e) Deflection due to future wearing surface at midspan

$$\Delta_{ws} = \frac{5w_{ws} L^4}{384 E_c(I_c)} = \frac{5 \left(\frac{0.192}{12} \right) [85 \times 12]^4}{384(4,696)(331,853)} = 0.14 \text{ in } \downarrow$$

(f) Deflection at midspan at the time of girder erection

The deflections at erection time can be estimated using the PCI multipliers in Table 1.7.

$$\text{Girder deflection} = 1.8\Delta_p + 1.85\Delta_g = 1.8(3.04) + 1.85(-1.41) = 2.86 \text{ in } \uparrow$$

After the deck pour, the deflection is $2.86" - 1.08" = 1.78"$. That means the minimum haunch thickness at girder support should be 1.78". With the assumption of a minimum of 1 in haunch thickness at midspan, the minimum haunch thickness should be 2.78 in at supports. Therefore, the minimum structure depth is 4'5" at midspan and the minimum structure depth is 4'7 3/8" at supports.

References

- AASHTO. 2012. *AASHTO RFD Bridge Design Specifications*, Customary U.S. Units, 2012, American Association of State Highway and Transportation Officials, Washington D.C.
- Collins, M. P. and Mitchell, D. 1991. *Prestressed Concrete Structures*, Prentice Hall, Englewood Cliffs, NJ.
- Lin, T. Y. and Burns, N. H. 1981. *Design of Prestressed Concrete Structure*, 3rd Ed., John Wiley & Sons, New York, NY.
- Martin, L. D. 1977. A rational method for estimating camber and deflection of precast prestressed members. *PCI Journal*, 22(1), 100–108.
- Mast, R. F. 1989. Lateral stability of long prestressed concrete beams, part 1. *PCI Journal*, 34(1), 34–53.
- Mast, R. F. 1993. Lateral stability of long prestressed concrete beams, part 2. *PCI Journal*, 38(1), 70–88.
- Naaman, A. E. 2004. *Prestressed Concrete Analysis and Design*, 2nd Ed., Techno Press 3000, Ann Arbor, Michigan.
- Nawy, E. G. 2009. *Prestressed Concrete: A Fundamental Approaches*, 5th Ed., Upgrade: ACI, AASHTO, IBC 2009 Codes Version. Prentice Hall, Englewood Cliffs, NJ.
- PCI. 2011. *PCI Bridge Design Manual*, 3rd Ed., Prestressed Concrete Institute, Chicago, IL.

@Seismicisolation

2

Cast-in-Place Posttensioned Prestressed Concrete Girder Bridges

2.1	Introduction	51
	Prestressing Systems • Posttensioning Operation • Materials	
2.2	Typical Box Girder Sections.....	56
2.3	Losses of Prestress	57
	Instantaneous Losses • Time-Dependent Losses: Refined Method	
2.4	Design Considerations.....	60
	Basic Theory • Stress Limits • Cable Layout • Secondary Moments • Flexural Resistance • Shear Resistance • Camber and Deflections • Anchorage Zones	
2.5	Design Limit States and Procedure.....	68
	Design Limit States • Design Procedure	
2.6	Design Example: Two-Span Continuous Box Girder Bridge.....	69
	Bridge Data • Requirements • Solution	
2.7	Summary.....	88
	References.....	88

Lian Duan
*California Department
of Transportation*

Kang Chen
MGE Engineering, Inc.

2.1 Introduction

Reinforced concrete combines concrete and steel bars by simply putting them together in a passive manner. Prestressed concrete combines high-strength concrete and high-strength steel in an active manner; this is achieved by tensioning the steel and holding it against the concrete, thus putting the concrete into compression. Prestressed concrete structures, using high-strength materials effectively, give improved serviceability, load-carrying capacity, and durability. It is an attractive alternative for long span bridges, and has been used worldwide since the 1950s. Prestressed concrete bridges have gone from being almost nonexistent in the 1940s to clearly being the predominant bridge type currently; these are being built in the United States and around the world. About 25% of highway bridges are prestressed concrete in the United States (FHWA 2010). There are three types of prestressed concrete bridges such as precast pretensioning girder bridges, cast-in-place (CIP) posttensioned girder bridges, and segmentally constructed concrete girder bridges. This chapter focuses only on CIP posttensioned prestressed concrete girder bridges. The precast pretensioned prestrengthened concrete girder bridges are presented in Chapter 1 and segmental concrete bridges are discussed in Chapter 3. For a more detailed discussion on prestressed concrete, references are made to textbooks by Collins and Mitchell (1997), Lin and Burns (1981), Navy (2009). For precast prestressed concrete, see PCI (2011). For posttensioned concrete, see CSI (2008) and PTI (2006).

2.1.1 Prestressing Systems

There are two types of prestressing systems: pretensioning and posttensioning systems. Pretensioning systems are methods in which the strands are tensioned before the concrete is placed. This method is generally used for mass production of linear concrete members. Pretensioning can neither be used to connect two precast concrete components nor to connect precast components to cast-in-place concrete members. Posttensioning systems are methods in which the tendons are tensioned after concrete has reached a specified strength. This technique is often used in projects with very large cast-in-place elements on falsework. The main advantage of posttensioning is its ability to posttension both precast and cast-in-place members.

2.1.2 Posttensioning Operation

Compressive stresses in a concrete member are induced by tensioning steel tendons of strands or bars placed in ducts embedded in the concrete (Figure 2.1). The tendons are installed after the concrete has been placed and sufficiently cured to a specified compressive strength. Hydraulic prestressing—jacking (Figure 2.2)—is the most common method used in bridge structures (Caltrans 2005). Figure 2.3 illustrates a complete jacking process (Caltrans 2005).



FIGURE 2.1 A posttensioned box girder bridge under construction.

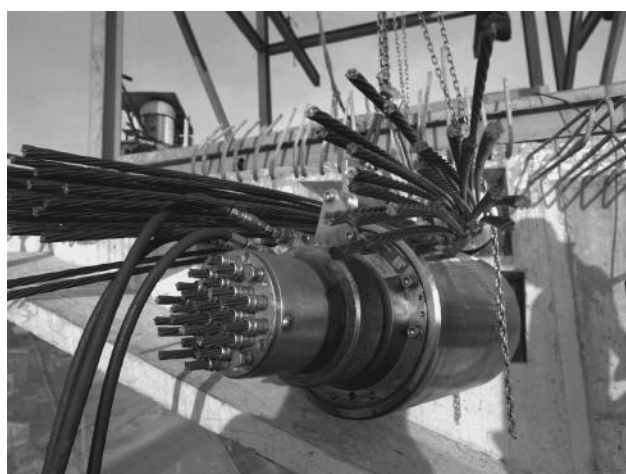


FIGURE 2.2 A typical hydraulic prestressing jack. (Courtesy of California Department of Transportation.)

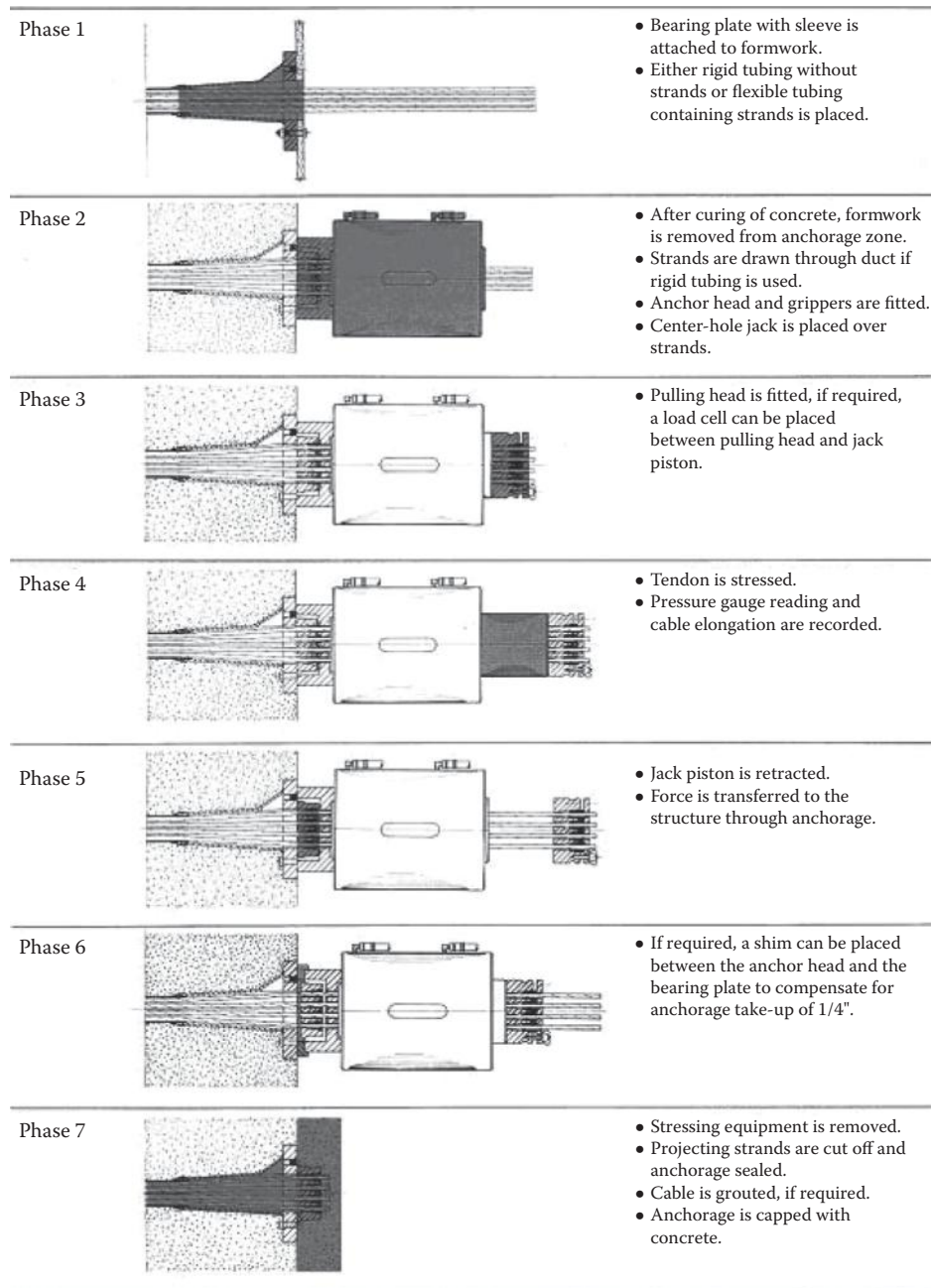


FIGURE 2.3 A complete jacking process. (Courtesy of California Department of Transportation.)

2.1.3 Materials

2.1.3.1 Concrete

A 28-day cylinder compressive strength (f'_c) of concrete, not less than 4.0 ksi (28 MPa), is commonly used for prestressed concrete in the United States. A higher early strength is often needed for the fast removal of formwork in the cast-in-place method. The basic concrete material properties are discussed

in Chapter 13 in *Bridge Engineering Handbook, Second Edition: Fundamentals*. Only concrete shrinkage and creep are discussed in this section.

Creep of concrete is a time-dependent inelastic deformation under sustained compression load and depends primarily on the concrete's maturity at the time of loading, and magnitude and duration of the compressive stress. The total creep strain generally ranges from about 0.5 to 4 times of the "instantaneous" deformation. The creep coefficient may be estimated as (AASHTO 2012)

$$\Psi(t, t_i) = 1.9 k_s k_{hc} k_f k_{td} t_i^{-0.118} \quad (2.1)$$

in which

$$k_s = 1.45 - 0.13(V/s) \geq 1.0 \quad (2.2)$$

$$k_{hc} = 1.56 - 0.08H \quad (2.3)$$

$$k_f = \frac{5}{1 + f'_c} \quad (2.4)$$

$$k_{td} = \frac{t}{61 - 4f'_{ci} + t} \quad (2.5)$$

where k_{hc} is humidity factor for creep and t_i is the age of concrete at the time of load application.

Concrete shrinkage has a time-dependent material behavior and mainly depends on mixture of concrete, moisture conditions, curing method, volume-to-surface ratio, and duration of curing period. The total shrinkage strains range from 0.0004 to 0.0008 over the life of concrete, and about 80% of this occurs in the first year.

For concrete devoid of shrinkage-prone aggregates, the strain due to shrinkage ϵ_{sh} may be estimated by (AASHTO 2012)

$$\epsilon_{sh} = k_s k_{sh} k_f k_{td} 0.48 \times 10^{-3} \quad (2.6)$$

in which

$$k_s = 1.45 - 0.13(V/s) \geq 1.0 \quad (2.7)$$

$$k_{hs} = (2.00 - 0.014H) \quad (2.8)$$

$$k_f = \frac{5}{1 + f'_c} \quad (2.9)$$

$$k_{td} = \frac{t}{61 - 4f'_{ci} + t} \quad (2.10)$$

where k_s is the effect factor of the volume-to-surface ratio of the component; V/S is the volume-to-surface area ratio (in.). H is the relative humidity (%); k_{hs} is the humidity factor for shrinkage; k_f is the effect factor of concrete strength; k_{td} is the time-dependent factor; t is the maturity of concrete (days), defined as the age of concrete at the time of loading for creep calculation, or end of curing for shrinkage calculation.

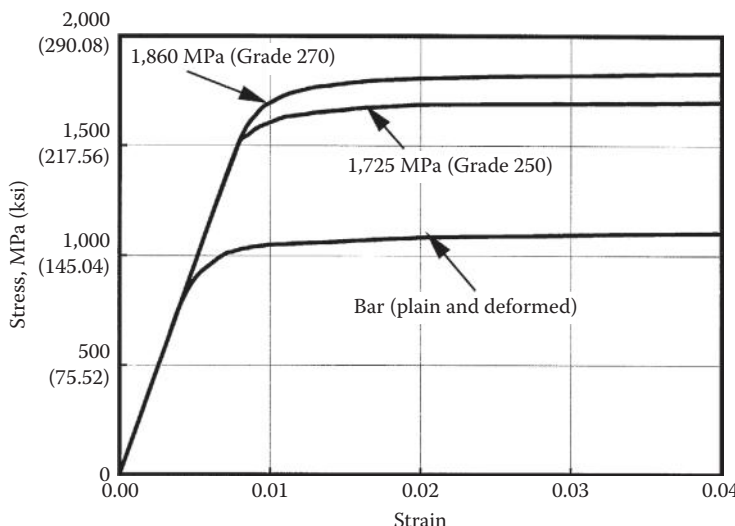
2.1.3.2 Steel for Prestressing

Uncoated, seven-wire stress-relieved strands (AASHTO M203 or ASTM A416), or low-relaxation seven-wire strands and uncoated high-strength bars (AASHTO M275 or ASTM A722) are commonly used in prestressed concrete bridges. Prestressing reinforcement, whether wires, strands, or bars, are also called *tendons*. The properties for prestressing steel are shown in Table 2.1.

TABLE 2.1 Properties of Prestressing Strand and Bars

Material	Grade and Type ksi (MPa)	Diameter in. (mm)	Tensile Strength f_{pu} ksi (MPa)	Yield Strength f_{py} ksi (MPa)	Modulus of Elasticity E_p ksi (MPa)
Strand	250 (1725)	1/4 to 0.6 (6.35 to 15.24)	250 (1,725)	80% of f_{pu} except 90% of f_{pu}	28,500 (197,000)
	270 (1860)	3/8 to 0.6 (10.53 to 15.24)	270 (1,860)	for low-relaxation strand	
Bar	Type 1, Plain	3/4 to 1-3/8 (19 to 25)	150 (1,035)	85% of f_{pu}	30,000 (207,000)
	Type 2, Deformed	5/8 – 1-3/8 (15 to 36)	150 (1,035)	80% of f_{pu}	

Source: Data from AASHTO, *AASHTO LRFD Bridge Design Specifications*, Customary U.S. Unit, 2012, American Association of State Highway and Transportation Officials, Washington DC, 2012.

**FIGURE 2.4** Typical stress-strain curves for prestressing steel.

Typical stress-strain curves for prestressing steel are shown in Figure 2.4. These curves can be approximated by the following equations:

For grade 250 (PCI 2011):

$$f_s = \begin{cases} 28,500 \epsilon_s (\text{ksi}) & \text{for } \epsilon_s \leq 0.0076 \\ 250 - \frac{0.04}{\epsilon_s - 0.0064} (\text{ksi}) & \text{for } \epsilon_s > 0.0076 \end{cases} \quad (2.11)$$

For grade 270 (PCI 2011):

$$f_s = \begin{cases} 28,500 \epsilon_s (\text{ksi}) & \text{for } \epsilon_s \leq 0.0086 \\ 270 - \frac{0.04}{\epsilon_s - 0.007} (\text{ksi}) & \text{for } \epsilon_s > 0.0086 \end{cases} \quad (2.12)$$

For bars grade 150:

$$f_s = \begin{cases} 30,000 \epsilon_s (\text{ksi}) & \text{for } \epsilon_s \leq 0.004 \\ 150 - \frac{0.028}{\epsilon_s - 0.003} (\text{ksi}) & \text{for } \epsilon_s > 0.004 \end{cases} \quad (2.13)$$

2.1.3.3 Advanced Composites for Prestressing

Advanced composites—fiber-reinforced plastics (FPR) with their high tensile strength and good corrosion resistance work well in prestressed concrete structures. Application of advanced composites for prestressing has been investigated since the 1950s (Eubunsky and Rubinsky 1954; Wines and Hoff 1966; Wines et al. 1966). Extensive research has also been conducted in Germany and Japan (Iyer and Anigol 1991). The Ulenbergstrasse bridge, a two span of 70 ft. (21.3 m) and 84 ft. (25.6 m) solid slab using 59 fiberglass tendons, was built in 1986 in Germany, which was the first prestressed concrete bridge to use advanced composite tendons in the world (Miesseler and Wolff 1991).

FPR cables and rods made of aramid, glass, and carbon fibers embedded in a synthetic resin have an ultimate tensile strength of 220 ksi (1,500 MPa) to 290 ksi (2,000 MPa), with the modulus of elasticity ranging from 9,000 ksi (62,055 MPa) to 24,000 (165,480 MPa) (Iyer and Anigol 1991). The main advantages of FPR are (1) a high specific strength (ratio of strength to mass density) of about 10 to 15 times greater than steel; (2) a low modulus of elasticity making the prestress loss small; and (3) good performance in fatigue tests (Kim and Meier 1991) show that, for CFRP, at least three times higher stress amplitudes and higher mean stresses than steel are achieved without damage to the cable for over 2 million cycles.

Although much effort has been put in to explore the use of advanced composites in civil engineering structures (see Chapter 16 of the first book in this series, *Bridge Engineering Handbook, Second Edition: Fundamentals*) and cost of advanced composites has come down significantly, the design and construction specifications have not yet been developed. Engineers and bridge owners still evaluate the cost effectiveness and extended life expectancy gained by using advanced composites.

2.1.3.4 Grout

For posttensioning construction, when the tendons are bound, grout is needed to transfer loads and to protect the tendons from corrosion. Grout is made of water, sand, and cements or epoxy resins. AASHTO-LRFD (2012) requires that details of the protection method be indicated in the contract documents. Readers are referred to the Posttensioning Manual (PTI 2006).

2.2 Typical Box Girder Sections

The multicell box section shown in Figure 2.5 is often used in CIP posttensioned prestressed concrete girder bridges for spans of 100 (30 m) to 600 ft. (180 m). The spacing of the girders (webs) can be taken as twice the girder depth. The thickness of the girder is usually taken as 12 in. (300 mm). The deck slab and soffit slab thickness depends on the clear distance between adjacent girders. The girder and soffit thickness are usually increased in the support regions. Structural depth-to-span ratios are 0.045 for simple spans, and 0.04 for continuous spans. The high torsional resistance of the box girder makes it particularly suitable for horizontally curved alignment (Figure 2.6) such as those needed on highway ramps.

For a longer span, box girders are usually haunched with a depth-to-span ratio of 0.05 to 0.07 at the piers. Truckee River Bridge of California, as shown in Figure 2.7, is 465 m (1,525.6 ft.) long and carries traffic on State Route 267. The 7-span bridge features a cast-in-place, posttensioned two-cell box girder with spans up to 71 m (232.9 ft.) long. The parabolic haunches with section depth of 2.33 to 4.57 m (7.64 ft. to 14.99 ft.) flow into the piers, resulting in a very elegant archlike structure.

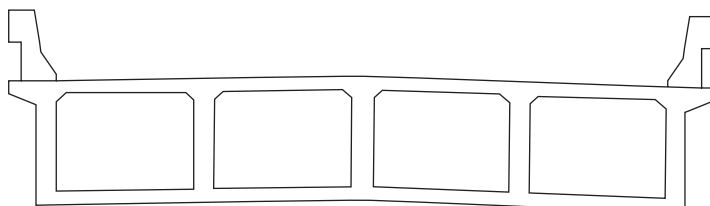


FIGURE 2.5 Typical cast-in-place posttensioned prestressed concrete box girder section.



FIGURE 2.6 Prestressed box girder bridge (I-280/110 Interchange, California).



FIGURE 2.7 Truckee River Bridge, California. (Courtesy of California Department of Transportation.)

2.3 Losses of Prestress

Loss of prestress refers to the reduced tensile stress in the tendons after stressing. Although this loss affects the service performance (such as camber, deflections, and cracking), it has no effect on the ultimate strength of a flexural member unless the tendons are unbonded or the final stress is less than $0.5f_{pu}$ (PCI 2011). It should be noted, however, that an accurate estimate of prestress loss is more pertinent in some prestressed concrete members than in others. Prestress losses can be divided into two categories:

- Instantaneous losses including losses due to anchorage set (Δf_{pA}), friction between tendons and surrounding concrete (Δf_{pF}), and elastic shortening of concrete (Δf_{pES}) during the construction stage.
- Time-dependent losses (Δf_{pLT}), including losses due to shrinkage (Δf_{pSR}), creep (Δf_{pCR}), and relaxation of the steel (Δf_{pR}) during the service life.

The total prestress loss (Δf_{pT}) for nonsegmental posttensioned members are as follows:

$$\Delta f_{pT} = \Delta f_{pA} + \Delta f_{pF} + \Delta f_{pES} + \Delta f_{pLT} \quad (2.14)$$

2.3.1 Instantaneous Losses

2.3.1.1 Anchorage Set Loss

As shown in Figure 2.8, assuming that the anchorage set loss changes linearly within the length (L_{pA}), the effect of anchorage set on the cable stress can be estimated by the following formula:

$$\Delta f_{pA} = \Delta f \left(1 - \frac{x}{L_{pA}} \right) \quad (2.15)$$

$$L_{pA} = \sqrt{\frac{E(\Delta L) L_{pF}}{\Delta f_{pF}}} \quad (2.16)$$

$$\Delta f = \frac{2 \Delta f_{pF} L_{pA}}{L_{pF}} \quad (2.17)$$

where ΔL is the thickness of the anchorage set; E is the modulus of elasticity of the anchorage set. Δf is the change in the stress due to the anchor set; L_{pA} is the length influenced by the anchor set; L_{pF} is the length to a point where loss, Δf_{pF} , is known; and x is the horizontal distance from the jacking end to the point considered.

2.3.1.2 Friction Loss

For a posttensioned member, friction losses are caused by the tendon profile *curvature effect* and the local deviation in tendon profile *wobble effects*. AASHTO-LRFD (2012) specifies the following formula:

$$\Delta f_{pF} = f_{pj} \left(1 - e^{-(Kx + \mu\alpha)} \right) \quad (2.18)$$

where f_{pj} is the stress in prestressing steel at jacking; K is the wobble friction coefficient and μ is the curvature friction coefficient (see Table 2.2); x is the length of a prestressing tendon from the jacking

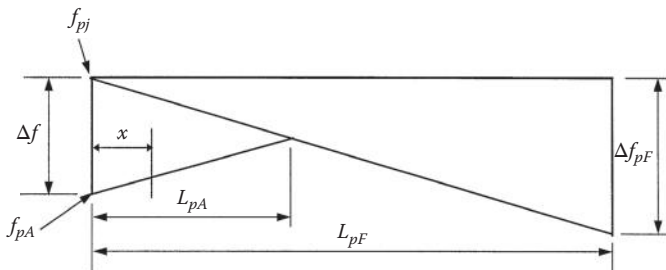


FIGURE 2.8 Anchorage set loss model.

TABLE 2.2 Friction Coefficients for Posttensioning Tendons

Type of Steel	Type of Duct	Wobble Coefficient, K (1/ft.)	Curvature Coefficient μ (1/rad)
Wire or strand	Rigid and semirigid galvanized metal sheathing	0.0002	0.15 ~ 0.25
	Polyethylene	0.0002	0.23
	Rigid steel pipe deviators for external tendons	0.0002	0.25
High-strength bars	Galvanized metal sheathing	0.002	0.30

Source: Data from AASHTO, *AASHTO LRFD Bridge Design Specifications*, Customary U.S. Unit, 2012, American Association of State Highway and Transportation Officials, Washington DC, 2012.

end to the point considered; α is the sum of the absolute values of angle change in the prestressing steel path from the jacking end.

2.3.1.3 Elastic Shortening Loss Δf_{pES}

The loss due to elastic shortening for posttensioned members can be calculated using the following formula (AASHTO 2012):

$$\Delta f_{pES} = \frac{N-1}{2N} \frac{E_p}{E_{ci}} f_{cgp} \quad (2.19)$$

where E_{ci} is the modulus of elasticity of concrete at prestress transfer; N is the number of identical prestressing tendons; and f_{cgp} is the sum of the concrete stress at the center of gravity of the prestressing tendons due to the prestressing force after jacking for posttensioned members and the self-weight of member at the section with the maximum moment. For posttensioned structures with bonded tendons, f_{cgp} may be calculated at the center section of the span for simply supported structures at the section with the maximum moment for continuous structures.

2.3.2 Time-Dependent Losses: Refined Method

AASHTO-LRFD (2012) provides the following refined estimates of each time-dependent loss for nonsegmental cast-in-place posttensioned members.

$$\Delta f_{pLT} = \Delta f_{pSD} + \Delta f_{pCD} + \Delta f_{pR2} - \Delta f_{pSS} \quad (2.20)$$

where Δf_{pSS} is the prestress gain due to shrinkage of deck in the composite section.

2.3.2.1 Shrinkage Loss

Shrinkage loss can be determined by formulas (AASHTO 2012):

$$\Delta f_{pSD} = \varepsilon_{bdf} E_p K_{df} \quad (2.21)$$

$$K_{df} = \frac{1}{1 + \frac{E_p A_{ps}}{E_{ci} A_c} \left(1 + \frac{A_c e_{pc}^2}{I_c} \right) \left(1 + 0.7 \Psi_b(t_f, t_i) \right)} \quad (2.22)$$

where ε_{bdf} is the shrinkage strain of the girder between the time of deck placement and the final time; K_{df} is the transformed section coefficient that accounts for the time-dependent interaction between concrete and bonded steel; e_{pc} is the eccentricity of the prestressing force with respect to the centroid of the composite section (this is positive where the prestressing force is below the centroid of the section); A_c and I_c are the area of the section and the moment of inertia of the section, calculated using the gross composite concrete section properties, respectively.

2.3.2.2 Creep Loss

Creep loss can be predicted by (AASHTO 2012):

$$\begin{aligned} \Delta f_{pCD} &= \frac{E_p}{E_{ci}} f_{cgp} [\Psi_b(t_f, t_i) - \Psi_b(t_d, t_i)] K_{df} \\ &\quad + \frac{E_p}{E_c} \Delta f_{cd} \Psi_b(t_f, t_d) K_{df} \end{aligned} \quad (2.23)$$

where Δf_{ca} is the change in the concrete stress at the centroid of prestressing strands due to long-term losses between transfer and deck placement, combined with the deck weight and the superimposed load. The concrete stress at the center of gravity of the prestressing steel at transfer, $\psi_b(t_f, t_d)$, is the girder final creep coefficient at the final time due to loading at deck placement.

2.3.2.3 Relaxation Loss

The total relaxation loss (Δf_{pR2}) can be determined as follows:

$$\Delta f_{pR2} = \frac{f_{pt}}{K_L} \left[\frac{f_{pt}}{f_{py}} - 0.55 \right] \quad (2.24)$$

where f_{pt} is the stress in prestressing strands immediately after transfer, taken to be not less than $0.55f_{py}$; K_L is equal to 30 for low-relaxation strands and 7 for other prestressing steel. The relaxation loss may be assumed to be equal to 1.2 for low-relaxation strands.

2.4 Design Considerations

2.4.1 Basic Theory

Compared to reinforced concrete, the main distinguishing characteristics of prestressed concrete are as follows:

- The stresses for concrete and prestressing steel and deformation of structures at each stage, that is, prestressing, handling, transportation, erection, and service, are investigated on the basis of the elastic theory.
 - The prestressing force is determined by concrete stress limits under service load.
 - At the strength limit states, flexure and shear resistances are based on the same basic principle as reinforced concrete.

For the prestressed concrete flexural member section shown in Figure 2.9, the stress at various service load stages can be expressed by the following formula:

$$f = \frac{P_j}{A} \pm \frac{P_j ey}{I} \pm \frac{My}{I} \quad (2.25)$$

where P_j is the prestress force; A is the cross-sectional area; I is the moment of inertia; e is the distance from the center of gravity to the centroid of the prestressing cable; y is the distance from the centroidal axis; and M is the externally applied moment.

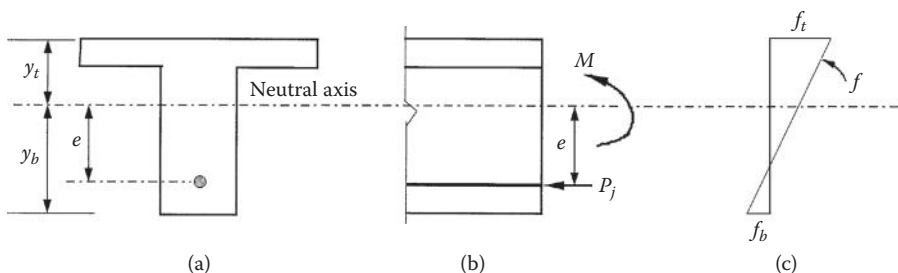


FIGURE 2.9 Prestressed concrete member section at service limit state: (a) Cross section; (b) Applied forces; (c) Stress diagram.

Section properties are dependent on prestressing methods and load stages. In the analysis, the following guidelines may be useful:

- Before bounding of the tendons, for a posttensioned member, the net section should be used theoretically, but the gross section properties can be used with a negligible tolerance.
- After bounding of tendons, the transformed section should be used, but gross section properties may be used approximately.
- At service load stage, transformed section properties should be used.

2.4.2 Stress Limits

The stress limits are the basic requirements for designing a prestressed concrete member. The purpose of stress limits on the prestressing tendons is to mitigate tendon fracture, to avoid inelastic tendon deformation, and to allow for prestress losses. Table 2.3 lists the AASHTO-LRFD (2012) stress limits for prestressing tendons.

The purpose for stress limits on the concrete is to ensure that there is no overstressing at the time of jacking and after transfer stages, and to avoid cracking (fully prestressed) or to control cracking (partially prestressed) at the service load stage. Tables 2.4 and 2.5 list the AASHTO-LRFD (2012) stress limits for concrete.

TABLE 2.3 Stresses Limits for Posttensioning Prestressing Tendon

Stress Type	Prestressing Tendon Type		
	Stress Relieved Strand and Plain High-Strength Bars	Low Relaxation Strand	Deformed High-Strength Bars
Prior to seating—short-term f_{pbt} may be allowed	$0.90f_{py}$	$0.90f_{py}$	$0.90f_{py}$
At anchorages and couplers immediately after anchor set	$0.76f_{pu}$	$0.80f_{pu}$	$0.75f_{pu}$
Elsewhere along length of member away from anchorages and couplers immediately after anchor set	$0.70f_{pu}$	$0.74f_{pu}$	$0.70f_{pu}$
At service limit state after all losses f_{pe}	$0.80f_{py}$	$0.80f_{py}$	$0.80f_{py}$

Source: Data from AASHTO, *AASHTO LRFD Bridge Design Specifications*, Customary U.S. Unit, 2012, American Association of State Highway and Transportation Officials, Washington DC, Table 5.9.3-1, 2012.

TABLE 2.4 Temporary Concrete Stress Limits at Jacking State before Losses—Fully Prestressed Components

Stress Type	Area and Condition	Stress (ksi)
Compressive		$0.60f'_{ci}$
Tensile	Precompressed tensile zone without bonded reinforcement	N/A
	Area other than the precompressed tensile zones and without bonded reinforcement	$0.0948\sqrt{f'_{ci}} \leq 0.2$
	Area with bonded reinforcement sufficient to resist the tensile force in the concrete computed assuming an uncracked section, where reinforcement is proportioned using a stress of 0.5fy, not to exceed 340 ksi.	$0.24\sqrt{f'_{ci}}$
	Handling stresses in prestressed piles	$0.158\sqrt{f'_{ci}}$

Note: Tensile stress limits are for nonsegmental bridges only.

Source: Data from AASHTO, *AASHTO LRFD Bridge Design Specifications*, Customary U.S. Unit, 2012, American Association of State Highway and Transportation Officials, Washington DC, Article 5.9.4, 2012.

TABLE 2.5 Concrete Stress Limits at Service Limit State after Losses—Fully Prestressed Components

Stress Type	Area and Condition		Stress (ksi)
Compressive	Under the sum of effective prestress and permanent loads		$0.45 f'_c$
Tensile	Under the sum of effective prestress, permanent loads, and transient loads as well as during shipping and handling		$0.60 \phi_w f'_c$
	Precompressed tensile zone	With bonded prestressing tendons or reinforcement under moderate corrosive conditions	$0.19 \sqrt{f'_c}$
	Assuming uncracked section	With bonded prestressing tendons or reinforcement under severe corrosive conditions With unbonded prestressing tendon	$0.0948 \sqrt{f'_c}$ No tension

Source: Data from AASHTO, *AASHTO LRFD Bridge Design Specifications*, Customary U.S. Unit, 2012, American Association of State Highway and Transportation Officials, Washington DC, Tables 5.9.4.2.1-1, 5.9.4.2.2-1, 2012.

Note: Tensile stress limits are for nonsegmental bridges only.

A prestressed member that does not allow cracking at service loads is called a *fully prestressed member*, while one which does is called a *partially prestressed member*. Compared with full prestress, partial prestress can minimize camber especially when the dead load is relatively small along with providing savings in prestressing steel, the work required to tension, and the size of end anchorages and utilizing more economical mild steel. On the other hand, engineers must be aware that partial prestress may cause earlier cracks and greater deflection under overloads and higher principle tensile stresses under service loads. Nonprestressed reinforcement is often needed to provide higher flexural strength and to control cracking in a partially prestressed member.

2.4.3 Cable Layout

A cable is a group of prestressing tendons and the center of gravity of all prestressing reinforcement. It is a general design principle that the maximum eccentricity of prestressing tendons should occur at locations of maximum moments. Typical cable layouts for nonsegmental concrete superstructures are shown in Figure 2.10. While straight tendons (Figure 2.10a) and harped multi-straight tendons (Figures 2.10b and 2.10c) are common in precast members, curved tendons are more popular for CIP posttensioned members (Figures 2.10d and 2.10e).

To ensure that the tensile stress in extreme concrete fibers under services does not exceed code stress limits (AASHTO 2012), cable layout envelopes are delimited. Figure 2.11 shows limiting envelopes for simply supported members. From Equation 2.25, the stress at extreme fiber can be obtained

$$f = \frac{P_j}{A} \pm \frac{P_j e C}{I} \pm \frac{M C}{I} \quad (2.26)$$

where C is the distance from top or bottom extreme fibers that form the center of gravity of the section (y_b or y_t as shown in Figure 2.9).

When no tensile stress is allowed, the limiting eccentricity envelope can be solved from Equation 2.26 with

$$e_{\text{limt}} = \frac{I}{AC} \pm \frac{M}{I P_j} \quad (2.27)$$

For limited tension stress f_t , additional eccentricities can be obtained as follows:

$$e' = \frac{f_t I}{P_j C} \quad (2.28)$$

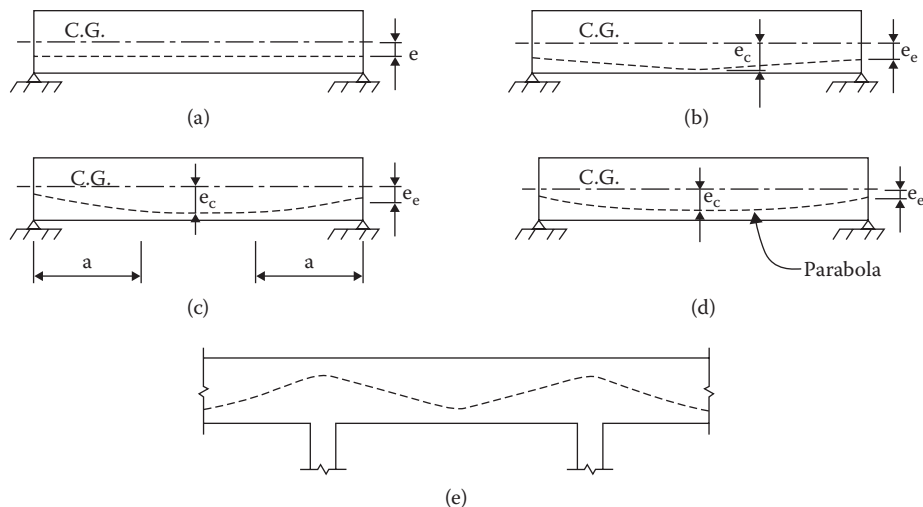


FIGURE 2.10 Cable layout for bridge superstructures: (a) straight tendon (b) harped multi-straight tendon (c) curved tendon (d) parabola tendon.

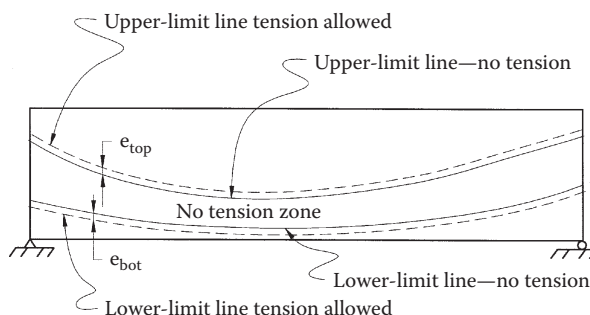


FIGURE 2.11 Cable layout envelopes.

2.4.4 Secondary Moments

The primary moment ($M_p = P_j e$) is defined as the moment in the concrete section caused by the eccentricity of the prestress for a statically determinate member. The secondary moment M_s (Figure 2.12d) is defined as the moment induced by prestress and structural continuity in an indeterminate member. Secondary moments can be obtained by various methods. The resulting moment is the sum of the primary and secondary moments.

2.4.5 Flexural Resistance

Flexural resistance in the strength limit state is based on the following assumptions (AASHTO 2012):

- For members with bonded tendons, strain is linearly distributed across a section. For members with unbonded tendons, the total change in tendon length is equal to the total change in member length over the distance between two anchorage points.
- The maximum usable strain at extreme compressive fiber is 0.003.
- The tensile strength of concrete is neglected.
- A concrete stress of $0.85 f'_c$ is uniformly distributed over an equivalent compression zone.
- Nonprestressed reinforcement reaches the yield strength and the corresponding stresses in the prestressing tendons are compatible based on plane section assumptions.

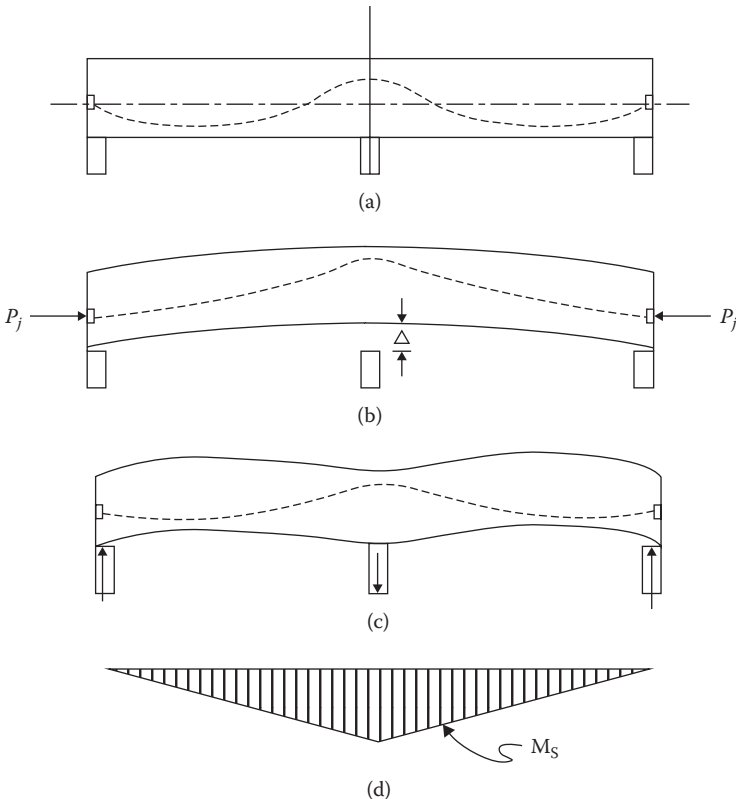


FIGURE 2.12 Secondary moments: (a) prestressed continuous beam (b) deformed simply supported beam due to primary moment (c) deformed continuous beam due to primary and secondary moments (d) secondary moment diagram.

For a member with a flanged section (Figure 2.13) subjected to uniaxial bending, the equations of equilibrium are used to obtain a nominal moment resistance of

$$\begin{aligned} M_n = & A_{ps}f_{ps}\left(d_p - \frac{a}{2}\right) + A_s f_s\left(d_s - \frac{a}{2}\right) \\ & - A'_s f'_s\left(d' - \frac{a}{2}\right) + 0.85 f'_c(b - b_w)h_f\left(\frac{a}{2} - \frac{h_f}{2}\right) \end{aligned} \quad (2.29)$$

$$a = \beta_1 c \quad (2.30)$$

For bonded tendons:

$$c = \frac{A_{ps}f_{pu} + A_s f_s - A'_s f'_s - 0.85 f'_c(b - b_w)h_f}{0.85 \beta_1 f'_c b_w + k A_{ps} \frac{f_{pu}}{d_p}} \geq h_f \quad (2.31)$$

$$f_{ps} = f_{pu} \left(1 - k \frac{c}{d_p}\right) \quad (2.32)$$

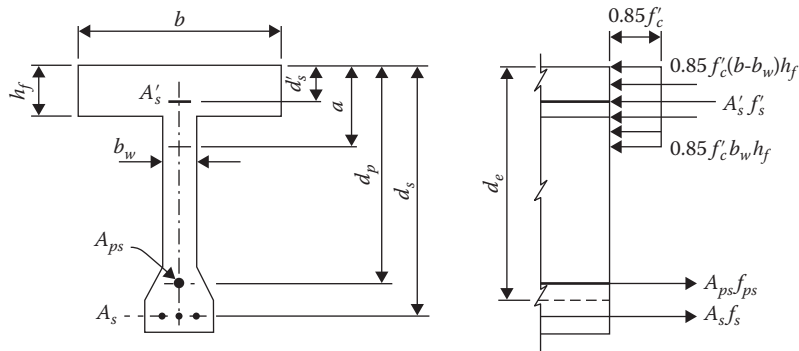


FIGURE 2.13 A flanged section at nominal moment capacity state.

$$k = 2 \left(1.04 - \frac{f_{py}}{f_{pu}} \right) \quad (2.33)$$

$$0.85 \geq \beta_1 = 0.85 - (f'_c - 4)(0.05) \geq 0.65 \quad (2.34)$$

where A represents area; f is the stress; b is the width of the compression face of the member; b_w is the web width of a section; h_f is the compression flange depth of the cross section; d_p and d_s are the distances from the extreme compression fiber to the centroid of prestressing tendons and to the centroid of tension reinforcement, respectively; subscript c indicates the specified strength for concrete; subscripts p and s mean prestressing steel and reinforcement steel respectively; subscripts ps , py , and pu correspond to states of nominal moment capacity, yield, and specified tensile strength of prestressing steel, respectively; superscript ' represents compression. The above equations can also be used for a rectangular section in which $b_w = b$ is taken.

For unbound tendons:

$$c = \frac{A_{ps}f_{ps} + A_s f_s - A'_s f'_s - 0.85 f'_c(b - b_w)h_f}{0.85 \beta_1 f'_c b_w} \geq h_f \quad (2.35)$$

$$f_{ps} = f_{pe} + 900 \left(\frac{d_p - c}{l_e} \right) \leq f_{py} \quad (2.36)$$

$$l_e = \frac{2l_i}{2 + N_s} \quad (2.37)$$

where l_e is the effective tendon length (in.); l_i is the length of the tendon between anchorage; N_s is the number of support hinges crossed by the tendon between anchorages or discretely bonded points.

Minimum reinforcement limit:

$$\phi M_n \geq 1.2 M_{cr} \quad (2.38)$$

in which ϕ is the flexural resistance factor 1.0 for prestressed concrete and 0.9 for the reinforced concrete; M_{cr} is the cracking moment strength given by the elastic stress distribution and the modulus of rupture of concrete.

$$M_{cr} = \frac{I}{y_t} (f_r + f_{pe} - f_d) \quad (2.39)$$

where f_{pe} is the compressive stress in concrete due to effective prestresses and f_d is the stress due to the unfactored self-weight; both f_{pe} and f_d are stresses at extreme fiber where tensile stresses are produced by externally applied loads.

2.4.6 Shear Resistance

The nominal shear resistance at the strength limit state is contributed by tensile stress in the concrete and tensile stresses in the transverse reinforcement and vertical component of prestressing force. It shall be determined by the following formula (AASHTO 2012):

$$V_n = \text{the lesser of } \begin{cases} V_c + V_s + V_p \\ 0.25 f'_c b_v d_v + V_p \end{cases} \quad (2.40)$$

where

$$V_c = 0.0316 \beta \sqrt{f'_c} b_v d_v \quad (2.41)$$

$$V_s = \frac{A_v f_y d_v (\cos \theta + \cot \alpha) \sin \alpha}{s} \quad (2.42)$$

where b_v is the effective web width determined by subtracting the diameters of un-grouted ducts or one-half the diameters of grouted ducts; d_v is the effective depth between the resultants of the tensile and compressive forces due to flexure, but it should not be taken into account if it is less than the greater of 0.9 d_e or 0.72 h ; A_v is the area of the transverse reinforcement within distance s ; s is the spacing of the stirrups; α is the angle of inclination of transverse reinforcement to the longitudinal axis; β is a factor indicating the ability of diagonally cracked concrete to transmit tension; θ is the angle of inclination of diagonal compressive stresses. The values of β and θ for sections with at least the minimum transverse reinforcement may be determined by

$$\beta = \frac{4.8}{(1 + 750 \varepsilon_s)} \quad (2.43)$$

$$\theta = 29 + 3500 \varepsilon_s \quad (2.44)$$

$$\varepsilon_s = \frac{\frac{|M_u|}{d_v} + 0.5 N_u + |V_u - V_p| - A_{ps} f_{po}}{E_s A_s + E_p A_{ps}} \quad (2.45)$$

where $|M_u|$ is the absolute value of the factored moment, not to be taken into account if it is less than where $|V_u - V_p| d_v$; N_u is the factored axial force (taken as positive if tensile) associated with the factored shear force V_u ; f_{po} is the stress in prestressing steel when the stress in the surrounding concrete is zero and can be conservatively taken as 0.7 f_{pu} ; V_p is the component in the direction of the applied shear of the effective prestressing force.

$$d_e = \frac{A_{ps} f_{ps} d_p + A_s f_y d_s}{A_{ps} f_{ps} + A_s f_y} \quad (2.46)$$

Minimum transverse reinforcement:

$$A_{v\min} = 0.0316 \sqrt{f'_c} \frac{b_v s}{f_y} \quad (2.47)$$

Maximum spacing of transverse reinforcement:

$$\text{For } v_u < 0.125 f'_c \quad s_{\max} = \text{the smaller of } \begin{cases} 0.8d_v \\ 24 \text{ in.} \end{cases} \quad (2.48)$$

$$\text{For } v_u \geq 0.125 f'_c \quad s_{\max} = \text{the smaller of } \begin{cases} 0.4d_v \\ 12 \text{ in.} \end{cases} \quad (2.49)$$

$$v_u = \frac{|V_u - \phi V_p|}{\phi b_v d_v} \quad (2.50)$$

where ϕ is the resistant factor for shear and is equal to 0.9.

2.4.7 Camber and Deflections

As opposed to load deflection, camber is usually referred to as *reversed deflection* and is caused by pre-stressing. A careful evaluation of camber and deflection for a prestressed concrete member is necessary to meet serviceability requirements. The following formulas developed by the moment-area method can be used to estimate midspan camber for simply supported members as shown in Figure 2.10.

For a straight tendon (Figure 2.10a):

$$\Delta = \frac{L^2}{8E_c I} M_e \quad (2.51)$$

For a one-point harping tendon (Figure 2.10b):

$$\Delta = \frac{L^2}{8E_c I} \left(M_c + \frac{2}{3} M_e \right) \quad (2.52)$$

For a two-point harping tendon (2.10c):

$$\Delta = \frac{L^2}{8E_c I} \left(M_c + M_e - \frac{M_e}{3} \left(\frac{2a}{L} \right)^2 \right) \quad (2.53)$$

For a parabola tendon (2.10d):

$$\Delta = \frac{L^2}{8E_c I} \left(M_e + \frac{5}{6} M_c \right) \quad (2.54)$$

where M_e is the primary moment at end, $P_j e_{end}$, and M_c is the primary moment at midspan $P_j e_c$. Uncracked gross section properties are often used in calculating camber. For deflection at service loads, cracked section properties, that is, moment of inertia I_{cr} should be used at the post-cracking service-load stage.

2.4.8 Anchorage Zones

In a pretensioned member, prestressing tendons transfer the compression load to the surrounding concrete over a length L_t gradually. In posttensioned member, prestressing tendons transfer the compression directly to the end of the member through bearing plates and anchors. The anchorage zone, based on the principle of St. Venant, is geometrically defined as the volume of concrete through which the prestressing force at the anchorage device spreads transversely to a more linear stress distribution across the entire cross section at some distance from the anchorage device (AASHTO 2012).

For design purposes, the anchorage zone can be divided into general and local zones (AASHTO 2012). The region of tensile stresses is the general zone. The region of high compressive stresses

(immediately ahead of the anchorage device) is the local zone. For the design of the general zone, a “Strut-and-Tie Model,” a refined elastic stress analysis, or approximate methods may be used to determine the stresses, while the resistance to bursting forces is provided by reinforcing spirals, closed hoops, or anchored transverse ties. For the design of the local zone, bearing pressure is a major concern. For detailed requirements, see AASHTO-LRFD (2012).

2.5 Design Limit States and Procedure

2.5.1 Design Limit States

A prestressed concrete girder highway bridge in the United States is designed to meet the requirements under various limit states specified by AASHTO-LRFD (2012) such as Strength I, Strength II, Service I and III, and Extreme Events. See Chapters 3, 4, and 6 in the first book in this series, *Bridge Engineering Handbook, Second Edition: Fundamentals* for a more detailed discussion.

2.5.2 Design Procedure

The CIP posttensioned prestressed concrete highway bridge girder may follow the flowchart as shown in Figure 2.14. The concrete design theory is discussed in Chapter 13 of *Bridge Engineering Handbook, Second Edition: Fundamentals*.

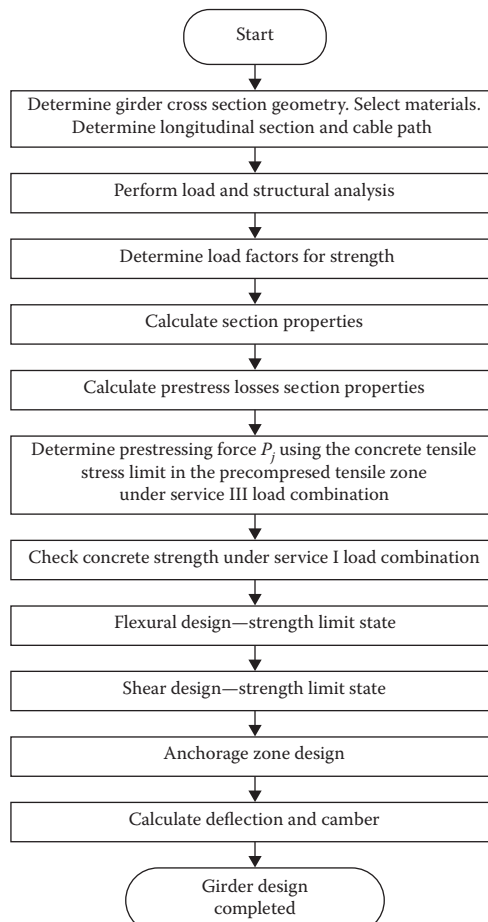


FIGURE 2.14 Typical CIP posttensioned prestressed concrete girder design flowchart.

2.6 Design Example: Two-Span Continuous Box Girder Bridge

2.6.1 Bridge Data

A two-span continuous cast-in-place prestressed concrete box girder highway bridge has two equal spans of length 157 ft. (47.9 m) with a column bent. The superstructure is 34 ft. (10.4 m) wide. The elevation of the bridge is shown in Figure 2.15.

2.6.2 Requirements

The following design calculations are performed for an interior plate girder at Span 1 in accordance with the *AASHTO LRFD Bridge Design Specifications*, 2012 Edition (AASHTO 2012).

- Determine cross-section geometry.
- Select materials.
- Determine longitudinal section and cable path.
- Perform load and structural analysis.
- Calculate unfactored moments and shears for interior girder.
- Determine load factors for strength and service limit states.
- Calculate section properties for interior girder.
- Calculate prestress losses.
- Determine prestressing force P_j —for interior girder.
- Check concrete strength for interior girder—Service Limit State I.
- Design for flexural—Strength Limit State I.
- Design for shear—Strength Limit State I.

2.6.3 Solution

2.6.3.1 Determine Cross-Section Geometry

1. Structural Depth— d

For prestressed continuous spans, the structural depth d can be determined using a depth-to-span ratio (d/L) of 0.04.

$$d = 0.04L = 0.04(157) = 6.28 \text{ ft. (1.91 m)}$$

Use $d = 6.25 \text{ ft. (1.91 m)}$

2. Girder Spacing— S

To provide effective torsional resistance and a sufficient number of girders for prestress paths, the spacing of girders should not be larger than twice their depth.

$$S_{max} < 2d = 2(6.25) = 12.5 \text{ ft. (3.81 m)}$$

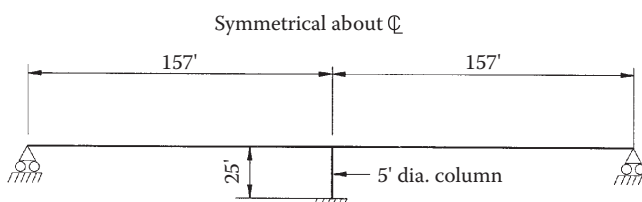


FIGURE 2.15 A two-span continuous CIP prestressed concrete box girder bridge.

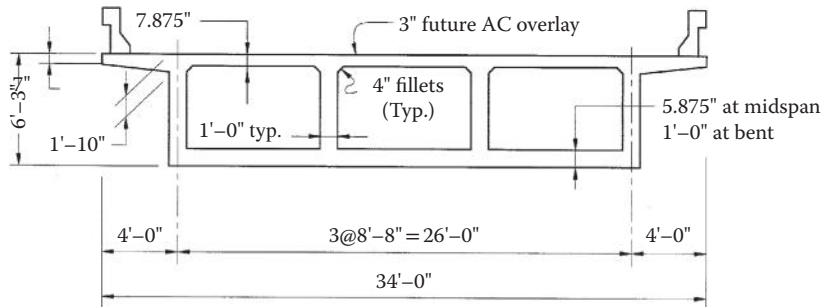


FIGURE 2.16 Typical section of box girder.

Using an overhang of 4 ft. (1.22 m), the center-to-center distance between two exterior girders is 26 ft. (7.92 m).

Try three girders and two bays, $S = 26/2 = 13$ ft. > 12.5 ft.

Try four girders and three bays, $S = 26/3 = 8.67$ ft. < 12.5 ft.

Use a girder spacing $S = 8.67$ ft. (2.64 m)

3. Typical Section

From past experience and design practice, we select a thickness of 7 in. (178 mm) at the edge and 12 in. (305 mm) at the face of the exterior girder for the overhang, the width of 12 in. (305 mm) for girders with the exterior girder flaring to 18 in. (457 mm) at the anchorage end. The length of this flare is usually taken as one-tenth of the span length 15.7 ft. (4.79 m). The deck and soffit thicknesses depend on the clear distance between adjacent girders. 7.875 in. (200 mm) and 5.875 in. (149 mm) are chosen for the deck and soffit thicknesses respectively. A typical section for this example is shown in Figure 2.16. The section properties of the box girder are as follows:

Properties	Midspan	Bent (face of support)
Cross section area – A ft. ² (m ²)	57.25 (5.32)	68.98 (6.41)
Moment of initial I ft. ⁴ (m ⁴)	325.45 (2.81)	403.56 (3.48)
Center of gravity – y_b ft. (m)	3.57 (1.09)	3.09 (0.94)

2.6.3.2 Select Materials

The following materials are selected for this example:

Concrete:

Initial concrete $f'_{ci} = 3,500$ psi (24.13 MPa), $E_{ci} = 3,372$ ksi (23,250 MPa)

Final concrete $f'_c = 4,000$ psi (27.58 MPa), $E_c = 3,600$ ksi (24,860 MPa)

Prestressing steel:

$f_{pu} = 270$ ksi (1,860 MPa) low relaxation strand

$E_p = 28,500$ ksi (197,000 MPa)

Prestressing stress at jacking $f_{pj} = 0.8 f_{pu} = 216$ ksi (1,489 MPa)

Reinforcement steel:

$f_y = 60$ ksi (414 MPa), $E_s = 29,000$ ksi (200,000 MPa)

Prestressing stress at jacking $f_{pj} = 0.8 f_{pu} = 216$ ksi (1,489 MPa)

Prestressing: Anchorage set thickness = 0.375 in. (9.5 mm)

2.6.3.3 Determine Longitudinal Section and Cable Path

To lower the center of gravity of the superstructure at the face of a bent cap in a CIP posttensioned box girder, the thickness of soffit slab is flared to 12 in. as shown in Figure 2.17. A cable path is generally

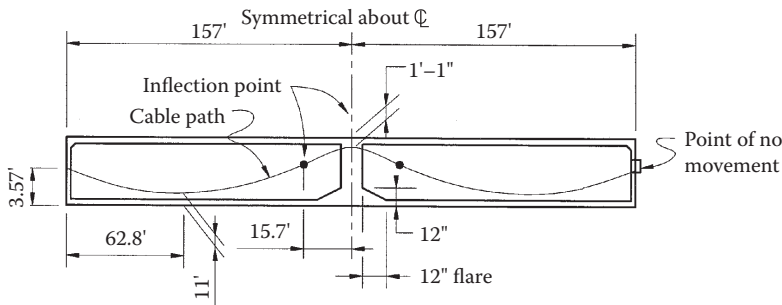


FIGURE 2.17 Cable path.

controlled by the maximum dead load moments and the position of the jack at the end section. Maximum eccentricities should occur at points of maximum dead load moment and almost no eccentricity should be present at the jacked end section. For this example, the maximum dead load moments occur at the bent cap, close to $0.4L$ for Span 1 and $0.6L$ for Span 2. A parabolic cable path is chosen as shown in Figure 2.17.

2.6.3.4 Perform Load and Structural Analysis

1. Calculate permanent loads

The permanent load or dead load includes the component dead load DC and the wearing surface load DW . The component dead load DC includes all structural dead loads with the exception of the future wearing surface and specified utility loads. For design purposes, two parts of the DC are defined as follows:

$DC1$ —girder self-weight (150 lbs./ft.³) acting at the prestressing state

$DC2$ —barrier rail weight (784 kip/ft.) acting at service state after all losses.

DW —future wearing surface of 3 in. (76 mm) with a unit weight of 140 lbs./ft.³

$$\begin{aligned} DW &= (\text{deck width} - \text{barrier width}) (\text{thickness of wearing surface}) (\text{unit weight}) \\ &= [34 - 2(1.75)] (0.25) (140) = 1067.5 \text{ lbs./ft.} \end{aligned}$$

2. Determine live load LL and dynamic load allowance IM

The design live load LL is the AASHTO HL-93 vehicular live load. To consider the wheel-load impact from moving vehicles, the dynamic load allowance $IM = 33\%$ [AASHTO-LRFD Table 3.6.2.1-1] is used.

3. Calculate live load distribution factors

AASHTO-LRFD (2012) recommends that approximate methods be used to distribute live load to individual girders. The dimension relevant to this prestressed box girder are depth $d = 6.25$ ft. (1.91 m), number of cells $N_c = 3$, spacing of girders $S = 8.67$ ft. (2.64 m), span length $L = 157$ ft. (47.9 m), half of the girder spacing plus the total overhang $W_e = 8.334$ ft. (2.54 m), and the distance between the center of an exterior girder and the interior edge of a barrier $d_e = 4 - 1.75 = 2.25$ ft. (0.69 m). This box girder is within the range of applicability of the AASHTO approximate formulas. The live load distribution factors are calculated as follows.

Live load distribution factor for bending moments

1. Interior girder (AASHTO Table 4.6.2.2.2b-1)

One lane loaded:

$$\begin{aligned} LD_M &= \left(1.75 + \frac{S}{3.6} \right) \left(\frac{1}{L} \right)^{0.35} \left(\frac{1}{N_c} \right)^{0.45} \\ &= \left(1.75 + \frac{8.67}{3.6} \right) \left(\frac{1}{157} \right)^{0.35} \left(\frac{1}{3} \right)^{0.45} = 0.432 \text{ lanes} \end{aligned}$$

Two or more lanes loaded:

$$\begin{aligned} LD_M &= \left(\frac{13}{N_c} \right)^{0.3} \left(\frac{S}{5.8} \right) \left(\frac{1}{L} \right)^{0.25} \\ &= \left(\frac{13}{3} \right)^{0.3} \left(\frac{8.67}{5.8} \right) \left(\frac{1}{157} \right)^{0.25} = 0.656 \text{ lanes (controls)} \end{aligned}$$

2. Exterior girder (AASHTO Table 4.6.2.2.2d-1)

$$LD_M = \frac{W_e}{14} = \frac{8.334}{14} = 0.595 \text{ lanes (controls)}$$

Live load distribution factor for shear

1. Interior girder (AASHTO Table 4.6.2.2.3a-1)

One lane loaded:

$$\begin{aligned} LD_V &= \left(\frac{S}{9.5} \right)^{0.6} \left(\frac{d}{12L} \right)^{0.1} \\ &= \left(\frac{8.67}{9.5} \right)^{0.6} \left(\frac{6.25}{12(157)} \right)^{0.1} = 0.535 \text{ lanes} \end{aligned}$$

Two or more lanes loaded:

$$\begin{aligned} LD_V &= \left(\frac{S}{7.3} \right)^{0.9} \left(\frac{d}{12L} \right)^{0.1} \\ &= \left(\frac{8.67}{7.3} \right)^{0.9} \left(\frac{6.25}{12(157)} \right)^{0.1} = 0.660 \text{ lanes (controls)} \end{aligned}$$

2. Exterior girder (AASHTO Table 4.6.2.2.3b-1)

One lane loaded: Lever rule

The lever rule assumes that the deck in its transverse direction is simply supported by the girders and uses statics to determine the live load distribution to the girders. AASHTO-LRFD also requires that, when the lever rule is used, the multiple presence factor m should apply. For a one loaded lane, $m = 1.2$. The lever rule model for the exterior girder is shown in Figure 2.18. From static equilibrium:

$$R = \frac{5.92}{8.67} = 0.683$$

$$LD_v = mR = (1.2)(0.683) = 0.820 \text{ (controls)}$$

Two or more lanes loaded: Modify interior girder factor by e

$$\begin{aligned} LD_V &= e(LD_v)_{\text{interior girder}} = \left(0.64 + \frac{d_e}{12.5} \right) (LD_v)_{\text{interior girder}} \\ &= \left(0.64 + \frac{2.25}{12.5} \right) (0.66) = 0.541 \end{aligned}$$

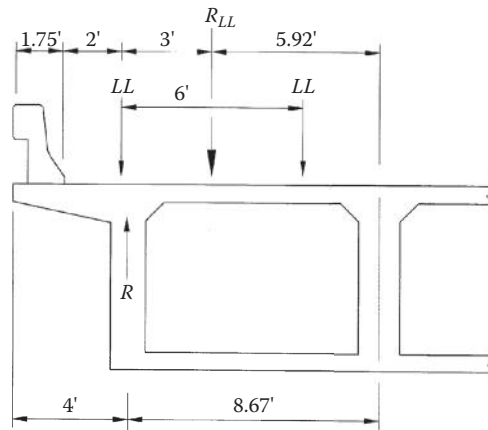


FIGURE 2.18 Live load distribution for exterior girder—lever rule.

Strength Limit State I	Interior Girder	Exterior Girder
Bending moment	0.656 lanes	0.595 lanes
Shear	0.660 lanes	0.820 lanes

The controlling live load distribution factors at the strength limit state are as follows:

4. Perform structural analysis

A line girder analysis for the two-span bridge is performed to obtain the unfactored dead load effects for the whole box girder and unfactored live load effects for one lane loaded.

The secondary moments due to prestressing at the bent are as follows:

$$M_{DA} = 1.118 P_j \text{ (kip-ft.)} \quad M_{DG} = 1.107 P_j \text{ (kip-ft.)}$$

2.6.3.5 Calculate Unfactored Moments and Shear for Interior Girder

It is practically assumed that all dead loads are carried by the box girder and equally distributed to each girder. The live load effects are distributed to individual girders according to live load distribution factors (AASHTO Article 4.6.2.2.2). Unfactored moment and shear effects for an interior girder are shown in Figures 2.19 and 2.20. Details are listed in Tables 2.6 and 2.7. Only the results for Span 1 are shown in these tables and figures since the bridge is symmetrical about the bent.

2.6.3.6 Determine Load Factors for Strength and Service Limit States

1. General design equation (ASHTO Article 1.3.2)

$$\sum \eta_i \gamma_i Q_i \leq \phi R_n = R_r \quad (2.55)$$

where γ_i is the load factor and ϕ is the resistance factor; Q_i represents the force effect; R_n is the nominal resistance; R_r is the factored resistance; η_i is the load modifier factor related to ductility, redundancy, and operational importance and is defined as follows when a maximum value of γ_i is used:

$$\eta_i = \eta_D \eta_R \eta_I \geq 0.95 \quad (2.56)$$

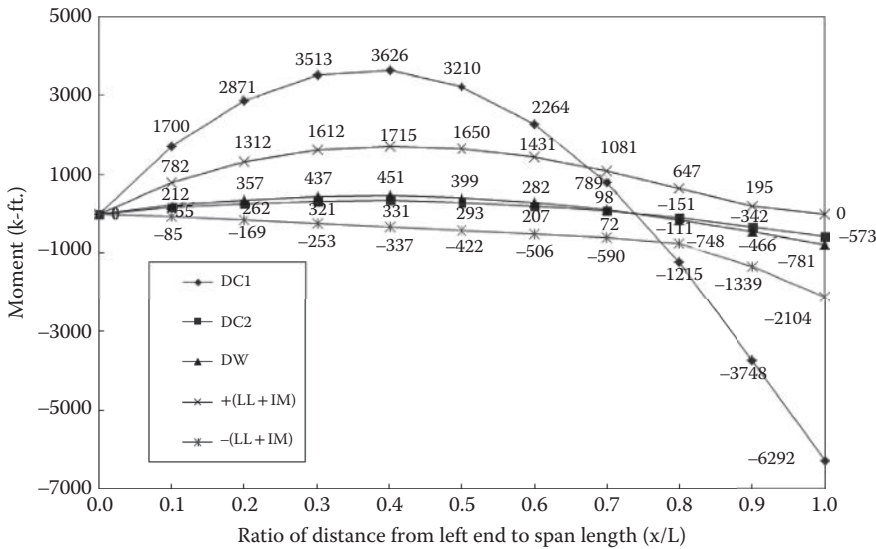


FIGURE 2.19 Unfactored moment envelopes for Span 1.

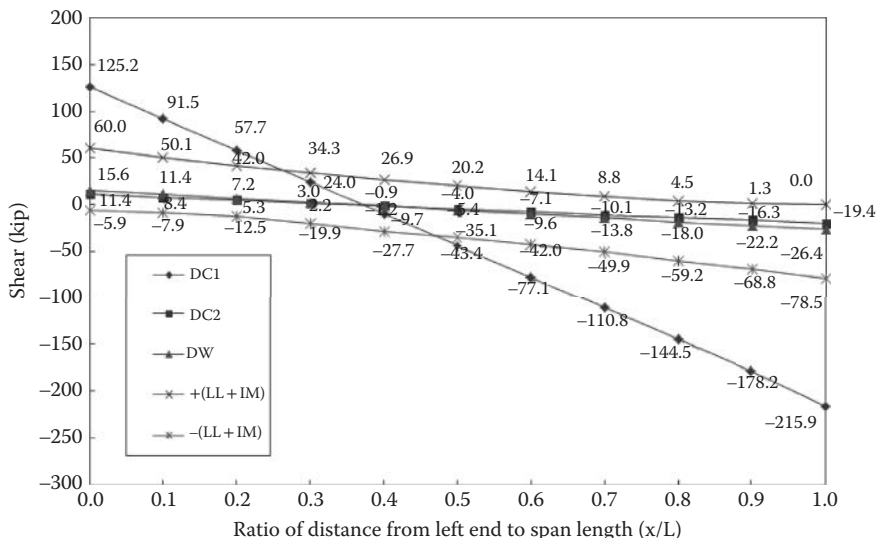


FIGURE 2.20 Unfactored shear envelopes for Span 1.

where

$$\eta_D = \begin{cases} 1.05 & \text{for non-ductile components and connections} \\ 0.95 & \text{for ductile components and connections} \end{cases} \quad (2.57)$$

$$\eta_R = \begin{cases} 1.05 & \text{for non-redundant members} \\ 0.95 & \text{for redundant members} \end{cases} \quad (2.58)$$

$$\eta_I = \begin{cases} 1.05 & \text{operational important bridge} \\ 0.95 & \text{general bridge} \\ \text{only apply to strength and extreme event limit states} & \end{cases} \quad (2.59)$$

TABLE 2.6 Unfactored Dead Load Moments and Shears for the Interior Girder

Span	Location (x/L)	Unfactored Dead Load					
		DC1		DC2		DW	
		M_{DC1}	V_{DC1}	M_{DC2}	V_{DC2}	M_{DW}	V_{DW}
1	0.0	0	125.2	0	11.4	0	15.6
	0.1	1700	91.5	155	8.4	212	11.4
	0.2	2871	57.7	262	5.3	357	7.2
	0.3	3513	24.0	321	2.2	437	3.0
	0.4	3626	-9.7	331	-0.9	451	-1.2
	0.5	3210	-43.4	293	-4.0	399	-5.4
	0.6	2264	-77.1	207	-7.1	282	-9.6
	0.7	789	-111	72	-10.1	98	-13.8
	0.8	-1215	-145	-111	-13.2	-151	-18.0
	0.9	-3748	-178	-342	-16.3	-466	-22.2
	1.0	-6833 (-6292)	-216	-622 (-573)	-19.4	-847(-781)	-26.4

Notes:

1. DC1—interior girder self-weight
2. DC2—barrier self-weight
3. DW—wearing surface load
4. Moments in brackets are for face of support at the bent
5. Moments in Span 2 are symmetrical about the bent
6. Shear in span is antisymmetrical about the bent

TABLE 2.7 Unfactored HL-93 Live Load Moments, Shears and Associated Forces for Interior Girder

Span	Location (x/L)	Positive Moment and Associated Shear		Negative Moment and Associated Shear		Shear and Associated Moment	
		M_{LL+IM}	V_{LL+IM}	M_{LL+IM}	V_{LL+IM}	V_{LL+IM}	M_{LL+IM}
1	0.0	0	0	0	0	60.0	0
	0.1	782	49.8	-85	-5.4	50.1	787
	0.2	1312	41.8	-169	-5.4	42.0	1320
	0.3	1612	29.3	-253	-5.4	34.3	1614
	0.4	1715	21.8	-337	-5.4	-27.7	1650
	0.5	1650	-30.0	-422	-5.4	-35.1	1628
	0.6	1431	-36.7	-506	-5.4	-42.0	1424
	0.7	1081	-42.6	-590	-5.4	-49.9	852
	0.8	647	-47.8	-748	-8.3	-59.2	216
	0.9	196	-32.9	-1339	-50.1	-68.8	-667
	1.0	0	0	-2266 (-2104)	-67.8	-78.5	-1788

Notes:

1. LL + IM—AASHTO HS20-44 live load plus dynamic load allowance
2. Moments in brackets are for face of support at the bent
3. Moments in Span 2 are symmetrical about the bent
4. Shear in Span 2 is antisymmetrical about the bent
5. Live load distribution factors are considered

For this bridge, the following values are assumed:

Limit States	Ductility η_D	Redundancy η_R	Importance η_I	η
Strength limit state	0.95	0.95	1.05	0.95
Service limit state	1.0	1.0	1.0	1.0

2. Load factors and load combinations

The load factors and combinations are specified as (AASHTO Table 3.4.1-1):

Strength Limit State I: $1.25(DC1 + DC2) + 1.5(DW) + 1.75(LL + M)$

Service Limit State I: $DC1 + DC2 + DW + (LL + IM)$

Service Limit State III: $DC1 + DC2 + DW + 0.8(LL + IM)$

2.6.3.7 Calculate Section Properties for Interior Girder

For the example bridge, the skew angle is zero and $L/S = 157/8.67 = 18.1 > 2$. For an interior girder, as shown in Figure 2.21, the effective flange width b_{eff} is taken as the tributary width of the concrete slab, that is, the girder spacing $S = 8.67$ ft. (AASHTO 4.6.2.6).

The section properties at the midspan and the bent (face of support) for the interior girder are calculated in Tables 2.8 and 2.9.

2.6.3.8 Calculate Prestress Losses

For a CIP posttensioned box girder, two types of losses, instantaneous losses (friction, anchorage set and elastic shortening) and time-dependent losses (creep and shrinkage of concrete, and relaxation of prestressing steel), are significant. Since the prestress losses are not symmetrical about the bent for this bridge, the calculation is performed for both spans.

1. Frictional loss Δf_{pF}

$$\Delta f_{pF} = f_{pj} \left(1 - e^{-(Kx + \mu\alpha)}\right) \quad (2.60)$$

where K is the wobble friction coefficient = 0.0002 1/ft. (6.6×10^{-7} 1/mm) and μ is the coefficient of friction = 0.25 (AASHTO Article 5.9.5.2.2b); x is the length of a prestressing tendon from

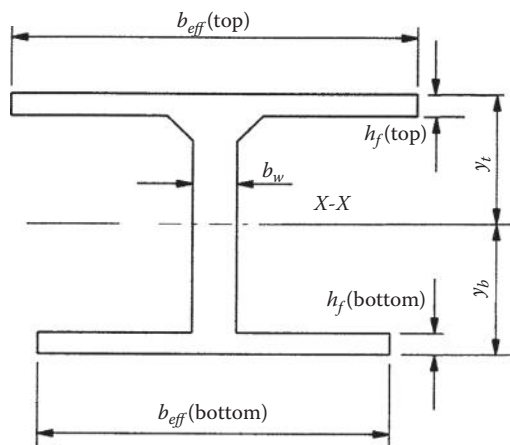


FIGURE 2.21 Cross section of interior girder.

TABLE 2.8 Midspan Section Properties for Interior Girder

Component	A_i (in. ²)	y_i (in.)	$A_i y_i$ (in. ³)	$y_i - y_b$ (in.)	$A_i (y_i - y_{NCB})^2$ (in. ⁴)	I_o (in. ⁴)
Top deck 104 × 7.875	819	71.06	58,200.2	30.77	775,487	4,233
Fillet 4 × 4	16	65.79	1,052.7	25.50	10,405	14
Web 61.25 × 12	735	36.5	26,827.5	-3.79	10,565	229,793
Bottom soffit 104 × 5.875	611	2.94	1,794.8	-37.35	825,529	1,757
Σ	2,181	-	87,875.2	-	1,648,986	235,787

$$y_b = \frac{\sum A_i y_i}{\sum A_i} = \frac{87,852.2}{2,181} = 40.29 \text{ in.}$$

$$y_t = (6.25)(12) - 40.29 = 34.71 \text{ in.}$$

$$I_x = \sum I_o + \sum A_i (y_i - y_b)^2 = 235,787 + 1,648,986 = 1,884,773 \text{ in.}^4$$

TABLE 2.9 Bent Section (at Face of Support) Properties for Interior Girder

Component	A_i (in. ²)	y_i (in.)	$A_i y_i$ (in. ³)	$y_i - y_b$ (in.)	$A_i (y_i - y_{NCB})^2$ (in. ⁴)	I_o (in. ⁴)
Top deck 104 × 7.875	819	71.06	58,200.2	37.21	1,133,902	4,233
Fillet 4 × 4	16	65.79	1,052.7	31.94	16,321	14
Web 55.125 × 12	661.5	39.56	26,170.6	5.71	21,559	167,512
Bottom soffit 104 × 12	1,248	6.00	74,988.0	-27.85	968,233	14,976
Σ	2,744.5	-	92,911.5	-	2,140,015	186,735

$$y_b = \frac{\sum A_i y_i}{\sum A_i} = \frac{92,911.5}{2,744.5} = 33.85 \text{ in.}$$

$$y_t = (6.25)(12) - 33.85 = 41.15 \text{ in.}$$

$$I_x = \sum I_o + \sum A_i (y_i - y_b)^2 = 186,735 + 2,140,015 = 2,326,750 \text{ in.}^4$$

the jacking end to the point considered; α is the sum of the absolute values of the angle change in the prestressing steel path from the jacking end.

For a parabolic cable path (Figure 2.22), the angle change is $\alpha = 2e_p/L_p$, where e_p is the vertical distance between two control points and L_p is the horizontal distance between two control points. The details are given in Table 2.10.

2. Anchorage set loss Δf_{pA}

The anchorage set loss can be approximated by assuming the anchorage set loss changes linearly within the length L_{pA} as shown in Figure 2.8.

Assume an anchor set thickness of $\Delta L = 0.375$ in., $E = 29,000$ ksi, and consider the point B where $L_{pF} = 141.3$ ft. and $\Delta f_{pF} = 14.9$ ksi:

$$L_{pA} = \sqrt{\frac{E(\Delta L)L_{pF}}{\Delta f_{pF}}} = \sqrt{\frac{29,000(0.375)(141.3)}{12(14.9)}} = 92.71 \text{ ft.} < 141.3 \text{ ft.}$$

$$\Delta f = \frac{2 \Delta f_{pF} x}{L_{pF}} = \frac{2(14.9)(92.71)}{141.3} = 19.55 \text{ ksi}$$

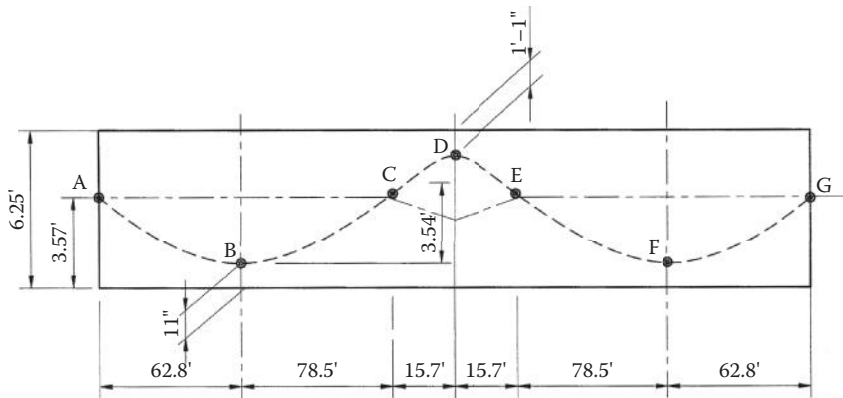


FIGURE 2.22 Parabolic cable path.

TABLE 2.10 Prestress Frictional Loss

Segment	e_p (in.)	L_p (ft.)	α (rad)	$\Sigma\alpha$ (rad)	ΣL_p (ft.)	Point	Δf_{pF} (ksi)
A	31.84	0	0	0	0	A	0.0
AB	31.84	62.8	0.0845	0.0845	62.8	B	7.13
BC	42.50	78.5	0.0902	0.1747	141.3	C	14.90
CD	8.50	15.7	0.0902	0.2649	157.0	D	20.09
DE	8.50	15.7	0.0902	0.3551	172.7	E	25.06
EF	42.50	78.5	0.0902	0.4453	251.2	F	32.18
FG	31.84	62.8	0.0845	0.5298	314.0	G	38.23

$$\Delta f_{pA} = \Delta f \left(1 - \frac{x}{L_{pA}}\right) = 19.55 \left(1 - \frac{x}{92.71}\right)$$

The anchorage set loss is calculated in Table 2.11.

3. Elastic shortening loss Δf_{pES}

The loss due to elastic shortening in posttensioned members is calculated using the following formula (AASHTO Article 5.9.5.2.3b):

$$\Delta f_{pES} = \frac{N-1}{2N} \frac{E_p}{E_{ci}} f_{cgp} \quad (2.61)$$

To calculate the elastic shortening loss, we assume that the prestressing jack force for an interior girder $P_j = 1800$ kips and the total number of prestressing tendons $N = 4$. f_{cgp} is calculated for the midsupport section. From Table 2.9, the distance between the prestressing tendons to the central gravity of the girder, $e = y_t - 13 = 41.15 - 13 = 28.15$ in.

$$\begin{aligned} f_{cgp} &= \frac{P_j}{A} + \frac{P_j e^2}{I_x} + \frac{M_{DC1} e}{I_x} \\ &= \frac{1,800}{2,744.5} + \frac{1,800 (28.15)^2}{2,326,750} + \frac{(-6,292)(12)(28.15)}{2,326,750} \\ &= 0.656 + 0.613 - 0.913 = 0.356 \text{ ksi (2.455 MPa)} \end{aligned}$$

TABLE 2.11 Cable Path and Prestress Losses

Span	Location (x/L)	Prestress Losses (ksi)					Force Coef.	
		Δf_{pF}	Δf_{pA}	Δf_{pES}	Δf_{pLT}	Δf_{pT}	F_{pCI}	F_{pCF}
1	0.0	0.00	19.55			39.01	0.904	0.819
	0.1	1.78	16.24			37.48	0.911	0.826
	0.2	3.56	12.93			35.95	0.918	0.834
	0.3	5.35	9.93			34.74	0.924	0.839
	0.4	7.13	6.31			32.90	0.933	0.848
	0.5	8.68	3.00	1.13	18.33	31.13	0.941	0.856
	0.6	10.24				29.70	0.947	0.863
	0.7	11.79				31.25	0.940	0.855
	0.8	13.35	0.00			32.81	0.933	0.848
	0.9	14.90				34.36	0.926	0.841
2	1.0	20.09				39.55	0.902	0.817
	0.0	20.09				39.55	0.902	0.817
	0.1	25.06				44.52	0.879	0.794
	0.2	26.49				45.95	0.872	0.787
	0.3	27.91				47.37	0.866	0.781
	0.4	29.34				48.80	0.859	0.774
	0.5	30.76	0.00	1.13	18.33	50.22	0.852	0.768
	0.6	32.18				51.64	0.846	0.761
	0.7	33.69				53.15	0.839	0.754
	0.8	35.21				54.67	0.832	0.747
	0.9	36.72				56.18	0.825	0.740
	1.0	38.23				57.69	0.818	0.733

Note:

$$F_{pCI} = 1 - \frac{\Delta f_{pF} + \Delta f_{pA} + \Delta f_{pES}}{f_{pj}}$$

$$F_{pCF} = 1 - \frac{\Delta f_{pT}}{f_{pj}} \quad f_{pj} = 216 \text{ ksi}$$

$$\Delta f_{pES} = \frac{N-1}{2N} \frac{E_p}{E_{ci}} f_{cgp} = \frac{4-1}{2(4)} \left(\frac{28,500}{3,372} \right) (0.356) = 1.13 \text{ ksi (7.778 MPa)}$$

4. Shrinkage loss Δf_{pSR}

For cast-in-place concrete box girder, concrete of deck and girders is usually cast prior to prestressing

Assume $\epsilon_{bid} = 0.0006$, $A_{ps} = P_j/f_{pj} = 1,800/216 = 8.33 \text{ in.}^2$, and $t_i = 28 \text{ days}$, $t_f = 120 \text{ days}$.

$$\frac{V}{s} = \frac{(2,181)(1.0)}{(2)(104 + 7.875 + 5.875 + 92 + 61.25)(1.0)} = 4.02 > 1.0$$

$$k_s = 1.45 - 0.13(V/s) \geq 1.45 - (0.13)(4.02) = 0.93 < 1.0 \quad \text{Use } k_s = 1.0$$

$$k_{hs} = (2.00 - .014H) = 2.0 - 0.014(70) = 1.12$$

$$k_f = \frac{5}{1+f'_c} = \frac{5}{1+4} = 1.0$$

$$k_{td} = \frac{t}{61 - 4f'_{ci} + t} = \frac{28}{61 - (4)(3.5) + 28} = 0.373$$

Creep coefficient

$$\psi(t_f, t_i) = 1.9 k_s k_{hc} k_f k_{td} t_i^{-0.118} = (1.9)(1.0)(1.0)(1.0)(0.373)(120)^{-0.118} = 0.403$$

Shrinkage loss can be determined by formulas (AASHTO 2012):

$$\begin{aligned} K_{id} &= \frac{1}{1 + \frac{E_p A_{ps}}{E_{ci} A_g} \left(1 + \frac{A_g e_{pg}^2}{I_g} \right) (1 + 0.7\psi_b(t_f, t_i))} \\ &= \frac{1}{1 + \frac{28,500}{3,372} \left(\frac{8.33}{2,744.5} \right) \left(1 + \frac{(2,744.5)(28.15)^2}{2,326,750} \right) (1 + 0.403)} \\ &= 0.935 \end{aligned} \quad (\text{AASHTO 5.9.5.4.3a-2})$$

$$\Delta f_{pSR} = \varepsilon_{bid} E_p K_{id} = (0.0006)(28,500)(0.935) = 16.0 \text{ ksi}$$

5. Creep loss Δf_{pCR}

$$\begin{aligned} \Delta f_{pCR} &= \left(\frac{E_p}{E_{ci}} \right) f_{cgp} \psi(t_d, t_i) K_{id} \\ &= \left(\frac{28,500}{3,372} \right) (0.356)(0.403)(0.935) = 1.13 \text{ ksi} \end{aligned} \quad (\text{AASHTO 5.9.5.4.2b-1})$$

6. Relaxation loss Δf_{pRI}

For low-relaxation strands, the relaxation loss is assumed to be equal to 1.2 ksi (AASHTO 5.9.5.4.2c).

7. Time-dependent losses Δf_{pLT}

Total time-dependent losses for nonsegmental cast-in-place posttensioned members is as follows:

$$\Delta f_{pLT} = \Delta f_{pSR} + \Delta f_{pCR} + \Delta f_{pRI} = 16.0 + 1.13 + 1.2 = 18.33 \text{ ksi}$$

8. Total losses Δf_{pT}

$$\Delta f_{pT} = \Delta f_{pF} + \Delta f_{pA} + \Delta f_{pES} + \Delta f_{pLT} \quad (2.62)$$

Details are given in Table 2.11.

 @Seismicisolation

2.6.3.9 Determine Prestressing Force P_j for Interior Girder

Since the live load is not in general equally distributed to girders, the prestressing force P_j required for each girder may be different. To calculate prestress jacking force P_j , the initial prestress force coefficient F_{pCI} and final prestress force coefficient F_{pCF} are defined as follows:

$$F_{pCI} = 1 - \frac{\Delta f_{pF} + \Delta f_{pA} + \Delta f_{pES}}{f_{pj}} \quad (2.63)$$

$$F_{pCF} = 1 - \frac{\Delta f_{pT}}{f_{pj}} \quad (2.64)$$

The prestress force coefficients are calculated and tabled in Table 2.12.

The secondary moment coefficients are defined as follows:

$$M_{sC} = \begin{cases} \frac{x}{L} \frac{M_{DA}}{P_j} & \text{for span 1} \\ \left(1 - \frac{x}{L}\right) \frac{M_{DG}}{P_j} & \text{for span 2} \end{cases} \quad (2.65)$$

where x is distance from the left end for each span.

TABLE 2.12 Prestress Force and Moment Coefficients

Span	Location (x/L)	Cable Path e (in.)	Force Coef.		Moment Coefficients (ft.)			
			F_{pCI}	F_{pCF}	$F_{pCI}e$	$F_{pCF}e$	M_{sC}	M_{psCI}
1	0.0	0.240	0.904	0.819	0.018	0.016	0.000	0.018
	0.1	-13.692	0.911	0.826	-1.040	-0.943	0.112	-0.928
	0.2	-23.640	0.918	0.834	-1.809	-1.642	0.224	-1.586
	0.3	-29.136	0.924	0.839	-2.244	-2.037	0.335	-1.908
	0.4	-31.596	0.933	0.848	-2.456	-2.232	0.447	-2.008
	0.5	-29.892	0.941	0.856	-2.344	-2.132	0.559	-1.785
	0.6	-24.804	0.947	0.863	-1.958	-1.783	0.671	-1.287
	0.7	-16.308	0.940	0.855	-1.278	-1.162	0.783	-0.495
	0.8	-4.404	0.933	0.848	-0.342	-0.311	0.894	0.552
	0.9	10.884	0.926	0.841	0.840	0.763	1.006	1.846
2	1.0	28.164	0.902	0.817	2.117	1.917	1.118	3.235
	0.0	-28.164	0.902	0.817	2.117	1.917	1.107	3.224
	0.1	10.884	0.879	0.794	0.797	0.720	0.996	1.793
	0.2	-4.404	0.872	0.787	-0.320	-0.289	0.886	0.566
	0.3	-16.308	0.866	0.781	-1.176	-1.061	0.775	-0.401
	0.4	-24.804	0.859	0.774	-1.776	-1.600	0.664	-1.111
	0.5	-29.892	0.852	0.768	-2.123	-1.912	0.554	-1.570
	0.6	-31.596	0.846	0.761	-2.227	-2.004	0.443	-1.784
	0.7	-29.136	0.839	0.754	-2.037	-1.831	0.332	-1.705
	0.8	-23.640	0.832	0.747	-1.639	-1.471	0.221	-1.417
	0.9	-13.692	0.825	0.740	-0.941	-0.844	0.111	-0.830
	1.0	0.240	0.818	0.733	0.016	0.015	0.000	0.016

Note: e is the distance between the cable path and the central gravity of the interior girder cross section, positive means cable is above the central gravity and negative indicates cable is below the central gravity.

The combined prestressing moment coefficients are defined as follows:

$$M_{psCI} = F_{pCI}(e) + M_{sC} \quad (2.66)$$

$$M_{psCF} = F_{pCF}(e) + M_{sC} \quad (2.67)$$

where e is the distance between the cable and the center of gravity of a cross section; positive values of e indicate that the cable is above the center of gravity, and negative ones indicate that the cable is below it.

The combined moment coefficients are calculated and tabled in Table 2.13. According to AASHTO, the prestressing force P_j can be determined using the concrete tensile stress limit in the precompressed tensile zone under Service III load combination (see Table 2.5):

$$f_{DC1} + f_{DC2} + f_{DW} + 0.8f_{LL+IM} + f_{psF} \geq -0.19\sqrt{f_c'} \quad (2.68)$$

TABLE 2.13 Determination of Prestressing Jacking Force for Interior Girder

Span	Location (x/L)	Top Fiber					Bottom Fiber					Jacking Force (kip) P_j	
		Stress (psi)				Jacking Force (kip) P_j	Stress (psi)						
		f_{DC1}	f_{DC2}	f_{DW}	$0.8f_{LL+IM}$		f_{DC1}	f_{DC2}	f_{DW}	$0.8f_{LL+IM}$	f_{psF}		
1	0.0	0	0	0	0	–	0	0	0	0	–	–	
	0.1	389	36	48	143	–	-512	-47	-64	-188	664	664	
	0.2	658	60	82	240	–	-865	-79	-108	-316	1191	1191	
	0.3	805	73	100	295	–	-1058	-97	-132	-388	1411	1411	
	0.4	831	76	103	314	–	-1092	-100	-136	-413	1438	1438	
	0.5	735	67	91	302	–	-967	-88	-120	-398	1345	1345	
	0.6	519	47	64	262	–	-682	-62	-85	-345	1057	1057	
	0.7	181	16	22	198	–	-238	-22	-30	-260	322	322	
	0.8	-278	-25	-35	-137	177	366	33	46	203	–	–	
	0.9	-859	-78	-107	-245	1121	1129	103	140	363	–	–	
2	1.0	-1336	-122	-166	-357	1703	1098	100	136	330	–	–	
	0.0	-1336	-122	-166	-357	1707	1098	100	136	330	–	–	
	0.1	-859	-78	-107	-245	1171	1129	103	140	363	–	–	
	0.2	-278	-25	-35	-137	186	366	33	46	203	–	–	
	0.3	181	16	22	198	–	-238	-22	-30	-260	367	367	
	0.4	519	47	64	262	–	-682	-62	-85	-345	1211	1211	
	0.5	735	67	91	302	–	-967	-88	-120	-398	1530	1530	
	0.6	831	76	103	314	–	-1092	-100	-136	-413	1626	1626	
	0.7	805	73	100	295	–	-1058	-97	-132	-388	1588	1588	
	0.8	658	60	82	240	–	-865	-79	-108	-316	1340	1340	
	0.9	389	36	48	143	–	-512	-47	-64	-188	746	746	
	1.0	0	0	0	0	–	0	0	0	0	–	–	

Notes:

1. Positive stress indicates compression and negative stress indicates tension

2. P_j is obtained from Equation 2.26

in which

$$f_{DC1} = \frac{M_{DC1}C}{I_x} \quad (2.69)$$

$$f_{DC2} = \frac{M_{DC2}C}{I_x} \quad (2.70)$$

$$f_{DW} = \frac{M_{DW}C}{I_x} \quad (2.71)$$

$$f_{LL+IM} = \frac{M_{LL+IM}C}{I_x} \quad (2.72)$$

$$f_{psF} = \frac{P_{pe}}{A} + \frac{(P_{pe}e)C}{I_x} + \frac{M_{sc}C}{I_x} = \frac{F_{pCF}P_j}{A} + \frac{M_{psCF}P_jC}{I_x} \quad (2.73)$$

where C ($= y_b$ or y_t) is the distance from the extreme fiber to the center of gravity of the cross section; f'_c is in ksi and P_{pe} is the effective prestressing force after all losses have been incurred; M_{DC1} , M_{DC2} , and M_{DW} are unfactored moments due to $DC1$ of girder self-weight acting at the prestressing state, $DC2$ of barrier rail weight acting at the service state after all losses, and DW of the future wearing surface acting at the service state after all losses, respectively; M_{LL+IM} is the unfactored moment due to HL93 live load and dynamic allowance. For stresses, positive sign implies compression and negative implies tension.

From Equations 2.68 and 2.73, we have

$$P_j = \frac{-f_{DC1} - f_{DC2} - f_{DW} - 0.8f_{LL+IM} - 0.19\sqrt{f'_c}}{\frac{F_{pCF}}{A} + \frac{M_{psCF}C}{I_x}} \quad (2.74)$$

Detailed calculations are given in Table 2.13. Most critical points coincide with locations of maximum eccentricity: $0.4L$ in Span 1, $0.6L$ in Span 2, and at the bent. For this bridge, the controlling section is through the right face of the bent. Herein, $P_j = 1707$ kip (7566 kN). Rounding P_j up to 1720 kips (7651 kN) gives a required area of prestressing steel of $A_{ps} = P_j/f_{pj} = 1720/216 = 7.96$ in.² (5236 mm²).

2.6.3.10 Check Concrete Strength for Interior Girder—Service Limit State I

Two criteria are imposed on the level of concrete stresses when calculating the required concrete strength (AASHTO 2012, Article 5.9.4.2):

$$\begin{cases} f_{DC1} + f_{psl} \leq 0.55f'_c & \text{at prestressing state} \\ f_{DC1} + f_{DC2} + f_{DW} + f_{LL+IM} + f_{psF} \leq 0.45f'_c & \text{at service state} \end{cases} \quad (2.75)$$

$$f_{psI} = \frac{P_{jl}}{A} + \frac{(P_{jl}e)C}{I_x} + \frac{M_{sl}C}{I_x} = \frac{F_{pCI}P_j}{A} + \frac{M_{psCI}P_jC}{I_x} \quad (2.76)$$

The concrete stresses in the extreme fibers (after instantaneous losses and final losses) are given in Tables 2.14 and 2.15.

For the initial concrete strength in the prestressing state, the controlling location is the bottom fiber at $0.9L$ section in Span 1. From Equation 2.75 we have

$$f'_{ci,req} \geq \frac{f_{DC1} + f_{psI}}{0.55} = \frac{942}{0.55} = 1713 \text{ psi} < 3500 \text{ psi}$$

\therefore choose $f'_{ci} = 3,500 \text{ psi}$ (24.13 MPa).

For the final concrete strength at the service limit state I, the controlling location is again in the bottom fiber at $0.9L$ section in Span 1. From Equation 2.75, we have

$$\begin{aligned} f'_{c,req} &\geq \frac{f_{DC1} + f_{DC2} + f_{DW} + f_{LL+IM} + f_{psF}}{0.45} \\ &= \frac{1608}{0.45} = 3573 \text{ psi} < 4000 \text{ psi} \end{aligned}$$

\therefore choose $f'_c = 4000 \text{ psi}$ (27.58 MPa).

TABLE 2.14 Concrete Stresses after Instantaneous Losses for the Interior Girder

Span	Location (x/L)	Top Fiber Stress (psi)				Total Initial Stress	Bottom Fiber Stress (psi)				Total Initial Stress
		f_{DCI}	$\frac{F_{pCI}P_j}{A}$	$\frac{M_{psCI}P_jY_t}{I_x}$	f_{psI}		f_{DCI}	$\frac{F_{pCI}P_j}{A}$	$\frac{M_{psCI}P_jY_b}{I_x}$	f_{psI}	
1	0.0	0	751	7	758	758	0	751	-9	742	742
	0.1	389	757	-366	391	781	-512	757	481	1238	726
	0.2	658	763	-625	138	796	-865	763	821	1584	720
	0.3	805	768	-752	16	820	-1058	768	989	1756	698
	0.4	831	775	-791	-17	814	-1092	775	1040	1815	723
	0.5	735	781	-703	78	814	-967	781	924	1706	739
	0.6	519	787	-507	280	798	-682	787	667	1454	772
	0.7	181	781	-195	586	767	-238	781	256	1037	800
	0.8	-278	775	217	992	714	366	775	-286	489	855
	0.9	-859	769	727	1496	638	1129	769	-956	-187	942
2	1.0	-1336	562	1181	1743	407	1098	562	-971	-409	689
	0.0	-1336	562	1177	1739	403	1098	562	-968	-406	692
	0.1	-859	730	707	1437	578	1129	730	-929	-199	930
	0.2	-278	724	223	947	669	366	724	-293	431	797
	0.3	181	719	-158	561	742	-238	719	208	97	689
	0.4	519	713	-438	276	794	-682	713	576	1289	607
	0.5	735	708	-618	90	825	-967	708	813	1521	555
	0.6	831	703	-703	0	830	-1092	703	924	1627	535
	0.7	805	697	-672	25	830	-1058	697	883	1580	522
	0.8	658	691	-558	133	790	-865	691	734	1425	560
	0.9	389	685	-327	358	747	-512	685	430	1115	603
	1.0	0	679	6	686	686	0	679	-8	671	671

Note: Positive stress indicates compression and negative stress indicates tension

TABLE 2.15 Concrete Stresses after Total Losses at Service I for the Interior Girder

Span	Location (x/L)	Top Fiber Stress (psi)				Bottom Fiber Stress (psi)				Total Final Stress
		$\frac{F_{pCF}P_j}{A}$	$\frac{M_{psCF}P_jY_t}{I_x}$	Total Final Stress	f_{LOAD}	$\frac{F_{pCF}P_j}{A}$	$\frac{M_{psCF}P_jY_b}{I_x}$	f_{psF}		
1	0.0	0	681	6	687	687	0	681	-8	672
	0.1	653	686	-328	359	1012	-858	686	431	1117
	0.2	1100	692	-559	133	1234	-1466	692	735	1427
	0.3	1348	697	-671	26	1374	-1772	697	882	1579
	0.4	1403	704	-703	1	1404	-1844	704	925	1629
	0.5	1272	711	-620	91	1363	-1672	711	815	1526
	0.6	958	716	-438	278	1237	-1260	716	576	1292
	0.7	467	710	-150	561	1028	-614	710	197	907
	0.8	-510	704	-230	934	425	670	704	-302	402
	0.9	-1351	698	697	1395	45	1776	698	-916	-218
2	1.0	-2070	509	1108	1617	-452	1702	509	-911	-402
	0.0	-2070	509	1104	1613	-456	1702	509	-908	-399
	0.1	-1351	659	676	1336	-15	1776	659	-889	-230
	0.2	-510	654	235	889	379	670	654	-309	345
	0.3	467	648	-113	536	1033	-614	648	148	797
	0.4	958	643	-369	274	1233	-1260	643	485	1128
	0.5	1272	638	-535	102	1374	-1672	638	704	1341
	0.6	1403	632	-615	17	1420	-1844	632	809	1441
	0.7	1348	626	-590	36	1383	-1772	626	776	1403
	0.8	1100	620	-493	128	1228	-1466	620	648	1268
	0.9	653	615	-289	326	978	-858	615	380	995
	1.0	0	609	6	615	615	0	609	-8	601

Notes:

1. $f_{LOAD} = f_{DC1} + f_{DC2} + f_{DW} + f_{LL} + f_{IM}$

2. Positive stress indicates compression and negative stress indicates tension

2.6.3.11 Design for Flexural—Strength Limit State I

AASHTO requires that for the strength limit state I

$$M_u \leq \phi M_n$$

$$M_u = \sum \gamma_i M_i = 0.95[1.25(M_{DC1} + M_{DC2}) + 1.5M_{DW} + 1.75M_{LLH}] + M_{ps}$$

where ϕ is the resistance factor which is linearly increased from 0.75 for compression controlled sections to 1.0 for tension controlled sections (AASHTO 2012, Article 5.5.4.2); M_{ps} is the secondary moment due to prestress. Factored moment demands M_u for the interior girder in Span 1 are calculated in Table 2.16. Although the moment diagram is not symmetrical about the bent (due to different secondary prestress moments), the results for Span 2 are similar and the differences are not considered in this example. The detailed calculations for the flexural resistance ϕM_n are shown in Table 2.17. It is seen that additional mild steel is required only in the interior support.

The minimum reinforcement is also provided to ensure a factored flexural resistance, M_r , at least equal to the lesser of $1.2M_{cr}$, and $1.33M_u$.

TABLE 2.16 Factored Moments for Interior Girder

Span	Location (x/L)	M_{DC1} (kip-ft.)	M_{DC2} (kip-ft.)	M_{DW} (kip-ft.)	M_{LL+IM} (kip-ft.)		M_{ps} (kip-ft.)	M_u (kip-ft.)	
		Dead Load-1	Dead Load-2	Wearing Surface	Positive	Negative	P/S	Positive	Negative
1	0.0	0	0	0	0	0	0	0	0
	0.1	1,700	155	212	782	-85	205	4,009	2,569
	0.2	2,871	262	357	1,312	-169	409	6,820	4,358
	0.3	3,513	321	437	1,612	-253	614	8,469	5,368
	0.4	3,626	331	451	1,715	-337	818	9,012	5,599
	0.5	3,210	293	399	1,650	-422	1,023	8,494	5,050
	0.6	2,264	207	282	1,431	-506	1,228	6,942	3,721
	0.7	789	72	98	1,081	-590	1,432	4,392	1,613
	0.8	-1,215	-111	-151	647	-748	1,637	922	-1,397
	0.9	-3,748	-342	-466	196	-1,339	1,841	-3,355	-5,906
	1.0	-6,292	-573	-781	0	-2,104	2,046	-7,219	-10,716

Note: $M_u = 0.95 [1.25(M_{DC1} + M_{DC2}) + 1.5 M_{DW} + 1.75 M_{LL+IM}] + M_{ps}$

TABLE 2.17 Flexural Strength Design for Interior Girder—Strength Limit State I

Span	Location (x/L)	A_{ps} (in.2)	d_p (in.)	A_s (i.2)	d_s (in.)	b (in.)	c (in.)	f_{ps} (ksi)	d_e (in.)	a (in.)	ϕM_n (kip-ft.)	M_u (kip-ft.)
1	0.0	32.16	0	72.06	104	6.73	253.2	32.16	5.72	4,940	0	
	0.1	46.09	0	72.06	104	6.85	258.1	46.09	5.83	7,412	4,009	
	0.2	56.04	0	72.06	104	6.90	260.1	56.04	5.87	9,183	6,820	
	0.3	61.54	0	72.06	104	6.93	261.0	61.54	5.89	10,163	8,469	
	0.4	64.00	0	72.06	104	6.93	261.3	64.00	5.89	10,602	9,012	
	0.5	7.96	62.29	0	72.06	104	6.93	261.1	62.29	5.89	10,298	8,494
	0.6	57.20	0	72.06	104	6.91	260.3	57.20	5.87	9,391	6,942	
	0.7	48.71	0	72.06	104	6.87	258.7	48.71	5.84	7,877	4,392	
	0.8	38.20	0	71.06	104	11.64	228.1	38.20	9.90	-5,477	-1,397	
	0.9	53.48	0	71.06	104	12.87	237.0	53.48	10.87	-8,030	-5,906	
	1.0	62.00	2.0	71.06	104	7.31	261.0	62.00	6.22	-10,848	-10,716	

Notes:

1. Prestressing steel $f_{pu} = 270$ ksi $f_{py} = 243$ ksi

$$f_{ps} = f_{pu} \left(1 - k \frac{c}{d_p} \right); k = 2 \left(1.04 - \frac{f_{py}}{f_{pu}} \right) = 0.28$$

2. For flanged section $c > h_f$

$$M_n = A_{ps} f_{ps} \left(d_p - \frac{a}{2} \right) + A_s f_s \left(d_s - \frac{a}{2} \right) - A' f'_s \left(d'_s - \frac{a}{2} \right) + 0.85 f'_c (b - b_w) h_f \left(\frac{a}{2} - \frac{h_f}{2} \right)$$

$$a = \beta_1 c; \beta_1 = 0.85$$

$$c = \frac{A_{ps} f_{pu} + A_s f_s - A'_s f'_s - 0.85 f'_c (b - b_w) h_f}{0.85 \beta_1 f'_c b_w + k A_{ps} \frac{f_{pu}}{d_p}}$$

3. For rectangular section, that is, when $c > h_f$, take $b = b_w$ in the above formulas

2.6.3.12 Design for Shear—Strength Limit State I

AASHTO requires that for the strength limit state I

$$V_u \leq \phi V_n$$

$$V_u = \sum \eta_i \gamma_i V_i = 0.95[1.25(V_{DC1} + V_{DC2}) + 1.5V_{DW} + 1.75V_{LL+IM}] + V_{ps}$$

where ϕ is the shear resistance factor 0.9 and V_{ps} is the secondary shear due to prestress. Factored shear demands V_u for the interior girder are calculated in Table 2.18. To determine the effective web width, assume that the VSL posttensioning system of 5–12 Tendon units will be used with a grouted duct diameter of 2.88 in. In this example, $b_v = 12 - 2.88/2 = 10.56$ in. (268 mm). Detailed calculations of the shear resistance ϕV_n (using 2-leg #5 stirrups $A_v = 0.62$ in.² (419 mm²) for Span 1 are shown in Table 2.19. The results for Span 2 are similar to Span 1 and the calculations are not repeated for this example. The longitudinal reinforcement at each section on the flexural tension side of the member is also checked to meet the requirement of AASHTO Article 5.8.3.5.

TABLE 2.18 Factored Shear for Interior Girder

Span	Location (x/L)	V_{DC1} (kip)	V_{DC2} (kip)	V_{DW} (kip)	V_{LL+IM} (kip)	M_{LL+IM} (k-ft.)	V_{ps} (kip)	V_u (kip)	M_u (kip-ft.)
		Dead Load-1	Dead Load-2	Wearing Surface	Envelopes	Associated	P/S	Associated	
1	0.0	125.2	11.4	15.6	60.0	0	13.03	297.1	0
	0.1	91.5	8.4	11.4	50.1	787	13.03	231.0	4,017
	0.2	57.7	5.3	7.2	42.0	1,320	13.03	168.0	6,883
	0.3	24.0	2.2	3.0	34.3	1,614	13.03	105.4	8,472
	0.4	-9.7	-0.9	-1.2	-27.7	1,650	130.3	-47.3	8,903
	0.5	-43.4	-4.0	-5.4	-35.1	1,628	13.03	-109.2	8,457
	0.6	-77.1	-7.1	-9.6	-42.0	1,424	13.03	-170.3	6,929
	0.7	-111	-10.1	-13.8	-49.9	852	13.03	-233.1	4,011
	0.8	-145	-13.2	-18.0	-59.2	216	13.03	-298.3	205.4
	0.9	-178	-16.3	-22.2	-68.8	-667	13.03	-364.0	-4,790
	1.0	-216	-19.4	-26.4	-78.5	-1,788	13.03	-434.3	-10,191

Note: 1. $V_u = 0.95 [1.25(V_{DC1} + V_{DC2}) + 1.5 V_{DW} + 1.75 V_{LL+IM}] + V_{ps}$

TABLE 2.19 Shear Strength Design for Interior Girder—Strength Limit State I

Span	Location (x/L)	d_v (in.)	y' (rad)	V_p (kip)	ϵ_x (1000)	θ (degree)	β	V_c (kip)	s (in.)	ϕV_n (kip)	$ V_u $ (kip)
1	0.0	54.00	0.084	124.1	0.090	-1.900	22.3	4.80	173.0	12	630.2
	0.1	54.00	0.063	93.9	0.071	0.660	31.3	3.21	115.8	12	432.6
	0.2	52.90	0.042	63.1	0.055	2.227	37.0	1.77	62.3	24	208.6
	0.3	58.87	0.021	31.8	0.034	1.650	34.8	2.14	83.4	24	221.4
	0.4	60.84	0.000	0.0	0.020	0.880	32.1	2.89	117.5	24	241.1
	0.5	59.14	0.018	27.8	0.037	-0.100	28.5	4.80	189.5	24	346.1
	0.6	54.06	0.036	56.2	0.058	-2.300	21.0	4.80	173.2	24	400.1
	0.7	54.00	0.054	83.5	0.077	-5.800	29.0	4.80	173.0	12	499.1

(Continued)

TABLE 2.19 (Continued) Shear Strength Design for Interior Girder—Strength Limit State I

Span	Location (x/L)	d_v (in.)	y' (rad)	V_p (kip)	ν/f'_c (1000)	ϵ_x (1000)	θ (degree)	β	V_c (kip)	s (in.)	ϕV_n (kip)	$ V_u $ (kip)
	0.8	54.00	0.072	110.4	0.097	-1.000	25.6	4.80	173.0	12	565.2	298.3
	0.9	54.00	0.090	136.8	0.117	4.500	44.8	1.10	39.5	8	380.8	364.0
	1.0	57.42	0.000	0.0	0.199	3.830	42.4	1.24	47.5	5	463.9	434.3

Notes:

1. $b_v = 10.56$ in. and y' is slope of the prestressing cable

2. $A_v = 0.62$ in.² (2#5)

$$V_n = \text{the lesser of } \begin{cases} V_c + V_s + V_p \\ 0.25 f'_c b_v d_v + V_p \end{cases}$$

$$V_c = 0.0316 \beta \sqrt{f'_c} b_v d_v; V_s = \frac{A_v f_y d_v \cos \theta}{s}$$

$$\epsilon_s = \frac{\frac{|M_u|}{d_v} + 0.5 N_u + |V_u - V_p| - A_{ps} f_{po}}{E_s A_s + E_p A_{ps}}$$

$$\beta = \frac{4.8}{1 + 750 \epsilon_s}; \quad \theta = 29 + 3500 \epsilon_s$$

$$A_{v\min} = 0.0316 \sqrt{f'_c} \frac{b_v s}{f_y}$$

$$\text{For } V_u < 0.1 f'_c b_v d_v \quad s_{max} = \text{smaller of } \begin{cases} 0.8 d_v \\ 24 \text{ in.} \end{cases}$$

$$\text{For } V_u \geq 0.1 f'_c b_v d_v \quad s_{max} = \text{smaller of } \begin{cases} 0.4 d_v \\ 12 \text{ in.} \end{cases}$$

2.7 Summary

This chapter presents typical cast-in-place posttensioned prestressed concrete girders used in highway bridges. It discusses prestressing systems and posttensioning operation, materials, and loss of prestress and provides general guidelines for typical box girder sections. It addresses general design considerations, design limit states and the design procedure. A design example of a two-span continuous box girder bridge is given to illustrate the design procedure.

References

- AASHTO. 2012. *AASHTO LRFD Bridge Design Specifications*, Customary U.S. Unit, 2012, American Association of State Highway and Transportation Officials, Washington D.C.
- Caltrans. 2005. *Prestress Manual*, California Department of Transportation, Sacramento, CA.
- Collins, M. P. and Mitchell, D. 1997. *Prestressed Concrete Structures*, Response Publication, Toronto, Canada.
- CSI. 2008. *Posttensioned Concrete Design Manual*, Version 12.0.0, Computers & Structures, Inc., Berkeley, CA.
- Eubunsky, I. A. and Rubinsky, A. 1954. A Preliminary Investigation of the Use of Fiberglass for Prestressed Concrete, *Magazine of Concrete Research*, 6(17), 71–78.
- FHWA. 2010. *FHWA Bridge Programs—Material Type of Structure by State as 12/2010*. Federal Highway Administration, Washington, DC. <http://www.fhwa.dot.gov/bridge/nbi/mat10.cfm>.

- Iyer, S. I. and Anigol, M. 1991. Testing and Evaluating Fiberglass, Graphite, and Steel Prestressing Cables for Pretensioned Beams, in *Advanced Composite Materials in Civil Engineering Structures*, Edited by Iyer, S.I. and Sen, R., ASCE, New York, NY.
- Kim, P. and Meier, U. 1991. CFRP Cables for Large Structures, in *Advanced Composite Materials in Civil Engineering Structures*, Edited by Iyer, S.I. and Sen, R., ASCE, New York, NY.
- Lin, T. Y. and Burns, N. H. 1981. *Design of Prestressed Concrete Structure*, 3rd Ed., John Wiley & Sons, New York, NY.
- Miesseler, H. J. and Wolff, R. 1991. Experience with Fiber Composite Materials and Monitoring with Optical Fiber Sensors, in *Advanced Composite Materials in Civil Engineering Structures*, Edited by Iyer, S.I. and Sen, R., ASCE, New York, NY.
- Nawy, E. G. 2009. *Prestressed Concrete: A Fundamental Approach*, 5th Edition, Upgrade: ACI, AASHTO, IBC 2009 Codes Version. Prentice Hall, Englewood Cliffs, NJ.
- PCI. 2011. *PCI Bridge Design Manual*, 3rd Edition, Prestressed Concrete Institute, Chicago, IL.
- PTI. 2006. *Posttensioning Manual*, Sixth Ed., Posttensioning Institute, Phoenix, AZ.
- Wines, J. C., Dietz, R.J. and Hawly, J. L. 1996. Laboratory Investigation of Plastic—Glass Fiber Reinforcement for Reinforced and Prestressed Concrete, *Report 2*, U.S. Army Corps of Engineers, Waterway Experimental Station, Vicksburg, MS.
- Wines, J. C. and Hoff, G. C. 1966. Laboratory Investigation of Plastic—Glass Fiber Reinforcement for Reinforced and Prestressed Concrete, *Report 1*, U.S. Army Corps of Engineers, Waterway Experimental Station, Vicksburg, MS.

@Seismicisolation

3

Segmental Concrete Bridges

3.1	Introduction	91
3.2	Structural Material.....	93
	General • Concrete • Posttensioning Systems • Prestressing Steel • Cementitious Grout • Ordinary Reinforcing Steel	
3.3	Construction Methods.....	97
	Balanced Cantilever Construction • Cast-in-Place on Falsework • Span-by-Span Construction • Incrementally Launched • Full-Span Erection • Precast Spliced U Girder	
3.4	Conceptual Design	110
	Span Configuration • Span-to-Depth Ratios • Proportional Sections • Structural System • Aesthetic Aspect	
3.5	Deck Design.....	115
	Design Approach • Live Load Analysis • Posttensioning Tendon Layout • Summary of Design Forces • Service Limit State Design • Strength Limit State Design	
3.6	Longitudinal Design	124
	Design Methodology • Tendon Layout and Envelope • LRFD Live Load • Shear Lag Effect • Temperature Load • Time-Dependent Effect • Secondary Forces • Summary of Design Forces • Service Limit State Design • Principal Tension Stress Check • Flexural Strength Check • Shear and Torsion Design	
3.7	Construction Stage Analysis.....	148
	Stability during Construction • Erection Tendons	
3.8	Detailing.....	158
	Combined Transverse Bending and Longitudinal Shear • Shear Key Design • Strut and Tie Model	
3.9	Durability.....	163
	Durability Problems of Posttensioned Bridges in the United States • Durability Problems of Posttensioned Bridges around the World • Lessons Learned • New Direction for the Next Generation of Posttensioned Concrete Bridges • Conclusions	
	References.....	169

Teddy S. Theryo
Parsons Brinckerhoff, Inc.

3.1 Introduction

Construction of segmental concrete bridges involves assembling smaller pieces of concrete members called segments using posttensioning tendons to form a bridge structural system, either superstructure or substructure. These segments can be produced by cast-in-place or precast/prefabricated methods, while the posttensioning system can be bonded, unbonded tendons, or a combination of both. Bonded

tendons typically consist of cementitious grouted internal tendons, while unbonded tendons could be cementitious grouted or greased, waxed, and sheathed, in the form of external or internal tendons. In segmental bridge design, it is critical to determine the construction means and methods, prior to proceeding with the design. The construction method will greatly affect the outcome of design and tendon layouts, unlike any other type of structures. In most cases, construction loads will also impact the design, material quantity, and details.

The following are some of the important events/milestones in the development of segmental concrete bridge construction from its infancy after World War II to the current state-of-the-art standard of practice.

In 1939, Eugene Freyssinet of France developed a conical wedge posttensioning anchorage system for wires which led to the wide application of posttensioned structures possible. Without posttensioning systems, the segmental bridge construction could not have been realized.

From 1941 to 1949, Freyssinet was the first to apply precast prestressed segmental construction for several bridges at Luzancy over the Marne River east of Paris, France.

The development of a modern long-span cast-in-place segmental bridge, the Lahn Bridge in Balduinstein, Germany, was pioneered by the German engineer Dr. Ulrich Finsterwalder of Dyckerhoff & Widmann AG in 1951. The bridge was constructed with the balanced cantilever method and the segments were cast on a form-traveler attached to the previously cast and stressed segments. Posttensioning was applied to the newly cast segment after the concrete had hardened against the previously stressed segments.

In 1954, French engineer Jean Muller applied for the first time the dry-joint match casting innovation to the construction of a small single-span bridge called Sheldon Bridge in upstate New York, USA, by assembling three precast girder segments and posttensioned them together on site to form a single span girder in order to facilitate the transportation of the girders and improve the speed of construction. It is much easier to handle and transport small pieces of girders than a long girder.

In 1962, Muller for the first time applied precast segmental box girder using epoxy-coated match cast joints between segments and posttensioned them together for the construction of the Choisy-le-Roi Bridge over the Seine River in Paris, France. The bridge was constructed by Campenon Bernard, a general contractor where Muller was the technical director of the company.

Since then, precast segmental construction has gained popularity over cast-in-place due to its speed of construction, mass production of segments in the casting yard, better quality control, ease of transportation, and overall economical structure. However, precast segmental technology is not suitable for every bridge project; it depends on the size of the project, span length, location, local standard practice, and so on. Under certain circumstances, cast-in-place segmental bridge construction is still popular, such as for a very long span bridge over river crossing or deep valley (see Section 3.4 on Conceptual Design for more discussions on selecting bridge types).

This chapter presents a practical knowledge to practicing engineers, owners, and graduate students on a complete spectrum of segmental concrete bridge design from conception to final design, including construction means and methods.

In Sections 3.4 to 3.8, the AASHTO LRFD Bridge Design Specifications (AASHTO 2012) on segmental bridge design provisions are extensively referenced (AASHTO LRFD Sections 4 and 5). AASHTO LRFD adopted segmental bridge design provisions from AASHTO Guide Specifications for Design and Construction of Segmental Bridges, 2nd Edition, 1999. The guide specifications have served as design guidelines and specifications and construction on segmental concrete bridges for many years since the first edition in 1989, prior to AASHTO LRFD Design Specifications.

Aside from design and construction, durability of segmental concrete bridges was discussed in Section 3.9 in order to fulfill the intended service life of the structures, minimize maintenance cost, and to build awareness on the importance of workmanship and quality control during the whole process of building a segmental bridge from design to the completion. Good detailing and high standard industry practice is an important part of a design process in order to maintain constructability during construction, structural integrity, and durability during its service life.

3.2 Structural Material

3.2.1 General

The basic structural materials for posttensioned segmental concrete bridges are very similar to posttensioned structures in general, which consist of high-strength concrete, high-strength prestressing steels, and ordinary reinforcing steel, including grout in the duct. Earlier, prestressed concrete structures failed due to lack of understanding of creep and shrinkage and long-term loss of prestress. Freyssinet was credited with the use of the first successful prestressed concrete by the application of high-strength steel to counteract the creep and shrinkage of concrete. Ordinary reinforcing steel also plays an important role in supplementing concrete and high-strength prestressing steel as the primary structural materials. Without ordinary reinforcing bars, a posttensioned prestressed concrete structure will not be able to function properly. For instance, local zones around the anchorages may crack, without ordinary reinforcement confinement in the form of spiral; and ordinary reinforcement will also contribute to the shear-carrying capacity in the webs, in addition to concrete and posttensioned inclined tendons. Ordinary reinforcement also plays an important role in partially prestressed concrete structures in controlling flexural crack width in concrete and contributes in flexural ultimate capacity of the structure.

There are two types of tendons used in segmental bridges, namely bonded and unbonded tendons. The earlier segmental bridges have mostly used grouted corrugated metal duct (internal), but since 2003 most owners in the US have switched to corrugated plastic duct made of either polyethylene (PE) or polypropylene (PP) for better tendon corrosion protection. For external tendons, smooth PE ducts are generally specified in the United States. European countries have also adopted petroleum grease, wax, and monostrand greased and sheathed tendons as another alternative of corrosion protection system.

3.2.2 Concrete

High-strength concrete for posttensioned bridges is required in posttensioned structures because of high compressive stresses transferred around the anchorages to the concrete members and precompression of the posttensioning forces to the member section. Without high-strength concrete, prestressed concrete is not efficient and economical. Typically, a minimum of 5,000 psi (35 MPa) concrete strength at 28 days is required in prestressed concrete structures. In addition, higher-strength concrete results in higher modulus of elasticity. This is a preferred concrete property to minimize long-term creep deformations. With the advancement of concrete technology, producing 10,000 psi (69 MPa) to 12,000 psi (83 MPa) concrete is a common practice nowadays in the precast industry. Therefore, more and more precast prestressed concrete structures are being constructed with concrete strength equal to or higher than 8,000 psi (55 MPa). For an aggressive environment, it may be necessary to select a mix design with high strength in combination with high-performance concrete (low permeability). High-performance concrete will improve the durability and protect the posttensioned tendons from corrosion. In case of concrete members with highly congested reinforcing bars such as diaphragms, blisters and deviators, self-consolidating concrete (SCC) is recommended in order to avoid honey combing.

3.2.3 Posttensioning Systems

PT anchorage systems in posttensioned bridges are a proprietary system. Any one of these systems such as VSL, DSI, Freyssinet, BBR, Schwager Davis, and other systems can be found in the industry/market in the United States. The PT anchorage systems are designed in different shapes, sizes, and material. In general, a basic posttensioning anchorage system comprises a bearing plate, trumpet, wedge plate (anchor head), grout cap, and grout ports as shown in Figure 3.1.

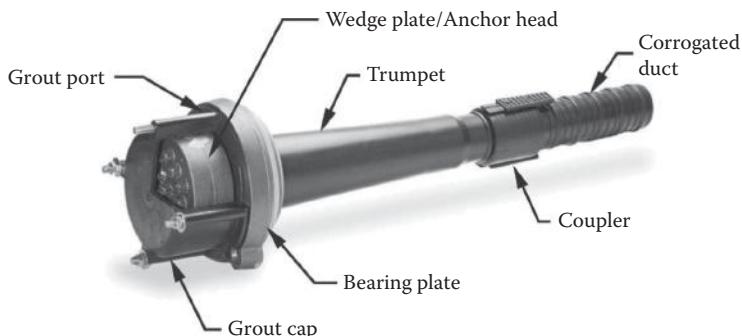


FIGURE 3.1 Basic posttensioning anchorage system. (Courtesy of VSL International.)

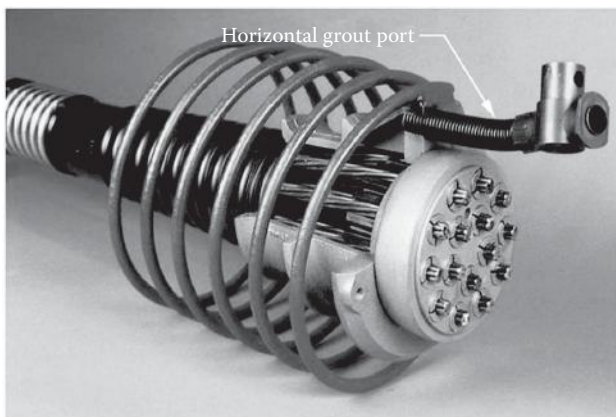


FIGURE 3.2 Old generation of PT anchorage system. (Courtesy of DSI.)

In 2003, the Florida Department of Transportation (FDOT) required an additional vertical grout port/vent located above the trumpet to facilitate postgrouting inspection and permanent grout cap in its posttensioning specifications. Notice the differences between the older and newer generations of PT anchorages systems as shown in Figures 3.2 and 3.3. Many other state DOTs have adopted PT anchorages similar to FDOT requirements. For the new anchorages, the inspection access will be a lot simpler through the vertical grout port.

In general, posttensioned bridges built in the United States consisted of grouted internal tendons, grouted external tendons, or a combination of the two.

Internal tendons are located inside the structural concrete section and are housed in corrugated metal ducts or corrugated plastic ducts and are bonded to the structural concrete by means of cementitious grout as shown in Figure 3.4. The plastic corrugated duct may be made from high density polyethylene (HDPE) or polypropylene (PP). The high-strength steel tendon could be strands, wires, or bars.

External tendons are typically located outside the perimeter of the concrete section and are housed in HDPE smooth duct and filled with cementitious grout. External tendons are not bonded with the concrete structural section (see Figures 3.5 and 3.6). In Europe the external tendons are also filled with flexible filler material, such as petroleum grease and wax.

3.2.4 Prestressing Steel

There are many forms of high-strength prestressing steel types in the industry worldwide that can be utilized for segmental and posttensioned bridges such as nineteen-wire strands, compact strands, two and three-wire strands, oval deformed bars, single wire, and so on. However, only two types of

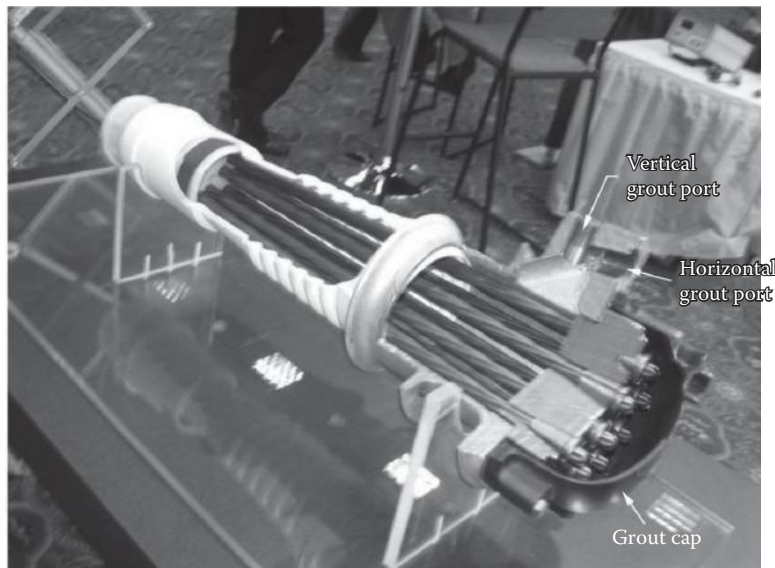


FIGURE 3.3 New generation of PT anchorage system. (Courtesy of DSI.)

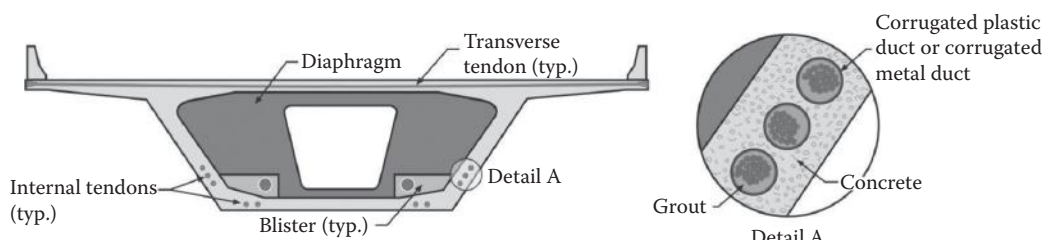


FIGURE 3.4 Internal tendon.

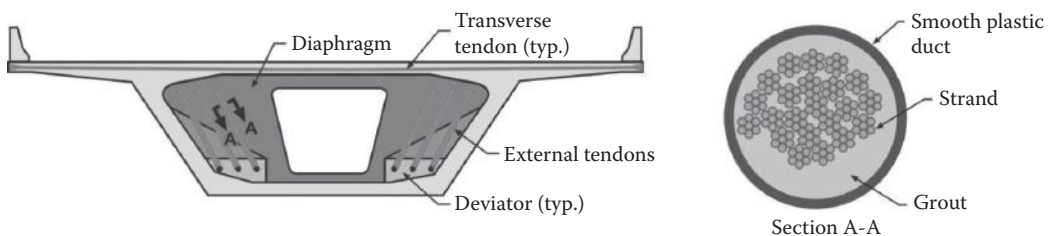


FIGURE 3.5 External tendon.

prestressing steel are commonly used in the United States, as shown below. Parallel wires were used in some older bridges in the past.

1. Uncoated seven-wire stress-relieved for prestressed concrete conforming to ASTM A416-90. It is recommended to use low relaxation for segmental bridges.

Material Properties:

- a. Ultimate tensile strength (f_{pu}): 270 KSI (1,860 Mpa)
- b. Yield strength (f_{py}): 243 KSI (1,674 Mpa)
- c. Apparent modulus of elasticity: 28,500 KSI (197,000 Mpa)



FIGURE 3.6 External tendons at deviator.

2. Uncoated high-strength steel bar for prestressed concrete according to ASTM A722-90.

It is recommended to use Type II (deformed) bar for segmental bridges.

Material Properties:

- a. Ultimate tensile strength (f_{pu}): 150 KSI (1,035 Mpa)
- b. Yield strength (f_{py}): 120 KSI (828 Mpa)
- c. Modulus of elasticity: 30,000 KSI (207,000 Mpa)

3.2.5 Cementitious Grout

Grout material consists of a mixture of Portland cement, mineral additives, admixtures, aggregates, and water. In bonded posttensioning tendons, grout serves as the primary corrosion protection of prestressing steel, in addition to forming a good bond between prestressing steel and its surrounding concrete. Type I or Type II cements according to ASTM C150/C150M can be used for grout mixture. For slower release of heat hydration application, Type II cement is used. Mineral additives could be Class C and Class F fly ash, Grade 120 slag cement, or silica fume. The role of admixtures in grout is to improve set control, reduce water, bleed control, air entrainment, corrosion inhabitation, and pumpability. Some grout contains fine sands, but sand is optional. Clean potable water is used for the grout mixture.

Posttensioning Institute (PTI) Grouting Specifications, 2nd Edition, 2012 listed four types of grout:

- Class A: Nonaggressive exposure such as indoor or nonaggressive outdoor.
- Class B: Aggressive exposure such as wet/dry cycle, marine environment, and deicing salts.
- Class C: Prepackaged for either nonaggressive or aggressive environments.
- Class D: Engineered grout.

The specifications also specified the material properties required for each type of grout, including the acceptance and test criteria and methods. Although most owners have their own grout specifications, PTI specifications are widely referenced and accepted.

3.2.6 Ordinary Reinforcing Steel

Deformed and plain billet-steel bars for concrete reinforcement conforming to ASTM A615.

Material properties:

Yield strength: 60 KSI (400 Mpa)

Modulus of elasticity: 29,000 KSI (200,000 Mpa)

Some owners have specified solid stainless steel reinforcing bars conforming to ASTM A955/A955M for structural elements located in the extremely corrosive environment.

3.3 Construction Methods

3.3.1 Balanced Cantilever Construction

Free cantilevering is a method of construction used to build outward from a fixed point to form a cantilever structure, without temporary support, using staged construction as shown in Figure 3.7. Definition of “cantilever” from Webster’s Dictionary is: “A rigid structural member projecting from a vertical support, especially one in which the projection is great in relation to the depth, so that the upper part is in tension and the lower part in compression.” Another meaning of “cantilever” is “bracket.”

When two opposing free cantilever structures are attached as a single structure and erected at the same step, it is termed “balanced cantilever construction method” as shown in Figure 3.8.

It is believed that the idea of cantilevering in bridge construction originated in the ancient Orient. Shogun’s Bridge located in Nikko, Japan, is the earliest recorded cantilever bridge, which dates to the fourth century. The Wandipore Bridge, shown in Figure 3.9, was constructed in the seventeenth century using timber cantilever members with the drop-in span girder in Bhutan, between India and Tibet (Petroski, Henry. 1995).

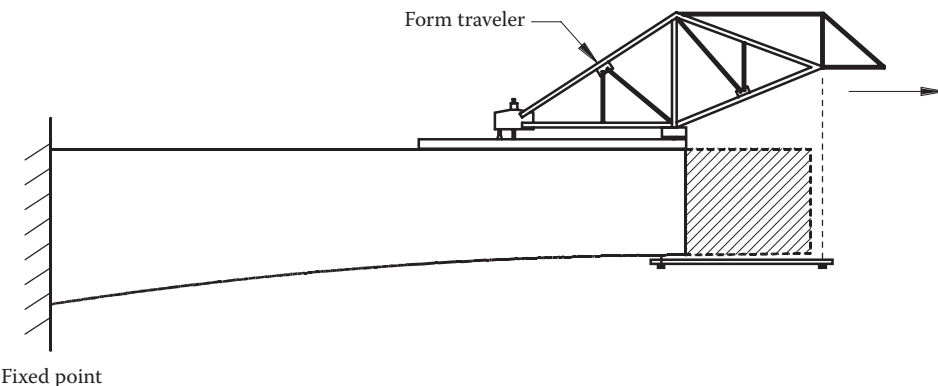


FIGURE 3.7 Cantilevering construction method.

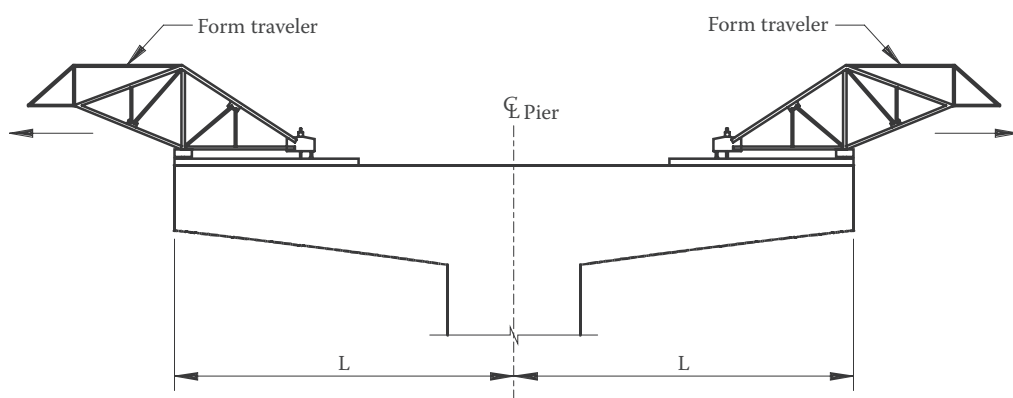


FIGURE 3.8 Balanced cantilever construction method.

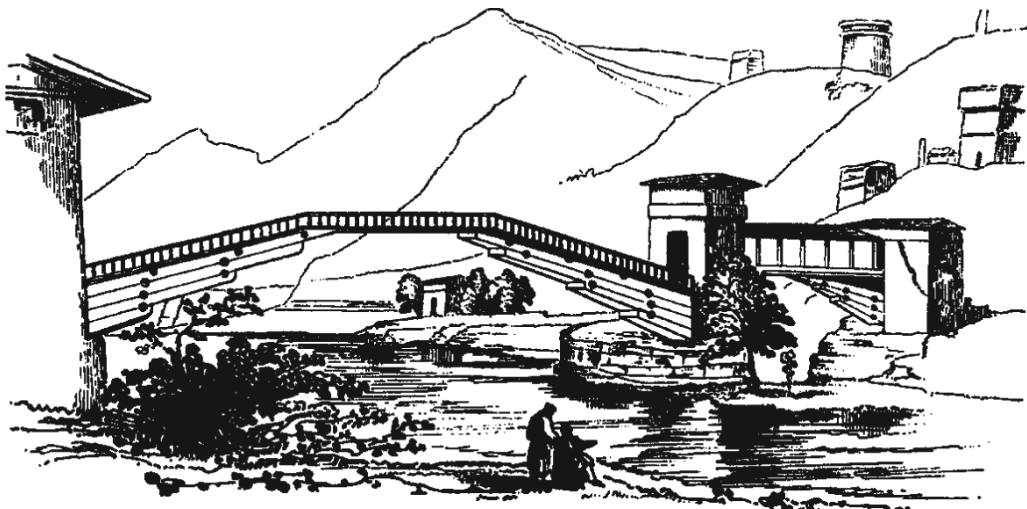


FIGURE 3.9 Wandipore Bridge (From Petroski, H., *Engineers of Dream*; Alfred A. Knopf, Inc., New York, 1995.)

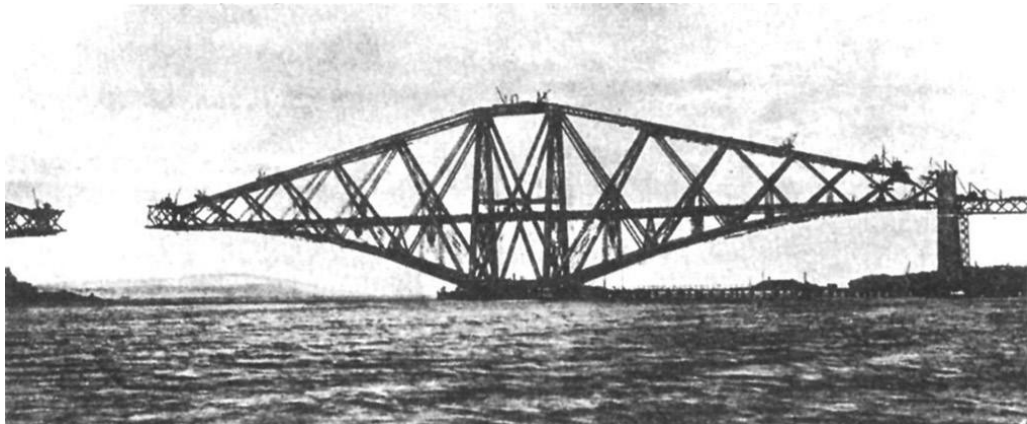


FIGURE 3.10 Firth of Forth Bridge in the United Kingdom under construction.

In the steel bridge construction industry, steel trusses were successfully erected using the cantilevering method by the end of the nineteenth century with construction of the Firth of Forth Bridge in England (Figure 3.10) and the Quebec Bridge over the Saint Lawrence River.

The application of the cantilevering method to cast-in-place reinforced concrete bridges took place for the first time with the construction of a 223 ft (68 m) span bridge across the Rio de Peixe in Brazil in 1930. However, the cantilevering method for reinforced concrete was not successful due to excessive deflection and heavy reinforcing required. Dr. Ulrich Finsterwalder of the firm Dyckerhoff & Widmann AG (DSI International) successfully applied posttensioning to a cast-in-place concrete bridge using the balanced cantilever method with construction of the Lahn Bridge at Balduinstein in Germany in 1950–1951, after World War II (see Figure 3.11). The bridge is fixed at both ends and has a span length of 203.65 ft (62.0 m). This bridge is considered the pioneer of modern long-span balanced cantilever segmental concrete bridge construction.

After successful completion of the Lahn Bridge, the system was improved over the years and has gained popularity for construction of long-span bridges across the world (see Figure 3.12). Cast-in-place balanced cantilever bridges are especially suitable for construction of long spans over deep valleys and

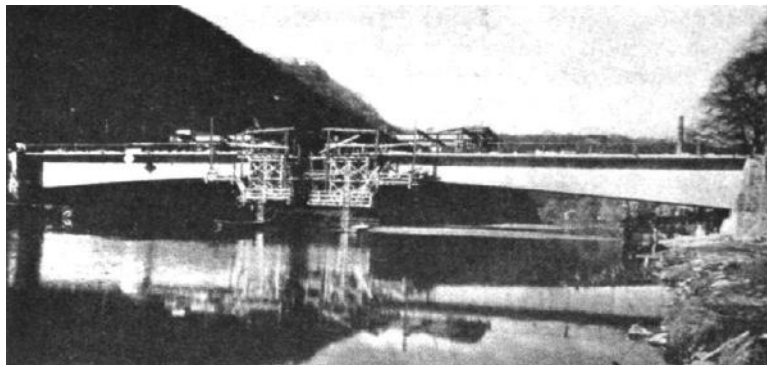


FIGURE 3.11 Lahn Bridge. (Courtesy of VSL International.)

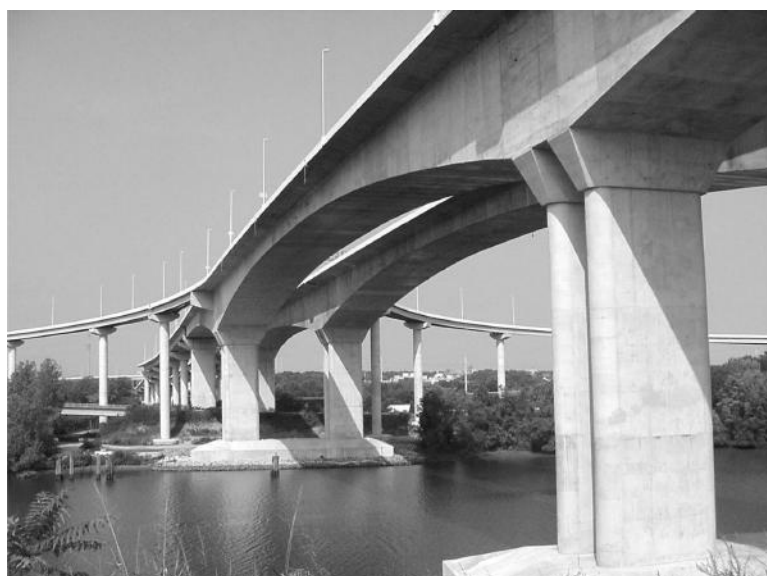


FIGURE 3.12 Vietnam Veterans Memorial Bridge, VA.

rivers where placing temporary supports is not possible or cost prohibitive. The only drawback of the system is the time required for superstructure construction. For instance, the time taken to cast every increment on site can be considered slow in comparison to precast concrete. In cast-in-place balanced cantilever construction, a starter segment is first constructed over a pier column. The starter segment over the pier is called a pier-table as shown in Figure 3.13. From this starting point, the bridge can be built from a single pier or multiple piers at the same time using form-travelers moving toward mid-span (see Figure 3.14). At mid-span, the two adjacent cantilever tips are connected to make a continuous structure with a closure pour segment. Typically a form-traveler and steel strong backs are attached to both cantilever tips to prevent differential movement during the closure pour (see Figure 3.15). These attachments can also be used to correct horizontal misalignment as well as elevation of both cantilever tips.

California's Pine Valley Creek Bridge rises 450 ft (137.2 m) above the valley floor, and is 1700 ft (518.2 m) long including five spans of 270 ft (82.3 m) + 340 ft (103.6 m) + 450 ft (137.2 m) + 380 ft (115.8 m) + 270 ft (82.3 m) and was the first cast-in-place segmental concrete bridge built in the United States in 1974.



FIGURE 3.13 Pier table of a cast-in-place balanced cantilever construction.

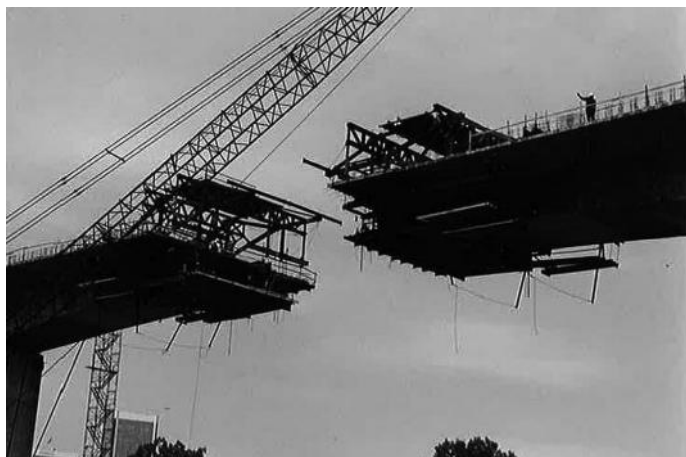


FIGURE 3.14 Segment placement supported by form-travelers.

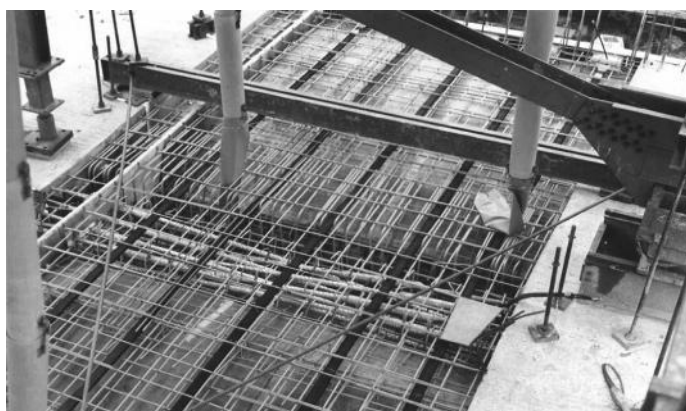


FIGURE 3.15 Strong back across a closure pour.

@Seismicisolation

In classical cantilever bridge construction, segments are placed symmetrically from the pier table with typical segment lengths ranging from 10 to 16 ft (3 to 4.9 m). Segment lengths longer than 16 ft (4.9 m) are not recommended due to longer segments producing large out-of-balance loads during construction. In addition, 16 ft segment form-travelers are widely available in the market, and can often be reused without ordering a new one. In special cases, cantilevering with form-travelers longer than 16 ft has been accomplished.

After successful construction of the first modern cast-in-place balanced cantilever (Lahn Bridge) in Germany in 1950–1951, Choisy-le-Roi Bridge over the Seine River near Paris in France was the first modern precast balanced cantilever bridge constructed using match cast epoxy joint in 1962–1964. The bridge was constructed by the Campenon Bernard contractor and designed by Jean M. Muller. Some advantages of precast segmental bridge over cast-in-place construction are the speed of superstructure erection, less creep and shrinkage effect, and better quality control when casting segment in the casting yard. In fact, bridge construction using posttensioning precast segment pieces was pioneered by Eugene Freyssinet in 1944 with the construction of Luzancy Bridge over the Marne River in France. Precast segmental construction was invented to overcome the slow construction schedule of the cast-in-place construction method. Other advantages of precast segmental construction are mass production in the casting yard, better curing system, independent of weather condition, ease of transporting the segments, flexibility in selecting erection equipments, and overall economical structure.

Precast segmental construction requires a casting yard to accommodate construction materials, casting cells (see Figure 3.16), reinforcing bar jigs, concrete plant, survey towers, curing facilities, segment transporter, segment storage site (see Figure 3.17), offices, and material testing facilities. The precast segments are stored on site at least one month prior to delivery to the project site for placement. Typically, the segments are match cast in 10 ft (3 m) to 12 ft (3.65 m) long segments for ease of handling and transportation. It is important to limit the segment weight to about 60 (534 KN) to 80 t (712 KN), since it impacts the erection equipment capacity to lift and place the segment in place. Therefore, it is common to split the pier segment into two segments in order to reduce the segment weight as shown in Figure 3.18. Depending on the site condition and the size of the project, segment erection can be accomplished with the following equipment:

1. Ground based crane
2. Overhead launching gantry (Figure 3.19)
3. Segment lifter (Figure 3.20)
4. Beam and winch



FIGURE 3.16 Casting yard



FIGURE 3.17 Segments storage site.



FIGURE 3.18 Split precast pier segment.



FIGURE 3.19 Segment erection with overhead launching gantry.

@Seismicisolation



FIGURE 3.20 Segment erection with segment lifter.



FIGURE 3.21 Cast-in-place on falsework.

3.3.2 Cast-in-Place on Falsework

Cast-in-place on false-work construction method is building a bridge superstructure on false-work supported directly on the ground for the entire length of the bridge. It is also common to construct the structure in stages/segments. Therefore, it could be considered as cast-in-place segmental construction. This type of construction is suitable for superstructure with complex geometry, relatively short columns, short to medium span length, and good soil conditions. The temporary false-work is removed after posttensioning is complete. Cast-in-place construction on false-work is relatively slow and labor intensive. The cast-in-place on false-work is depicted in Figure 3.21.

3.3.3 Span-by-Span Construction

Span-by-span construction method is typically meant for erection of precast segments by posttensioning the segments for the whole span. Each segment is temporarily posttensioned with posttensioned bars against the adjacent segment after epoxy glue is applied at the match-cast joint between segments.

Some of the earlier span-by-span bridges have no epoxy applied at the joints. This type of joint is called dry-joint. However, precast segmental with dry joint is no longer allowed in the United States due to water leaking from the deck resulted in durability concern, although some countries are still using dry joint. The permanent tendons typically consist of external tendons entirely (Figure 3.22) or a combination of external and internal tendons. Span-by-span bridge construction can also be designed as a continuous structure up to ten spans, by splicing the longitudinal tendons at the diaphragms. For the external tendons, deviators are required in between the piers (see Figure 3.23). The span-by-span segment erection can be done either using an overhead launching gantry (see Figure 3.24) or underslung gantry. In the case of underslung gantry, support brackets are needed at the columns to support the gantry.



FIGURE 3.22 External tendons inside a box girder.



FIGURE 3.23 Typical deviator



FIGURE 3.24 Span-by-span segment erection using overhead gantry.

3.3.4 Incrementally Launched

The incremental launching bridge construction method has been used for steel bridge erection for many years. This is not surprising since the steel material can handle both tension and compression well, which is not the case for concrete structures. The first concrete incrementally launched bridge was applied to the construction of a reinforced concrete bridge over the Rio Caroni in Venezuela, South America, in 1962. Soon after that, the first modern prestressed concrete incrementally launched bridge was constructed in 1965 at the Inn Bridge in Kufstein, Austria. Professor Dr. Fritz Leonhardt and his partner Willi Baur were credited with the development of both bridges. Since then, they have designed many posttensioned concrete incrementally launched bridges, and hold a patent for the method in Germany. Many posttensioned concrete incrementally launched bridges have been built around the world, but the construction method has seen few applications in North America.

The basic idea of the incrementally launched bridge is very simple. The bridge is constructed in successive short segments on a stationary casting form located behind one of the abutments, as shown in Figure 3.25. Typically, each segment is about 50 (15) to 80 ft (25 m) in length. The first segment is cast and posttensioned with a steel-launching nose attached to the segment end nearest the abutment. Subsequently, the form is lowered and the first segment is launched by being either pushed or pulled forward. A new segment is cast against the first segment and then posttensioning is stressed to connect the two segments together. The second and first segments are then ready to be launched forward. The construction sequences are repeated until the first segment reaches its final position at the other abutment. The advantage of this construction method is that the launching of the superstructure can be done over the piers from abutment to abutment without disturbing the area below the bridge.

During the conceptual design phase of a project, the advantages and disadvantages are carefully evaluated for each construction alternative to determine the most economical solution for a particular site. Incrementally launched bridges have their own set of interesting features.

Some advantages of incrementally launched bridge are as follows:

1. Requires short casting form of about 100 ft (30 m) long and less heavy equipment.
2. Allows for the ability to cast segments during inclement weather and through the winter by providing shelter and insulation over the casting form.



FIGURE 3.25 Casting form. (Courtesy of C2HC Alliance, Australia.)

3. Provides better quality control, similar to precast segment.
4. Possesses simple geometry control.
5. Increases efficiency by repetitive works.
6. Requires no segment storage and transportation.
7. Relatively fast construction (average one segment per week).
8. Superstructure erection can be done over the piers without ground-based lifting equipment. Therefore, no maintenance of traffic required and suitable for bridge construction over railways, rivers, valleys, and soft soil conditions.
9. Suitable for top-down construction over environmentally sensitive areas.
10. Requires no temporary false-work.
11. Reinforcing bars are continuous across the segment joints.

Incrementally launched bridges require launching equipment, which consists of a launching nose, hydraulic jacks, pushing or pulling devices, temporary sliding bearings, and lateral guides.

In order to reduce the cantilever bending moment during launching prior to reaching the pier top, a steel launching nose is attached on the forward face of the first segment. The steel launching nose consists of two steel plate girders or two steel trusses, each attached to the leading end of the concrete box girder webs by posttensioned bars embedded in the webs (Figure 3.26). Both of the steel plate girders or trusses are laterally braced together. A light and sufficiently stiff nose is preferred. The nose length is about 60%–80% of the longest span length of the bridge.

Hydraulic jacks at the front of the nose facilitate jack-up of the nose as it reaches the piers or temporary supports (Figure 3.27). The jacks are loaded to a predetermined force to provide support for the launching nose and reduce the bending moments in the girder. When the girder reaches the support, the vertical geometry can be further adjusted to proper grade. A mast and stay cable system can also be used instead of a launching nose to reduce the bending moments in the front segments.

The superstructure can be moved forward, by pulling the superstructure using hydraulic jacks reacting against the abutment where the casting form is located, as shown in Figure 3.28. Another way of launching the superstructure is by pushing the superstructure using a special device, as shown in Figure 3.29.



FIGURE 3.26 Launching nose and segment connection. (Courtesy of C2HC Alliance, Australia.)



FIGURE 3.27 Hydraulic jack at launching nose's tip. (Courtesy of C2HC Alliance, Australia.)

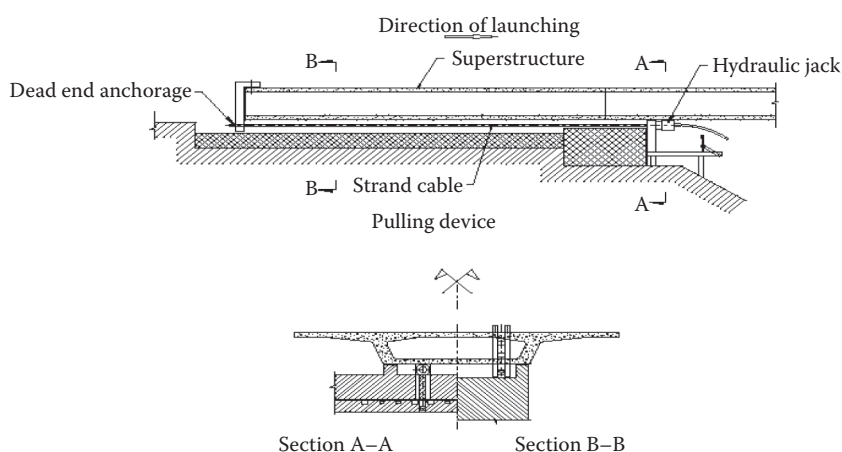


FIGURE 3.28 Bridge pulling device. (Courtesy of VSL International.)

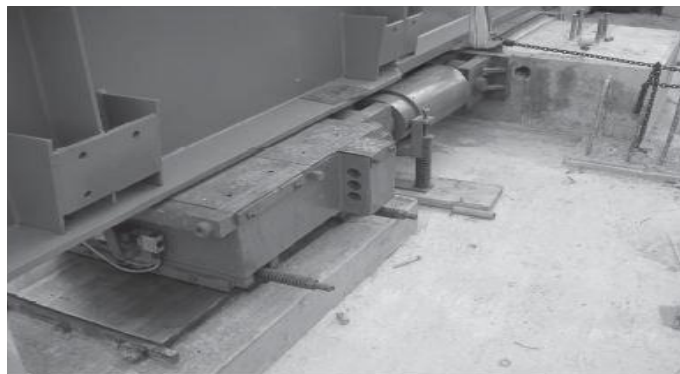


FIGURE 3.29 Bridge pushing device. (Courtesy of C2HC Alliance, Australia.)



FIGURE 3.30 Full-span girder erection. (Courtesy of DEAL.)

3.3.5 Full-Span Erection

Full-span erection method is another form of span by span erection for short span bridges up to about 120 ft (36 m). The difference with the span-by-span erection is that the girder is cast in one piece for the whole span, instead of in short segments. The full-span erection is ideal for a very long viaduct such as structure for high speed rail project as shown in Figure 3.30. The girder transportation and girder placement can be handled by one erection equipment. The girder transportation usually can be done over the completed spans. The advantages of full span erection are that it is simpler to produce the girder and the speed of erection. However, the disadvantage of this erection method is dealing with a very heavy girder. It is important to study the optimum span length for the viaduct by considering the availability of the erection equipment.

3.3.6 Precast Spliced U Girder

Precast spliced U girder bridges have been gaining popularity recently for medium-span length bridges, especially horizontally curved bridges (see Figures 3.31 and 3.32). Several long segments of pretensioned or posttensioned tub girders are posttensioned using draped internal tendons in the web to



FIGURE 3.31 Precast spliced U girder bridge during erection. (Courtesy of Summit Engineering Group.)



FIGURE 3.32 Precast U girder supported on temporary false-work. (Courtesy of Summit Engineering Group.)

form a continuous multi-span girder from end to end. The joints between the girders are cast-in-place concrete. The diaphragms are typically cast at the splice locations. These diaphragms are reinforced concrete or posttensioned transversely. A temporary support is provided at the cast-in-place joint locations to stabilize the structure until the girders are made continuous. In reality, the spliced girder construction concept is also a form of segmental bridge construction using longer segments. The segments are typically lifted with a ground-based crane. This option is particularly attractive for a span range of 150 to 250 ft.

3.4 Conceptual Design

3.4.1 Span Configuration

In the conceptual design stage, span arrangement and configuration should be closely studied first by considering the site location of the bridge. A bridge crossing over a navigable waterway is very much dictated by the horizontal and vertical clearance required. It is also important to know the soil condition and landscapes (e.g., over water, land, valley, or mountainous area). For segmental concrete bridges uniformity of the span lengths is critical in order to maximize the benefit of precasting the segments. The more uniform the span distribution, the more economical the bridge. It is also preferable to have an uneven number of spans from the architectural point of view. Leonhard discussed different approaches (See Figure 3.33) for deep V shape valley and shallow valley conditions (a,b and c,d views respectively). For deep valley and steep slope and unstable soil conditions, it is not a good practice to place many piers with short span lengths. Therefore, the number of piers should be reduced and the span length increased. Notice also the shape and size of the piers. For shorter span length, the lateral pier dimensions should be slender in order to reduce the wall view effect from an oblique view. For shallow valley, it is important to consider the L/H ratio of the opening between two piers, where L is the span length and H is the pier height. It is preferable to have an L/H ratio equal to or greater than 1.5. The end spans should be less than the typical span length (60% to 80% of typical span length) in order to achieve an efficient design.

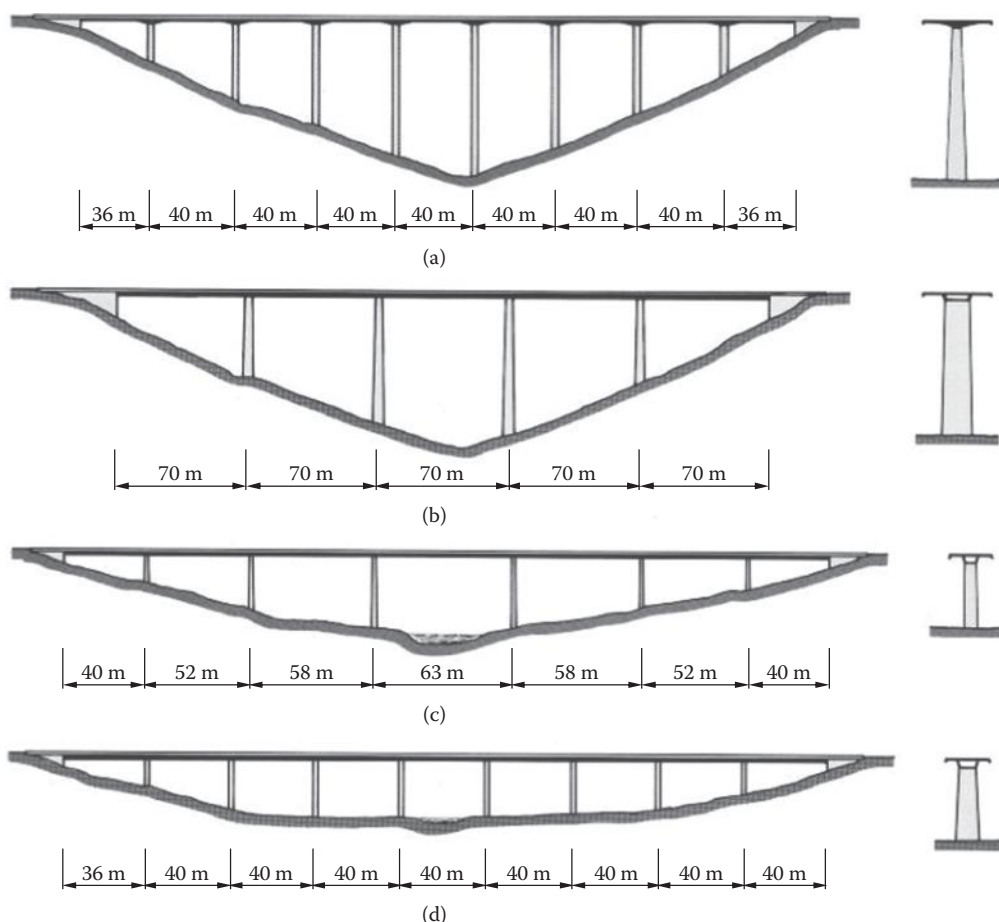


FIGURE 3.33 Span distribution. (From Leonhardt, F. 1984. *Bridges*, The MIT Press, Cambridge, MA, 1984.)

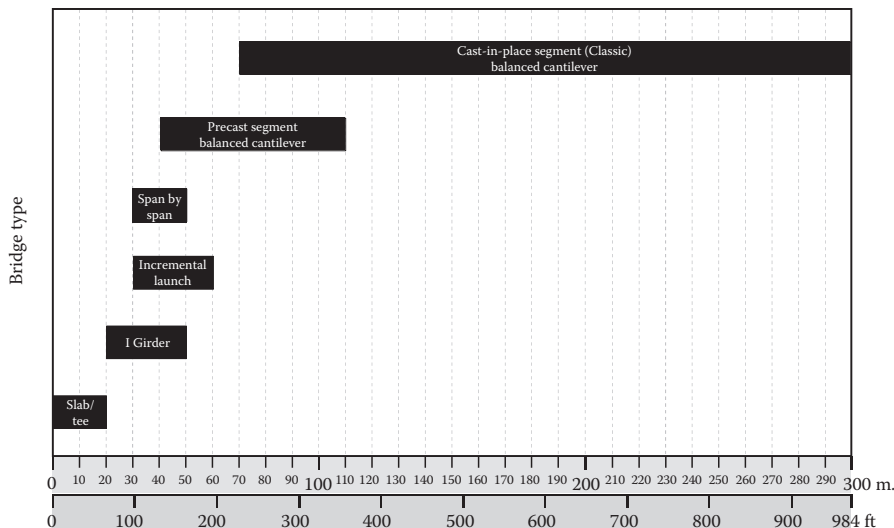


FIGURE 3.34 Economical span length ranges for typical concrete bridge types.

Once the typical span length is selected, use the following chart (Figure 3.34) to determine the kind of construction method that is suitable for the particular span. Of course, this is only one of the parameters to consider when selecting the construction method.

3.4.2 Span-to-Depth Ratios

For spans up to 250 ft (75 m), constant depth section is typically utilized. However, when the span length is larger than 250 ft, a variable depth section is more economical and efficient. Span length over depth ratio (L/D) plays an important role in conceptual design. The preliminary section depth is selected on the basis of the L/D ratio rule of thumb to establish the superstructure structural depth. The initial depth selected is continuously refined in the preliminary and final design. Figure 3.35 shows the preliminary L/D ratio for constant depth section of simply supported girder and continuous girder. Figure 3.36 shows the L/D ratio for a variable-depth girder.

3.4.3 Proportional Sections

After all structural components of the bridge have been roughly determined, including shape and exterior dimensions, the conceptual design process continues to study the overall proportional dimensions and shape compatibility and suitability of the proposed structure at a particular site. Typically, several alternatives are studied by varying span configurations, superstructure types, materials, construction means and methods, and the approximate cost for each alternative. In most cases, rendering in three dimensions (3D) (See Figure 3.37 for a 3D rendering) is required so that the owners can also participate in the decision making on the preferred alternative.

3.4.4 Structural System

As the conceptual design progresses to a more advanced stage, the next step is to study the structural system of the bridge. The final bridge structural system is studied carefully, particularly the stability during construction and how the statical system changes from stage to stage of the construction until the bridge is completed. This is the nature of segmental bridges, unlike other types of structures such as reinforced concrete or steel conventional types of bridges. The erection and stitching of the segment pieces require many stages and the structural system is constantly changing from time to time until completion.

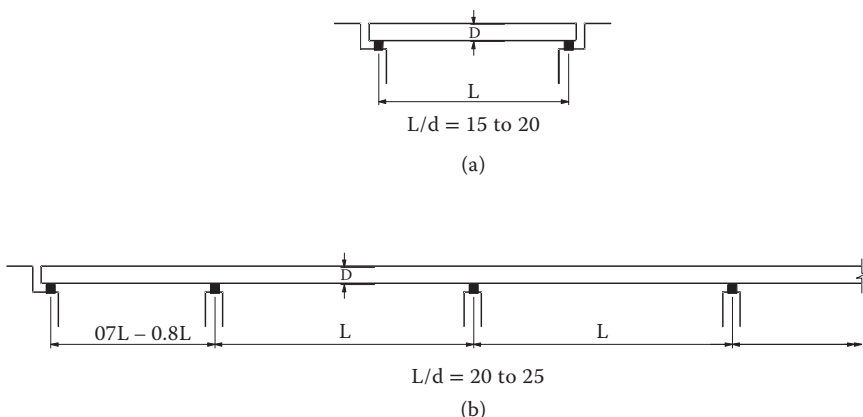


FIGURE 3.35 Span over depth ratio for constant-depth bridge girder: (a) simply supported girder; (b) continuous girder.

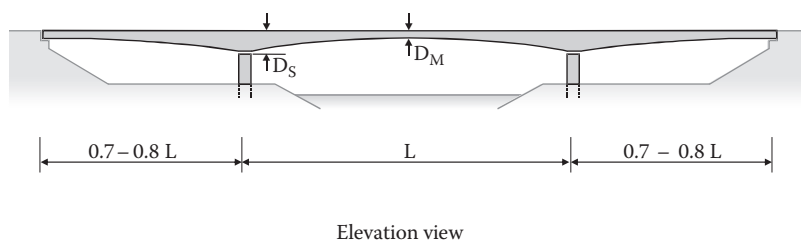


FIGURE 3.36 Span over depth ratio for variable-depth bridge girder (for span $\geq 250'$).



FIGURE 3.37 Rendering of Cincinnati Airport Ramp. (Courtesy of Parsons Brinckerhoff, Inc.)

@Seismicisolation

Figure 3.38a-l shows some of the structural system possible for segmental bridges from simply supported girder to the most complicated portal frame system. Although providing in span hinges is theoretically possible, (Figure 3.38e-h) practically such in-span hinges should be avoided for segmental bridges. The earlier cast-in-place balanced cantilever bridges in Europe had adopted midspan hinges in their bridges. It was later discovered that those bridges had suffered maintenance problems due to excessive deflection at the midspan hinges due to long-term creep and shrinkage (Guyon 1972). The subsequent generation of segmental bridges has eliminated midspan or other in-span hinges. If for some reason, the midspan hinges cannot be eliminated, it is necessary to provide a strong back over the hinge to avoid excessive long-term deflection due to creep and shrinkage.

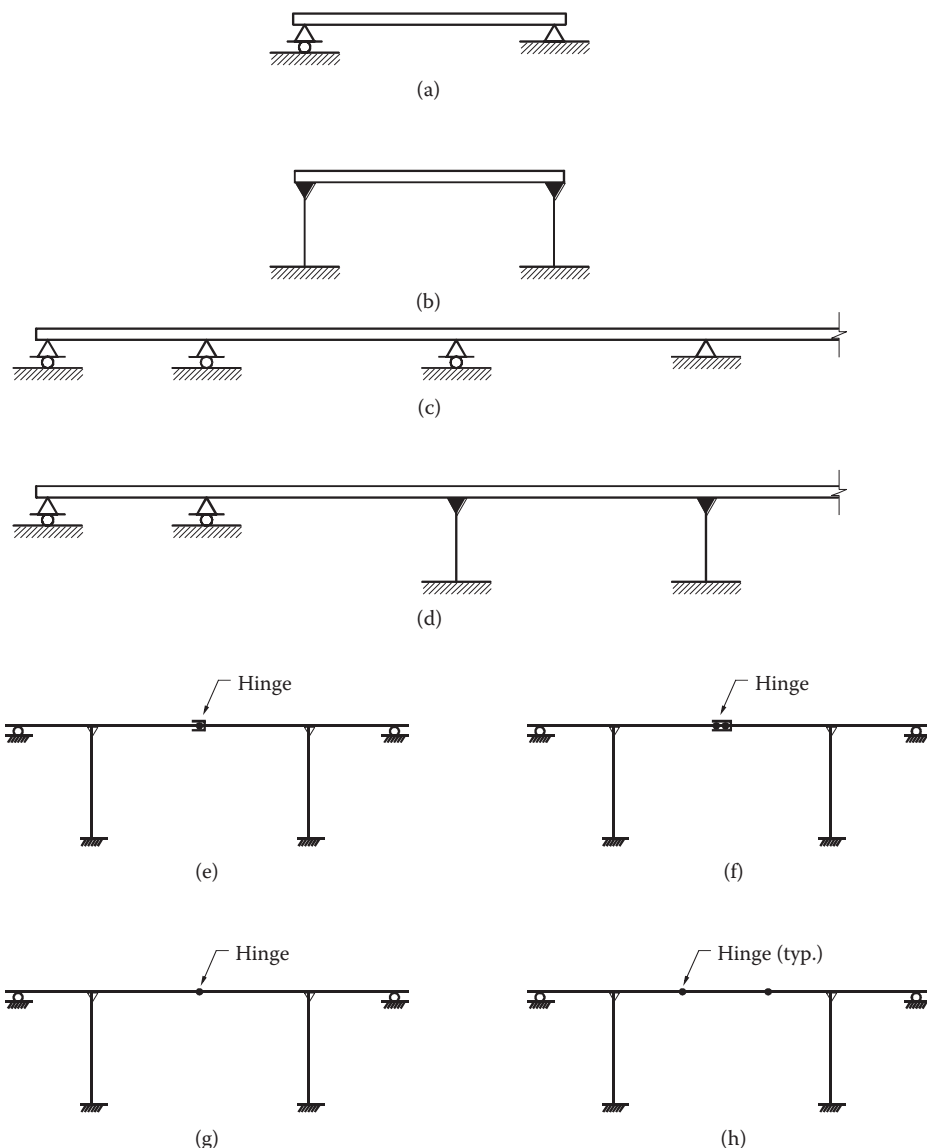


FIGURE 3.38 Possible structural systems.

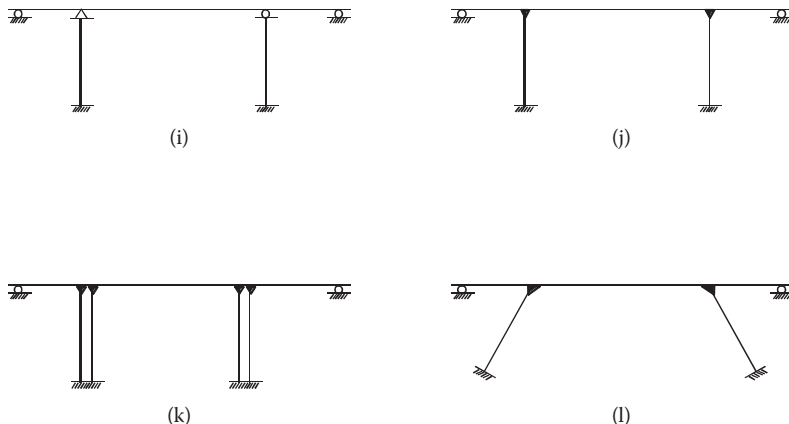


FIGURE 3.38 (Continued) Possible structural systems.

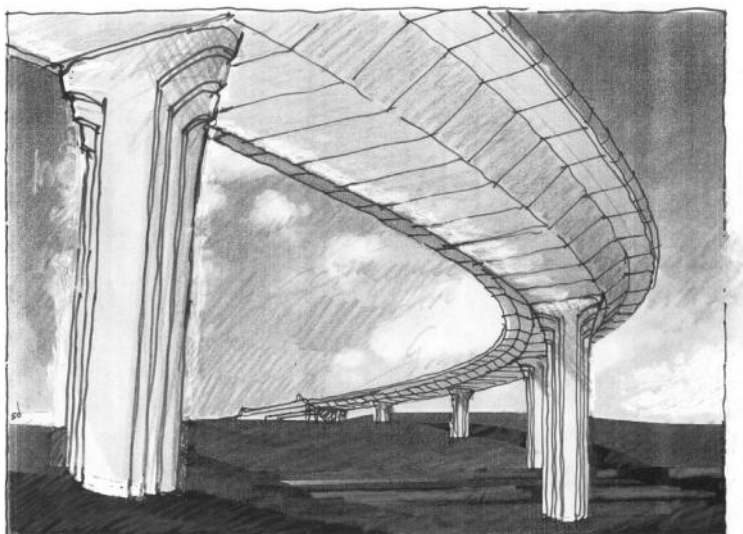
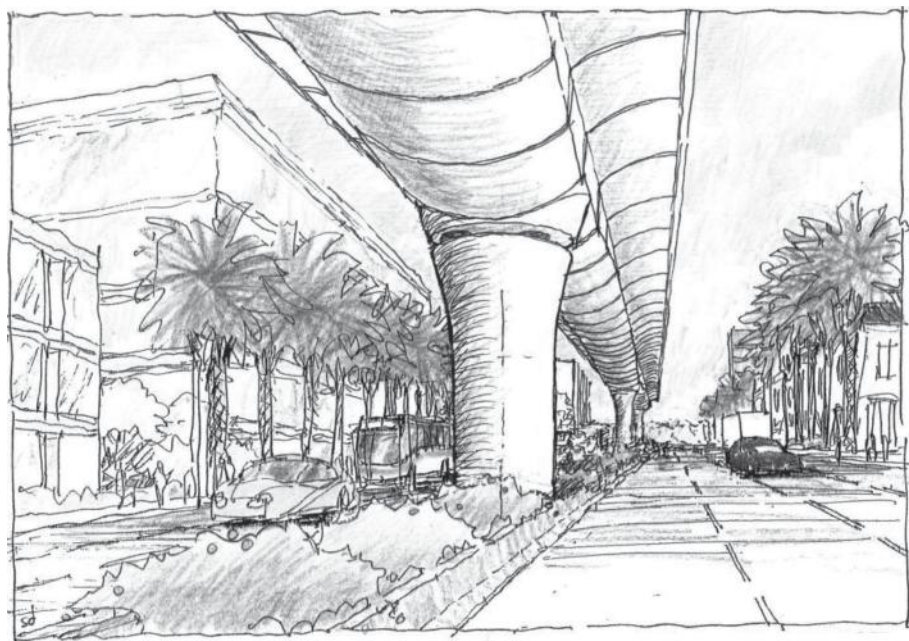


FIGURE 3.39 Segmental bridge concept in an urban area (architect: Scott Danielson).

3.4.5 Aesthetic Aspect

Segmental bridge construction is not only popular for long span bridges over rivers and canyons but also in urban and city interchanges and for transit structures such as light rail and high-speed rail guideway structures. Aesthetic value has become one of the most important parameters in selecting the bridge structure. The owners and stakeholders are placing more and more importance on aesthetically pleasing structures. Fortunately for segmental box girder bridges, the shape of the box girder is already inherently attractive. The architect should properly design the pier shape to ensure that the overall look of the bridge is compatible and suitable for a particular location. Several samples of this are shown in Figures 3.39 through 3.42. The structural engineers view aesthetics from a different angle. Structural engineers consider aesthetics from the functionality of each bridge element from superstructure to substructure and the logical flow of forces subjected to the bridges, from live loads, dead loads, seismic load, wind loads, temperature loads, long-term creep, and shrinkage of concrete and ship impact, including constructability and durability. A successful bridge design involves the close collaboration of planners, structural engineers, architects, contractors, and the stakeholders/owners.



PB
Sd 8.14.02
R 8.28.02

Highly sculpted
Seg, conc. box

FIGURE 3.40 Segmental bridge concept in a city (architect: Scott Danielson).

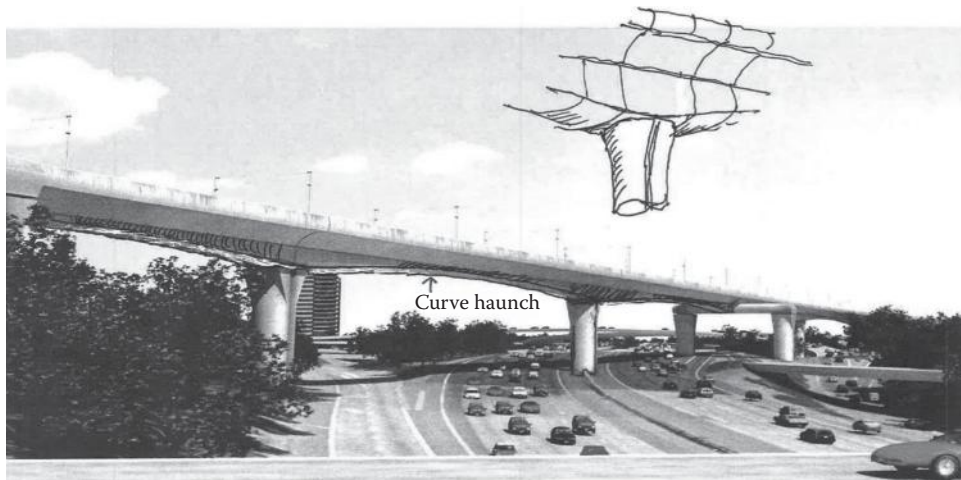


FIGURE 3.41 Segmental bridge concept over a highway (architect: Scott Danielson).

3.5 Deck Design

The top deck of a box girder is subjected to complex external forces, static and dynamic loads, thermal gradients, and creep and shrinkage effects. Proper consideration should be given to these effects to prevent cracking and deterioration. De-icing chemicals and freeze-thaw action should also be considered in design to counteract degradation.

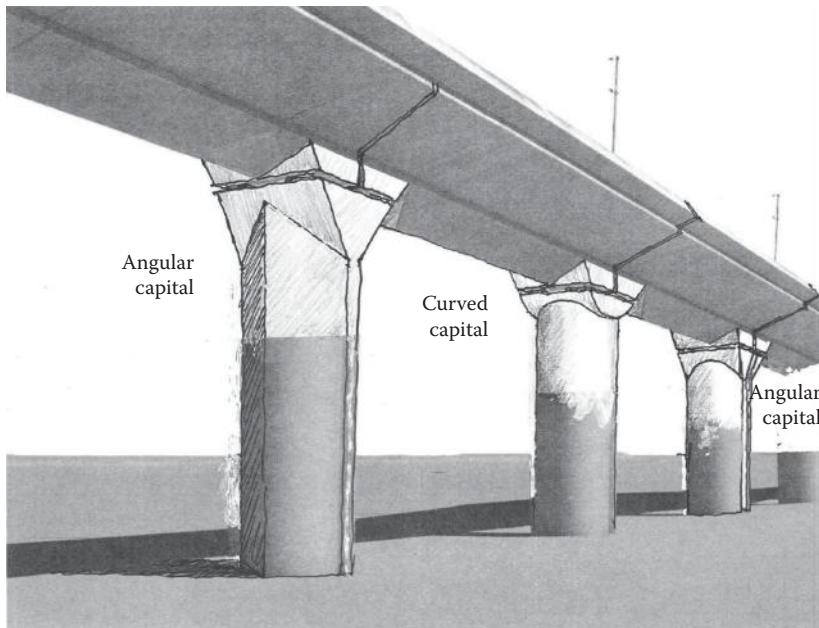


FIGURE 3.42 Segmental bridge concept for high-speed rail guideway (architect: Scott Danielson).

Deck replacement is not only costly but also results in inconvenience to the traveling public. For segmental bridge superstructures, deck replacement is not practical and almost impossible to do without closing the entire bridge. Therefore, when designing decks for segmental bridges, it is always a good strategy to be conservative/robust and allow for reserved capacity.

Studies have shown that transverse posttensioning of top decks improves long-term deck durability and results in low life cycle cost (Posten, Carrasquillo and Breen 1987). It is recommended that for all posttensioned box girders the top deck be transversely posttensioned, even for short overhangs. For bridges not subjected to freeze-thaw action and de-icing chemicals, at least the deck should be partially prestressed. The top deck should be designed using elastic methods and then checked for ultimate limit states, not the other way around.

In general, it is standard practice to select a minimum top deck thickness of 8 in (200 mm), although AASHTO-PCI-ASBI Standard Sections Committee recommends a minimum deck thickness of 9 in (230 mm).

3.5.1 Design Approach

To correctly represent the final system of the box girder, a three-dimensional analysis incorporating all loads with proper boundary conditions is needed. Owing to the complexity of this type of analysis, in particular, the application of prestressing to three-dimensional systems, this is seldom done. In lieu of this complex analysis, it is common practice to model the box as a two-dimensional (2D) plane frame of unit length, as shown in Figure 3.43. If the thicknesses of the web and bottom slab vary along the length of the bridge, several 2D frames may have to be analyzed in order to obtain a more representative interpretation of these varying cross-sectional properties. The 2D frame model allows for load distribution to the webs and slab members relative to their stiffness.

A typical 2D frame model is assumed to be supported at the lower end of the webs as shown in Figure 3.43. While it could be argued that different boundary conditions exist for this model, this simplified assumption produces reasonable results.

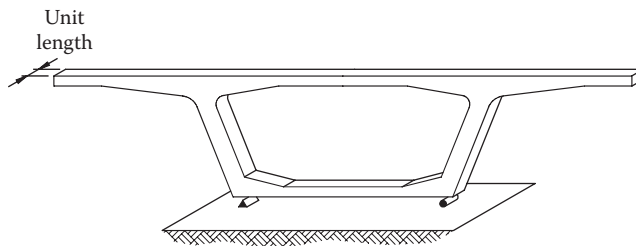


FIGURE 3.43 Simplified two-dimensional plane frame of unit length.

The design loads considered in transverse design include, but are not limited to

- *DC* = Dead load of structural components and nonstructural components, such as traffic barrier wall
- *DW* = Dead load of wearing surface or future wearing surface and utilities, if any
- *LL* = Live load
- *IM* = Dynamic load allowance
- *PT* = Primary prestressing forces
- *EL* = Miscellaneous locked-in force effects resulting from the construction process, including jacking apart of cantilevers in segmental construction
- *TG* = Thermal gradient ($\pm 10^{\circ}\text{F}$ differential between the inside and outside of box girder) Note: currently not required by AASHTO LRFD Design Specifications, but commonly done in standard practice
- *PS* = Secondary forces from posttensioning
- *CR* = Creep effect of concrete
- *SH* = Shrinkage effect of concrete

Secondary forces of posttensioning are included in ultimate limit state load combinations with a load factor of 1.0.

In addition to service and strength limit state load combinations, the deck design should be checked for construction load combinations, such as segment lifting, construction equipment, and segment stacking (see LRFD Article 5.14.2).

3.5.2 Live Load Analysis

When a static concentrated load is applied on a deck, the deck will deflect transversely as well as longitudinally, similar to the structural behavior of a two-way slab. The load distribution becomes more complex when multiple point loads are applied to the deck, such as a truck load. When the structural model is simplified to a 2D frame model, as stated in Section 3.5.1, it is important to obtain the resulting 3D forces to the 2D model.

Commonly, there are two ways of handling live load distributions in the transverse direction:

1. In the past, influence surfaces from Pucher or Homberg Charts have been extensively used in box girder transverse design. These charts are based on elastic theory of plates (homogeneous and isotropic). Some charts are valid for constant depth plate thickness and some for variable depth plate thickness with a parabolic soffit. Depending on the boundary conditions of the selected plate, the dimensionless charts provide bending moments per unit length at the fixed end and midspan only. The fixed end moment (FEM) is then applied as external forces to the 2D frame. The bending moments between supports are approximated by interpolation. The method has limitations for haunched deck slabs, regarding the support depth over midspan depth ratio. This method is approximate and can be useful for preliminary design.

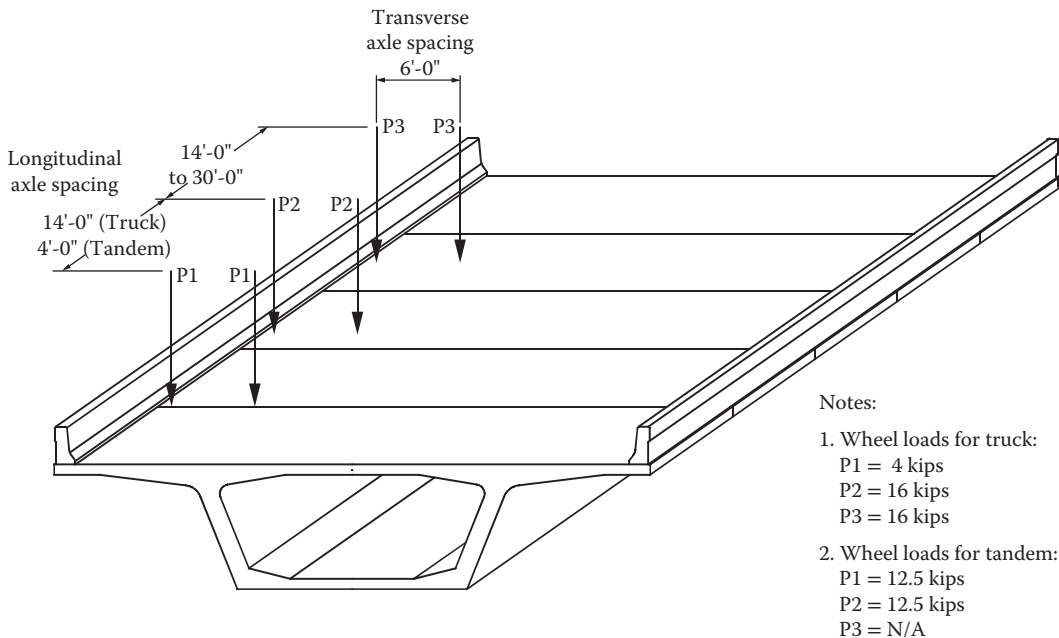


FIGURE 3.44 LRFD live load configuration in 3D.

2. A more accurate method is based on a partial 3D finite element model of the box girder. The term “partial” implies that the entire bridge superstructure need not be modeled; rather it should be interpreted as a partial length of the box that will be long enough to include three-dimensional effects. From this model, influence lines can be generated at any section of interest. The influence lines should be generated using a line load consisting of front and rear wheels of a design truck. Since general finite element programs are readily available presently, it is recommended that this method be used for final design.

It should be noted that, theoretically, a continuous vehicle barrier could be incorporated into this model to further distribute live load longitudinally. However, owing to discontinuities of the barrier and uncertain future quality, this edge stiffening effect is neglected and not recommended.

It is very important that the live load configuration be strategically placed in order to produce the worst condition (see Figures 3.44 and 3.45). Some common points where stresses are checked include the following:

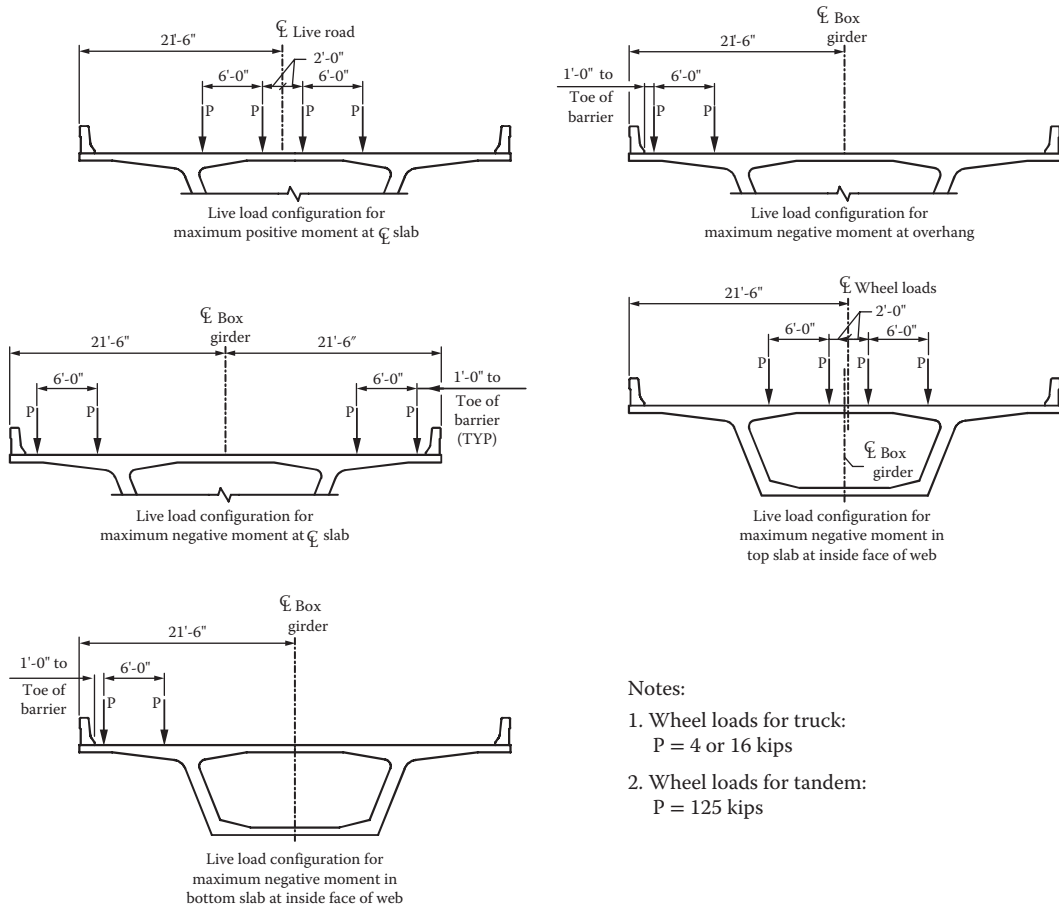
- Maximum negative bending moment at the root of deck overhang
- Maximum positive and negative bending moments at the center line between two webs
- Maximum negative bending moment in the top deck at the interior face of the webs
- Maximum negative and positive bending moments in the webs and bottom slab
- Maximum negative moment in the deck overhang where the taper begins

Figures 3.46 through 3.51 show typical influence lines corresponding to the above locations using method 2.

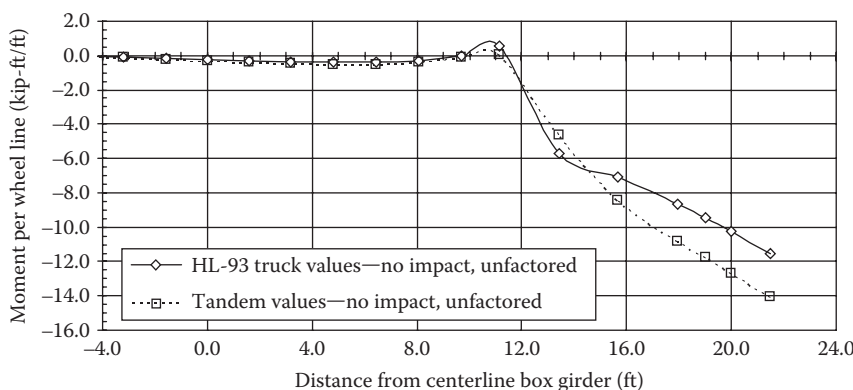
In the *AASHTO LRFD Specifications* (AASHTO 2012), only the effect of a design truck (or tandem) is to be considered for transverse design and no lane loads (see Article 3.6.1.3.3).

3.5.3 Posttensioning Tendon Layout

Posttensioning in the transverse direction typically consists of three to four 0.5- (13) or 0.6-in (15 mm) diameter strands per tendon passing through the top slab and anchored at the face of the overhang on each side of the box girder. These tendons are usually housed in flat ducts due to the thin top slab. To efficiently utilize the tendon, it should be suitably profiled for maximum structural efficiency.

**Notes:**

1. Wheel loads for truck:
 $P = 4$ or 16 kips
2. Wheel loads for tandem:
 $P = 125$ kips

FIGURE 3.45 LRFD live load transverse configurations.**FIGURE 3.46** Live load influence lines for moment at root of outside wing.

A typical tendon is generally anchored at mid height of the slab at wing tips and then gradually rises to a level above the neutral axis of the deck over the webs. This helps the tendon resist the negative moments at the webs. The tendon then gradually drops to a level below the neutral axis of the top slab near the centerline of the box girder in order to resist the positive bending in that region. Figure 3.52 shows one example of the tendon path,

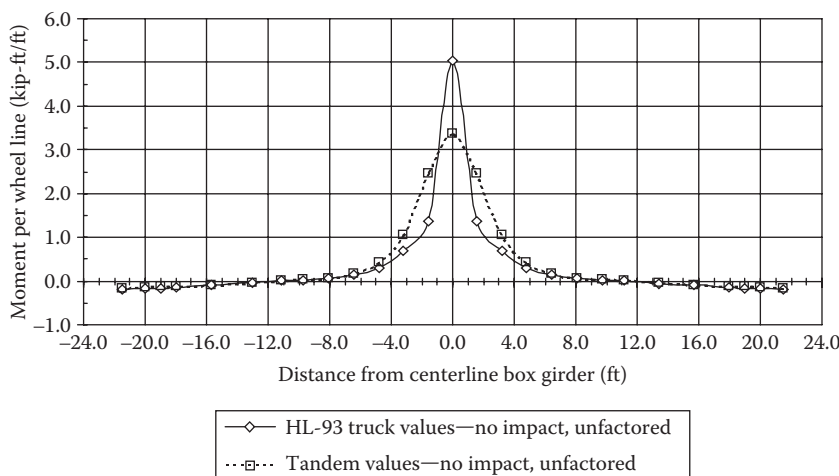


FIGURE 3.47 Live load influence lines for moment at box centerline.

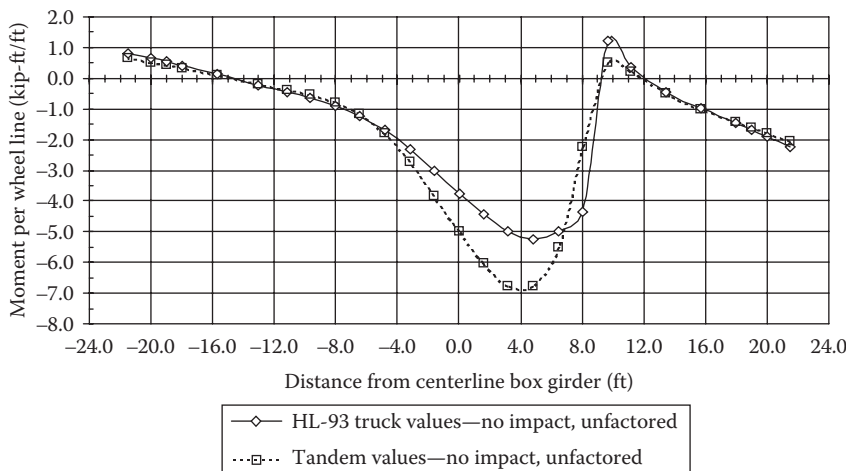


FIGURE 3.48 Live load influence lines for moment at inside face of web.

Longitudinally, the tendon spacing is determined using the appropriate service and strength limit state checks. The maximum spacing of tendons is typically restricted to 4 ft (1.2 m) in an effort to limit shear lag effects between anchorages. However, it is a good practice to space transverse tendons based on 30° stress distribution from the anchorage point on each side of the tendon considered. If maximum tendon spacing is not addressed, zones near outside edges of the slab may be without effective prestressing.

3.5.4 Summary of Design Forces

The design forces obtained from the 2D frame analysis and 3D live load influence lines may be combined in a spreadsheet using the LRFD Service Limit State and Strength Limit State combinations. The maximum tensile and compressive stresses at each predetermined section in the top slab are summarized and compared to the stress limits at Service Limit States specified in AASHTO-LRFD Bridge Design Specifications (AASHTO 2012). The prestressing force is usually estimated in preliminary hand calculations, and then analyzed in a 2D time-dependent run using proprietary software. All other loads are incorporated into the 2D model, except live loads. The results are then compiled in a spreadsheet to check stresses. By varying the prestressing force, the combined stresses of service limit states are

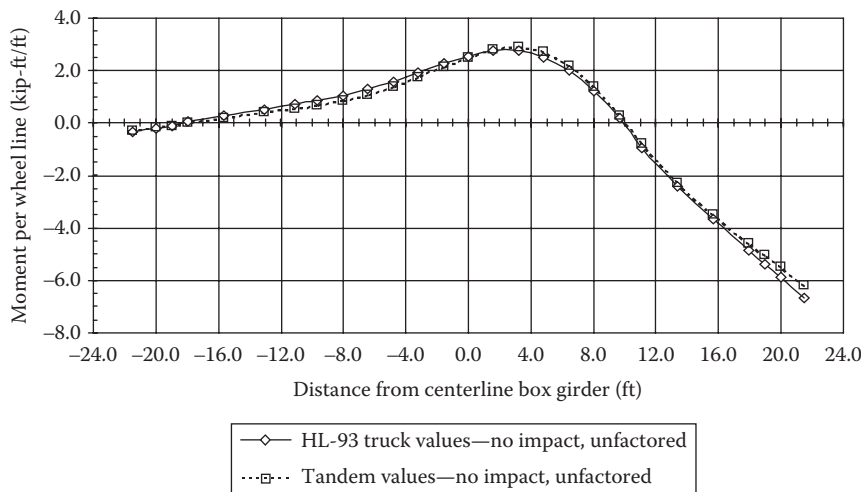


FIGURE 3.49 Live load influence lines for moment at top of web.

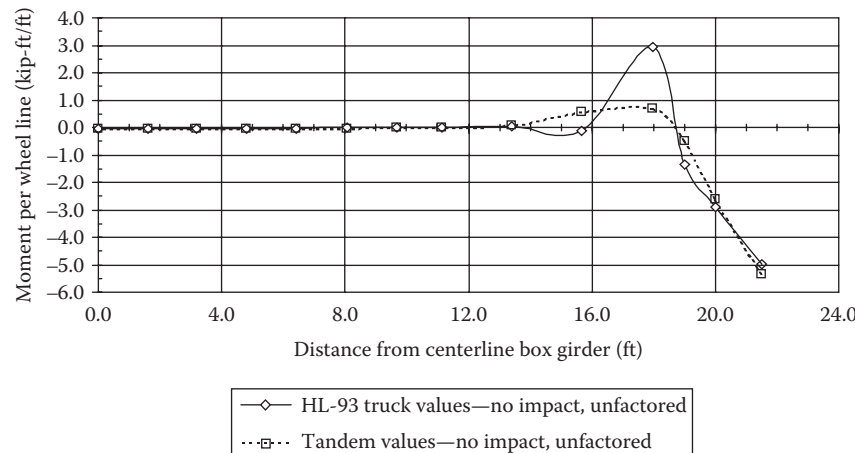


FIGURE 3.50 Live load influence lines at outside wing/thickness transition.

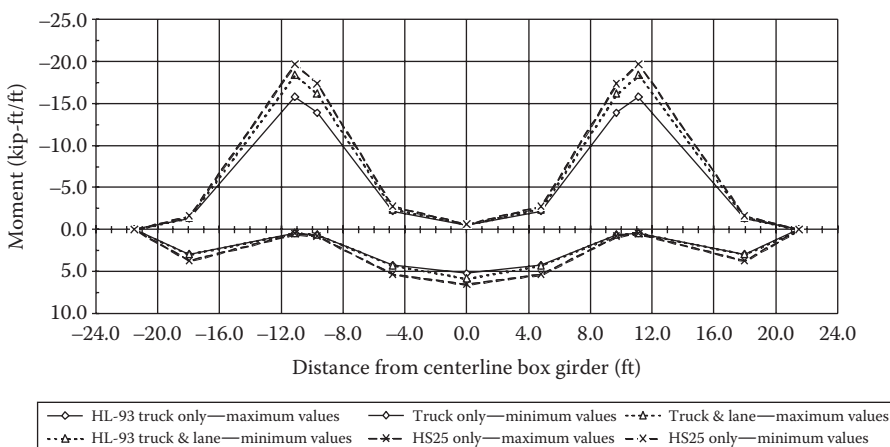


FIGURE 3.51 Transverse deck live load moment envelope (unfactored without impact).

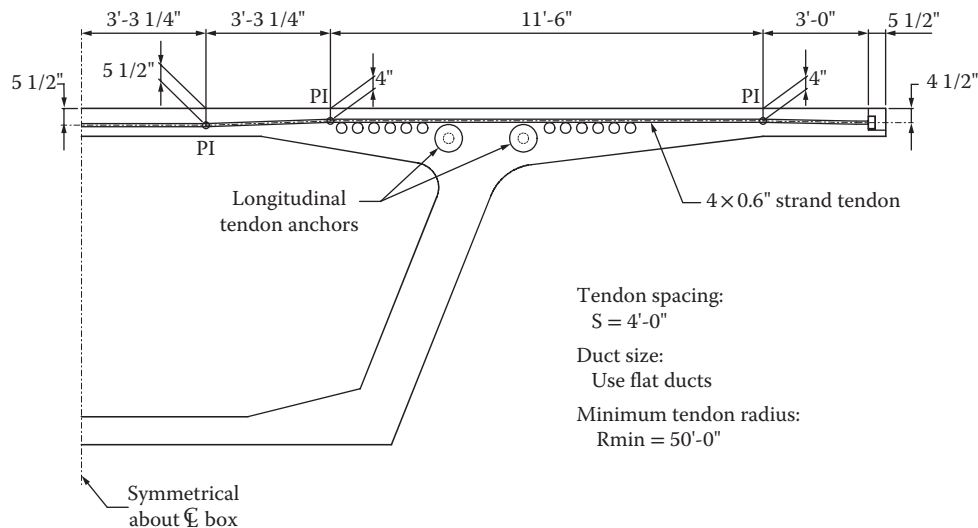


FIGURE 3.52 Typical transverse tendon layout.

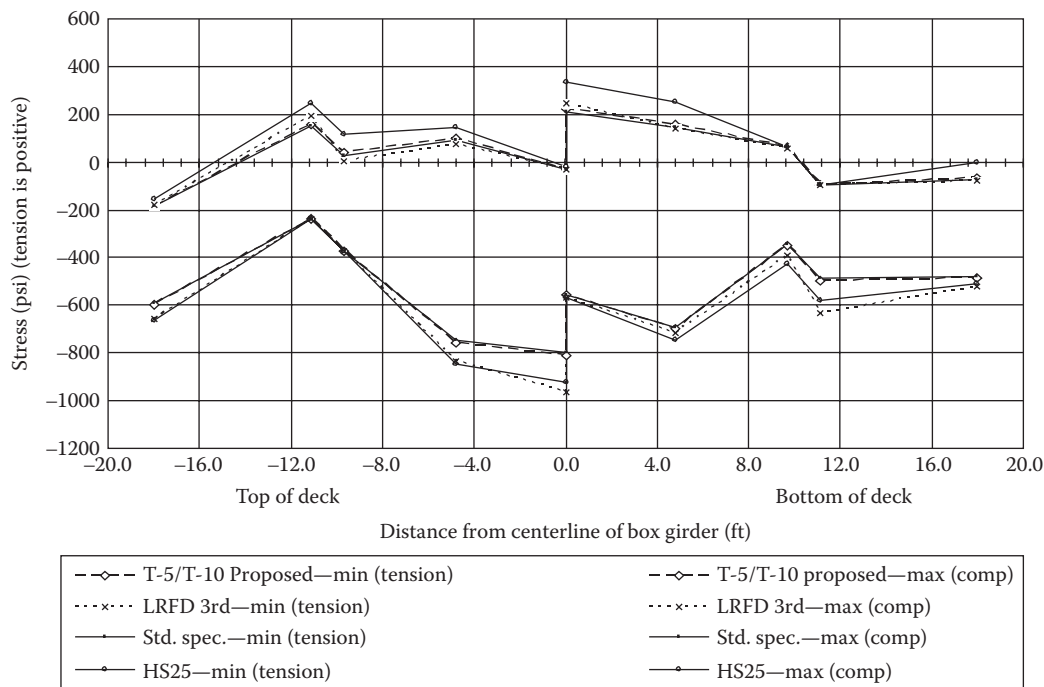


FIGURE 3.53 Concrete service stresses (code comparison).

calculated. Using the selected tendon forces per unit length, the size and spacing of transverse tendons in the segment are determined.

The LRFD Strength Limit States may be also tabulated in a spreadsheet and an envelope of maximum and minimum values is determined for each chosen section. The values of the moment envelope can then be compared to the calculated bending capacities for each of the corresponding transverse components. Concrete service stresses were computed using several AASHTO Standard Specifications and the current LRFD Specifications for comparison purposes (see Figure 3.53).

3.5.5 Service Limit State Design

When checking concrete stresses, only Service Limit State I is checked with a live load factor of 1.0 for tension as well as compression. Also, a linear temperature gradient of 10° F between interior and exterior surfaces of the box is used in Service Limit State I. The current LRFD specification does not specify this loading, leaving it up to the owner or designer to establish if it should be included on a project-by-project basis. This example is based on a load factor of 0.5 for transverse temperature gradient when accompanying live load. Also, in addition to Service Limit State I, LRFD requires a check for service load stresses due to dead load and full temperature gradient. This limit state can often govern at locations where live load influences are small.

In addition to service limit states under maximum loading, temporary stresses such as those prior to barrier placement and vehicular traffic should be checked to ensure that allowable stresses are not exceeded during the construction process.

Service load combinations used in this example include the following:

Service I (Tension & Compression)

$$1.0(\text{DC} + \text{DW} + \text{EL}) + 1.0(\text{PT}) + 1.0(\text{LL} + \text{IM}) + 1.0(\text{CR} + \text{SH}) + / - 0.5(\text{TG})$$

Segmental Load Combination (LRFD Equation 3.4.1-2)

$$1.0(\text{DC} + \text{DW} + \text{EL}) + 1.0(\text{PT}) + 1.0(\text{CR} + \text{SH}) + / - 1.0(\text{TG})$$

3.5.6 Strength Limit State Design

3.5.6.1 Flexural Strength Design Check

For purposes of the transverse design, Strength Limit State IV is the same as Strength Limit State I without live load, with 25% more self-weight. This loading does not govern in this example.

For temperature gradient load factors, LRFD Specifications suggest determining a load factor on a project-specific basis, with a recommendation of 0.0 for most instances. Since these loads are a result of restrained deformations, the loads should disappear if the reinforcement begins to yield at ultimate. In addition, the Segmental Guide Specifications do not include this component in ultimate load combinations. For these reasons, the temperature gradient was not used in the strength limit state combinations below.

The LRFD specifications require minimum reinforcement equal to that required to resist 1.2 times the cracking moment. This requirement governs only the bottom slab (soffit) design. To satisfy the minimum steel requirement, the transverse bar spacing in the bottom soffit was decreased from 12 (205) to 8 in (203 mm), which represents an increase in reinforcement of 50%.

Also, under ultimate flexure, the amount of web steel reinforcing required for transverse bending should be calculated. This should be combined in an appropriate manner with reinforcing required for longitudinal shear.

Listed below is the ultimate load combination per LRFD:

Strength I

$$\gamma_p \text{DC} + \gamma_p \text{DW} + 1.0 \text{EL} + 1.75(\text{LL} + \text{IM}) + 0.5(\text{CR} + \text{SH})$$

3.5.6.2 Shear Strength Design Check

Traditionally, shear behavior has been ignored in the design of concrete decks for AASHTO bridges. Box girder decks are similar in this sense, but can often have large construction loads placed on them. In these special cases, both one-way and two-way action shear should be investigated.

3.6 Longitudinal Design

3.6.1 Design Methodology

The following design example illustrates the longitudinal design process for a typical precast segmental bridge. The structure is assumed to be erected using the precast balanced cantilever construction method with a ground-based crane. Owing to changes in the statical system during erection, as cantilevers are made continuous through cast-in-place closure joints, it is necessary to analyze the structure for time-dependent effects. Time-dependent analysis is a function of the segment casting date, times that the segments are incorporated into the structure, as well as dates associated with changes in the statical system throughout the construction process.

It is customary to establish an assumed sequence of construction and to estimate a reasonable construction schedule. Casting and erection dates of the segments are established on the basis of the construction schedule and the segment production rate. Casting dates are a function of an assumed number of casting cells and the time required to cast each segment. For purposes of estimating these dates, the segment production rate is assumed as one typical segment per day per casting cell and one pier/expansion joint segment per week per casting cell. Segments are not to be erected earlier than one month after casting. During construction, when actual casting and erection dates become available, the stage-by-stage analysis should be rerun in order to obtain correct camber values.

Time-dependent properties of concrete are established on the basis of the environmental humidity and dimensions of the cross section, and can be adjusted for concrete composition (e.g. limestone aggregate), rate of hardening, and ambient temperature. Section properties are determined for each segment considering the effects of shear lag in the top and bottom slab.

The above information is entered into a time-dependent analysis proprietary software. A stage-by-stage analysis is performed using an assumed posttensioning layout while carefully modeling appropriate boundary conditions for each step of the construction process. After the construction has been modeled, the structure is stepped through time day 10,000 to allow all time-dependent effects to occur. It is also essential in statically indeterminate structures to sum up all locked-in forces that result from various stages of structural systems until day 10,000. Additional loads are placed on the structure such as live load, temperature gradient, and support settlement, as appropriate, and analyzed for initial (at end of construction) and final conditions at day 10,000.

3.6.2 Tendon Layout and Envelope

An approximate tendon layout can be based on preliminary calculations for construction loading of a typical cantilever. Span continuity tendons can be estimated by preliminary design based on the final structure approximate creep and shrinkage effects using load factor dead and live load combinations. The assumed layout can then easily be modified during the final design to satisfy all applicable LRFD Limit State Load Combinations.

The preliminary design for this example indicates the need for twelve cantilever tendons and five bottom continuity tendons per web. On the basis of previous experience, two eight-strand continuity tendons were added in the top slab across the closure pour to control stresses resulting from temperature gradients. The final design resulted in an increase of one cantilever tendon and one bottom span continuity tendon at interior spans only (see Figures 3.54 through 3.56).

The tendons used are based on a 12-strand system using 0.6 in (15.24 mm) diameter strands. Only 11 strands were used for bottom continuity tendons to provide space for 5% contingency posttensioning as required for internal tendons. One out of 12 strands will provide approximately 8% of the contingency posttensioning if needed. An empty duct was provided for the cantilever tendons combined with an anchorage on the last segment of the cantilever to allow for contingency posttensioning. This empty duct should be grouted if no contingency tendons are required.

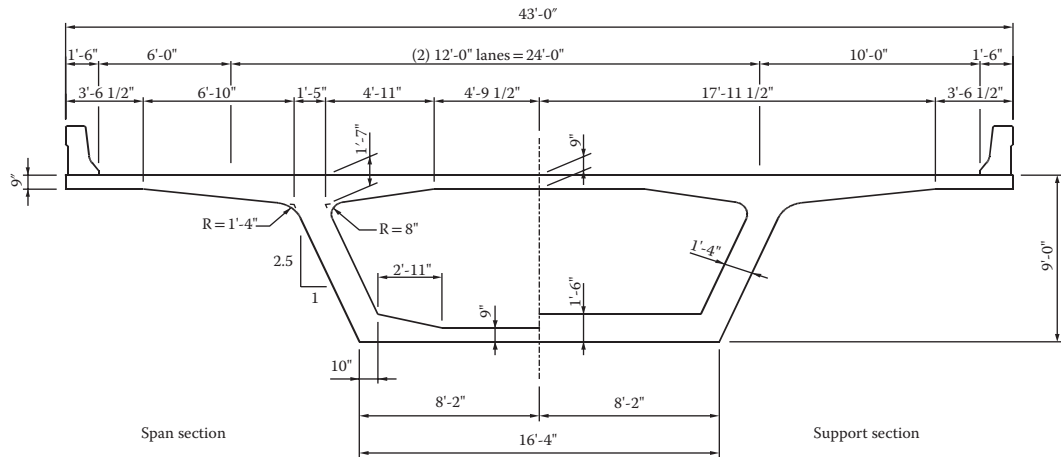


FIGURE 3.54 Typical section.

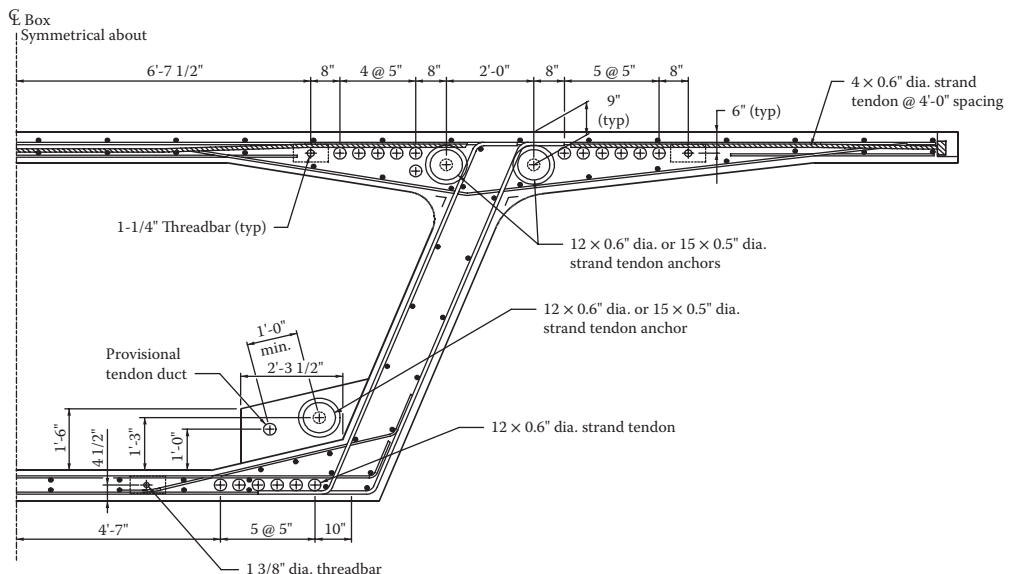


FIGURE 3.55 Posttensioning tendon locations.

Provisions are also made for future posttensioning by addition of anchorages and deviation points for external tendons (inside the box section), which can be used for adjustment of deflections or for other unforeseen conditions. Provisional posttensioning ducts and anchorages are covered under Article 5.14.2.3.8 of AASHTO LRFD Bridge Design Specifications (AASHTO 2012).

3.6.3 LRFD Live Load

LRFD live load (HL-93) consists of a single design truck per lane or tandem combined with a uniformly distributed lane load. For negative moments only, a second truck is added and the total effect is reduced by 10%. The second truck is required only between points of uniform load contraflexure, and should leave a space of at least 50 ft (15 m) between trucks measured between the rear axle of

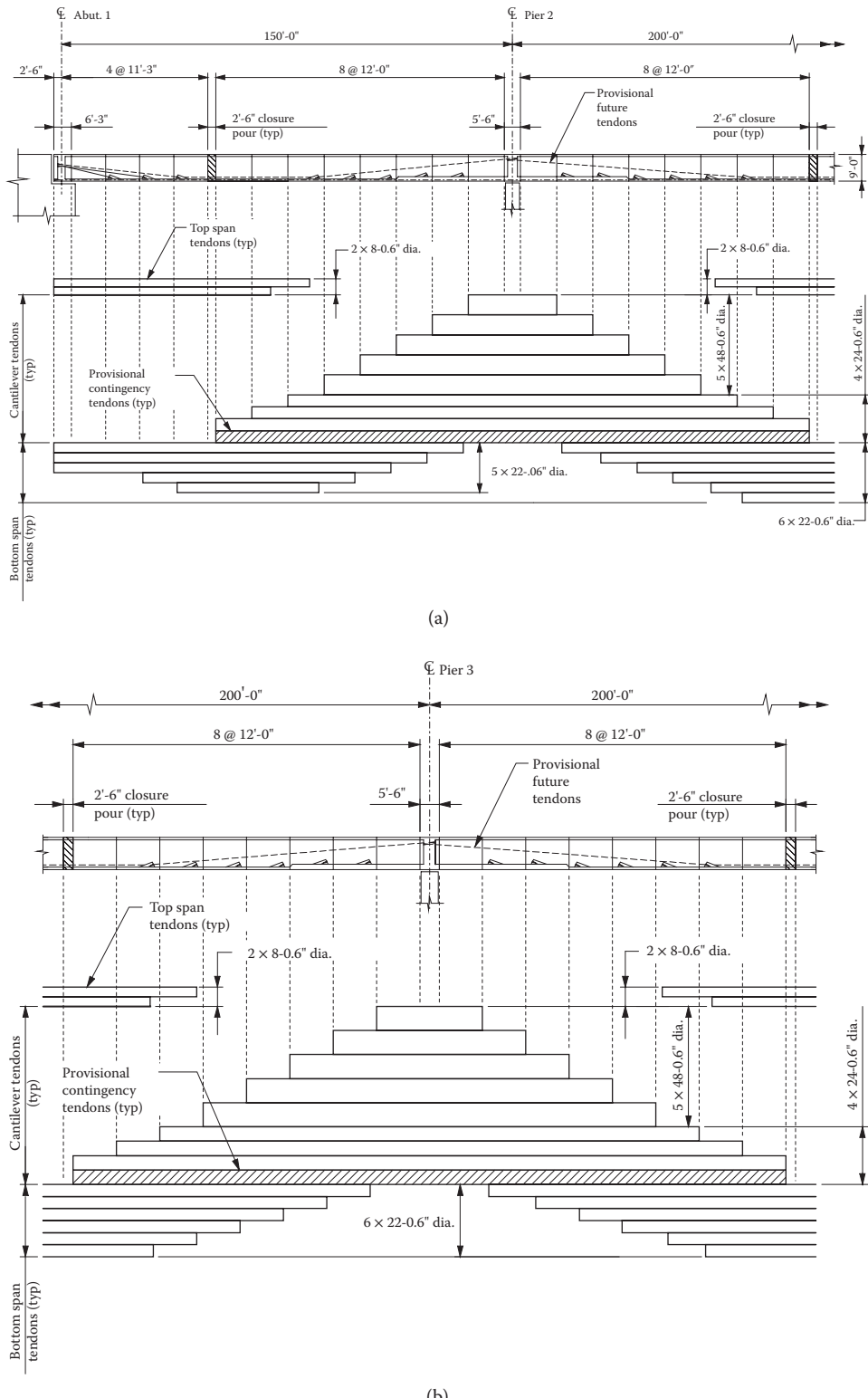
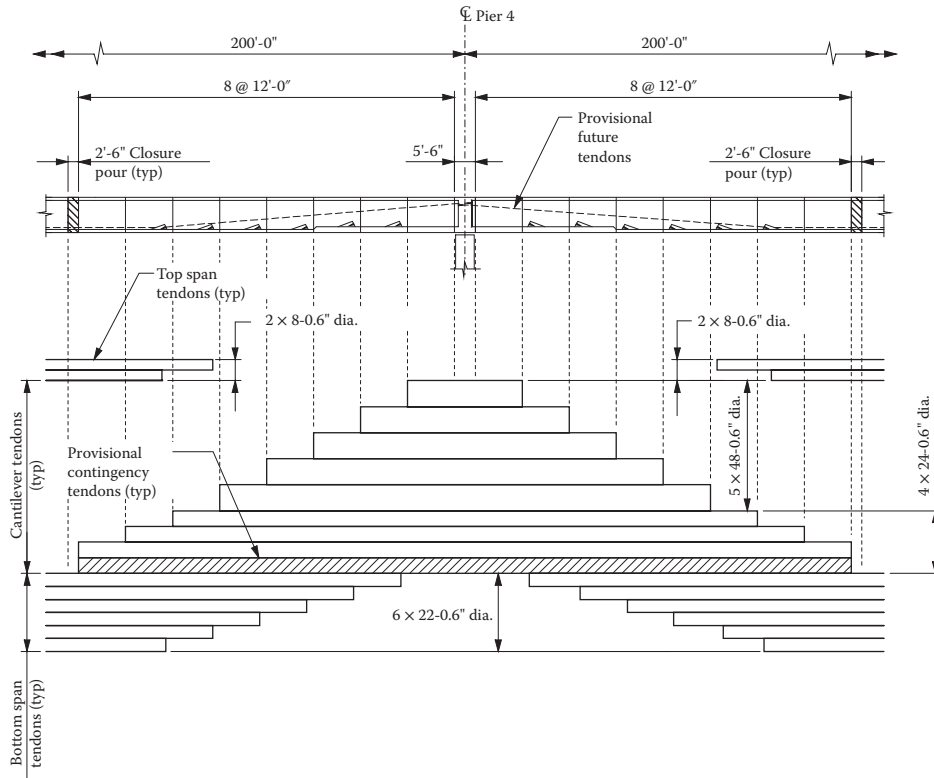
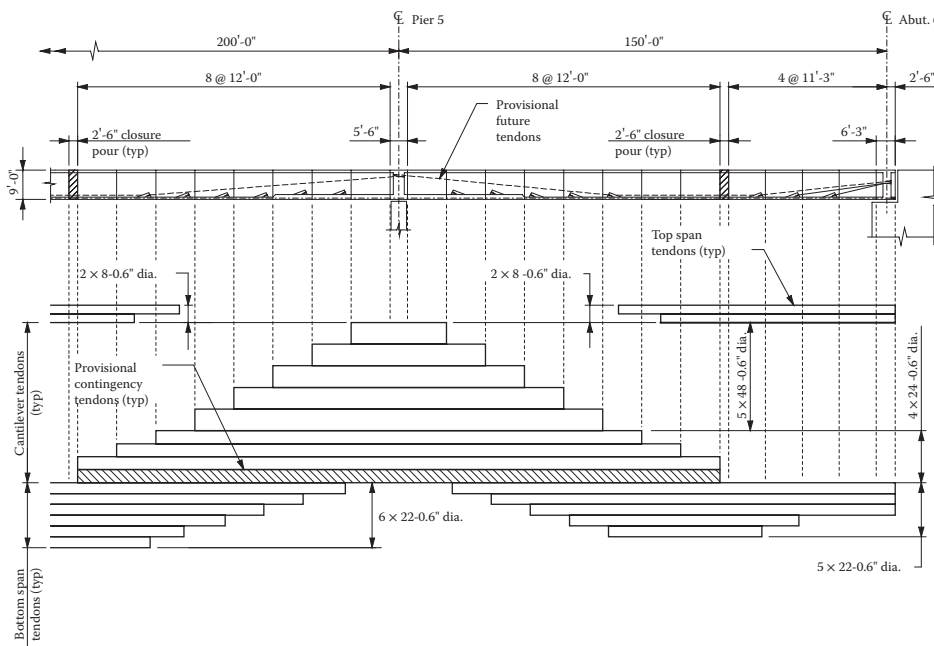


FIGURE 3.56 Typical tendon layout to balanced cantilever bridge construction.



(c)



(d)

FIGURE 3.56 (Continued) Typical tendon layout to balanced cantilever bridge construction.

the leading truck and the front axle of the trailing truck. A fatigue truck is also specified but was not considered for this example.

A dynamic load allowance (impact) of 33% is added to the design truck, but is not required for design lane load. Multiple presence factors range from 1.2 for a single lane to 0.85 for three lanes and 0.65 for more than three lanes. This example is based on three lanes, and has a multiple presence factor of 0.85. The application of LRFD live loads is shown in Figures 3.57 and 3.58.

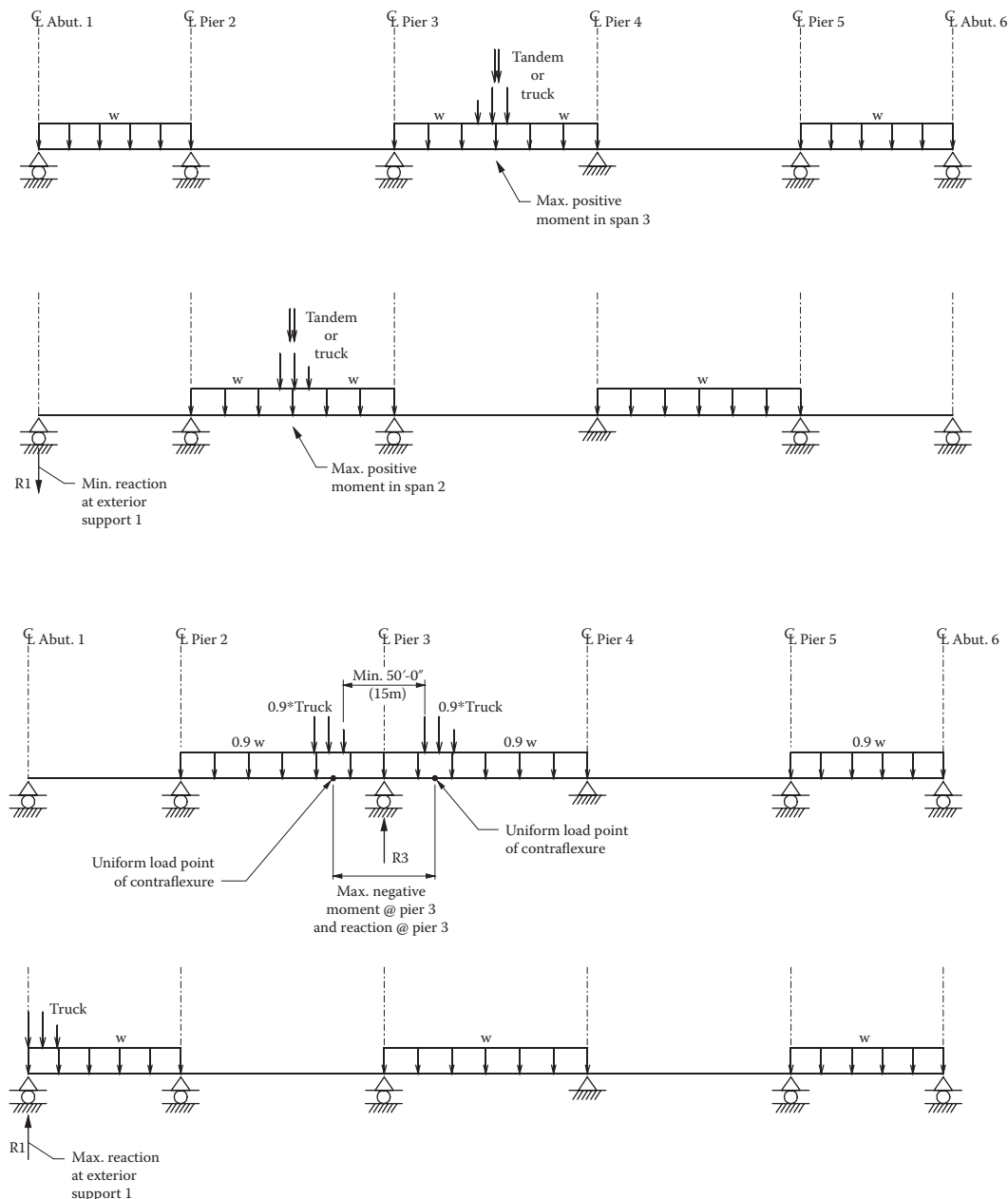


FIGURE 3.57 Application of LRFD live loads on a continuous structure.

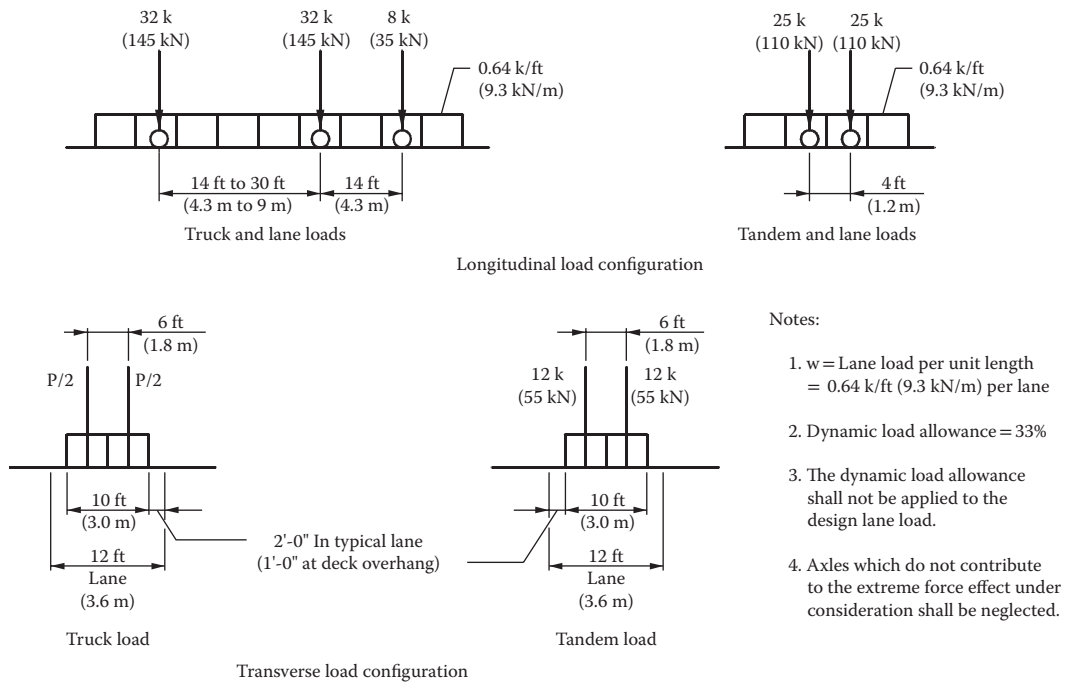


FIGURE 3.58 Longitudinal and transverse live load configurations.

3.6.4 Shear Lag Effect

The AASHTO *Guide Specifications for Design and Construction of Segmental Concrete Bridges, First Edition* (AASHTO 1989a) adopted shear lag provisions of DIN 1075 (German Concrete Code) using a linear transition of effective flanges. However, in the second edition, shear lag provision changed to a step function between span and support regions. In contrast to this change, the AASHTO LRFD *Bridge Design Specifications, Third Edition* (AASHTO 2004) adopted shear lag provisions similar to DIN 1075, as shown in Article 4.6.2.6.2. The difference between the two methods is insignificant, but the LRFD shear lag provision is considered to be more accurate.

When determining section properties, it is commonly assumed that shear lag applies to the moment of inertia and location of the neutral axis of the section. However, the cross-sectional area remains based on the full gross cross section, so as to not overestimate the "P/A" component of posttensioning stresses, where $P = PT$ effective force and $A = \text{gross cross section area}$.

Shear lag is a function of the structural system at the time it is under consideration. If the software used permits, section properties can be changed in the construction model to approximate true statical conditions at all intermediate steps. This additional accuracy may not be warranted for all designs, but could be evaluated on a case-by-case basis.

The following shear lag effect calculation is in accordance with article 4.6.2.6 of AASHTO LRFD *Bridge Design Specifications* (AASHTO 2012).

A. Completed structure

A.1- End span (see Figure 3.59)

where

$b = \text{flange width on each side of web (See Figure 3.60)}$

$b_1 = 10.37'$

$b_2 = 9.71'$

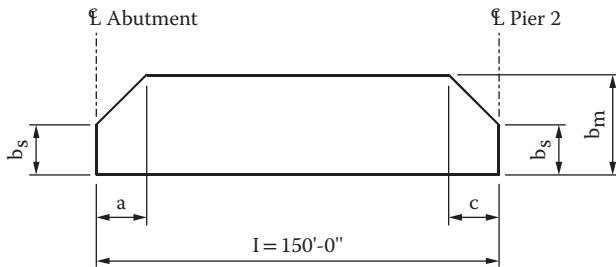


FIGURE 3.59 End span effective flange width diagram.

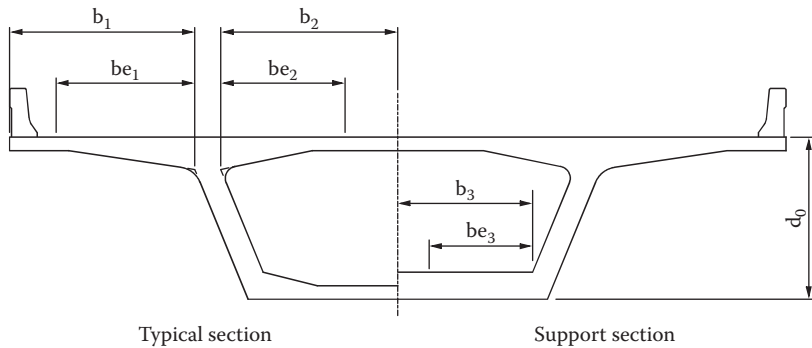


FIGURE 3.60 Typical box girder section effective flange widths.

$$b_3 = 7.34'$$

$$a = \text{the largest of } b, \text{ but not exceeding } 0.25 \times l \\ = 10.37' < 0.25 \times 150' = 37.5'$$

$$c = 0.1 \times l = 0.1 (150') = 15' 0''$$

$$l_i = 0.8 \times l = 0.1 (150') = 120'$$

	b	b/l_i	b_s/b	b_m/b	b_{se}	b_{me}
b_1	10.37'	0.086	0.8	1.0	8.3'	10.37
b_2	9.71'	0.081	0.8	1.0	7.77'	9.71'
b_3	7.34'	0.061	1.0	1.00	7.34	7.34

Obtained b_s/b and b_m/b ratios from LRFD Figure 4.6.2.6.2-2.

Effective flange: b_{me} (no reduction)

$$b_{s1e} = 8.3'$$

$$b_{s2e} = 7.77'$$

$$b_{s3e} = 7.34' \text{ (no reduction)}$$

A.2-Inner span (see Figure 3.61)

where

$$c = 0.1 \times l = 0.1 \times 200' = 20'$$

$$l_i = 0.6 \times l = 0.6 \times 200' = 120'$$

	b	b/l_i	b_s/b	b_m/b	b_{se}	b_{me}
b_1	10.37'	0.086	0.8	1.0	8.3'	10.37'
b_2	9.71'	0.080	0.8	1.0	7.77'	9.71'
b_3	7.34	0.060	1.0	1.00	7.34'	7.34'

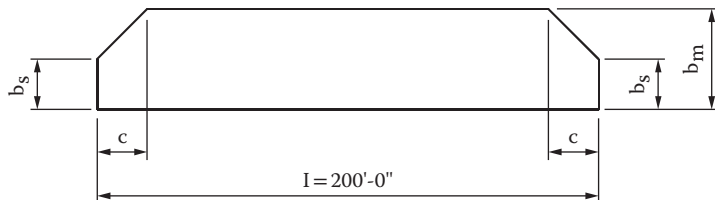


FIGURE 3.61 Inner span effective flange width diagram.

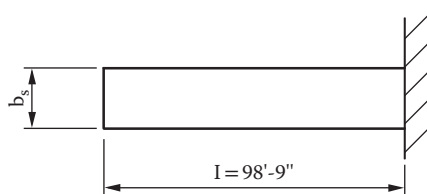


FIGURE 3.62 Cantilever span effective flange width diagram.

Effective flange: b_{me} (no reduction)

$$b_{s1e} = 8.3'$$

$$b_{s2e} = 7.77'$$

$$b_{s3e} = 7.34' \text{ (no reduction)}$$

	b	b/l_i	b_s/b	b_{se}
b_1	10.37	0.07	0.75	7.77'
b_2	9.71	0.07	0.75	7.28'
b_3	7.34	0.05	1.00	7.34'

B. During construction

B.1- Cantilever (see Figure 3.62)

$$\text{where } l_i = 1.5 \times l = 1.5 \times 98.75 = 148.125'$$

$$\text{Effective flange: } b_{s1e} = 7.77'$$

$$b_{s2e} = 7.28'$$

$$b_{s3e} = 7.34' \text{ (no reduction)}$$

3.6.5 Temperature Load

Temperature loads for superstructures consist of uniform temperature change as well as temperature gradients. A uniform temperature change of the superstructure is defined as the entire cross-section heating or cooling at the same rate. In contrast to this, a temperature gradient is defined as a vertical temperature change from top to bottom of the box. A positive temperature gradient results from solar heating of the deck surface and will cause higher temperatures in the top deck. A negative temperature gradient results from rapid cooling of deck concrete while ground temperatures may remain relatively unchanged from daytime conditions. The aforementioned gradients vary in a nonlinear manner with respect to depth of the superstructure, which requires a rather complex method of analysis to determine resulting stresses. The AASHTO LRFD Bridge Design Specifications (Article 3.12.3) adopted a temperature gradient profile (see Figure 3.63) that differs from that used by the AASHTO Guide Specifications for Thermal Effects in Concrete Bridge Superstructures (AASHTO 1989b), which is an abridged version of NCHRP Report 276.

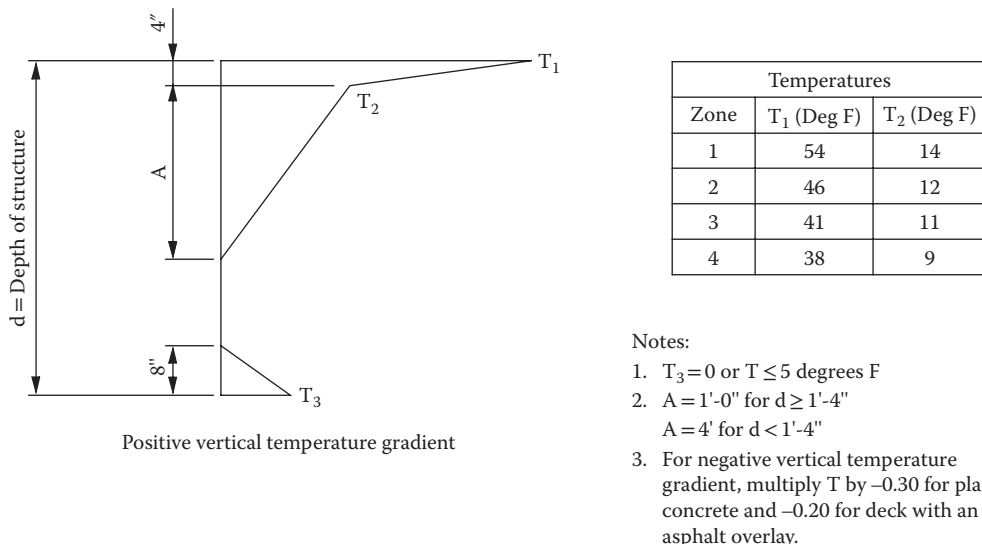


FIGURE 3.63 Vertical temperature gradient profile for segmental bridge (AASHTO LRFD Figure 3.12.3-2).

Both uniform temperature and temperature gradient are included in service limit state load combinations. Temperature gradient may be reduced by 50% if live load is present in service load combinations. For segmental bridge design only, a special load combination (LRFD Equation 3.4.1-2) for service shall be checked. This load combination has no live load; therefore 100% of the temperature gradient is included. In general, this load combination controls for segmental concrete bridges where live load force effects are small. In this example, such an area occurs at closure pours in the top of the box. Please note, for uniform temperature use a load factor of 1.0 when checking stresses, and 1.2 for structural deformations. The 1.2 factor will assure that bearing and expansion joint are not under design.

Temperature gradient is not included in strength limit state load combinations, while uniform temperature is included. Two load factors are assigned to uniform temperature in strength limit states. A factor of 0.5 is used for strength capacity calculations and 1.2 for structural deformations.

3.6.6 Time-Dependent Effect

Creep and shrinkage of concrete, including relaxation of prestressing steel are commonly referred to as *time-dependent long-term effects*. These effects are important factors that demand consideration in design of segmental bridges (see Figure 3.64). Nonlinear time-dependent deformations result in force redistribution due to changes in the statical system during the course of the construction, and continue through day 10,000 when long-term effects are considered to be diminished (see Figure 3.65).

Shrinkage, which causes shortening of concrete due to dehydration, is independent of stress (applied loads). Creep is a result of concrete deformation under permanent stress (loads) in addition to elastic deformation.

The redistribution of sectional forces due to change in statical system and creep effect can be estimated by Dischinger's equation:

$$M_f = M_{II} + (M_I - M_{II})e^{-\phi}$$

where

M_f = Final moment at day 10,000

M_I = Moment as constructed at the end of construction

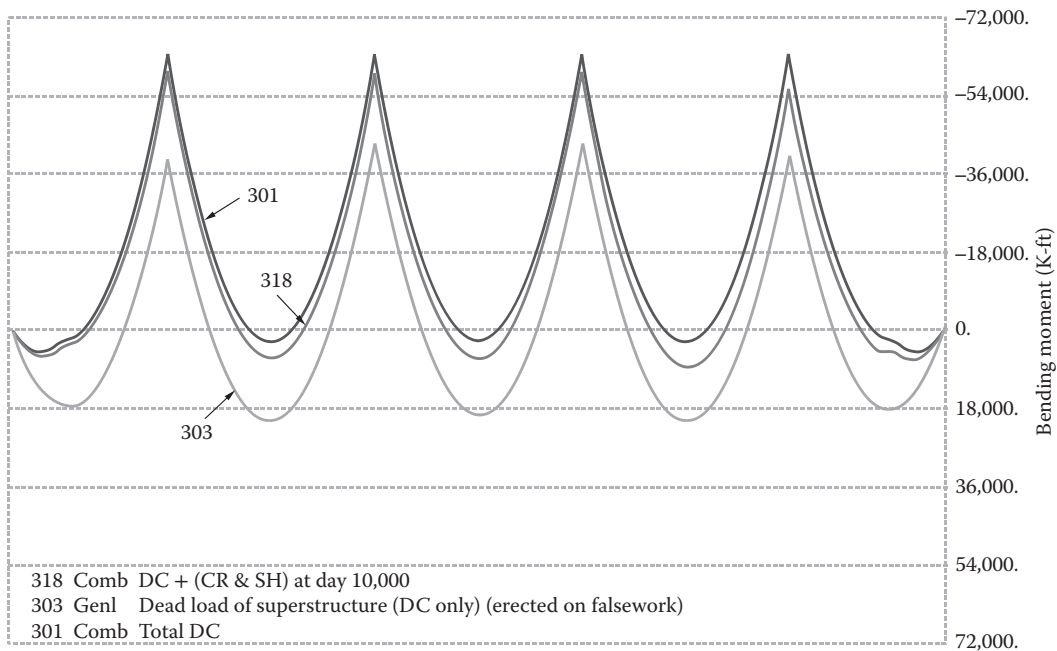


FIGURE 3.64 Superimposed final moment (diagram 318), moment (diagram 301) and moment constructed on false-work (diagram 303).

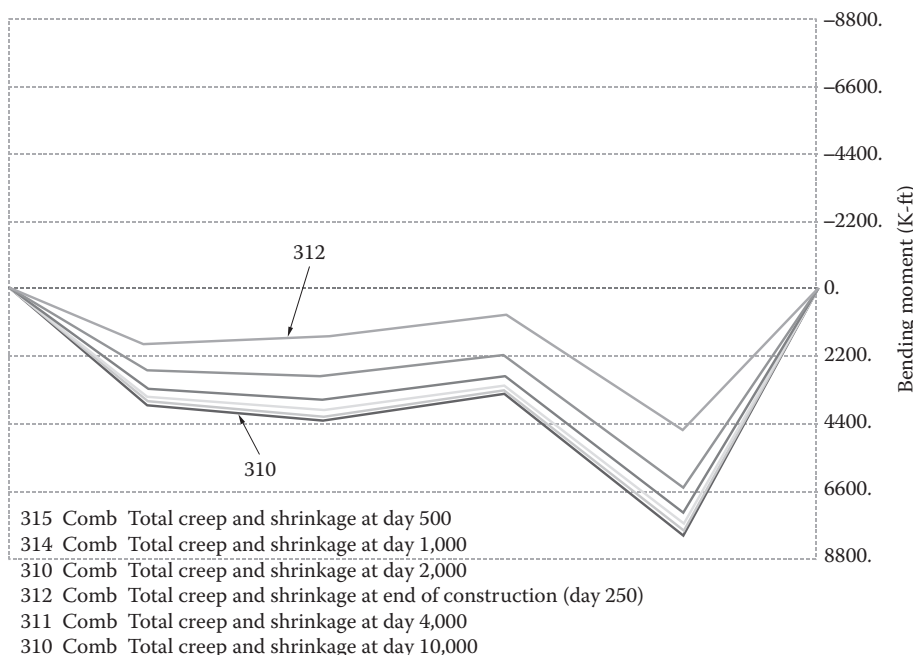


FIGURE 3.65 Development of time-dependent bending moment due to creep and shrinkage from end of construction (diagram 312) to day 10,000 (diagram 310).

M_{II} = Moment assuming the bridge is constructed on false work

ϕ = Creep coefficient

M_{cr} = Moment due to creep effect

The above equation can be rewritten to obtain M due to creep effects: $M_{cr} = (1 - e^{-\phi}) (M_{II} - M_P)$.

Steel relaxation is the loss of tension in prestressing steel under constant length and temperature over a period of time. To prevent excessive relaxation loss in segmental bridges, low-relaxation strands are used. The low-relaxation strands meet the ASTM Standard requirement that relaxation loss after 1000 hours under 70°F is no more than 2.5% when initially stressed to 70% guaranteed ultimate tensile strength (GUTS) and not more than 3.5% when stressed to 80% GUTS.

Although AASHTO LRFD Bridge Design Specifications allow creep and shrinkage effects to be evaluated using the provisions of CEB-FIP Model Code or ACI 209, for segmental bridge design, the CEB-FIP Model Code provisions are commonly used. This design example utilizes the CEB-FIP Model Code 1990.

3.6.7 Secondary Forces

Secondary forces are internal forces generated as a result of applied deformations or imposed loads to statically indeterminate systems.

Several recognized secondary forces in segmental bridge design are as follows:

- Secondary forces due to primary posttensioning (see Figures 3.66 and 3.67)
- Secondary forces due to construction process such as locked-in forces (see Figures 3.66 and 3.67)
- Secondary forces due to creep and shrinkage effects
- Secondary forces due to temperature loads (uniform and gradient temperature)
- Secondary forces due to support settlement

All of the above secondary forces are included in service limit state load combinations without exception. However, inclusion of different types of secondary forces in strength limit state load combinations may differ from code to code.

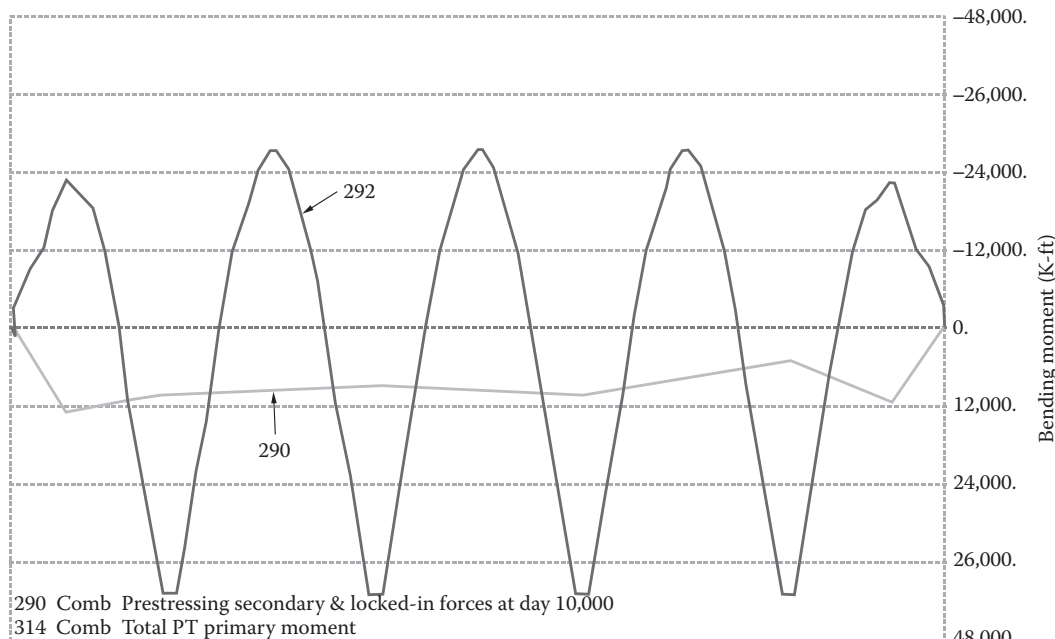


FIGURE 3.66 Superimposed of PT primary moment (292) and secondary moment and locked-in forces (290) at day 10,000.

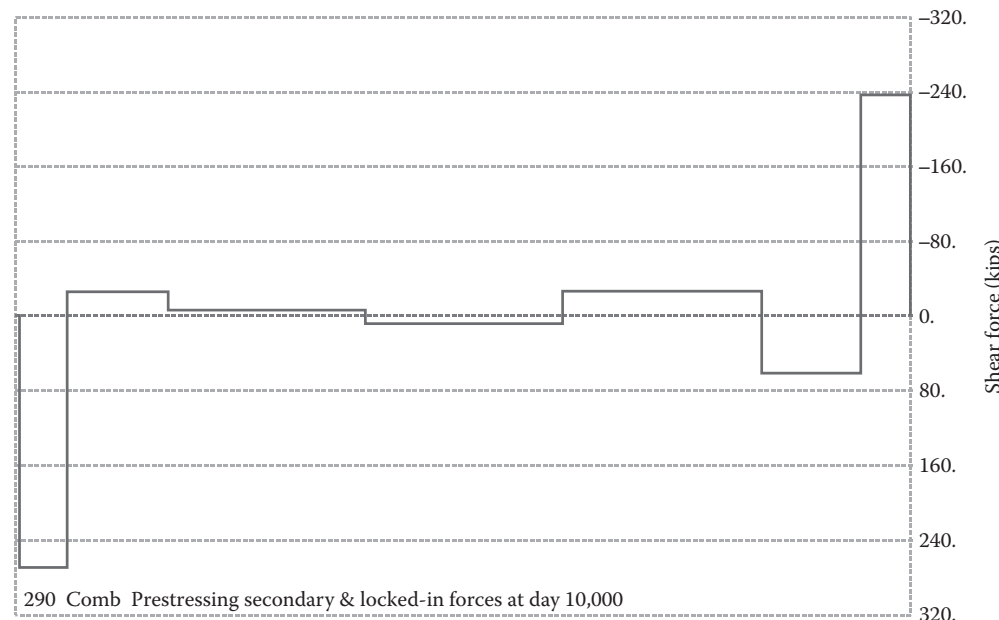


FIGURE 3.67 PT Secondary and locked-in shear forces at day 10,000.

Under AASHTO LRFD 6th Edition (2012), the locked-in forces (EL) are separated from prestressing secondary forces (PS), unlike in the previous editions. For strength limit state load combinations, both EL and PS have a load factor of 1.0, while dead loads (DC) have a load factor of 0.9 (minimum) and 1.2 (maximum). In most segmental bridge software, dead loads are not distinguished from locked-in forces. Owing to many construction stages during the erection process, it is possible to accumulate large quantities of dead load cases and locked-in force load cases. Once the construction process is complete, back-tracking to separate dead load cases from locked-in load cases creates complex book-keeping, and serves of little benefit to end results. EL load factor should follow DC, since it modifies the final design forces due to many construction stages, unlike other types of structures such as steel.

Secondary forces due to temperature gradient are not included in strength limit state load combinations, while support settlement secondary forces are to be considered on a project-specific basis.

Uniform-temperature secondary forces, including creep and shrinkage effects, are included in strength limit state load combinations with a load factor of 0.5.

3.6.8 Summary of Design Forces

The summary of all design forces are presented in the form of maximum design forces envelopes as shown in Figures 3.68 and 3.69.

3.6.9 Service Limit State Design

Service limit state design of the superstructure requires a stress check for three load combinations. These consist of Service Limit State I, Service Limit State III, and a special load case for segmental bridges. Service Limit State III allows tension to be evaluated using a 0.8 live load factor, while Service Limit State I checks compression with a 1.0 live load factor. In combination with these three limit states, a nonlinear temperature gradient will be applied. For Service Limit States I and III, which use maximum live load influence, LRFD recommends a factor of 0.5 for temperature gradient in lieu of project-specific data. For the special load case applying to segmental bridges, temperature gradient receives a load factor of 1.0, since live load is not included. For a description of this load case, see LRFD Equation 3.4.1-2.

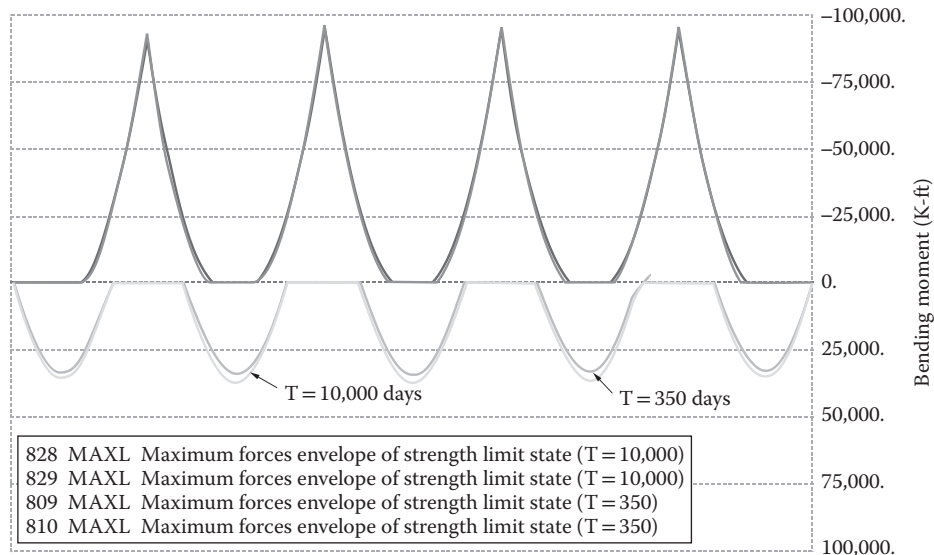


FIGURE 3.68 Maximum bending moments envelope for strength limit state load combinations.

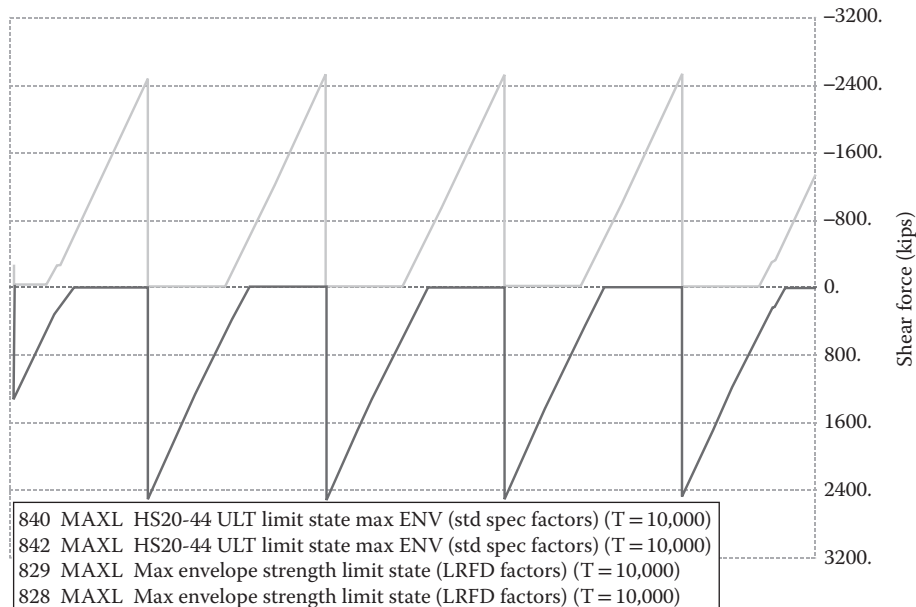


FIGURE 3.69 Maximum shear forces envelop for strength limit state load combinations.

It is important to note that, although the special load case may not control at locations where large amounts of posttensioning are present, it may indeed control at locations where live load effects are small or at locations outside the precompressed tensile zone. Such locations for this example include tension in the top of closure pours and compression in the top of the box at pier locations. For this example, tendons were added at the top of the box crossing the closure pour to counteract the tension produced by the bottom of the box being warmer than the top.

3.6.10 Principal Tension Stress Check

In order to control diagonal tension cracks from developing in the webs adjacent to pier support at service limit state load combinations for shear and torsion, principal tension stresses should be checked. Stresses are calculated using Mohr's circle to determine the principle tension (see Figure 3.70). If the allowable tensile capacity of the concrete is exceeded, diagonal tension cracks may be anticipated. Typically, the maximum principal tension stress is limited from $3\sqrt{f'_c}$ to $4\sqrt{f'_c}$ (psi). AASHTO LRFD limits the principal tension stresses to a maximum value of $3.5\sqrt{f'_c}$ (psi) at service loads (Tables 5.9.4.1.2-1 and 5.9.4.2.2-1) and $4\sqrt{f'_c}$ (psi) during construction (Table 4.14.2.3.3-1) for segmental bridges. Although this check is only required at the neutral axis of the web, it is recommended that the top slab and web interface location be investigated as well. For this example, $3.5\sqrt{f'_c}$ tension is used as a maximum allowable value under service loading.

Since principal stress is a function of longitudinal, vertical, and shear stress, it is necessary to determine concurrent moments for the maximum live load shear. It should be noted that high principle stresses commonly occur at interior pier locations, and the HL-93 live load moment corresponding to shear should only use one truck, rather than two, as used in calculating the negative moment at interior piers. The live load also has a load factor of 0.8 similar to Service III Limit State or it would be practically impossible to satisfy principal stresses while the extreme fiber could be in tension.

The maximum principal stresses in this example occurred near the interior piers at the top of the web for final conditions. From analysis at the critical section, the maximum principle tension stress was approximately $4.5\sqrt{f'_c}$; larger than the previously discussed limit. For this particular example, vertical posttensioning bars are used to control the principal tension stress. Calculations show that three 1 $\frac{1}{4}$ " diameter bars, are needed in each web to the reduce principle tension to an acceptable value (see Figure 3.71). The overstress could also be addressed by modifying the cross section (web thickness) or adding more longitudinal compressive stress (additional strands). The solution presented was deemed acceptable since only a small number of segments require vertical posttensioned bars can be seen in Figure 3.72.

Principal tensile stress check

$$\nu = \frac{VQ}{Ib}$$

where

V = Vertical shear force

Q = First moment of an area with respect to CG of the section

I = Moment of inertia about CG of the section

b = Perpendicular web thickness

$$f_1 = \frac{\sigma_x + \sigma_y}{2} - \frac{1}{2}\sqrt{4\nu^2 + (\sigma_x - \sigma_y)^2}$$

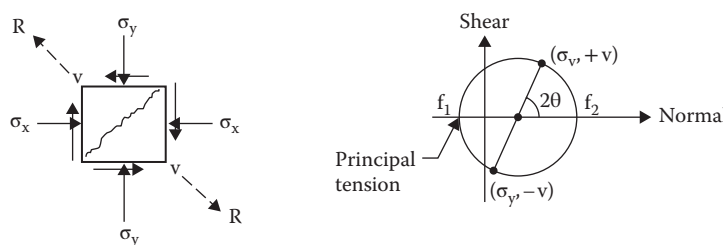


FIGURE 3.70 Principal stresses and Mohr's Circle.

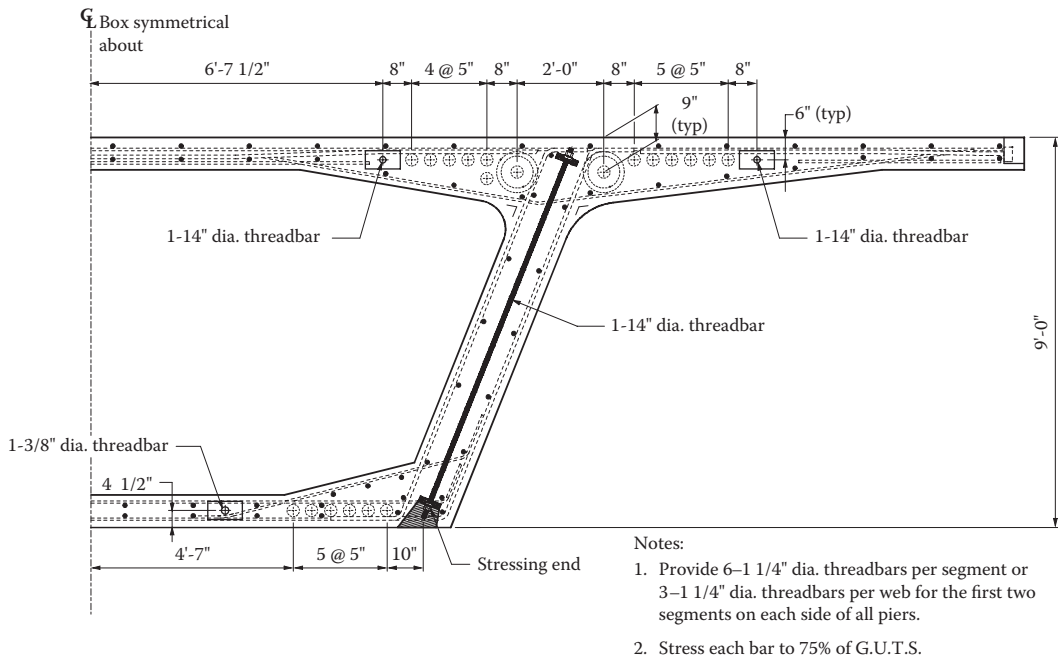


FIGURE 3.71 Vertical PT bar in the web.

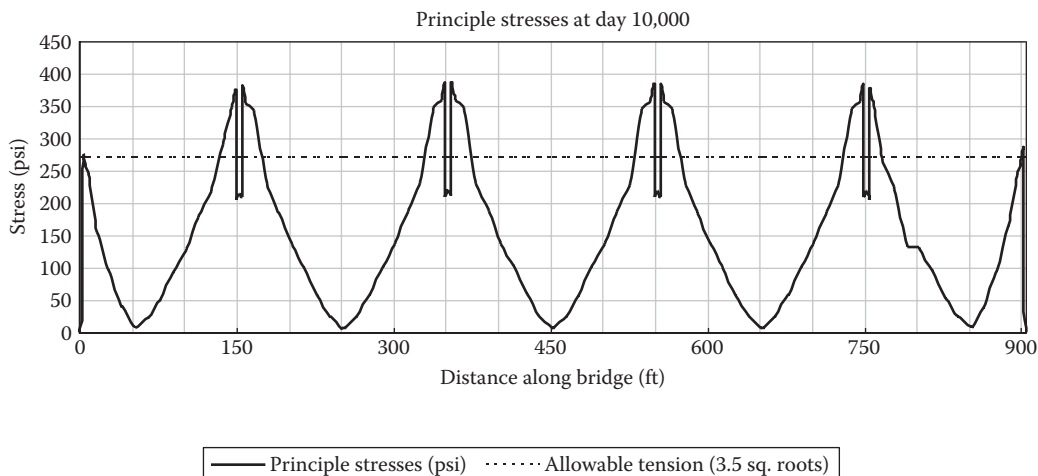


FIGURE 3.72 Principal tension stress at service limit state load combinations along the bridge.

where compression stress is positive

For $\sigma_y = 0$: (at sections where no vertical web posttensioning is present)

$$v_a = \sqrt{f_a \times (f_a + f)}$$

where

f_a = Allowable principal tension

f = Compressive stress at level on web under investigation

3.6.11 Flexural Strength Check

Once service stresses are satisfied in the superstructure, the limit state of flexural strength must be checked. For most cases with superstructures, Strength Limit State I is the only load combination that needs to be considered. However, for longer spans where the ratio of the dead load to live load is large, Strength Limit State IV may control. For this example, the magnitudes of live load force effects are greater than a 25% difference in structural component dead load. Hence, Strength Limit State IV will not control.

The load factors for support settlement and temperature gradient are not provided by LRFD; they are to be determined on a project-specific basis. In lieu of project specific data, LRFD recommends using a load factor of 0.0 for the temperature gradient. With regard to the temperature gradient, the loads imposed result from restrained deformations and should disappear if the reinforcement starts to yield at ultimate. Owing to this occurrence, the temperature gradient is not considered in strength limit states. Also, support settlements are not considered in this example.

The LRFD specifications, Article 5.7.3.3.2, require minimum reinforcement in order to prevent flexure brittle failure, especially in deeper girder where a very small amount of flexural reinforcement is required.

3.6.12 Shear and Torsion Design

3.6.12.1 AASHTO LRFD Shear and Torsion General Design Procedure

The modified compression field theory (MCFT) was developed by Collins and Mitchell (Collins and Mitchell, 1991) in Canada. The MCFT for shear and torsion design was adopted for the first time by the *Ontario Highway Bridge Design Code* in 1991. The *AASHTO LRFD Bridge Design Specifications* (AASHTO 2012) also adopted the new method of shear and torsion design in addition to traditional ACI and AASHTO *Guide Specifications for segmental bridge* empirical equations. Unlike previous empirical equations, MCFT is a rational approach that gives physical significance to the parameters being calculated. The MCFT is based on variable-angle truss instead of a 45° truss model. Owing to this truss model, the longitudinal reinforcement becomes an important element of shear design. Prior to 2008 *AASHTO LRFD* Interim, the general procedure for concrete shear capacity contribution required iteration to determine α and θ parameters. Currently, AASHTO provides noniterative algebraic expressions. The iterative procedure has been moved to Appendix B5 and it is acceptable as an alternative to General Procedure Section 5.8.3.4.2. *AASHTO LRFD* also allows V_c to be calculated using a simplified procedure as per Section 5.8.3.4.3 compatible with *ACI Code 318-05* and *AASHTO Standard Specification*. For segmental box girder bridges, shear and torsion design procedure of Section 5.8.6 may be applied in lieu of Section 5.8.3.

3.6.12.1.1 Sections Subjected to Shear Only

In a box girder, the stresses due to shear and torsion are additive on one side of the web and counteract each other on the other side. Therefore, the final transverse web reinforcement should be based on the summation of reinforcement due to shear and torsion.

Normally, the loading that produces the maximum shear is not the same loading which produces the maximum torsion. Therefore, it is conservative to design on the basis of the maximum shear and maximum torsion. However, it is sufficient to design using the maximum shear with its associated torsion and the maximum torsion with its associated shear.

For shear design, the following basic relationship must be satisfied at each section:

$$V_u \leq \phi V_n$$

where

V_n is determined as the lesser of

$$V_n = V_c + V_s + V_p$$

(LRFD 5.8.3.3-1)

$$V_n = 0.25 f'_c b_v d_v + V_p \quad (\text{LRFD 5.8.3.3-1})$$

$$V_c = 0.0316 \beta \sqrt{f'_c} b_v d_v \quad (\text{LRFD 5.8.3.3-3})$$

The value of β at a given section is obtained from equation:

$$\beta = \frac{4.8}{1 + 750 \epsilon_s} \quad (\text{LRFD 5.8.3.4.2-1})$$

where β is a factor indicating the ability of diagonally cracked concrete to transmit tension and shear, and ϵ_s is the net longitudinal tensile strain in the section at the centroid of the tension reinforcement. Tensile strain ϵ_s may be determined by equation:

$$\epsilon_s = \frac{M_u/d_v + 0.5N_u + |V_u - V_p| - A_{ps}f_{po}}{E_s A_s + E_p A_{ps}} \quad (\text{LRFD 5.8.3.4.2-4})$$

The contribution of transverse reinforcement is calculated using equation:

$$V_s = \frac{A_v f_y d_v (\cot \theta + \cot \alpha) \sin \alpha}{s} \quad (\text{LRFD 5.8.3.3-4})$$

where α is the angle of inclination of transverse reinforcement and θ is the angle of inclination of diagonal compressive stresses as determined by equation:

$$\theta = 29 + 3500 \epsilon_s \quad (\text{LRFD 5.8.3.4.2-3})$$

3.6.12.1.2 Longitudinal Reinforcement

One of the cornerstone principles of modified compression field theory is the recognition that shear causes tension in longitudinal steel. At each section of the beam not subjected to torsion, the capacity of the longitudinal reinforcement must be checked for sufficiency. This relationship is expressed as follows:

$$A_s f_y + A_{ps} f_{ps} \geq \left[\frac{|M_u|}{d_v \phi_f} + 0.5 \frac{N_u}{\phi_c} + \left(\left| \frac{V_u}{\phi_v} - V_p \right| - 0.5 V_s \right) \cot \theta \right] \quad (\text{LRFD 5.8.3.5-1})$$

3.6.12.1.3 Sections Subjected to Combined Shear and Torsion

For sections subjected to combined shear and torsion, refer Article 5.8.3.6. Strain should be calculated taking into account the combination of these effects. Shear stress, longitudinal reinforcing, and area of shear reinforcing should also be modified.

3.6.12.2 AASHTO Shear and Torsion Design Procedure for Segmental Box Girder Bridges

Refer to LRFD Article 5.8.6

The nominal shear resistance is the algebraic sum of the contributing components:

$$V_n = V_c + V_s + V_p$$

In sections where the effects of torsion may be neglected, the nominal shear resistance is limited to

$$V_n = 0.379 \sqrt{f'_c} b_v d \quad (\text{LRFD 5.8.6.5-2})$$

The shear provided by concrete section is determined as follows:

$$V_c = 0.0632 K \sqrt{f'_c} b_v d \quad (\text{LRFD 5.8.6.5-3})$$

where K is the stress variable parameter expressed by equation:

$$K = \sqrt{1 + \frac{f_{pc}}{0.0632 \sqrt{f'_c}}} \leq 2.0 \quad (\text{LRFD 5.8.6.3-3})$$

where

f_{pc} = Compressive stress in concrete after allowance for all prestress losses at the centroid of cross-section resisting shear

f'_c = Specified concrete strength

Shear provided by transverse reinforcement is determined from equation:

$$V_s = \frac{A_v f_y d}{s} \quad (\text{LRFD 5.8.6.5-4})$$

A_v = Area of transverse reinforcement within a distance s (in²)

Torsional effects is investigated in sections where factored torsional moment at the section is greater than the torsional cracking moment:

$$T_u \geq \phi T_{cr} \quad (\text{LRFD 5.8.6.3-1})$$

where

T_u = Factored torsional moment (kip-ft)

T_{cr} = Torsional cracking moment (kip-ft)

Torsional cracking moment T_{cr} is given by equation:

$$T_{cr} = 0.0632 K \sqrt{f'_c} 2 A_o b_e \quad (\text{LRFD 5.8.6.3-2})$$

where

A_o = Area enclosed by shear flow path (in²)

b_e = Minimum effective shear flow web or flange width to resist torsional stresses (in)

When torsional effects are considered, the longitudinal and transverse reinforcement must satisfy the following conditions:

$$T_u \leq \phi T_n \quad (\text{LRFD 5.8.6.4-1})$$

where T_n is the nominal torsional resistance of transverse reinforcement calculated as follows:

$$T_n = \frac{2 A_o A_t f}{s} \quad (\text{LRFD 5.8.6.4-2})$$

The longitudinal reinforcement should satisfy:

$$A_l = \frac{T_n p_h}{2A_o f_y} \quad (\text{LRFD 5.8.6.4-3})$$

where

A_l = Total additional longitudinal reinforcement required for torsion (in²)

p_h = Perimeter of centerline outermost continuous closed transverse reinforcement (in)

Additionally the section is sized to satisfy:

$$\left(\frac{V_u}{b_v d} \right) + \left(\frac{T_u}{2A_o b_e} \right) \leq 0.474 \sqrt{f'_c} \quad (\text{LRFD 5.8.6.5-5})$$

3.6.12.2.1 Design Examples (Using LRFD Modified Compression Field Theory)

3.6.12.2.1.1 Node Number: 41 (At Critical Shear Section) Ultimate moment: $M_u = 82,091$ kip·ft (negative moment, bottom slab is in compression)

$$V_u = 2,391 \text{ kip}$$

$\phi = 0.90$ for shear

Nominal shear resistance:

$$V_n = V_c + V_s + V_p$$

or

$$V_n = 0.25 f'_c b_v d_v + V_p$$

where

$f'_c = 6$ ksi, compression strength of concrete

$b_v = 32$ in, effective web width

$d_v = 108 - 6 - 17.1/2 = 93.4$ in = 7.79 ft > $\text{Max} \{ 0.9(108 - 6), 0.72 \times 108 \}$,
effective shear depth

$$V_p = 0$$

$$V_n = 0.25 \times 6 \times 32 \times 93.4 = 4,483 \text{ kip}$$

$$V_n = 4,483 \text{ kip} > V_u / \phi = 2,391 / 0.9 = 2,657 \text{ kip}$$

Cross-section dimension is sufficient.

Concrete contribution:

$$V_c = 0.0316 \beta \sqrt{f'_c} b_v d_v$$

Transverse reinforcement contribution:

$$V_s = \frac{A_v f_y d_v \cot \theta}{s}$$

@Seismicisolation

where

- β = factor indicating the ability of diagonally cracked concrete to transmit tension
 θ = angle of inclination of diagonal compressive stresses

Step 1: Calculate the net longitudinal tensile strain in the section at the centroid of the tension reinforcement:

$$\begin{aligned}\epsilon_s &= \frac{\frac{M_u}{d_v} + 0.5N_u + |V_u - V_p| - A_{ps}f_{ps}}{E_s A_s + E_p A_{ps}} = \frac{\frac{82,091}{7.79} + 2,391 - 67.7 \times 189}{28,500 \times 67.7} \\ &= \frac{133.7}{1,929,450} = 0.00007\end{aligned}$$

Step 2: Compute the value of β :

$$\beta = \frac{4.8}{1 + 750\epsilon_s} = \frac{4.8}{1 + 750 \times 0.00007} = 4.53$$

Step 3: Compute the value of θ :

$$\theta = 29 + 3,500\epsilon_s = 29 + 3,500 \times 0.00007 = 29.24^\circ$$

Step 4: Compute the contribution of concrete steel V_c :

$$\begin{aligned}V_c &= 0.0316\beta\sqrt{f'_c b_v d_v} \\ &= 0.0316 \times 4.53 \sqrt{6 \times 32 \times 93.4} = 1,048 \text{ kip}\end{aligned}$$

$$\begin{aligned}V_s &= V_n - V_c = V_u / \phi - V_c \\ &= 2,391 / 0.9 - 1,048 = 1,609 \text{ kip} = 805 \text{ kip/web}\end{aligned}$$

$$\begin{aligned}\frac{A_v}{s} &= \frac{V_s}{f_y d_v \cot \theta} \\ &= \frac{805}{60 \times 93.4 \times \cot 29.24^\circ} = 0.08 \text{ in}^2/\text{in} = 0.96 \text{ in}^2/\text{ft}\end{aligned}$$

Use double #6 bars at 9" centers per web $A_v = 1.17 \text{ in}^2/\text{ft}$

3.6.12.2.1.2 Longitudinal Reinforcement For sections not subjected to torsion, longitudinal reinforcement needs to satisfy:

$$A_s f_y + A_{ps} f_{ps} \geq \left[\frac{M_u}{d_v \phi} + 0.5 \frac{N_u}{\phi} + \left(\frac{V_u}{\phi} - 0.5 V_s - V_p \right) \cot \theta \right] \quad (\text{LRFD 5.8.3.5-1})$$

$\phi = 0.95$ for flexure; (Table 5.5.4.2.2-1)

$\phi = 0.90$ for shear; (Table 5.5.4.2.2-1)

$$A_s f_y + A_{ps} f_{ps} = 0 \times 0 + 67.7 \times 253 = 17,136 \text{ kip}$$

$$V_s = \frac{A_v f_y d_v \cot \theta}{s} = \frac{2 \times 0.44 \times 60 \times 93.4 \times \cot(29.24)}{9} \times 2 = 1,958 \text{ kip}$$

$$\begin{aligned} & \frac{M_u}{d_v \phi} + 0.5 \frac{N_u}{\phi} + \left(\frac{V_u}{\phi} - 0.5 V_s - V_p \right) \cot \theta \\ &= \frac{82,091}{7.79 \times 0.95} + 0 + \left(\frac{2,391}{0.90} - 0.5 \times 1,958 - 0 \right) \times \cot 29.24^\circ \\ &= 13,909 \text{ kip} \end{aligned}$$

Therefore, the condition (5.8.3.5-1) is satisfied.

3.6.12.2.1.3 Node Number: 29 (At Section 60 Feet from the Face of Diaphragm) Ultimate moment: $M_u = 20,816$ kip-ft (positive moment, top slab is in compression)

$$V_u = 1,087 \text{ kip}$$

$$\phi = 0.90$$

Nominal shear resistance:

$$V_n = V_c + V_s + V_p$$

or

$$V_n = 0.25 f'_c b_v d_v + V_p$$

where

$f'_c = 6$ ksi, compression strength of concrete

$b_v = 32$ in, effective web width

$d_v = 108 - 5 - 2.6/2 = 101.7$ in = 8.48 ft > $\text{Max}\{0.9(108 - 5), 0.72 \times 108\}$, effective shear depth;

$$V_p = 0$$

$$V_n = 0.25 \times 6 \times 32 \times 101.7 = 4,882 \text{ kip}$$

$$V_n = 4,882 \text{ kip} > V_u / \phi = 1,087 / 0.9 = 1,208 \text{ kip}$$

Cross-section dimensions are sufficient

Concrete contribution:

$$V_c = 0.0316 \beta \sqrt{f'_c} b_v d_v$$

Transverse reinforcement contribution:

$$V_s = \frac{A_v f_y d_v \cot \theta}{s}$$

where

- β = Factor indicating ability of diagonally cracked concrete to transmit tension
 θ = Angle of inclination of diagonal compressive stresses

Step 1: Calculate the net longitudinal tensile strain in the section at the centroid of the tension reinforcement:

$$\begin{aligned}\varepsilon_s &= \frac{\frac{M_u}{d_v} + 0.5N_u + |V_u - V_p| - A_{ps}f_{po}}{E_s A_s + E_p A_{ps}} = \frac{\frac{20,816}{8.48} + 1,087 - 19.1 \times 189}{28,500 \times 19.1} \\ &= \frac{-68.2}{544,350} = -0.00013 \rightarrow \varepsilon_s = 0\end{aligned}$$

Step 2: Compute the value of β :

$$\beta = \frac{4.8}{1 + 750\varepsilon_s} = \frac{4.8}{1 + 750 \times 0.0} = 4.8'$$

Step 3: Compute the value of θ :

$$\theta = 29 + 3,500\varepsilon_s = 29 + 3,500 \times 0.0 = 29.0^\circ$$

Step 4: Compute the contribution of concrete steel V_c :

$$\begin{aligned}V_c &= 0.0316\beta\sqrt{f'_c}b_v d_v \\ &= 0.0316 \times 4.8\sqrt{6} \times 32 \times 101.7 = 1,209 \text{ kip}\end{aligned}$$

$$V_u/\phi = 1,087/0.9 = 1,207 \text{ kip} \equiv V_c$$

$$\text{Minimum reinforcing } A_v = 0.0316\sqrt{f'_c}b_v \frac{s}{f_y} = 0.0316\sqrt{6} \times 16 \times \frac{12}{60} = 0.248 \text{ in}^2/\text{ft}$$

Conservatively use double #5 at 18" centers $A_v = 0.413 \text{ in}^2/\text{ft}$

$$V_s = \frac{A_v f_y d_v \cot \theta}{s} = \frac{2 \times 0.413 \times 60 \times 101.7 \times \cot 29^\circ}{12} \times 2 = 1,515.5 \text{ kip}$$

3.6.12.2.1.4 Longitudinal Reinforcement For sections not subjected to torsion, longitudinal reinforcement needs to satisfy:

$$A_s f_y + A_{ps} f_{ps} \geq \left[\frac{M_u}{d_v \phi} + 0.5 \frac{N_u}{\phi} + \left(\frac{V_u}{\phi} - 0.5 V_s - V_p \right) \cot \theta \right] \quad (\text{LRFD 5.8.3.5-1})$$

$\phi = 0.95$ for flexure; (Table 5.5.4.2.2-1)

$\phi = 0.90$ for shear; (Table 5.5.4.2.2-1)

$$A_s f_y + A_{ps} f_{ps} = 0 \times 0 + 19.1 \times 268 = 5,118 \text{ kip}$$

$$\begin{aligned}
 & \frac{M_u}{d_v\phi} + 0.5 \frac{N_u}{\phi} + \left(\frac{V_u}{\phi} - 0.5V_s - V_p \right) \cot \theta \\
 &= \frac{20,816}{8.48 \times 0.95} + 0 + \left(\frac{1,087}{0.90} - 0.5 \times 1,515.5 - 0 \right) \times \cot 29^\circ \\
 &= 3,396 \text{ kip}
 \end{aligned}$$

Therefore, the condition (5.8.3.5-1) is satisfied.

3.6.12.2.2 Design Examples (Using AASHTO LRFD Section 5.8.6)

3.6.12.2.2.1 Node Number: 41 (At Critical Shear Section)

$$V_u = 2,391 \text{ kip}$$

$\phi = 0.90$ for shear

$f_{pc} = 906$ psi at neutral axis

$f'_c = 6$ ksi, compression strength of concrete

$b_v = 32$ in, effective web width

Concrete contribution:

$$V_c = 0.0632K\sqrt{f'_c}b_w d$$

$$K = \sqrt{1 + \frac{f_{pc}}{0.0632\sqrt{f'_c}}} \leq 2.0$$

$$K = \sqrt{1 + \frac{0.9}{0.0632\sqrt{6}}} = 2.62 \Rightarrow 2.0$$

Note: Tensile stress at the extreme fiber under factored loads with effective prestressing was checked to insure it was under $6\sqrt{f'_c}$.

$$V_c = 2 \times 0.0632\sqrt{6} \times 32 \times 102 = 1,011 \text{ kip}$$

Transverse reinforcement contribution:

$$\begin{aligned}
 V_s &= V_n - V_c = V_u/\phi - V_c \\
 &= 2,391/0.90 - 1,011 = 1,646 \text{ kip} = 823 \text{ kip/web}
 \end{aligned}$$

$$\begin{aligned}
 \frac{A_v}{s} &= \frac{V_s}{f_y d} \\
 &= \frac{823}{60 \times 102} = 0.134 \text{ in}^2/\text{in} = 1.61 \text{ in}^2/\text{ft}
 \end{aligned}$$

Use double #6 bar at 6" centers per web $A_v = 1.76 \text{ in}^2/\text{ft}$

$$\begin{aligned}
 V_s &= \frac{A_v f_y d}{s} \\
 V_s &= \frac{2 \times 1.76 \times 60 \times 102}{12} = 1,795 \text{ kip}
 \end{aligned}$$

Ultimate shear resistance:

$$\phi V_n = \phi(V_c + V_s + V_p)$$

$$V_p = 0$$

$$\phi V_n = 0.9(1,011 + 1,795) = 2,525 \text{ kip} > V_u = 2,391 \text{ kip}$$

Check maximum nominal shear resistance:

$$V_n = V_c + V_s + V_p \leq 0.379 \sqrt{f'_c} b_v d_v$$

$$V_n = 1,011 + 1,795 = 2,806 \text{ kip}$$

$$0.379 \sqrt{f'_c} b_v d_v = 0.379 \times \sqrt{6} \times 32 \times 103 = 3,060 \text{ kip}$$

The section is adequate to carry the factored shear force.

3.6.12.2.2 Node Number: 29 (At Section 60 Feet from the Face of Diaphragm)

$$V_u = 1,087 \text{ kip}$$

$\phi = 0.90$ for shear

$f_{pc} = 533$ psi at neutral axis

$f'_c = 6$ ksi, compression strength of concrete

$b_v = 32$ in, effective web width

Concrete contribution:

$$V_c = 0.0632 K \sqrt{f'_c} b_w d$$

$$K = \sqrt{1 + \frac{f_{pc}}{0.0632 \sqrt{f'_c}}} \leq 2.0$$

$$K = \sqrt{1 + \frac{0.533}{0.0632 \sqrt{6}}} = 2.11 \Rightarrow 2.0$$

Note: Tensile stress at the extreme fiber under factored loads with effective prestressing was checked to insure it was under $6\sqrt{f'_c}$.

$$V_c = 2 \times 0.0632 \sqrt{6} \times 32 \times 103 = 1,021 \text{ kip}$$

Transverse reinforcement contribution:

$$\begin{aligned} V_s &= V_n - V_c = V_u / \phi - V_c \\ &= 1,087 / 0.90 - 1,021 = 187 \text{ kip} = 93 \text{ kip/web} \end{aligned}$$

$$\begin{aligned}\frac{A_v}{s} &= \frac{V_s}{f_y d} \\ &= \frac{93}{60 \times 103} = 0.015 \text{ in}^2/\text{in} = 0.18 \text{ in}^2/\text{ft}\end{aligned}$$

$$\text{Minimum reinforcing } A_v = \frac{50b_w s}{f_y} = \frac{50 \times 16 \times 12}{60,000} = 0.16 \text{ in}^2/\text{ft}$$

Minimum reinforcing does not control. However, conservatively use double #5 at 18 in centers
 $A_v = 0.413 \text{ in}^2/\text{ft}$

$$V_s = \frac{V_s f_y d}{s} = \frac{2 \times 0.413 \times 60 \times 103}{12} = 425 \text{ kip}$$

Ultimate shear resistance:

$$\phi V_n = \phi(V_c + V_s + V_p)$$

$$V_p = 0$$

$$\phi V_n = 0.9(1,021 + 425) = 1,301 \text{ kip} > V_u = 1,087 \text{ kip}$$

Check maximum nominal shear resistance:

$$V_n = V_c + V_s + V_p \leq 0.379 \sqrt{f'_c b_v d_v}$$

$$V_n = 1,021 + 425 = 1,446 \text{ kip}$$

$$0.379 \sqrt{f'_c b_v d_v} = 0.379 \times \sqrt{6} \times 32 \times 103 = 3,060 \text{ kip}$$

The section is adequate to carry the factored shear force.

3.7 Construction Stage Analysis

3.7.1 Stability during Construction

A stability analysis during construction is one of the design criteria for segmental bridge design. During construction of a segmental bridge, the boundary conditions are constantly changing from the beginning of construction to the end. At all times during construction, the structure and foundation must be in a stable state and have ample safety factors against material failure, overturning, and buckling. Stability analysis, therefore, becomes an important design issue due to the lower degree of redundancy and the load imbalance of the structure during this period.

A free cantilever structure is one example that requires a stability check during erection of a segment (see Figure 3.73). The longer the span length, the larger are the unbalanced loads. In many cases, temporary supports are required to handle the load imbalance during erection. In addition to balanced cantilever conditions, other partially completed structures may also need to be investigated.

It is important for the engineer to specify the design plans and the construction loads that were assumed during design associated with the construction method selected. It is common practice that at least one construction method be designed and shown in the plans. The limits of these loads

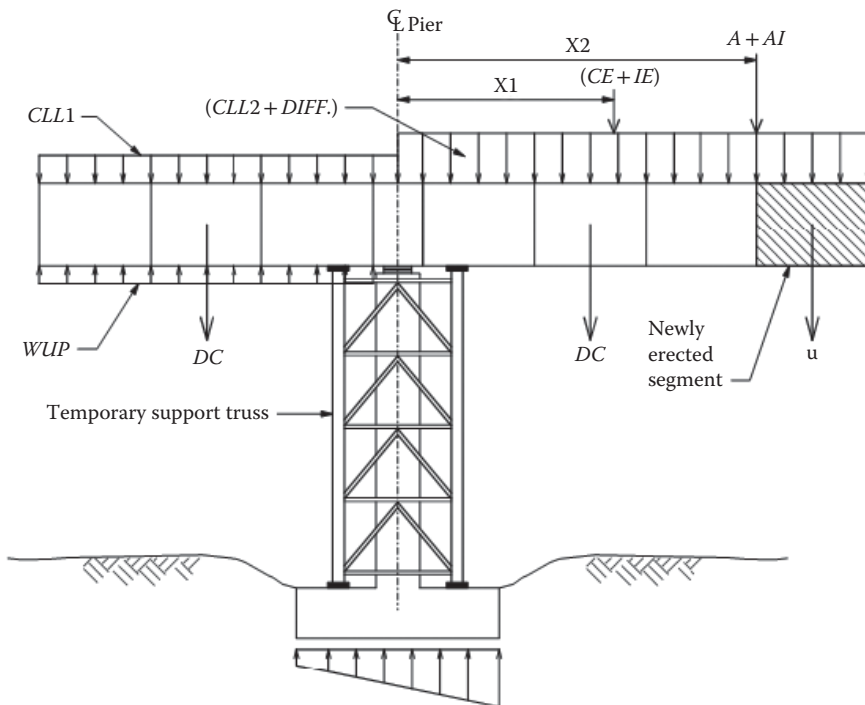


FIGURE 3.73 Unbalanced construction load for balanced cantilever construction.

and locations where loads are applied on the structure should also be shown. Additionally, the engineer's construction schemes should be clearly stated, including approximate support reactions due to construction equipment. The stresses caused by critical construction loads and strengths of the members should also be checked. Figures 3.74 through 3.76 show critical construction loads for this example.

The stability analysis specifications were originally covered in Article 7.4 of the *AASHTO Guide Specifications for Design and Construction of Segmental Concrete Bridges, Second Edition* (AASHTO 1999). Later, those specifications were adopted by the *AASHTO LRFD Bridge Design Specifications*, under Article 5.14.2.3. Table 3.1 shows service limit state load combinations during construction and its associated stress limit.

The following construction loads should be considered in a stability analysis:

DC = Weight of the supported structure (kip).

DIFF = Differential load: applicable only to balanced cantilever construction, taken as 2% of the dead load applied to one cantilever (kip).

DW = Superimposed dead load (kips or klf).

CLL = Distributed construction live load; taken as 0.01 ksf of deck area applied to one side of cantilever and 0.005 ksf on the other side.

CE = Specialized construction equipment, load from launching gantry, form-traveler, beam and winch, etc. (kip).

IE = Dynamic load from equipment; determined according to the type of machinery. (For gradual lifting, it may be taken as 10% of the lifting load.)

CLE = Longitudinal construction equipment loads (kip).

U = Segment unbalanced load (kip).

WS = Horizontal wind load on structure in accordance with the provisions of Section 3 (LRFD) (ksf).

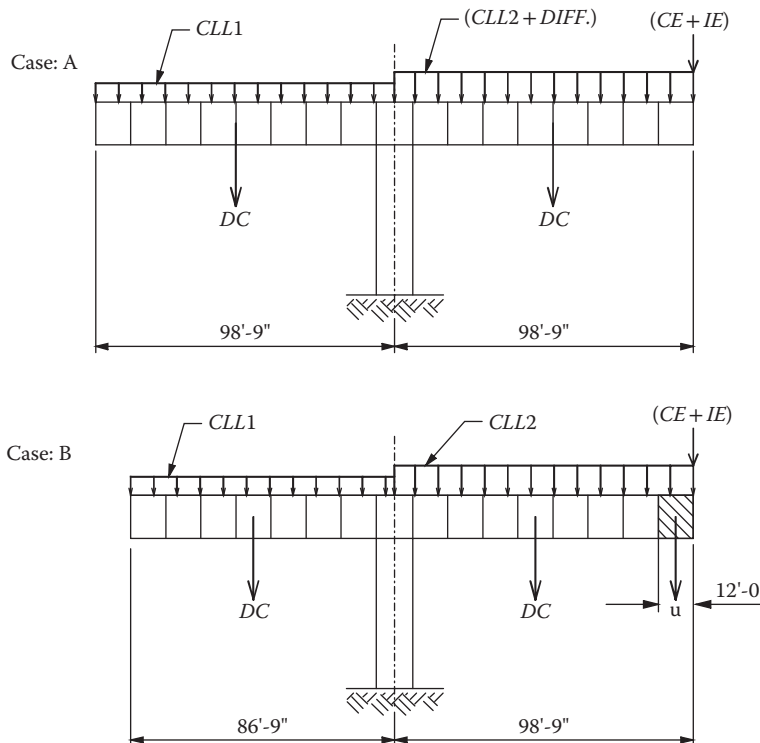


FIGURE 3.74 Construction loads Case A and Case B.

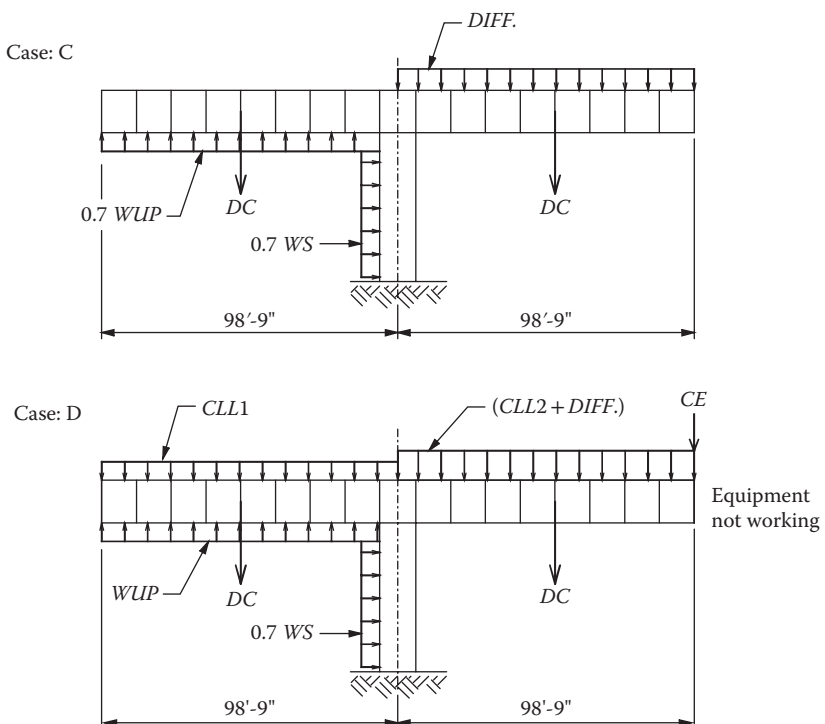


FIGURE 3.75 Construction loads Case C and Case D.

@Seismicisolation

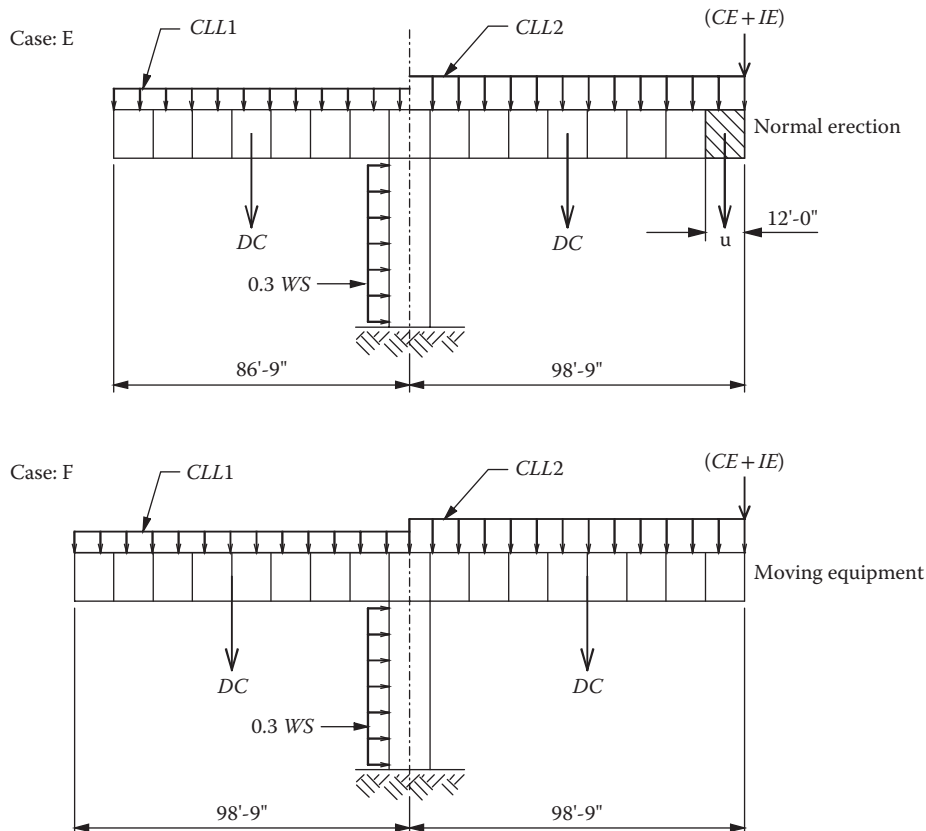


FIGURE 3.76 Construction loads Case E and Case F.

TABLE 3.1 Service Limit State Load Combinations during Construction

	Load Combinations	Allowable Flexural Tension Stress (ksi)	Allowable Principal Tension Stress (ksi)
a1	DC + DIFF + CLL + (CE + IE)	$0.19\sqrt{f'_c}$	$0.11\sqrt{f'_c}$
a2	DC + DIFF + CLL + (CE + IE) + OTHER LOADS	$0.22\sqrt{f'_c}$	$0.126\sqrt{f'_c}$
b1	DC + U + CLL + (CE + IE)	$0.19\sqrt{f'_c}$	$0.11\sqrt{f'_c}$
b2	DC + U + CLL + (CE + IE) + OTHER LOADS	$0.22\sqrt{f'_c}$	$0.126\sqrt{f'_c}$
c1	DC + DIFF + 0.7WS + 0.7WUP	$0.19\sqrt{f'_c}$	$0.11\sqrt{f'_c}$
c2	DC + DIFF + 0.7WS + 0.7WUP + OTHER LOADS	$0.22\sqrt{f'_c}$	$0.126\sqrt{f'_c}$
d1	DC + DIFF + CLL + CE + 0.7WS + WUP + 0.7WE	$0.19\sqrt{f'_c}$	$0.11\sqrt{f'_c}$
d2	DC + DIFF + CLL + CE + 0.7WS + WUP + 0.7WE + OTHER LOADS	$0.22\sqrt{f'_c}$	$0.126\sqrt{f'_c}$
e1	DC + U + CLL + (CE + IE) + 0.3WS + 0.3WE	$0.19\sqrt{f'_c}$	$0.11\sqrt{f'_c}$
e2	DC + U + CLL + (CE + IE) + 0.3WS + 0.3WE + OTHER LOADS	$0.22\sqrt{f'_c}$	$0.126\sqrt{f'_c}$
f1	DC + CLL + (CE + IE) + CLE + 0.3WS + 0.3WE	$0.19\sqrt{f'_c}$	$0.11\sqrt{f'_c}$
f2	DC + CLL + (CE + IE) + CLE + 0.3WS + 0.3WE + OTHER LOADS	$0.22\sqrt{f'_c}$	$0.126\sqrt{f'_c}$

Notes:

1. OTHER LOADS = CR + SH + TU + TG + EH + EV + ES + WA
2. Allowable compressive stress in concrete where f'_c is the compressive strength at the time of load application.
3. d: equipment not working
- e: normal erection
- f: moving equipment

WE = Horizontal wind load on equipment taken as 0.1 ksf of exposed surface.

WUP = Wind uplift on cantilever taken as 0.005 ksf of deck area applied to one side only.

A = Static weight of precast segment being handled (kip).

AI = Dynamic response due to accidental release of precast segment taken as static load to be added to the dead load as 100% of load *A* (kip).

CR = Creep effects in accordance with Article 5.14.2.3.6 (LRFD).

SH = Shrinkage in accordance with Article 5.14.2.3.6 (LRFD).

T = Thermal loads; the sum of the effects due to uniform temperature variation (TU) and temperature gradients (TG).

WA = Water load and stream pressure.

Strength limit state load combinations (see Figure 3.77)

1. For maximum force effects:

$$\Sigma \phi F_u = 1.1(DC + DIFF) + 1.3CE + A + AI \quad (\text{LRFD 5.14.2.3.4a-1})$$

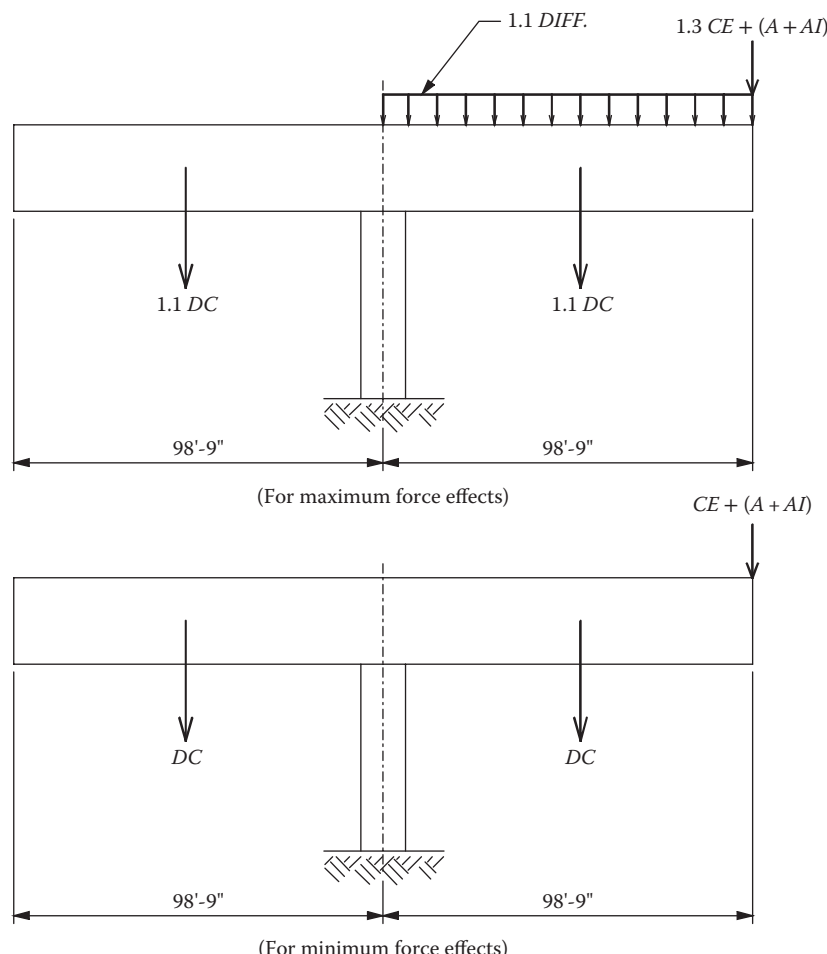


FIGURE 3.77 Strength limit state construction load combinations.

2. For minimum force effects:

$$\sum \phi F_u = DC + CE + A + AI \quad (\text{LRFD 5.14.2.3.4a-2})$$

WS, WE and other loads were ignored in this analysis.
Stress Limits for $f'_c = 6$ ksi:

$$\text{Compressive stress} = -0.5 f'_c = -0.5 \times 6 = -3 \text{ ksi}$$

$$\text{Tensile stress} = 0.19 \sqrt{f'_c} = 0.19 \sqrt{6} = 0.465 \text{ ksi}$$

Since the design example has a 200 ft typical span, only one balanced cantilever structure will be considered in the stability analysis during construction.

The load combinations "a" to "f" as specified in the *AASHTO LRFD Bridge Design Specifications* Table 5.14.2.3.3-1 were computed.

The following construction loads were applied in the stability analysis.

$$CLL1 = 0.005 \text{ ksf} \times 43 = 0.215 \text{ klf}$$

$$CLL2 = 0.01 \text{ ksf} \times 43 = 0.43 \text{ klf}$$

CE = construction equipment such as stressing jack and stressing platform
= 5 Kip.

$$CE + IE = 5 \times 1.1 = 5.5 \text{ kip}$$

$$W_{up} = 0.005 \text{ ksf} \times 43 = 0.215 \text{ klf}$$

$$A = 78 \times 12 \times 0.155 = 145 \text{ kip}$$

1. For maximum force effects:

$$\sum \phi F_u = 1.1 \times (DC + DIFF) + 1.3 \times CE + A + AI$$

2. For minimum force effects:

$$\sum \phi F_u = DC + CE + A + AI$$

where

A = static load of typical segment = 145 kip
 CE = 5 kip.

Although calculations have not been shown in this example, of load cases *a* to *f*, strength limit state load combination *e* controls.

3.7.2 Erection Tendons

It is common practice in precast balance cantilever segmental bridges to use temporary or permanent posttensioning bars to attach the segment being erected to the previously erected segment. In the case of permanent erection PT bars, the posttensioned bars could be designed as part of the permanent cantilever tendons and stressed to full allowable jacking force. However, if reusable temporary posttensioned bars are utilized, the jacking force should be limited to approximately 50% of GUTS of the bars.

The epoxy resin is applied to the match cast faces of the joint between two segments before posttensioning bars are stressed. Purposes of the epoxy resin are as follows:

1. Lubrication to facilitate the proper alignment between segments.
2. Hardened epoxy provides a water-tight joint, preventing moisture, water, and chlorides from reaching the tendons.
3. Hardened epoxy helps distribute compressive stresses and shear stresses more uniformly.
4. Hardened epoxy prevents cementitious grout in the tendon duct from leaking out.

The application of epoxy is normally 1/16 in thick applied on both faces of match cast joints.

In accordance with the Article 5.14.2.4.2 of the LRFD Specifications for a Type A joint, the temporary posttensioning bars should be designed to provide a minimum stress of 0.03 ksi and an average stress of 0.04 ksi across the joint until the epoxy has cured. The intention of the stress limitation is to prevent uneven epoxy thickness across the match-cast joint, which could lead to systematic error in geometry control.

Essentially, there are two load cases that need to be considered when designing temporary posttensioning bars:

1. Dead load of the segment plus construction loads and temporary posttensioning bars, (see Figure 3.78). The erection PT bars should be stressed during the open time of the epoxy (approximately 45 to 60 min). The allowable joint stresses for this load case should conform to Article 5.14.2.4.2 of the LRFD specifications.
2. Case 1 plus permanent cantilever tendons. Normally, one or two hours after the open time of the epoxy is completed, the allowable joint stress is zero tension, preferably some compression.

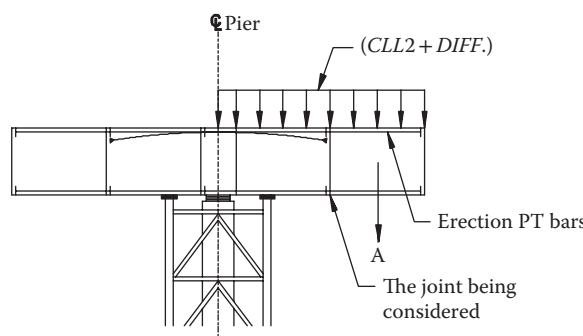


FIGURE 3.78 Construction loads during segment erection.

3.7.2.1 Design of Erection PT Bars

Section Properties (use typical section: including shear lag effect)

$$A_c = 78 \text{ ft}^2$$

$$A_{c\text{eff}} = 70.38 \text{ ft}^2$$

$$I = 791.892 \text{ ft}^4$$

$$Y_t = 3.4 \rightarrow S_t = 232.89 \text{ ft}^3$$

$$Y_b = 5.6 \text{ ft} \rightarrow S_b = 141.40 \text{ ft}^3$$

$$CLL2 = 0.01(43) = 0.43 \text{ plf}$$

$$\text{Segment weight + DIFF} = 1.02 \times 78 \times 12 \times 0.155 = 148 \text{ kip}$$

$$M_{\max} \text{ at the joint} = -148 \times 12 \times \frac{1}{2} - \frac{1}{2} \times 0.43 \times 1 = -918.96 \text{ kip-ft}$$

3.7.2.2 Design Assumptions

Permanent erection bars were selected in this design example.

$$f_{pu} \text{ for PT bars} = 150 \text{ ksi}$$

$$P_u \text{ of } 1.375" \text{ dia. bar} = 1.58(150) = 237 \text{ kip}$$

$$P_u \text{ of } 1.25" \text{ dia. bar} = 1.25(150) = 187.5 \text{ kip}$$

$$P_u \text{ of } 1.0" \text{ dia. bar} = 0.85(150) = 127.5 \text{ kip}$$

Jacking force: 75% of GUTS

Check anchoring forces after anchor set for 1 ¼ in dia. PT bars.

Losses due to friction:

$$\Delta F_{PF} = F_{pj} \left(1 - e^{-(\kappa x + \mu \alpha)} \right) \quad (\text{LRFD5.9.5.2.2b-1})$$

where

F_{pj} = Force in the prestressing steel at jacking, (kip)

x = Length of a prestressing tendon from the jacking end to any point under consideration, (ft)

κ = Wobble coefficient, (ft^{-1})

n = Coefficient of friction (1/rad);

α = Sum of the absolute values of angular change of prestressing steel path from jacking end, (rad)

e = Base of the Napierian logarithm

$$\text{Jacking force: } P_j = 0.75 \times 187.5 = 140.625 \text{ kip}$$

$L = 12 \text{ ft}$ (segment length)

$\kappa = 0.0002$ per ft

$\mu = 0.3$

$\alpha = 0.0$

Anchor set $\delta = 1/16$ in 0.0052 ft

$$\Delta P_F = 140.625 \times (1 - e^{-(0.0002 \times 12)}) \\ = 0337 \text{ kip}$$

$$\therefore P_{(L)} = 140.625 - 0337 = 140.29 \text{ kip}$$

Friction loss is negligible.

$$\text{Loss of stress due to anchor set} = E_s \epsilon = 30,000 \left(\frac{0.0052}{12} \right) = 13 \text{ ksi}$$

$$P_i = 140.624 - 1.25(13) = 124.375 \text{ kip (66% G.U.T.S)}$$

Therefore, anchoring forces, immediately after seating equal to 66% of GUTS

Try: 4 - 1 1/4" dia. top bars and

2 - 1 3/8" dia. bottom bars, as shown in Figure 3.79

$$\therefore P_i \text{ top} = 4 \times 0.66 \times 187.5 = 495 \text{ kip}$$

$$P_i \text{ bottom} = 2 \times 0.66 \times 237 = 312.84 \text{ kip}$$

$$\sum P_i = 807.84 \text{ kip}$$

Compute CGS location relative to the top fiber

$$807.84 \times Y_s = 495 \times 0.5 + 312.84 \times (9 - 0.375)$$

$$Y_s = 3.65 \text{ ft}$$

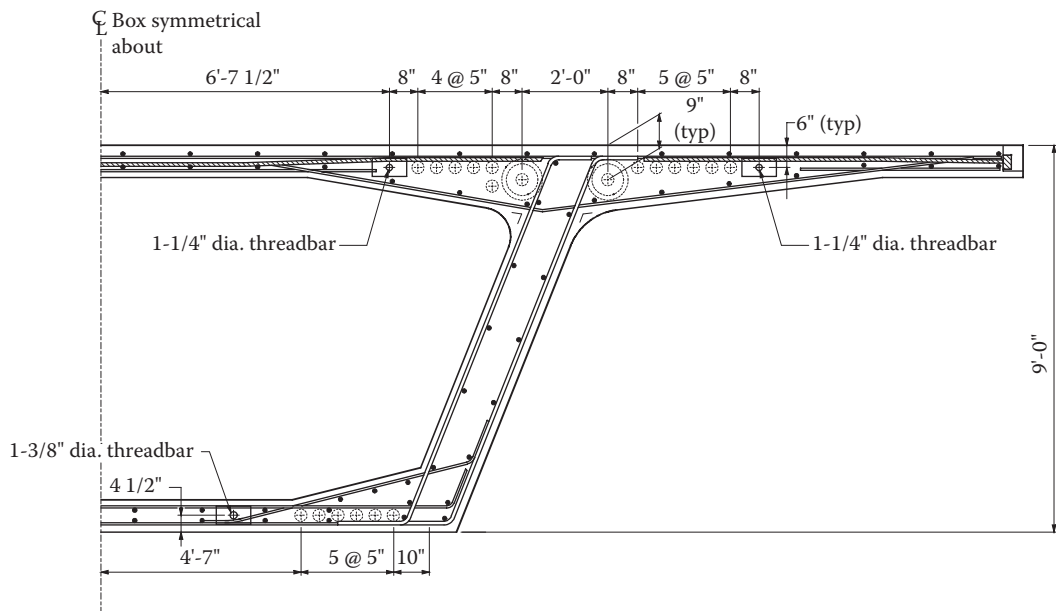


FIGURE 3.79 Erection PT bars

@Seismicisolation

PT bars eccentricity = $3.65 - 3.4 = 0.25$ ft (below C.G.C.)

a. Check joint stresses due to dead loads and PT bars

$$|f_t| = |-0.046 \text{ ksi}| > 0.03 \text{ ksi} \quad (\text{LRFD 5.14.2.4.2})$$

$$\begin{aligned} f_b &= -\frac{\sum P_i}{A_c} - \frac{\sum P_i e}{S_b} - \frac{M_{DL}}{S_b} \\ &= -11.478 - \frac{807.84 \times 0.25}{141.40} - \frac{918.96}{141.40} \\ &= -11.478 - 1.428 - 6.450 \\ &= -19.406 \text{ ksf} = -0.134 \text{ ksi} \end{aligned}$$

$$|f_b| = |-0.134 \text{ ksi}| > 0.03 \text{ ksi}$$

$$\text{Average stress} = \frac{0.046 + 0.134}{2} = 0.09 \text{ ksi} > 0.04 \text{ ksi} \quad (\text{LRFD 5.14.2.4.2})$$

b. Check stresses at the joint due to dead loads, PT bars and cantilever tendons

Tendon size: 4 – 12Ø0.6" strands.

$$P_i = 0.7 \times 50.6 \times 48 = 1,968.96 \text{ kip}$$

$$\text{Tendon eccentricity} = 3.4 - 0.5 = 2.9 \text{ ft}$$

Stress due to cantilever tendons:

$$\begin{aligned} f_t &= -\frac{\sum P_i}{A_c} - \frac{\sum P_i e}{S_t} \\ &= -\frac{1,968.96}{70.38} - \frac{1,968.96 \times 2.9}{232.89} \\ &= -27.98 - 24.52 \\ &= -52.5 \text{ ksf} = -0.3646 \text{ ksi} \end{aligned}$$

$$\begin{aligned} f_b &= -\frac{\sum P_i}{A_c} + \frac{\sum P_i e}{S_b} \\ &= -27.98 + \frac{1,968.96 \times 2.9}{232.89} \\ &= -27.98 + 24.52 \\ &= -3.46 \text{ ksf} = -0.024 \text{ ksi} \end{aligned}$$

Tendon size: 2 – 12Ø0.6" strands. (50% less PT)

$$f_t = 0.5(-0.3646) = -0.1823 \text{ ksi}$$

$$f_b = 0.5(-0.024) = -0.012 \text{ ksi}$$

Summation of stresses.

For segments with 4 – 12Ø0.6" tendons

$$\sum f_t = -0.046 - 0.3646 = -0.4106 \text{ ksi}$$

$$|\sum f_t| = |-0.4106 \text{ ksi}| > -0.03 \text{ ksi}$$

$$\sum f_b = -0.134 - 0.024 = -0.158 \text{ ksi}$$

$$|\sum f_b| = |-0.158 \text{ ksi}| > 0.03 \text{ ksi}$$

For segments with 2 – 12Ø0.6" tendons

$$\sum f_t = -0.046 - 0.1823 = -0.2283 \text{ ksi}$$

$$|\sum f_t| = |-0.2283 \text{ ksi}| > -0.03 \text{ ksi}$$

$$\sum f_b = -0.134 - 0.012 = -0.146 \text{ ksi}$$

$$|\sum f_b| = |-0.146 \text{ ksi}| > 0.03 \text{ ksi}$$

Conclusion:

The proposed permanent PT bars satisfy the allowable joint stresses.

3.8 Detailing

3.8.1 Combined Transverse Bending and Longitudinal Shear

On the basis of previously determined shear reinforcement and flexural reinforcement, the standard practice has been to use the worst case of adding 50% of shear steel to 100% of the flexural steel, or 100% of the shear steel to 50% of the flexural steel.

A rational approach can also be used, where the compression strut in an equivalent truss model would be shifted to the extreme edge of the web. This compression would then be eccentric to a section through the web which would counteract an applied moment. If the applied moment were to exceed the amount that could be resisted in this manner, additional reinforcing could be added.

3.8.2 Shear Key Design

There are two types of shear keys in match-cast joints between precast segments:

- Web shear keys – Located on the faces of the webs of precast box girders. Corrugated multiple shear keys are preferred due to their superior performance. When designing shear keys, only web shear keys are considered in transferring the shear forces.
- Alignment keys – Located in the top and bottom flanges. Alignment keys are not expected to transfer the major shear forces; rather they facilitate the correct alignment of the two match-cast segments being erected in vertical and horizontal directions. For a single-cell box, normally a minimum of three alignment keys are required on the top slab and one on the bottom slab. However, alignment shear keys help in preventing local relative vertical displacement on the deck.

slab between two adjacent precast segments due to concentrated load on one side of the match cast joint. Therefore, in longer slabs spanning between two webs or longer cantilevers wings, it is necessary to provide more than one alignment shear key.

Both shear and alignment keys should not be located in the tendon duct zones. (see Figure 3.83) The design of web shear keys should satisfy two design criteria:

1. Geometric design: As per LRFD Figure 5.14.2.4.2-1, the total depth of shear keys extends approximately 75% of the section depth and at least 75% of the web thickness.
2. Shear strength design: As per AASHTO *Standards Specifications, 17th Edition* (AASHTO 2002), Article 9.20.1.5, reverse shearing stresses should be considered in the shear key design. At the time of erection, shear stress carried by the shear key should not exceed $2\sqrt{f_c}$ (psi). Alternatively, strength of the shear key could also be computed in accordance with article 12.2.21 of AASHTO *Guide Specifications for Design and Construction of Segmental Concrete Bridges, Second Edition* (AASHTO 1999). However, the AASHTO *Guide Specification* shear key provision was developed for dry joints only. Note that dry joint is no longer permitted by AASHTO *LRFD Specifications*.

Shear key design example was illustrated in Figure 3.80

1. Geometric consideration (see Figures 3.81 to 3.83)

$$h = 9 \text{ ft}$$

$$\text{Shear key depth} = 0.75 \times 9 \text{ ft} = 6.75 \text{ ft}$$

$$b_w = 16 \text{ in}$$

$$\text{Shear key width} = 0.75 \times 16 = 12 \text{ in}$$

2. Shear strength design of the shear keys

AASHTO LRFD Bridge Design Specification does not specify any guideline on the strength design of shear keys. Use *AASHTO Standard Specifications*, article 9.20.1.5.

- AASHTO Standard Specifications*, article 9.20.1.5

$$V_u = 1.1(V_{DC} + DIFF)$$

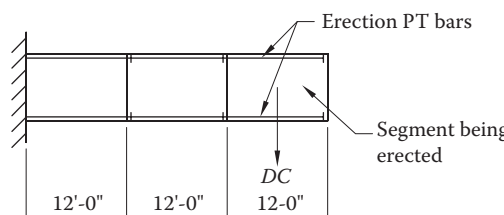


FIGURE 3.80 Precast segment being erected.

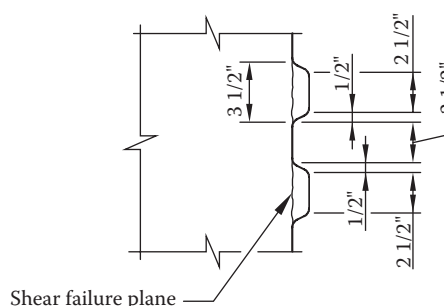
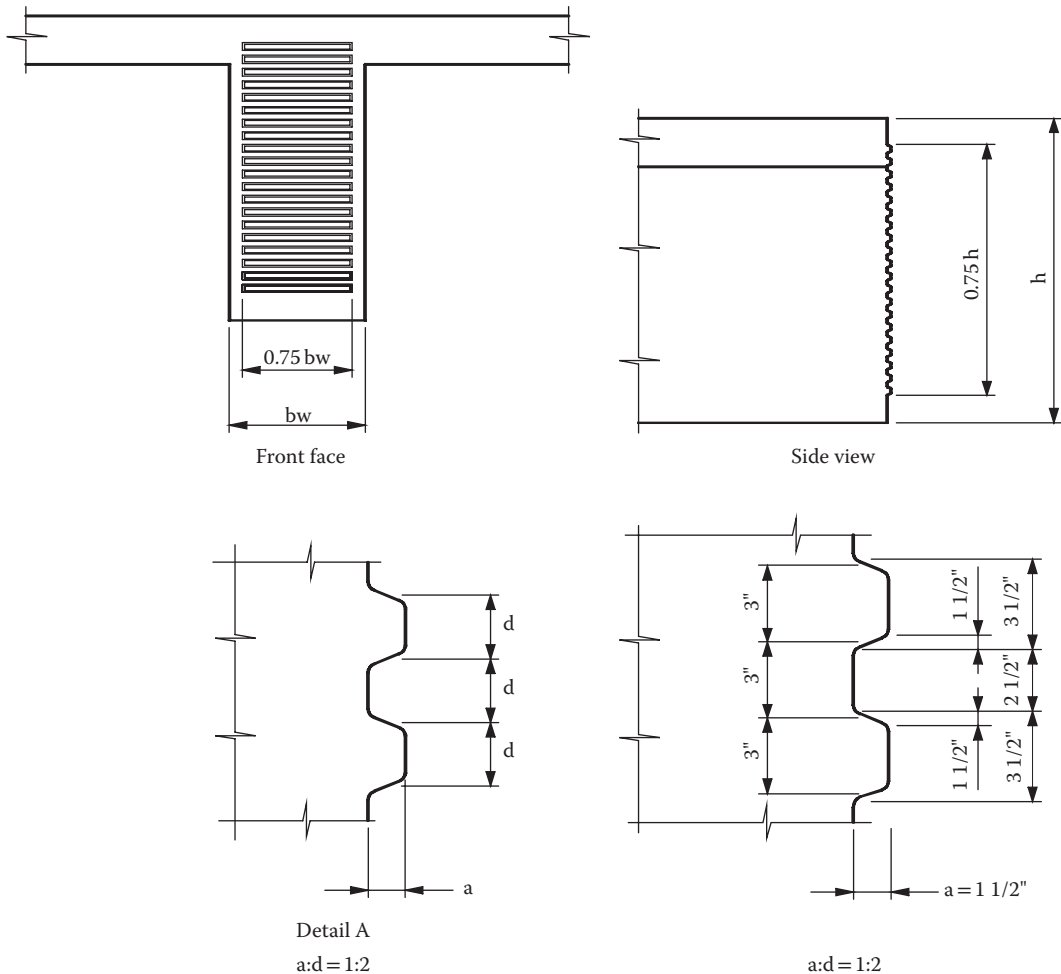


FIGURE 3.81 Details of shear keys.



Notes:

1. $1\frac{1}{4}'' \leq a \geq$ twice the diameter of the top size aggregate.
2. As per AASHTO LRFD specifications Fig. 5.14.2.4.2-1.

FIGURE 3.82 Web shear key detail.

where

$$\begin{aligned} V_{DC} &= \text{shear force due to self-weight of one typical segment (kips)} \\ &= 78 \times 12 \times 0.155 = 145 \text{ kip} \end{aligned}$$

$$\text{DIFF} = 2\% \text{ of } V_{DC}$$

$$V_u = 1.1 \times 145 \times 1.02 = 162.8 \text{ kip}$$

$$V_n = V_c$$

$$V_u/\phi = V_c$$

Consider one web only,

$$V_c = 0.5 V_u/\phi, \text{ per web,}$$

$$V_c = A_k \cdot v, \text{ per key,}$$

@Seismicisolation

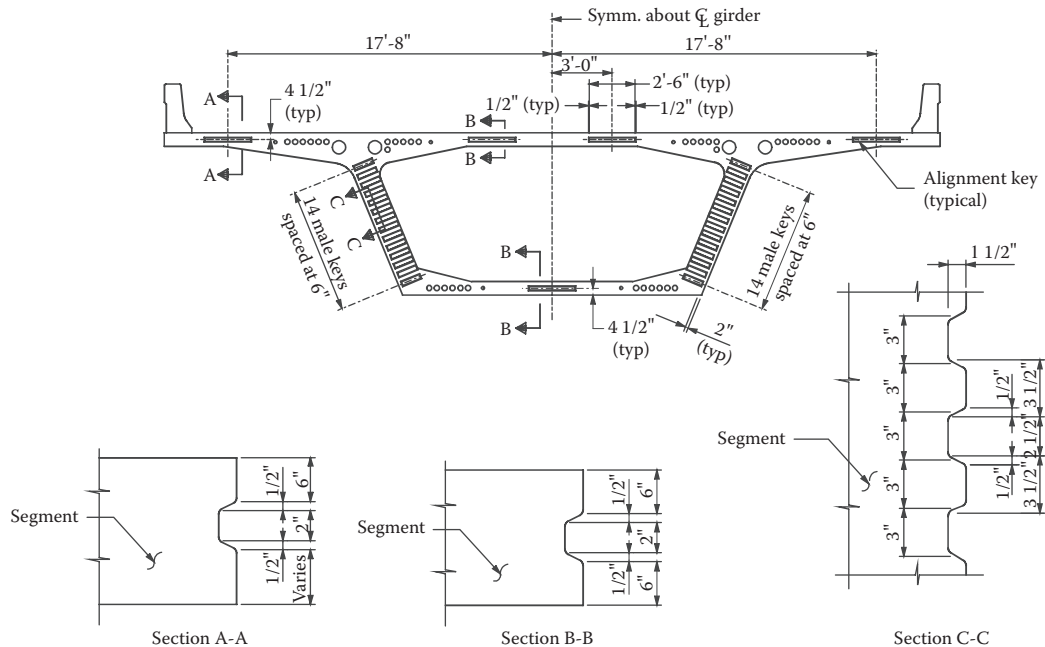


FIGURE 3.83 Bulkhead details.

where

$$\phi = 0.9 \text{ article 9.14 of AASHTO Standard Specifications}$$

ν = allowable shear stress

$$\nu = 2\sqrt{f_c'} \text{ (psi)}$$

A_k = shear area of one key

$$A_k = 3.5 \times (12) = 42 \text{ in}^2$$

$$V_c \text{ per web} = (0.5 \times 162.8) / 0.9 = 90.44 \text{ kip}$$

$$V_c \text{ per key} = 42 \times 2\sqrt{6000} = 6506.6 \text{ lbs} = 6.5 \text{ kip}$$

$$\text{Number of male keys required per web} = \frac{90.44}{6.5} = 13.9 \text{ say } 14 \text{ keys}$$

3.8.3 Strut and Tie Model

In segmental bridge design and detailing, strut and tie model is extensively used in studying the flow of forces from one structural element to the other. The flow of forces from the box girder to the diaphragm, bearings, pier cap, pier column, pile cap to pile foundations can be modeled by the strut and tie model. The strut and tie model is a truss system analogy applied to concrete members consisting of compression and tension members, and is tied together by nodes. Some examples of strut and tie models are shown in Figures 3.84 through 3.91.

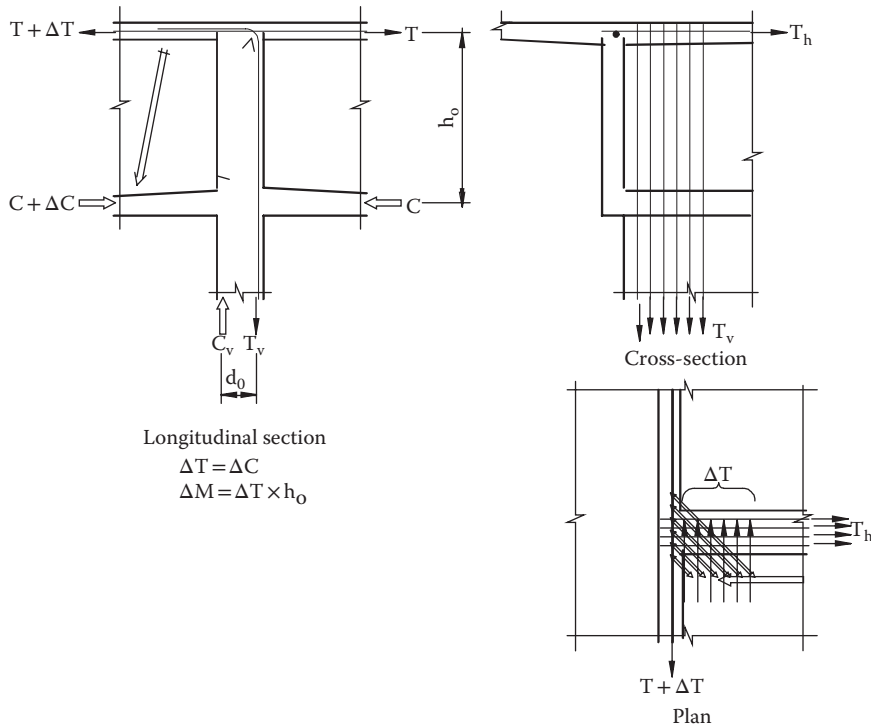


FIGURE 3.84 Transfer of moment from the box girder to the pier column (From Menn, C. 1986. *Prestressed Concrete Bridges*; Birkhauser-Verlag, Boston, MA, 1986.)

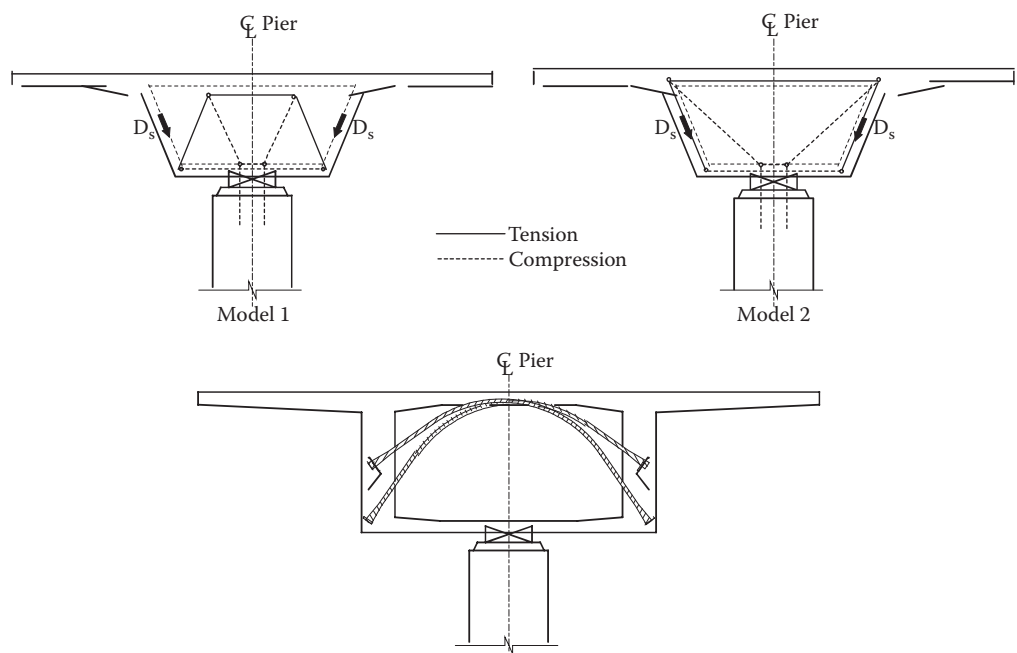


FIGURE 3.85 Transfer of forces from the diaphragm to a single bearing. (From Menn, C. 1986. *Prestressed Concrete Bridges*; Birkhauser-Verlag, Boston, MA, 1986.)

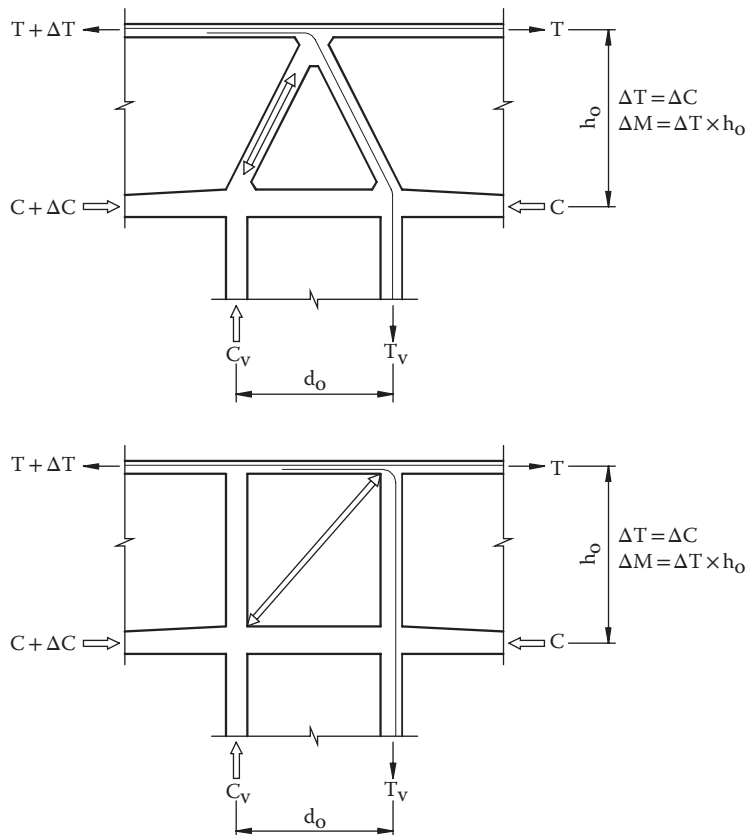


FIGURE 3.86 Transfer of moment from the box girder to the box column. (From Menn, C. 1986. *Prestressed Concrete Bridges*; Birkhauser-Verlag, Boston, MA, 1986.)

3.9 Durability

3.9.1 Durability Problems of Posttensioned Bridges in the United States

After the findings of corrosion in posttensioning tendons in some of Florida's bridges in 1999 to 2000, durability of posttensioned concrete bridges in the United States has become a great concern to owners and bridge engineers around the country. Other deficiencies of posttensioned bridges such as cracked polyethylene ducts and grout voids were also found in other states. For half a century, since the construction of Walnut Lane Bridge in Philadelphia (1949–1950), the first posttensioned bridge in the United States, this type of bridge has enjoyed its popularity as an economical and durable structural system that requires minimum maintenance.

In the summer of 1999, one of the external tendons in the superstructure box girder of the Niles Channel Bridge in Florida Keys was found to have failed due to corrosion. The bridge was constructed in early 1983 and is believed to be one of the first span-by-span segmentally erected concrete bridges in Florida (Fib 2001).

In August 2000, during a routine inspection of the Mid-Bay Bridge located in Destin, Florida, a post-tensioning tendon in span 28 was found in a significant state of distress. The polyethylene external duct was cracked and several strands were fractured. Further inspection of the bridge revealed that a post-tensioned tendon in Span 57 had failed completely at the north end of the tendon. The tendon pulled out from the expansion joint diaphragm as a result of severe corrosion of the tendon in the anchorage

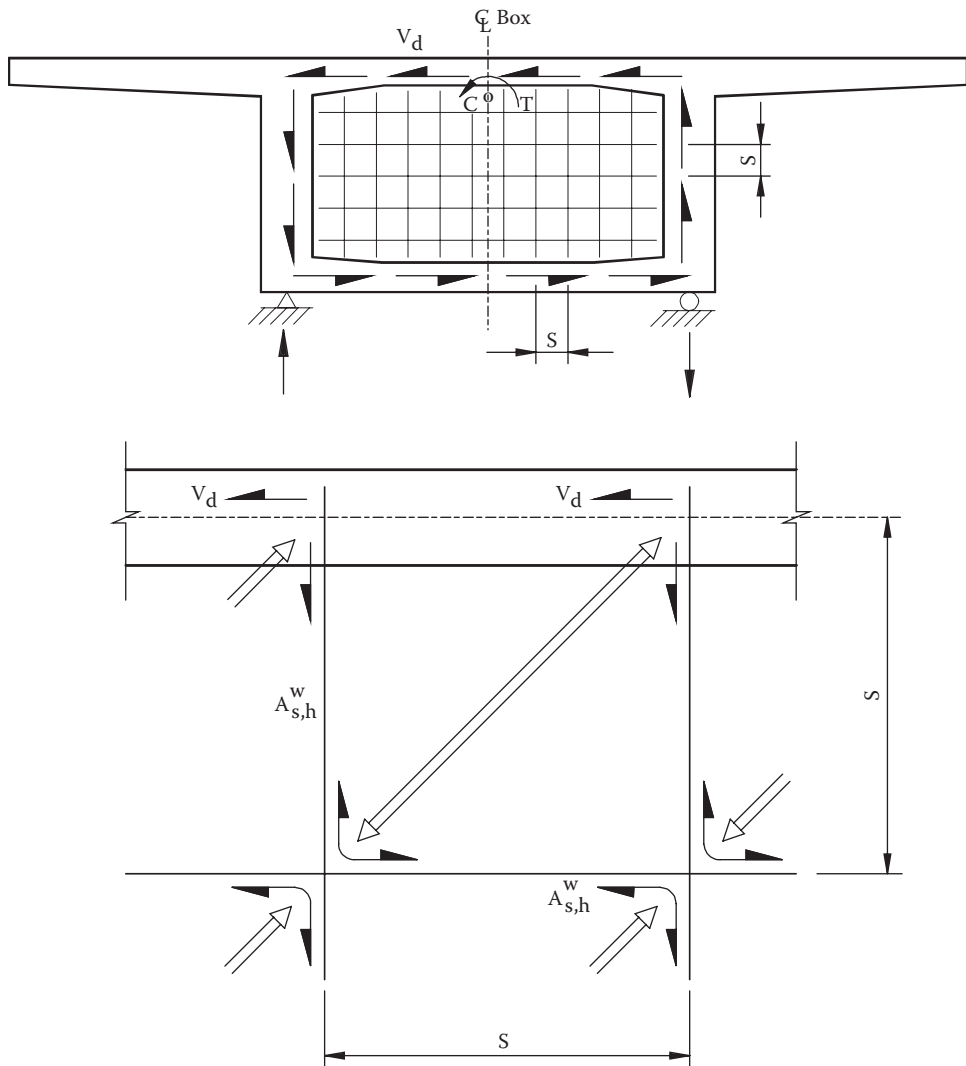


FIGURE 3.87 Transfer of torsion moment from the box girder through the diaphragm to bearings. (From Menn, C. 1986. *Prestressed Concrete Bridges*; Birkhauser-Verlag, Boston, MA, 1986.)

area. After extensive investigation and inspection, it was found that 11 tendons required replacement. The bridge was constructed in 1992 using span-by-span precast segmental construction. In addition to tendon corrosion, cracked polyethylene ducts and grout voids were also discovered (FDOT 2001).

In September 2000, during a special inspection of the high level approach columns in the Sunshine Skyway Bridge in St. Petersburg, Florida, it was discovered that severe corrosion resulted in the failure of 11 strands of the southeast external vertical tendon located in column 133 northbound (PBQD 2002). This finding triggered an extensive investigation of all other high-level approach columns, the bridge superstructure, and cable anchorage of the main span bridge. The investigation of the rest of the columns revealed severe tendon corrosion in the anchorages and at the base of the columns, including cracked polyethylene duct, grout void, and grout chloride contamination. The 76 high-level approach columns have been repaired, including deficiencies found in the superstructure external tendons. The bridge was constructed in 1982 to 1987 and utilized the precast segmental construction method, including for the high-level approach columns.

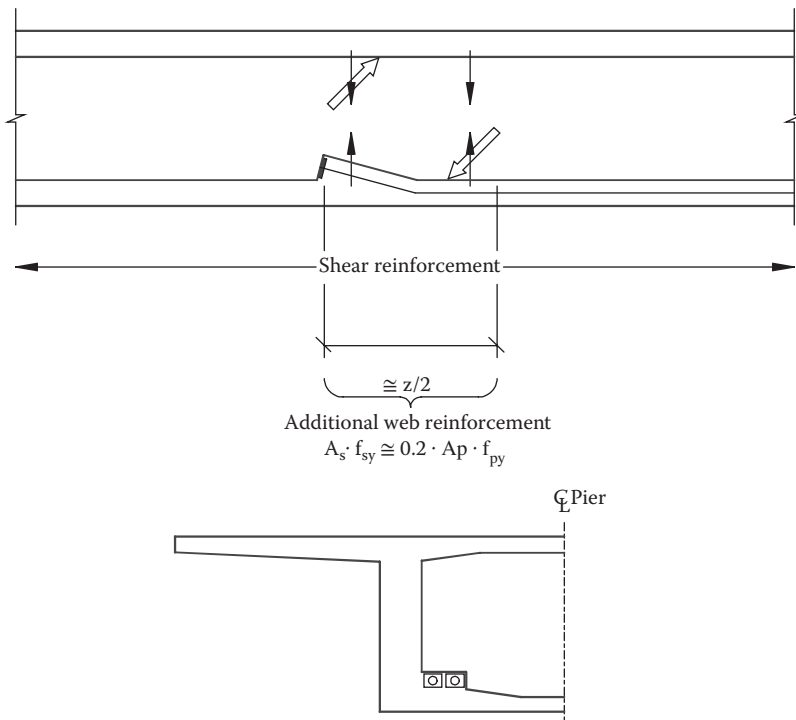


FIGURE 3.88 Transfer of blister forces to the web. (From Menn, C. 1986. *Prestressed Concrete Bridges*; Birkhauser-Verlag, Boston, MA, 1986.)

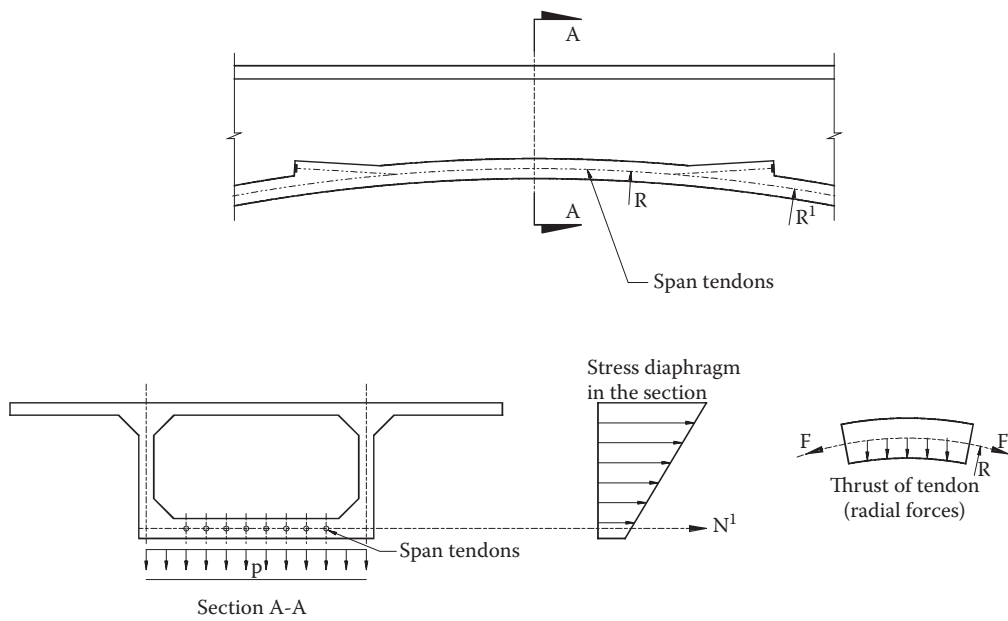


FIGURE 3.89 Radial forces in curved bottom slab. (From Mathivat, J. *The Cantilever Construction of Prestressed Concrete Bridges*; John Wiley & Sons, New York, NY, 1979.)

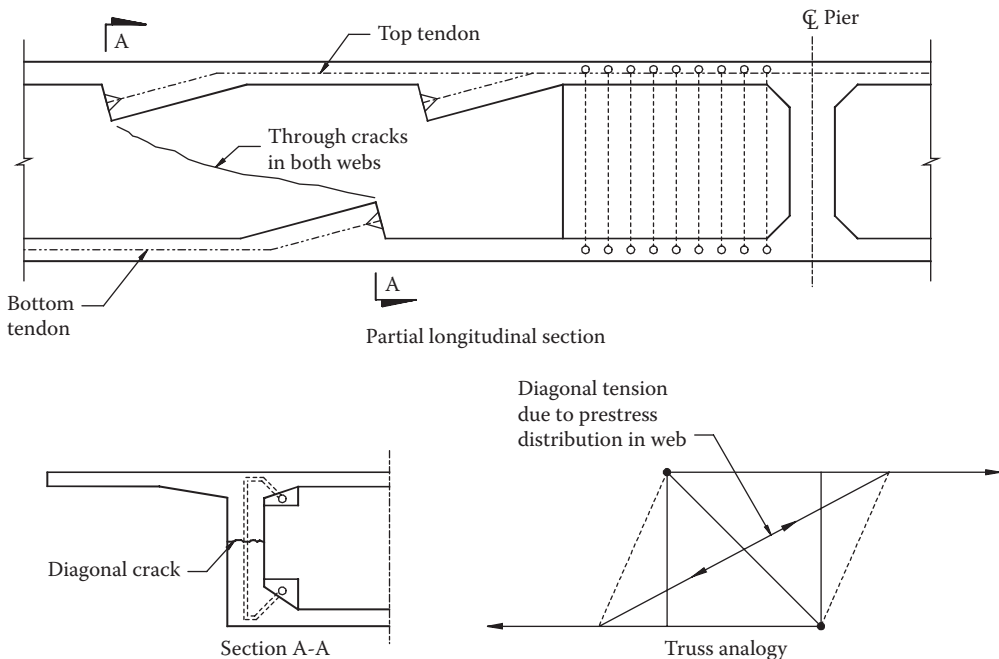


FIGURE 3.90 Transfer of forces by opposing blisters. (From Podolny, W., Muller, J. M. 1982. *Construction and Design of Prestressed Concrete Bridges*; John Wiley & Sons, Inc, New York, NY, 1982.)

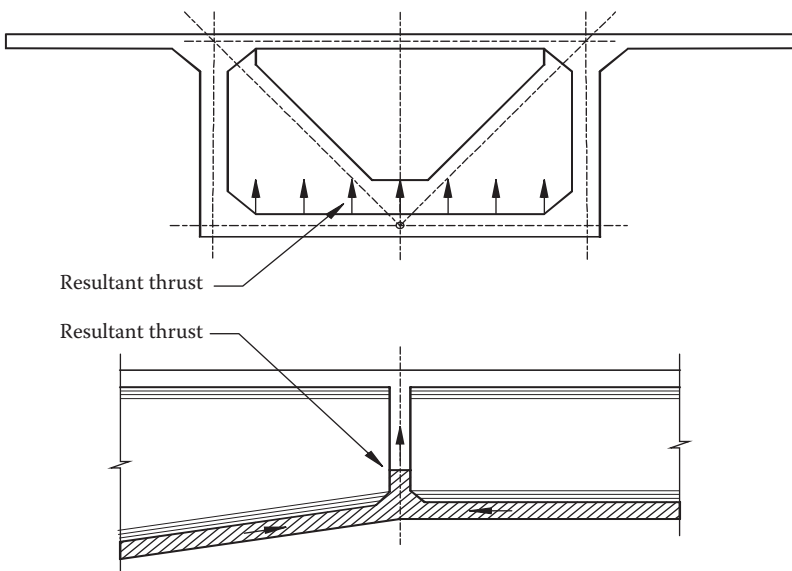


FIGURE 3.91 Resal shear effect at a kink in bottom slab. (From Mathivat, J. *The Cantilever Construction of Prestressed Concrete Bridges*; John Wiley & Sons, New York, NY, 1979.)

The findings of the different bridges in Florida raised concerns about the grouting situation in the Central Artery/Tunnel project in Boston where there are considerable numbers of segmental and cast-in-place posttensioned concrete structures. It was important to determine if the Central Artery structures have grout voids and whether or not the tendons are corroded, although the structures are relatively young. Posttensioned tendons inspection was conducted at 380 locations. This is less than 1.5% of

the total number of tendons on the project. The initial investigation revealed excessive amounts of grout voids but no corrosion of strands.

3.9.2 Durability Problems of Posttensioned Bridges around the World

Signs of durability problems in Europe were discovered about 20 to 30 years prior to the discovery of posttensioned corrosion problems in the United States.

In December 1985, a single-span precast segmental bridge in the United Kingdom, namely Ynys-y-gwas, collapsed without warning (The Highway Agency, Setra, TRL, and LCPC. 1999). Since then a sample of nine segmental bridges were inspected; grout voids in seven bridges and severely corroded tendons in two bridges were discovered. In the late 1980s and early 1990s, about a dozen posttensioned concrete bridges in the United Kingdom were discovered with serious tendon corrosion, which required major repairs or replacement. The inspection results led to the UK Department of Transport (currently called Highway Agency) initiated a ban on internally grouted posttensioned concrete bridges in September 1992. The moratorium was lifted for cast-in-place posttensioned concrete bridges in 1996. However, the moratorium for precast segmental posttensioned concrete bridges, including segmental bridges with epoxy joints, is still in place. In 1992 the UK Department of Transport launched a five-year special inspection program for all existing posttensioned concrete bridges located on the Trunk Road. As a result of the inspection program, 447 posttensioned concrete bridges were completely inspected and documented.

In 1970, the first serious sign of durability problems of posttensioned concrete bridges in France was discovered with the finding of several concrete cracks in the side span of the Chazey Bridge caused by severe tendon corrosion. The bridge was demolished and reconstructed in 1972. Additionally, tendon corrosion, grout deficiency, and other posttensioning system defects were also found in the Choisy-le-Roi Bridge, the Vaux Sur Seine Bridge, the Port a Binson Bridge, the Villeneuve Saint-Georges Bridge, the Can Bia Bridge, the Saint-Cloud Viaduct, the bridge over the Durance, and the Riviere d' Abord Bridge, including the first generation of simple-span posttensioned bridges constructed in the period between 1946 and 1960 (Fib 2001).

Japan Highway Public Corporation conducted inspections and investigated 120 posttensioned concrete bridges. The results showed 31% of the tendons investigated have grout deficiency such as no grout, imperfect grout, and grout voids. Other deficiencies such as tendon corrosion, reinforcement corrosion, concrete cracks, and spalling were also found. As a result of these findings, the Japan Highway Public Corporation has placed a moratorium on new construction of grouted posttensioned bridges (Fib 2001).

Other countries such as Germany, Austria, and Italy also have their share of corrosion problems with their posttensioned bridges. For instance, the collapse of Congress Hall in Berlin is one of the most spectacular posttensioned structure failures in Germany, although it was not a posttensioned bridge. FIB Task Group 9.5 reported that several posttensioned concrete bridges in Germany were affected by severe tendon corrosion, for example failure of the flyover at the Heerdter in Dusseldorf in 1976, tendon corrosion of the flyover junction in Berlin-Schmargendorf, tendon corrosion of the A73 motorway at South Nurenberg, and tendon corrosion of the bridge over Muckbachthal on motorway Wurzburg-Heilbronn. Consequently, German Federal Ministry for Transport and Construction has placed a moratorium on internal tendons in the webs of posttensioned bridges, with the exception of replaceable external tendons and internal tendons in the top and bottom flanges of box girder.

3.9.3 Lessons Learned

The United Kingdom is one of the few countries in the world that has undertaken an extensive study and investigation of its posttensioned concrete bridges. As mentioned above, from the Special Inspection Program, 447 posttensioned concrete bridges were systematically documented. Such a study allows the

UK Highway Agency to determine the important factors affecting their posttensioned concrete bridges. Although there are common problems associated with durability of posttensioned bridges shared between countries, it is believed that each country has its own unique problems. The study concluded that corrosion of posttensioned tendons in internally grouted duct has occurred in a small number of posttensioned concrete highway bridges in the United Kingdom. Therefore, the report finds that the majority of the structures have a good record of durability.

In the United States, special inspection and investigation of posttensioned bridges were conducted in the States of Florida, Texas, Virginia, Georgia, Mississippi, Delaware, Kansas, South Carolina, Indiana, Iowa, Rhode Island, and Massachusetts. While there is no national guideline for this type of investigation, the Florida Department of Transportation (FDOT) has become the leader for this type of investigation in the United States. Unfortunately, there is no single coordinated effort in the United States to collect and study the inspections/investigations completed from different States. To date, the findings of posttensioned concrete bridges investigations in the United States, such as Florida, Texas and other states are very similar to the findings in the European countries' investigations.

The following is the brief summary findings of posttensioned bridges investigation in the United States:

- Cracked polyethylene duct of external tendon
- Grout voids in the posttensioned duct and anchorages as result of water bleed
- Grout voids as a result of poor construction practice, quality control, design, and detailing
- Tendon corrosion and failure as a result of water and oxygen intrusion due to failure of tendon protection system
- Tendon corrosion as a result of unsuitable grout materials and chloride contamination
- Tendon corrosion as a result of shortcomings in specifications and corrosion detection methods

Grout voids do not necessarily compromise the durability of posttensioned structures, as long as one or more of the tendon protection systems are still intact and undamaged. This has been verified in the investigation findings of posttensioned bridges in the United Kingdom and in the United States.

It is believed that there are three factors that may have contributed to the durability problems of post-tensioned bridges today:

1. The original philosophy of prestressed concrete design of full prestressing (no tension allowed at working loads) created a perception that prestressed concrete should be crack free and therefore required minimal or no maintenance.
2. Lack of historical data and testing on emerging new technologies in posttensioned bridge designs and construction methods.
3. Generally, grouted tendons are perceived as adequate corrosion protection to the prestressing steel, notwithstanding the inability to inspect the condition and quality of the grout inside the ducts.

3.9.4 New Direction for the Next Generation of Posttensioned Concrete Bridges

While the well-known 1992 UK DOT moratorium on posttensioned bridges was considered an over-reaction by most countries at that time, the moratorium has impacted the concrete bridge industries of the world in very positive ways. It has also challenged the Bridge Engineering Society and Industry to review and make revisions to the construction and materials specifications, including design and detailing of posttensioned bridges. Technical Report 47 (TR 47) is one of the most important documents ever produced by the UK Concrete Society to deal with durability of posttensioned concrete bridges in response to the moratorium (The Concrete Society 1996).

FDOT and TxDOT (Texas Department of Transportation) are leading in developing and implementing the new direction for the future generation of posttensioned concrete bridges in the United States. Similar to the United Kingdom, FDOT has rewritten its posttensioned grouting specifications, posttensioned system specifications, quality control manuals, and certification requirements, including semistandard posttensioning details. The Posttensioning Institute (PTI) also has rewritten its grouting specifications. In support of FDOT and PTI, the American Segmental Bridge Institute (ASBI) contributed in improving grouting practice, workmanship, quality control, and posttensioning details by setting up ASBI Grouting Training Certification Seminars conducted once a year since 2001. The new posttensioned concrete bridge projects in Florida have fully implemented the new posttensioned specifications and details since 2003 (FDOT 2003).

3.9.5 Conclusions

The durability problems found in Florida and in other parts of the country do not necessarily represent the condition of all posttensioned concrete bridges in the United States. Observe that almost all of the posttensioned bridges mentioned above that are affected by corrosion are located in the very corrosive environment of Florida coastal areas and are associated mostly with the precast segmental construction method. A durable posttensioned structure can be constructed to last the service life provided the required improvements are done across the board including materials, construction methods, design, detailing, workmanship, quality assurance, quality control, corrosion detection system, inspection, and preventive maintenance. Neglecting any one of the above will indeed compromise the durability of posttensioned concrete bridges. Similar to other types of bridges, posttensioned concrete bridges require routine inspection and maintenance.

References

- AASHTO. 1989a. *Guide Specification for the Design and Construction of Segmental Bridges and Interim Specifications*; 1st Edition, American Association of State Highway and Transportation Officials; Washington, D.C.
- AASHTO. 1989b. *Guide Specifications for Thermal Effects in Bridge Superstructures*; American Association of State Highway and Transportation Officials; Washington, D.C.
- AASHTO. 1999. *Guide Specification for the Design and Construction of Segmental Bridges and Interim Specifications*; 2nd Edition, American Association of State Highway and Transportation Officials; Washington, D.C.
- AASHTO. 2002. *Standard Specifications for Bridge Design*; 17th Edition, American Association of State Highway and Transportation Officials; Washington, D.C.
- AASHTO. 2004. *AASHTO LRFD Bridge Design Specifications*; 3rd Edition, American Association of State Highway and Transportation Officials; Washington, D.C.
- AASHTO. 2012. *AASHTO LRFD Bridge Design Specifications*; Customary US Units, 2012, American Association of State Highway and Transportation Officials; Washington, D.C.
- CEB. 1991. *CEB-FIP Model Code 1990*; CEB, Lausanne, Switzerland.
- Collins, M. P. and Mitchell, D. 1991. *Prestressed Concrete Structures*; Prentice-Hall; Englewood Cliffs, NJ.
- The Concrete Society. 1996. *Durable Post-tensioned Concrete Bridges*; Technical Report 47, The Concrete Society, London, U.K.
- FDOT. 1989. *Segmental Manual: A Guide to the Construction of Segmental Bridges*; Bureau of Construction; Florida Department of Transportation, Tallahassee, FL.
- FDOT. 2001. *Mid-Bay Bridge Post-Tensioning Evaluation*; Final report, Corven Engineering, Inc, Tallahassee, FL.
- FDOT. 2003. *New Directions for Florida Post-Tensioned Bridges*; Seminar Proceeding, June 13–14, Florida Department of Transportation, Tallahassee, FL.

- Fib. 2001. *Durability of post-tensioning tendon*; fib Workshop 15–16 November, Ghent, Belgium.
- FIP. 1976. *Report on Prestressing Steel, 1. Types and Properties*; FIP, Wexham Springs, Slough SL3 6PL, England.
- Guyon, Y. 1972. *Limit-State Design of Prestressed Concrete*; Vol. 1, Applied Science Publishers, LTD; London, UK.
- Highway Agency, SETRA, TRL, and LCPC. 1999, *Post-tensioned Concrete Bridges*; Anglo-French liaison report, Thomas Telford, London.
- Leonhardt. F. 1984. *Bridges*; The MIT Press, Cambridge, MA.
- Mathivat, J. 1979. *The Cantilever Construction of Prestressed Concrete Bridges*; John Wiley & Sons, New York, NY.
- Menn, C. 1986. *Prestressed Concrete Bridges*; Birkhauser-Verlag, Boston, MA.
- PBQD. 2002. *Sunshine Skyway Bridge Post-Tensioned Tendons Investigation, Part 2: Investigation of the High Level Approach Span piers*; Final report, Parsons Brinckerhoff Quade and Douglas, Inc, Tampa, Florida, FL.
- Petroski, H. 1995, *Engineers of Dream*; Alfred A. Knopf, Inc., New York, NY.
- Podolny, W. and Muller, J. M. 1982. *Construction and Design of Prestressed Concrete Bridges*; John Wiley & Sons, Inc, New York, NY.
- Posten, R.W., Carrasquillo, R.L., and Breen, J. E. 1987. Durability of Post-Tensioned Bridge Decks; *ACI Material Journal*, 84(4), 315–326.
- PTI. 2012. *Specifications for Grouting of Post-tensioned Structures*; 2nd Edition, April 2012. Post-Tensioning Institute, Farmington Hills, MI.
- VSL. 1977. *The Incremental Launching Method in Prestressed Concrete Bridge Construction*; Losinger Ltd., VSL International, Bern, Switzerland, April 1977.
- VSL. 1978. *The Free Cantilevering Method in Prestressed Bridge Construction*; Losinger, Ltd. VSL International, Bern, Switzerland.
- Webster's New Universal Dictionaries. 1996. Barnes & Nobel, New York.

4

Composite Steel I-Girder Bridges

4.1	Introduction.....	171
4.2	Structural Components and Materials..... Structural Components • Structural Steel • Concrete: Deck Slabs	172
4.3	Section Proportion..... Classification of Sections • Depth-to-Span Ratio • Flanges • Webs • Stiffeners	174
4.4	Span and Framing Arrangement	179
	Span Configuration • Girder Spacing • Diaphragms and Cross Frames • Lateral Bracing • Field Splice Locations • Expansion Joints and Hinges	
4.5	Structural Modeling and Analysis	182
4.6	Design Limit States and Procedures..... Design Limit States • Design Procedures	182
4.7	Design Example: Three-Span Continuous Composite Plategirder Bridge	183
	Bridge Data • Design Requirements • Design Calculations	
4.8	Summary	214
	References.....	214

Lian Duan
*California Department
of Transportation*

Yusuf Saleh
*California Department
of Transportation*

Steve Altman
*California Department
of Transportation*

4.1 Introduction

Girder bridges are structurally the simplest and the most commonly used in short-to-medium span bridges. An I-section is the simplest and most effective solid section of resisting bending and shear. Figures 4.1 and 4.2 show a steel–concrete composite I-girder bridge under construction and completion, respectively. In this chapter, straight steel–concrete composite I-girder bridges are discussed. Materials and components of I-section girders are described. Design guidelines for section proportion, span configuration, girder spacing, diaphragms and cross frames, lateral bracings, stiffeners, and shear connectors are presented. A design example of a three-span continuous composite girder bridge is given to illustrate the design procedure. For a more detailed discussion, reference may be made to texts by Xanthakos (1994), Taly (1997), FHWA (2003), Unsworth (2010), Barker and Puckett (2011), and NSBA (2012). The basic steel design theory is presented in Chapter 14 of *Bridge Engineering Handbook, Second Edition: Fundamentals*.



FIGURE 4.1 Steel-concrete composite I-girder bridge under construction (I-880 Replacement, Oakland, California).



FIGURE 4.2 Steel-concrete composite I-girder bridge (I-880 Replacement, Oakland, California).

4.2 Structural Components and Materials

4.2.1 Structural Components

Figure 4.3 shows a typical portion of a composite I-girder bridge superstructure. Major structural components include concrete deck slab, shear studs, steel I-section girder, longitudinal stiffeners, transverse stiffeners, and cross frames. Figure 4.4 shows dimensions and symbols used for a steel I-girder.

4.2.2 Structural Steel

Four types of structural steels (structural carbon, high-strength low-alloy, heat-treated low-alloy, and high-strength heat-treated alloy steel) are commonly used for bridge structures. Designs are based on minimum properties as specified in AASHTO LRFD Bridge Design Specifications (AASHTO 2012). ASTM material property standards differ from AASHTO in notch toughness and weld-ability requirements. Steel meeting the AASHTO-M requirements is prequalified for use in welded steel bridges.

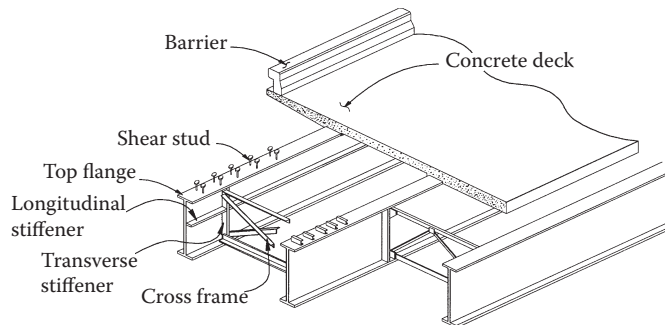


FIGURE 4.3 Typical components of composite I-girder bridge.

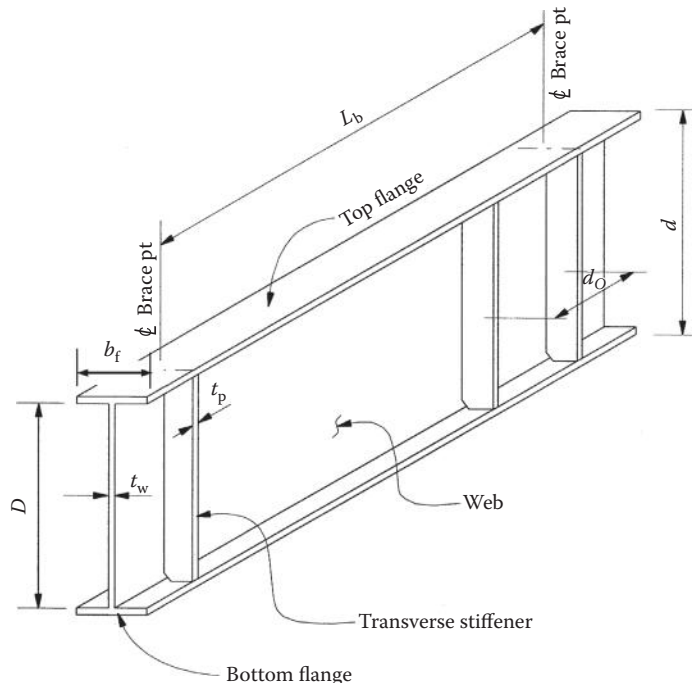


FIGURE 4.4 Dimensions and symbols for I-girder.

The use of ASTM A 709 Grade 50 for all structural steel, including flanges, webs, bearing stiffeners, intermediate stiffeners, cross frames, diaphragms, and splice plates is preferred. The use of ASTM A 709 Grade 36 for secondary members does not reduce material unit costs. The hybrid section consisting of flanges with a higher yield strength than that of the web may be used to save materials and is being promoted more due to the new high performance steels. Using HPS 70W for top and bottom flanges in negative moment regions and bottom flanges in positive moment regions and Grade 50 top flanges in positive moment regions, and Grade 50 for all webs may provide the most efficient hybrid girder. The use of ASTM A 709 Grade 100 or 100W steel may lead to much thinner sections and may have stiffness problems. The use of HPS Grade 100W is recommended if there is a need for specific components in complex built-up or box girders.

The use of high performance steel (HPS) and weathering steel is encouraged if it is acceptable for the location. FHWA Technical Advisory T5140.22 (FHWA 1989) provides guidelines on acceptable locations.

4.2.3 Concrete: Deck Slabs

Concrete with 28-day compressive strength $f'_c = 4.0$ ksi (41 MPa) is commonly used in concrete deck slab construction. The transformed area of concrete is used to calculate the composite section properties. For unshored construction, the short-term modular ratio $n = E_s/E_c$ is used for transient loads and long-term modular ratio $3n$ for permanent loads. For normal weight concrete, the short-term ratio of modulus of elasticity of steel to that of concrete are recommended by AASHTO-LRFD (2012):

$$n = \begin{cases} 8 & \text{for } 3.5 \leq f'_c < 4.5 \text{ ksi} \\ 7 & \text{for } 4.5 \leq f'_c < 6.0 \text{ ksi} \\ 6 & \text{for } f'_c \leq 6.0 \text{ ksi} \end{cases} \quad (4.1)$$

4.3 Section Proportion

4.3.1 Classification of Sections

I-sectional shapes can be classified in four categories based on different fabrication processes or their structural behavior as discussed below:

- A steel I-section may be a *rolled* section, also known as an I-beam (Figure 4.5a) with or without cover plates, or a *built-up* section, also known as a plate girder (Figure 4.5b) with or without haunches consisting of top and bottom flange plates welded to a web plate. It should be noted that the web of a rolled section always meets compactness requirements while the flanges may not. To increase the flexural strength of a rolled section, it is common to add cover plates to the flanges. *Rolled* steel I-beams are applicable to shorter spans less than 100 ft. (30 m) and *plate girders* to longer spans of about 100 to 300 ft. (30 to 90 m). Plate girder sections provide engineers freedom and flexibility to proportion the flanges and web plates efficiently. A plate girder can be considered as a deep beam. The most distinguishing feature of a plate girder is the use of the transverse stiffeners

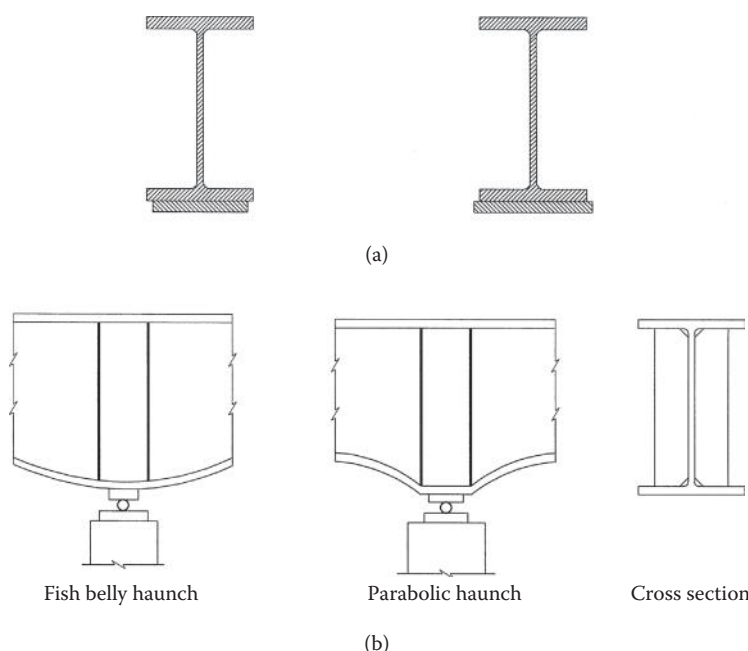


FIGURE 4.5 Typical steel girder sections: (a) Rolled beam with cover plate; (b) Built-up plate girder with haunches.

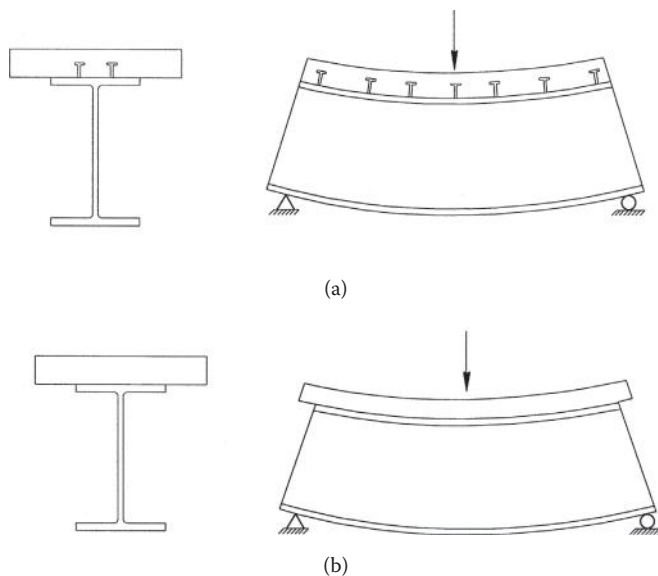


FIGURE 4.6 Composite and noncomposite section: (a) Composite girder; (b) Noncomposite girder.

that provides tension-field action increasing the postbuckling shear strength. The plate girder may also require longitudinal stiffeners to develop inelastic flexural buckling strength.

- I-sections can be classified as *composite* or *noncomposite*. A steel section that acts together with the concrete deck to resist flexure is called a *composite* section (Figure 4.6a). A steel section disconnected from the concrete deck is *noncomposite* (Figure 4.6b). Since *composite* sections most effectively use the properties of steel and concrete, they are often the best choice. Steel-concrete *composite* sections are used in positive moment regions and girder bridges are recommended by AASHTO-LRFD (2012), whereas *noncomposite* sections are used in negative moment regions (AASHTO 2012).
- I-sections can also be classified as *compact*, *noncompact*, and *slender* sections (AASHTO 2012, AISC 2010a). A qualified *compact* section can develop a full plastic stress distribution and expected to be able to achieve a level of rotational deformation ductility of at least 4. *Noncompact* sections only develop the yield stress in extreme fiber of compression elements before buckling locally, but will not resist inelastic local buckling at the strain level required for a fully plastic stress distribution. *Slender* element sections buckle elastically before the yield stress is achieved. The slender steel sections are not permitted in bridge girders (AASHTO 2012).
- I-sections can also be classified as hybrid or nonhybrid sections. A hybrid section consisting of flanges with a higher yield strength than that of the web may be used to save materials and is being promoted more due to the new high strength steels.

The first step in the structural design of an I-girder bridge is to select an I-rolled shape or to initially size the web and flanges of a plate girder. The following sections present the basic principles of selecting I-rolled shapes and sizing the dimensions of a plate girder.

4.3.2 Depth-to-Span Ratio

For straight girders in highway bridges, AASHTO LRFD (AASHTO 2012) Table 2.5.2.6.3-1 specifies that the minimum ratio of the depth of steel girder portion to the span length is 0.033 for simply supported spans and 0.027 for continuous spans; the minimum ratio of the overall depth (concrete slab plus steel girder)-to-span length is 0.04 for simply supported spans and 0.032 for continuous spans. For horizontally curved girders, the minimum depth will more than likely need to be increased by 10 to



FIGURE 4.7 A haunched steel continuous girder bridge (U.S. 50 Bridge over Sacramento River).

20%. I-rolled shapes are standardized and can be selected from the AISC Manual (2010b). In the straight girders in railway bridges, the depth-to-span ratio is usually 0.05 to 0.055.

The variable cross sections may be used to save material where the bending moment is smaller and/or larger near the end of a span (Figure 4.5b). A haunched section may be used for continuous spans. Figure 4.7 shows a haunched steel continuous girder bridge. For haunched I-girders, the depth-to-span ratios are typically taken as 0.05–0.06 at the piers and 0.025–0.033 at the midspans. However, the manpower required for welding and fabrication may be increased. The cost of manpower and material must be balanced to achieve the design objectives. The designer should consult local fabricators to determine common practices in the construction of a plate girder. Figure 4.8 shows typical depth-to-span ratios.

Plate girders must have sufficient flexural and shear strength and stiffness. A practical choice of flange and web plates should not result in any unusual fabrication difficulties. An efficient girder is one that meets these requirements with the minimum weight. An economical one minimizes construction costs and may or may not correspond to the lowest weight alternative (Blodgett 1996).

4.3.3 Flanges

The flanges provide bending strength. The width and thickness are usually determined by choosing the area of the flanges within the limits of the width-to-thickness ratio, b/t , and requirement as specified in the design specifications to prevent local buckling. Lateral bracing of the compression flanges is usually needed to prevent lateral torsional buckling during various load stages. The practical guidelines are as follows:

- Flanges should be at least 12 in. wide. A constant flange width for the entire length of the girder is preferred. If the flange area needs to be increased, it is preferable to change the flange thickness. If flange widths need to be changed, it is best to change the width at field splices only. Width increments should be in multiples of 2 or 3 in. For horizontally curved girders, the flange width should be about one-fourth of the web depth. For straight girders, a flange width of approximately one-fifth to one-sixth of the web depth should be sufficient.
- For straight girders, the minimum flange thickness should be 3/4 in. For curved girders, 1 in. thickness is a practical minimum. The desirable maximum flange thickness is 3 in. Grade 50 and HPS 70W steels are not available in thicknesses greater than 4 in. Flange thickness should have an increment of 1/8 in. for thicknesses up to 1 in., 1/4 in. from 1 to 3 in., and 1/2 in. from 3 to 4 in. At the locations where the flange thickness is changed, the thicker flange should provide about 25%

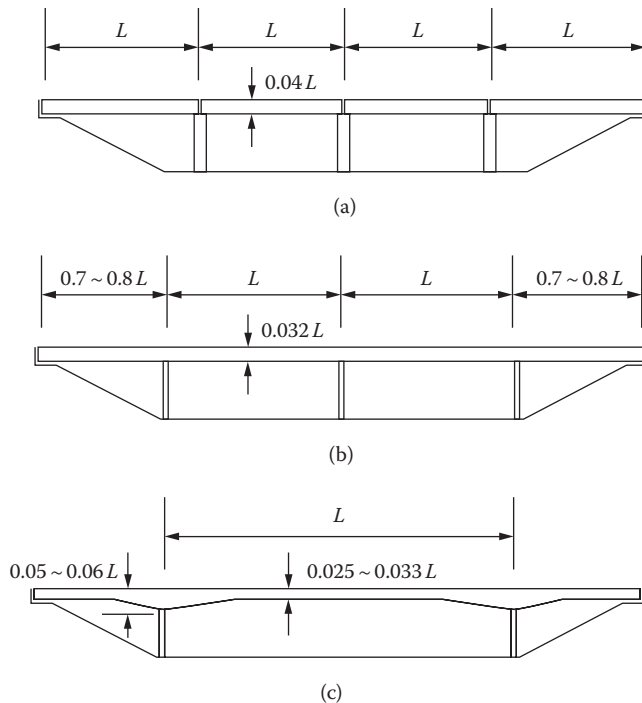


FIGURE 4.8 Depth-to-span ratios and span arrangements: (a) simply supported spans; (b) continuous spans with constant depth; (c) continuous spans with variable depth.

more area than the thinner flange. In addition, the thicker flange should not be greater than twice the thickness of the thinner flange.

- Both the compression and tension flanges should meet the following proportion requirements (AASHTO-LRFD Article 6.10.2.2) as follows:

$$\frac{b_f}{2t_f} \leq 12 \quad (4.2)$$

$$b_f \geq \frac{D}{6} \quad (4.3)$$

$$t_f \geq 1.1t_w \quad (4.4)$$

$$0.1 \leq \frac{I_{yc}}{I_{yt}} \leq 10 \quad (4.5)$$

- where b_f and t_f are full width and thickness of the flange (in.); t_w is web thickness (in.); I_{yc} and I_{yt} are the moment of inertia of the compression flange and the tension flange about the vertical axis in the plane of web respectively (in.⁴); D is the web depth (in.). Equation 4.2 is to ensure that the flange will not distort excessively when welded to the web. Equation 4.3 ensures that stiffened interior web panels can develop postelastic buckling shear resistance by the tension field action. Equation 4.4 ensures that flanges can provide some restraint and proper boundary conditions to resist web shear buckling. Equation 4.5 ensures more efficient flange proportions and prevents the use of sections that may be difficult to handle during construction. It also ensures that the lateral torsional buckling formulas used in AASHTO (AASHTO 2012) are valid.

4.3.4 Webs

The web mainly provides shear strength for the girder. Since the web contributes little to the bending resistance, its thickness should be as small as practical to meet the web-depth-to-thickness ratio limits $D/t_w \leq 150$ for webs without longitudinal stiffeners, and $D/t_w \leq 300$ for webs with longitudinal stiffeners, respectively (AASHTO Article 6.10.2.1). It is preferable to have web depths in increments of 2 or 3 in. for convenience. Web depths greater than 120 in. will require both longitudinal and vertical splices.

In order to avoid an excessive distortion from welding, the web thickness is preferred not to be less than 1/2 in. A thinner plate is subjective. The thickness should be sufficient to preclude the need for longitudinal stiffeners. Web thickness should be constant or with a limited number of changes. It is more desirable to have one or two web sizes for a continuous girder and one web size for a simple span. Web thickness increments should be 1/16 or 1/8 in. for plate thicknesses up to 1 in., and 1/4 in. increments for plates greater than 1 in.

4.3.5 Stiffeners

For built-up I-sections, the longitudinal stiffeners may be provided to increase bending resistance by preventing local buckling, while transverse stiffeners are usually provided to increase shear resistance by the tension field action (Basler 1961a and 1961b). The following three types of stiffeners are usually used for I-Sections:

- *Transverse intermediate stiffeners:* They are typically welded to the web and work as anchors for the tension field force so that postbuckling shear resistance can be developed. It should be noted that elastic web shear buckling cannot be prevented by transverse stiffeners. Transverse stiffeners are designed to (1) meet the slenderness requirement of projecting elements to prevent local buckling, (2) provide stiffness to allow the web developing its postbuckling capacity, and (3) have strength to resist the vertical components of the diagonal stresses in the web. Stiffeners connecting cross frames/diaphragms should be welded or bolted to the both flanges. Stiffeners without connecting cross frames/diaphragms are welded to the compression flange and fitted tightly to the tension flange. Stiffener plates are preferred to have even inch widths from the flat bar stock sizes.
- *Bearing stiffeners:* They are required at all bearing locations and at all locations supporting concentrated loads. For rolled beams, bearing stiffeners may not be needed when factored shear is less than 75% of factored shear resistance. They work as compression members to support vertical concentrated loads by bearing on the ends of stiffeners (Figure 4.5). They are transverse stiffeners and connect to the web to provide a vertical boundary for anchoring shear force from tension field action. They are designed to satisfy the slenderness, bearing, and axial compression requirements. Bearing stiffeners are welded or bolted to both sides of the web. Bearing stiffeners should be thick enough to preclude the need for multiple pairs of bearing stiffeners to avoid multiple-stiffener fabrication difficulties. AASHTO-LRFD Article 6.10.11.2 requires that the stiffeners extend to the full depth of the web and as close as practical to the edge of the flanges.
- *Longitudinal stiffeners:* They work as restraining boundaries for compression elements so that inelastic flexural buckling stress can be developed in a web. It consists of either a plate welded longitudinally to one side of the web, or a bolted angle. It should be located at a distance of $2D_c/5$ from the inner surface of the compression flange, where D_c is the depth of web in compression at the maximum moment section to provide optimum design. The slenderness and stiffness need to be considered for sizing the longitudinal stiffeners. It is recommended that sufficient web thickness be used to eliminate the need for longitudinal stiffeners as it can cause difficulty in fabrication and create fatigue-prone details.

4.4 Span and Framing Arrangement

4.4.1 Span Configuration

Span configuration plays an important role in the efficient and cost-effective use of steel. For cases where pier locations are flexible, designers should optimize the span arrangement. Two-span continuous girders/beams are not the most efficient system because of high negative moments. Three and four span continuous girders are preferable, but may not always be possible. For multispan continuous girders, a good span arrangement is to have the end span lengths approximately 70% to 80% of the interior span lengths. Equal interior span arrangements are also relatively economical. A span configuration with uplift due to live load plus impact should be avoided. Figure 4.8 also shows some typical span arrangements.

The use of simply supported girders under construction load and continuous girders through steel reinforcement for live load can be an economical framing method (Azizinamini 2007). This type of framing presents possible advantages over continuous beam designs by eliminating costly splices and heavy lifts during girder erection. The potential drawbacks are that deeper section may be required and the weight of steel per unit deck area may be higher. This framing method needs to be investigated on a case-by-case basis to determine whether it can be economically advantageous.

When simply supported span configurations are used, special attention should be given to seismic performance detailing.

4.4.2 Girder Spacing

As a general rule, the most economical superstructure design can be achieved using girder spacing within 11 to 14 ft. range. For spans less than 140 ft., 10 to 12 ft. spacing is preferred. For spans greater than 140 ft., 11 to 14 ft. spacing is recommended. The use of metal deck form panels will limit the spacing to about 16 ft. Girder spacing over 16 ft. may require a transversely posttensioned deck system. Parallel girder layout should be used wherever possible.

4.4.3 Diaphragms and Cross Frames

The term diaphragm and cross frame are synonymous. Figure 4.9 shows commonly used types of diaphragms and cross frames used in I-shaped plate girder and rolled beam spans. The K-frames and X-frames usually include a top strut as shown in Figure 4.9. Intermediate cross frames provide bracing against lateral torsional buckling of compression flanges during erection and deck concrete placement, and for all loading stages in negative flexure regions. They also provide lateral bracing for wind loads and participate to some degree in live load distribution. End cross frames or diaphragms at piers and abutments are provided to transmit lateral wind loads and seismic loads to the bearings.

In horizontally curved girder bridges, cross frames and diaphragms are considered primary load-carrying members because they constitute an essential part of the overall structural system. In skewed girder bridges, the cross frames carry significant load, as they resist differential deflection of adjacent girders and form secondary load paths.

End cross frames or diaphragms in slab on-girder steel bridges may be designed as ductile systems for better inelastic performance and energy dissipation capacity to limit the seismic forces transferred to the substructure in transverse direction. Ductile end diaphragm systems are usually effective in longer span bridges and may not be effective for short-span bridges when the superstructure is significantly stiffer than the substructure. More detailed guidelines and references are made to Zahrai and Bruneau (1998 and 1999); Carden et al. (2001); Carden, Itani and Buckle (2006); Bahrami, Itani and Buckle (2009).

4.4.3.1 Spacing

Arbitrary 25 ft. spacing limit for diaphragms and cross frames was specified in the AASHTO Standard Design Specifications (2002). The AASHTO-LRFD (2012), however, no longer specifies a limit on the

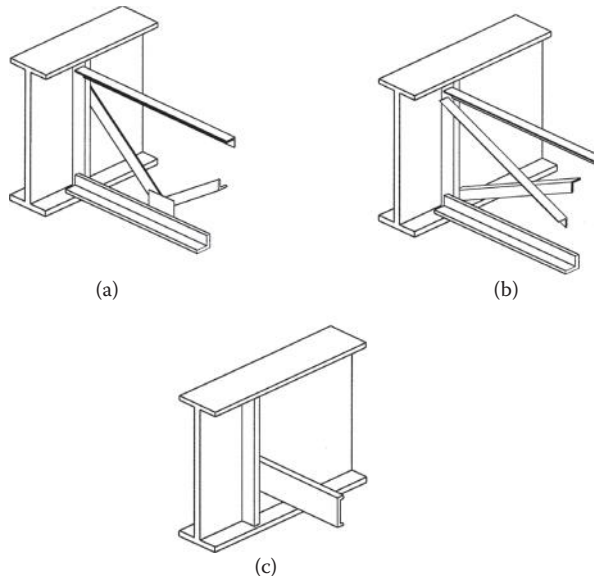


FIGURE 4.9 Cross frames and diaphragms: (a) V-type; (b) X-type; (c) channel diaphragm.

cross-frame spacing, but instead requires rational analysis to investigate needs for all stages of assumed construction procedures and the final conditions. Spacing is compatible with the transverse stiffeners.

4.4.3.2 Orientation

Intermediate cross frames are placed parallel to the skew up to a 20° skew and normal to the girders for the skew angle larger than 20° . On skewed bridges with cross frames placed normal to the girders, there may be situations where the cross frames are staggered or discontinuous across the width of the bridge. At these discontinuous cross frames, lateral flange bending stresses may be introduced into the girder flanges and should be considered. Install stiffeners on the back side of connection plates if staggered cross frames are used. Horizontally curved girders should always have the cross frames placed on radial lines.

A good economical design will minimize the number of diaphragms with varying geometries. Superelevation changes, vertical curves, different connection plate widths, and flaring girders all work against this goal.

4.4.3.3 Connections

Cross frames are typically connected to transverse stiffeners. The stiffeners have a positive connection to the girder flange and may either be bolted or welded, although welding is preferred.

For bridges built in stages or with larger skew angles, differential deflections between girders due to slab placement can be significant. If differential deflections are significant, slotted holes and hand tight erection bolts with jamb nuts are provided during concrete placement, and permanent bolts fully tensioned or field welded connection are installed after the barriers are placed. The bolt holes can be field drilled to insure proper fit. Intermediate cross frames between stages are eliminated if possible. The connection between cross frames and stiffeners typically are bolted for construction fit up purpose to address potential out-of-plane fatigue cracking of the welds.

4.4.3.4 Design Guidelines

- The diaphragm or cross frame is as deep as practicable to transfer lateral load and to provide lateral stability. They are at least 0.5 of the beam depth for rolled beams and 0.75 of the girder depth for plate girders.

- Cross frames should be designed and detailed such that they can be erected as a single unit, and all welding during fabrication should be done from one side to minimize handling costs. As minimum, cross frames are designed to resist lateral wind loads. A rational analysis is preferred to determine actual lateral forces.
- End diaphragms and cross frames at bearings are designed to resist all lateral forces transmitted to the substructure. Unless they are detailed as ductile elements, the end diaphragms or cross frames are designed to resist the overstrength shear capacity of the substructures. Shear connectors should be provided to transfer lateral loads from the deck to the end diaphragm. When an expansion joint occurs at a support, the end diaphragm is designed to resist truck wheel and impact loads.
- Effective slenderness ratios (KL/r) for compression diagonals are less than 120 and 140 for horizontally curved girders and straight girders, respectively (AASHTO-LRFD Article 6.9.3); and for tension members (L/r) less than 240 (AASHTO-LRFD Article 6.8.4).
- Cross frame members and gussets consisting of single angle or WT shapes should be designed for the eccentricity inherent at the gusset connections. Use rectangular gusset plates in lieu of multisided polygons.
- Steel plate, I girder, and concrete diaphragms may be used at abutments and piers. The use of integral abutments, piers, and bents is encouraged.

4.4.4 Lateral Bracing

The main function of the lateral bracing is to transfer wind loads to bearings and provides lateral stability to compression flange in a horizontal plan. The use of lateral bracing systems is no longer common, since it is now recognized that the role of lateral bracing systems in resisting wind loads is negligible in the completed bridge. However, all construction stages should be investigated for the need of lateral bracing, in particular for curved girders and long straight girders. The lateral bracing should be placed as near the plane of the flange being braced as possible.

Bottom flange lateral bracing should be avoided because the bracing creates fatigue-sensitive details and is costly to fabricate, install, and maintain. Flange sizes should be sufficient to preclude the need for bottom flange lateral bracing.

4.4.5 Field Splice Locations

Field splices should preferably be located at points of dead load contraflexure and at points of section change and spaced more than 50 ft. (15.2 m) apart. The splice locations are also dependent on shipping and fabrication limits. The length of shipping piece is usually less than 125 ft. (38 m) and weight less than 40 t. It is unnecessary to locate the splices at the exact contraflexure point, but they should be reasonably close. Field splices are sometimes required to be placed near points of maximum moment in longer spans in order to meet erection requirements. Field bolted splices as shown in Figure 4.10 are preferred. Adjacent girders should be spliced in approximately the same location.

4.4.6 Expansion Joints and Hinges

In-span hinges are generally not recommended for steel bridges since there are not many acceptable solutions for the design of hinges to resist seismic loads. Steel bridges have been designed without expansion joints and hinges at lengths up to 1200 ft. (366 m). When dropped cap bents are utilized, the superstructure may be separated from the substructure with expansion bearings to prevent undue temperature effects on the substructure.



FIGURE 4.10 Field bolted splices.

4.5 Structural Modeling and Analysis

Straight steel girder bridges are commonly analyzed by the line girder method. The method evaluates the girder individually and uses live load distribution factors to consider the effects from the rest of the superstructure system. In the analysis, flexural stiffness of the composite section is assumed over the entire bridge length even though the negative moment regions may be designed as noncomposite for the section capacity. Longitudinal reinforcing steel in the top mat of concrete deck within the effective deck width is generally not included in calculating section properties.

In the preliminary analysis, a constant flexural stiffness may be assumed. In the final analysis of composite I-girders, the stiffness properties of the steel section alone for the loads applied to noncomposite sections, the stiffness properties of the long-term composite section for permanent loads applied to composite sections, and the stiffness properties of the short-term composite section properties for transient loads are used over the entire bridge length, respectively.

Dead loads are usually distributed to the girders based on the tributary area. Live load distribution is dependent on the girder spacing S , span length L , concrete slab depth t_s , longitudinal stiffness parameter K_g , and number of girders N_b . Some approximate formulae are recommended by AASHTO Article 4.6.2.2.1 (AASHTO 2012).

The more refined analysis using the finite element method may be used in analyzing complex bridge systems such as skewed and horizontally curved bridges. Reference is made to the recent AASHTO/NSBA *Guidelines for Steel Girder Bridge Analysis* (AASHTO/NBSA 2011).

4.6 Design Limit States and Procedures

4.6.1 Design Limit States

A highway bridge in the United States is designed to meet the requirements under various limit states specified by AASHTO-LRFD (2012) such as Strength I, Strength II, Service II, Fatigue I and II, and extreme events. Constructibility (AASHTO 6.10.3) must be considered. See Chapters 5, 6, and 14 in *Bridge Engineering Handbook, Second Edition: Fundamentals*, for a more detailed discussion.

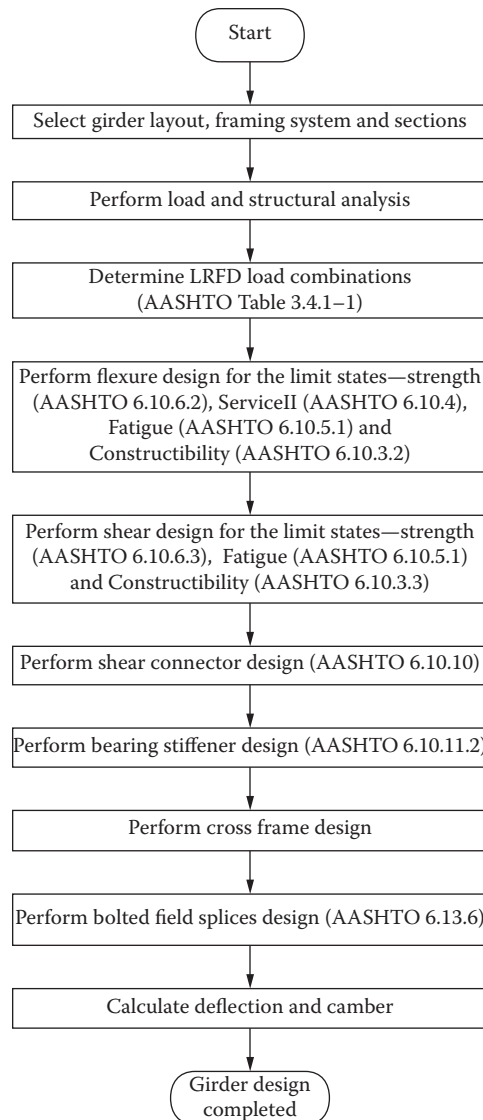


FIGURE 4.11 Typical steel girder design flowchart.

4.6.2 Design Procedures

The highway steel girder design may follow the flowchart as shown in Figure 4.11.

4.7 Design Example: Three-Span Continuous Composite Plategirder Bridge

4.7.1 Bridge Data

A three-span continuous composite plate girder bridge has two equal side spans of length 160 ft. (48.8 m) and one midspan of 210 ft. (64 m). The superstructure is 44 ft. (13.4 m) wide. The elevation and plan views are shown in Figure 4.12.

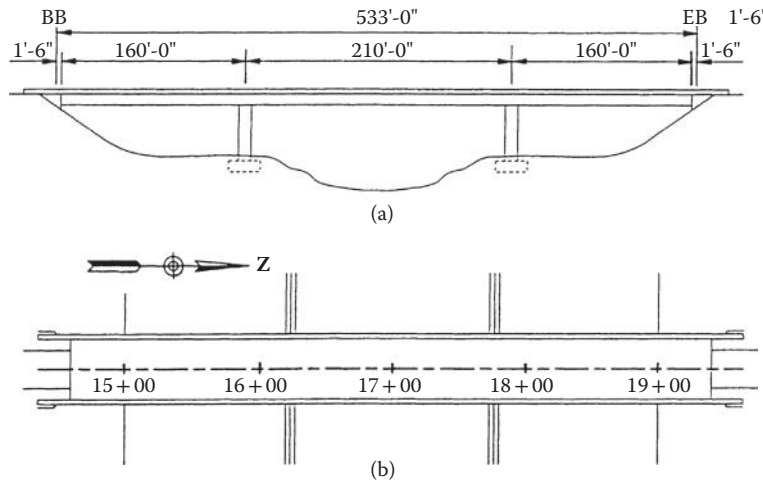


FIGURE 4.12 A three-span continuous plate girder bridge: (a) elevation; (b) plan.

Structural steel: A709 Grade 50 for web and flanges

$F_{yw} = F_{yt} = F_{yc} = F_y = 50 \text{ ksi}$ (345 MPa)

A709 Grade 36 for stiffeners, and so on. $F_{ys} = 36 \text{ ksi}$ (248 MPa)

Concrete: $f'_c = 4000 \text{ psi}$ (27.6 MPa), $E_c = 3625 \text{ ksi}$ (25.0 MPa)

modular ratio $n = 8$

Loads: Dead load = self-weight + barrier rail + future wearing 3 in. AC overlay

Live load = AASHTO HL-93 + dynamic load allowance

Single-lane average daily truck traffic ADTT = 3600 (one way)

Deck: Concrete deck slab with thickness = 10.875 in. (276 mm)

Construction: Unshored construction

4.7.2 Design Requirements

Perform the following design calculations for an interior plate girder at Span 1 in accordance with the *AASHTO LRFD Bridge Design Specifications*, 2012 Edition (AASHTO 2012).

- Select girder layout and sections for positive flexure region.
- Perform load and structural analysis.
- Determine load and resistance factors and load combinations.
- Calculate factored moments and shears.
- Design for flexure—composite section at 0.4 point—strength limit state.
- Design for shear—left end of span 1—strength limit state.
- Check fatigue limit state—typical girder details—positive flexure region.
- Design bearing stiffener.
- Design intermediate transverse stiffener.
- Design shear connectors for positive flexural region of Span 1.
- Check service limit state requirements.
- Check constructability requirements.

4.7.3 Design Calculations

4.7.3.1 Select Girder Layout and Sections for Positive Flexure Region

1. Select Girder Spacing

A girder spacing of 16 ft is selected and typical section is shown in Figure 4.13.

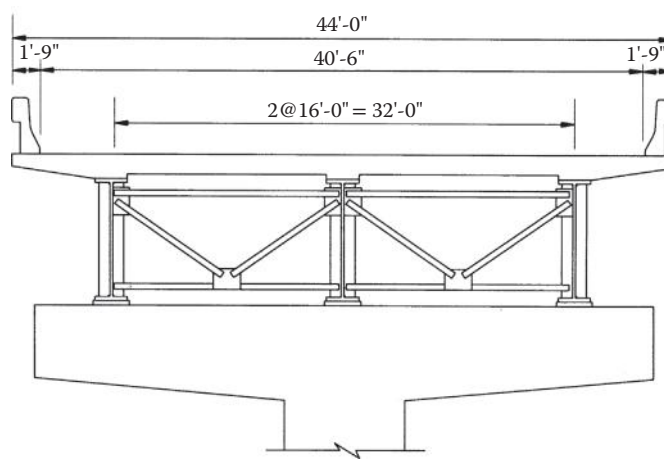


FIGURE 4.13 A three-span continuous plate girder bridge—typical section.

2. Select Intermediate Cross Frame Spacing

Cross frames at spacing of 20 ft. for Spans 1 and 3, and 21 ft. for Span 2 are selected to accommodate transverse stiffener spacing for web design and to facilitate a reduction in the required flange thickness of the girder section at the bent.

3. Select Steel Girder Section for Positive Flexure Region

The cross section is usually proportioned on the basis of past practice and proportion limits specified in AASHTO 6.10.2.

Top Compression Flange

The maximum transported length of a steel plate girder is generally limited to a length of about 120 ft. and a weight of about 180 kip and may vary due to the locations. It is common practice that the unsupported length of each shipping piece divided by the minimum width of compression flange should be less than about 85. For a length of 120 ft., the width of compression flange is preferably larger than $(120 \times 12)/85 = 17$ in. Try top compression flange $b_{fc} \times t_{fc} = 18 \times 1$ (in. \times in.).

Web

AASHTO Table 2.5.2.6.3-1 specifies that, for composite girders, the minimum ratio of the depth of the steel girder portion to the length of the span is 0.033 for a simple span and 0.027 for a continuous spans. For this design example, the depth of the steel girder is larger than $0.027(210) = 5.67$ ft. = 68 in. Try web $D \times t_w = 90 \times 0.625$ (in. \times in.).

Bottom Tension Flange

Try bottom tension flange $b_{ft} \times t_{ft} = 18 \times 1.75$ (in. \times in.).

Check Section Proportion Limits (AASHTO 6.10.2.2)

- Web without longitudinal stiffeners

$$\frac{D}{t_w} = \frac{90}{0.625} = 144 < 150$$

- Compression flange

$$\frac{b_{fc}}{2t_{fc}} = \frac{18}{2(1.0)} = 9 < 12$$

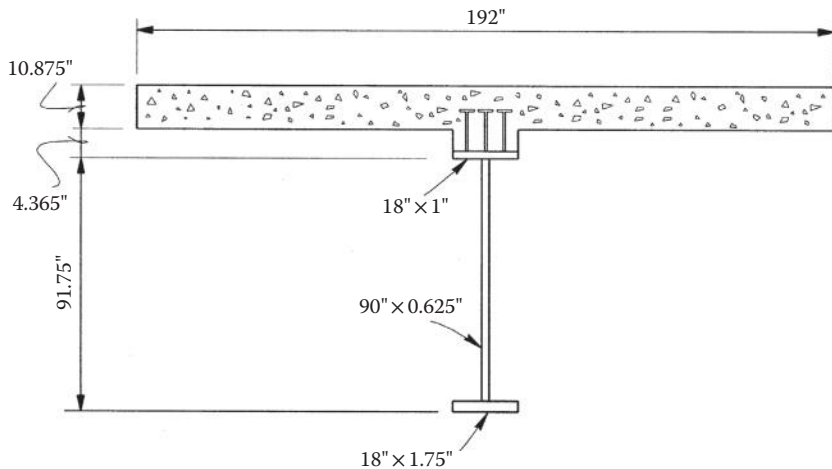


FIGURE 4.14 Cross section in positive flexural region.

$$b_{fc} = 18 > \frac{D}{6} = \frac{90}{6} = 15$$

$$t_{fc} = 1.0 \text{ in.} > 1.1 t_w = 1.1(0.625) = 0.69 \text{ in.}$$

- Tension flange

$$\frac{b_{ft}}{2t_{ft}} = \frac{18}{2(1.75)} = 5.14 < 12$$

$$b_{ft} = 18 > \frac{D}{6} = \frac{90}{6} = 15$$

$$t_{ft} = 1.75 \text{ in.} > 1.1 t_w = 1.1(0.625) = 0.69 \text{ in.}$$

- Flanges Ratio

$$0.1 < \frac{I_{yc}}{I_{yt}} = \frac{(1)(18)^3 / 12}{(1.75)(18)^3 / 12} = 0.57 < 10$$

Interior girder section is shown in Figure 4.14.

4.7.3.2 Perform Load and Structural Analysis

1. Calculate Permanent Loads for an Interior Girder

The permanent load or dead load of an interior girder includes *DC* and *DW*. *DC* is the dead load of structural components and nonstructural attachments. *DW* is the dead load of the wearing surface. For design purposes, the two parts of *DC* are defined as, *DC1*, structural dead load,

acting on the noncomposite section and $DC2$, nonstructural dead load, acting on the long-term composite section.

- $DC1$ — Deck concrete (self-weight 150 lbs./ft.³) and steel girder including the bracing system and details (estimated weight 300 lbs./ft. for each girder). Assume that $DC1$ is acting on the noncomposite section, and is distributed to each girder by the tributary area. The tributary width for the interior girder is 16 ft. (4.9 m).

$$\begin{aligned} DC1 &= [(10.875/12)(16) + (1.5)(15.2 - 10.975)/12(1.5)](0.15) + 0.3 \\ &= 2.557 \text{ kips/ft. (37.314 kN/m)} \end{aligned}$$

- $DC2$ —Barrier rail weight (784 kip/ft.). Assume that $DC2$ is acting on the long-term composite section and is equally distributed to each girder.

$$DC2 = 0.784/3 = 0.261 \text{ kip/ft. (3.809 kN/m)}$$

- DW — A future wearing surface of 3 in. (76 mm) with a unit weight of 140 lbs./ft.³. Assume that DW is carried by the long-term composite section, and is equally distributed to each girder.

$$\begin{aligned} DW &= (\text{deck width} - \text{barrier width}) (\text{thickness of wearing surface}) (\text{unit weight})/3 \\ &= [44 - 2(1.75)] (0.25) (0.14)/3 = 0.473 \text{ kip/ft. (6.903 kN/m)} \end{aligned}$$

2. Determine Live Load and Dynamic Load Allowance

The design live load LL is the AASHTO HL-93. To consider the wheel-load impact for moving vehicles, the dynamic load allowance $IM = 33\%$ for the Strength I Limit State, and 15% for the fatigue limit states is used (AASHTO Table 3.6.2.1-1).

3. Calculate Live Load Distribution Factors

Check Ranges of Applicability of Live Load Distribution Factors

For beam-slab bridges, the distribution of live load is dependent on the girder spacing S , span length L , concrete slab depth t_s , and longitudinal stiffness parameter K_g and number of girders N_b . This example is categorized as Type "a" (concrete deck on steel beams) (AASHTO Table 4.6.2.2-1).

The preliminary section shown in Figure 4.15 is assumed to estimate the longitudinal stiffness parameter, K_g (AASHTO 4.6.2.2.1-1) for the positive moment region in Span 1.

Check ranges of applicability of AASHTO Tables 4.6.2.2.2b-1 and 4.6.2.2.3a-1 for Type "a" (concrete deck on steel beams) structure as follows:

Girder spacing: 3.5 ft. < $S = 16$ ft. = 16 ft.

Span length: 20 ft. < $L = (160, 210, \text{ and } 160)$ ft. < 240 ft.

Concrete deck: 4.5 in. < $t_s = 10.875$ in. < 12.0 in.

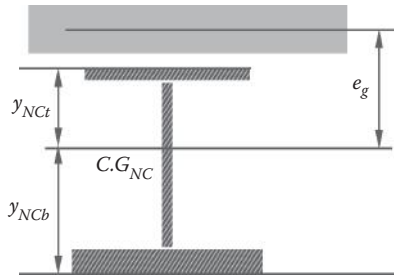
Number of girders: $N_b = 3 < 4$

Stiffness parameter: 10,000 in.⁴ < $K_g = 4,750,927$ in.⁴ < 7,000,000 in.⁴

It is seen that the number of girders $N_b = 3$ satisfies the limitation of ranges of applicability of the approximate live load distribution factors specified in AASHTO Tables 4.6.2.2.2b-1 and 4.6.2.2.3a-1. The live load distribution factor for moments, DF_m , is the lesser of AASHTO approximate formula and the lever rule. The live load distribution factor for shears, DF_s , is determined by the lever rule.

For preliminary design, AASHTO 4.6.2.2.2b permits that term $K_g/(12Lt_s)^3$ may be taken as 1.0. Although the K_g term varies slightly along the span and between spans, the distribution factor is typically not sensitive to the value of K_g . For simplicity, the K_g of Span 1 is used for all spans of this example.

Component	A_i (in. ²)	y_i (in.)	$A_i y_i$ (in. ³)	$y_i - y_{NCb}$ (in.)	$A_i (y_i - y_{NCb})^2$ (in. ⁴)	I_o (in. ⁴)
Top flange 18 × 1	18.00	92.25	1,660.5	51.42	47,593	1.5
Web 90 × 0.625	56.25	46.75	2,629.7	5.92	1,972	37,969
Bottom flange 18 × 1.75	31.50	0.875	27.6	-39.95	50,286	8.04
Σ	105.75	—	4,317.8	—	99,850	37,978



$$y_{NCb} = \frac{\sum A_i y_i}{\sum A_i} = \frac{4,317.8}{105.75} = 40.83 \text{ in.}$$

$$I_{NC} = \sum I_o + \sum A_i (y_i - y_{NCb})^2 \\ = 37,978 + 99,850 = 137,828 \text{ in.}^4$$

$$e_g = 51.92 - 1.0 + 4.375 - \frac{10.875}{2} \\ = 60.73 \text{ in.}$$

$$K_g = n(I_{NC} + A e_g^2) = 9[137,838 + (105.75)(60.73)^2] = 4,750,927 \text{ in.}^4$$

FIGURE 4.15 Preliminary section properties.

Lever Rule

The lever rule assumes that the deck in its transverse direction is simply supported by the girders and uses statics to determine the live load distribution to the girders. AASHTO also requires that, when the level rule is used, the multiple presence factor m (1.2 for one loaded lane; 1.0 for two loaded lanes; 0.85 for three loaded lanes; and 0.65 for more than three loaded lanes) should apply.

Figure 4.16 shows locations of traffic lanes for the interior girder. For a 12 ft. (3.6 m) traffic lane width, the number of traffic lanes for this bridge is three.

- a. One lane loaded (Figure 4.16a)

$$R = \frac{13}{16} = 0.8125 \text{ lanes}$$

$$DF = mR = 1.2(0.8125) = 0.975 \text{ lanes}$$

b. Two lanes loaded (Figure 4.16b)

$$R = \frac{13}{16} + \frac{9}{16} = 1.375 \text{ lanes}$$

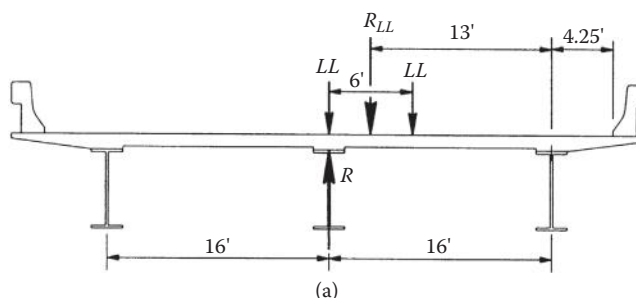
$$DF = mR = 1.0(1.375) = 1.375 \text{ lanes (controls)}$$

c. Three lanes loaded (Figure 4.16c)

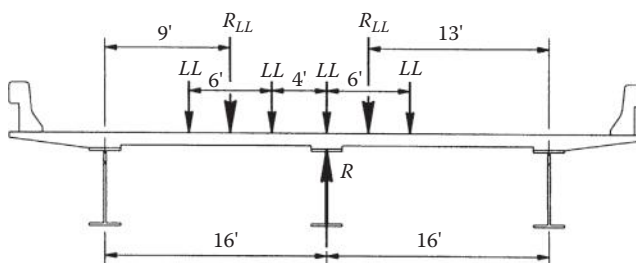
$$R = \frac{(13+3)}{16} + \frac{7}{16} = 1.4375 \text{ lanes}$$

$$DF = mR = 0.85(1.4375) = 1.222 \text{ lanes}$$

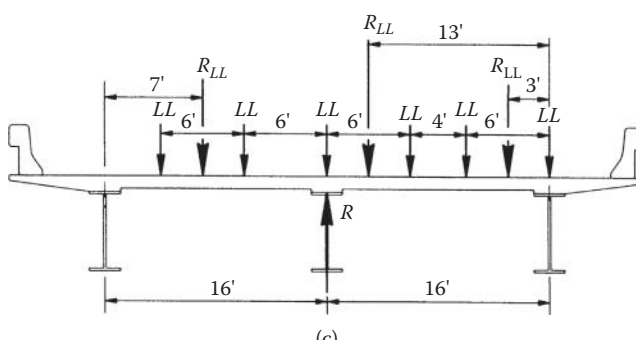
Live load distribution factors obtained by the lever rule are also listed in Table 4.1.
AASHTO Approximate Method



(a)



(b)



(c)

FIGURE 4.16 Live load distribution—lever rule: (a) one traffic lane; (b) two traffic lanes; (c) three traffic lanes.

TABLE 4.1 Live Load Distribution Factors for Interior Girder

Span and Location	Span Length (ft.)	Strength Limit State				Fatigue Limit State	
		Approximate Formulas		Lever Rule		DF_m	DF_v
		Moment DF_m	Two or More Lanes	One Lane	DF_{mp} DF_v		
1*	160	0.624	1.000	0.975	1.375	0.520	0.813
1 & 2**	185	0.593	0.957			0.494	
2*	210	0.566	0.924			0.472	
2 and 3**	185	0.593	0.957			0.494	
3*	160	0.624	1.000			0.472	

Notes:

*The span length span for which moment is being calculated for positive moment, negative moment—other than near interior supports of continuous spans, shear, and exterior reaction.

**Average span length for negative moment—near interior supports of continuous spans from point of contraflexure to point of contraflexure under a uniform load on all spans, and interior reaction of continuous span.

i. One design lane loaded

$$DF_m = 0.06 + \left(\frac{S}{14} \right)^{0.4} \left(\frac{S}{L} \right)^{0.3} \left(\frac{K_g}{12Lt_s^3} \right)^{0.1}$$

ii. Two or more design lanes loaded

$$DF_m = 0.075 + \left(\frac{S}{9.5} \right)^{0.6} \left(\frac{S}{L} \right)^{0.2} \left(\frac{K_g}{12Lt_s^3} \right)^{0.1}$$

$$K_g = 4,750,927 \text{ in.}^4$$

$$S = 16 \text{ ft.}$$

$$t_s = 10.875 \text{ in.}$$

Live load distribution factors in accordance with AASHTO Tables 4.6.2.2.2b-1 and 4.6.2.2.3a-1 are calculated and listed in Table 4.1.

It is seen that live load distribution factors for moments obtained by approximate formulas for case of two or more lanes loaded control the strength limit states. For the fatigue limit states, since live load is one HL-93 truck, multiple lane presence factor of 1.2 is removed for the case of one lane loaded (AASHTO 3.6.1.1.2).

4. *Perform Structural Analysis*

A line girder analysis for three-span continuous beams is performed to obtain the unfactored dead load for the interior girder and unfactored live load moments and shears for one lane loaded. A constant flexural stiffness is assumed for simplicity.

5. *Calculate Unfactored Moments and Shears*

For an interior girder, unfactored moment and shear envelopes are shown in Figures 4.17 and 4.18 for the strength limit state, and Figures 4.19 and 4.20 for the fatigue limit state, respectively. Unfactored live load moments and shears for the interior girder are obtained by multiplying the appropriate live load distribution factor to one lane live load moments and shears; this is listed in Tables 4.2 to 4.4. Only the results for Span 1 and one-half of Span 2 are shown in these tables and figures since the bridge is symmetrical about the centerline of Span 2.

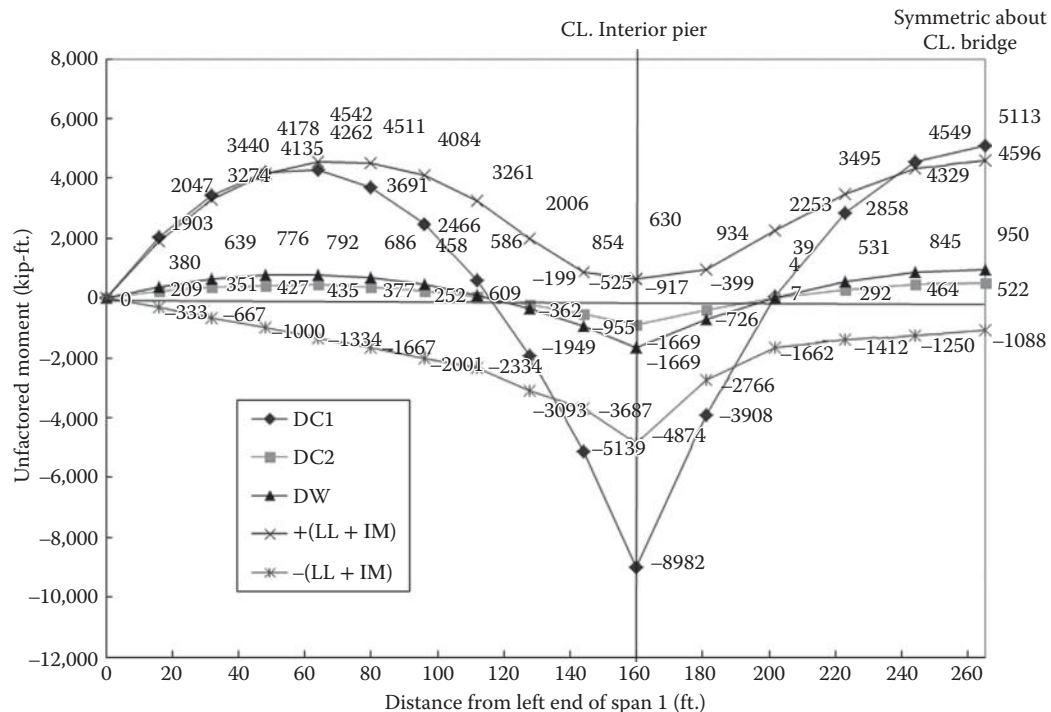


FIGURE 4.17 Unfactored moment envelopes for interior girder—Strength I.

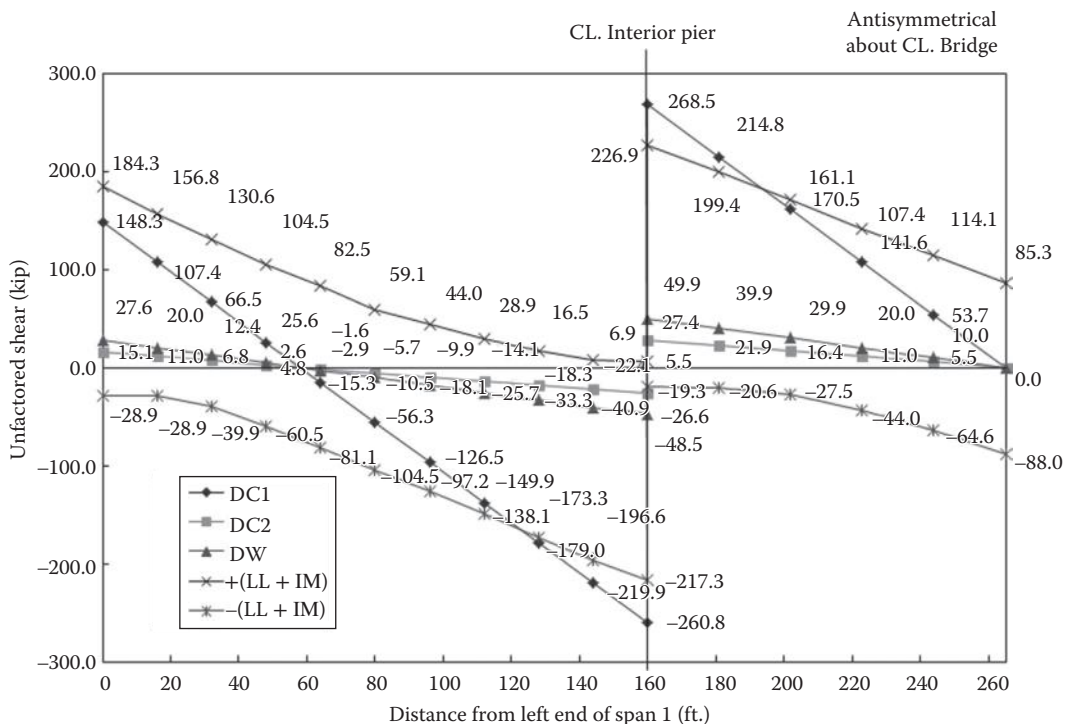


FIGURE 4.18 Unfactored shear envelopes for interior girder—Strength I.

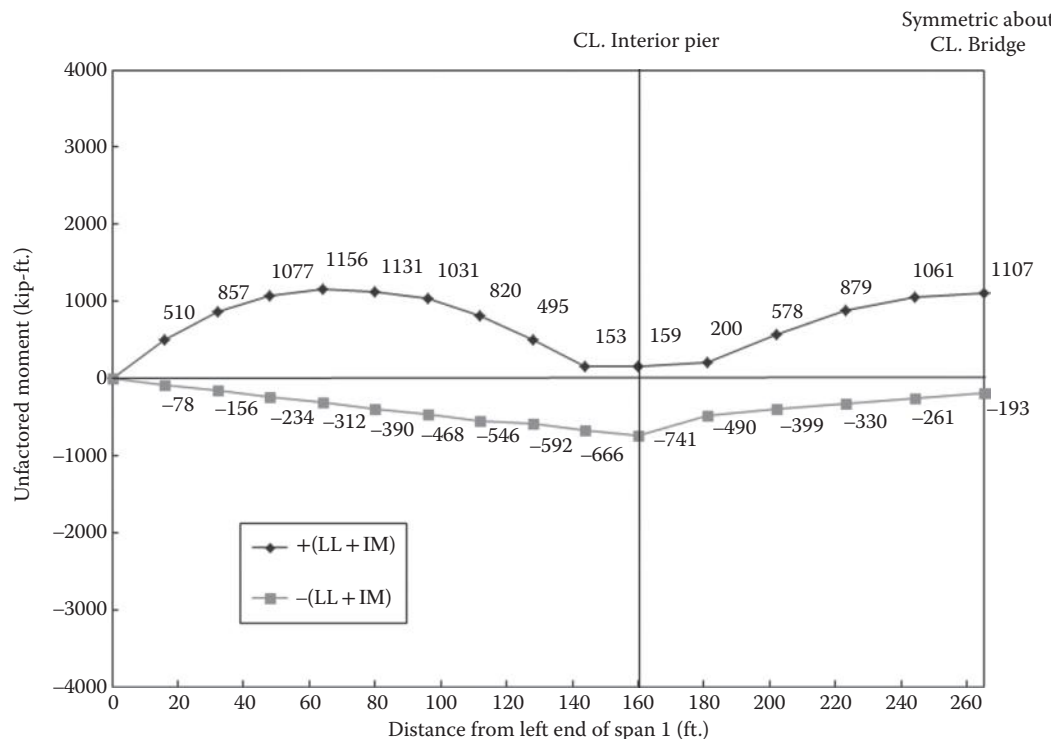


FIGURE 4.19 Unfactored moment ranges for interior girder—fatigue.

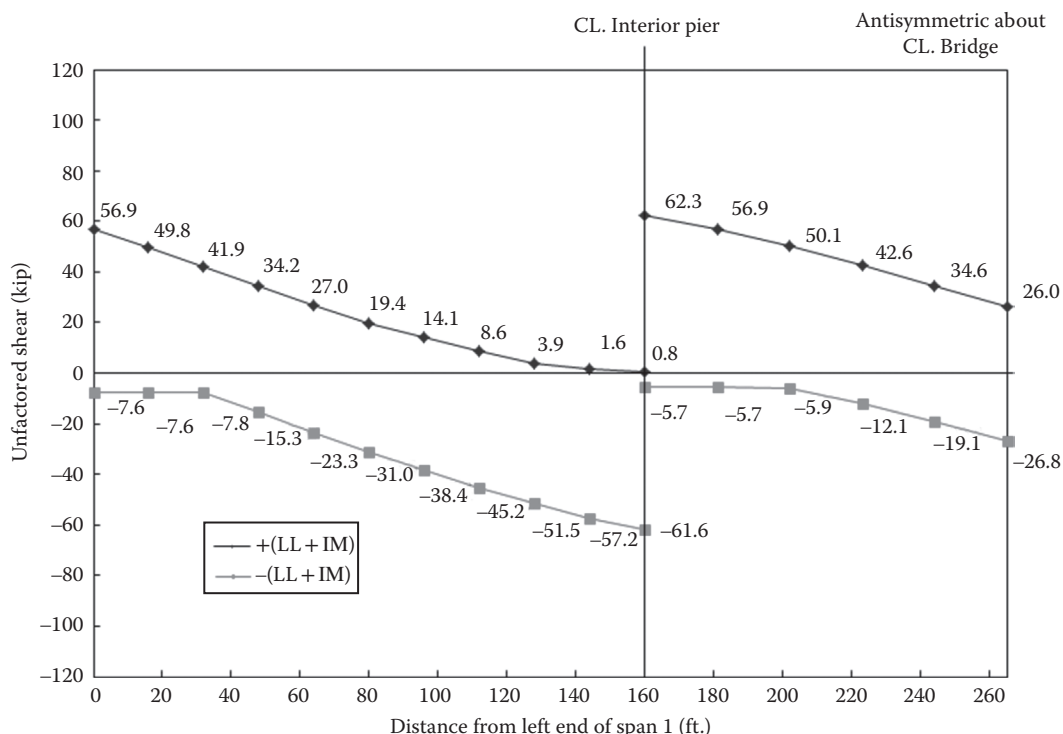


FIGURE 4.20 Unfactored shear ranges for interior girder—fatigue.

TABLE 4.2 Moment Envelopes for Interior Girder at Strength Limit State I

Span	Location (x/L)	M_{DC1} (kip-ft.)	M_{DC2} (kip-ft.)	M_{DW} (kip-ft.)	M_{LL+IM} (kip-ft.)		M_u (kip-ft.)	
		Dead Load-1	Dead Load-2	Wearing Surface	Positive	Negative	Positive	Negative
1	0.0	0	0	0	0	0	0	0
	0.1	2047	209	380	1903	-333	6385	2668
	0.2	3440	351	639	3274	-667	10856	4304
	0.3	4178	427	776	4135	-1000	13449	4912
	0.4	4262	435	792	4542	-1334	14257	4489
	0.5	3691	377	686	4511	-1667	13308	3037
	0.6	2466	252	458	4084	-2001	10669	553
	0.7	586	60	109	3261	-2334	6343	-2959
	0.8	-1949	-199	-362	2006	-3093	268	-8209
	0.9	-5139	-525	-955	854	-3687	-6666	-14215
	1.0	-8982	-917	-1669	630	-4874	-13086	-22236
	0.0	-8982	-917	-1669	630	-4874	-13086	-22236
2	0.1	-3908	-399	-726	934	-2766	-4596	-10747
	0.2	39	4	7	2253	-1662	3806	-2702
	0.3	2858	292	531	3495	-1412	10308	2250
	0.4	4549	464	845	4329	-1250	14355	5080
	0.5	5113	522	950	4596	-1088	15686	6236

Notes:

1. Live load distribution factors for moments are listed in Table 4.1

2. Dynamic load allowance $IM = 33\%$

3. $M_u = 0.95 [1.25(M_{DC1} + M_{DC2}) + 1.5 M_{DW} + 1.75 M_{LL+IM}]$

TABLE 4.3 Shear Envelopes for Interior Girder at Strength Limit State I

Span	Location (x/L)	V_{DC1} (kip)	V_{DC2} (kip)	V_{DW} (kip)	V_{LL+IM} (kip)		V_u (kip)	
		Dead load-1	Dead load-2	Wearing surface	Positive	Negative	Positive	Negative
1	0.0	148.4	15.1	27.4	184.3	-28.9	539.7	185.4
	0.1	107.5	11.0	19.9	156.8	-28.9	429.7	121.1
	0.2	66.6	6.8	12.3	130.6	-39.9	321.9	38.4
	0.3	25.6	2.6	4.7	104.5	-60.5	214.1	-60.3
	0.4	-15.3	-1.6	-2.8	82.5	-81.1	113.0	-159.1
	0.5	-56.2	-5.7	-10.4	59.1	-104.5	9.7	-262.3
	0.6	-97.1	-9.9	-18.0	44.0	-126.5	-79.8	-363.3
	0.7	-138.0	-14.1	-25.5	28.9	-149.9	-169.4	-466.5
	0.8	-178.9	-18.3	-33.1	16.5	-173.3	-254.3	-569.8
	0.9	-219.8	-22.4	-40.7	6.9	-196.6	-334.6	-672.9
	1.0	-260.7	-26.6	-48.2	5.5	-217.3	-401.3	-771.6
	0.0	268.5	27.4	49.7	226.9	-19.3	799.7	390.5
	0.1	214.7	21.9	39.7	199.4	-20.6	669.4	303.6
2	0.2	161.1	16.4	29.8	170.5	-27.5	536.8	207.7
	0.3	107.4	11.0	19.9	141.6	-44.0	404.6	96.0
	0.4	53.7	5.5	9.9	114.1	-64.6	274.3	-22.9
	0.5	0	0	0	85.3	-88.0	141.7	-146.3

Notes:

1. Live load distribution factors are listed in Table 4.1

2. Dynamic load allowance $IM = 33\%$

3. $V_u = 0.95 [1.25(V_{DC1} + V_{DC2}) + 1.5 V_{DW} + 1.75 V_{LL+IM}]$

TABLE 4.4 Moment and Shear Envelopes for Interior Girder at Fatigue Limit State

Span	Location (x/L)	Unfactored				Fatigue I -Factored			
		M_{LL+IM} (kip-ft)		V_{LL+IM} (kip)		$(M_{LL+IM})_u$ (kip-ft)		$(V_{LL+IM})_u$ (kip)	
		Positive	Negative	Positive	Negative	Positive	Negative	Positive	Negative
1	0.0	0	0	56.9	-7.6	0	0	105.0	-14.1
	0.1	510	-78	49.8	-7.6	764	-117	92.0	-14.1
	0.2	857	-156	41.9	-7.8	1285	-234	77.3	-14.4
	0.3	1077	-234	34.2	-15.3	1616	-351	63.2	-28.2
	0.4	1156	-312	27.0	-23.3	1734	-468	49.8	-42.9
	0.5	1131	-390	19.4	-31.0	1697	-585	35.9	-57.2
	0.6	1031	-468	14.1	-38.4	1547	-702	26.1	-70.8
	0.7	820	-546	8.6	-45.2	1230	-819	15.9	-83.4
	0.8	495	-592	3.9	-51.5	743	-888	7.2	-95.1
	0.9	153	-666	1.6	-57.2	230	-1000	3.0	-105.6
	1.0	159	-741	0.8	-61.6	239	-1111	1.5	-113.7
	0.0	159	-741	62.3	-5.7	239	-1111	114.9	-10.5
	0.1	200	-490	56.9	-5.7	300	-735	105.0	-10.5
2	0.2	578	-399	50.1	-5.9	867	-599	92.4	-11.0
	0.3	879	-330	42.6	-12.1	1319	-496	78.6	-22.4
	0.4	1061	-261	34.6	-19.1	1592	-392	63.9	-35.3
	0.5	1107	-193	26.0	-26.8	1660	-289	48.0	-49.5

Notes:

1. Live load distribution factors are listed in Table 4.1
2. Dynamic load allowance $IM = 15\%$
3. Fatigue I - $(M_{LL+IM})_u = 1.5(M_{LL+IM})_u$ and $(V_{LL+IM})_u = 1.5(V_{LL+IM})_u$

4.7.3.3 Determine Load and Resistance Factors and Load Combinations

1. Determine Design Equation

AASHTO Article 1.3.2.1 requires that the following design equation be satisfied for all limit states:

$$\sum \eta_i \gamma_i Q_i \leq \phi R_n = R_r \quad (4.6)$$

where γ_i is the load factor and ϕ is the resistance factor; Q_i represents the force effect; R_n is the nominal resistance; η_i is the load modifier factor related to ductility, redundancy, and operational importance and is defined as follows when a maximum value of γ_i is used:

$$\eta_i = \eta_D \eta_R \eta_I \geq 0.95 \quad (4.7)$$

where η_D , η_R , and η_I are ductility, redundancy, and operational factors, respectively.

$$\eta_D = \begin{cases} 1.05 & \text{for non-ductile components and connections} \\ 0.95 & \text{for ductile components and connections} \end{cases} \quad (4.8)$$

$$\eta_R = \begin{cases} 1.05 & \text{for non-redundant members} \\ 0.95 & \text{for redundant members} \end{cases} \quad (4.9)$$

$$\eta_I = \begin{cases} 1.05 & \text{operational important bridge} \\ 0.95 & \text{general bridge} \end{cases} \quad (4.10)$$

only apply to strength and extreme event limit states

For this bridge, the following values are assumed:

Limit States	Ductility η_D	Redundancy η_R	Importance η_I	η
Strength limit state	0.95	0.95	1.05	0.95
Fatigue limit state	1.0	1.0	1.0	1.0

2. Determine Applicable Load Factors and Load Combinations

According to AASHTO Table 3.4.1-1, considering live load distribution factors for the interior girder and denoting ($LL + IM$) as unfactored force effect due to one design lane loaded, the following load combinations are obtained as follows:

$$\text{Strength I: } 1.25(DC) + 1.5(DW) + 1.75(LL + IM)_{HL-93}$$

$$\text{Fatigue I: } 1.5(LL + IM)_{HL-93\text{Truck}}$$

3. Determine Applicable Resistance Factors

According to AASHTO 6.5.4.2, the following resistance factors are used for the strength limit states in this example.

For flexure: $\phi_f = 1.0$

For shear $\phi_v = 1.0$

For shear connector $\phi_{sc} = 0.85$

4.7.3.4 Calculate Factored Moments and Shears

Factored moments and shears for an interior girder are calculated and listed in Tables 4.2 to 4.4 based on the following load combination:

$$\text{Strength I: } 1.25(DC) + 1.5(DW) + 1.75(LL + IM)_{HL-93}$$

$$\text{Fatigue I: } 1.5(LL + IM)_{HL-93\text{Truck}}$$

Shears, V_u , due to the unfactored permanent load plus the factored fatigue load (Fatigue I) is also calculated for checking special fatigue requirement for web as required by AASHTO Article 6.10.5.3.

$$V_u = V_{dc1} + V_{dc2} + V_{dw} + (1.5)(LL + IM)_{HL-93\text{Truck}}$$

4.7.3.5 Design for Flexure—Composite Section at 0.4 Point—Strength Limit State

In the following, flexural design for 0.4 Point Section is illustrated.

1. General Requirement

At the strength limit state, the composite compact section in positive flexure regions satisfies the requirement as follows:

$$M_u + \frac{1}{3}f_l S_{xt} \leq \phi_f M_n \quad (4.11)$$

In this example of the straight bridge, flange lateral bending stress for interior girders $f_l = 0$. The design equation, therefore, is simplified as follows:

$$M_u \leq \phi_f M_n \quad (4.11)$$

2. Calculate Elastic Composite Section Properties

Steel section (Figure 4.14) as:

Top flange: $b_{fc} = 18$ in. $t_{fc} = 1$ in.

Web: $D = 90$ in. $t_w = 0.625$ in.

Bottom flange: $b_{ft} = 18$ in. $t_{ft} = 1.75$ in.

Effective Flange Width (AASHTO Article 4.6.2.6)

For an interior girder, the effective flange width is taken as girder spacing, that is, $b_{eff} = 16(12) = 192$ in.

Elastic Composite Section Properties

For the typical section (Figure 4.14) in the positive flexure region of Span 1, its elastic section properties for the noncomposite (steel section alone), the short-term composite ($n = 8$), and the long-term composite ($3n = 24$) are calculated in Figures 4.21 to 4.23.

The concrete haunch may be included in calculating composite section properties. However, the concrete haunch is ignored in this example for simplicity.

3. Check Section Compactness

For composite sections in the positive flexure region, it is usually assumed that the top flange is adequately braced by the hardened concrete deck; there are, therefore, no requirements for the compression flange slenderness and bracing for compact composite sections at the strength limit state. Three requirements (AASHTO Article 6.10.6.2.2) for a compact composite section in straight bridges are checked as follows:

Specified minimum yield strength of flanges:

$$F_{yf} = 50 \text{ ksi} < 70 \text{ ksi}$$

$$\text{Web: } \frac{D}{t_w} = 124.8 < 150$$

$$\text{Section: } \frac{2D_{cp}}{t_w} \leq 3.76 \sqrt{\frac{E}{F_{yc}}} \quad (4.12)$$

where D_{cp} is the depth of the web in compression at the plastic moment state and is determined in the following.

Compressive force in concrete slab:

$$P_s = 0.85 f'_c b_{eff} t_s = 0.85(4.0)(192)(10.875) = 7,099 \text{ kip (31,578 kN)}$$

Yield force in the top flange:

$$P_c = A_{fc} F_{yc} = (18 \times 1)(50) = 900 \text{ kip (4,003 kN)}$$

Yield force in the web:

$$P_w = A_w F_{yw} = (90)(0.625)(50) = 2,813 \text{ kip (16,961 kN)}$$

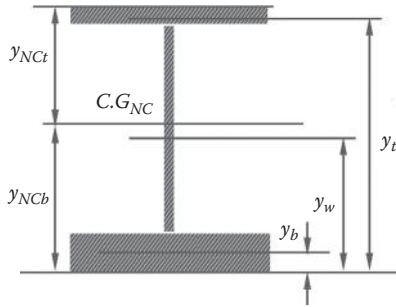
Yield force in the bottom flange:

$$P_t = A_{ft} F_{yt} = (18 \times 1.75)(50) = 1,575 \text{ kip (7,006 kN)}$$

$$\therefore P_s = 7,099 \text{ kip} > P_c + P_w + P_t = 900 + 2,813 + 1,575 = 5,287.5 \text{ kip}$$

\therefore The plastic neutral axis (PNA) is within the concrete slab (Figure 4.24) and D_{cp} is equal to zero.

Component	A_i (in. ²)	y_i (in.)	$A_i y_i$ (in. ³)	$y_i - y_{NCb}$ (in.)	$A_i (y_i - y_{NCb})^2$ (in. ⁴)	I_o (in. ⁴)
Top flange 18 × 1	18.00	92.25	1,660.5	51.42	47,593	1.5
Web 90 × 0.625	56.25	46.75	2,629.7	5.92	1,972	37,969
Bottom flange 18 × 1.75	31.50	0.875	27.6	-39.95	50,286	8.04
Σ	105.75	—	4,317.8	—	99,850	37,978



$$y_{NCb} = \frac{\sum A_i y_i}{\sum A_i} = \frac{4,317.8}{105.75} = 40.83 \text{ in.}$$

$$y_{NCt} = (1.75 + 90 + 1) - 40.83 = 51.92 \text{ in.}$$

$$\begin{aligned} I_{NC} &= \sum I_o + \sum A_i (y_i - y_{NCb})^2 \\ &= 37,978 + 99,850 = 137,828 \text{ in.}^4 \end{aligned}$$

$$S_{NCb} = \frac{I_{NC}}{y_{NCb}} = \frac{137,828}{40.84} = 3,376 \text{ in.}^3$$

$$S_{NCt} = \frac{I_{NC}}{y_{NCt}} = \frac{137,828}{51.92} = 2,655 \text{ in.}^3$$

FIGURE 4.21 Noncomposite section (steel section alone) properties.

$$\frac{2D_{cp}}{t_w} = 0.0 < 3.76 \sqrt{\frac{E}{F_{yc}}}$$

The nominal flexural resistance, M_n , of the composite compact section is computed in accordance with AASHTO 6.10.7.1.2.

4. Calculate Plastic Moment Capacity M_p

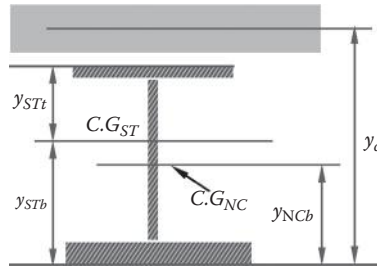
The plastic moment capacity M_p is determined using equilibrium equations. The reinforcement in the concrete slab is neglected in this example.

1. Determine the location of the plastic neutral axis (PNA)

As calculated above, PNA is within the concrete slab as shown in Figure 4.24. From equilibrium, $P_s = P_c + P_w + P_t = 900 + 2,813 + 1,575 = 5,287.5$ kip and obtain

$$\bar{y} = \frac{P_s}{0.85 f'_c b'_{eff}} = \frac{5,287.5}{0.85(4.0)(192)} = 8.10 \text{ in. (206 mm)}$$

Component	A_i (in. ²)	y_i (in.)	$A_i y_i$ (in. ³)	$y_i - y_{STb}$ (in.)	$A_i(y_i - y_{STb})^2$ (in. ⁴)	I_o (in. ⁴)
Steel section	105.75	40.83	4,317.8	-43.22	197,545	137,829
Concrete slab 192/8 × 10.875	262.00	101.56	26,507.8	17.51	80,040	2,572
Σ	366.75	—	30,825.6	—	277,585	140,401



$$y_{STb} = \frac{\sum A_i y_i}{\sum A_i} = \frac{30,825.6}{366.75} = 84.05 \text{ in.}$$

$$y_{STt} = (1.75 + 90 + 1) - 84.05 = 7.70 \text{ in.}$$

$$\begin{aligned} I_{ST} &= \sum I_o + \sum A_i (y_i - y_{STb})^2 \\ &= 140,401 + 277,585 = 417,986 \text{ in.}^4 \end{aligned}$$

$$S_{STb} = \frac{I_{ST}}{y_{STb}} = \frac{417,986}{84.05} = 4,973 \text{ in.}^3$$

$$S_{STt} = \frac{I_{ST}}{y_{STt}} = \frac{417,986}{7.70} = 48,044 \text{ in.}^3$$

FIGURE 4.22 Short-term composite section properties ($n = 8$).

2. Calculate M_p

Summing all forces about the PNA, obtain

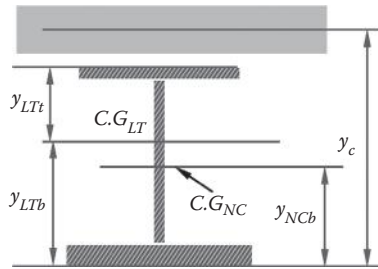
$$M_p = \sum M_{PNA} = P_s \frac{\bar{y}}{2} + P_c d_c + P_w d_w + P_t d_t$$

where

$$d_c = t_s + \text{haunch height} - \frac{t_{fc}}{2} - \bar{y} = 10.875 + 4.375 - \frac{1.0}{2} - 8.10 = 6.65 \text{ in. (169 mm)}$$

$$d_w = d_c + \frac{t_{fc}}{2} + \frac{D}{2} = 6.65 + \frac{1.0}{2} + \frac{90}{2} = 52.15 \text{ in. (1,325 mm)}$$

Component	A_i (in. ²)	y_i (in.)	$A_i y_i$ (in. ³)	$y_i - y_{LTb}$ (in.)	$A_i (y_i - y_{LTb})^2$ (in. ⁴)	I_o (in. ⁴)
Steel section	105.75	40.83	4,317.8	-27.41	79,465	137,829
Concrete slab 192/24 × 10.875	87.00	101.56	8,835.9	33.32	96,591	857
Σ	192.75	—	13,153.7	—	176,056	138,686



$$y_{LTb} = \frac{\sum A_i y_i}{\sum A_i} = \frac{13,153.7}{192.75} = 68.24 \text{ in.}$$

$$y_{LTt} = (1.75 + 90 + 1) - 68.24 = 24.51 \text{ in.}$$

$$\begin{aligned} I_{LT} &= \sum I_o + \sum A_i (y_i - y_{LTb})^2 \\ &= 138,686 + 176,056 = 314,752 \text{ in.}^4 \end{aligned}$$

$$S_{LTb} = \frac{I_{LT}}{y_{LTb}} = \frac{314,742}{68.24} = 4,612 \text{ in.}^3$$

$$S_{LTt} = \frac{I_{LT}}{y_{LTt}} = \frac{314,742}{24.51} = 12,841 \text{ in.}^3$$

FIGURE 4.23 Long-term composite section properties ($3n = 24$).

$$d_t = d_w + \frac{D}{2} + \frac{t_{ft}}{2} = 52.15 + \frac{90}{2} + \frac{1.75}{2} = 98.03 \text{ in. (2,490 mm)}$$

$$\begin{aligned} M_p &= (5,287.5) \left(\frac{8.10}{2} \right) + (900)(6.65) + (2,813)(52.15) + (1,575)(98.03) \\ &= 328,496 \text{ kip-in.} = 27,375 \text{ kip-ft. (37,116 kN-m)} \end{aligned}$$

5. Yield Moment M_y

The yield moment M_y (AASHTO Article D6.2.2) corresponds to the first yielding of either steel flange. It is obtained by the following formula:

$$M_y = M_{D1} + M_{D2} + M_{AD} \quad (4.12)$$

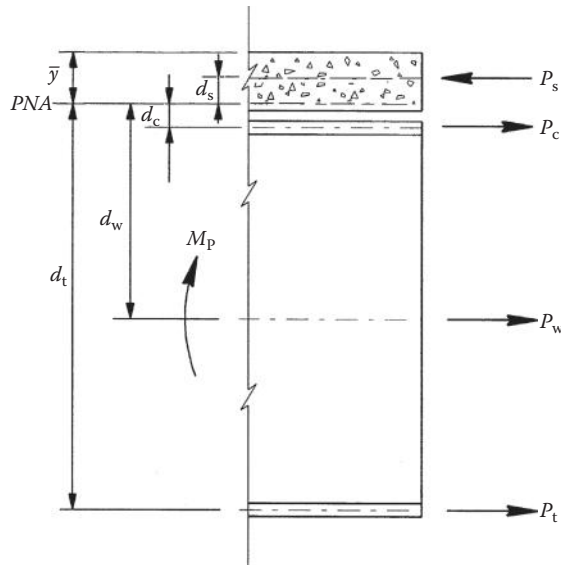


FIGURE 4.24 Plastic moment capacity state.

where M_{D1} , M_{D2} , and M_{AD} are moments due to the factored loads applied to the steel, the long-term, and the short-term composite section, respectively. M_{AD} can be obtained by solving equation

$$F_y = \frac{M_{D1}}{S_{NC}} + \frac{M_{D2}}{S_{LT}} + \frac{M_{AD}}{S_{ST}} \quad (4.13)$$

$$M_{AD} = S_{ST} \left(F_y - \frac{M_{D1}}{S_{NC}} - \frac{M_{D2}}{S_{LT}} \right) \quad (4.14)$$

where S_{NC} , S_{ST} , and S_{LT} (see Figures 4.21 to 4.23) are section moduli for the noncomposite steel, the short-term, and the long-term composite section, respectively. From Table 4.2, the maximum factored positive moments M_{D1} and M_{D2} in Span 1 are obtained at the location of $0.4L_I$.

$$M_{D1} = (0.95)(1.25)(M_{DC1}) = (0.95)(1.25)(4,260) = 5,061 \text{ kip-ft. (6,863 kN-m)}$$

$$\begin{aligned} M_{D2} &= (0.95)(1.25M_{DC2} + 1.5M_{DW}) \\ &= (0.95)[1.25(435) + 1.5(792)] = 1,645 \text{ kip-ft. (2,230 kN-m)} \end{aligned}$$

For the top flange:

$$\begin{aligned} M_{AD} &= (48,044) \left(50 - \frac{5,061(12)}{2,655} - \frac{1,645(12)}{12,841} \right) \\ &= 1,229,358 \text{ kip-in.} = 102,446 \text{ kip-ft. (138,897 kN-m)} \end{aligned}$$

For the bottom flange:

$$\begin{aligned} M_{AD} &= (4,973) \left(50 - \frac{5,061(12)}{3,376} - \frac{1,645(12)}{4,612} \right) \\ &= 137,904 \text{ kip-in.} = 11,492 \text{ kip-ft. (15,581 kN-m) (controls)} \\ \therefore M_y &= 5,061 + 1,645 + 11,492 = 18,198 \text{ kip-ft. (24,673 kN-m)} \end{aligned}$$

6. Calculate Nominal Flexural Resistance

In this example, it is assumed that the adjacent interior-bent sections are noncompact non-composite sections that do not satisfy requirements of AASHTO B6.2. The nominal flexural resistance of the composite compact section in positive flexure is calculated in accordance with AASHTO 6.10.7.1.2:

$$M_n = \begin{cases} M_p & \text{for } D_p \leq 0.1D_t \\ M_p \left[1.07 - 0.7 \frac{D_p}{D_t} \right] & \text{for } D_p > 0.1D_t \end{cases} \leq 1.3R_h M_y \text{ for a continuous span} \quad (4.15)$$

where R_h is the hybrid factor and is equal to 1.0 for this example; D_p is the depth from the top of the concrete deck to the PNA; D_t is total depth of the composite section.

$$D_t = t_s + \text{Hunch Depth} + D + t_{fl} = 10.875 + 4.375 + 90 + 1.75 = 107 \text{ in.}$$

$$D_p = \bar{y} = 8.10 \text{ in.} < 0.1D_t = 10.7 \text{ in.}$$

$$\therefore M_n = M_p = 27,375 \text{ kip-ft.} > 1.3R_h M_y = 1.3(1.0)(18,198) = 23,657 \text{ kip-ft.}$$

Use $M_n = 27,375 \text{ kip-ft. (37,116 kN-m)}$

7. Check Ductility Requirement

For the compact and noncompact sections, the following ductility requirement is checked to ensure that the tension flange of the steel section reaches significant yielding before the crushing strain is reached at the top of the concrete deck.

$$D_p = 8.10 \text{ in.} < 0.42D_t = 0.42(107) = 44.94 \text{ in.}$$

8. Check Design Requirement

From Table 4.2, for 0.4 point, factored moment $M_u = 14,257 \text{ kip-ft.}$

$$M_u = 14,257 \text{ kip-ft.} < \phi_f M_n = (1.0)(27,375) = 27,375 \text{ kip-ft.}$$

4.7.3.6 Design for Shear—Left End of Span 1—Strength Limit State

1. Select Stiffener Spacing

AASHTO C6.10.2.1.1 states that by limiting the slenderness of transversely-stiffened webs to $D/t_w \leq 150$, the maximum transverse stiffener spacing d_o (as shown in Figure 4.4) up to $3D$ is permitted (AASHTO C.6.10.2.1.1). For end panels adjacent to simple supports, stiffener spacing d_o do not exceed $1.5D$ (AASHTO 6.10.9.3.3).

Try end panel transverse stiffener spacing $d_o = 120$ in. (for Spans 1 and 3) and 126 in. (for Span 2) $1.5D = 1.5(90) = 135$ in. and for the interior span transverse stiffener spacing

$$d_o = 240 \text{ in.} < 3D = 3(90) = 270 \text{ in.}$$

Calculation for interior span shear strength is not covered in this example.

2. Calculate Shear Resistance

V_n for end-stiffened web panel adjacent simple support is follows: (AASHTO Article 6.10.9.3.3)

$$V_n = CV_p \quad (4.16)$$

$$C = \begin{cases} 1.0 & \text{For } \frac{D}{t_w} < 1.12\sqrt{\frac{Ek}{F_{yw}}} \\ \frac{1.12}{(D/t_w)}\sqrt{\frac{Ek}{F_{yw}}} & \text{For } 1.12\sqrt{\frac{Ek}{F_{yw}}} \leq \frac{D}{t_w} \leq 1.40\sqrt{\frac{Ek}{F_{yw}}} \\ \frac{1.57}{(D/t_w)^2}\sqrt{\frac{Ek}{F_{yw}}} & \text{For } \frac{D}{t_w} > 1.40\sqrt{\frac{Ek}{F_{yw}}} \end{cases} \quad (4.17)$$

$$k = 5 + \frac{5}{(d_o/D)^2} \quad (4.18)$$

For the left end of Span 1, $d_o = 120$ in.

$$k = 5 + \frac{5}{(120/90)^2} = 7.81$$

$$\frac{D}{t_w} = \frac{90}{0.625} = 144 < 1.4\sqrt{\frac{Ek}{F_{yw}}} = (1.4)\sqrt{\frac{(29,000)(7.81)}{50}} = 94.23$$

$$\therefore C = \frac{1.57}{(D/t_w)^2} \left(\frac{Ek}{F_{yw}} \right) = \frac{1.57}{144^2} \left(\frac{29,000(7.81)}{50} \right) = 0.343$$

$$V_p = 0.58F_{yw}Dt_w = 0.58(50)(90)(0.625) = 1,631.3 \text{ kip}$$

$$\therefore V_n = CV_p = (0.343)1,631.3 = 559.5 \text{ kip (2,489 kN)}$$

Check Design Requirement

$$V_u = 539.7 \text{ kip} < \phi_v V_n = (1.0)(559.5) = 559.5 \text{ kip}$$

4.7.3.7 Check Fatigue Limit State—Typical Girder Details—Positive Flexure Region

1. Typical Girder Details and Nominal Fatigue Resistance

For load-induced fatigue consideration, the most common types of components and details in a typical I girder are (AASHTO Table 6.6.1.2.3-1) listed in Table 4.5.

TABLE 4.5 Typical Girder Details—Fatigue Limit States

Type of details	Category (AASHTO Table 6.6.1.2.3-1)	Constant $-A \times 10^8$ (ksi ³)	Fatigue I $(\Delta F_n) = (\Delta F)_{TH}$ (ksi)	$N_{TH} = \frac{A}{[(\Delta F)_{TH}]^3}$ ($\times 10^6$)
1 Base metal and weld metal at full-penetration groove-welded splices	B	120.0	16.0	2.93
2 Base metal at gross section of high-strength bolted slip-critical connections (bolt gusset to flange)	B	120	16.0	2.93
3 Base metal at fillet-welded stud-type shear connectors	C	44.0	10.0	4.40
4 Base metal at toe of transverse stiffener-to-flange and transverse stiffener-to-web welds	C'	44.0	12.0	2.55

Nominal fatigue resistance is calculated as follows:

For finite fatigue life ($N \leq N_{TH}$)

$$(\Delta F_n) = \left(\frac{A}{N} \right)^{\frac{1}{3}} \quad (4.19)$$

For infinite fatigue life ($N > N_{TH}$)

$$(\Delta F_n) = (\Delta F)_{TH} \quad (4.20)$$

$$N = (365)(75)n(ADTT)_{SL} \quad (4.21)$$

$$N_{TH} = \frac{A}{[(\Delta F)_{TH}]^3} \quad (4.22)$$

where A is a constant depending on the detail category as specified in AASHTO Table 6.6.1.2.5-1, and $(\Delta F)_{TH}$ is the constant-amplitude fatigue threshold taken from AASHTO Table 6.6.1.2.5-3. N_{TH} is minimum number of stress cycles corresponding to constant-amplitude fatigue threshold, $(\Delta F)_{TH}$ and is listed in Table 4.5.

$$ADTT_{SL} = p(ADTT) \quad (4.23)$$

where p is the fraction of truck traffic in a single lane (AASHTO Table 3.6.1.4.2-1) = 0.8 for three or more lanes' traffic, n is the number of stress-range cycles per truck passage = 1.0 for the positive flexure region for span > 40 ft. $ADTT$ is the number of trucks per day in one direction averaged over the design life.

For this example, $ADTT = 3600$,

Since $N = (365)(75)(1.0)(0.8)(3600) = 78.784(10)^6 > N_{TH}$, the fatigue limit state—infinite fatigue life is checked and $(\Delta F_n) = (\Delta F)_{TH}$ as summarized in Table 4.5.

2. Check Fatigue Stress Range—0.4 Point of Span 1

The most critical flexural section for the positive moment region is located at 0.4 Point (64 ft. from the left end) of Span 1, where positive live load moments are applied to the short-term composite section and negative live load moments are applied to the steel section and deck slab longitudinal reinforcement.

Fatigue stress ranges at the bottom flanges and the top flanges are checked as follows:

Fatigue I - HL-93 Truck for Infinite Life:

Flexural fatigue stress ranges at the bottom flange:

$$\gamma(\Delta f) = \left| \frac{+M_u}{S_{STb}} \right| + \left| \frac{-M_u}{S_{NCb}} \right| = \frac{1,734(12)}{4,973} + \frac{468(12)}{3,376}$$

< 16.0 ksi O.K. for Category B

$$= 4.18 + 1.66 = 5.84 \text{ ksi} \quad < 12.0 \text{ ksi O.K. for Category C'}$$

$$< 10.0 \text{ ksi O.K. for Category C}$$

Flexural fatigue stress ranges at the top flange:

$$\gamma(\Delta f) = \left| \frac{+M}{S_{STt}} \right| + \left| \frac{-M}{S_{NCt}} \right| = \frac{1,734(12)}{48,044} + \frac{468(12)}{2,655}$$

< 6.0 ksi O.K. for Category B

$$= 0.43 + 2.11 = 2.54 \text{ ksi} \quad < 12.0 \text{ ksi O.K. for Category C'}$$

$$< 10.0 \text{ ksi O.K. for Category C}$$

The above stresses are calculated at the extreme fiber of the flange for Category B and can be conservatively used for Categories C and C'. It is obvious that if the calculation is made at the toe of the weld for the transverse stiffeners (Category C'), the stress ranges will be smaller than the stress ranges calculated at the extreme fiber of the flange.

3. Check Special Fatigue Requirement for Web (AASHTO 6.10.5.3)

The objective of this requirement is to ensure that significant elastic flexing of the web due to shear does not occur and the member is able to sustain an infinite number of smaller loadings without fatigue cracking due to the shear. A stiffened interior panel at 0.1 point is checked as follows:

- Fatigue I load combination

$$V_u = V_{DC1} + V_{DC2} + V_{DW} + 1.5(V_{LL+IM})_u$$

$$= 107.5 + 11.0 + 19.9 + (1.5)(49.8) = 213.1 \text{ kip (948 kN)}$$

- Shear resistance for interior panel

$$C = 0.343$$

$$V_p = 1,631.3 \text{ kip}$$

$$V_{cr} = CV_p = (0.343)(1,613.3) = 559.5 \text{ kip} > V_u = 213.1 \text{ kip}$$

4.7.3.8 Design Bearing Stiffener

Try two 0.875 in. \times 8.25 in. stiffness plates welded to each side of the web as shown in Figure 4.25a.

1. Check local buckling requirement (AASHTO Article 6.10.11.2.2)

$$b_t = 8.25 \text{ in.} < 0.48 t_p \sqrt{\frac{E}{F_y}} = 0.48(0.875) \sqrt{\frac{29,000}{36}} = 11.9 \text{ in.}$$

2. Check bearing resistance (AASHTO Article 6.10.8.2.3)

Contact area of the stiffeners on the flange $A_{pn} = 2(8.25 - 1.5)(0.875) = 11.81 \text{ in.}^2$

$$(R_{sb})_r = \phi_b (1.4) A_{pn} F_{ys} = (1.0)(1.4)(11.81)(36) = 595.2 \text{ kip} > V_u = 539.7 \text{ kip}$$

3. Check axial resistance of effective column section (AASHTO 6.10.11.2.4, 6.9.4.1)

Effective column section area is shown in Figure 4.25b.

$$A_s = 2[(8.25)(0.875) + 9(0.625)(0.625)] = 21.47 \text{ in.}^2$$

$$I = \frac{(0.875)[(2)(8.25 + 0.625)]^3}{12} = 366.2 \text{ in.}^4$$

$$r_s = \sqrt{\frac{I}{A_s}} = \sqrt{\frac{366.2}{21.47}} = 4.13 \text{ in.}$$

$$\frac{P_o}{P_e} = \lambda = \left(\frac{KL}{r_s \pi} \right)^2 \frac{F_y}{E} = \left(\frac{0.75(90)}{4.13\pi} \right)^2 \frac{36}{29,000} = 0.034$$

$$\therefore \frac{P_e}{P_o} = \frac{1}{0.034} = 29.41 > 0.44$$

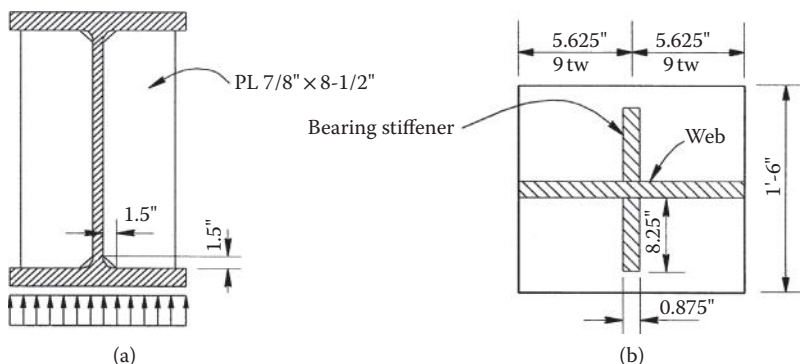


FIGURE 4.25 Bearing stiffener: (a) elevation; (b) cross section.

$$P_n = \left[0.658^{\left(\frac{P_e}{P_n}\right)} \right] P_o = \left[0.658^{\left(\frac{P_e}{P_e}\right)} \right] A_s F_y = [0.658^{0.034}] (21.47)(36) = 762 \text{ kip}$$

$$P_r = \phi_c P_n = 0.9(762) = 685.8 \text{ kip} > V_u = 539.7 \text{ kip}$$

Therefore, using two 0.875 in. \times 8.25 in. plates is adequate for bearing stiffeners at abutment.

4.7.3.9 Design Intermediate Transverse Stiffener

The intermediate transverse stiffener consists of two plates welded to both sides of the web. The design of the first intermediate transverse stiffener in the left end of Span 1 is discussed in the following.

1. Projecting Width b_t Requirements (AASHTO Article 6.10.11.1.2)

To prevent local buckling of the transverse stiffeners, the width, b_t , of each projecting stiffener satisfies these requirements:

$$\begin{cases} 2.0 + \frac{D}{30} \\ 0.25b_f \end{cases} \leq b_t \leq 16t_p \quad (4.24)$$

where b_f is the full width of the steel flange; t_p is the thickness of the projecting stiffener element and D is web depth.

To allow adequate space for cross frame connections, try stiffener width $b_t = 6$ in. (152 mm)

$$b_t = 6 \text{ in.} > \begin{cases} 2.0 + \frac{D}{30} = 2.0 + \frac{90}{30} = 5.0 \text{ in.} \\ 0.25b_f = 0.25(18) = 4.5 \text{ in.} \end{cases}$$

Try $t_p = 0.5$ in. (13 mm) and obtain

$$b_t = 6 \text{ in.} < 16t_p = 16(0.5) = 8 \text{ in.}$$

Use two 6 in. \times 0.5 in. (152 mm \times 13 mm) transverse stiffener plates (Figure 4.26).

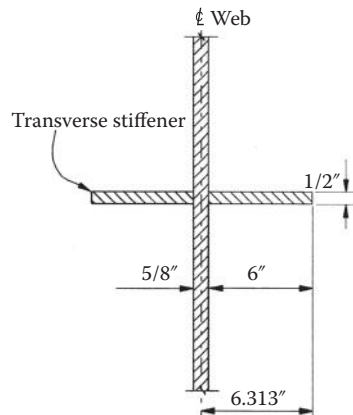


FIGURE 4.26 Intermediate transverse stiffener.

2. Moment of Inertia Requirements (AASHTO Article 6.10.11.1.3)

The purpose of this requirement is to ensure sufficient rigidity of transverse stiffeners to adequately develop a tension field in the web.

$$I_t \geq \begin{cases} I_{t1} = bt_w^3 J \\ I_{t2} = \frac{D^4 \rho_t^{1.3}}{40} \left(\frac{F_{yw}}{E} \right)^{1.5} \end{cases} \quad (4.25)$$

$$J = \frac{2.5}{\left(\frac{d_o}{D} \right)^2} - 2.0 \geq 0.5 \quad (4.26)$$

where I_t is the moment of inertia for the transverse stiffener taken about the edge in contact with the web for single stiffener and about the midthickness of the web for stiffener pairs (Figure 4.26); b is smaller of d_o and D .

$$\because J = \frac{2.5}{\left(\frac{90}{240} \right)^2} - 2.0 = -1.6 < 0.5 \quad \therefore \text{Use } J = 0.5$$

$$I_{t1} = bt_w^3 J = (90)(0.625)^3(0.5) = 10.99 \text{ in.}^4$$

$$F_{crs} = \frac{0.31E}{\left(\frac{b_t}{t_p} \right)^2} = \frac{0.31(29,000)}{\left(\frac{6}{0.5} \right)^2} = 62.43 \text{ ksi} > F_{ys} = 36 \text{ ksi}$$

Use $F_{crs} = F_{ys} = 36 \text{ ksi}$

$$\rho_t = \text{larger} \begin{cases} \frac{F_{yw}}{F_{crs}} = \frac{50}{36} = 1.39 \\ 1.0 \end{cases} = 1.39$$

$$I_{t2} = \frac{D^4 \rho_t^{1.3}}{40} \left(\frac{F_{yw}}{E} \right)^{1.5} = \frac{(90)^4 (1.39)^{1.3}}{40} \left(\frac{50}{29,000} \right)^{1.5} = 180.12 \text{ in.}^4$$

$$I_t = 2 \left(\frac{6^3 (0.5)}{12} + (6)(0.5)(3.313)^2 \right) = 83.86 \text{ in.}^4$$

$$> \text{smaller of} \begin{cases} I_{t1} = 10.89 \text{ in.}^4 \\ I_{t2} = 180.12 \text{ in.}^4 \end{cases} = 10.89 \text{ in.}^4$$

4.7.3.10 Design Shear Connectors for Positive Flexural Region of Span 1

In a composite girder, stud or channel shear connectors must be provided at the interface between the concrete deck slab and the steel section to resist the interface shear. For a straight composite bridge girder, the shear connectors should be normally provided throughout the length of bridges (AASHTO Article 6.10.10.1). Stud shear connectors are chosen in this example and will be designed for the fatigue limit state and then checked against the strength limit state. The detailed calculations of the shear stud connectors for the positive flexure region of Span 1 are given in the following. A similar procedure can be used to design the shear studs for other portions of the bridge.

1. Stud Size (AASHTO Article 6.10.10.1.1)

To meet the limits for cover and penetration for shear connectors specified in AASHTO Article 6.10.10.1.1 and 6.10.10.1.4, try:

$$\text{Stud height } H_{\text{stud}} = 7 \text{ in.} > t_h + 2 = 3.375 + 2 = 5.375 \text{ in.}$$

$$\text{Stud diameter } d_{\text{stud}} = 0.875 \text{ in.} < H_{\text{stud}}/4 = 7/4 = 1.75 \text{ in.}$$

2. Pitch of Shear Stud, p —Fatigue Limit State

a. Basic requirements for straight girder (ASHTO Article 6.10.10.1.2)

$$6d_{\text{stud}} \leq p = \frac{n_{\text{stud}} Z_r I_{ST}}{V_{sr} Q} \leq 24 \text{ in.}$$

where n_{stud} is the number of shear connectors in a cross section; Q is the first moment of the transformed section (concrete deck) about the neutral axis of the short-term composite section; V_{sr} is the shear force range in the fatigue limit state; and Z_r is the shear fatigue resistance of an individual shear connector.

b. Fatigue shear resistance Z_r (AASHTO Article 6.10.10.2)

For the Fatigue I load combination

$$Z_r = 5.5d_{\text{stud}}^2 = 5.5(0.875)^2 = 4.211 \text{ ksi}$$

c. First moment Q and moment of initial I_{ST} (see Figure 4.22)

$$\begin{aligned} Q &= \left(\frac{b_{\text{eff}} t_s}{8} \right) \left(y_{ST} + t_h + \frac{t_s}{2} \right) \\ &= \left(\frac{192(10.875)}{8} \right) \left(7.7 + 3.375 + \frac{10.875}{2} \right) = 4,310 \text{ in.}^3 \end{aligned}$$

$$I_{ST} = 417,986 \text{ in.}^4$$

d. Required pitch for the fatigue limit state

Assume that shear studs are spaced at 6 in. transversely across the top flange of steel section (Figure 4.13) and using $n_{\text{stud}} = 3$ for this example and obtain

$$p_{\text{required}} = \frac{3(4.211)(417,986)}{V_{sr}(4.31)} = \frac{1,225.16}{V_{sr}}$$

The detailed calculations for the positive flexure region of Span 1 are shown in Table 4.6.

TABLE 4.6 Shear Connector Design for the Positive Flexure Region in Span 1

Span	Location (x/L)	V_{sr} (kip)	$p_{required}$ (in.)	p_{final} (in.)	$n_{total-stud}$
1	0.0	119.1	10.3	9	3
	0.1	106.1	11.5	9	66
	0.2	91.7	13.4	12	114
	0.3	91.4	13.4	12	162
	0.4	92.7	13.2	12	210
	0.4	92.7	13.2	9	210
	0.5	93.0	13.2	8	147
	0.6	96.9	12.6	8	75
	0.7	99.3	12.3	8	3

Notes:

$$1. \quad V_{sr} = |(V_{LL+IM})_u| + |-(V_{LL+IM})_u|$$

$$2. \quad p_{required} = \frac{n_{stud} Z_r I_{com-n}}{V_{sr} Q} = \frac{1,225.16}{V_{sr}}$$

3. $n_{total-stud}$ is the summation of the number of shear studs between the locations of the zero moment and that location.

3. Strength Limit State Check

a. Basic requirement (AASHTO Article 6.10.10.4.1)

The resulting number of shear connectors provided between the section of maximum positive moment and each adjacent point of zero moment satisfy the following requirement:

$$n_{total-stud} \geq \frac{P}{\phi_{sc} Q_n} \quad (4.27)$$

where ϕ_{sc} is the resistance factor for shear connectors, 0.85; P is the nominal horizontal shear force, and Q_n is the nominal shear resistance of one stud shear connector.

b. Nominal horizontal shear force (AASHTO Article 6.10.10.4.2)

For straight composite girder:

$$P = \text{the lesser of } \begin{cases} P_{1p} = 0.85 f'_c b_{eff} t_s \\ P_{2p} = F_{yw} D t_w + F_{yt} b_{ft} t_{ft} + F_{yc} b_{fc} t_{fc} \end{cases} \quad (4.28)$$

$$P_{1p} = 0.85 f'_c b_{eff} t_s = 0.85(4.0)(192)(10.875) = 7,099 \text{ kip}$$

$$\begin{aligned} P_{2p} &= F_{yw} D t_w + F_{yt} b_{ft} t_{ft} + F_{yc} b_{fc} t_{fc} \\ &= 50[(18)(1.0) + (90)(0.625) + (18)(1.75)] = 5,287.5 \text{ kip} \end{aligned}$$

$$\therefore P = 5,287.5 \text{ kip (18,708 kN)}$$

c. Nominal shear resistance (AASHTO Article 6.10.10.4.3)

$$Q_n = 0.5 A_{sc} \sqrt{f'_c E_c} \leq A_{sc} F_u \quad (4.29)$$

where A_{sc} is the cross-sectional area of a stud shear connector and F_u is the specified minimum tensile strength of a stud shear connector = 60 ksi (420 MPa).

$$\therefore 0.5\sqrt{f'_c E_c} = 0.5\sqrt{3.25(3,250)} = 51.4 \text{ kip} < F_u = 60 \text{ kip}$$

$$\therefore Q_n = 0.5A_{sc}\sqrt{f'_c E_c} = 51.4\left(\frac{\pi(0.875)^2}{4}\right) = 30.9 \text{ kip}$$

- d. Check the resulting number of shear stud connectors (see Table 4.6)

$$n_{total-stud} = \begin{cases} 210 & \text{from left end 0.4 } L_1 \\ 210 & \text{from 0.4 } L_1 \text{ to 0.7}L_1 \end{cases} > \frac{P}{\phi_{sc} Q_n} = \frac{5,287.5}{0.85(30.9)} = 202$$

4.7.3.11 Check Service Limit State Requirements

1. *General Requirements (AASHTO 6.10.4)*

Service Limit State II is to control the elastic and permanent deflections under the design live load HL-93 (AASHTO 6.10.4). Elastic deformations are controlled by meeting of span-to-depth ratios specified in AASHTO Table 2.5.2.6.3-1. Permanent deformations are controlled by limiting stresses to prevent permanent deflections due to expected server traffic loadings that would impair rideability.

2. *Calculate Factored Moments—Service Limit State II*

It is noted that, for unshored construction, $DC1$, $DC2 + DW$, and live load are applied to the noncomposite (steel section alone), long-term, and short-term composite sections, respectively. At the Service Limit State II, factored moments for 0.4 Point of Span 1 are illustrated as follows:

$$M_{DC1} = 4,260 \text{ kip-ft.}$$

$$M_{DC2} + M_{DW} = 435 + 788 = 1,223 \text{ kip-ft.}$$

$$M_{(LL+IM)HL-93} = (1.3)(1.0)(3,056) = 3,973 \text{ kip-ft.}$$

3. *Check Flange Stresses*

In this example, $f_i = 0$ for this interior girder. The requirement becomes:

$$f_f = \frac{M_{DC1}}{S_{NC}} + \frac{M_{DC2} + M_{DW}}{S_{LT}} + \frac{M_{(LL+IM)HL-93}}{S_{ST}} \leq 0.95 R_h F_y = 0.95(1.0)(50) = 47.5 \text{ ksi}$$

- For the top flange

$$\begin{aligned} f_f &= \frac{(4,262)(12)}{2,655} + \frac{(1,227)(12)}{12,841} + \frac{(4,542)(12)}{48,044} \\ &= 19.26 + 1.15 + 1.13 = 21.54 \text{ ksi} < 47.5 \text{ ksi} \end{aligned}$$

- For the bottom flange

$$\begin{aligned} f_f &= \frac{(4,262)(12)}{3,376} + \frac{1,227(12)}{4,612} + \frac{(4,542)(12)}{4,973} \\ &= 15.15 + 3.19 + 10.96 = 29.30 \text{ ksi} < 47.5 \text{ ksi} \end{aligned}$$

- For the web

AASHTO 6.10.4.2.2 states that for composite sections in positive flexure in which the web satisfies the requirement of AASHTO 6.10.2.1.1, that is, $D/t_w \leq 150$, the web bend-buckling check is not required. In this example,

$$\frac{D}{t_w} = \frac{90}{0.625} = 144 < 150$$

\therefore The web bend-buckling check is not required.

4. Check Compressive Stress in Concrete Deck

For compact composite section in positive flexure regions utilized in shored construction, compressive stress in the concrete deck is due to long-term dead load and the live load satisfies

$$f_c = \frac{M_{DC2} + M_{DW}}{S_{LTc}} + \frac{M_{(LL+IM)HL-93}}{S_{STc}} \leq 0.6f'_c = 0.6(4.0) = 2.4 \text{ ksi}$$

Section modulus of concrete deck is

$$S_{STc} = \frac{I_{ST}(n)}{\gamma_{STc}} = \frac{417,986(8)}{7.7 + 3.325 + 10.875} = 152,689 \text{ in.}^3$$

$$S_{LTc} = \frac{I_{LT}(3n)}{\gamma_{LTc}} = \frac{314,752(24)}{24.51 + 3.325 + 10.875} = 195,145 \text{ in.}^3$$

$$f_c = \frac{(1,227)(12)}{195,145} + \frac{4,542(12)}{152,689} = 0.43 \text{ ksi} < 0.6f'_c = 1.95 \text{ ksi}$$

4.7.3.12 Check Constructability Requirements

1. General Requirements

At construction stages, steel girders of Span 1 with an unbraced compression flange length, $L_b = 240$ in., carry out the construction load including dead load (self-weight of steel girders and concrete deck slab) and other loads acting on the structure during construction. To prevent nominal yielding or reliance on postbuckling resistance of the steel girder during critical stages of construction, the following AASHTO 6.10.3 requirements for flexural stresses are checked. For 0.4 Point Section, shear effects are very small and shear strength check is not illustrated.

2. Calculate Factored Moment—Constructability

In the constructability check, all loads are factored as specified in AASHTO Article 3.4.2. In this example, no other construction load is assumed and only factored dead loads are applied on the noncomposite section. Compression flange is discretely braced with an unbraced length $L_b = 240$ in. within Span 1. Factored moment at 0.4 Point of Span 1 is as follows:

$$M_u = (1.25)M_{DC1} = (1.25)(4,262) = 5,328 \text{ kip-ft.}$$

3. Check Compression Flange

- Web Compactness

Limiting slenderness ratio for a noncompact web (AASHTO 6.10.1.10.2-4) is

$$\lambda_{rw} = 5.7 \sqrt{\frac{E}{F_{yc}}} = 5.7 \sqrt{\frac{29,000}{50}} = 137.3$$

$$D_c = y_{NCt} - t_{fc} = 51.92 - 1.0 = 50.92$$

(See Figure 4.21)

$$\therefore \frac{2D_c}{t_w} = \frac{2(50.92)}{(0.625)} = 162.9 > \lambda_{rw} = 137.3$$

The web is slender and AASHTO Eq. (6.10.3.2.1-2) and (6.10.3.2.1-3) are checked.

- Calculate Flange-Strength Reduction Factors R_h and R_b

Since homogenous plate girder sections are used for this example, hybrid factor R_h is taken as 1.0 (AASHTO 6.10.1.10.1).

When checking constructability according to AASHTO 6.10.3.2, web load-shedding factor R_b is taken as 1.0 (AASHTO 6.10.1.10.2).

- Calculate Flexural Resistance

Nominal flexural resistance of the compression flange is the smaller of the local buckling resistance (AASHTO 6.10.8.2.2) and the lateral torsional buckling resistance (AASHTO 6.10.8.2.3).

Local buckling resistance

$$\therefore \lambda_f = \frac{b_{fc}}{2t_{fc}} = \frac{18}{2(1)} = 9 < \lambda_{pf} = 0.38 \sqrt{\frac{E}{F_{yc}}} = 0.38 \sqrt{\frac{29,000}{50}} = 9.15$$

$$F_{nc(FLB)} = R_b R_h F_{yc} = (1.0)(1.0)(50) = 50 \text{ ksi}$$

Lateral torsional buckling resistance

$$r_t = \frac{b_{fc}}{\sqrt{12 \left(1 + \frac{1}{3} \frac{D_c t_w}{b_{fc} t_{fc}} \right)}} \quad (4.30)$$

$$r_t = \frac{b_{fc}}{\sqrt{12 \left(1 + \frac{1}{3} \frac{D_c t_w}{b_{fc} t_{fc}} \right)}} = \frac{18}{\sqrt{12 \left(1 + \frac{1}{3} \frac{(50.92)(0.625)}{(18)(1.0)} \right)}} = 4.12 \text{ in.}$$

$$L_p = 1.0 r_t \sqrt{\frac{E}{F_{yc}}} = (1.0)(4.12) \sqrt{\frac{29,000}{50}} = 99.2 \text{ in.}$$

$$F_{yr} = \text{smaller} \begin{cases} 0.7 F_{yc} = (0.7)(50) \\ F_{yw} = 50 \end{cases} = 35 \text{ ksi} > 0.5 F_{yc} = 25 \text{ ksi}$$

Use $F_{yr} = 35 \text{ ksi}$

$$L_r = \pi r_t \sqrt{\frac{E}{F_{yr}}} = (\pi)(4.12) \sqrt{\frac{29,000}{35}} = 372.6 \text{ in.} \quad (4.31)$$

$$\therefore L_p = 99.2 \text{ in.} < L_b = 240 \text{ in.} < L_r = 372.6 \text{ in.}$$

$$\begin{aligned} F_{nc(LTB)} &= C_b \left[1 - \left(1 - \frac{F_{yr}}{R_h F_{yc}} \right) \left(\frac{L_b - L_p}{L_r - L_p} \right) \right] R_b R_h F_{yc} \\ &= (1.0) \left[1 - \left(1 - \frac{35}{(1.0)(50)} \right) \left(\frac{240 - 99.2}{372.6 - 99.2} \right) \right] (1.0)(1.0)(50) \\ &= 42.3 \text{ ksi} < R_b R_h F_{yc} = (1.0)(1.0)(50) = 50 \text{ ksi} \end{aligned}$$

Use $F_{nc(LTB)} = 42.3 \text{ ksi}$ (292 Mpa)

C_b factor is taken as 1.0 conservatively for 0.4 Point of Span 1. The nominal flexural resistance of the compression flange is as follows:

$$F_{nc} = \min(F_{nc(FLB)}, F_{nc(LTB)}) = \min(50, 42.3) = 42.3 \text{ ksi}$$

$$f_{bu} = \frac{M_u}{S_{NCt}} = \frac{5,325(12)}{2,193} = 24.1 \text{ ksi} < \phi_f F_{nc} = 4.23 \text{ ksi}$$

Calculate web bend-buckling resistance

$$k = 9 \left(\frac{D}{D_c} \right)^2 = 9 \left(\frac{90}{50.92} \right)^2 = 28.12$$

$$\begin{aligned} F_{crw} &= \frac{0.9 E k}{\left(\frac{D}{t_w} \right)^2} = \frac{0.9(29,000)(28.12)}{\left(\frac{90}{0.625} \right)^2} = 35.4 \text{ ksi} \\ &< \text{smaller} \left\{ \begin{array}{l} R_h F_{yc} = (1.0)(50) = 50 \text{ ksi} \\ F_{yw} / 0.7 = 50 / 0.7 = 71.4 \text{ ksi} \end{array} \right\} = 50 \text{ ksi} \end{aligned}$$

Use $F_{crw} = 35.4 \text{ ksi}(244 \text{ MPa})$

$$f_{bu} = 24.1 \text{ ksi} < \phi_f F_{crw} = 35.4 \text{ ksi}$$

4. Check Tension Flange

$$f_{bu} = \frac{M_u}{S_{NCb}} = \frac{5,328(12)}{3,376} = 18.9 \text{ ksi} < \phi_f R_h F_{yt} = 50 \text{ ksi}$$

4.8 Summary

This chapter presents typical steel–concrete composite I-girders used in highway bridges. It discusses and provides general guidelines for girder section proportion, overall span configuration, girder spacing, cross frames and diaphragms, structural modeling and analysis, and design considerations. A design example of a three-span continuous composite girder bridge is given to illustrate the design procedure.

References

- AASHTO. 2002. *Standard Specifications for Highway Bridges*, 17th Edition, American Association of State Highway and Transportation Officials, Washington, DC.
- AASHTO. 2012. *AASHTO LRFD Bridge Design Specifications*, Customary U.S. Unit, 2012, American Association of State Highway and Transportation Officials, Washington, D.C.
- AASHTO/NSBA. 2011. *G13.1 Guidelines for Steel Girder Bridge Analysis*, 1st Edition, American Association of State Highway and Transportation Officials/National Steel Bridge Alliance, Washington, D.C.
- AISC. 2010a. *Design Specification for Structural Steel Buildings (ANSI/AISC 360-10)*, American Institute of Steel Construction, Chicago, IL.
- AISC. 2010b. *Manual of Steel Construction*, 14th ed., American Institute of Steel Construction, Chicago, IL.
- Azizinamini, A. 2007. *Development of a Steel Bridge System Simple for Dead Load and Continuous for Live Load. Volume 1: Analysis and Recommendations*. National Bridge Research Organization, Lincoln, NE., College of Engineering and Technology, Nebraska State Department of Roads, Lincoln, NE.
- Bahrami, H., Itani, A., and Buckle, I. 2009. Guidelines for the Seismic Design of Ductile End Cross Frames in Steel Girder Bridge Superstructures, *Report No. CCEER-09-04*, September, Center for Civil Engineering Earthquake Research, Department of Civil and Environmental Engineering, University of Nevada, Reno, NV.
- Barker, R. M. and Puckett, J. A. 2011. *Design of Highway Bridges*, 3rd Edition, John Wiley & Sons, Inc., New York, NY.
- Basler, K. 1961a. Strength of Plates Girder in Shear, *J. Struct. Div.* 87(ST7), 151–180.
- Basler, K. 1961b. Strength of Plates Girder under Combined Bending and Shear, *J. Struct. Div.* 87(ST7), 181–198.
- Blodgett, O.W. 1996. *Design of Welded Structures*, The James, F. Lincoln Arc Welding Foundation, Cleveland, OH.
- Carden, L., Garcia-Alvarez, S., Itani, A., and Buckle, I. 2001. Cyclic Response of Steel Plate Girder Bridges in the Transverse Direction, *The Sixth Caltrans Seismic Research Workshop*, June 12-13, California Department of Transportation, Sacramento, CA.
- Carden, L., Itani, A., and Buckle, I. 2006. Seismic Performance of Steel Girder Bridges with Ductile End Cross Frames using Single Angle X-Braces, *J. Struct. Engrg.* 132(3), 329–327.

- FHWA, 1989. *Technical Advisory T5140.22*, Federal Highway Administration, Washington, DC.
- FHWA, 2003. *LRFD Design Example for Steel Girder Superstructure Bridge*, FHWA NHI-04-042, Federal Highway Administration, Washington, DC.
- NSBA, 2012. *Steel Bridge Design Handbook*, National Steel Bridge Alliance, Chicago, IL.
- Taly, N. 1997. *Design of Modern Highway Bridges*, WCB/McGraw-Hill, Burr Ridge, IL.
- Unsworth, J.F. 2010. *Design of Modern Steel Railway Bridges*, CRC Press, Boca Raton, FL.
- Xanthakos, P. P. 1994. *Theory and Design of Bridges*, John Wiley & Sons, Inc., New York, NY, 1994.
- Zahrai, S. M. and Bruneau, M. 1998. Impact of Diaphragms on Seismic Responses of Straight Slab-on-Girder Steel Bridges, *J. Struct. Engrg.* 124(8), 938–947.
- Zahrai, S. M. and Bruneau, M. 1999. Ductile End-Diaphragms for Seismic Retrofit of Slab-on-Girder Steel Bridges, *J. Struct. Engrg.* 125(1), 71–80.

@Seismicisolation

5

Composite Steel Box Girder Bridges

5.1	Introduction	217
	Early Steel Box Girder Superstructure Developments • Where Can Composite Box Girder Superstructures Be Used? • Why Are Steel Box Girders Inherently Efficient? • Design for Economy • Redundancy and Reserve Capacity • Constructibility	
5.2	Behavior.....	220
	Live Load Distribution • Box Girder Properties • Bending Effects • Torsion Effects on an Open Box Girder Section • Shear Effects • Composite Behavior • Boundary Conditions	
5.3	Design: Proportioning a Box Girder Superstructure.....	229
	General Arrangement • Cross Section (Including Single Box Sections) • Skew and Curvature • Fatigue and Vibration • Bracing Systems • Detailing	
5.4	Modeling and Analysis	237
	General • Modeling Approach • Live Load Analysis • Model 1: Proportion the Structure • Model 2: Strength Design • Model 3: Construction Stage Models 3.1 through 3.n—Sequentially Composite Checks • Model 4: Superimposed Dead Load Checks (Time Dependent) • Model 5: Full Composite Checks	
5.5	Redundancy and Reserve Capacity.....	241
	Performance Criteria • Loading Criteria • Modeling and Analysis	
5.6	Construction	247
	The Procurement Process • Shop • Drawings • Fabrication Erection • Special Construction Techniques	
5.7	Other Considerations.....	255
	Accelerated Bridge Construction (ABC) • Access and Inspection	
5.8	Summary.....	255
	Economy • Constructability • Safety and Reserve	
	References.....	256

Kenneth Price
HNTB Corporation

Tony Shkurti
HNTB Corporation

5.1 Introduction

5.1.1 Early Steel Box Girder Superstructure Developments

Perhaps the single most defining factor in the development of highway bridge design practice in the United States was the AASHO (American Association of State Highway Officials) Road Test, performed between 1951 and 1958 in Ottawa, Illinois. Subsequent to the field tests, further laboratory and field fatigue testing was carried out at the University of Illinois between 1958 and 1961.

These tests were carried out on 16 standard bridges including 4 noncomposite steel girder bridges, 4 composite steel girder bridges, 4 precast concrete I-girder bridges, and 4 cast-in-place concrete T-beam bridges. These tests represented the typical bridge designs in use at the time on the U.S. Highway System. On June 29, 1956, President Dwight D. Eisenhower signed into law the Federal-Aid Highway Act, and the 41,000-mile (65,983 km) National Interstate Highway System was born. Construction on the Interstate System began in earnest and continued unabated for the next 16 years. Nearly half a century later these bridge types continue to represent the typical bridge still being designed and built today on the U.S. Interstate Highway system.

In the spring of 1964, the “Criteria for Design of Steel-Concrete Composite Box Girder Bridges” was presented by Mattock and Fountain to the AASHO Regional Meetings and was subsequently published as an interim to the AASHO bridge specifications in 1967. These criteria were based on folded plate analysis methods and 1/4-scale model testing completed at that time. This research provided the basis for the emergence of a new and different bridge form, the composite steel box girder bridge.

At the University of Waterloo, ON, in the early 1970s, Green and Branco continued with further research and testing to demonstrate the efficiency of these structures, and determine simple and efficient bracing systems necessary to construct these bridges safely and economically. Other work ongoing at the time included work by Johnson and Mattock (1967); Lally (1973); and Heins and Hall (1981).

5.1.2 Where Can Composite Box Girder Superstructures Be Used?

Composite steel box girder superstructures, as shown in Figure 5.1, can be designed for almost any span length and configuration, but are particularly efficient for medium- and long-span highway bridges, both tangent and curved, in spans of over 150 ft (45.7 m) and up to 500 ft (152.4 m). Steel box girders are not the answer for every bridge, but as this bridge type becomes better understood, and designers take full advantage of their inherent efficiencies, it is expected that they will become more economical and competitive in a wider range of applications.

5.1.3 Why Are Steel Box Girders Inherently Efficient?

The primary reason for the efficiency of steel boxes, and particularly for horizontally curved superstructures, is their torsional stiffness. The lateral bending stiffness of the deck is significantly enhanced by the fixity of the support at the girder lines provided by the torsional stiffness of the box. This in turn distributes live loads over a much greater tributary area engaging adjacent girders and correspondingly increasing the amount of the superstructure cross section resisting the vertical loads. I-girders provide more of a simply supported condition at the girder lines, and cannot distribute loads to adjacent girders as effectively.

5.1.4 Design for Economy

The designer should always set an objective of reducing the number of girders (web lines) and increasing the girder spacing; thus, proportioning the box girder cross section for maximum economy. The following comments were made by Mattock and Fountain (1967):

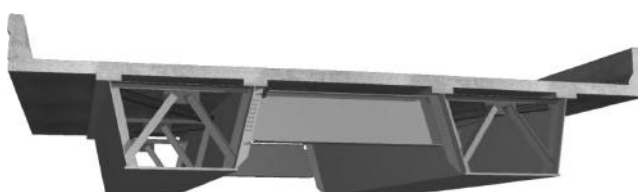


FIGURE 5.1 Typical configuration of a composite box girder superstructure.

By using the least number of boxes practical to support a cross section, it should be possible to obtain designs requiring the least amount of steel. Such designs will require the least number of boxes to be fabricated and erected.

This statement is fundamental to the design principles presented in this chapter. Mattock and Fountain (1967) concluded that efficiencies in steel materials on the order of 15% can be achieved over conventional plate girder bridges when box-girder bridges are properly proportioned and designed.

5.1.5 Redundancy and Reserve Capacity

Currently, redundancy and safety have taken on new significance as the nation's infrastructure continues to deteriorate. Safety and reliability have become a top priority. On a recent project in the Midwest, an analytical study (Shkurti et al. 2005) demonstrated that box girder bridges consisting of two box girders could in fact be considered redundant and have a remarkably high reserve capacity even when one of the girders was completely fractured.

Subsequent to the publication of these findings, and acceptance by the FHWA, full-scale testing on a similar bridge by the University of Texas at Austin (Frank and Widianto 2004) confirmed both of the above hypotheses, that is, the exceptional redundancy and reserve capacity demonstrated by this type of bridge, even in a single-span configuration subject to severe damage and extreme loading.

5.1.6 Constructability

As the complexity of highway bridges continues to escalate, and design-build becomes an increasingly popular project delivery method, it is necessary for the practicing bridge engineer to consider constructability issues as well as economy. It is safe to say that the critical stage in the life cycle of any steel girder bridge is the erection phase (Figures 5.2 and 5.3). The designer needs to be aware of how the bridge is to be delivered and erected. Awareness of stability, strength, and deformation characteristics at each stage of erection can make the difference between a successful design and a design that may lead to potential problems in the field.



FIGURE 5.2 Marquette Interchange, Milwaukee WI (2008)



FIGURE 5.3 Marquette Interchange, Milwaukee WI (2008).

5.2 Behavior

Composite steel box girder superstructures are used in a wide range of applications, with the number of boxes in the cross section varied to suit the width of the roadway. Their remarkable rigidity and strength in resisting St. Venant torsional moments (closed section, unidirectional shear flow) makes them the structural form of choice for curved alignments and numerous other applications involving significant eccentric loading conditions. A closed section subject to torsion is not only exceptionally rigid but is also considerably less susceptible to the larger warping effects associated with torsionally weaker I-girders.

5.2.1 Live Load Distribution

Load distribution in typical tangent box girder bridges that fall within a limiting range of geometric criteria (see AASHTO Art.6.11.2.3) was originally defined as follows (Johnson and Mattock 1967; Mattock and Fountain 1967).

$$W_L = 0.1 + \frac{1.7N_w}{R} + \frac{0.85}{N_w} R$$

where $0.5 < R < 1.5$

W_L = fraction of wheel load

R = N_w /(number of box girders)

N_w = number of design lanes

$N_w = W_c/12$, reduced to nearest whole number

W_c = roadway width between curbs (ft)

If one were to perform a parametric study on a four lane bridge as shown in Figure 5.4 with a variable number of girders in the cross section, the fraction of wheel load (w_L) carried by each



FIGURE 5.4 Typical multi-box girder superstructure (four lane bridge).

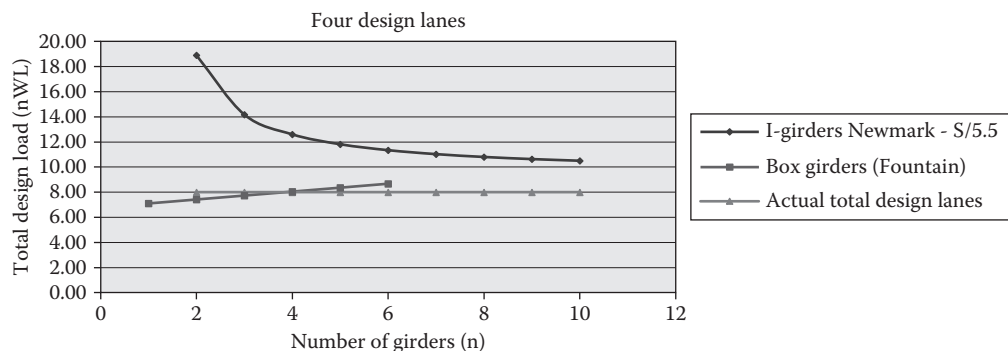


FIGURE 5.5 Comparison of total load for I-girders versus box girder bridges as predicted by the AASHTO Specifications.

girder in the cross section could be calculated using the AASHTO 2012 provisions (Art.6.11.2.3). If this fraction is multiplied by the number of girders in the cross section, the total notional load that can be placed on the structure can be obtained and compared to the actual number of lanes on the bridge.

The results of such a parametric study are summarized in the above chart, and compared to a similar series of cross sections utilizing I-girders. Figure 5.5 demonstrates that for a typical I-girder bridge the total notional live load on a four-lane structure is always more than what the bridge can physically accommodate (eight wheel loads = four axle loads), and grossly exaggerates the load that can be physically placed on the bridge as the number of girders decreases. On the other hand, the total live load on a four-lane box girder bridge is very accurately predicted by the AASHTO Specifications (AASHTO 2012) and corresponds to the load that can be physically placed on the bridge, regardless of the number of girders.

These trends are similar for bridges with any number of lanes.

This simple comparison demonstrates the inherent efficiencies of a torsionally stiff box girder superstructure system. Single box girder and twin I-girder structures have been included for the purpose of this analysis, although some owners would consider them nonredundant, or fracture critical systems.

For box girder bridges, the live load distribution formula in AASHTO 6th Edition (2012) is based on limiting criteria such as girder spacing. It should be noted that box girder superstructures are not required to conform to these limiting criteria, and additional economies can be realized by increasing the spacing, using narrower boxes, and longer overhangs. In these circumstances, the designer is required to use a more rigorous form of analysis, and the superstructures should ideally be analyzed using a three-dimensional (3D) model as described in the following sections. While the above live load distribution algorithm provides a reasonable estimate of the live load effect, the 3D behavior of a composite box girder structure is somewhat complex, and the inherent efficiencies may not otherwise be captured, resulting in an overly conservative and noncompetitive design.

The additional benefit of a 3D model is the advantage associated with the use of a live load utility program for planar deck systems. A 3D live load utility program will provide an influence surface for all the maximum and minimum design responses, producing a load set for maximum economy and design efficiency. Automated live loader systems that produce influence surfaces that can be mapped accurately to a 3D structural model are becoming more common.

5.2.2 Box Girder Properties

The following Figures 5.6, 5.7, and 5.8 demonstrate conceptually the physical properties of a steel box girder prior to placing the concrete deck. The section properties for each of these conditions can be calculated manually; however, the first two conditions represent complex manual calculations, and the third condition is seldom used in typical highway bridges.

The use of a 3D FE modeling approach renders the need for any manual calculations unnecessary.

The open section shown in Figure 5.6 is susceptible to warping. The top flanges are also susceptible to lateral-torsional buckling when subject to compression. The shear center for this section is approximately one-half the section height below the bottom flange as shown, which makes it very unstable for any eccentric vertical loads or horizontal loads applied to the section.

On the other hand, a closed section, as shown in Figure 5.7, resists torsional loads primarily by a unidirectional (St. Venant) shear flow around the cross section. The warping torsional stiffness of the closed section is negligible. However, the section is subject to normal warping stresses and through-thickness bending stresses due to cross-section distortion. Top flanges in compression are not susceptible to lateral-torsional buckling once the section is closed.

The closed section in Figure 5.7 is not a practical or cost-effective solution for design or construction, hence the quasi-closed section shown in Figure 5.8.

The quasi-closed section shown in Figure 5.8 captures the behavior of a closed section, and at the same time is a practical and cost-effective section for steel box construction. The top lateral bracing effectively closes the section and moves the shear center back into the cross section as shown, and significantly reduces the weight and cost of the cross section for construction.

In the closed or quasi-closed condition, the shear center is more or less coincidental with the geometric center of the section. This means that, although the designer must be aware of the loads occurring eccentrically to the shear center, it has to be determined whether horizontal loads are associated with wind loads during construction, for example, or eccentric vertical loads such as wet concrete or other construction loads prior to the composite closed condition and necessary steps taken to ensure the stability of the cross section during construction prior to the closed composite condition so that the negative effects of these construction loads are mitigated considerably.

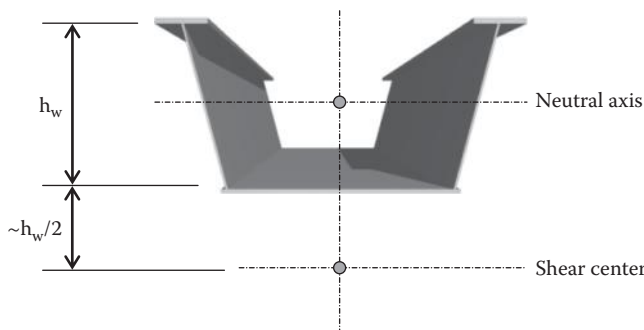


FIGURE 5.6 Open section

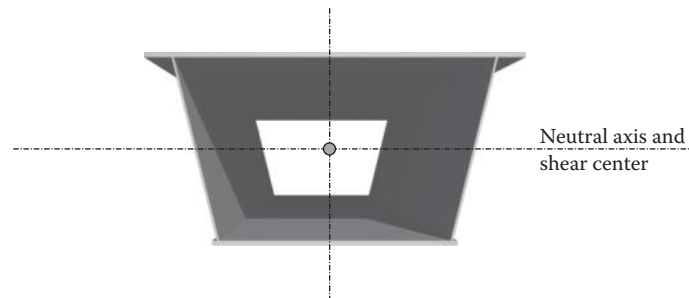


FIGURE 5.7 Closed section.

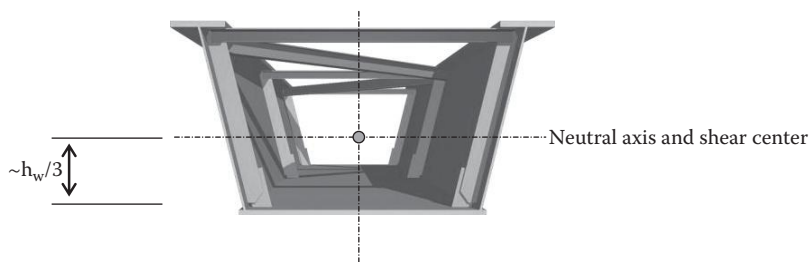


FIGURE 5.8 Quasi-closed section.

5.2.3 Bending Effects

Concentric vertical loads on a box girder section seldom occur; however, in order to understand the effects of bending on a box girder section, consider concentric vertical loads applied to the box as a stand-alone Case 1.

5.2.3.1 Case 1: Vertical Loads Applied Concentrically to an Open Box Section

As illustrated in Figure 5.9, a concentric vertical load applied to an open box section produces two responses.

1. Bending of the cross section resulting in vertical displacements.
2. Spreading of the top flanges (only when webs are inclined).

Vertical bending loads on an open box section with inclined webs will always result in a “spreading effect” at the top flanges in the open-section condition. This spreading effect is resisted in the final composite condition by the concrete deck, but during construction, including erection and placement of the concrete deck, must be resisted in some other manner, usually orthogonal struts.

These struts also provide lateral support to the top flange in compression. The unsupported length of the compression flange during placement of the deck concrete is an important check (see discussion in Section 5.3.5).

The requirements for top lateral bracing are discussed in a later section, but for now it is assumed that this bracing is always required for horizontally curved superstructures and should be considered for one or more lines of girders in tangent box girder superstructure alignments (see AASHTO LRFD Art.6.7.5.3). Figure 5.10 illustrates a typical configuration for this bracing, and describes how it behaves with respect to longitudinal bending on the section. It is essential that the designer understands that lateral bracing of any sort will engage in flexure with the superstructure cross section, with some potentially desirable and undesirable effects (fatigue for example).

As noted above, any top lateral (diagonal) bracing used to resist torsion loads during construction will participate in longitudinal bending of the girder, which can induce significant axial loads in the

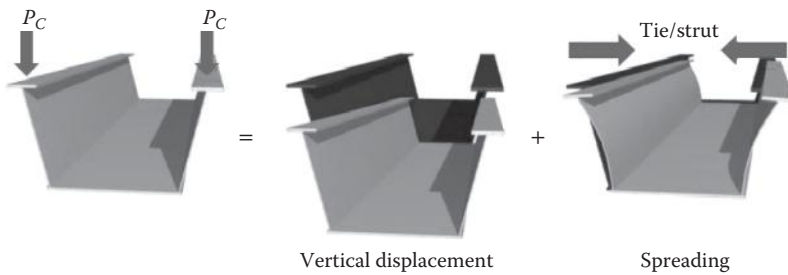


FIGURE 5.9 Bending and spreading effects on an open unbraced trapezoidal box section.

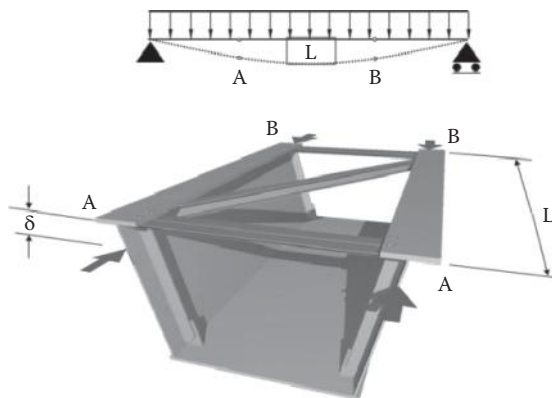


FIGURE 5.10 Concentric bending effects on top lateral bracing members.

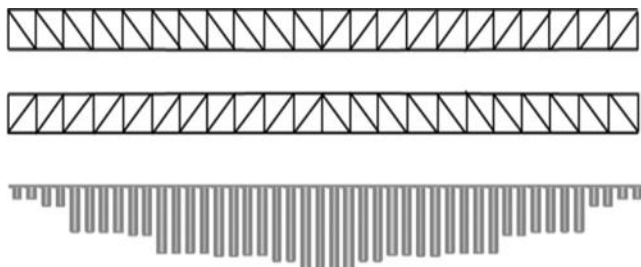


FIGURE 5.11 Distribution of bending effects in the top lateral bracing (simple-span quasi-closed superstructure).

bracing, primarily during construction. The resulting compression forces in a simple span box with top lateral bracing are illustrated in Figure 5.11.

For this reason, the designer should consider minimizing the use of top lateral bracing members (i.e. diagonal members) that are susceptible to the “bending effect,” and at the same time consider providing sufficient bracing members (i.e. orthogonal members) to resist the “spreading effect.”

At the locations of peak negative moment, the bottom flange is subjected to large compression forces. Inclined webs will decrease the bottom flange width, which in turn enhances resistance to local buckling, and should be considered accordingly. The current AASHTO provisions limit the maximum stress in the bottom compression flange to F_y , or below, so the designer needs to evaluate the labor and material associated with stiffening requirements relative to simply increasing the plate thickness.

This consideration is typically applied to webs (i.e., the use of transverse stiffening versus increased web thickness), and should likewise be considered for stiffened compression flanges.

AASHTO provisions indicate that shear lag on wider flanges is not an issue if the flange width is less than 20% of the span length for simple spans, and 20% of the distance between points of contraflexure for continuous spans (see AASHTO LRFD Art.6.11.1).

The designer should also be aware of the “resal” effect, which is the incremental compression effect in the bottom flange of a variable depth girder due to shear, which is described more fully in the next section.

Bending effects are only one component of the normal (plane section) stresses in a box girder. Stresses produced by torsional effects are discussed in the next section.

5.2.4 Torsion Effects on an Open Box Girder Section

5.2.4.1 Case 2: Vertical and/or Horizontal Loads Applied Eccentrically (Open Sections)

Torque loads (P_T) are characterized by a vertical couple as noted in Figure 5.12. This representation is intended to cover torque from all vertical and/or horizontal effects.

There are two components of this torque load both of which result in normal warping stresses.

1. Rotation of the section about the shear center (as shown in the unbraced case)
2. Distortion of the cross section due to “hard points” at cross frames or lateral brace points.

This combined effect is significantly reduced when the section is closed; however, some limited distortion of the closed cross section does occur for which AASHTO requires internal cross frames at a limited spacing in order to maintain the shape of the cross section and to minimize normal warping stresses associated with this distortion effect.

This torque accumulates along the span to the “torsion supports” such as the end diaphragms, or at the locations of the internal cross frames. These internal bracing elements help maintain the geometric integrity of the cross section, which in turn reduces the distortion effect. These bracing components, however, create corresponding local distortion stresses. These stresses are reported by most finite element programs as normal warping stresses, which are typically relatively small, but which are additive to the normal bending stresses.

Normal warping stresses and through-thickness bending stresses due to cross-section distortion in closed sections are difficult to obtain directly from finite-element models unless the mesh is quite refined. These stresses normally must be obtained from the Beam-On-Elastic Foundation methodology as outlined in Heins and Hall (1981). Normal warping stresses due to cross-section distortion are different and must be distinguished from normal warping stresses due to warping torsion, which are indeed quite small in closed sections due to the relatively small warping-torsional stiffness of a closed section.

The internal cross frames shown in Figure 5.1 are required to control this distortion effect during construction. In the case of eccentric vertical loads, they also produce a vertical bending effect as described

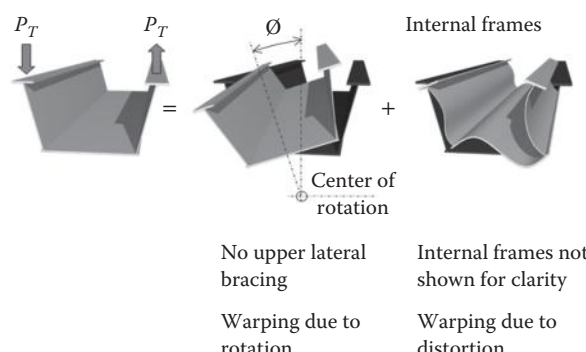


FIGURE 5.12 Torsion effects on an open trapezoidal box girder.

in the previous section. In the case of horizontal eccentric loads, there is only torsion with no associated vertical bending moment.

The designer must be aware that the special case is a curved girder configuration for both of these effects, but that the general case (a straight girder bridge) can also be critical, as there are invariably eccentric vertical loads due to construction and wind loads that will produce a similar destabilizing effect, or lateral-torsional instability on the cross section that must be considered.

Shear flow around the closed section due to torsion must be added or subtracted as appropriate to the effects of vertical shear in the webs. It must also be considered in the design of the bottom flange and in the design of the shear connectors for fatigue. In boxes subject to large torques, it may also need to be considered in the design of the transverse reinforcement in the concrete deck.

Figure 5.13 illustrates that the top lateral bracing will participate in torsion on the cross section in much the same way as it participates in vertical bending. This can be an important effect. The design objective is to plan the layout of the top lateral bracing to avoid large compression loads and associated buckling issues in the diagonals (orient for tension), and to minimize the absolute magnitude of the diagonal forces.

Figure 5.14 shows the sum of the diagonal forces from the torsion effect (P_T) and the diagonal forces from the bending effect (P_B) in a simple span.

The first plot represents the torque responses in the diagonals. The dashed line below represents the compression load in the diagonals if their orientation was not antisymmetrical (as shown in Figure 5.13) to produce tension. This will be beneficial to the amount of material required for the bracing, as buckling under compression loads will not be a concern.

In the case of bending in a simple span, the diagonals will always be in compression from the bending effect regardless of their orientation, as shown in the second plot.

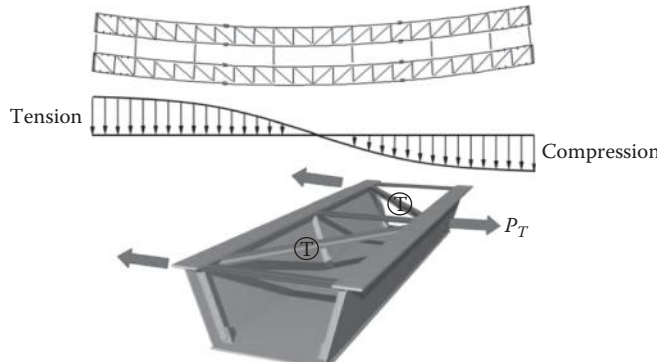


FIGURE 5.13 Distribution of torsion member forces in top lateral bracing system.

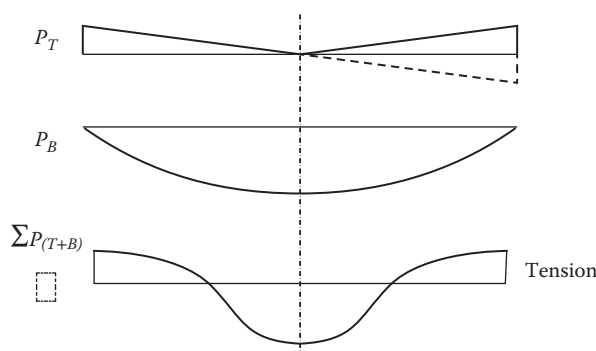


FIGURE 5.14 Combined member forces (torsion and bending) in top lateral bracing system.

These results can be extrapolated to the case of a multispan continuous bridge. The objective at all times is to mitigate the combination of bending and torsion effects in the top lateral bracing by orienting the bracing in the most effective manner to avoid large compression forces, which increases cost due to member size and connection details.

5.2.5 Shear Effects

In any solid-web girder, there is an inherent inefficiency over much of the span resulting from the lower shear demand away from the reactions (supports). In order to maximize economy, this makes minimizing the number of web lines an absolute priority, as well as reducing the web depth in the low-shear zones.

Automated fabrication methods using numerical control continue to reduce the cost of variable depth girders, to the point where this is no longer a significant fabrication cost component. The designer should focus on the fewest web lines and a uniform demand (variable) web depth everywhere to design for efficiency in shear. A shallower web depth also minimizes the demand for transverse stiffeners and longitudinal stiffeners in deeper sections.

Often, it is less expensive to provide a slightly thicker web to minimize the use of transverse stiffeners, which are labor intensive and time consuming to fabricate.

The shear stresses in the web also increase by the inclination to the vertical plane. This inclination is typically in the range of 1:4, and must be accounted for.

Another factor related to shear is the “resal” effect. In the case of a variable depth girder, the compression flange of a girder is inclined in regions of high shear (near the supports). It is intuitive that the vertical component of this curvature will attract a component of the vertical shear. This “resal” effect, or shear component of axial stress in the compression flange, must be considered in addition to the axial effects due to bending.

This effect is automatically generated by a well-conceived 3D model, but the designer must be aware that the compression stresses in the bottom flange are not generated by flexure alone in a variable-depth girder. At points where the inclined flange becomes horizontal, the vertical component of force is transferred back into the web as a concentrated load, which causes additional stress in the web and web-to-bottom flange welds and may require additional local stiffening of the web, or out-of-plane flange buckling away from the webs.

Moment-shear interaction at the support locations is no longer an explicit check in accordance with AASHTO 2012 Specifications (see AASHTO LRFD Article 6.10.9.3.2). The equations in the AASHTO Specification sufficiently capture the shear resistance of a reasonably comprehensive set of experimental test results so that moment-shear interaction effects need not be considered (White et al. 2004). The additional shear resistance and anchorage of the postbuckling tension field action in the web provided by the composite deck are also conservatively neglected, and the maximum moment and shear envelope values are typically used for design, whereas the maximum concurrent moment and shear values tend to be less critical.

The tension field action in shear introduces an incremental longitudinal load in the flange. At interior support locations, this effect is equal and opposite, so the flange is “anchored” by the adjacent span; however, this is not the case at a simple support, so the designer must ensure that this tension field effect is “anchored” at the location of end supports.

As noted in Section 5.2.4, the St. Venant shear flow at supports will increase the vertical shear due to bending on one web, and reduce it on the other, depending on the direction of the torque loads.

5.2.6 Composite Behavior

Composite behavior is relevant to both the serviceability and strength limit states.

For the service limit state, it is desirable to check the deck stresses in tension zones, and the reinforcing be proportioned to meet exposure criteria and limit cracking if the deck stress is above the concrete modulus of rupture. It is common practice to consider the bridges as fully elastic, uncracked sections for analysis purposes (AASHTO Art.6.10.1.5). Field testing has demonstrated (see AASHTO

Commentary 6.10.1.5) that a concrete deck poured directly on the top flange of a steel girder exhibits considerable unintended composite action under service loads even when constructed without shear connectors.

Research has also shown (Baldwin et al., 1987; Roeder and Eltvik, 1985; Yen et al., 1995) that considerable composite action occurs in negative bending regions, suggesting that localized deck cracking does not significantly change the stiffness properties of a composite superstructure. On the basis of these findings, it is customary to model and analyze the bridge with a fully uncracked deck section in tension zones, and provide reinforcing steel assuming a fully cracked deck in tension zones for strength design. When certain conditions specified in AASHTO Articles 6.6.1.2.1 and 6.10.4.2.1 are satisfied, the fully uncracked deck in tension zones may be utilized for fatigue and service design.

If the designer wishes to take a more rigorous approach to cracking effects for the service limit states, and introduces a stiffness regression model to evaluate the composite moment of inertia for the analysis, the following software tools are available, including Response 2000 (UT 2000), XTRACT (TRC 2012), LPile (Ensoft 2011), and SAP2000 (CSI 2013).

Permanent dead loads on the composite section should take account of creep and shrinkage and corresponding time-dependent effects using some rational method; for example, transforming the concrete deck area using the long-term modular ratio, $3n$, in the computation of composite section properties for the calculation of flexural stresses due to the permanent dead loads acting on the composite section (AASHTO Article. 6.10.1.1.b).

For transverse bending, composite bridge decks have traditionally been designed using a one-way equivalent strip method assuming continuous beam behavior of the deck and elastic, uncracked deck properties (AASHTO Article 4.6.2.1). This approach results in considerably more deck reinforcing than the so-called empirical deck design method.

The empirical deck design method has been incorporated into the current AASHTO LRFD Specifications (6th Edition - 2012), with limiting conditions including requirements for isotropic reinforcing, cross-frame spacing, deck placement methods, deck depths and span-to-depth ratios, among others. This method is a recognition that decks typically do not behave as beams only, but as a strut-and-tie, including arching section between supports. This behavior introduces a very high degree of stiffness and strength into the bridge response for both service and strength limit states. Combined with the torsional stiffness of composite box girders, this action may actually be enhanced, but this has not yet been the subject of an investigation or testing program.

The designer might wish to consider empirical deck design for deck economy and durability (see also AASHTO Commentary 9.7.2.4.)

When modeling composite box girder systems, utilizing an eight-node brick element for modeling the concrete deck captures the arching effect and provides realistic live load distribution and deck design responses. This in turn provides a true depth of the concrete-composite section, provides simple node points for mesh generation to accurately model deck haunches or tapers, and provides corresponding locations for steel flange elements.

5.2.7 Boundary Conditions

5.2.7.1 Bearings and Support Diaphragms

For construction purposes, it is generally desirable to provide dual bearings and solid bearing diaphragms. This provides for a point of torsional fixity at all supports, and takes advantage of the natural stability of a closed or quasi-closed box girder section.

Alternatively, single bearings can be used, but may represent a false economy if the external diaphragm has to carry substantial transverse bending moments, or entails complex and costly detailing.

It should be noted that torsional fixity, during construction specifically, can be significantly enhanced by the use of at least one panel of top lateral bracing (torsion box) on each span adjacent to each support. While it may be conservative to extend this top lateral bracing through the full length

of every box, the effective span for torque is significantly reduced by the use of a torsion box, and the lateral-torsional stability increases. It should be noted, however, that AASHTO LRFD Art.6.7.5.3 (as discussed earlier) requires top lateral bracing for all curved boxes, and is recommended for at least one line of boxes in tangent girder alignments. This is discussed further in the section on bracing (Section 5.3.5).

This in turn, combined with the effect of the internal cross frames, has the effect of reducing the cross-section distortion associated with torsion loads, and allows the designer to increase the spacing of the internal cross frames.

The designer may also wish to consider dual bearings, for the following reasons. Typically they are more expensive, and entail more detailing and fabrication at points of support, but on the other hand dual bearings provide a relatively simple means of fixity for torsional loads. This may be an advantage during construction and in-service. If single bearings are used, and there are significant torsion and transverse bending effects at the line of support dual bearings may be a more cost-effective alternative to a heavy end diaphragm.

Wherever feasible, skew should be eliminated by an incremental increase to the span, or widening the bearing seats to accommodate squared-off bearings.

5.3 Design: Proportioning a Box Girder Superstructure

5.3.1 General Arrangement

The most efficient span arrangement for a multispan continuous prismatic (constant moment of inertia) beam is based on equalizing midspan and interior support moments. The classic 0.65 to 1 ratio is a good starting point. Since continuous span bridges are not often designed with a prismatic section, this is not a hard and fast ratio.

Since the designer can tune the stiffness of the bridge with variable plate sizes and depths over a wide range of span ratios, it is possible to optimize the design for any specific site without any significant effects on the structural efficiency of the bridge or running up the cost.

It is always advisable to avoid very short end spans or internal spans to avoid uplift and hogging effects respectively. The designer should be aware that the relative adjacent span lengths may occasionally result in a “negative” (hogging) camber, that is, the web plates may need to be cut into a “sag” curve, rather than a “crest” curve, immediately adjacent to a pier, due to girder rotation from placement of deck concrete at the support.

This introduces two other considerations that must be accounted for, namely bearing and diaphragm rotation during the deck pour. Most bearing types have limited or desirable amplitudes for rotation, so bearings may need to be reset after the deck pour. The fabricator should be provided the rotation so that the bearing diaphragms can be detailed to be plumb as well.

5.3.1.1 Unit Weight of Steel

Figure 5.15 represents the relationship between the unit weight of steel in a bridge relative to its longest span. These curves represent a database of steel bridges constructed in Ontario between 1980 and 1990. Several observations can be made from this figure:

- Single-span bridges become inefficient compared to multispan bridges in the range of 130–150 ft.
- The unit weight of steel for multispan continuous bridges is linearly proportional to the span, contrary to the theoretical ratio, which varies with the moment, or the square of the span length. This is explained by load distribution and composite section properties.
- The unit weight of steel is consistently reduced where the value of R is reduced (i.e., the ratio of box girder width to lane width $R > 1.5$). In other words, use fewer boxes per lane and space them as widely as possible. Current AASHTO Article 4.6.2.2.2b has simplified this formula to replace R with a comparable ratio N_L/N_B (number of lanes to number of boxes).

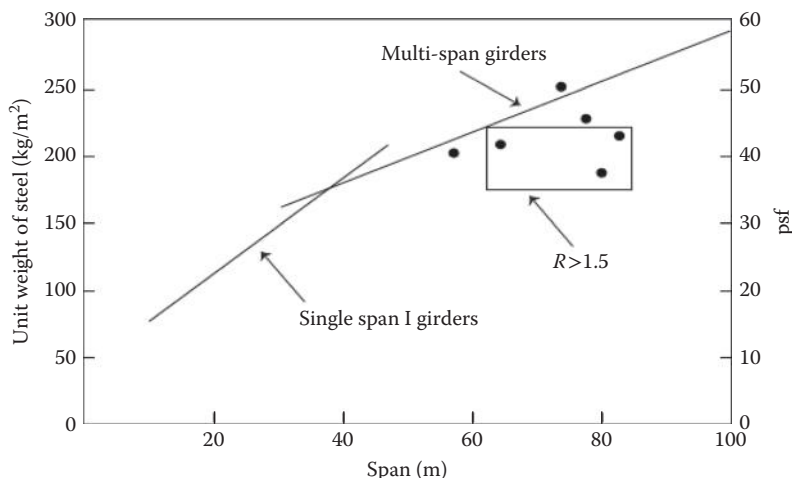


FIGURE 5.15 Relationship between span length and steel weight.

Intermediate- and long-span bridge girders with the same approximate shape (girder soffit profile) as the bending moment diagram use material most efficiently. In most cases, it is possible to reduce, and in some cases even eliminate, changes in the flange-plate thickness. This has the benefit of reducing fabrication costs associated with a variety of plate sizes and shop splice transitions.

In addition, variable depth girders are typically shallower at those locations where there is reduced shear demand, generating material savings in the web as noted earlier.

Johnson and Mattock (1967) predicted that a span-to-depth ratio (L/d) for box girders in the range of 25 would result in the most economical design. They also noted that box girders would conform to current AASHTO provisions for live load deflection with a span-to-depth ratio as high as 40. Typically composite span-to-depth ratios are in the order of 28 and noncomposite ratios are in the order of 30 to 40. Deeper girders can be used when incremental launching is proposed, to control cantilever deflections when necessary.

A nonprismatic girder can be proportioned in such a way as to require a single thickness of bottom flange throughout the entire bridge. This minimizes the need for bottom flange shop splices at thickness changes. For example, a three-span bridge with spans of 105 + 151 + 105 ft was designed (La Croix Street Bridge – Chatham ON) with a continuous bottom flange plate with a 5/8-in single-plate thickness throughout the entire bridge. The span-to-depth ratio at the piers was 27 and at midspan, 42. This resulted in a very economical steel box.

Use of a nonprismatic girder usually results in material savings when the design is properly executed. With the use of modern digitally controlled cutting machines, there is little, if any, cost penalty in fabricating webs with variable depths. Webs are frequently cut to a profile for curvature or camber in any event.

5.3.2 Cross Section (Including Single Box Sections)

There are two fundamental considerations for an optimized superstructure cross section:

1. Box girder shape and size
2. Box girder spacing

5.3.2.1 Box Girder Shape and Size

Narrower boxes are preferred to wider boxes. The advantages associated with a narrow box section (height greater than width) are as follows.

- Narrower bottom flange (increased buckling resistance)
- Greater resistance to distortion and torsional effects
- Smaller cross section, hence easier to fabricate, ship, and erect
- Advantages associated with wider girder spacing and efficiencies based on deck contribution to LL distribution

Current AASHTO specifications (2012) limit the ratio of box girder width to lane width ($R \leq 1.5$) when the specified live-load distribution factor is used. This should not be considered a limitation if the designer is using a rational method of analysis that takes into account real live load distribution and accurate modeling of the cross section.

The fraction of wheel load carried by each box is reduced as the box width increases. This is based on the torsional stiffness of the box section and supports the premise that the number of boxes in a cross section should be reduced, otherwise the demand per box reduces the efficiency of the total cross section suffers (see Section 5.3.2.2).

It is clear from the UT Austin full-scale tests discussed previously that there is a very large reserve capacity in the typical tub girder bridge with two or more tubs designed in accordance with AASHTO LRFD provisions (AASHTO 2012).

Shear lag and stability of the compression (bottom) flange in box girders is an important consideration. Shear lag increases with flange width. Likewise, a wider flange is susceptible to buckling, which incurs the cost of longitudinal stiffening, increases the effect of shear lag, and reduces the capacity of the section if the critical stress is less than F_y .

The typical trapezoidal section used in many box girder bridges has the benefit of allowing the designer to provide the same amount of material required in the bottom flange for bending in a thicker plate. This increases the stability of the wider bottom flange, reduces the effect of shear lag, and reduces the need for longitudinal stiffening.

The neutral axis tends to move up in a composite trapezoidal section and makes the bottom flange more efficient. This does not necessarily have a negative effect on the efficiency of the top flanges because most of the load in the top flanges is dead load acting on the noncomposite section before the deck has hardened or is made composite.

In addition, the trapezoidal shape is inherently more stable for fabrication and erection and reduces the fatigue problems arising from secondary vibrations.

As noted earlier, a variable depth girder more closely matches the moment-shear demand along the length of the span, and typically provides a more cost-effective use of material. Fabricators are becoming more sophisticated with the use of technology to shape girder webs and flanges without major cost implications, and develop cutting diagrams that minimize waste.

5.3.2.2 Box Girder Spacing and Single Box Sections

There are three key components of transverse design. This is a term coined by concrete segmental engineers in the last century, but is not exclusive to concrete box girders. Composite steel box girders behave according to the same rules of structural mechanics.

The three elements of transverse design (in the concrete segmental world) have been reduced to the classic Homberg, or Puchert charts, and are itemized as follows.

- Point load conditions
- Line load conditions
- Single box versus dual box configuration

These are very simple graphic algorithms that cover the majority of segmental designs, and which are directly applicable to the same range of composite steel box girder designs.

The key to an economical design is wider spacing of the boxes and fewer girder lines. This premise is based on the torsional stiffness of the boxes, which as noted above, provides a “framed” or “fixed end”

boundary condition for transverse bending moments in the superstructure, which in turn stiffens the superstructure transversely, which has the effect of engaging all the girders for a given point load or line load on the structure. This, along with the shell behavior (arching action) of the deck provides the designer the opportunity to increase the transverse deck spans.

The ultimate in efficiency is obtained with a single box girder section. Clearly a single box carries all the load regardless of where it is placed on the section, and the section can thus be optimized. Furthermore, a box is the most efficient section for carrying longitudinal bending. This can be proven theoretically as follows. This explains why segmental bridges are nearly always single cell boxes.

The flexural efficiency of any superstructure can be conveniently measured by the following dimensionless coefficient.

$$\rho = \frac{r^2}{c_1 c_2}$$

where

$$r^2 = \frac{I}{A}$$

and

I = Moment of Inertia

A = Cross-sectional area

c_1 = Distance from centroid to top extreme fiber

c_2 = Distance from centroid to bottom extreme fiber

The efficiency coefficient is $\rho = 1$ if the section consists of a top and bottom flange connected with a web of negligible thickness. Rectangular sections (without a slab overhang) and single cell box girders (with a slab overhang) typically have efficiency coefficients of $\rho = 0.33$ and $\rho = 0.60$ respectively.

By comparison, slab structures typically have poor flexural efficiency ($\rho = 0.24$). However, this is offset by relatively inexpensive formwork and shallower structural depth, but these advantages disappear on spans in excess of 50 to 75 ft, the higher end of the range represented by variable depth slabs.

(See Podolny and Muller [1982]).

For many years, owners and designers have avoided single box girder structures for various reasons. Current research and experience referenced elsewhere in this chapter, has led to a wider acceptance, and single cell steel box girder structures are now permitted by AASHTO. These structures offer significant advantages on ramp structures. They allow for wider overhangs, smaller substructures, fewer pieces to fabricate and erect, fewer web lines, and are less affected by fatigue since the single box must resist all the dead load (much higher DL to LL ratios).

Fracture critical concerns must be dealt with in certain areas, but modern bridge steels are simultaneously very tough (resistant to fatigue and brittle fracture—cracks tend not to propagate) and quite ductile (with relatively high elongations). No fractures have been reported in HPS steels that are 20 years or less in age.

Single box composite steel structures are much more competitive with segmental concrete where a single concrete box is often used.

Figure 5.16 illustrates an actual bridge for which an alternative preliminary design was completed using two boxes with a vaulted precast deck instead of four boxes with a constant-depth conventional cast-in-place deck.

This bridge is a five-span structure with variable spans up to 236 ft and an overall length of 1047 ft. The alternative design reduced the total weight of steel in the structure by 500 t (550 t), or about 20% of the total. This exceeds the predictions by Mattock and Fountain (1967) as noted above.

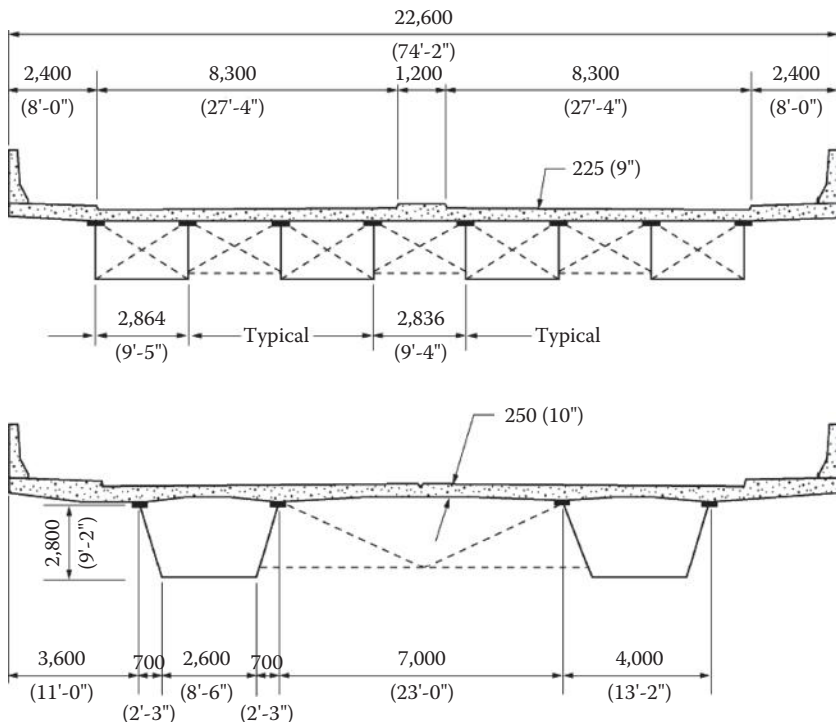


FIGURE 5.16 Box girder spacing. Two options for a four lane bridge. Option 1: Multiple girders with shorter transverse deck spans (top). Option 2: Two girders with longer transverse deck spans (below).

The two-box alternative was bid competitively against a two-box concrete segmental alternative. It was constructed as the winning bid. No bids were received for the concrete segmental option.

5.3.3 Skew and Curvature

Box girder bridges should avoid skew wherever possible. The torsional stiffness of a box girder superstructure will attract potentially excessive loads to the obtuse corners of the structure and increase the reactions and corresponding shear with corresponding rotational effects that can introduce significant longitudinal moment and shearing effects on fixed bearings. The designer should be careful to avoid fixed bearings at an obtuse support, as there can be dramatic horizontal shear forces developed on the bearing.

Wherever possible, skew should be eliminated by an incremental increase to the span, or widening the bearing seats to accommodate squared-off bearings.

5.3.4 Fatigue and Vibration

Tub-type box girders are generally not fatigue critical, especially as the number of girders is decreased and the dead-to-live load ratio is increased accordingly.

Having said this, there are a number of details in these superstructure types that can give rise to stress components that should be considered.

The primary components of stress concentration arise from the use of both internal and external cross frames, and lateral bracing. Strictly speaking, internal cross frames are the primary elements used to resist cross-section distortion during construction, although they are not so important in service. The same is true for top lateral bracing that resists twist due to torsion, (also during construction), temperature distortions and provides global stability. It is not economical to remove these bracing elements

after construction, and they tend to provide lateral bending stiffness in the superstructure in-service, when they may not even be needed. As the old adage goes, “stiffness attracts stress.” Minimize these “hot-points.”

In other words, the solution to this dilemma is to minimize these components wherever possible. As noted elsewhere in this chapter, AASHTO allows the designer to increase the spacing of internal cross frames up to a maximum of 40 ft in single box sections, curved box sections, and multiple box sections not satisfying the requirements of AASHTO LRFD (Art. 6.11.2.3), or with box flanges that are not fully effective; otherwise, there is no limit.

5.3.4.1 Normal Stresses

As noted in Section 5.2 Behavior, the normal stresses (to a plane section) in a closed or quasi-closed box girder are comprised of bending and cross-section distortion stresses. Normal stresses should be checked relative to transverse stiffening and cross-frame connections both inside and outside the box.

5.3.4.2 Distortion (or warping) Stresses

These stresses can largely be mitigated by providing sufficient internal cross frames and ensuring that transverse stiffeners and connection plates are either welded or bolted to the top and bottom flanges.

5.3.4.3 Top Lateral Bracing

Ideally, lateral bracing should be connected directly to the top flanges, but often this creates a constructability issue with deck soffit formwork as noted elsewhere. The upper elements of the lateral bracing should be detailed to be clear of formwork.

In the final composite section, the top lateral bracing is located in relatively close proximity to the neutral axis of the section, and does not participate significantly in flexure due to live load, unlike dead load on the noncomposite section. The designer should be aware, however, of the connection details to the top flanges or webs, which are subject to live load stresses.

5.3.4.4 Shear Connectors

In the case of significant torsional loads on the cross section, there is additional shear flow around the section, which should be added to the horizontal shear due to vertical bending (see AASHTO LRFD Art. 6.11.10) in the critical web. Torsional warping and distortion shear flow effects are not found to be significant.

5.3.4.5 Vibration

Vibration of girders in rapid transit systems can be significant, up to 100 g. This is a very large number, but refers to low amplitude—high-frequency vibrations, a separate phenomenon from the fundamental modal frequencies of the superstructure (see TCRP Report 71 Track Related Research — TRB 2005). Most transit agencies specify a minimum fundamental frequency for flexure (Heins and Hall 1981).

5.3.5 Bracing Systems

There are several types of bracing systems that are required for construction of tub-type box girders. These bracing systems are primarily used to stabilize the tubs prior to hardening of the deck concrete. Figure 5.17 shows a typical tub-girder bracing system.

Typically, as noted previously, these bracing systems are less important for the in-service composite performance of the superstructure system, but they still carry live load forces. Less bracing is generally needed in a box-girder system than an I-girder system to resist torsional effects. Nevertheless, bracing members are still required (AASHTO LRFD 6th Edition) to be considered primary members in horizontally curved box-girder bridges.

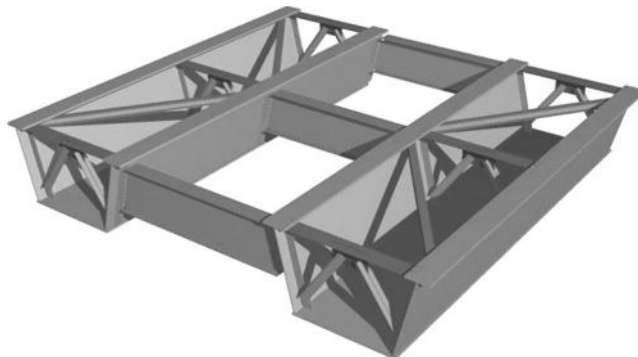


FIGURE 5.17 Tub girder bracing system.

5.3.5.1 Spreading Ties

The ties to resist the spreading force are typically a single or double angle or tee attached to the transverse stiffeners and oriented orthogonally to the longitudinal axis.

The spreading force in a tie, as shown in Figure 5.9, can be calculated simply from the weight of the wet concrete over the tributary area between ties, times the inclination of the web. Once the deck concrete has hardened, this tie serves no further function, but does carry a locked-in force.

5.3.5.2 Distortion Bracing (Internal)

In order to maintain the geometric integrity of the cross section under the cross-section distortion effects shown in Figure 5.12, an internal cross frame or diaphragm can be utilized with the spacing criteria and limitations discussed in an earlier section. It makes sense to utilize the spreading tie above as the top member of this cross frame, which can be a K, an X, a full-depth diaphragm, or a partial-depth diaphragm depending on the cross-sectional size and shape of the box and the demand.

5.3.5.3 Cross Frames (External)

External cross frames are not required by the current AASHTO specifications for straight or horizontally curved tub-girder bridges, except at the supports only (see AASHTO LRFD Article 6.7.4.3). Intermediate external cross frames should be minimized to the extent possible as they do not significantly participate in live load distribution, or redistribution of loads in a damaged structure. In the case of a two-girder system subjected to the complete failure of one box, the external cross frames are the first component to fail and do not contribute to the reserve capacity of the bridge (Shkurti et al. 2005).

5.3.5.4 Top Lateral Bracing

Top lateral bracing is typically required to stabilize the open tub section and limit distortions due to temperature effects during construction. It serves no useful function once the composite deck is in place, so it should also be minimized to the extent possible.

For straight, nonskewed, tub-girder bridges, a single line of girders with top lateral bracing will usually suffice. This bracing should be included in the first box to be erected (see also AASHTO Article C6.7.5.3 for further discussion). Subsequent girders can be stabilized during the deck pour by lean-on bracing comprising external cross frames and/or simple struts. Research on this multigirder bracing configuration for construction was carried out at the University of Waterloo ON in the 1980s (Branco and Green 1984 and 1985).

For curved girder bridges, the torsional effects can be substantial during the deck pour, and AASHTO requires continuous top lateral bracing in all tubs. The diagonals participate in flexure and torsion, so the designer should be careful to orient the bracing elements to minimize compression as noted in Section 5.2.4, as compression members are heavier and more costly than tension ties.

Current AASHTO provisions disallow the use of stay-in-place formwork in lieu of top lateral bracing.

5.3.5.5 End Cross Frames or Diaphragms (External)

As noted earlier, external-end cross frames or diaphragms are only required at supports.

5.3.5.6 End Diaphragms (Internal)

Internal to the boxes, the end diaphragms are designed as columns and beams to take the vertical reactions and to transmit external diaphragm forces respectively to the bearings.

5.3.6 Detailing

5.3.6.1 Plate Thickness and Width

The designer should attempt to use common thicknesses available from plate mills, and minimize the number of thickness transitions. This minimizes shop splices. If possible, transition bottom-flange plate sizes at field splices only. In variable depth girders, it is possible to use a constant bottom flange plate thickness throughout the length of the bridge.

Top flanges should ideally be at constant width within each field section to facilitate deck formwork.

5.3.6.2 Bottom Flange

There is a current simplified design methodology for checking the local buckling resistance of compression flanges in the presence of torsional shear in the 2012 Edition of AASHTO LRFD. By narrowing the box width to the extent feasible, the inherent stability of the bottom flange is increased, and the need for longitudinal stiffening reduced.

5.3.6.3 Top Flanges

The current AASHTO specification utilizes the equations governing the stability of top flanges of I-girder sections for the design of tub-girder top flanges during construction (see AASHTO LRFD Article 6.11.3.2). Article 6.11.3.2 states that the unbraced length is measured between the interior cross frames, although this will be conservative in the case of a trapezoidal tub, where buckling can only occur to the outside (see paragraph below).

Article C6.11.3.2 further states that top lateral bracing attached to flanges at points where only struts, and not internal cross frames, exist between the flanges may be considered as brace points at the discretion of the engineer.

The designer may wish to consider, however, the additional benefit due to the inclination of the webs to the outside in equal and opposite directions. Since the spreading effect is always to the outside, and is equal and opposite, there can never be a condition when considering the top flange where the effective length factor (K) can be 1, or even 0.7, but always 0.5. This is an inherent benefit for lateral-torsional stability of inclined web trapezoidal boxes during deck placement.

5.3.6.4 Shear Connectors

As noted elsewhere, shear connectors should be designed for torsional effects at the fatigue limit state by calculating the torsional shear and adding it to the longitudinal shear from bending acting on the composite section in the web algebraically. When calculating the horizontal shear flow for the design of the studs— $VQ/I - V$ is computed simply and conservatively as the algebraic sum of the flexural and torsional shears in the web. The same number of studs would then be used on the top flange over the other web.) Fatigue usually governs the pitch of the shear connectors.

5.3.6.5 Web Design

AASHTO defines the limits of web slenderness for webs without longitudinal stiffeners and webs with longitudinal stiffeners. Transverse stiffeners cost several more times the cost of web steel, so they should be minimized to the extent possible. An optimization analysis of stiffened versus unstiffened and

partially stiffened webs should be performed. Longitudinal web stiffeners should only be considered on longer-span girders. Longitudinal shop splices should be avoided wherever possible.

The web should always be checked for elastic behavior (Euler buckling) under dead load and the fatigue live load. Buckled webs under dead load can be unsightly, and elastic buckling (oil canning) should be avoided under the fatigue live loads, for various reasons.

Postbuckling capacity is provided by current AASHTO provisions.

5.3.6.6 Shop Splices

Shop splices should be minimized as noted above.

5.3.6.7 Field Splices

The conventional upper limits of shipping size and weight are being pushed upward on a continuing basis. The advantages associated with fabricating and/or subassembly of larger and heavier steel tub units continue. A recent example is the shipping of a large tub girder for the Columbus Ohio Gateway bridge from Wisconsin along the Interstate System, a distance of about 600 miles, using a large SPMT Traveler. The unit weighed 350,000 lbs.

Minimize the number of field splices to the extent possible.

5.4 Modeling and Analysis

5.4.1 General

AASHTO provisions have simple live load distribution methods for designers to proportion superstructures as simple-span or continuous-span line girders, including boxes.

These provisions are typically based on limiting conditions, and continue to work well for simple highway bridges.

Because of the inherent anisotropic stiffness of composite steel box superstructures, and the efficiencies associated with live load distribution as previously discussed, current AASHTO provisions allow the designer to step outside these limiting conditions to enhance the efficiency and economy of typical highway bridges when rational methods of analysis are approved (AASHTO 2012). This is particularly important for box girder bridges, as there is an incremental benefit to be gained on the basis of their fundamental behaviors, as described in Section 5.4.2. (see below).

A 3D model using plate-bending (shell) elements for steel components and simple eight-node brick elements for the concrete deck, is very helpful to realistically capture the live and dead load distribution, primary bending responses, shears, torques, and reactions.

A 3D model based on the above is described in the following section. For a more detailed discussion, reference is made to the recent AASHTO/NSBA *Guidelines for Steel Girder Bridge Analysis* (AASHTO/NBSA 2011).

In the early 1960s, as numerical methods and computer modeling came to be an increasingly important part of bridge analysis and design, and finite element analysis was still in the early stages of development, a simplified approach to modeling bridge decks as anisotropic plates was developed, known as the *grillage analogy*. This method attempted to model the in-plane and out-of-plane behavior of shells, or plate-bending elements, using a two dimensional (2D) orthogonal grillage of beams using an empirical algorithm to assign torsional stiffness for the beams. This application of torsional stiffness to the grillage was intended to model the two-way behavior of the deck plate by approximating the "tributary area" of the individual grillage members.

These approximations continue to be problematical, especially for tub girders, as grillage models can provide very different results due to the complexity of these bridge types, depth effects in the composite superstructure (separation of the neutral axes of the boxes and the deck) all of which is relatively complex, and difficult to model accurately with a two-way plate analogy.

This modeling approach for composite bridges is still being used in some commercial applications, but continues to be deficient for several reasons. Not only is the two-way plate and out-of-plane arching action of the deck modeled using approximate methods, but also the torsional stiffness of the longitudinal girder elements themselves. The eccentricity between the neutral axes of the composite deck and the girders is not accounted for and the results can be problematic as the interaction between the plate behavior of the deck and the torsional stiffness of the box girders is approximate only.

A comparison of the results between an approximate grillage model and a finite element model can be very different depending on the geometry of the bridge.

Grillage methods are not generally recommended for modeling of composite box girder bridges.

It should be noted that current efforts continue to refine these 2D modeling tools to rectify these deficiencies in existing 2D software systems (White and Coletti 2013).

5.4.2 Modeling Approach

For a 3D analysis, the entire superstructure can be modeled as follows.

- Four or five node plate-bending elements with a specified thickness for all steel flanges and webs
- Rigid links (with appropriate stiffness and spacing) to realistically model horizontal shear between the top flanges and the deck
- Beam elements for diaphragms, internal, and external cross frames
- Beam elements for top lateral bracing
- Eight-node brick elements for the composite deck, meshed to match flange widths and web lines
- Elastic spring coefficients for bearings (optional refinement)

It is important to limit the aspect ratios for the deck elements to conventional proportions and keep the element size to a reasonable maximum, which is more than satisfactory for global analysis of all composite load effects.

Designers should understand forces and deformed shapes, before they learn about FE modeling. If not, they may well be fooled into believing stress results before there is any evidence that the model is accurate. A quick check on total reactions, and deformed shapes always provide a sanity check on the model before detailed results are considered.

The designer (or the software provider) can back-calculate moment, shear, and bending effects from the FE results, on the cracked and uncracked sections for service and strength limit states (as noted, from the stress results) in the FE model. This provides the designer with the necessary forces for design purposes.

Finite element stress results from the deck using a coarse meshing approach may not be entirely reliable at specific locations, but are perfectly satisfactory for global behavior of the total superstructure as noted. If more refined results are required for deck responses at specific locations, the deck meshing can be enhanced at a limited number of locations to provide the necessary responses without burdening the model and run time with unnecessary nodes, elements, and degrees of freedom.

5.4.3 Live Load Analysis

Having established the fundamental importance of box girder behavior, and the physical modeling necessary to capture the real behavior of composite steel box girder bridges, the designer should carefully consider the application of live loads.

Historically designers have used the fundamentals of influence lines and live load envelopes to capture specific maximum and minimum structural responses at any point in the structure. Extending this analogy to three dimensions provides designers with the notional model of a “load line” of unit loads applied to the full deck width at discrete locations along each span, as opposed to a “point load” applied along the length of a beam. Aggregating the results of this load line analysis for bending, shear,

torsion, deflections, or reactions provides the designer with an influence surface for each maximum and minimum response.

These surfaces can accommodate all live loads including truck loads, lane loads, fatigue loads, and so on for both strength and serviceability design.

There are several live loaders, as described above, that are commercially available, or which can be easily developed with the current modeling tools, to provide very realistic and accurate results for live loads.

Typically, the designer should consider several separate models for analysis and design as follows. This can vary depending on the size, complexity, and construction sequence for the bridge.

Another pitfall that designers sometime fall into is the issue of coincident loads. It is essential to identify coincident load cases for shear, moment and torsion, otherwise the end result will be an unnecessarily conservative design. Exceptions can be made for members where the effort outweighs the advantages, for example, on the design of bracing systems. The savings may be relatively small, and may not justify the engineering effort.

5.4.4 Model 1: Proportion the Structure

This model is typically used to initially proportion all the key components of the bridge. A single model of the bridge is constructed using a fully composite, uncracked concrete deck section.

Load cases can be set up and checked simultaneously for various strength, fatigue, and service limit states.

Select plate sizes, shop splices, field splices, bearing locations, and bracing elements based on previous experience.

This model can be sufficiently detailed to provide nodes for connection locations of cross frames and subsequent modifications, rigid links for solid diaphragms (that can be modeled as beam elements), and any other details that are specific to the particular bridge. The meshing in the longitudinal and transverse direction is normally in the range of 5% to 10% of the span length depending on the refinements that are anticipated in subsequent iterations.

The deck meshing as noted above should be as coarse as possible to limit the model size, and the deck elements should be proportioned using conventional ratios of width to length.

The use of a continuous, instantaneously placed, uncracked composite deck will result in somewhat conservative negative moments, and somewhat unconservative positive moments. This can be kept in mind as the designer iterates through the postprocessing of results to refine plate sizes, splice locations, and bearing layout. The incrementally composite behavior of the structure can be modeled more accurately in Model 3 (Construction Staging) as described below.

For the purposes of initial modeling and proportioning of the bridge, the designer may assume that the deck concrete is placed on the structure as an instantaneous uniform gravity load for the purpose of calculating dead load effects on the structural framing system, including stability of compression flanges, bracing loads, and cambers.

This assumption should not be used for the final design, or the construction loading sequence as described below, as the incremental stiffness of the superstructure resulting from the deck pour sequence, including the effects on camber, may not otherwise be accurately predicted.

5.4.5 Model 2: Strength Design

Once the structure has been proportioned using Model 1, it is recommended that the deck stresses be checked in the negative moment region, and a fully cracked section with reinforcing steel only in the negative moment region be used for the design checks at the strength limit state.

The critical checks using the load responses and reactions from this model include design of the compression flanges, the negative moment reinforcing steel, and web design.

5.4.6 Model 3: Construction Stage Models 3.1 through 3.n—Sequentially Composite Checks

It is becoming increasingly important for the designer to take account of the sequential nature of bridge construction in order to capture intermediate effects on the partially completed, or partially composite, superstructure. This is particularly true of larger spans and bridges with more complex geometry.

The designer should determine a practical sequence for the placement of deck concrete. For longer and larger bridges, it may be appropriate to place the concrete in stages based on a proposed pour sequence, and model the bridge deck as incrementally composite to determine more accurately the ultimate camber requirements and to check the effects of subsequent deck pours on composite deck sections in place already and curing.

Traditionally, designers have required deck pours to follow a checkerboard pattern, where positive moment sections are placed first, and negative moment areas last, to minimize deck cracking. This is a rather laborious and time-consuming procedure for a contractor using traveling finishing equipment. In the event that this occurs, the designer should check the slenderness and unbraced length of the top flanges for adequacy when the positive moment pours are placed. Lateral bending of the fascia top flanges due to the torsion created by deck overhang load effects should also be considered.

Generally, contractors will elect to pour the deck continuously from one end of the bridge to the other if given the choice. Typically a three- to four-hundred cubic yard pour is feasible in a single shift, but this can be increased considerably if necessary.

If the deck concrete is placed continuously from one abutment, it is critical that the bracing of the top flanges in the end spans be spaced to limit the unbraced length as described in AASHTO LRFD Article 5.3.5 to suit the demand. If the bracing requirements become too onerous to support the wet concrete in the entire end-span, the designer might limit the first pour to say the point of contra-flexure to minimize the noncomposite bending moment demand.

It is unlikely that the deck will be entirely placed in one pour, so the benefit of modeling an incremental composite bridge, in addition to more accurately predicting real camber effects, provides a check on the locked-in stresses generated during the real construction sequence.

The “hogging effect” in the first interior span should also be checked. This load case corresponds to the end span fully loaded with wet concrete. This effect can put the bottom flange in the first interior span into a temporary compression condition as subsequent casts are made, where it is normally in tension under service loads. A wide, relatively slender, unbraced box girder tension flange may be incapable of carrying the compression loads in this condition, and precipitate a buckling failure.

A fully elastic uncracked composite deck section is appropriate for the incremental composite stiffness used in the deck staging analysis.

5.4.7 Model 4: Superimposed Dead Load Checks (Time Dependent Effects)

The structure as modeled at the end of construction has now been defined as fully composite with all the locked-in stresses and corresponding geometric responses. A common practice has been to use a modular ratio of $n = 3n$ to approximate the time-dependent response of the composite structure to additional permanent loads; however, a more rigorous time-dependent analysis can be utilized to capture creep and shrinkage effects.

Depending on the size and complexity of the structure, the designer may wish to consider the application of permanent superimposed dead loads on the fully composite structure, possibly even including the elements of the cross section that may contribute to the total composite moment of inertia such as barriers, sidewalks, and median structures. These can significantly increase the moment of inertia of the bridge in some cases.

Generally speaking, this does not result in any significant difference in redistribution of live loads, as the relative longitudinal stiffness does not change; however, a stress check on the modified composite section

for live loads will ensure that, as the neutral axis moves up, extreme fiber stresses remain within design limits. The increased section will also participate in time-dependent effects under sustained (permanent) loads.

5.4.8 Model 5: Full Composite Checks

Finally, all live load, transient loads, and extreme event load cases are typically applied to the fully composite, uncracked structure.

This model should include all the locked-in effects from Model 3: Construction Sequence as appropriate.

5.5 Redundancy and Reserve Capacity

There is significant internal redundancy and reserve capacity in the composite cross section, and even two-box girder systems have a remarkable capacity to bridge a complete failure of one girder around the location of the failure by a combination of deck bending, membrane action, torsional stiffness, engagement of traffic barrier, and structural continuity.

This reserve capacity is demonstrated analytically in the work by Shkurti et al (2005). This analytical study was accepted by WSDOT and the FHWA as proof that the twin girder boxes in the Marquette Interchange were redundant, non-fracture-critical structures. Subsequently, the full-scale tests completed at the Ferguson Laboratory at the UT Austin (Barnard et al. 2010; Samaris et al. 2012) corroborated these findings and demonstrated a remarkable reserve capacity in a single-span, twin-tub, curved bridge structure.

5.5.1 Performance Criteria

The Federal Highway Administration (FHWA) has defined one- and two-girder bridge superstructures as “fracture critical” or “nonredundant,” meaning that this type of bridge does not provide sufficient redundancy to prevent collapse upon the loss of a main load carrying member. Unfortunately there is currently (2013) no theoretical or research basis for this assumption. The good news is that the current AASHTO specification recognizes this indirectly. Currently, the AASHTO Specifications (AASHTO 2012) allow for the design and construction of nonredundant bridges subject to the implementation of a defined fracture control plan.

Owners are reluctant to add new nonredundant bridges to their inventories. Nonredundant bridges (perceived or actual), pose an increased risk to the traveling public and increase the scope and cost of inspection required. However, the definition of a “redundant,” or conversely a “nonredundant” bridge, is still a matter of some debate.

Some owners might define a two-girder bridge as nonredundant, but the work above shows that this is not the case for tub girder structures. Others might define a truss or single box girder bridge as non-redundant; however, one might demonstrate analytically, or through testing, that the failure of one or more “members” does not necessarily lead to a catastrophic collapse.

Daniels, Kim, and Wilson (1989) have put forward the following definition of redundant steel girder bridges:

New, existing or rehabilitated steel highway bridges where at least one alternate load path exists and is capable of safely supporting the specified dead and live loads and maintaining serviceability of the deck following fracture of a main load carrying member.

As shown in this definition, although multiple load paths are the major factor, a practical definition of redundancy must entail a quantification of reserve structural capacity, and a definition of both the alternate load path, and its corresponding capacity, for the case of member loss or failure. This failure

may be caused by fracture or other forms of damage to the bridge. A minimum measure of reserve capacity based on public safety and serviceability considerations must be established in order to have a set of criteria for comparison.

Recent research by the University of Texas at Austin by Barnard et al. (2011) has demonstrated that a curved ($r = 1365$ ft), simple span twin steel trapezoidal box girder superstructure is clearly redundant, and has a very high reserve capacity after complete failure of one member.

Reference is made to a landmark redundancy analysis performed on a highway system interchange including a number of twin box girder bridges. Shkurti et al. (2005) have documented the findings of a redundancy analysis of the proposed twin steel box girder bridge Structure B-40-1222, carrying traffic from southbound I-43 to westbound I-94, of the Marquette Interchange Project in Milwaukee, WI. This bridge is one of eight directional ramps constructed using two-box girder superstructures.

The NCHRP Report 406-Redundancy of Highway Girder Bridges by Ghosn and Moses (1998) proposes four limit states as follows.

1. Member limit state—Individual members are designed for strength.
2. Collapse limit state—The bridge should not reach its ultimate system capacity under extreme loading conditions.
3. Functionality limit state—Maximum deformation under expected traffic load conditions should not render the bridge nonfunctional.
4. Damaged limit state—The bridge should have a minimum reserve live load capacity after damage to or the loss of a component.

5.5.2 Loading Criteria

The NCHRP report by Ghosn and Moses (1998) proposed a loading criterion as shown in Figure 5.18 for the purpose of analyzing for redundancy. This load is intended to represent the live load that could occur on the span in the event of a defined damage limit state with a view to avoiding a total collapse and provide an assumed level of functionality until the span can be closed and the safety of the traveling public assured.

This load is defined as a pair of HS-20 vehicles side by side on the damaged span, and the measure of redundancy is defined by the number of stacked pairs that the bridge is capable of carrying in a given limit state as defined above. This configuration is based on the load that was used to calibrate the live load for the AASHTO LRFD specifications.

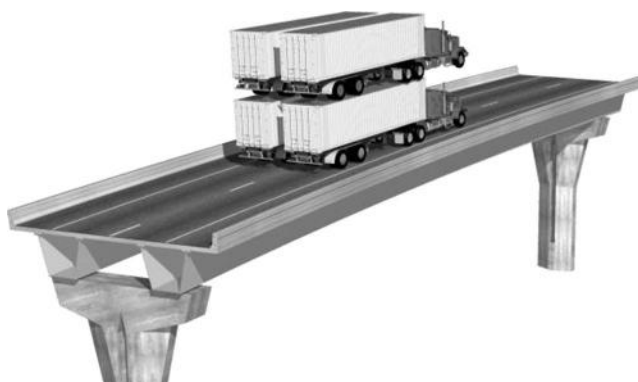


FIGURE 5.18 Loading proposed by NCHRP 406 for evaluation of system redundancy and reserve capacity (multiples of HS-20 pairs)

For the purpose of the Marquette study (Shkurti et al. 2005), this load was assumed to be a pair of HS-25 vehicles. Figure 5.20 later in the chapter shows how the reserve capacity of the structure is defined by a stepwise loading and member failure sequence (pushover analysis) for additional pairs of HS-25 loading incremental applied to the damaged structure.

The methodology employed and the results found by studying the damaged limit state are summarized below. The damaged limit state was defined as one complete box girder section fractured through both webs and all three flanges.

A dynamic effect was evaluated as well. This analysis showed an equivalent total dynamic effect of 2.68 load units, including dead load and one live load unit (pair of HS-25 trucks) on the bridge at the time of fracture, which is less than the calculated reserve capacity of 3.35.

5.5.3 Modeling and Analysis

The self-weight of the structure was modeled internally by LARSA (Shkurti et al. 2005) through the use of a gravity loading feature by specifying the material densities and section dimensions. A superimposed dead load of 25 psf was applied through the use of distributed plate pressure loads. The truck loading was modeled using two HS-25 trucks placed adjacently such as to cause the maximum load effects on the fractured (damaged) structure. The first truck load was placed 2 ft from the inside edge of the outer parapet and the trucks were spaced at 4 ft. A wheel spacing of 6 ft transversely and a conservative axle spacing of 14 ft longitudinally was chosen. The loads were applied to the structure by distributing each point load proportionately to the surrounding nodes of the respective shell.

5.5.3.1 Summary of Procedure

The structure was observed through a series of load steps to determine the response of various elements and to adjust properties or remove elements as necessary. Modifications to elements were made accordingly and the structure was reanalyzed. In the *in-depth* models where lateral bracing, cross frames, and inter-box diaphragms as shown in Figure 5.19 were modeled, if a member's connection capacity was exceeded, the failure was assumed to be brittle, the affected element was then removed and the structure reanalyzed.

Step One is to define the damage criteria. This is based on engineering judgment, and is usually agreed with the Owner, and the FHWA. In the case of the system ramps at Marquette, it was agreed to be the fracture of one complete box, with the exception of the top flanges, including the corresponding dynamic effect.

When the structure was observed to come into equilibrium with the load level being applied, the element live load effects were increased by a multiple until the next element failure. The process was continued until the onset of nonlinear behavior in the box girder, since no structure-compromising failures were observed in other elements. If the live load multiple at this point was greater than the NCHRP Report 406 (Ghosn and Moses 1998) recommended live load capacity for a damaged structure



FIGURE 5.19 Deformed shape, showing load paths and components included in redundancy and reserve capacity assessment.

and greater than the predicted step loading magnitude required capacity, the structure was deemed to be adequate without taking the structure to complete collapse.

5.5.3.2 Member Limit State

For the member failure limit state, each element is evaluated using elastic analysis and against its design member capacity. The capacity of the structure is defined as the amount of both dead and live load that the structure can support before the failure of any one member.

The required capacity for a member designed using AASHTO can be expressed as follows:

$$\phi R_{req} = \gamma_d D_n + \gamma_l L_n (1+I) \quad (5.1)$$

where

R_{req} is the required member capacity

ϕ is the resistance factor

γ_d is the dead load factor

γ_l is the live load factor

D_n is the nominal or design dead load

$L_n(1 + I)$ is the nominal or design live load including impact

The required member load factor $LF_{l,req}$ is defined as follows:

$$LF_{l,req} = \frac{R_{req} - D}{L_{HS-25}} \quad (5.2)$$

where

D is the dead load effect on the member.

L_{HS-25} is the effect of 1 set of 2 HS-25 trucks on the member.

$LF_{l,req}$, the member reserve capacity, represents the probable excess capacity of an AASHTO-designed member required by AASHTO load and resistance factors, beyond that required by unfactored dead loads. This capacity is expressed in terms of the multiple of a set of two side-by-side HS-25 truck loads. This $2 \times$ HS-25 truck loading stems from governing load conditions determined during the AASHTO LRFD bridge code calibration. NCHRP Report 406 proposes the use of HS-20 truck loading; however, the Ramp D bridge is being designed for HS-25 loading. Therefore, a set of $2 \times$ HS-25 trucks will be used as the basic live loading unit.

5.5.3.3 Required Reserve Capacity—NCHRP Method

For the damaged condition, the report establishes a load factor LF_d , that represents the multiple by which the load condition of two side-by-side AASHTO trucks can be applied, in excess of the structure's self-weight, before exceeding the damaged limit state criteria. This can be considered as the reserve capacity of the damaged system.

Furthermore, the required system reserve ratio for the damaged condition can be defined as follows:

$$R_{d,req} = \left(\frac{LF_{d,req}}{LF_{l,req}} \right) \quad (5.3)$$

where $LF_{d,req}$ is the required load factor, or required damaged system reserve capacity, and represents the required number of units of $2 \times$ HS-25 trucks the damaged structure should be able to carry, in excess

of its own dead load, to be classified as redundant. $R_{d,req}$ represents the amount of live load capacity the structure exhibits after damage versus the amount of probable excess capacity required in a particular member in the undamaged structure by AASHTO design criteria. Both capacities are taken to be in excess of that required to support the structure's dead load.

In order to determine whether or not the structure can be considered redundant, a criterion with which to compare $R_{d,req}$ must be established. NCHRP Report 406 uses a reliability analysis along with a study of bridges that are generally accepted in the engineering community as redundant to establish this criterion as follows:

$$R_d = \left(\frac{LF_d}{LF_{l,req}} \right) \geq 0.5 \quad (5.4)$$

where R_d is the system reserve ratio.

Therefore,

$$R_{d,req} = 0.5 \quad (5.5)$$

Equations 5.3, 5.4 and 5.5 effectively state that a damaged structure must have a capacity greater than or equal to one-half of the probable excess member capacity required by AASHTO design criteria, in excess of the structure's dead load, in order to be considered redundant.

Combining Equations 5.2, 5.3, and 5.4, it can be seen that

$$\begin{aligned} LF_{d,req} &= 0.5 \times \left(\frac{D(\gamma_d - 1) + \gamma_l L_{HS-2S}(1 + 0.35)}{L_{HS-2S}} \right) \\ &= 0.5 \times \left(\frac{D}{L_{HS-2S}} (\gamma_d - 1) + 1.35\gamma_l \right) \\ &= 0.15 \times \left(\frac{D}{L_{HS-2S}} \right) + 1.465 = R_{d,req} \times LF_l \end{aligned} \quad (5.6)$$

where

$$I = 0.35$$

$$\gamma_d = 1.3$$

$$\gamma_l = 2.17$$

$$\phi = 1.0 \text{ (for steel girders, LFD)}$$

Therefore, for a structure to be considered redundant:

$$LF_d \geq LF_{d,req} \quad (5.7)$$

From Equation 5.6, it can be seen that the damaged condition load factor can be calculated by determining the dead load effect and the effect of 1 set of 2 HS-25 trucks on an AASHTO designed member

in the undamaged structure. For example, if the live load effect were equal to the dead load effect in a particular member,

$$\frac{D}{L_{HS-25}} = 1$$

$$LF_{d,req} = 0.15 \times 1 + 1.465 = 1.615$$

This means that the damaged structure must hold 1.615 sets of $2 \times$ HS-25 trucks in addition to supporting the unfactored dead load in order to be considered redundant.

It should be noted that the member selected in the determination of $LF_{d,req}$ must be the member considered in the determination of LF_d in order for the comparison to be self-consistent. For example, if the structure is seen to collapse due to a plastic hinge forming in the damaged box girder at the pier, LF_d is taken as the number of units of live load that could be placed on the structure up to the point this occurs. This LF_d must be compared against the $LF_{d,req}$ calculated considering the box girder at the pier where the plastic hinge occurs and using Equation 5.7.

5.5.3.4 Methodology

In order to evaluate whether or not the structure being studied should be classified as redundant, and therefore nonfracture critical, and to provide recommendations accordingly, the following methodology was employed.

- Step 1. Construct a 3D finite element model of the structure for the *In-Depth Analyses*. A grid model with beam-type elements can be used for a *Simplified Analysis*.
- Step 2. Determine the benchmark condition for the response in the undamaged structure due to dead and live load ($1 \text{ set of } 2 \times \text{HS-25}$) conditions.
- Step 3. Calculate the required live load magnitude, $LF_{d,req}$, that the damaged structure must support in order to be considered redundant. Use the NCHRP Report 406 criteria (Eq. 5.7).
- Step 4. Determine the equivalent static load due to the dynamic effects of the dead load and live load ($1 \text{ set of } 2 \times \text{HS-25}$), resulting from the instantaneous nature of the fracture at the assumed critical section. Calculate $LF_{d,req}^{dyn}$ that the damaged structure must support due to the dynamic effect.
- Step 5. Determine the static response in the damaged structure due to dead and live load ($1 \text{ set of } 2 \times \text{HS-25}$ trucks) conditions.
- Step 6. Monitor the structural elements to determine when the load effects surpass their capacity.
Remove or yield elements as necessary and reanalyze.
- Step 7. Increment the load unit (Figure 5.20) until the governing failure criterion is exceeded.
- Step 8. Check that the maximum live load supplied in Step 7, LF_d , is greater than the live load magnitude required.
- Step 9. Establish the bridge as redundant/nonfracture critical or propose design measures to provide the necessary redundancy.

Notes:

1. Each Steel Box girder assumed to be a line girder of equivalent E and I .
2. Cross-frame elements between box girders omitted, except for pier diaphragms.
3. Lateral bracing and internal diaphragms are omitted conservatively.
4. Slab is modeled as beams elements spanning between interior box girder flanges with equivalent E and I .

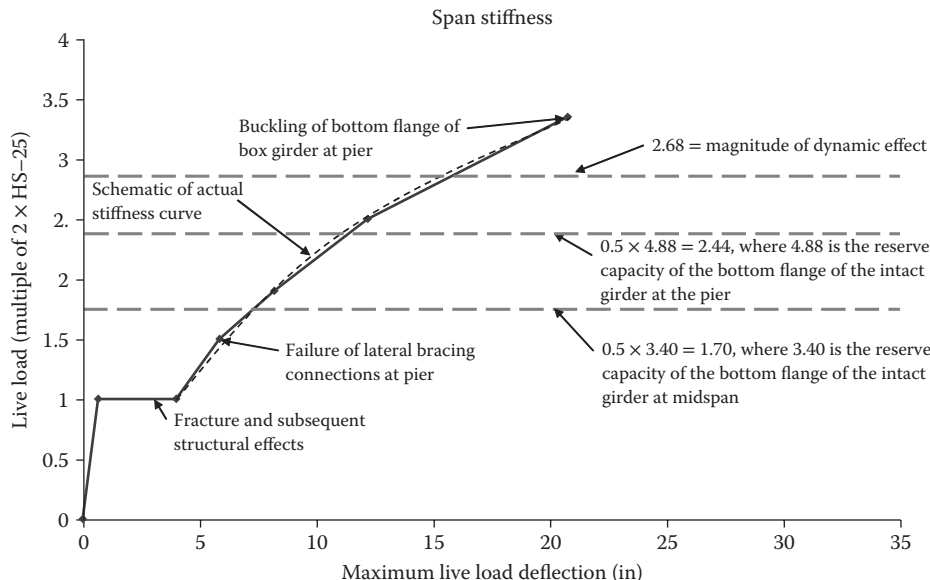


FIGURE 5.20 Pushover loading and failure of damaged section.

5. Dead loads and superimposed loads are applied as uniformly distributed linear loads onto the line girders, whereas truck wheel loads are applied as point loads onto appropriate joints of the girders.

- Step 1 – Midspan fracture of the damaged girder
- Step 2 – Failure of internal top lateral bracing connections at the pier
- Step 3 – Buckling failure of the bottom flange of the intact girder

Notes:

1. The capacity of the bottom flange of the girders at midspan and the support are equivalent.
2. The cross frames fail almost immediately.
3. Intermediate steps of the pushover analysis include cracking moment and plastic moments of the slab.
4. The capacity of the shear studs to resist pullout is important to develop plastic moments in the slab.

5.5.3.5 Summary

On the basis of the above, it was determined that the structure has sufficient reserve capacity in the defined damaged limit state to be classified as redundant and therefore, nonfracture critical. No modifications to the current design of the bridge are required. The necessary reserve capacity is supplied through available alternate load paths.

5.6 Construction

5.6.1 The Procurement Process

The first step in the procurement process stipulates a structural steel plan set that outlines the design requirements and the intent of the designer and provides the contractor–fabricator–supplier–erector sufficient information to place a mill order, price the fabrication and erection, and award a contract. In the typical design-bid-build process, these plans are produced by the engineer of record (EOR) and approved by the owner prior to advertising the project, and often includes a significant amount of detail. In case of design-build, the level of design detail required to bid and award a contract is significantly less.



FIGURE 5.21 MacMillan Rail Yards, Toronto, 1997.

In a long multiyear construction project, it is often desirable for the owner to stipulate a payment schedule that mitigates the change in material costs, and reduces this risk to the contractor. This payment schedule can also include payment milestones for various components of fabrication, erection, and completion. Otherwise the contractor may end up with significant carrying costs that will be passed along to the owner and result in a higher bid price.

The second step is a mill order. A mill order is the quantity of material that the fabricator requires to cut and fabricate field sections. It can easily be prepared with a high degree of confidence from a 20% or 30% complete set of design plans, or less. Sometimes it is desirable, especially in a design-build procurement to place a mill order as soon as realistically possible to get a place “in line” and mitigate delays in delivery if there is any significant backlog with the producers.

The third step in the process is the detailed shop drawings. These plans are typically produced for the fabricator by a detailing specialist, and can represent another significant cost in terms of schedule. In some cases, the production of shop drawings has been successfully contracted directly by the owner, and can facilitate the overall project schedule by producing an early mill order, and delivery of materials to the fabricator. It is recommended that the designer/EOR be the reviewer, although sometimes the owner takes on this responsibility.

The fourth step is the erection plan. It is likely very true that the critical stage in the entire life cycle of any bridge is the erection stage. This is the stage where the design objectives, the accuracy of detailing, and the erection methods converge.

The MacMillan Rail Yards (see Figure 5.21) represent a large-scale twin-box girder section that was competitively bid against a cast-in-place incrementally launched concrete superstructure with the same cross section and span arrangement. Because of severe restrictions to contractor activity in the rail yards, including high volumes of commuter rail traffic, the steel bridge was also designed for incremental launching. No intermediate piers were required for this operation, unlike the concrete alternative, and ultimately several bids were received for the steel alternative, and none for the concrete.

In the case of a design-build procurement process, this process becomes intuitive. The risk, responsibility, and cost for delivering at each stage becomes contractual, if not intuitive.

5.6.2 Shop Drawings

The EOR (in the case of a bid-build project), should provide design plans that are sufficient for the purpose of ordering material, developing shop drawings and assembly drawings, and providing guidance to the erection-construction engineer.

The Owner's Engineer is typically not responsible for shop drawings, or erection engineering in a design–bid–build procurement process, although the EOR is responsible for showing sufficient information on the design drawings to fully convey the intent for assembly and erection. In a design-build project, the EOR is typically responsible for design, mill-orders, erection plans, and shop drawings.

5.6.2.1 Detailing Cross Frames

As noted earlier bracing elements provided in a composite box girder are important for construction, meaning erecting and stabilizing the framing system until the concrete deck has been placed and cured. However, typically less bracing is needed in a box girder system than an I-girder system to resist torsional effects.

5.6.2.2 External Cross Frames

The current AASHTO specifications require a maximum spacing for external cross frames based on lateral-torsional stability, and live load distribution. Neither of these requirements applies to straight box girders.

Also, as noted earlier, lateral–torsional stability can be provided to the entire superstructure by a single line of box girders that is provided with upper lateral bracing and erected first. Subsequently a simple system of “lean-on” bracing struts can be provided to subsequent girder lines for erection purposes. The assumed sequence of girder erection should be shown on the plans, and if the erection contractor wishes to change the sequence, he must propose a change to the bracing.

Cross frames between boxes are not effective for live load distribution purposes, although they are designated by AASHTO as primary members (for construction) in curved girder bridges. Their contribution to the anisotropic and two-way behavior of the superstructure is insignificant. This is very different from an I-girder bridge where they are primary members for both construction and live load distribution. As a footnote, this adds “hot-spots” to an I-girder bridge for fatigue that must be considered.

5.6.2.3 Support Diaphragms inside and outside the Boxes

It is not required by AASHTO to have solid plate diaphragms inside and outside the boxes at support locations; however, the designer must address two primary considerations, that is, torsional fixity and concentrated bearing loads. Solid plate diaphragms are simple and effective. They must be detailed carefully to avoid fabrication and constructability issues.

5.6.2.4 Top Lateral Bracing inside the Boxes

The sole purpose of this bracing system is to provide lateral torsional stability to a multibox superstructure system during erection. As noted earlier, this can be accomplished by providing top lateral bracing in one line of boxes, and lean-on bracing in the form of simple struts to adjacent box girder lines.

5.6.2.5 Distortion Bracing (Cross Frames) within the Boxes

Distortion is induced by one of two effects, as noted earlier.

1. Warping effects produced by torque and bimoment on an open section. This can be very significant and will require distortion bracing to maintain the geometric stability of the cross section. Open box sections should not be used unless the framing plan ensures that even small eccentricities of vertical (and horizontal) loads during construction are taken elsewhere in the system and pose no threat of lateral instability to an unbraced line of boxes.
2. Warping effects produced by torque and bimoment on a closed “St. Venant” section. This is usually negligible and will not require distortion bracing.

The designer should take full account of the proposed bracing configurations and the relative stiffness of each for the distribution of both dead and live loads (fatigue effects) within the structure. In many cases, the dead load governs the design—particularly for larger spans, bigger boxes, and wide cross sections. Staged placement of the deck concrete can produce very different responses within the steel girder and bracing systems than the responses predicted by simultaneous placement of the deck. This factor

becomes important as the spans increase over 60 m (200 ft) in conjunction with transverse eccentricity of the dead load relative to the shear center of the boxes.

One bracing option and associated details are shown schematically in Figure 5.17 above. This continuous transverse framing system is carried into each box and occurs at quarter points.

5.6.2.6 Detailing Splices

The EOR should be able to tabulate all design loads and criteria in a tabulated format on the design drawings. Designers should not be required to detail splices. This is a detailing exercise that can be provided by the fabricator–detailer.

5.6.2.7 Detailing Bearings and Joints

The EOR should likewise tabulate all loads, movements, and associated design criteria on the design plans to provide the supplier with an unambiguous set of requirements for bidding, shop drawings, production, and installation. Suppliers should also be required to provide a brief inspection and maintenance manual to cover the expected life span of their product.

5.6.3 Fabrication

This is an art that is based on practical experience. The EOR should avail himself of every opportunity to visit the fabricating sites for his superstructures, and will learn much about how bridge components are fabricated and assembled.

Some of the key issues are fabricator certification, quality control (QC), welding procedures and heat control, material delivery, and payment and contracting issues.

For example, the EOR should understand enough of this process to know what the industry standards are for delivery and payment on a project-by-project basis. If the industry requires the fabricator to place an early order to get in line to meet the owner's delivery schedule, but is not paid until the final product is delivered or installed, this represents a potentially large risk and cost to the fabricator and the contractor, all of which is marked up and passed along to the owner.

This can be avoided by a reasonable and unambiguous payment schedule for material, completed components, delivery, and erection, which can make life a whole lot easier for everyone in the supply chain.

5.6.4 Erection

Experience has shown that the EOR cannot be divorced from the realities of erecting the bridge and associated risks. This is true of a bid-build or a design-build procurement contract. It is essential to include sufficient information on the design plans to ensure that a reasonably practical and economical solution has been provided for bidding purposes.

At the same time, the proposed solution should not be mandatory. The contract documents, based on AASHTO Construction Specifications (AASHTO 2012), should clearly articulate the requirements and erection criteria, and at the same time allow for innovation, ingenuity, and contractor means and methods to attain a safer, more economical, and efficient erection solution.

In this scenario, the contractor–erector should be required to provide a sufficiently detailed erection plan and criteria for the owner–engineer to complete a satisfactory review for compliance with contract requirements.

5.6.5 Special Construction Techniques

5.6.5.1 Incremental Launching

The incremental launching construction method was developed in Europe in the 1960s and is now used for construction of prestressed concrete, steel, and steel-composite bridges. The method involves

the process of building a bridge at a single construction location. The technology involves the typical configuration of field splices and field sections that designers are used to, then pushing or pulling the bridge forward incrementally as each field section is subassembled from the rear of the assembly yard.

Historically, the incremental launching method was developed for concrete bridges to facilitate the industrialization of segmental construction on site, and to eliminate the need for large and expensive launching gantries.

It is now recognized that this technology is readily and effectively adapted to steel bridges, including composite tub girder bridges based on the fact that steel spans are much lighter, forgiving of larger deflections during launching, and that temporary intermediate piers are typically unnecessary.

The incremental launching of the Schrotetal Bridge in Germany (1995–1997) illustrates conventional incremental launching of a dual-single composite steel box girder bridge, including a rolling form system, as illustrated in Figures 5.22 and 5.23.

Incremental launching construction for steel girder bridges typically involves adjustable supports that support the girder field sections during their assembly. The diaphragms and lateral bracing also are assembled behind the abutment. The deck slab of steel-composite bridges is typically cast in place upon completion of the launch of the steel girders.

Simply supported spans also can be launched without the costs and limitations of self-propelled modular transporters. Such versatility is advantageous in accelerated bridge construction (ABC) applications—from urban bridges to isolated or environmentally sensitive sites—and for widening existing structures.

5.6.5.2 Case Studies—Examples

The steel U-girders of the Schrotetal Bridge were launched in Germany in the years 1995–1997 (Figures 5.22 and 5.23). The two 1600-foot superstructures comprise five 225-ft spans, a 180-ft special span, and two end spans.

One-half of each U-girder was launched from the left abutment, a shorter thinner portion was launched from the right abutment over a railroad, and a varying-depth closure segment was assembled on the ground and lifted. The deck slab was cast in place with a movable forming system running along the girders.



FIGURE 5.22 Schrotetal Bridge—Germany 1997



FIGURE 5.23 Short stroke hydraulic systems for lightweight superstructures in the Schrotetal Bridge (1995–1997).



FIGURE 5.24 Chavانون.

Figure 5.24 illustrates the incremental launching of a more complex composite steel box girder bridge, the 984 foot main span, dual axial suspension bridge at Chavانون, France (2000). The span was launched from each end using a dual, swinging suspender mechanism, and spliced at mid-span before placement of the composite deck.

The reasons for incrementally launching a bridge include the following.

5.6.5.3 Sustainable Construction

- Cross-environmentally sensitive sites with minimum impact
- Disruption of the area under the bridge limited to pier erection in tight work windows
- Small subassembly yard with no additional right-of-way
- Improved control of noise and dust
- Easy demolition and replacement: a launched bridge can be moved back to the abutment and demolished on the ground

5.6.5.4 Safety

- Improved worker safety—limited work zone risks
- Avoiding detours and risks to traffic when building over highways or railroads
- Eliminating construction clearances for the forming systems

High-volume transit and rail corridors represent high-risk construction, and are often spanned by single or simple spans. Simply supported spans may be launched with the help of a temporary pier and/or a simple launching nose. The span is built in its entirety behind the abutment and then launched, thus avoiding the cost and limitations of self-propelled modular transporters.

5.6.5.5 Efficiency in Accelerated Construction

- Low labor demand, repetitive operations, and short learning curve
- Parallel activities for flexible critical path and enhanced quality of ABC applications
- Continuous production with inclement weather
- Possible 24/7 organization for ABC applications

When the bridge is short, the level of industrialization is lower and the labor demand therefore increases, but it is still lower than conventional construction.

5.6.5.6 Improved Quality

- Improved quality for welding, connection, and geometry control
- Controlled environment

The assembly of steel girders is simpler and more accurate when working on the ground. Adjustable saddles support the segments before bolting or welding and permit accurate cambers in the girders. A launched bridge is built on the ground. In addition to the absence of risks for workers and the environment, the fabrication shop can be sheltered from inclement weather to permit continuous production.

5.6.5.7 Reduced Cost

- Enhanced level of site industrialization
- No need for heavy cranes
- No need for heavy-haul loads in urban areas or mountain sites
- No operational restraints from difficult terrain

5.6.5.8 Combination Launching–Sliding

The 660-ft Tiziano Bridge was built in Italy during 1999–2001 and is another example of the versatility of the incremental bridge launching method.

The value-engineering design for this 56-ft-wide, four-span bridge resulted in a construction method that included launching a first box-girder, shifting the box-girder transversely by 30 ft to clear the launch alignment, launching a second box-girder, and joining the two box-girders with a cast-in-place curb.

5.6.5.9 Launching Nose

During launching, the leading end of a launched bridge is supported in some manner so the bridge does not need to cantilever the entire span. There are several ways to achieve this:

- Supporting the overhang with a cable-stayed system
- Reducing the cantilever weight with a light steel extension, a launching nose

The use of a steel launching nose is safe, fast, and economical. Other options include cable stayed or temporary pier systems that can be used independently or in conjunction. Temporary piers are not economical and should be avoided at all costs, but can be used effectively if the above measures are not sufficient. The designer should also avoid the addition of permanent material to the girder section for launching, as this is also not economical.

5.6.5.10 Bearings and Sliding

The girders of steel-composite bridges are launched without the deck slab, so the launch bearings are subjected to low support reactions but large rotations. They are typically pivoted saddles containing reinforced elastomeric blocks that distribute the support reaction to a long web section. Pivoted assemblies of rollers also may be used.

5.6.5.11 Push–Pull Systems

When the superstructure is light weight, (almost always the case with a composite steel box girder bridge) a pair of hydraulic pistons (Figure 5.23) anchored to the foundation is used to push the end of the bridge forward.

With heavier (concrete segmental) structures, prestressing jacks applied to the rear end of the deck pull strands or bars anchored to the abutment.

The steel girders of composite bridges can be launched on spans longer than 300 ft without temporary piers. Temporary piers are normally used for the launch of arch bridges and cable-stayed bridges.

The optimum bridge length varies between 300 and 3000 ft.

5.6.5.12 Geometric Criteria and Launching-Sliding Control

Incremental bridge launching requires simple structural geometries and constant-depth superstructures. The simplest launch conditions are described as follows.

- The bridge is straight in plan and with constant radius of vertical curvature
- There is a constant radius of curvature both in plan and in profile

Bridges with varying curvature or width also have been launched.

5.6.5.13 Summary

Incremental bridge launching works best for regular-shaped steel bridges with span lengths ranging from 100 to 300 ft (30.5 to 91.5 m) or more and bridge lengths varying from 300 to 3000 ft (91.5 to 915 m). For steel composite bridges, the spans can easily exceed 300 ft (91.5 m) without temporary piers. The primary reasons for selecting this time-tested construction method are as follows:

- Sustainable construction method for environmentally sensitive areas; context-sensitive design, small casting yard, site disruption limited to pier erection, control of noise and dust, no need for heavy transportation, and easy demolition and replacement at the end of service life
- Simple and inexpensive basic equipment; including formwork, thrust systems, and a steel launching nose
- Steel superstructures can be subassembled in a fixed, sheltered location
- Safe, simple, and repetitive operations may be organized in parallel for a short learning curve and flexible critical path in ABC applications
- Precast decks can be installed after launching
- No temporary falsework between the piers
- Limited risks for workers and traffic
- Reduced traffic restrictions on railroads or highways
- No need for detour of traffic or clearance reduction
- Compatible with tall piers, steep slopes, and urban areas

5.6.5.14 Lateral Sliding

In the case of lateral sliding, the bridge is built off-alignment adjacent to the existing bridge, using more or less conventional technology. The criterion for this technology is typically based on reducing the interruption to traffic on the existing adjacent alignment to a minimum. Depending on the circumstances, the existing bridge can be slid out in a single combined operation, all of which can be accomplished in a very short period of time (hours, or days) regardless of the size or complexity of the structure.

Figure 5.25 illustrates this technology. The existing swing bridge was kept in operation as long as possible, then the new bridge completed and traffic re-routed immediately while the new substructures and foundations were completed on the existing alignment, which could not be changed. In a short period of 3 hours and 20 minutes, the new bridge was slid laterally into its permanent position using a simple manifolded hydraulic system and stainless-steel-teflon elastomeric bearings.



FIGURE 5.25 Trenton, Ontario 1993. (a) Aerial view of bridge. (b) Bottom view of bridge.

5.7 Other Considerations

5.7.1 Accelerated Bridge Construction (ABC)

This technology is currently at the forefront of highway bridge replacement and renewal. The impact of closures, slowdowns, and safety issues on construction sites has been recognized as a significant challenge and cost at all levels. As bridge owners continue to struggle with limited resources, funding shortfalls, and a deteriorating infrastructure, the benefits associated with modularized bridges, prefabricated bridge elements, and systems, ABC will continue to increase in importance.

Reference is made to the SHRP2 R-04 Rapid Renewal and Replacement project, which is currently entering its final stages, with final deliverables due in the second half of 2012.

One of the significant components of this research is the tool kit of designs applicable to typical highway bridge replacement projects. While this tool kit has not explicitly addressed composite box girder bridges, many of the concepts and technologies are directly adaptable.

5.7.2 Access and Inspection

Owners are increasingly conscious of the need to provide safe and easy access to their bridges for inspection purposes. Designers should collaborate with their clients in order to address this important element of design.

5.8 Summary

5.8.1 Economy

Considerable effort has gone into the development of composite box girder construction in North America and elsewhere in the world over the past few decades. It is safe to say that there is still considerable work to be done in understanding the behavior, design, and safety capacity of these structures. For example, composite tub girders do not behave as line girders. Live load distribution and load paths (and boundary conditions) must be clearly understood by the designer.

As the understanding of these structures continues to evolve, and the entire industry including owners, engineers, contractors, fabricators, and erectors become more and more conversant and comfortable with this technology, the cost will continue to come down and composite box girders should be a more economical and competitive solution in a wider range of applications.

Single and dual composite box sections hold the most promise as they are inherently the most efficient structures in terms of structural performance by weight of material.

5.8.2 Constructability

Composite tub girders are typically much more stable for construction. The designer should consider not only single-girder conditions for erection, but also multigirder systems where struts and lean-on bracing can considerably simplify bracing requirements and the associated cost.

5.8.3 Safety and Reserve

Recent research has demonstrated the large reserve capacity that is apparent in composite box girder systems. Not only is it very difficult to fail these systems, but internally there is a very high level of redundancy for load redistribution and increased capacity.

References

- AASHTO. 2011. *AASHTO LRFD Bridge Construction Specifications, 3rd Edition, with 2010 and 2011 Interim Revisions*, American Association of State Highway and Transportation Officials, Washington, D.C.
- AASHTO. 2012. *AASHTO LRFD Bridge Design Specifications*, Customary US Units, 2012, American Association of State Highway and Transportation Officials, Washington, D.C.
- AASHTO/NSBA. 2011. *G13.1 Guidelines for Steel Girder Bridge Analysis, 1st Edition*, American Association of State Highway and Transportation Officials/National Steel Bridge Alliance, Washington, D.C.
- Baldwin, J. W., Salame, H. J., and Duffield, R. C., June 1987. *Fatigue Test of a Three Span Composite Highway Bridge*, Report 73-1. Department of Civil Engineering, University of Missouri, Columbia, MO.
- Barnard, T., Hovell, C. G., Sutton et al. 2011. *Modeling the Response of Fracture Critical Steel Box-Girder Bridges*, Report FHWA/TX-08/0-5498-1, Center for Transportation Research, University of Texas at Austin, Austin, TX.
- Branco, F. A. and Green, R. 1984. Bracing for composite box girder bridges, *Can J Civ Eng*, 11(4), 844–853.
- Branco, F. A. and Green, R. 1985. Composite Box Girder Bridge Behavior During Construction, *J. Struct. Eng*, 111(3), 577–593.
- CSI. 2013. *SAP2000 V16 Enhancements*, Computers and Structures, Inc., Berkeley, CA.
- Daniels, J. H., Kim, W., and Wilson, J. L. 1989. *Recommended Guidelines for Redundancy Design and Rating of Two-Girder Steel Bridges*, National Cooperative Highway Research Program Report 319, Transportation Research Board, National Research Council, Washington, DC.
- Frank, K. and Widianto, 2004. Lateral Torsional Buckling of Straight Steel Trapezoidal Box Girders during Construction, *Proceedings of AASHTO T-14 Meeting*, July, Baltimore, MD.
- Ghosn, M. and Moses, F. 1998. *Redundancy in Highway Bridge Superstructures*, National Cooperative Highway Research Program Report 406, Transportation Research Board, National Research Council, Washington, DC.
- Heins, C. P., Jr. and Hall, D. H. 1981. *Designer's Guide to Steel Box Girder Bridges*, Booklet No. 3500, Bethlehem Steel Corporation, Bethlehem, PA.
- Johnson, S. B. and Mattock, A. H. 1967. *Lateral Distribution of Load in Composite Box Girder Bridges*, Highway Research Record—Bridges and Structures No. 167, Transportation Research Board, National Research Council, Washington, DC.
- Lally, A. 1973. *Steel Box Girder Bridges*, Presentation to AISC (American Institute of Steel Construction), May, Chicago, IL.
- Mattock, A. H. and Fountain, R. S. 1967. *Criteria for Design of Steel-Concrete Composite Box Girder Highway Bridges*, United States Steel Corporation, Pittsburgh, PA.
- Podolny, W., Jr. and Muller, J. M. 1982. *Construction and Design of Prestressed Concrete Segmental Bridges*, Wiley-Interscience Publication, John Wiley & Sons, New York, Toronto, Brisbane, London.

- Price, K. D. and Sivakumar, B. 2013. associated with Genesis Structures, Structural Engineering Associates and Iowa State University, Report S2-R04-RR-2, *Innovative Bridge Designs for Rapid Renewal SHRP R-04, Prepared for Strategic Highway Research Program 2*, Transportation Research Board of the National Academies, Washington, DC.
- Roeder, C. W., and Eltvik, L. 1985. *An experimental evaluation of Autostress Design*, Transportation Research Record 1044. Transportation Research Board, National Research Council, Washington, DC.
- Samaris, V. A., Sutton, J. P., Williamson, E. B., and Frank, K. H. 2011. Simplified Method for Evaluating the Redundancy of Twin Steel Box-Girder Bridges, *J Bridge Eng.*, 17(3), 470–480.
- Shkurti, T., Dal, O., Elza, P., and Price, K. D. May 2005. *Redundancy Analysis - Marquette Interchange Final Design, Project ID: 1060-05-05*, Milwaukee Transportation Partners, Milwaukee, WI.
- TRC. 2012. *XTRACT, Version 3.09*, TRC, Rancho Cordova, CA.
- UT 2000. *Response 2000*, University of Toronto, Toronto, Canada.
- White, D., and Coletti, D. 2013, Building a Better Grid. *Modern Steel Construction*, 53(9), 46–51.
- White, D., Barker, M., and Azizinamini, A., 2004. *Shear Strength and Moment-Shear Interaction in Transversely Stiffened Steel I-Girders*, Structural Engineering, Mechanics and Materials Report No. 27, School of Civil and Environmental Engineering, Georgia Institute of Technology, Atlanta, GA.
- Yen, B., Huang, T., and VanHorn, D., 1995. *Field Testing of a Steel Bridge and a Prestressed Concrete Bridge*, Research Project No. 86-05, Final Report , Vol II, Pennsylvania Department of Transportation Office of Research and Special Studies, Fritz Engineering Laboratory Report No 519.2, Lehigh University, Bethlehem, PA.

@Seismicisolation

6

Horizontally Curved Girder Bridges

Eric V. Monzon
University of Nevada

Ahmad M. Itani
University of Nevada

Mark L. Reno
Quincy Engineering

6.1	Introduction	259
6.2	Structural Analysis for Curved Bridges	263
	Straight versus Curved Bridge • V-Load Analysis Method: Approximate Analysis for Gravity Loading • Refined Analysis Methods	
6.3	Curved Steel I-Girder Bridges	274
	Geometric Parameters • Design Criteria • Design Example	
6.4	Curved Steel Box Girder Bridges.....	277
6.5	Curved Concrete Box Girder Bridges.....	277
	Acknowledgments.....	280
	References.....	280

6.1 Introduction

As a result of complicated geometrics, limited right of way, and traffic mitigation, horizontally curved bridges are becoming the norm of U.S. highway interchanges and urban expressways. This type of superstructure has gained popularity since the early 1960s because it addresses the needs of transportation engineering. The superstructures of curved highway bridges are usually steel I-girders, steel box girders, or concrete box girders. Figure 6.1 shows the 20th Street HOV (High Occupancy Vehicle) Viaduct in Denver, Colorado, which is composed of curved I-girders that are interconnected by cross frames and bolted to the concrete bent cap. The cross frames are usually bolted to the transverse stiffeners, while the concrete deck is supported on a permanent metal deck as shown in Figure 6.2. Figure 6.3 shows the elevation of the bridge and the connection of the plate girders into an integral bent cap. Figure 6.4 shows the United States Naval Academy Bridge in Annapolis, Massachusetts, which is a horizontally curved twin steel box haunched girder bridge. Figure 6.5 shows Ramp Y at I-95 Davies Boulevard Interchange in Broward County, Florida. The structure is a single steel box girder with an integral bent cap that is pin connected to the concrete column. Figure 6.6 shows the Route 92/101 Interchange in San Mateo, California. The structure is composed of several cast-in-place prestressed curved box girder bridges.

The American Association of Highway and Transportation Officials (AASHTO) Guide Specifications for Horizontally Curved Highway Bridges was first published in 1980. This was developed by the Consortium of University Research Teams (CURT) in 1976. In its first edition, the Guide Specifications were presented in allowable stress design (ASD) design philosophy. The Guide Specifications were updated in 1993 and were presented in both the ASD and load factor design (LFD) (AASHTO 1993). However, these new specifications did not include the latest extensive research in this area nor the important changes that affected the design of straight I-girder

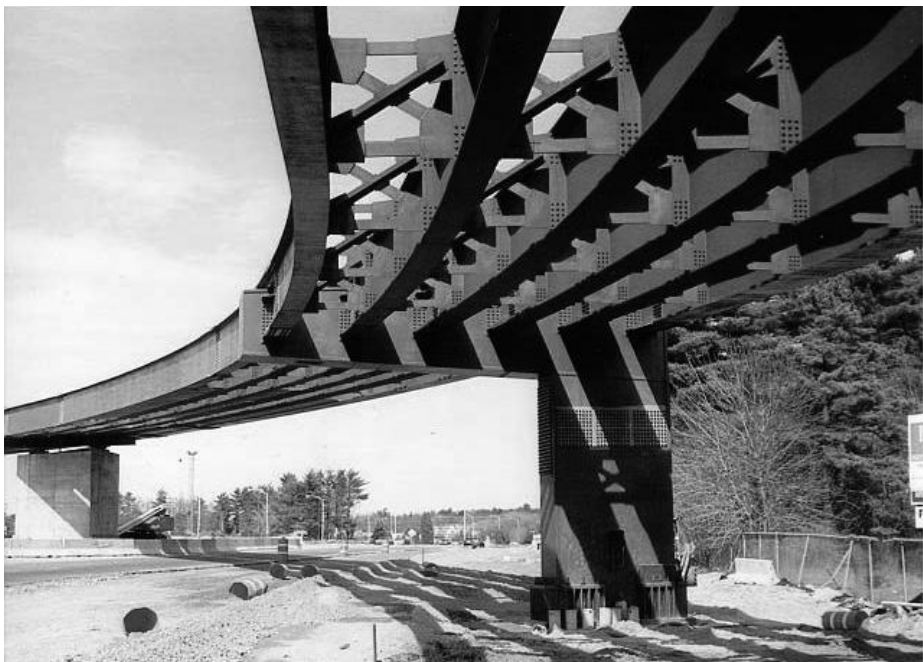


FIGURE 6.1 Curved I-girder bridge under construction—20th Street HOV, Denver, CO.



FIGURE 6.2 Bottom view of curved I-girder bridge.

@Seismicisolation



FIGURE 6.3 Curved I-girder bridge with integral bent cap.



FIGURE 6.4 Twin box girder bridge—United States Naval Academy Bridge, Annapolis, MD.

@Seismicisolation



FIGURE 6.5 Single box girder bridge with integral bent cap—Ramp Y, I-95 Davies Blvd, Broward County, FL.



FIGURE 6.6 Curved Concrete Box Girder Bridges—Route 92/101 Interchange, San Mateo, CA.

steel bridges. In 2003, the Guide Specifications were updated again based on the work by National Cooperative Highway Research Program (NCHRP) Project 12-38 (Hall, Grubb, and Yoo 1999) and was written in LFD format.

The NCHRP Project 12-52 (Kulicki, Wassef, Kleinhans et al. 2006) was commissioned by AASHTO and Federal Highway Administration (FHWA) in 1999 to develop design provisions for curved bridges that can be incorporated into the load and resistance factor design (LRFD) format of the AASHTO Bridge Design Specifications. These design provisions were calibrated to merge into the existing straight girder provisions. NCHRP Project 12-52 was divided into two phases. Phase I produced design provisions based on the information available at that time and design examples of curved steel box-girder and curved steel

I-girder bridges. Phase II revised these specifications based on the results of the then ongoing research on curved bridges. The FHWA-funded research projects include experimental testing of a full-scale single-span superstructure with three steel I-girders. In 2006, the curved girder provisions were included in the interim to AASHTO LRFD Bridge Design Specifications (AASHTO 2006).

For curved concrete box-girder bridges, NCHRP Project 12-71 (NCHRP 2008) developed design specifications, commentary, and design examples. The Project 12-71 report includes literature review and state of practice, results of global and local response analysis, recommended LRFD design provisions, and design examples.

Recently, FHWA funded the seismic investigation of curved steel highway bridges. In this investigation, a large-scale model of a three-span, horizontally curved steel I-girder bridge was tested on multiple shake tables at University of Nevada Reno (Monzon, Buckle, and Itani 2013). The 2/5-scale model was tested for a variety of configurations. First, a benchmark bridge was tested using conventional columns and bearing details. Then the influence of seismic isolation, partial isolation combined with ductile end cross-frames, abutment backfill soil interaction, and rocking footing were studied by comparison to the response of benchmark bridge. In addition, the effect of live load was studied by placing a series of trucks on the deck of bridge model. The findings of the experimental studies coupled with analytical investigations are used to develop seismic design guidelines for horizontally curved steel girder bridges.

The objective of this chapter is to present guidelines for the design of curved highway bridges. Structural design of steel I-girder, steel, and prestressed concrete box girder bridges is the main thrust of this chapter.

6.2 Structural Analysis for Curved Bridges

The accuracy of structural analysis depends on the analysis method selected. The main purpose of structural analysis is to determine the member actions due to applied loads. In order to achieve reliable structural analysis, the following items should be properly considered:

- Mathematical model and boundary conditions
- Application of loads

The mathematical model should reflect the structural stiffness and the boundary conditions properly. Lateral bearing restraint is one of the most important conditions in curved bridges because it may cause lateral shear in the superstructure. The deck overhang, which carries a rail, can provide a significant torsion resistance. Moreover, the curved flanges would participate not only in resisting the vertical load but also in the inherent torsion in the superstructure. This participation increases the applied stresses beyond those determined by using simple structural mechanics procedure (Hall, Grubb, and Yoo 1999).

Owing to curved geometry, the gravity loads induce torsional shear stresses, normal warping stresses, and lateral bending stresses in addition to the vertical shear and bending stresses. In curved steel I-girder bridges, the internal torsion in the superstructure is distributed to the girders through the cross frames or diaphragms. The outer girders take more load than the inner girders, causing each girder to deflect differently. In curved box girders, internal torsion increases the lateral deck shear but equilibrium is less dependent on the interaction between girders.

6.2.1 Straight versus Curved Bridge

A common assumption in the analysis of curved highway bridges is to ignore the curvature and analyze these bridges as if they are straight. The AASHTO LRFD Bridge Design Specifications (AASHTO 2012) permits curved I-girders to be analyzed as a straight girder for determining the major-axis bending

moments and shears due to dead and live loads provided that the girders are concentric, the bearing lines are not skewed more than 10° from the radial direction, all of the girders are about the same stiffness, and the subtended angle of the span is less than 4° . Otherwise, the effect of curvature must be accounted for through either approximate or refined analysis methods. Approximate methods such as the *V-Load* method (USS 1984) for I-girders and the *M/R* method for box girder bridges may be used for “regular” bridges. Refined analysis is required for highly curved bridges and when other geometric irregularities such as skew supports are present.

Multicell concrete box girder may be analyzed as straight segments for central angles less than 34° within one span. Steel box and tub girders are permitted to be analyzed as if they are straight provided the girders are concentric, bearings are not skewed, the span central angle is less than 17° , and the girder depth is less than the width of the box.

For seismic analysis, the AASHTO Specifications permit curved bridges to be analyzed as if they are straight when the subtended angle is less than 90° and the bridge has “regular” properties, as defined in the specifications.

Depending on various parameters such as boundary conditions, curvature, skew, and other geometric irregularities, the straight bridge assumption might be able to capture some of the global response. However, this assumption could either underestimate or overestimate the response of local superstructure components such as bearings and cross-frame forces. Bearing forces obtained from a curved bridge can be significantly different than from the corresponding straight bridge due to the difference in boundary conditions, frame action between the piers, and abutments and inherent superstructure torsion. Cross-frame forces must be determined accurately and designed accordingly since they are primary load-carrying members in a curved bridge.

To illustrate the effect of curvature on local components such as cross frames, three-dimensional (3D) finite element models of a curved and a straight bridge were developed. The curved bridge geometry and section properties are as shown in Section 6.3.3 Design Example. The straight bridge has the same section properties as the curved bridge such that the only difference is the curvature.

Figure 6.7 shows the comparison of axial forces in one of the diagonal members of the cross frames under dead load. As shown, the cross-frame forces in a curved bridge can be twice as those in the corresponding straight bridge. The discrepancy is most pronounced at the midspan of the center span (cross-frame number 13) and the piers (cross-frame numbers 8 and 18). The torsional deformations in a curved bridge are largest at the mispan, causing axial forces in the nearby cross frames, which are not generated in straight bridges. Since a curved bridge tends to twist toward the outside of the curve, more loads are shifted to the outside bearings at the piers. The pier cap then will have a larger displacement at one end (on the outside of the curve) and smaller displacement at the other end (on the inside of the curve). The differential displacements generate forces in the cross frames. In a straight bridge, cross-frame forces are also generated due to pier cap flexibility but they are smaller because of relatively uniform distribution of bearing forces.

Figure 6.8 shows the comparison of axial forces in one of the diagonal members under seismic loading. Similar to the observation made under dead load, the discrepancy in the cross-frame forces is largest at the midspan of the center span. Seismic loading in the transverse direction creates frame action in curved bridges due to the offset between the abutments and piers. This frame action results in seismic axial forces in the columns and vertical reactions in the abutment bearings, which must be resisted by superstructure torsion (Priestley, Seible, and Calvi 1996). This torsion is then resisted by the cross frames increasing the force of the gravity load even further.

However, at the abutment locations, the seismic cross-frame axial forces in straight bridges are normally larger than those in curved bridges. This is due to the difference in the boundary conditions in the transverse direction, highlighting the importance of proper representation of boundary conditions as mentioned before. Since the guided bearings in the example curved bridge allow translation in the tangential direction but restrain the radial direction, the transverse direction is only partially restrained. However, in the straight bridge, the abutments are fully restrained in the transverse direction as the guided bearings allow translation in the longitudinal direction only.

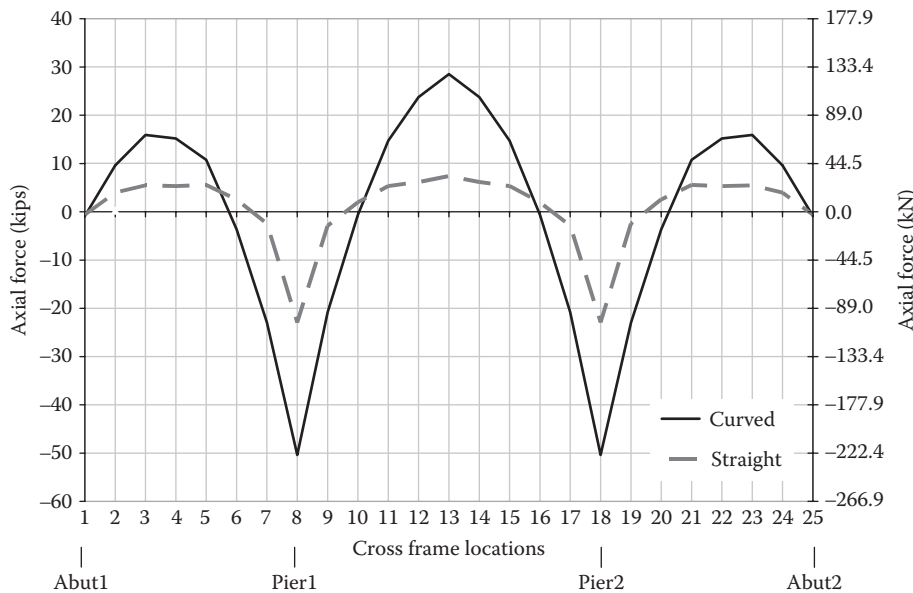


FIGURE 6.7 Comparison of forces in one of the diagonal members of cross frames under dead load.

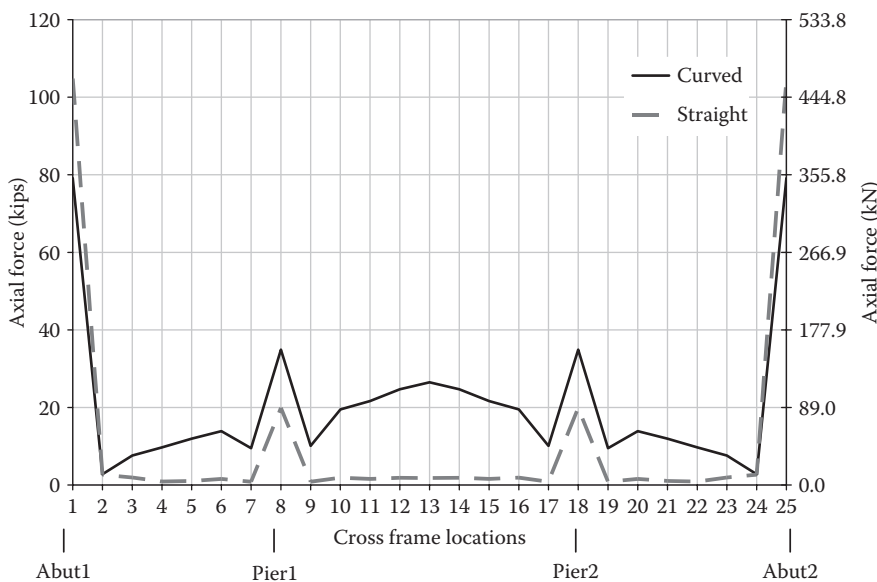


FIGURE 6.8 Comparison of forces in one of the diagonal members of cross frames under earthquake load.

6.2.2 V-Load Analysis Method: Approximate Analysis for Gravity Loading

In 1984, the United States Steel published Chapter 12 “V-Load Analysis” in USS Highway Structures Design Handbook (USS 1984). This chapter presents an approximate simplified analysis method to determine moments and shears for horizontally curved, open-framed highway bridges. In this method, the individual girders are analyzed first as straight to determine the primary major-axis bending moments and shears. These moments and shears are then adjusted using the V-loads, which are a set of fictitious self-equilibrating shears between adjacent girders. The rationale for V-loads is discussed below.

Consider a curved bridge with two prismatic girders continuous over an interior support with two equal spans as shown in Figure 6.9. The girder height is h and Girder 1 has a radius R . When the gravity load is applied, assuming the flanges of the plate girder resist the full moment, the flanges are subjected to axial forces M/h (see Figure 6.10). Owing to the curvature of the bridge, these forces are not collinear along any given segment of the flange. Thus, radial forces must be developed along the girder to maintain equilibrium. The magnitude of the distributed radial forces is as follows:

$$q = \frac{M}{hR} \quad (6.1)$$

Because the distributed radial forces are proportional to moment M , its shape is the same as the bending moment diagram as shown in Figure 6.11. These forces cause lateral bending of the girder flanges resulting in warping stresses.

The distributed load creates equal and opposite reaction forces at every cross frame as shown in Figure 6.12. By assuming the spacing between the cross frames is equal to d , the reaction force at the cross frame is as follows:

$$H = \frac{Md}{hR} \quad (6.2)$$

To maintain equilibrium of the cross frame forces, vertical shear forces must develop at the end of the cross frames as a result of its rigidity and end fixity as shown in Figure 6.13. The resulting shears then become the fictitious self-equilibrating V-loads applied to the straightened individual girders. Using

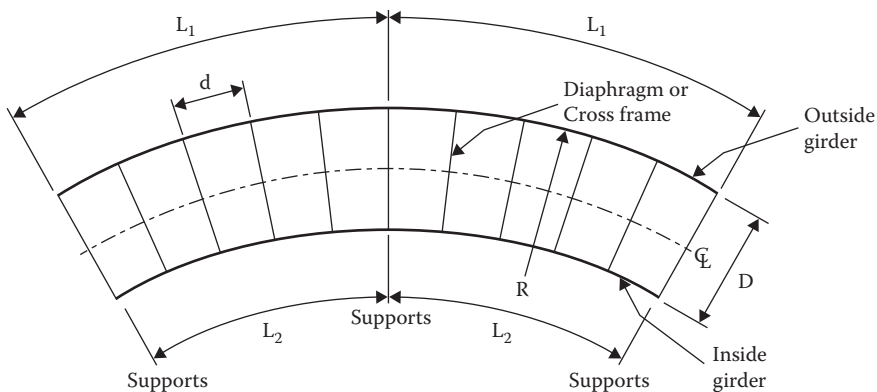


FIGURE 6.9 Plan view of two span curved bridge.

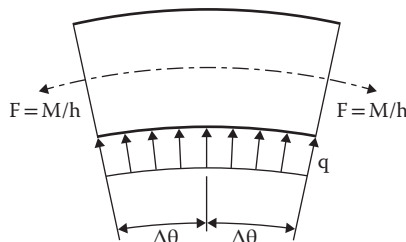


FIGURE 6.10 Plan view of curved bridge top flange.

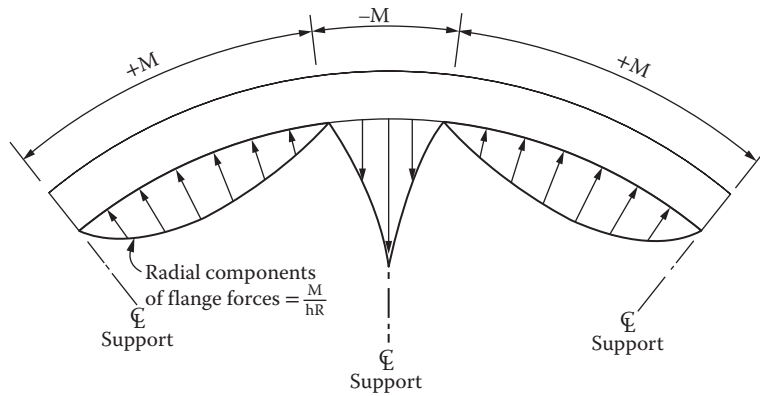


FIGURE 6.11 Lateral forces on curved girder flange.

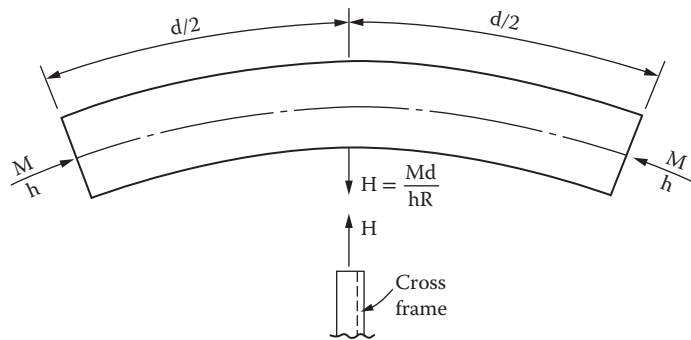


FIGURE 6.12 Reaction at cross frame location.

this procedure, the V-loads for bridges with three or more girders can be calculated. In general, the V-load equation can be expressed as follows:

$$V = \frac{\Sigma M_p}{CK} \quad (6.3)$$

$$K = \frac{RD}{d} \quad (6.4)$$

where ΣM_p is the summation of primary bending moments (see example below), C is a coefficient that depends on the number of girders (see Table 6.1), and D is the distance between the outside and inside girders. The radius R and cross-frame spacing d along the outside girder are always used for simplicity because the ratio R/d is the same for all the girders.

Equation 6.3 is the general equation for the V-loads on the exterior girders. On the interior girders, the V-loads are calculated by multiplying Equation 6.3 by a proportionality factor, which is based on triangular load distribution (see example below). At positive moment regions, the V-loads act downward on the girders outside the bridge centerline and upward on the girders inside the bridge centerline. The opposite is true in the negative moment region (i.e., the V-loads act upward on the outside girders and downward on the inside girders).

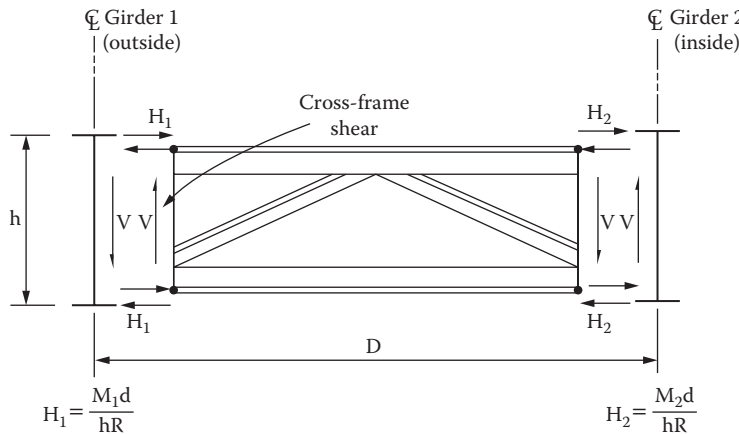


FIGURE 6.13 Equilibrium at cross frame location and the formation of V-loads.

TABLE 6.1 Coefficient C for Multigirder Systems

No. of Girders in the System	Coefficient, C
2	1
3	1
4	10/9
5	5/4
6	7/5
7	14/9
8	12/7
9	15/8
10	165/81

The moments and shears obtained by applying the V-loads are then added to the primary moments and shears to determine the final design forces. The lateral bending moment in the flanges is then approximated using the equation

$$M_{lat} = \frac{M_f l^2}{NRD} \quad (6.5)$$

where M_f is the final major-axis bending moment, l is the girder unbraced length, R is the girder radius, D is the web depth, and N is a constant taken as either 10 or 12 depending on the desired level of conservatism.

As the curvature increases, the accuracy of the V-load method in predicting the superstructure major-axis bending moments and shear decreases.

6.2.2.1 V-Load Method Example

Figure 6.14 shows the superstructure of a horizontally curved, three-span, steel I-girder bridge. This bridge is used to compare the results of the V-load method against that from the finite element (FE) model. The total width of the deck is 39 ft [11.89 m] with girder spacing of 11 ft [3.354 m]. The center-line radius is 146 ft [44.51 m], the total length of 290 ft [88.41 m], and the total subtended angle is 114°. The span lengths are 84 [25.61], 122 [37.20], and 84 ft [25.61 m]. Girder 1 (G1) is at the outside of the

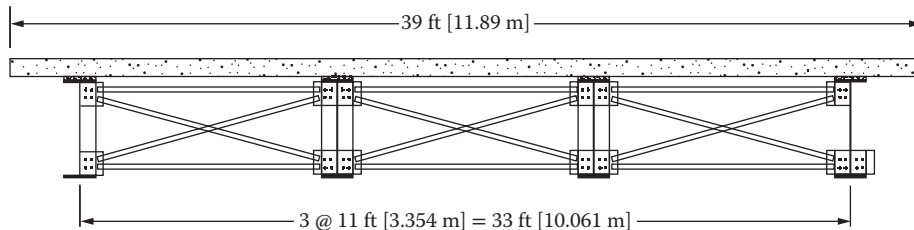


FIGURE 6.14 Typical cross section.

curve, while Girder 4 (G4) is at the inside of the curve. For the V-load analysis, the individual girders were straightened out first and the primary moments under dead load were calculated. The dead loads were based on the weight of the girder plus the weight of deck. The effective deck width specified in AASHTO Specifications was used in calculating the deck weight. From the primary moments, the V-loads were calculated at each cross-frame location and applied to the individual girders to determine the V-load moments. The V-load moments were then added to the primary moments to determine the final moments.

The step-by-step procedure below illustrates the calculation of the V-load final moment at the center of the bridge, at the location of cross-frame number 13.

Step 1. Determine the Primary Bending Moments M_p

The individual girders were straightened out such that the total length was equal to the girder arc length. The dead load was applied as uniformly distributed load then the primary bending moments M_p at cross-frame locations were determined. At the center of the bridge, the primary moments are as follows:

$$M_{p,G1} = 830 \text{ kip-ft [1126 kN-m]}$$

$$M_{p,G2} = 888 \text{ kip-ft [1204 kN-m]}$$

$$M_{p,G3} = 764 \text{ kip-ft [1036 kN-m]}$$

$$M_{p,G4} = 528 \text{ kip-ft [716 kN-m]}$$

Although G1 is the longest girder, its M_p is smaller than that in G2 because of smaller tributary area. The total M_p at the center of the bridge is as follows:

$$M_{p,total} = 3010 \text{ kip-ft [4082 kN-m]}$$

Step 2. Calculate the V-Loads

The V-loads for the four-girder system is calculated using Equations 6.3 and 6.4. The radius of the outside girder is 162.5 ft [49.54 m] and the cross-frame spacing along the outside girder is 14.47 ft [4.41 m]. Thus, the V-loads on the exterior girders are as follows:

$$VL_{exterior} = \frac{3010}{\frac{10}{9} \left(\frac{162.5 \times 33}{14.47} \right)} = 7.31 \text{ kips [32.51 kN]}$$

Because the interior girders are one-third as far from the bridge centerline as the exterior girders, the proportionally factor for calculating the interior girder V-loads is 1/3.

$$VL_{interior} = 7.31 \times 1/3 = 2.44 \text{ kips [10.84 kN]}$$

Since the center of bridge is at positive moment region, the V-load on the girders are as follows:

$$VL_{G1} = 7.31 \text{ kips [32.51 kN] acting downward}$$

$$VL_{G2} = 2.44 \text{ kips [10.84 kN] acting downward}$$

$$VL_{G3} = 2.44 \text{ kips [10.84 kN] acting upward}$$

$$VL_{G4} = 7.31 \text{ kips [32.51 kN] acting upward}$$

Step 3. Determine the V-Load Moments

After all the girder V-loads at cross-frame locations are calculated, the V-loads are then applied to the straightened girders to determine the V-load moments, M_{VL} .

$$M_{VL_G1} = 394 \text{ kip-ft [535 kN-m]}$$

$$M_{VL_G2} = 122 \text{ kip-ft [166 kN-m]}$$

$$M_{VL_G3} = -114 \text{ kip-ft [-154 kN-m]}$$

$$M_{VL_G4} = -314 \text{ kip-ft [-426 kN-m]}$$

Note that the V-load moments on G3 and G4 are negative because their V-loads at the center of the bridge are acting upward as shown in Step 2.

Step 4. Determine the Final Moments

The final moments M_f are calculated by adding M_{VL} to M_p .

$$M_{f_G1} = 830 + 394 = 1224 \text{ kip-ft [1660 kN-m]}$$

$$M_{f_G2} = 888 + 122 = 1010 \text{ kip-ft [1370 kN-m]}$$

$$M_{f_G3} = 764 - 114 = 650 \text{ kip-ft [881 kN-m]}$$

$$M_{f_G4} = 528 - 314 = 214 \text{ kip-ft [290 kN-m]}$$

The bridge final moments are shown in Figure 6.15 together with the moments obtained from FE analysis.

The FE model of the bridge with the actual curvature and substructure was developed using the computer program SAP2000 (CSI 2010). The bridge was analyzed for dead load and the girder moments were determined. Figure 6.15 shows the comparison of the results of V-load and FE model for Girders 1 to 4. Overall, the V-load method gives a reasonable result despite the tight bridge curvature. The V-load method overestimated the positive bending moments at the center of the bridge by 10% to 30%. Except for the outside girder (G1), the V-load method constantly underestimated the negative support moments. The V-load method constantly underestimated the bending moments for the inside girder (G4).

6.2.3 Refined Analysis Methods

Unless approximate analysis methods are appropriate, AASHTO Specifications require that computer-based refined analysis methods be used for the analysis of curved steel bridges. Refined methods of bridge analysis usually involve the use of computer programs. The AASHTO/NSBA Guidelines for the Analysis of Steel Girder Bridges (AASHTO/NSBA 2012) provides a detailed discussion of analysis methods for steel girder bridges including guidance on modeling the superstructure from construction to completion.

In general, there are three modeling techniques recommended for the analysis of bridges:

1. Spine beam
2. Grillage model
3. 3D finite element

6.2.3.1 Spine Beam Model

In the spine beam model, the superstructure is modeled as a single beam with equivalent section properties. This is appropriate for torsionally stiff superstructures such as single and multicell concrete box girders and steel box girders with appropriate internal bracings.

The spine beam centerline is located at the center of gravity of the cross section. The loads are applied to the nodes and their eccentricity, if there is any, should be taken into account. Many of computer programs used to create a spine beam model include only the translational mass but not the rotational mass inertia of the superstructure. This should be added to the nodes of the spine beam, particularly for curved bridges.

The spine beam model can capture the global response of the bridge with reasonable accuracy including column forces but it does not give good results for local behavior in the superstructure such as torsional rotation, cross-frame forces, and bearing forces. In the case of curved steel I-girder bridges, the

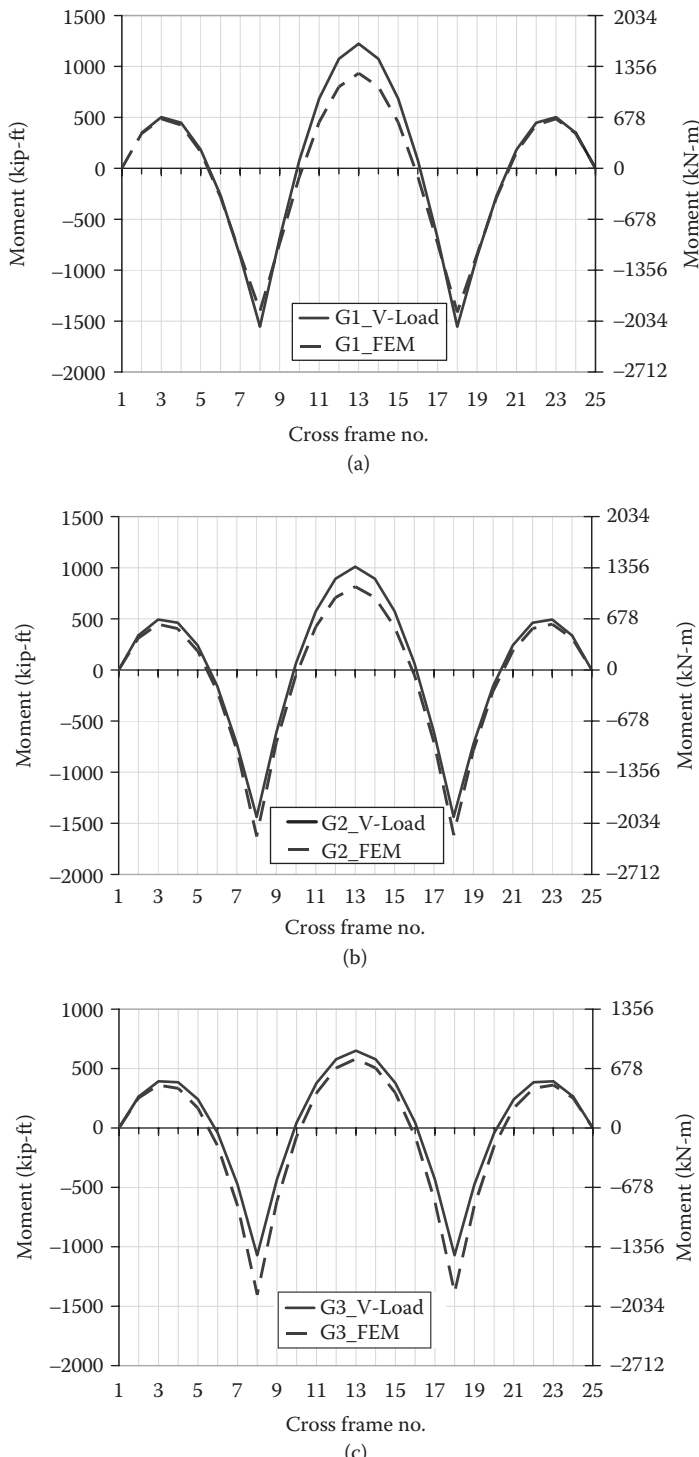


FIGURE 6.15 (a) Girder 1: Comparison of girder moments from V-load method and FE Model. (b) Girder 2: Comparison of girder moments from V-load method and FE Model. (c) Girder 3: Comparison of girder moments from V-load method and FE Model. (d) Girder 4: Comparison of girder moments from V-load method and FE Model.

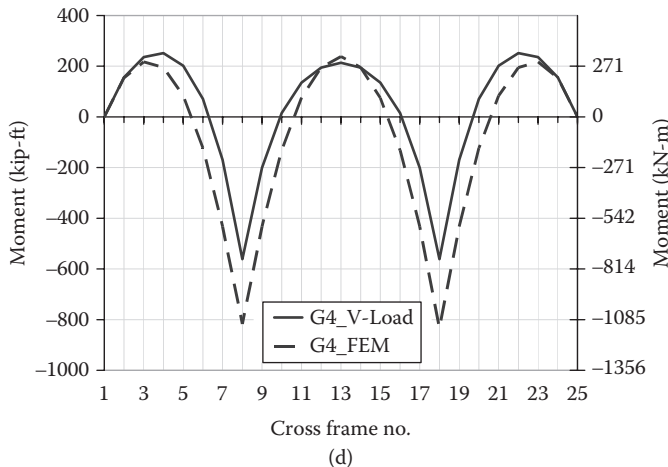


FIGURE 6.15 (Continued) (a) Girder 1: Comparison of girder moments from V-load method and FE Model. (b) Girder 2: Comparison of girder moments from V-load method and FE Model. (c) Girder 3: Comparison of girder moments from V-load method and FE Model. (d) Girder 4: Comparison of girder moments from V-load method and FE Model.

superstructure internal torsion results in an uneven distribution of loads between the girders. More loads are transferred to the outside girder and thus has larger deflections than the adjacent girders. Therefore, the deflections obtained from the spine beam model should not be used to determine the camber in the girders. Additionally, the effect of cross frames on the overall structural system is neglected and the analysis does not provide cross-frames forces. The cross frames provide resistance to the torsional moments in the superstructure. Depending on the amount of curvature, the cross-frame forces may be large.

6.2.3.2 Grillage Model

In the grillage model, the individual girders are modeled and are connected transversely by beam elements representing the deck and/or cross frames. All the grid elements lie on the same plane. The transverse beam elements that represents the cross frames are assigned with either flexural or shear stiffness. There is better representation of the mass across and along the superstructure and thus rotational inertia is implicitly included in the model.

However, since the cross frames are modeled as transverse beam elements, this modeling technique does not provide the cross-frame forces directly and may not be able to capture the actual cross-frame behavior. In addition, the actual location of the bearing supports, which are at the bottom of the girders, may not be modeled correctly because the grid elements are located on the same plane. Horizontal bearing reactions create moments in the superstructure because they are at some distance from the superstructure neutral axis. These errors, however, can be lessened through a variation of the grillage model, called the *plate-and-beam model*.

In the plate-and-beam model (see Figure 6.16), the deck is modeled as shell elements, while the girders are modeled as beam elements. The shell elements are located at the deck center of gravity. The beam elements can also be located at the girder center of gravity. It is preferred to maintain the vertical distance between the deck shell elements and girder beam elements. When the girder section varies along the bridge length, the beam elements can be placed at a location where its vertical position is constant along the bridge length. For example, at the center of top flange, provided the eccentricities are accounted for in the equivalent section properties. The shell elements and beam elements are then connected with link elements.

The deck flexibility in the plate-and-beam model is modeled accurately and has better distribution of mass than the traditional grillage model. Since the superstructure has “depth,” the actual geometry of the cross frames can be modeled and the bearings can be positioned at their correct location.

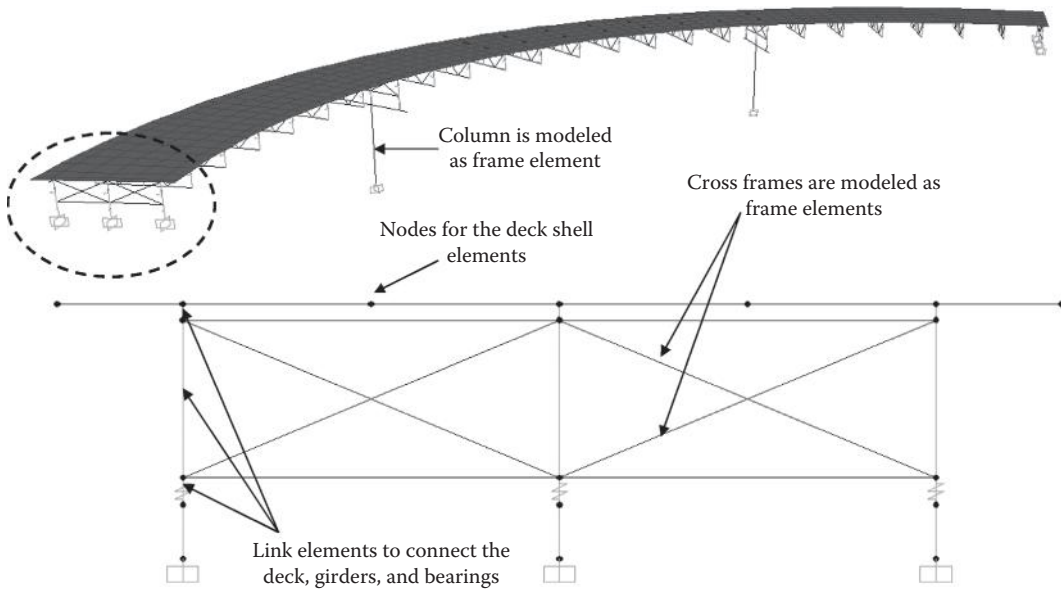


FIGURE 6.16 Plate-and-beam model.

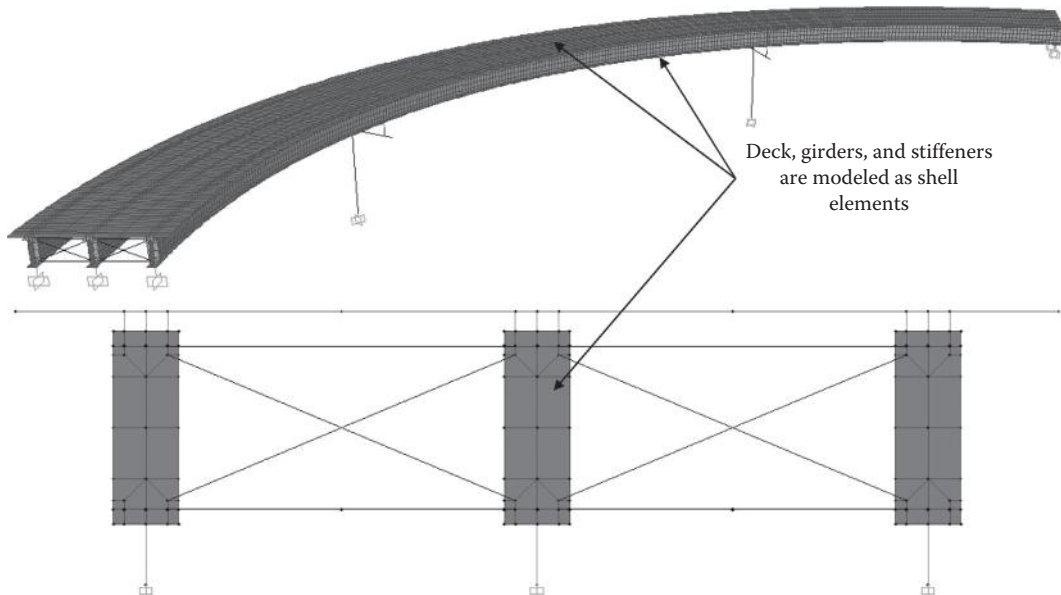


FIGURE 6.17 3D finite element model.

6.2.3.3 Three-Dimensional Finite Element Model

The 3D finite element model (see Figure 6.17) is the most rigorous of the modeling techniques and is regarded as the most accurate. This modeling technique is preferred for complex and highly curved bridges. The deck is modeled as shell elements, while the girders are modeled by either shell elements for the web and flanges or by combination of shell elements for the web and beam elements for the flanges. In the case of steel I-girders, the stiffeners can be included in the model using shell elements. Analyses have shown that, at support locations, the contribution of bearing stiffeners on the transverse girder stiffness is significant compared to that due to girder rotation (Monzon, Itani, and Buckle 2013). Because

the superstructure is modeled in detail, the cross-section distortion and its effect on structure behavior is recognized and the information about the stress state of the components is provided.

However, this modeling technique can be time consuming and complicated. The results can be sensitive to various input parameters. Thus, the engineer should understand the assumptions and limitations of the computer program used to model the bridge. Additionally, postprocessing is required since the output is in terms of stresses and not moments, shears, and axial loads that are typically used in design calculations.

6.3 Curved Steel I-Girder Bridges

6.3.1 Geometric Parameters

The framing system for curved I-girder bridges may follow the preliminary design of straight bridges in terms of span arrangement, girder spacing, girder depth, and cross-frame types. The choice of the exterior spans length is normally set to give relatively equal positive dead load moments in the exterior and interior spans. The arrangement results in the largest possible negative moment, which reduces both positive moments and related deflections. Normally, the depth of the superstructure is the same for all spans. Previous successful designs have shown a depth-to-span ratio equal to 0.04 for the exterior girder to be adequate. This ratio has been based on vibration and stiffness needed to construct the plate girders. Also, this ratio helps ensure that the girders do not experience excessive vertical deflections.

Girder spacing plays a significant role in the deck design and the determination of the number of girders. For curved steel I girder bridges, the girder spacing varies between 10 [3.05] to 16 ft [4.87 m]. Wider spacing, common in Europe and Japan, requires a posttensioned concrete deck, which is not common practice in the United States. The overhang length is preferred not to exceed 4 ft [1.22 m] because it tends to increase the load on the exterior girders by adding more dead load and permitting truckload to be applied on the cantilever. The girder spacing is considered to be one of the most important items in the superstructure design because it controls the required minimum thickness of the deck and the number of the girders. Wider spacing tends to increase the dead load on the girders, while closer spacing requires additional girders, which increase the fabrication and erection cost.

The flanges of the plate girder should have a minimum width to avoid out-of-plane buckling during construction. Many steel erectors limit the length of girder shipping pieces to 85 times the flange width. On the basis of the above, many bridge engineers tend to limit the width of the flange to 16 in [40.6 mm] based on a maximum shipping length equal to 120 ft [36.6 m]. It is also recommended that the minimum web thickness is limited to 7/16 in [11.1 mm] because of weld distortion problems. The thickness of the web depends on its depth and the spacing of the transverse stiffeners. This represents a trade-off between having extra material and adding more stiffeners. Many bridge engineers use the ratio of D/t equal 150 to choose the thickness of the web.

The spacing of the cross frame plays an important factor in the amount of force that is carried out by them and the value of flange lateral bending. Normally, cross frame spacing are maintained at a constant spacing between 15 ft [4.57 m] to 25 ft [7.62 m].

6.3.2 Design Criteria

The design guidelines are established based on the following principles:

- Statics
- Stability
- Strength of Materials

External and internal static equilibrium should be maintained under every expected loading condition. Stability of curved steel girder bridges is a very important issue especially during

construction. By their nature, curved girders experience lateral deflection when subjected to gravity loading. Therefore, these girders should be braced at specified intervals to prevent lateral torsional buckling. The compactness ratio of the web and the flanges of curved I-girders are similar to the straight girders. The linear strain distribution is normally assumed in the design of curved girder bridges. The design specification recognizes that compact steel sections can undergo inelastic deformations; however, current U.S. practice does not utilize a compact steel section in the design of curved I-girder bridges.

The design criteria for curved girder bridges can be divided into two main sections.

- Strength
- Serviceability

Limit state design procedures are normally used for the strength design, which includes flexure and shear. Service load design procedures are used for fatigue design and deflection control. The primary members should be designed to be such that their applied stress ranges are below the allowable fatigue stress ranges according to AASHTO fatigue provisions (AASHTO 2012). The deflection check is used to ensure the serviceability of the bridge. According to the Guide Specifications (AASHTO 1993), the superstructure should be first analyzed to determine the first mode of flexural vibration. The frequency of this mode is used to check the allowable deflection of the bridge as indicated in the Ontario Bridge Code (OMTC 1991).

6.3.3 Design Example

This design example was based on the prototype of the curved bridge model (see Figure 6.18) used for experimental seismic testing at University of Nevada, Reno. The bridge is on a tight curvature representing a highway on-ramp or off-ramp. The centerline radius is 200 ft [60.98 m] and the total subtended angle is 104°. The total bridge length is 362.5 ft [110.52 m] with span lengths of 105 ft [32.01 m], 152.5 ft [46.49 m], and 105 ft [32.01 m]. The deck width is 30 ft [9.15 m] and can accommodate two lanes of traffic. The piers are single column with column clear height of 20 ft [6.10 m]. The column diameter is 5 ft [1.52 m]. At the piers, the bottom flange of the girder is pin connected to the bent cap. The boundary condition at the abutments is free in the tangential direction but restrained in the radial direction. On the basis of the deck width, the chosen girder spacing was 11.25 ft [3.43 m], with three girders. The overhang width is therefore 3.75 ft [1.14 m]. The deck design showed that an 8.125-in [206-mm]-thick, reinforced concrete deck is sufficient. To start the analysis, a girder dimension was assumed first based on the cross-section proportion limits set by AASHTO Specifications (AASHTO 2012).

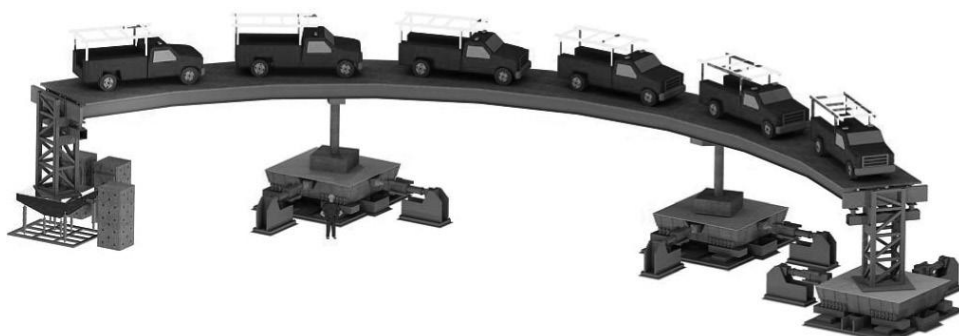


FIGURE 6.18 3D view of the curved bridge model on shake tables (trucks used for live load tests are also shown).

The bridge was then modeled using the computer program SAP2000 (Computers and Structures 2010). The plate-and-beam model was deemed sufficient to provide the superstructure forces needed for design. For live load analysis, the computer program allows the user to define the number of lanes, lane width, lane length, and type of loading (HL-93 in this example). The computer program calculates the influence surface by placing unit loads on the defined lanes. Using the influence surface, the trucks and lane loads are then positioned to determine the maximum and minimum force effects on a particular bridge component.

The seismic analysis was performed using the multimode spectral analysis. The bridge was assumed to be located on a rock site with seismic parameters $PGA = 0.4$ g, $S_s = 1.3$ g, and $S_1 = 0.4$ g. A total of 30 modes were used such that the total of the participating mass in the directions of earthquake loading are more than 95%. For earthquake loading, the effective section properties of the columns were used. Section analysis was performed and it was found that the effective moment of inertia I_e is 30% of the gross moment of inertia I_g . The column effective torsional stiffness was specified by using a 20% multiplier for the torsional constant J .

The design forces were determined using the load combinations specified in the AASHTO Specifications (AASHTO 2012). The girders were designed as noncompact sections, even though compactness checks indicate that it is a compact section. The AASHTO Specifications require that the girders in a horizontally curved bridge be designed as noncompact sections, thus the flexural resistance is limited to the moment at first yield. The capacity check is in terms of stress instead of moment. Under positive flexure, lateral bending is not considered because it is continuously braced by the deck; however, the tension flange is checked for the combined effect of vertical and lateral bending. Under negative flexure, the tension and compression flanges are checked for the combined effect of vertical and lateral bending. The girders are made of ASTM A709 Grade 50 steel. The typical superstructure cross section is shown in Figure 6.19.

The cross-frame spacing is 15 ft [4.57 m] throughout the span except the two at the midspan of main span where spacing is 16.25 ft [4.95 m]. There are two cross-frame sizes—one at supports and one at intermediate locations. The support cross frames transmit the deck seismic forces to the bearings, thus are subjected to larger forces than those at intermediate.

Transverse stiffeners were provided at each cross-frame location. The interior girder web is considered as stiffened and the shear resistance is taken as the sum of the postbuckling tension field force and either the shear-yielding or shear-buckling force. At the end panels, the shear resistance is taken from either the shear-yielding or shear-buckling force. At each support, a pair of bearing stiffeners welded to both sides of the web transmits the full bearing loads and prevents web local yielding and web crippling.

Shear connectors were provided throughout the bridge length. Because torsional shear is present in a horizontally curved bridge, the shear connectors are needed even in the negative moment regions. Three shear connectors per row were provided and their design was governed by fatigue limit state.

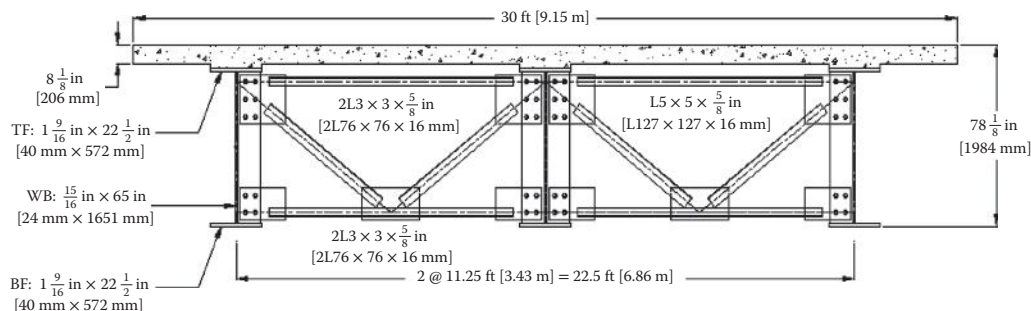


FIGURE 6.19 Typical cross section.

6.4 Curved Steel Box Girder Bridges

The most common type of curved steel box girder bridges are tub girders that consist of independent top flanges and cast-in-place reinforced concrete decks. The design guidelines are covered in the AASHTO Specifications (AASHTO 2012). Normally the tub girder is composed of bottom plate flange, two web plates, and independent top flange attached to each web. The top flanges are required to be braced to become capable of resisting loads until the girder acts in composite manner. Internal bracing in the form of cross frame or diaphragm is required to limit the distortion of the box due to the bending stresses. Finite element analysis, which account for the distortion is normally utilized to calculate the stresses and displacement of the box.

The webs of the box girder may be inclined with a width-to-depth ratio of one to four. The AASHTO provisions for straight box girders apply for curved boxes regarding the shear capacity of the web and the ultimate capacity of the tub girders. The maximum bending stresses are determined according to the factored loads with the considerations of composite and noncomposite actions. Bending stresses should be checked at critical sections during erection and deck placement. The bending stresses may be assumed to be uniform across the width of the box. Prior to curing of concrete, the top flanges of tub girders are to be assumed laterally supported at top flange lateral bracing. The longitudinal warping stresses in the bottom flange are computed on the basis of the stiffness and spacing of internal bracing. It is recommended that the warping stresses should not exceed 10% of the maximum bending stresses.

The M/R method is usually used to analyze curved box girder bridge. The basic concept behind this method is the conjugate beam analogy. The method loads a conjugate simple-span beam with a distributed loading, which is equal to the moment in the real simple or continuous span induced by the applied load divided by the radius of curvature of the girder. The reactions of the supports are obtained and thus the shear diagram can be constructed, representing the internal torque diagram of the curved girder. After the concentrated torque at the ends of the floor beam is known, the end shears are computed from statics. These shears are applied as vertical concentrated loads at each cross frame location to determine the moment of the developed girder. This procedure constitutes a convergence process whereby the M/R values are applied until convergence is attained.

6.5 Curved Concrete Box Girder Bridges

Although the NCHRP Project 12-71 (NCHRP 2008) provided recommended LRFD design specifications for the analysis and design of curved concrete box girder bridges, these recommendations have not yet been included in the current AASHTO Specifications (AASHTO 2012). It is generally believed that the concrete monolithic box girders have high torsional rigidity, which significantly reduces the effect of curvature. However, during the last 15 years a problem has occurred with small-radius, horizontally curved, posttensioned box girder bridges. Prestress tendon breakout in curved bridges has occurred on a number of bridges over the years (Podolny 1985; NCHRP 2008). Immediate inspection of the failure indicated that the tendons exerted radial horizontal pressure along the wall of the outer most webs.

In recognition to this problem, Caltrans has prepared and implemented design guidelines (Caltrans 2010). Charts and reinforcement details were developed to check girder webs for containment of tendons and adequate stirrup reinforcement to resist flexural bending. Caltrans' Memo-To-Designers 11-31 (MTD 11-31) specifies that designers of curved posttensioned bridges should consider the lateral pre-stress force for each girder. This force is approximately equal to the jacking force, P_{jack} , of each girder divided by the horizontal radius of the girder, R . The guidelines presented are applicable to girders with horizontal radii not exceeding 2000 ft [610 m].

The first step is to calculate the in-plane deviation force effect per unit length of the tendon, F_{u-in} .

$$F_{u-in} = \frac{P_u \cos\theta}{R} = \frac{(1.2 P_{jack}) \cos\theta}{R} \quad (6.6)$$

where θ is the angle of inclination of the web measured from the vertical. Then, enter the chart in Figure 6.20 with the value of clear girder height h_c in the vertical axis and F_{u-in} in the horizontal axis. If the point plots above the curve for corresponding R , Detail A shown in Figure 6.21 is required.

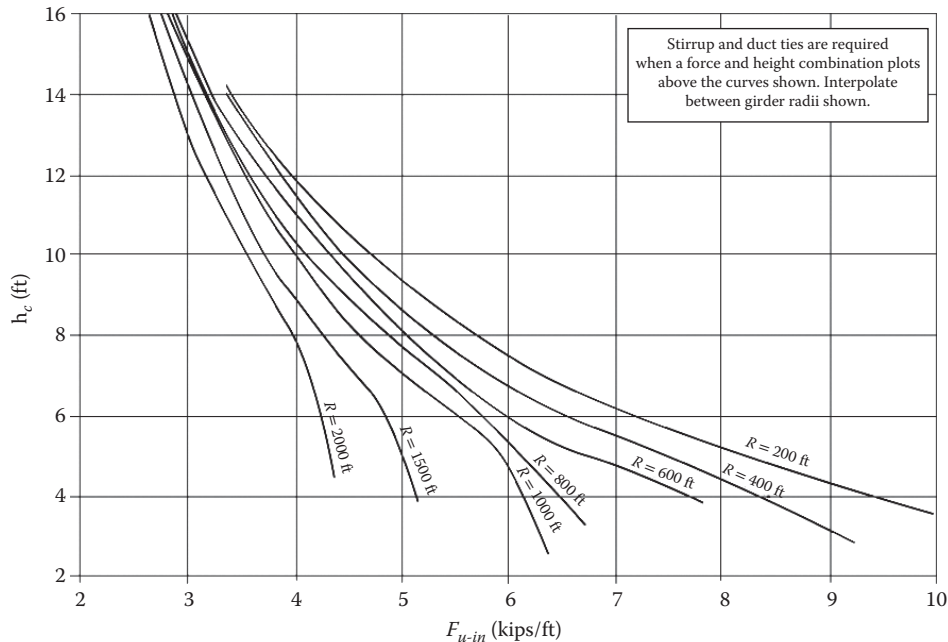


FIGURE 6.20 Caltrans chart to determine if detail as shown in Figure 6.21 is required.

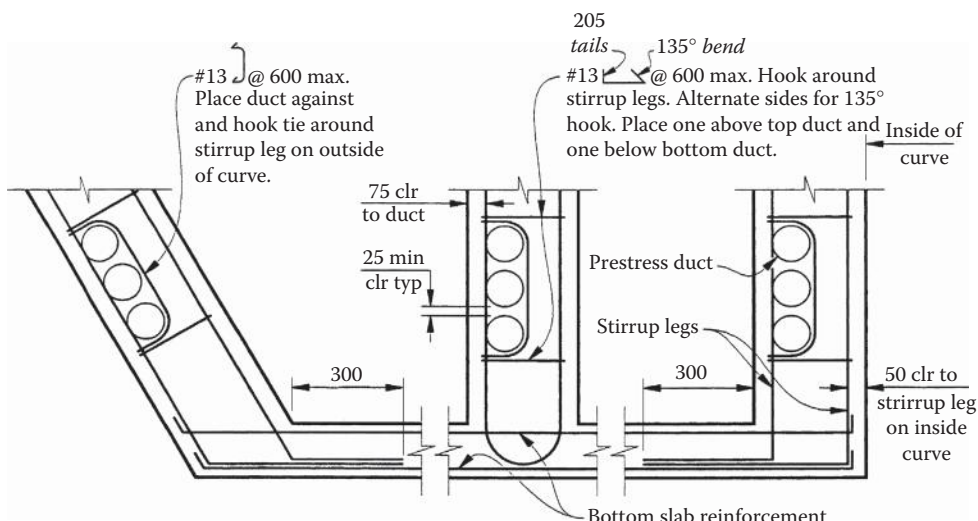


FIGURE 6.21 Caltrans duct detail in curved concrete bridges (Detail A).

Maximum stirrup tie spacing, s_{max} , of 24 in [610 mm] is adequate for most bridges but for high values of F_{u-in} Figure 6.22 can be used to determine the maximum spacing. The required stirrup spacing, s , is then determined using one of the charts provided in MTD 11-31. Figure 6.23 shows the required spacing of #5 [No. 16] stirrups for a girder with radius equal to 500 ft [152 m].

The stirrup spacing calculated above is then combined with those needed for other loads. However, the interaction between the effect of lateral loads and other loads cannot be added directly.

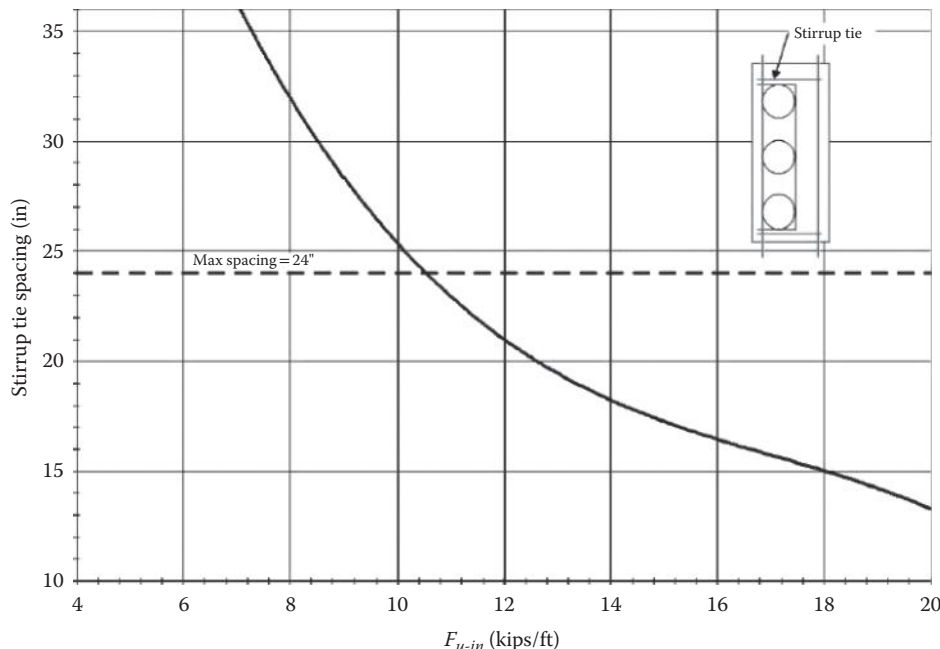


FIGURE 6.22 Caltrans chart to determine the maximum stirrup tie spacing.

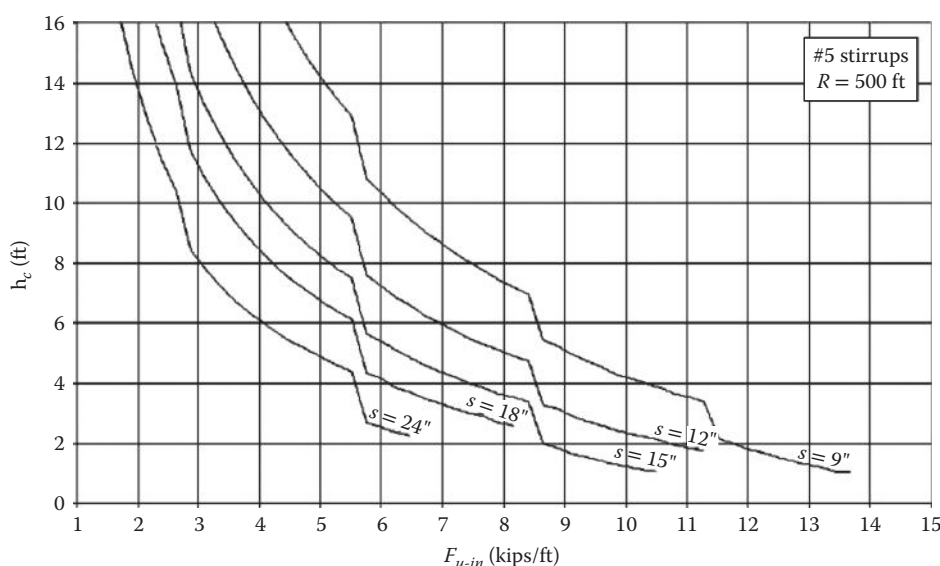


FIGURE 6.23 Caltrans chart to determine required stirrup tie spacing for girder radius of 500 ft (152 m).

The Podolny–Muller combination (Podolny and Muller 1982) can be used to combine the stirrup reinforcement required from transverse bending and shear stresses from other loads.

$$s = \max \left\{ \begin{array}{l} a + \frac{1}{2}b \\ \frac{1}{2}a + b \\ 0.7(a+b) \end{array} \right\} \quad (6.7)$$

where a is the required stirrup reinforcement for transverse bending and b is the stirrup reinforcement required for other loads. The maximum of the above combinations is used to design the stirrup reinforcement.

Acknowledgments

The authors thank Dr. Duan and Prof. Chen for selecting them to participate in this *Bridge Engineering Handbook*. The National Steel Bridge Alliance provided the photographs of curved bridges in this document for which the authors are sincerely grateful. Finally, the authors warmly appreciate the continued support of Caltrans.

References

- AASHTO. 1993. *Guide Specifications for Horizontally Girder Highway Bridges*, American Association of State Highway and Transportation Officials, Washington, D.C.
- AASHTO. 2006. *AASHTO LRFD Bridge Design Specifications, 2006 Interim*, American Association of State Highway and Transportation Officials, Washington, D.C.
- AASHTO. 2012. *AASHTO LRFD Bridge Design Specifications, 5th Edition*, American Association of State Highway and Transportation Officials, Washington, D.C.
- AASHTO/NSBA. 2012. *Guidelines for the Analysis of Steel Girder Bridges, G13.1*, American Association of State Highway and Transportation Officials/National Steel Bridge Alliance (AASHTO/NSBA) Steel Bridge Collaboration, Chicago, IL.
- Caltrans. 2010. *Bridge Memo-to-Designers 11-31*, Curved Post-tensioned Bridges, California Department of Transportation, Sacramento, CA.
- CSI. 2010. *SAP2000 Structural Analysis Program*, Computers and Structures, Inc., Berkeley, CA.
- Hall, D.H., Grubb, M.A., and Yoo, C.H. 1999. *NCHRP Report 424: Improved Design Specifications for Horizontally Curved Steel Girder Highway Bridges*, Transportation Research Board, Washington, D.C.
- Kulicki, J.M., Wassef, W.G., Kleinhans, D. et al. 2006. *NCHRP Report 563: Development of LRFD Specifications for Horizontally Curved Steel Girder Bridges*, Transportation Research Board, Washington, D.C.
- Monzon, E.V., Buckle, I.G., and Itani, A.M. 2013. *Seismic Performance of Curved Steel Plate Girder Bridges with Seismic Isolation*, CCEER Report No. 13-06, Center for Civil Engineering Earthquake Research, University of Nevada, Reno, NV.
- Monzon, E.V., Itani, A.M., and Buckle, I.G. 2013. *Seismic Analysis and Modeling of Curved Steel Plate Girder Bridges*, CCEER Report No. 13-05, Center for Civil Engineering Earthquake Research, University of Nevada, Reno, NV.
- NCHRP. 2008. *NCHRP Report 620: Development of Design Specifications and Commentary for Horizontally Curved Concrete Box-Girder Bridges*, National Cooperative Highway Research, Transportation Research Board, Washington, D.C.

- OMTC. 1991. *Ontario Highway Bridge Design Code, 3rd Edition*, Ministry of Transportation and Communications, Highway Engineering Division, Toronto, Ontario, Canada.
- Podolny, W. 1985. The Cause of Cracking in Post-Tensioned Concrete Box Girder Bridges and Retrofit Procedures, *Journal of the Prestressed Concrete Institute*, 30(2):82–139.
- Podolny, W. and Muller, J. 1982. *Construction and Design of Prestressed Concrete Segmental Bridges*, John Wiley & Sons, Inc., New York, NY.
- Priestley, M.J.N., Seible, F., and Calvi, G.M. 1996. *Seismic Design and Retrofit of Bridges*, John Wiley & Sons, Inc., New York, NY.
- USS. 1984. V-Load Analysis, *USS Highway Structures Design Handbook, Chapter 12, Vol. 1*, United States Steel, Pittsburgh, PA.

@Seismicisolation

7

Highway Truss Bridges

John M. Kulicki
Modjeski and Masters, Inc.

7.1	Truss Configurations	283
	Historical • Modern	
7.2	Typical Components, Nomenclature, and Materials	284
	Components and Nomenclature • Truss Members	
7.3	Methods of Analysis.....	287
	Two-Force Member Methods—Pin-Connected Truss • Computer Methods	
7.4	Floor Systems and Framing Details.....	291
	Conventional Deck Systems Not Integral with Truss Chords • Decks Integral with Truss Chords	
7.5	Special Details	292
	Hangers and Dummy Chords for Cantilever Bridges	
	• Bearings • Wind Tongues and Bearings for Transverse Forces • Gusset Plates	
7.6	Camber and Erection	306
	Camber for Vertical Geometry • Camber of Joints • Common Erection Methods	
7.7	Summary.....	308
	References.....	308

7.1 Truss Configurations

7.1.1 Historical

During the 1800s, truss geometries proliferated. The Historic American Engineering Record illustrates 32 separate bridge truss geometries in its 1976 print shown in Figure 7.1 (NPS 1976). These range from the very short King Post and Queen Post Trusses and Waddell “A” Trusses to very complex indeterminate systems, including the Town Lattice and Burr Arch Truss. Over a period of years following Squire Whipple’s breakthrough treatise on the analysis of trusses as pin-connected assemblies, that is, two force members, a number of the more complex and less functional truss types gradually disappeared and the well-known Pratt, Howe, Baltimore, Pennsylvania, K Truss, and Warren configurations came into dominance. By the mid-twentieth century, the Warren Truss with verticals was a dominant form of truss configuration for highway bridges, and the Warren and “K” Trusses were dominant in railroad bridges. The Historic American Engineering Record indicates that the Warren Truss without verticals may have appeared as early as the mid-1880s, but was soon supplanted by the Warren Truss with verticals, as this provided a very convenient way to brace compression chords, reduce stringer lengths, and frame sway frames into the relatively simple geometry of the vertical members.

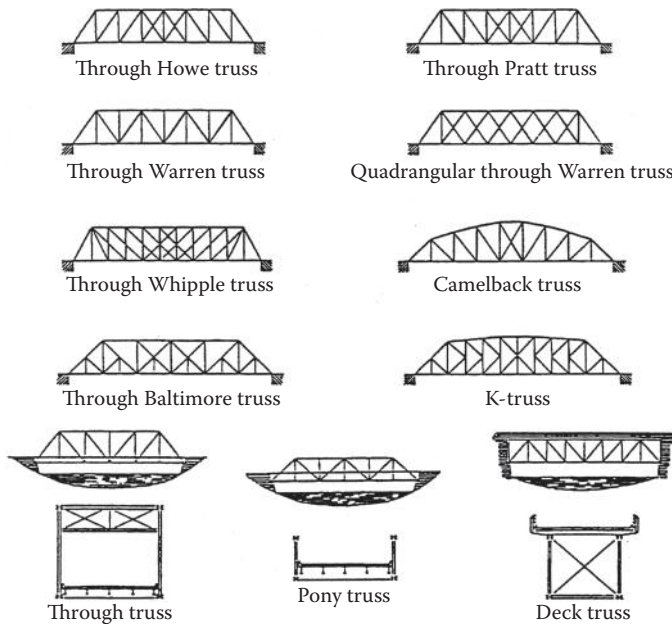


FIGURE 7.1 Historic trusses.

7.1.2 Modern

Few single-span trusses are used as highway bridges today, although they are still used for railroad bridges. Modern highway trusses are usually either continuous or cantilever bridges and are typically Warren Trusses with or without verticals. Some typical configurations are shown in Figure 7.2.

Throughout the 1980s and 1990s, the Warren Truss without verticals has resurfaced as a more aesthetically pleasing truss configuration, especially in the parallel-chord configuration, and this has led to a significant simplification in truss detailing, because sway frames are typically omitted in this form of truss, except for portals. The Warren Truss without verticals was used extensively on the Japanese Railroad System and, more recently, in U.S. highway practice as exemplified in the Cooper River Bridge near Charleston, South Carolina, and the Kanawha River Bridge near Charleston, West Virginia; such a bridge configuration is shown in Figure 7.3 as it was considered as one option for the Second Blue Water Bridge (281 m main span) between Port Huron, Michigan, and Point Edward, Ontario, Canada.

The truss bridge behaves much like a closed-box structure when it has four planes capable of resisting shear and end portals sufficient to transmit shear back into vertical loads at the bearings. Given the need for a box configuration to resist vertical and lateral loads, it is possible that the configuration could be either rectangular, that is, four-sided, or triangular, if that geometry is able to accommodate the roadway clearances. Issues of redundancy should be addressed, either by supplementary load paths, for example, prestressing, or by sufficiently improved material properties, primarily toughness, to make a triangular configuration acceptable to owners, but it is certainly within the technical realm of reason.

7.2 Typical Components, Nomenclature, and Materials

7.2.1 Components and Nomenclature

The truss bridge is usually characterized by a plethora of bracing and wind-carrying members in addition to those members seen in front elevation. Typical members of a simple single-span through-truss are identified in Figure 7.4, taken from Hartle et al. (1995).

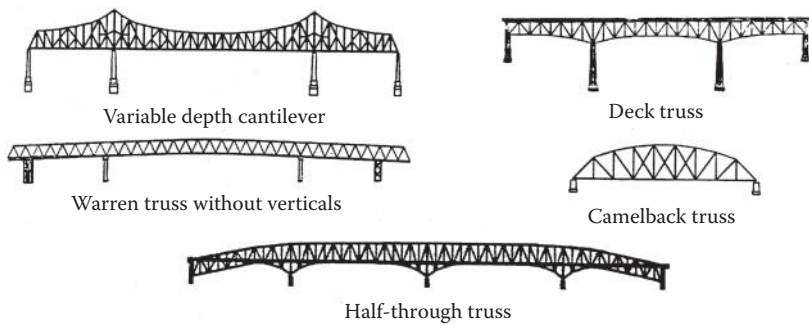


FIGURE 7.2 Typical modern highway truss configuration.



FIGURE 7.3 Second Blue Water Bridge—parallel chord truss study option.

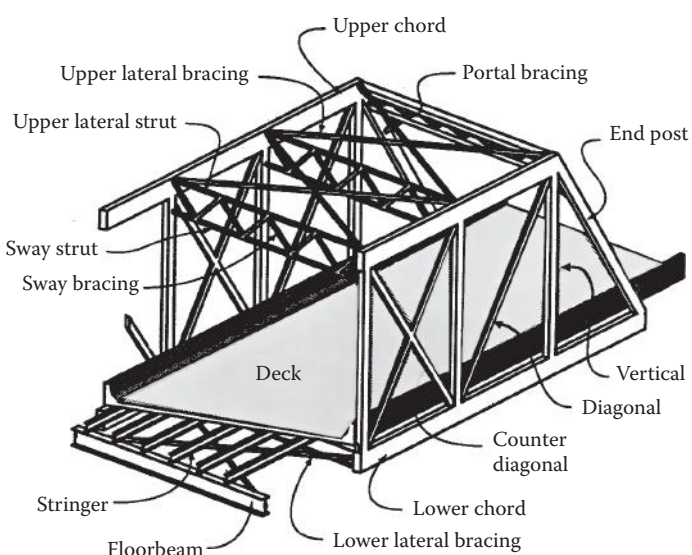


FIGURE 7.4 Typical truss members.

@Seismicisolation

The lateral members in the planes of the top and bottom chords resist wind loads and brace the compression chords. Sway frames are assumed to square the truss and increase its torsional rigidity. End portals carry torsional loads resulting from uneven vertical loads and wind loads into the bearings.

It is the visual impact of the various members, especially bracing members, which contribute to aesthetic opposition to many truss designs. However, if unforeseen events cause damage to a main truss member, these bracing members can serve as additional load paths to carry member load around a damaged area.

7.2.2 Truss Members

Some of the cross sections used as modern truss members are shown in Figure 7.5. Truss members have evolved from rods, bars, and eyebars to box and H-shaped members. Generally speaking, the box members are more structurally efficient and resist the tendency for wind-induced vibration better than H-shapes, whereas H-shapes are perceived as being more economical in terms of fabrication for a given tonnage of steel, generally easier to connect to the gusset plates because of open access to bolts, and easier to maintain because all surfaces are accessible for painting. The use of weathering steel offsets these advantages.

Even in the late 1990s, box members were widely used and, in some cases, the apparent efficiency of the H-shape was offset by the need to make the members aerodynamically stable. The choice is clearly project specific, although the H-shaped sections have a relatively clear advantage in the case of tension members because they are easier to connect to gusset plates and easier to paint as indicated above, without the stability design requirements needed for compression members. They are, however, more susceptible to wind-induced vibrations than box shapes. Box shapes have an advantage in the case of compression members because they usually have lower slenderness ratios about the weak axis than a corresponding H-shaped member.

The sealing of box shapes to prevent corrosion on the inside of the members has been approached from many directions. In some cases, box shapes may be fully welded, except at access locations at the ends used to

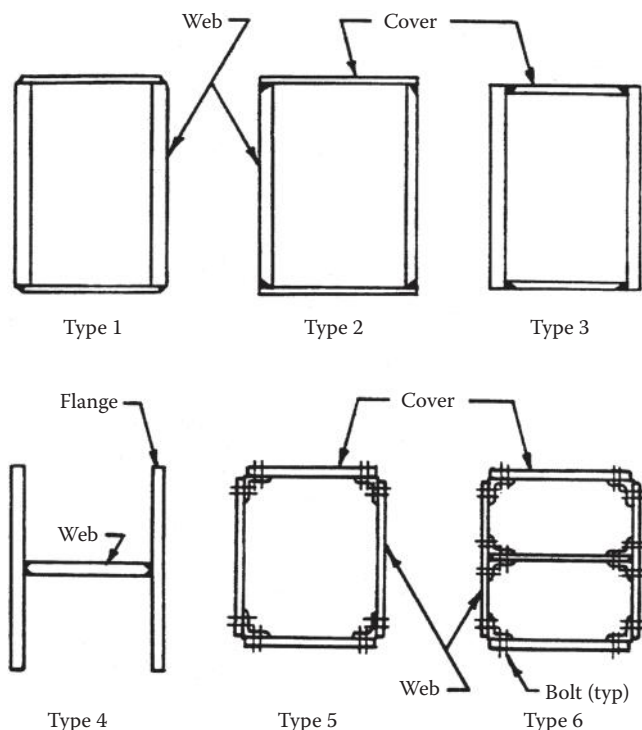


FIGURE 7.5 Cross sections of modern truss members.

facilitate connection to gusset plates. Sealing of box members has met with mixed success. In some instances, even box members that have been welded on all four sides and have had welded internal squaring and sealing diaphragms have been observed to collect moisture. The issue is that the member need not be simply watertight to prevent the infiltration of water in the liquid form, it must also be airtight to prevent the natural tendency for the member to “breath” when subjected to temperature fluctuations, which tends to draw air into the member through even the smallest cracks or pinholes in the sealing system. This air invariably contains moisture and can be a recurring source of condensation, leading to a collection of water within the member. In some cases, box members have been equipped with drainage holes, even though nominally sealed, in order to allow this condensate to escape. In some instances, box members have been sealed and pressurized with an inert gas, typically nitrogen, in order to establish that adequate seals have been developed, as well as to eliminate oxygen from the inside of the member, thus discouraging corrosion. Box members have been built with valve stems in order to monitor the internal pressure, as well as to purge and refill the inert gas corrosion protection. Various types of caulking have been used to try to seal bolted joints with mixed success.

Owing to the increased interest in redundancy of truss bridges, stitch-bolted members have been used in some cases. Because a bolt does not completely fill a hole, this leaves a path for water ingress, making adequate ventilation and drainage of the member important.

7.3 Methods of Analysis

7.3.1 Two-Force Member Methods—Pin-Connected Truss

In the 1840s, a method of analyzing trusses as pin-connected assemblages was developed and is still in wide use today. This method is based on assuming that the truss joints are frictionless pins. This assumption means that, as long as loads are applied to the joints and not along the member length, the only bending is caused by self-weight. Thus, the major force in the member is assumed to act along its length. This is often called a “two-force member.” The two forces are the axial load at each end of the member.

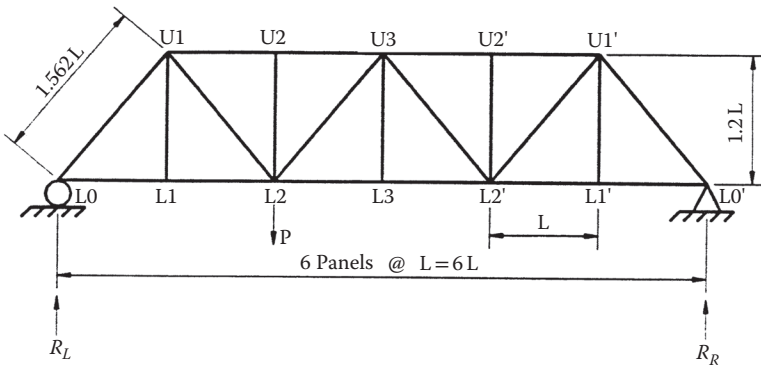
Throughout the nineteenth century and even into the early part of the twentieth century, it was common to use physical pins in truss joints in order to facilitate the interconnection of components of members, and to also replicate the mathematical assumptions. As a truss deflects under loads, the joints rotate through what are typically very small angles. If the pins truly were frictionless, the truss members would rotate relative to each other and no end moments would be developed on the members. The physical pins never really were friction-free, so some moments developed at the ends in truss members and these were typically regarded as secondary forces. When pin-ended construction gave way to riveted joints and then to bolted or welded joints, the truss joints were detailed, so that the working lines of the members intersected either at a common point, so as to reduce eccentricities, or to utilize eccentricities to compensate for the bending caused by the dead weight of the members. In either event, it was widely regarded that the pin-connected analysis model was applicable. As will be discussed later, as long as a bridge is properly cambered, it often is an accurate analysis tool.

Two variations of the pin-connected truss model are in common usage; the method of joints, and the method of sections. Each of these is illustrated below.

7.3.1.1 Method of Joints

As the name implies, the method of joints is based on analysis of free-body diagrams of each of the truss joints. As long as the truss is determinate, there will be enough joints and equations of equilibrium to find the force in all the members. Consider the simple example shown in Figure 7.6. This six-panel truss supports a load “ P ” at Joint L3. By taking the summation of the moments about each end of the bridge, it is possible to determine that the left-hand reaction is $2/3$ “ P ” and the right-hand reaction is $1/3$ “ P ”

Isolating Joint L0, it can be seen that there are two unknowns, the force in Member L0-U1 and the force in Member L0-L1. For this small truss, and as typically illustrated in most textbooks, the truss is assumed to be in a horizontal position, so that it is convenient to take one reference axis through



Summing moments about right end:

Computer reactions

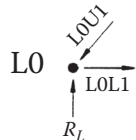
$$4PL = 6R_L L$$

$$R_L = \frac{2}{3}P$$

$$2PL = 6R_R L$$

$$R_R = \frac{1}{3}P$$

Summing moments about left end:



From $\Sigma V = 0$:

$$\frac{1.2LOU1}{1.562} = R_L = \frac{2}{3}P$$

$$LOU1 = 0.868P$$

From $\Sigma H = 0$:

$$\frac{LOU1}{1.562} = LOL1$$

$$LOL1 = 0.555P$$

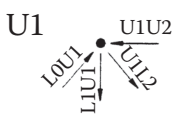


From $\Sigma V = 0$:

$$L1U1 = 0$$

From $\Sigma H = 0$:

$$L1L2 = LOL1 = 0.555P$$



From $\Sigma V = 0$:

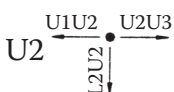
$$\frac{1.2LOU1}{1.562} = \frac{1.2U1L2}{1.562}$$

$$U1L2 = LOU1 = 0.868P$$

From $\Sigma H = 0$:

$$U1U2 = \frac{LOU1}{1.562} + \frac{U1L2}{1.562} = \frac{2(0.868)}{1.562}P$$

$$U1U2 = 1.111P$$

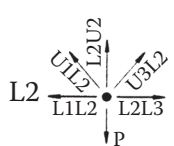


From $\Sigma V = 0$:

$$L2U2 = 0$$

From $\Sigma H = 0$:

$$U2U3 = U1U2 = 1.111P$$



Determined so far:

$$L2U2 = 0$$

$$U1U2 = 0.858P$$

$$L1L2 = 0.555P$$

From $\Sigma V = 0$:

$$\frac{1.2U1L2}{1.562} + \frac{1.2U3L2}{1.562} = P$$

$$U3L2 = 0.434P$$

From $\Sigma H = 0$:

$$L1L2 + \frac{U1L2}{1.562} = \frac{U3L2}{1.562} + L2L3$$

$$L2L3 = 0.833P$$

FIGURE 7.6 Method of joints.

Member L0-L1 and establish an orthogonal axis through L0. These are commonly called the horizontal and vertical axes. The forces parallel to each must be in equilibrium. In this case, this means that the vertical component of the force in Member L0-U1 is equal to the reaction R_L . By considering the forces in the horizontal direction, the force in Member L0-L1 is equal to the horizontal component of the force in Member L0-U1. Thus, all of the member forces at L0 can be determined.

If we proceed to Joint L1, at which there is no applied load, it is clear that vertical equilibrium of the joint requires that the force in L1-U1 be equal to 0, and that the force in L1-L2 be equal to L0-L1.

Proceeding to Joint U1, it can be seen that, although four members frame into that joint, the force in two of the members are now known, and the force in the other two members can be found from the equation of equilibrium of forces along the two axes.

The analysis continues in this way from joint to joint.

7.3.1.2 Method of Sections

The method of sections proceeds by identifying free-body diagrams that contain only two unknowns, so that equilibrium of the sum of the moment about one joint and the equilibrium of the sum of the shears through a panel are sufficient to determine the two unknown truss forces. Consider Section AA in Figure 7.7, which shows a portion of the same truss shown in Figure 7.6. If we consider the free-body diagram to the left of Section AA, it is clear that the shear in the panel is equal to the reaction R_L and that this can be reacted only by the force L0-U1. Similarly, since the section and hence the free-body diagram is taken just to the left of the Joints L1 and U1, summing moments about Joint U1, or more accurately, the end of Member L0-U1 an infinitesimally small distance to the left of the section line, enables us to compute the force in L0-U1.

If we consider Section BB, it can be seen that the sum of the moments about the lower chord joint enables us to find the force in the top chord, and the shear in this panel enables us to find the force in the diagonal directly.

The analysis then proceeds from section to section along the truss. As a practical matter, a combination of the method of sections and the method of joints usually results in the most expeditious calculations.

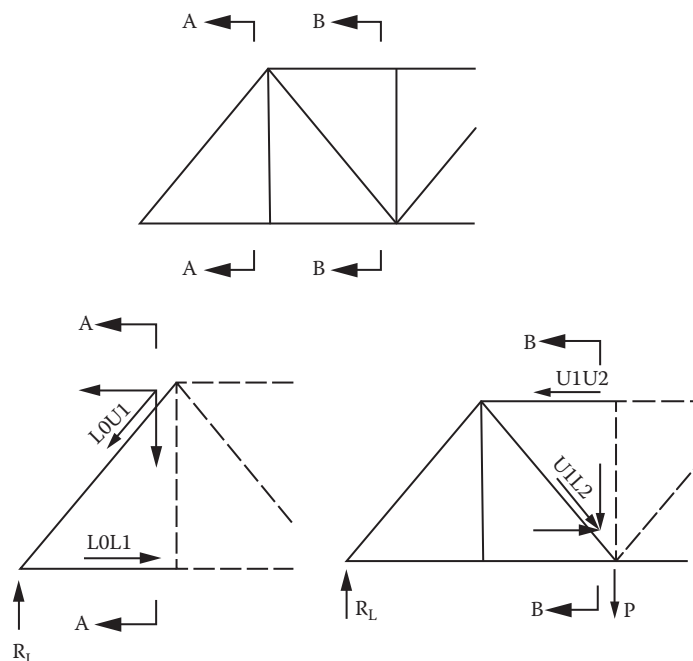


FIGURE 7.7 Method of section.

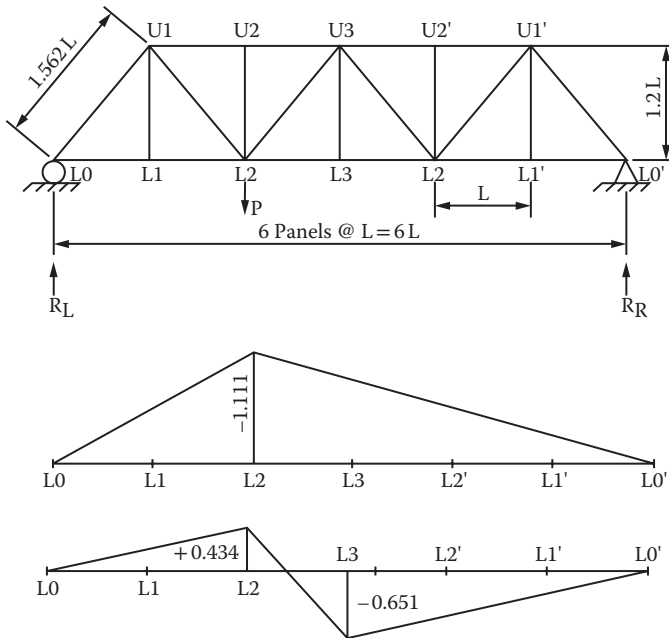


FIGURE 7.8 Influence lines for forces in one chord and one diagonal.

7.3.1.3 Influence Lines for a Truss

An influence line is a graphical presentation of the force in a truss member as the load moves along the length of the structure.

Influence lines for forces in the members are usually found by applying a unit load at each of the affected chord joints. This information is then shown pictorially, as indicated in Figure 7.8, which shows the influence line for a Chord Force \$U_1-U_2\$ (or \$U_2-U_3\$) and Diagonal Force \$L_2-U_3\$. If the truss is statically determinate, the influence line is a series of straight line segments. Since panel point loading is usually used in a truss, the influence lines for diagonals typically pass through a truss panel, as shown in Figure 7.8. If the truss is statically indeterminate, then the influence lines will be a series of chords to a curve, not a straight line.

7.3.2 Computer Methods

The method of joints and the method of sections identified above appear to be very simple as long as the geometry of the truss is also simple and the structure is statically determinate. This is particularly true if one or both chords are horizontal. On most modern trusses, the span is sufficiently long that the change in the vertical geometry can be significant. In fact, most larger trusses are on vertical curves if they cross a waterway. The chord joints are usually parallel to the deck profile. Thus, in many practical truss bridges, one or both truss chords are a series of chord segments representing a parabolic curve over at least part of the length of the bridge. This significantly complicates the geometry with respect to the use of either the method of joints or the method of sections. It does not negate the use of either of these methods, but certainly makes them less attractive.

There are many software packages for computers that permit the analysis of trusses. The analysis can be done typically as either the pin-connected assemblage or as a frame with moment-resisting joints.

If the bridge is determinate in the plane of a truss, and if the truss is analyzed with two force members, then the cross-sectional area of the members does not affect the analysis. Assuming the unit area for all members will give the proper forces, but not necessarily the proper displacements. If the truss is

indeterminate in a plane, then it will be necessary to use realistic areas for the truss members and may be important to include the camber of the members in order to get realistic results in some cases. This will be true of the so-called “geometric case” that is usually taken as the state of the bridge under all dead load, at which time it is supposed to have the proper grades and profile. An analysis for a subsequent load, such as unit loads for the assembly of influence lines, or a transient load, does not require inclusion of the member camber. In fact, inclusion of the camber for other than the loads acting in the geometric condition would yield erroneous results for the indeterminate truss.

Where software has the ability to put in a unit length change within a member and an analysis similar to this is required to properly account for camber of the members, then it is often found efficient to calculate the influence lines for truss members using the Mueller-Bresslau principle as found in any text on structural mechanics.

When a truss is analyzed as a three-dimensional (3D) assemblage with moment-resisting joints, then the method of camber becomes even more important. It is common practice for some of the members to be cambered to a “no load position” and in order for these members to have no load in them as analyzed, all the other members in the truss will have to be properly cambered in the computer model. With the usual fabrication techniques and adequate care for camber in both primary and secondary members (which may have no camber), a 3D computer analysis of a roadway truss will typically result in determining truss member forces that are very close to those obtained by the pin-connected truss analogy. The secondary stresses from joint rotation resulting from transient loads will be determined directly from the computer analysis.

7.4 Floor Systems and Framing Details

7.4.1 Conventional Deck Systems Not Integral with Truss Chords

Initially floor system framing was intended to be as structurally simple as possible. In the past, floorbeams were often hung from truss pins with yokes and the simple-span stringers framing between floorbeams often supported by saddle brackets on floorbeam webs. As time went on, the advantages of continuous stringers, particularly in highway bridges, became very evident, and framing involving stringers-over-floorbeams developed, as did improved details for framing simply-supported stringers between floorbeams. The composite design of stringers and/or stringers and floorbeams continued to add strength, stiffness, and robustness to trusses, while simultaneously eliminating many of the sources of uncontrolled drainage and hence, corrosion, which had been the perceived source of excessive maintenance in trusses. Currently, floorbeams are either vertical or set normal to roadway grade, and stringers are usually normal to crown and parallel to grade. If they are vertical, some sort of bevelled fill is necessary between the floorbeam and the stringers. A typical through truss cross section is shown in Figure 7.9.

Most modern truss designs continue to use concrete decks, as well as filled grid, or grid and concrete composite systems, as efficient durable decks. Relatively little use has been made of orthotropic decks in conjunction with the original design (as opposed to rehabilitation) of trusses in the United States, but this is certainly a feasible alternative. The use of newer lightweight deck systems, such as the proprietary Aluma-Deck or possibly advanced composite orthotropic deck systems can lead to further reduction in weight and, hence, savings in a competitive environment, as well as holding the potential for significantly reduced maintenance in future trusses.

7.4.2 Decks Integral with Truss Chords

So far, deck systems have almost always been designed to be structurally separate from the main supporting truss systems. As a need for efficiency and reduced cost, as well as increased redundancy, continues, a possible merging of the deck and truss system is a technical possibility. Orthotropic deck has been used as part of the bottom or top chord on some foreign bridges. Redundancy issues should be thoroughly considered as more traditional load paths are reduced. The available computer capabilities allow modeling

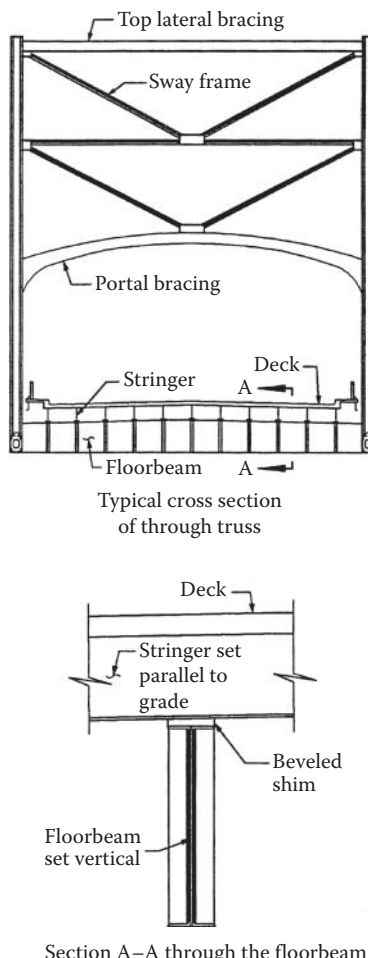


FIGURE 7.9 Typical truss cross section.

of damage scenarios and the emerging knowledge on the computation of reliability indices for damaged structures can provide designs with high levels of confidence, but such sophisticated calculations will have to be justified by cost savings and/or other benefits. Merging chords and deck has the potential to eliminate more joints within the deck system, perhaps at the expense of accommodating certain differential temperature features. Generally, as in all types of bridge structures, the elimination of joints is perceived as a favorable development. If the use of orthotropic decks as part of the chord system, and the lateral system for that matter, were to evolve, designers would have to consider the possibility of using either reinforced or prestressed concrete in a similar manner. This would, of course, tend to lead toward loading the chord at other than the panel points, but this situation has been handled in the past where, in some situations, deck chord members directly supported the roadway deck over their full length, not simply at the panel points.

7.5 Special Details

7.5.1 Hangers and Dummy Chords for Cantilever Bridges

The cantilevered truss has been used effectively on long-span structures since the Firth of Forth Bridge was built in Scotland in the late 1800s. This structural system was developed to provide most of the economy of continuous construction, as well as the longer spans possible with

continuity, while simultaneously providing the simplicity of a statically determinate structural system. Consider the system shown in Figure 7.10. Figure 7.10a shows what appears to be a Warren truss configuration for a three-span continuous unit. The parallel diagonal configuration shown in the detail in Figure 7.10a is an indication that the framing system for the standard Warren truss has been interrupted. The statical system for the cantilever truss, indicated by the parallel diagonals, is shown in Figure 7.10b. The continuity has been interrupted by providing two points along the structure where the chords carry no axial force, resulting in a "shear only" connection. This is, by definition, a structural hinge. The unit between the two hinges is commonly referred to as a "suspended span." The remaining portions of the structure are called the "cantilever arms" and the "anchor spans," as indicated in Figure 7.10a. The mechanism for supporting the suspended span is shown in concept in Figure 7.10c, which indicates that two chords are missing and hinges have been placed in the strap, or hanger, carrying the load of the suspended span into the anchor arm. The configuration with the link and two hinges allows the portions of the structure to expand and contract relative to each other.

In practice, the unnecessary top and bottom chords are added to the structure to allay public concerns, and are articulated in a manner that prevents them from carrying any axial load. These elements are typically called "false chords" or "dummy chords." A typical top chord joint at the hanger point is shown in Figure 7.11. Figure 7.11a is a plan view of the top chord element, and the corresponding elevation view

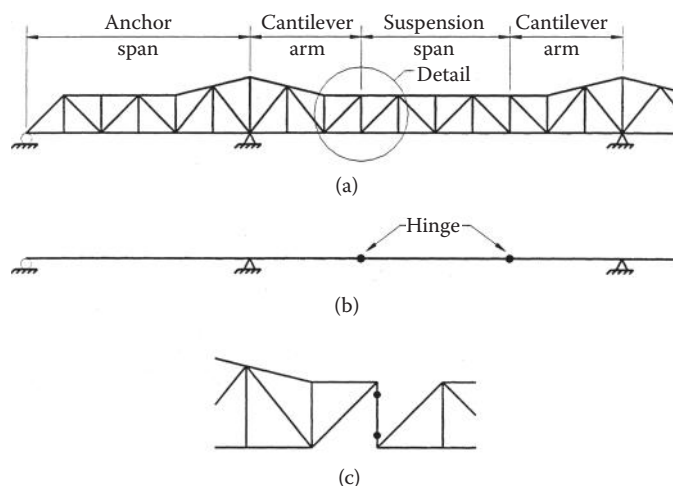


FIGURE 7.10 Cantilever suspension.

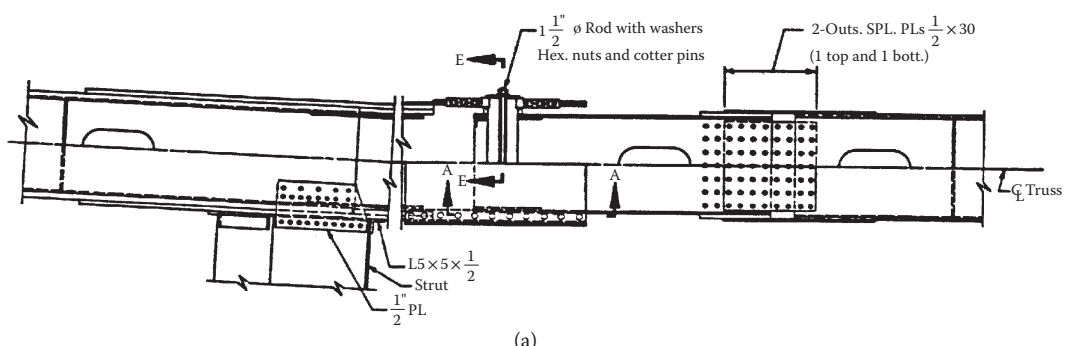


FIGURE 7.11 (a) Top false chord details—plan view. (b) Top false chord details—elevation view. (c) Hanger details.

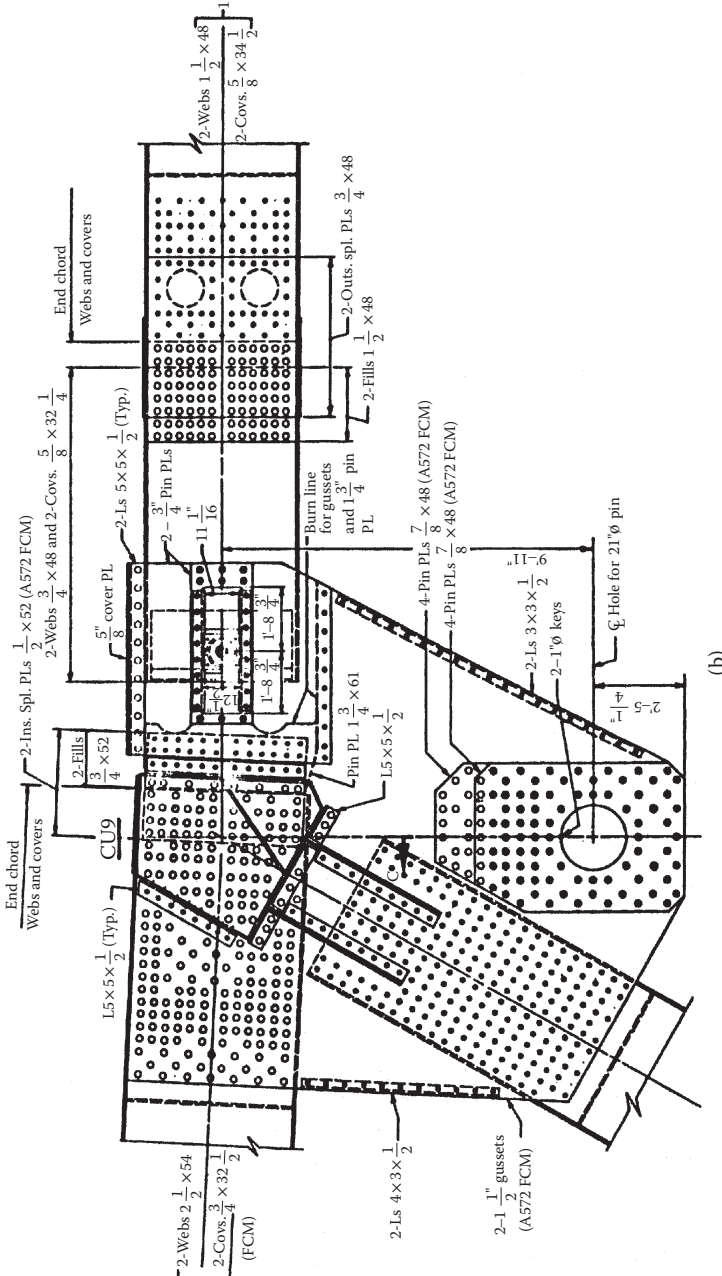


FIGURE 7.11 (Continued) (a) Top false chord details—plan view. (b) Top false chord details—elevation view. (c) Hanger details.

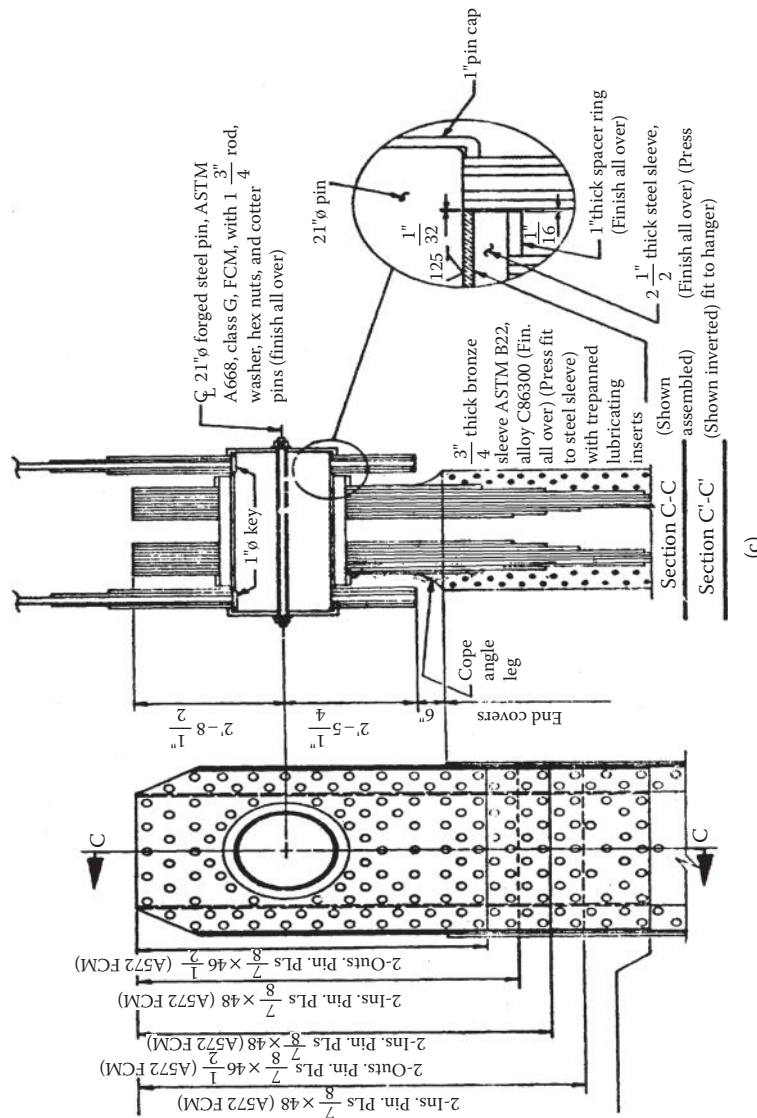


FIGURE 7.11 (Continued) (a) Top false chord details—plan view. (b) Top false chord details—elevation view. (c) Hanger details.

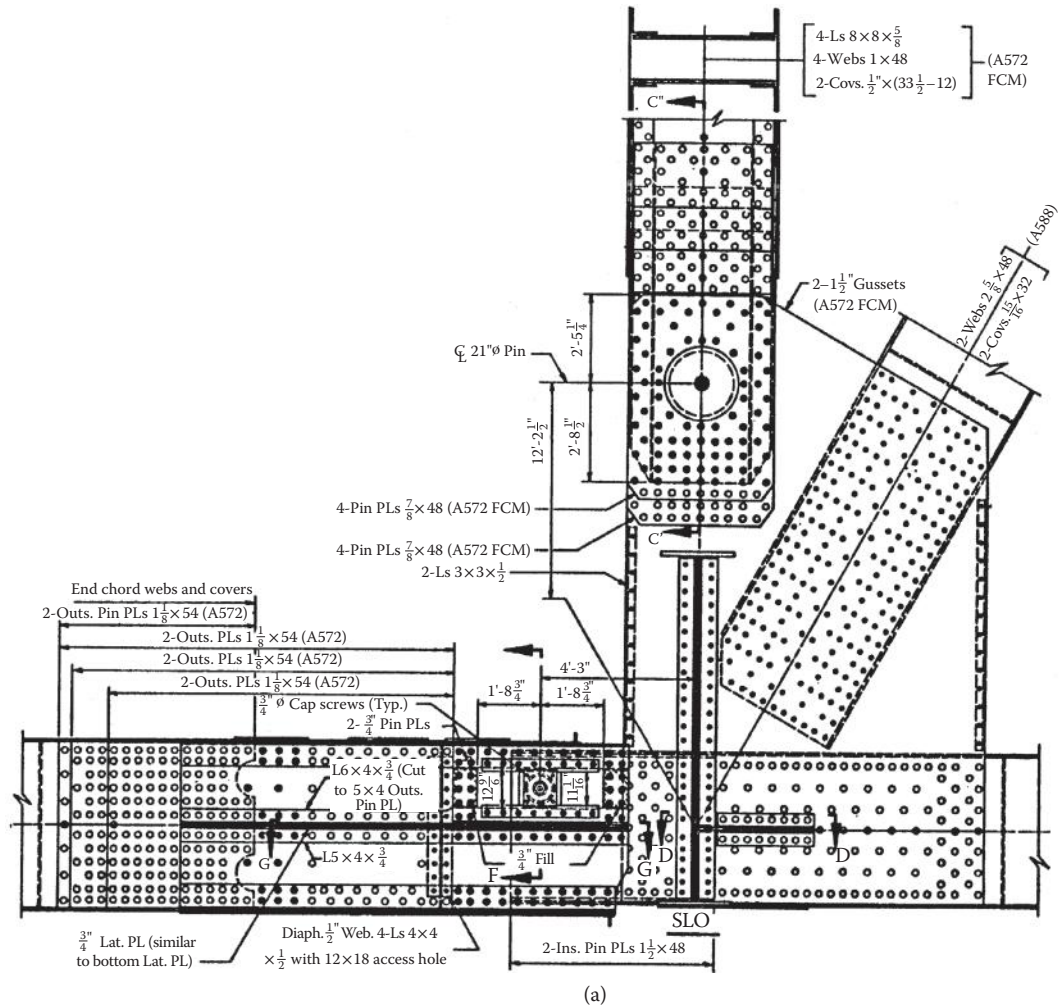
is shown in Figure 7.11b. The false chord in this case is supported by the anchor arm, utilizing a pin. The false chord is slotted, so that it may move back and forth with expansion and contraction without carrying any load. It simply moves back and forth relative to the pin in the slot provided. The pin carries the vertical weight of the member to the top chord joint. Also shown in Figure 7.11b, and extending further into Figure 7.11c, are details of the hanger assembly and the top pin of the pins in the hanger used to allow it to swing back and forth. Hangers are potentially fracture-critical members, as a failure of this member would almost certainly result in a collapse of at least the suspended span portion of the structure. These members are usually built of multiple components to add redundancy. The particular assembly shown has multiple plates bolted together to compensate for the hole occupied by the pin. In recent years, many truss bridges have been retrofitted with redundancy-adding assemblies usually consisting of rods or cables parallel to the hanger and attaching to the top and bottom chord. These assemblies are intended to pick up the load if the hanger or pin were to fail. Some of the details for the hanger pin are also shown in Figure 7.11c.

The corresponding portions of the structure at the bottom chord are shown in Figure 7.12. An elevation view of the lower chord joint is shown in Figure 7.12a, and a partial plan view is shown in Figure 7.12b. The concepts are very similar to those utilized in the upper joints, in that there are pins and slots to allow the false chord to move without picking up axial load and pins and gusset plates to transfer the load from the suspended span into the hanger.

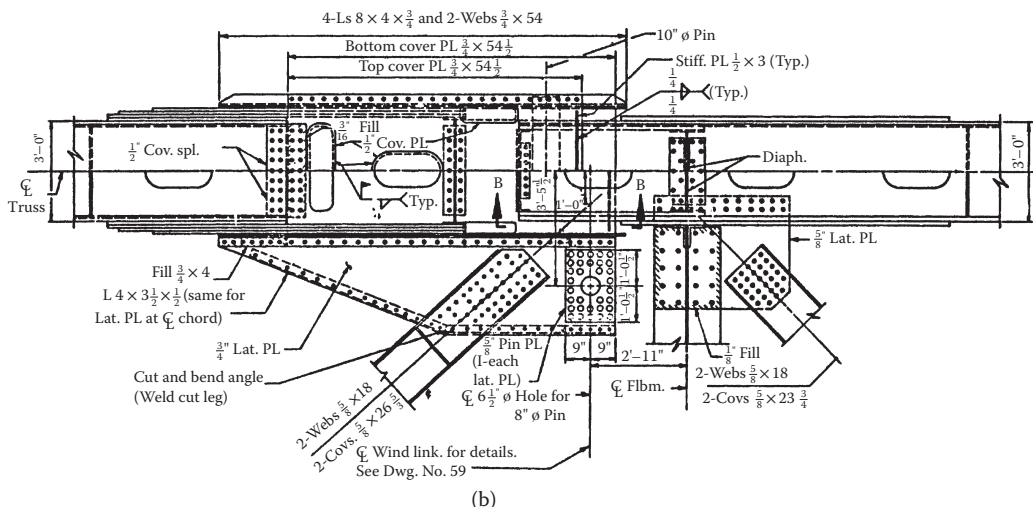
After completion of erection of the anchor span and the cantilever arm, the suspended span may be erected component by component, often referred to as “stick erection,” or the entire suspended span may be assembled off-site and hoisted into position until it can be brought into bearing at the hanger pins. If stick erection is used, the bridge will sag toward the middle as the cantilevers reach midspan. The bridge will be in the sag position because once assembled to midspan, the cantilevers will be much shorter than they are at the midspan closure. It will thus be necessary to raise or lower portions of the bridge in order to get the closure members in and to transfer loads to the intended statical system. Also, during this time, the false chords have to carry loads to support the cantilevering. With this type of erection, the false chords may be temporarily fixed, and one or both of the chords may have mechanical or hydraulic jacks for transferring load and for repositioning the two cantilevers for closure. Provisions for this type of assembly are often made in the false chord, at least to the point of being certain that the required space is available for jacks of sufficient capacity and that bearing plates to transmit the load are either in place or can be added by the contractor. A typical detail for providing for jack assemblies is shown in Figure 7.13, which indicates how jacks would fit in the bottom chord false chord shown in Figure 7.12, and bear against the rest of the structure, so as to swing the cantilevered portion of the suspended span upward to facilitate closure.

7.5.2 Bearings

From the viewpoint of bearings, the cantilever form of erection offers several other advantages. The bearings used on the main piers can be fixed to the pier tops, and the chords framing into that point can be pinned into gusset plates. This provides a very simple and relatively maintenance-free connection to carry the major reaction of the bridge. The bearings on the end piers at the ends of the anchor spans are sometimes unique. Depending upon the requirements of the site or to reduce costs, the end spans are sometimes quite short, so that even under dead load, the reaction on the end piers is negative, which is to say an uplift condition exists under the dead load. Under some patterns of live load, this uplift will increase. When this condition exists, hanger assemblies similar to those described in Article 7.5.1 may be used to connect to a bearing fixed to the pier, and connected to an embedded steel grillage or similar device used to engage the weight of the pier to hold down the superstructure. Such a bearing is shown in Figure 7.14. The link accommodates the movement of the superstructure relative to the substructure required by expansion and contraction. The length of the arch swing of the link is designed so that the vertical displacement associated with the swing of the link can be accounted for and accommodated.



(a)



(b)

FIGURE 7.12 (a) Bottom false chord details—elevation view. (b) Bottom false chord details—plan view.

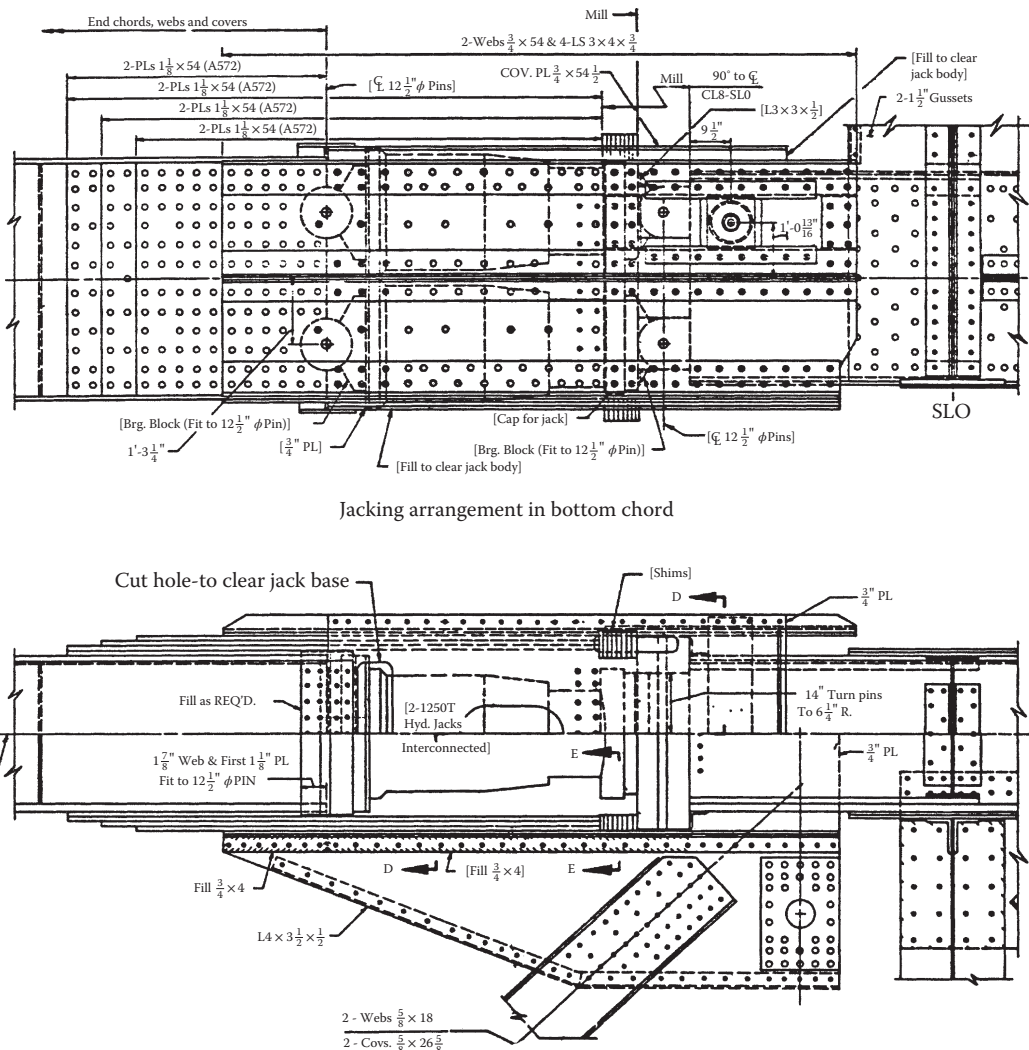


FIGURE 7.13 False chord jacking details.

Where positive reactions are possible under all loadings, the bearing on the back span pier may be a rocker, roller nest, such as that shown in Figure 7.15, roller and gear assembly, or low profile modern bearings, such as a pot bearing shown in Figure 7.16 as applied to a girder bridge or the disc bearing shown in Figure 7.17. It is usually necessary for this bearing to provide for expansion and contraction while minimizing the forces put on the piers and to allow for rotation about the major bending axis of the bridge. Depending upon the designer's preferences, these bearings may or may not also carry the horizontal forces on the structure, such as wind loads, into the piers in the transverse direction. In some instances, the chord bearings serve this function through guide bars or pintles and, in some cases, a separate wind bearing, such as that shown in Figure 7.18, is provided to carry the transverse loads into piers separate from the main chord bearings.

Where structures are continuous, as opposed to cantilevered, it is usually necessary for three of the four-span bearings supporting the typical three-span truss to move. Individual movement is greater in these bearings than it would be for a comparable-length cantilevered truss, and additional requirements are placed on the bearing at one of the two main piers that moves, because of the large vertical reaction that is transmitted at that point. Additionally, the continuous bridge has two expansion joints, instead of four on the

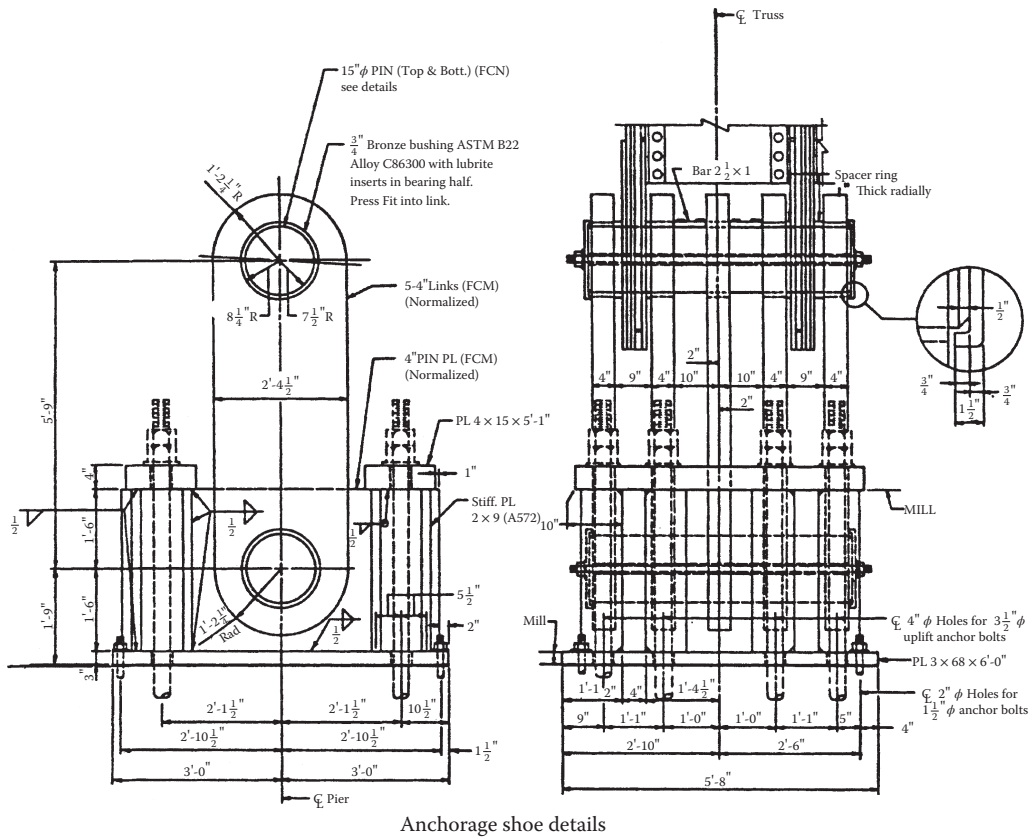


FIGURE 7.14 Link-type tie down bearing.

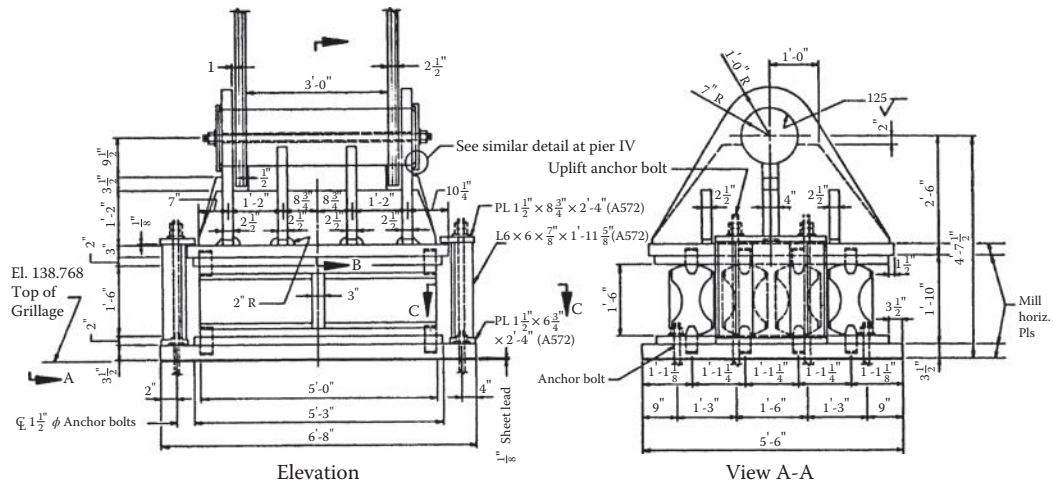


FIGURE 7.15 Roller bearing.

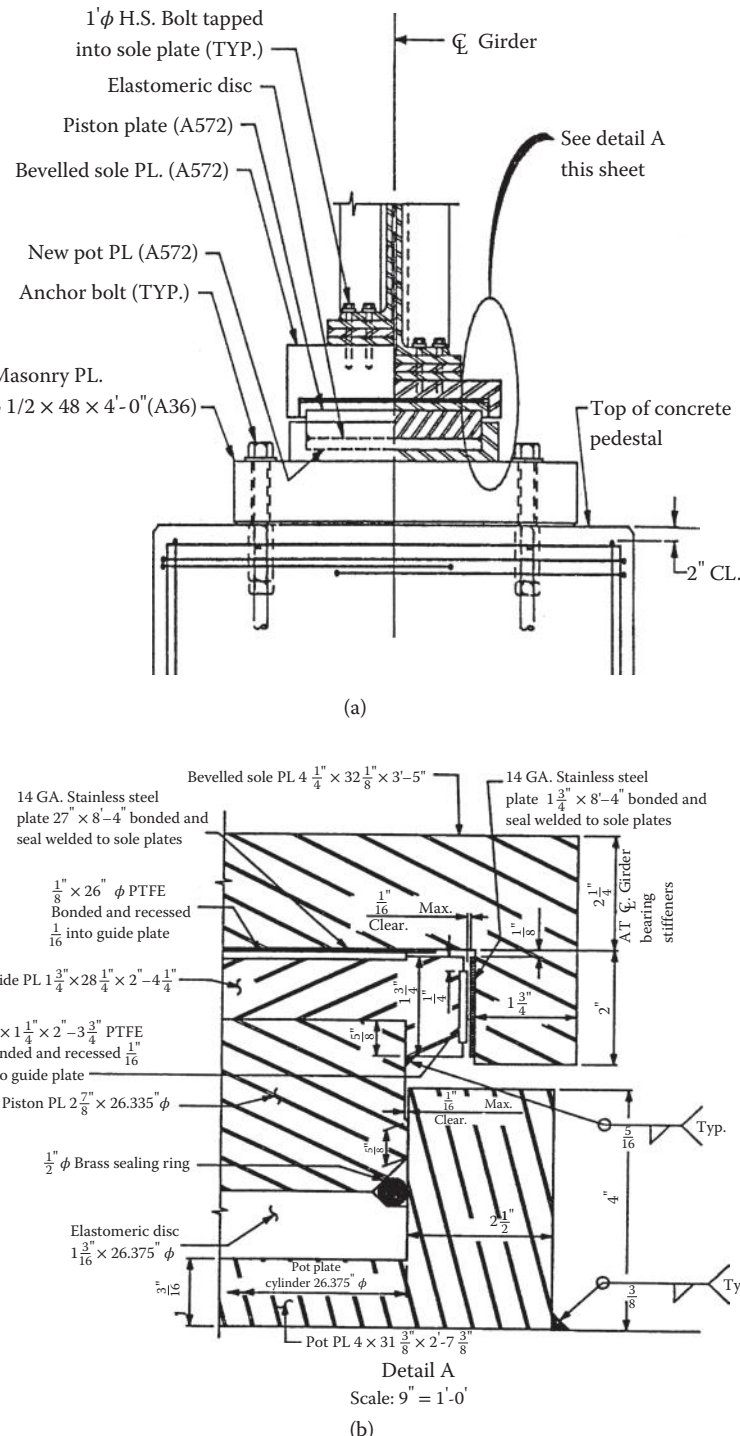


FIGURE 7.16 (a) Typical pot bearing. (b) Typical pot bearing details.

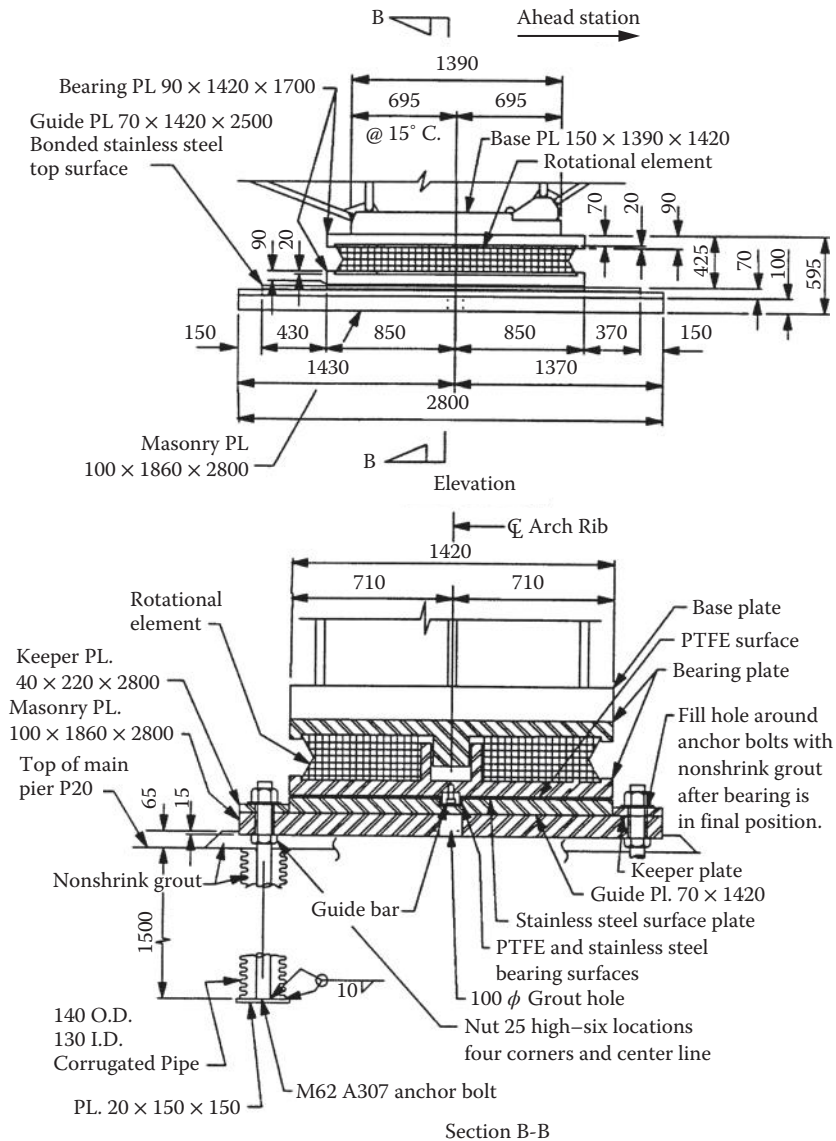


FIGURE 7.17 Typical disc bearing.

cantilever bridge, which is both an advantage and a disadvantage. These joints have to be larger for the continuous bridge than for the cantilevered bridge and, therefore, more expensive. On the other hand, the tendency toward minimizing the number of joints in structures in order to reduce damage from deck drainage favors the continuous structure. Generally speaking, the extra points of expansion and contraction, associated deck joints and articulation hardware in the cantilevered bridge have required above-average maintenance.

7.5.3 Wind Tongues and Bearings for Transverse Forces

Wind loads carried by the suspended span in the cantilevered bridge have to be carried to the bearings on the piers. Thus, it is necessary for the wind loads to be carried through the panels framed with the false chords. Typically, in a through truss, all of the wind loads on the suspended span are reacted by the hangers and by a special purpose mechanism used to transmit horizontal forces at the lower chord level from the

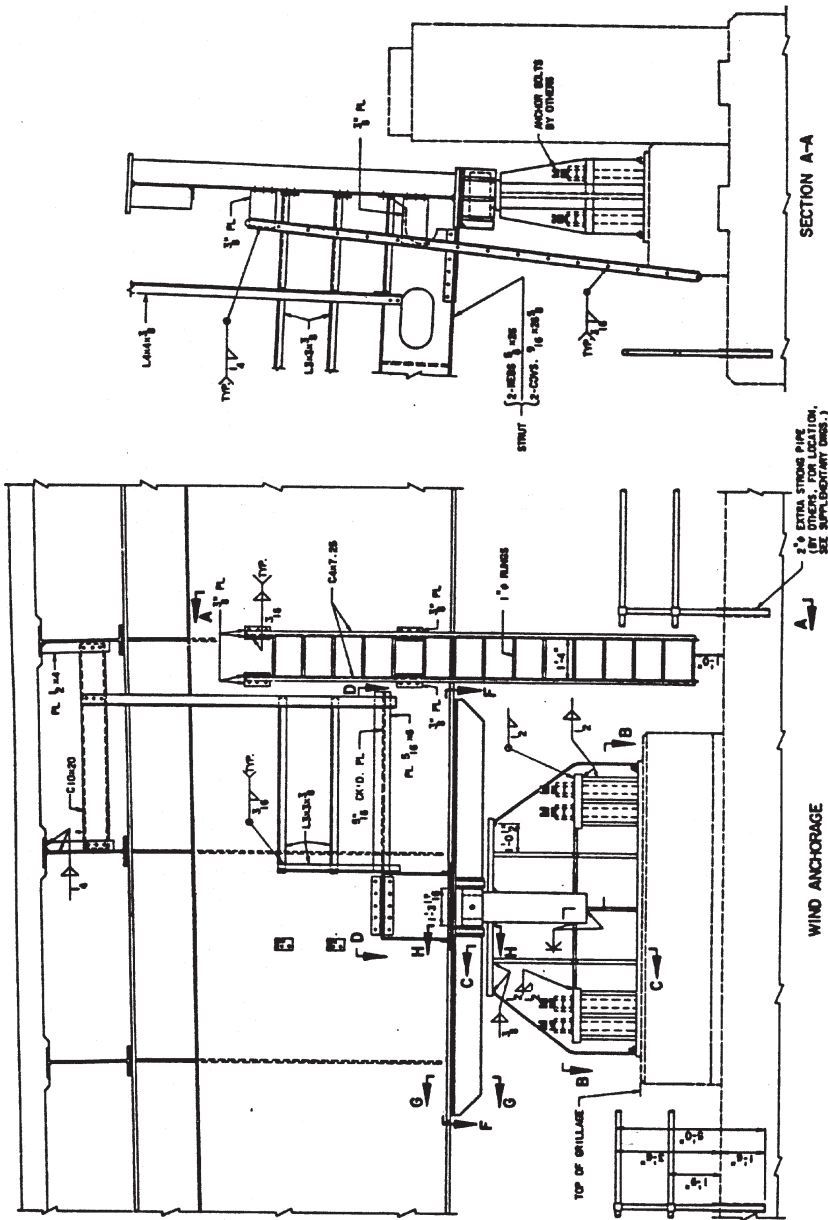


FIGURE 7.18 Truss wind bearing.

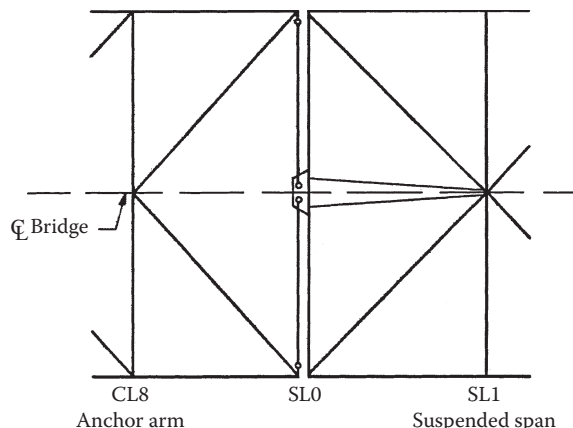


FIGURE 7.19 Schematic of wind tongue.

suspended span into the anchor arms. Wind load tributary to the upper lateral truss system in the plane of the top chord joints is carried into the anchor arms as a shear at the lower chord joint and the torque necessary to react to the transfer of loads from the top chord to the lower chord is carried as equal and opposite vertical reactions on the hangers. The horizontal forces at the lower chord level are then transmitted from the suspended span to the cantilever arm by a device called a “wind tongue” shown schematically in Figure 7.19. Because of the offset in chord joints at the suspended span, the horizontal force creates a torque in the plane of the bottom lateral system as the shear is transmitted across the expansion joint. Additionally, because expansion and contraction movements are accommodated at this point, allowance has to be made for some of the lateral members to swing along with that expansion and contraction. Thus, in Figure 7.19, there are four pin assemblies shown in the detail. The two horizontal links thus swing back and forth to accommodate the relative movement occurring at the open joint. The torque caused by the offset shear is reacted by the members framing from the open joint back into the next panel point of the suspended span. These members form a lever to react to torque and prevent significant rotation of the wind tongue.

The typical details for accomplishing this wind transfer are shown in Figure 7.20a and b. Figure 7.20a shows the assembly that spans the open joint between the suspended span and the anchor arm. Also shown is one of the horizontal link members. The reacting members that form the lever to react the torque are also shown in this view, and are shown again in Figure 7.20b as they converge back to a common work point in the lateral truss of the suspended span. A typical pin assembly is shown in Figure 7.21.

In the case of the continuous truss, since the open joint does not exist, no assembly similar to the wind tongue, described above, is necessary. As can be seen in a plan view, the colinear force system can be developed that transmits wind and other transverse forces into the piers without creating torque in the bottom lateral system. Despite this, designers will often support the bearing point in order to accommodate accidental eccentricities that might exist. As seen in a vertical plane, there will almost certainly be an eccentricity between the center of transverse forces and the bearing. This will also be typically framed into a triangular system to carry this eccentricity through truss action, rather than bending. These details are usually much simpler than the wind tongue at the suspended span, because it is not necessary to simultaneously account for expansion and contraction in the lateral truss system. This is usually handled by allowing the reaction points to move relative to the bearing while they are stationary relative to the lateral truss.

7.5.4 Gusset Plates

Gusset plates are used to connect truss members at a joint and accomplish the transfer of forces among the members as required by the global shear and moments imposed by the loads. Sometimes the splicing of chords also takes place in the gusset plates. The August 1, 2007 failure of the I-35 Mississippi River Bridge in Minneapolis has resulted in a renewed focus on the behavior and in-service condition

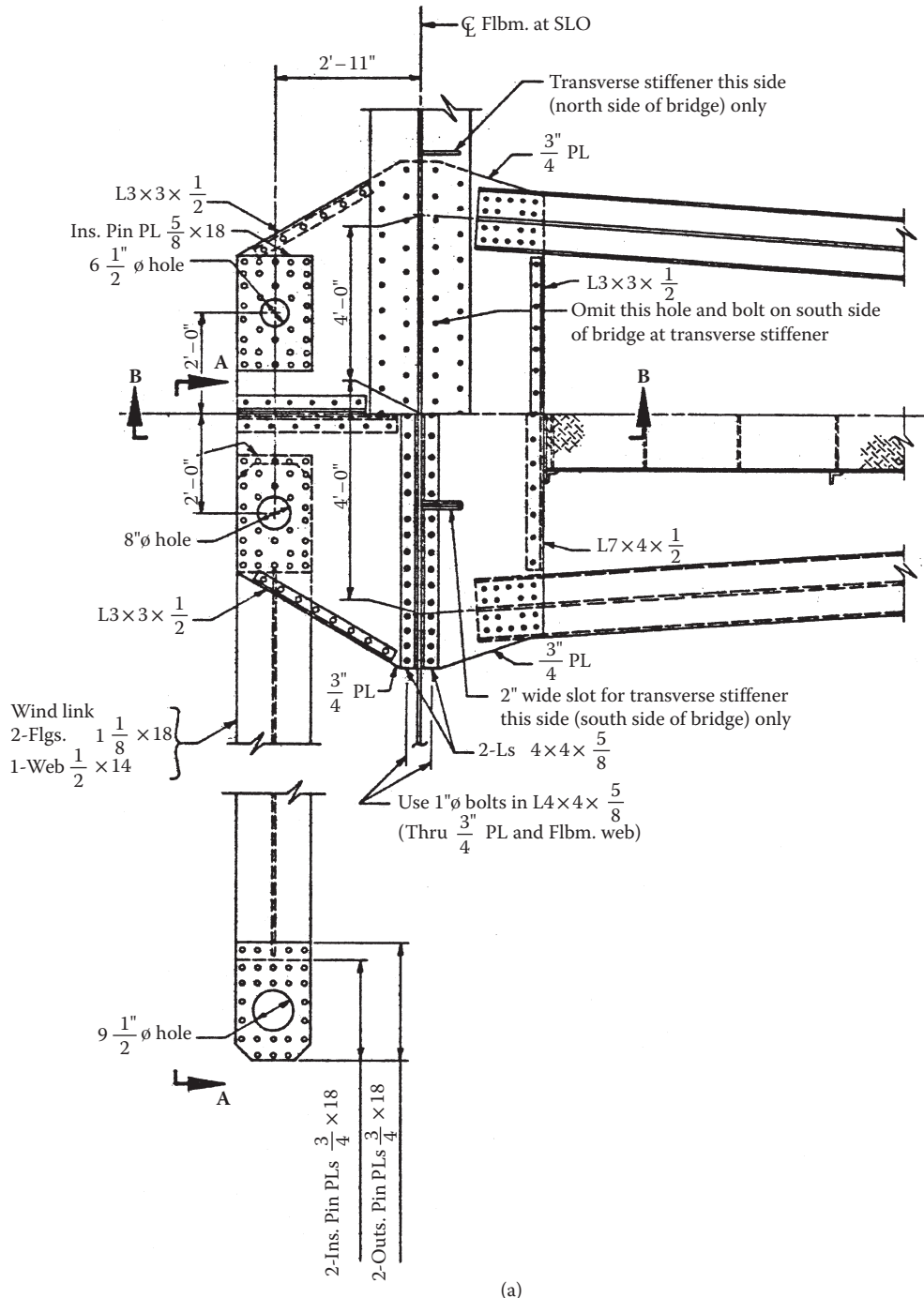


FIGURE 7.20 (a) Details of wind bearing. (b) Details of wind tongue.

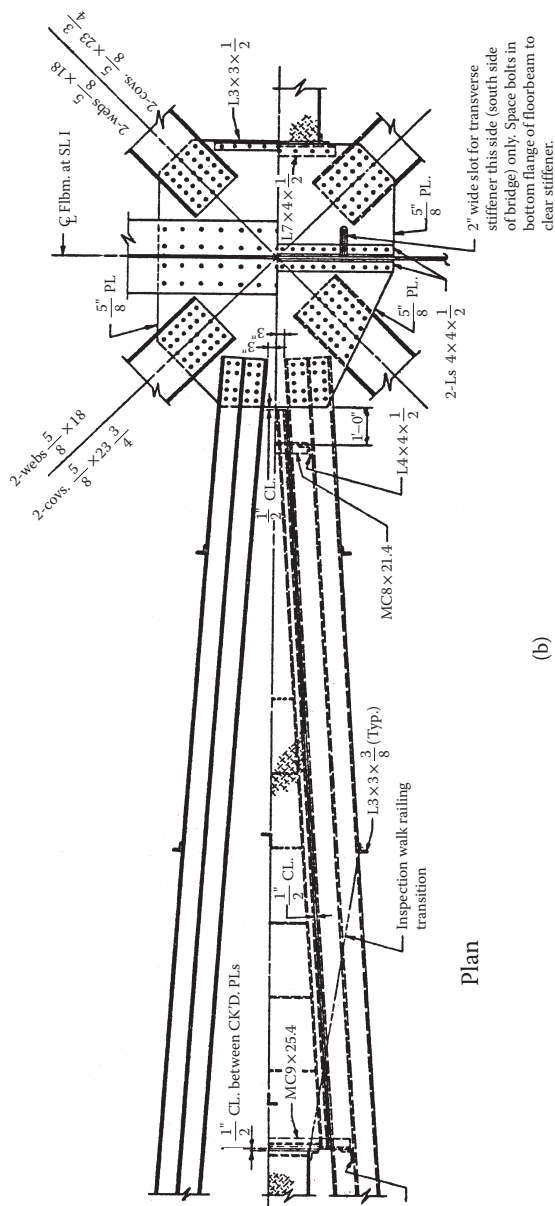


FIGURE 7.20 (Continued) (a) Details of wind bearing. (b) Details of wind tongue.

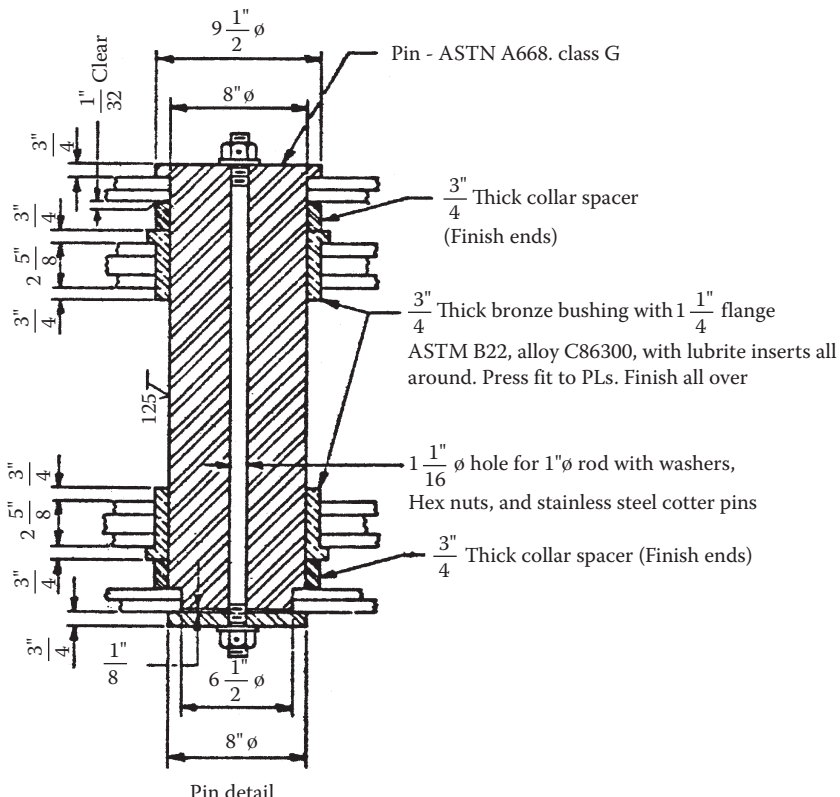


FIGURE 7.21 Typical wind tongue pin details.

of these important bridge components. Inspection of gusset plates throughout the country has shown that corrosion, often between the members and the gusset plates, and deformed gusset plates were more widespread in the U.S. bridge inventory than previously thought.

Gusset plates have historically been designed using simple rules based on experience and a limited amount of research, especially on bridge-specific details. A study by Whitmore (1952) resulted in a commonly assumed spread of load from a connected member into the gusset plate material. The National Academies through its National Cooperative Highway Research Program and the FHWA have undertaken a major research program, NCHRP 12-84, involving large-scale testing and numerical simulation to develop the guidelines for the load and resistance factor design and rating of riveted, bolted, and welded gusset-plate connections for steel bridges since 2008. Guidance for design and evaluation based on research (Ocel 2013) was adopted by AASHTO in 2013.

7.6 Camber and Erection

7.6.1 Camber for Vertical Geometry

It is obvious that all bridges have a theoretical geometric location as determined by the final design drawings. Every member has a theoretical length and location in space. One goal of the designer, fabricator, and erector is to produce a bridge as close to the theoretical position as possible, thereby ensuring actual stresses similar to design stresses.

To accomplish this, main members are usually cambered. Tensioned members that stretch under load are fabricated such that their unstressed length is shorter than their length under the effect of dead load.

of the structure. The opposite is true for compression members. The cambered lengths are then accounted for during the erection stress and geometry studies. The state of the bridge when the camber “comes out” is called the geometric position. In this state, the loads on the bridge are sufficient to return all of the members to their theoretical length. At any other state, the bridge will be out of shape and additional forces may result from the difference between its shape at any time and the final shape. This is relatively easy to see in the case of a continuous truss because it is clearly statically indeterminate and the shears and moments producing member forces are dependent on its shape. However, this is also true for a simple-span truss because the joints are not frictionless pins as may have been assumed in the analysis. Because of this, even the simplest form of truss can have significant temporary member forces and moments until it reaches the geometric position. As discussed in the next section, there may be secondary moments in the geometric position, depending on the positioning of connector patterns on member ends in the shop.

Secondary members such as laterals and sway frame members are usually not cambered. They are usually intended to be stress free in the geometric position. Thus, at intermediate stages of erection, they may also be subject to temporary forces.

The importance of camber in achieving the designer's intent for the structure is shown in the following discussion. In a determinant structure, the forces in components are uniquely determined by the geometry, loading, and support condition through the equations of equilibrium. The designer cannot alter the structural actions.

In a redundant structure, the designer can theoretically alter the forces associated with any one loading case. After this, the distribution of forces is again uniquely determined by all the conditions above, plus the relative stiffness of the various structural components. In truss construction, this adjustment of natural forces is seldom actually done. On certain occasions, camber to produce a determinant structure at steel closure has been used to facilitate erection. Camber for force control is very common in other types of bridges.

7.6.2 Camber of Joints

When the principal operations on a main member, such as punching, drilling, and cutting are completed, and when the detail pieces connecting to it are fabricated, all the components are brought together to be fitted up, that is, temporarily assembled with fit-up bolts, clamps, or tack welds. At this time, the member is inspected for dimensional accuracy, squareness, and, in general, conformance with shop detail drawings. Misalignment in holes in mating parts should be detected then and holes reamed, if necessary, for insertion of bolts. When fit-up is completed, the member is bolted or welded with final shop connections.

The foregoing type of shop preassembly or fit-up is an ordinary shop practice, routinely performed on virtually all work. There is another class of fit-up, however, mainly associated with highway and railroad bridges that may be required by project specifications. These may specify that the holes in bolted field connections and splices be reamed while the members are assembled in the shop. Such requirements should be reviewed carefully before they are specified. The steps of subpunching (or subdrilling), shop assembly, and reaming for field connections add significant costs. Modern computer-controlled drilling equipment can provide full-size holes located with a high degree of accuracy. AASHTO Specifications, for example, include provisions for reduced shop assembly procedures when computer-controlled drilling operations are used.

7.6.3 Common Erection Methods

Construction on falsework, stick erection (piece-by-piece), float-ins, cantilever erection, and the use of tie-backs have all been used to erect truss bridges. It is common for more than one method to be used in the construction of any single bridge. The methods selected to erect a bridge may depend on several factors, including the type of bridge, bridge length and height, type and amount of river traffic, water depth, adjacent geographical conditions, cost, and weight, availability, and cost of erection equipment.

Regardless of the method of erection that is used, an erection schedule should be prepared prior to starting the erection of any long-span bridge. The study should include bridge geometry, member stress and stability

at all stages of erection. Bridges under construction often work completely differently than they do in their finished or final condition, and the character of the stress is changed, as from tension to compression. Stresses induced by erection equipment must also be checked, and, it goes without saying, large bridges under construction must be checked for wind stresses and sometimes wind-induced vibrations. An erection schedule should generally include a fit-up schedule for bolting major joints, and a closing procedure to join portions of a bridge coming from opposite directions. Occasionally, permanent bridge members must be strengthened to withstand temporary erection loads. Prior to the erection of any bridge, proper controls for bridge line and elevation must be established, and then maintained for the duration of the construction period.

Most long-span bridge construction projects have a formal closing procedure prepared by bridge engineers. The bridge member or assembled section erected to complete a span must fit the longitudinal opening for it, and it must properly align with both adjoining sections of the bridge. Proper alignment of the closing piece is generally obtained by vertical jacking of falsework, lifting the existing bridge with a tie-back system, or horizontal jacking of truss chords.

The forces obtained during various stages of construction may be entirely different than those applicable to the final condition and, in fact, the entire mechanism for resisting forces within the structure may change. During the erection of a truss, falsework bents may be used to support a portion of the structure. The gravity and lateral loads still act in the sense that they do on the final condition, and the basic internal mechanism of resisting forces remains unchanged, that is, the primary load path involves axial load in the chords and diagonals, with the vertical components of those forces adding up to equal the applied shear within the panel, and the bending moment accounted for by the horizontal component of those forces. The camber of the truss will not pertain to an intermediate construction case, and, therefore, there is bound to be more joint rotation and, hence, more secondary bending moments within the truss members. Nonetheless, the primary load-carrying mechanism is that of axial forces in members. As the truss is erected, it is entirely possible that members that are in tension in the permanent condition will be under compression during erection and vice versa. In fact, the state of stress may reverse several times during the erection of the bridge. Clearly, this has to be taken into account, not only in the design of the members but also in the design of the connections. Compression members are apt to have been designed to transmit part of the forces in bearing. This will not be applicable when the member is in tension during erection. Similarly, a compression member that has tension during erection has to be reviewed for net section provisions and shear lag provisions.

7.7 Summary

Truss bridges have been an effective and efficient force of long-span bridges for over 150 years. As plate girder bridges have been utilized for spans of about 550 ft, box girders for spans of up to 750 ft (22.9 m), segmental concrete box girders for spans of up to about 800 ft, and cable-stayed bridges for spans of about 500 ft (152.4 m) to 2000 ft (609.6 m), the use of trusses has declined over the last 25 years. Nonetheless, they remain a cost-effective bridge form, one with which many fabricators and erectors are experienced. Emerging materials and the use of computer analysis to treat the bridge as a 3D structure will keep the truss form viable for the foreseeable future.

References

- Hartle, R. A., Amrheim, W. J., Willson, K. E., Baughman, D. R. and Tkacs, J. J. 1995. *Bridge Inspector's Training Manual/90*, FHWA-PD-91-015, Federal Highway Administration, Washington, DC.
- NPS. 1976. *Historic American Engineering Record*, National Park Service, Washington, DC.
- Ocel, J. M. 2013. Guidelines for the Load and Resistance Factor Design and Rating of Riveted and Bolted Gusset-Plate Connections for Steel Bridges, *NCHRP Web-Only Document 197*, Transportation Research Board, Washington, DC.
- Whitmore, R. E. 1952. *Experimental Investigation of Stresses in Gusset Plates*, Bulletin No. 16, Engineering Experiment Station, The University of Tennessee, Knoxville, TN.

8

Arch Bridges

8.1	Introduction	309
	Definition of Arch • Comparison of Arch Bridges to Other Bridge Types • A Brief History • Technical Trends	
8.2	Types	319
8.3	Design	322
	Masonry Arches • Concrete Arches • Steel Arches • CFST Arches	
8.4	Construction	337
	Scaffolding Method • Cantilever Method • Swing Method • Embedded Scaffolding Method for Concrete Arch Bridge • Construction Methods for Tied Arch Bridges	
8.5	Examples	345
	Mike O'Callaghan-Pat Tillman Memorial Bridge at Hoover Dam • Skradin Bridge near Šibenik in Croatia • Infante Dom Henrique above Douro in Portugal • Wanxian Yangtze River Bridge in China • Gateway Bridge in Detroit, Michigan, USA • Lupu Bridge in Shanghai, China • New Saikai Bridge in Nagasaki, Japan • Second Yellow River Highway Bridge in Zhengzhou, China • Yajisha Bridge in Guangzhou, China	
	Acknowledgments	359
	References	359

Baochun Chen
Fuzhou University

8.1 Introduction

8.1.1 Definition of Arch

An arch bridge is usually defined as a vertically curved and axially compressed structural member spanning an opening and providing a support for the moving loads above the opening. According to the spandrel structure, deck arch bridges can be characterized as filled spandrel arch bridge and open spandrel arch bridge as illustrated in Figure 8.1. The terminology used to describe arch bridges is shown in Figure 8.1.

The clear span of an arch bridge, l_0 , is the horizontal projection distance between the two intrados springing points. As a curved structure, the rise is also an important structural parameter in addition to the span. The clear rise, f_0 , is the vertical distance from the intrados crown to the connecting line between two intrados adjacent springing points. Besides, the rise-to-span ratio, which is defined as f_0/l_0 , is a key indicator of mechanical properties of an arch bridge.

The design span, l , and the rise, f , used in arch design usually refer to the span and rise of arch axis, as given in Equation 8.1:

$$\left. \begin{aligned} l &= l_0 + d \cdot \sin \varphi_j \\ f &= f_0 + \frac{d}{2} (1 - \cos \varphi_j) \end{aligned} \right\} \quad (8.1)$$

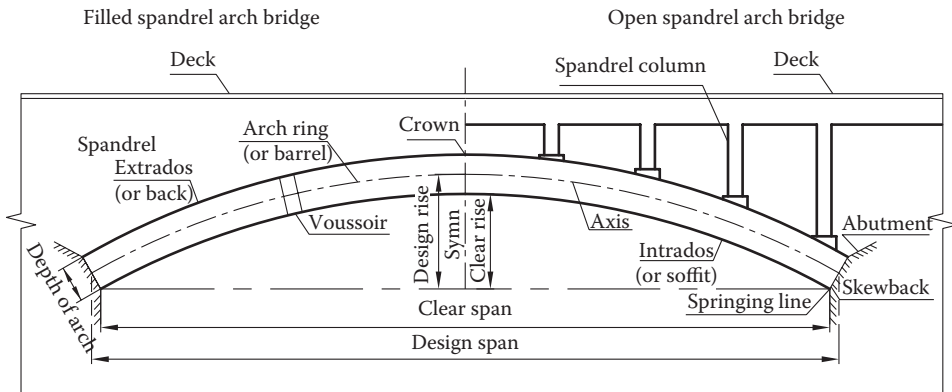


FIGURE 8.1 Arch bridge nomenclature.

where l is the design span, also called calculated span; d is the depth of main arch; φ_1 is the horizontal angle of the center line at the arch springing; and f is the design rise, also named calculated rise.

8.1.2 Comparison of Arch Bridges to Other Bridge Types

An arch is mainly subjected to compression and can be built with many kinds of materials, such as timber, masonry, concrete, metal, composite, and so on. The essential construction difficulty of arch bridges lies in the fact that arch structures do not work until a whole arch system is formed, that is, the closure of the arch.

Timber arch bridges are rarely built in modern time as road bridges because of their low load-bearing capacity, rot, combustibility, and high maintenance cost.

Masonry arch bridges, mainly constructed using stones and bricks, were mostly used as permanent bridges in ancient times. But the large self-weight limits the length of arch spanning. The expensive construction costs make masonry arch bridges less competitive than other types of bridges in developed countries where labor cost is high. However, masonry arch bridges may still be adopted in developing countries, particularly in mountainous areas with suitable construction sites and rich stone-like materials.

Since concrete has a high compressive strength and is inexpensive, it remains an ideal material for modern arches. However, the heavy self-weight of a concrete arch bridge also results in construction difficulty and large thrusts to the abutments and piers. The span record of concrete arch bridge is 420 m for Wanxian Yangtze River Bridge.

The construction technology for concrete arch bridge has been well developed for spans less than 200 m. In mountain or island areas, concrete arch bridges are cost-effective alternatives to concrete or steel girder bridges with tall piers. It is expected that long span concrete arch bridges will continue to be built over deep valleys whenever appropriate.

Steel is a material stronger than masonry and concrete; hence, a steel arch may span a longer span and be more slender and elegant than a masonry or concrete arch. In fact, the six of seven arch bridges in the world spanning more than 500 m are steel arch bridges. However, steel arch bridges with dominate compression forces require more steel for stability and may be more difficult in fabrication and erection than girder-type bridges or cable-stayed bridges. This is why only a few long span steel arch bridges have been built around the world since 1970s. Steel arch bridges are very competitive against truss bridges for spans up to about 275 m. If the construction cost is comparable to a truss bridge, an arch is commonly preferred for aesthetic reasons. For heavily and dynamically loaded long span railway bridges, steel arches (usually tied arches) are often the type chosen.

Innovative usage of composite materials in arch bridges takes advantage of the properties of both steel and concrete. A good example is concrete filled steel tubular (CFST) arch bridge. Many CFST arch bridges have been built in China since 1990 (Chen and Wang 2009). The longest CFST arch bridge with a main span of 530 m, the First HeJiang Yangtze River Bridge, China, will open to traffic in 2012.

In plain regions or areas with soft soil, tied arches are commonly employed. However, this type of bridge has a big disadvantage in that the tie girders must be constructed before the arch ribs can be loaded. Hence, for very long spans, usually across water, cable-stayed bridges may be more cost-effective than tied arch bridges because they do not have the thrust balancing problem and their deck elements and stay cables may be erected simultaneously during the process of construction.

8.1.3 A Brief History

The application of arches to bridge structures came much later than girder and suspension types, but an arch is the first and greatest of Man's inventions in the field of structures because arch transfers loads relating to its shape. The Sumerians, a society that lived in the Tigris-Euphrates Valley, used sun-baked bricks for their main building material. To span an opening, they relied on corbel construction techniques. Around 4000 BC, they discovered the advantages of arch shape in construction, and began to build arch entranceways and small arch bridges with their sun-baked bricks (Steinman and Watson 1941).

Other communities with access to stone soon began to build arches with stone elements. By the time of the Romans most bridges were constructed as stone arches, also known as masonry or voussoir arches. Empirical rules were developed for dimensioning the shape of the arch and the wedge-shaped stones. The Romans were magnificent builders and many of their masonry bridges are still standing. Probably the most famous is the Pont du Gard at Nîmes in France (Figure 8.2), which was built shortly before the Christian era to allow the aqueduct of Nîmes (which is almost 50 km long) to cross the Gard River. The Roman architects and hydraulic engineers, who designed this bridge almost 50 m high with three levels, created a technical as well as an artistic masterpiece. Excellent descriptions of other great Roman bridges can be found in Steinman and Watson (1941).

In China, ancient stone arch bridges with many shapes and configurations are ubiquitous. The Zhaozhou Bridge (Anji Bridge) shown in Figure 8.3 completed in 605 AD is the first shallow segmental stone arch bridge, and the first open spandrel arch bridge in the world.

In the Middle Ages, only a few arch bridges were constructed in Europe, such as the Saint Bénézet Bridge (Pont d'Avignon) in France, the old London Bridge in England, the Pont Valentré in France, the Charles Bridge in Prague, Czech Republic and the Scaliger Bridge (Castelvecchio Bridge) in Verona, Italy. During the Renaissance, many arch bridges were built again in Europe, some notable bridges still



FIGURE 8.2 Pont du Gard Aqueduct, France. (Courtesy of Jure Radić.)

existing today and very famous are the Ponte di Rialto in Venice, Italy (Figure 8.4), the Ponte di Santa Trinita in Florence, Italy and the Pont Notre Dame and Pont Neuf in Paris, France. In 1676, the theory of arch design was derived by Robert Hooke who discovered the famous Hooke Law.

In the eighteenth century, iron was used in bridges. In 1779, the first cast iron bridge (Figure 8.5) was constructed at Coalbrookdale, England, across the Severn River with a semicircular arch spanning 43 m, heralding the beginning of a new era of arch bridge construction.

The nineteenth century was a century of advanced iron/steel bridges including arch bridges, suspension bridges, truss bridges, large cantilever bridges and viaducts, built for railway traffic. Eiffel designed two notable railway wrought iron two hinged sickle shaped arch bridges, the Maria Pia Bridge in Porto, Portugal with a span of 160 m and the 165 m span Garabit Viaduct across the Truyeres River at St. Flour, France. The Eads steel bridge at St. Louis is another notable arch bridge of this period, which comprises three 158.5 m spans. This bridge is notable not only for being the first steel bridge but also the first bridge in the world using the cantilever construction method.

In addition to steel, concrete is the other most important construction material for civil engineering works today. The emergence of concrete bridges was at the end of the nineteenth century. The weak-in-tension but strong-in-compression nature of concrete makes it perfectly suitable for arch bridges. In 1875, the first reinforced concrete (RC) arch bridge—Marquis of Tilière de Chazelet was designed by Monier.



FIGURE 8.3 Zhaozhou Bridge, China.



FIGURE 8.4 Ponte di Rialto in Venice, Italy.

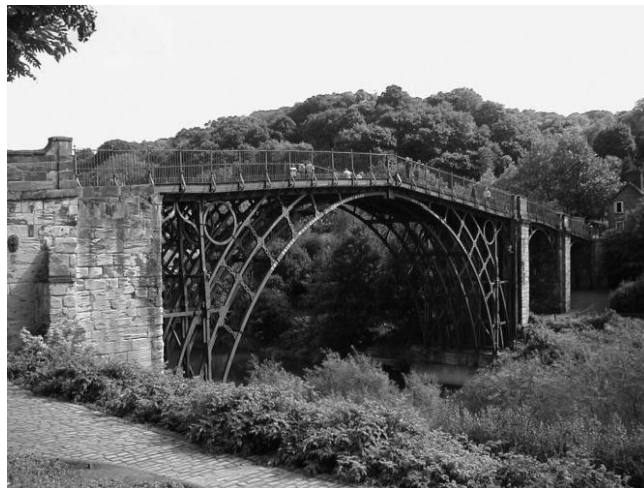


FIGURE 8.5 Iron bridge at Coalbrookdale, England. (Courtesy of Shozo Nakamura.)

With the booming development of railway and canal systems in the first half of the twentieth century, more and more bridges were built, especially in Europe. Most of the short and medium bridges were masonry arch bridges. Very few long-span arch bridges were built using masonry because they were not competitive with the new materials, iron, steel and concrete.

In the twentieth century, more and more concrete arch bridges were built. In 1904, Hennebique built the Risorgimento Bridge in Rome with a span over 100 m. Freyssinet designed a series of arch bridges in the first half of the twentieth century. A typical example is the Albert Louppe Bridge at Plougastel in France used for both highway and railway traffic. The main arch of the bridge is 31.5 inch height, 9.5 inch width and spans 180 m (net span of 172.6 m). He also contributed to the arch bridge construction method by employing hydraulic jacks in the crown to lift the completed arch from its false work. The arches designed in this period by Maillart should also be noted for their novelty and beauty (Billington 1985). Later on, the Martin Gil Viaduct with a span of 210 m in Spain was completed in 1942; and the Sandö Bridge with a span of 264 m in Sweden was completed in 1943.

With the development of concrete arch bridges, the application of steel arch bridges was also advanced. A major leap forward in steel arch bridge came with the construction of the Hell Gate Bridge in New York, which was a 298 m span half-through truss arch bridge supporting four railway tracks. This engineering masterpiece was designed by Gustav Lindenthal. At the beginning of 1930s, a further breakthrough in steel arch bridges was accomplished with the Bayonne Bridge with a main span of 503.6 m in New York (Figure 8.6) and the Sydney Harbor Bridge in Australia with a main span of 503 m.

In the last half of the twentieth century, the record spans of both the steel and concrete arch bridges were successively eclipsed. The New River Gorge Bridge in Fayetteville, West Virginia, completed in 1977, extended the world record of steel arch bridge span to 518.3 m. The primary structure of the bridge is a two-hinged truss arch, with a rise-to-span ratio of 1:4.6.

A few representative concrete arch bridges built in the second half of the twentieth century are the Arrabida Bridge over the Douro River in Porto, Portugal with a main span of 270 m completed in 1963; the Gladesville Bridge in Australia with a clear span of 305 m, completed in 1964; and the Amizade Bridge connecting Brazil and Paraguay with a span of 290 m, completed in 1965. In 1979, the span record for concrete arch bridges was broken by Krk I Bridge in Croatia (see Figure 8.7 with a main span of 390 m. It was built using the cantilever truss method. The cross-section of the arch consists of assembled precast elements with in-situ concreted joints.



FIGURE 8.6 Bayonne Bridge, New York/New Jersey. (Copyright Keith Pholpott. Photo courtesy of HDR.)



FIGURE 8.7 Krk I Bridges, Croatia. (Courtesy of Qingwei Huang.)

With the continuing economic development since 1980s, numerous bridges have been built, including a large number of arch bridges accompanying the development of material, construction methods as well as design theory. The Wanxian Yangtze River Bridge (Figure 8.8) is a concrete arch bridge with the longest span of 420 m in the world. An innovative construction method was used: a stiff three-dimensional arch steel truss frame, consisting of longitudinal steel tubes filled with concrete as the upper and lower chords, was erected over this span. The steel tubes served as the embedded scaffolding of the arch and held the cast-in-place concrete. More details of this bridge can be found in Section 8.5.4.

In 2003, the Lupu Bridge in Shanghai, China, crossing the Huangpu River, was opened to traffic. The main span of the bridge is 550 m, the longest span of an arch bridge in the world at that time (see Section 8.5.6 for more details). However, this record was broken again 6 years later by the Chaotianmen Yangtze River Bridge (Figure 8.9) with a main span of 552 m in Chongqing, China (Xiang et al. 2010). This bridge is a half-through tied arch bridge with double decks carrying six lanes of highway traffic on the upper level, and two reserved highway lanes and a two railway tracks on the lower level.

As the concrete filled steel tube (CFST) is efficient to sustain compression, it was first used in two arch bridges in the former Soviet Union in 1930s and 1940s. From 1990 to March 2005, 229 CFST arch bridges, with spans over 50 m, were built in China. Of these bridges, 131 bridges have a main span over 100 m and 33 of them span over 200 m. The current span record for a CFST arch bridge is held by the Wushan Yangtze River Bridge (Figure 8.10) with a span of 460 m (Chen and Wang 2009). The Hejiang Yangtze River No. 1 Bridge with a CFST arch span of 530 m will be opened to traffic in 2012.



FIGURE 8.8 Wanxian Yangtze River Bridge, China. (Courtesy of Tingmin Mou.)



FIGURE 8.9 Chaotianmen Bridge, China. (Courtesy of Zhongfu Xiang.)



FIGURE 8.10 Wushan Yangtze River Bridge, China. (Courtesy of Tingmin Mou.)

@Seismicisolation

8.1.4 Technical Trends

Arch was a main bridge type for a long time. However, as bridge technologies have advanced, more and more prestressed concrete (PC) girder, steel-concrete composite girder, and steel girder bridges have been constructed. Cable-stayed bridge technologies have also been fully mastered and implemented since the Second World War. Nevertheless, arch bridges are still very competitive, especially in mountainous areas. For example, the 323 m span concrete arch bridge at the historic Hoover Dam in the United States was completed in 2010. It is the fourth longest concrete arch bridge in the world and also the longest in North America (see Section 8.5.1 for more details). In Asia and Europe, many new long span arch bridges have been built in recent years with development of bridge technologies, especially in China in recent two decades (Chen 2009).

Fewer and fewer wooden and stone arches are built nowadays. New arch bridges are mainly constructed of steel, concrete, and steel-concrete composite. Steel arch bridges will continue to be built for heavily and dynamically loaded long span railway or road bridges and also for light loaded pedestrian bridges for aesthetics. The use of steel-concrete composites and the utilization of high performance concrete are two major advances in arch bridge design and construction.

8.1.4.1 Steel-Concrete Composite Arch Bridges

Modern arch bridges tend to have lightweight superstructures. The Skradin Bridge described in Section 8.5.2 has a span of 204 m, using a steel-concrete composite deck system, weighing only 22,910 tons, excluding foundations and abutments. This weight is 35% less than that of the previously built Maslenica Bridge which is a concrete arch bridge with a span of 200 m span and has the same roadway width of 20.4 m (Šavor et al. 2008).

Other bridges using steel-concrete composite deck system include the above-mentioned Colorado River Bridge (Section 8.5.1), the Wilde Gera Bridge in Germany, the Chateaubriand Bridge and the Morbihan Bridge in France (Šavor and Bleiziffer 2008), and the Fujikawa Bridge in Japan (Takahashi et al. 2000). Some bridges like the Second Svinesund Bridge connecting Norway and Sweden even use steel orthotropic deck systems to reduce the weight of the superstructure (Jordet and Jakobsen 2007).

Composite arches have less self-weight than arches of concrete or masonry materials, so construction is facilitated. The CFST arch bridge is one of the most remarkable implementations of composite arches in the last two decades in China. The steel tube not only supports the load together with the concrete, but also acts as the skeletal system during construction, thus simplifying and facilitating the construction (Chen and Wang 2009).

In China, research continues on a new steel-concrete composite arch by replacing concrete webs with steel webs (plates or trusses) in conventional concrete box arch. A series of concrete arch structures with steel webs have been proposed and studied at Fuzhou University in China since 2003. In this new type of steel-concrete composite arch, the arch box section is composed of upper and bottom reinforced concrete flanges and steel webs. The steel web may be corrugated plates, plain plates or tubular truss. Trial designs by employing real arch bridges as prototypes and experimental researches on arch models have been conducted. Research results show that the arch rib of the RC flange composited with steel web can be 30% lighter than the standard RC arch rib. At the same time, the construction is easier and faster because no web concreting is required (Chen and Mou 2008).

8.1.4.2 HPC and UHPC Arch Bridges

The application of high performance concrete (HPC) and ultra-high performance concrete (UHPC) to arch structures is a main development with regard to new materials. In a trial design research on a 600 m span concrete arch bridge by the Japan Society of Civil Engineers, C60 concrete was used for the arch ring (JSCE 2003). On the Barqueta Bridge in Spain built in 1992, which is an arch bridge with a main span of 270 m long, 43 m wide, the main arch rib is made of C75 concrete and the deck is made of C60 concrete. In 1996, as one of the 60 tenders for the Millau Viaduct project in France, Muller and



FIGURE 8.11 Wild Bridge, Austria.

Spielmann presented a concrete arch solution with a span of 602 m, in which C60 concrete was adopted (Muller 2001). A comparative study (Legeron et al. 2000) on a 110 m span arch bridge using C40 and C80 concretes shows that the costs are roughly the same but HPC is structurally more favorable. In the Los Tilos Bridge in Spain built in 2004, the main arch rib and the spandrels are all made of C75 HPC. In the Colorado River Bridge, the main span rib is made of 70 MPa concrete.

The use of UHPC in arch bridges has been a hot research topic recently. Research works on trial design of UHPC arch bridges spanning 432 m, 500 m, 750 m or 1000 m have been carried out in Croatia (Čandrlić et al. 2004). Chinese researchers are attempting to use reactive powder concrete (RPC) in arch bridges. Experimental research on two RPC arch models has been carried out to understand the structural behavior of RPC arch bridges (Du et al. 2010). At present, there are two UHPC arch bridges built in the world. One is the Sunyu footbridge in Korea with a main span of 120 m completed in 2002 (Huh and Byun 2005); the other is the Wild Bridge in Graz, Austria completed in 2009, which serves for load traffic. The Wild Bridge (Figure 8.11) consists of two foreland bridges and two UHPFRC segmental arches side by side with a span of 70 m. The halves of the arches consist of precast elements which were linked together by the use of external tendons. Half-arches were assembled vertically and swiveled into design elevation to connect together (Sparowitz et al. 2011).

8.1.4.3 New Structural Forms

Structural innovations for arch bridges have been continually conducted by bridge engineers; one effective way to create a new structure form is to combine an arch with other structural types. Tied arch or truss arch is a common arch composite structure, in conjunction with a girder or a truss. Almost all of other bridge structural types have been adopted or proposed to be used in conjunction with arches, such as the rigid frame continuous girder bridge, cable-stayed bridge as well as a suspension bridge. Arch supported stress ribbon bridge is a new structure formed by this method proposed by Strasky (2010). As the name implied, in such a bridge type the stress ribbon is supported or suspended on an arch. The two structures form a self-anchorage system where the horizontal force from the stress ribbon is transferred by inclined concrete struts to the foundation, balancing the thrust from the arch. In return, the arch helps to enhance the stiffness of the stress ribbon and decrease the sagging of the ribbon. Meanwhile, because of the light weight of the ribbon, thinner ribs and lower rise-to-span ratio can be used.

The structure formed by an arch and a stress ribbon looks artful and smoothly curved, which is competitive in scenic footbridges. Figure 8.12 shows the Svatka River Pedestrian Bridge in Brno, Czech Republic, in which a stress ribbon is supported on the concrete arch. The bridge was built in 2007,

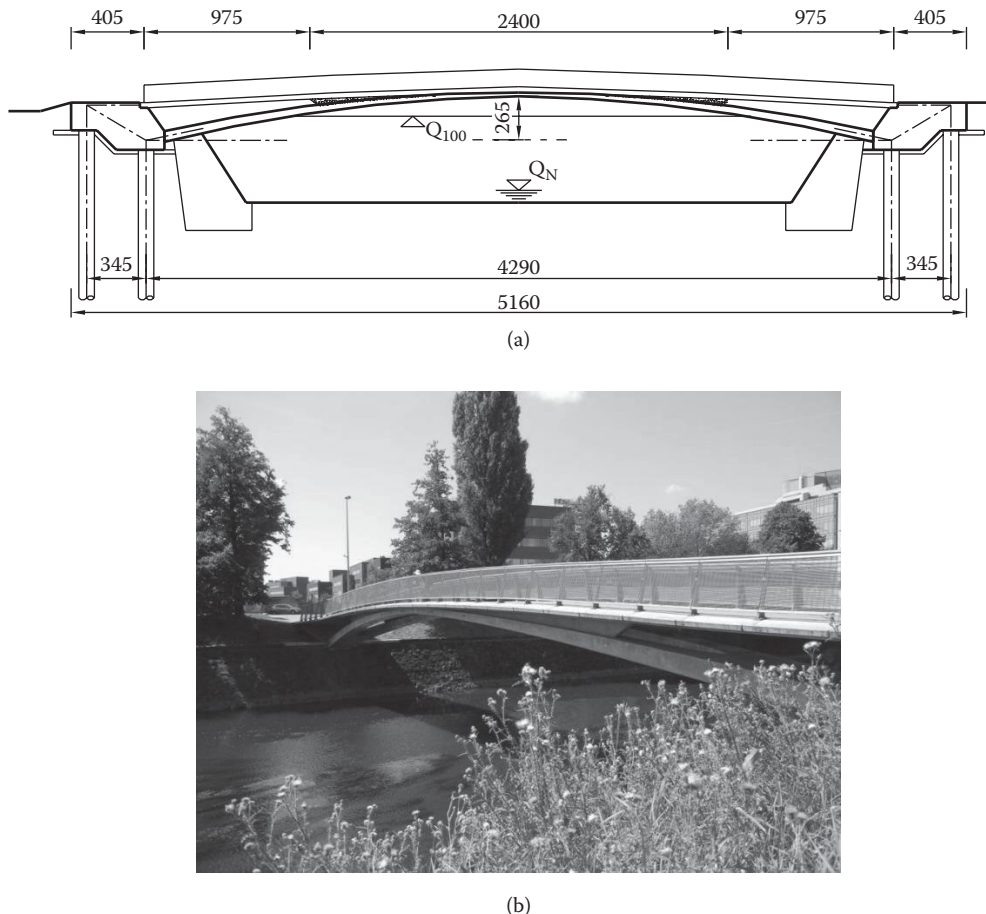


FIGURE 8.12 Svatka River Pedestrian Bridge in Brno, Czech Republic: (a) elevation (unit: cm) (Courtesy of Jiri Strasky) and (b) completed bridge.

has a span of 42.90 m with a rise to span ratio of 1:16.19. The arch is formed by two legs that have a variable mutual distance and merge at the arch springings. The 43.50 m long stress-ribbon is assembled of segments of length of 1.5 m and its central part is supported by low spandrel walls. The end abutments are located beyond the old stone riverbank walls, supported by pairs of drilled shafts. The rear shafts are stressed by tension forces, the front shafts are stressed by compression forces. This pair of forces balances a couple of tension and compression forces originating in the stress ribbon and the arch. Although the structure is extremely slender, and first bending frequencies are close to 2 Hz, the users do not have an unpleasant feeling when standing or walking on the bridge.

To combine different arch structures is another way to create a new structural form. An example is the Gate Bridge in Michigan, which is a modified tied arch combining the beauty of a true arch with the efficiency of a tied arch (Section 8.5.5).

8.1.4.4 Construction Technique

It is well known that the essential difficulty in arch bridge deployment is the construction works. Improvement in construction methods encourages engineers to design more challenging and elegant arch bridges. An interesting innovation is the *FlexiArch* for small span bridges, which consists of precast individual concrete voussoirs with tailored correct taper for a given span and rise connected by a polymeric membrane that forms an arch when lifted, thus no centering is needed in construction (Bourke et al. 2010).

Using CFST as embedded scaffolding in long span concrete arch bridges is an economic solution which was developed in China two decades ago. Another effective construction method for long span concrete arch bridges is the partial cantilever method. With this method, two partial half arches are erected by cantilever method, and the rest crown part is erected by embedded scaffolding method.

8.1.4.5 Preservation and Maintenance

There are many existing arch bridges built in ancient times, some of them are masterpieces in structures, architecture, and/or culture. The survived ancient bridges are all historic heritages and deserve protection. Assessing and maintaining of those ancient arch bridges is a big challenge to modern engineers.

From the last century till today, many arch bridges have been built in modern roadways and railways, utilizing various materials, concrete, steel, masonry or even stone. All of these bridges were expensively built and most of them are still in service. Therefore, inspection, evaluation, rating, repairing, strengthening and maintenance of those existing arch bridges have been becoming hot topics today. Those urgent needs and future trends have been discussed at a series of international conferences on arch bridges (<http://www.arch-bridges.cn>).

8.2 Types

Like other kinds of bridges, arch bridges can be classified in a number of ways (O'Connor 1971). From an engineering point of view, arch bridges can be classified on the basis of their structural arrangement.

According to the relative positions of the deck and the arch rib, arch bridges can be classified into either deck arch bridges, through arch bridge, and half-through arch bridges, as shown in Figure 8.13.

A deck arch bridge has its deck located above the crown of the arch (Figure 8.13a). This is the usual type of true arch bridge. It is the most common type of arch and is ideal for crossing a valley with sound rock walls.

The space between the deck and the arch is called spandrel. When the spandrel is filled with soil or other solid materials, the traffic loading is transmitted through this material onto the extrados of the arch. This type of arch is called filled spandrel arch or solid spandrel arch (Figure 8.1, left half). If there are openings in this space, then the arch is called an open spandrel arch (Figure 8.1, right half), in which the loads from the deck are transferred to the arch by struts, or spandrel columns.

In an open spandrel arch bridge, the deck may be simple or continuously supported on the spandrel columns, or rigidly connected to tall spandrel columns. If diagonals are added, the arch rib, deck, verticals and diagonals form a truss structure, called a braced spandrel arch or truss arch as shown in Figure 8.14a (Chen 2009). In the case when the horizontal girder at deck level meets the arch rib at the crown and is supported by straight inclined legs, this structure is called a rigid-frame arch, as shown in Figure 8.14b and c. It is convenient to use this type as an overpass with a shallow rise-to-span ratio, satisfying the clearance requirement for traffic underneath.

A through arch bridge has the bridge deck located at the springing line of the arch. Its thrust is generally absorbed by a tie rod or girder connecting the two ends of the arch, resulting in a tied arch bridge, also called a bowstring arch bridge or Langer girder bridge. It is usually adopted on sites with poor soil foundations. In a through arch, the loads from the deck are transferred to the arch through tension hangers. The tie rod is usually a steel plate girder, a steel box girder or sometimes a prestressed concrete girder. Depending on its stiffness, it is capable of carrying a portion of live loads. Whether a weak tie girder is

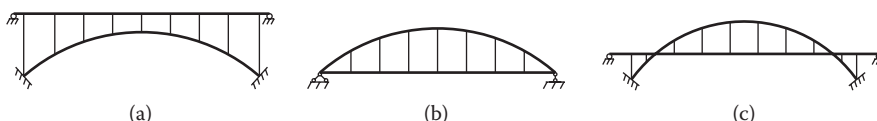


FIGURE 8.13 Classification of arch bridges by deck location: (a) deck arch bridge, (b) through arch bridge, and (c) half-through arch bridge

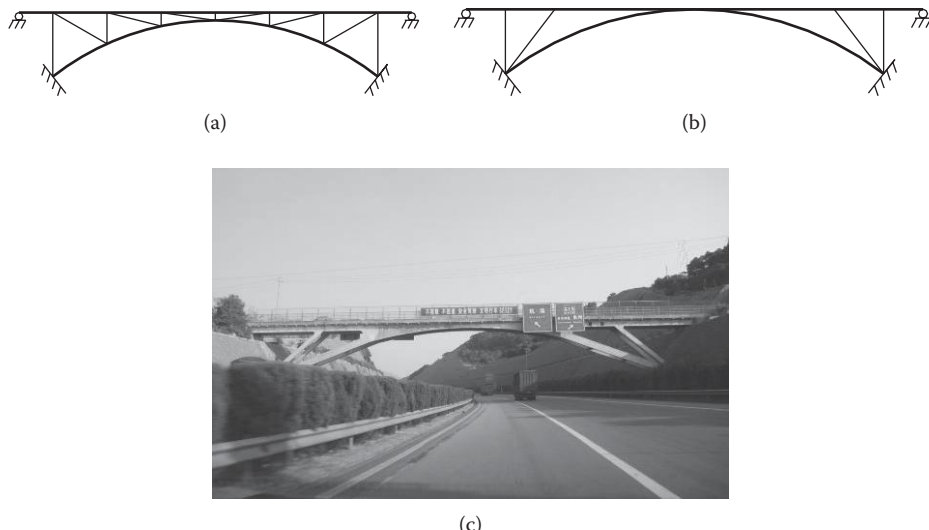


FIGURE 8.14 Braced spandrel arch and rigid-framed arch: (a) braced spandrel arch, (b) rigid-framed arch, and (c) photo of a rigid-frame arch bridge over a highway.

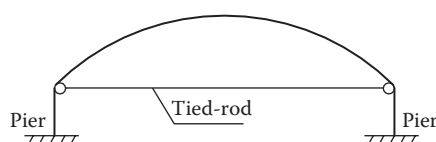


FIGURE 8.15 Through rigid-framed tie arch bridge (deck and hangers not shown).

used—usually in conjunction with a deep arch rib or a stiff deep tie girder is chosen instead, it is possible to optimize the size of the arch and the tie girder according to the desired aesthetic and economic goals.

Besides the traditional through arch bridge supported by bearings on piers or abutments, there exists another arrangement, called rigid-framed tied arch bridge (Figure 8.15), in which arch ribs are rigidly connected to piers to form a rigid frame, so that the arch ribs can be erected as in a true arch using cantilever cable-stayed method. High strength prestressed strands can be used as a tie rod to balance the thrusts of the arch ribs. The construction of this type of bridge is easier than that of a tied arch bridge. The trouble with the latter arises from the fact that the horizontal reactions cannot be taken up until the deck is finished.

A half-through arch bridge has a bridge deck located at an elevation between the crown of the arch and the springing line of the arch. It can be a true arch (Figure 8.13c) or a tied arch with flanking spans (Figure 8.16). The flanking span can be further classified as a cantilever arch (Figure 8.16a) or a half-through rigid-framed arch (Figure 8.16b). A cantilever arch is supported by bearings and tied by rigid girders. A half-through rigid-framed arch, nickname of flying-bird arch, is rigidly connected to the piers and tied by cables; an arrangement widely used in concrete filled steel tube (CFST) arch bridges in China.

Arch bridges can also be classified as three-hinged, two-hinged or hingeless arch bridges, based on the articulation of main arch, as shown in Figure 8.17.

A three-hinged arch allowing rotations at A, B, and C is a statically determinate structure (Figure 8.17a). A two-hinged arch allowing rotations at A and B and is indeterminate to one degree of freedom (Figure 8.17b). A hingeless arch, or a fixed arch (Figure 8.17c), cannot rotate at the supports A and B. A hingeless arch is indeterminate to three degrees of freedom. The arch's sensitivity to secondary effects, such as arch shortening and foundation settlement yielding of supports, and

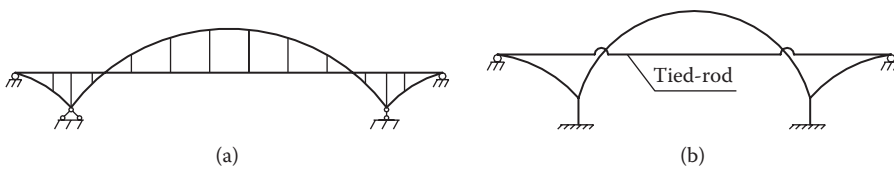


FIGURE 8.16 Half-through tied arch: (a) cantilever arch and (b) half-through rigid-framed arch (deck and hangers not shown).

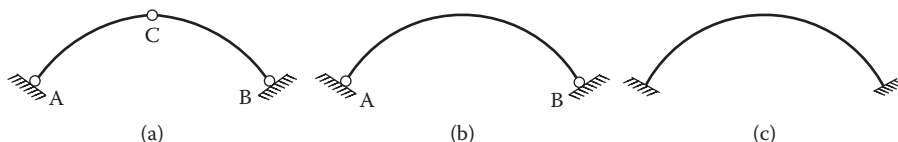


FIGURE 8.17 Classification of arches based on articulation: (a) three-hinged arch, (b) two-hinged arch and (c) fixed arch.

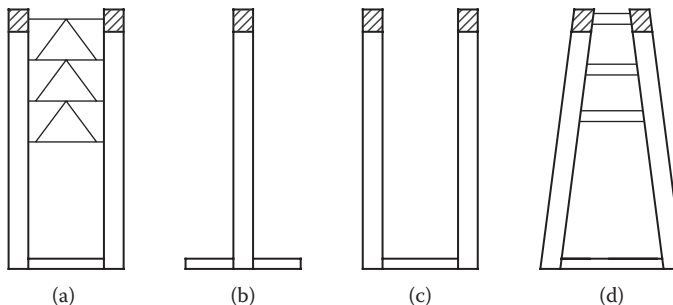


FIGURE 8.18 Classification of arch bridges by rib form in transverse direction: (a) parallel-rib arch bridge, (b) single-rib arch bridge, (c) open arch bridge and (d) basket-handle-like arch bridge.

temperature variations, increases with its degree of static indeterminacy, that is, with less hinges. Therefore, as hinges are added to the arches, the secondary effects tend to decrease or nearly vanish.

More steel arch bridges have been constructed with hinges than without them. During the early twentieth century, reinforced concrete arches, like steel arches, were often constructed with two or three hinges. These hinges ensure that the thrust line is on the arch axis and eliminate bending moments because of secondary effect caused essentially by shrinkage and temperature. However, hinges usually make the structure more flexible, increasing construction and maintenance costs, especially for stone and concrete arch bridges. Therefore, stone arch bridges are preferably fixed or hingeless and for same reasons modern concrete arch bridges are also generally designed without hinges.

Most arch bridges are constructed of two planes of vertical arch ribs connected by bracings in the transverse direction (Figure 8.18a). However, for through or half-through arch bridges, there are some bridges constructed of only one rib with roadways cantilevered on each side of the rib (Figure 8.18b), or as open arch twin ribs with no bracing (Figure 8.18c). In these two instances, the arch ribs should have sufficient out-of-plane stiffness or improved lateral stability by using stiff hangers in conjunction with the bridge deck system to form a half-frame in the transverse direction. There are arch bridges constructed of arch ribs tilted towards the crown (Figure 8.18d), called basket-handle-like arch bridge. This is done mainly because of aesthetic considerations, but it also increases the lateral stiffness of the arch bridge and could result in reduced bracing. Some examples in Section 8.5 are basket-handle-like arch bridge, such as the Gateway Bridge in Michigan and the Lupu Bridge in Shanghai, China.

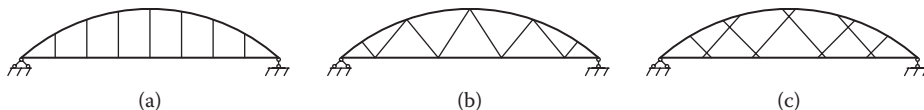


FIGURE 8.19 Classification of arch bridges by hanger arrangement: (a) vertical-hanger arch bridge, (b) nielsen arch bridge, and (c) network arch bridge.

Hangers in through or half-through arch bridges usually consist of wire ropes or rolled sections. They are usually vertical (Figure 8.19a), but truss-like diagonal hangers are also used, as shown in Figure 8.19b. Diagonal hangers result in smaller deflections and a reduction in the bending moments in the arch rib and deck. In addition, the diagonal hangers help to reduce the tendency of buckling in the arch plane. Accordingly, both the arch and the tie girder can be made more slender, optimizing configuration and saving materials. An arch with diagonal hangers is often called a Nielsen arch named after the engineer developed the underlying theory and founded a company of the same name. When each of the diagonal hangers crosses with others more than one time, the arch is also called a network arch (Figure 8.19c).

8.3 Design

There are many factors affecting the design of the general layout of an arch bridge. In general, these factors are related to function, cost economy, safety, aesthetics, traffic demand capacity, foundation conditions, erection procedure, under clearance requirements, and so on.

Arch bridges of various structural forms are applicable over a wide range of span lengths from a few meters for masonry arches to over 500 m for steel and CFST arches.

Spans of masonry arch bridges cover the range from a few meters for culverts to a maximum of 146 m of the New Danhe Bridge in China. Filled spandrel masonry arch bridges are suitable for spans smaller than approximately 20 m and may still be used in developing countries where labor work force is cheap, while for longer span bridges with open spandrel structure is likely obsolete to go out of adoption for new bridges due to expensive construction nowadays.

Concrete arch bridge can be used advantageously in the span range from 35 m to 200 m, though more than 40 bridges with a span over 200 m have been built and the longest one, the Wanxian Yantze River Bridge in China (Section 8.5.4) has a span of 420 m. The most common type of concrete arch bridges is the deck true arch with spandrel columns and girders, the arch can be either ribs or box ring, generally a fixed arch.

Steel and CFST arch bridges with their load-carrying bearing structures of higher strength materials have larger spanning capacity than masonry and concrete arch bridges. Spans of steel arch bridges cover the range from 50 m to 552 m, with either solid or truss ribs. Solid ribs are generally used for spans up to 230 m, while truss arches should be used for spans above 300 m, except in some special cases. Simultaneously, they allow the selection of more structural forms to suit various construction conditions. The small self-weight leaves a large room for innovation in structural form. Many footbridges with various novel arch structure forms have been built to achieve extraordinary aesthetical results, some successful and some less so.

Similar as in steel arch bridges, spans of CFST arch bridges also cover the range from 50 m to over 500 m. The economic spans for true deck arch, half-through true arch, fly-bird type arch, rigid-frame tied through type and tied arch are the spans up to 300 m, 260 m, 260 m, 160 m, and 120 m, respectively.

When an arch bridge crosses over a river, generally speaking, a large span is favored for a deep gorge, while multi-spans would be selected as the optimal solution for a wide flat river in which one or several main spans will cross over the main navigation channel, accompanied by other smaller span approaches.

There are four levels of elevation for an arch bridge, that is, the deck height, the intrados crown elevation, the springing elevation and the foundation base elevation (Figure 8.20). The design of an arch bridge is affected by appropriate selections of these elevations.

The deck elevation is controlled by the vertical profile of the roads or railway lines on both banks but the structure also must provide clearances dictated by stream flow and transportation vehicles. Once the deck elevation is determined, the extrados crown elevation can be obtained by subtracting the deck elevation by the superstructure depth.

The springing elevation is generally selected at a lower elevation to minimize the moment at the pier and/or abutment foundations and their bodies. However, the springing position is also dictated by the requirement of navigation clearance (Figure 8.21), flood, ice debris and other relevant considerations. In the selection of the arch elevations, the rise-to-span ratio of an arch is a very important parameter to consider, which is also a key parameter affecting the behaviors and aesthetics of an arch structure and will be discussed in the Sections 8.3.1 and 8.3.2.

There is no doubt that arch bridges are beautiful, functional, understandable and in expressive form. Long-span arch bridges over deep valleys have no competitors as far as aesthetics is concerned. Many of the masonry arch bridges built in the past 2000 years are located in cities whose residents consider these bridges not only necessary for traffic but also beautiful in appearance. Arch bridges have enriched their surrounding landscapes and even become emblems of their cities. Prime examples are the beautiful shallow steel arch—the Pont Alexandre III in Paris over the Seine River, the great Sydney Harbor steel arch bridge, and the modern Lupu Bridge in Shanghai.

Arch bridges remain popular structure types that are frequently adopted for modern bridges even though designers now have many more structural types to choose from. Many of them are built primarily for their elegant appearance and favored by designers and owners. With the passage of time, the beauty afforded by arches will probably continue to evolve.

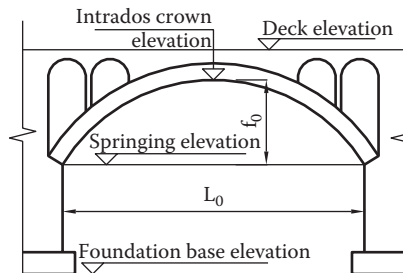


FIGURE 8.20 Arch bridge elevations.

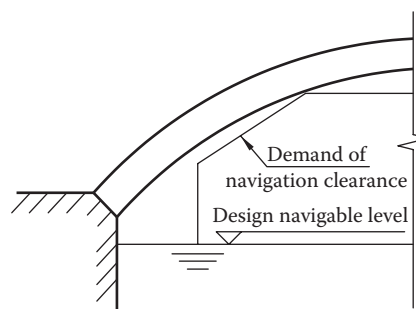


FIGURE 8.21 Clearance underneath.

The rise-to-span ratio is a key parameter in the arch configuration not only for structural behavior but also for appearance. From existing ancient arch bridges, it can be noted that high rise-to-span ratios and even semi-circular arches were commonly used in masonry arches. However, it is believed that a shallow arch is ambitious and the trend to design shallow arches continues until today. Typical historic bridges are the Pont Alexandre III (steel arch bridge) in Paris built in 1900 with a rise-to-span ratio of 1:17.62 and the Veurdre Bridge (concrete arch bridge) over the Allier River near Vichy, France built in 1910 with a rise-to-span ratio of 1:15. Modern shallow arch bridges are the Infant Henrique Bridge in Portugal with a rise-to-span ratio of 1:11.2 (Section 8.5.3); the Passerelle Léopold-Sédar-Senghor Bridge in Paris with a rise-to-span ratio of 1:15.14; and the Fourth Grand Canal Bridge in Venice (Figure 8.22) which has a rise-to-span ratio of 1:16. But large thrust of a shallow arch will cause significant horizontal movement of the abutments, such as in the Fourth Grand Canal Bridge in Venice; and reduce the rise of the arch, such as in the destroyed Veurdre Bridge in France. Moreover, a shallow arch also has the disadvantages of low rigidity, large deformation and significant vibration. Salonga and Gauvreau (2010) proposed a minimum practical limits of rise-to-span ratio of 20 to ensure that given arch designs behave efficiently on shallow concrete arches. Therefore, it should be noted by the designer that a shallow arch should have sufficient rise to display its strength, and a combined assessment to incorporating both appearance and structural behavior is needed when he attempts to design a very shallow arch.

With the development of computer technology and its applications to structural analysis, various challenging arch shapes have turned up in practice that previously perhaps may have been imagined but were impossible to design. With every advance in arch design and construction, more and more advantages of arches are known. The arch has regained its prior eminence in more and more designers' eyes.

The Bac de Roda-Felippe II Bridge (Figure 8.23) in Barcelona designed by Santiago Calatrava is a steel arch bridge with two pairs of inclined arches carrying traffic lanes crossing over a railway. The twin arches have enough rigidity for stability without bracing over the travel lanes, giving an open view for drivers, while the twin arches on each side appear as a gate and provide a well-defined space for pedestrians to walk and rest.

As mentioned in Section 8.2.3, it is functional to tilt two arch ribs toward each other to form a stable spatial structure—basket-handle-like arch (Figure 8.15). Contrary to this structure, however, there is a current trend to tilt arches outward to form nontraditional, surprising structures. The arch spatial stability is generally provided by cable hangers tied from the arch to a rigid bridge deck system. One example is the Dagu Bridge in Tianjin, China, designed by T. Y. LIN International China. It consists of two outward inclined arches without bracing, forming one integrated structure in antiphony. The two arches, one big and one small, symbolize the Sun and Moon, respectively (Figure 8.24) (Ma 2010).

Outwardly inclined arch may give a showy and dramatic effect because of their shapes and angles not normally seen in bridges. At the same time an additional budget may be needed because the increase of structure material consuming and the difficulty in construction because of the complexity of the structures. Fortunately, this arrangement is usually used only for small span steel arch ribs to resist light



FIGURE 8.22 Fourth Grand Canal Bridge in Venice, Italy.



FIGURE 8.23 Bac de Roda-Felipe II Bridge in Barcelona, Spain.



FIGURE 8.24 Dagu Bridge in Tianjin, China. (Courtesy of Zhendong Ma.)

loads such as in pedestrian bridges. If the appearance and aesthetics of a bridge are very important and the increased costs are limited and acceptable, variant arches may be considered. But they should not be used excessively, or for long spans or for heavily loaded bridges, because the likely result would be very expensive but not exactly beautiful bridges.

An arch may also be used as a pylon of a cable-stayed bridge. In the Haneda Sky Arch at Tokyo International Airport completed in 1993, a large steel arch is employed as a pylon to anchor stayed cables to support two road decks. The arch resembles a gate and may provide a key focal point for the newly expanded airport (Figure 8.25).

Besides the span, the rise-to-span ratio is another very important parameter of an arch. It may vary widely because an arch can be very shallow or, at the other extreme, a semi-circle. The rise of a deck arch would generally be controlled by the under-deck clearance requirement (or the shape of the obstacle) as mentioned in the previous section, while the rise of a through and half-through arch need to consider the clearance beneath the bracings of arch ribs for the traffic over the bridge deck.

A small ratio or a flat arch will develop relatively large compressive forces in the arch, which is beneficial for arch made of massive construction materials like stone and concrete. Nevertheless, the large horizontal thrust necessitates large costly abutments unless the rock foundation soil is rock, allowing for relatively simple foundations. At the same time, the dominant compressive forces will be reduced in statically indeterminate structures because the stresses caused by temperature, shrinkage, and elastic shortening are relatively large. Some typical extreme shallow arch bridges are described in Section 8.3.2.



FIGURE 8.25 Haneda Sky Arch at Tokyo International Airport, Japan.

Conversely, an arch with a large rise-to-span ratio develops relatively smaller less horizontal thrust but large bending moments because of increased arch length and, self-weight and structure behaviors. Therefore extreme ratios are not favored. From economic and structural points of view the rise-to-span ratio should generally be in the range of 1:2–1:10, but more commonly between 1:3 and 1:6.

Numerous arch axes have been employed in arch bridges, such as circular (semicircular, segmental or compound circular), elliptical, (second order) parabolic, (inverse) catenary, and even polygonal if necessary.

A perfect arch, in which only a compressive force is acting at the centroid of each section of the arch, is theoretically possible only for a special loading condition. Three common perfect arches with three-hinges are a circular arch subjected to a radial uniform load, a parabolic arch subjected to a vertical uniform load, and a catenary arch subjected to a varying load density in direct proportion to the axis curve elevation y .

However, it is practically impossible to have a perfect arch in bridge structures. The arch bridge is usually subject to multiple loadings or actions (dead load, live load, temperature, support settlements, etc.), which will produce bending stresses in the arch rib in addition to the axial compressive stress. For a two-hinged arch and a fixed arch, although the shape and loading are similar to a three-hinged arch, the bending moment cannot be completely avoided because the elastic deformation of the arch under compression causes shortening of the arch axis leading to additional bending moment in the arch. Therefore, in bridge design, an arch shape or axis is generally chosen in such a way that the structure is subjected to predominant compression under permanent loads (especially in masonry and concrete arch bridges in which the permanent load is predominant) or permanent loads plus half of the live load. The general practice in design is to make let the arch axis coincide with the thrust line of the design loads. The most popularly adopted arch axes in modern arch design are circular, parabolic, and catenary.

A simple circular shape is easily configured. Still, the axis of a circular arch differs significantly from the permanent thrust line, which causes non-uniform stresses along the rib. This is the reason why circular arch axes are only used in bridges with small spans of less than 20 m.

The parabolic arches are widely used in bridges where the permanent load distribution is nearly uniform, such as in steel arch bridges, through or half-through arch bridges with flexible hangers and spandrel columns.

In filled spandrel arch bridges, the permanent load density increases continuously from the crown to the springing, as shown in Figure 8.26. The load at any point along the arch, g_x , can be expressed as $g_x = g_d + \gamma f$. When x is approaching the springing location, this equation becomes

$$g_j = g_d + \gamma f = mg_d \quad (8.2)$$

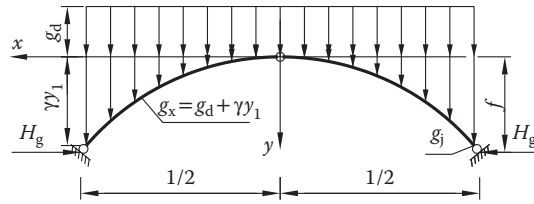


FIGURE 8.26 Permanent load distribution along filled spandrel arch bridge.

where g_j is the permanent load at springing; g_d is the permanent load at crown; γ is the density of spandrel filling materials per unit height; f is the rise of the arch; and m is the arch axis parameter, $m = g_j/g_d$.

The load density at any point is

$$g_x = g_d + (m-1) \frac{g_d}{f} y_1 = g_d \left[1 + (m-1) \frac{y_1}{f} \right] \quad (8.3)$$

where y_1 is the vertical coordinate originated from the crown.

For a perfect arch, the moment in any cross section is zero, therefore

$$y_1 = \frac{M_x}{H_g} \quad (8.4)$$

where H_g is the horizontal thrust.

The second order derivation of Equation 8.4 leads to

$$\frac{d^2 y_1}{dx^2} = \frac{1}{H_g} \cdot \frac{d^2 M_x}{dx^2} = \frac{g_x}{H_g} \quad (8.5)$$

Substituting Equation 8.3 into Equation 8.5, and for simplification, introducing $x = \xi l_1$, or $dx = l_1 d\xi$, then

$$\frac{d^2 y_1}{d\xi^2} = \frac{l_1^2}{H_g} g_d \left[1 + (m-1) \frac{y_1}{f} \right]$$

Let

$$k^2 = \frac{l_1^2 g_d}{H_g f} (m-1) \quad (8.6)$$

Then

$$\frac{d^2 y_1}{d\xi^2} = \frac{l_1^2 g_d}{H_g} + k^2 y_1 \quad (8.7)$$

By solving Equation 8.7, the arch axis equation can be obtained as

$$y_1 = \frac{f}{m-1} (\operatorname{ch} k \xi - 1) \quad (8.8)$$

It is a catenary curve.

At springings where $\xi = 1$ and $y_1 = f$, then from Equation 8.8, $\operatorname{ch} k = m$. The value m is usually known; then, k can be solved by

$$k = (\operatorname{ch})^{-1} m = \ln(m + \sqrt{m^2 - 1}) \quad (8.9)$$

Therefore, the catenary arch axis is a group of curves with different values of m . If $m = 1$, then $g_x = g_d$, which represents a uniform permanent load distribution. In this case, the perfect arch axis is parabolic curve.

The continuously curved arch axis is statically ideal where the load is distributed continuously along the arch. However, in an open spandrel arch, the dead load of the spandrel structures is applied to the arch as a series of concentrated loads transferred by the spandrel columns. In that case, even when only the dead load is considered, a continuous load distribution is not possible for a perfect arch. Therefore, polygonal axis arches are sometimes used, such as in the Wild Bridge (Figure 8.10) and the Infante Dom Henrique (Figure 8.59). The bending moment induced from the hanger or spandrel columns is less in a polygonal arch than in a continuous curved arch. However, a polygonal arch is aesthetically inferior to a continuous arch, especially when the span length is small, hence it is not commonly used nowadays.

If the spandrel girders have small spans and the spandrel columns are spaced at short distance, the dead load can be approximately considered as continuously distributed. If hangers or light spandrel columns are used, a parabolic arch axis may be adopted because the dead load distribution is approximately uniform, while if the self-weight of the spandrel columns is heavy and occupies a large portion of the total dead load, a catenary curve may be selected.

In current design practice, it is possible (e.g., by computer) to configure an arch axis, such as splines, a four or even higher order parabola or a compound curve, to optimize the force distribution and to minimize the arch bending moments in the arch under superimposed loads.

The cross section of an arch can be uniform or non-uniform. The former is easier to fabricate and construct, therefore widely used; whereas the latter can save materials and will be economical for a long span. The shape of the cross section often depends on the material used.

8.3.1 Masonry Arches

Masonry arches generally have a solid slab section. There exist several empirical formulae for determining the thickness of arch ring or rib. The one given in Equation 8.10 is widely used in China to estimate the depth of the stone arch ring in highway bridges with spans less than 40 m.

$$d = k_1 k_2 \sqrt[3]{l_0} \quad (8.10)$$

where d is the depth of the arch ring with the unit of cm; l_0 is the clear span of the arch rib with the unit of m; k_1 is a factor related to the rise-to-span ratio, usually between 4.5 and 6, large value for shallow arch; k_2 is a traffic load factor; $k_2 = 1.4$ for Class I Highway Traffic and $k_2 = 1.2$ for Class II Highway Traffic by Chinese design code, which can be found in Chen and Wang (2009).

8.3.2 Concrete Arches

Concrete arches usually have two individual ribs connected together by lateral bracings. The rib cross section may be solid rectangular section, I section or box section, as shown in Figure 8.27. Solid sections are only employed in relatively short span bridges; while box sections are often used in long span bridges because of its high rigidity and capacity to resist bending and torsion, such as the two box arch ribs in the American Colorado River Bridge (see Section 8.5.1 for more details).

Concrete arch section may also have a single box with several cells like the Krk I Bridges (Figure 8.6) and the Wanxian Yangtze River Bridge (Figure 8.7). Figure 8.28 illustrates a three-cell box cross-section.

For large span concrete arches, non-uniform cross sections are usually employed. The depth of the arch is generally optimized according to the changing compressive force along the ring so that it is

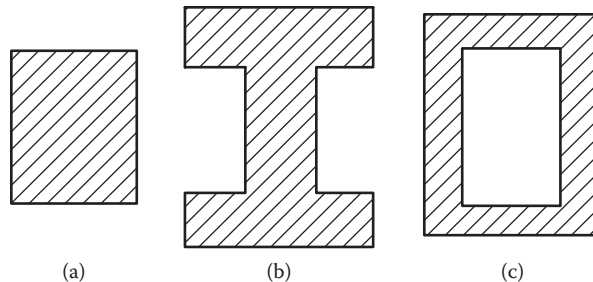


FIGURE 8.27 Cross sections used in RC arch bridge ribs: (a) rectangular section, (b) I-shaped section and (c) box section.

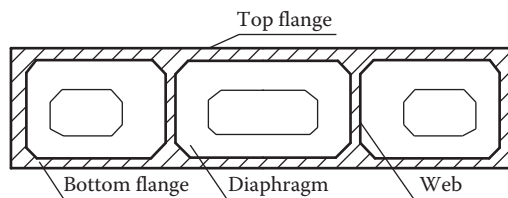


FIGURE 8.28 Three-cell box cross section.

relatively larger at springings and decreases gradually toward the crown. In China, the empirical depth of concrete arches is determined as follows:

- Hingeless deck arch: about $1/29$ – $1/75$ of the span at springings and about $1/44$ – $1/75$ of the span at crown
- Tied arch (Langer girder): about $1/59$ – $1/122$ of the span at springings and about $1/59$ – $1/112$ of the span at the crown
- Half-through hingeless arch: about $1/34$ – $1/67$ of the span at springings and about $1/34$ – $1/80$ of the span at the crown

8.3.3 Steel Arches

A steel arch usually consists of either solid ribs or truss ribs and bracings. The cross section shape of the ribs is usually I-shaped, circular, box, or else, made up of steel plates. Stiffening members are required for steel arch ribs to avoid local buckling under dominate compression forces.

Solid steel ribs are mainly used in arches spanning less than 200 m. For very small spans, I-shaped sections may be more cost effective than box sections, however the development of welding technologies has made boxlike sections with large flexural and torsional stiffness more viable, so I-section arch ribs are rarely used in modern steel arch design while the welded box members are widely used. Today even for steel arch bridge with spans exceeding 200 m, solid box may be used in arch rib as in the 550 m Lupu Bridge in China (Section 8.5.6).

A circular section is closed with isotropic behavior. The peripheral distribution of steel maximizes the radius of gyration, which is advantageous for resistance to both compression and torsion. It is favored to be used in windy areas such as offshore or mountainous valley because a circular section rib effectively reduces wind pressure.

The depth of a uniform solid steel arch rib is usually between $1/25$ and $1/80$ of the span length and a normally range is $1/70$ and $1/80$ (Konishi 1981; Wright and Brunner 2006). This value generally decreases with the increase of a span. For a tied arch whose bending moment is partially held by the

tie rods, the depth can be suitably reduced. If deep tie rods are employed, the depth of a solid steel arch rib ranges from 1/140 to 1/190 of the span (Wright and Brunner 2006). In a non-uniform section arch rib, the depth can be reduced towards the hinges in hinged arches and toward the crown in fixed arches.

Truss ribs can be more effectively used in arch bridges and are preferred when the arch span exceeds 200 m. Members in truss ribs are smaller and lighter than those in solid section ribs, therefore, they facilitate delivery and erection. Out of the five steel arch bridges with a span over 500 m, four of them are truss rib bridges, that is, the Sydney Harbor Bridge, the New York's Bayonne Bridge (Figure 8.5), the New River Gorge Bridge and the Chaotianmen Bridge (Figure 8.8). The depth of a truss arch are generally between 1/25 and 1/50 for both a true arch or a tied arch because the ties has little effect on depth of truss arch required except the tie members are also truss structure (Konishi 1981; Wright and Brunner 2006).

In an indeterminate arch, if the depth is too large, then the thermally induced stress increases. At the same time, deflection related extra stresses decrease. Once the rise-to-span ratio is determined, by calculating the maximum stress at 1/4 span caused by main loads, the appropriate depth of the cross section can be roughly determined (Konishi 1981).

8.3.4 CFST Arches

Similar to the ribs in steel arches, the ribs in a CFST arch are solid or trussed. The two main types of solid sections are the single tube section and the dumbbell-shaped section. A dumbbell-shaped rib is formed by connecting two CFST tubes with two steel web plates, as shown in Figure 8.29.

Generally, a single tube section is suitable for short span bridges. For a steel tube rib with a diameter of 600–800 mm, the maximum span should not exceed 80 m. Dumbbell-shaped section ribs are widely used in bridges with a span of about 100 m, but no longer than 160 m.

The depth-to-span ratio of a dumbbell-shaped CFST arch is generally between 1/30 and 1/60. The rib depth to tube diameter ratio ranges between 2.11 and 2.67 but usually close to 2.5. Similar to the I-shaped section, the dumbbell-shaped section has larger bending moment resistance compared to single tube section. Since the rib depth to tube diameter ratio is only around 2.5, the contribution of flexible stiffness of the chord tube to the whole section cannot be omitted, it is not to be treated as a truss section.

For spans above about 120 m a truss rib is likely to be economic which is composed of CFST chords and hollow tube web members. The rib can be composed of three, four or six CFST tubes. The four-tube truss is usually used, as shown in Figure 8.30, while three-tube or six-tube trusses are seldom utilized.

For a CFST arch bridge spanning less than 300 m, the rib depth of a four-tube truss rib can be initially sized by Equation 8.11.

$$H = k_1 \cdot k_2 \cdot \left[0.2 \left(\frac{l_0}{100} \right)^2 + \frac{l_0}{100} + 1.2 \right] \quad (8.11)$$

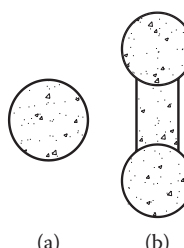


FIGURE 8.29 Solid rib sections of CFST arches: (a) single tube and (b) dumbbell shape.

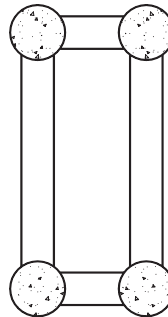


FIGURE 8.30 Cross-section of CFST four-tube truss arch rib.

where H is the depth of the cross section in meters; l_0 is the design rise of the arch in meters; k_1 is the traffic load factor, which is 1.0 or 0.9 for Class I and II Highway Traffic by Chinese design code, respectively. The traffic load grading can be found in Chen and Wang (2009); k_2 is the traffic lane factor, which is 0.9, 1.0, or 1.1 for decks with 2–3 lanes, 4 lanes or 6 lanes, respectively.

The rib width is related to its depth, which is usually between 0.4 and 1.0 of the depth. Lower values are used for greater depths.

Bracings of rib arches are used to ensure the monolithic structural response to lateral actions. Bracings of large dimensions and arranged in small spacing are helpful to ensure the global out-of-plane stability of the arch, as well as the local buckling of the arch rib between two adjacent bracing members. However, it is aesthetically less attractive. It is easy to arrange the bracing system in a deck arch. However for a through or half-through bridge, the clearance requirement for the carriageway affects the bracing arrangement. At the same time, low bracings are not esthetically pleasing and result in awkward feeling to travelers. In modern times, designers tend to use fewer bracing members at large spacing to improve the bridge appearance. Hence, the placement of the bracing members should be optimized to ensure high efficiency. Research and much experience prove that the bracing arrangement is more important than the bracing number.

For a low arch, three bracing members may be enough to provide the needed stiffness. Out-of-plane buckling shape of an arch bridge is normally in a half-sine curve. The stiff bracing at the crown should have a large flexural stiffness to efficiently restrict the arch rib from torsion, as illustrated in Figure 8.31. In the sloping parts, for example 1/4 span between the crown and springing, the bracing with diagonals, like K-shape or X-shape system, has a large flexural stiffness in the transverse direction to resist the shear deformation of the arch ribs as shown in Figure 8.32. The bracing system of the Second Highway Bridge over the Yellow River in Zhengzhou, China (described in Section 8.5.8) follows this principle.

In long span bridges, more bracing members are needed. The bracing can be X-shaped or K-shaped (Figure 8.33), diamond-shaped (Figure 8.34) and Vierendeel typed (Figure 8.35), which is formed by either diagonal and/or straight transverse members. It is obvious that bracing systems with diagonal members, like K-shape, X-shape or diamond shape, are more effective than the Vierendeel typed (only straight members) bracing system. However, the latter is esthetically favorable. Therefore, it is necessary to carefully design bracings to balance the aspects of safety and appearance.

A three-hinged arch (Figure 8.17a) is statically determinate and can be analyzed easily by hand structural mechanics to obtain the support reactions, the internal forces and deflections under dead load or live load.

A two-hinged arch is statically indeterminate to the first degree and therefore has one redundant reaction. With the force method, the structure is firstly made determinate by freeing the right horizontal support and letting it move horizontally, as shown in Figure 8.36. The horizontal deflection Δ_{1p} at the

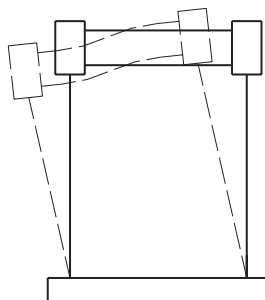


FIGURE 8.31 Section view of out-of-plane buckling.

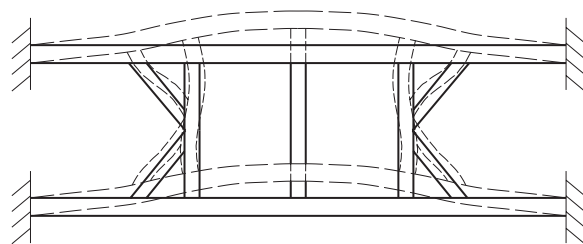


FIGURE 8.32 Plane view of out-of-plane buckling.

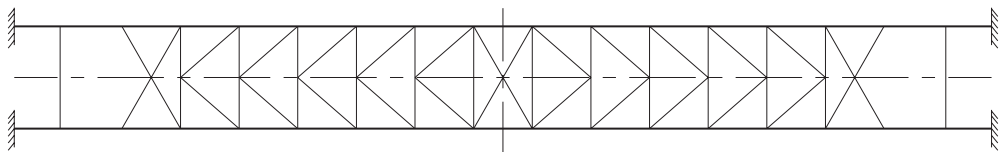


FIGURE 8.33 K type bracing.

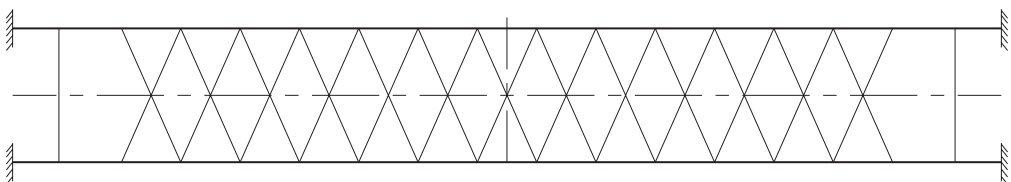


FIGURE 8.34 Diamond type bracing.

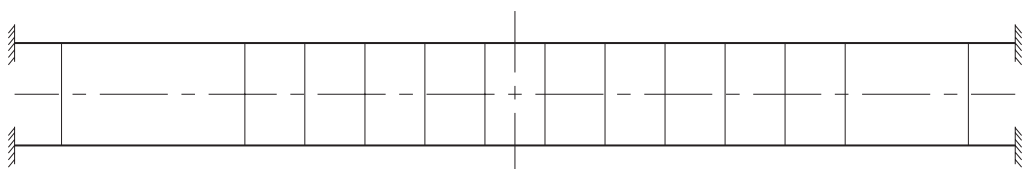


FIGURE 8.35 Vierendeel type bracing.

@Seismicisolation

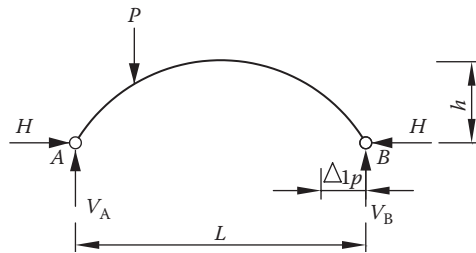


FIGURE 8.36 Basic structural model of a two-hinged arch.

support is then calculated with the applied loads. Next the horizontal deflection δ_{11} at the support is calculated for a horizontal force of $N = 1$ acting at the support. Since the sum of these two deflections must vanish, then the total horizontal reaction H at the support for the applied loading must be

$$H = -\frac{\Delta_{1p}}{\delta_{11}} \quad (8.12)$$

Having the horizontal reaction the moments and axial forces in the arch can be calculated. A good example of early design procedures for a tied two-hinged arch can be found in “Design of St. Georges Tied Arch Span” (Carrelts 1942; Karol 1942). The bridge was completed in 1941. It spans the Chesapeake and Delaware Canal and was the first of its type in the United States to have a very stiff tie and shallow rib. While this design procedure may be crude compared with modern methods, many fine arches were constructed following this method.

A fixed arch is three times statically indeterminate. In general, the analysis is also done by using the force method. Cutting the arch at the crown and taking cantilever curved beams as the basic structure, some coefficients to the redundant forces are zero because of the symmetry of the structure, that is, $\delta_{13} = \delta_{31} = \delta_{23} = \delta_{32} = 0$. Removing the redundant forces to a distance y_s from the crown to the end of a rigid bar as shown in the Figure 8.37, the other two coefficients to the redundant forces should also be zero, that is, $\delta_{12} = \delta_{21} = 0$. Therefore, only one redundant force remains in one equation as shown in Equation 8.13, which simplifies the computation.

$$\left. \begin{aligned} \delta_{11}X_1 &= \Delta_{1p} \\ \delta_{22}X_2 &= \Delta_{2p} \\ \delta_{33}X_3 &= \Delta_{3p} \end{aligned} \right\} \quad (8.13)$$

where δ_{ij} is the deflection at location i , caused by unit force X_j ($i, j = 1, 2, 3$); and Δ_{ip} is the deflection at location i , caused by exterior load P ($i = 1, 2, 3$).

For a symmetric arch, the distance of the rigid bar from the crown can be calculated by Equation 8.14.

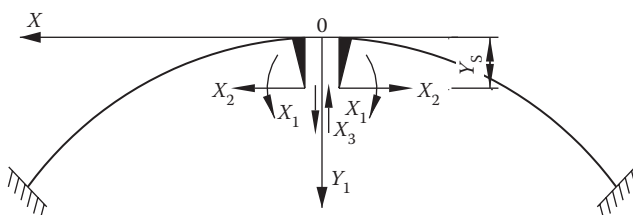


FIGURE 8.37 Decomposition of a hingeless arch in force method analysis.

$$\gamma_s = \frac{\int_s \frac{y_1 ds}{EI}}{\int_s \frac{ds}{EI}} \quad (8.14)$$

Further calculation can be carried out using the method described in textbooks on structural analysis. The stressing mechanism in arch bridges is complicated, even though simplifications such as those mentioned above are available. Calculation by hand is still very complex and therefore calculation graphs and tables are often used in engineering practice.

Modern analysis, of course, utilizes finite element computer programs (for information on finite-element method refers to Structural Theory in Chapter 7 and Nonlinear Analysis in Chapter 36 of this Handbook). For stocky arches such as short span masonry or concrete arches, the first-order deflection or linear analysis can be accurate enough, while geometric nonlinear analysis is necessary for long span slender steel arches. A nonlinear analysis procedure with accompanying computer programs on disk is available in Levy and Spillers (1995). Karol (1942) derived an approximation formula for calculating the geometric nonlinear influence values for the horizontal forces in arches, which depend on the rise-to-span ratio only.

In the same discussion paper, an approximation formula for the distribution of the total moment between the tie and the rib depending only on the depths of the rib and the tie girder was also proposed. These formulae are very useful in preliminary design of a tied arch and preparing input information for finite element analysis.

Since the arch rib of an arch bridge is subject to high axial compression, the possibility of buckling failure should not be ignored. According to the equilibrium paths, an arch losing its stability, or buckling, generally corresponds to either a bifurcation point or a stability limit point.

For a perfect arch or a slender arch with predominately compressive forces under symmetrically uniformly distributed load, buckling tends to occur at a bifurcation point, which is similar to overall buckling of a column. Therefore, the buckling of such an arch is usually analyzed as an equivalent column with an effective length. The stability of elastic arches is presented handled very well in Galambos (1998) with tabular values to calculate critical buckling loads for arches with different cases of loading and arch configurations. As an example, the critical in-plane buckling load for a two-hinged parabolic arch rib supporting a uniform vertical deck load distributed on a horizontal projection will be calculated as follows:

Arch span: $L = 120$ m

Arch rise: $S = 24$ m

Rise-to-span ratio = $24/120 = 0.2$

Rib moment of inertia: $I = 7.6 \times 10^9$ mm⁴

Modulus of elasticity: $E = 20 \times 10^4$ N/mm²

Horizontal buckling force:

$$H = c_1 \frac{EI}{L^2}$$

Uniform load causing $q = c_2 \frac{EI}{L^3}$ buckling:

From Table 17.1 of Galambos (1998), $C_1 = 28.8$ and $C_2 = 46.1$, and then

$$H = \frac{28.8 \times 20 \times 10^4 \times 7.6 \times 10^9}{(120 \times 10^3)^2} = 3.04 \text{ MN}$$

$$q = \frac{46.1 \times 3.04 \times 10^3}{28.8 \times 120} = 40.55 \text{ kN/m}$$

The above calculation of critical loads is valid for in-plane arch buckling which under the assumption of adequate bracing between ribs to prevent out-of-plane buckling. No restraint from the deck is considered in the calculation. If the deck is taken into account, the critical buckling load will increase.

It is now quite easy to get the elastic buckling loads by using the eigenvalue analysis method in finite element programs. For a real arch, however, the elastic buckling load is only the upper limit of the ultimate load since geometric and material imperfections are unavoidable. The action in the cross section of an arch is usually a combination of axial compression and bending moment, not compression only. Concurrently, the material of an arch may reach also become inelastic range prior to elastic before buckling. Moreover, the geometric nonlinearity must be considered for slender arches at large deflections. Therefore, both material and geometric nonlinearities need to be considered in some cases. No doubt this will increase the complexity and difficulty of hand calculation. Therefore, the utilization of the finite element method has become very popular nowadays. Various nonlinear finite element methods have been developed to analyze a variety of problems and can be found in textbooks on bridge engineering, for example (Xanthakos 1994).

An arch, especially a narrow arch, subject to in-plane loading would also buckle with a deformation out of its original plane, namely out-of-plane buckling or spatial buckling, while the material stays elastic. Similar to in-plane buckling, out-of-plane buckling of an arch may also analogous to columns buckling. Again, the eigenvalue analysis method by computer programs can be used. However, it is hard to predict accurately the load-carrying capacity considering the out-of-plane stability of a real arch as it is affected by too many factors. In design practice, a safety factor is generously selected as high as 4–6.

Arch bridges can be of single span or with multiple spans. Single-span bridges are usually adopted to cross over valleys by making use of the strong rock foundation on both banks; multi-span bridges have piers.

The piers for tied arch bridges are similar to those for girder bridges. However, the piers for true arch bridges have to be larger enough to ensure greater stiffness, strength and stability to resist the horizontal thrust in addition to vertical loads. If it is a fixed arch, additional moments must also be considered as well. The piers are usually made of stone, concrete or reinforced concrete. The structure and shape of piers depend on geological, hydrological conditions of the site, and the type of arch, span length, rise-to-span ratio, load and construction method adopted.

If the adjacent two spans are symmetric then the pier need only balance the thrust caused by live loads. Otherwise, stronger interchanging piers must be used as shown in Figure 8.38c. When there are three or more spans, to avoid the risk of progressive collapse of arches and for construction convenience, there needs to be an extra-strong pier every several spans to resist the horizontal thrust from a given direction because of asymmetric conditions. This kind of pier is a single direction thrust pier.

The most commonly-used pier in arch bridges is gravity, or solid pier, which balances external actions and keeps the stability by its own gravity. A gravity pier is composed of the cap, pier as well as the footing, as shown in Figure 8.38.

The pier cap supports the arch springing with its oblique plane normal to the arch axis. It must be sufficiently strong, and sometimes multiple reinforcement layers are used to resist diffuse the localized action. To reduce the shaft volume, the pier cap is sometimes raised a bit and called a cantilever pier cap. The pier body generally is made of masonry or plain or concrete, based on the shallow shaft foundation or caisson foundation.

Different from the gravity pier, a frame pier is sometime used in small span arch bridge with pile footing (Figure 8.39).

A popular abutment, with a cross section resembling the letter U, is simply called a U-shaped abutment. It also balances and keeps stability by its own gravity and is one major type of gravity abutments. The abutment body is composed of the front wall and two parallel wing walls (Figure 8.40). The U-shape abutment usually connected to the embankment through a cone slope, which depends on the reinforcing pattern, height of the slope and the landform. The slope is usually 1:1–1:1.5.

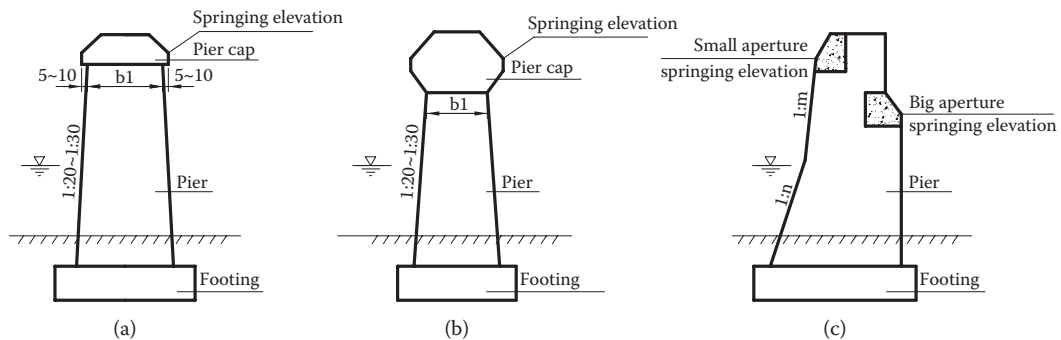


FIGURE 8.38 Gravity piers for arch bridges: (a) general type, (b) cantilever pier cap, and (c) interchanging pier.

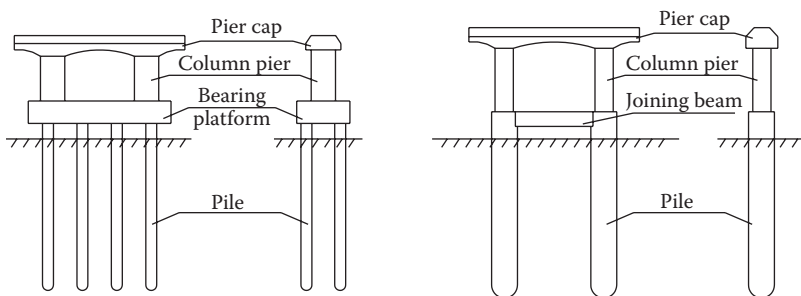


FIGURE 8.39 Frame piers for arch bridges.

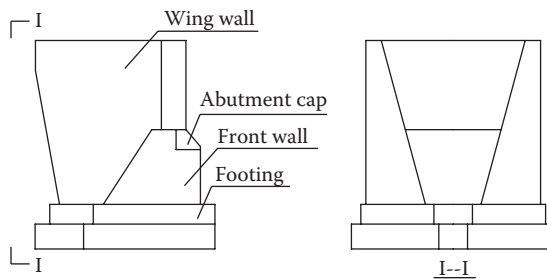


FIGURE 8.40 U-shaped abutment (gravity abutment).

Among various light abutments used in soft foundation soil, composite abutment (Figure 8.41) is one of the commonly used types. It comprises the front part and the back part with a settlement joint between them. The front part is generally supported by pile foundation to resist the vertical forces from the superstructure, while the back part is composed of two side parallel wings and shaft foundation to resist the horizontal thrust forces from the arch. This concept to separate the vertical and horizontal reactions of arch structure is adopted for some extra-long span concrete arch bridges. A typical example is the Wanxian Yangtze River Bridge in China (Figure 8.62 in Section 8.5.4).

The deck design concept provided in several chapters in Part II of this Handbook, *Superstructure Design*, also applies to the design of decks on arches. A “deck” is the roadway concrete slab or the orthotropic steel plate and their structural supports.

In the 1970s there were reports that cracks appeared in welded tied girders in several arch bridges. Repairs were made, some at great cost. However, there was no complete failure of any of the tied girders. Nonetheless, it caused the engineering community to think about the need for redundancy. One

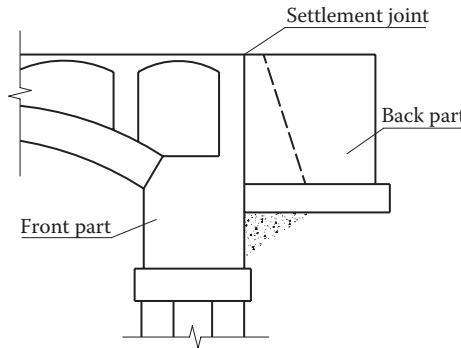


FIGURE 8.41 Composite abutment.

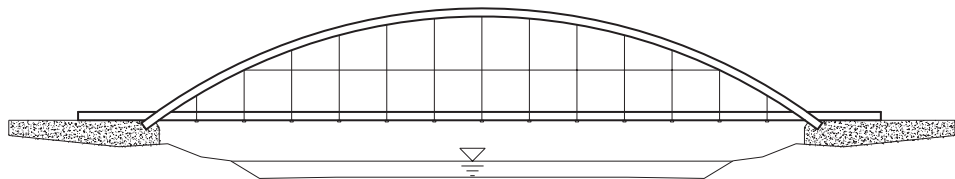


FIGURE 8.42 Connecting hangers with horizontal cables.

proposal for arch bridges is not to weld the plates of the steel tied girders together but rather to use angles to connect them, secured by bolts. Another proposal is to prestress the tie girder with post-tensioning cables. It was also proposed to have the deck participate with the tied girder.

For through and half-through arch bridges, the hangers can be stiff or flexible. Hangers may experience vibrations especially those of I-shaped cross section. The vibrations result from vortex shedding. The usual retrofit is to connect the hangers as shown in Figure 8.42, which effectively reduces the length of the hangers and changes the natural frequency of the hangers. Another method is to add spoiler devices on the hangers (Simiu and Scanlan 1986). In addition to the hangers, there have also been vortex shedding problems on very long steel columns that carry loads from the arch deck down to the arch rib. Nowadays, more and more through and half-through arch bridges employ high strength steel wire strands, which may still experience vibration problems but not so serious as the shaped steel hangers. Corrosion and fatigue may cause problems collapse tendency rises, however, due to the small area and high stress of a slender hanger. A similar problem also appears in the high strength prestressed tied cables for rigid-frame tied arch bridges. Great attention should be paid to detail design and service maintenance.

8.4 Construction

Obviously, the arch will not perform its behavior until the arch is closed at the crown. Generally speaking, intermediate (alternative) members or structures are required during the construction process of an arch. Various construction methods for arch structures have been developed, such as the scaffolding, cantilever, swing, and embedded scaffolding methods (only for concrete arches). The fundamental idea for cost-effective arch construction is to include as much as possible the already constructed parts of the arch into the load-carrying system during construction (Troyano 2003).

8.4.1 Scaffolding Method

The scaffolding method is a classic construction method for arch bridges. All masonry arch bridges are built by this method. Large size of wood-and-steel composite centering was used in the construction of the New Danhe stone arch bridge with a record span of 146 m (Chen 2009). Some important concrete

arch bridges were also built using this method in history, such as the Albert Louppe (Plougastel) Bridge, the Salginatobel Bridge with 90 m span built in 1930 in Switzerland, the Sandó Bridge, the Arrabida Bridge and the Gladesville Bridge (Troyano 2004). The scaffolding method is still used for various arch bridges today. However, this construction method loses its advantages for a long span bridge.

The scaffolding may be formed of timber, bamboo or steel, as well as of combinations of these materials in various structural types. Since it is the main temporary support during the construction, it must have sufficient strength and stiffness to carry the whole or primary part of the weight of the arch, as well as construction loads. The deformation of scaffolding during the construction should be taken into account to ensure that the completed arch is centered with the designed arch axis. Moreover, the scaffolding must be carefully designed and constructed to avoid local or global buckling, and it must be simple to fabricate and erect and easily removed, transported, and reused.

8.4.2 Cantilever Method

The cantilever method is the most popular method for arch bridge building. With this method, halves of an arch rib are built separately from two springings to crown and finally closed at the crown. Because the arch before closure is not an efficient load-carrying structure, auxiliary members or structures are necessary during construction. According to the load-carrying structure composed of temporary members and the arch rib under erection, the cantilever method can be further categorized into free cantilever method, cable-stayed cantilever method, cantilever truss method, partial cantilever method, and so on.

8.4.2.1 Free Cantilever Method

The free cantilever method is the first choice for a steel truss arch rib because it has a great stiffness and load-carrying capacity, therefore the need for auxiliary structures is minimized. The Hell Gate Bridge and the Bayonne Bridge in New York, as well as the Sydney Bridge, were all built using the free cantilever method. The two main-spans of steel truss arches of the Dashengguan Bridge in China were also erected by this method as shown in Figure 8.43. This bridge crossing realizes the Yangtze River carries rossing of the high-speed railway line from Beijing to Shanghai. It is a steel truss tied arch bridge with a span arrangement of $108 + 192 + 336 + 336 + 192 + 108$ m. Each of the side arches was erected using the free cantilever method via a short pylon and a pair of cables. The two central arches were erected via horizontal cables in three levels anchored back to back to each other. The deck truss was installed synchronously with the arch ribs, which were closed in August 2009.

8.4.2.2 Cable-Stayed Cantilever Method

The cable-stayed cantilever method using pylons and stay cables is also called the pylon construction method. Temporary pylons can be built on piers or abutments, and the stayed cables are back anchored to the ground, other piers or adjacent bridges to hold the cantilevered arch in position.



FIGURE 8.43 Free cantilever method used in the Dashengguan Bridge in China. (Courtesy of Kangming Chen.)



FIGURE 8.44 Caiyuanba Yangtze River Bridge in Chongqing, China: (a) in construction (Courtesy of Qingxiong WU) and (b) completed bridge.

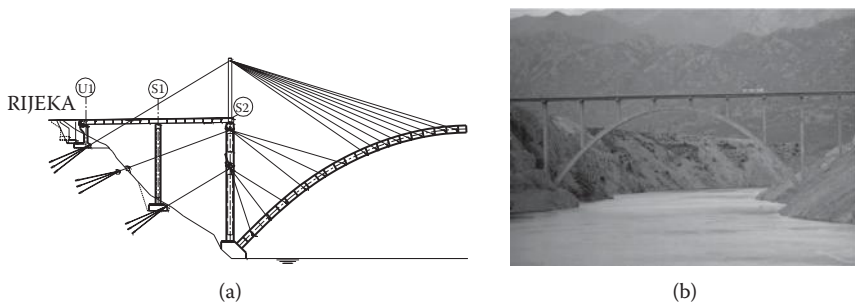


FIGURE 8.45 Maslenica Bridge, Croatia: (a) arch construction scheme (Courtesy of Zlatko Šavor) and (b) completed bridge.

Many steel and CFST arches were erected by this method, such as the New River Gorge Bridge in the USA (see Section 8.5.1), the Lupu Bridge (see Section 8.5.6) and the Chaotianmen Bridge (Figure 8.9) in China. The lifting equipment can be cranes on the ribs or cable cranes spanning between tower bents. The latter is often used in arch bridges located in mountainous areas. In the construction process of the three-span double-deck Chongqing Caiyuanba Yangtze River Bridge in China, a cable crane with 4200 kN capacity was employed to erect the steel box arch and the steel truss girder, as shown in Figure 8.44. The bridge opened to traffic on October 29, 2007. The central span of the bridge is 420 m.

For concrete arches, when the cable-stayed cantilever method is adopted, the arches can be assembled by lifting up precast arch segments, and can also cast in-situ on barges one segment after the other. The new Maslenica Highway Bridge in Croatia was constructed by this method. The concrete arch bridge spans 200 m and rises 65 m. The arch rib is a double cell box with a uniform depth of 4.0 m and width of 9.0 m rigidly connected to the abutments. During construction, the piers at the arch abutments were extended by auxiliary cable-stayed pylons 23 m high to facilitate successive cantilevering. A movable cable-crane of 500 m span and 6.0 tons capacity was utilized for delivering on site. The arch was constructed symmetrically from the arch abutments (Figure 8.45). Each of the 55.0 tons and 5.26 m long segments was carried by traveling formwork carriages and assembled in position next to previously completed segments and connected by stressed bars (Radić et al. 2008).

8.4.2.3 Cantilever Truss Method

The cantilever truss method is generally used in deck arch bridges. The cantilever trusses are composed of arch ribs, spandrel columns, and temporary diagonal and horizontal cables or a deck structure. After the two bridge halves are united by the crown segment, diagonal and horizontal cables can be removed.

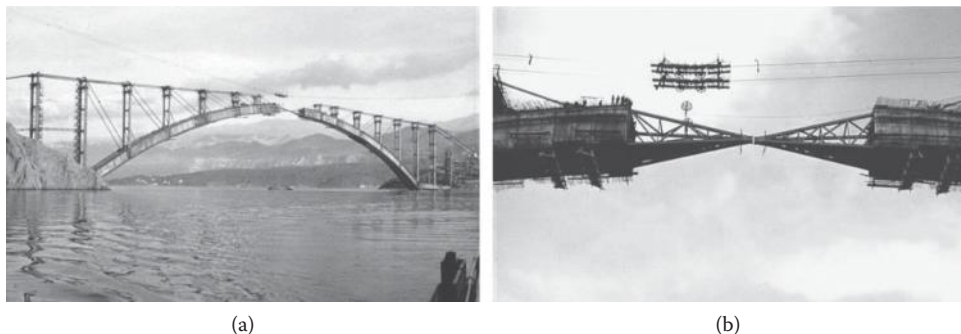


FIGURE 8.46 Cantilever truss method used in Krk I Bridge, Croatia: (a) overview (b) detailed view. (Courtesy of Zlatko Šavor.)

This method can also be further divided into assembling method and casting method with respect to the manufacturing methods for a concrete arch. The famous Krk I (390 m) and Krk II (244 m) arch bridges in Croatia were erected by the cantilever truss assembling method (Figure 8.46a). The arch segments were prefabricated on a barge, placed in position by cable-crane and then assembled in-situ by concreting “wet” joints. The arch rib is a three-cell box section.

First the central cell arch was erected after which it served as scaffolding for building the two lateral cells. Before the arch closure, two steel trusses were assembled by cable cranes to provide support for the installation of hydraulic jacks at the crown, see Figure 8.46b, thus speeding up the construction. Moreover, the mismatch between the two cantilevered ends could be corrected on time and the stresses in all elements of the scaffolding, stays and spandrel columns decreased and the vertical deflections of cantilevers significantly reduced. Hence, the utilization of steel trusses for closure significantly made the construction time shorter and speeding up the cost lowered. The completed bridge is shown in Figure 8.17 (Šavor and Bleiziffer 2008).

The cantilever method can sometimes be used to erect partial half arches and leave a central part erected by other methods. This is known as the composite cantilever method. This method was first used by Freyssinet for the construction of three arch bridges on the Caracas-La Guaira Highway in Venezuela in 1950s and have been widely employed in construction of concrete arch bridges from then on. A typical example is the Kashirajima Bridge with a span of 218 m and a rise-to-span ratio of 1:8. The bridge was opened to service in 2005. The arch construction comprised of three parts. Using the cable-stayed cantilever method, the two side parts of the concrete arch, each one with ground plan length of 57.3 m, were cast in-situ segment by segment on moving barges. Then 130.4 m long steel truss profiles were erected to unite the two side parts and to close the arch, which was subsequently concreted to form the final concrete arch rib (Mizushima et al. 2000).

8.4.3 Swing Method

The swing method of arch bridge construction start from prefabrication of two half-arches or two half-bridge structures on each bank of the river. When completed, both are rotated into their final position for closure. This method transforms the construction work from a spatial work over the obstacle of the bridge crossing to a more accessible position above level ground. According to the direction of rotation, the swing method can be classified as horizontal swing method, vertical swing method, or a combination of these two methods—the hybrid swing method.

8.4.3.1 Vertical Swing Method

If the vertically built half arches on the springings are rotated from high position to low position for closure, then it is called downward method. On the contrary, if the halves are rotated from springing position to high position for closure, then it is called the lift-up method.

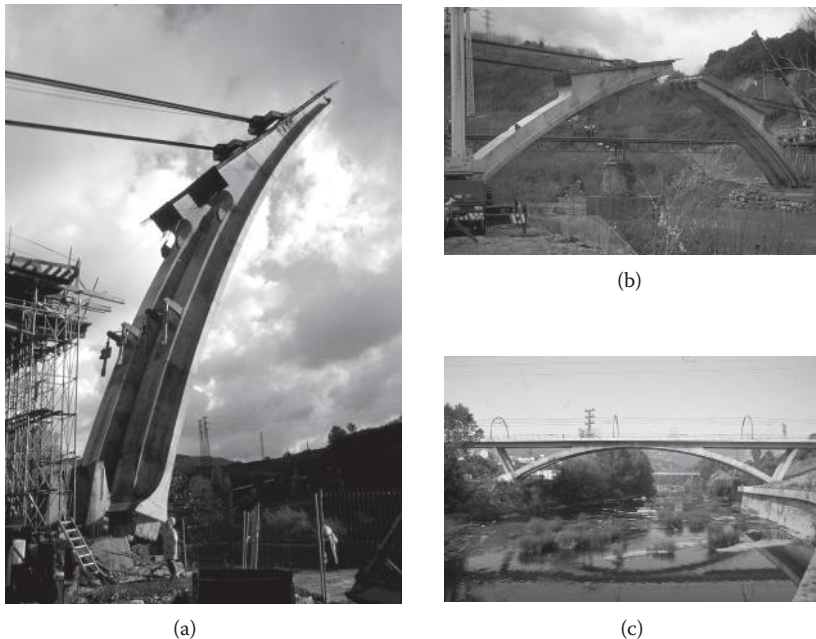


FIGURE 8.47 Downward swing method in Bulueta Bridges, Spain (Courtesy of Leonardo Fernández Troyano): (a) arch half in rotation, (b) two arch halves near closure, and (c) completed bridge.

In the vertical downward swing method, the two halves of a concrete arch can be cast in-situ by means of a climbing formwork in a quasi-vertical position on provisional or permanent hinges over the abutments. The gravity center of the half arch is generally outside of the bridge span to assure safety during construction. The rotation will start by jacking from behind the arch half or by pulling by cables from the opposite abutment until the center of gravity is within the span. Then staying cables are used to control the downward rotation of the arch half.

The history of this method dates back to the early twentieth century in the erection of wooden arches. Since then, this method has been used in the construction of concrete arch bridges. The first concrete arch bridge with a span of 100 m erected by this method is the Morandi's Storms River Bridge in South Africa built in 1954. This method was also used to build the 145 m Argentobel Bridge in Germany in 1987. Figure 8.47 shows the photos of the two bridges Bulueta 1 and 2 built by this method, which are for the Bilbao underground over the Nervion River in Spain with span 63 m and 58 m respectively (Troyano 2004).

The lift-up swing method requires higher lifting capacities forces than the downward method. But it is convenient to fabricate ribs on site if water traffic does not preclude it and the river is shallow. This method has been used mainly in constructing lightweight steel ribs of steel arch bridges or tubular ribs of CFST arch bridges in China. In the following section on the hybrid swing method, the lift-up swing method employed in Yajisha Bridge will be introduced as a typical example.

8.4.3.2 Horizontal Swing Method

When the horizontal swing method is applied, a counterweight is needed to balance the self-weight of the cantilever arch half. This method is called horizontal swing method with counterweight, which has been used in construction of many concrete and CFST arch bridges in China. The counterweight can be the abutment, or if more weight is required, heavy blocks may be added temporarily. An example of this method is also presented in the following section on hybrid swing method on the example of Yajisha Bridge.

However, because it is difficult to balance the self-weight of concrete arch ribs for a long span, when the span is long, a swing method without counterweight was developed. By this method, the arch rib with a hinge on its seat is back stayed by cables at the end of the arch half. For a three-cell box concrete arch, the



(a)



(b)

FIGURE 8.48 Wujiang Bridge and its construction method: (a) completed bridge and (b) during construction.

two side cells would be cast-in situ as two arch ribs and rotated to closure, and after that the upper and bottom flanges of the central cell would be concreted in-situ to form a complete three-cell box ring. The Wujiang Bridge (Figure 8.48a) in Sichuan, China was erected by this method. The bridge is a RC arch and has a clear span of 200 m. The arch has a three-cell box section, with a width of 9 m and height of 3 m. Each side cell of the arch halves formed a single-cell box structure during the horizontal swing (Figure 8.48b). After closure, two single-cell box arch ribs were united together in the transverse direction and cast concrete of the upper flange and bottom flange in the central cell to form a three-cell box arch section.

8.4.3.3 Hybrid Swing Method

In the hybrid swing method, the two arch halves are fabricated and/or assembled in a position favorable to construction. Then they are rotated to the design plan axix and elevation by vertical swing method and horizontal swing method. Finally, they are connected by a crown segment to form an arch.

For flying-bird (Figure 8.16b) CFST arch bridges, the flanking spans can be used as the counterweight in horizontal swing and as the anchorage for vertical swing. Thereby, this composite swing method can be more feasible than others and is an ideal solution in some special cases.

A typical example using the hybrid swing method is the Yajisha Bridge in China, which is a three span arch bridge with a span arrangement of 76 + 360 + 76 m. The more details of this bridge are given in Section 8.5.9. The half arch rib of the main span and the half arch rib of the side span next to it comprises a rotation unit. First, the flanking RC arch was constructed on site and the central half steel tubular arch truss was assembled on centering along the riverbank at the springing line elevation. Then, it was rotated vertically from a lower position (Figure 8.49a) up into the design elevation (Figure 8.49b). The total weight in vertical swinging was 20,580 kN and the vertical swing angle was 24.70°. The vertical rotation of a unit was completed in just 1 day. After swinging vertically, the main half arch rib was fixed to the springing to form a horizontal swinging unit together with the concrete arch seat, the side span RC arch, the temporary pylon and the stay cables.

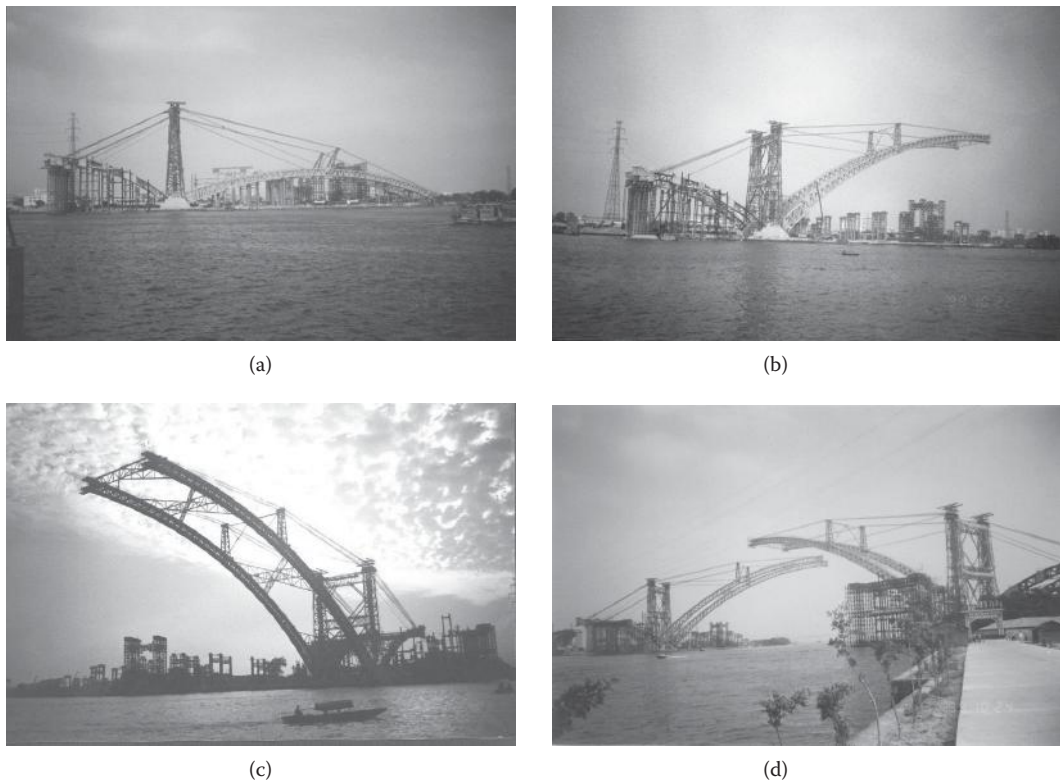


FIGURE 8.49 Erection of Yajisha Bridge, China: (a) half of the central span arch before vertical swing, (b) after vertical swing to position, (c) first half in horizontal swing, and (d) second half in horizontal swing.

A slide way with a radius of 33 m and width of 1100 mm was prepared before the horizontal swing. It was covered with oiled stainless steel panels. The steel panels were 25 mm thick, 1100 mm wide and 1410 mm long connected by 6 pairs of bolts. The bottom side of the steel panel was strengthened by steel profiles, and bolted onto the skeleton of the supporting platform. The slide way was expected to support most of the weight of the rotation unit, aided by the central shaft. The rotation was done gradually until the rib reached the design position as shown in Figure 8.49c and d. This procedure was so well controlled that there was only 5 mm mismatch between the arch axes of the two halves after rotation. Then the backstays, the wind strands and the temporary fixed members in the springings were all dismantled in sequence. The two arch halves were connected at the crown by a segment about 1 m long.

Each of the rotating units was fastened to its basement by connecting steel bars to the embedded reinforcement members and the space between the rotation set and its basement was concreted. Finally, the central span of the steel tubular hingeless arch was formed. The Yajisha Bridge was completed and opened to traffic on June 24, 2000 (Chen 2009).

8.4.4 Embedded Scaffolding Method for Concrete Arch Bridge

The embedded scaffolding method for a concrete arch bridge is also called the Melan Method, for Joseph Melan who first used it at the end of the nineteenth century. The Echelsbach Bridge in Germany with a span of 130 m and the Martin Gil Viaduct in Spain with a span of 210 m were constructed using improved versions of this method. An embedded steel truss in large concrete arches is very expensive and often renders this method infeasible.

Using CFST members as scaffolding is an innovative alternative of this method. It is accomplished by erecting a steel tubular arch, then pumping concrete into the tube to form a CFST scaffolding, which can serve for concreting an encasement of the scaffolding to form the concrete arch rib. Compared with steel rib profiles, CFST as scaffolding provides improved stiffness and strength with lower cost, contributing greatly to the construction technology of concrete arch bridges. Recently, many long span concrete arch bridges were built in China using this method, such as the Yongjiang Bridge and the Wanxian Yangtze River Bridge.

The Yongjiang Bridge located in Guangxi, China, is a half-through reinforced concrete arch bridge with a main span of 312 m and a width of 18.9 m (Figure 8.50). The two arch ribs are of box shaped with embedded CFST trusses.

A truss is composed of steel tube chords of $\Phi 402 \text{ mm} \times 12 \text{ mm}$, steel profile bracings, web bars and steel plate gussets at corners as shown in the Figure 8.51. Each truss comprised of nine segments

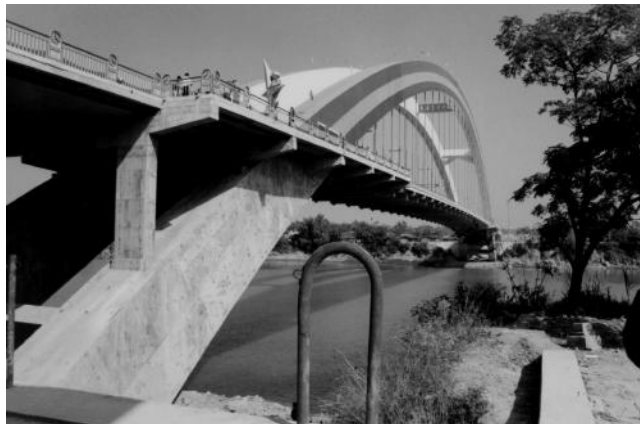


FIGURE 8.50 Yongjiang Bridge, China.

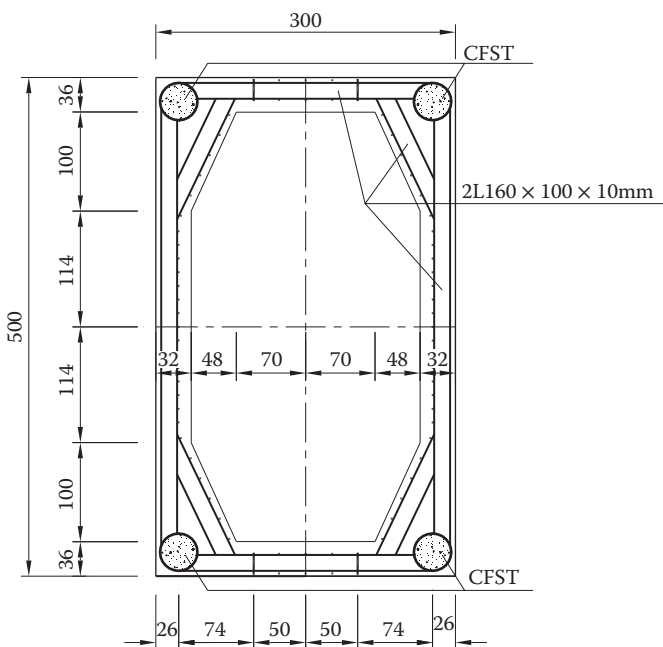


FIGURE 8.51 Box rib cross section of Yongjiang Bridge (unit: cm).

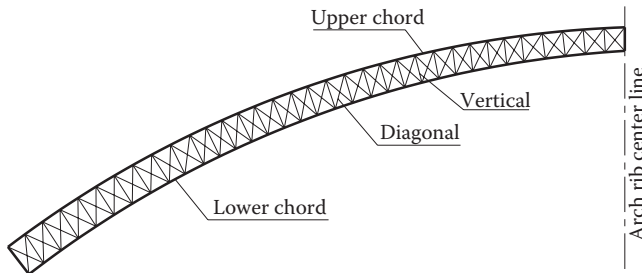


FIGURE 8.52 Embedded scaffolding of Yongjiang Bridge.



FIGURE 8.53 Apollo Bridge, Slovakia (<http://www.most.pokorny.sk/>): (a) assembly at river bank and (b) floating of arch span to its final position.

(Figure 8.52) and was erected by the cable-stayed cantilever method. After it was closed, the C60 concrete was pumped into the tubes from the springing to the crown. Next, the two hinges were fixed to form a hingeless CFST truss arch. After removing auxiliary members from the CFST truss arch, concrete was cast in-situ encasing the embedded scaffolding to form a complete concrete box rib (Chen 2009).

8.4.5 Construction Methods for Tied Arch Bridges

For a typical tied steel arch, the deck and steel tie can be erected on temporary erection bents. Once this operation is completed, the arch ribs, including bracings as well as hangers can be constructed directly on the deck. Alternatively, steel ties, and ribs may be erected simultaneously by means of tieback cables. A more spectacular erection scheme, that is economical when it can be used, involves constructing the tied arch span on the shore or on the piles adjacent and parallel to the shore. When completed, the tied arch is floated on barges to the bridge site and then pulled up vertically to its final position in the bridge. For example, Figure 8.53 shows the 231 m span Apollo Bridge in Slovakia, which is a basket-handle-like tied arch, assembled at the river bank and floated to its final position (Šavor and Bleiziffer 2008).

8.5 Examples

8.5.1 Mike O'Callaghan–Pat Tillman Memorial Bridge at Hoover Dam

A concrete arch bridge in the Hoover Dam Bypass, crossing the Colorado River, was completed and opened to traffic on October 19, 2010. The bridge was officially named the Mike O'Callaghan–Pat Tillman Memorial Bridge. This signature bridge with a main span of 323.1 m (1060 ft.) crosses the Black Canyon, connecting the Arizona and Nevada Approach Highways nearly 275 m above the Colorado River.



FIGURE 8.54 Mike O'Callaghan–Pat Tillman Memorial Bridge, Nevada. (Courtesy of T. Y. Lin International.)

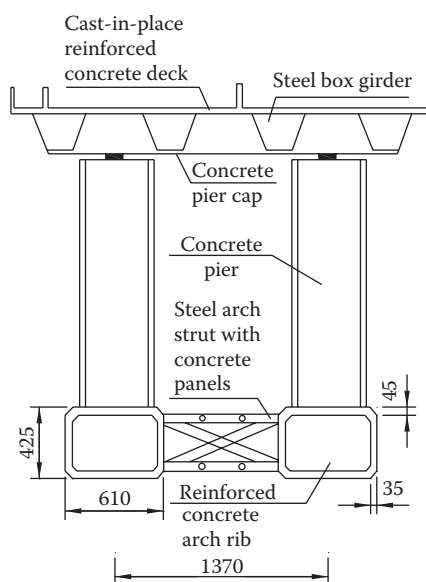


FIGURE 8.55 Typical section of Mike O'Callaghan–Pat Tillman Memorial Bridge (unit: cm). (Courtesy of T. Y. Lin International.)

In the process of the bridge type selection, a comprehensive study of all types was conducted, including truss, box girder, cable-stayed, suspension, deck arch and half-through arch. The two most favored options were to span the canyon by a suspension bridge or by an arch bridge. After a careful study of the engineering demands, the fixed deck arch remained the only option. Then, a family of fixed deck arch designs was reviewed and the final selection was a twin rib framed structure (Figure 8.54) (Goodyear and Turton 2010).

The arch has a rise of 84.5 m with a rise-to-span ratio of 0.323. The arch consists of twin reinforced concrete ribs connected by steel struts and concrete panel bracings (Figure 8.55). There were two reasons in design to prefer a twin rib layout over a single box section. The first consideration was of practical construction and the second was because of the improved performance under extreme lateral forces of seismic ground motion. The bridge has a composite deck system of steel box girders and a conventionally reinforced concrete deck plate.

The bridge was built by cable-stayed cantilever method. Four travelers were advanced to the crown of the cast-in-situ arch supported by 88 carefully tuned stay cables, while precast segments were erected for the tallest columns per schedule.

8.5.2 Skradin Bridge Near Šibenik in Croatia

The Skradin Bridge (Krka Bridge) near Šibenik in Croatia is located in an environmental reservation area very close to the Krka National Park, carrying the motorway across the Krka River Canyon on the Skradin-Šibenik section of the Adriatic Highway. The overall width of the four lane roadway is 21.0 m, including the median strip of 3.0 m; and the total width of the superstructure is 22.56 m. Designers decided to enrich the beautiful environment with this new bridge across the canyon, so an aesthetically-pleasing arch type structure became the logical choice. A concrete arch of 204.0 m span and 52.0 m rise was selected with a rise-to-span ratio of 0.25 (Figure 8.56) (Šavor et al. 2008).

The arch rib has a double-cell box section with constant outer dimensions $b \times h = 10 \text{ m} \times 3 \text{ m}$, with its springings fixed. The thickness of top and bottom flanges chords is 40.0 cm. The thicknesses of the outer and inner webs are 50.0 cm and 30.0 cm, respectively. The flange chord thickness is increased to a maximum of 60.0 cm in the last 10.0 m (measured horizontally) close to the abutments (Figure 8.57).



FIGURE 8.56 Skradin Bridge, Croatia.

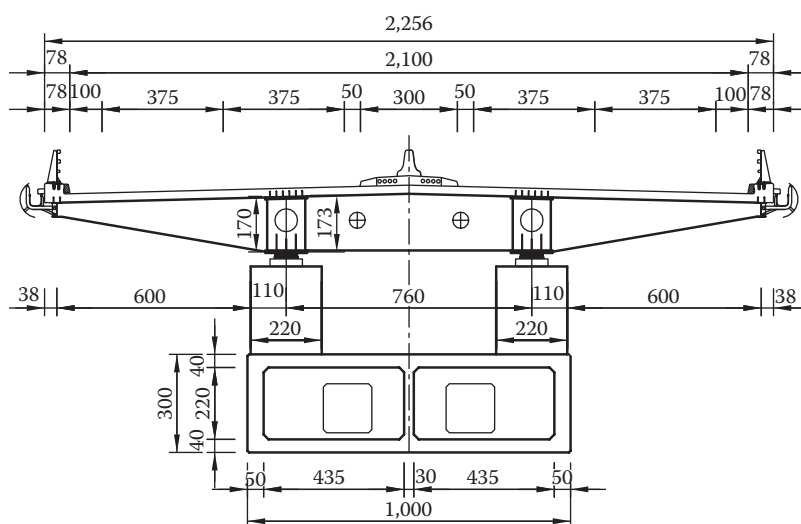


FIGURE 8.57 Typical cross section of Skradin Bridge (unit: cm). (Courtesy of Zlatko Šavor.)

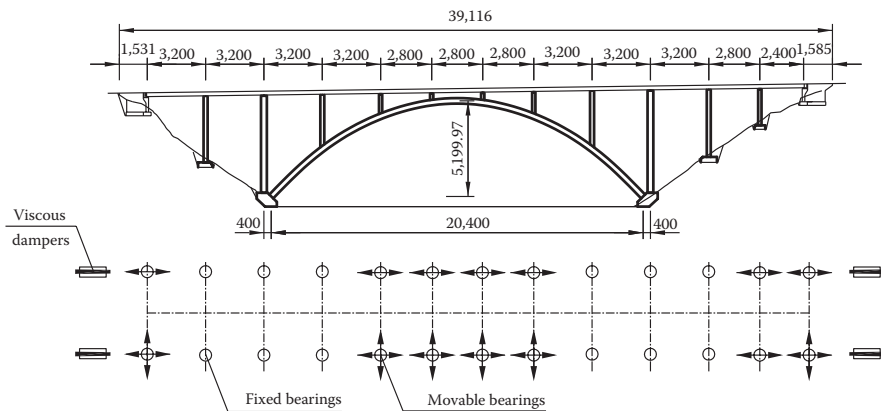


FIGURE 8.58 Elevation and bearings layout of Skradin Bridge (unit: cm). (Courtesy of Zlatko Šavor.)

The total length of the superstructure is 360.0 m ($L = 4 \times 32.0 + 3 \times 28.0 + 3 \times 32.0 + 28.0 + 24.0$ m). The deck structure is concrete deck slab composite, composed with of a steel grillage and a concrete deck plate, so that the self-weight of the bridge and consequently the arch cross section dimensions are significantly reduced. Special longitudinally fixed structural bearings were installed on top of the double spandrel columns. The stiffness of the structural system is ensured in the longitudinal direction under normal service working conditions. Viscous dampers are installed at both abutments to provide seismic resistances (Figure 8.58).

The arch was constructed by the cantilever method, using temporary stays and backstays. The deck was launched to its final position. The construction of the bridge across the Krka River Canyon commenced in the year 2003 and was completed in 2005.

8.5.3 Infante Dom Henrique above Douro in Portugal

The Infante Dom Henrique (Prince Henry) Bridge is located in Porto, Portugal, linking the historic center of Porto to the Serra do Pilar Escarpment in Gaia. The bridge is situated between the remarkable Maria Pia Bridge and the Luis I Bridge. Therefore, aesthetical harmony of them, together with the scenery, was an essential design consideration (Fonseca 2007).

This design-build project was opened to public bidding internationally and launched in May 1997. The extremely shallow Maillart-type deck-stiffened arch bridge was selected from 14 alternatives. This solution and the previous two bridges complement each other and blend in with the surroundings (Figure 8.59). All members of the structure are straight without any curvature, giving a clear and concise emotive presentation; consequently one of the most prominent highlights of this bridge is its structural and geometric simplicity.

The bridge was designed by António Adão da Fonseca. The prestressed concrete box girder deck, 4.5 m deep, 380 m long and 20 m wide, is supported by an arch of 280 m span with a rise-to-span ratio of 1:11.2, soaring 75 m above the Douro River (see Figure 8.60). The flexible arch is comprised of straight segments with a constant depth of only 1.5 m, yet it perfectly maintains an arch-like appearance. The width varies from 20 m at the springings to 10 m at the central 70 m segment integrated with the deck. At the springing areas the arch ribs are hollow to reduce self-weight.

The cantilever truss method was used to construct the bridge (see Figure 8.61) (Fonseca 2007). During construction, the cantilever truss consisted of the deck girder (in tension), arch (in compression), permanent and temporary supports, and cables which were anchored into massive granite. Temporary columns were erected from both river banks to reduce the cantilever span from 140 m to 105 m. Both the girder and the arch were cast in situ by travelers. After the closure of the arch, the temporary columns and diagonal cables were removed. The bridge was under construction from January 2000 to September 2003.



FIGURE 8.59 Infante Dom Henrique Bridge in Porto, Portugal.

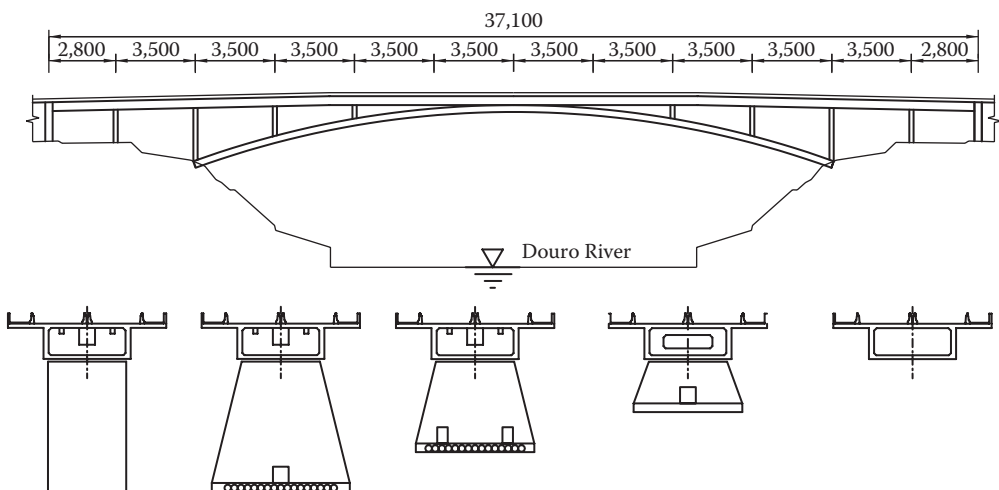


FIGURE 8.60 Elevation of Infante Dom Henrique Bridge (unit: cm).



FIGURE 8.61 Cantilever truss construction method of Infante Dom Henrique Bridge.

@Seismicisolation

8.5.4 Wanxian Yangtze River Bridge in China

The Wanxian Yangtze River Bridge (Figure 8.62) crosses the Yangtze River in the area of the Three-Gorge Reservoir (see Figure 8.18). During the planning phase, various bridge types with different spans were examined, including suspension bridge, PC rigid frame bridge, cable-stayed bridge, and arch bridge. A concrete arch bridge spanning the river without any pier above water was finally selected from 18 design alternatives. This choice made use of the geological condition and rock cliff banks avoiding the need for underwater foundations and extremely tall piers, and therefore, was the most economic.

The total length of the bridge is 856 m. The north approach consists of eight 30.7 m simple spans and the south approach consists of five 30.7 m simple spans. The deck is 24 m wide, providing four-lane highway traffic and two pedestrian sidewalks. The main bridge is a concrete deck arch with a 420 m clear span. Evidently, such a long span concrete arch is a formidable challenge for both design and construction engineers, as it represents a milestone in long span arch bridges (Xie 2008).

The rise of the arch is 84 m. The arch axis is a catenary curve with a rise-to-span ratio of 1:5. The arch section is a three-cell box 7.0 m deep and 16.0 m wide, with 40 cm thick upper and lower flanges. Details are shown in Figure 8.63.

Since the geological conditions at the abutments were not adequate to support the arch structure with traditional foundations, vertical piles under the abutments and massive horizontal blocks behind abutments were designed to resist vertical and horizontal reactions without considering the inclined bearing capacity of the abutments themselves (Figure 8.62).

A concrete filled steel tubular arch truss frame served as the rigid skeleton, weighing 2160 tons. It was designed mainly to support the weight of the concrete arch during construction. The steel arch truss frame, 6.45 m deep and 15.2 m wide, is composed of 5 truss panels spaced 3.8 m apart and the its 10 steel tube chords are of 402 mm diameter and 16 mm thick, as shown in Figure 8.63. The truss was erected by the conventional cantilever method as shown in Figure 8.64.

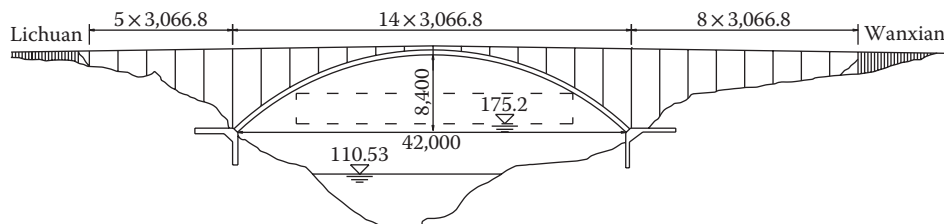


FIGURE 8.62 Elevation of Wanxian Yangtze River Bridge in China (unit: cm). (Courtesy of Bangzhu XIE.)

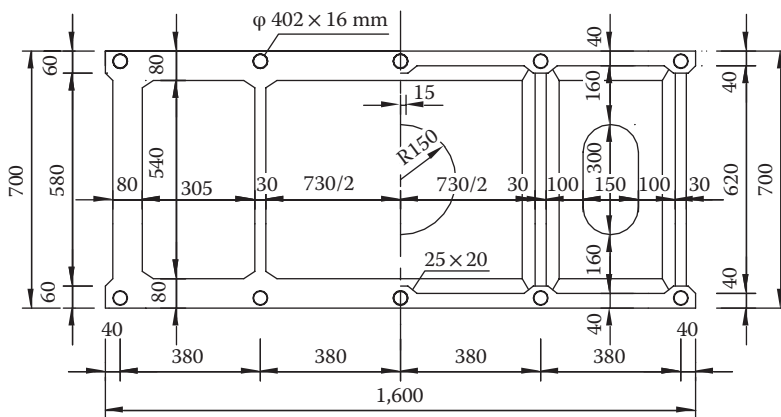


FIGURE 8.63 Arch ring cross section of Wanxian Yangtze River Bridge (unit: cm). (Courtesy of Bangzhu XIE.)

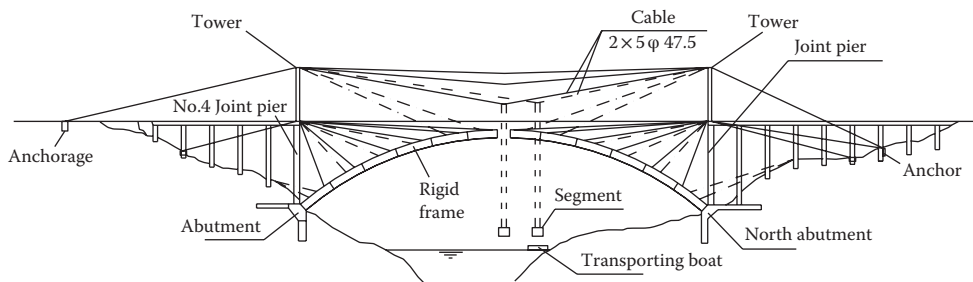


FIGURE 8.64 Erection of steel tubular arch truss of Wanxian Yangtze River Bridge. (Courtesy of Bangzhu XIE.)

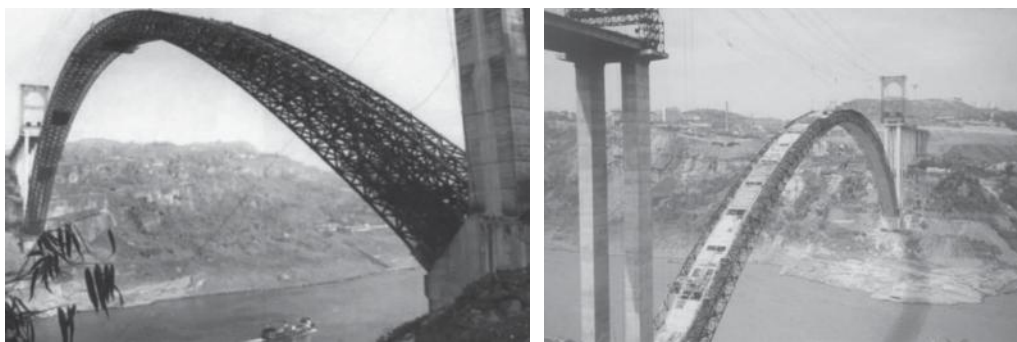


FIGURE 8.65 Construction of Wanxian Yangtze River Bridge arch ring (Courtesy of Bangzhu XIE): (a) completed steel tubular arch truss and (b) encasing of concrete.

After the steel tube truss frame was erected and formed arch truss (Figure 8.65a), C60 concrete was pumped into the steel tubes to form a CFST arch truss to increase its load-carrying capacity and stiffness. The CFST arch truss served as the embedded scaffolding of the arch in the subsequent concreting of the cross section. Once the RC arch was ready, the columns, spandrel beams, and deck system were constructed.

Careful attention was exercised to avoid premature yielding of the steel tubes and reduce the stresses between the concrete layers during the concrete placement process. A study was conducted to optimize the concrete placement sequence leading to a better load distribution, minimized deflection, and minimized use of steel. As a result of this study, the cross section concrete was cast in eight stages, from the central cell to the two side cells, from the bottom slabs to webs and top slabs. At each stage the concrete was not cast along the whole span length at the same time but in six working sectors along the arch axis. Figure 8.65b shows the arch under construction when the concreting of the central cell of the arch ring was completed.

All spandrel columns and deck structures were constructed by conventional methods. Columns were designed as thin-walled RC box structures, and the bridge deck is composed of ten post-tensioned T-shaped girders.

8.5.5 Gateway Bridge in Detroit, Michigan, USA

The Gateway Bridge in Detroit, Michigan, carries interstate traffic over a newly reconstructed (in 2006) I-94 Interchange at the Telegraph Road. One of the project requirements was to maintain the 4.5 m existing clearance under the bridge. With a conventional bridge the I-94 profile would need to have been raised or the Telegraph Road profile lowered, to maintain the required clearance. An arch bridge avoided



FIGURE 8.66 Gateway Bridge in Michigan. (Courtesy of M. Kasi.)

a raised profile, maintained a clear sight distance by eliminating the center pier, improved aesthetics at the interchange and minimized changes to the physical environment. The superstructure depth of the arch bridge is 1.524 m, which accommodates the existing vertical clearance under the bridge (Kasi and Darwish 2010).

In order to provide an arch bridge as a gateway of Michigan on the site with poor soil conditions, the project team combined the advantages of the aesthetics of a true arch and the economy of a tied arch together and developed the concept of a longitudinal tie under the roadway.

Twin steel arch structures were selected as the structural solution, each one is a single-span inclined through arch, as shown in Figure 8.66. The interior and exterior arch ribs are inclined 25° towards each other and connected using five football shape braces. The inclination is limited to 25° to maintain the desirable vertical clearance.

Each arch rib has a box-section of 0.914 × 1.219 m, with webs 19 mm thick. The flange thicknesses for the exterior ribs and interior ribs are 63.5 mm and 57 mm, respectively. The floor system comprises a 0.229 m thick, cast-in-place reinforced concrete deck, four W18 × 65 stringers and two 0.9779 m deep stiffening girders, all supported by 14 transverse steel beams equally spaced at 5.0 m. The transverse beams, stiffening girders, and stringers act compositely with the concrete deck.

The longitudinal arch thrust is resisted by multiple foundation elements: the longitudinal foundation ties, the transverse foundation ties and battered piles. The concrete foundation ties, buried beneath Telegraph Road, are sized so that the maximum tensile stress of the reinforcement is less than 138 MPa. The arch design makes possible an overall clear span of 75 m between the east and west abutments.

8.5.6 Lupu Bridge in Shanghai, China

The Lupu Bridge in Shanghai, China, crosses the Huangpu River and links the Luwan District on the north bank with the Pudong New District on the south bank. The steel arch type bridge was selected by the desire for creating a bridge which looks different from the three existing cable-stayed bridges nearby, the Nanpu, Yangpu, and Xupu Bridges.

The span arrangement is (100 + 550 + 100) m. The main arch rise is 100 m, giving a rise-to-span ratio of 1:5.5. The main span of 550 m was the longest one of any arch bridge in the world when it was completed in 2003. The bridge won the 2008 IABSE Outstanding Structure Award for being a soaring box-arch bridge with a record span, clean impressive lines and innovative use of the side arch spans and the deck to resist the thrust of the main arch (Figure 8.67) (Yue 2008).

The twin arch ribs of the central span have an inward inclination of 1:5 to form an arch structure resembling basket handle. The central distance between two ribs is 51 m at the springings and 11 m at the crown.



FIGURE 8.67 Lupu Bridge in Shanghai, China.

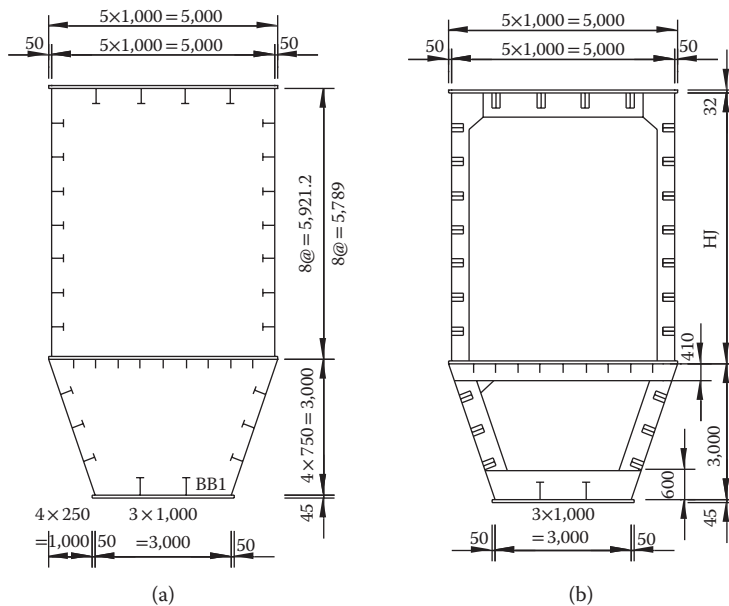


FIGURE 8.68 Arch rib cross section of Lupu Bridge (unit: mm): (a) general section and (b) section with diaphragm.

Unlike previous record span bridges with truss arch ribs, the Lupu Bridge has arch ribs of welded steel box section. Each of the twin steel boxes is 5.0 m wide and 6 m deep at the crown and 9 m deep at the springings. In order to make the arch rib visually smaller, a gyro box-type section consisting of an upper rectangular section and a lower trapezoidal section, as shown in Figure 8.68. The 3 m depth of the lower box section is constant throughout the rib.

Two arch ribs are connected with 25 straight steel box bracings above the deck spaced at 13.5 m and 8 K-shaped bracings below the deck as well as 2 cross beam bracings at the deck level. A wind bracing is 2 m wide and 3 m to 4.3 m deep.

To balance the horizontal thrust of the bridge (about 200 MN), a total of 16 tied cables are allocated inside and outside the stiffening girder (Figure 8.69), of which 8 tied cables in the upper row were installed during the erection phase of the arch ribs and the stiffening girder in the central span to balance the horizontal thrust caused by self-weight, while the other 8 tied cables in the lower row were installed and tensioned after the mid-span stiffening girder was completed and took its role in balancing the thrust caused by the subsequent dead loads and the live loads, together with the 8 tied cables in the upper row.



FIGURE 8.69 Tie bars on Lupu Bridge deck.

The deck structure of 39.5 m wide and 3 m deep, consists of a steel orthotropic plate and longitudinal beam grillage, linked to the arch by 28 pairs of hangers. The main pier foundation uses a Q345C steel pipe piles. The outer diameter of the piles is 900 mm. The wall thickness of the pile varies from 22 mm at the bottom to 16 mm at the top in consideration of stress variation along the pipe.

Bridge construction began in October 2000 and was completed in June 2003. The cable-stayed cantilever method was used for the main arch ribs above the arch deck after the triangular structures were constructed on scaffoldings. Half-arch side spans, main arch sections below deck, and the stiffening girder together with vertical columns form triangular configurations near the springings of the arches.

8.5.7 New Saikai Bridge in Nagasaki, Japan

The New Saikai Bridge is a CFST arch bridge with a span of 240 m and a width of 20.2 m (Figure 8.70). It is a highway bridge, located in the Japan National Saikai Park, close to the old Saikai Bridge (a deck type steel arch bridge with a span of 216 m, completed in 1955). In order to harmonize with the landscape and the existing steel arch bridge nearby, a half-through CFST arch bridge was adopted in the design.

The New Saikai Bridge has two parallel arch ribs, each of a triangular cross-section consisting of three CFST chords. The steel tubes have an outer diameter of 812.8 mm and a thickness that differs depending upon the position in the arch rib. The deck system consists of steel cross I-section floor-beams and two box longitudinal stiffened girders, upon which a concrete composite deck slab is placed. A footbridge with a total length of about 300 m and 3 m wide is suspended under the bridge deck since it is not allowed to build sidewalks on the highway bridge. The steel truss arch ribs were erected by cable-stayed cantilever method. The bridge was completed in 2006 (Wu et al. 2006).

8.5.8 Second Yellow River Highway Bridge in Zhengzhou, China

The Second Highway Bridge over the Yellow River in Zhengzhou, China, is a key national highway engineering project. The highway links the north from Beijing to the south Zhuhai in Guangdong Province. The bridge is composed of two separate one-way bridges, each of 19.484 m clear width carrying 4 lanes. It has a total length of 9848.16 m, comprised of 800 m long main bridge, 9035 m long approach spans and two abutments. The approach bridge contains 127 spans of 35 m and 81 spans of 50 m simple PC

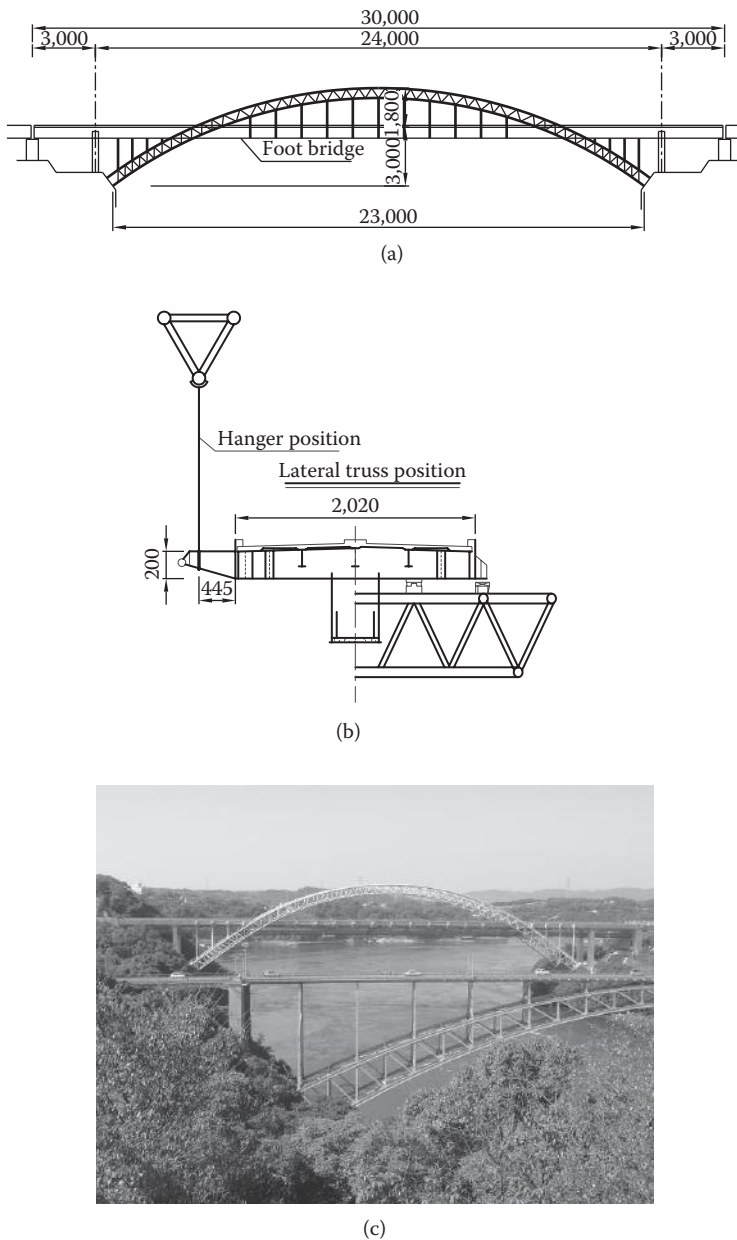


FIGURE 8.70 New Saikai Bridge, Japan: (a) elevation, (b) cross-section, and (c) completed bridge.

beam bridges, and 27 spans of 20 m PC slab bridges. The main bridge crosses the major stream channel and the dike on the south bank.

It is obvious that simple beam and slab structures are the cost-effective solution for the approach spans; while for the main bridge, various design alternatives were carefully examined and compared, including a PC simply supported bridge with a span of 50 m, a PC continuous girder bridge with a main span of 125 m, a cable stayed bridge with a main span of 210 m and a CFST arch bridge with a main span of 135 m. Finally a CFST arch bridge, with 8 spans of 100 m tied arches, was selected for the main bridge (Figure 8.71) design (Zhang et al. 2004).



FIGURE 8.71 Second Yellow River Highway Bridge in Zhengzhou, China.

The distance between two neighboring piers along the bridge is 100 m and the design span is 95.5 m. The rise-to-span ratio of the arch rib is 1:4.5. The main arch employs a catenary axis with the parameter m of 1.347. The two ribs are spaced at 22.377 m connected by three hollow steel tubular braces (one straight and two K-shaped bracings). The configuration of the superstructure is illustrated in Figure 8.72.

Each superstructure is supported by four 1750 tons rubber pot bearings. Both fixed and expansion bearings are used. The fixed bearings of two adjacent spans share a same pier where the deck is continuous. Thus, the deck is continuous between expansion joints spaced at 200 m.

There are two dumbbell shape arch ribs and each rib has a deep of 2.4 m. The steel tube of the arch rib with a diameter of 1000 mm and thickness of 16 mm was filled C50 concrete (Figure 8.73a). The tied beam is a PC box girder which is 2.0 m wide and 2.75 m deep (Figure 8.73b). The hangers are arranged at 7.1 m intervals. The end floor beam is also PC box girder which has 2.9 m deep and 3.22 m wide. A total of 12 PC cross beams are connected to the longitudinal tie beams. These cross beams support the precast RC π -shaped slabs. The hangers are made of 91-Φ7 mm high tensile strength wires protected by two layers of polyethylene.

The two separate superstructures share one RC substructure. Each pier is composed of three RC box pier columns and a cap. Friction piles with a diameter of 2.0 m serve as the foundations.

All RC substructures and foundations were built on site. A working platform was constructed at each pier for piling. The erection of so many members was very challenging. Therefore two temporary bridges were constructed on both sides of the bridge to be built. A gantry crane with lifting capacity of 600 kN

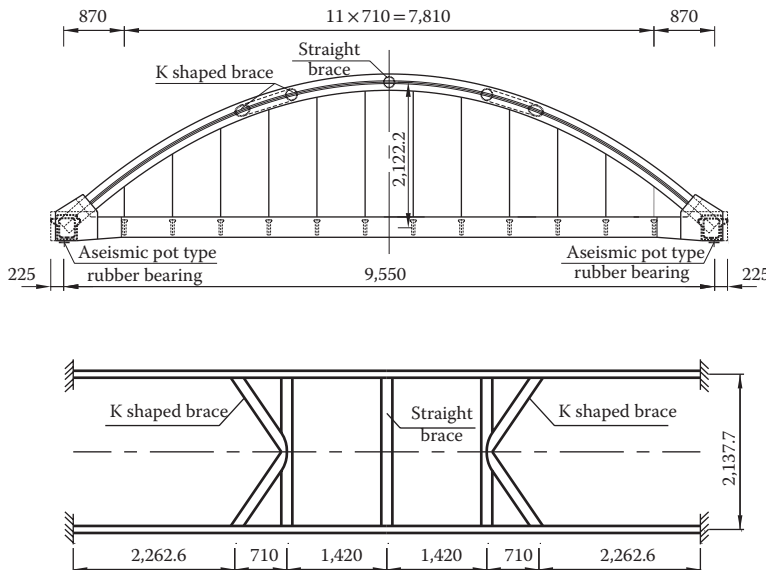


FIGURE 8.72 Configuration of Second Yellow River Highway Bridge superstructure (unit: cm).

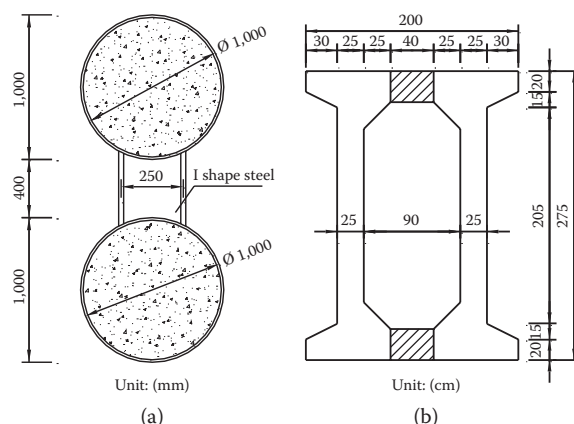


FIGURE 8.73 Cross sections of major structural members of Second Yellow River Highway Bridge: (a) CFST arch rib and (b) PC tied beam.

was specially designed. During the construction, the crane 47 m high with a reach of 66 m and a lifting height of 43 m moved along rails on the temporary bridges to handle the steel tubular rib segments and other PC or RC members. At the same time, a steel tube arch rib was divided into five segments and fabricated in the shop. After the PC tied beams and PC floor beams erected and formed a plan frame, the steel tube arch segments were erected by the gantry crane on the scaffoldings on the deck structure. After that concrete was pumped into the steel tube to form CFST arch ribs and the RC deck slabs were erected.

8.5.9 Yajisha Bridge in Guangzhou, China

The Yajisha Bridge is located in the southwest section of the loop expressway of Guangzhou City, crossing the Pearl River over the Yajisha Isle. The isle separates the Pearl River into two channels. The main navigation channel is about 350 m wide and can accommodate ten-thousand-ton ships, while the

sub-channel is only about 200 m wide. The Yajisha Bridge was designed to cross the broad portion of the river with its longitudinal axis intersecting the mainstream river at 70°.

The Yajisha Bridge is 1084 m long with a deck of 32.4 m wide, including 3 vehicle lanes in each direction. The bridge consists of two parts, the main bridge across the main navigation channel and the approach bridge across the sub-channel. The main bridge is a half-through CFST arch bridge with two half cantilever flanking arches. The span arrangement is 76 m + 360 m + 76 m (Figure 8.74). The approach bridge is a continuous rigid frame PC bridge with a span arrangement of (86 + 160 + 86) m, extended for 6 additional 40 m simply supported PC girders. Because the secondary bridge is unremarkable, Yajisha Bridge usually refers only to the main bridge (Chen and Wang 2009; Chen 2009).

The bridge elevation is shown in Figure 8.75. The arches are fixed on the piers. The bridge is tied by prestressed steel bars from two ends of the side spans. There are two arch ribs in the main span, in which the arch axis is an inverse catenary curve. The design span is 344 m and the rise of the arch is 76.45 m, giving a rise-to-span ratio of 1:4.5.

Each arch rib has six 750 mm diameter steel tubes filled with C60 concrete. Each three tubes of the upper chord and the lower chord are connected with two steel plates in between to form a box that is filled with C60 concrete. The vertical and the diagonal web members of the arch truss are also made of steel tubes. The cross section of the rib is 3.45 m wide and its depth varies from 8.039 m at the springings to 4.0 m at the crown section. The center spacing of the two ribs is 35.95 m. They are connected by seven groups of steel tubular bracings, five positioned above the deck and the other two below the deck.



FIGURE 8.74 Ya-ji-sha Bridge in Guangzhou, China.

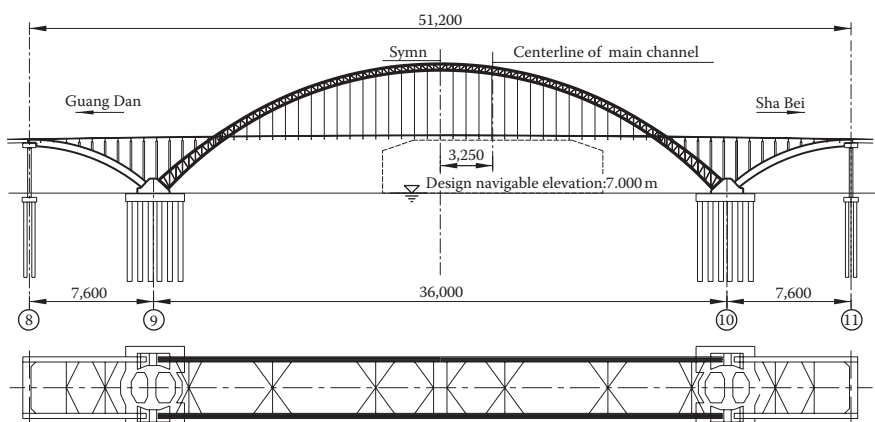


FIGURE 8.75 Longitudinal and plan sections of the Yajisha Bridge (unit: cm).

The spandrel columns in the central span are CFST columns with diameters of 1000 mm or 1300 mm. Each of the cable hangers contains 91-Φ7 mm steel wires with a strength of $R_y^b = 1670$ MPa, anchored by using cold-cast steel sockets. The deck is a steel-concrete composite structure. The 32.4 m or 38.0 m steel cross beams spaced at 8 m are connected to the π-shaped precast RC deck plates by shear studs and cast-in-situ steel fiber concrete. The deck is surfaced with 6 cm thick asphalt concrete.

Each side span arch consists of two stiffened CFST skeleton concrete box ribs. Each box is 4.5 m deep and 3.45 m wide. The arch axis is also an inverse catenary curve and the rise-to-span ratio is 1:5.2. The tie rod anchored at the two ends of the side span arches is formed by 20 strand cables. Each strand cable consists of 37 Φ 15.2 mm strands (1 Φ 15.2 mm strand consists of 7 wires of 5.2 mm diameter). The 30–50 m deep piles with 2.5 m or 3.0 m diameter are used as the pier foundations. The arch seats are reinforced concrete structures.

The erection method employed in the Yajisha Bridge is a combination of the vertical swing and the horizontal swing methods introduced in Section 8.4.3.

Acknowledgments

The first edition original version of this chapter was written by Gerard F. Fox (deceased). The author of this updated chapter is deeply indebted to many people for their direct or indirect contribution to the text. In particular, the author sincerely thanks Dr. Lian Duan, California Department of Transportation, USA, of Caltrans, Professor Wai-Fah Chen, of Purdue University of Hawaii, USA and the staff at CRC Press. Special thanks are also extended to Dr. Xinxing Yu, Professor Yizhou Zhuang and Bruno Brieseghella of Fuzhou University, China; Professor Zlatko Šavor of Zagreb University, Croatia, Dr. Dongzhou Huang of BSD Engineering, USA for their valuable comments during the editing of this chapter, as well as Mr. Jucan Dong of the Shenzhen Municipal Design and Research Institute for preparing all of the figures.

References

- Billington, D. P. 1985. *The Tower and the Bridge*, Princeton University Press, Princeton, NJ.
- Bourke, J., Taylor, S., Robinson, D. and Long, A. 2010. Analysis of a Flexible Concrete Arch, *Proceedings of 6th International Conference on Arch Bridges*, 11–13 Oct, Fuzhou, China: 133–139.
- Čandrlić, V., Radić, J. and Gukov, I. 2004. Research of Concrete Arch Bridges up to 1000 m in Span, *Proceedings of the Fourth International Conference on Arch Bridge*, 17–19 Nov, Barcelona, Spain: 538–547.
- Carrelts, J. M. 1942. Design of St. Georges tied arch span, *Proceedings of ASCE*, December: 1801–1812.
- Chen, B. C. 2009. Construction Methods of Arch Bridges in China, *Proceedings of 2nd Chinese-Croatian Joint Colloquium on Long Span Arch Bridges*, 5–9 Oct, Fuzhou, China: 1–186.
- Chen, B. C. and Mou, T. M. 2008. Research on Concrete Arches with Steel Webs, *Proceedings of Chinese-Croatian Joint Colloquium on Long Span Arch Bridges*, 10–14 July, Brijuni Islands, Croatia: 189–196.
- Chen, B. C. and Wang, T. L. 2009. Overview of Concrete Filled Steel Tube Arch Bridges in China, *Practice Periodical on Structural Design and Construction*, ASCE, 14(2): 70–80.
- Du, R. Y., Yu, J. and Chen, B. C. 2010. Trial Design of a Reactive Powder Concrete (RPC) Arch Bridge with a Span of 420 m, *Proceedings of 6th International Conference on Arch Bridges*, 11–13 Oct, Fuzhou, China: 126–132.
- Fonseca, A. D. 2007. The Infante Dom Henrique Bridge over River Douro at Porto, *Proceedings of the Fifth International Conference on Arch Bridges*, 12–14 Sept, Madeira, Portugal: 931–960.
- Galambos, T. V. 1998. *Stability Design Criteria for Metal Structures*, 5th ed., John Wiley & Sons, New York, NY.
- Goodyear, D. and Turton, R. 2010. The New Mike O'Callaghan Pat Tillman Memorial Bridge at Hoover Dam, *Proceedings of 6th International Conference on Arch Bridges*, 11–13 Oct, Fuzhou, China: 1–8.

- Huh, S. B. and Byun, Y. J. 2005. Sun-Yu Pedestrian Arch Bridge, Seoul, Korea. *Structural Engineering International*, 15(1): 32–34.
- Jordet, E. A. and Jakobsen, S. E. 2007. The Svinesund Bridge, Norway/Sweden, *Structural Engineering International*, 17(4): 309–313.
- JSCE. 2003. *Design and Construction of Long Span Concrete Arch Bridges—The 600 m Class Span*, Japan Society of Civil Engineers, Tokyo, Japan.
- Karol, J. 1942. Discussion of St. Georges Tied Arch Paper, *Proceedings of ASCE*, April: 593.
- Kasi, M. and Darwish, I. 2010. Engineering Innovation in Arch Design, *Proceedings of 6th International Conference on Arch Bridges*, 11–13 Oct, Fuzhou, China: 58–66.
- Konishi, I. 1981. *Steel Bridges (Volume 4)*, Translated by Dan, Z. F., People's Railway Press, Beijing, China (in Chinese).
- Legeron, F., Toutlemonde, F., Bouchon, E. et al. 2000. Application of High Performance Concrete in an Arch of Medium Span—Comparative Study, *Proceedings of the Third International Conference on Arch Bridges*, Paris, France: 701–707.
- Levy, R. and Spillers, W. R. 1995. *Analysis of Geometrically Nonlinear Structures*, Chapman & Hall, New York, NY.
- Ma, Z. D. 2010. Aesthetics Conceivability and Structural Characteristics of Dagu Bridge, *Proceedings of 6th International Conference on Arch Bridges*, 11–13 Oct, Fuzhou, China: 67–73.
- Mizushima, O., Fuchimoto, Y., Sugita, K. and Yamawaki M. 2000. Design of Kashirajima Bridge by Steel-Concrete Mixed Arch, *Bridge and Foundation*, 34(10): 10–18 (in Japanese).
- Muller, J. 2001. On Design and Construction of Long Span Concrete Arch Bridge. *Proceedings of the Third International Conference on Arch Bridge*, Paris, France: 17–28.
- O'Connor, C. 1971. *Design of Bridge Superstructures*, John Wiley & Sons, New York, NY.
- Radić J., Šavor, Z., Prpić V. et al. 2008. Design and construction of the Maslenica Highway Bridge, *Proceedings of Chinese-Croatian Joint Colloquium on Long Span Arch Bridges*, 10–14 July, Brijuni Islands, Croatia: 229–240.
- Salonga, J. and Gauvreau, P. 2010. Span-to-Rise Ratios in Concrete Arches: Threshold Values for Efficient Behaviour, *Proceedings of 6th International Conference on Arch Bridges*, 11–13 Oct, Fuzhou, China: 665–673.
- Šavor, Z. and Bleiziffer, J. 2008. Long Span Concrete Arch Bridges of Europe, *Proceedings of Chinese-Croatian Joint Colloquium on Long Span Arch Bridges*, 10–14 July, Brijuni Islands, Croatia: 171–180.
- Šavor, Z., Mujkanović N. and Hrelja, G. 2008. Design and Construction of Krka River Arch Bridge, *Proceedings of Chinese-Croatian Joint Colloquium on Long Span Arch Bridges*, 10–14 July, Brijuni Islands, Croatia: 217–228.
- Simiu, E. and Scanlan, R. H. 1986. *Wind Effects on Structures*, 2nd ed., John Wiley & Sons, New York, NY.
- Sparowitz, L., Freytag, B., Reichel, M. and Zimmermann, W. 2011. Wild Bridge—A Sustainable Arch Made of UHPFRC, Sustainable of Arch Bridges—*Proceedings of 3rd Chinese-Croatian Joint Colloquium on Long Span Arch Bridges*, 15–16 July, Zagreb, Croatia: 45–70.
- Steinman, D. B. and Watson, S. R. 1941. *Bridges and Their Builders*, G. P. Putnam's Sons, New York, NY.
- Strasky, J. 2010. Stress Ribbon and Arch Pedestrian Bridges, *Proceedings of 6th International Conference on Arch Bridges*, 11–13 Oct, Fuzhou, China: 38–48.
- Takahashi, S. et al. 2000. Design and Construction of Fujikawa Concrete Arch Bridge. *Proceedings of the Third International Conference on Arch Bridges*, Paris, France: 889–894.
- Troyano, L. F. 2003. *Bridge Engineering—A Global Perspective*, Thomas Telford, London, UK.
- Troyano, L. F. 2004. Procedures for the Construction of Large Concrete Arches, *Proceedings of the Fourth International Conference on Arch Bridge*, 17–19 Nov, Barcelona, Spain: 53–63.
- Wright, K. J. and Brunner, M. A. 2006. Arch Bridges. In *Structural Steel Designer's Handbook* (Fourth Edition), Brockenbrough, R. L. and Merritt, F. S.(Eds.), 14.1–14.75, McGraw-Hill, New York, NY.

- Wu, Q. X., Yoshimura, M., Takahashi, K., Nakamura, S. and Nakamura, T., 2006. Nonlinear Seismic Properties of the Second Daikai Bridge—A Concrete Filled Tubular (CFT) Arch Bridge, *Engineering Structures*, 28(2006): 163–182.
- Xanthakos, P. P. 1994. *Theory and Design of Bridges*, John Wiley & Sons, New York, NY.
- Xiang, Z. F., Xu, W., Wang, C. S. and Dong Y. 2010. The Construction Technology of Chongqing Chaotianmen Bridge, *Proceedings of 6th International Conference on Arch Bridges*, 11–13 Oct, Fuzhou, China: 788–796.
- Xie, B. Z. 2008. Wanxian Long Span Concrete Arch Bridge over Yangtze River in China, *Proceedings of Chinese-Croatian Joint Colloquium on Long Span Arch Bridges*, 10–14 July, Brijuni Islands, Croatia: 181–188.
- Yue, G. P. 2008. Key Technology for Design of Lupu Bridge, *Proceedings of Chinese-Croatian Joint Colloquium on Long Span Arch Bridges*, 10–14 July, Brijuni Islands, Croatia: 431–438.
- Zhang, W. Z., Chen, B. C. and Huang, W. J. 2004. Design of the Second Highway Bridge over Yellow River in Zhengzhou, China, *Proceedings of the Fourth International Conference on Arch Bridge*, 17–19 Nov, Barcelona, Spain: 531–537.

@Seismicisolation

9

Suspension Bridges

Atsushi Okukawa
*Oriental
Consultants Co., Ltd.*

Shuichi Suzuki
*Kensetsu-toso
Kogyo Co., Ltd.*

Ikuro Harazaki
*Japan Bridge
Engineering Center*

9.1	Introduction	363
	Origins • Evolution of Modern Suspension Bridges • Dimensions of Suspension Bridges in the World	
9.2	Structural System.....	366
	Structural Components • Types of Suspension Bridges • Main Towers • Cables • Suspended Structures • Anchorages	
9.3	Design	371
	General • Analytical Methods • Design Criteria • Wind-Resistant Design • Seismic Design • Main Towers • Cables • Suspended Structures	
9.4	Construction	389
	Main Towers • Cables • Suspended Structure	
9.5	Field Measurement and Coatings.....	393
	Loading Test • Field Observations • Coating Specification • Main Cable Corrosion Protection • Inspection for Suspender Rope Corrosion	
	References.....	397

9.1 Introduction

9.1.1 Origins

The origins of the suspension bridge go back a long way in history. Primitive suspension bridges, or simple crossing devices, were the forebears to today's modern suspension bridge structures. Suspension bridges were built with iron chain cables over 2000 years ago in China and a similar record has been left in India. The iron suspension bridge, assumed to have originated in the Orient, appeared in Europe in the sixteenth century and was developed in the eighteenth century. Though the wrought iron chain was used as main cables in the middle of the eighteenth century, a rapid expansion of the center span length took place in the latter half of the nineteenth century triggered by the invention of steel. Today, the suspension bridge is the most suitable type for very long span bridge and actually represents 20 or more of all the longest span bridges in the world.

9.1.2 Evolution of Modern Suspension Bridges

9.1.2.1 Beginning of the Modern Suspension Bridge

The modern suspension bridge originated in the eighteenth century when the development of the bridge structure and the production of iron started on a full-scale basis. Jacobs Creek Bridge was constructed by Finley in the U.S. in 1801, which had a center span of 21.3 m. The bridge's distinguishing feature was the adoption of a truss stiffening girder that gave rigidity to the bridge so as to disperse the load through

the hanger ropes and thus preventing excessive deformation of the transmission line. The construction of the Clifton Bridge with a center span of 214 m, the oldest suspension bridge now in service for cars, began in 1831 and was completed in 1864 in the United Kingdom using wrought iron chains.

9.1.2.2 Progress of the Center Span Length in the First Half of the Twentieth Century in the United States

The Aerial Spinning Method (AS method) used for constructing parallel wire cables was invented by Roebling during the construction of the Niagara Falls Bridge, which was completed in 1855 with a center span of 246 m. The technology was installed in the Brooklyn Bridge, completed in 1883 with a center span of 486 m, where steel wires were first used. The Brooklyn Bridge, which is hailed as the first modern suspension bridge, was constructed across New York's East River through the self-sacrificing efforts of the Roebling family—father, son, and the daughter-in-law—over a period of 14 years.

In 1903, the Manhattan Bridge, with a center span of 448 m, and in 1909 the Williamsburg Bridge, with a center span of 488 m, were constructed on the upper stretches of the river. The first center span longer than 1000 m was the George Washington Bridge across the Hudson River in New York. It was completed in 1931 with a center span of 1067 m. In 1936, the San Francisco-Oakland Bay Bridge, which was a twin suspension bridge with a center span of 704 m respectively and in 1937, the Golden Gate Bridge with a center span of 1280 m were constructed in the San Francisco bay area.

In 1940, the Tacoma Narrows Bridge, with a center span of 853 m, the third longest in the world at that time, exhibited bending mode oscillations of up to 8.5 m with subsequent torsional mode vibrations. It finally collapsed under a 19 m/s wind just 4 months after its completion. After the accident, wind-resistant design became crucial for suspension bridges. The Tacoma Narrows Bridge, which was originally stiffened with I-girder, was reconstructed with the same span length while using a truss type stiffening girder in 1950.

The Mackinac Straits Bridge with a center span of 1158 m was constructed as a large suspension bridge comparable to the Golden Gate Bridge in 1956 and the Verrazano Narrows Bridge with a center span of 1298 m, which updated the world record after an interval of 27 years, was built in 1964.

While long-span suspension bridges were not constructed in the late twentieth century, new projects of suspension bridges with latest technology have begun in the twenty-first century. As a part of the Seismic Retrofit Program for the bridges in San Francisco area, New Carquinez Bridge, officially named Alfred Zampa Memorial Bridge, with a center span of 728 m, was constructed replacing a structurally deficient truss bridge in 2003. An aerodynamically streamlined box girder was firstly used in the United States.

In the San Francisco Bay Bridge Seismic Safety Project, Self Anchored Suspension span (SAS), employing cutting-edge seismic safety technology, is now under construction. This bridge has a long main span of 385 m in the world as a self-anchored suspension bridge. The bridge will be open to traffic in 2013.

To carry heavy traffic between Tacoma and the Kitsap Peninsula, New Tacoma Narrows Bridge, with a center span of 853 m, was completed in 2007 on a parallel with the original bridge. It is the fifth longest suspension bridge in the United States.

9.1.2.3 New Trends in Structures in Europe from the End of World War II to the 1960s

Remarkable suspension bridges were being constructed in Europe even though their center span lengths were not outstandingly large.

In the United Kingdom, though the Forth Road Bridge, with a center span of 1006 m, was constructed using truss stiffening girder, the Severn Bridge, with a center span of 988 m, was simultaneously constructed with a box girder and diagonal hanger ropes in 1966. This unique design revolutionized suspension bridge technology. The Humber Bridge, with a center span of 1410 m, which was the longest in the world until 1997, was constructed using the similar technology as the Severn Bridge. In Portugal, the 25 de Abril Bridge was designed to carry railway traffic and future vehicular traffic and was completed in 1966 with a center span of 1013 m.

In 1998, the Great Belt East Bridge with the third longest center span of 1624 m was completed in Denmark using a box girder.

9.1.2.4 Developments in Asia Since the 1970s

In Japan, research for the construction of the Honshu-Shikoku Bridges was begun by the Japan Society of Civil Engineers in 1961. The technology developed for long-span suspension bridges as part of the Honshu-Shikoku Bridge Project contributed first to the construction of the Kanmon Bridge, completed in 1973 with a center span of 712 m, then the Namhae Bridge, completed in 1973 in the Republic of Korea with a center span of 400 m, and finally the Hirado Bridge, completed in 1977 with a center span of 465 m.

The Innoshima Bridge, with a center span of 770 m, was constructed in 1983 as the first suspension bridge of the Honshu-Shikoku Bridge Project, followed by the Ohnaruto Bridge, which was designed to carry future railway traffic in addition to vehicular loads and was discharged in 1985 with a center span of 876 m. The center route of the Honshu-Shikoku Bridge Project, opened to traffic in 1988, incorporates superior technology enabling the bridges to carry high-speed trains. This route includes long-span suspension bridges such as the Minami Bisan-Seto Bridge, with a center span of 1100 m, the Kita Bisan-Seto Bridge, with a center span of 990 m, and the Shimotsui-Seto Bridge, with a center span of 910 m. The Akashi Kaikyo Bridge, completed in 1998 with the world longest center span of 1991 m, represents the accumulation of bridge construction technology to this day.

In Turkey, the Bosphorus Bridge, with a center span of 1074 m, was constructed in 1973 with a similar bridge type of the Severn Bridge, while the Second Bosphorus Bridge with a center span of 1090 m, called the Fatih Sultan Mehmet Bridge now, was completed in 1988 using vertical instead of diagonal hanger ropes.

In China, the Tsing Ma Bridge (Hong Kong), a combined railway and highway bridge with a center span of 1377 m, was completed in 1997. The construction of long-span suspension bridges over 1000 m is currently considered remarkable. The Jiangyin Yangze River Bridge with a center span of 1385 m and the Runyang Yangze River Bridge with a center span of 1490 m were constructed in 1999 and 2005, respectively. The Zoushan Xihoumen Bridge with a center span of 1650 m, which is the second longest bridge in the world, was completed in 2008. These three suspension bridges have a box or twin-box stiffening girder and concrete main towers.

9.1.3 Dimensions of Suspension Bridges in the World

Major dimensions of long-span suspension bridges in the world are shown in Table 9.1.

TABLE 9.1 Dimensions of Long-Span Suspension Bridges

No.	Bridge	Country	Year of Completion	Span Length (m)	Type	Remarks
1	Akashi Kaikyo	Japan	1998	960 + 1991 + 960	3-Span, 2-Hinged	
2	Zoushan Xihoumen	China ^a	2008	578 + 1650 + (485)	Continuous	
3	Great Belt East	Denmark	1998	535 + 1624 + 535	Continuous	
4	Runyang Yangtze River	China ^a	2005	(470) + 1490 + (470)	Single-span	
5	Humber	U.K.	1981	280 + 1410 + 530	3-Span, 2-Hinged	
6	Jiangyin Yangtze River	China ^a	1999	(336.5) + 1385 + (309.4)	Single-span	
7	Tsing Ma	China ^a	1997	355.5 + 1377 + (300)	Continuous	Highway + Railway
8	Verrazano Narrows	U.S.	1964	370.3 + 1298.5 + 370.3	3-Span, 2-Hinged	
9	Golden Gate	U.S.	1937	342.9 + 1280.2 + 342.9	3-Span, 2-Hinged	

(Continued)

TABLE 9.1 (Continued) Dimensions of Long-Span Suspension Bridges

No.	Bridge	Country	Year of Completion	Span Length (m)	Type	Remarks
10	Yangtze River	China ^a	2007	(250) + 1280 + (440)	Single-span	
11	Hoga Kusten	Sweden	1997	310 + 1210 + 280	3-Span, 2-Hinged	
12	Mackinac Straits	U.S.	1957	548.6 + 1158.2 + 548.6	3-Span, 2-Hinged	
13	Zhujiang Huangpu	China ^a	2008	(290) + 1108 + (350)	Single-span	
14	Minami Bisan-Seto	Japan	1988	274 + 1100 + 274	Continuous	Highway + Railway
15	Fatih Sultan Mehmet	Turkey	1988	(210) + 1090 + (210)	Single-span	
16	Guizhou Balinghe	China ^a	2009	(248) + 1088 + (228)	Single-span	
17	Bosphorus	Turkey	1973	(231) + 1074 + (255)	Single-span	
18	George Washington	U.S.	1931	185.9 + 1066.8 + 198.1	3-Span, 2-Hinged	
19	3rd Kurushima	Japan	1999	(260) + 1030 + (280)	Single-span	
20	2nd Kurushima	Japan	1999	250 + 1020 + (245)	2-Span, 2-Hinged	
21	25 de Abril	Portugal	1966	483.4 + 1012.9 + 483.4	Continuous	Highway + Railway
22	Forth Road	U.K.	1964	408.4 + 1005.8 + 408.4	3-Span, 2-Hinged	
23	Kita Bisan-Seto	Japan	1988	274 + 990 + 274	Continuous	Highway + Railway
24	Severn	U.K.	1966	304.8 + 987.6 + 304.8	3-Span, 2-Hinged	
25	Yichang Yangtze River	China ^a	2001	(246.3) + 960 + (246.3)	Single-span	
26	Shimotsui-Seto	Japan	1988	(230) + 940 + (230)	Single-span with Cantilever	Highway + Railway
27	Xi Ling Yangtze River	China ^a	1997	(225) + 900 + (255)	Single-span	
28	Si Du River Bridge	China ^a	2009	(208) + 900 + (114)	Single-span	
29	Hu Men Zhu Jiang	China ^a	1997	(302) + 888 + (348.5)	Single-span	
30	Ohnaruto	Japan	1985	(93) + 330 + 876 + 330	3-Span, 2-Hinged	Highway + Railway ^b

^a The People's Republic of China.

^b Railway has been planned.

9.2 Structural System

9.2.1 Structural Components

The basic structural components of a suspension bridge system are shown in Figure 9.1.

1. Stiffening girders/trusses: Longitudinal structures that support and distribute moving vehicle loads, act as chords for the lateral system and secure the aerodynamic stability of the structure.
2. Main cables: A group of parallel-wire bundled cables that support stiffening girders/trusses by hanger ropes and transfer loads to towers.

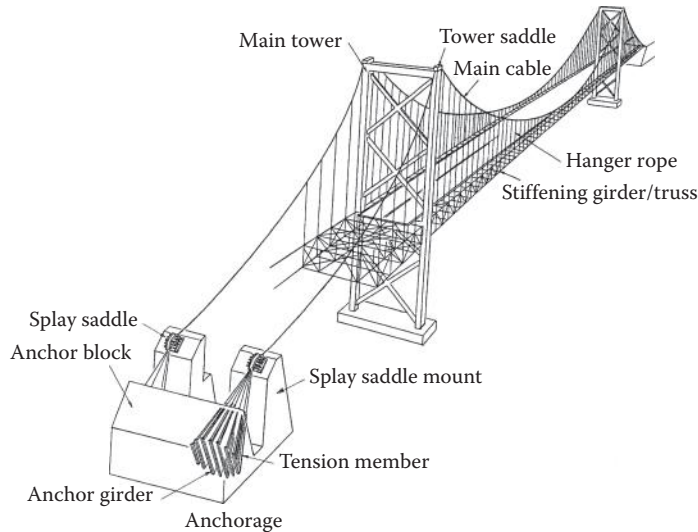


FIGURE 9.1 Suspension bridge components.

3. Main towers: Intermediate vertical structures that support main cables and transfer bridge loads to foundations.
4. Anchorages: Massive concrete blocks that anchor main cables and act as end supports of a bridge.

9.2.2 Types of Suspension Bridges

Suspension bridges can be classified by the number of spans, continuity of stiffening girders, types of suspenders and types of cable anchoring.

9.2.2.1 Number of Spans

Bridges are classified into single-span, two-span or three-span suspension bridges with two towers, and multi-span suspension bridges that have three or more towers (Figure 9.2). Three-span suspension bridges are the most commonly used. In multi-span suspension bridges, the horizontal displacement of the tower tops might increase due to the load conditions, and countermeasures to control such displacement may become necessary.

9.2.2.2 Continuity of Stiffening Girders

Stiffening girders are typically classified into two-hinge or continuous types (Figure 9.3). Two-hinge stiffening girders are usually used for highway bridges. For combined highway-railway bridges, the continuous girder is often adopted to ensure train runnability.

9.2.2.3 Types of Suspenders

Suspenders, or hanger ropes, are either vertical or diagonal (Figure 9.4). Generally, suspenders of most suspension bridges are vertical. Diagonal hangers have been used, such as in the Severn Bridge, to increase the damping of the suspended structures. Occasionally vertical and diagonal hangers are combined for more stiffness.

9.2.2.4 Types of Cable Anchoring

These are classified into externally-anchored or self-anchored types (Figure 9.5). External anchorage is most common. Self-anchored main cables are secured to the stiffening girders instead of the anchorage; the axial compression is carried into the girders.



FIGURE 9.2 Types of suspension bridges.



FIGURE 9.3 Types of stiffening girders.

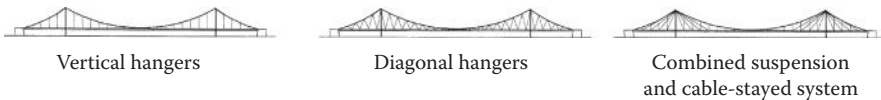


FIGURE 9.4 Types of suspenders.



FIGURE 9.5 Types of cable anchoring.

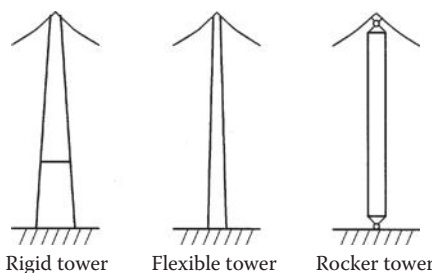


FIGURE 9.6 Main tower structural types.

9.2.3 Main Towers

9.2.3.1 Longitudinal Direction

Towers are classified into rigid, flexible, or locking types (Figure 9.6). Flexible towers are commonly used in long-span suspension bridges, rigid towers of multi-span suspension bridges to provide enough stiffness to the bridge, and locking towers occasionally for relatively short-span suspension bridges.

9.2.3.2 Transverse Direction

Towers are classified into portal or diagonally-braced types (Figure 9.7). Moreover, the tower shafts can either be vertical or inclined. Typically, the center axis of inclined shafts coincide with the center line of the cable at the top of the tower. Careful examination of the tower configuration is significant, in that towers dominate the bridge aesthetics.

9.2.4 Cables

In early suspension bridges, chains, eye-bar chains, or other materials were used for the main cables. Wire cables were used for the first time in suspension bridges in the first half of the nineteenth century, and parallel-wire cables were adopted for the first time, the Niagara Falls Bridge, in 1854. Cold-drawn

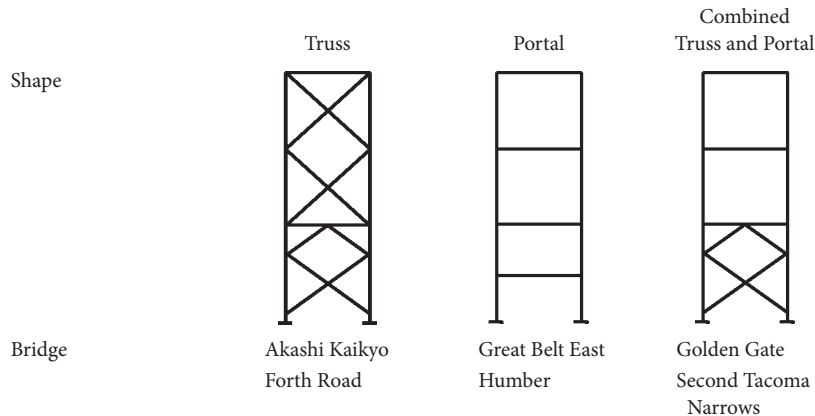


FIGURE 9.7 Types of main tower skeletons.

Name	Shape of Section	Structure	Bridge
Parallel Wire Strand		Wires are hexagonally bundled in parallel.	Brooklyn
Strand Rope		Six strands made of several wires are closed around a core strand.	Humber Great Belt East Akashi Kaikyo
Spiral Rope		Wires are stranded in several layers mainly in opposite lay directions.	St. Johns Little Belt Tancarville
Locked Coil Rope		Deformed wires are used for the outside layers of Spiral Rope	Wakato Kvalsund Emmerich Älzburg New Köln Rodenkirchen

FIGURE 9.8 Suspension bridge cable types.

and galvanized steel wires were adopted for the first time in the Brooklyn Bridge in 1883. This type has been used in almost all modern long-span suspension bridges. The types of parallel wire strands and stranded wire ropes that typically comprise cables are shown in Figure 9.8. Generally, strands are bundled into a circle to form one cable. Hanger ropes might be steel bars, steel rods, stranded wire ropes, parallel wire strands, and others. Stranded wire rope is most often used in modern suspension bridges.

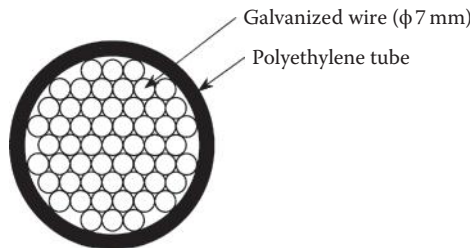


FIGURE 9.9 Parallel wire strands covered with polyethylene tubing.

In the Akashi Kaikyo Bridge and the Kurushima Bridge, parallel wire strands covered with polyethylene tubing were used (Figure 9.9).

9.2.5 Suspended Structures

Stiffening girders may be the I-girders, trusses, and box girders (Figure 9.10). In some short-span suspension bridges, the girders do not have enough stiffness itself and are usually stiffened by storm ropes. In long-span suspension bridges, trusses or box girders are typically adopted. Plate girders (with I-section) become disadvantageous due to aerodynamic stability. There are both advantages and disadvantages to trusses and box girders, involving trade-offs in aerodynamic stability, ease of construction, maintenance, and so on (details are in Section 9.3.8).

9.2.6 Anchorages

In general, anchorage structure includes the foundation, anchor block, bent block, cable anchor frames and protective housing. Anchorages are classified into gravity or tunnel anchorage system as shown in Figure 9.11. Gravity anchorage relies on the mass of the anchorage itself to withstand the tension of the

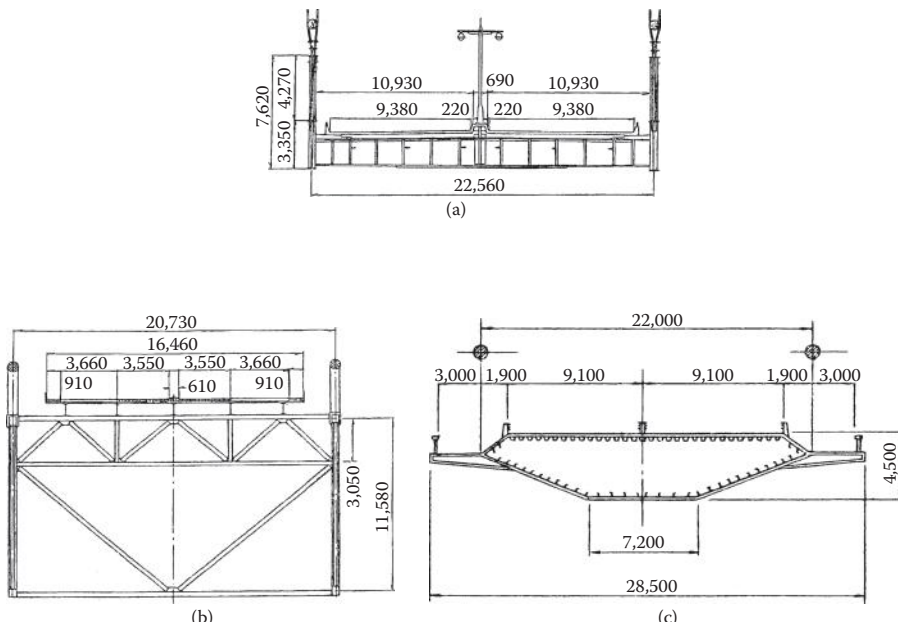


FIGURE 9.10 Types of stiffening girders (a) I-girder (Bronx-Whitestone Bridge), (b) Truss girder (Mackinac Straits Bridge), and (c) Box girder (Humber Bridge).

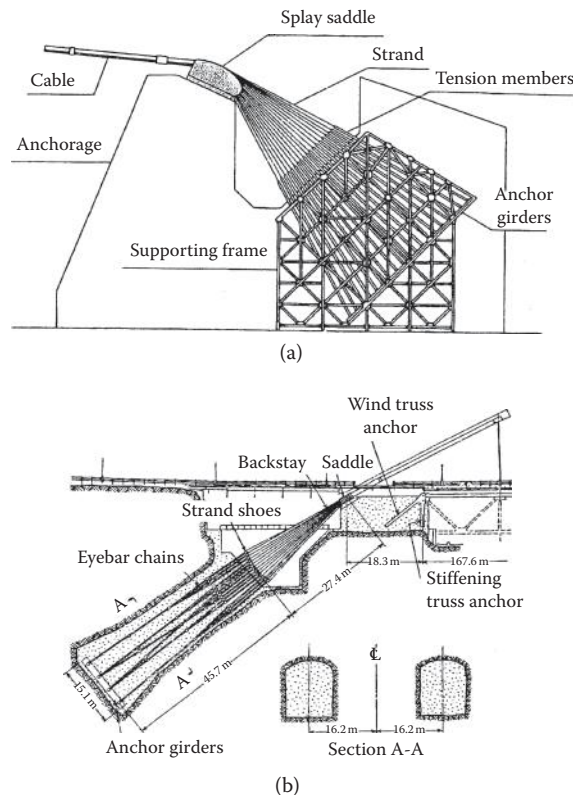


FIGURE 9.11 Types of anchorages.

main cables. This type is commonplace in many suspension bridges. Tunnel anchorage takes the tension of the main cables directly into the ground. Adequate geotechnical conditions are required.

9.3 Design

9.3.1 General

Naveir (1823) was the first to consider a calculation theory of an unstiffened suspension bridge in 1823. Highly rigid girders were adopted for the suspended structure in the latter half of the nineteenth century because the unstiffened girders that had been used previously bent and shook under not much load. As a result, Rankine (1858) attempted to analyze suspension bridges with a highly rigid truss, followed by Melan who helped complete elastic theory in which the stiffening truss was regarded as an elastic body. Ritter (1877), Lévy (1886), and Melan (1888) presented deflection theory as an improved alternative to elastic theory. Moisseiff (1925) realized that the actual behavior of a suspension bridge could not be explained by elasticity theory in studies of the Brooklyn Bridge in 1901, and confirmed that deflection theory was able to evaluate the deflection of that bridge more accurately. Moisseiff designed the Manhattan Bridge using deflection theory in 1909. This theory became a useful design technique with which other long-span suspension bridges were successfully built (Moisseiff 1925). Moreover, together with increasing the span length of the suspension bridge, horizontal loads such as wind load and vertical loads came to govern the design of the stiffening girder. Moisseiff and Lienhard (1933) were among the first to establish the out-of-plane analysis method for suspension bridges.

Currently, thanks to rapid computer developments and the accumulation of matrix analysis studies of nonlinear problems, the finite deformation theory with a discrete frame model is generally used for the analysis of suspension bridges. Brotton was the first to analyze the suspension bridge to be a plane structure in the matrix analysis and applied his findings to the analysis at the erection stage for the Severn Bridge with good results (Brotton 1966). Saafan's (1966) and Tezcan's (1966) thesis, which applied the general matrix deformation theory to the vertical in-plane analysis of a suspension bridge was published almost at the same time in 1966. The Newton-Raphson's method or original iteration calculation method may be employed in these nonlinear matrix displacement analyses for a suspension bridge.

9.3.2 Analytical Methods

9.3.2.1 Classical Theory

9.3.2.1.1 Elastic Theory and Deflection Theory

The elastic theory and the deflection theory are in-plane analyses of the global suspension bridge system. In the theories that are sometimes called membrane theory, the entire suspension bridge is assumed as a continuous body and the hanger ropes are closely spaced. Both of these analytical methods assume the following:

- The cable is completely flexible.
- The stiffening girder is horizontal and straight. The geometrical moment of inertia is constant.
- The dead load of the stiffening girder and the cables are uniform. The coordinates of the cable are parabolic.
- All dead loads are taken into the cables.

The difference between the two theories is whether cable deflection resulting from live load is considered. Figure 9.12 shows forces and deflections due to load in a suspension bridge. The bending moment, $M(x)$, of the stiffening girder after loading the live load is shown as follows.

$$\text{Elastic Theory: } M(x) = M_0(x) - H_p y(x) \quad (9.1)$$

$$\text{Deflection Theory: } M(x) = M_0(x) - H_p y(x) - (H_w + H_p) \eta(x) \quad (9.2)$$

where $M_0(x)$ is the bending moment resulting from the live load applied to a simple beam of the same span length as the stiffening girder, $y(x)$ is the longitudinal position of the cable, $\eta(x)$ is the deflection of the cable and the stiffening girder due to live load and H_w, H_p are the cable horizontal tension due to dead load and live load, respectively.

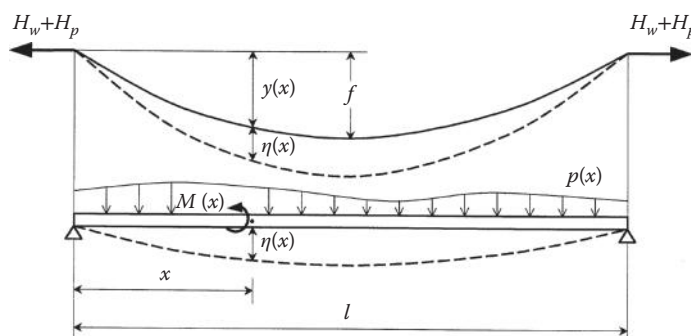


FIGURE 9.12 Deformations and forces of a suspension bridge.

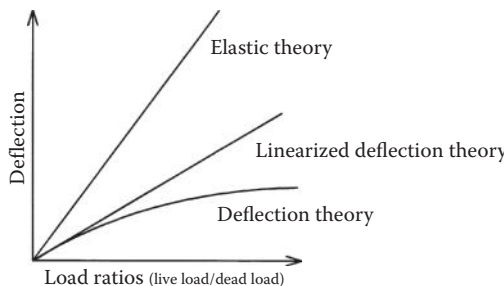


FIGURE 9.13 Deflection-load ratios relations among theories.

It is understood that the bending moment of the stiffening girder is reduced because the deflection induced due to live load is considered in the last product of Equation 9.2. Since deflection theory is a nonlinear analysis, the principle of superposition using influence lines cannot be applied. However, because the intensity of live loads is smaller than that of dead loads for long-span suspension bridges, sufficient accuracy can be obtained even if it is assumed that $H_w + H_p$ is constant under the condition of $H_w \gg H_p$. In that circumstance, because the analysis becomes linear, the influence line can be used. Figure 9.13 shows the deflection-load ratios relations among elastic, deflection, and linearized deflection theories (Bleich, McCullough, Rosecrans, and Vincent 1950). When the live load to dead load ratio is small, linearized theory is particularly effective for analysis. In deflection theory, the bending rigidity of towers can be ignored because it has no significance for behavior of the entire bridge.

9.3.2.1.2 Out-of-Plane Analysis Due to Horizontal Loads

The lateral force caused by wind or earthquake tends to be transmitted from the stiffening girder to the main cables, because the girder has larger lateral deformation than the main cables due to the difference of the horizontal loads and their stiffness. Moisseiff first established the out-of-plane analysis method considering this effect (Moisseiff and Lienhard 1933).

9.3.2.1.3 Analysis of Main Tower for the Longitudinal Direction

Birdsall (1942) proposed a theory on behavior of the main tower in the longitudinal direction. Birdsall's theory utilizes an equilibrium equation for the tower due to vertical and horizontal forces from the cable acting on the tower top. The tower shaft is considered a cantilevered beam with variable cross section, as shown in Figure 9.14. The horizontal load (F) is obtained on the precondition that the vertical load (R), acting on the tower top, and the horizontal displacement (Δ) are calculated by using Steinman's generalized deflection theory method (Steinman 1935).

9.3.2.2 Modern Design Method

9.3.2.2.1 Finite Deformation Method

With the development of the computer in recent years, finite displacement method on framed structures has come to be used as a more accurate analytical method. This method is used for plane analysis or space frame analysis of the entire suspension bridge structure. The frame analysis according to the finite displacement theory is performed by obtaining the relation between the force and the displacement at the ends of each component of the entire structural system. In this analytical method, the actual behavior of the bridge such as elongation of the hanger ropes, which is disregarded in deflection theory, can be considered. The suspension bridges with inclined hanger ropes, such as the Severn Bridge, and bridges in the erection stage are also analyzed by the theory. While the relation between force and displacement at the ends of the element is nonlinear in the finite displacement theory, the linearized finite

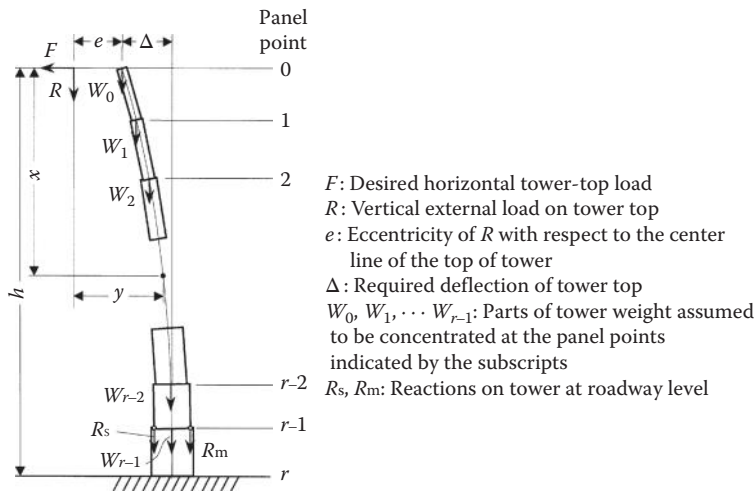


FIGURE 9.14 Analytical model of the main tower.

deformation theory is used in the analysis of the eccentric vertical load and the out-of-plane analysis; because the geometrical nonlinearity can be considered to be relatively small in those cases.

9.3.2.2 Elastic Buckling and Vibration Analyses

Elastic buckling analysis is used to determine an effective buckling length, which is required in the design of the compression members, such as the main tower shafts. Vibration analysis is needed to determine the natural frequency and vibrational modes of the entire suspension bridge as part of the design of wind- and seismic resistance. Both of these analyses are eigenvalue problems in the linearized finite deformation method for framing structures.

9.3.3 Design Criteria

9.3.3.1 Design Procedure

A general design procedure for a suspension bridge superstructure is shown in Figure 9.15. Most rational structure for a particular site is selected from the result of preliminary design over various alternatives. Then final detailed design proceeds.

9.3.3.1.1 Design Load

Design loads for a suspension bridge must take into consideration of the natural conditions of the construction site, the importance of a bridge, its span length, and function (vehicular or railway traffic). It is important in the design of suspension bridges to accurately determine the dead load because the dead load typically dominates the forces on the main elements of the bridge. Securing structural safety against strong winds and earthquakes is also an important issue for long-span suspension bridges.

1. In the case of wind, consideration of the vibrational and aerodynamic characteristics is extremely important.
2. In the case of earthquake, assumption of earthquake magnitude and evaluation of energy content are crucial for bridges in regions prone to large-scale events.

Other design loads include effects due to errors in fabrication and erection of members, temperature change, and possible movement of the supports.

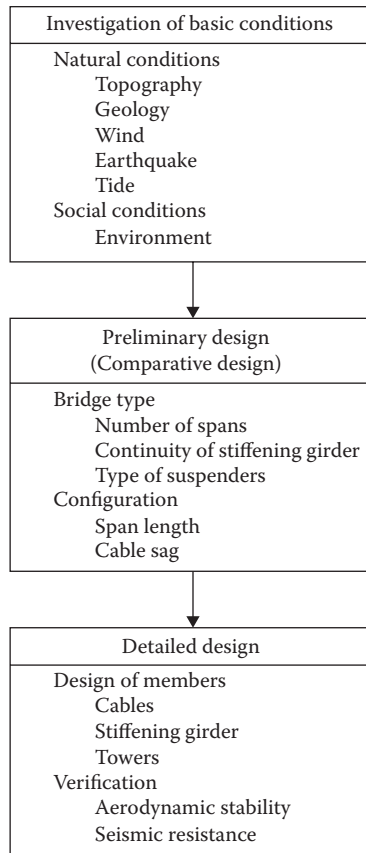


FIGURE 9.15 Design procedure for the superstructure of a suspension bridge.

9.3.3.1.2 Analysis Procedure

General procedure used for the design of a modern suspension bridge is as follows (Figure 9.16):

1. *Select Initial Configuration:* Span length and cable sag are determined, and dead load and stiffness are assumed.
2. *Analysis of the Structural Model:* In the case of in-plane analysis, the forces on and deformations of the members under live load are obtained by using finite deformation theory or linear finite deformation theory with a two-dimensional model. In the case of out-of-plane analysis, wind forces on and deformations of the members are calculated by using linear finite deformation theory with a three-dimensional model.
3. *Dynamic Response Analysis:* The responses of earthquakes are calculated by using response spectrum analysis or time-history analysis.
4. *Member Design:* The cables and girders are designed using forces obtained from previous analyses.
5. *Tower Analysis:* The tower is analyzed using loads and deflection, which are determined from the global structure analysis previously described.
6. *Verification of Assumed Values and Aerodynamic Stability:* The initial values assumed for dead load and stiffness are verified to be sufficiently close to those obtained from the detailed analysis. Aerodynamic stability is to be investigated through analyses and/or wind tunnel tests using dimensions obtained from the dynamic analysis.

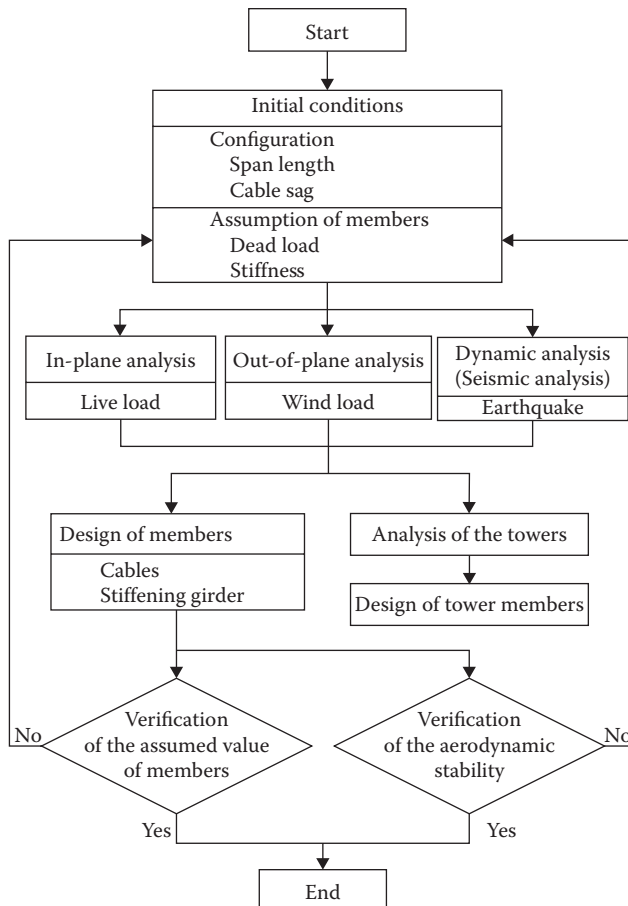


FIGURE 9.16 General procedure for designing a suspension bridge.

9.3.4 Wind-Resistant Design

9.3.4.1 General

In the first half of the nineteenth century, suspension bridges occasionally collapsed under wind loads because girders tended to have insufficient rigidity. In the latter half of the nineteenth century, such collapses decreased because the importance of making girders sufficiently stiff was recognized.

In the beginning of the twentieth century, stiffening girders with less rigidity reappeared as deflection theory was applied to long-span suspension bridges. The Tacoma Narrows Bridge collapsed 4 months after its completion in 1940 under a wind velocity of only 19 m/s. The deck of the bridge was stiffened with plate girders formed from built-up plates. The plate girders had low rigidity and aerodynamic stability was very inferior as shown in recent wind resistant design. After this accident, wind tunnel tests for stiffening girders became routine in the investigation of aerodynamic stability. Truss-type stiffening girders, which give sufficient rigidity and combined partially with open deck grating, have dominated the design of modern suspension bridges in the United States.

A new type of stiffening girder, however, a streamlined box girder with sufficient aerodynamic stability was adopted for the Severn Bridge in the United Kingdom in 1966 (Walshe and Rayner 1962; Roberts 1970). In the 1980s, it was confirmed that a box girder, with big fairings (stabilizers) on each side and longitudinal openings on upper and lower decks, had excellent aerodynamic stability. This concept was

adopted for the Tsing Ma Bridge, completed in 1997 (Simpson, Curtis, and Choi 1981). The Akashi Kaikyo Bridge has a vertical stabilizer in the center span located along the truss-type stiffening girder's center line just below the deck to improve aerodynamic stability (Ohashi et al. 1988).

In the 1990s, in Italy, a new girder type has been proposed for the Messina Straits Bridge, which would have a center span of 3300 m (Diana 1993). The 60 m wide girder would be made up of three oval box girders that support the highway and railway traffic. Aerodynamic dampers combined with wind screens would also be installed at both edges of the girder. Stiffening girders in recent suspension bridges are shown in Figure 9.17.

9.3.4.2 Design Standard

Figure 9.18 shows the wind-resistant design procedure specified in the Honshu-Shikoku Bridge Standard (HSBA 1990a). During the design procedure, a wind tunnel testing is required for two purposes: one is to verify the airflow drag, lift and moment coefficients that strongly influence the static design, and the other is to verify that harmful vibrations would not occur.

9.3.4.3 Analysis

Gust response analysis is an analytical method to ascertain the forced vibration of the structure under wind gusts. The results are used to calculate structural deformations and stress in addition to those caused by mean wind. Divergence, one type of static instability, is analyzed by using the finite displacement analysis to examine the relationship between wind force and deformation. Flutter is the most critical phenomena in considering the dynamic stability of suspension bridges, because of the possibility of collapse. Flutter analysis usually involves solving the bridge's motion equation as a complex eigenvalue problem where unsteady aerodynamic forces from wind tunnel tests are applied.

9.3.4.4 Wind Tunnel Testing

In general, the following wind tunnel tests are conducted to investigate the aerodynamic stability of the stiffening girder.

1. Two-dimensional test of rigid model with spring-support: The aerodynamic characteristics of a specific mode can be studied. The scale of the model is generally higher than 1/100.
2. Three-dimensional global model test to examine coupling effects of different modes.

For the Akashi Kaikyo Bridge, a global 1/100 model about 40 m in total length, was tested in a boundary layer wind tunnel laboratory. Together with the verification of the aerodynamic stability of the Akashi Kaikyo Bridge, new findings in flutter analysis and gust response analysis were established from the test results.

9.3.4.5 Countermeasures against Vibration

Countermeasures against vibration due to wind are classified as shown in Table 9.2.

1. *Increase Structural Damping*: Damping, a countermeasure based on structural mechanics, is effective in decreasing the amplitude of vortex-induced oscillations that are often observed during the construction of the main towers, and so on. Tuned mass dampers (TMD) and tuned liquid dampers (TLD) have also been used to counter this phenomenon in recent years. Active mass dampers (AMD), which can suppress vibration amplitudes over a wider frequency band, have also been introduced.
2. *Increase Rigidity*: One way to increase rigidity is to increase the girder height. This is an effective measure for suppressing flutter.
3. *Aerodynamic Mechanics*: It may also be necessary to adopt aerodynamic countermeasures, such as providing openings in the deck, and supplements for stabilization in the stiffening girder.

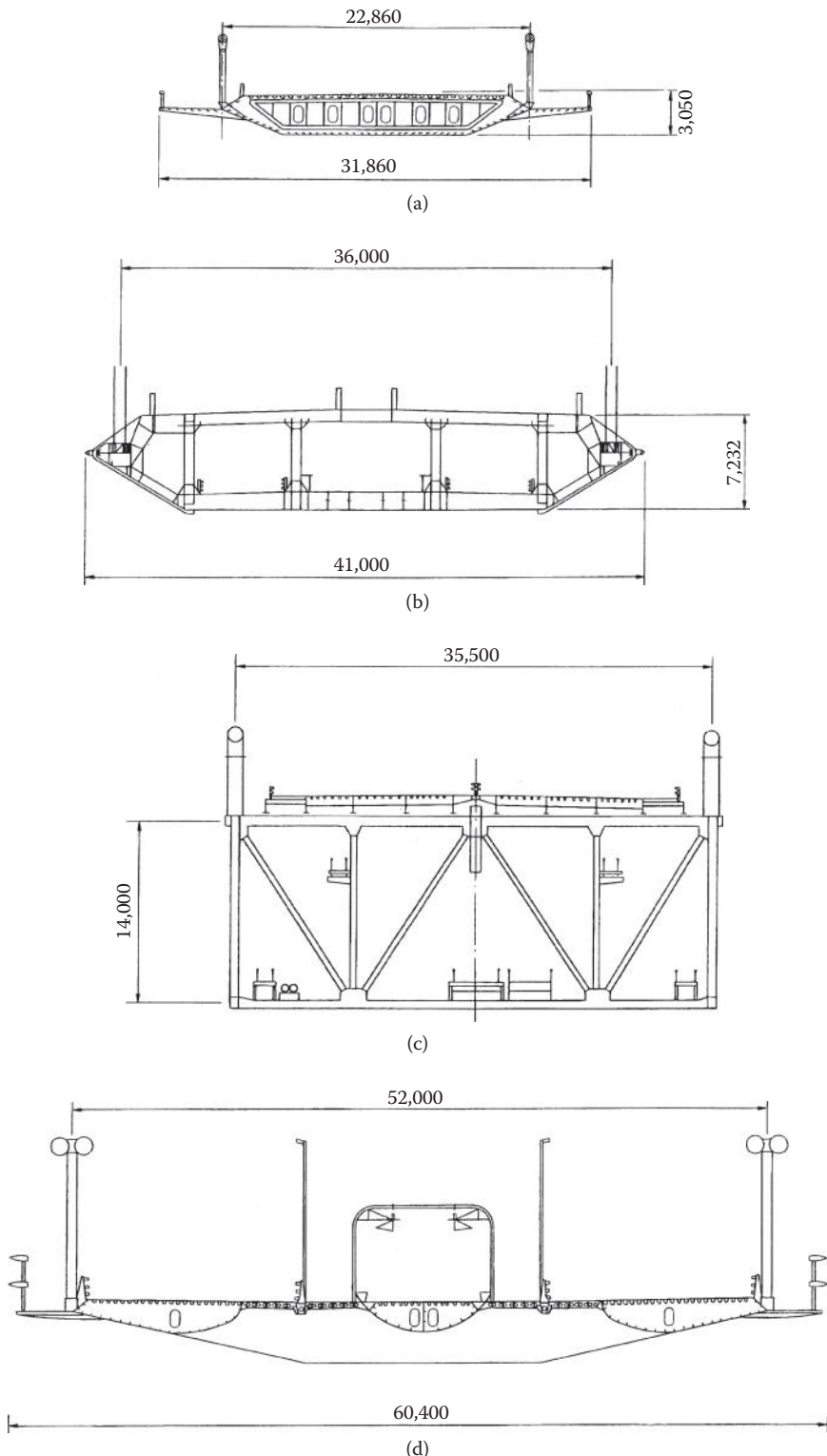


FIGURE 9.17 Cross-sections through stiffening girders.

@Seismicisolation

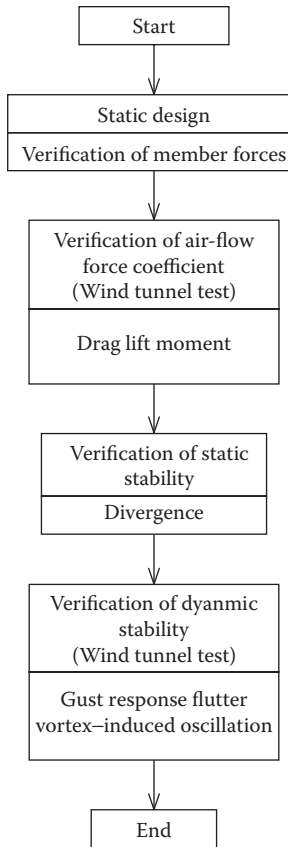


FIGURE 9.18 Procedure for wind-resistant design.

TABLE 9.2 Vibration Countermeasures

Category	Item	Counter Measures
Structural mechanics	Increase damping	TMD ^a , TLD ^b , AMD ^c
	Increase rigidity	Increase cross-sectional area of girder
	Increase mass	
Aerodynamic mechanics	Cross section	Streamlined box girder Open deck
	Supplements	Spoiler Flap

^a Tuned mass damper.

^b Tuned liquid damper.

^c Active mass damper.

9.3.5 Seismic Design

9.3.5.1 General

For a seismic design of long-span suspension bridges, the site-specific design ground motions are analytically estimated based on the past earthquakes in history, and the geometry and properties of the geological materials, including the detailed condition of the active faults at the bridge site.

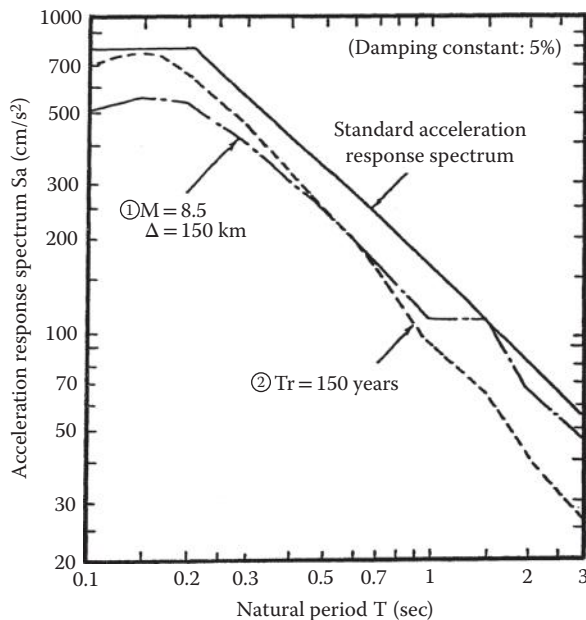


FIGURE 9.19 Design acceleration response spectrum.

In recent years, there are no instances of suspension bridges collapsing or even being seriously damaged due to earthquakes. During construction of the Akashi Kaikyo Bridge, the relative placement of four foundations changed slightly due to crustal movements in the 1995 Hyogo-ken Nanbu Earthquake. Fortunately, the quake caused no critical damage to the structures.

The verification to the seismic characteristics of the Akashi Kaikyo Bridge was conducted by using the earthquake motion of the same scale as that of the 1995 Hyogo-ken Nanbu Earthquake, and consequently the structure in its completed state was verified to be stable (Kawatoh and Kawaguchi 2003).

9.3.5.2 Design Method

The superstructure of a suspension bridge should take into account long period motion in the seismic design. A typical example of a seismic design is as follows. The superstructure of the Akashi Kaikyo Bridge was designed with consideration given to large ground motions including the long-period contribution. The acceleration response spectrum from the design standard is shown in Figure 9.19 (Kashima, Yasuda, Kanazawa, and Kawaguchi 1987). Time-history analysis was conducted on a three-dimension global bridge model including substructures and ground springs.

The moderate ground motions induced in the earthquakes with high probability to occur has been employed in the elastic design method. On the other hand, the intensive ground motions induced in the earthquakes with extremely low probability to occur is recently considered in the seismic retrofit projects and newly built bridges. In these cases, principal support structures, such as foundations, towers, and cables, are kept in sound while damage is allowed in secondary members.

9.3.6 Main Towers

9.3.6.1 General

Flexible type towers have predominated among main towers in recent long-span suspension bridges. This type of tower maintains structural equilibrium while accommodating displacement and the downward force from the main cable. Both steel and concrete are feasible material. Major bridges like the Golden Gate Bridge and the Verrazano Narrows Bridge in the United States as well as the Akashi Kaikyo Bridge in Japan consist

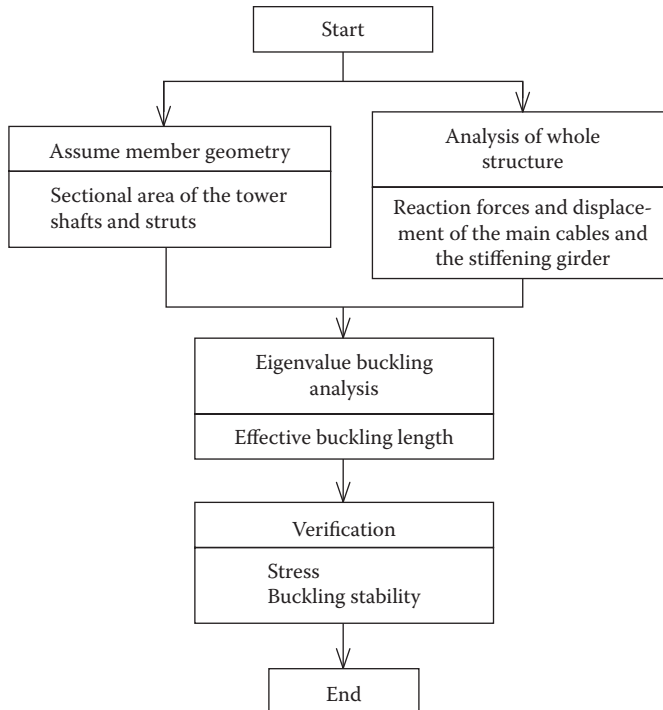


FIGURE 9.20 Design procedure for the main towers.

of steel towers. Examples of concrete towers include the Humber and Great Belt East Bridges in Europe, and the Tsing Ma Bridge in China. Because boundary conditions and loading of main towers are straightforward in the suspension bridge systems, the main tower can be analyzed as an independent structural system.

9.3.6.2 Design Method

The design method for the steel towers follows. The basic concepts for design of concrete towers are similar. For the transverse direction, main towers are analyzed using small deformation theory. This is permissible because the effect of cable restraint is negligible and the flexural rigidity of the tower is high. For the longitudinal direction, Birdsall's analytical method, discussed in Section 9.3.2, is generally used. However, more rigorous methods, such finite displacement analysis with a three-dimensional model that permits analysis of both the transverse and longitudinal directions, can be used, as was done in the Akashi Kaikyo Bridge. An example of the design procedure for main towers is shown in Figure 9.20 (HSBA 1984).

9.3.6.3 Tower Structure

The tower shaft cross-section may be T-shaped, rectangular, or cross-shaped, as shown in Figure 9.21. Though the multi-cell made up of small box sections has been used for some time, multi-cells and single cell have become noticeable in more recent suspension bridges.

The detail of the tower base that transmits the axial force, lateral force, and bending moment into the foundation, are either of grillage (bearing transmission type) or embedded types (shearing transmission type) as shown in Figure 9.22. Field connections for the tower shaft are typically bolted joints. Large compressive forces from the cable act along the tower shafts. Tight contact between two metal surfaces acts together with bolted joint to transmit the compressive force across joints with the bearing stresses spread through the walls and the longitudinal stiffeners inside the tower shaft. This method can secure very high accuracy of tower configuration. Another type of connection detail for the steel towers using tension bolts was used in the Forth Road Bridge, the Severn Bridge, the Bosphorus Bridge, and the first Kurushima Bridge (Figure 9.23).

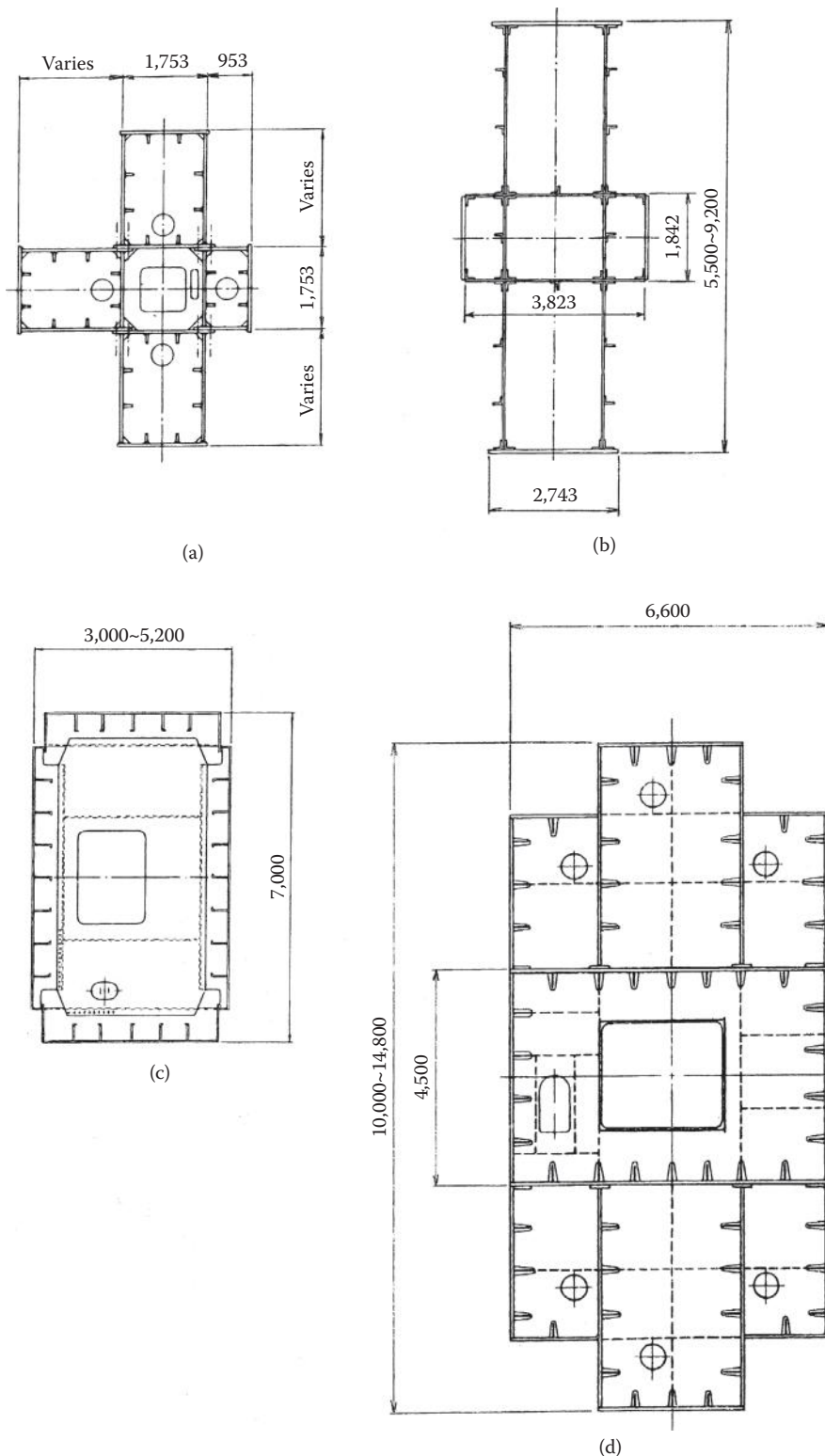


FIGURE 9.21 Tower shaft sections.

@Seismicisolation

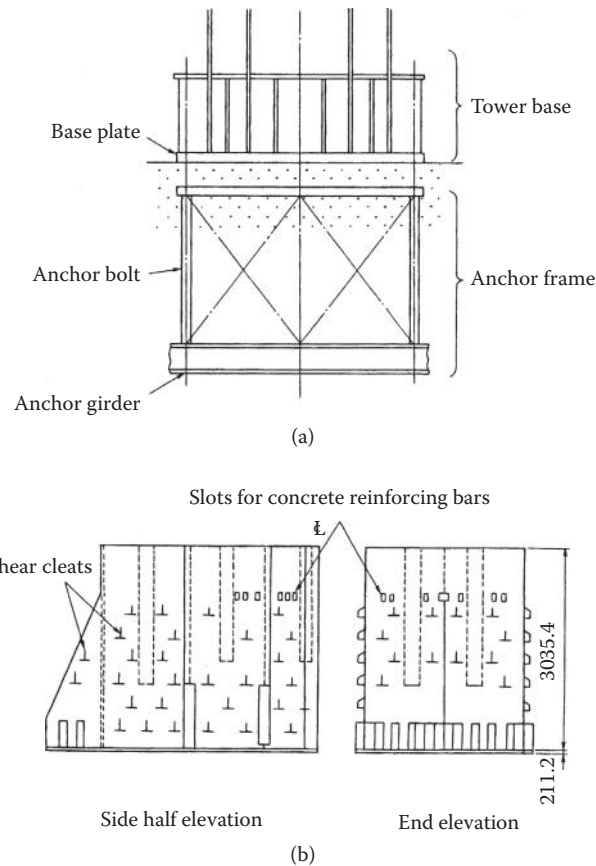


FIGURE 9.22 Tower base.

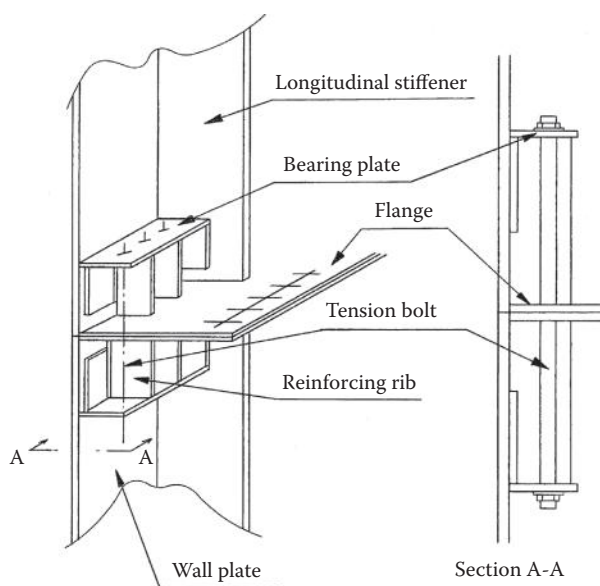


FIGURE 9.23 Connection using tension bolts.

9.3.7 Cables

9.3.7.1 General

Parallel wire cable has been used exclusively as the main cable in long-span suspension bridges. Parallel wire has the advantage of high strength and high modulus of elasticity compared to stranded wire rope. The design of the parallel wire cable is discussed next, along with structures supplemental to the main cable.

9.3.7.2 Design Procedure

Alignment of the main cable must be decided first (Figure 9.24). The sag-span ratios should be determined in order to minimize the construction costs of the bridge. In general, this sag-span ratio is roughly 1/10. However, the vibration characteristics of the entire suspension bridge change occasionally with changes in the sag-span ratios, so the influence on the bridge's aerodynamic stability should be also considered. After structural analyses are executed according to the design process shown in Figure 9.16, the sectional area of the main cable is determined based on the maximum cable tension, which usually occurs on the side span face of tower top.

9.3.7.3 Design of Cable Section

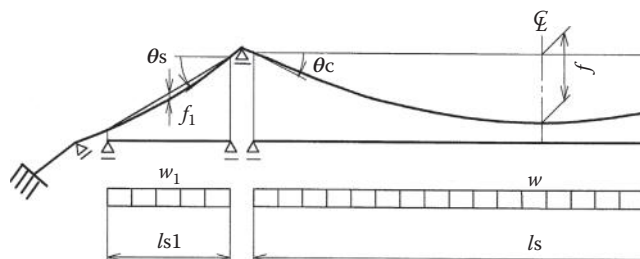
The tensile strength of cable wire has been about 1570 N/mm^2 (160 kgf/mm^2) in recent years. For a safety factor, 2.5 was used for the Verrazano Narrows Bridge and 2.2 for the Humber Bridge, respectively. In the design of the Akashi Kaikyo Bridge, a safety factor of 2.2 was used using the allowable stress method considering the predominant stress of the dead load. The main cables used a newly developed high-strength steel wire whose tensile strength is 1770 N/mm^2 (180 kgf/mm^2) and the allowable stress was 804 N/mm^2 (82 kgf/mm^2) led to this discussion. An increase in the strength of cable wire over the year is shown in Figure 9.25. In the design of the Great Belt East Bridge that was done using limit state design methods, a safety factor of 2.0 was applied for the critical limit state (Petersen and Yamasaki 1994). Cable statistics of major suspension bridges are shown in Table 9.3.

9.3.7.4 Supplemental Components

Figure 9.26 shows the auxiliary components of the main cable.

1. Cable strands are anchored in the cable anchor frame that is embedded into the concrete anchorage.
2. Hanger ropes are fastened to the main cable with the cable bands.

Cable saddles support the main cable at the towers and at the splay bents in the anchorages; the former is called the tower saddle and the latter is called the splay saddle.



f : center span sag

f_1 : side span sag

w : Uniform dead load (center span)

w_1 : Uniform dead load (side span)

θ_c : Tangential angle of cable (center span)

θ_s : Tangential angle of cable (side span)

l_s : center span length

l_{s1} : side span length

FIGURE 9.24 Configuration of suspension bridge.

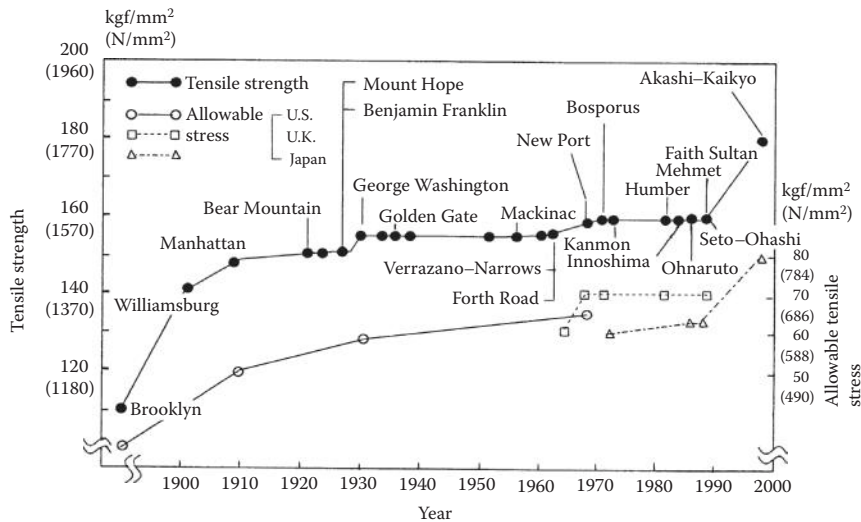


FIGURE 9.25 Increase in strength of cable wire.

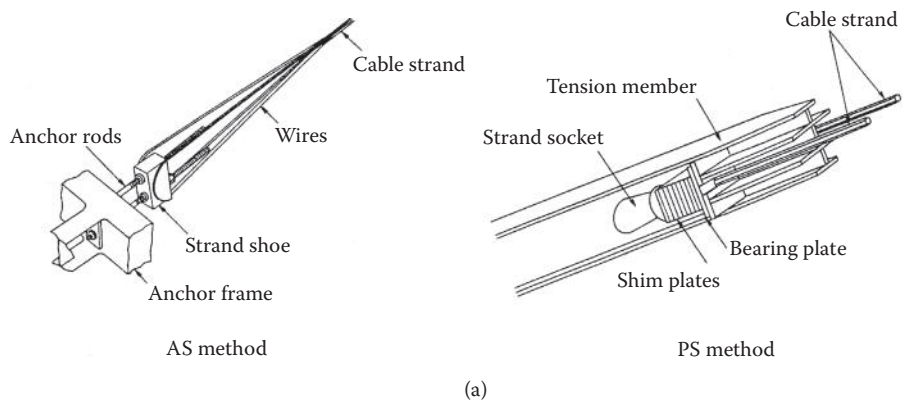
TABLE 9.3 Main Cable of Long-Span Suspension Bridges

No.	Bridge	Country	Year of Completion	Center Span Length (m)	Erection Method ^b	Composition of Main Cable ^c
1	Akashi Kaikyo	Japan	1998	1991	P.S.	127 × 290
2	Zoushan Xihoumen	China ^a	2008	1650	P.S.	North 127 × 175 Center 127 × 169 South 127 × 171
3	Great Belt East	Denmark	1998	1624	A.S.	504 × 37
4	Runyang Yangtze River	China ^a	2005	1490	P.S.	127 × 184
5	Humber	U.K.	1981	1410	A.S.	404 × 37
6	Jing Yin Yangtze River	China ^a	1999	1385	P.S.	127 × 169 (c/s), 177 (s/s)
7	Tsing Ma	China ^a	1997	1377	A.S.	368 × 80 + 360 × 11 (c/s, Tsing Yi s/s) 368 × 80 + 360 × 11 + 304 × 6 (Ma Wan s/s)
8	Verrazano Narrows	U.S.	1964	1298.5	A.S.	428 × 61 × 2 cables
9	Golden Gate	U.S.	1937	1280.2	A.S.	452 × 61
10	Yangtze Yangtze River	China ^a	2007	1280	P.S.	127 × 154
11	Höga Kusten	Sweden	1997	1210	A.S.	304 × 37 (c/s) 304 × 37 + 120 × 4 (s/s)
12	Mackinac Straits	U.S.	1957	1158.2	A.S.	340 × 37
13	Zhujiang Huangpu	China ^a	2008	1108	P.S.	North 127 × 153 Center 127 × 147 South 127 × 149
14	Minami Bisan-Seto	Japan	1988	1100	P.S.	127 × 271
15	Fatih Sultan Mehmet	Turkey	1988	1090	A.S.	504 × 32 (c/s), 36 (s/s)
16	Guizhou Balinghe	China ^a	2009	1088	P.S.	91 × 208 (c/s), 216 (s/s)
17	Bosphorus	Turkey	1973	1074	A.S.	550 × 19
18	George Washington	U.S.	1931	1066.8	A.S.	434 × 61 × 2 cables
19	3rd Kurushima	Japan	1999	1030	P.S.	127 × 102

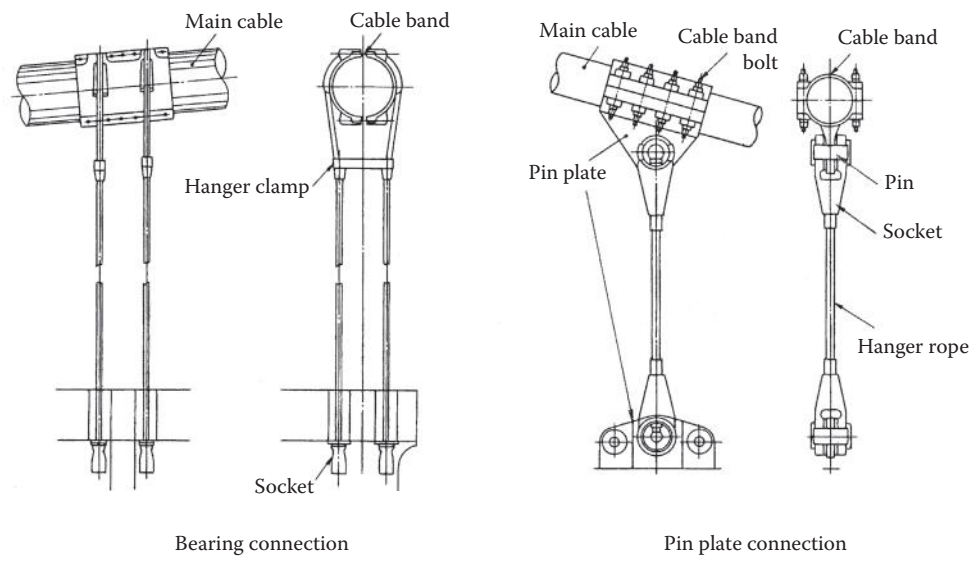
(Continued)

TABLE 9.3 (Continued) Main Cable of Long-Span Suspension Bridges

No.	Bridge	Country	Year of Completion	Center Span Length (m)	Erection Method ^b	Composition of Main Cable ^c
20	2nd Kurushima	Japan	1999	1020	P.S.	127 × 102
21	25 de Abril	Portugal	1966	1012.9	A.S.	304 × 37
22	Forth Road	U.K.	1964	1005.8	A.S.	(304 – 328) × 37
23	Kita Bisan-Seto	Japan	1988	990	P.S.	127 × 234
24	Severn	U.K.	1966	987.6	A.S.	438 × 19
25	Yichang Yangtze River	China ^a	2001	960	P.S.	127 × 104
26	Shimotsui-Seto	Japan	1988	940	A.S.	552 × 44

^a The People's Republic of China.^b P.S.: Prefabricated parallel wire strand method; A.S.: Aerial spinning erection method.^c Wire/strand × strand/cable.

(a)



(b)

FIGURE 9.26 Supplemental components of the main cable.

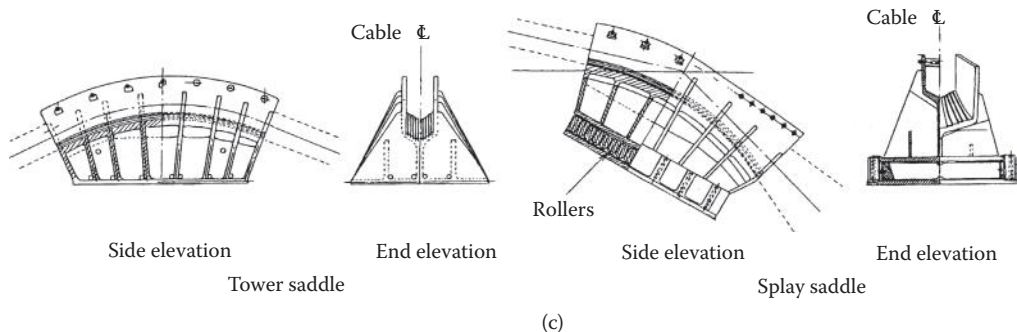


FIGURE 9.26 (Continued) Supplemental components of the main cable.

9.3.8 Suspended Structures

9.3.8.1 General

The suspended structure of a suspension bridge can be classified as a truss stiffening girder or a box stiffening girder, as described in Section 9.3.4. Basic considerations in selecting girder types are shown in Table 9.4. The length of the bridge and the surrounding natural conditions are also factors.

9.3.8.2 Design of the Stiffening Girder

9.3.8.2.1 Basic Dimensions

The width of the stiffening girder is determined to accommodate carriageway width and shoulders. The depth of the stiffening girder, which affects its flexural and torsional rigidity, is decided so as to ensure aerodynamic stability. After examining alternative stiffening girder configurations, wind tunnel tests are conducted to verify the aerodynamic stability of the girders.

In judging the aerodynamic stability, in particular the flutter, of the bridge design, a bending-torsional frequency ratio of 2.0 or more is recommended. Nevertheless, it is not always necessary to satisfy this condition if the aerodynamic characteristics of the stiffening girder are satisfactory.

9.3.8.2.2 Truss Girders

The design of the sectional properties of the stiffening girder is generally governed by the live load or the wind load. Linear finite deformation theory is usually employed to determine reactions due to live loads in the longitudinal direction, in which theory the influence line of the live load can be applied. The reactions due to wind loads, however, are decided using finite deformation analysis with a three-dimensional model given that the stiffening girder and the cables are loaded with a homogeneous part of the wind load. Linearized finite deformation theory is used to calculate the out-of-plane reactions due to wind load because the change in cable tension is negligible.

9.3.8.2.3 Box Girders

The basic dimensions of a box girder for relatively small suspension bridges are determined only by the requirements of fabrication, erection, and maintenance. Aerodynamic stability of the bridge is not generally a serious problem. The longer the center span becomes, however, the stiffer the girder needs to be to secure aerodynamic stability. The girder height is determined to satisfy rigidity requirement. For the Second and Third Kurushima Bridges, the girder height required was set at 4.3 m based on wind tunnel tests. Fatigue due to live loads need to be especially considered for the upper flange of the box girder because it directly supports the bridge traffic. The diaphragms support the floor system and transmit the reaction force from the floor system to the hanger ropes.

TABLE 9.4 Basic Considerations in Selecting Stiffening Structure Types

Item	Truss Girder	Box Girder
Girder height	High	Low
Aerodynamic stability	Flutter should be verified	Vortex induced oscillation tends to occur
Maintenance	Coating area is large	Flutter should be verified
Construction	Both plane section and section erection methods can be used	Only section erection method is permissible

9.3.8.3 Supplemental Components

Figure 9.27 shows supplemental components of the stiffening girder.

1. The stay ropes fix the main cable and the girder to restrict longitudinal displacement of the girder due to wind, earthquake, and temperature changes.
2. The tower links and end links support the stiffening girder at the main tower and the anchorages.
3. The wind bearings, which are installed in horizontal members of the towers and anchorages. They prevent transverse displacement of the girders due to wind and earthquakes.
4. Expansion joints are installed on the main towers of two-hinged bridges and at the anchorages to absorb longitudinal displacement of the girder.

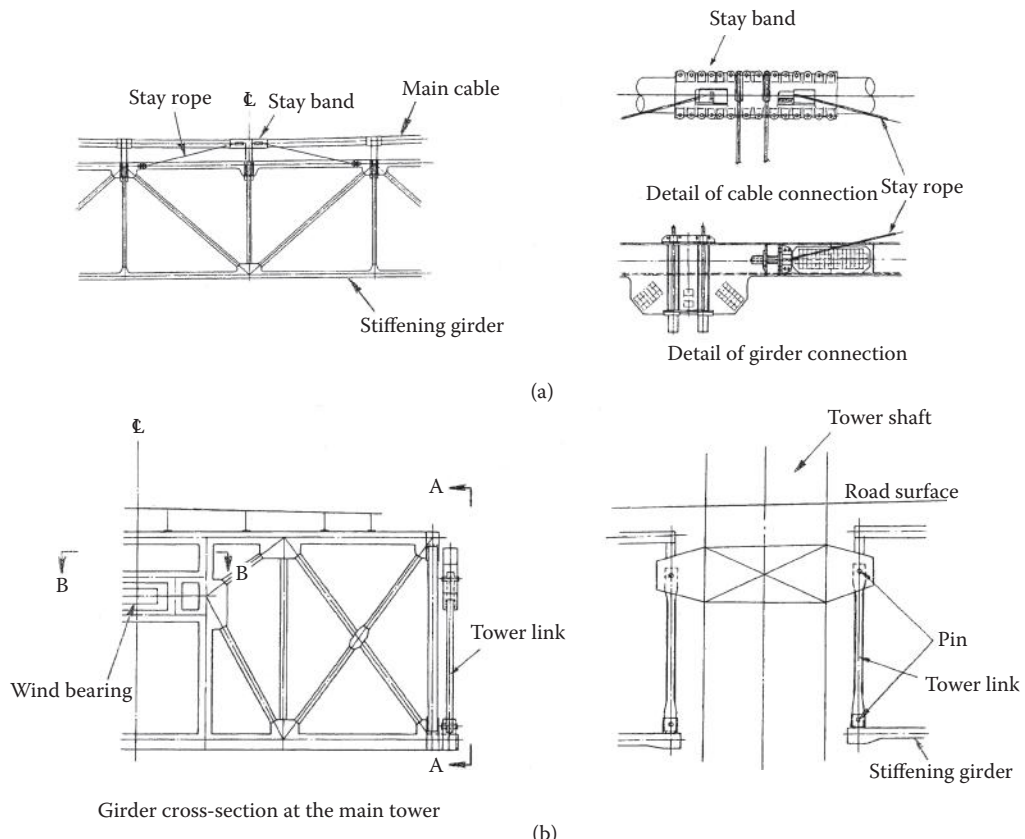


FIGURE 9.27 Supplemental components of the stiffening girder: (a) main cable and stay rope (b) tower link.

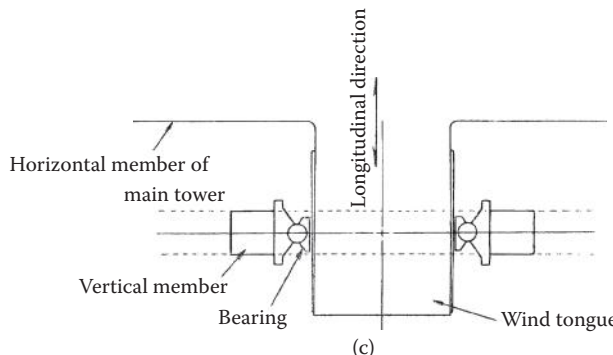


FIGURE 9.27 (Continued) Supplemental components of the stiffening girder: (c) wind tongue.

9.4 Construction

9.4.1 Main Towers

Suspension bridge tower supports the main cable and the suspended structure. Controlling erection accuracy to ensure that the tower shafts are perpendicular is particularly important. During construction, because the tower is cantilevered and thus easily vibrates due to wind, countermeasures for vibration are necessary. Recent examples taken from constructing steel towers of the Akashi Kaikyo Bridge and concrete towers of the Tsing Ma Bridge are described below.

9.4.1.1 Steel Towers

Steel towers are typically either composed of cells or have box sections with rib stiffening plates. The first was used in the Forth Road Bridge, the 25 de Abril Bridge, the Kanmon Bridge, and most of the Honshu-Shikoku Bridges. The latter was employed in the Severn Bridge, the Bosphorus Bridge, the Fatih Sultan Mehmet Bridge and the Kurushima Bridges. For the erection of steel towers, floating, tower and creeper traveler cranes are used. Figure 9.28 shows the tower erection method used for the Akashi Kaikyo Bridge. The tower of the Akashi Kaikyo Bridge is 297 m high. The cross section consists of three cells with clipped corners (Figure 9.21). The shaft is vertically divided into 30 sections. The sections were prefabricated and barged to the site. The base plate and the first section were erected using a floating crane. The remainder was erected using a tower crane supported on the tower pier. To control harmful wind-induced oscillations, tuned mass dampers (TMD) and active mass dampers (AMD) were installed in the tower shafts and the crane.

9.4.1.2 Concrete Towers

The tower of the Tsing Ma Bridge is 206 m high, 6.0 m in width transversely, and tapered from 18.0 m at the bottom to 9.0 m at the top longitudinally. The tower shafts are hollow. Each main tower was slip-formed in a continuous around-the-clock operation, using two tower cranes and concrete buckets (Figure 9.29).

9.4.2 Cables

9.4.2.1 Aerial Spinning Method

The Aerial Spinning Method (AS method) of parallel wire cables was invented by John A. Roebling and used for the first time in the Niagara Falls Bridge that was completed in 1855 with a center span of 246 m (Figure 9.30). He installed this technology in the Brooklyn Bridge where steel wire was first applied. Most

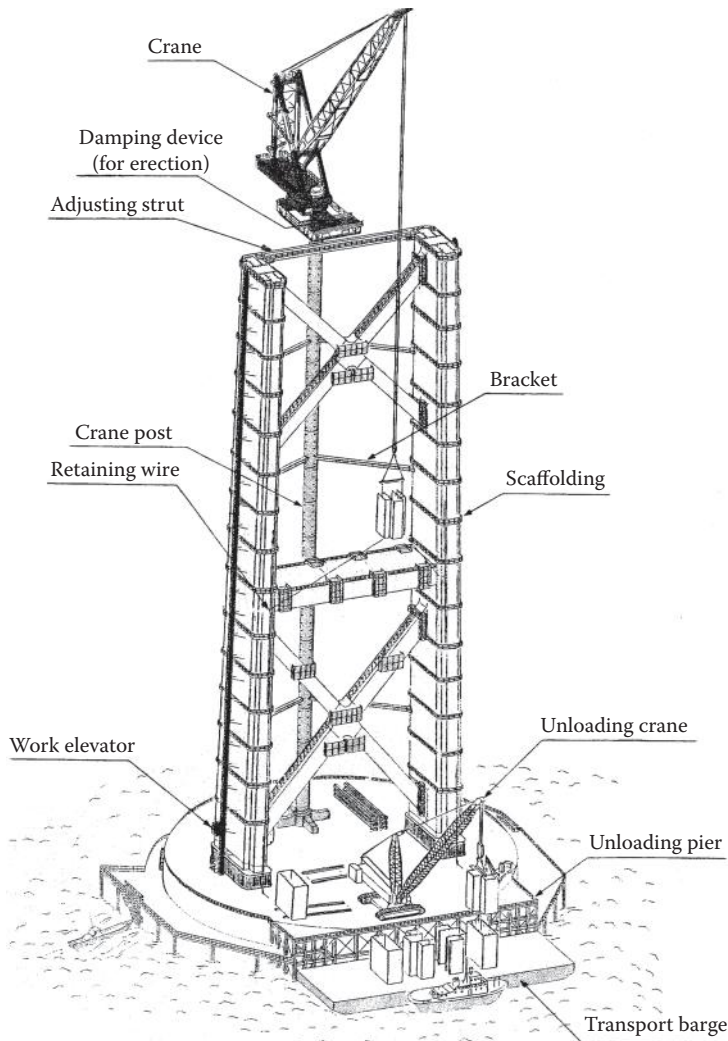


FIGURE 9.28 Overview of main tower construction.

suspension bridges built in the U.S. since Roebling's development of the AS method have used parallel wire cables. In contrast, in Europe, the stranded rope cable was used until the Forth Road Bridge was built in 1966.

In the conventional AS method, individual wires were spanned in free hang condition, and the sag of each wire had to be individually adjusted to ensure all were of equal length. In this so-called sag-control method, the quality of the cables and the erection duration are apt to be affected by site working conditions, including wind conditions and the available cable-spinning equipment. It also requires a lot of workers to adjust the sag of the wires.

A new method, called the tension-control method, was developed in Japan (Figure 9.31). The idea is to keep the tension in the wire constant during cable-spinning so as to obtain uniform wire lengths. This method was used on the Hirado, Shimotsui-Seto, Second Bosporus and Great Belt East Bridges (Figure 9.32). It does require adjustment of the individual strands even in this method.



FIGURE 9.29 Tower erection for the Tsing Ma Bridge.

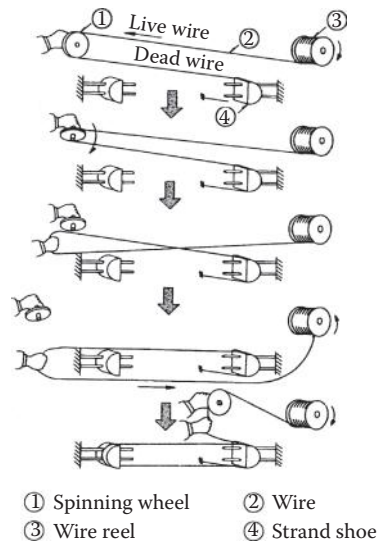


FIGURE 9.30 Operating principle of aerial spinning.

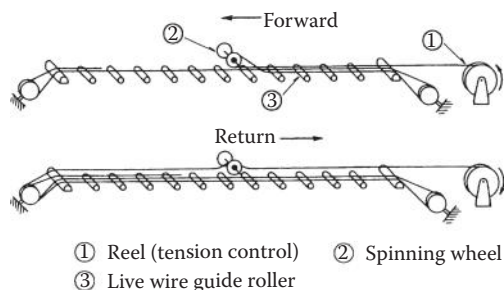


FIGURE 9.31 Operating principle of tension control method.

@Seismicisolation



FIGURE 9.32 Aerial spinning for the Shimotsui-Seto Bridge.

9.4.2.2 Prefabricated Parallel Wire Strand Method

Around 1965, a method of prefabricating parallel wire cables was developed to cut the on-site work intensity required for the cable-spinning in the AS method. The Prefabricated Parallel Wire Strand Method (PS method) was first used in the New Port Bridge. That was the first step toward further progress achieved in Japan in enlarging strand sections, developing high-tensile wire and lengthening the strand.

9.4.3 Suspended Structure

There are various methods of erecting suspended structures. Typically they have evolved out of the structural type and local natural and social conditions.

9.4.3.1 Girder Block Connection Methods

The connections between stiffening girder section may be classified as one of two methods.

9.4.3.1.1 All Hinge Method

In this method the joints are loosely connected until all girder sections are in place in general. This method enables simple and easy analysis of the behavior of the girders during construction. Any temporary reinforcement of members is usually unnecessary. However, it is difficult to obtain enough aerodynamic stability unless structures to resist wind force are given to the joints that were used in the Kurushima Bridges for example.

9.4.3.1.2 Rigid Connection Method

In this method full-splice joints are immediately completed as each girder block is erected into place. This keeps the stiffening girder smooth and rigid, providing good aerodynamic stability and high construction accuracy. However, temporary reinforcement of the girders and hanger ropes to resist transient excessive stresses or controlled operation to avoid over-stress are sometimes required.



FIGURE 9.33 Block erection method on the Kurushima Bridge.



FIGURE 9.34 Cantilevering method in the Akashi Kaikyo Bridge.

9.4.3.2 Girder Erection Methods

Stiffening girders are typically put in place using either girder section method or cantilevering from the towers or the anchorages.

9.4.3.2.1 Girder-Section Method

The state-of-the-art for girder-section method with hinged connections is shown in Figure 9.33. At the Kurushima bridge construction sites, the fast and complex tidal current of up to 5 m/s made it difficult for the deck-barges and tugboats maintain their desired position for a long time. As a result, a self-controlled barge, able to maintain its position using computer monitoring, and a quick joint system, which can reduce the actual erection period, were developed and fully utilized.

9.4.3.2.2 Cantilevering Method

A recent example of the cantilevering method of girders on the Akashi Kaikyo Bridge is shown in Figure 9.34. Pre-assembled panels of the stiffening girder truss were erected by extending the stiffening girders as a cantilever from the towers and anchorages. This avoided disrupting marine traffic, which would have been required for girder-section method.

TABLE 9.5 Structural Damping Obtained from Vibration Tests

Bridge	Center Span Length (m)	Logarithmic Decrement ^a
Minani Bisa-Seto	1100	0.020–0.096
Ohnaruto	876	0.033–0.112
Kanmon	712	0.016–0.062
Ohshima	560	0.017–0.180

^a Structural damping.

9.5 Field Measurement and Coatings

9.5.1 Loading Test

The purpose of loading tests is chiefly to confirm the safety of a bridge for both static and dynamic behavior. Static loading tests were performed on the Wakato, the Kanmon and the President Mobutu Sese Seko Bridges by loading heavy vehicles on the bridges. Methods to verify dynamic behavior include vibration tests and the measurement of micro oscillations caused by slight winds. The former test is based on the measured response to a forced vibration. The latter is described in Section 9.5.2. Dynamic characteristics of the bridge, such as structural damping, natural frequency and mode of vibration, are ascertained using the vibration test. As the real value of structural damping is difficult to estimate theoretically, the assumed value should be verified by an actual measurement. Examples of measured data on structural damping obtained through vibration tests are shown in Table 9.5.

9.5.2 Field Observations

Field observations are undertaken to verify such characteristics of bridge behavior as aerodynamic stability and seismic resistance, and to confirm the safety of the bridge. To gather the necessary data for certification, various measuring instruments are installed on the suspension bridge. Examples of measuring instruments used are given in Figure 9.35 (Abe and Amano 1998). A wind vane and anemometer, which measure local wind conditions, and a seismometer, to monitor seismic activity, gather data on natural conditions. An accelerometer and a displacement speedometer are installed to measure the dynamic response of the structure to wind and earthquake loads. A deck end displacement gauge tracks the response to traffic loads. The accumulated data from these measuring instruments will contribute to the design of yet longer-span bridges in the future.

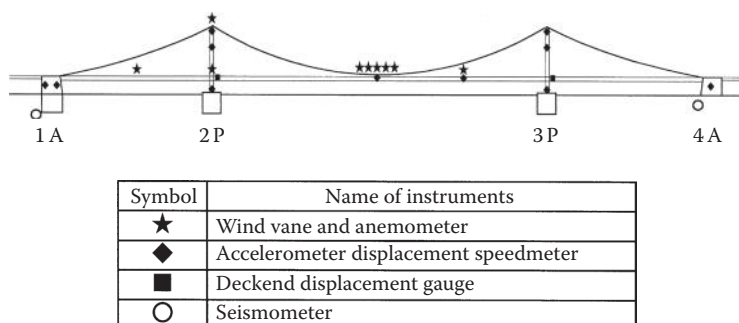


FIGURE 9.35 Placement of measuring instruments in the Akashi Kaikyo Bridge.

TABLE 9.6 Coating Systems of Major Suspension Bridges

Country	Bridge	Year of Completion	Coating Specification
U.S.	George Washington	1931	Base: oil based anticorrosive paint Top: phthalic resin paint
	San Francisco-Oakland Bay	1936	Base: red lead anticorrosive paint
	Golden Gate	1937	Top: oil-modified phenolic resin aluminum paint
	Mackinac Straits	1957	Base: oil based anticorrosive paint
	Verrazano Narrows	1964	Top: phthalic resin paint
Canada	Pierre La Porte	1970	Base: basic lead chromate anticorrosive paint Top: alkyd resin paint
	Bosphorus	1973	Base: zinc spraying Top: phenolic resin micaceous iron oxide paint
Turkey	Fatih Sultan Mehmet	1988	Base: organic zincrich paint Intermediate: epoxy resin paint Intermediate: epoxy resin micaceous iron oxide paint Top: paintchlorinated rubber resin paint
U.K.	Forth Road	1964	Base: zinc spraying
	Severn	1966	Top: phenolic resin micaceous iron oxide paint
	Humber	1981	
Japan	Kanmon	1973	Base: zinc spraying Intermediate: micaceous iron oxide paint Top: chlorinated rubber resin paint
	Innoshima	1983	Base: hi-build inorganic zincrich paint Intermediate: hi-build epoxy resin paint
	Akashi Kaikyo	1998	Top: polyurethane resin paint Intermediate: epoxy resin paint Top: fluoropolymer paint

9.5.3 Coating Specification

Steel bridges usually get a coating regimen that includes a rust-preventive paint for the base coat, and a long oil-base alkyd resin paint or chlorinated rubber resin paint for the intermediate and top coats. This painting regimen needs to be repeated at several-year intervals. Because long-span suspension bridges are generally constructed in a marine environment, which is severely corrosive, and have enormous painting surfaces, which need to be regularly redone, a heavy-duty coating method with long-term durability is required. The latest coating technology adopted for major suspension bridges is shown in Table 9.6. Previous painting methods relied on oil-base anticorrosive paints or red lead anticorrosive paints for base coats with phthalic resin or aluminum paints as intermediate and top coats. The latest coating specification aimed at long-term durability calls for an inorganic zinc-enriched base paint, which is highly rust-inhibitive due to the sacrificial anodic reaction of the zinc, with an epoxy resin intermediate coat and a polyurethane resin or fluoropolymer top coat. Because the superiority of fluoropolymer paint for long-term durability and in holding a high luster under ultraviolet rays has been confirmed in recent years, it was used for the Akashi Kaikyo Bridge (HSBA 1990b).

9.5.4 Main Cable Corrosion Protection

Since the main cables of a suspension bridge are most important structural members, corrosion protection is extremely important for the long-term maintenance of the bridge. The main cables are composed of

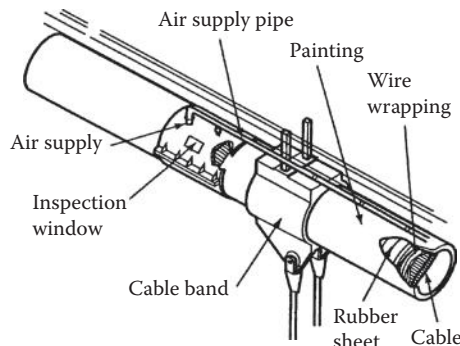


FIGURE 9.36 Dehumidified air injection system for the main cables of the Akashi Kaikyo Bridge.

TABLE 9.7 Corrosion Protection Systems for Main Cable of Major Suspension Bridges

Bridge	Year of Completion	Erection method	Cable		Wrapping/Air Injection System
			Wire	Paste	
Brooklyn	1883	A.S.	Galvanized	Red lead paste	Galvanized wire
Williamsburg	1903	A.S.	- ^a	Red lead paste	Cotton duck + sheet iron coating
Golden Gate	1937	A.S.	Galvanized	Red lead paste	Galvanized wire
Chesapeake Bay II	1973	A.S.	Galvanized	-	Neoprene rubber
Verrazano Narrows	1964	A.S.	Galvanized	Red lead paste	Galvanized wire
Severn	1966	A.S.	Galvanized	Red lead paste	Galvanized wire Air injection system
New Port	1969	P.S.	Galvanized	-	Glass-reinforced acrylic
Kanmon	1973	P.S.	Galvanized	Polymerized organic lead paste	Galvanized wire
Minami Bisan-Seto	1988	P.S.	Galvanized	Calcium plumbate contained polymerized organic lead paste	Galvanized wire
Hakicho	1998	P.S.	Galvanized	Aluminum triphosphate contained organic lead paste	Galvanized wire (S shape)
Akashi Kaikyo	1998	P.S.	Galvanized	-	Air injection system Galvanized wire + rubber wrapping Air injection system

^a Coated with a raw linseed oil.

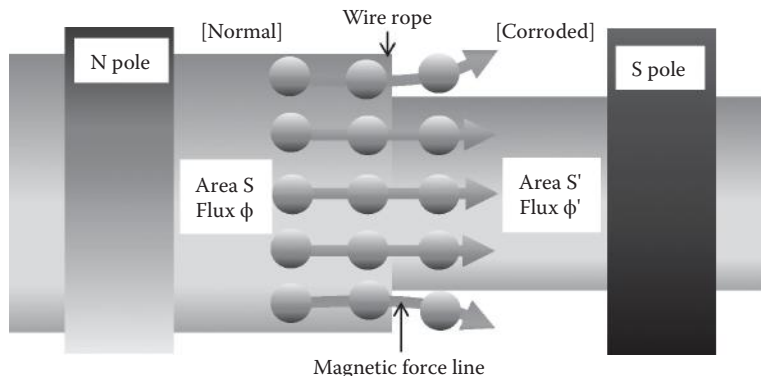


FIGURE 9.37 Main flux method for inspection of suspender rope corrosion.

galvanized steel wire about 5 mm in diameter with a void of about 20% that is longitudinally and cross-sectionally consecutive. Main cable corrosion is caused not only by water and ion invasion from outside, but also by dew resulting from the alternating dry and humid conditions inside the cable void. The standard corrosion protection system for the main cables ever since it was first worked out for the Brooklyn Bridge has been to use galvanized wire covered with a paste, wrapped with galvanized soft wires and then coated.

New approaches such as wrapping the wires with neoprene rubber or fiberglass acrylic or S-shaped deformed steel wires have also been undertaken. A dehumidified air injection system is developed and used on the Akashi Kaikyo Bridge (Ito, Saeki, and Tatsumi 1996). This system includes wrapping to improve water-tightness and the injection of dehumidified air into the main cables as shown in Figure 9.36. To all existing and new suspension bridges in Honshu-Shikoku Bridges, the system was introduced. This system has also been applied to three suspension bridges in Japan, and to eight bridges in the world including three noted suspension bridges in United Kingdom. Examples of a corrosion protection system for the main cables in major suspension bridges are shown in Table 9.7.

9.5.5 Inspection for Suspender Rope Corrosion

At the Innoshima Bridge, one of the Honshu-Shikoku Bridges, which was opened in 1983, corrosion was found on the inner layer strands of its suspenders when a few suspenders were disassembled.

To examine corrosion of all suspenders, a non-destructive inspection method, the main flux method that can directly detect any reduction of sectional area caused by corrosion, was tested. In this method, a coil wrapped around a suspender detects magnetic flux, and decrease of magnetic flux can be measured by calculating the accumulated amounts of electricity induced in the suspender over time, as shown in Figure 9.37 (Kitagawa, Suzuki, and Okuda 2001).

This method was used in two suspension bridges in Honshu Shikoku Bridges, and its accuracy was demonstrated.

References

- Abe, K. and Awmano, K. 1998. "Monitoring system of the Akashi Kaikyo Bridge," *Honshi Technical Report*, 86, 29 [in Japanese].
- Birdsall, B. 1942. "The suspension bridge tower cantilever problem," *Trans. ASCE*. 107(1), 847–862.
- Bleich, F., McCullough, C. B., Rosecrans, R., and Vincent, G. S. 1950. *The Mathematical Theory of Vibration in Suspension Bridges*, Department of Commerce, Bureau of Public Roads, Washington, DC.
- Brotton, D. M. 1966. "A general computer programme for the solution of suspension bridge problems," *Struct. Eng.*, 44, 161–167.

- Diana, G. 1993. "Aeroelastic study of long span suspension bridges, the Messina Crossing," in *Proceedings ASCE Structures Congress '93*, Irvine, CA.
- HSBA. 1984. *Design Standard of the Main Tower for a Suspension Bridge*, Honshu-Shikoku Bridge Authority, Japan [in Japanese].
- HSBA. 1990a. *Wind-Resistant Design Standard for the Akashi Kaikyo Bridge*, Honshu-Shikoku Bridge Authority, Japan [in Japanese].
- HSBA. 1990b. *Steel Bridges Coating Standards of Honshu-Shikoku Bridge*, Honshu-Shikoku Bridge Authority, Japan. [in Japanese].
- Ito, M., Saeki, S., and Tatsumi, M. 1996. "Corrosion protection of bridge cables: from Japanese experiences," in *Proceedings of the International Seminar on New Technologies for Bridge Management*, IABSE, Seoul.
- Kashima, S., Yasuda, M., Kanazawa, K., and Kawaguchi, K. 1987. "Earthquake resistant design of Akashi Kaikyo Bridge," Paper Presented at *Third Workshop on Performance and Strengthening of Bridge Structures*, Tsukuba, Japan.
- Kawatoh, C. and Kawaguchi K., 2003. "Seismic verification of long-span bridge of Honshu-Shikoku Bridges," *19th US-Japan Bridge Engineering Workshop*, Tsukuba, Japan.
- Kitagawa, M., Suzuki, S., and Okuda, M. 2001. "Assessment of cable maintenance technologies for Honshu-Shikoku Bridges," *J. Bridge Eng. ASCE*, 6(6), 418–424.
- Lévy, M. 1886. "Calculation method for rigidity of the suspension bridge (Mémoire sur le calcul des ponts suspendus rigides)," *Annals of Roads and Bridges (Ann. Ponts Chaussées)*, (in French).
- Melan, J. 1888. *Theory of the Iron Arch Bridges and Suspension Bridges (Theorie der eisernen Bogenbrücken und der Hängebrücken)*, Scientific engineering handbook (Handb. Ingenieurwissenschaft) (in German).
- Moisseiff, L. S. 1925. "The towers, cables and stiffening trusses of the bridge over the Delaware River between Philadelphia and Camden," *J. Franklin Inst.*, 200(4), 433–466.
- Moisseiff, L. S. and Lienhard, F. 1933. "Suspension bridge under the action of lateral forces," *Trans. ASCE*, 98(2), 1080–1095.
- Navier, M. 1823. *Report on the Suspension Bridges (Rapport et Mémoire sur les Ponts Suspendus)*, Royal Printing (de l' Imprimerie Royale), Paris, France (in French).
- Ohashi, M., Miyata, T., Okauchi, I., Shiraishi, N., and Narita, N. 1988. "Consideration for wind effects on a 1990 m main span suspension bridge," *Pre-report 13th International Congress IABSE*, 911 pp.
- Petersen, A. and Yamasaki, Y. 1994. "Great Belt Bridge and Design of its Cable Works," *Bridge Foundation Eng.*, 1, 18–26. [in Japanese].
- Rankine, W. J. M. 1858. *A Manual of Applied Mechanics*. Richard Griffin and Company, London, UK.
- Ritter, W. 1877. "Cambered multiple stiffening trusses and suspension bridges (Versteifungsfachwerke bei Bogen und Hängebrücken)," *J. Constr. (Z. Bauwesen)*, 27, 187–207.
- Roberts, G. 1970. *Severn Bridge, Institution of Civil Engineers*, London, UK.
- Saafan, A. S. 1966. "Theoretical analysis of suspension bridges," *J. Struct. Div. ASCE*, 92(4), 1–11.
- Simpson, A. G., Curtis, D. J., and Choi, Y.-L. 1981. *Aeroelastic Aspects of the Lantau Fixed Crossing*, Institution of Civil Engineers, London, UK.
- Steinman, D. B. 1935. "A generalized deflection theory for suspension bridges," *Trans. ASCE*, 100(1), 1133–1170.
- Tezcan, S. S. 1966. "Stiffness analysis of suspension bridges by iteration," in *Symposium on Suspension Bridges*, Lisbon, Portugal.
- Walshe, D. E., and Rayner, D. V. 1962. *A Further Aerodynamic Investigation for the Proposed Severn River Suspension Bridge*, National Physical Laboratory, Aerodynamics Division, Teddington, UK.

10

Cable-Stayed Bridges

10.1	Introduction	399
	Evolution of Cable-Stayed Bridges	
10.2	Configuration.....	407
	General • Extradosed Bridges	
10.3	General Layout	412
	Girder • Stay Cables • Pylons • Piers and Foundations • Articulation	
10.4	Design Requirements.....	422
	Functional Requirements • Loading Conditions • Analysis	
10.5	Superlong Spans.....	423
10.6	Multi-Span Cable-Stayed Bridges	425
10.7	Cable-Stayed Bridges for Railway	429
10.8	Aerodynamic Aspects	431
	Cable Vibrations • Girder • Pylon • Wind Tunnel Testing	
10.9	Architectural Lighting.....	432
	References.....	434

Tina Vejrum
COWI A/S

Lars Lundorf Nielsen
COWI A/S

10.1 Introduction

The use of cables as the primary load carrying elements in bridge structures has proven very efficient as the high strength-to-weight ratio of the cable material will decrease the escalation of the dead load otherwise related to longer spans. Today cable supporting is applied to most spans above 250 m (820 ft).

Cable-stayed bridges have become very popular since completion of the first modern cable-stayed bridge, the Strömsund Bridge in Sweden, in 1955. Due to the versatile nature of cable-stayed bridges this type of bridge design is adopted for a variety of span lengths from footbridges less than 50 m in length up to spans of more than 1000 m carrying traffic load. There are currently well over 1000 cable-stayed bridges around the world.

The basic structural form of a cable-stayed bridge consists of a number of triangles composed of the pylon, the stiffening girder, and the stay cables. Bridges mainly carry vertical loads and these are transferred locally by the stiffening girder to the elastic supports provided by the stay cables and subsequently through tension in the cables to the pylons as shown in Figure 10.1. Compressive axial forces in the stiffening girder and in the pylons are in equilibrium with tensile forces in the cables. Hence the loads are mainly transferred as axial forces rather than bending, which generally results in a more efficient and economical structure. The dead load of the stiffening girder induces pretensioning of the stay cables that increases the stiffness of the structural system.

Cable-stayed bridges are usually self-anchored structures and therefore offer a good solution at locations where the soil conditions are not good and as a consequence the cost of the foundations for an earth-anchored structure—like a typical suspension bridge—would become excessive.

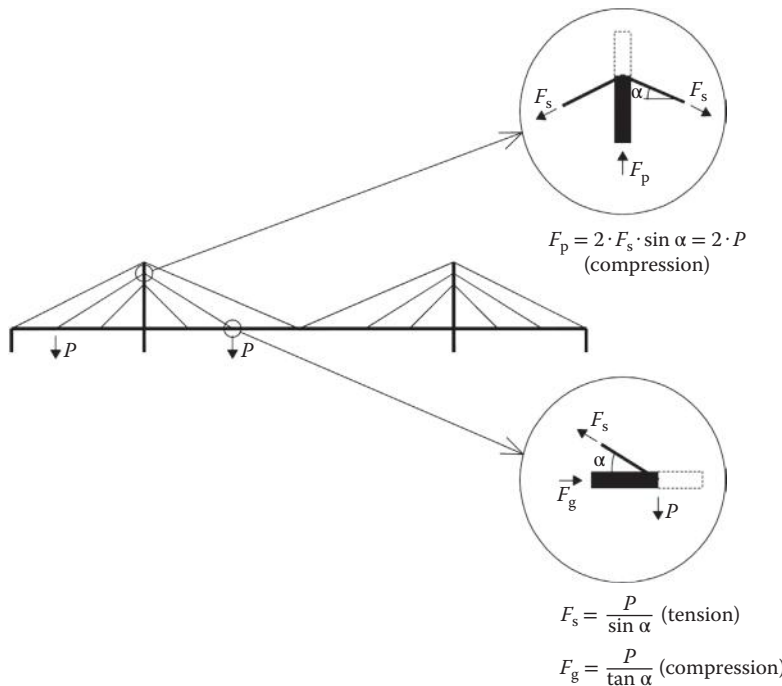


FIGURE 10.1 Basic load transfer in a cable-stayed system subject to balanced vertical loads.

As a consequence of the self-anchored system a cable-stayed bridge is typically faster to construct in comparison with a suspension bridge because erection of the superstructure can start as soon as the pylons reach the height of the first cable anchor points. However, the arrangement of the stay cables in combination with the self-anchored system introduces compression in the girder that makes cable-stayed bridges less favorable for very long spans where suspension bridges dominate.

10.1.1 Evolution of Cable-Stayed Bridges

10.1.1.1 Design and Span Length

Even though cable-stayed systems had been adopted in bridge construction earlier in history, none of these early examples set a precedent and the Strömsund Bridge (Figure 10.2) in Sweden is usually considered the first modern cable-stayed bridge. The Strömsund Bridge completed in 1955 has one main span and two side spans—a global arrangement that has often been used for suspension bridges. The main span of 182.6 m (599 ft) is supported by two sets of stay cables radiating from the top of each pylon. The pylons are of the portal type and the stay cables are anchored on either side of the bridge deck, thus providing both vertical and torsional support to the deck. Stiffening girders and pylons are in steel, whereas the deck consists of a concrete slab.

In the following years the center of development in cable-stayed bridges was in Germany where a remarkable number of cable-stayed bridges and with a variety of different designs were constructed.

The first cable-stayed bridge in Germany is the Theodor Heuss Bridge across the Rhine River in Düsseldorf. The bridge is a three span structure with a main span of 260 m (853 ft) as shown in Figure 10.3. The stiffening girder and pylons are in steel. The pylons are of the freestanding post (or mast) type with the posts located at the edge of the girder providing two vertical cable planes. The stay cables are arranged in a harp configuration with three sets of stay cables from each post, for terminology refer to Section 10.2—Configuration.

The Severins Bridge with a span of 302 m (991 ft) across the Rhine in Cologne followed in 1961, 4 years after completion of the Theodor Heuss Bridge. The design stands out as it is the first cable-stayed bridge with an A-shaped pylon and furthermore an asymmetrical arrangement with one pylon only and two spans



FIGURE 10.2 Strömsund Bridge, Sweden, completed in 1955. The main span is 182.6 m (599 ft) and the stay cables are arranged in a pure fan system. Pylons and stiffening girders are in steel. (Courtesy of www.pwpeics.se [P. Wåhlin].)



FIGURE 10.3 The Theodor Heuss Bridge across the Rhine River in Düsseldorf, Germany (also known as the North Bridge). Completed in 1957, the bridge has a main span of 260 m (853 ft) and the stay cables are arranged in a harp system. (Courtesy of www.structurae.de [N. Janberg].)

as shown in Figure 10.4. The pylon and stiffening girder are constructed in steel and the deck arrangement is similar to the Theodor Heuss Bridge with stay cables anchored along the edges. Due to the A-shaped pylon the stay cables are arranged in a fan system that is inclined in the transverse direction. The overall arrangement leads to a very efficient structural system.

The third German cable-stayed bridge is the Norderelbe Bridge in Hamburg, in 1962, having a traditional three-span arrangement with a main span of 172 m (564 ft). What makes this bridge noteworthy is that it was the first cable-stayed bridge constructed with central post (or mono-column) pylons and a single cable plane located in the central reserve of the motorway. Accordingly, the torsional stiffness is provided by the stiffening girder that is a 3 m (10 ft) deep closed steel box located under the central portion of the deck. Even though the single plane cable system is less efficient than a system providing torsional support the arrangement makes sense for motorway applications where the traffic is divided into two directions separated by a central reserve of a certain minimum width providing sufficient space for the cable anchorages. Subsequently, the arrangement with a single vertical cable plane was often the preferred system.



FIGURE 10.4 Severins Bridge across the Rhine River in Cologne, Germany, completed in 1961. Main span 302 m (991 ft). (Courtesy of S. Prinzler.)

The first cable-stayed bridges only have a few discrete cables imitating the support that additional piers would have provided to the girder. Cable-stayed bridges are statically indeterminate structures and limitations in the numerical tools available at that time required the number of redundants to be kept at a minimum. These limitations have subsequently been overcome by the development of analysis tools and the increasing capability of modern computers. As a consequence the trend has moved towards multi-cable systems where the cable system provides an almost continuous elastic support of the girder, which in turn can be designed with moderate bending stiffness about the horizontal axis since it is basically only required to carry the vertical loads over the short distance between cable anchor points. This simplifies construction as well as future cable replacement and has contributed to a more economic design overall.

The Friedrich Ebert Bridge across the Rhine River in Bonn in Germany, completed in 1967, is the first cable-stayed bridge to adopt a multi-cable system.

The development in Germany continued with construction of a number of cable-stayed bridges, with the Duisburg-Neuenkamp Bridge, completed in 1970, holding the world record for 5 years with its main span of 350 m (1148 ft). This bridge stands out in the list of record spans as it is the sole record holder to date designed with just one cable plane.

At the same time as the Norderelbe Bridge was built another remarkable structure was under construction: The Maracaibo Bridge (Figure 10.5) built in Venezuela in 1962. Not only is this the first multi-span cable-stayed bridge having six pylons and five main spans of 235 m (771 ft), it is also the first application of concrete as structural material in the pylons and stiffening girder of a cable-stayed bridge. Overall stability in the longitudinal direction is provided by the very stiff triangular pylon structures. Only one set of stay cables from each pylon provides intermediate support to the girder and consequently the girder is of a very heavy design enabling it to span between the pylons and the cable support points. A small suspended span at the center of each main span connects the ends of the cable-stayed cantilevers. The Maracaibo Bridge held the world record for concrete cable-stayed bridges until the Wadi Cuf Bridge in Libya was completed in 1971 by the same designer. The Wadi Cuf Bridge with a single main span of 287 m (942 ft) followed the same design principles as Maracaibo. Yet, despite the pioneering these bridges have not set a precedent in design of cable-stayed bridges.

The Saint Nazaire Bridge across the Loire River and Brotonne Bridge across the Seine River, both in France and both completed in 1977, became the longest cable-stayed bridge overall (404 m [1326 ft]) and longest concrete cable-stayed bridge (320 m [1050 ft], Figure 10.6), respectively. The Brotonne Bridge has central



FIGURE 10.5 Maracaibo Bridge in Venezuela (General Rafael Urdaneta Bridge), completed in 1962, is an all-concrete multi-span cable-stayed bridge with five main spans of 235 m. (Courtesy of C. Añez.)



FIGURE 10.6 Brotonne Bridge across the river Seine, France, completed in 1977. The main span is 320 m and the bridge is an all-concrete structure. (Courtesy of P. Bourret.)

mono-column pylons and a central cable plane, whereas the Saint Nazaire Bridge has inverted V-shaped steel pylons located on top of concrete piers and two transversely inclined cable planes.

Until 1983 the longest cable-stayed bridge span had always been constructed in steel. In 1983 the Barrios de Luna Bridge in Spain became the first concrete bridge to hold the record with 440 m (1444 ft) main span. This was followed by the Alex Fraser Bridge in Canada with a composite main span of 465 m (1526 ft) (Figure 10.7). The Alex Fraser Bridge was completed in 1986. Both the Barrios de Luna and the Alex Fraser Bridge have H-shaped pylons located on land and with two cable planes arranged in a modified fan multi-cable system providing an efficient structural system.

On a smaller scale a very interesting concrete cable-stayed bridge was completed in 1985: The Diepoldsau Bridge across the Rhine River in Switzerland. With its main span of 97 m (318 ft) and stiffening girder composed of a concrete slab with a depth of only 0.55 m (1.81 ft) at the centerline and 0.36 m (1.18 ft) at the edges the superstructure is extremely slender (Walther et al. 1985). This was made possible by the closely spaced stay cables anchored at 6 m (20 ft) centers effectively providing continuous elastic support to the girder



FIGURE 10.7 Alex Fraser Bridge in Vancouver, Canada, has a composite main span of 465 m (1526 ft). The bridge was completed in 1986. (Courtesy of Buckland & Taylor Ltd.)

and the application of two cable planes providing torsional support. Prior to the project, an extensive research program was implemented to provide a better understanding of the buckling stability of such a slender girder and the dynamic behavior of the structure in general.

Another all-concrete bridge took over the record in 1991: Skarnsundet in Norway having a main span of 530 m (1739 ft). The pylons are A-shaped and the cable system provides vertical and torsional support to the girder. The girder transfers lateral loads, like transverse wind loading, in bending and with a girder width of only 13 m (43 ft) the superstructure is extremely slender in the lateral direction.

The Yangpu Bridge across the Huangpu River in Shanghai, China, was constructed with a composite main span of 602 m (1975 ft). The bridge was completed in 1993 and held the record for 2 years, when completion of the Normandy Bridge in France increased the record span by an impressive 42% to 856 m (2808 ft). The superstructure of the Normandy Bridge is in concrete in the side spans and 116 m (381 ft) into the main span with the central 624 m (2047 ft) of the main span fabricated in steel. The structural system is unusual by having a monolithic connection between the concrete superstructure and the pylons. This is facilitated by the fact that the concrete superstructure continues into the main span, but as a result of the restraint strains in the girder due to, for example, temperature will introduce axial forces in the girder and bending moments in the pylons.

A large number of cable-stayed bridges were constructed in Japan and quite frequently a double deck concept was adopted. The Tatara Bridge completed in 1999 has a slender box girder and it increased the record span length to 890 m (2920 ft).

Completion of the Sutong Bridge in China in 2008 is an important milestone. With a main span of 1088 m (3570 ft) this is the first cable-stayed bridge passing the 1 km (3281 ft) mark. Simultaneously, Stonecutters Bridge in Hong Kong S.A.R., China, was constructed with a main span of 1018 m (3340 ft). The third cable-stayed bridge with a main span over 1 km (3281 ft) is the bridge to Russky Island in Vladivostok, Russia, which was completed in 2012. The main span of the Russky Island Bridge is 1104 m (3622 ft). More details of these cable-stayed bridges are presented in Section 10.5—Superlong Spans.

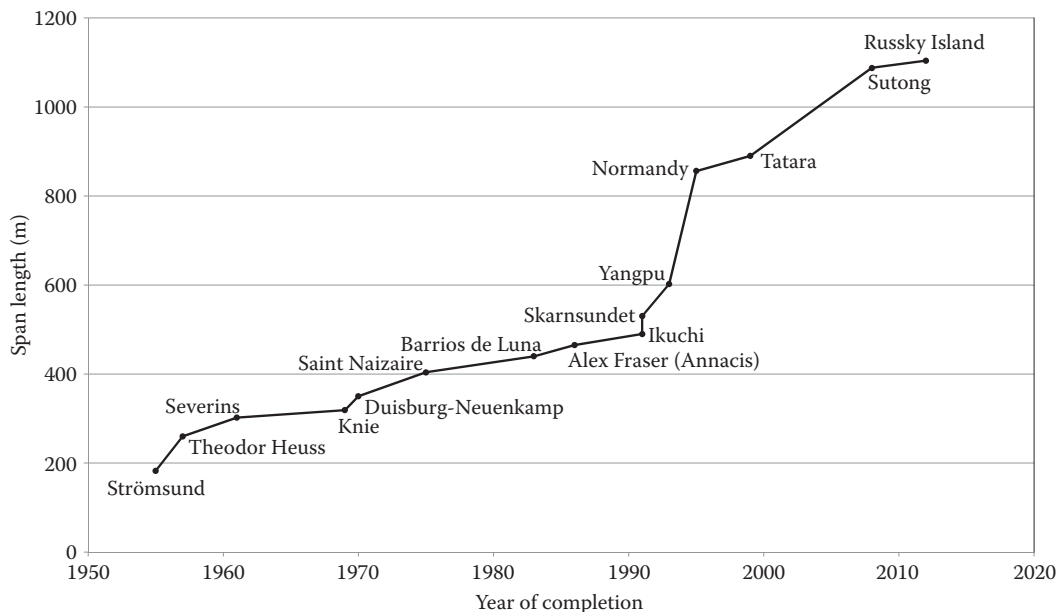


FIGURE 10.8 The longest cable-stayed bridge spans since 1955.

Figure 10.8 illustrates the development in world record cable-stayed bridge spans as a function of the year of completion since 1955. It is worth noting that except for the Duisburg-Neuenkamp Bridge all the record spans are designed with two cable planes providing both vertical and torsional support to the superstructure. Comprehensive overviews of the history and development of cable-stayed bridges are found in (Gimsing 1996; Fernández Troyano 1999; Leonhardt 1986).

10.1.1.2 Iconic Designs

The previous sections have mainly dealt with the evolution in design and materials adopted for record span cable-stayed bridges and ultimately the development in achievable span length. Record spans obviously require efficient structural systems. However, it is also worth mentioning some of the large number of cable-stayed bridges with more moderate span length, but very spectacular designs that have been completed. These structures fully demonstrate the diversity in terms of span arrangement, pylon shape, cable configuration and girder arrangement offered by this bridge type.

One of the most famous examples is probably the Alamillo Bridge in Seville, Spain, completed in 1991. The bridge features a single inclined pylon, leaning backwards away from the main span and arranged without backstays (Figure 10.9). The balance for permanent loads is achieved by a combination of a lightweight steel girder and a heavy concrete pylon. Live loads result in global bending in the girder and pylon. Due to the arrangement construction was relatively complicated and the structural system is obviously not very efficient. The main span length is 200 m (656 ft).

The Fabian Way Bridge in Swansea, United Kingdom, carries pedestrian traffic and a bus lane. In this case the pylon leans forward by 22° and is provided with backstays twisted into a warped arrangement. There is a single central plane of stay cables in the main span whereas there are two planes of backstays. Both deck and pylon are constructed in steel and the span length is 71 m (233 ft). The bridge was completed in 2007 (Figure 10.10).



FIGURE 10.9 Alamillo Bridge in Seville, Spain. Arranged with a main span of 200 m (656 ft) and no side span or backstays. Completed in 1991. (Courtesy of www.pwpeics.se [P. Wåhlin].)



FIGURE 10.10 Fabian Way Bridge in Swansea, United Kingdom. The bridge, completed in 2007, carries pedestrian traffic and a bus lane. (Courtesy Flint & Neill Ltd. [C. Walker].)

The Glorias Catalanas Footbridge in Barcelona has a single mast type pylon supporting three walkways of which the two are curved. The arrangement is similar to a guyed mast and the geometrical layout in plan gives the horizontal balance of the forces acting on the pylon.

The Nelson Mandela Bridge in Johannesburg, South Africa, completed in 2003 carries the city traffic over 41 railway tracks that imposed severe restrictions on the positioning of pylons and piers. This resulted in an asymmetric configuration with short and heavy concrete side spans in combination with a composite main span 176 m (577 ft) long (Figure 10.11).



FIGURE 10.11 Nelson Mandela Bridge in Johannesburg, South Africa, completed in 2003. (Courtesy of J. Jung.)

10.2 Configuration

10.2.1 General

Depending on the obstacle to be crossed and site conditions cable-stayed bridges are usually arranged as two-span, three-span or multi-span bridges as shown in Figure 10.12. The two-span arrangement consists of a main span and a shorter side span (also referred to as back span). The three-span arrangement, which is the most common, consists of a main span and two side spans, where the length of each

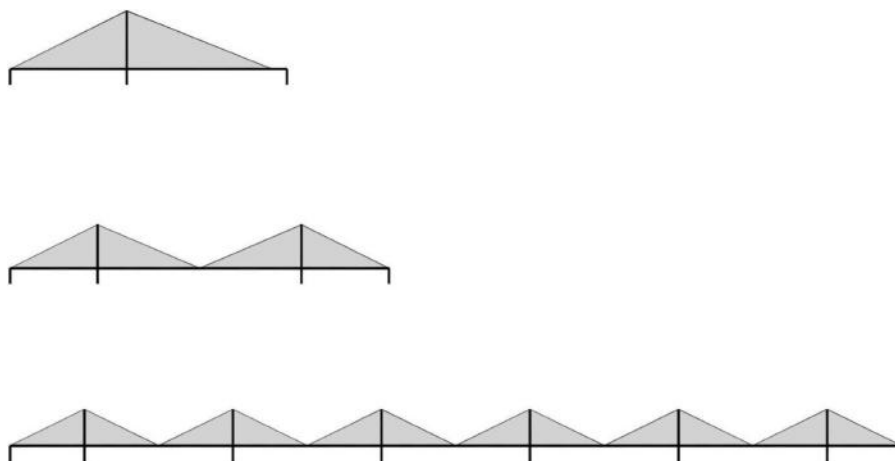


FIGURE 10.12 From top: Two-span, three-span, and multi-span cable-stayed bridge arrangements. The three-span arrangement is the most common.

side span equals half of the main span length or less. A multi-span cable-stayed bridge has a number of main spans and a side span at either end.

Vertical restraints are arranged towards the ends of the cable supported portion of the bridge. The vertical restraint is usually located at the abutment or, in case of a longer crossing with approach viaducts, over one or a number of side span piers. Anchor cables attached over the vertical fix point provide an efficient horizontal restraint of the pylon top.

The purpose of the stay system is to assist the stiffening girder transferring the loads from the girder to the supports of the structure. The loads to consider when choosing the arrangement of the cable planes are vertical and lateral forces and torsional moment. Typically the vertical loads originating from dead load and traffic load are dominating. Furthermore, eccentric live load will result in rotation (twist) about the longitudinal bridge axis. For very long spans or very narrow bridges, where the width-to-span ratio is small, horizontal load like wind load and the dynamic effects of wind may become dominant.

Section 10.1.1 Evolution of Cable-Stayed Bridges briefly touched on the arrangement of cable planes and stiffening girder. This is described in detail in the following sections. Figure 10.13 illustrates how different arrangements of cable planes, in terms of number and arrangement in the transverse direction, may be combined with different types of stiffening girders and how the main loads are transferred.

In a girder bridge the girder itself obviously transfers all external loading to the supports. The simplest addition to the girder bridge is to arrange a single central cable plane, which will assist in transferring vertical loads only. The stay cables are tensioned by the dead load of the stiffening girder and any other permanent loads applied to the girder. If two vertical cable planes are provided, the stiffening girder can be designed without torsional stiffness, but it still has to transfer lateral loads in bending about its strong axis. A purely torsional moment is transferred by the cable system as a pair of forces with opposite direction where the compressive component results in a reduction of the pretensioning in the stay cables. The system with two vertical cable planes is typically combined with either an H-shaped pylon (Barrios de Luna Bridge, Alex Fraser Bridge, and the Øresund Bridge) or a pylon of the portal type (Strömsund Bridge).

If instead an A-shaped or inverted Y-shaped pylon is adopted in combination with two cable planes, the cable planes become inclined in the transverse direction. Transfer of vertical loads takes place as in the system with two vertical cable planes. The stiffening girder transfers transverse loads and, if the girder has no torsional stiffness, a torsional moment has to be transferred by the cable system. However, due to the inclined cable planes transfer of the torsional moment as a pair of forces acting in the direction of the inclined cable planes will lead to an additional transverse load acting on the girder. If the inclined cable planes are combined with a box girder with significant torsional stiffness, transfer of lateral loads and torsional moments become more complex and the load share will depend on the torsional stiffness ratio between girder and cable system. Examples of bridges with two inclined cables planes include the Severins, Normandy, Sutong, and Stonecutters bridges where the latter has a mono-column type pylon and a twin box girder. The superstructure of the Severins Bridge is composed of two relatively small steel box girders at the edges and an orthotropic deck structure, whereas the others have full-width closed box girders with significant torsional stiffness.

In combination with a portal type pylon the cable planes can be arranged to be leaning outwards whereby vertical and transverse loads can be transferred by the cable system, whereas torsional moments have to be transferred by the girder that consequently needs to be designed as torsionally stiff.

The highest degree of efficiency of the cable support is generally achieved by a cable system offering both vertical and torsional support to the girder. The two systems with inclined cable planes, inwards and outwards leaning, described above can be combined and if a minimum of three mutually inclined cables planes are arranged this results in a truly spatial cable system that can transfer vertical and transverse loads as well as torsional moments globally without assistance from the stiffening girder (Vejrum 1997). For symmetry it would typically be preferred to arrange four cable planes as shown in Figure 10.13. Spatial cable systems have been adopted for some pipeline bridges where the stiffening girder, that is, the pipe, is characterized by a negligible bending stiffness; however, so far none of the projects proposing truly spatial systems for bridges carrying vehicular traffic have reached the construction phase.

Girder and stay cable arrangement	Global load transfer by:			Typical pylon arrangement			
	Cable system	Girder	Torsion	Vertical	Lateral	Torsion	
Central cable plane	✓			✓	✓		
Two vertical cable planes	✓	✓	✓		✓		
Two inclined cable planes, inward	✓	✓	✓				
Two inclined cable planes, outward	✓	✓			✓		
Four inclined cable planes	✓	✓	✓				

FIGURE 10.13 Transfer of global vertical, lateral, and torsional loads as a function of the configuration of girder and stay cable system. (Adapted from Gimsing, N. J., *Skråstagsbroer*. Series F, No. 113. Department of Structural Engineering, Technical University of Denmark [in Danish].)

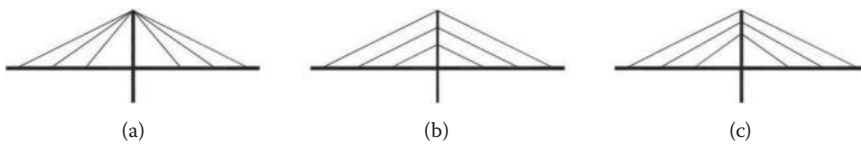


FIGURE 10.14 Stay cable arrangements: (a) Pure fan system (also referred to as radial system); (b) Harp system; (c) Modified fan system (also referred to as semi-fan system or modified harp system).

It should be emphasized that all the cable systems described above, including the spatial system, are relying on the stiffening girder being able to transfer the compressive forces required for equilibrium with the cable forces as illustrated in Figure 10.1.

Looking at the bridge in elevation the stay cables are usually arranged according to one of the basic systems shown in Figure 10.14: Pure fan system, harp system and modified fan system, which is sometimes also referred to as semi-fan or modified harp system.

As a general rule of thumb the longest cables should not be arranged with an angle with horizontal less than 21°–23° in order to be effective in transferring vertical loads. This means that the ratio of the pylon height above the bridge deck to the main span length is typically in the order of 1:5. If cables are flatter than this they rather act as external prestress and the bridge type is commonly referred to as extradosed (see Section 10.2.2).

In the fan system all stay cables are radiating from an anchorage point at the pylon top and due to space limitations and practical detailing the pure fan system is mainly found in bridges with only few sets of stay cables. As the trend moved towards multi-cable systems with many relatively small stay cables it was found more favorable to spread the anchorage zone out in the upper part of the pylon leading to the modified fan system.

With the harp system the stay cables are parallel and the anchorages are spread over practically the entire height of the pylon above the stiffening girder.

From a structural point of view the fan and modified fan system offer a more efficient cable system: If an anchor cable is arranged, that is, a cable connecting the pylon top to a point of vertical fixity over a side span pier, the system is stable even if the bending stiffness of the girder and pylon is ignored. In a harp system only the stay pairs including an anchor cable can transfer vertical loads without relying on the bending stiffness of girder and pylon. Furthermore, the inclination of the stay cables is more favorable with the fan and modified fan system as the flat angle is only necessary for the longest cables whereas the shorter cables are more vertical and thus more efficient in transferring vertical loads. In a harp system all stay cables are parallel and have the same flat angle resulting in a higher compressive normal force accumulating in the stiffening girder towards the pylon.

However, from an aesthetic perspective it can be argued that the harp system has an advantage because the array of parallel cables will always appear parallel irrespective of the viewing angle. Fan and modified fan systems with two cable planes tend to appear more disorganized and due to the variety of angles the cables appear to cross when the bridge is viewed under an angle. This is to some degree mitigated when a multi-cable system and stay cables of a light color are adopted, but the effect is still there.

From a construction and programming point of view the harp system allows girder and stay cable installation to start earlier before the pylon reaches full height because the cable anchorages in the pylon begin at a lower elevation.

10.2.2 Extradosed Bridges

Extradosed bridges can be considered as an intermediate form between a cable-stayed bridge and a pre-stressed launched concrete girder bridge. It is argued whether the first extradosed bridge constructed is the Ganter Bridge in Switzerland (main span 174 m [571 ft]) completed in 1980 or the Odawara Blueway Bridge in Japan (main span 122 m [400 ft]) completed in 1994. The latter was based on a concept described in 1988 where the term “extradosed” appeared for the first time. In the Ganter Bridge the cables radiating from

the pylon top to the girder are embedded in concrete and consequently this particular bridge type is also referred to as a “fin back” bridge.

In an extradosed bridge the pylon height above deck relative to the main span length is significantly smaller than in a cable-stayed bridge, typically less than 1:10. Due to the flat angle of the cables these mainly carry permanent loads and the stress variations experienced by the cables due to live loads are very limited. In some designs the cables have been classified as prestressing tendons rather than stay cables and due to the low fatigue stress range it has been accepted to utilize the cable material up to $0.60f_u$, where f_u is the ultimate tensile strength (see, for instance, Ogawa et al. 1998). However, for longer spans and depending on the connection between deck and piers, fatigue stress ranges may be higher and the allowable stress has been decreased to $0.45f_u$, which is a value typically adopted for cable-stayed bridges. In determining an appropriate allowable stress in the cables, designers need to consult relevant codes and standards while taking durability issues into due consideration, also refer to Section 10.3.2.

Due to restricted space available in the pylons of extradosed bridges it has in some cases been found advantageous to replace traditional cable anchorages with cable saddles. This allows cables to pass continuously through the pylon from deck anchorage to deck anchorage simplifying the detailing.

Extradosed bridges are often arranged as multi-span bridges, which they are well adapted to due to the similarities with continuous girder bridges. The Sunniberg Bridge near Klosters in Switzerland has four pylons and three main spans curved in plan, the longest being 140 m (459 ft), as shown in Figure 10.15. The Golden Ears Bridge in Vancouver, Canada, completed in 2009 also has four pylons and three main spans, but with 242 m (794 ft) the main spans are significantly longer and comparable to what would typically be found in a small cable-stayed bridge (Figure 10.16).



FIGURE 10.15 Sunniberg Bridge near Klosters in Switzerland was completed in 1998. The bridge is a multi-span extradosed bridge with a curved alignment. The curved alignment is clearly visible from the bridge deck (right). One of the pylons with the array of flat cables (left). (Courtesy of www.structureae.de [N. Janberg].)



FIGURE 10.16 Golden Ears near Vancouver in British Columbia, Canada, completed in 2009. (Courtesy of Armtec Ltd. Partnership.)

In a number of instances extradosed bridges have been found competitive compared to medium range span continuous girder bridges and small cable-stayed bridges. From an aesthetic point of view the smaller pylon height compared with a cable-stayed bridge and the smaller girder depth and lighter structure compared with a haunched girder may be considered an advantage.

Comprehensive discussions of extradosed bridges are provided in Chapter 11.

10.3 General Layout

10.3.1 Girder

10.3.1.1 Materials

Apart from the Maracaibo Bridge the first decades of modern cable-stayed bridge design and construction were dominated by steel bridges with orthotropic decks combined with plate or box girders and steel pylons of cellular construction. However, as compression is dominating in large areas of both the stiffening girder and pylons concrete as structural material offers some advantages. When assessing the economic benefits of applying concrete in the stiffening girder it should be remembered that a concrete girder is heavier and consequently requires more steel in the stay cables than with a steel superstructure. This is also the case for a composite stiffening girder.

As it was described in the section on the Evolution of Cable-Stayed Bridges steel, concrete and composite have all been adopted for the design of the stiffening girder. What is optimum depends on a number of project-specific factors such as span length, the Owner's requirements with respect to aesthetics and maintenance, geometry, the contractor's preferred methods of construction including segment length, prefabrication versus in-situ construction, qualifications of the local labor, and of course ultimately the cost. The super long span cable-stayed bridges have all been designed with steel in the main span, whereas concrete and composite superstructures are typically found in the medium range of span lengths. For the shorter spans other factors such as fast construction with minimum disruption of existing traffic links may be decisive and due to this steel may be competitive despite the higher material cost.

Some cable-stayed bridges have been arranged with a steel superstructure in the main span and concrete in the side spans so that the weight of the longer main span is balanced by the heavier section in the side spans. Examples where this arrangement has been adopted include the Flehe Bridge across the Rhine River in Germany, the Normandy Bridge where the concrete section continues 116 m into the main span, whereas the central 624 m is in steel and the Stonecutters Bridge where the steel superstructure continues past the pylons and 50 m into the side spans. The Nelson Mandela Bridge mentioned earlier has a composite main span with short and heavy concrete side spans.

Concrete girders can be either cast-in-place or of precast construction or a combination of these. Cast-in-place (or in-situ) construction originates from the free cantilever construction method of concrete box girder bridges. In terms of shape cellular cross sections with one, two or more closed box sections have been used frequently. Some examples are Barrios de Luna and the Second Bridge across the Panama Canal (Figure 10.17). Simpler cross sections consisting of beams and slabs have also been adopted for instance on the Dames Point Bridge in Florida and the Talmadge Memorial Bridge in Georgia (Tang 1995). An even simpler stiffening girder consisting of a solid slab was used on the Diepoldsau Bridge, see also Section 10.1.1—Evolution of Cable-Stayed Bridges.

When precast concrete segments are adopted the cross section can be somewhat more complex because casting is done in the prefabrication yard and typically off the critical path for construction. However, the design should aim for a high degree of standardization in the segment layout to minimize the need for adjustments to the precasting forms. The segment length is limited by the maximum size and weight that can be handled during transportation to site and lifting to the final position. Examples of cable-stayed bridges with a precast concrete girder are the Brotonne Bridge (completed in 1977, 320 m [1050 ft] main span, length of girder segments 3.0 m [10 ft]) and Sunshine Skyway in Florida (completed 1987, 367 m [1204 ft] main span, length of girder segments 3.60 m [11.8 ft]).



FIGURE 10.17 Second Bridge across the Panama Canal (Puente Centenario), completed 2004. The main span is 420 m (1378 ft). (Courtesy of COWI A/S [K. Fuglsang].)

Concrete superstructures typically need post-tensioning to control tension cracking in areas where the compressive stresses are low, that is, around midspan where the normal force is small, and in areas where large bending moments occur as for instance where the girder is supported in the vertical direction. In precast segmental construction the typical design criteria is for no tension to develop in the joints.

In a composite girder a concrete deck slab is used to transfer compressive axial forces. The concrete slab is connected to the steel girder by shear studs. The steel girder can either be a torsionally stiff box girder as adopted on the Sungai Johor Bridge in Malaysia (Figure 10.18) or consist of a grid of edge girders and floor beams as on the Alex Fraser Bridge. Whether the girder is required to have torsional stiffness depends on the cable system as explained in Section 10.2—Configuration.

The concrete slab in a composite girder can be cast in-situ, but more commonly the slab consists of precast panels connected by in-situ cast joints. As for concrete girders the concrete slab in a composite girder will typically require post-tensioning in areas where tensile stresses can occur. Prefabricated slabs furthermore have the advantage that the effects of creep and shrinkage are reduced if the slabs are cast sufficiently in advance of installation and loading. It is critical to achieve a good quality of the in-situ joints and these require careful detailing and execution. A number of details have been developed and are described in the literature, see for instance (Virlogeux 2002) for a general overview. Reference is also made to the relevant codes and standards.

10.3.1.2 Construction

Site joints (or field splices) in stiffening girders in steel and in the steel portion of composite girders are carried out by welding or bolting. The site joints in the skin plates of steel box girders are typically carried out by welding. Splices in the stiffeners can be both welded and bolted. Site joints in plate girders can be welded or bolted and what is optimal depends on the specific project.

With a multi-cable system supporting a girder carrying roadway traffic the typical stay spacing for a stiffening girder in concrete is 6–8 m (20–26 ft), for composite 10–12 m (33–39 ft) and for steel 16–20 m (53–66 ft). When selecting the stay cable spacing the number of stay cables anchored in each segment, maximum breaking load of the stays, the maximum lifting weight of the segments, forces on the structure during stay rupture, and stay replacement load cases are all factors that need to be considered.

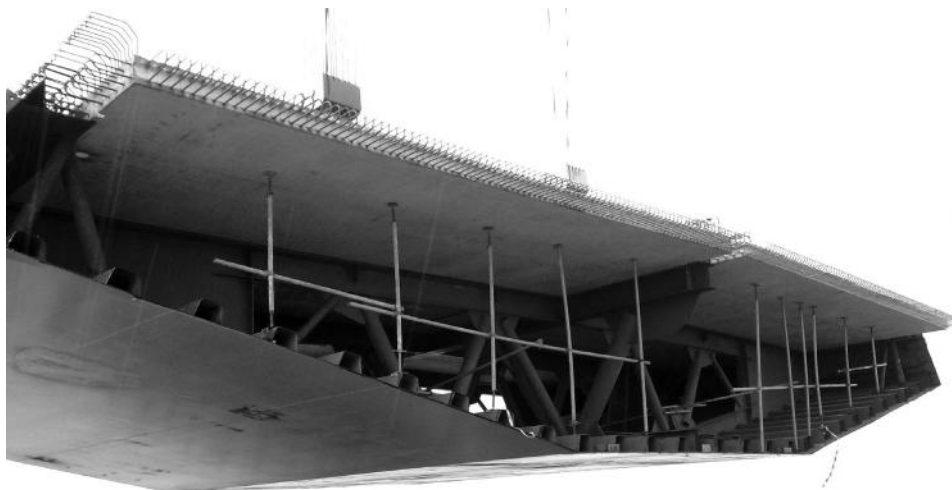


FIGURE 10.18 The composite girder of the Sungai Johor Bridge in Malaysia. The photo shows a partly completed girder segment during the lifting operation. The main span of the three-span cable-stayed bridge is 500 m. (Courtesy of COWI A/S [S. C. Christensen].)

The choice of girder type and method for joining segments on site highly influences the cycle time for segment installation. Together with the number of segments to be installed, being a function of the chosen segment length, this determines the total time required for the erection of the superstructure.

10.3.1.3 Two-Level Girders and Twin Decks

Two-level stiffening girders, arranged as a deep truss, have been adopted for cable-stayed bridges on a number of projects where either a deck of normal width is not enough to accommodate the traffic volume or where the bridge carries railway load and the additional stiffness provided by a deep truss girder is an advantage. In the latter case the bridge often carries the roadway on one deck and railway on the other. The first double-deck cable-stayed bridge to be constructed was the Rokko Bridge in Japan completed in 1977 (Gimsing 1996). Further details of bridges carrying railway load are presented in Section 10.7—Cable-Stayed Bridges for Railway.

A few cable-stayed bridges have been constructed with twin decks where the superstructure is composed of parallel girders connected by cross girders acting partly as a Vierendeel girder. The arrangement is suited for central pylons of the mono-column type that can conveniently be located in the void between the two girders. The Ting Kau Bridge in Hong Kong S.A.R., China, has a twin deck of composite construction consisting of four parallel steel plate girders acting as main girders. The main girders are connected by cross girders and this grid supports the deck slab composed of precast panels. The stiffening girder has negligible torsional stiffness. There are four cable planes in the transverse direction of the bridge, however, due to the very modest inclination of the cable planes these act like a plane cable system and not as a spatial system (Bergman 1999). The superstructure of Stonecutters Bridge consists of twin box girders connected by cross girders at the stay anchorage points. The gap between the two main girders is 14.3 m and the total width of the superstructure is 53.3 m. This results in a deck structure with a significant bending stiffness in the horizontal plane that was necessary to ensure the stability of the structure considering the span length and the fact that the bridge is located in an area prone to typhoon winds (Vejrum et al. 2006).

10.3.1.4 Aerodynamics

Stiffening girders have been designed and constructed with both streamlined and bluff sections. The benefit of applying an aerodynamically shaped box girder in terms of reduced wind loading and improved aerodynamic performance of the structure increases with span length. For moderate spans a bluff section is usually acceptable from a structural point of view. In some cases girders with a bluff cross section are provided with non-structural wind fairings or other features to modify the flow around the section and thereby improve the overall aerodynamic behavior, such as in the main span of the Alex Fraser Bridge. It has also been found necessary to provide box girders with guide vanes in some instances to prevent separation of the flow at the downwind corner that may initiate vortex shedding excitation of the girder. Stonecutters Bridge is an example. Section 10.8 provides more details on aerodynamic aspects.

10.3.1.5 Alignment

Due to the compressive axial force in the stiffening girder the natural horizontal alignment of the cable supported portion of a cable-stayed bridge is a straight line. However, a number of cable-stayed bridges have been designed and constructed with a curved alignment as for instance the two 70 m (230 ft) main span cable-stayed bridges providing road access to the Malpensa Airport in Milan, Italy. With a main span of 285 m (935 ft) the Térénez Bridge carries road traffic to the peninsula of Crozon in France. Because of the arrangement of the existing access roads on land a horizontally curved alignment of the bridge was the logical solution. The two pylons are lambda-shaped and located next to the girder towards the center of the curve (Figure 10.19).



FIGURE 10.19 Térénez Bridge in France, completed in 2010. The bridge has a horizontally curved alignment with a main span of 285 m (935 ft) and carries road traffic. (Courtesy of Photothèque VINCI [F. Vigouroux].)

10.3.2 Stay Cables

10.3.2.1 General Design

The overall deformations of a cable-stayed bridge are governed by the axial stiffness of the stay cables. Cable elements sag under their dead weight due to the negligible bending stiffness, see Figure 10.20. Because of the sag the relationship between cable force and elongation is nonlinear reducing the axial stiffness of cable elements. The effective axial stiffness of the inclined stay cables depends on the weight, the angle of inclination (in the following expressed as the horizontal projection of the stay cable) and the tension in the cable.

The effective stiffness of a stay cable relative to the E-modulus of the cable material can be calculated by the following expression, see for instance (Gimsing 1996):

$$\frac{E_{\text{eff}}}{E} = \frac{1}{1 + K \cdot a^2}$$

where E is the E-modulus (or Young's modulus), (MN/m^2), typically $E \approx 195,000 \text{ MN/m}^2$ (28,200 ksi); E_{eff} is the effective E-modulus of the stay cable, (MN/m^2); a is the horizontal projection of the stay cable, (m); K is a curve parameter in (m^{-2}) that can be calculated either for the tangent modulus or the secant modulus.

K is given by

$$\text{Tangent modulus: } K = \frac{1}{12} \cdot \frac{\gamma^2}{\sigma_0^3} \cdot E$$

$$\text{Secant modulus: } K = \frac{1}{24} \cdot \frac{\gamma^2 \cdot (\sigma_0 + \sigma)}{\sigma_0^2 \cdot \sigma^2} \cdot E$$

where γ is the density of the cable material, (MN/m^3); σ_0 is the initial stress in the stay cable, (MN/m^2); σ is the stress in the stay cable after the external load is applied, (MN/m^2).

Figure 10.21 shows a graphical representation of the effective E-modulus as a function of K and the horizontal projection of the stay cable.

The typical density of stay cables including corrosion protection is around 90 kN/m^3 (5618 kip/ft³). For a typical stay cable design the curve parameter K is in the order of $1.0 \times 10^{-6} \text{ m}^{-2}$. For a three-span cable-stayed bridge with a main span of 400 m (1312 ft) the effective E-modulus of the longest cables is then 96% of E . This reduction is so small that it can in most cases be ignored. However, for a main span of 1000 m (3281 ft) the effective E-modulus drops to 80% of E , which is a significant reduction that will influence the overall stiffness of the bridge.

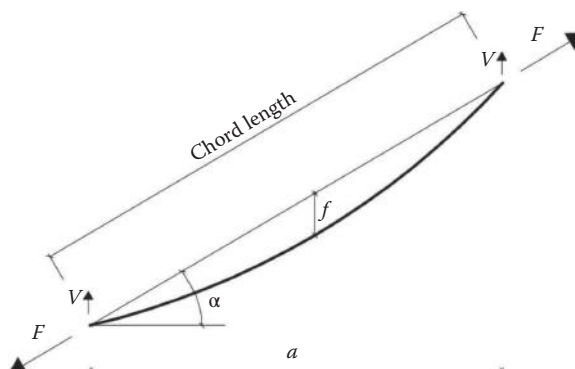


FIGURE 10.20 Inclined cable sagging under its dead weight. Definition of geometry and forces.

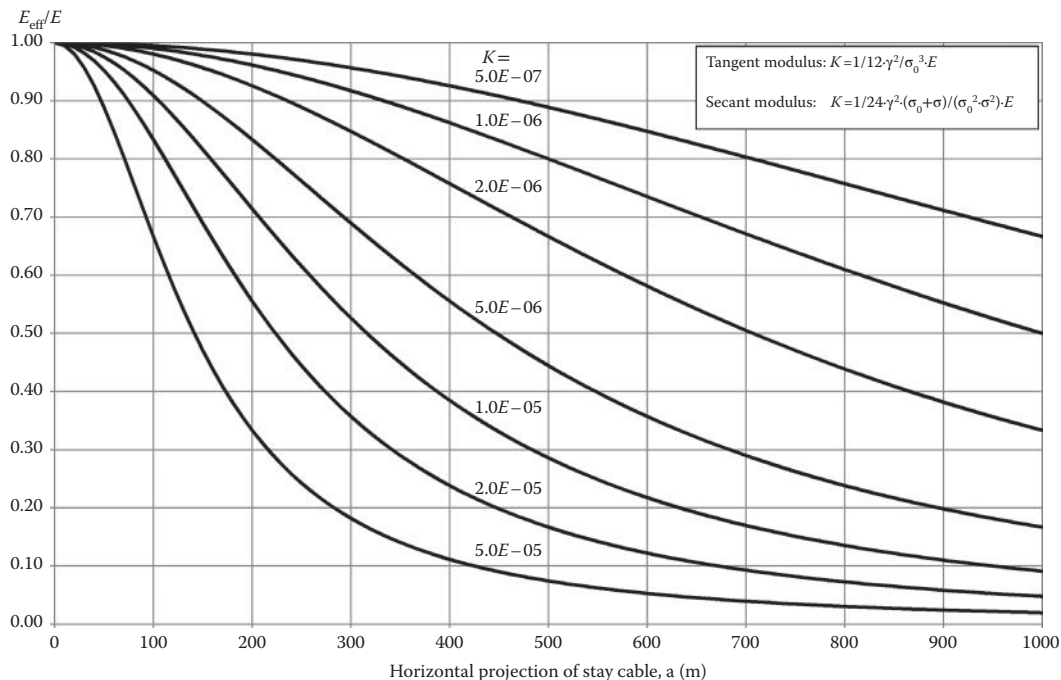


FIGURE 10.21 Effective E-modulus as a function of horizontal projection of the stay cable and cable stress, expressed by the parameter K .

The dead load of the stiffening girder is carried by the stay cables. The initial stress due to dead load is typically in the range 450–550 MPa (65–80 ksi), equivalent to 25%–30% of the ultimate tensile strength, where a steel girder will be at the lower end of the range and a concrete girder at the upper end due to the different ratios of dead load to live load. Assuming an initial stress of 500 MPa and a horizontal projection of 300 m (984 ft) the effective tangent E-modulus becomes 91% of E . If the initial stress had been as low as 300 MPa (44 ksi) the effective tangent E-modulus would only have been 69% of E . This illustrates the influence of the initial stress condition in the cables on the global stiffness of a cable-stayed bridge. In this connection it should be emphasized that during construction all the permanent load is not yet in place and therefore the initial stress in the stay cables just after installation will typically be lower than the dead load stress after completion when surfacing, parapets and ancillary works have been installed. Consequently, the effective axial stiffness of the stay system will be lower during construction than in the final condition and this reduced stiffness needs to be taken into account when analyzing the construction stages.

Some cables may experience significant de-tensioning during construction or in-service. In particular the anchor cables, that is, the cables in the side span attached near a vertical support, where the stress is reduced when live load is located in the side span only. This configuration of live load forces the pylon top to deflect toward the side span decreasing the stress in the anchor cables. This effect must be taken into account in the design both in terms of the decreased effective stiffness of the anchor stays and the fatigue action due to stress variations.

Stress variations in the stay cables due to live load may lead to fatigue. The principal fatigue actions originate from traffic load and dynamic wind load. Stress variations in the stay cables of a bridge carrying railway load may be significant due to the load intensity.

Bending effects need to be taken into account when calculating the stress in the stay cables. Bending effects occur at the points of restraint, that is, at the anchorages, at stay saddles, and at the attachment of dampers and cross-ties.

Most finite element programs used for analysis of cable-stayed bridges include cable elements or other means of taking the nonlinear behavior of the stay cables into account in the structural analysis.

10.3.2.2 Types of Stay Cables

The first cable-stayed bridges were constructed using locked-coil cables. The layers of wires are twisted and in combination with wedge- and z-shaped wires in the outer layers the cable is self-compacting leading to a good corrosion resistance. However, due to the twist the effective E-modulus of the cable is lower than the E-modulus of steel, typically 165,000–170,000 MPa (23,900–24,600 ksi). This effect is in addition to the reduction in effective E-modulus due to sag. Furthermore, the wedge- and z-shaped wires have a lower fatigue resistance than standard circular wires. Locked-coil cables are prefabricated to the specified length by a specialist manufacturer.

Solid bars have also been used for stay cables. As explained above it is important for the global stiffness that the initial stress in the stays is high and consequently a high strength steel grade is essential. The main drawback of solid bars is the limited length necessitating the bars to be joined by couplers into the required length, see Figure 10.31.

Parallel wire strands (PWS cables) consist of 7 mm (0.28 in.) wires and are prefabricated to the specified length in the workshop by a specialist manufacturer. Length adjustment is provided either by a nut and external threads on the sockets or by shim plates between the socket and a bearing plate fixed to the structure. The first generation PWS cables were arranged with truly parallel wires of equal length and consequently some difficulties were experienced in coiling the cables on reels for transportation. The new generation cables, referred to as New PWS, are fabricated with a long lay that overcomes the problems of coiling. During installation on site and stressing it is important to prevent the cables from rotating as this will cause an uneven stress distribution in the wires due to these being of different length. The slight twist of the wires reduces the E-modulus of the cable to around 200,000 MPa (29,000 ksi).

The socket is a key element for the fatigue performance of the cables. The sockets are filled with a compound of steel balls mixed with zinc or epoxy bonding to the wire whereby the stress in the wires is transferred to the socket. This is the primary anchorage of the wires. Furthermore, each individual wire is threaded through an anchor plate and button heads on the wire ends provide additional anchorage.

The corrosion protection usually consists of a double system: The individual wires are galvanized and the wire bundle is protected by an extruded pipe of high density polyethylene (HDPE). The HDPE may be black or have an external layer of colored polyethylene.

Multi-strand (MS) cables consisting of seven-wire strands have become very popular due to good performance and simple installation. The strands were originally developed for prestressed concrete applications, but special systems for stay cables are now available. MS cables are installed strand by strand that requires only light equipment as compared to the installation of a full prefabricated cable. The strands can either be stressed individually by use of a mono-strand jack or the full stay cable can be stressed by a multi-strand jack. As for the PWS cables the anchorage detail is a key element. The strands are typically anchored by split-cone wedges inserted into an anchor block. It is important to ensure that the wedges do not come loose due to de-tensioning or vibrations of the stay cable during construction or in-service. A minimum tension, in the order of 10%–20% of the stress due to permanent load, is therefore often required during all normal and extreme events or alternatively a keeper plate has to be installed.

Modern MS cables have several barriers providing corrosion protection: The individual wires are usually galvanized. The seven-wire strand is covered by a tightly extruded PE-coating and the voids are filled with wax or grease. Finally, the bundle of strands is protected by an outer HDPE pipe that may be black or colored. In addition dehumidified air may be ventilated through the cable.

The use of seven-wire strand, where wires are twisted around the central wire, reduces the E-modulus of the cable to around 195,000 MPa (28,300 ksi).

The various types of stay cables are shown in Figure 10.22.

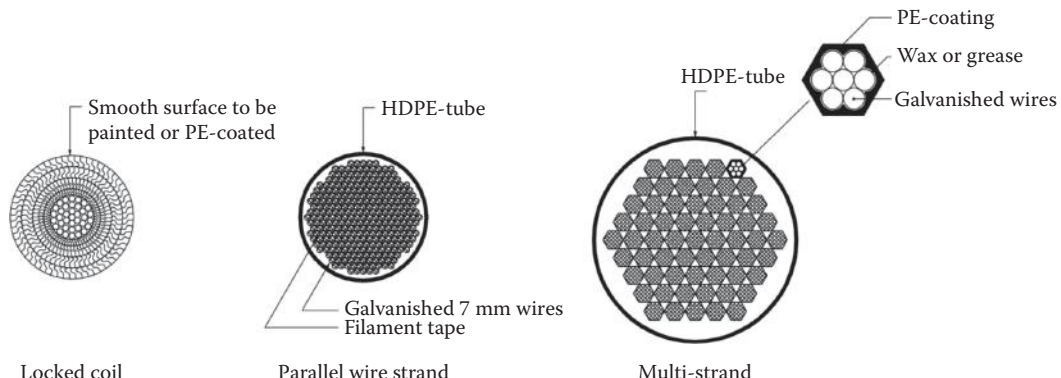


FIGURE 10.22 Cross section of locked coil, parallel wire strand and multi-strand cables.

The design life of stay cables is typically assumed to be in the order of 50–60 years. Specifications often require that stay cables can be replaced while the bridge is in operation, if necessary with reduced live load. In this connection multi-stay systems have an advantage because additional loading in the remaining cables and associated bending moments in the girder during stay replacement are smaller as compared with a system with few but large stay cables. Furthermore, with multi-strand stays strands can in principle be replaced individually.

In the early days it was common practice to fill the outer HDPE sheathing with cement grout after installation of the stay for improved corrosion protection. This practice is now generally being abandoned for a number of reasons such as the grout not being an effective means of preventing water ingress due to cracking, and the grout preventing inspection of the tension elements and replacement of individual strands in a multi-strand stay cable.

All the stay types described above use high strength steel as the tensile element. Some research into the use of composite materials such as carbon fibers has been carried out and a number of smaller scale bridges have been constructed using carbon fiber strands in the stay cables (Keller 2003). One of the main challenges is the design of the anchorages. Further research and development is required before alternative materials are ready for use at a larger scale.

10.3.2.3 Codes and Guidelines

Various organizations have published recommendations for the design, testing and installation of stay cables. The *Recommendations for Stay Cable Design, Testing and Installation* by the Post-Tensioning Institute (PTI recommendations), *CIP Recommendations on Cable Stays* (CIP recommendations) and *Acceptance of Stay Cable Systems using Prestressing Steels* (fib recommendations) represent the state-of-the-art based on the design principles and safety philosophy adopted in their respective countries of origin. As a consequence of the different design and safety principles the recommendations allow slightly different maximum stresses and the designer shall ensure that the adopted design criteria for the stay cables are consistent with the general design assumptions for the project. The Eurocodes provide a consistent basis of design and Eurocode 3 Part 1-11 *Design of Structures with Tension Components* (EN 1993-1-11) includes specific requirements for cable elements.

10.3.2.4 Testing

Relevant standards specify the required routine checks of the individual components of stay cables. In addition, the recommendations listed above specify qualification testing of representative samples of the entire stay system, including mechanical testing (fatigue and ultimate tensile strength) and water tightness testing to document the effectiveness of the protective barriers of the actual stay cable assembly.

10.3.3 Pylons

10.3.3.1 Pylon Shapes and Arrangement

The pylons are the most visible structural element of a cable-stayed bridge simply because of their scale and together with the arrangement of the cable planes the pylons define the characteristics of a particular bridge. Consequently, aesthetic considerations including good proportions and careful detailing are very important for a successful overall appearance of the bridge. The pylons are sometimes referred to as towers or bridge towers.

A number of different pylon shapes have been described in the previous sections. The optimum form depends on whether the pylon supports one or more cable planes and on the foundation conditions.

H-shaped and portal type pylons are the most common for cable-stayed bridges with two vertical cable planes. Freestanding post-type pylons located at the edge of the stiffening girder have also been adopted.

Central mono-column pylons, A-shaped and inverted Y-shaped pylons may be used with one or more cable planes. The diamond shaped pylon can be considered a variation of the A- and inverted Y-shaped pylons where the pylon legs are kinked at the level of the girder to allow them to be supported on a single foundation of minimum dimensions.

The harp system is used in combination with pylons with vertical legs above deck level, whereas A- and inverted Y-shaped pylons are logical choices when fan and modified fan systems are adopted.

Pylons are usually vertical, but examples of inclined pylons toward the main span or the side span also exist as illustrated in Section 10.1.1.2. Intuitively a pylon leaning backward seems more logical as it visually seems to pull the main span up, but a forward leaning pylon results in a more favorable angle for the stay cables in the main span and also reduces the length of the main span stay cables while the stays in the side span increase in size.

Pylons of more sculptural shapes have been proposed for a number of small and medium scale cable-stayed bridges. An example is the asymmetrical, kinked and inclined pylon of the Erasmus Bridge in Rotterdam, the Netherlands (Figure 10.23). The bridge has a single set of heavy stays in the back span and it should be emphasized that a pylon of this design will experience a high degree of bending.

10.3.3.2 Materials

Although the early cable-stayed bridges were with a few exceptions constructed with steel pylons, concrete has turned out to be an economical alternative as the pylons are compression members. Concrete is now generally the preferred material in pylons for large cable-stayed bridges and are usually constructed by climb forming. However, steel pylons may be a better option in areas exposed to large earthquakes.



FIGURE 10.23 The Erasmus Bridge in Rotterdam, the Netherlands, completed in 1996. The bridge features a single, kinked pylon with a height of 139 m (456 ft). (Courtesy of COWI A/S [M. B. Jensen].)

As it is the case for choice of material for the stiffening girder other factors such as fast construction and minimum disturbance of existing traffic may be decisive in some cases and due to this steel may be competitive despite the higher material cost, in particular for small and medium scale projects.

10.3.3.3 Stay Cable Anchorage

The stay cables may be anchored in the pylon or pass through the pylon supported on a cable saddle. Cable saddles have been used on smaller and medium range projects and simplifies geometry in the otherwise congested area in the anchorage zone. However, cost and additional stresses in the stay cables due to contact pressure on the saddle limit the use.

In pylons with limited external dimensions the stay cables may be taken through the pylon and anchored on the opposite face. This is sometimes referred to as a “crisscrossing” arrangement. In order to avoid creating a torsional moment in the pylon it is desirable to arrange the stay cables in a symmetrical pattern. This can be achieved by arranging two cable planes in at least one of the spans (main span, side span or in both main span and side span).

If the pylon is composed of a box section in the anchorage zone the stay cables can be anchored behind the front and back wall of the pylon. In case of a concrete pylon, which is the most common, the stay cables can either be anchored directly on concrete corbels in which case horizontal prestressing is often introduced in the pylon walls. Alternatively, the stay cables can be anchored inside a steel anchor box that is connected to the concrete walls with shear studs. In this case the side walls of the anchor box transfer the tensile component of the stay force in the direction of the bridge axis.

10.3.3.4 Balance of Loads

The most efficient balance for permanent loads is normally achieved by ensuring that the horizontal component of the stay forces in the main span equals the horizontal component of the stay forces in the side span (the backstays) and thereby achieving zero bending moment in the pylons for permanent loads. The pylon design shall consider unbalanced permanent load that will occur during construction. Live load as well as load cases involving stay rupture and stay replacement will also result in unbalanced load on the pylon.

The backstays provide the balance of forces and ensure that the pylon is mainly working in compression and experiences only limited bending. It is reiterated that the whole idea of cable staying is that the structural elements work as tension and compression members rather than in bending. The few cases where a cable-stayed bridge has been arranged without backstays have led to very uneconomical structures, even though it may still be a spectacular design.

10.3.4 Piers and Foundations

The piers in the side spans provide points of vertical fixity and the stay cables anchored near the piers provide increased restraint of the pylon in the longitudinal direction of the bridge.

The piers may be arranged with a single shaft or multiple shafts to accommodate the arrangement of the stiffening girder. A crosshead can be provided below the girder to keep the overall width of the pier down. Pier structures are wider in the transverse direction of the bridge than in the direction along the bridge alignment. When the bridge is viewed from a skew angle the piers may appear very massive and almost block the view under the bridge deck in the side spans. Consequently, designers usually attempt to provide as slender pier designs as possible.

The anchor cables give rise to large uplift forces and a number of bridges have been designed with a heavier girder in the side spans to balance the weight of the main span and to provide the necessary additional counterweight to accommodate live load in the main span only. Examples are the Normandy Bridge, Nelson Mandela Bridge, Stonecutters Bridge, and Sungai Johor. If the dead weight in the side span is not sufficient to balance the vertical component of the maximum stay forces in the anchor cables, whereby there is a resulting uplift, it is necessary to include a holding-down arrangement. This may be

achieved by providing non-structural counterweight over the anchor piers or by installing a tie-down arrangement between the girder and the pier to ensure that the structures remain in contact and prevent the bearings from lifting off. In the latter case the anchor piers are often referred to as tie-down piers. The tie-down is arranged either as cables or in some instances as a pendulum.

Cable-stayed bridges are almost always designed as self-anchored structures under the vertical loads and therefore the horizontal loads acting on the foundations are very small as compared to earth-anchored systems. However, ship impact and seismic events may give rise to significant horizontal forces and moments on the foundations.

10.3.5 Articulation

The stiffening girder is arranged as a continuous beam over the cable supported length due to the compressive normal force. The cable system provides an elastic vertical support, in some cases torsional support but rarely horizontal support. Transverse restraint is arranged at the pylons and side span piers. The transverse restraint is sometimes referred to as wind bearings since the load transverse to the bridge axis mainly originates from wind loading. If the stay system does not provide torsional support then this would usually be provided at the pylons and in any case at the side span piers. Some cable-stayed bridges are designed with a vertical support of the girder at the pylons. However, the stiff support at the pylon—as opposed to the elastic support provided by the stay cables in the spans—results in large negative bending moments in the girder at the pylon. Consequently, it is often found advantageous to omit the vertical support at the pylons and let the girder be elastically suspended over the entire length. An example of a bridge with torsion restraint but without vertical support at the pylons is the Sungai Johor Bridge.

Longitudinal forces, such as braking load, can be transferred to the pylons, side span piers or abutments. The maximum displacements where the girder is free to move need to be considered when deciding on the most optimal position of the point of fixity. In some cases it has been found advantageous to arrange a structural system without a fixed support in the longitudinal direction and let the girder “float.” The stay cables will provide some restraint against longitudinal displacement of the girder that causes bending in the pylons. Additional restraint can be arranged if a hydraulic buffer or shock absorber is installed between the girder and pylons. This device can be designed to allow slowly varying movements, like temperature movements, to take place freely whereas dynamic forces, like seismic load and dynamic wind load, will cause the device to lock whereby forces can be transferred from the girder to the pylon. This system has for instance been adopted on Stonecutters Bridge.

Some cable-stayed bridges have been designed with a monolithic connection between the stiffening girder and pylon. Examples are the Normandy Bridge and the Second Bridge across the Panama Canal (Puente Centenario). Due to the longitudinal restraint of the girder at both pylons of these three-span cable-stayed bridges, temperature variations will cause bending of the pylons. However, the monolithic connection is an advantage during construction as it increases the stability during cantilevering.

10.4 Design Requirements

10.4.1 Functional Requirements

The functional requirements for the bridge are defined in the owner's requirements (also referred to as the employer's requirements) and relevant codes and standards. The owner's requirements will provide information on alignment, required clearance under the bridge, type of loading, information on lanes, tracks and walkways and any special loading conditions specific for the structure or the site. In addition there are requirements to maximum allowable deflections, twist of the deck and often also to maximum displacements and accelerations due to vibrations. It is also common practice to specify requirements for durability and replacement of elements that have a shorter design life than the overall design life of the structure.

10.4.2 Loading Conditions

The loading is a combination of permanent loads, live loads and environmental loads. Special loading conditions include fire and accidental loading and actions during construction.

Cable-stayed bridges are flexible structures and therefore respond to dynamic loads that include traffic loading, dynamic wind and seismic loading.

Road traffic, railway traffic and pedestrians may all introduce dynamic loading that result in dynamic forces in the structure and possibly in vibrations. For bridges carrying railway traffic it is usually a requirement to carry out a runability analysis.

The dynamic component of the wind results in dynamic wind forces in the structure and the buffeting response of the bridge shall be analyzed both in the serviceability limit state and the ultimate limit state. However, vibrations can occur also in smooth flow and at low wind speeds and even small stress variations may ultimately lead to fatigue failure of components. More details on wind loading are presented in Section 10.8—Aerodynamic Aspects.

Earthquakes impose dynamic loading on the structure and the seismic load spectrum is site specific. Typically different levels of seismic loading are specified allowing for different levels of acceptable damage to the structure. For a seismic event with short return period the structure is required to remain elastic, whereas some local damage and yielding can be accepted for a seismic event with a long return period (no collapse scenario).

Repeated stress variations may cause elements to fail in fatigue. Large stress ranges are more detrimental than small stress ranges, but even small stress variations may have a significant contribution to the total fatigue damage if the number of stress cycles is large. Vibrations usually only result in small stress variations, but the number of cycles may be very significant.

10.4.3 Analysis

As explained above the preload in the stay cables is essential for the global stiffness of the structural system. Consequently, the first step in the analysis is to establish the permanent load condition of the structure. The permanent load condition includes all structural dead load and superimposed dead load as well as prestressing effects. Because the structure is statically indeterminate the designer can—with certain limitations—assign a desired value to the unknowns and there are in principle an infinite number of possible combinations of permanent load forces in the structure. The designer can select the condition that is most favorable overall when all other load effects are considered.

Actual construction shall reproduce the selected final condition in terms of geometry and load distribution in the structure. The construction stage analysis is carried out backwards from the final condition to determine the initial geometry and load in the elements when these are built into the structure.

Time dependent effects, such as creep and shrinkage of concrete and relaxation of steel, have to be considered in a forward calculation that takes into account when elements are cast, built in and when load transfer takes place.

The analysis of a cable-stayed bridge is usually a combination of backward and forward calculation.

10.5 Superlong Spans

Looking at the historical development in world record cable-stayed spans two projects mark a big step forward, refer to Figure 10.8: The Normandy Bridge that increased the span length by more than 250 m over the Yangpu Bridge completed 2 years earlier, and the Sutong Bridge increased the record span by approximately 200 m. The Normandy Bridge (Figure 10.24) passed the 800 m mark while Sutong (Figure 10.25) passed the milestone span length of 1000 m in 2008. Today it would be reasonable to define superlong span cable-stayed bridges as the ones having a main span over 1000 m.



FIGURE 10.24 Normandy Bridge, France, completed in 1995. Main span 856 m. The photo shows the final stage of construction just prior to main span closure. (Courtesy of COWI A/S [S. Lausten].)



FIGURE 10.25 Sutong Bridge over the Yangtze River, China, completed in 2008. The main span is 1088 m (3570 ft). (Courtesy of Sutong Bridge Co. Ltd.)

A number of elements become increasingly critical with the super long spans: The efficiency of the stay cables, compression in the stiffening girder and the aerodynamic stability. The effect of cable sag has already been described. A possible way forward, beyond what can be achieved by the current technology, is the development of super high strength steel for stay cables or new materials with a more favorable ratio between strength and density.

The compression in the stiffening girder is a function of the vertical loading (refer to Figure 10.1) and can therefore be considered proportional to the span length. The cross sectional area of the girder usually varies along the span with the heaviest sections located around the pylons where axial compression is highest.

Aerodynamic stability is linked to the torsional stiffness of the structural system and the superlong span bridges have all been constructed with torsionally stiff box girders in combination with two cable planes. Since the cable systems usually do not provide lateral support the lateral stiffness of the stiffening girder may become an issue for superlong spans. Adding to the horizontal load on the girder itself



FIGURE 10.26 Stonecutters Bridge, Hong Kong S.A.R., China. The bridge with a main span of 1018 m (3340 ft) was completed in 2009. (Courtesy of M. R. Larsen.)

is also half of the wind load on the cable system, as each cable will transfer half of its wind load to the pylon and half to the girder. For superlong span cable-stayed bridges a significant amount of the total wind load on the structure originates from wind load on the cable system. However, a long span does not necessarily call for a wide deck and as the span-to-width ratio increases the minimum deck width necessary to accommodate the traffic lanes may not be sufficient to ensure the required bending stiffness and stability. Consequently, it may become necessary to increase the deck width beyond the functional requirements or to adopt a spatial cable system enabling transverse loads to be transferred through the cable system.

The three existing superlong span cable-stayed bridges, Sutong, Stonecutters Bridge and the bridge to Russky Island, have all been designed with aerodynamically shaped closed steel box girders in the main span. The stiffening girders on the Bridge to Russky Island, Sutong Bridge and also Tatara and Normandy are all single box girders, whereas Stonecutters Bridge has a twin box girder interconnected by cross girders at the stay cable anchorage points. This increases the total width of the stiffening girder and thereby lateral stiffness and aerodynamic stability.

The pylon design adopted on the superlong span cable-stayed bridges Sutong and Russky Island as well as previous world record holders Normandy Bridge and Tatara has been of the inverted Y- or A-shaped configuration. Stonecutters Bridge has central mono-column pylons, see Figure 10.26. The stay cables are arranged in modified fan systems with two transversely inclined cable planes leading to efficient structural systems that are necessary for achieving very long spans.

10.6 Multi-Span Cable-Stayed Bridges

In the case of two-span and three-span cable-stayed bridges the anchor stays provide an efficient restraint by connecting the pylon top to a vertically fixed point at the anchor pier(s). Thereby the deflection of the main span under unbalanced live loads is significantly reduced. In the absence of anchor stays live load in the main span would result in significant bending in the pylon. In a multi-span arrangement there are no anchor stays to provide restraint of the central pylons and overall stability has to be provided by other means as illustrated in Figure 10.27.

The following measures to stabilize a multi-span cable-stayed bridge have all been adopted in practice:

- Arrange pylons with substantial stiffness in the longitudinal direction of the bridge.
- Introduce additional tie-down piers to provide efficient anchorage to stabilize the central pylons.
- Stabilize the central pylons by introducing tie cables from the top of the central pylons to the girder-pylon intersection point at the adjacent pylons.

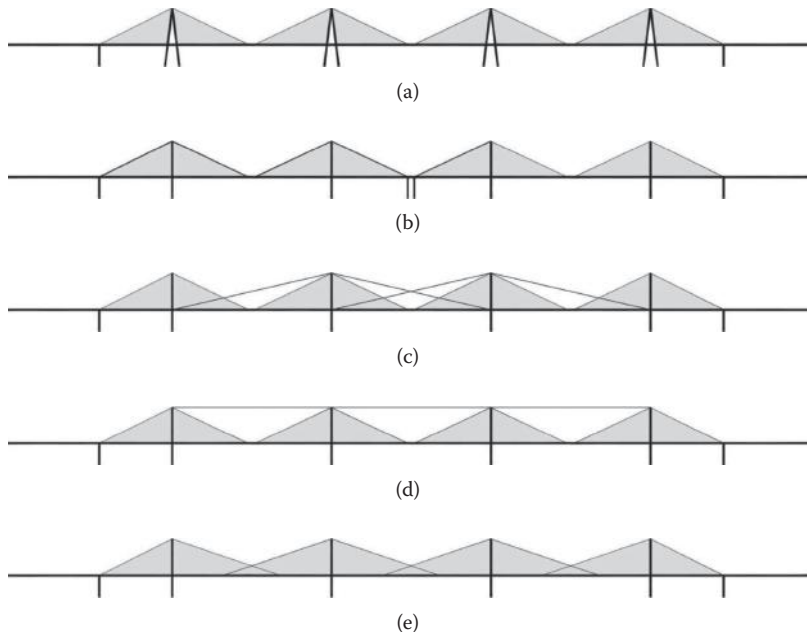


FIGURE 10.27 Measures to stabilize a multi-span cable-stayed bridge: (a) rigid pylons; (b) additional tie-downs; (c) introduce tie cables from the top of the central pylons to the girder-pylon intersection point at the adjacent pylons; (d) introduce a horizontal top stay; (e) crossover stay cables in the main spans.

- d. Stabilize the pylons by adding a horizontal stay connecting the pylon tops.
- e. Arrange crossover stay cables in the main spans.

In the Maracaibo Bridge (Figure 10.5) overall stability is provided by the extremely rigid pylons designed with an inverted V-shape in the longitudinal direction. An additional V-shaped bracket supports the deck and provides a moment stiff connection for the cantilevers on either side of the pylons. Simply supported spans (drop-in spans) connect the cantilevers at the center of the main spans. The pylons of the Rion-Antirion Bridge in Greece, completed in 2004, have an inverted V-shape in both directions and a significant bending stiffness but in this case the stiffening girder is continuous (Figure 10.28). The three main spans are 560 m (1837 ft) long each.

The spectacular Millau Viaduct completed in 2004 consists of six main spans of 342 m (1122 ft) and two side spans of 204 m (669 ft) (Figure 10.29). The superstructure with a total length of 2460 m (8071 ft) is continuous from abutment to abutment. The inverted V-shape pylons are 90 m (295 ft) tall and supported on the superstructure that in turn is fixed to the piers. The piers, where the tallest is 245 m (805 ft) above ground, are of a very sophisticated design allowing a favorable distribution of stiffness between superstructure, piers and pylons. The taller piers have to resist significant forces from wind loading and second order effects, whereas the shorter piers towards the abutments experience high bending moments due to the longitudinal displacement of the superstructure, notably originating from temperature variations. To accommodate these demands the piers are designed with a solid section in the lower part that is split into two flexible shafts in the upper 90 m portion below the deck.

The Second Orinoco Bridge in Venezuela has two 300 m (984 ft) long cable-stayed navigation spans separated by a central cable-stayed section containing a common anchor pier corresponding to the concept (b) in the list above. The anchor pier has an inverted V-shape providing stiffness in the longitudinal direction of the bridge. In this way the structure is similar to two three-span cable-stayed bridges placed back-to-back, but the structures are not independent as forces are transferred across at the anchor pier.



FIGURE 10.28 The Rion-Antirion Bridge in Greece, completed in 2004. The bridge has three main spans of 560 m (1837 ft). (Courtesy Photothèque VINCI [C. Dupont].)



FIGURE 10.29 The Millau Viaduct, completed in 2004, has a central cable plane and comprises six main spans of 342 m (1122 ft). The photo to the left shows the bridge during the construction stage with temporary supports in place until pylons and stay cables were installed. The photo to the right shows the split arrangement of the upper portion of the pier shaft. (Courtesy of COWI A/S [M. B. Jensen].)

A design based on tie-cables from the central pylon to the girder-pylon intersection point at the adjacent pylons, concept (c), is found in the Ting Kau Bridge in Hong Kong S.A.R., China (completed in 1998) (Figure 10.30). The Second Macau-Taipa Crossing can be considered as a crossover between system (b) and (c) in the list above as the tie-cables connect the two central pylons only.

The Munksjön Bridge in Sweden with a total length of 260 m (853 ft) consists of four main spans of 44 m (144 ft) and the central pylons are stabilized by a top stay (Figure 10.31).

The New Forth Crossing across the Firth of Forth in Scotland consists of two main spans and three pylons (Figure 10.32). Stability of the central pylon is provided by crossover stay cables in the main spans that ensure that the flanking pylons and their anchor stays are activated for unbalanced live loads



FIGURE 10.30 Ting Kau Bridge in Hong Kong S.A.R., China. The bridge has two main spans of 475 m (1558 ft) and 448 m (1470 ft), respectively. The superstructure consists of a twin deck supported by four cable planes. The bridge was completed in 1998. (Courtesy of Buckland & Taylor Ltd.)



FIGURE 10.31 Munksjön Bridge in Sweden, completed in 2006. The central pylons are stabilized by horizontal top stays. The stay cables are fabricated from solid bars in high strength steel joined by couplers into the required length (refer to detail to the right). (Courtesy of COWI A/S [H. E. Jensen].)

thereby providing overall stiffness to the system. The New Forth Crossing is scheduled for completion in 2016.

In some projects all pylons are designed with the same overall dimensions thus leading to the same appearance irrespective of whether it is a central pylon or a flanking pylon. Examples of this approach are the Maracaibo Bridge, Rion-Antirion and the New Forth Crossing. In other projects it has been decided to accentuate the difference by deliberately adopting different pylon designs as for instance the Ting Kau Bridge and the concept design developed for the Fehmern Belt Crossing (Figure 10.34 later in the chapter).

The arrangement of multi-span cable-stayed bridges together with an overview of completed projects is found in (Virlogeux 1999).



FIGURE 10.32 New Forth Crossing near Edinburgh, Scotland, scheduled for completion in 2016. Rendering showing the crossover stay cables in the two main spans. (Visualization by Knight Architects, courtesy of Forthspan and Transport Scotland.)

10.7 Cable-Stayed Bridges for Railway

Most cable-stayed bridges carry only road traffic and/or pedestrian traffic. However, cable-stayed bridges have also been designed to carry light rail or heavy railway load, often in combination with road traffic. The requirements to maximum slope, deflections and rotations are stricter for a bridge carrying railway than for roadway traffic only. In particular the differential angular rotations under live load at movement joints between adjacent girders need special attention. Furthermore, the loads in the longitudinal direction of the bridge due to trains braking and accelerating are significant.

The dynamic amplification of the loads shall be taken into account in the structural design and the accelerations shall be evaluated in terms of comfort and safety of the train passengers. A runability analysis is carried out to verify the dynamic train-track-structure interaction due to moving loads on the flexible structure. Special accidental load cases are defined to cover various scenarios of derailment.

One of the earliest examples is the twin bridges across the Paraná River in Argentina (Zárate-Brazo Largo Bridge I and II), which opened for railway traffic in 1978. These two identical cable-stayed bridges with main spans of 330 m (1083 ft) carry four lanes of roadway traffic and a single railway track over the two main branches of the Paraná River. The railway track is located eccentrically next to the traffic lanes on the one-level girder. One of the stay cables suddenly failed in 1996 and subsequently all stay cables were replaced.

The Skytrain Bridge in Vancouver, Canada, opened in 1990 and carries two tracks of light rail across the Fraser River. The superstructure is a one-level prestressed concrete girder. The main span is 340 m (1115 ft) and the bridge carries no road or pedestrian traffic.

The cable-stayed bridge of the Øresund Fixed Link between Denmark and Sweden opened for traffic in 2000 and has a main span of 490 m (1608 ft). The stiffening girder is a two-level truss structure with the double track railway located on the lower deck. The trusses and the lower deck are in steel whereas the upper deck is in concrete. The depth of the girder is 11 m (36 ft), which provides significant stiffness and distribution of local, concentrated loads. The pylons are H-shaped with the cross girder located underneath the girder. The stay cable spacing is 20 m (66 ft) at deck level and the stays are arranged in a harp system (Figure 10.33).

The current (2013) world record for a combined road and rail cable-stayed bridge is the Tianxingzhou Bridge across the Yangtze River in Wuhan, China, with its main span of 504 m (1654 ft). The bridge carries

six traffic lanes and four railway tracks, including high speed railway. The bridge opened to traffic in 2008 (Montens et al. 2012).

A number of long span cable-stayed bridges carrying railway are currently in the planning stage. The Third Tagus River Crossing in Lisbon, Portugal, is planned to carry four tracks of railway, two tracks for conventional railway and two for high speed railway, in addition to six lanes of roadway traffic according to the project requirements in the 2008/2009 project. A significant bending stiffness of the girder is needed for the planned 540 m main span requiring a deep two-level truss girder.

A number of bridge and tunnel solutions have been investigated for the planned Fehmarnbelt Fixed Link between Denmark and Germany. The preferred bridge solution is a two-span cable-stayed bridge to accommodate two tracks of railway and four lanes of roadway traffic. The conceptual design investigations comprise a structure with two main spans of 724 m (2375 ft) and a two-level truss girder with the railway located on the lower deck (Figure 10.34).

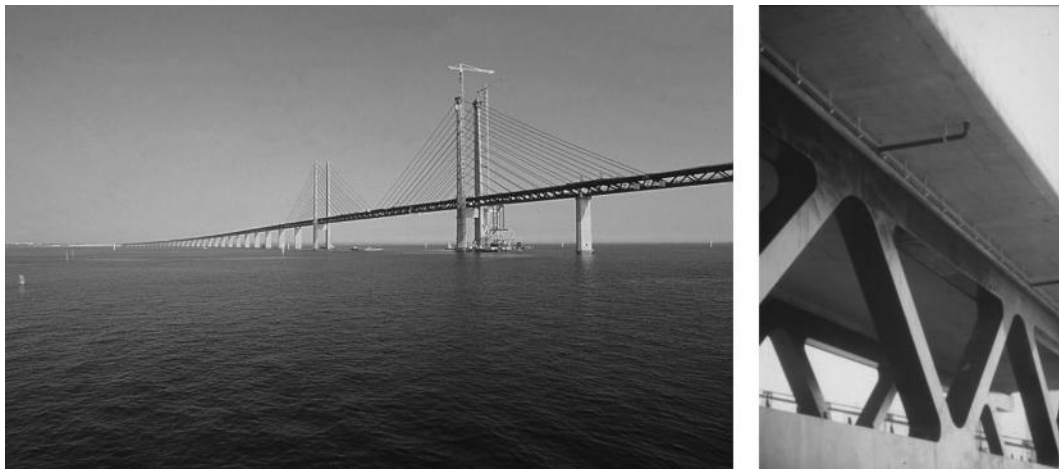


FIGURE 10.33 The Øresund Fixed Link between Denmark and Sweden, completed in 2000, carrying two tracks of railway on the lower deck and four lanes of road traffic on the upper deck. (Courtesy of COWI A/S.)



FIGURE 10.34 Proposed bridge solution for the Fehmarn Belt Fixed Link: Multi-span cable-stayed bridge with two main spans of 724 m (2375 ft) carrying two tracks of railway on the lower deck and four lanes of road traffic on the upper deck. (Visualization by Dissing + Weitling, courtesy of Femern Bælt A/S.)

10.8 Aerodynamic Aspects

10.8.1 Cable Vibrations

As explained previously modern cable-stayed bridges typically adopt multi-cable systems whereas the first cable-stayed bridges were only provided with a few discrete, but relatively heavy stay cables. The advantage of the multi-cable system is that it leads to a more continuous support of the girder whereby bending moments are reduced, also during construction and future cable replacement. At the same time cable forces to be transferred at each anchorage point are smaller, which simplifies the detailing. However, the total wind area of a multi-cable system is larger than for a system composed of a few large stay cables and also the smaller cables in a multi-cable system are more prone to vibrations. A number of different vibration phenomena have been reported on completed cable-stayed bridges and during construction, including rain-wind induced vibrations, vortex shedding induced vibrations, galloping and indirect excitation.

Rain-wind induced oscillations are probably the most common cause of stay cable vibrations. The phenomenon is related to the formation of water rivulets on the upper and lower surface of the stay cable under the combined action of rain and wind. This changes the characteristics of the cable that in turn causes a change in the forces acting on the cable. Modifying the surface of the stay cables from smooth to non-smooth and thereby disrupting the formation of rivulets has proven to be an efficient mitigation measure. Dimples and helical fillets have been used with success on a number of projects, sometimes in combination with increased stay cable damping.

Vortex shedding induced vibrations and galloping occur in the crosswind direction. Vortices form behind the stay cable in smooth airflow and when the frequency of vortex shedding is close to a natural frequency of the stay cable vortex resonance or lock-in occurs. Vortex shedding induced vibrations occur at limited wind speed ranges matching the natural frequencies of the stay cable. Galloping may be observed when ice-coating changes the cross section of the stay cable. Galloping may occur at all wind speeds above a certain critical value.

Vibration of the cable anchorage points may cause the stay cables to vibrate. This is referred to as indirect excitation. Both vibrations of the anchorage points in the direction of the cable and perpendicular to the cable can result in stay cable oscillations of high amplitude.

Vibrations may not necessarily result in large stress variations but due to the large number of cycles vibrations may ultimately lead to fatigue failure of a stay cable or components of the cable.

Mitigation measures to counteract stay cable vibrations can be classified into three groups: Aerodynamic control, structural control and mechanical control. Aerodynamic control involves changes of the shape of the element that is susceptible to vibrations. Modification of the cable surface by introducing dimples or helical fillets to mitigate rain-wind induced vibrations belong to this group. Structural control modifies the mass or stiffness of the element and an example is the provision of cross-ties that changes the natural frequency of the stay cables. Mechanical control is achieved by the application of damping devices. These devices are attached directly to the stay cables and thereby dampen cable oscillations. In the case of indirect excitation damping devices can be located at the stiffening girder and/or pylons to reduce the vibrations of the cable support points.

For a detailed description of the phenomena including the physics behind the various types of oscillations and possible mitigation measures refer to de Sá Caetano 2007.

10.8.2 Girder

Buffeting is the dynamic response of the bridge to gusty wind. The governing response is usually in the along-wind direction, but depending on the aerodynamic characteristics of the stiffening girder and the turbulence characteristics of the wind on the bridge site a significant buffeting response may be found in the crosswind direction.

Box girders adopted for long span cable-stayed bridges are often aerodynamically shaped to reduce the wind load effects. An aerodynamically shaped “nose” can be either structural or non-structural

in which case it is often referred to as a wind fairing. However, vortices can form if the flow detaches from the surface at the downwind corners. Vortex shedding excitation of the stiffening girder occurs when the vortex shedding frequency matches the natural frequency of one of the vertical girder modes. Typically the lower order modes are more critical and vortex shedding excitation will occur at relatively low wind speeds where the flow is smooth. Guide vanes, wind fairings and splitter plates have been adopted in practice and have proven efficient in preventing the formation of vortices. Active control systems have been proposed but not yet implemented in practice (Ostenfeld and Larsen 1992).

Flutter is an extreme event characterized by high amplitude oscillations at high wind speeds. The critical wind speed of onset of flutter is defined as the point where the total damping becomes negative because of negative aerodynamic damping. The total damping is the sum of structural and aerodynamic damping. The total damping further decreases when the wind speed increases beyond this point resulting in self-exciting oscillations that will ultimately lead to collapse of the structure. Reference is made to the specialist literature (Simiu and Scanlan 1996).

Cable-stayed bridges are often constructed by balanced cantilevering. However, the bridge is less stable aerodynamically during the cantilevering phase than in the completed stage after main span closure. In some cases the buffeting response or critical wind speed of onset of flutter during construction has been found to be unacceptable unless stabilizing measures such as tie-down cables or tuned mass dampers were installed.

10.8.3 Pylon

Depending on the cross sectional shape pylons may be susceptible to vortex shedding that may in turn cause the stay cables to oscillate due to indirect excitation. This can be counteracted by modifying the cross section to a more favorable shape, for instance by introducing corner cuts, by installation of deflector plates or tuned mass dampers.

10.8.4 Wind Tunnel Testing

Most cable-stayed bridges are prototypes in terms of the characteristics of the structure and the bridge site and it is common practice to carry out wind tunnel testing to verify the design, including the stability during construction. Computational fluid dynamics (CFD) is a useful tool, which can be used to study and optimize the cross sectional shape of girders and pylons. Section model wind tunnel testing provides the wind load coefficients and can also provide input for the assessment of vortex shedding excitation and flutter stability. Full aeroelastic bridge model tests are used to check the buffeting response and flutter stability of the bridge during construction and in the completed stage. Terrain models can be used to provide specific information on the wind climate including the turbulence intensities at the bridge site if site measurements are not available or need to be supplemented.

10.9 Architectural Lighting

Cable-stayed bridges are often landmark structures and it has become popular to provide these with architectural lighting to highlight special architectural features. Consequently, it may be quite a different experience to cross a bridge or view it from a distance at daytime and at night, respectively.

Lighting schemes can be static or the lighting controls can be dynamic, and should be programmed such as not to distract traffic. The light intensity shall be adjusted to match the surroundings of the bridge.

Environmental and sustainability aspects are obviously an important part of the design of architectural lighting that should consider issues such as energy consumption and how light pollution can be avoided. The recent development in LED lighting technology and lighting controls has added to the popularity of architectural lighting.

A number of cable-stayed bridges ranging from small scale to large bridges have been provided with architectural lighting, in particular bridges located in urban areas. An example is the Stonecutters Bridge. The lighting scheme installed on Stonecutters Bridge is based on LED luminaires that allow both a neutral

white light and various colored lighting themes for special occasions. The key elements of the bridge design are the mono-column pylons and the cross girders connecting the unique twin box girders. As a consequence the architectural lighting focuses on the pylons by means of the light beacon at the pylon top and a vertical light strip in the upper section of the pylons that is of composite construction with an outer stainless steel skin (see Figure 10.35), flood light on the pylons themselves, and on the cross girders.

Other examples of bridges with sophisticated architectural lighting schemes include the Sutong Bridge (China, Figure 10.36), the Rama 8 Bridge (Thailand), the Normandy Bridge (France), and the Erasmus Bridge (The Netherlands, Figure 10.37).

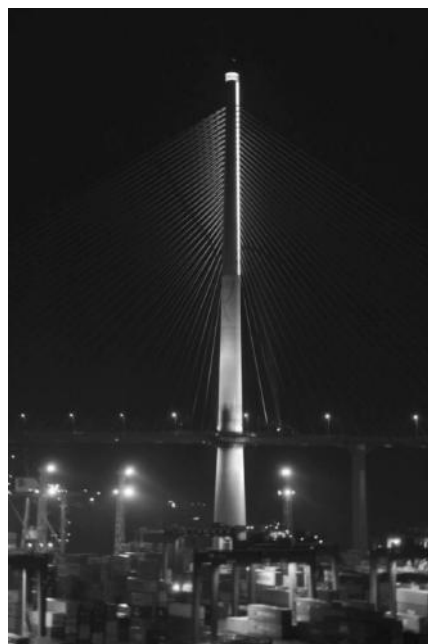


FIGURE 10.35 Stonecutters Bridge, Hong Kong S.A.R., China. Night view showing the architectural lighting on the pylon. (Courtesy of M. R. Larsen.)



FIGURE 10.36 The Sutong Bridge, China. General view of the architectural lighting. (Courtesy of Sutong Bridge Co., Ltd.)



FIGURE 10.37 The Erasmus Bridge in Rotterdam, The Netherlands. Night view showing the normal architectural lighting on pylon and stay cables. Colored lighting schemes have been adopted for special occasions: The Erasmus Bridge was illuminated in yellow to mark that Rotterdam hosted the prologue of the 2010 Tour de France. In 2007 when Rotterdam was the City of Architecture the Erasmus Bridge was illuminated in purple. (Courtesy of D. Broers.)

References

- Bergman, D. 1999. Ting Kau Cable Stayed Bridge: Challenges in the Construction Process. *Proceedings of the IABSE Conference Cable-Stayed Bridges—Past, Present and Future*, Malmö, 1999. IABSE Reports, Volume 82, Zürich, Switzerland.
- CIP Recommendations on Cable Stays. 2002. *Recommendations of French interministerial commission on Prestressing*. Setra (Service d'Etudes Techniques des Routes et Autoroutes), Bagneux, France.
- de Sá Caetano, E. 2007. *Cable Vibrations in Cable-Stayed Bridges*. Structural Engineering Documents No. 9. IABSE, Zürich, Switzerland.
- EN 1993-1-11. 2006. *Eurocode 3—Design of steel structures—Part 1-11: Design of Structures with Tension Components*. European Standard.
- Fédération internationale du béton. 2005. *Acceptance of stay cable systems using prestressing steels*. Fib Bulletin No. 30, Lausanne, Switzerland.
- Fernández Troyano, L. 1999. *Bridge Engineering: A Global Perspective*. [Tierra sobre el Agua. Visión Histórica Universal de los Puentes] (in Spanish). Colegio de Ingenieros de Caminos, Canales y Puertos. Colección de Ciencias, Humanidades e Ingeniería No. 55, Madrid, Spain.
- Gimsing, N. J. 1988. *Cable-Stayed Bridges (Skråstagsbroer)*. Series F, No. 113. Department of Structural Engineering, Technical University of Denmark, Lyngby, Denmark.
- Gimsing, N. J. 1996. *Cable Supported Bridges—Concept & Design* (2nd ed.). John Wiley & Sons, Chichester, U.K.
- Janberg, N. Structurae: International Database and Gallery of Structures. <http://www.structurae.de/>.
- Keller, T. 2003. *Use of Fibre Reinforced Polymers in Bridge Construction*. Structural Engineering Documents No. 7. IABSE, Zürich, Switzerland.
- Leonhardt, F. 1986. *Bridges (Ponts—Puentes)*. Presses polytechniques romandes (in French and Spanish). Lausanne, Switzerland.
- Montens, S., Moine, P., Lam, H. and Vollery, J.-C. 2012. Tianxingzhou Bridge: World Record Span for Railway Cable-Stayed Bridges. *Proceedings of the IABSE Symposium Large Structures and Infrastructures for Environmentally Constrained and Urbanised Areas*, Venice, 2012.
- Ogawa, A., Matsuda, T. and Kasuga, A. 1998. The Tsukuhara Extradosed Bridge near Kobe. *Structural Engineering International*, 8(3), 172–173.

- Ostenfeld, K. H. and Larsen, A. 1992. Bridge Engineering and Aerodynamics. In Larsen A. (Ed.) *Aerodynamics of Large Bridges. Proceedings of the First International Symposium on Aerodynamics of Large Bridges*, Copenhagen, 1992. Balkema.
- Post-Tensioning Institute. 2007. *Recommendations for stay cable design, testing and installation* (5th ed), Phoenix, AZ.
- Simiu, E. and Scanlan, R. 1996. *Wind Effects on Structures: Fundamentals and Applications to Design* (3rd ed.). John Wiley & Sons, New York.
- Tang, M.-C. 1995. Talmadge Memorial Bridge, Savannah, Georgia. *Structural Engineering International*, 5(1), 15–16.
- Vejrum, T. 1997. *Bridges with Spatial Cable Systems. Theoretical and Experimental Studies with Special Emphasis on Lateral Buckling Stability of the Girder*. PhD Thesis. Series R, No. 19. Department of Structural Engineering and Materials, Technical University of Denmark.
- Vejrum, T., Carter, M. and Kite, S. 2006. Detailed Design of Stonecutters Bridge Superstructure. *Proceedings of the International Conference on Bridge Engineering—Challenges in the 21st Century*, Hong Kong, 2006.
- Virlogeux, M. 1999. Bridges with Multiple Cable-Stayed Spans. *Proceedings of the IABSE Conference Cable-Stayed Bridges—Past, Present and Future*, Malmö, 1999. IABSE Reports, Volume 82, Zürich, Switzerland.
- Virlogeux, M. 2002. New Trends in Prestressed Concrete Bridges. *Structural Concrete*, Thomas Telford/fib, 3(2), 67–97.
- Walther, R., Houriet, B., Isler, W. and Moïa, P. 1985. *Cable-Stayed Bridges [Ponts Haubanés]* (In French). Presses polytechniques romandes, Lausanne, Switzerland.

@Seismicisolation

11

Extradosed Bridges

11.1	Introduction	437
11.2	Structural Configuration.....	437
	Cable-Stayed vs. Extradosed Bridge • Structural Configuration	
	• Extradosed Unit Section • Tower • Stay Cable Layout	
	• Composite Extradosed Bridge	
11.3	Design	446
	Girder Bending Moment under Dead Load • Stress Change of Stay	
	Cables • Stay Cable Design • Optimization of Stay Cable Damper	
11.4	Structural Member Detailing	452
	Saddle • Steel Box Anchorage in Tower • Extradosed Cable	
11.5	Construction	455
11.6	Summary.....	456
	References.....	457
	Appendix	459

Akio Kasuga
*Sumitomo Mitsui
Construction*

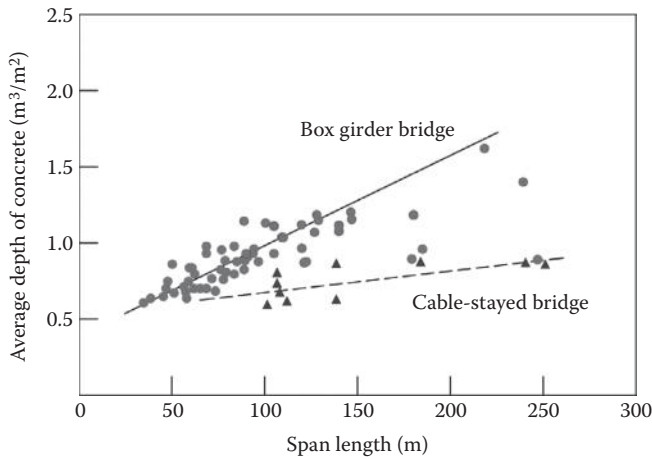
11.1 Introduction

The boldness of the extradosed concept for the new structure type, first proposed by Mathivat (1988), in its use of a stay cable allowable stress of $0.6f_{pu}$ —the same value as for ordinary prestressed concrete steel—was well received, and the extradosed solution flowered in Japan. More than 40 extradosed bridges in Japan (Kasuga 2006) and many in the world have been constructed since this new concept was introduced. Extradosed bridges are similar to cable-stayed bridges in that stay cables are used for strengthening. However, they have the characteristics of cable-stayed and ordinal girder bridges. Figures 11.1 through 11.3 show the data of extradosed bridges in Japan. Moreover, experience up to now in the construction of extradosed bridges has made their relationship to cable stayed bridges, which use $0.4f_{pu}$ as the allowable stress for the stays, increasingly clear. As a result, considering the fact that suspending the structure from stays greatly increases the degree of freedom of the design.

11.2 Structural Configuration

11.2.1 Cable-Stayed versus Extradosed Bridge

Since the time of the construction of the first extradosed bridge, the differences between cable-stayed bridges and extradosed bridges have been debated. Both of these bridge types have structures that use stays for reinforcement (Figure 11.4). However, rather than simply assuming that an allowable stress of $0.6f_{pu}$ could be used in the case of an extradosed bridge, it became desirable to provide some structural rationale. At that point, attention focused on the distribution ratio of vertical load borne by the girders and the stay cables. Then after investigation of many existing bridges, the fact that there are no clear boundaries between extradosed and cable-stayed bridges was found (Ogawa and Kasuga 1998).



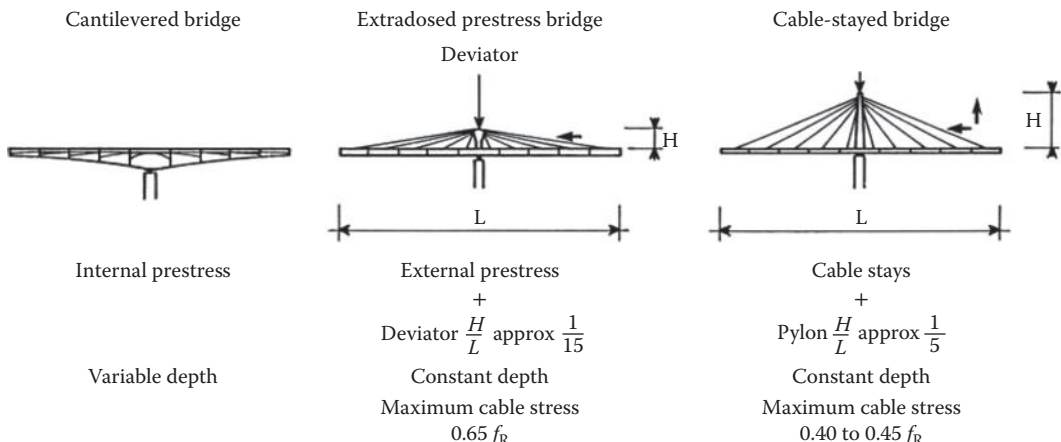


FIGURE 11.4 Ordinal girder, extradosed and cable-stayed bridge. (From Mathivat, J., *FIP Notes*, 1988.)

The major advantages of extradosed bridges compared with cable-stayed bridges and ordinary box girder bridges are as follows:

- Low fatigue stress ranges of stay cables because of live load
- No stay cable adjustment during construction because of stiffer girder
- Aesthetically suitable to environmental sensitive surrounding area because of lower tower
- Continuous design concept between cable-stayed and ordinary box girder bridges
- Economical solution for around 150–200 m span

11.2.2 Structural Configuration

Figure 11.5 shows a general view and photograph of Japanese five typical extradosed bridges. The ratio of center span of side span of the Odawara Blueway Bridge (Kasuga et al. 1994) is the same as that of a normal box girder bridge. However, on the Tsukuhara Bridge (Ogawa, Matsuda, and Kasuga 1998), the side span is extremely short because of the topography. As a result, a large counterweight was placed on the inside of the side span girders. Both the Ibi River (Hirano et al. 1999) and Shin-Meisei Bridges (Iida et al. 2002) span rivers, so they have long side spans. Moreover, as in both cases it was not possible to locate the structures being erected near to the embankments, the side spans were constructed using a special erection method called the core section advance cantilever method. On the Himi Bridge (Maeda et al. 2002), the ratio between the center and side spans was 1:2:1. However, even this ratio results in side spans that are rather short for extradosed bridges as opposed to cable stayed bridges.

The height of the main towers is in accordance with Mathivat's theory on the Odawara Blueway Bridge and Tsukuhara Bridge—in other words, 1/2 of the main tower height of a cable-stayed bridge. The Ibi River Bridge is the same as the other bridges in terms of the proportion of main tower height to span length, but as the sections where the stay cables are placed are the concrete girder sections, the average angle of the stays is 25° or almost the same as that for a cable stayed bridge. On the Shin-Meisei Bridge and Himi Bridge, the girders are somewhat slender, so the main tower height is slightly higher.

The interval between stays is affected by not only structural considerations but by construction-related factors as well. The interval between stays for the Odawara Blueway Bridge and the Shin-Meisei Bridge is about 4 m, and the stays are anchored to each segment. At the Tsukuhara Bridge, the stays are anchored to every other segment, so the interval between stays is 7 m. The Ibi River Bridge uses the precast segmental construction method, so the interval between stays is 5 m controlled by the segment length. The Himi Bridge is a corrugated steel web bridge, so the interval is set at 6.4 m based on the waveform of the corrugated steel web.

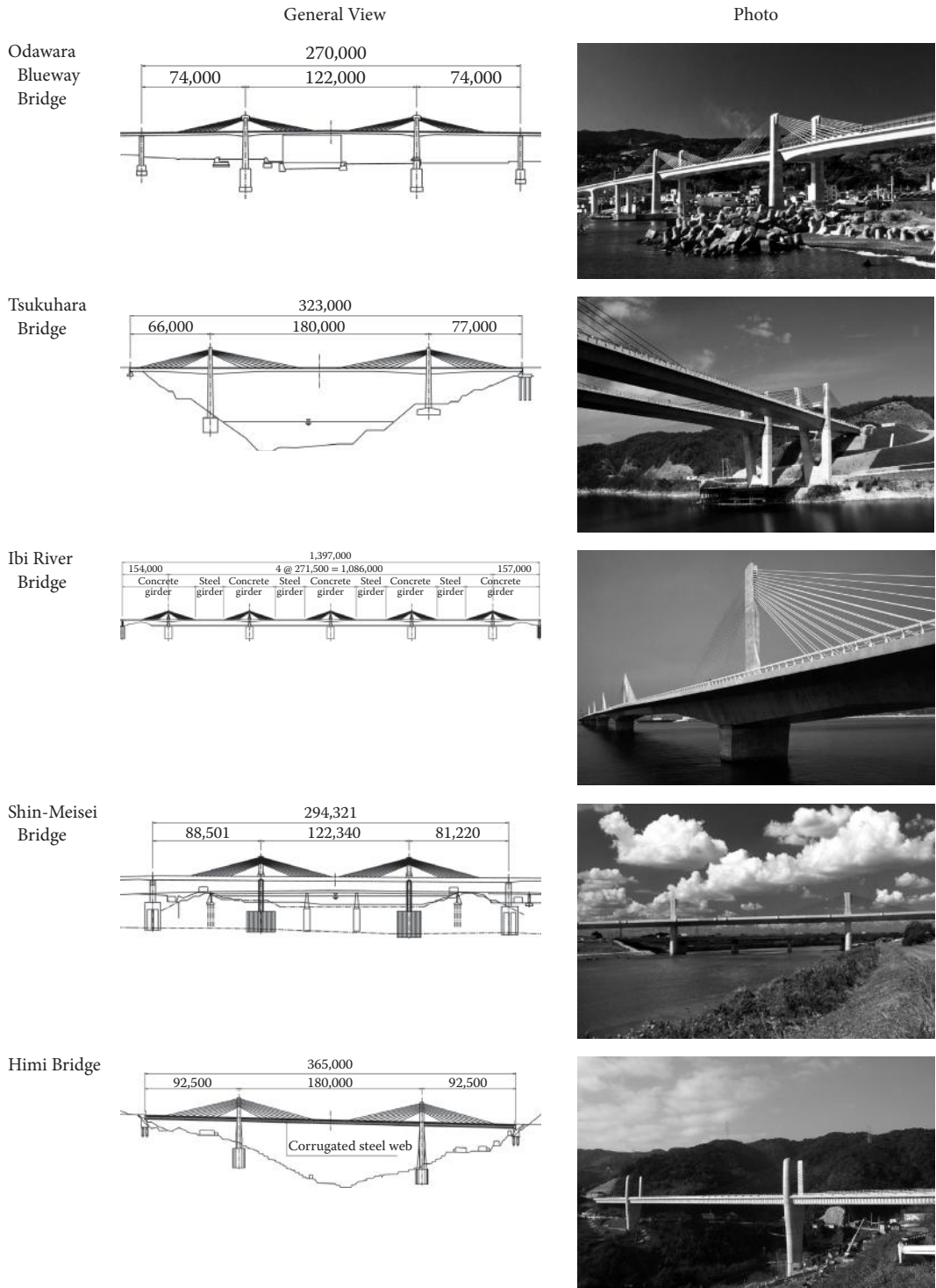


FIGURE 11.5 Five typical extradosed bridges in Japan.

The ratio of the back span of center span is similar to typical box girder bridges. Although the girders are supported by extradosed cables, the features of the extradosed box girder bridge are different from cable-stayed bridges. The girder is much stiffer and is not as influenced by the cables. Therefore, half of the main span of extradosed bridges is slightly shorter than the back span with the back span mostly in the range of 0.55–0.60 of main span length.

11.2.3 Extradosed Unit Section

The several sectional configurations of the bridges are shown in Figure 11.6. The Odawara Blueway Bridge, Tsukuhara Bridge and Ibi River Bridge have two planes of stays, while the Ibi River Bridge and Shin-Meisei Bridge use a single plane. Moreover, with extradosed bridges like the Odawara Blueway Bridge and Tsukuhara Bridge, on which the stays are anchored near the web, it was learned that the

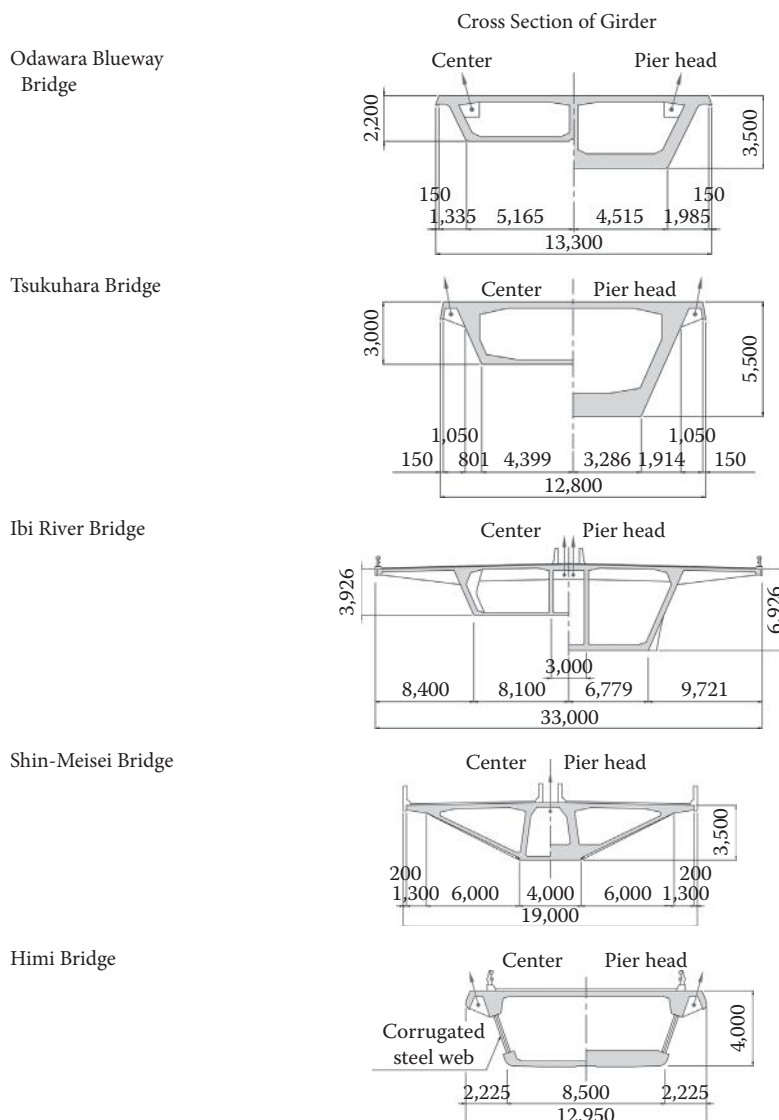


FIGURE 11.6 Cross section of girder.

vertical component of stay cable forces is low and is transmitted immediately to the main girder, making it unnecessary to install structural diaphragms at the stay anchorage positions as in the case of a cable-stayed bridge. This has greatly increased the ease with which extradosed bridges can be constructed.

In the case of single-plane stay, the most important consideration for the section configuration is how to efficiently transmit the stay cable forces to the main girder. For the Ibi River Bridge of 33 m wide, structure for main girders that would transmit the stay cable forces efficiently without diaphragms at each stay location was adopted. As a result, it was decided to set the internal webs spaced at 3 m, the minimum size, and it was also determined that the upper deck ribs, web ribs and three structural diaphragms in one cantilever were needed to ensure the rigidity of the main girder section. Moreover, on the Shin-Meisei Bridge, as on the Ibi River Bridge, it was decided to make the intervals of the internal web as narrow as possible, and to use an inverted trapezoid section to concentrate the shear forces at the internal web to enable the ribs and structural diaphragms to be eliminated.

11.2.4 Tower

Figure 11.7 shows the towers of the five extradosed bridges. The towers of extradosed bridges are low, so there are not so many variations in the shape of the tower as in the case of cable-stayed bridges, and the interface between the towers and the bridge piers will affect the overall design of the bridge aesthetics, particularly in the case of two-plane stay. On the Odawara Blueway Bridge and Tsukuhara Bridge, on which the main towers are connected directly to the two-legged bridge piers, and in terms of form it has an exceptionally high degree of purity. On the Ibi River Bridge and Shin-Meisei Bridge, towers are arranged on the center of girders. And the bottom length of towers is widened to resist transverse seismic loads because of earthquakes.

In terms of stay cable anchorage configuration of the tower, the Odawara Blueway Bridge and Tsukuhara Bridge use a saddle, while the other bridges use a steel box anchorage. In the saddle, there is no access to the tower, however, the use of a steel box anchorage made it possible to provide an inspection manhole on the inside of the towers, allowing the stay cables to be inspected from the inside during maintenance. Figure 11.8 shows the inspection path on the Ibi River Bridge. The later Shin-Meisei Bridge and Himi Bridge have followed this precedent.

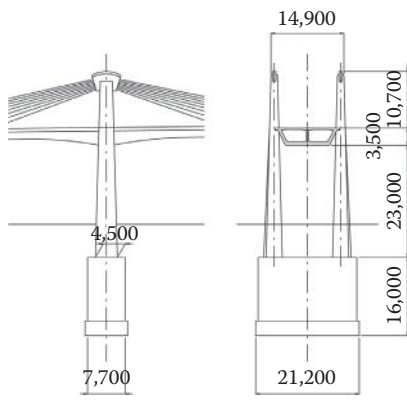
11.2.5 Stay Cable Layout

Figure 11.9 shows cable layouts of five extradosed bridges. Odawara Blueway Bridge and Tsukuhara Bridge use saddle and the rest of them use steel box anchorages in towers. The cable distance at the tower is 0.5–1.0 m. The shorter distance induces larger eccentricity for bridge towers. And the cable distance at the girder is affected by not only structural considerations but by construction-related factors as well. The interval between stays is about 4–7 m. However, the cable distance is related to bridge width, extradosed cable capacity, segment length and number of extradosed cable plane.

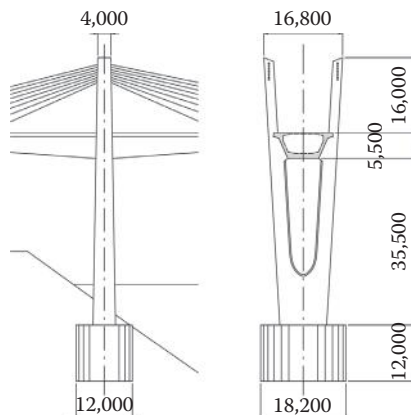
11.2.6 Composite Extradosed Bridge

On the Himi Bridge, whose girder has a corrugated steel web, a major problem was how to ensure that the vertical component of the stay forces is not be applied directly to the joint between the corrugated steel web and the concrete deck. Finally, it was decided to adopt a steel diaphragm anchorage structure as shown in Figure 11.10. The concept behind this structure is that the steel diaphragm mainly carries the vertical component of the stay forces and the shear forces from the corrugated steel, while the concrete slab resists the girder bending and the horizontal component of the stay forces. At the same time, this diaphragm also functions as a stiffening rib reinforcing the upper and lower decks.

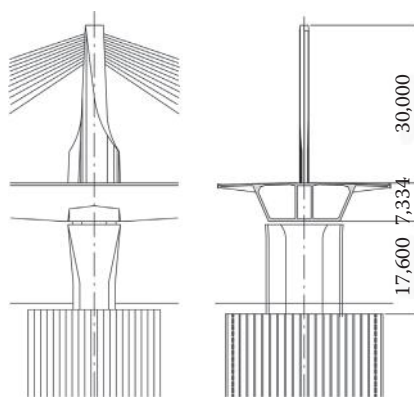
Odawara Blueway Bridge



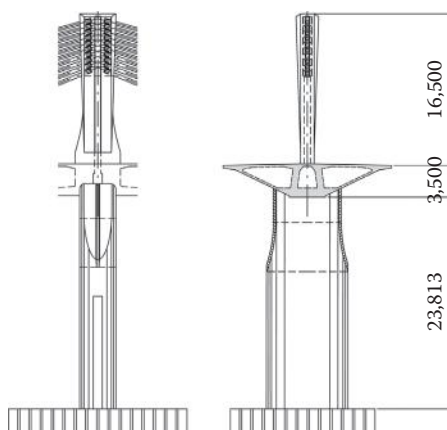
Tsukuhara Bridge



Ibi River Bridge



Shin-Meisei Bridge



Himi Bridge

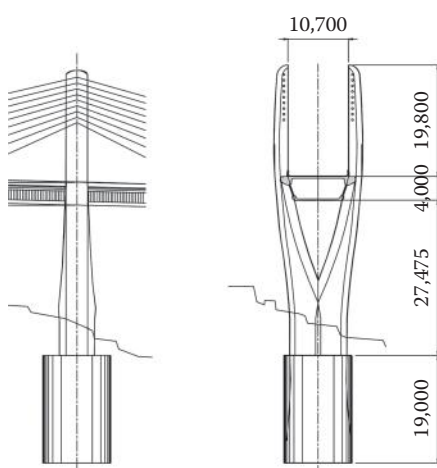


FIGURE 11.7 Tower configuration.

@Seismicisolation

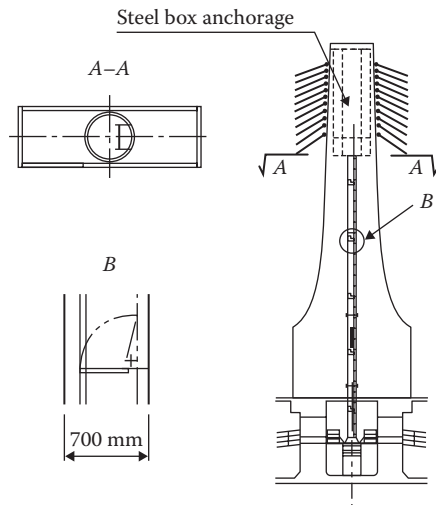


FIGURE 11.8 Example of inspection path (Ibi River Bridge).

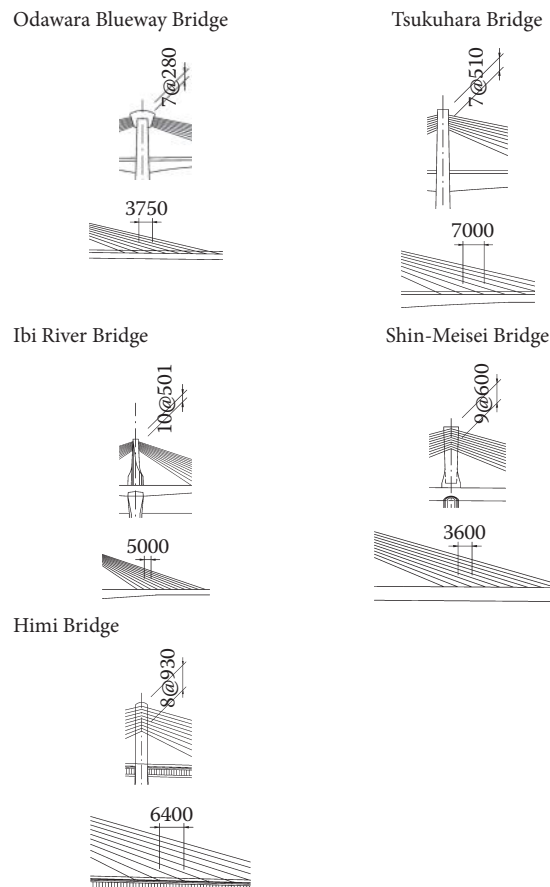


FIGURE 11.9 Stay cable layout at tower and girder.

@Seismicisolation

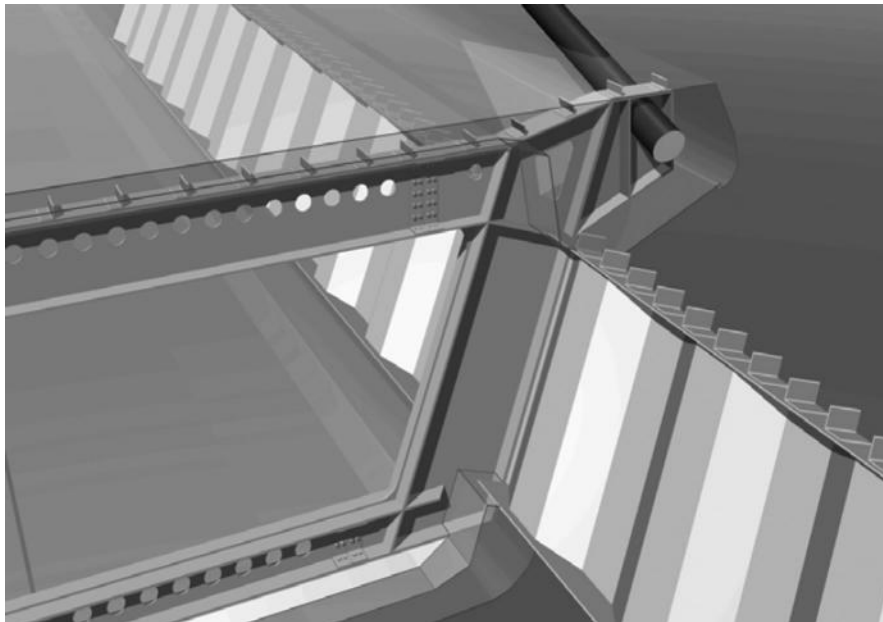


FIGURE 11.10 Steel diaphragm anchorage for corrugated steel web (Himi Bridge).



FIGURE 11.11 Connection segment (Ibi River Bridge).

On the IBI River Bridge, the central part of each span is composed of 100 m long steel box girder, whereas the remaining part of the span is made of concrete segments. Figure 11.11 shows the connection segment and Figure 11.12 indicates the detail of the connection between concrete and steel girders. The top parallel cables are anchored in the steel girder section. To reduce the steel weight, external cables are applied in the part of the steel box girders.

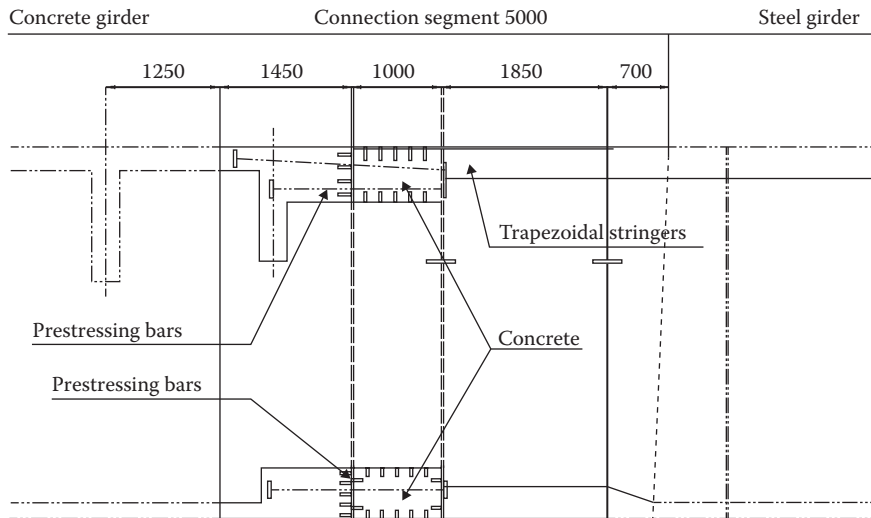


FIGURE 11.12 Detail of connection between steel and concrete girder.

11.3 Design

11.3.1 Girder Bending Moment under Dead Load

Figures 11.13 and 11.14 show the bending moment diagrams change before and after creep.

In the Tsukuhara Bridge, the percentage before creep, which means just after construction, is about 73%. However, this value changes to 67% after creep. And in the Odawara Blueway Bridge, this value changes from 69% to 60%.

The percentage of stay cable forces is determined by the balance between tower height and girder stiffness. Usually, the amount of stay cables and internal or external tendons are determined by the girder and tower height and construction process. In the free cantilevering method, cantilevering tendons are needed before stay cable tensioning. And the amount of these tendons is based on the girder height. Usually, the distance of stay cable is related to the segment length, for example, one stay in each segment or one stay in each two segments. And the size of stay cable depends on the longitudinal distance and girder width. Usually 19 or 27 strands of 15 mm, and sometimes 37 are used in extradosed bridges.

11.3.2 Stress Change of Stay Cables

For the cable stayed bridges and extradosed bridges constructed up to now, plotting the value β (Ogawa and Kasuga 1998)—which expresses the distribution ratio of the stay cables for the horizontal axis—and the value for maximum stress change of the stay cables because of design live loads for the vertical axis reveals that there is a considerable correlation between these values, as shown in Figure 11.15. Two observations can be concluded from this figure. First, it is difficult to clearly distinguish extradosed bridges and cable-stayed bridges in terms of structural mechanics, since many of extradosed bridges constructed up to now are very similar to now cable-stayed bridges. Second, in designing stay cables for extradosed bridges, stress change because of design live loads provides an effective index that can be easily determined through the design process.

11.3.3 Stay Cable Design

In the design of stays, the fatigue limit state is usually critical. When designing structures that are reinforced using stays, it may be unnecessary to define in advance whether the bridge will be a

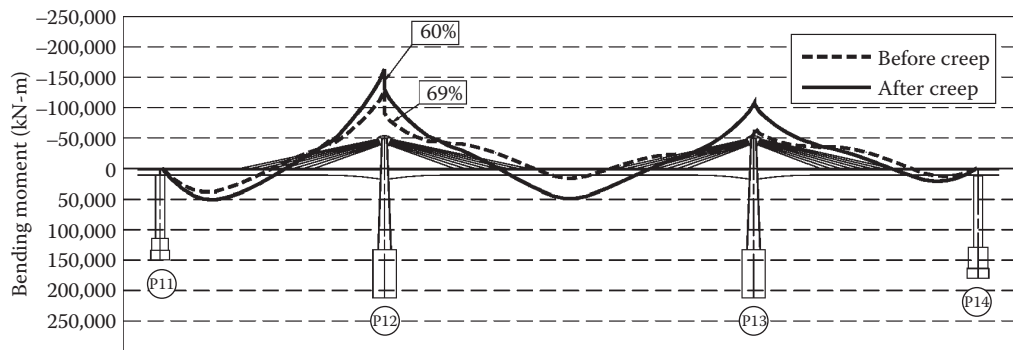


FIGURE 11.13 Bending moment (dead load + stay cable forces, Odawara Blueway Bridge).

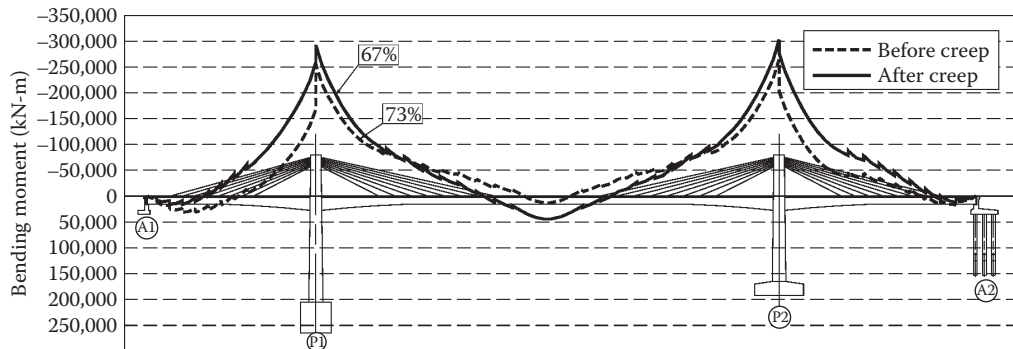


FIGURE 11.14 Bending moment (dead load + stay cable forces, Tsukuhara Bridge).

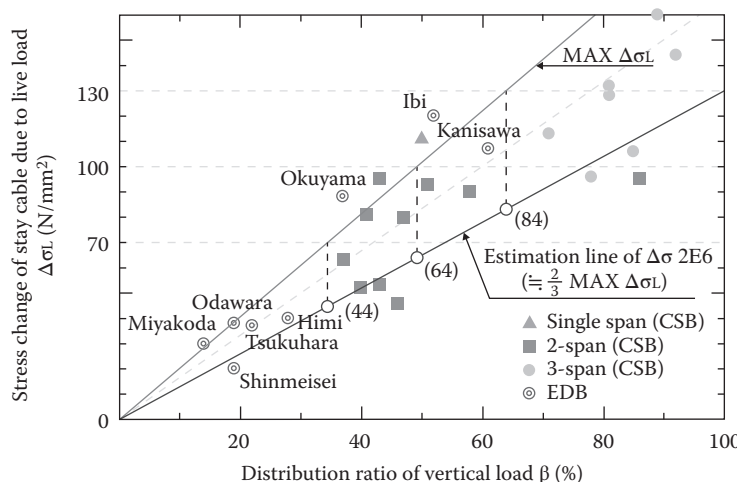


FIGURE 11.15 Distribution ratio versus stress changes because of live load.

cable-stayed bridge or an extradosed bridge and then to determine the allowable stress for the stays. A more rational approach is to design the stays for fatigue limit state first by focusing on the stress change caused by live loads. It makes possible to design each stay separately and enable the allowable stress to be set individually for each stay. From the outset, unlike suspension bridges, the stress change on a cable-stayed bridge will differ depending on the stays, so it is not rational to define the allowable stress using a single value of $0.4f_{pu}$. This knowledge is reflected in the "Specifications for Design and Construction of Cable-Stayed Bridges and Extradosed Bridges" (JPCEA 2000). The specification allows two kinds of design methods. One is normal fatigue design using fatigue load and design lifetime of a bridge (Method A). However, it is usually difficult to estimate the amount of future traffic and heavy trucks, especially local roads. In that case, another approximation method using stay cable stress change because of design vehicular live loads is introduced (Method B). Figure 11.16 shows the design flow for stay cable design. In order to derive tensile stress of stay cables at service loads, design under fatigue limit state should be performed first. Figure 11.17 shows the relationship between the allowable tensile stress for stays of highway bridges and the stress change because of live load $\Delta\sigma_L$ regulated in the specifications. The fatigue strength difference between prefabricated wire type and strand type is considered. On the basis of prior successful experiences in Japan with cable-stayed, extradosed and similar bridges having spans of up to about 250 m, Method B is defined so as to ensure adequate safety in comparison with bridges designed using Method A.

Fatigue design was performed in the estimation line of stress range for two million cycles ($\Delta\sigma_{2E6}$) including secondary flexural bending because of girder deflection, determined according to design conditions on a design service life of 50 years and average daily traffic of 70,000 mixing 50% trucks, by using the structural models of the Odawara Blueway Bridge, the Tsukuhara Bridge, and the IBI River Bridges, as shown in Figure 11.15. It is seen that, based on the calculations that stress change because of fatigue load is about 1/3 of that because of design live loads and the stress level because of secondary flexural bending is the same as that due to axial forces of stay cables, the estimation line of $\Delta\sigma_{2E6}$ assumes 2(1/3) (Max $\Delta\sigma_L$). The safety margin of Method B can be confirmed compared with $\Delta\sigma_{2E6}$ and fatigue strength (f_{scrd}) divided by a safety factor (γ_b).

For a strand stay cable fabricated on site by using wedges, the relationship between f_{scrd}/γ_b and the $\Delta\sigma_{2E6}$ estimation line is shown in Figure 11.18, on the basis of a system with fatigue strength of at least 120 N/mm^2 at $0.6f_{pu}$ or at least 200 N/mm^2 at $0.4f_{pu}$. In this situation, γ_b is 1.4. The shaded section of the figure is the range determined by Method A with the fatigue design conditions indicated above, and since this is 2/3 of the $\Delta\sigma_L$, as prescribed by Method B, there is a safety factor of around 2.0 with respect to f_{scrd}/γ_b .

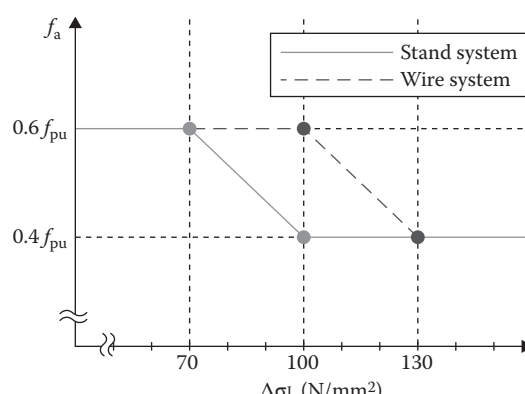


FIGURE 11.16 Design flowchart for stay cables.

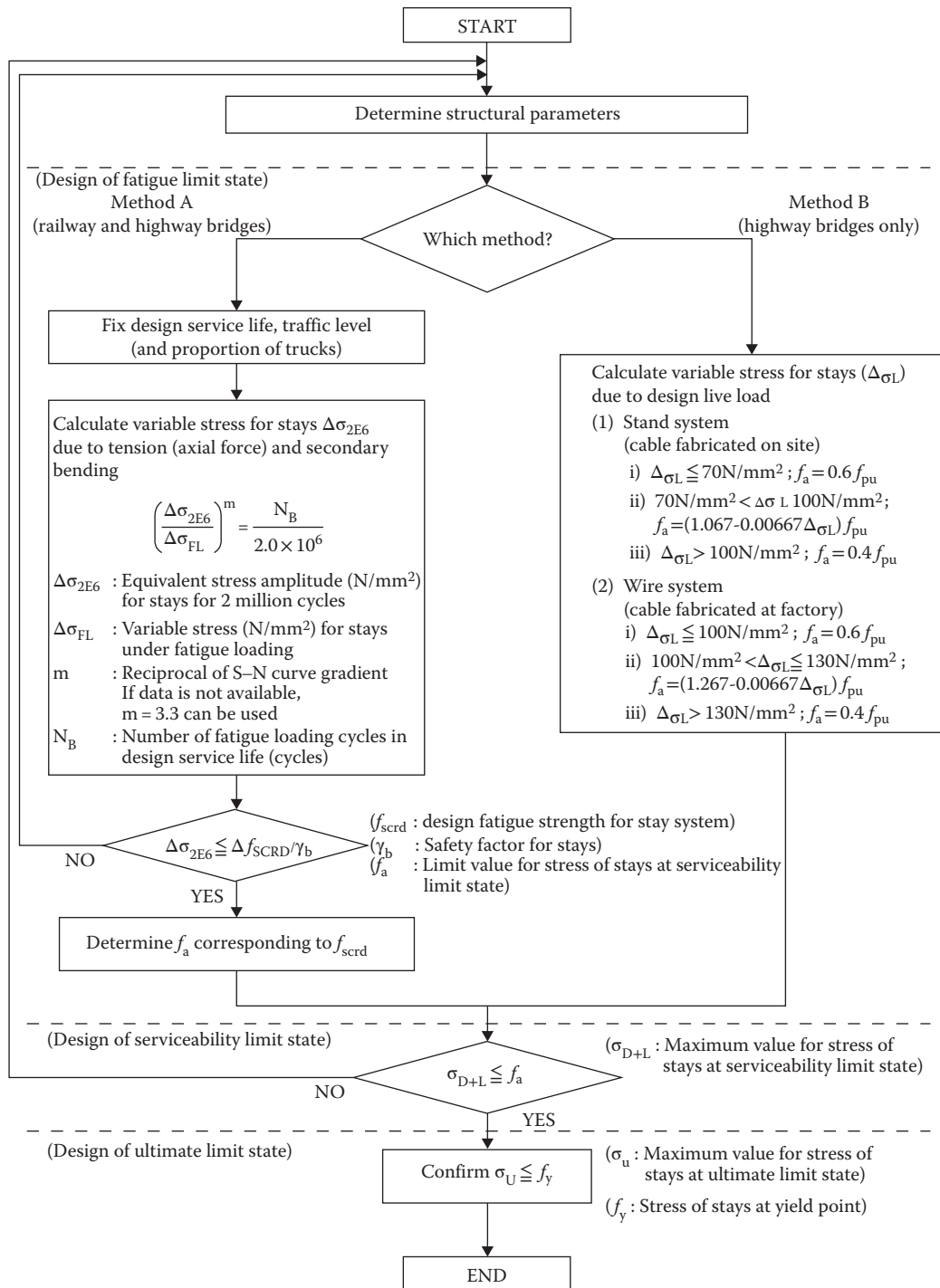


FIGURE 11.17 Allowable stress versus stress changes because of live load.

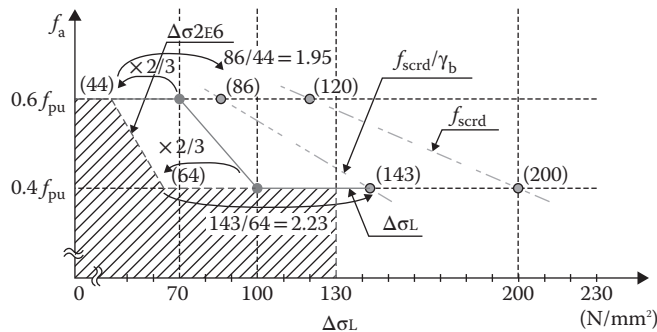


FIGURE 11.18 Safety margin of Method B in strand system.

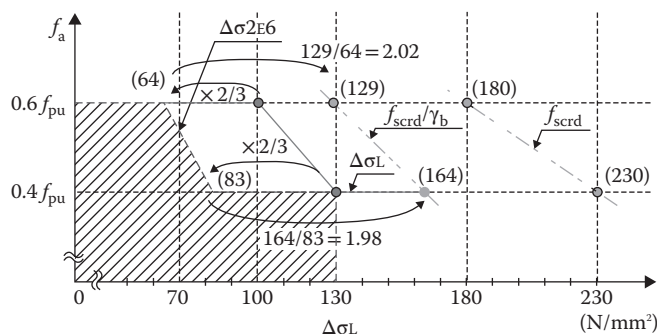


FIGURE 11.19 Safety margin of Method B in wire system.

For a galvanized wire stay cable made at a factory as a cold-cast cable or as a cable with buttonhead anchorages, the relationship between the f_{scrd}/γ_b and the $\Delta\sigma_{2E6}$ estimation line is shown in Figure 11.19, on the basis of a system with fatigue strength of at least 180 N/mm^2 at $0.6f_{\text{pu}}$ or at least 230 N/mm^2 at $0.4f_{\text{pu}}$, and similar to the figure for the cable fabricated on site. It can be seen from the figure that the factory-made cable also has a safety factor of around 2.0 with respect to f_{scrd}/γ_b .

As described above, stays designed by Method B require a safety factor of about 2.0 for $\Delta\sigma_L$ with respect to f_{scrd}/γ_b , to take into consideration the fact that the method includes more uncertainties than Method A, and in order that the safety of stays does not vary greatly from that of cable-stayed and extradosed bridges constructed to date. In the most of extradosed bridges and some cable-stayed bridges, $0.6f_{\text{pu}}$ as the tensile stress can be used because their stress changes are low, $20\text{--}50 \text{ N/mm}^2$. Moreover, the most rational point of this specification is that we can choose the tensile stress in each stay cable from $0.4f_{\text{pu}}$ to $0.6f_{\text{pu}}$ continuously. This is based on the concept that one value of tensile stress in one bridge is not structurally rational.

Figure 11.20 shows the allowable stress for stay cables according to the Japanese and French Recommendations (SETRA 2002). The Japanese Specifications have linear change between $0.6f_{\text{pu}}$ and $0.4f_{\text{pu}}$ and two types of stay cable systems, strand and wire, which are defined with different allowable stress in the stress range from 70 N/mm^2 to 130 N/mm^2 . The stress range considered is the variation in cable stress because of live load. The Japanese Specifications take into account the flexural bending of stay cables because of girder deflection by live load. However, this graph is an approximate method when using Japan's L-25 live load. When the magnitude of fatigue loading and number of load cycles during the design life time are defined, more precise fatigue design for stay cables can be determined in place by this simplified method. For comparison, the French Recommendations have nonlinear change after 50 N/mm^2 with the allowable stress decreasing gradually to $0.45f_u$.

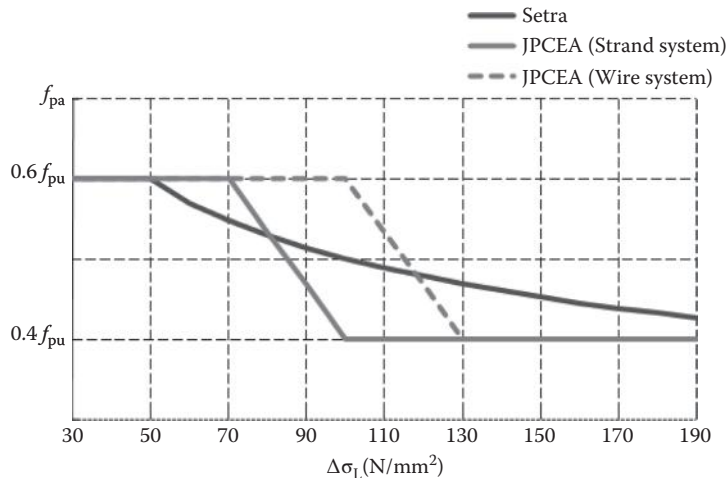


FIGURE 11.20 Allowable stresses of Japanese and French recommendations.

11.3.4 Optimization of Stay Cable Damper

An allowable stress of $0.6f_{pu}$ is usually used for the extradosed cable. However, in fatigue design, it is difficult to evaluate the vibration of the stay cables because of the wind. For this reason, dampers should be provided for the extradosed cables. Many types of dampers for stay cables, for example, viscous dampers, friction dampers, oil dampers and so on, are available nowadays. And also in order to derive suitable performance of dampers, optimization of stay cable dampers is needed. In this section, the example of high damping rubber damper will be discussed.

The high damping rubber dampers (Figure 11.21) developed for the Odawara Blueway Bridge were also used on the Tsukuhara Bridge, the Ibi River Bridge, the Shin-Meisei Bridge and the Himi Bridge. In economic and aesthetic reasons, the high damping rubber dampers are suitable for up to 200 m lengths of the stay cables to obtain 0.03 logarithmic decrements against rain-induced vibrations. The approximation method to design for high damping rubber dampers and the test results (Figure 11.22) were shown in the Odawara Blueway Bridge (Kasuga, Kimizu, and Matsui 1995). The advantage of this damper makes it possible to tune the optimized elastic spring constant by selecting the number of high damping rubbers. The development of such damping technologies also played a role in the development of extradosed bridges.

On the model shown in Figure 11.23, the optimum elastic spring constant K_{opt} (Figure 11.24) is obtained by the following equation (Kasuga, Kimizu, and Matsui 1995):

$$K_{opt} = \frac{(\omega n)(\gamma)}{0.72(\alpha)(2\nu)} \quad (11.1)$$

where

$$\nu = \frac{4\gamma}{4 + \gamma^2} \quad (11.2)$$

and

$$\alpha = \frac{(\omega n)(X_i)(L - X_i)}{(T)(L)} \quad (11.3)$$

where γ is the loss factor for the rubber, ωn is the n th circular frequency mode, L is the length of the stay cable, X_i is the location of a damper and T is the cable tension.

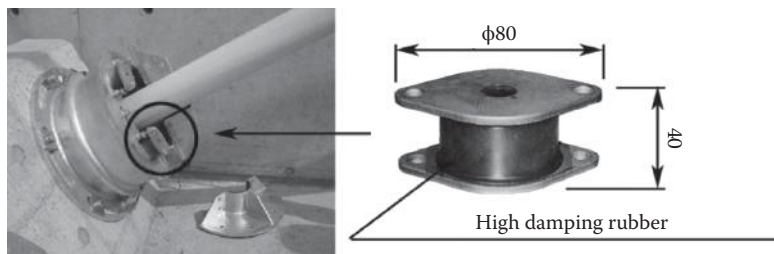


FIGURE 11.21 High damping rubber damper.

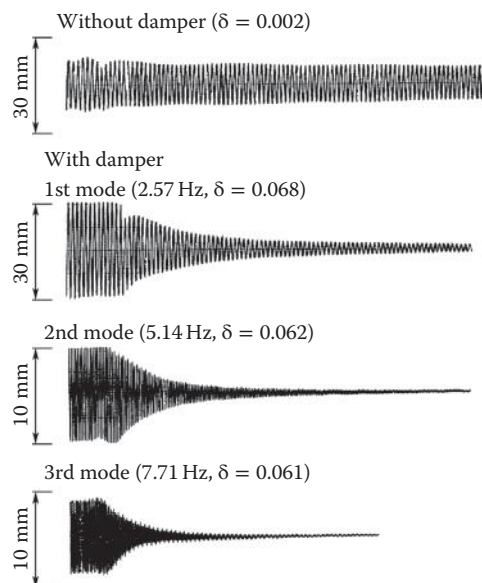


FIGURE 11.22 Test results of high damping rubber damper.

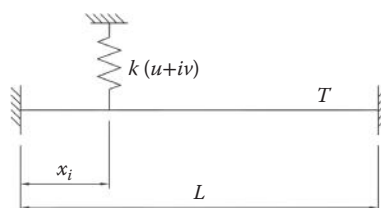


FIGURE 11.23 Analysis model.

11.4 Structural Member Detailing

11.4.1 Saddle

The tower saddle developed for the Odawara Blueway Bridge (Figure 11.25) was also used on the Tsukuhara Bridge. The “Specifications for Design and Construction of Cable-Stayed Bridges and Extradosed Bridges” (JPCEA 2000) specifies that, the saddle can be used under the condition on less than 50 N/mm² of stress change because of design live loads. This is based on the research

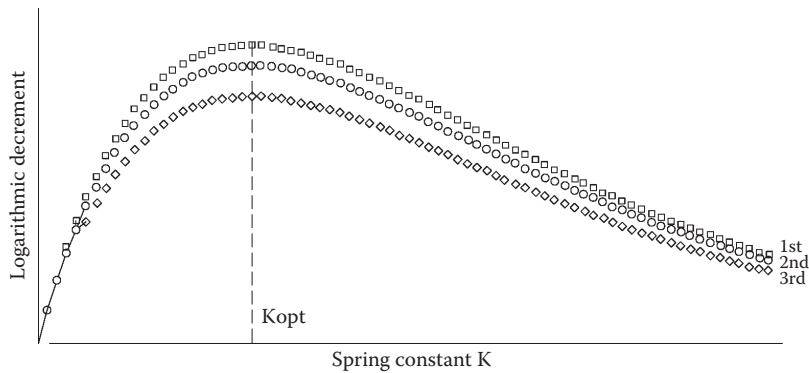


FIGURE 11.24 Relationship between elastic spring constant versus logarithmic decrement.

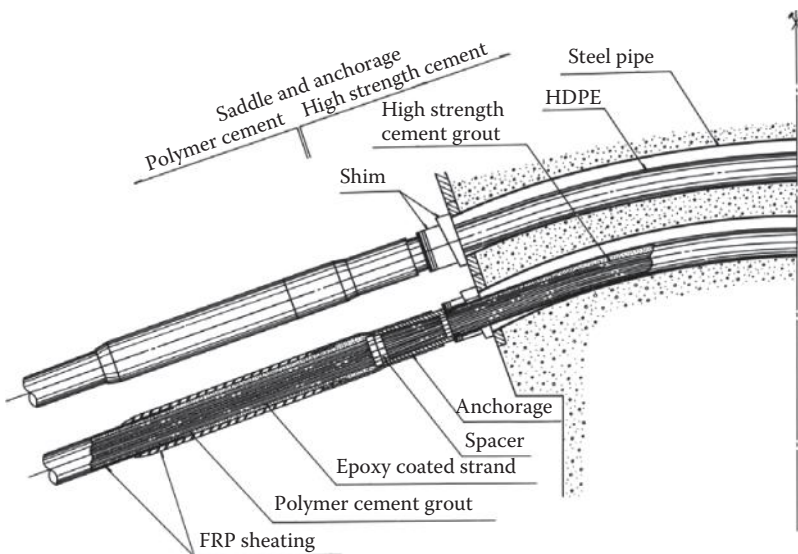


FIGURE 11.25 Example of saddle (Odawara Blueway Bridge).

(Fujita et al. 1999) for fretting fatigue test data up to the tendon system of 37 strands of 15.2 mm diameter. The radius of the saddle may be the same as that of deviators of external cables. Moreover, in the saddle, stay cable force difference between right and left side because of creep and earthquakes should be fixed.

11.4.2 Steel Box Anchorage in Tower

From an ease of maintenance perspective, the steel anchorage box structure of the tower is useful. However, it is a heavy structure, and although there is no problem when it can be erected in one piece using a floating crane (Figure 11.26), when it must be erected on land where big cranes cannot be used, such as in the case of the Shin-Meisei Bridge (Figure 11.27) and Himi Bridge, the structure must be separated into some sections of a weight that allows them to be erected on land. Moreover, when the stay forces are carried by the steel box, as in the case of the Ibi River Bridge, the separate sections must be assembled and then a thick steel plate must be bolted or welded to connect the sections. In such cases, bolts and welding become a major obstacle, from a detail standpoint in the case of bolts and from a



FIGURE 11.26 Anchorage box erection (Ibi River Bridge).

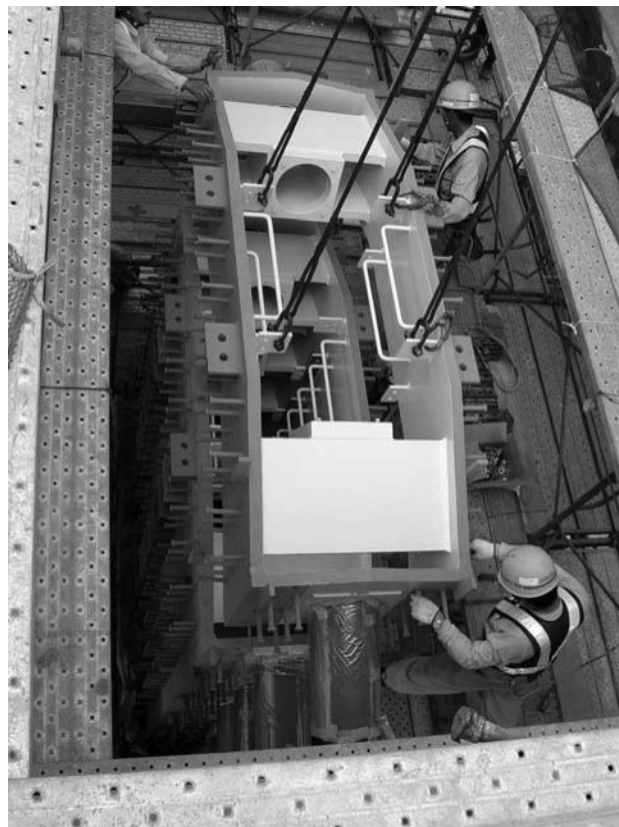


FIGURE 11.27 Installation of a separated steel box (Shin-Meisei Bridge).

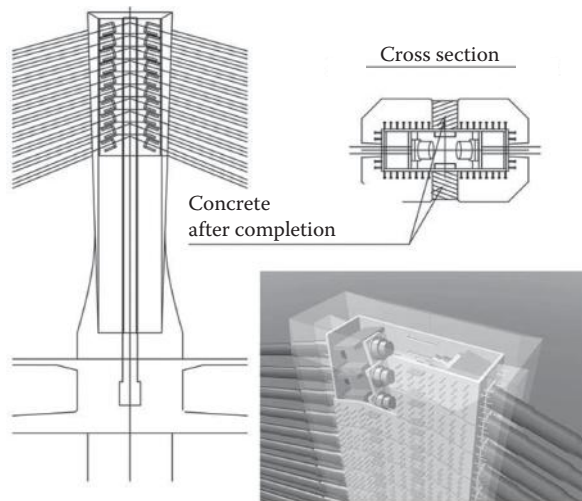


FIGURE 11.28 Composite anchorage at tower (Shin-Meisei Bridge).

time and cost standpoint in the case of welding. For this reason, on the Shin-Meisei Bridge, concrete was placed around the anchorages to form composite structures for anchoring the extradosed cables (Figure 11.28). In this method, the horizontal component of stay cable forces is carried by only steel, and vertical ones are carried by steel and concrete. Each steel anchorage boxes are metal touched. So the surface was ground by machine. This method was also used on the Himi Bridge.

11.4.3 Extradosed Cable

The development of the extradosed bridge, whose main feature is the ability to use an external cable system for the extradosed cables has been made possible by the development of the stay cable system. It is no exaggeration to say that the development of the extradosed cable system is synonymous with the development of corrosion protection technologies. There are various types system available, from epoxy coated strand and galvanized strand with polyethylene coating of prefabricated galvanized wire with polyethylene sheeting. And also cable installation methods also vary depending on whether the strand-by-strand type or the prefabricated type is used.

In the Japanese Specifications of Design and Construction for Cable-stayed and Extradosed Bridges, design requirements for cable replacement are provided in the commentary. And cable replacement is considered in the most of extradosed bridges in Japan.

11.5 Construction

Construction process of extradosed bridges is similar to that of cable-stayed bridges. However, extradosed cable force adjustment is not usually necessary during construction or after completion of the bridges.

Extradosed cable force history during construction is checked. Figures 11.29 and 11.30 show cable force history during construction for Odawara Blueway Bridge and Tsukuhara Bridge. After tensioning of extradosed cables, cable forces are decreasing and increasing within a certain range because of the addition of dead load, prestressing, and installation of subsequent cables.

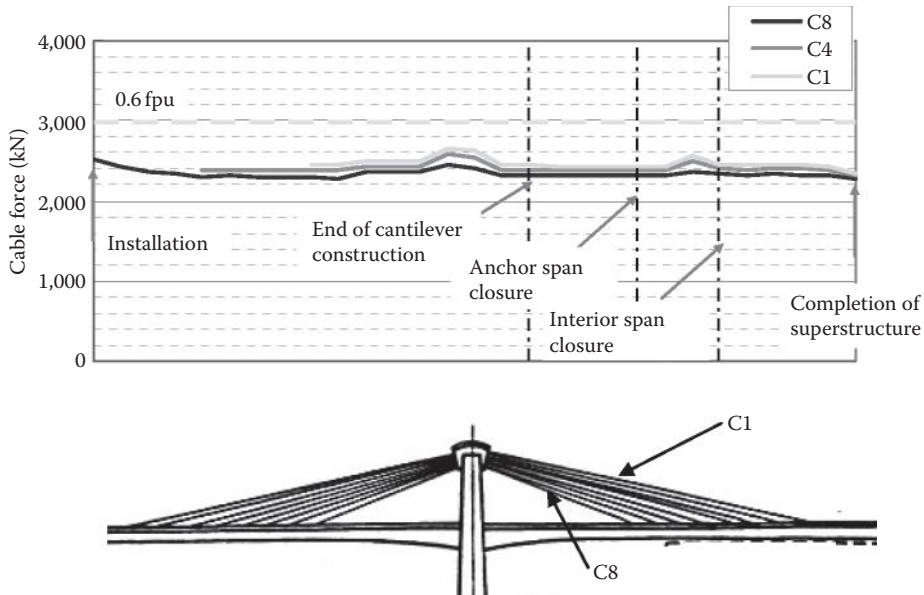


FIGURE 11.29 Extradosed cable force history during construction (Odawara Blueway Bridge).

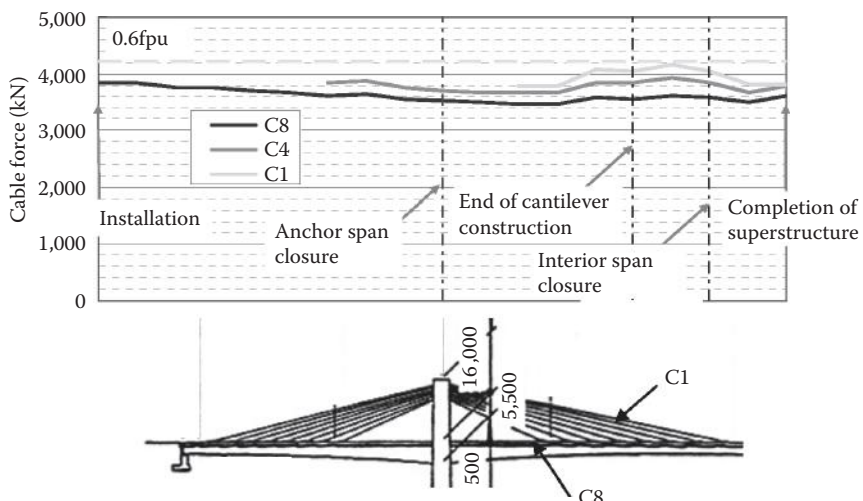


FIGURE 11.30 Extradosed cable force history during construction (Tsukuhara Bridge).

11.6 Summary

The significance of partially prestressed concrete was that it successfully combined prestressed concrete and reinforced concrete into a single concept. A similar success has been achieved with the development of extradosed bridge technology, which is significant because it enables engineers to apply design principles already established for cable-stayed bridges and ordinary girder bridges. The extradosed bridge is a revolutionary high-performance structural system that greatly increases the degree of freedom for the design of cable-stayed and cable-supported structures. Building on J. Mathivat's ideas and the achievement of the Odawara Blueway Bridge, extradosed bridges have written a major new page in the history of bridge engineering. The Appendix lists the design data of Japanese extradosed bridges and the 21 longest spans for extradosed bridges in the world.

References

- BD&E. 2008. "Korea's Newest City to Have Two Dramatic Bridges," *Bridge Design & Engineering*, 2nd Quarter, 14(51), 35.
- Calafat-Vidin Bridge. 2013. Available at <http://en.structurae.de/structures/data/index.cfm?id=s0004900>.
- Fujita, M., Umezawa, K., Arai, H., and Ueda, T. 1999. "Fretting Fatigue Characteristics in the Curved Layout of Large-capacity Prestressing Strands," *15th U.S.-Japan Bridge Engineering Workshop*, Tsukuba, Japan.
- Golden Ears Bridge. 2013. Available at http://en.wikipedia.org/wiki/Golden_Ears_Bridge.
- Hino, S. 2005. "The Great Himiyume Bridge, Highway Entrance to Nagasaki, The World First Extradosed Bridge Using Corrugated Steel Plate Webs," Available at www.jsce.or.jp/kokusai/civil_engineering/2005/4-2.pdf.
- Hirano, M., Ikeda, H., Kasuga, A., and Komatsu, H. 1999. "Composite Extradosed Bridge," *FIB Symposium*, Prague, Czech, pp. 661–666.
- Iida, J., Nakayama, H., Wakasa, T. et al. 2002. "Design and Construction of Shinmeisei Bridge," *FIB Congress*, Osaka, Japan, pp. 557–562.
- Ikeda, S. and Kasuga, A. 2000. "Development of Extradosed Structures in the Bridge Construction," *25th Conference on Our World In Concrete & Structures*, August, 23–24. Singapore. Available at <http://cipremier.com/100025008>.
- JPCEA. 2000. *Specifications for Design and Construction of Prestressed Concrete Cable-Stayed Bridges and Extra dosed Bridges*. Japan Prestressed Concrete Engineering Association, Tokyo, Japan, November 2000 (in Japanese).
- Kasuga, A. 2006. "Extradosed Bridges in Japan," *Structural Concrete*, 7(3), 91–103.
- Kasuga, A., Kimizu, T., and Matsui, Y. 1995. "Testing of High Damping Rubber Damper for Stay Cables," *Building for the 21st Century EASEC-5*, Gold Coast, Australia, pp. 243–246.
- Kasuga, A., Shirano, Y., Nishibe, G., and Okamoto, H. 1994. "Design and Construction of the Odawara Port Bridge—The First Extradosed Prestressed Bridge," *FIP International Congress*, Washington D.C., pp. F56–F62.
- Keong-An Bridge. 2013. Available at <http://en.structurae.de/structures/data/index.cfm?id=s0002145>.
- Kiso River Bridge. 2013. Available at <http://en.structurae.de/structures/data/index.cfm?id=s0000844>.
- Koror Babeldaob Bridge. 2013. Available at http://en.wikipedia.org/wiki/Koror%2680%93_Babeldaob_Bridge.
- Maeda, Y., Imaizumi, Y., Kasuga, A., and Tazoe, K. 2002. "Design and Construction of the Himi Bridge—Extradosed Bridge with Corrugated Steel Web," *FIB Congress*, Osaka, Japan, pp. 95–100.
- Mathivat, J. 1988. "Recent Development in Prestressed Concrete Bridges," *FIP Notes*, pp. 15–21.
- Ningjiang Songhua River Bridge. 2013. Available at http://www.jljt.gov.cn/bdzz/yb_1/wz/201108/t20110819_35602.html (In Chinese).
- North Arm Bridge. 2013. Available at http://en.wikipedia.org/wiki/North_Arm_Bridge.
- Ogawa, A. and Kasuga, A. 1998. "Extradosed Bridges in Japan," *FIP Notes*, pp. 11–15.
- Ogawa, A., Matsuda, T. and Kasuga, A. 1998. "The Tsukuhara Extradosed Bridge near Kobe," *Structural Engineering International*, 8(3), 172–173.
- Qiancao Bridge. 2013. Available at <http://baike.baidu.com/view/1933073.htm> (in Chinese), also http://highestbridges.com/wiki/index.php?title=2012_High_Bridge_Trip_Photo_Album.
- Qin, Q., Mei, G. and Xu G. 2014. "Chapter 20, Bridge Engineering in China," *Handbook of International Bridge Engineering*, Ed, Chen, W.F. and Duan, L. CRC Press, Boca Raton, FL. Available at http://en.wikipedia.org/wiki/Wuhu_Yangtze_River_Bridge
- Sannai-Maruyama Bridge. 2013. Available at <http://www.jsce.or.jp/committee/concrete/e/newsletter/newsletter19/award.html>.
- Sannohe-Boukyo Bridge. 2013. Available at <http://en.structurae.de/structures/data/index.cfm?id=s0034430>.

- Second Mactan-Mandaue Bridge. 2013. Available at <http://en.structurae.de/structures/data/index.cfm?id=s0005543>.
- SETRA. 2002. Cable Stays—*Recommendations of French Interministerial Commission on Prestressing*, SETRA, Bagneux Cedex, France, June.
- Shah Amanat Bridge. 2013 Available at http://en.wikipedia.org/wiki/Shah_Amanat_Bridge.
- Tang M.C. 2011. “Poised For Growth,” HYPERLINK “<http://cedb.asce.org/cgi/www.display.cgi?168625>” *Civil Engineering*, ASCE, 81(9), 64-67, 73.
- Tokunoyama Hattoku Bridge. 2013. Available at http://www.highestbridges.com/wiki/index.php?title=Tokunoyamahattoku_Bridge.

Appendix

TABLE II A.1 Design Data of Japanese Extradosed Bridges

No.	Bridge Name	Completion	Bridge Length (m)	Span Length (m)	Total Width (m)	Effective Width	Width (m)	Girder Support on Pier			Girder Section of Girder			Girder Height (m)			Tower Height from Ground (m)	Shape Nos. of Plane	Cable Interval (m)	Extradosed Cable Arrangement		Safety Factor of Extradosed Cables		Stress Change in Extradosed Cable (%)
								At Pier	Mid. Span	At Pier	Cross Section of Girder	At Pier	Mid. Span	At Pier	Mid. Span	At Pier	Mid. Span	Under Design	Under Construction	Under Load	During Earthquake Level 1	During Earthquake Level 2		
1	Odawara Blueway Bridge	1994	270.0	73.3+122.3+	130.0	9.5	Rigid	2 Cells	3.5	2.2	10.7	37.2	Fan 2 plane	3.75	1.67	1.67	1.67	38	38	19.0				
2	Tsukuhara Bridge	1998	323.0	65.4+180.0+	128.0	9.25	Rigid	1 Cell	5.5	3.0	16.0	57.0	Fan 2 plane	7.0	1.67	1.67	1.67	37	37	22.0				
3	Shoyo Bridge (Kanisawa Bridge)	1998	380.0	99.3+180.0+	175.0	99.3	Bearing	2 Cells	5.6	3.3	22.1	43.2	Fan 2 plane	4.0	2.50	1.67	1.67	71	71	61.0				
4	Karato Bridge (west)	1998	285.0	74.1+140.0+	115.0	8.7	Rigid	2 Cells	3.5	2.5	12.0	31.4	Fan 2 plane	4.0	1.67	1.67	1.67	88	88	37.0				
5	Karato Bridge (East)	1998	260.0	66.1+120.0+	115.0	72.1	Rigid	2 Cells	3.5	2.5	12.0	43.5	Fan 2 plane	4.0	1.67	1.67	1.67	75	75					
6	The Second Mactan Bridge	1999	410.0	111.5+	210.0	18.0	Rigid	3 Cells	5.1	3.3	18.2	42.6	Fan 2 plane	5.0	1.67	1.67	1.67	1.67	1.67					
7	Mactanica Bridge	2000	200.0	109.3+89.3	113.0	8.0	Rigid	2 Cells	6.0	3.5	26.4	59.4	Fan 2 plane	4.0	1.67	1.67	1.67	1.67	1.67	16.0				
8	Ashikita Bridge	2000	225.0	60.8+105.0+	110.0	57.5	Bearing	2 Cells	3.2	2.1	12.3	25.0	Fan 2 plane	3.75	2.50	2.50	2.50	2.50	2.50	38.97				
9	Yukisawa Third Bridge	2000	177.1	70.3+71.0+	158.0	34.4	Bearing	2 Cells	3.5	2.0	11.3	20.3	Fan 2 plane	4.0	1.67	1.67	1.67	1.19	1.19	44				
10	Suriage Dam Bridge	2000	110.0	84.2	9.2	7.0	Rigid	1 Cell	5.0	2.8	16.5	16.5	Fan 2 plane	4.0	1.67	1.67	1.67	1.11	1.11	23				
11	Pakse Bridge	2000	1380.0	70+102×9 +123+143+ 915+34.5	146.0	13.8	Rigid	1 Cell	6.5	3.0	15.0	27.6, 26.4	Fan 2 plane	3.5	1.67	1.67	1.67	1.67	1.67					
12	Shikari Bridge	2001	610.0	94.0+140.0×	23.0	39.40	Bearing	3 Cells	6.0	3.0	10.0	32.7	Harp 1 plane	3.5	1.67	1.67	1.67	1.43	1.43	3.0				
13	Nakanoiike Bridge	2001	123.0	60.6+60.6	21.4	17.4	Rigid	3 Cells	4.0	2.5	11.8	11.0	Fan 1 plane	7.0	1.67	1.67	1.67	1.19	1.19	27				

(Continued)

TABLE 11A.1 (Continued) Design Data of Japanese Extradosed Bridges

No.	Bridge Name	Completion	Bridge Length (m)	Span Length (m)	Total Width	Effective Width	Girder Support on Pier	Cross Section of Girder	Girder Height (m)	Tower Height From Ground (m)			Extradosed Cable Arrangement			Safety Factor of Extradosed Cables				
										Mid	Span	At Pier	Shape Nos. of Plane	Cable Interval (m)	Under Design Load	Under Construction	During Earthquake Level 1	During Earthquake Level 2		
14	Miyakoda River Bridge	2001	268.0	133.0 + 133.0	19.91	16.5	Rigid	2 Cells	6.5	4.0	20.0	83.0	Fan 2 plane	6.0	1.67	1.42	1.33	1.25	31	15.5
15	Houz Bridge	2001	368.0	33+50+76 +100+76+	15.3	14.5	Rigid	1 Cell	2.8	2.8	10.0	31.5	Fan 2 plane	3.5	1.67	1.67	1.67	1.67	15.0	
16	Kiso River Bridge	2001	1145.0	160+275× 3+160	33.0	290	Bearing	3 Cells	7.3	4.3	30.0	54.3	Fan 1 plane	5.0	1.67	1.67	1.00	26-109	31.7	
17	Ibi River Bridge	2001	1397.0	154+271.5× 4+157	33.0	29.0	Bearing	3 Cells	7.3	4.3	30.0	54.8	Fan 1 plane	5.0	1.67	1.67	1.00	112	52.0	
18	Japan Palau Friendship Bridge in Republic of Palau	2001	412.7	82+247+82	11.6	8.0	Rigid	1 Cell	7.0	3.5	27.0	6.7	Fan 2 plane	40, 4.5	2.22	1.67	2.22	22.0		
19	Hukaura Bridge	2002	294.0	62.1+90.0+ 66.4+45.0+ 29.1	13.7	10.8	Rigid	3 Cells	3.0	2.5	8.5	40.5	Fan 2 plane	4.0	1.67	1.67	1.67	7.0		
20	Gotoh River Bridge (Sashikubo Bridge)	2002	230.3	114.0+114.0	11.33	8.0	Rigid	1 Cell	6.5	3.2	22.0	73.0	Fan 2 plane	7.0	1.67	1.67	1.67	28	10.6	
21	Tobhuo Bridge	2002	386.0	38.5+45.0+ 90.0+130.0+ 80.5	25.8	20.5	Bearing	3 Cells	4.0	2.4	13.0	29.0	Fan 1 plane	3.5	1.67	1.67	1.67	35.1		
22	Akabono Bridge (Shinnensei Bridge)	2004	294.32	88.340+ 122.340+ 81.220	19-23	16-20	Rigid	3 Cells	3.5	3.5	16.5	23.8	Fan 1 plane	3.6	1.67	1.67	1.00	24.0	21.0	
23	Himi Bridge	2004	365.0	91.75+ 180.0+91.75	12.95	9.75	Rigid	1 Cell	4.0	4.0	19.8	42.475	Fan 2 plane	6.4	1.67	1.67	1.67	26.0		
24	Sannohe Bohkyo Bridge	2005	400.0	99.25+ 200.0+99.25	13.45	10.25	Rigid	2 Cells	6.5	3.5	25.0	66.0	Fan 2 plane	3.75	1.67	1.67	1.67	25.3		
25	Noikura Bridge	2005	273.0	62.2+135.0+ 74.2	10-12.4	9.0	Rigid	1 Cell	4.5	2.5	11.1	340, 36.0	Fan 2 plane	3.75	1.67	1.67	1.18	32.3	19.2	
26	Nanchiku Bridge	2006	248.0	68.05+ 110.0+68.05	20.55	19.75	Bearing	3 Cells	3.5	2.6	11.0	17.2	Fan 2 plane	12.75	2.50	2.50	1.19	29.2		

27	Satonojo Bridge	2006	186.0	54.9+77.0+	11.75-14.75	10.75-13.75	Rigid	1 Cell	3.5	2.5	8.0	23.8	Fan 2 plane	12.15	1.67	1.67	1.67	16.0
28	Asagiri Bridge	2006	166.0	80.200+	17.8	15.0	Rigid	2 Cells	4.5	3.0	14.5	16.5	Fan 2 plane	4.0	1.67	1.67	1.67	6.2
29	Tokunoyama Hattoku Bridge	2006	503.0	139.7+	8.2	7.0	Rigid	1 Cell	6.5	3.5	22.5	101.0	Fan 2 plane	7.0	1.67	1.67	1.67	25.7
30	Ohmi-Otori Bridge (Kitto Bridge)	2007	495.0	137.6+	19.63	16.5	Rigid	3 Cells	7.5	4.5	30.5	65.0	Fan 2 plane	4.8	1.667	1.67	1.67	1.000
31	Ohmi-Otori Bridge (Kitto Bridge)	2007	505.0	152.6+160+	19.63	16.5	Rigid	3 Cells	7.5	4.5	30.5	61.5	Fan 2 plane	4.8	1.667	1.67	1.67	1.000
32	Yanagawa Dam 9th Bridge	2007	264.0	130.7+130.7	17.4	15.0	Rigid	2 Cells	6.5	4.0	24.6	57.0	Fan 2 plane	3.0	1.67	1.67	1.67	1.19
33	Hedase Bridge	2008	285.0	69.15+145+	12.4	9.0	Bearing	1 Cell	5.5	3.0	14.181	48.0	Fan 2 plane	4.0	1.67	1.67	1.67	1.18
34	Rades La Goulette Bridge	2009	260.0	70.0+120.0+	23.5	18.0	Rigid	3 Cells	3.7	2.6	20.0	20.9	Fan 1 plane	3.5	1.67	1.67	1.67	44
35	Yunekake Bridge (Route 1681- 1 Bridge)	2010	290.0	42.25+	14.2	10.51	Rigid	1 Cell	4.8	2.8	25.0	50.5	Fan 2 plane	6.0	1.67	1.67	1.67	1.19
36	Shin Yokoyama Bridge	2010	232.6	88.2+142.0	11.5-12.2	8-11	Rigid	1 Cell	8.0	4.0	40.0	95.0	Fan 2 plane	40.8, 8.0	1.67	1.67	1.18	30.5
1	Yashironimami Bridge	1995	340.0	64.2+105.0×	12.8	-	Rigid	3 Cells	2.5	2.5	12.0	28.8	Fan 2 plane	4.0	2.50	1.67	1.43	48
2	Yashinokita Bridge	1995	200.0	54.3+90.0+	12.8	-	Rigid	3 Cells	2.5	2.5	10.0	30.6	Fan 2 plane	4.0	2.50	1.67	1.43	24
3	Shinkawa Bridge	1999	111.0	51.4+58.4	13.2	-	Bearing	U shape	2.6	2.6	9.9	15.1	Fan 2 plane	4.0	2.50	1.43	2.50	1.00
4	Sakai River Bridge	2003	182.9	55.3+70.0+	12.5	9.3	Bearing	U shape	3.5	3.15	9.3	19.85	Fan 2 plane	4.5	2.50	2.50	2.50	48
5	Arako River Bridge	2004	245.9	54.42+90+	12.7	9.1	Rigid	U shape	3.6	2.6	12.6	6.3	Fan 2 plane	4.0	1.43	2.50	1.43	42-83
6	Sannaimatuyama Over Bridge	2008	450.0	74.18+	13.85	-	Rigid, bearing	2 Cells	8.0	3.8	17.5	15.0	Fan 2 plane	4.0	2.50	1.43	2.50	1.19
7	Ono River Bridge	2009	286.0	29+113+	11.3-12.4	9.9-11	Rigid	2 Cells	6.0	3.5	15.0	9.0	Fan 2 plane	7.0	1.60	1.60	1.60	45

TABLE 11A.2 List of 21 Longest Spans for Extradosed Bridges in the World

No.	Name	Main Span Length m (ft)	Structure Features	Total Length m (ft)	Opened Year	Usage	Country	References
1	Wuhu Yangtze River Bridge	312 (1,023.6)	Double decks	10,521(34,517.7)	2000	Hwy/Rail	China	Qin et al (2014)
2	Kiso River Bridge	275 (902.2)		1,145 (3,756.6)	2001	Hwy	Japan	Kiso River Bridge (2013)
3	Ibi River Bridge	271.5 (890.7)		1,397 (4,583.3)	2001	Hwy	Japan	Figure 11.5
4	Keong-An Bridge	270 (885.8)		778 (2,552.5)	2009	Hwy	Korea	Keong-An Bridge (2013)
5	Jiayue Bridge	250 (820.2)		1,190 (3,904.2)	2010	Hwy	China	Tang (2011)
6	Qiancaao Bridge	248 (813.7)		413 (1,35.05)	2011	Hwy	China	Qiancaao Bridge (2013)
7	Korror Babedao Bridge	247 (810.4)		2410 (7,906.9)	2009	Hwy	Palau	Korror Babedao Bridge (2013)
8	Golden Ears Bridge	242 (794.0)		526.6 (1,727.8)	2006	Hwy	Canada	Golden Ears Bridge (2013)
9	Tokunoyama Hattoku Bridge	220 (721.8)	146 m high	950 (3,116.8)	2010	Hwy	Japan	Tokunoyama Hattoku Bridge (2013)
10	Shah Amanat Bridge	200 (656.2)		400 (1,312.3)	2005	Hwy	Bangladesh	Shah Amanat Bridge (2013)
11	Sannohe-Boukyo Bridge	200 (656.2)		1010 (3,313.6)	1999	Hwy	Japan	Sannohe-Boukyo Bridge (2013)
12	Second Mactan-Mandaue Bridge	185 (607.0)		735 (2,411.4)	2012	Hwy	Philippines	Second Mactan-Mandaue Bridge (2013)
13	Gumgang No.1 Bridge	185 (607.0)		323 (1,059.7)	1997	Hwy	Korea	BD&E (2008)
14	Tsukuhara Bridge	180 (590.6)	Single-cell PS box girder	380.1 (1,247)	1998	Hwy	Japan	Ogawa et al. (1998)
15	Shoyo (Kanisawa) Bridge	180 (590.7)	Corrugated steel plate webs	365 (1,197.5)	2004	Hwy	Japan	Ikeda and Kasuga (2000)
16	Himi Yume Bridge	180 (590.6)		562 (1,843.8)	2009	Rail	Japan	Hino (2005)
17	North Arm Bridge	180 (590.6)		3,598 (11,804.5)	2013	Hwy/Rail	Canada	North Arm Bridge (2013)
18	Calafat–Vidin Bridge	180 (590.6)	Corrugated steel plate webs	490.2 (1,608.3)	2007	Hwy	Romania and Bulgaria	Calafat–Vidin Bridge (2013)
19	Ohmi Ohtori (Rittoh) Bridge	170 (557.7)		450 (1,476.4)	2008	HSR	Japan	Appendix-Design Data of Japanese Extradosed Bridges
20	Sannai-Maruyama Bridge	150 (492.1)	Concrete box girder	2,236 (7,336.0)	2013	Hwy	Japan	Sannai-Maruyama Bridge (2013)
21	Ningjiang Songhua River Bridge	150 (492.1)					China	Ningjiang Songhua River Bridge (2013)

12

Stress Ribbon Pedestrian Bridges

12.1	Introduction	463
12.2	Structural Arrangement.....	466
	Stress Ribbon • Structural Arrangement of the Deck • Structural Arrangement at Piers and Abutments • Transferring Stress Ribbon Force into the Soil	
12.3	Erection	477
	Construction Sequences A • Construction Sequences B	
12.4	Static and Dynamic Analysis.....	479
	Single Cable • Analysis of Stress Ribbon as a Cable • Analysis of the Stress Ribbon as a Geometrically Non-Linear Structure • Dynamic Analysis • Designing of Structural Members • Example of the Analysis	
12.5	Stress Ribbon Supported by Arch	495
12.6	Examples	498
	DS-L Bridges: Bridge across the Vltava River in Prague-Troja, Czech Republic • Sacramento River Trail Bridge, Redding, California • Lake Hodges Bridge, San Diego, California • Bridge across the Medway River, Maidstone, Kent, UK • Kikko Bridge, Japan • Bridge across the Expressway R35 near Olomouc, Czech Republic • McLoughlin Boulevard Bridge, Portland, Oregon	
	References.....	514

Jiri Strasky
Strasky, Hustý and
Partners, Ltd.

12.1 Introduction

“What would be the best bridge? Well, the one which could be reduced to a thread, a line, without anything left over; which fulfilled strictly its function of uniting two separated distances.”

Pablo Picasso

Stress-ribbon bridge is the term that has been coined to describe structures formed by directly walked prestressed concrete deck with the shape of a catenary. The conception was first introduced by Ulrich Finsterwalder, who repeatedly proposed such a structure for bridging large spans (Walther 1969; Strasky 2011). Among the bridges suggested they were those over Bosphorus (see Figure 12.1), Lake Geneva and Zoo in Köln.

The load-carrying structure consists of slightly sagging tensioned cables, bedded in a very thin concrete slab compared with the span length. This slab serves as a deck, but apart from distributing the load locally and preserving the continuity it has no other function. It is a kind of suspension structure where the cables are tended so tightly that the traffic can be placed directly on the concrete slab embedding the

cables. Compared with other structural types its load path is extremely simple. On the other hand, the force in the cables is very large making the anchoring of the cable very expensive.

The stress ribbon structures combine a structural form of primitive bridges formed by ropes from liana or bamboo with the structural arrangement of prestressed suspended roofs. The characteristic feature of the stress ribbon structures is a variable slope that disqualifies using of this structural type for highway bridges. It is difficult to imagine that the structure presented in Figure 12.1 would be acceptable for highway agencies. A stress ribbon structure might represent a right solution only in special cases when the highway is straight and the profile is a concave (sag) curve. On the other hand, the variable slope is acceptable or even advantageous for pedestrian bridges built in a countryside where there is no straight line.

The first stress ribbon bridge built for the public was designed by Prof. Walther across the freeway N3 near Pfäfikon, Switzerland in 1965 (Walther 1969). From that time the stress ribbon bridges were built in many countries all over the world. In the United States the first stress ribbon bridge of span of 127 m (417 ft.) was built in 1990 across the Sacramento River in Redding, CA (Redfield and Strasky 1992) (see Figure 12.2).

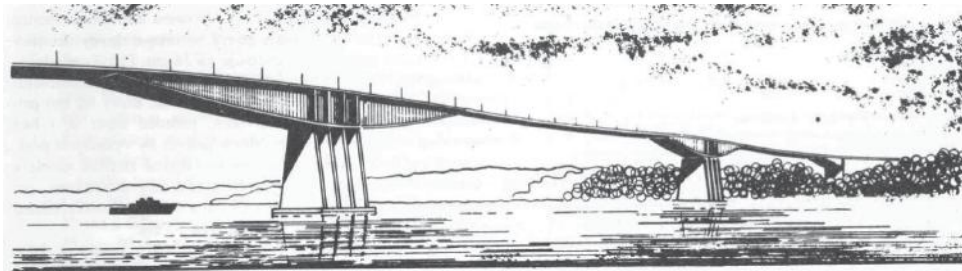


FIGURE 12.1 Bosporus Bridge—U. Finsterwalder 1958.

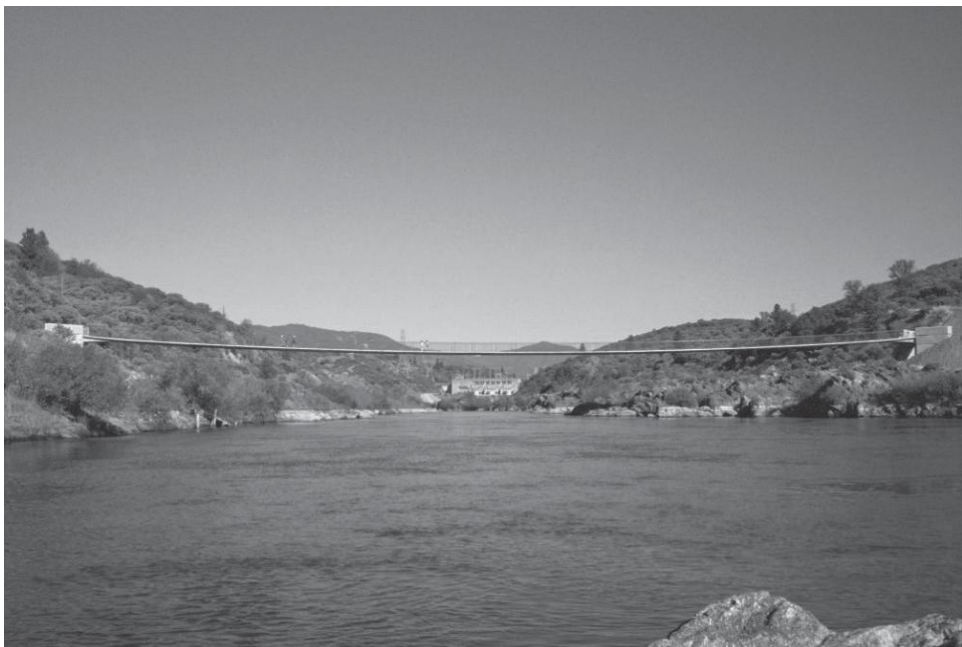


FIGURE 12.2 Bridge across the Sacramento River in Redding, CA.

The stress ribbon structures can be designed with one or more spans and are characterized by successive and complementary smooth curves. The curves blend into the surrounding environment and their forms, the most simple and basic of structural solutions, clearly articulate the flow of internal forces. Their fine dimensions also correspond to a human scale.

It is evident that the stress ribbon structure represents the simplest structural form. Both engineering and aesthetic beauty of this bridge type lies in the fact that the suspended walkway itself is the structure. It carries itself without the need for any arms, props, masts, cables, dampers, and so on. Its stiffness and stability result from its geometry.

Such structures can be either cast in-situ or formed of precast units. In the case of precast structures, the deck is assembled from precast segments that are suspended on bearing cables and shifted along them to their final position (see Figure 12.3). Prestressing is applied after casting the joints between the segments to ensure sufficient rigidity of the structures.

The main advantage of these structures is that they have minimal environmental impact because they use very little material and can be erected independently from the existing terrain. Since they do not need bearings or expansion joints they need only minimal long-term maintenance.

They are able to resist not only uniformly distributed load but also large concentrated loads created by the wheels of heavy trucks (Strasky 1987a) (see Figure 12.4). Extremely large floods that occurred in the Czech Republic in summer 1997 and 2002 also confirmed that they are able to resist a large ultimate load. Although the bridge was totally flooded, their static function remains without any changes.

Even though the stress ribbon structures have low natural frequencies, our experience confirmed that the speed of motion of the deck created by walking is within acceptable limits. Also our detailed dynamic test confirmed that vandals cannot damage these structures.

Although the above structures have a very simple shape, their design is not straightforward. It requires a deep understanding of structural forms, function of structural details and behavior of prestressed concrete structures post-tensioned by internal and/or external tendons. Also the static and dynamic analysis requires understanding of the function of cables and resolves various problems in regard to both geometric and material non-linearity.

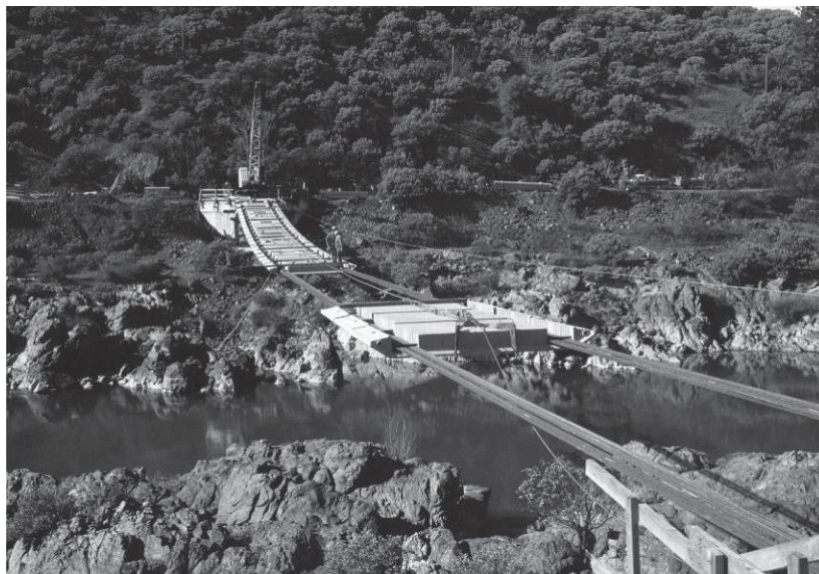


FIGURE 12.3 Erection of the bridge across the Sacramento River in Redding, CA.



FIGURE 12.4 Loading test of the bridge across the Vltava River in Prague-Troja, Czech Republic.

12.2 Structural Arrangement

12.2.1 Stress Ribbon

The beauty of the suspension and arch structures comes from their economic structural shape. It is well known that a suspension cable can span several miles. However, its shape has to be funicular to the given load and the structures need to have an economic rise or sag.

The layout of pedestrian bridges is influenced by two requirements. In cable supported structures where the deck follows the shape of the cables only limited slope with corresponding sag can be accepted. Furthermore, these bridges need to have sufficient stiffness that guarantees comfortable walking and stability of the shape (see Figure 12.5). It is therefore necessary to stiffen them.

The deformation of the suspension structures (see Figure 12.6a) can be reduced by stiffening the cables using dead load (see Figure 12.6b), external cables (see Figure 12.6c) or by creating a prestressed concrete band with a certain amount of bending stiffness to guarantee the distribution of local loads and the stability of the overall shape (see Figure 12.6d.).

The importance of the stiffening of directly walked suspension structures shown in Figure 12.6 is evident from Figure 12.7 in which four stress ribbon structures are compared. The bridge has a span of 99 m (325 ft.) with a maximum dead load slope of 8%, which yields maximum sag at mid-span of 1.98 m (6.50 ft.). The bridge may be formed by following five cases:

1. Timber boards are placed on two cables with a total area of $A_s = 0.0168 \text{ m}^2$ (26 in.²). The dead load $g = 5 \text{ kN/m}$ (0.343 kip/ft.) and the horizontal force $H_g = 3094 \text{ kN}$ (696 kip).
2. Concrete panels of 125 mm (5 in.) thickness are supported by two cables with a total area of $A_s = 0.0252 \text{ m}^2$ (39 in.²).
3. A concrete band of 125 mm (5 in.) thickness is supported by two cables with a total area of $A_s = 0.0252 \text{ m}^2$ (39 in.²). The cables are embedded in the band that is fully prestressed and therefore uncracked.
4. A concrete band of 125 mm (5 in.) thickness is supported by two cables with a total area of $A_s = 0.0252 \text{ m}^2$ (39 in.²). The cables are embedded in the band that is partially prestressed and therefore cracks can form in the concrete. It is assumed that the crack spacing is 125 mm (5 in.) and that the concrete between cracks resists resistance of the tension. The area of concrete that resists the tension is taken as shown in Figure 12.7b-4.

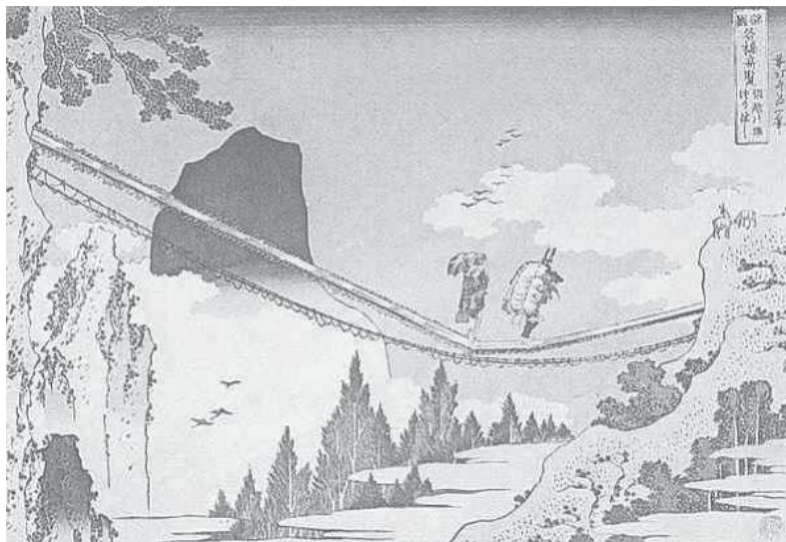


FIGURE 12.5 Hukusai Bridge, Japan.

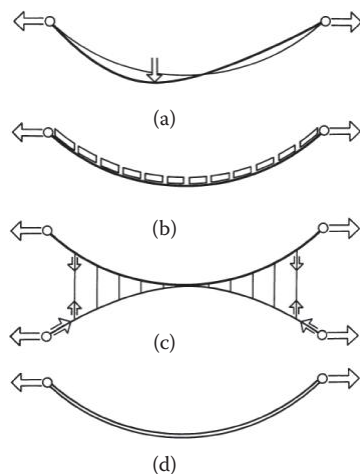


FIGURE 12.6 Cable stiffening.

5. A concrete band of 250 mm (10 in.) thickness is supported by two cables with a total area of $A_s = 0.0392 \text{ m}^2$ (67.6 in.²). The cables are embedded in the band that is fully prestressed and therefore uncracked.

Structures 2–4 are stressed by a dead load $g = 17 \text{ kN/m}$ (1.165 kip/ft.) with corresponding horizontal force $H_g = 10,519 \text{ kN}$ (2,365 kip). Structure 5 is stressed by a dead load $g = 33.345 \text{ kN/m}$ (2.286 kip/ft.) with corresponding horizontal force $H_g = 20,635 \text{ kN}$ (4,639 kip). The contribution of the prestressing tendons and reinforcing steel to the tension stiffness of the band is neglected in structures 3–5.

The $A_e = A_s + \frac{E_c}{E_s} A_c = A_s + \frac{36}{195} A_c$. above structures were analyzed for the effects of the dead load g and live load $p = 20 \text{ kN/m}$ (1.371 kip/ft.) placed on one half of the structure. The analysis was performed for the structure modeled as a cable of effective tension stiffness $E_s A_e$ and zero bending stiffness. The effective stiffness $E_s A_e$ was determined from the modulus of elasticity of the cable $E_s = 195,000 \text{ MPa}$ (28,000 ksi) and an effective area A_e that depends on the area of the cable A_s and concrete band A_c (or $A_{c,cr}$, respectively) as well as the ratio of the modulus of elasticity of steel E_s and concrete E_c .

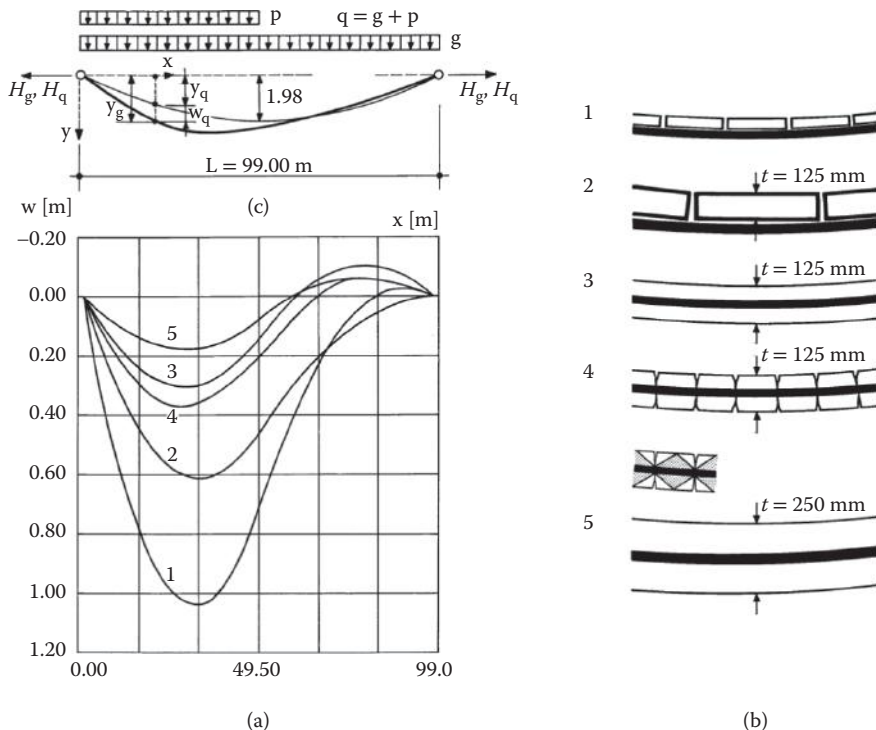


FIGURE 12.7 Stiffness of the stress ribbon structure: (a) load and deformation and (b) different types of stress ribbons structures.

Resulting deformations presented in Figure 12.7 shows that the fully prestressed band of thickness of 250 mm (10 in.) has the smallest deformations. Also fully and partially prestressed structures 3 and 4 of thickness of 125 mm (5 in.) have reasonable deformations. Although the deformations of structures 1 and 2 could be reduced by substituting the cables with strips of structural steel that have lower allowable stresses and therefore requires a larger cross section, the deformations are still significant.

It is evident that the prestressed concrete deck (fully or partially prestressed) has a superior behavior. The monolithic concrete deck gives the structure not only sufficient tension stiffness but its membrane stiffness also guarantees the transverse stiffness of the bridge. These structures are further called *stress ribbon* structures.

Stiffening of the suspension structures by tension cables of the opposite curvature (see Figure 12.6c) has similar effects to the stiffening of the structure dead load (see Figure 12.6b). However, this arrangement requires complicated connections of the cables and good maintenance.

12.2.2 Structural Arrangement of the Deck

Since the stress ribbon bridges with prestressed concrete deck have superior behavior they will be further discussed in a greater detail.

The deck of a stress ribbon structure can be formed by a monolithic band or can be assembled of precast segments. The band is fixed to the abutments and is supported by intermediate piers. Due to limits on the maximum slope, the ribbon is stressed by a large horizontal force that has to be transferred into the soil.

Only in special cases the deck is cast in formwork supported by a false work. Usually, the stress ribbon structures are erected independently from the existing terrain. The formwork of precast segments is suspended on bearing tendons and shifted along them into their design position (see Figure 1.3).

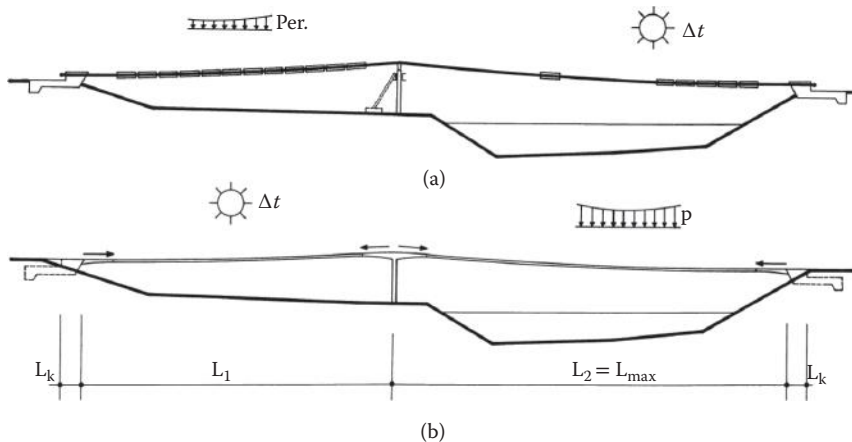


FIGURE 12.8 Static function: (a) erection and (b) service.

Prestressing applied after the casting of the whole band, or the joints between the segments, guarantees the structural integrity of the complete deck.

The structural arrangement of the stress ribbon bridges is determined by their static function and by their process of construction. During the erection the structure acts as a perfectly flexible cable (see Figure 12.8a), during service as a prestressed band (stress ribbon) that is stressed not only by normal forces but also by bending moments (see Figure 12.8b). However, the shape and the stresses in the structure at the end of the erection determine the magnitude of the stresses that will occur in the structure during the service.

Although a prestressed band can resist very heavy loads it can be very slender (see Figure 12.4). In order to understand the behavior of the stress ribbon structures, the bending moments in the deck due to prestressing, live load, and temperature changes are shown in Figure 12.9. The structure has a span of 99 m (325 ft.); its sag is 1.98 m (6.50 ft.). The deck is the same as the deck of the structure studied in Figure 12.7(5). The concrete band of modulus of elasticity of $E_c = 36,000 \text{ MPa}$ (522 ksi) had section properties taken from a basic rectangular section of a width of 5.00 m (16.4 ft.) and a depth of 0.25 m (0.82 ft.).

The deck was suspended on bearing tendons of area $A_{s,bt} = 0.0196 \text{ m}^2$ and post-tensioning was applied with tendons of area $A_{s,pt} = 0.0196 \text{ m}^2$.

The horizontal force H_g due to the dead load $g = 33.345 \text{ kN/m}$ (2.286 kip/ft.) is 17.30 MN (3889 kip). The structure was loaded by dead load (1), temperature changes $\Delta t = \pm 20^\circ\text{C}$ (2) and (3), live load $p = 20 \text{ kN/m}$ (1.371 kip/ft.) on the whole (4) and half (5) of the span and by a point load $F = 100 \text{ kN}$ (22.5 kip) at mid-span (6). The structure was analyzed as a geometrically non-linear structure of the program system ANSYS without and with post-tensioning of the deck with a prestressing force $P = 25.52 \text{ MN}$ (5737 kip).

Figure 12.9a shows the position of the loadings, deformations and bending moments for the non-prestressed deck; Figure 12.9b for the prestressed deck.

From the presented results it is evident that significant bending moments originate only at the supports. The bending moments due to the concentrate load representing a typical maintenance car are relatively very low. Since the deck is always post-tensioned, the negative bending moments at the supports are very low. However, positive bending moments are very large and have a significant influence on the detailing of the stress-ribbon structure at the supports.

Since along the whole length of the structure the deck is stressed only by normal forces, the deck can be formed by a very slender solid section that can be further reduced by *waffles* that create a coffered soffit. The minimum area of the deck is determined from the requirements that under the various loading condition (including prestress) there are limited or zero tension stresses in the deck, and that maximum compressive stresses are not exceeded. Since the bending moments due to the point load are low, the

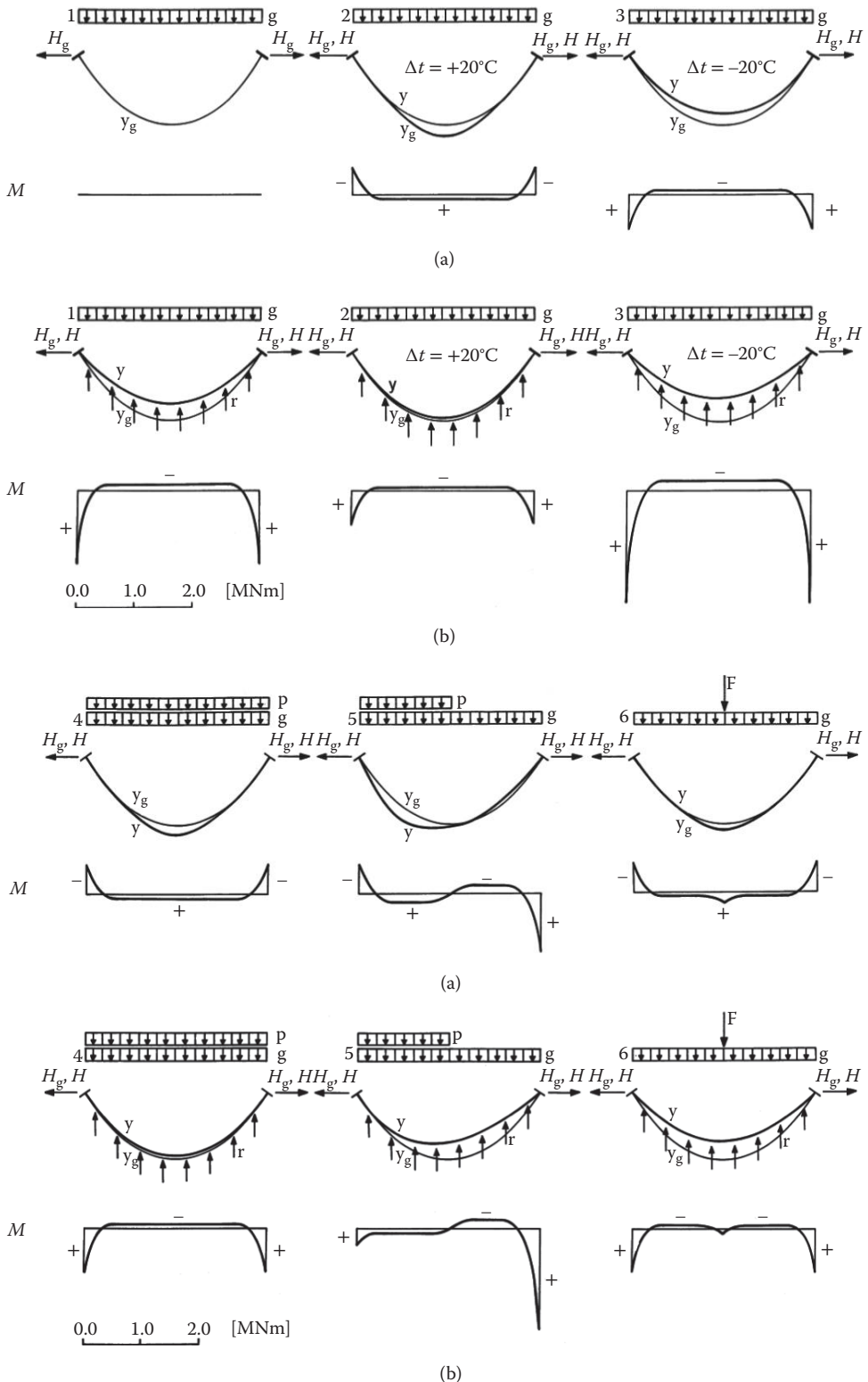


FIGURE 12.9 Deformation and bending moments. (a) Without prestressing. (b) With prestressing.

depth of the deck is essentially determined by the cover requirements of the prestressing steel. Usually the minimum depth guarantees a sufficient stiffness of the deck.

The deck of stress ribbon structures can be cast in a form that is suspended on the bearing cables (see Figure 12.10a) or be assembled of precast segments. Usually the deck is suspended from bearing tendons and is prestressed by prestressing tendons. However, the function of bearing and prestressing tendons can be combined as well. Initially, the segments can be hung from bearing tendons situated in troughs, and after erection the deck is post-tensioned by the second group of cables situated either in the ducts within the segments (Figure 12.10b) or in the troughs (see Figure 12.10c). The bearing tendons are then protected by a cast-in-place concrete poured simultaneously with the joints between the segments. Since longitudinal shrinkage cracks are likely to occur between the cast-in-place and precast concrete, it is recommended to protect the surface with a waterproof overlay.

The deck can be also assembled from precast segments that hang on temporary erection cables that are removed after post-tensioning of the deck with the internal tendons (see Figure 12.10d). Another system utilizes external tendons to support and prestress the deck (Figure 12.10f). These external tendons either can be uniformly distributed along the width of segment or be situated close to the edges of the segments.

Another arrangement consists of precast segments with a composite slab (see Figure 12.10e). The segments are suspended on bearing tendons and serve as a false-work and formwork for the composite slab that is cast simultaneously with the segment joints. Both the precast segments and the composite slab are post tensioned by tendons that are situated along the bearing tendons within the cast-in-place slab. A continuous deck slab without any joints provides an excellent protection to the prestressing steel and requires minimum maintenance.

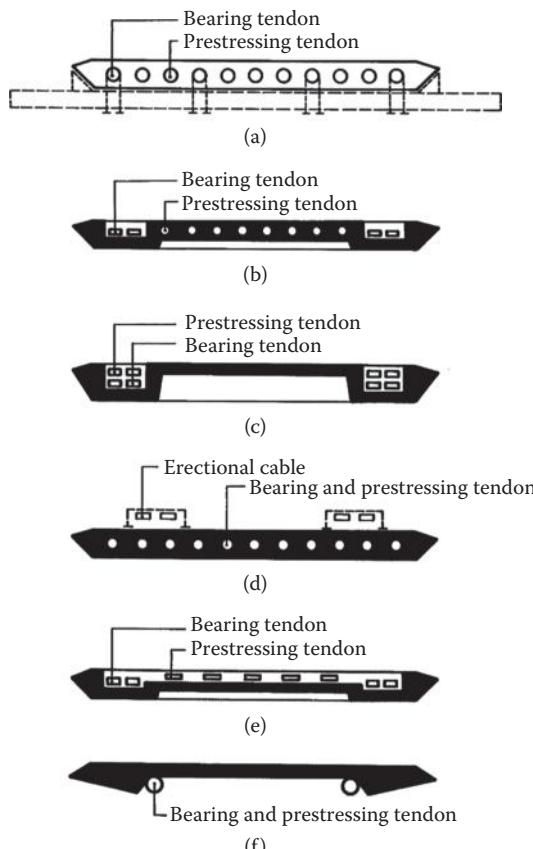


FIGURE 12.10 Prestressed band: typical sections.

Usually the bearing tendons consist of strands that are protected by the post-tensioned concrete of the troughs or composite slab. The prestressing tendons are formed by strands grouted in a traditional duct. If a higher degree of protection is required, the bearing tendons can also be made from strands grouted in ducts or both bearing and prestressing tendons can be made from monostrands additionally grouted in PE (polyethylene) ducts.

12.2.3 Structural Arrangement at Piers and Abutments

A typical section of stress-ribbon is not able to resist the bending moments that occur at the supports (see Figure 12.9). The support bending moments can be reduced by

- Supporting the stress ribbon with a saddle from which the band can lift during post-tensioning and temperature drop, and to which the band can return for a temperature increase (see Figures 12.11a and 12.12a)
- Strengthening the stress ribbon with a short support haunch (see Figures 12.11b and 12.12b)

The detailing of these regions depends on the local conditions and the chosen technology (see Figure 12.13).

Figure 12.13a shows a cast in place deck supported by saddles. Figures 12.13b and 12.14 present a solution in which precast segments are supported by saddles. To accommodate the larger curvatures in the region, the length of pier segments is one third of that of the typical segments. The segments are erected before the bearing tendons are placed and tensioned.

The segments directly above for pier columns are placed on cement mortar; the remaining segments are placed on neoprene strips. The stress ribbon is connected to the saddles using reinforcement between the segments situated above the pier columns.

Figures 12.13b and 12.15 show examples of a cast-in place haunch cast in a formwork, which was suspended on the already erected segments and the pier. In this case the bearing tendons were supported by steel saddles anchored in the pier columns. The friction forces between the strands and the saddle are reduced using Teflon plates (see Figure 12.13e). Until the deck itself provides a restraint, the piers can be stabilized using temporary struts.

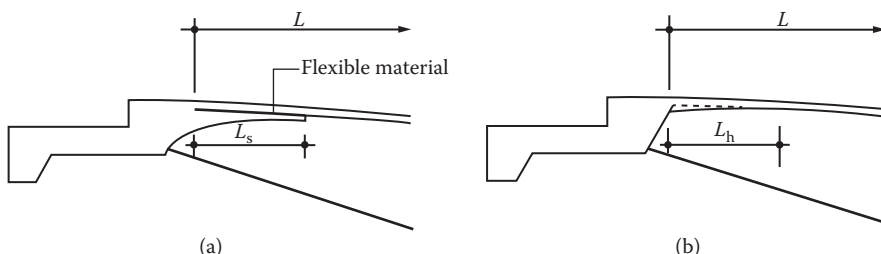


FIGURE 12.11 Abutments: (a) support with a saddle and (b) support with a short haunch.

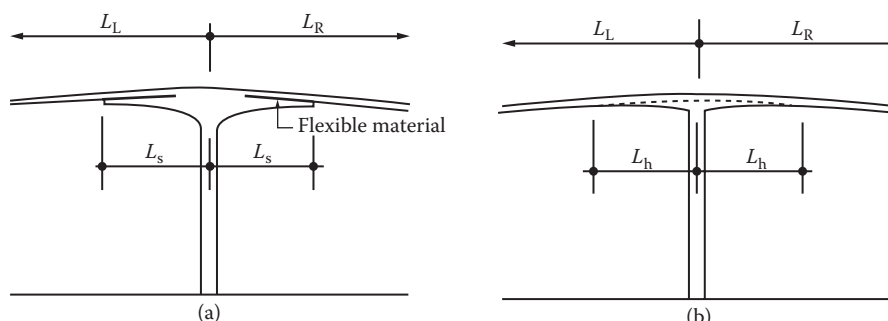


FIGURE 12.12 Intermediate piers: (a) support with a saddle and (b) support with a short haunch.

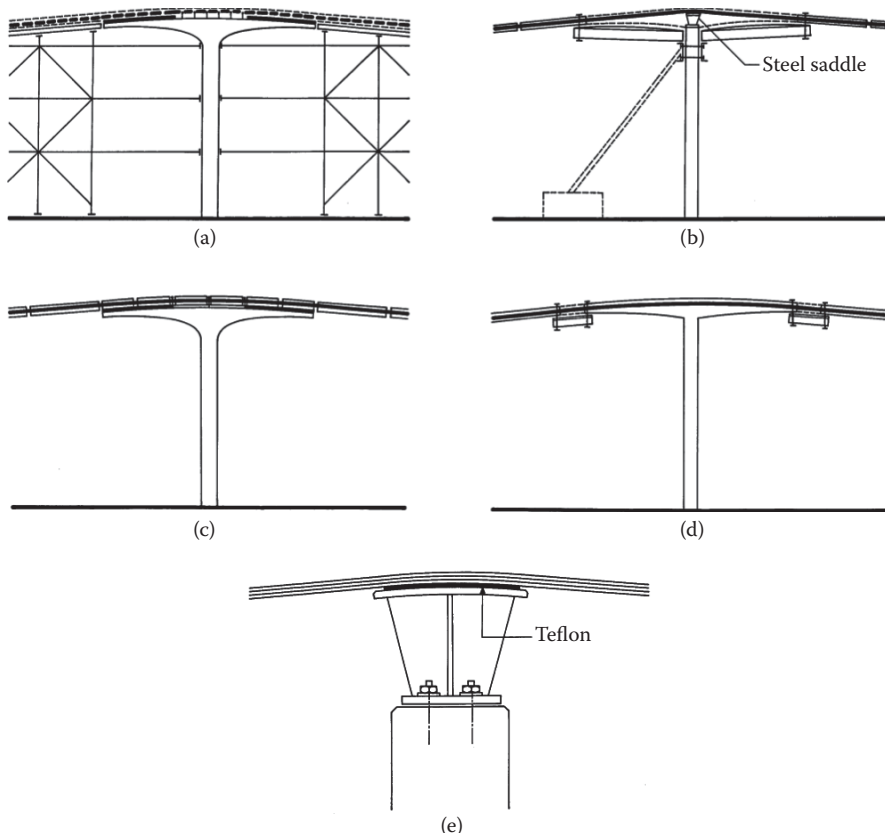


FIGURE 12.13 Erection of the stress ribbon at intermediate piers: (a) cast in place deck supported by saddles, (b) cast in place haunch, (c) precast deck, (d) cast in place deck, and (f) Teflon plates.



FIGURE 12.14 Grants Pass Pedestrian Bridge—intermediate pier.

@Seismicisolation

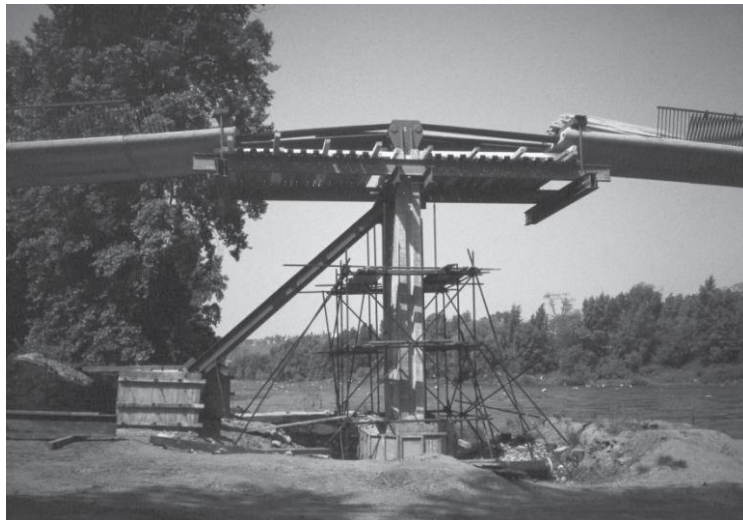


FIGURE 12.15 Prague-Troja Bridge—intermediate pier during the erection.

Figure 12.13c shows a solution in which the abutment and pier haunches were cast in place before the erection of the segments. The ducts, in which the bearing tendons are placed, have to allow a change of slope during the construction of the deck. A closure was therefore provided between the saddles and the segments.

The main advantage of the solution shown in Figure 12.13b is that the shape of the saddle can be easily adjusted according to the geometry of the already erected deck that is dependent not only on the value of the initial stressing and actual weight of segments, but also on the temperature at the time of casting.

Although the described measures can significantly reduce the bending stresses, it is necessary to carefully design the stress ribbon in the vicinity of the supports. For designing of the ribbon, the positive bending moments that cause tension stresses at bottom fibers are critical. Since the bearing and prestressing tendons are situated a sufficient distance away from the bottom fibers it is possible to accept cracks there and design the ribbon as a partial post-tensioned member in which crack width and fatigue stresses in the reinforcement are checked. If the ribbon above the saddle is assembled from precast members, it is necessary to guarantee compression in the joints. This can be provided with additional short tendons situated in the pier segments.

12.2.4 Transferring Stress Ribbon Force into the Soil

The stress ribbon is usually fixed at anchor blocks that are integral parts of the abutments. The abutments therefore need to transfer some very large horizontal forces into the soil by rock or ground anchors. Unfortunately, only in exceptional cases sound rock is close to grade and then the anchor block has the simple shape shown in Figure 12.16.

In most cases the competent soil is situated at a certain distance and the abutments have an arrangement as shown in Figure 12.17. In this case it is necessary to check the soil pressure as well as the resistance against overturning and sliding not only for the maximum loading but for all stages of construction. It is important to realize that the rock anchors or ties have to be post-tensioned. That means that they load the footing with an eccentric inclined force N_{an} that has vertical and horizontal components V_{an} and H_{an} .

During post-tensioning the capacity of the anchors is checked. By post-tensioning—or anchoring the footings to the soil—the variation of stresses at the anchor is eliminated and resistance against sliding is guaranteed.

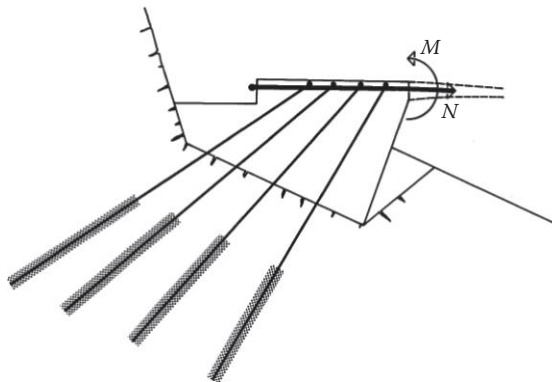


FIGURE 12.16 Rock anchors.

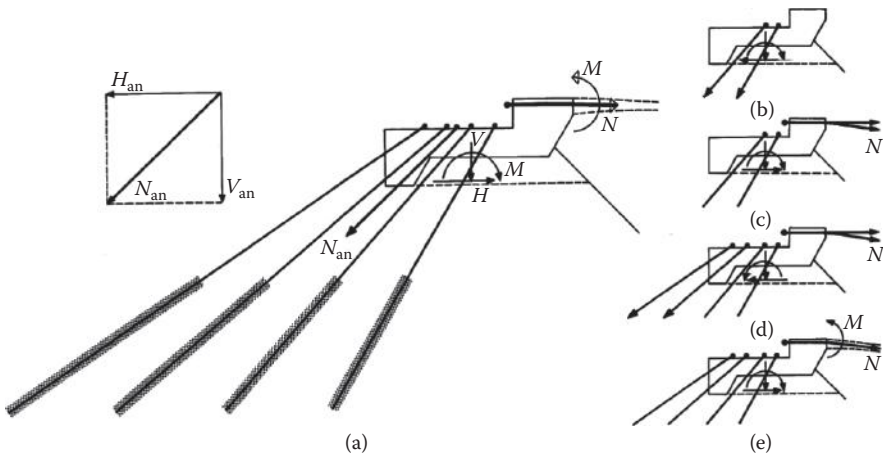


FIGURE 12.17 Installation of rock anchors: (a) anchor system, (b) post-tensioning of the first half of the rock anchors, (c) erection of the deck, (d) post-tensioning of the second half of the rock anchors, and (e) bridge in service.

In Figure 12.17 the footing is provided with a shear key. Therefore the resistance against sliding has to be checked at the bottom of the key. The safety against sliding:

$$s = \frac{V \cdot \operatorname{tg}\varphi + Ac}{H} = \frac{(V_q + V_{an}) \cdot \operatorname{tg}\varphi + Ac}{H_q - H_{an}} \geq s_0$$

where V_q is a vertical force from the dead and live load, H_q is the horizontal component of the force in the stress ribbon, φ is the angle of internal friction of the soil, A the area of the footing at the level of the key and c is the cohesion.

The factor of safety against sliding s_0 depends on national codes and typically varies from 1.5 to 2.0.

The factor of safety has to be determined for all stages of the construction. In general, it is impossible to post-tension all rock anchors before erection of the deck, since the horizontal force H_{an} is too large and can cause sliding of the footing in the direction of the post-tensioning. Therefore, the post-tensioning is usually done in two stages and the safety against sliding has to be checked for the following:

1. Post-tensioning of the first half of the rock anchors (see Figure 12.17b).
2. Erection of the deck (see Figure 12.17c).

3. Post-tensioning of the second half of the rock anchors (see Figure 12.17d).
4. Service of the bridge, full live load and temperature drop (see Figure 12.17e).

The use of rock or ground anchors requires a soil with adequate bearing capacity to resist not only the pressure from the stress ribbon, but also the pressure from the vertical component of the anchor force.

If there is insufficient capacity, drilled shafts can be used to resist both the vertical and horizontal components of the stress ribbon force. Although the drilled shafts have a relatively large capacity for resisting in a horizontal force, their horizontal deformations are significant and it is necessary to consider them in the analysis. Elastic horizontal deformations can be eliminated with an erection process in which the structure is pre-loaded before the casting of the closure joints. Nevertheless, with time plastic deformations can cause considerable horizontal displacements of the abutments that consequently cause an increase of the sag of the stress ribbon.

An elegant solution is presented in Figure 12.18 in which the stress ribbon is supported by battered micropiles. They transfer the load from the stress ribbon into the soil because of their tension and compression capacity. The maximum tension in the piles occurs in at the last row where the tension force from to horizontal force ${}^H T_i$ is increased by a tension force coming from the uplift (V_i) created by the vertical force V and bending moment M .

$$V_i = -\frac{V}{n} \pm \frac{M}{I} z_i$$

$$I = \sum z_i^2$$

where n is number of micropiles, and z_i is distance of the micropile from the center of gravity of the micropile group.

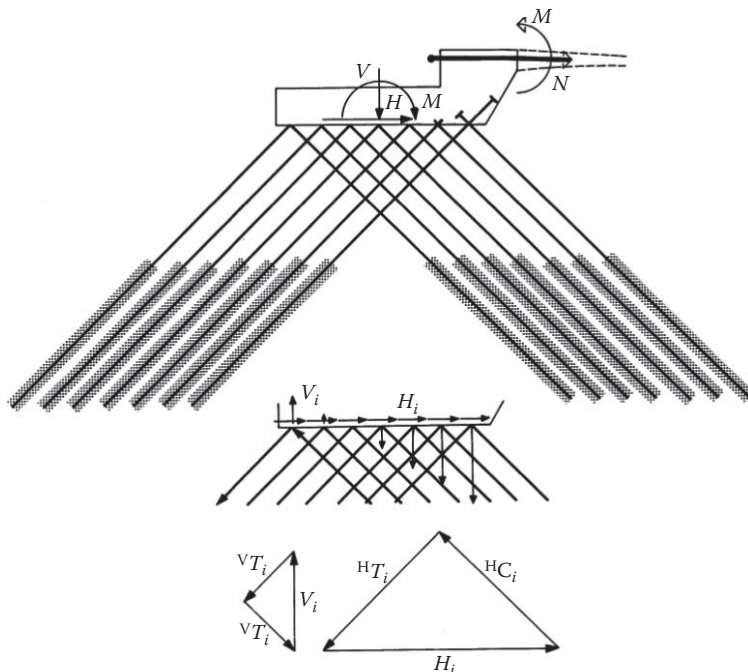


FIGURE 12.18 Battered micropiles.

12.3 Erection

One of the main advantages of the stress ribbon structure is that the erection of the deck can be done independently of the conditions of the terrain under the bridge since the formwork of precast segments can be suspended from the bearing tendons.

Although there are some differences given by the arrangement of the stress ribbon above supports, they are two basic erection possibilities that are distinguished by the arrangement of the bearing tendons.

12.3.1 Construction Sequences A

When the bearing tendons are situated in the troughs, where they are protected by cast-in-place concrete, they can also be used as erection cables (Figure 1.3). The general arrangement of the erection of segments can be seen in Figure 12.19. The construction process could be as follows:

- First the bearing tendons are drawn by a winch. The strands are wound off from coils and are slowed down at the abutment by a cable brake that also ensures equal length for all strands. An auxiliary rope can also be attached to the erected tendon that enables to back drawing of the hauling rope. After drawing each tendon is tensioned to the prescribed stress.
- The segments are erected in each span by means of a crane truck. The erected segment is first placed under the bearing tendons and lifted until the tendons are touching the bottom of the troughs. Then "hangers" are placed into the position and secured; the segment is attached to hauling and auxiliary ropes and by pulling of the winch the segment is shifted along the bearing tendon into the pre-determined position (see Figure 12.20a). Before the segment is attached to the previously erected segments, the tubes for coupling the ducts of prestressing tendons are placed. This process is repeated until all segments are assembled.
- When all segments are erected the formwork for the saddle is hung on neighboring segments and piers and/or abutments. In structures with saddles the formwork of the closures is suspended. Then the prestressing tendons and rebar are placed. After that, the joints, saddles and troughs or composite slab are all cast together. It is necessary to use a retarder in the concrete mix, which postpones the beginning of concrete setting until the concrete in all members is placed. In order to reduce the effects of shrinkage, temperature drop and accidental movement of pedestrians, it is recommended to partially prestress the deck as early as possible. When a minimum specified strength is attained, the stress ribbon is then prestressed to the full design stress.

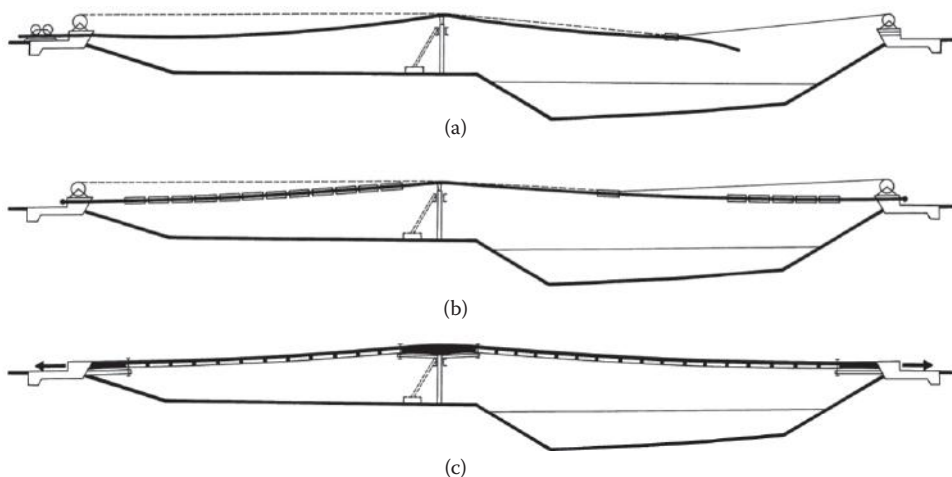


FIGURE 12.19 Construction sequences A.

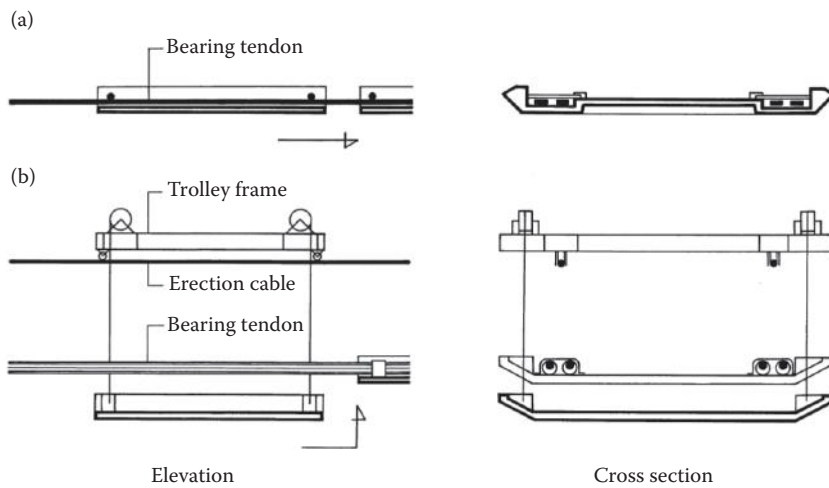


FIGURE 12.20 Erection of a segment: (a) erection A and (b) erection B.

12.3.2 Construction Sequences B

When the bearing tendons are placed in the ducts, the process of construction has to be modified. The general procedure of the erection of segments is shown in Figure 12.21. The construction process can be as follows:

- First an erection cable is erected and anchored at the abutments. Then the ducts are progressively suspended, spliced and shifted along the erection cable into the design position (see Figure 12.20a). When the ducts are completed, the strands are pulled or pushed through the ducts and tensioned to the prescribed stress.
- The segments can be also erected by a crane truck. If the span across the obstacle is relatively short and the crane has sufficient reach it can erect all the segments (see Figure 12.22). The erected segment is placed in a C frame and slipped in under the bearing tendon. Then it is lifted up such that it touches the bearing tendons. Thereafter, the “hangers” are placed into position and secured.

If the spans are longer, it is possible to apply an erection technique used for erection of suspension structures (see Figure 12.20b). The segment is suspended on an erection frame supported

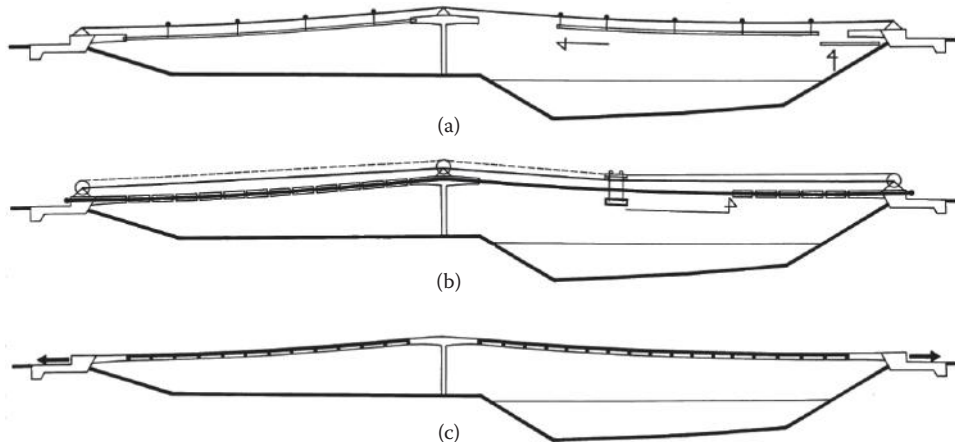


FIGURE 12.21 Construction sequences B.



FIGURE 12.22 Bridge across the Medway River, Maidstone, Kent, UK—erection of a segment.

on erection cables that is attached to hauling and auxiliary ropes. Using a winch, the segment is shifted along the erection cables into a pre-determined position where it is lifted until it touches the bearing tendons. The hangers are then placed and secured. This process is repeated until all segments are assembled.

- c. When all segments are assembled the forms for the closures are hung, and the prestressing tendons and rebars are placed. After that, the joints, saddles, and troughs or a composite slab are cast (see Figure 12.20c) and post-tensioned. The remainder of this process is similar to previously described erection method.

12.4 Static and Dynamic Analysis

The static behavior of the stress ribbon structures is dependent of their structural arrangement and the process of construction. It is clear that it is necessary to distinguish between the behavior of the structure during erection and during the service. During erection the structure acts as a cable (see Figure 12.8a), during service as a stress ribbon (see Figure 12.8b) that is stressed not only by normal forces but also by bending moments. The shape and the stresses in the structure at the end of the erection determine the stresses in the structure when in use. The change from cable to stress ribbon occurs when the concrete of joints starts to set.

All the design computations have to start from this basic stage. During the erection analysis the structure is progressively unloaded down to the stage in which the bearing tendons are stressed. This is the way the required jacking force is obtained (see Figure 12.23a through 12.23c).

The designer sets the shape of the structure after prestressing (see Figure 12.23e). Since this shape depends on the deformation of the structure due to prestress, the basic stage has to be estimated; then the deformation of the structure due to prestress computed and checked against the required final stage. This computation has to be repeated until reasonable agreement is obtained.

The basic stage is also the initial stage for the subsequent analysis of the structure for all service loads (see Figures 12.23d through 12.23f).

This section describes a simplified analysis that the author used in his first structures. This approach can be used for preliminary analysis or for checking results obtained from modern analytical programs that are discussed in more details in author's book (Strasky 2011).

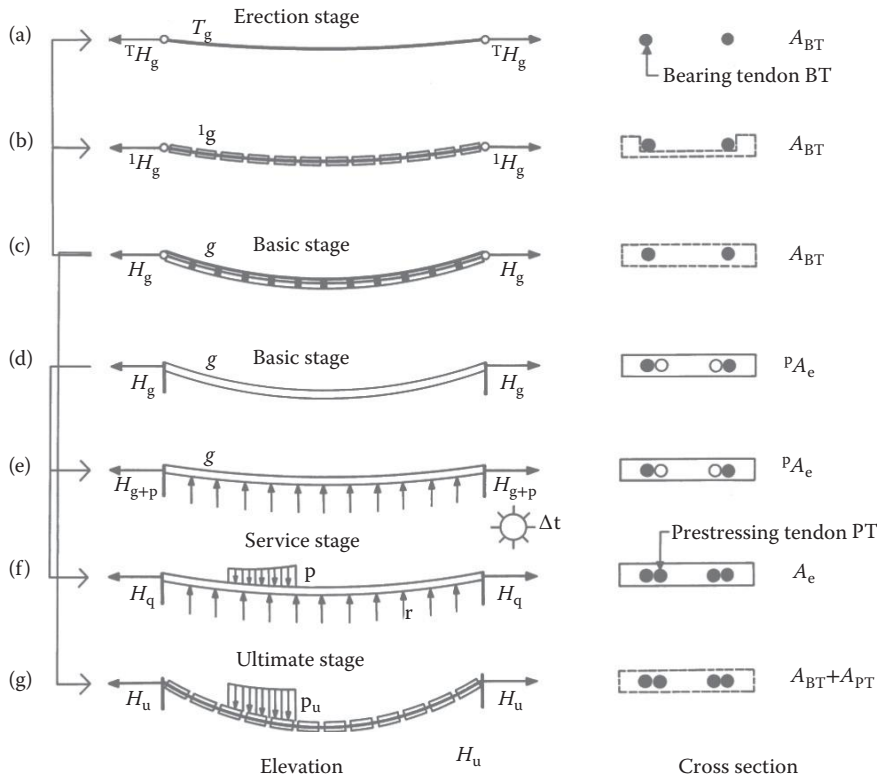


FIGURE 12.23 Static function.

12.4.1 Single Cable

The analysis of the single cable is described in many books. The approach used in this chapter comes from the author's book (Strasky 2011). In the analysis we suppose that the cable of the area A and modulus of elasticity E acts as perfectly flexible member that is able to resist the normal force only. Under this assumption the cable curve will coincide with the funicular curve of the load applied to the cable and to chosen value of the horizontal force H (see Figure 12.24).

Suppose a cable that is supported at two fix hinges a, b and it is loaded by a vertical load $q(x)$.

$$l = X(b) - X(a) = x(b) \quad (12.1)$$

$$h = Y(b) - Y(a) = y(b) \quad (12.2)$$

$$\operatorname{tg}\beta = \frac{h}{l} \quad (12.3)$$

For the given load $q(x)$ and chosen horizontal force H the cable curve is determined by coordinate $y(x)$, sag $f(x)$, by the slope of the tangent $y'(x) = \operatorname{tg}\varphi(x)$ and radius of the curvature $R(x)$. These values are derived from the general equilibrium conditions on the element ds .

The cable is stressed by a normal force $N(x)$ that has vertical and horizontal components $V(x)$ and $H(x)$.

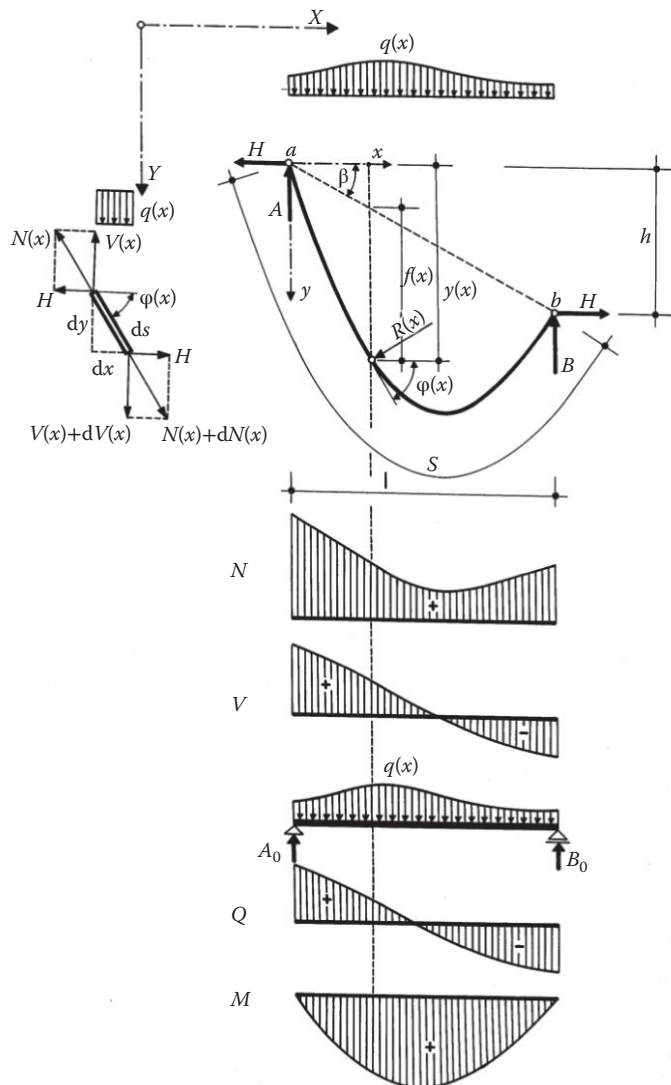


FIGURE 12.24 Basic characteristics of the single cable.

$$N(x)^2 = H(x)^2 - V(x)^2 \quad (12.4)$$

$$H(x) = N(x)\cos\phi(x) \quad (12.5)$$

$$V(x) = N(x)\sin\phi(x) \quad (12.6)$$

For vertical load $H = \text{const.}$

$$p^0(x) = \frac{Q(x)}{H} \quad (12.7)$$

$$p(x) = y'(x) = p^0(x) + \frac{h}{l} = p^0(x) + tg\beta \quad (12.8)$$

$$f(x) = \frac{M(x)}{H} \quad (12.9)$$

$$y(x) = \frac{M(x)}{H} + \frac{h}{l}x = f(x) + x \tan \beta \quad (12.10)$$

where $Q(x)$ and $M(x)$ are shear force and bending moment on simple beam of the span l .

For $q(x) = \text{const.}$

$$p^0(x) = \frac{1}{H} \left(\frac{1}{2} ql - qx \right) = \frac{q}{2H} (l - 2x) \quad (12.11)$$

$$p(x) = p^0(x) + \frac{h}{l} = p^0(x) + \tan \beta \quad (12.12)$$

$$f(x) = \frac{M(x)}{H} = \frac{1}{H} \left(\frac{1}{2} qlx - \frac{1}{2} qx^2 \right) = \frac{q}{2H} x(l - x) \quad (12.13)$$

12.4.1.1 Length of Cable

$$s = \int_0^s ds = \int_0^s \sqrt{dx^2 + dy^2} = \frac{l}{\cos \beta} + \frac{\cos \beta}{2H} D \quad (12.14)$$

$$D = \int_0^l Q^2(x) dx = \int_0^l Q(x) \cdot Q(x) dx \quad (12.15)$$

is usually determined by a Vereshchagin rule. (The area of the $Q(x)$ is multiplied by a value of the value Q_p , that occurs at the center of the gravity of the area.)

For example, for uniform load $q(x) = \text{const.}$:

$$D = \int_0^l Q(x) dx = 2 \times \left[\left(\frac{1}{2} \left(\frac{1}{2} ql \right) \frac{l}{2} \right) \times \left(\frac{2}{3} \times \frac{1}{2} ql \right) \right] = \frac{q^2 l^3}{12} \quad (12.16)$$

For the cable of the length l , sag f , horizontal force H and uniform load q the length of the cable is

$$s = \frac{l}{1} + \frac{1}{2H^2} \frac{q^2 l^3}{12} = l + \frac{q^2 l^3}{24H^2} \quad (12.17)$$

for $H = \frac{ql^2}{8f}$

$$s = l + \frac{8f^2}{3l} \quad (12.18)$$

12.4.1.2 Elastic Elongation of Cable

$$\Delta s = \int_0^s \frac{N(s)}{EA} ds = \int_0^s \frac{H}{EA} \frac{ds^2}{dx} \quad (12.19)$$

$$ds = \int_0^l (1 + y'^2(x)) dx \quad (12.20)$$

For vertical load

$$\Delta s = \frac{H}{EA} \left(\frac{l}{\cos^2 \beta} + \frac{1}{H^2} \int_0^l Q(x) ds \right) = \frac{2H}{EA \cos \beta} \left(s - \frac{l}{2 \cos \beta} \right) \quad (12.21)$$

For the cable of the length l , sag f , horizontal force H and uniform load q the length of the cable is

$$\Delta s = \frac{2H}{EA} \left(s - \frac{l}{2} \right) = \frac{2H}{EA} \left(l + \frac{8f^2}{3l} - \frac{l}{2} \right) = \frac{H}{EA} \left(l + \frac{16f^2}{3l} \right) \quad (12.22)$$

12.4.1.3 Determining Horizontal Force H_i

For the load $q(x)_0$, horizontal force H_0 and temperature t_0 the length of the non-tension cable:

$$\ln = s_0 - \Delta s_0 = \frac{l}{\cos \beta} + \frac{\cos \beta}{2H_0^2} D_0 - \frac{H_0 l}{EA \cos^2 \beta} - \frac{1}{H_0 EA} D_0 \quad (12.23)$$

$$D_0 = \int_0^l Q_{x,0}^2 dx \quad (12.24)$$

For the load $q(x)_i$, unknown horizontal force H_i and the temperature t_i the length of the non-tension cable:

$$\ln_i = s_i - \Delta s_i \quad (12.25)$$

$$\ln_i = \ln(1 + \alpha_t \Delta t_i) \quad (12.26)$$

$$D_i = \int_0^l Q_{x,i}^2 dx \quad (12.27)$$

where the temperature change $\Delta t_i = t_i - t_0$ and α_t is a coefficient of thermal expansion.

$$s_i = \frac{l}{\cos \beta} + \frac{\cos \beta}{2H_i^2} D_i \quad (12.28)$$

$$\Delta s_i = \frac{H_i l}{EA \cos^2 \beta} + \frac{1}{H_i EA} D_i \quad (12.29)$$

$$\ln_i = s_i - \Delta s_i = \frac{l}{\cos \beta} + \frac{\cos \beta}{2H_i^2} D_i - \frac{H_i l}{EA \cos^2 \beta} - \frac{D_i}{EA H_i} \quad (12.30)$$

$$\left(\ln_i - \frac{l}{\cos \beta} \right) - \frac{\cos \beta}{2H_i^2} D_i + \frac{H_i l_i}{EA \cos^2 \beta} + \frac{D_i}{EA H_i} = 0 \quad (12.31)$$

If we denote

$$a = \frac{l}{EA \cos^2 \beta} \quad (12.32)$$

$$b = \ln_i - \frac{l}{\cos \beta} \quad (12.33)$$

$$c = \frac{D_i}{EA} \quad (12.34)$$

$$d = \frac{\cos \beta}{2} D \quad (12.35)$$

we get a cubic equitation for determining of H_i

$$aH_i^3 + bH_i^2 + cH_i + d = 0 \quad (12.36)$$

From this equation the unknown horizontal force H_i can be easily solved.

12.4.1.4 Influence of Deformation of Supports and Cable Elongation at Anchor Blocks

In actual structures it is necessary to include possible deformations of supports and elongations of the cable at the anchor blocks (see Figure 12.25).

Deformations of supports for load 0 and i :

$$\begin{aligned} \Delta_{a0}^V &= A_0 \delta_a^V & \Delta_{ai}^V &= A_i \delta_a^V \\ \Delta_{a0}^H &= H_0 \delta_a^H & \Delta_{ai}^H &= H_i \delta_a^H \\ \Delta_{b0}^V &= B_0 \delta_b^V & \Delta_{bi}^V &= B_i \delta_b^V \\ \Delta_{b0}^H &= H_0 \delta_b^H & \Delta_{bi}^H &= H_i \delta_b^H \end{aligned}$$

depend on values of the reactions and positive unit deformations.

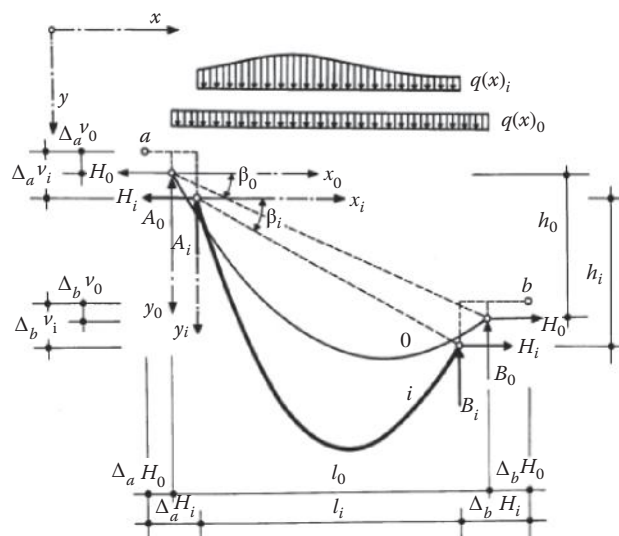


FIGURE 12.25 Initial and final stage of the cable.

For load 0:

$$l_0 = X_b - X_a - \Delta_{a0}^H - \Delta_{b0}^H \quad (12.37)$$

$$h_0 = Y_b - Y_a - \Delta_{a0}^V - \Delta_{b0}^V \quad (12.38)$$

$$\operatorname{tg}\beta_0 = \frac{h_0}{l_0} \quad (12.39)$$

For load i :

$$l_i = X_b - X_a - \Delta_{ai}^H - \Delta_{bi}^H \quad (12.40)$$

$$h_i = Y_b - Y_a - \Delta_{ai}^V - \Delta_{bi}^V \quad (12.41)$$

$$\operatorname{tg}\beta_i = \frac{h_i}{l_i} \quad (12.42)$$

The elastic deformations of the cable in the anchor blocks a and b for load 0:

$$\Delta_{\text{an},0} = kH_0$$

and load i :

$$\Delta_{\text{an},i} = kH_i$$

where $k = k_a + k_b$ express of the elongation of the cable at the anchor blocks a and b due to unit horizontal force $H = 1$.

$$k_a = \int_0^{l_{ka}} \frac{S_{ka}}{EA} ds \quad (12.43)$$

$$k_b = \int_0^{l_{kb}} \frac{S_{kb}}{EA} ds \quad (12.44)$$

For the load $q(x)_0$, horizontal force H_0 and temperature t_0 the length of the non-tension cable:

$$\ln = s_0 - \Delta s_0 - \Delta_{\text{an},0} = \frac{l_0}{\cos\beta_0} + \frac{\cos\beta_0}{2H_0^2} D_0 - \frac{H_0 l_0}{EA \cos^2 \beta_0} - \frac{1}{H_0 EA} D_0 - kH_0 \quad (12.45)$$

$$D_0 = \int_0^{l_0} Q_{x,0}^2 dx \quad (12.46)$$

For the load $q(x)$, unknown horizontal force H_i and the temperature t_i the length of the non-tension cable:

$$\ln_i = \ln(1 + \alpha_i \Delta t_i) \quad (12.47)$$

$$\ln_i = s_i - \Delta s_i - \Delta_{an,i} = \frac{l_i}{\cos \beta_i} + \frac{\cos \beta_i}{2H_i^2} D_i - \frac{H_i l_i}{EA \cos^2 \beta_i} - \frac{1}{H_i EA} D_i - kH \quad (12.48)$$

$$D_i = \int_0^{l_i} Q_{x,i}^2 dx \quad (12.49)$$

$$\left(\ln_i - \frac{l_i}{\cos \beta_i} \right) - \frac{\cos \beta_i}{2H_i^2} D_i + \frac{H_i l_i}{EA \cos^2 \beta_i} + kH_i + \frac{D_i}{EA H_i} = 0 \quad (12.50)$$

If we denote

$$a = \frac{l_i}{EA \cos^2 \beta_i} + k \quad (12.51)$$

$$b = \ln_i - \frac{l_i}{\cos \beta_i} \quad (12.52)$$

$$c = \frac{D_i}{EA} \quad (12.53)$$

$$d = \frac{\cos \beta_i}{2} D_i \quad (12.54)$$

we get a cubic equation for determining of H_i

$$aH_i^3 + bH_i^2 + cH_i + d = 0 \quad (12.55)$$

Since the members a, b, c, d depend on the span l_i and vertical difference h_i which again depend on horizontal force H_i , it is not possible to determine the unknown H_i directly by solving of the equation. Therefore it is necessary to determine H_i by iteration. First, the unknown H_i is determined for zero deformation of supports and zero elongation of the cable at the anchor blocks. For this force the vertical reactions A_i and B_i , span length l_i and vertical difference h_i and members a, b, c, d and new horizontal force H_i . The computation is repeated till the difference between the subsequent solutions is smaller than the required accuracy.

12.4.1.5 Bending of the Cable

The bending of the cable is derived from the analysis of Single cable that is stressed by known horizontal force H (Strasky 2011).

Figure 12.26 shows a single cable of the area A , moment of inertia I and modulus of elasticity E that is fixed into the supports a and b . The cable is loaded by load $g(x)$ and $q(x)$. Corresponding horizontal forces are H_g and H .

It is supposed that erection of the cable is done in such a way that the load g does not cause any bending of the cable. For $g = const.$ the shape of the cable given by $y(x)$ is the second degree parabola.

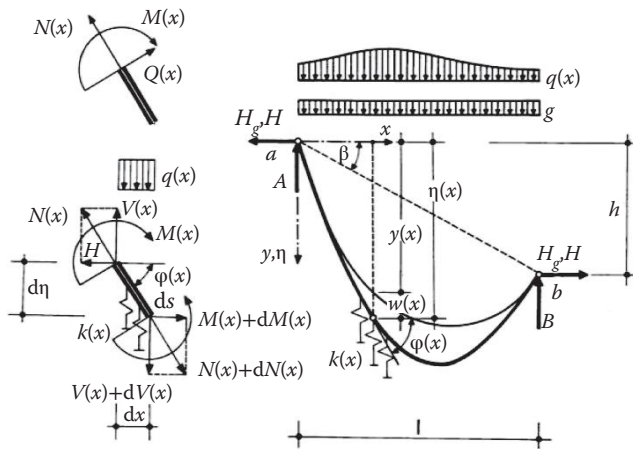


FIGURE 12.26 Geometry and internal forces at flexibly supported cable.

The portion of the cable can be supported by Winkler's springs. The characteristic of the spring \$k(x)\$ is a "stress" that corresponds to its unit deformation.

Then the bending of the cable is given by

$$EI \frac{d^4 w(x)}{dx^4} - H \frac{d^2 w(x)}{dx^2} + kw(x) = q(x) + \frac{H}{R_g} = q(x) - \frac{H}{H_g} g \quad (12.56)$$

The solution of the equation is possible to write

$$w(x) = w_h(x) + w_p(x) \quad (12.57)$$

the particular solution \$w_p(x)\$ corresponds to deformation of the cable without bending stiffness; the homogenous solution can be written as

$$w_h(x) = Ae^{\lambda x} + Be^{-\lambda x} + C + Dx \quad (12.58)$$

$$\lambda = \sqrt{\frac{H}{EI}} \quad (12.59)$$

Direct solution is possible only for special cases (see Figure 12.27). For example the course of the bending moment \$M(x)\$ in the vicinity of the support of the cable that is loaded by uniform loads \$g\$ and \$q\$ and corresponding horizontal forces are \$H_g\$ and \$H\$ is solved for infinitely long cable. The bending moment is given by an expression:

$$M(x) = \Delta\phi \sqrt{H \cdot EI} \cdot e^{-\lambda x} + \Delta q EI \quad (12.60)$$

The bending moment at an infinitely long cable loaded that is loaded by point load \$F\$ and by uniform load \$q\$ is given by an expression:

$$M(x) = \frac{F}{2\lambda} e^{-\lambda x} + EI\Delta q \quad (12.61)$$

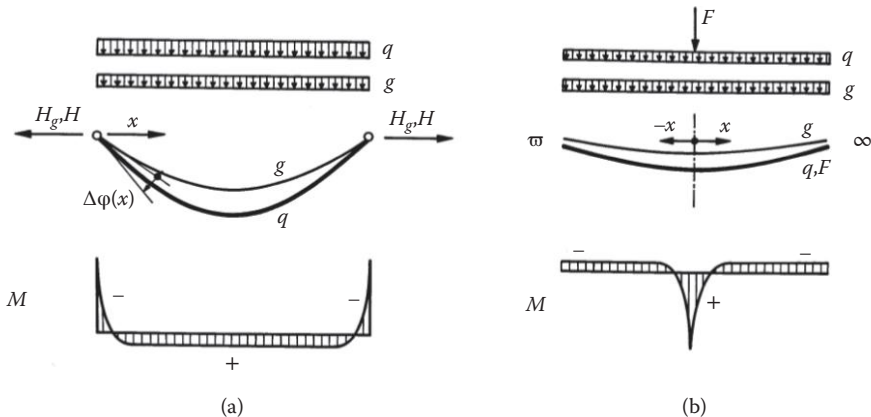


FIGURE 12.27 Bending moments (a) at support and (b) under point load.

where

$$\lambda = \sqrt{\frac{H}{EI}}$$

$$\Delta q = \frac{q}{H} - \frac{g}{H_g}$$

The author, rather than solve the equations for different loading conditions, developed a program in which the deformation and corresponding shear forces and bending moments were solved using *finite difference method*. This approach enables to express a local stiffening of the cable and supporting of portion of the cable by Winkler springs.

12.4.1.6 Natural Modes and Frequencies

The natural modes and frequencies of Single cable (see Figure 12.28) can be determined according to the following formulas:

$$f_{(1)} = \frac{1}{2} \sqrt{\frac{1}{\mu} \left(\frac{H}{l^2} + \frac{EAf^2\pi^2}{2l^4} + \frac{EI\pi^2}{l^4} \right)} \quad (12.62)$$

$$f_{(n)} = \frac{1}{2} \sqrt{\frac{1}{\mu} \left(\frac{Hn^2}{l^2} + \frac{EI\pi^2 n^2}{l^4} \right)} \quad (12.63)$$

where H is the horizontal force, M is the mass of the cable per unit length, f is the sag of the cable, E is the modulus of elasticity, A is the area and I is the moment of inertia.

The member $(EAf^2\pi^2)/2l^4$ in equation expresses the normal stiffness of the cable that has to elongate when vibrate in the first mode. This is the reason why in some cases the first mode is higher than the second one.

The member $(EI\pi^2n^2)/l^4$ expresses the bending stiffness of cable that is in engineering calculations insignificant.

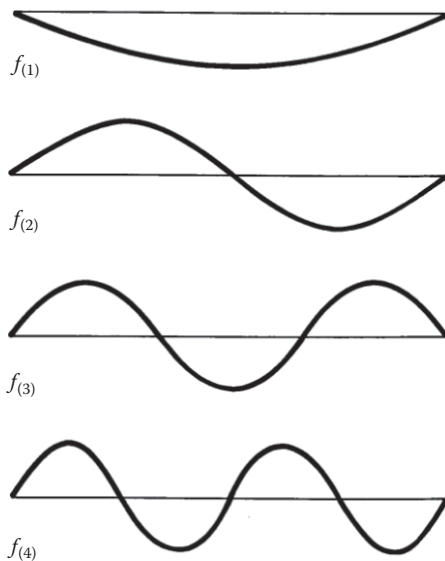


FIGURE 12.28 Natural modes.

12.4.2 Analysis of Stress Ribbon as a Cable

12.4.2.1 Erection Stage

During the erection all loads are resisted by the bearing tendons that act as a cable. Since the tendons are not usually connected to the saddles they can slide freely according to the imposed load (see Figure 12.29a). This is true both for structures in which the bearing tendons are supported by steel or concrete saddles and for structures in which the bearing tendons pass through ducts in the support haunches.

Hence, the cables act as a continuous cable of m spans that crosses fixed supports (see Figure 12.23a). A change of any load causes friction in the saddles, the magnitude of which depends on the vertical reaction R and on a coefficient of friction μ . In all supports friction forces ΔH act against the direction of the cable movement.

$$\Delta H = R\mu \quad (12.64)$$

The stresses in the bearing tendons are also affected by their elongation in the anchorage blocks and by possible displacements of the end supports. The unknown horizontal force H_i is given by an equation that is used for the analysis of the simple cable.

$$aH_i^3 + bH_i^2 + cH_i + d = 0 \quad (12.65)$$

Since both the length s and the elongation of the cable Δs are calculated for the whole length of continuous cable,

$$s = \sum_{j=1}^m s_j = \sum_{j=1}^m \frac{l_j}{\cos \beta_j} + \frac{\cos \beta_j}{2H_j} D_j \quad (12.66)$$

$$\Delta s = \sum_{j=1}^m \Delta s_j = \sum_{j=1}^m \frac{2H_j}{EA \cos \beta} \left(s_j - \frac{l_j}{2 \cos \beta_j} \right) \quad (12.67)$$

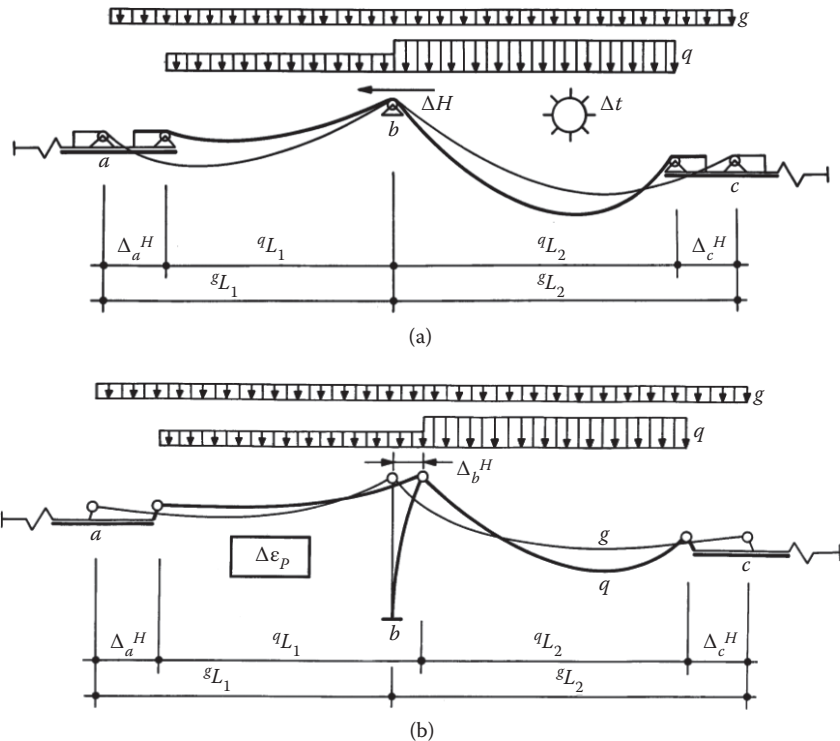


FIGURE 12.29 Static function: (a) stage of erection and (b) stage of service.

$$D_j = \int_0^{l_j} Q_j^2 dx \quad (12.68)$$

the terms a, b, c, d have to be modified to

$$a = \sum_{j=1}^m \frac{l_{j,i}}{EA \cos^2 \beta_{j,i}} + k \quad (12.69)$$

$$b = \ln_i - \sum_{j=1}^m \frac{l_{j,i}}{\cos \beta_{j,i}} \quad (12.70)$$

$$c = \sum_{j=1}^m \frac{D_{i,j}}{EA} \quad (12.71)$$

$$d = \sum_{j=1}^m \frac{\cos \beta_{j,i}}{2} D_{j,i} \quad (12.72)$$

The horizontal force H_i in span j is taken as the largest horizontal force acting in the most loaded span reduced by the sum of the losses due to friction at the supports situated between the span j and the most loaded span.

Since the terms a, b, c, d depend on the span lengths $l_{j,i}$ and vertical differences $h_{j,i}$ which in turn depend on horizontal force H_i , it is not possible to determine the unknown H_i directly by solving the above equation. It is therefore necessary to determine H_i by iteration. First, the unknown H_i is calculated

for zero deformation of supports and zero elongation of the cable at the anchor blocks. For this force the vertical reactions A_p , B_p , and R_p ; span length $l_{j,i}$ and vertical difference $h_{j,i}$ members a , b , c , d and the new horizontal force H_p , are calculated. This iteration is repeated until the difference between subsequent solutions is smaller than the required tolerance.

This analysis should be repeated for all erection stages. The goal of the analysis is not only to determine the jacking force for the bearing tendons, but also the deformations of the structure and the corresponding stresses that affect the substructure.

12.4.2.2 Service Stage

Since the structure is very slender, local shear and bending stresses develop only under point loads and at the supports. Because these stresses are relatively small, they do not affect the global behavior of the structure. This makes it possible to analyze the structure in two closely related steps.

In step 1, the stress ribbon is analyzed as a perfectly flexible cable hinge connected with supports (see Figure 12.29b). The effect of prestressing is a shortening of the cable, which can be simulated as a temperature drop. The effect of creep and shrinkage can be analyzed in a similar way. However, due to the redistribution of stresses between the individual components of the concrete section, an iterative approach has to be used. To facilitate this analysis, standard computer programs for continuous cables are used.

In step 2, shear and bending stresses in single spans are calculated using the analysis of the bending of the simple cable. The cable is analyzed for the load $q(x)$, and for the horizontal force and deformations of the supports that were determined in step 1.

Since the bending moments were relatively large, the support sections should be analyzed as partially prestressed members and therefore a reduction of the bending stiffness caused by cracks should be considered in the analysis.

12.4.3 Analysis of the Stress Ribbon as a Geometrically Non-Linear Structure

Modern structural programs allow us to follow the behavior of the stress ribbon structures both during erection and during service. These programs also need to capture the large deformation and the tension stiffening effects. The structure can be modeled as a chain of parallel members that represent bearing tendons (BT), prestressing tendons (PT), precast segments (PS) and cast-in-place slab (CS) or trough (see Figure 12.30b). Bearing and prestressing tendons can be modeled as “cable” members, for which the initial force or strain has to be determined. Precast segments and cast-in-place slab can be modeled as 3D bars or as shell elements that have both bending and membrane capabilities.

Since the programs use so called “frozen members” it is possible to model a change of static system (from the cable into the stress ribbon) as well as the progressive erection of structure. The program systems also contain so called “contact” members that only resist compression forces. These members can be used for the modeling of saddles from where the stress ribbons can lift up.

In the analysis the initial stress in the tendons has to be determined. The initial forces are usually determined for the basic stage (see Figure 12.23c and 12.23d) where the structure changes from cable to stress ribbon. The initial forces in the cable are determined using the cable analysis.

Some programs have “cable members” that have zero stiffness (area and modulus of elasticity) in the initial stage. They are stressed by initial forces that exactly balance the external load. For all subsequent loads these elements are part of the structure—part of the global stiffness of the structure. This is the way to model the prestressing tendon.

Unfortunately in some programs the initial stage is modeled with an initial strain of tendons that also have actual stiffness (area and modulus elasticity), and therefore are part of the stiffness of the structure. Since a portion of the strain and corresponding stress is absorbed by their stiffness, it is necessary to artificially increase their initial strain such that the strain and corresponding stress in tendons exactly balances the load at the basic stage. That means that the initial stage has to be determined by iteration.

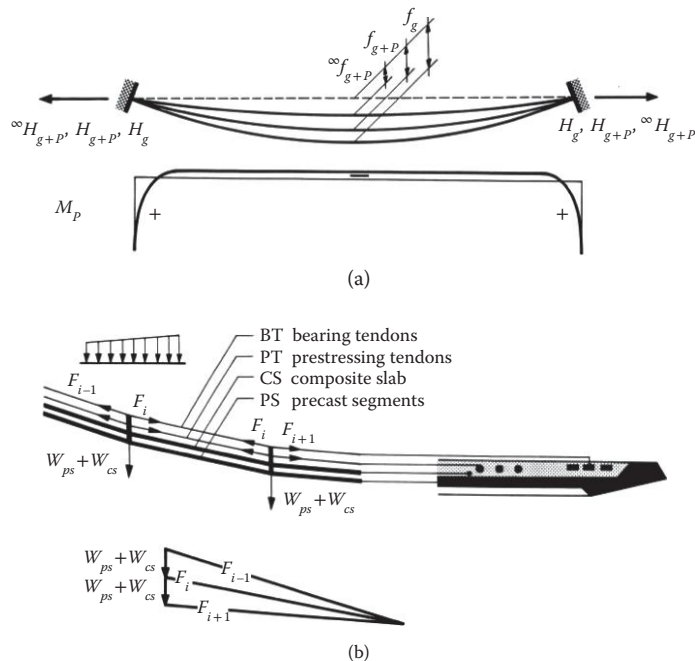


FIGURE 12.30 Stress ribbon structure: (a) deformation and bending moments and (b) modeling of the deck.

The analysis that starts from the basis stage can be used for both the analysis of the erection and service stages. The stresses in the structure during erection and the bearing tendons jacking forces are determined by simulating a progressive unloading of the structure. Since the superposition principle does not apply, the analysis of the service stage should be carried out according to the following flow chart.

Figure 12.30 shows deformed shapes and bending moment (a), and a calculation model (b) of a one span structure loaded by dead load, prestress, and creep and shrinkage of concrete. It is evident that due to creep and shrinkage the sag is reduced and therefore all internal forces are higher at time t_∞ .

Furthermore, since the area of the bearing and prestressing tendons is higher than in traditional concrete structures, a significant redistribution of stresses between steel and concrete occurs with time. In structures assembled from precast segments and cast-in-place slab the redistribution of stresses between these members also has to be considered.

For the analysis of the creep and shrinkage it is necessary to perform a time dependent analysis (Strasky et al. 2011). It is not possible to analyze the structure in a single step for the initial strain caused by creep and shrinkage. This would cause significantly larger deformations and higher bending moments at the supports.

12.4.4 Dynamic Analysis

Recently several pedestrian bridges exhibited unacceptable performance due to vibration caused by people walking or running on them. Also wind can cause an unpleasant movement. Dynamic actions induced by people result from rhythmical body motions of persons (Bachmann 2002; fib 2005).

Typical pacing frequencies f_s of walking person is 2 Hz, of running person is $f_r = 2.5$ Hz. To avoid the resonance some standards specify that pedestrian bridges with fundamental frequencies below 3 Hz should be avoided (AASHTO 2009). However, all stress ribbon and suspension pedestrian bridges designed by the author have these fundamental frequencies below 2 Hz. Although they have been built since 1979, no complaints on their dynamic behavior have been reported.

It is obvious that rather than checking the natural modes and frequencies, a speed of motion or acceleration of the bridge deck caused by forced vibration, which represents the effects of moving people, should be checked.

According to (UKDOT 1988) the maximum vertical acceleration should be calculated assuming that the dynamic loading applied by a pedestrian can be represented by a pulsating point load F , moving across the main span of the superstructure at a constant speed v_t as follows.

$$F = 180 \cdot \sin 2\pi f_0 T \quad (12.73)$$

$$v_t = 0.9 f_0 \quad (12.74)$$

where point load F is in N, T is the time in s and speed v_t is in m/s.

The maximum vertical acceleration should be limited to $0.5\sqrt{f_0}$ m/s².

With every step, there is also a horizontal power that interacts with the bridge. While the vertical power has a downward effect by each footstep, the horizontal power sends our force alternatively to the right and to the left. This is why we are dealing with a case of resonance if

Vertical vibration: $f_v = f_s$

Horizontal vibration: $f_h = f_{s/2}$

Step frequencies f_s of about 2.0 Hz will affect bridges with vibrations of 1.0 Hz with substantial horizontal deformations. Circumstances $f_v = 2f_h$ should be avoided.

It is evident that a response of the stress ribbon structures for a dynamic load caused by people and wind has to be checked. Also, response to earthquake loading has to be verified. Typically, the first step is to determine the natural modes and frequencies followed by the check of the dynamic response due to the moving load.

For final design the dynamic analysis should be done with a calculation model that includes non-linear analysis. It is important to realize that the dynamic analysis is usually linear and that most programs are able to describe the special behavior of the stress ribbon and cable supported structures only by using the so called tension stiffening effect.

When analyzing multi-span structures it is noted that the bridge behaves as a continuous structure only when there is horizontal displacement of the supports. For a small load, as caused by a group of pedestrians, the change of stresses is very small and the individual spans behave as isolated cables. Therefore, when the structure is checked for motions that can cause unpleasant feeling, the dynamic analysis should be done for the individual spans in addition to the overall structure.

12.4.5 Designing of Structural Members

The stress ribbon structures are designed as ordinary structural concrete. As such, it is reasonable to check all members as partially prestressed where crack width and fatigue stresses in tendons and reinforcing steel are checked. Also maximum compression stresses in the concrete should be verified.

Since the stress range in the prestressed band is within the stress range of ordinary prestressed concrete structures, the stresses in the bearing and prestressing tendons should be treated as ordinary prestressing tendons in accordance with the appropriate national standard. Usually for bonded tendons maximum service stresses should not exceed $0.7f_u$, for unbonded tendons the stresses should not exceed $0.6f_u$.

Since at increasing load the joints and cracks in the concrete band open, the stress ribbon behaves as a cable at ultimate loading (see Figure 12.24g). The load is resisted both by the bearing and prestressing tendons. Since the additional load causes larger sag, the stresses in the tendons increase less than linearly with the load. This explains why it is possible to use relatively high allowable stresses in the tendons for service load.

12.4.6 Example of the Analysis

In Figures 12.31 through 12.33 calculation models and some results of the analysis of the Bridge across the Medway River, Maidstone, Kent, UK are presented in Strasky (2003). The structure was modeled as 3D structures assembled from parallel 3D elements that modeled precast segments (PS), composite slab (CS), bearing (BT) and prestressing tendons (PT). The length of the elements corresponded to that of the segments.

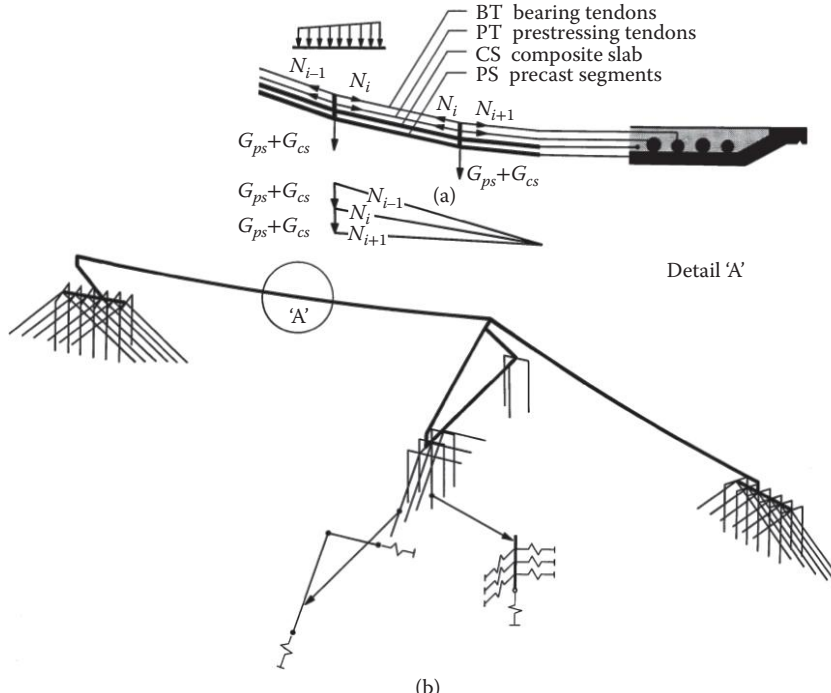


FIGURE 12.31 Bridge across the Medway River, Maidstone, Kent, UK: calculation model. (a) Local model, Detail 'A' and (b) global model.

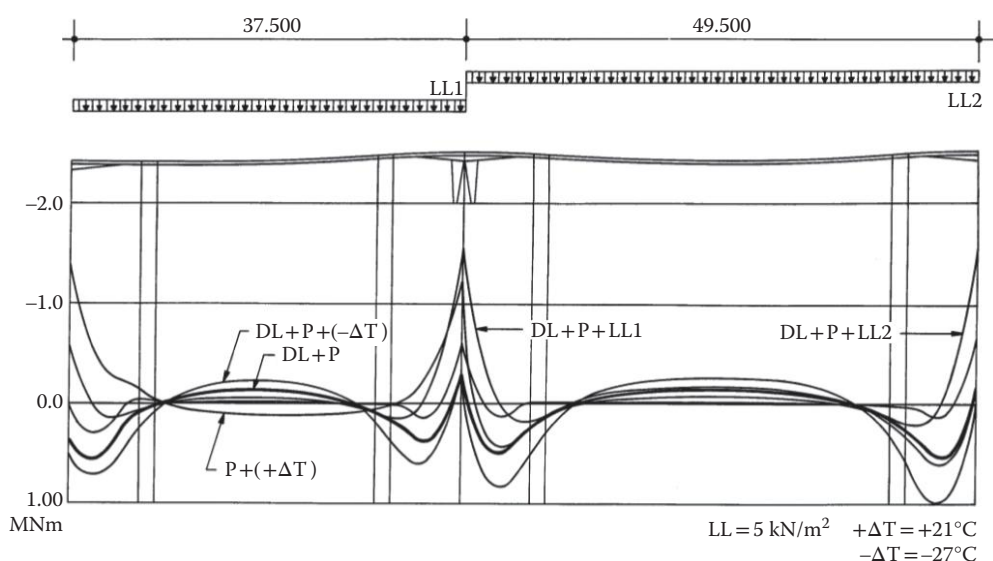


FIGURE 12.32 Bridge across the Medway River, Maidstone, Kent, UK: bending moments in the deck.

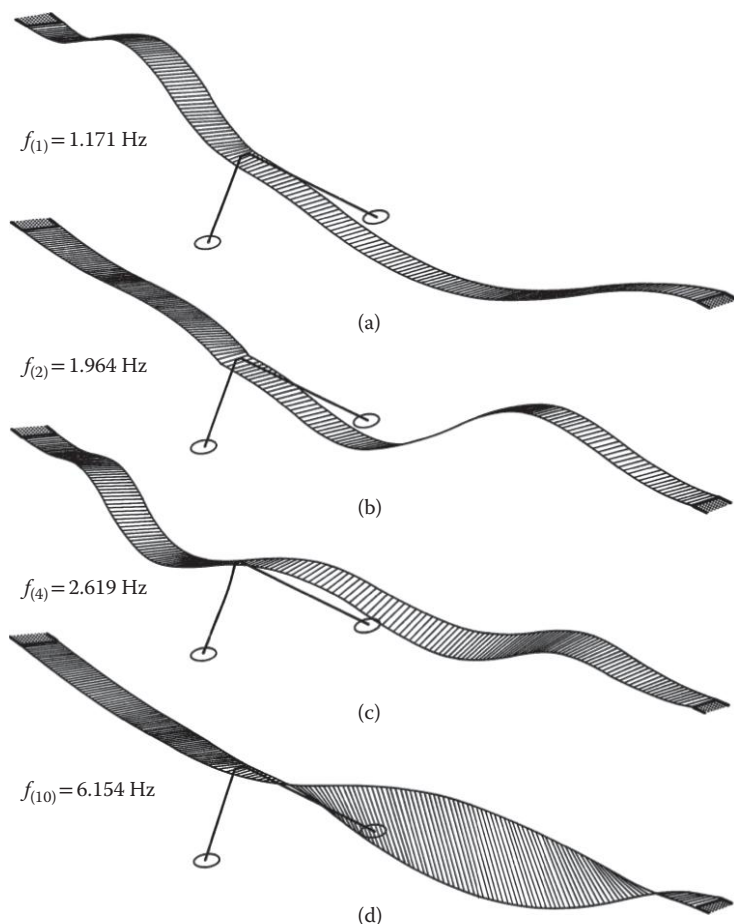


FIGURE 12.33 Bridge across the Medway River, Maidstone, Kent, UK: natural modes and frequencies.

In this bridge the saddles were modeled by 3D beam elements of 0.5 m length that had varying depth corresponding to that of the haunches. From the figures it is evident that the calculation models can describe the actual arrangement of the stress ribbon structures including their flexible connection to the soil.

Figure 12.32 presents the bending moment diagrams in the stress ribbon deck of the Maidstone Bridge. Due to the arrangement of the prestressing tendons at the abutments and pier haunches, the positive bending moments that usually appear at those locations were significantly reduced. From the natural modes and frequencies shown in Figure 12.33 it is evident that this complex structure vibrates in compound modes. This also demonstrates the good behavior of this slender structure.

The forced vibration (Strasky, Necas, and Kolacek 2012) determined the maximum amplitude $\max u = 3.710 \text{ mm}$ (0.15 in.), maximum speed of motion $\max v = 0.031 \text{ m/s}$ (1.02 ft./s) and maximum acceleration $\max a = 0.260 \text{ m/s}^2$ (0.85 ft./s²). This value is smaller than limited acceleration $a_{\lim} = 0.471 \text{ m/s}^2$ (1.545 ft./s²). Although the structure is extremely slender, and first bending frequencies are close to 2 Hz, the users do not have an unpleasant feeling when standing or walking on the bridge.

12.5 Stress Ribbon Supported by Arch

The intermediate support of a multi-span stress ribbon (see Figure 12.14) can also have the shape of an arch (see Figure 12.34). The arch serves as a saddle from which the stress ribbon can rise during post-tensioning and during temperature drop, and where the band can rest during a temperature rise.

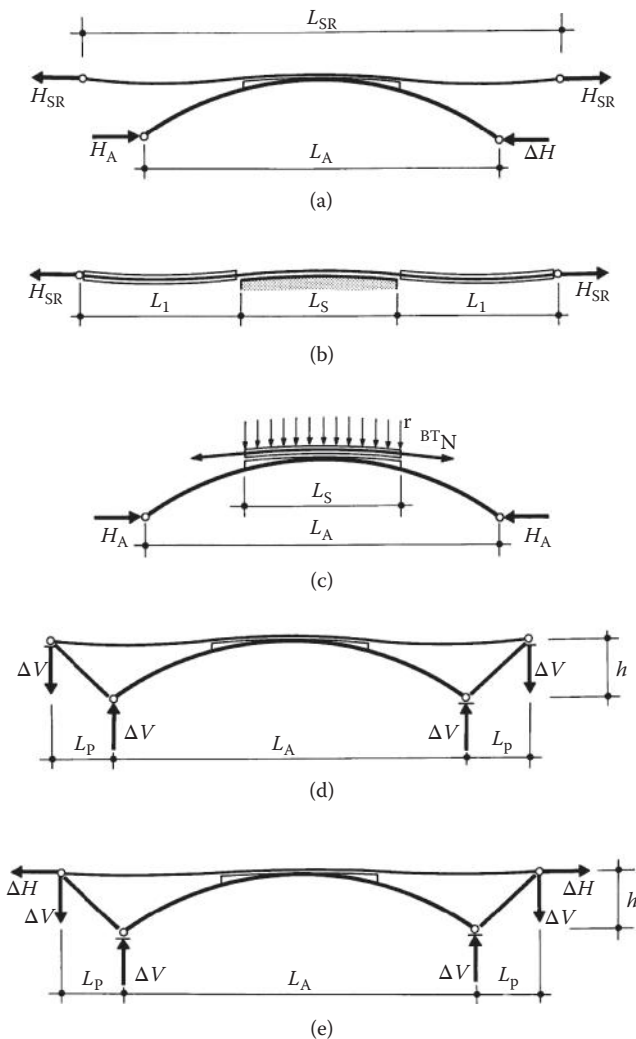


FIGURE 12.34 Stress ribbon supported by arch: (a) stress ribbon and arch, (b) stress ribbon, (c) arch, (d) self-anchored system, and (e) partially self-anchored system.

In the initial stage the stress ribbon behaves as a two span cable supported by the saddle that is fixed to the end abutments (see Figure 12.34b). The arch is loaded by its self-weight, the weight of the saddle segments and the radial forces caused by the bearing tendons (see Figure 12.34c). After post tensioning the stress ribbon with the prestressing tendons, the stress ribbon and arch behave as one structure.

The shape and initial stresses in the stress ribbon and in the arch can be chosen such that the horizontal forces in the stress ribbon H_{SR} and in the arch H_A are the same. It is then possible to connect the stress ribbon and arch footings with compression struts that balance the horizontal forces. The moment created by horizontal forces $H_{SR} \cdot h$ is then resisted by the $\Delta V \cdot L_p$. In this way a self-anchored system with only vertical reactions is created (see Figure 12.34d). This self-anchored system eliminates the anchoring of horizontal forces in the upper soil layers.

In some cases—due to the slope limitations of the stress ribbon—the deck has to have very small sag and the corresponding horizontal force becomes very large. A supporting arch that would balance this force would result extremely flat. If the topography requires an arch of higher rise, it is then possible to develop a partially self-anchored system.

The arch is designed for an optimum rise and its corresponding horizontal force. This horizontal force H_a is then transferred by the inclined props into the stress ribbon's anchor blocks. The anchor blocks have to resist only the difference

$$\Delta H = H_s - H_a$$

The moment created by horizontal forces $H_a \cdot h$ is then resisted by the couple $\Delta V \cdot L_p$.

It is possible to develop many partially self-anchored systems in which the arch helps to reduce the stress ribbon's horizontal force. Figure 12.35 describes a static function of one possibility. In the initial stage the arch is loaded only by its self-weight and the weight of the saddle segments. In this case, the stress ribbon forms a one span structure where the bearing tendons only carry the weight of the segments at either side of the saddle.

The horizontal force H_A is then transferred by means of the inclined struts into the stress ribbon's anchor blocks that now have to resist only the difference

$$\Delta H = H_{SR} - H_A$$

The moment created by horizontal forces $H_A \cdot h$ is then resisted by a couple of vertical forces $\Delta V \cdot L_p$.

It is also obvious that the stress ribbon be suspended from the arch. It is then possible to develop several of fully or partially self-anchored systems. Figure 12.36 presents some concepts using such systems.

Figure 12.36a shows an arch fixed at the anchor blocks of the slender prestressed concrete deck. The arch is loaded not only by its own self weight and the stress ribbon's, but also with the radial forces of the prestressing tendons.

Figure 12.36b shows a structure that has a similar static behavior as the structure presented in Figure 12.36d. The two span stress ribbon is suspended on an arch that serves as a "saddle" on which the prestressed band changes curvature. In the initial stage the stress ribbon behaves as a two span cable supported by the saddle (see Figure 12.34b). The arch is loaded by its self-weight, the weight of the saddle segments and the radial forces caused by the bearing tendons. When the stress ribbon is post-tensioned the stress ribbon and arch behave as one structure.

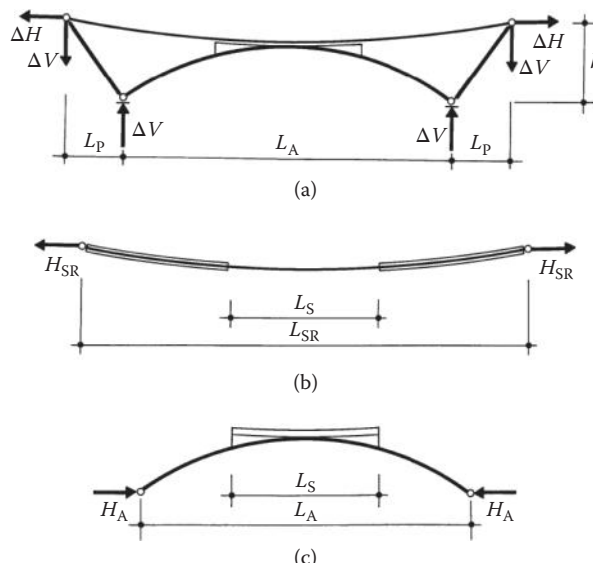


FIGURE 12.35 Stress ribbon supported by arch: (a) partially self-anchored system, (b) stress ribbon, and (c) arch.

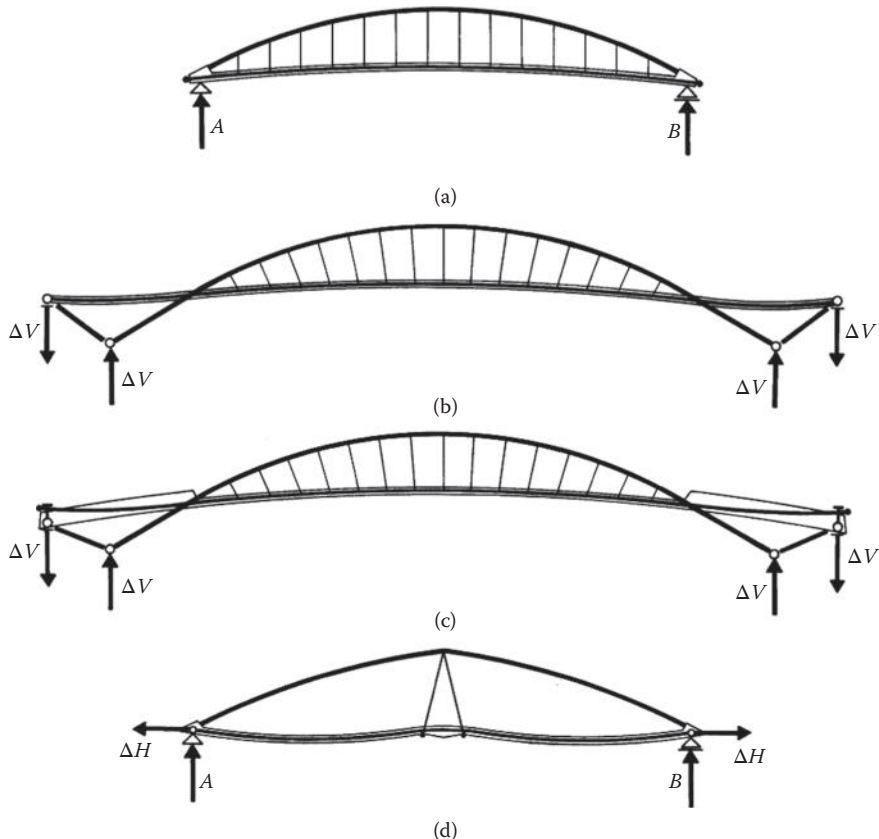


FIGURE 12.36 Stress ribbon suspended on arch: (a) tied arch, (b) tied arch with side spans, (c) tied arch with flexural stiff side spans, and (d) two span stress ribbon suspended on arch.

To reduce the tension force at the stress ribbon anchor blocks, it is possible to connect the stress ribbon and arch footings by compression struts that fully or partially balance the stress ribbon horizontal forces.

Figure 12.36c shows a similar structure in which the slender prestressed concrete band has increased bending stiffness in the non-suspension portion of the structure not suspended from the arch.

Figure 12.36d presents a structure in which the change of curvature of the prestressed band is accomplished in a short saddle that is suspended from the arch. Since the arch is loaded by its self-weight and by a point load from the stress ribbon, it should have the funicular shape corresponding to this load.

The described structures were carefully analyzed and statically and dynamically tested on physical models. The first applications presented in Section 12.6—Examples proved the economy of the solution.

12.6 Examples

12.6.1 DS-L Bridges: Bridge across the Vltava River in Prague-Troja, Czech Republic

In the course of years 1978–1985 the author, as a chief designer of the firm Dopravní stavby Olomouc, Czechoslovakia designed seven stress ribbon bridges of the similar arrangement (Stráský 1987b and 2011). The firm marked these structures as DS-L Bridges. The bridges have one, two, or three spans of maximum length of 102 m (335 ft.); the maximum length of the bridge is 261.20 m (857.0 ft.). All these

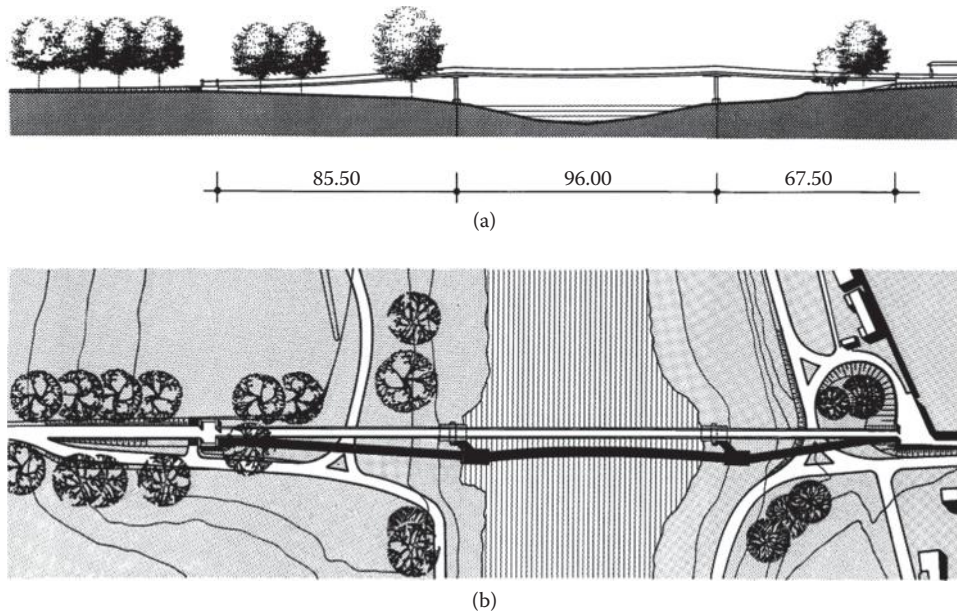


FIGURE 12.37 Prague-Troja Bridge: (a) elevation and (b) plan.

bridges are assembled of the same precast segments and have similar structural arrangement that is demonstrated on the examples of the bridge built in 1984 in Prague—Troja (Strasky 1987a).

The bridge of the total length of 261.20 m (857.0 ft.) crosses the Vltava River in the north suburb Prague—Troja. It connects the Prague ZOO and Troja Chateau with sports facilities situated on the Emperor Island and with the park Stromovka (see Figure 12.37).

The bridge has three spans of lengths of $85.50 + 96.00 + 67.50$ m (280.51 + 314.96 + 221.46 ft.); the sags at mid-spans are 1.34, 1.69, and 0.84 m (4.40, 5.55, and 2.76 ft.). The stressed ribbon is formed by precast segments and by cast-in-place saddles (pier tables) frame connected with intermediate piers (see Figure 12.38). At the bottom of the piers concrete hinges, which allow rotation in the longitudinal direction of the bridge, were designed. The horizontal force from the stress ribbon is resisted by wall diaphragms and micropiles.

The decks of all bridges are assembled of two types of segments: *waffle* segments that form the prevailing part of the deck and *solid* segments designed at the abutments. The precast segments are 3.00 m (9.84 ft.) long, 3.80 m (12.47 ft.) wide and have the depth 0.30 m (9.84 ft.) (see Figure 12.39). The section of the *waffle* segments is formed by edge girders and a deck slab. At joint between the segments the section is stiffened by low diaphragms.

During the erection the segments were suspended on bearing tendons situated at troughs, after the casting of the joints between the segments, the deck was post-tensioned by prestressing tendons situated in the deck slab (see Figure 12.40). Bearing and prestressing tendons are formed by 6-0.6" strands.

Erection of the deck started by placing the solid segments on the neoprene pads situated on the front portion of the abutments. Then the first half of the bearing tendons was pulled across the river and tensioned to the design stress. The tendons were supported by steel saddles situated on the piers.

Then the segments were erected by a mobile crane. The segments were suspended on bearing tendons and shifted along them into the design position. At first, the segments of the side spans were erected, and then the segments of the main span.

After all segments were erected the second half of the bearing tendons was pulled and tensioned to the design stress. In this way the structure reached the design shape. Then the steel tubes that form the ducts in the joints between the segments were placed and prestressing tendons were pulled through the deck.

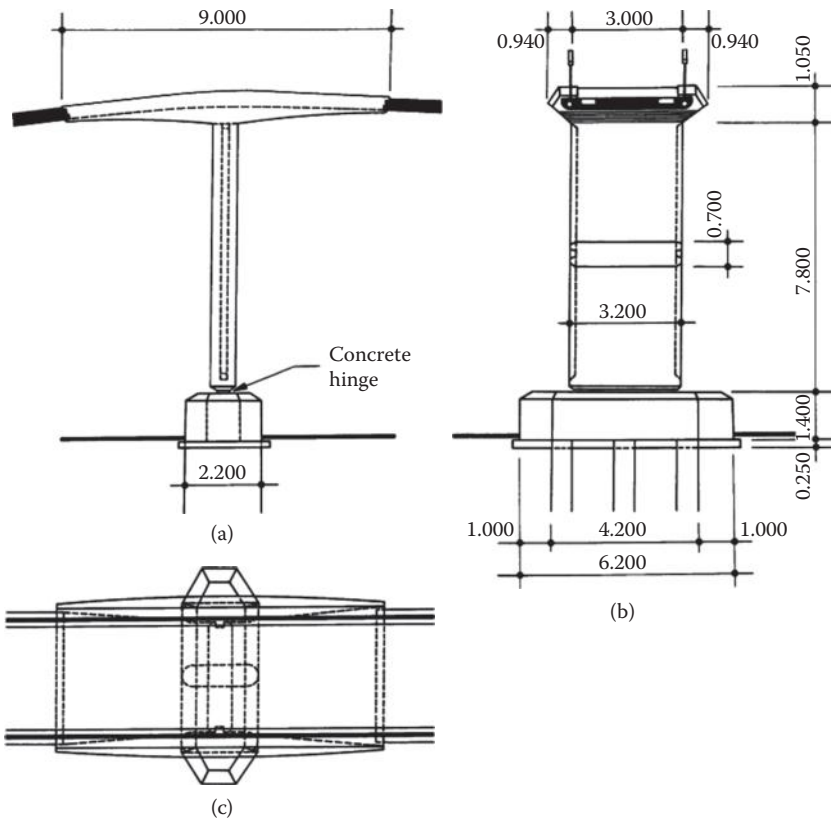


FIGURE 12.38 Prague-Troja Bridge—pier table: (a) elevation, (b) cross section, and (c) plan.

Then the reinforcing steel of the troughs and saddles was placed and the joints, troughs and saddles were cast. At first the side spans were cast, then the central span and saddles. The saddles were cast in formworks that were suspended on the already erected segments and were supported by the piers (see Figure 12.19).

The static assumptions and quality of the workmanship were also checked by a static and dynamic loading test see Figure 1.4. In 2001 when exceptional flood has occurred in Prague, the pedestrian bridge was totally flooded. Careful examination of the bridge done after the flood has confirmed that the structure was without any structural damages.

The DS-L bridges were well accepted by the public and so far no problems with their static or dynamic performance have occurred. The dynamic tests have confirmed that is not possible to damage the bridges by an excessive vibration caused by people (a case of vandalism) and that the speed and acceleration of motion caused by people is within acceptable limits.

12.6.2 Sacramento River Trail Bridge, Redding, California

The Sacramento River trail and connecting bridge form part of the City of Redding's park system. The riverbanks have extensive rock outcropping that dramatically increases the beauty of the basin. To preserve this natural terrain and to mitigate adverse hydraulic conditions, it was important to avoid founding any piers in the river basin (Redfield and Strasky 1992) (see Figures 12.41 and 12.42).

The bridge is formed by a stress-ribbon of the span of 127.40 m (481 ft.). During the service of the bridge the sag at mid span varies from 3.35 m (11 ft.) (time 0 with maximum temperature and full live load) to 2.71 m (8.9 ft.) (time infinity with minimum temperature). Apart from a distance of 4.20 m

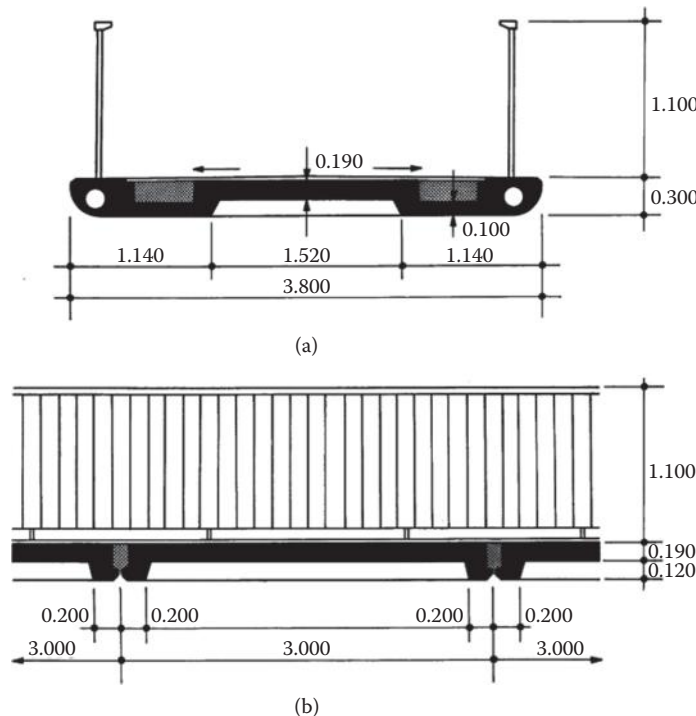


FIGURE 12.39 Prague-Troja Bridge—deck: (a) cross section and (b) partial elevation.

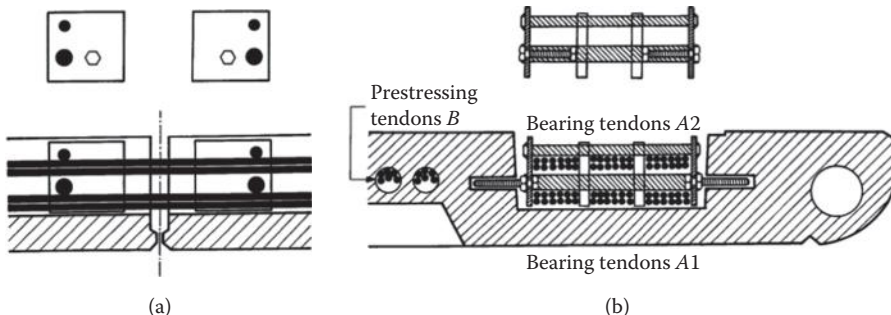


FIGURE 12.40 Prague-Troja Bridge—bearing and prestressing tendons: (a) partial elevation and (b) partial cross section.

(13.8 ft.) at each end abutment, where the deck is haunched to 0.914 m (3 ft.), the deck has a constant depth of 0.381 m (1.25 ft.). The stress ribbon is assembled of precast segments suspended on bearing tendons (see Figure 1.3) and it is post-tensioned by prestressing tendons. Both bearing and prestressing tendons are placed in troughs situated at the edges of segments. Horizontal force from the stress ribbon is resisted by rock anchors.

The bridge was designed as a geometrically non-linear structure. The haunches were designed as partially prestressed members in which tension forces at bottom fibers are resisted by reinforcing steel. Bridge vibration studies were carefully considered in the design for a wide range of pace frequencies, including jogging and the remote possibility of vandals attempting to physically excite the bridge. Because the bridge is an extremely shallow band with a long span, an aeroelastic study was deemed necessary to check the stability under dynamic wind loads.



FIGURE 12.41 Redding Bridge—completed structure (slide).

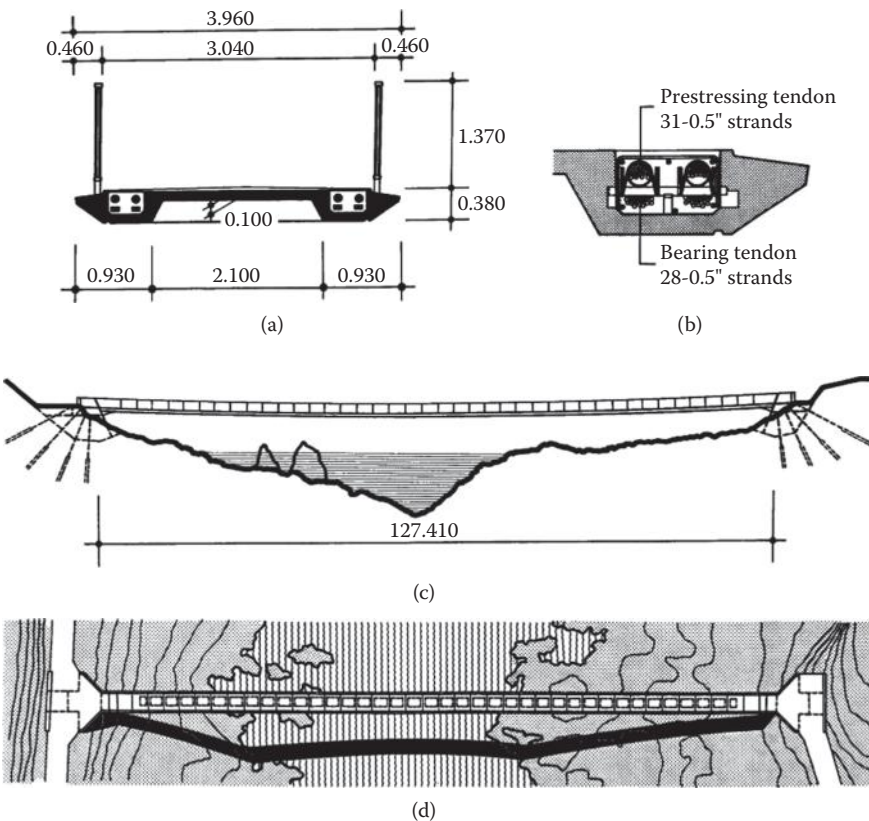


FIGURE 12.42 Redding Bridge: (a) cross section, (b) bearing and prestressing tendons, (c) elevation, and (d) plan.

@Seismicisolation

The construction of the bridge was commenced by casting of the abutments and installation of the rock anchors. Then the bearing tendons were pulled across the river and post-tensioned to the design stress. Subsequently the segments were suspended on bearing tendons and shifted along them into the design position. All segments were erected within 2 days. Then the prestressing tendons were placed directly above the bearing tendons, and joints and troughs were cast. By post-tensioning of prestressing tendons the structure received the required stiffness.

Due to the first use of the stress ribbon in the United States, it was considered prudent to load test the bridge and verify the structural behavior with the design assumptions. A successful test was conducted on the completed bridge with 24 vehicles spaced over the whole length of the structure. The bridge was built in 1990.

The bridge was designed by Charles Redfield, Consulting Engineer and Jiri Strasky, Consulting Engineer; the contractor was Shasta Constructors Inc.

12.6.3 Lake Hodges Bridge, San Diego, California

The world's longest stress ribbon bridge is located in the northern part of San Diego County and it is a part of the San Dieguito River Valley Regional Open Space Park (Sánchez, Tognoli, and Strasky 2008) (see Figure 12.43). The bridge is formed by a continuous stress ribbon of three equal spans of length of 108.58 m (356.23 ft.) (see Figure 12.44). The sag at mid-spans is 1.41 m (4.63 ft.). The stress ribbon of the total length of 301.75 m (990 ft.) is assembled of precast segments and cast-in-place saddles situated at all supports. The stress ribbon is fixed into the end abutments and it is frame connected with intermediate piers. The structural solution was developed from the pedestrian bridges built in Prague-Troja and in Redding.

The precast segments of the depth of 0.407 m (1.34 ft.) are 3.048 m (10 ft.) long and 4.266 m (14 ft.) wide. Each segment is formed by two edge girders and a deck slab. At joints the segments are strengthened by diaphragms. During the erection the segments were suspended on bearing cables and shifted along them to the design position. After casting of saddles and joints between segments, the stress



FIGURE 12.43 Lake Hodges Bridge, CA

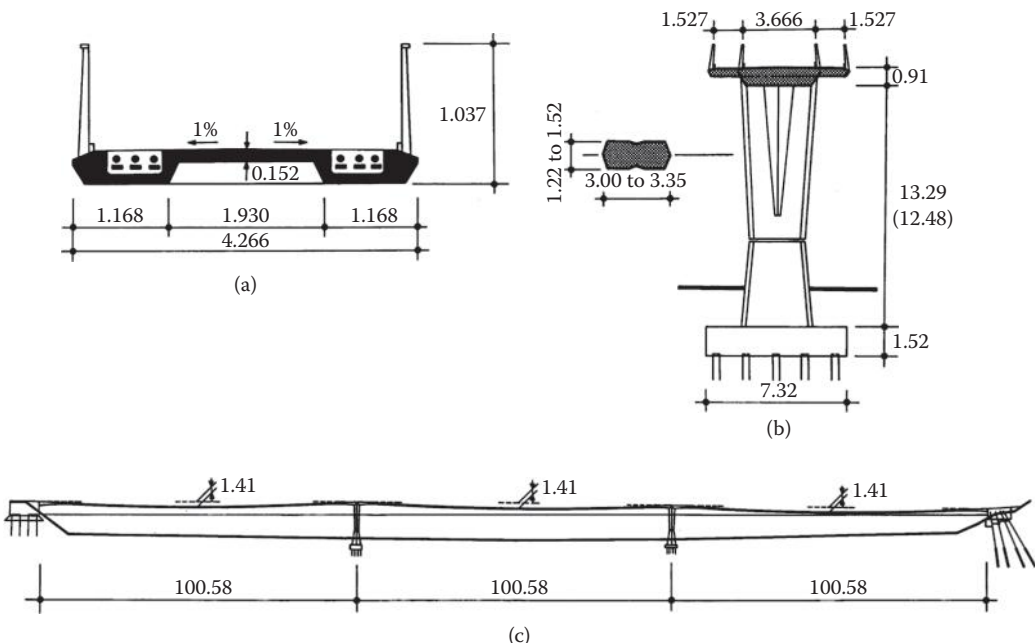


FIGURE 12.44 Lake Hodges Bridge, CA: (a) cross-section of the deck, (b) pier elevation, and (c) elevation.

ribbon was post-tensioned by prestressing tendons. The bearing cables are formed by 2×3 cables of 19-0.6" strands, the prestressing tendons are formed by 2×3 tendons of 27-0.6" strand. Both bearing cables and prestressing tendons are placed in the troughs situated at the edge girders.

The saddles have a variable depth and width. The depth varies from 0.407 to 0.910 m (1.34–3 ft.), the width change from 4.266 to 7.320 m (14–24 ft.). Above supports viewing platforms with benches were created. The saddles were cast after erection of all segments in the formwork suspended on the already erected segments and supported by piers or abutments (see Figure 12.13b). During the erection the bearing cables were placed on Teflon plates situated on steel saddles (see Figure 12.13e).

The horizontal force as large as 53 MN (11,915 kip) is transformed into the soil at the left abutment by four drilled shafts of a diameter of 2.70 m (8.86 ft.), at the right abutment the horizontal force is resisted by rock anchors.

Extensive detailed static and dynamic analyzes have been performed. The structure was checked not only for service load but also for significant seismic load. The analyses have proved that the bridge will be comfortable to users and will remain elastic under seismic loading. To verify that the bridge would be stable under heavy winds, a special wind analysis was performed by West Wind Labs, CA. Wind tunnel tests on a 1/10 scale model of the bridge section were performed to determine the aerodynamic load characteristics of the bridge deck.

The bridge was completed in May 2009. The bridge was designed by T. Y. Lin International, San Diego with a collaboration of Jiri Strasky, Consulting Engineer; the contractor was Flatiron, Longmont, Colorado.

12.6.4 Bridge across the Medway River, Maidstone, Kent, UK

The pedestrian bridge that was built in 2001 forms part of a river park project along Medway in Maidstone, United Kingdom. The deck of the bridge is formed by a two span stress ribbon that was—for the first time—designed with a *cranked* alignment (see Figure 12.45) (Strasky 2003). The length of the bridge is 101.50 m (333 ft.), the span length of the main span bridging the river is 49.5 m (162.4 ft.), and the span length of the side span is 37.5 m (123 ft.). The angle plan between the spans is 25 degrees (see Figure 12.46).



FIGURE 12.45 Bridge across the Medway River, Maidstone, Kent, UK.

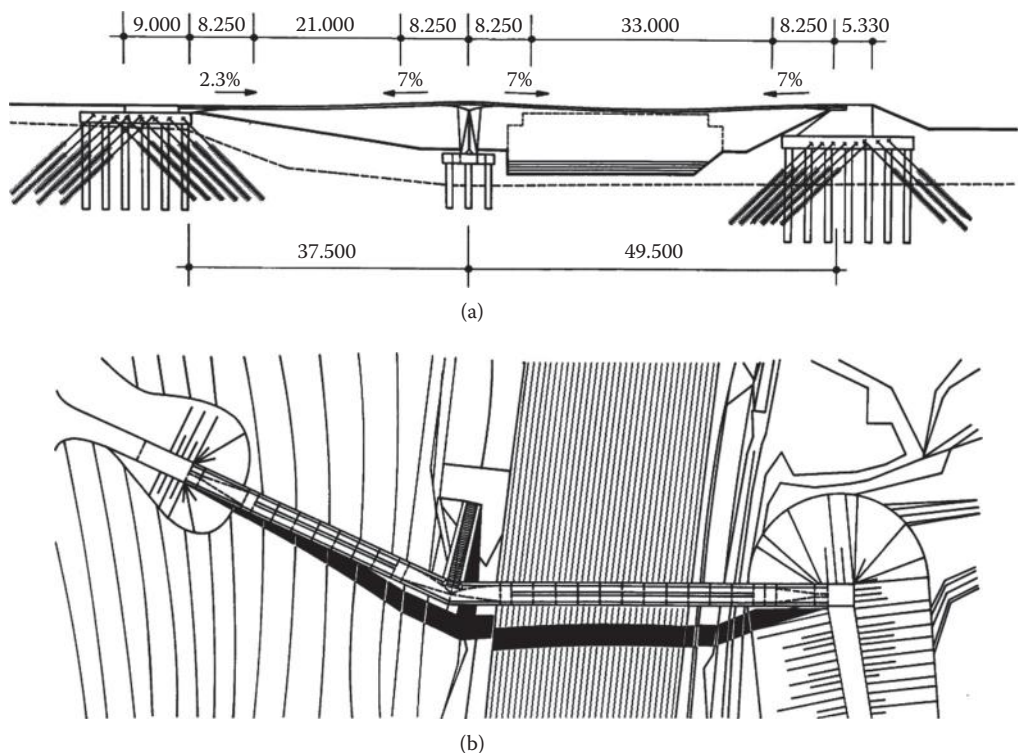


FIGURE 12.46 Bridge across the Medway River, Maidstone, Kent, UK; (a) elevation and (b) plan.

@Seismicisolation

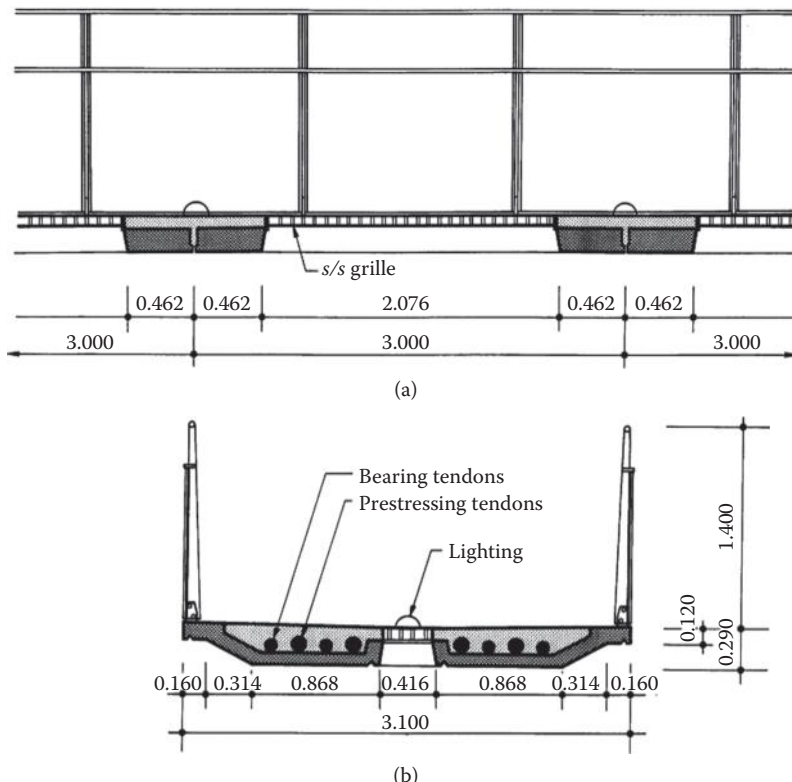


FIGURE 12.47 Bridge across the Medway River, Maidstone, Kent, UK—prestressed band: (a) partial elevation and (b) cross section.

The stress ribbon is formed by precast segments with a composite deck slab (see Figure 12.47). The segments are suspended on bearing cables and serve as a false-work and formwork for casting of the composite slab that was cast simultaneously with the joints between the segments. The stress ribbon is fixed into the abutments' anchor blocks and it is frame connected with the intermediate support. At all supports cast-in-place haunches are designed.

The precast segments of the length of 3.00 m (9.84 ft.) are formed by 80 mm (3.15 in.) thick slab that gives a form of the soffit and edges of the deck. In longitudinal axis of each segment a rectangular opening covered by stainless grid is designed. The opening serves for drainage of the deck and lighting of the underneath ground. Between the openings airport runway lights are situated.

Both the precast segments and the composite slab are post tensioned by prestressing tendons that are situated together with the bearing cables within the cast-in-place slab. The bearing cables and prestressing tendons are formed by 7 and 12 monostrands grouted in Polyethylene ducts. The arrangement of cables and tendons and their anchoring comply with special UK requirements for post-tensioned structures.

The intermediate support that is situated in the axis of the angle break resists the resultant horizontal force from the adjacent spans into the foundation by a system formed by a compression strut and a tension tie. The compression strut is formed by stairs, the tension tie is formed by a stainless steel tube. Since the value of the horizontal force depends on the position of the live load, for several loading cases the tube acts as a compression member too.

Large tension force from the stress ribbon is transferred into the soil formed by weald clay by a combination of vertical drilled shafts and inclined micro-piles.

The structure was designed on the basis of very detailed static and dynamic analyzes. The structure was modeled by a 3D frame flexibly fixed into the soil. The stress ribbon was modeled by mutually connected parallel members that can express the function of the bearing and prestressing cables, precast deck, and cast-in-place concrete. The analysis was performed by the program system ANSYS as a geometrically non-linear structure. In the initial stage, bearing-cable forces are in equilibrium with the self-weight of the deck.

The change of direction in the bridge deck plan creates transverse and torsional forces for which the structure was carefully checked. Similar to all stress ribbon structures significant bending stresses originate close to the supports. These stresses were reduced by designing of cast-in-place haunches that were checked as partially prestressed members.

In a dynamic analysis natural frequencies and modes were determined first. Then the speed and acceleration of the deck motion were checked. The response of the structure to a pulsating point moving along the deck, that represents the pedestrian loading, was checked.

Before the erection of the deck the abutments and the intermediate support including the haunches were cast. Until the tensioning of the bearing cables, the stability of the intermediate support was guaranteed by temporary supports. The bearing cables were erected as stay cables. At first, erection strands were pulled across the river and the left bank, then the PE ducts were suspended and moved into the design position. After that the monostrands were pushed through the ducts.

After the tensioning of the bearing cables the segments were erected by a mobile crane. At first the erected segment was placed on "C" frame, then transported into the design position under the bearing cables, lifted and suspended on the bearing cables (see Figure 12.22). All segments were erected in 1 day.

The geometry of the erected segments and horizontal deformation of the abutments were carefully checked. After the erection of the segments the tension force in the cables was corrected, the prestressing tendons and reinforcing steel of the composite slab were placed and the joints between the segments, closure and slab were cast. The slab was cast simultaneously in both spans symmetrically from the mid-spans to the closures. To guarantee that the concrete remains plastic until the entire deck is cast a retarder was used.

After 2 days the bearing and prestressing tendons were grouted. When the cement mortar reached a sufficient strength the prestressing tendons were post-tensioned to 15% of the final prestressing force. Partial prestressing prevented arising of cracks due to the temperature changes. When the concrete reached sufficient strength the structure was post-tensioned to the full design level. The function of the bridge was also verified by a dynamic test that proved that the users do not have a feeling of discomfort when walking or standing on the bridge.

The bridge was designed by Cezary M. Bednarski, Studio Bednarski, London, UK and by Strasky Husty and Partners, Consulting Engineers, Ltd., Brno, Czech Republic. UK liaison and checking was done by Flint & Neill Partnership, London, UK. The bridge was built by Balfour Beatty Construction Ltd., Surrey, UK.

12.6.5 Kikko Bridge, Japan

The Kikko Bridge is a three-directional stress-ribbon pedestrian bridge, built in 1991 at the Aoyama-Kohgen golf club in Japan (see Figures 12.48 and 12.49) (Arai and Ota 1994). It provides a convenient pedestrian link between the club-house and the courses, which are arranged around a pond.

The deck is formed by three stress ribbons mutually connected by central platform formed by a steel frame that is composite with a bottom precast slab and additionally cast top slab (see Figure 12.50). The stress ribbons are assembled of precast segments suspended on bearing tendons that are anchored at the abutments and the central steel frame. The continuity of the structure is given by post-tensioning of prestressing tendons anchored at the abutments and central platform. The bearing tendons are placed in the troughs situated close to edges of the section, prestressing tendons are situated in the deck slab. At the abutments cast-in-place haunches were designed. The horizontal force from stress ribbons is resisted by rock anchors.



FIGURE 12.48 Kikko Bridge. Courtesy of Sumitomo Mitsui Construction Co. Ltd.

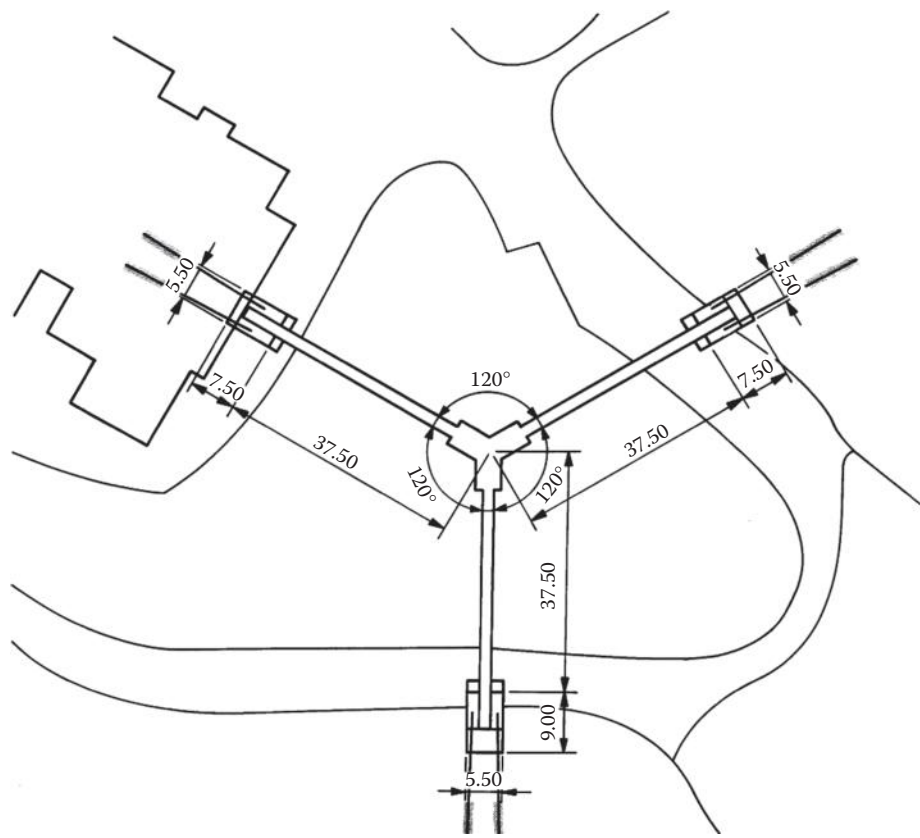


FIGURE 12.49 Kikko Bridge: plan.

@Seismicisolation

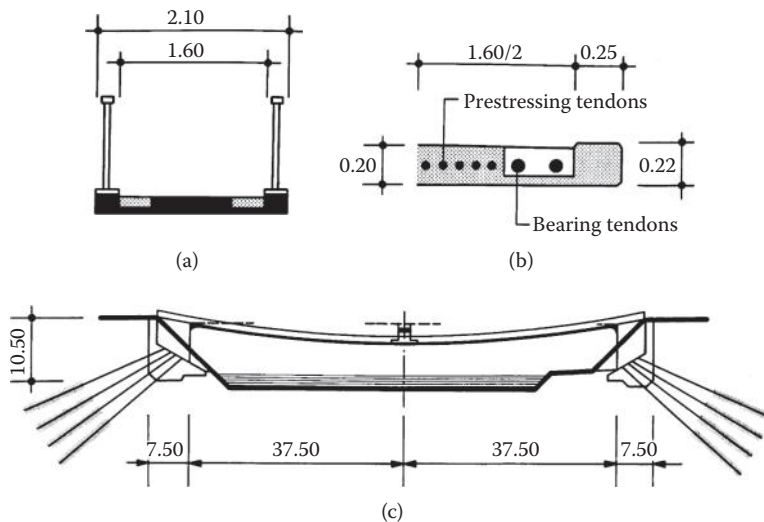


FIGURE 12.50 Kikko Bridge: (a) cross section, (b) bearing and prestressing tendons, and (c) elevation.

The construction of the bridges started by casting the abutments and by post-tensioning of the rock anchors. Then a central link formed by the steel frame and precast concrete slab was erected and temporary supported at the central of the bridge. Subsequently the bearing tendons were installed and post-tensioned. By post-tensioning the central link was lifted from the temporary support to the designed position.

After that the precast segments were suspended on bearing tendons. Then the troughs, joints between the segments, slab of the central platform and haunches were cast. By post-tensioning of prestressing tendons the structure got the designed shape and required stiffness.

The design of the structure required a complex static and dynamic analysis. The bridge was designed and built by Sumitomo Construction Co., Ltd.

12.6.6 Bridge across the Expressway R35 near Olomouc, Czech Republic

The bridge crosses an expressway R3508 near a city of Olomouc arch (Strasky 2010) (see Figure 12.51). The bridge is formed by a stress-ribbon of two spans that is supported by an arch (see Figure 12.52). The stress-ribbon of the length of 76.50 m (251 ft.) is assembled of precast segments 3.00 m (9.84 ft.) long supported and prestressed by two external tendons (see Figures 12.53 and 12.54).

The precast deck segments and precast end struts consist of high-strength concrete of a characteristic strength of 80 MPa (11.6 ksi). The cast-in-place arch consists of high-strength concrete of a characteristic strength of 70 MPa (10.15 ksi). The external cables are formed by two bundles of 31-0.6" diameter mono-strands grouted inside stainless steel pipes. They are anchored at the end abutments and are deviated on saddles formed by the arch crown and short spandrel walls.

The steel pipes are connected to the deck segments by bolts located in the joints between the segments. At the abutments, the tendons are supported by short saddles formed by cantilevers that protrude from the anchor blocks. The stress-ribbon and arch are mutually connected at the central of the bridge. The arch footings are founded on drilled shafts and the anchor blocks on micro-piles.

The bridge was erected in several steps. After the piles were placed, the end struts were erected and the arch footings and end anchor blocks were then cast. The arch was cast in a formwork supported by light scaffolding. When the concrete of the arch had sufficient strength, the external cables were assembled and tensioned. Then the precast segments were erected. After the forces in the external cables were adjusted, the joints between the segments were cast and subsequently the external tendons were tensioned up to the design stress.



FIGURE 12.51 Bridge Olomouc, Czech Republic.

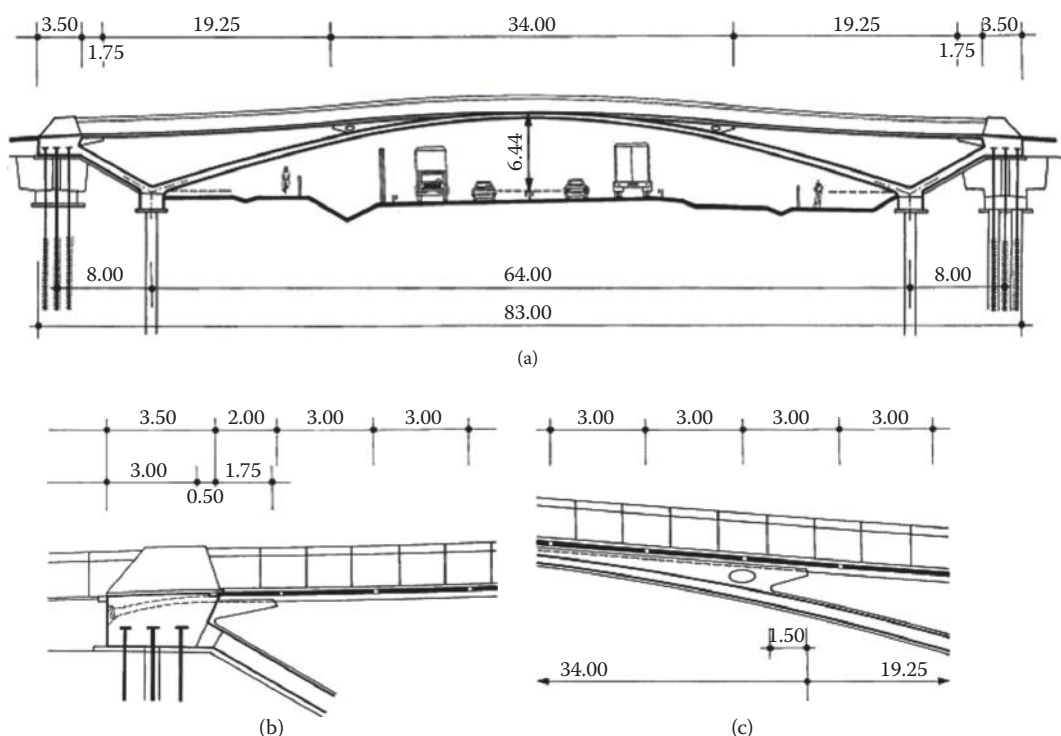


FIGURE 12.52 Bridge Olomouc, Czech Republic: (a) elevation, (b) partial elevation at anchor block, and (c) partial elevation at spandrel wall.

The structural solution was developed on the basis of a very detailed static and dynamic analysis. A great attention was also devoted to the analysis of the buckling of the arch. The stability analysis has proved that the structure has a sufficient margin of safety. Although the structure is extremely slender, the users do not have an unpleasant feeling when standing or walking on the bridge. The bridge was built in 2007.

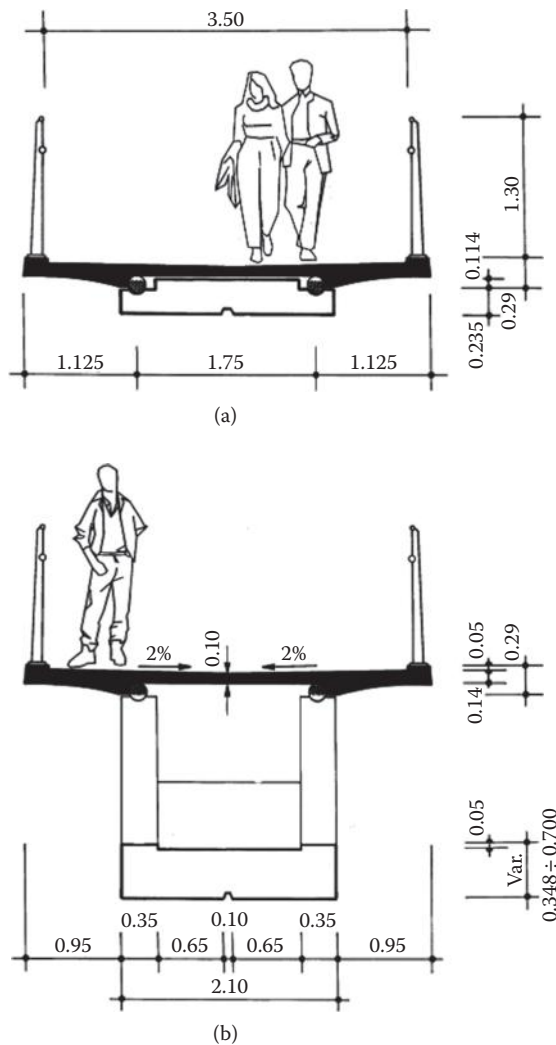


FIGURE 12.53 Bridge Olomouc, Czech Republic—cross-section: (a) at mid-span and (b) at spandrel wall.



FIGURE 12.54 Bridge Olomouc, Czech Republic—segment on external cables.

@Seismicisolation

The bridge was designed by the author's design firm Strasky, Hustý and Partners, Ltd., Brno, the bridge was built by firm Max Bögl a Josef Krýsl, k.s., Plzeň.

12.6.7 McLoughlin Boulevard Bridge, Portland, Oregon

The McLoughlin Boulevard Pedestrian Bridge (see Figure 12.55) is a part of a regional mixed-use trail in the Portland, Oregon metropolitan area (Strasky and Rayor 2007). The bridge is formed by a stress-ribbon deck that is suspended on two inclined arches (see Figures 12.56 and 12.57). Since the stress-ribbon anchor blocks are connected to the arch footings by struts, the structure forms a self-anchored system that loads the footing by vertical reactions only. The deck is suspended on arches via suspenders of a radial arrangement; therefore, the steel arches have a funicular/circular shape. The slender arches are formed by 450 mm-diameter pipes that are braced by two wall diaphragms.

The stress-ribbon deck is assembled from precast segments and a composite deck slab. In side spans, the segments are strengthened by edge composite girders. The deck tension due to dead load is resisted by bearing tendons. The tension due to live load is resisted by the stress-ribbon deck being prestressed by prestressing tendons. Both bearing and prestressing tendons are situated in the composite slab. The bearing tendons that were post-tensioned during the erection of the deck are formed by two bundles of 12 by 0.6" diameter strands that are protected by the cast-in-place slab; deck prestressing tendons are formed by six bundles of 10 by 0.6" diameter tendons that are grouted in ducts.

Edge pipes and rod suspenders make up part of the simple hanger system (see Figure 12.58). The suspenders connect to "flying" floor beams cantilevered from the deck panels to provide the required path clearance. The edge pipes contain a small tension rod that resists the lateral force from the inclined



FIGURE 12.55 McLoughlin Bridge, OR.

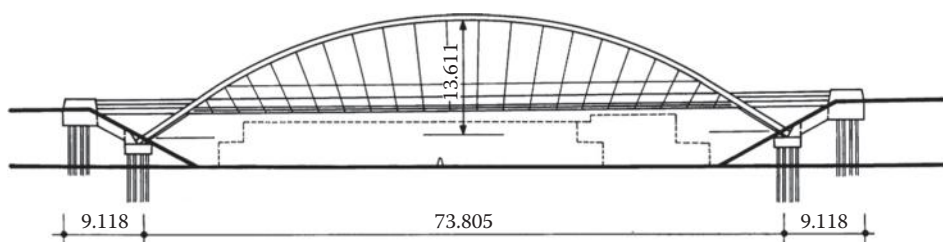


FIGURE 12.56 McLoughlin Bridge, OR—cross-sections: (a) main span, (b) bridge, and (c) side spans.

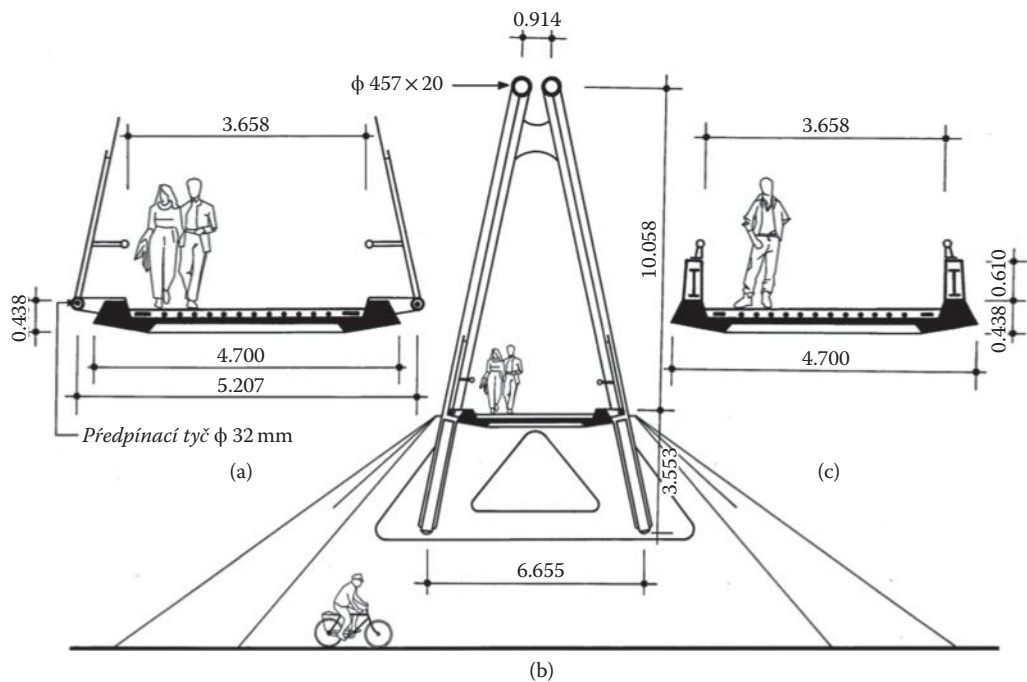


FIGURE 12.57 McLoughlin Bridge: elevation.

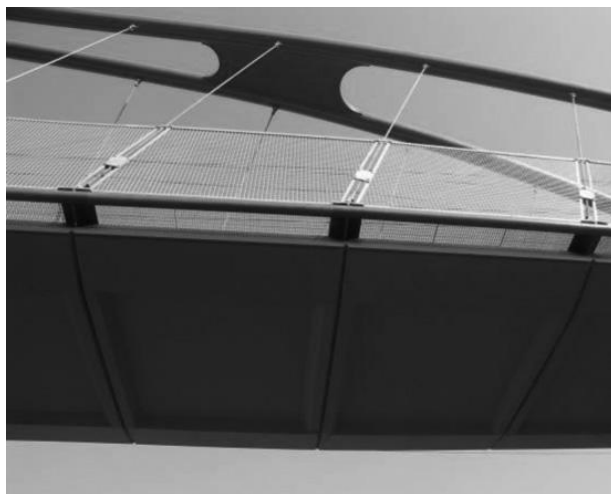


FIGURE 12.58 McLoughlin Bridge: stress ribbon deck.

suspenders on the end of the floor beams. Grating is used to span the gap between the edge pipe and the deck panels. Protective fencing is placed in the plane of the suspenders to open up the deck area, and the rail is cantilevered from the plane of the suspenders to open up the deck area, and the rail is cantilevered from the suspenders.

The structural solution was developed on the basis of very detailed static and dynamic analyzes. Great attention was also devoted to analysis of the buckling of the arch and the dynamic analyzes. The non-linear stability analysis has proved that the completed structure has a very large margin of safety. However, during construction when the load is resisted by the arches only, the margin of safety was

relatively low. Therefore, the erected structure was stiffened by a mid-span erection tower that loaded the arch by a controllable force.

Although the first bending frequency is below the walking frequency, the pedestrians do not have an unpleasant feeling when standing or walking on the bridge.

Construction of the bridge commenced in March, 2005, and was completed in September, 2006. The bridge was designed by OBEC, Consulting Engineers, and Jiri Strasky, Consulting Engineer. The bridge was built by Mowat Construction Company, Vancouver, Washington.

References

- AASHTO. 2009. *LRFD Guide Specifications for Design of Pedestrian Bridges*, 2nd Edition, American Association of State Highway and Transportation Officials, Washington, DC.
- Arai, H. and Ota, Y. 1994. "Prestressed Concrete Stress Ribbon Bridge—Kikko Bridge Prestressed Concrete in Japan 1994. Japan Prestressed Concrete Engineering Association. National Report," *XII FIP Congress*, Washington, DC.
- Bachmann, H. 2002. "Lively' Footbridges—A Real Challenge," *Footbridge 2002. Design and Dynamic Behavior of Footbridges*, OTUA Paris, France.
- fib*. 2005. *Guidelines for the Design of Footbridges, fib*—Guide to good practice prepared by Task Group 1.2. Fédération internationale du béton (*fib*) (ISBN 2-88394-072-X), Lausanne, Switzerland.
- Redfield, C. and Strasky, J. 1992. "Stressed ribbon pedestrian bridge across the Sacramento river in Redding, CA," *L'Industria Italiana del Cemento* pp. 82–99, N 663/1992, Roma, Italy.
- Sánchez, A., Tognoli, J. and Strasky, J. 2008. "The Lake Hodges Stress Ribbon Bridge, San Diego, California," *Conference Footbridge 2008*, Porto, Portugal.
- Strasky, J. 1987a. "The Stress Ribbon Footbridge across the River Vltava in Prague," *L'Industria Italiana del Cemento*, pp. 638–653, N 615/1987, Roma, Italy.
- Strasky, J. 1987b. "Precast Stress Ribbon Pedestrian Bridges in Czechoslovakia," *PCI Journal*, May–June, 32(3), 52–73.
- Strasky, J. 2003. "Millennium Bridge," *L'Industria Italiana del Cemento*, pp. 860–873, N792/November 2003, Roma, Italy.
- Strasky, J. 2010. "Recent Development in Design of Stress Ribbon Bridges," 3rd *fib* International Congress, Washington, DC.
- Strasky, J. 2011. *Stress Ribbon and Cable Supported Pedestrian Bridges*, 2nd Edition. Thomas Telford Publishing, London, UK (ISBN: 0 7277 3282 X).
- Strasky, J., Navratil, J., Susky, S. 2011. "Applications of Time-Dependent Analysis in the Design of Hybrid Bridge Structures," *PCI Journal*, July/August, 46(4), 56–74.
- Strasky, J., Necas, R. and Kolacek, J. 2012. "Dynamic Response of Footbridges," *Structural Concrete: Journal of the fib*, 13(2), 109–118.
- Strasky, J. and Rayor, G. 2007. "Design & Construction of OMSI-Springwater Trail McLoughlin Boulevard Bridge," *Western Bridge Engineers' Seminar*, September, Boise, Idaho.
- UKDOT. 1988. *Design Criteria for Footbridges*, Department of Transport, London, UK.
- Walther, R. 1969. "Spannbandbrücken," *Schweizerische Bauzeitung*, 87(8), 133–137.

13

Movable Bridges

Michael J. Abrahams
Parsons Brinckerhoff

Scott Snelling
Parsons Brinckerhoff

Mark VanDeRee
Parsons Brinckerhoff

13.1	Introduction	515
13.2	Types of Movable Bridges	516
	Bascule Bridges • Swing Spans • Vertical Lift Bridges • Retractile Bridges • Uncommon Types	
13.3	Structural Design.....	527
	Design Criteria • Bridge Balance • Counterweights • Foundations • Pier Protection • Vessel Collision • Movable Bridge Decks • Seismic Design	
13.4	Bridge Machinery	533
13.5	Bridge Operation, Power, and Controls	542
	Bridge Operations • Bridge Power • Bridge Control	
13.6	Traffic Control.....	545
	Glossary	546
	References	547
	Further Reading	547

13.1 Introduction

Movable bridges, sometimes referred to as draw bridges, are an integral part of the transportation system and have proven to be an economical solution to the problem of how to carry a railroad line or highway across an active waterway. Their development has been in concert with that of (1) the development of the railroads and (2) the development of our highway system. In the United States, movable bridges are found most commonly in states that have low coastal zones such as California, Florida, Louisiana, Washington State, Virginia, New York, and New Jersey, or a large number of inland waterways such as Michigan, Illinois, Wisconsin, and Minnesota.

Jurisdiction for movable bridges that cross navigable waterways currently lies with the U.S. Coast Guard. In most instances, marine craft have priority, and the movable span must open to marine traffic upon demand. This precedence was established in 1839 when a lawsuit (*Renwick vs. Morris*) was brought concerning a fixed dam and bridge that had been constructed across the Harlem River in New York City and the owner was forced to provide an opening so that navigation could pass through the dam. There is a famous 1852 Currier and Ives print, *View on the Harlem River, N. Y., the Highbridge in the Distance*, that shows the dam as modified to provide for navigation, illustrating the movable bridge that was constructed. And the ability to open for navigation is reflected in the terms “closed” and “open,” used to describe the position of the movable span(s). A “closed” movable bridge has closed the waterway to marine traffic, while an “open” bridge has opened the waterway to marine traffic. As a distinction, one would refer to a bridge that is not movable as a “fixed” bridge.

Highway bridges are typically designed to remain in the closed position and to only be opened when required by marine traffic. However, movable railroad bridges can be designed to remain in either the

open or closed position, depending on how frequently they are used by train traffic. The difference is important as different wind and seismic load design conditions are used to design for a bridge that is usually open versus one that is usually closed.

There are more than 3000 highway and railroad movable bridges in the U.S. It is the current policy of the Federal Highway Administration (FHWA) that “*a fixed bridge shall be provided wherever practicable*.” If there are “*social, economic, environmental, or engineering reasons*” and “*a cost benefit analysis to support the need for a new movable bridge*,” the FHWA may allow it. For many sites a low-level movable bridge will be significantly less expensive to construct versus a high-level fixed bridge or tunnel. However, a movable bridge is typically more expensive to maintain when compared to a fixed bridge of a similar size due to the need for staff to operate the bridge and to maintain the moving and electrical components. New movable bridges continue to be built in the United States, most often as replacements to existing, obsolete movable bridges. Sites particularly well suited for movable bridges include densely developed urban streets where high-level approaches may not be practical, as well as rural areas where traffic is light and the added expense of high-level approach spans is not justified.

The first American specification for the design and construction of movable bridges was published by the American Railway Association (ARA) in its 1922 *Manual of Railway Engineering* (ARA 1922). Until 1938 this specification was used to design and construct both movable highway and railroad bridges, when the American Association of State Highway Officials (AASHO) published its *Standard Specifications for Movable Highway Bridges* (AASHO 1938). Both specifications are very similar, but have remained separate. Today, the specifying body for railroads is the American Railway Engineering and Maintenance-of-Way Association (AREMA). Movable railroad bridges are currently designed in accordance with the AREMA Manual, Chapter 15, Part 6 (AREMA 2011), and new movable highway bridges are designed in accordance with the American Association of State Highway and Transportation Officials (AASHTO) *LRFD Movable Bridge Design Specifications* (AASHTO 2012a). However, prior to the publication of the AASHTO LRFD specifications, movable highway bridges were designed in accordance with the AASHTO *Standard Specifications for Movable Highway Bridges* (AASHTO 1988), and for the repair or retrofit of highway bridge designed using this older code one may elect to still use it rather than trying to utilize the newer LRFD code.

These specifications primarily cover the mechanical and electrical aspects of a movable bridge; the bridge's structural design is covered in other parts of the AREMA Manual for Railroad Bridges or the AASHTO *LRFD Bridge Design Specifications* (AASHTO 2012b). However, there are some specific areas where the movable bridge codes modify some issues regarding structural design and these will be included in Section 13.3.

13.2 Types of Movable Bridges

The three major categories of movable bridges are bascule, swing, and vertical lift, and these three types are specifically covered in the AREMA and AASHTO specifications. This list is not inclusive as there are other types of movable bridges. Uncommon types such as jackknife, reticulated, retracting, transporting, folding, gyratory, and floating will be briefly overviewed. The reader should be aware that movable bridges can be crafted to suit specific site needs and are not restricted to the types discussed in Section 13.2.4.

13.2.1 Bascule Bridges

Bascule bridges are related to medieval drawbridges that protected castles and are familiar illustrations in school books. The function is the same; the bascule span leaf (or leaves if there are two) rotates from the horizontal (closed) position to the vertical (open) position to allow use of the waterway below, or in the case of drawbridges to prevent access across a moat. Figure 13.1 illustrates a typical double-leaf through girder bascule bridge, the South Slough (Charleston) Bridge, Coos County, Oregon, which spans 126 feet (38.4 m) between trunnions.

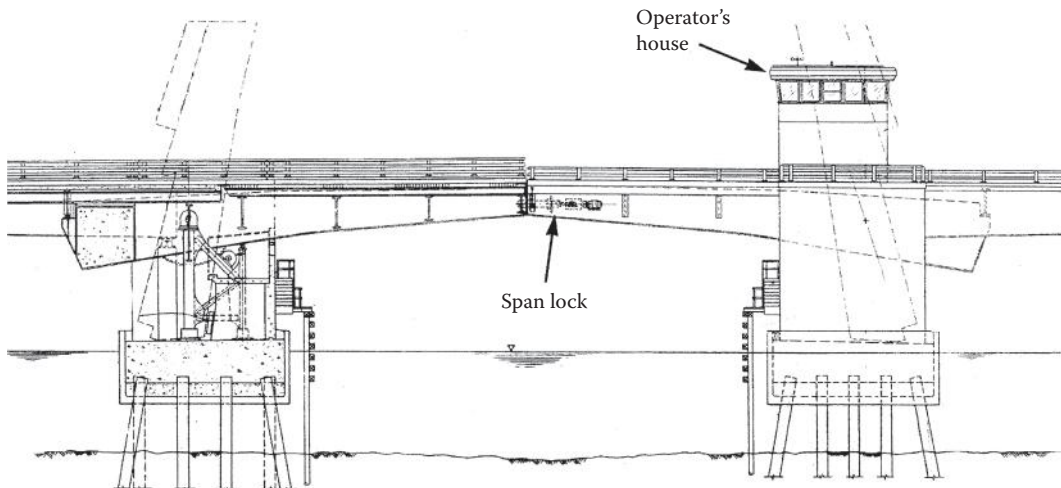


FIGURE 13.1 South Slough (Charleston) Bridge, Coos County, Oregon.

This highway bridge includes a number of features. It is a trunnion type, as the bascule span rotates about a fixed axis that is made up of a pair of horizontal shafts, which are commonly referred to as trunnions. The counterweight, which is at the back end of the leaf and serves to balance the leaf about the trunnion, is placed outside of the pier so that it is exposed. This is advantageous in that it minimizes the width of the pier. However, other trunnion type bascule bridges enclose the counterweight in a concrete pier. Also note that the tail or back end of the leaf reacts against the flanking span to stop the span and to resist uplift when there is traffic (live load) on the span. There is a lock bar mechanism between the two leaves that transfers live load shear between the leaves as the live load moves from one leaf to the other. The locks (also called center locks to distinguish them from end locks that are provided at the tail end of some bascule bridges) transfer shear only and allow rotation, expansion and contraction to take place between the leaves. The bridge shown in Figure 13.1 is operated mechanically, with drive machinery in each pier to open and close the leaves.

Another feature to note is the operator's house, also referred to as the control house. It is situated so that the operator has a clear view both up and down the roadway and waterway, which is required when the leaves are both raised and lowered. The lower levels of the operator's house typically house the electrical switchgear, emergency generator, bathroom, workshop, and storage space. This bridge has a freestanding fender system that is intended to guide ships through the channel while protecting the pier from impact. Although not directly related to the bascule bridge, the use of precast footing form and tremie fill shown in the figure can be an excellent solution to constructing the pier as it minimizes the pier depth and avoids excavation at the bottom of the waterway.

Figure 13.2, the 3rd Street Bridge, Wilmington, Delaware, shows a similar through girder double-leaf bascule span illustrating other typical bascule span design features. It has a center to center trunnion distance of 188 feet (57.3 m). For this bridge the tail or back end of the leaf, including the counterweight, is totally enclosed in the pier and the live load reaction is located at the front wall of the pier. In addition this bascule is shown with a mechanical drive. A larger pier is required to protect the enclosed counterweight. The advantage of an enclosed pier is that it allows the counterweight to swing below the waterline within the confines of the bascule pier pit. And, as can be seen, the bascule pier is constructed within a cofferdam. For this bridge there was not enough depth to place a full tremie seal so underwater tie downs were used to tie the seal to the rock below. Also note the architectural detailing of the cast in place concrete substructure, this was achieved using form liners. This was done because the bridge is located in a park and needed to be compatible with a park setting.

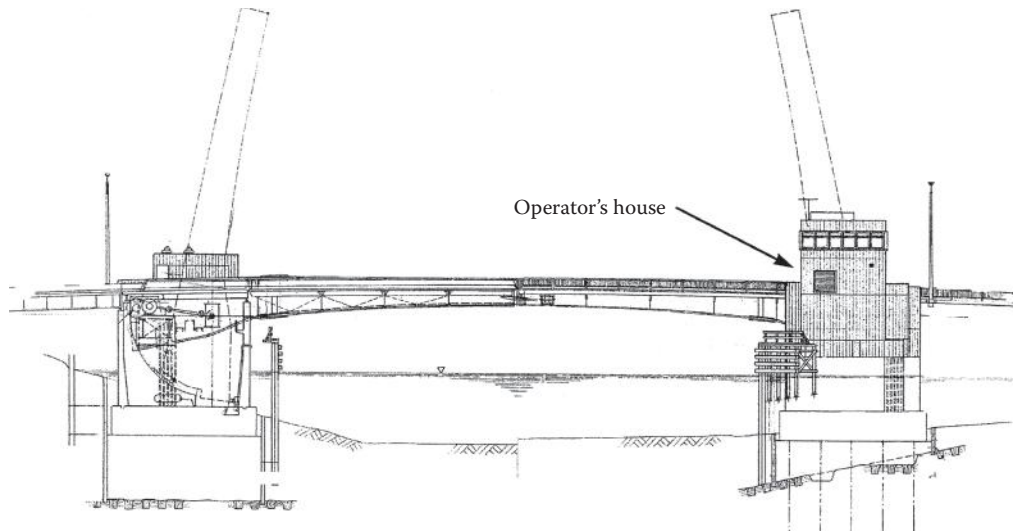


FIGURE 13.2 3rd Street Bridge, Wilmington, Delaware.

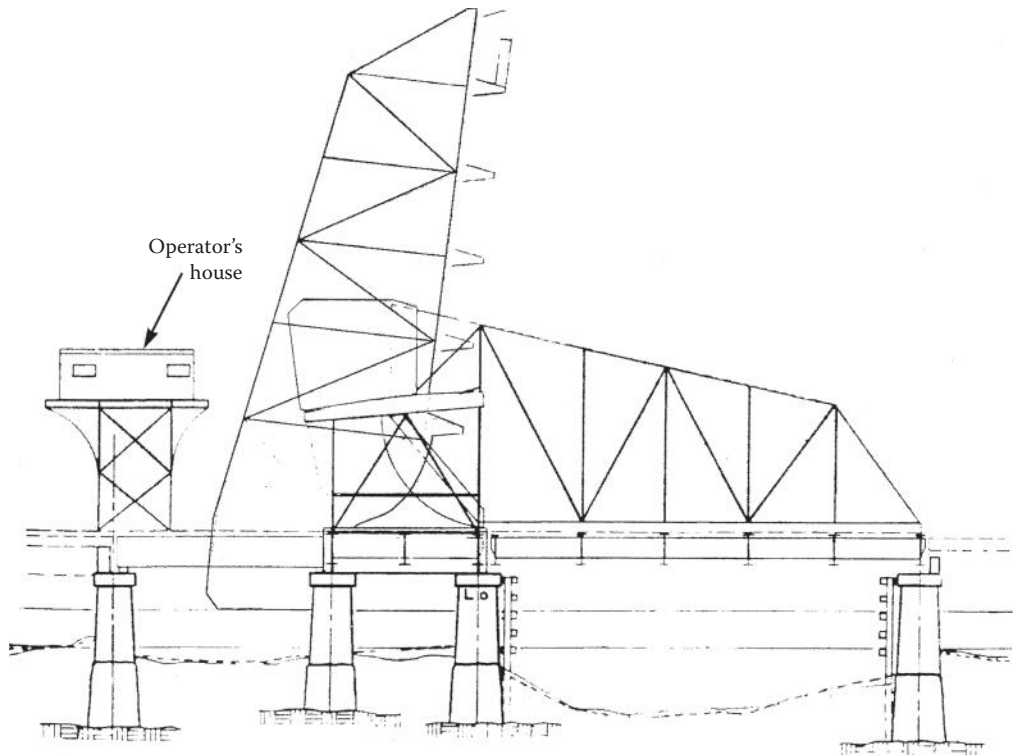


FIGURE 13.3 Pelham Bay Bridge, New York.

Figure 13.3, the Pelham Bay Bridge, New York, illustrates a single-leaf Scherzer rolling lift bridge or rolling lift bascule railroad bridge, typical of many movable railroad bridges. The design was developed and patented by William Scherzer in 1893 and is both simple and widely used. This is a through truss with a span of 81.6 feet (24.9 m). Railroad bascule bridges are always single leaf, which is required by the AREMA Manual, as the heavy live loads associated with heavy rail preclude a joint at mid span. This

problem does not occur with light rail (trolley) live loads and combined highway/trolley double-leaf bascule bridges were frequently used in the 1920s. Also, railroad bascule bridges such as the one shown are usually through truss spans, again due to the heavy rail live loads. This bridge has an overhead counterweight, a typical feature of Scherzer-type bridges. This allows the bridge to be placed relatively close to the water and permits a very simple pier. The bascule track is supported by a steel girder and two simple open piers. As illustrated, each leaf rolls back on a track rather than pivoting about a trunnion. The advantage of this feature is that it is not restricted by the capacity of the trunnion shafts and it minimizes the distance between the front face of the pier and the navigation channel. As the span opens, it rolls back away from the channel. The drive machinery is located on the moving leaf and typically uses a mechanically or hydraulically driven rack and pinion to move the span. The machinery must thus be able to operate as it rotates and for hydraulic machinery this means the reservoir needs to be detailed accordingly. However this is not always the case and designs have been developed that actuate the span with external, horizontally mounted hydraulic cylinders. A disadvantage of a rolling lift is that the pier needs to be designed to accommodate the large moving load of the bascule leaf as it rolls back and tread members need to withstand repeated concentrated loads so that older bridges of this style may experience cracking and/or plastic flow. Conversely, the reaction from the leaf in a trunnion type span is concentrated in one location, simplifying the design of the pier. More complicated bascule bridges with overhead counterweight designs have been developed where the counterweight is supported by a scissors type frame and by trunnions that allow the counterweight to pivot.

Figure 13.4, the Manchester Road Bridge at the Canary Wharf, London, illustrates a modern interpretation of an overhead counterweight bascule bridge. It has a span of 109 feet (33.2 m). In addition to being attractive, it is a very practical design with all of the structure above the roadway level, allowing the profile to be set as close to the water line as desired. The design concept is not new and is found in many small hand operated bridges in Holland, perhaps the most famous of which appears in van Gogh's 1888 painting *The Langlois Bridge*.

Figure 13.5, the Nitschke (Main Street) Bridge, Green Bay, Wisconsin is a double-leaf rolling lift (Scherzer) bascule span. The bridge spans 171 feet (52 m), center-to-center of pinions and provides a 115 foot (35 m) channel across the Fox River. Each leaf consists of two girders, 6 feet (1880 mm) deep at the center break and 14 feet (4.3 m) deep at the pinion. Each leaf rolls on a 10 foot (3 m) radius tread casting. The floor beams are spaced at 13.5 feet (4.1 m) and vary in depth from 4 feet (1.2 m) at the girder to 4.5 feet (1.4 m) at the center of the roadway. The 8-foot-wide (2.4 m) sidewalks on each side are supported on brackets, cantilevered from the girders. The counterweight is supported by a combination of beams and horizontal trusses. Each leaf is

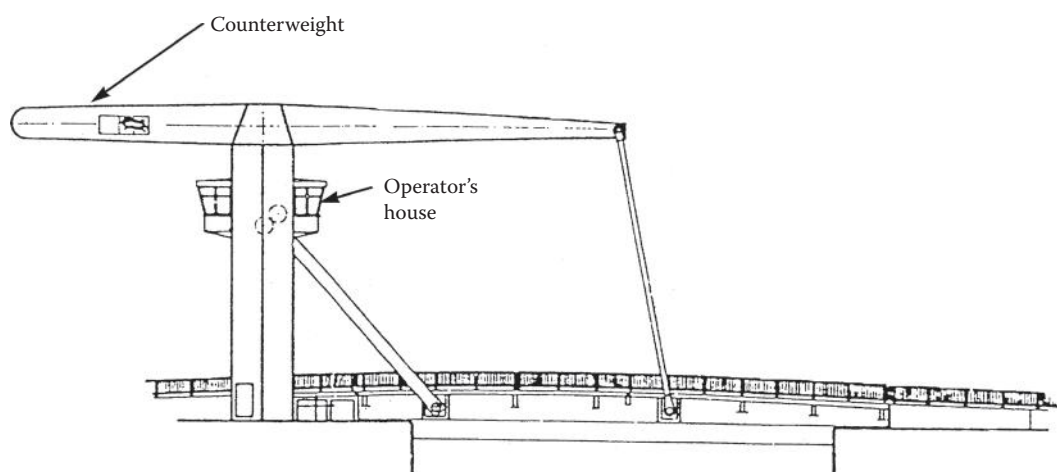


FIGURE 13.4 Manchester Road Bridge at the Canary Wharf, London



FIGURE 13.5 Nitschke (Main Street) Bridge, Green Bay, Wisconsin. (Courtesy of David Sailors.)

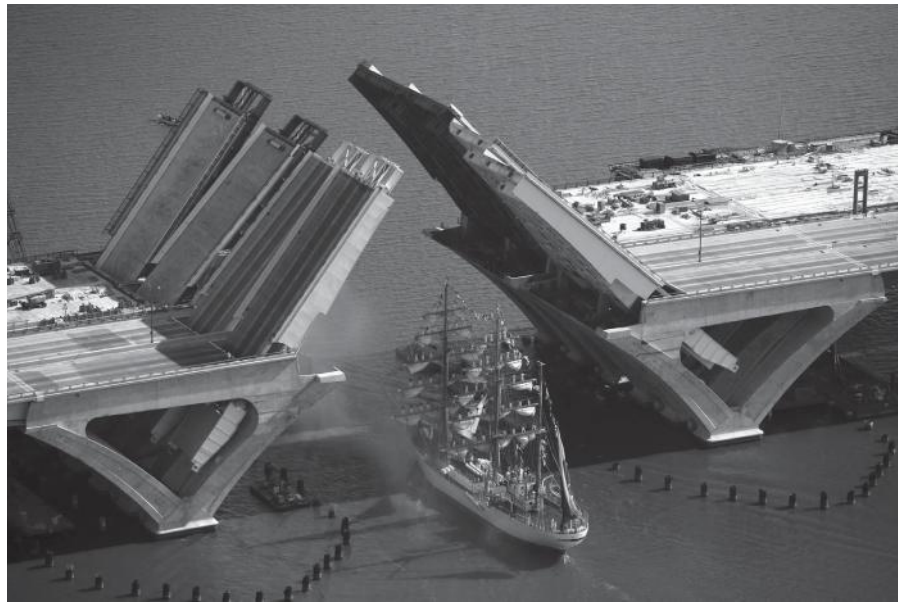
braced by longitudinal cross frames and lateral bracing at the bottom of the floor beams. The soils below the Fox River are very poor and each bascule pier is supported on twelve 8 foot (2.4 m) diameter drilled shafts, extending 85 feet (26 m) to bedrock. The bridge utilizes an Exodermic grid deck, incorporating a reinforced concrete deck cast composite with the steel grid and the floor beams. The bridge employed what is believed to be the first use of a closed loop hydraulic drive system on a bascule bridge. In recognition of the landmark status of the original bridge a number of architectural features were carried over to the new bridge, including the octagonal tender house, a clay tile roof and re-use of the terra cotta cornice.

The Woodrow Wilson Bridge Replacement (Figure 13.6), completed in 2008, carries the Capitol Beltway over the Potomac River, connecting Virginia, District of Columbia, and Maryland. This 6000-foot-long (183 m) bridge was constructed with a bascule span of 270 feet (82 m) between trunnions. The navigable channel has a horizontal clearance of 175 feet (53 m) and a minimum vertical clearance of 70 feet (21 m) when the bridge is closed. The bascule span is notable for its exceptional width of 249 feet (76 m), carrying 12 lanes of highway traffic. This width is accommodated by four double-leaf bascule spans oriented side-by-side, for a total of eight bascule leaves. Three notable design features include the aesthetic pier configuration, mid-span moment locks, and the stainless steel reinforcement of the concrete deck. The bascule piers use curved compression ribs and tension ties to create an airy, arch-like appearance that provides visual continuity with the numerous approach spans. The bridge is designed to carry light rail trains; in order to minimize mid-span deflections and maintain rail continuity, mid-span moment locks were selected (see Figure 13.6b). Moment locks reduced the expected deflections by more than half when compared to shear locks that are typically used on bascule bridges at mid span. The deck uses a lightweight concrete deck cast compositely with the steel superstructure. Stainless steel reinforcing bars were selected to prevent corrosion and increase service life of the deck, thus avoiding deck replacement.

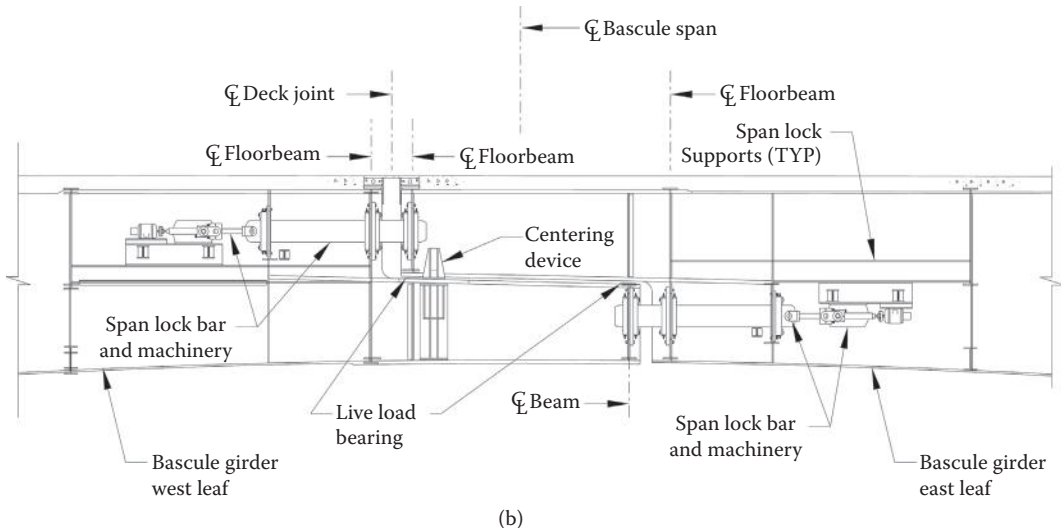
Figure 13.7, the Johns Pass Bridge to Treasure Island, Florida and constructed in 2008, has four bascule leaves spanning a tidal navigation channel on Florida's West Coast. The bridge profile was kept exceptionally low in order to maintain the local area ambiance while accommodating most navigational traffic. The movable leaf box girder structural design is an unusual feature for a bascule girder and was intended to improve aesthetics and reduce maintenance costs. The operating machinery design uses a traditional rack and pinion configuration with redundancy in the drive motors and controls. The drives are modern electronic D.C. drives connected to a modern industrial hardened programmable logic control system.

13.2.2 Swing Spans

Swing spans were widely used by the railroads. However, they only allowed a limited opening and the center pivot pier was often viewed as a significant impediment to navigation. The pivot pier could also



(a)



(b)

FIGURE 13.6 Woodrow Wilson Bridge Replacement: (a) bridge opening (b) moment locks. (Courtesy of Hardesty & Hanover.)

require an elaborate, difficult to maintain, and expensive fender system. As a result, swing spans are infrequently selected for new sites. However, they can be a cost-effective solution, particularly for a double swing span, and should be considered when evaluating options for a new movable bridge.

Figure 13.8 shows a typical through truss swing span, the Macombs Dam Bridge over the Harlem River in New York City, constructed in 1895 at the site of the original bridge discussed in the introduction. This span is 415 feet (126.5 m) long. The large pivot pier in the middle of the channel illustrates the navigation issue with this design. The piers at either end of the swing span are referred to as the rest piers. By using a through truss, the depth of structure (the distance between the profile grade line and the underside of the structure) is minimized—thus minimizing the height and length of the approaches.



FIGURE 13.7 Johns Pass Bridge to Treasure Island, Florida. (Courtesy of David Sailors.)

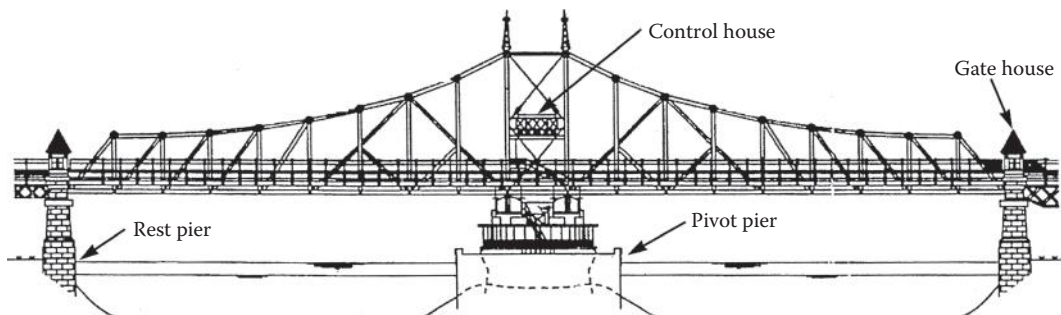


FIGURE 13.8 Macombs Dam Bridge over the Harlem River, New York City.

The turning mechanism is located at the pivot pier and the entire dead load of the swing span is supported on the pivot pier. As the two arms of the swing span are equal, they are balanced, although this is not always the case with swing spans. This bridge is operated with a mechanical drive that utilizes a rack and pinion system. As is typical for many swing spans, there are end lifts at the ends of the swing span that are engaged when the span is closed in order to pick up some of the dead load and allow the movable span to act as a two-span continuous bridge under live load. The end lifts, as the name suggests, lift the ends of the swing span, which are free cantilevers when the span operates. The operator's house is typically located on the swing span within the truss but above the roadway, as this location provides good visibility. On older bridges one may also find tenders' houses located at the ends of the swing span. In the case of the Macombs Dam Bridge, these were for gate tenders who would stop traffic, manually close the traffic gates and hold the horses if necessary. Gate tenders have been replaced with automatic traffic signals and gates, but their houses remain.

Figure 13.9, the Potato Slough Bridge, San Joaquin County, California, illustrates a good example of a more modern highway swing span. This bridge has a 310 foot (94.5 m) long swing span that uses a simple

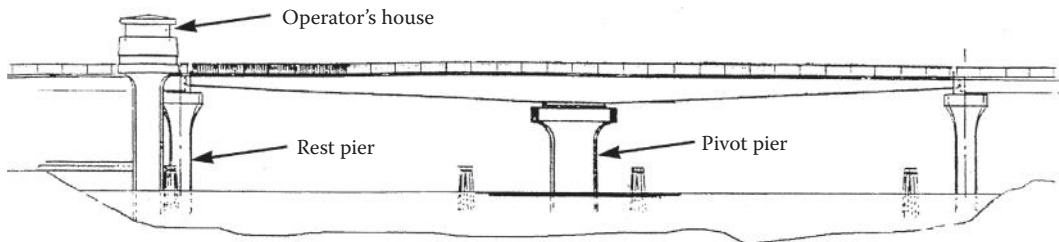


FIGURE 13.9 Potato Slough Bridge, San Joaquin County, California.

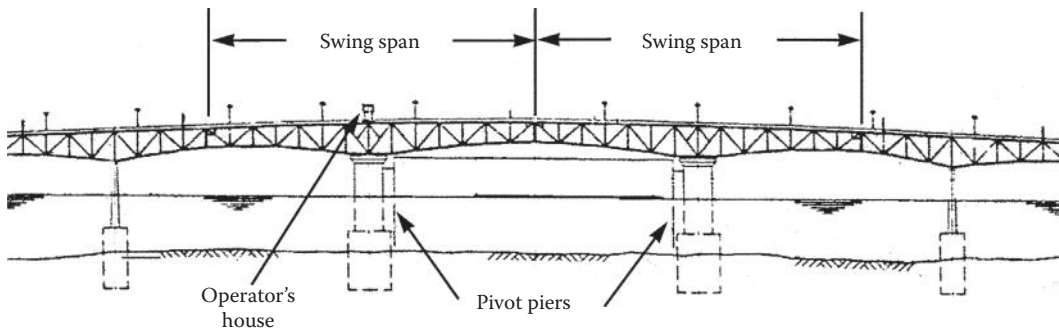


FIGURE 13.10 Coleman Bridge over the York River, Virginia (drawing).

composite deck, steel girder construction. It is very economical on a square foot basis compared to a bascule or vertical lift bridge, due to its simplicity and lack of a large counterweight. One way of looking at this is that on a bascule or vertical lift bridge a large amount of structure is composed of the counterweight and its supports. These elements do not contribute to the effective load carrying area. The swing span back span, on the other hand, not only acts as a counterweight but also carries traffic making for a more cost effective solution. One disadvantage of the deck girder design is that it does not minimize the depth of construction, as does a through truss or through girder design. On this bridge the swing span is symmetrical and thus balanced. Nevertheless, on swing spans some small counterweights may be required to correct any longitudinal or transverse imbalance. The operator's house is located in an adjacent independent structure again in an area that provides good visibility upstream, downstream and along the roadway. The pivot pier can accommodate switchgear and a generator. The roadway joints at the ends of the span are on a radius. These could also be detailed as beveled joints, provided that the span only needs to swing in one direction. However, some designers are of the opinion that it is preferable to design a swing bridge to swing in either direction to allow the bridge to be opened away from oncoming marine traffic and to minimize damage if the structure is struck and needs to swing free.

Figures 13.10 and 13.11 illustrate the double swing span Coleman Bridge across the York River in Virginia. The two swing spans are each 500 feet (152.4 m) long and provide a 420-foot (128.0 m) wide navigation channel, wide enough to accommodate the wide range of U.S. Navy vessels that traverse the opening. The bridge is a double swing deck truss. At this site the river banks are relatively high, so the depth of the structure was not a significant issue. Because the bridge is located adjacent to a national park, the low profile of a deck truss was a major advantage. The bridge uses hydraulic motors to drive the span, driving through a rack and pinion system similar to that used in large slewing excavators. Unlike the single swing bridges above, there are lock bars at all three movable span joints. These are driven when the span is in the closed position and function in the same manner as lock bars between the leaves of a double-leaf bascule. There are wedges at each pivot pier to support the live load. As shown, the operator's house is located above one of the swing spans. The control equipment is located inside the operator's house and the generator and switchgear is located on the swing spans below deck. This bridge



FIGURE 13.11 Coleman Bridge over the York River, Virginia (photo). (Courtesy of David Sailors.)

superstructure was replaced in 1996 and uses a lightweight concrete deck. The piers were constructed in 1952 when the bridge was first built using concrete filled steel shell caissons that were placed by dredging through open wells.

13.2.3 Vertical Lift Bridges

Vertical lift bridges, the last of the three major types of movable bridges, are most suitable for longer spans, particularly for railroad bridges.

Figures 13.12 and 13.13 show a through truss highway lift span—the James River Bridge in Virginia, which has a span of 415 feet (126.5 m). The maximum span for this type of design to date is approximately 550 feet (167.7 m) long. The weight of the lift span is balanced by counterweights, one in each tower. Wire ropes that pass over sheaves in the towers are attached to the lift span at one end and the counterweight at the other. A secondary counterweight system is often required to balance the weight of the wire ropes as the span moves up and down and the weight of the wire ropes shifts from one side of the sheaves to the other.

Two types of drive systems are commonly employed, tower drive and span drive. A span drive places all of the drive machinery in the center of the lift span and through drive shafts, operates a winch and hauling rope system to raise and lower the span. A tower drive—as the name implies—uses drive machinery in each tower to operate the span. The advantage of the span drive is that it ensures that the two ends lift together, whereas a tower drive requires coordinating the movement at each end. The disadvantages of the span drive are that it tends to be ugly and the lift span, ropes, sheaves and counterweights must carry the additional weight of the operating machinery. Consequently tower drives are favored on new bridges.

The machinery drive can be either mechanical or hydraulic with mechanical being the normal choice. Guide wheels guide the span as it moves along the tower legs, and they must be detailed so as to allow expansion and contraction at one end of the lift span to accommodate changes in temperature. Span locks are used at each end of the lift span to ensure that the lift span does not drift up when in the down (closed) position. If the bridge is normally in the open position, an additional set of span locks needs to be provided. As shown, the operator's house is located on one of the towers. For this bridge, the house partially wraps around the tower to provide good visibility of both the waterway and roadway.

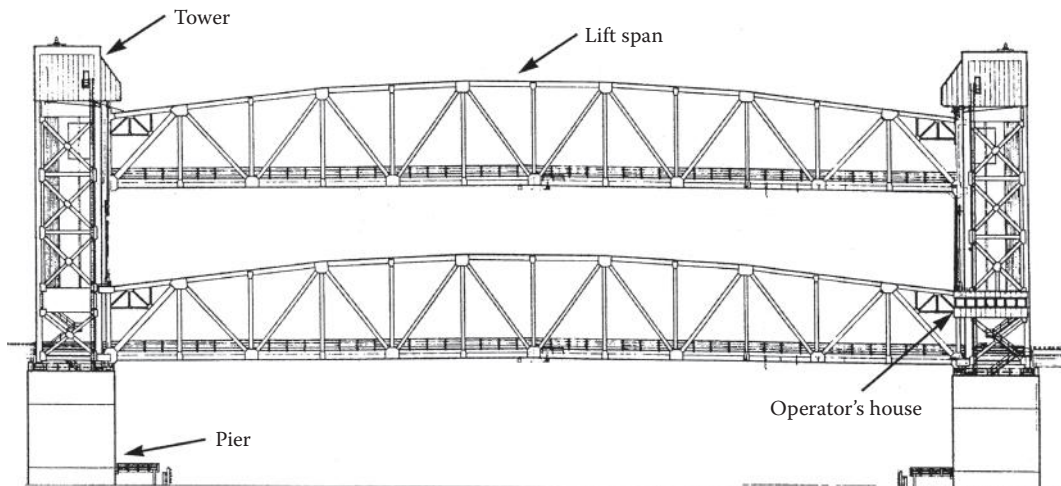


FIGURE 13.12 James River Bridge, Virginia (drawing).



FIGURE 13.13 James River Bridge, Virginia (photo). (Courtesy of David Sailors.)

Figure 13.14, the Danziger Bridge, New Orleans, is a vertical lift bridge that uses an orthotropic deck with steel box girders for the lift span and welded steel boxes for the tower. The lift span is 320 feet (97.6 m) long. The depth of construction is less than that of an equivalent through truss so that the appearance is cleaner, the load to lift should be less and the height of the towers lower than that of an equivalent through truss. The foundations for both of these vertical lift bridges used deep cofferdam construction, which may be advantageous for longer spans because the mass and rigidity of such a foundation should be better able to resist the forces from collision by a large ship.

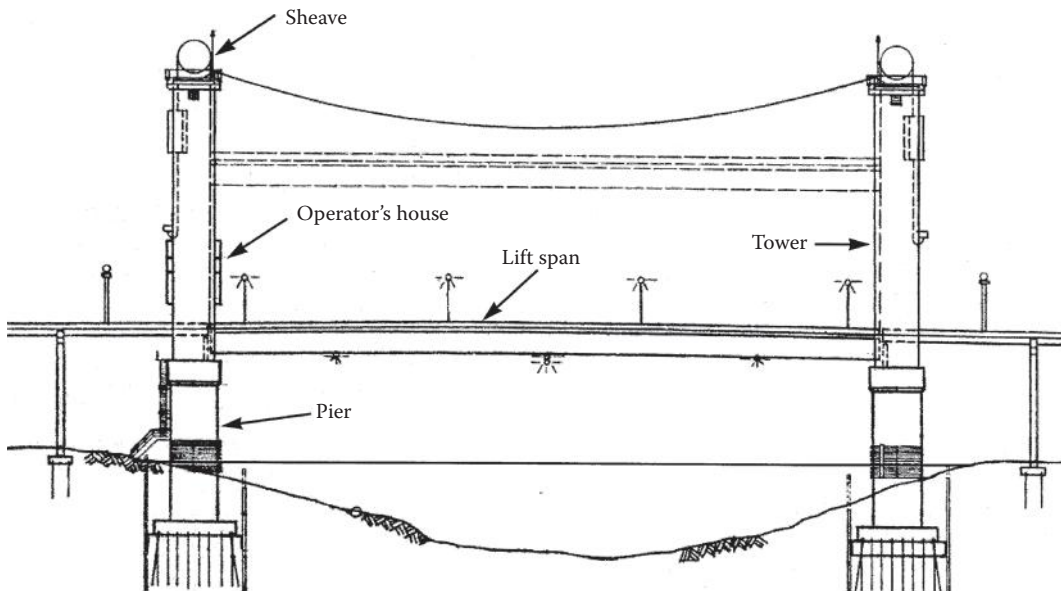


FIGURE 13.14 Danziger Bridge, New Orleans, Louisiana.

13.2.4 Retractile Bridges

Retractile bridges open by translating horizontally, or said more plainly, pulling back away from the navigable channel. There are two types of retractile bridge: rolling and floating. Rolling retractile bridges are obsolete. However, this type was once common in Boston, with a dozen examples and a handful of rolling retractile bridges remaining in service in the United States, including the historically landmarked Carroll Street Bridge in Brooklyn, NY. The construction of floating retractile movable spans is justified in response to certain unique site conditions, namely the necessity for a very wide channel and/or the presence of a very deep channel. Examples include the Admiral Clarey Bridge in Pearl Harbor, Hawaii and the Hood Canal Bridge in Washington State.

The Carroll Street Bridge, constructed in 1889, spans the 36-foot-wide (11 m) channel of the Gowanus Canal and has a total length of 107 feet (33 m). The bridge uses a wooden deck to support one traffic lane and two sidewalks. The steel superstructure uses a king-post truss. In plan, the span has a trapezoidal shape, due to the angled joint between the movable span and the fixed abutment. The operating machinery is contained in an adjacent control house, from which wire ropes connect to the movable span. Wheels, riding on rails, are mounted underneath the movable span. The rails allow the bridge to roll away from the channel at an angle of approximately 45° from the center of the roadway.

The 7869 feet (2399 m) long Hood Canal Bridge, is believed to be the world's longest floating bridge in an ocean environment. The Hood Canal is a natural fjord-like inlet off Puget Sound and the site of a U.S. Navy submarine base, several miles inland from the bridge crossing. A floating bridge was selected for the site because the width and depth of the Canal, over 300 feet (91 m) deep, precluded a normal fixed structure. The bridge includes a 600 foot (183 m) floating retractile span, one of the largest movable spans in the world, to allow for marine traffic. Each of the two movable pontoons retracts 300 feet (91 m) and is secured to the fixed pontoons using four feet (1.2 m) diameter guide rollers. Hydraulic cylinders lift the roadway adjacent to the movable spans up to clear space for the movable span to retract below. The floating pontoons are constructed of concrete post-tensioned in three directions. The bridge uses wire ropes to secure to numerous gravity anchors on the ocean floor. The first Hood Canal Bridge was designed by the Washington State Department of Transportation, construction was completed in 1963.

In 1979, a 100-year storm struck the area causing the West Half of the bridge to sink. The West Half Replacement was completed, to a new design, 3 years later, in 1982. In 2010, the original East Half was replaced using design plans that had been prepared at the time of the West Half replacement. However, due to increased traffic, the existing West Half superstructure was widened and the East Half design was modified to provide a wider roadway. The reader is referred to Chapter 14—Floating Bridges.

13.2.5 Uncommon Types

There are many uncommon, obsolete, variations, and novel types of movable bridge. Too many, in fact, to warrant more than a brief overview here. The early twentieth century saw the development and patent of a multitude of designs, many overly complicated. More recently, several imaginative movable pedestrian bridges have been built to unique designs, such as the folding bridge at Paddington Basin, London, which rolls up into a compact cylindrical profile. Movable pedestrian bridges in this vein are sometimes selected for their ability to delight the public, not by strict engineering and economic considerations. As recently as 2011, the Congress for the International Association for Bridge and Structural Engineering included two different papers proposing “new” forms of movable bridge for pedestrian and bicycle use. One was functionally similar to the counterweight-less bascule erected in Milwaukee, Wisconsin in the 1890s and replaced in 1929 due to safety concerns with the design. The other, termed a “butterfly bridge,” was a unique hybrid of suspended arch, gyratory, and vertical lift type bridges conceived for pedestrian use within a private development.

13.3 Structural Design

13.3.1 Design Criteria

In the closed position movable bridges are designed for the same design conditions as a fixed bridge. However a movable bridge must also be designed for the other loads and load combinations.

13.3.1.1 Movable Highway Bridges

The load combinations described below are from Article 2.4 Loads, Load Factors, and Combinations of the AASHTO Specifications (AASHTO 2012a).

Load combinations for bascule and vertical lift bridge structures:

- Strength BV-I—Load combination related to structure in the open or closed position and dynamic effects of operating machinery.
- Strength BV-II—Load combination related to structure in any open position, dynamic effects of operating machinery, and wind.
- Strength BV-III—Load combination related to structure in the closed position, with live load and counterweight independently supported.

Load combinations for swing bridge structures:

- Strength S-I—Load combination related to structure in any open or closed position and dynamic effects of operating machinery.
- Strength S-II—Load combination related to live load on simple span configuration.
- Strength S-III—Load combination related to live load on continuous span configuration.
- Strength S-IV—Load combination related to structure in the open position, dynamic effects of operating machinery, and wind.
- Strength S-V—Load combination related to live load on a simple span configuration and wind.
- Strength S-VI—Load combination related to live load on a continuous span configuration and wind.

13.3.1.2 Movable Railroad Bridges

The load combinations described below are from Article 6.3 of the AREMA Manual (AREMA 2011).

1. Moving Dead Load: dead load plus 20%. This is applied to structural parts in which the member stress varies with the movement of the span. It is not combined with live load stresses. For structural parts with the stresses caused by machinery or forces applied for moving or stopping the span, 100% impact is used. For end floor beams live load plus 100% impact is used.
2. Wind Loads:
 - a. Movable Span Closed
 - i. Structure to be designed as a fixed span
 - b. Movable Span Open
 - ii. When the movable span is normally left in the closed position, the structure is designed for 30 psf (Pounds Per Square Foot) (1.44 kPa) wind load on the structure, combined with dead load, and 20% of dead load to allow for impact, at 1.25 times the allowable unit stresses. For swing bridges the design is also checked for 30 psf (1.44 kPa) wind load on one arm and 20 psf (0.96 kPa) wind load on the other arm.
 - iii. When the movable span is normally left in the open position, the structure is designed for 50 psf (2.39 kPa) wind load on the structure, combined with dead load, at 1.33 times allowable unit stresses. For swing bridges the design is also checked for 50 psf (2.39 kPa) wind load on one arm and 35 psf (1.68 kPa) wind load on the other arm, applied simultaneously.
3. Ice Load

These are typically not considered in structural design, since they are assumed to be accompanied by reducing traffic and impact loads. However, an ice load of 2.5 psf (0.12 kPa) must be considered in designing the bridge operating machinery in locations where such conditions exist.
4. Swing Bridges:
 - a. The stresses in trusses or girders of swing bridges continuous on three or four supports shall be calculated for the bridge in the following conditions.

Condition 1—Bridge open, or closed with the ends just touching.
Condition 2—Bridge closed with ends lifted.
 - b. The computation of stresses shall be divided into the following cases:

Case I Condition 1, dead load.
Case II Condition 2, dead load, ends lifted to give a positive reaction equal to the maximum negative reaction of the live load and impact load plus 50% of their sum.
Case III Condition 1, live load plus impact load on one arm as a simple span.
Case IV Condition 2, live load plus impact on one arm, bridge as a continuous structure.
Case V Condition 2, live load plus impact load on both arms, bridge as a continuous structure.
 - c. The following combinations of these cases shall be used in determining the maximum stresses:

Case I alone, plus 20%
Case I with Case III
Case I with Case V
Case II with Case IV
Case II with Case V
5. Bascule Bridges and Vertical Lift Bridges:
 - a. The stresses in trusses or girders of bascule bridges and vertical lift bridges shall be calculated for the bridge in the following conditions:

Condition 1—Bridge open in any position
Condition 2—Bridge closed
Condition 3—Bridge closed, with counterweights independently supported

- b. The computation of stresses shall be divided into the following cases:
 - Case I Condition 1, dead load
 - Case II Condition 2, dead load
 - Case III Condition 3, dead load
 - Case IV Condition 2 or 3, live load plus impact load
- c. The following combinations of these cases shall be used in determining the maximum stresses:
 - Case I alone, plus 20%
 - Case II with Case IV
 - Case III with Case IV

All of the above applies to the structural design of the moving span and its supports. For the design of the operating machinery, there are other load cases contained in the AREMA Manual (AREMA 2011) and the AASHTO Specifications (AASHTO 1992).

13.3.2 Bridge Balance

Almost all movable bridges are counterbalanced so that the machinery that moves the span only needs to overcome inertia, friction, wind, ice and a relatively small imbalance. Recently at least one bascule bridge and one lift span have been designed without counterweights, relying instead on the force of the hydraulic machinery to move the span. While this saves the cost of the counterweight and reduces the design dead loads, one needs to carefully compare the reduced construction costs against the present value of the added machinery costs and future annual electric utility demand and service costs (utility rates are based on not only how much energy is consumed but also on how much it costs the utility to be able to supply the energy on demand).

Counterweights are designed with pockets to allow for adjustment of the bridge balance, recognizing that during its lifetime, the bridge's weight and weight distribution can change, usually increasing. The typical reasons for these changes are deck replacement, paint, repairs, or new span locks, among others. Typically contract drawings show the configuration, estimated concrete volume and location of the counterweights, but require that the contractor be responsible for balancing the span. This is reasonable as the designer does not know the final weight of the elements to be used, such as the size of the splice plates, the lock bar machinery, concrete unit weight, and other variables. And published unit weights of manufactured items such as grid decks can vary. Balance checks can be made during construction or retrofit using detailed calculations accounting for every item that contributes to the weight of the moving span. These calculations need to account for the location of the weight in reference to the span's horizontal and vertical global axes and, for an asymmetrical span such as a swing span, the transverse axis.

For bascule and vertical lift bridges, current practice is to attach strain gauges to the machinery drive shafts and measure the strain in the shafts as the span is actuated through a full cycle, thereby accurately determining the balance. Strain gauge balance testing cannot detect transverse imbalance. For vertical lift spans and swing spans, hydraulic jacks can be used to measure imbalance, including transverse imbalance. Measuring the tension in each rope of a vertical lift bridge is another method for determining the weight of the counterweight, including transverse distribution.

Rope tension is measured by vibrating each rope to determine the natural frequency. This procedure can be performed by hand with a pencil and a stop watch; alternatively accelerometers can be temporarily attached to the ropes. The formula for calculating tension from natural frequency is $T = 4W(L-F)^2$, where T is the rope tension in pounds, W is rope weight in pounds per foot, L is rope free length, in feet, or the vertical distance from the span connection to the sheave tangent point and F is the natural frequency in cycles per second at which the rope vibrates when excited.

13.3.3 Counterweights

Figure 13.15 illustrates typical counterweight configuration for a vertical lift bridge. Both the AREMA Manual (AREMA 2011) and AASHTO Specifications (AASHTO 1988 and 2012a) require that a pocket be provided in the counterweight for adjustment. The pockets are then partially filled with smaller counterweight blocks, which can be moved by hand to adjust the balance of the bridge. Counterweights are typically made up of a concrete surrounding a steel frame or a reinforced steel box that is filled with normal weight concrete. Heavyweight concrete can be used to minimize the size of the counterweight and this is typically done using heavyweight aggregates such as taconite. At one time, punchings from steel fabrication were mixed in with concrete to increase its density although this is seldom done due to cost considerations. However, some more recent designs have used steel billets in lieu of concrete to minimize the size of the counterweight and there is at least one vertical lift bridge where cast iron counterweights were used because the counterweights needed to be as small as possible as they were concealed in the towers. If there is not enough space left for added blocks or if there are no longer any blocks available, counterweight adjustments can always be made by adding steel plates, shapes, or rails and on older bridges one may encounter these types of added weights.

Figure 13.16 below shows the results of a balance check of a rolling lift bridge. In this case, the bridge had been in operation for many years and the owner wanted to replace the timber ties with

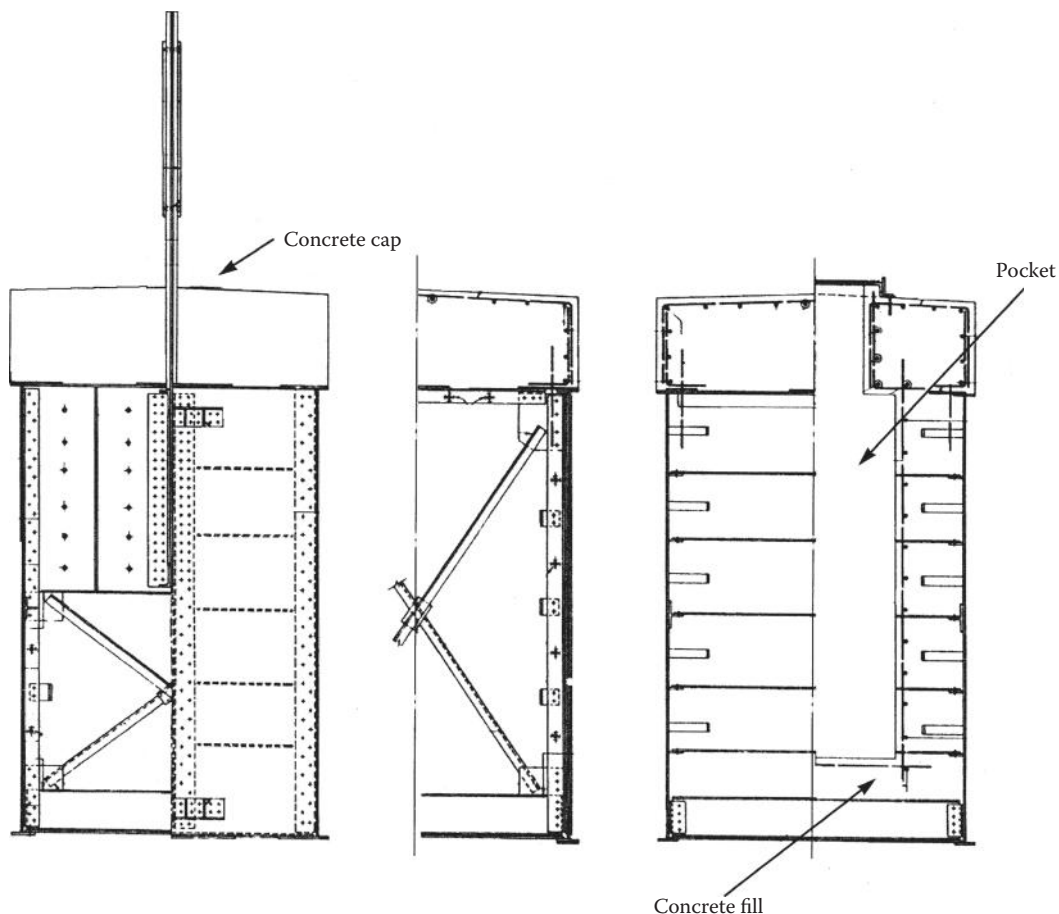


FIGURE 13.15 Typical counterweight configuration for a vertical lift bridge.

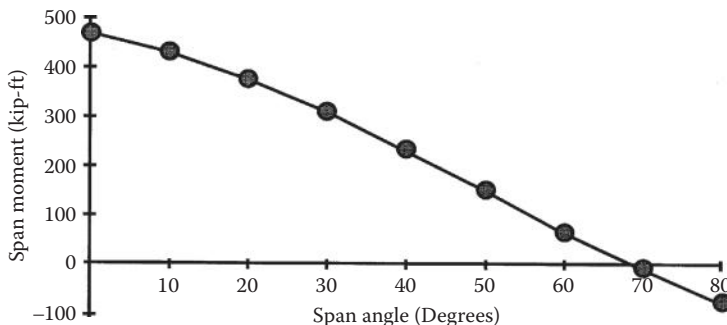


FIGURE 13.16 Results of balance check of a rolling lift bridge.

newer, heavier ties. As shown the imbalance varied with the position of the span and in the open position the center of gravity was behind the center of rotation. It would be preferable to have the entire imbalance on the span side, and to reduce the imbalance. One needs to be careful as an increased imbalance can have a chain reaction and cause an increase in the drive machinery and bridge power requirements.

In general it is good practice to balance a span so that it is slightly toe heavy for a bascule bridge and slightly span heavy for a vertical lift bridge, the idea being that the span will tend to stay closed under its own weight and will not bounce under live load, although, once the span locks are engaged the span cannot rise. The amount of imbalance needs to be included in designing the bridge operating machinery, so that it can tolerate the imbalance in combination with all the other machinery design loads.

13.3.4 Foundations

Foundations and substructures on movable bridges are more complex and typically more expensive than a similar sized fixed bridge. The foundations have to cope with the additional deadweights of counterweights and machinery, as well as the load imposed when the leaf is moved, started, and stopped. Wind and seismic loads, especially in the raised position, can in some cases control overturning moments, and the impact loads due to frequently misaligned road joints and non-functional lockbars impart loads not common to fixed bridge designs.

Movable bridges have operating tolerances. Those clearances change with the seasons, and even with which side of the bridge is exposed to direct sunlight. Movable bridge foundations have to be stiffer than a fixed bridge foundation to maintain these tolerances, as well as resist the dynamic loads of leaf movement. Differential deflections are typically not tolerated well by movable bridges, as the leaves tend to be torsionally stiffer than a fixed bridge to deal with the dynamic loads and changed support conditions that go with leaf movement.

Rolling lift (Scherzer) bridges, due to the translation of their center of gravity, tend to require larger, more expensive, foundations when compared to a trunnion bascule. For bascule bridges with low clearance, care must be taken to ensure that the counterweight does not become submerged, particularly if one considers future sea level rise due to the effects of climate change. Hollow bascule piers with sump pumps can allow for under-deck counterweights to swing below the water line, yet stay dry. Alternatively, designs with above-deck counterweights can be selected.

In many cases, movable bridges are replaced on the same alignment or immediately adjacent to an existing movable bridge, and the existing bridge has to remain operable for at least a portion of the construction period. Thus the new bridge foundations must be staged or selected such that settlement or other impacts to the existing adjacent structure are acceptable.

13.3.5 Pier Protection

Movable bridges are constructed to allow marine traffic to pass through what otherwise would be a low clearance span. Frequently the high cost of the movable bridge and channel constraints end up placing large ships very close to the foundations and movable superstructures. Fenders or other protection systems can be designed to handle vessel impact loads. However, one can also design the fender system to be attached to the movable bridge pier, in which case the fender will transfer any ship impact load to the pier and the fender would only be designed to minimize damage to the ship. And typically dolphins are provided to assist in redirecting any errant vessels back into the navigation channel. Every waterway has its own set of conditions that will provide the design constraints for a given pier protection system.

13.3.6 Vessel Collision

Movable bridges are typically designed with the minimum allowable channel. As a result, vessel collision is an important aspect as there may be a somewhat higher probability of ship collision than with a fixed bridge with a larger span. There are two factors that are unique to movable bridges with regard to fender (and vessel collision) design. The first is that if a large vessel is transiting the crossing, the bridge will be in the open position and traffic will be halted away from the main span. As a result, the potential consequences of a collision are less than would be with a fixed bridge ship collision. On the other hand, a movable bridge is potentially more vulnerable to misalignment or extensive damage than a fixed bridge. This is because not only are the spans supported by machinery, but movable spans by their very nature lack the continuity of a fixed bridge. There is no code to govern these issues, but they need to be considered in the design of a movable bridge. As suggested in the discussion on vertical lift bridges, the configuration of the piers is an important aspect of this consideration. The reader is referred to Chapter 4 Vessel Collision Design of Bridges in *Bridge Engineering Handbook, Second Edition: Substructure Design*.

13.3.7 Movable Bridge Decks

An important part of the design of movable bridges is to limit the moving dead load, which affects the size of the counterweight, the overall size of the main structural members and, to a lesser extent, the machinery depending upon the type of movable bridge. For movable railroad bridges this is typically not a problem, as movable span decks can be designed with open decks (timber ties on stringers) and the design live load is such a large part of the overall design load that the type of deck is not an issue. For highway bridges, however, the type of deck needs to be carefully selected to provide a minimum weight while providing an acceptable riding surface. Early movable spans used timber decks, but they are relatively heavy, have poor traction and wear. Timber decks also had variable weight depending on weather and humidity, causing difficulty with movable span balance. Timber was replaced by open steel grid, which at 20–25 psf (0.96–1.20 kPa) was a good solution that is both lightweight and long wearing. In addition the open grid reduced the exposed wind area, particularly for bascule bridges in the open position. However, with higher driving speeds, changes in tires, and greater congestion, steel grid deck has become the source of accidents, particularly when wet or icy. Steel grid decks also allow rainwater and roadway debris to accumulate on below-deck structural steel, often leading to premature corrosion problems. Now most new movable bridge decks are designed with some type of solid surface. Depending on the bridge, this can be a partially filled steel grid, an orthotropic steel deck, concrete, lightweight concrete or the Exodermic system. If a solid concrete deck is used, it is considered advantageous to use stainless steel reinforcing bars and lightweight concrete to allow a minimum cover and hence control the deck weight.

Recently several movable bridges have been developed with composite decks as these are relatively lightweight. Aluminum orthotropic decks and FRP decks are also now being developed and may prove

to be a good solution. While steel orthotropic steel decks would seem to be a good solution, as the deck can be used as part of the overall structural system, they have not yet seen widespread use in new designs. Congress Avenue Bridge, a double leaf bascule in Chicago, was recently retrofitted with a steel orthotropic deck. A common issue with orthotropic, composite decks is the wearing surface, which need to be lightweight, durable and adhere to bascule decks while in the vertical position without slippage. The reader is referred to Chapters 15 and 16 for information on bridge decks.

13.3.8 Seismic Design

The seismic design of movable bridges is also a special issue because they represent a large mass, which may include a large counterweight, supported on machinery that is not intended to behave in a ductile manner. In addition, the movable span is not joined to the other portions of the structure thus allowing it to respond in a somewhat independent fashion. The AREMA Manual (AREMA 2011) Chapter 9 covers the seismic design of railroad bridges. However, these guidelines specifically exclude movable bridges. For movable highway bridges, AASHTO's Standard Specification for Movable Highway Bridges (AASHTO 1988 and 2012a) requires that movable bridges that are normally in the closed position shall be designed for one-half the seismic force in the open position. However, this is only an approximation and the recommended approach (Abrahams 1998) is to consider the time period that the bridge is normally in the open and closed positions in order to design for a consistent vulnerability.

Shown below is a table of normalized peak ground acceleration (normalized with respect to the 500-year value) for a normally closed movable bridge in the open position for New York and San Francisco. The normalized peak ground acceleration values were derived using the criterion that the peak ground acceleration has a 90% probability of not being exceeded in the given exposed time.

Span Open Time (years)	Return Period (years)	Normalized Peak Ground Acceleration	
		New York	San Francisco
0%	0	0	0
10%	5	11%	45%
20%	10	22%	57%
30%	15	34%	67%
40%	20	45%	75%
50%	25	55%	80%
60%	30	65%	85%
70%	35	75%	90%
80%	40	85%	95%
90%	45	93%	98%
100%	50	100%	100%

The reader is referred to Part IV of AASHTO LRFD *Movable Bridge Design Specifications* for an additional discussion of seismic investigation.

13.4 Bridge Machinery

Currently bridge machinery is designed with either a mechanical or hydraulic drive for the main drive and usually a mechanical drive for the auxiliary machinery items such as span locks and wedges. This is true for all types of movable bridges and the choice of mechanical versus hydraulic drive is usually based on a combination of owner preference, and cost—although other factors may also be considered. Mechanical drives are typically simple configurations based on machinery design principles that were

developed long before movable bridges, although now drives use modern enclosed speed reducers and bearings. Overall, these systems have performed very well with sometimes limited maintenance. More recently, hydraulic machinery has been introduced in movable bridge design and it has proven to be an effective solution, as the hydraulics can be closely matched to the power demands, which require good speed control over a wide range of power requirements. Also, there are many firms that furnish hydraulic machinery. However, the systems also require a more specialized knowledge and maintenance practice than was traditionally the case with mechanical drives. After experiencing maintenance problems, the Florida Department of Transportation guidelines no longer allows for new movable bridges to use hydraulic drive systems. Nevertheless, hydraulic machinery is often used for temporary operation such as for a temporary movable bridge or when operating machinery is being replaced.

Figure 13.17 shows a section through a bascule pier illustrating the layout of the bascule girder trunnions (about which the bascule girders rotate) as well as the hydraulic cylinders used to operate the span. The typical design practice is to provide multiple cylinders so that one or more can be removed for maintenance while the span remains in operation. The cylinder end mounts incorporate spherical bearings to accommodate any misalignments. Note that the hydraulic power unit, consisting of a reservoir, motors, pumps and control valves, is located between the cylinders. Typically redundant motors and pumps are used and the valves can be hand operated if the control system fails. As movable bridges are located on waterways, the use of biodegradable hydraulic fluids is an option in case of a leak or spill.

Figure 13.18 shows a similar section through a bascule pier that utilizes a mechanical drive. What is not shown is the rack attached to the bascule girder. Note the different arrangement here of the trunnions, with bearings on either side of the girders. The central reducer contains a differential, similar to the differential in a vehicle that serves to equalize the torque in these two drive shafts. As shown there are two drive motors and typically the span will be designed to operate with only one motor in operation either as a normal or emergency condition. Also note the extensive use of welded steel frames to support the machinery. It is important that they are stress relieved after assembly but prior to machining and that they be carefully detailed to avoid re-entrant corners that could, in time, be a source of cracks.

Figure 13.19 is an illustration of a trunnion and trunnion bearing. The trunnions are fabricated from forged steel and in this case, are supported on one end by a trunnion bearing and on the other by a trunnion girder that spans between the bascule girders. In this figure a sleeve type trunnion bearing is shown. The use of sleeve bearings in this type of arrangement is not favored by some designers due to a concern with uneven stress on the lining due to deformation of the trunnions and trunnion girder, particularly as the span rotates. However, this can be addressed by orienting the bearing so that its slope

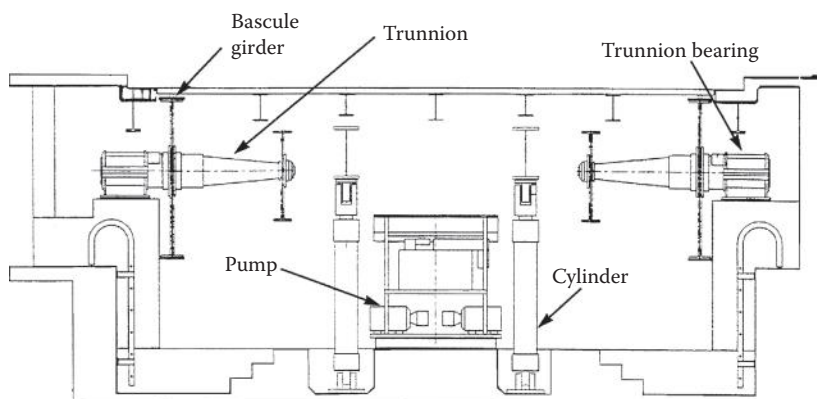


FIGURE 13.17 Section through a bascule pier showing girder trunnions and hydraulic cylinders.

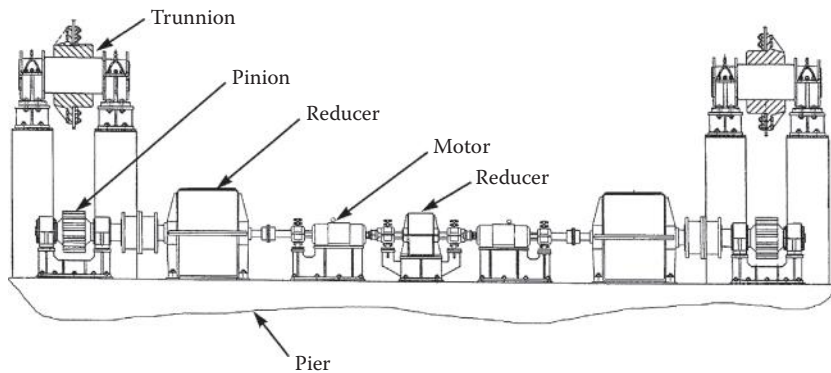


FIGURE 13.18 Section through a bascule pier that utilizes a mechanical drive.

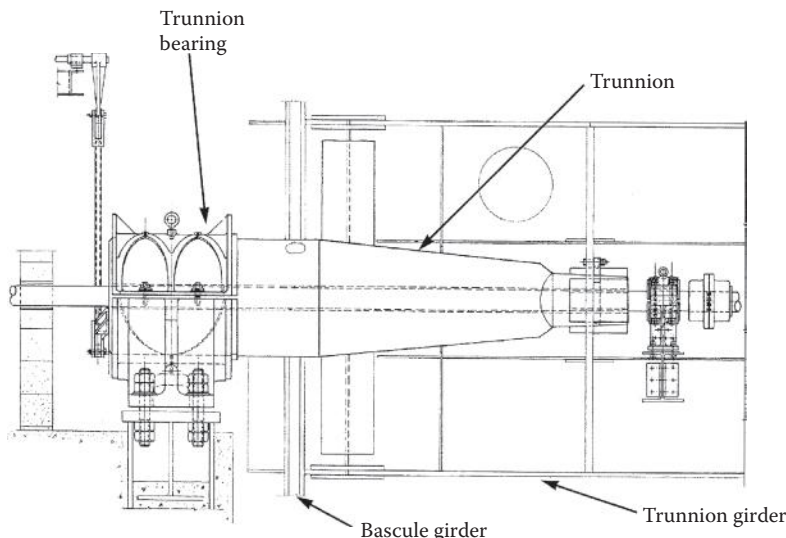


FIGURE 13.19 Trunnion and trunnion bearing.

matches that of the trunnion in its deformed dead load position. Alternative solutions include high capacity spherical roller bearings and large spherical plain bearings. However, trunnion roller bearings, when used in combination with a computer based control system, can lead to span control problems. The low frictional resistance of a trunnion roller bearing results in low damping. Several constructed bridges of this type experienced poor motion control and jerky movements. More recent computer control systems have overcome these issues, however, field adjustments by a control system technician are typically required during commissioning. The crank arrangement shown on the left side of the figure is associated with a position indicator.

Figure 13.20 shows a typical arrangement of the treads for a rolling lift bascule. There are a number of variants to this type of arrangement and one needs to be cognizant that the treads and associated track may experience plastic flow when in operation over a long period of time. Thus the treads and tracks are detailed in sections so that they can be replaced.

Figure 13.21 is a typical drive mechanism for a vertical lift bridge, with a tower drive. The drive is somewhat similar to that used for a bascule bridge except that a differential is not typically used and the

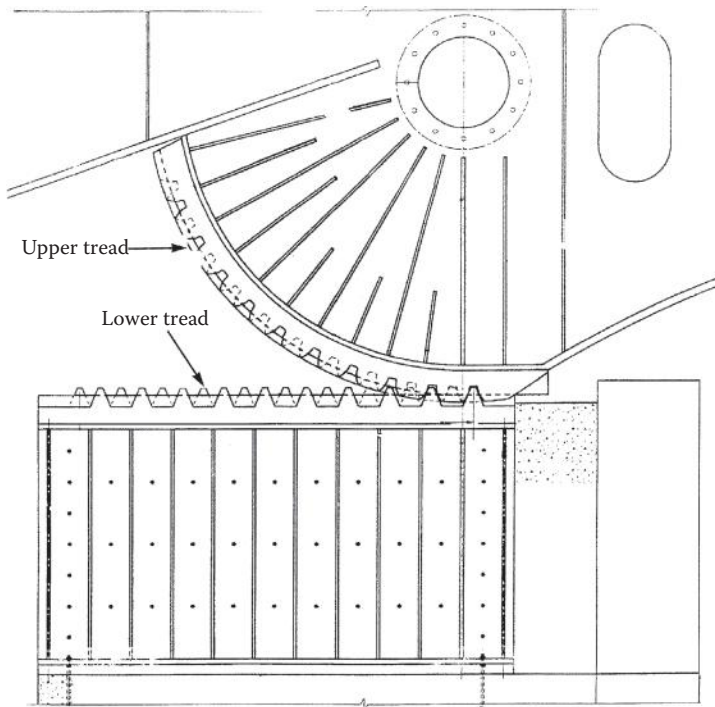


FIGURE 13.20 Treads for a rolling lift bascule.

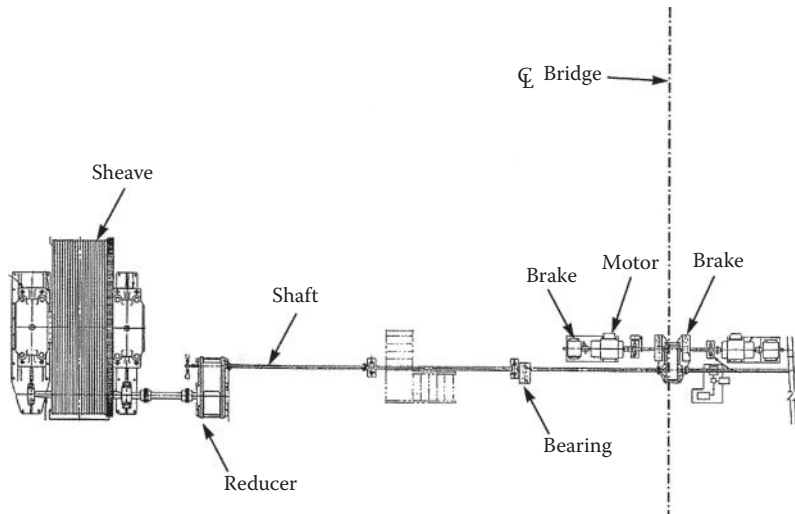


FIGURE 13.21 Drive mechanism for vertical lift bridge.

pinion drives the rack attached to a sheave rather than a rack attached to a bascule girder. Although a mechanical drive is shown, a similar arrangement could be accomplished with hydraulic motors.

Figure 13.22 is a typical welded sheave used for a vertical lift bridge. As shown there are 16 rope grooves so this would be associated with a large vertical lift bridge. Typically there are 4 sheaves for a vertical lift bridge, one at each corner of the lift span, although heavier bridges sometimes use 8 sheaves.

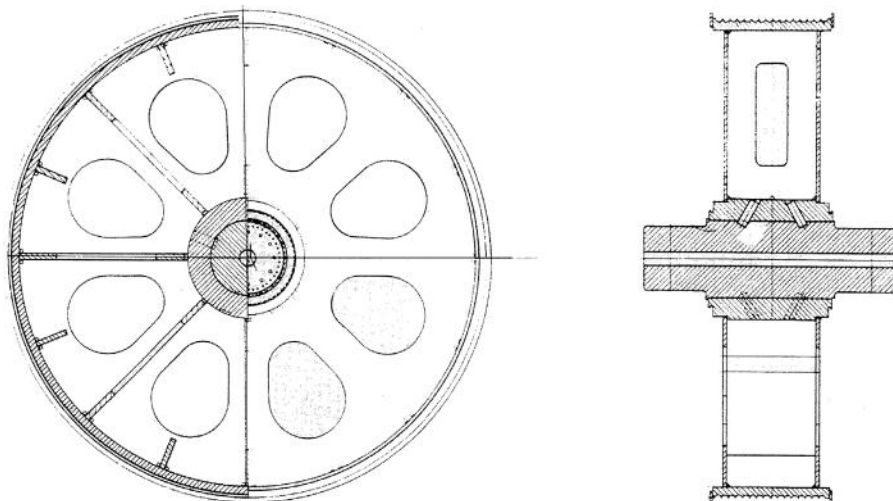


FIGURE 13.22 Welded sheave for a vertical lift bridge.

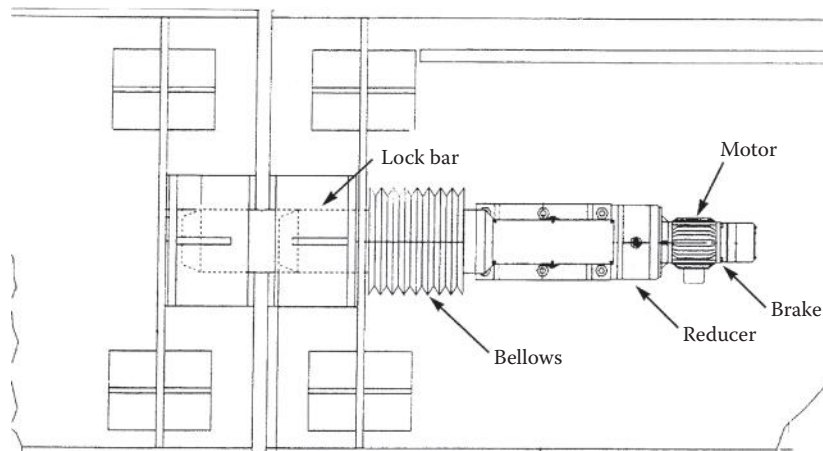


FIGURE 13.23 Span lock between leaves of a double leaf bascule bridge.

The trunnion bearing is not shown but would be similar to that shown in a bascule bridge trunnion. While sleeve bearings are commonly used, spherical roller type bearings are also considered to allow for trunnion flexure and reduce friction loads.

Figure 13.23 shows a span lock typically used between the leaves on a two leaf bascule bridge. In this case a manufactured unit is illustrated. It incorporates a motor, brake, reducer and lock bars. Alternative arrangements with a standard reducer are also used, although for this type of an installation the compactness and limited weight favor a one piece unit. It is important that provisions be included for replacement of the wearing surfaces in the lock bar sockets and realignment as they receive considerable wear.

Figures 13.24 and 13.25 show a pivot bearing, balance wheel and live load wedge arrangement typically used for a center pivot swing span. For highway bridges AASHTO states that “*Swing bridges shall preferably be the center bearing type.*” No such preference is indicated by AREMA. The center pivot, which contains a bronze bearing disc, carries the dead load of the swing span. The balance wheels are

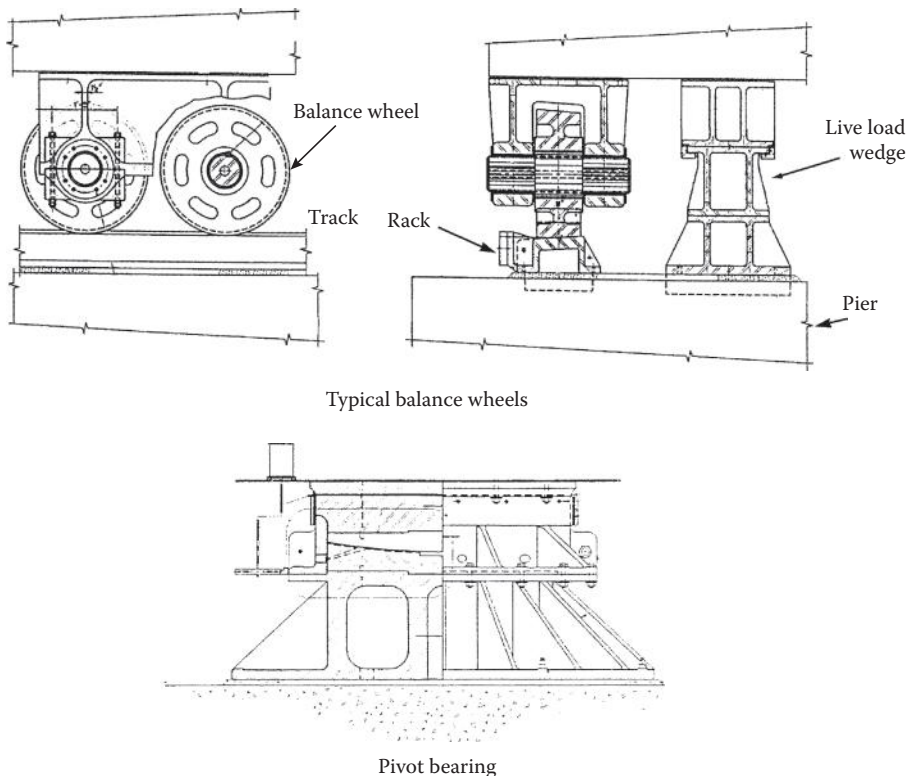


FIGURE 13.24 Balance wheels and pivot bearing for a center pivot swing span.

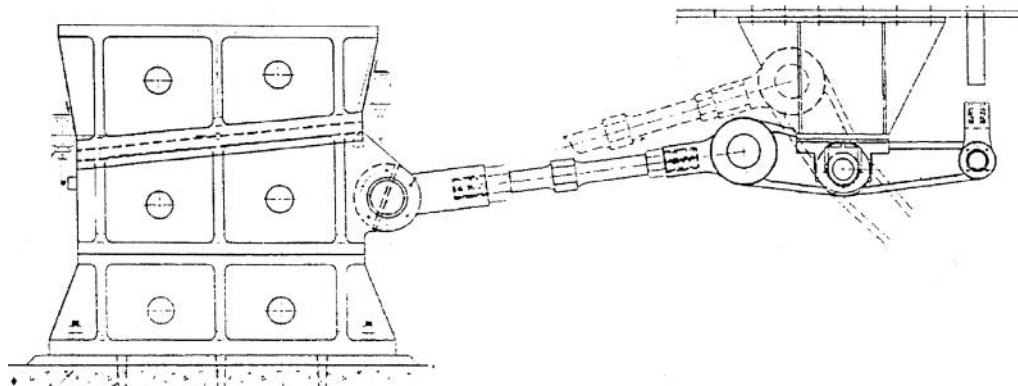


FIGURE 13.25 Live-load wedge arrangement for center pivot swing span.

only intended to accommodate unbalanced wind loads when the span moves so that they are adjusted to be just touching the roller track. The wedges are designed to carry the bridge live load and are retracted prior to swinging the span.

Figure 13.26 shows a rim bearing type swing span arrangement. Note that it is much more complicated than the center pivot arrangement shown above. The rollers must be designed to carry dead, live, and impact loads and, unlike the intermittent rollers used for a center pivot bridge, need to be placed in a continuous fashion all around the rim. The purpose of the center pivot is to keep the rollers centered,

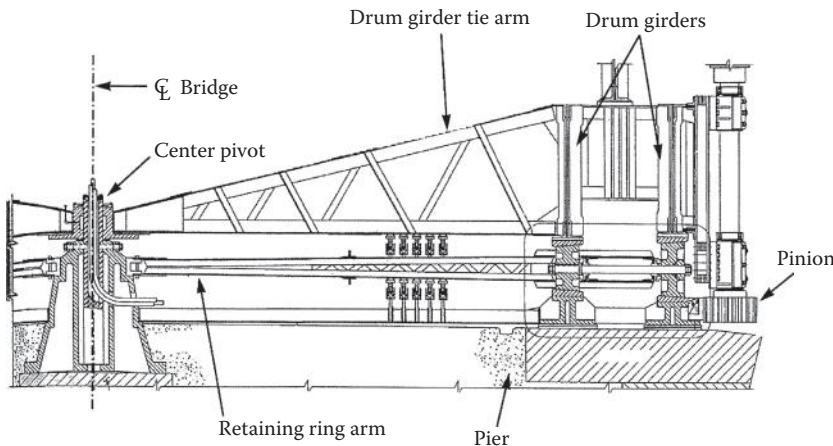


FIGURE 13.26 Rim-bearing swing span arrangement.

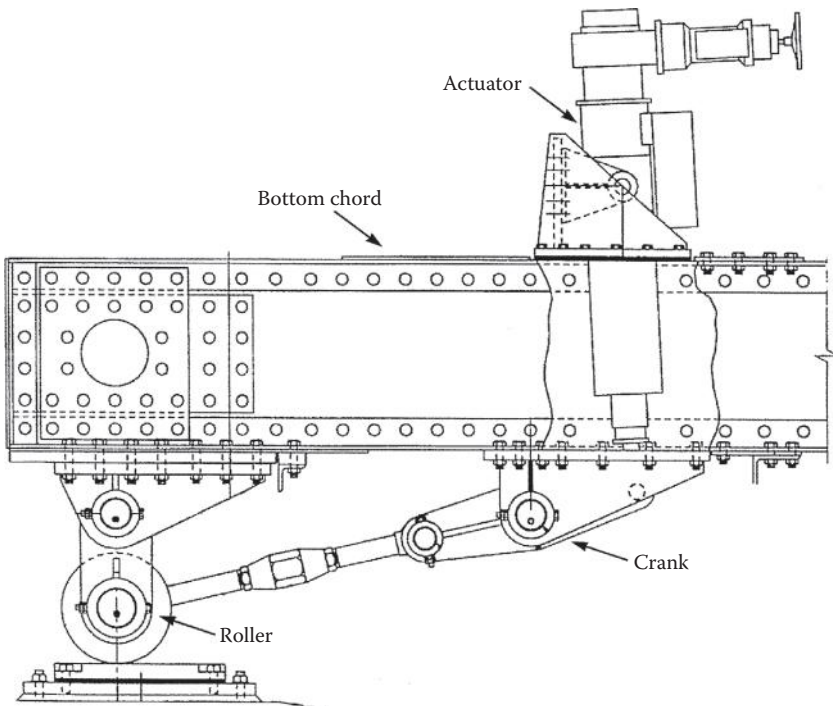


FIGURE 13.27 End lift device for a swing span.

and for some bridges to carry a portion of the dead and live load. In seismic areas the center pivot also needs to resist seismic forces. Figure 13.27 shows an end lift device used for a swing span.

Figure 13.28 shows a mechanical drive arrangement for a swing span, and similar arrangements can be adapted to both pivot and rim bearing bridges. A common problem with this arrangement is the pinion attachment to the structural supports as very high forces can be induced in braking the swing span when stopping and these supports tend to be a maintenance problem. Figure 13.29 illustrates one of 4 hydraulic drives from the Coleman Bridge. This drive has an eccentric ring mount so that the pinion/rack backlash can be adjusted.

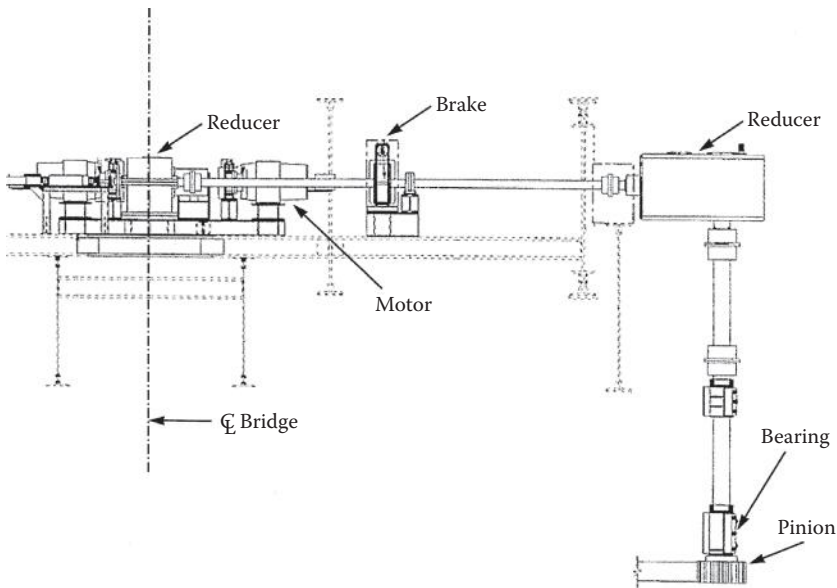


FIGURE 13.28 Mechanical drive arrangement for a swing span.

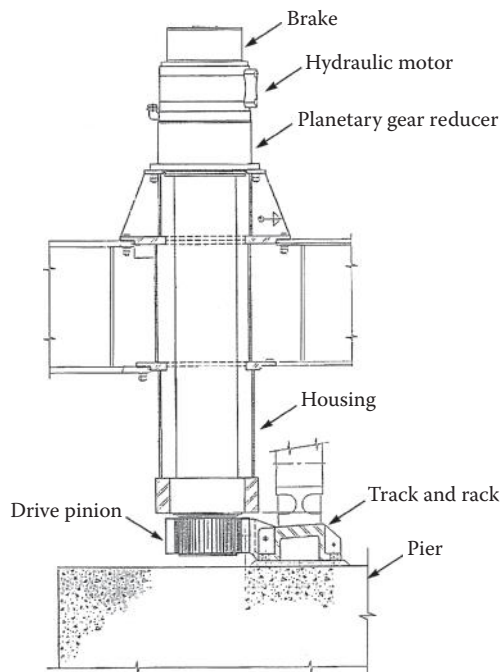


FIGURE 13.29 One of four hydraulic drives from the Coleman Bridge, York River, Virginia.

Figure 13.30 shows a hydraulic drive for a swing span using hydraulic cylinders. This would be more likely used for temporary operation.

Figure 13.31 shows a typical air buffer. These are provided at the ends of the movable span. With modern control systems, particularly with hydraulics, buffers may not be required to assist in seating. For many years these were custom fabricated but one can now utilize off the shelf commercial air or hydraulic buffers, as is shown here.

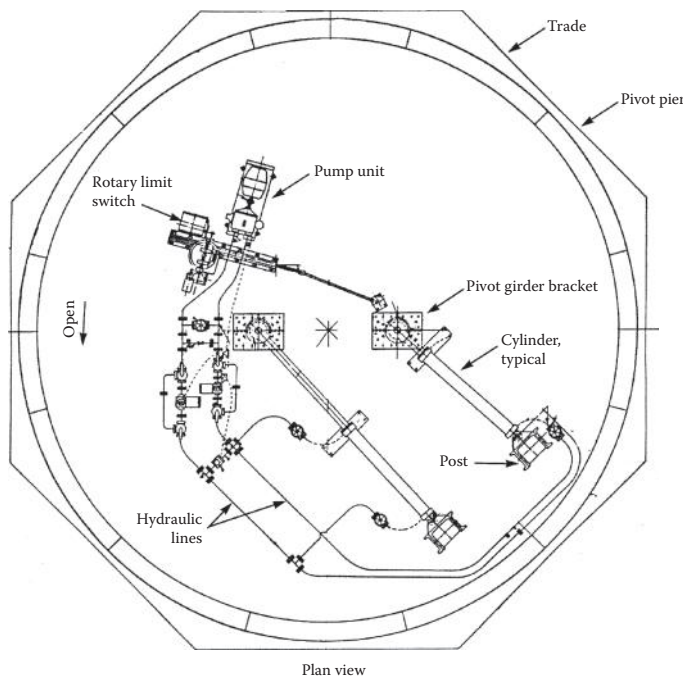


FIGURE 13.30 Hydraulic drive for a swing span using hydraulic cylinders.

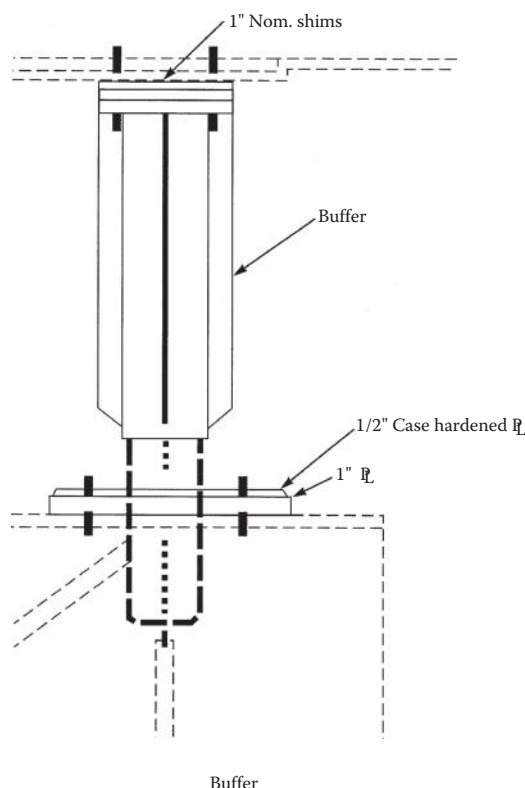


FIGURE 13.31 Typical air buffer

@Seismicisolation

13.5 Bridge Operation, Power, and Controls

13.5.1 Bridge Operations

Movable bridges are designed to be operated following a set protocol and this protocol is incorporated into the control system as a series of permissive interlocks. The normal sequence of operation is as follows: vessel signals for an opening, usually through a marine radio but it can be with a horn. For a highway bridge, the operator sounds a horn, activates the traffic signals halting traffic, lowers the roadway traffic warning gates, then lowers the barrier gates. For a railroad bridge the operator needs to get a permissive signal from the train dispatcher. This permissive signal is typically both verbal and through enabling the bridge controls for the operator.

After the barrier gates are lowered, a permissive signal allows the operator to withdraw the span locks and wedges and lifts, and once that is completed to open the span. The vessel then can proceed through the navigation channel opening. To close the bridge, the steps are reversed.

The controls are operated from a control desk and Figure 13.32 shows a typical control desk layout. Note that the control desk includes a position indicator to demonstrate the movable span(s) position as well as an array of push buttons to control the operation. A general objective in designing such a desk is to have the position of the buttons mimic the sequence of operations. Typically the buttons are lit to indicate their status.

13.5.2 Bridge Power

In the early years, when the streets of most cities had electric trolleys, movable bridges were operated on the 500 V d.c. trolley power and used trolley type (drum) controls where the operator manually moved a lever to control the speed. As the trolleys were removed, rectifiers were installed on the bridges to transform the power utility company alternating current (a.c.) to direct current (d.c.). Many of the historical movable bridges that are still operating on their original d.c. motors and drum switch/relay speed controls have these rectifiers. Most of the movable bridges that have been rehabilitated in recent years, but

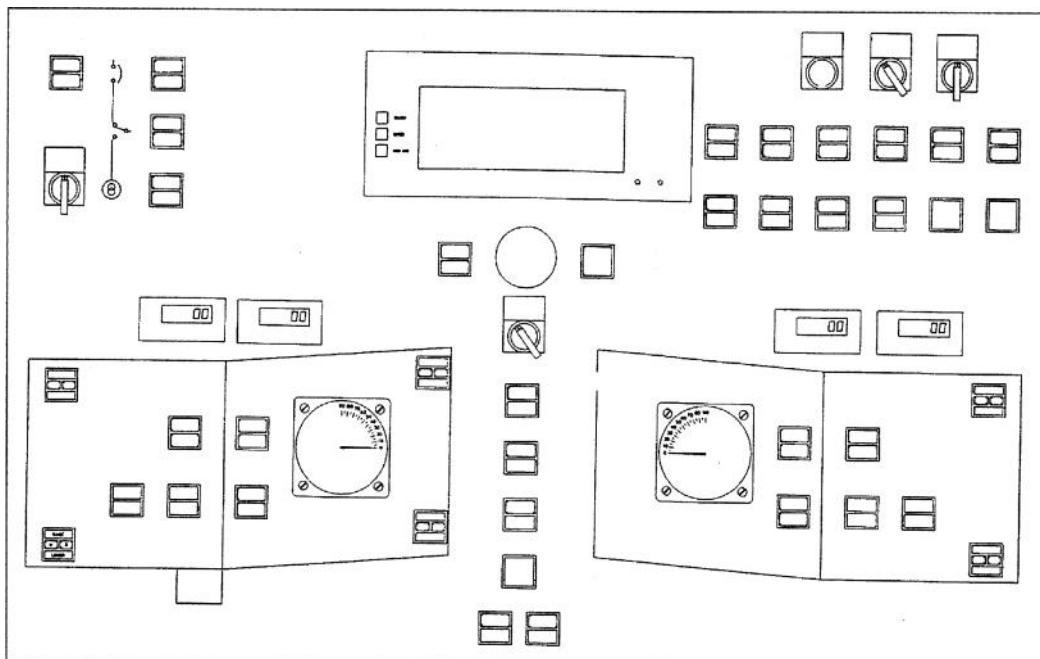


FIGURE 13.32 Layout of a typical control desk.

still retain the original d.c. motors, now have Silicon Controlled Rectifier (SCR) controllers that use a.c. voltage input and produce a variable d.c. voltage output directly to the motor.

The most common service voltage for movable bridges is 480 V a.c., 3 phase. Although in some locations, the service is 240 or 208 V a.c., 3 phase. Economics and the utility company policies are the primary determinant factors for the voltage used. The choice of one voltage over the other has no bearing on the cost of power for a movable bridge. Power is power and the rate per kilowatt-hour is the same regardless of voltage. A service cost factor that is sometimes overlooked is the demand charge that utility companies impose on very large intermittent loads. These charges are to offset the utility companies cost of reserving power generation and transmission capacity to serve the demands of a facility that is normally not on line. In the case of a bridge that has a very high power demand, even if it is opened only once or twice a year, the annual electricity costs are very high because the owner has to pay for the demand capacity whether it is used or not. Referring to the earlier discussion on counterweights, it is very important that the bridge design is as energy efficient as possible.

Both AREMA (2011) and AASHTO (1988 and 2012a) require a movable bridge to have an emergency means of operation should primary power be lost. Most bridges are designed with a backup engine driven generator and operate the bridge on the normal electric motor drives. For safety and reliability, diesel engines are preferred by most bridge owners. Hand operation can be provided as back-up for auxiliary devices such as locks, gates, and wedges.

There are other types of backup systems such as the following:

1. Internal combustion engines or air motors on emergency machinery that can be engaged when needed.
2. Smaller emergency electrical motors on emergency machinery to reduce the size of the emergency generator.
3. A receptacle for a portable emergency generator. The purpose is to use the portable generator for several bridges to reduce the capital investment for emergency power. The practical applications of this method are very limited because it can be difficult to get a portable generator to a bridge site during an emergency.

13.5.3 Bridge Control

The predominant control system in use in newly constructed or rehabilitated movable bridges is the programmable logic controller (PLC). This is a computer based system that has been adapted from other industrial type applications. The PLC offers the ability to automate the operation of a bridge. Many agencies have used the PLC as a replacement for a relay based system to reduce the cost of initial construction and to reduce the space required for the control system. Other common applications for the PLC include generation of alarm messages to help reduce time in trouble shooting and maintenance of the systems.

As an example of their widespread use, the New Jersey Department of Transportation has PLC systems on all of their bridges and have a proactive training program for their operations and technical staff. However, not all states are using PLC systems. Some movable bridge owners are returning to the hardwired relay based systems. These owners favor the relay based systems because they do not have the technical staff to maintain the PLC, and because the electronics tend to become obsolete quickly with each new PLC offering.

A more recent development is the use of PLC systems for remote operation. For example, the City of Milwaukee, WI, has several bridges that are controlled remotely by means of computer modem links and closed-circuit TV. This reduces their staff to one tender for three bridges per shift. The potential liability of this type of system needs to be carefully evaluated as the bridge operator may not be able to adequately observe all parts of the bridge in all weather conditions when the spans operate. It is typically necessary for the operator to maintain visual contact at all times with pedestrians, motor vehicles, and vessels.

Environmental regulations have made the installation permits for submarine cables difficult to obtain. PLC and radio modems have been used in several states to replace the control wiring that would otherwise be in a submarine cable. These types of installations have varying degrees of success and depend on the ability to have reliable wireless communications across the waterway. The great proliferation of wireless devices is making it difficult to maintain reliable communications without performing detailed surveys or using dedicated licensed frequencies.

The advent of horizontal directional boring technology offers an alternative to trenching waterways for submarine cables. Directional boring systems use GPS (global positioning systems) or inertial navigation systems to accurately drill and install underground ducts for electrical conduit and cables, or of other utility piping. The cable lengths are somewhat greater with a directional bore due to the bore radius required to reach depths below the waterway. Additional cable length is needed to double back to the bridge approaches and piers from the landing points on the shores of the waterway.

The selection of a span drive system is performance oriented. Reliability and cost are key issues. The most common drives for movable bridges over that past 90 years have been d.c. and wound rotor a.c. motors with relays, drum switches, and resistors. These two technologies remain common today although there have been many advances in d.c. and a.c. motor controls and the old systems are rapidly being replaced with solid state electronic drives.

The modern d.c. drives on movable bridges are digitally controlled, fully regenerative, four quadrant, SCR (silicon controlled rectifiers) motor controllers. In more general terms, this is a solid state drive that provides infinitely variable speed and torque control in both forward and reverse directions. They use microprocessor programming to provide precise adjustments of operating parameters. Once a system is set up, it rarely needs further adjustment. Programmable parameters include acceleration, deceleration, preset speeds, response rate, current/torque limits, braking torque, and sequence logic. This type of drive has been proven to provide excellent speed and torque control for all bridge operating conditions.

The wound rotor motor drive technology has also moved into digital control. The SCR variable voltage controllers are in essence crane control systems. While they are not quite as sophisticated as the d.c. drives, they have similar speed and torque control capabilities. It is common for movable bridges to be retrofitted with these drives using the existing motors.

Adjustable frequency controllers (AFC) control speed by varying the frequency of the a.c. voltage and current to a squirrel cage induction motor. The original AFC drives were used on movable bridges with some success, but they were not well suited for this type of application. There are two primary reasons. First, this type of drive was designed for the control of pumps and fans, not high inertia loads. Second, at low speeds, it does not provide sufficient braking torque to maintain control of an overhauling load. This is a significant concern when controlling and seating a span with an ice, snow, or wind load.

The newer type of AFC is the flux vector controlled drive which has been in use on movable bridges since the late 1990s. Their use has become one of the favorites among movable bridge engineers for both new and rehabilitated bridges. It is a sophisticated drive system that controls magnetic flux to artificially create slip and thus control torque at any speed. This control includes providing full rated motor torque at zero speed which was not previously possible with a.c. squirrel cage induction motors. The drive controller uses input from a digital shaft encoder to locate the motor rotor position and then calculates how much voltage and current to provide to each motor lead. The drive's capability to provide 100% rated torque at zero speed gives it excellent motion control at low speeds.

Much empirical knowledge has been learned about the a.c. vector drives since the late 1990s. The successful application of this technology may require the use of motors specially made for inverter and vector duty. Consideration must also be given to the motor horsepower and speed/torque characteristics when replacing existing motors during rehabilitations. In some cases, it may be necessary to increase the horsepower rating of a replacement motor. It may also be necessary for a replacement motor to have a customized operating frequency other than the standard 60 Hz to provide the needed motor speed. Motors specifically made for use with the vector drives typically have higher rated electrical insulation for the motor windings and may require a means for auxiliary cooling. However, care must be taken in

selecting the motor size if retrofitting an existing bridge as an oversized motor may accelerate wear on the drive machinery.

Vector drives may require power filters to reduce adverse effects from harmonics they generate. It is generally advisable to keep the distances between the drives and motors as short as possible, or to use feeders with higher voltage insulation ratings than those conventionally used. These precautions may be needed to mitigate potentially damaging reflected voltage spikes generated in vector drive systems (BMC 2002). Additional precautions are advisable when selecting motors for use with vector drives to be sure the motor bearings are electrically isolated or grounded. Premature motor bearing failures have been reported when using vector drives (USMC 2002; Boyanton 2010). The failures are due to motor shaft voltages causing current to arc from the rotor to the stator through the bearings. The arcing is essentially equivalent to many “micro lighting storms” that cause bearing pitting. The premature bearing failures are being addressed by motor manufacturers making the necessary design changes to the motor grounding and insulation.

13.6 Traffic Control

Rail traffic control for movable railroad bridges involves interlocking the railroad signal system with the bridge operating controls. Interlocking must include the traction power system for a movable bridge that is on a railroad line that has third rail or catenary power. In principal, railroad signal interlocks need to indicate that the track is closed and the power is de-energized prior to operating the span. The particulars of how this is accomplished depends upon the railroad in question and can vary widely.

Highway traffic control for a movable highway bridge is governed by AASHTO's Standard Specifications for Movable Highway Bridges (AASHTO 2012a), as well as the Manual for Uniform Traffic Control Devices (MUTCD) (FHWA 2009). Each owner may impose additional requirements but the MUTCD is typically used in the United States. Requirements include a DRAWBRIDGE AHEAD warning sign, traffic signals, traffic warning gates, and resistance barrier gates. One possible arrangement is shown below (Figure 13.33) for a two leaf bascule bridge. Note that there are no resistance

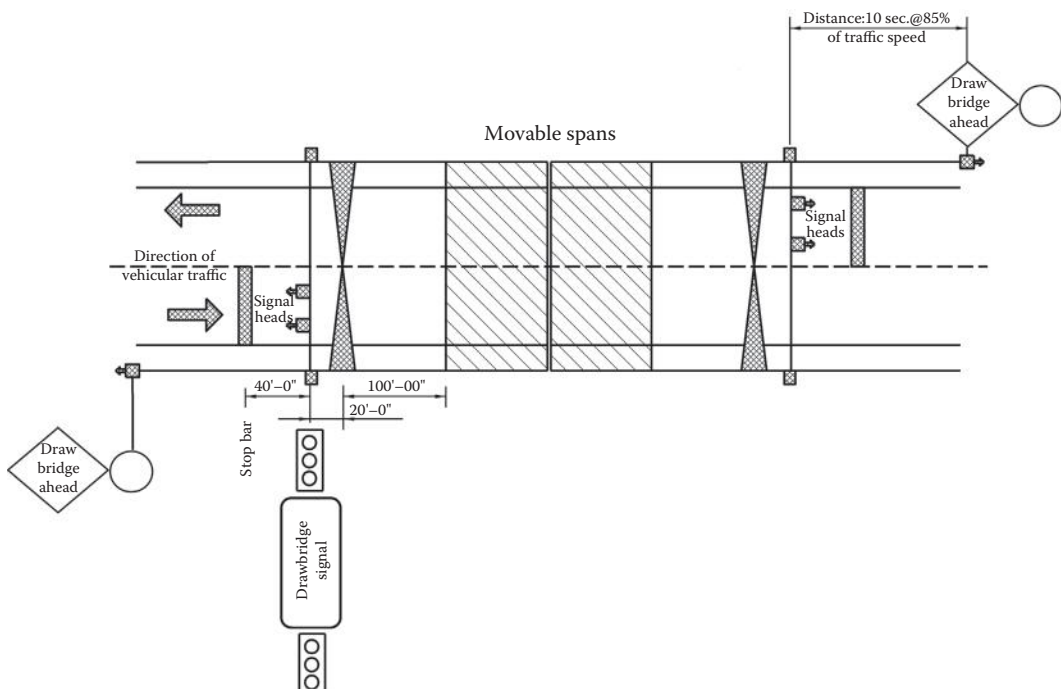


FIGURE 13.33 Typical layout of movable bridge signals and gates.

barrier gates in this figure. AASHTO (1988) requires that a resistance gate providing a positive barrier be placed prior to a movable span opening except where the span itself, such as a bascule leaf, blocks the opening.: AASHTO (2012) is interpreted by many movable bridge engineers to have the same requirement for resistance barriers, although the requirement is not as clearly stated as in the AASHTO (1988).

Navigation lights for marine traffic must follow the requirements of the bridge permit as approved by the U.S. Coast Guard. The permit typically follows the Coast Guard requirements as found in the U.S. Code of Federal Regulations 33, Part 118, Bridge Lighting and Other Systems (CFR 1986). These regulations identify specific types and arrangements for navigation lights depending upon the type of movable bridge.

Glossary

This glossary includes terms particular to movable bridge engineering.

Bascule Bridge—Pivot upward from a horizontal axis to open. Highway bascules can be either single or double leaf; however, railroad bascules are single leaf so that the heavy railroad live load and impact are taken on fixed substructure elements. Bascule is a French word for a seesaw or a balance type scale.

Bushing (mechanical)—A soft metal sleeve that resists radial, and sometimes axial, loads on rotating or sliding components.

Cross-bearing—A misalignment condition in which gear teeth or shaft bearings are out of parallel lengthwise.

Hydraulics—The study of fluid flow and pressure. Industrial hydraulics use fluids to transmit and control energy. Typical components include an HPU, piping/tubing, cylinders, and or hydraulic motors.

Hydraulic Power Unit (HPU)—A system that controls and converts energy into the form of hydraulic pressure and flow. HPU is typically powered by an electrical motor(s) or internal combustion engine, this prime mover is connected to a hydraulic pump. Other typical HPU components include a hydraulic reservoir, valves, filters, a manifold, piping/tubing, and an electrical control system.

Leaf—The movable portion of a bascule bridge.

Megger—A small d.c. power supply used for testing insulation resistance. The meter scale is usually calibrated to read megohms directly.

Motor Control Center (MCC)—Electrical switchgear used to start and control electric motor operation.

Movable Bridge—A bridge having one or more spans that are capable of being translated and/or rotated to provide passage for boats or other navigable vessels. The three most typical movable bridge types are bascule, swing, and vertical lift.

Pinion—The smaller gear in a gear set. The pinion is typically the driver.

Programmable Logic Controller (PLC)—An electronic device based on a microprocessor that uses pre-programmed logic to control the operation of a device, system, or the entire movable span. A PLC is an alternative to relays.

Pump—A mechanical device converts rotational energy into hydraulic pressure and flow.

Rack—A gear with teeth spaced along a straight line or very large radius.

Relay—An electro-mechanical device used in “hard-wired” logic circuit to control the operation of a device, system, or the entire movable span. Relays are an alternative to a PLC.

Scour—Removal of material from the bed and banks across all or most of the width of the waterway, at restricted parts of the channel, or around obstructions such as a bridge piers, piles, or abutments. This issue is significant for all bridges, but has particular importance for movable bridges due because of increased sensitivity to settlement and tight fit tolerances.

Swing Bridge—A movable span that rotates in a horizontal plane about a vertical axis.

Trunnion—A shaft or pin about which an object can be rotated or tilted. The word trunnion comes from the French circa 1625 and was used for the shafts on either side of a cannon. For bascule bridges, the trunnions support the entire weight of the moving span. The sheave shafts for vertical lift bridges are sometimes also referred to as trunnions.

Vertical Lift Bridge—A movable span that translates vertically.

References

- AASHTO. 1938. *Standard Specifications for Movable Highway Bridges*, American Association of State Highway Officials, Washington, DC.
- AASHTO. 1988. *Standard Specifications for Movable Highway Bridges*, 5th Edition, with 1992, 1993, and 1995 Interims, American Association of State Highway and Transportation Officials, Washington, DC.
- AASHTO. 2002. *Standard Specifications for Highway Bridges*, 17th Edition, American Association of State Highway and Transportation Officials, Washington, DC.
- AASHTO. 2012a. *AASHTO LRFD Movable Bridge Design Specifications*, 2nd Edition with 2008, 2010, 2011 and 2012 Interim Revisions, American Association of State Highway and Transportation Officials, Washington, DC.
- AASHTO. 2012b. *AASHTO LRFD Bridge Design Specifications*, Customary U.S. Units, 2012, American Association of State Highway and Transportation Officials, Washington, DC.
- Abrahams, M. J. 1998. "Seismic Performance of Movable Bridges," in *Heavy Movable Structures, Seventh Biennial Symposium, Heavy Movable Structures*, Inc., Lake Buena Vista, FL.
- ARA. 1922. *Manual of Railway Engineering*, American Railway Association, New York, NY.
- AREMA. 2011. *Manual for Railway Engineering*, Chapter 15, Steel Structures, Part 6, Movable Bridges, Lanham, MD.
- BMC. 2002. *Fundamentals of Inverter-Fed Motors*, Technical Manual (Manual Number MN780), Baldor Motor Company, St. Joseph, MO.
- Boyanton, H. 2010. Shaft Grounding Systems, Inc., *Bearing Damage Due to Electric Discharge—Electrical Discharge Machining of Bearings*, Shaft Grounding Systems, Inc., Albany, OR.
- CFR. 1986. *Code of Federal Regulations* 33, Part 118, Bridge Lighting and Other Systems, Federal Highway Administration, Washington, DC.
- FHWA. 2009. *Manual on Uniform Traffic Control Devices*, Federal Highway Administration, Washington, DC.
- USMC. 2002. "Bearing Failures," *Product Service Bulletin*, Volume 3, U.S. Motor Corporation (Emerson), Los Angeles, CA.

Further Reading

Significant engineering books and chapters for further reading on the subject of movable bridges.

- Birnstiel, C. 2008. "Chapter 12—Movable Bridges," in *Manual of Bridge Engineering*, Ed. Ryall, M.J., Parke, G.A.R. and Harding, J.E., Institute of Civil Engineers, Thomas Telford Ltd, London, UK.
- Hoole, G. A., Kinne, W. S., Zippoldt, R. R. et al. 1943. *Movable and Long Span Steel Bridges*, McGraw-Hill, New York, NY.
- Hovey, O. S. 1926. *Movable Bridges, Volumes 1 & 2*, John Wiley & Sons, Inc., New York, NY.
- Koglin, T. L. 2003. *Movable Bridge Engineering*, John Wiley & Sons, Inc., New York, NY.

@Seismicisolation

14

Floating Bridges

14.1	Introduction	549
14.2	Basic Concepts.....	551
14.3	Types	552
	Floating Structure • Anchoring Systems	
14.4	Design Criteria	555
	Loads and Load Combinations • Winds and Waves • Potential	
	Damage • Control Progressive Failure • Design of Concrete	
	Members • Anchoring System • Movable Span • Deflection and	
	Motion	
14.5	Structural Design and Analysis.....	561
	Preliminary Design • Dynamic Analysis • Frequency Domain	
	Analysis	
14.6	Fabrication and Construction	565
14.7	Construction Cost	567
14.8	Inspection, Maintenance, and Operation.....	567
14.9	Closing Remarks	568
	References.....	570

M. Myint Lwin
*U.S. Department of
Transportation*

14.1 Introduction

Floating bridges are cost effective solutions for crossing a large body of water with unusual depth and very soft bottom where conventional piers are impractical. For a site where the water is 2–5 km (1.24–3.11 miles) wide, 30–60 m (100–200 ft.) deep and a very soft bottom extending another 30–60 m (100–200 ft.), a floating bridge is estimated to cost 3–5 times less than a long span fixed bridge, tube, or tunnel.

A modern floating bridge may be constructed of wood, concrete, steel or a combination of materials, depending on the design requirements. A 124 m (407 ft.) long floating movable wood pontoon railroad bridge was built in 1874 across the Mississippi River in Wisconsin. It was rebuilt several times before it was abandoned. A 98 m (322 ft.) long wood floating bridge is still in service in Brookfield, Vermont. The present Brookfield Floating Bridge is the seventh replacement structure, and was built by the Vermont Agency of Transportation in 1978. The first 2018 m (6621 ft.) long Lake Washington Floating Bridge in Seattle (Andrew 1939; Lwin 1993) Washington State, was built of concrete and opened to traffic in 1940 (Figure 14.1). Since then, three more concrete floating bridges were built (Lwin 1993; Nichols 1962). These concrete floating bridges form major transportation links in the State and Interstate highway systems in Washington State. The Kelowna Floating Bridge on Lake Okanagan in British Columbia, Canada (Pegusch 1957), was built of concrete and opened to traffic in 1958. It was 640 m (2100 ft.) long and carries 3 lanes of traffic. This 3-lane bridge was replaced with a five-lane floating bridge to mitigate congestion and improve safety and efficiency of traffic movement across Lake Okanagan, and support economic growth in the region. The new bridge was opened to traffic on May 25, 2008, and was renamed the William R. Bennett Bridge in honor of the former Premier William Richards Bennett, who was a



FIGURE 14.1 First Lake Washington Floating Bridge. (Courtesy of Washington State DOT.)



FIGURE 14.2 The Bergsoysund Floating Bridge.

native of Kelowna. The 1246 m (4088 ft.) long Salhus Floating Bridge and the 845 m (2772 ft.) long Bergsoysund Floating Bridge in Norway (Figure 14.2) were constructed of concrete pontoons and steel superstructures (Landet 1994). They were opened to traffic in the early 1990s.

Washington State's experience has shown that reinforced and prestressed concrete floating bridges are cost effective, durable and low in maintenance as permanent transportation facilities. Concrete is

highly corrosion resistant in a marine environment when properly designed, detailed, and constructed. Concrete is a good dampening material for vibration and noise, and is also far less affected by fire and heat than wood, steel, or other construction materials.

14.2 Basic Concepts

The concept of a floating bridge takes advantage of the natural law of buoyancy of water to support the dead and live loads. There is no need for conventional piers or foundations. However, an anchoring or structural system is needed to maintain transverse and longitudinal alignments of the bridge.

A floating bridge is basically a beam on elastic continuous foundation and supports. Vertical loads are resisted by buoyancy. Transverse and longitudinal loads are resisted by a system of mooring lines or structural elements.

The function of a floating bridge is to carry vehicles, trains, bicycles, and pedestrians across an obstacle—a body of water. In as much as a floating bridge crosses an obstacle, it creates an obstacle for marine traffic. Navigational openings must be provided for the passage of pleasure boats, smaller water crafts and large vessels. These openings may be provided at the ends of the bridge. However, large vessels may impose demands for excessive horizontal and vertical clearances. In such cases, movable spans will have to be provided to allow the passage of large vessels. The Hood Canal Floating Bridge in Washington State has a pair of movable spans capable of providing a total of 183 m (600 ft.) of horizontal clearance (Figure 14.3). Opening of the movable spans for marine traffic will cause interruption to vehicular traffic. Each interruption may be as long as 20–30 minutes. If the frequency of openings is excessive, the concept of a floating bridge may not be appropriate for the site. Careful consideration should be given to the long term competing needs of vehicular traffic and marine traffic before the concept of a highway floating bridge is adopted.



FIGURE 14.3 Movable spans for large vessels.

14.3 Types

14.3.1 Floating Structure

Floating bridges have been built since time immemorial. Ancient floating bridges were generally built for military operations (Gloyd 1988). All of these bridges took the form of small vessels placed side by side with wooden planks used as a roadway. Subsequently, designers added openings for the passage of small boats, movable spans for the passage of large ships, variable flotation to adjust for change in elevations, and so on.

Modern floating bridges are generally consisted of concrete pontoons with or without elevated superstructure of concrete or steel. The pontoons may be reinforced concrete or post-tensioned in one or more directions. They may be classified into two types, namely, the continuous pontoon type and the separate pontoon type. Openings for the passage of small boats and movable spans for large vessels may be incorporated into each of the two types of modern floating bridges. Table 14.1 summarizes the leading floating bridge spans in the world.

A continuous pontoon floating bridge consists of individual pontoons joined together to form a continuous structure (Figure 14.4). The size of each individual pontoon is based on the design requirements, the construction facilities and the constraints imposed by the transportation route. The top of the pontoons may be used as a roadway or a superstructure may be built on top of the pontoons. All the present floating bridges in Washington State are the continuous pontoon floating bridge type.

A separate pontoon floating bridge consists of individual pontoons placed transversely on the structure and spanned by a superstructure of steel or concrete (Figure 14.5). The superstructure must be of

TABLE 14.1 Leading Floating Bridge Spans

Rank	Bridge Name	Total Length, m (ft.)	Structure Features	Draw Span, m (ft.)	Year Opened	Usage	Country
1	Albert D. Rosselini Bridge	2309.8 (7578)		61.0 (200)	1963	Hwy	USA
2	First Lake Washington Bridge	1999.8 (6561)		61.0 (200)	1940	Hwy	USA
3	New Lacey V. Murrow Bridge	1999.8 (6561)		None	1993	Hwy	USA
4	Hood Canal Bridge	1990.3 (6530)		182.9 (600)	1962	Hwy	USA
5	Demerara Harbour Bridge	1851 (6072.8)			1978	Hwy	Guyana
6	Homer M. Hadley Bridge	1748.3 (5736)		None	1989	Hwy	USA
7	Nordhordland Bridge	1246 (4087.9)		None	1994	Hwy	Norway
8	Bergøysund Floating Bridge	933 (3061.0)		None	1992	Hwy	Norway
9	William R. Bennett Bridge	690 (2263.8)		None	2008	Hwy	Canada
10	Yumemai Bridge	410 (1345.1)	Arch	280 (918.6)	2001	Hwy	Japan
11	Dongjin Bridge	400 (1312.3)	Wood-boat	None	1173	Pedestrian	China
12	Eastbank Esplanade	365.8 (1200)		None	2001	Pedestrian	USA
13	Dubai Floating Bridge	365 (1197.5)		None	2007	Hwy	United Arab Emirates
14	Ford Island Bridge	283.5 (930)		283.5 (930)	1998	Hwy	USA
15	Queen Emma Bridge	167 (547.9)			1939	Hwy	Curaçao



FIGURE 14.4 Continuous pontoon type structure.

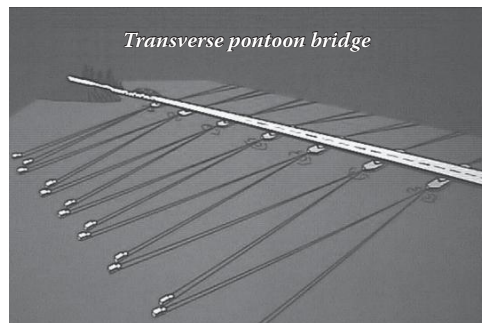


FIGURE 14.5 Separate pontoon type structure.

sufficient strength and stiffness to maintain the relative position of the separated pontoons. The two floating bridges in Norway are of the separate pontoon floating bridge type.

Both types of floating structures are technically feasible and relatively straight forward to analyze. They can be safely designed to withstand gravity loads, wind and wave forces, and extreme events, such as vessel collisions and major storms. They perform well as highway structures with high quality roadway surface for safe driving in most weather conditions. They are uniquely attractive and have low impact on the environment. They are very cost effective bridge types for water-crossing where the water is deep (say over 30 m [100 ft.]) and wide (say over 900 m [2953 ft.]), but the currents must not be very swift (say over 6 knots), the winds not too strong (say average wind speed over 160 km [99.4 miles] per hour) and the waves not too high (say significant wave height over 3 m [10 ft.]).

14.3.2 Anchoring Systems

A floating structure may be held in place in many ways—by a system of piling, caissons, mooring lines and anchors, fixed guide structures, or other special designs. The most common anchoring system consists of a system of mooring lines and anchors. This system is used in all the existing floating bridges in Washington State. The mooring lines are galvanized structural strands meeting ASTM A586. Different types of anchors may be used, depending on the water depth and soil condition. Four types of anchors are used in anchoring the floating bridges on Lake Washington, Seattle, Washington State.

Type A anchors (Figure 14.6) are designed for placement in deep water and very soft soil. They are constructed of reinforced concrete fitted with pipes for water jetting. The anchors weigh from 60 to 86 tons each. They are lowered to the bottom of the lake and the water jets are turned on allowing the anchors to sink into the soft lake bottom to fully embed the anchors. Anchor capacity is developed through passive soil pressure.

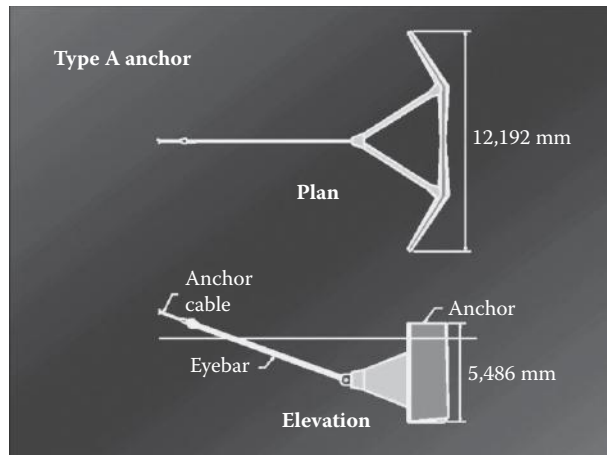


FIGURE 14.6 Type A anchor.

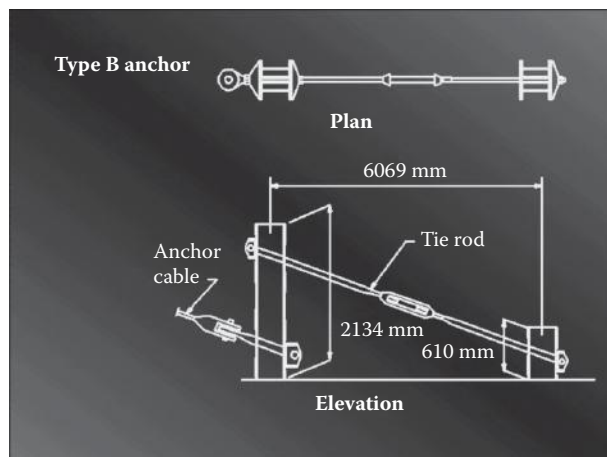


FIGURE 14.7 Type B anchor.

Type B anchors (Figure 14.7) are pile anchors designed for use in hard bottom and in water depth less than 27 m (89 ft.). A Type B anchor consists of two steel H-piles driven in tandem to a specified depth. The piles are tied together to increase capacity.

Type C anchors (Figure 14.8) are gravity type anchors, constructed of reinforced concrete in the shape of a box with top open. They are designed for placement in deep water where the soil is too hard for jetting. The boxes are lowered into position and then filled with gravel to the specified weight.

Type D (Figure 14.9) anchors are also gravity type anchors like the Type C anchors. They consist of solid reinforced concrete slabs, each weighing about 270 tons. They are designed for placement in shallow and deep water where the soil is too hard for water jetting. The first slab is lowered into position and then followed by subsequent slabs. The number of slabs is determined by the anchor capacity required. Type D anchors are the choice over Type B and Type C anchors, because of the simplicity in design, ease in casting and speed in placement.

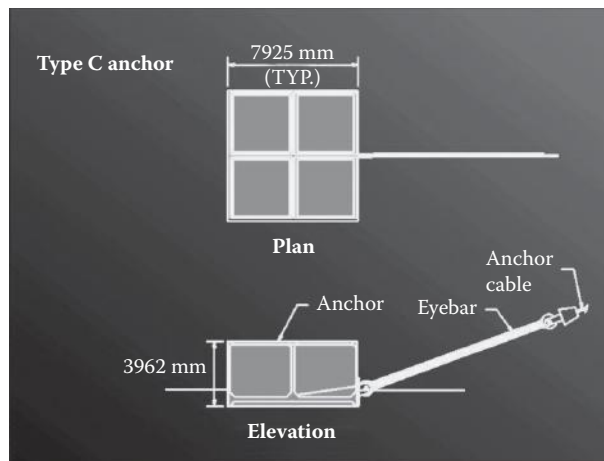


FIGURE 14.8 Type C anchor.

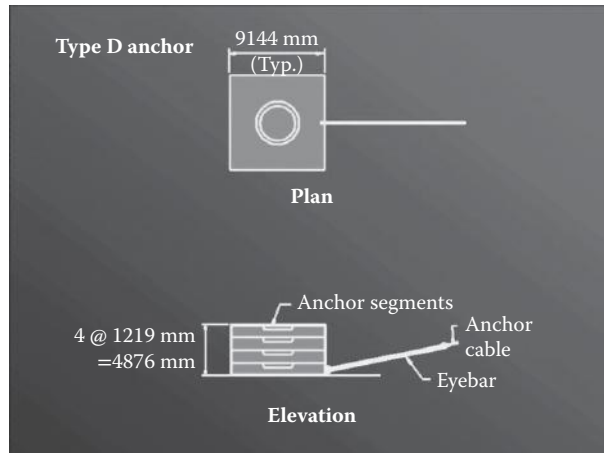


FIGURE 14.9 Type D anchor.

14.4 Design Criteria

The design of a floating bridge follows the same good engineering practices as for land-based concrete or steel bridges. In the United States, the design and construction provisions stipulated in the AASHTO Standard Specifications for Highway Bridges (AASHTO 2002) or the LRFD Bridge Design Specifications (AASHTO 2012) are applicable and should be adhered to as much as feasible. However, due to the fact that a floating bridge is floating on fresh or marine waters, the design criteria must address some special conditions inherent with floating structures. The performance of a floating bridge is highly sensitive to the environmental conditions and forces, such as, winds, waves, currents and corrosive elements. The objectives of the design criteria are to assure that the floating bridge will

- Have a long service life of 75–100 years with low life-cycle cost
- Meet functional, economical, and practical requirements
- Perform reliably and be comfortable to ride on under normal service conditions
- Sustain damage from accidental loads and extreme storms without sinking
- Safeguard against flooding and progressive failure

14.4.1 Loads and Load Combinations

The structure shall be proportioned in accordance with the loads and load combinations for service load design and load factor design outlined in the AASHTO Standard Specifications for Highway Bridges (AASHTO 2002) or the AASHTO LRFD Bridge Design Specifications (AASHTO 2012), except the floating portion of the structure shall recognize other environmental loads and forces, and modify the loads and load combinations accordingly.

Winds and waves are the major environmental loads, while currents, hydrostatic pressures and temperatures also have effects on the final design. Depending on the site conditions, other loadings, such as tidal variations, marine growth, ice, drift, and so on, may need to be considered.

14.4.2 Winds and Waves

Winds and waves exert significant forces on a floating structure (Figure 14.10). Yet these environment loads are the most difficult to predict. Generally there is a lack of long term climatological data for the bridge site. A long record of observations of wind data is desirable for developing more accurate design wind speeds and wave characteristics. It is advisable to install instruments on potential bridge sites to collect climatological data as early as possible.

Wind blowing over water generates a sea state that induces horizontal, vertical, and torsional loads on the floating bridge. These loads are a function of wind speed, wind direction, wind duration, fetch length, channel configuration and depth. Consideration must be given to the normal and extreme storm wind and wave conditions for the site. The normal storm conditions are defined as the storm conditions that have a mean recurrence interval of 1 year, which is the maximum storm that is likely to occur once a year. The extreme storm conditions are defined as the storm conditions that have a mean recurrence interval of 100 years, which is the maximum storm that is likely to occur once in 100 years. These wind and wave forces may be denoted by the following:

WN = Normal Wind on Structure—1-Year Storm

NW = Normal Wave on Structure—1-Year Storm

WS = Extreme Storm Wind on Structure—100-Year Storm

SW = Extreme Storm Wave on Structure—100-Year Storm



FIGURE 14.10 Wind and wave forces.

TABLE 14.2 Example of Wind and Wave Design Data

Return Interval	Wind Speed (1 min average), km/hr (miles/hr)	Significant Wave Height, m (ft.)	Period (s)
1-Year wind storm	76 (47)	0.85 (2.79)	3.23
20-Year wind storm	124 (77)	1.55 (5.09)	4.22
100-Year wind storm	148 (92)	1.95 (6.40)	4.65

The following modifications are recommended for the AASHTO Load Combinations where wind loads are included:

1. Substitute WS + SW for W, and WN + NW for 0.3W.
2. Use one-half the temperature loads in combination with WS and SW.
3. Omit L, I, WL, and LF loads when WS and SW are used in the design.

A 20-year wind storm condition is normally used to make operational decisions for closing the bridge to traffic to insure safety and comfort to the traveling public. This is especially important when there is excessive motion and water spray over the roadway. When there is a movable span in the floating bridge for providing navigation openings, a 20-year wind storm is also used to open the movable span to relieve the pressures on the structure.

Table 14.2 shows an example of a set of wind and wave design data.

14.4.3 Potential Damage

A floating bridge must have adequate capacity to safely sustain potential damages (DM) resulting from small vessel collision, debris or log impact, flooding and loss of a mooring cable or component. Considering only one damage condition and location at any one time, the pontoon structure must be designed for at least the following:

1. Collision: Apply a 45 kN (100 kip) horizontal collision load as a service load to the pontoon exterior walls. Apply a 130 kN (290 kip) horizontal collision load as a factored load to the pontoon exterior wall. The load may be assumed to be applied to an area no greater than 0.3 m × 0.3 m (1 ft. × 1 ft.).
2. Flooding:
 - Flooding of any two adjacent exterior cells along the length of the structure
 - Flooding of all cells across the width of the pontoon
 - Flooding of all the end cells of an isolated pontoon during towing
 - Flooding of the outboard end cells of a partially assembled structure
3. Loss of a Mooring Cable or Component.
4. Complete separation of the floating bridge by a transverse or diagonal fracture. This condition should apply to the factored load combinations only.

The above potential damage (DM) loadings should be combined with the AASHTO Groups VI, VIII, and IX combinations for Service Load Design and Load Factor Design. If the AASHTO LRFD Bridge design specifications are used in the design, the loads from Items (2) to (4) may be considered as extreme events.

Every floating structure is unique and specific requirements must be established accordingly. Maritime damage criteria and practices, such as those for ships and passenger vessels, should be reviewed and applied where applicable in developing damage criteria for a floating structure. However, a floating bridge behaves quite differently from a vessel in that structural restraint is much more dominant than hydrostatic restraint. The trim, list, and sinkage of the flooded structure are relatively small.

With major damage, structural capacity is reached before large deformations occurred or observed. This is an important fact to note when comparing with stability criteria for ships.

14.4.4 Control Progressive Failure

While water provides buoyancy to keep a floating bridge afloat, water leaking into the interior of a floating bridge can cause progressive failure and eventual sinking of the bridge. Time is of the essence when responding to damage or flooding. Maintenance personnel must respond to damage of a floating bridge quickly, especially when water begins to leak into the structure. An electronic cell monitoring system with water sensors to detect water entry and provide early warning to the maintenance personnel should be installed to assure timely emergency response. A bilge piping system should also be installed in the bridge for pumping out water.

It is important to control progressive failure in a floating bridge caused by flooding resulting from structural damage. Damage to the floating bridge could occur from a wind storm, a collision with a boat, the severing of mooring lines or other unforeseen accidents. The interior of the pontoons shall be divided into small watertight compartments or cells (Figure 14.11) to confine flooding to only a small portion of the bridge. Access openings in the exterior or interior wall or bulkheads shall be outfitted with watertight doors.

Water sensors may be installed in each watertight compartment for early detection and early warning of water entry. A bilge piping system may be installed in the compartments for pumping out water when necessary. In such cases, pumping ports and quick disconnect couplings shall be provided for pumping from a boat or vehicle equipped with pumps.

14.4.5 Design of Concrete Members

The design of reinforced concrete members should be based on behavior at service load conditions as per AASHTO Standard Specifications (AASHTO 2002), or the service limit state as per AASHTO LRFD Bridge Design Specifications (AASHTO 2012), except sections where reinforcement is to resist sustained hydrostatic forces the allowable stress in the reinforcing steel should not exceed 97 MPa (14,000 psi) to limit the crack width to a maximum of 0.1 mm (0.004 in.).

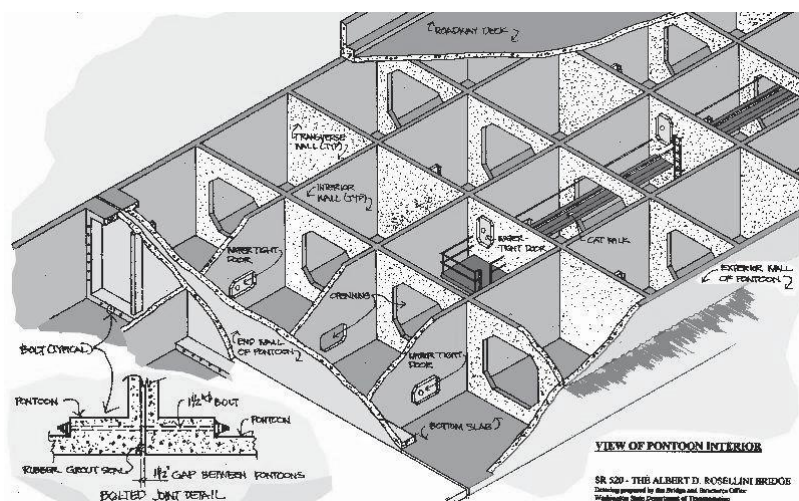


FIGURE 14.11 Small watertight compartments.

Prestressed members shall be designed under the applicable service load and load factor provisions in the AASHTO Standard Specifications (AASHTO 2002) or the limit states provisions in the AASHTO LRFD Bridge Design Specifications (AASHTO 2012), except the allowable concrete tensile stress under final conditions in the pre-compressed tensile zone should be limited to zero.

The ultimate flexural strength of the overall pontoon section should be computed for a maximum crack width of 0.25 mm (0.01 in.) and should not be less than the loads from the Factored Load Combinations or 1.3 times the cracking moment, M_{cr} .

In a moderate climate, the following temperature differentials between the various portions of a floating bridge may be used:

1. Between the exposed portion and the submerged portion of a pontoon: $\pm 19^{\circ}\text{C}$ ($\pm 62^{\circ}\text{F}$). The exposed portion may be considered as the top slab, and the remaining part of the pontoon as submerged. If the top slab is shaded by an elevated structure, the differential temperature may be reduced to $\pm 4^{\circ}\text{C}$ ($\pm 57^{\circ}\text{F}$).
2. Between the top slab and the elevated structure of the pontoon: $\pm 14^{\circ}\text{C}$ ($\pm 57^{\circ}\text{F}$). The effects of creep and shrinkage should be considered while the pontoons are in the dry only. Creep and shrinkage may be taken as zero once the pontoons are launched. The time dependent effects of creep and shrinkage may be estimated in accordance with the AASHTO Specifications (AASHTO 2012). A final differential shrinkage coefficient of 0.0002 should be considered between the lower portion of the pontoon and the top slab of the pontoon.

High performance concrete containing fly ash and silica fume is most suitable for floating bridges (Lwin, Bruesch, and Evans 1995; Lwin 1997). The concrete is very dense, impermeable to water, highly resistant to abrasion and relatively crack free. High performance concrete also has high strength, low creep and low shrinkage. Concrete mixes may be customized for the project.

Recommended minimum concrete cover of reinforcing steel:

	Fresh Water	Salt Water
Top of roadway slab, mm (in.)	65 (2.6)	65 (2.6)
Exterior Surfaces of pontoons and barrier, mm (in.)	38 (1.5)	50 (2.0)
All other surfaces, mm (in.)	25 (1.0)	38 (1.5)

Corrosion-free stainless steel or FRP reinforcement may be used for improved durability in a marine environment.

14.4.6 Anchoring System

An anchoring system should be installed in the floating bridge to maintain transverse and horizontal alignment. The anchoring system should be designed to have adequate capacity to resist transverse and longitudinal forces from winds, waves, and current.

Adequate factors of safety or load and resistance factors consistent with the type of anchoring should be included in the design of the components of the system.

14.4.7 Movable Span

A floating bridge creates an obstruction to marine traffic. Movable spans may need to be provided for the passage of large vessels. The width of the opening that must be provided depends on the size and type of vessels navigating through the opening. Movable spans of up to a total opening of 190 m have been used.

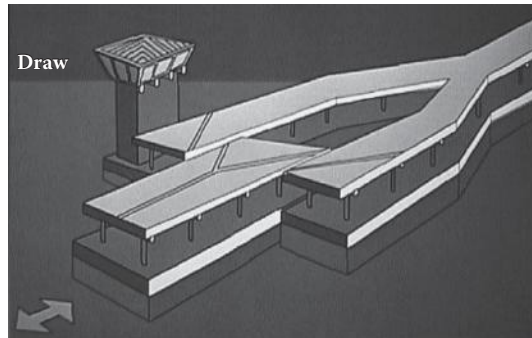


FIGURE 14.12 Draw type movable span.

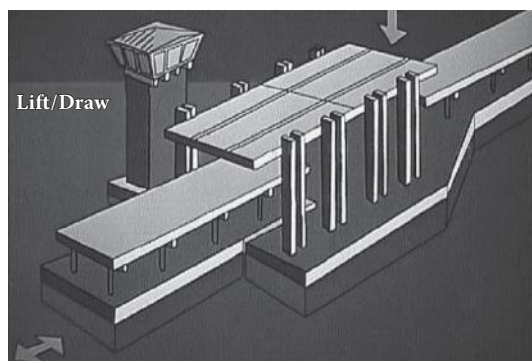


FIGURE 14.13 Lift/draw type movable span.

Two types of movable spans are used in Washington State—the draw type and the lift/draw type. In the draw type movable span, the draw pontoons retract into a “lagoon” formed by flanking pontoons (Figure 14.12). Vehicles must maneuver around curves at the “bulge” where the “lagoon” is formed. In the lift/draw type of movable span, part of the roadway will be raised for the draw pontoons to retract underneath it (Figure 14.13). As far as traffic safety and flow are concerned, the lift/draw type movable span is superior over the draw type. Traffic moves efficiently on a straight alignment with no curves to contend with.

The movable spans may be operated mechanically or hydraulically. The design of the movable spans should be in accordance with the latest AASHTO LRFD Movable Highway Bridge Design Specifications (AASHTO 2011). Chapter 13 provides a detailed discussion about movable bridges.

14.4.8 Deflection and Motion

Floating bridges should be designed so that they are comfortable to ride on during a normal storm (1-year storm) conditions and also to avoid undesirable structural effects during extreme storm (100-year storm) conditions. Deflection and motion criteria have been used to meet these objectives. Table 14.3 lists deflection and motion limits for normal storm (1-year storm) conditions and may be used as guidelines.

The objective of the motion limits is to assure that the people will not experience discomfort walking or driving across the bridge during a normal storm. The motion limit for rotation (roll) under the dynamic action of waves should be used with care when the roadway is elevated a significant distance above the water surface. The available literature contains many suggested motion criteria for comfort

TABLE 14.3 Deflection and Motion Limits for Normal Storm (1-Year Storm)

Loading Condition	Type of Deflection or Motion	Maximum Deflection, m (ft.)	Maximum Motion, m/s (ft./s)
Vehicular load	Vertical	L/800	-
Winds-static	Lateral (drift)	0.3 (1)	-
Winds-static	Rotation (heel)	0.5°	-
Waves-dynamic	Vertical (heave)	±0.3 (±1)	0.5 (1.6)
Waves-dynamic	Lateral (sway)	±0.3 (±1)	0.5 (1.6)
Waves-dynamic	Rotation (roll)	±0.5°	0.05 rad/s

based on human perceptions (Bachman and Amman 1987). A more detailed study on motion criteria may be warranted for unusual circumstances.

14.5 Structural Design and Analysis

The design and analysis of floating bridges have gone through several stages of progressive development since the first highway floating bridge was designed and built in the late 1930s across Lake Washington, Seattle, Washington State. The design has advanced from empirical methods to realistic approach, from the equivalent static approach to dynamic analysis, from computer modeling to physical model testing, and from reinforced concrete to prestressed concrete.

The most difficult part of early designs was the prediction of winds and waves, and the response due to wind-wave-structure interaction. Climatological data was very limited. The wind-wave-structure interaction was not well understood. Current state-of-the-knowledge in atmospheric sciences, computer science, marine engineering, finite element analysis, structural engineering, and physical model testing provides more accurate prediction of wind and wave climatology, more realistic dynamic analysis of wind-wave-structure interactions and more reliable designs.

Designing for static loads, such as dead and live loads, is very straightforward using the classical theory on beam on elastic foundation (Hetenyi 1979). For example, the maximum shear, moment and deflection due to a concentrated load, P , acting away from the end of a continuous floating structure are given by

$$V_{\max} = \frac{P}{2} \quad (14.1)$$

$$M_{\max} = \frac{P}{4\lambda} \quad (14.2)$$

$$\gamma_{\max} = \frac{P\lambda}{2k} \quad (14.3)$$

where k is the *modulus of foundation*

$$\lambda = 4\sqrt{\frac{k}{4EI}}$$

Designing for the response of the structure to winds and waves is more complex, because of the random nature of these environment loads. To realistically determine the dynamic response of the bridge to wind generated waves, a dynamic analysis is necessary.

14.5.1 Preliminary Design

The design starts with selecting the type, size and location of the floating bridge (Figure 14.14). Assuming a concrete box section of cellular construction with dimensions as shown in (Figure 14.15), the first step is to determine the freeboard required. The height of the freeboard is selected to avoid water spray on the roadway deck from normal storms. The draft can then be determined as necessary to provide the selected freeboard.

The freeboard and draft of the floating structure should be calculated based on the weight of concrete, weight of reinforcing steel, the weight of appurtenances, weight of marine growth as an appropriate and vertical component of anchor cable force. The weight of the constructed pontoon is generally heavier than the computed weight, because of form bulging and other construction tolerances. Based on the experience in Washington State, the weight increase varies from 3% to 5% of the theoretical weight. This increase should be included in the draft calculation. Additionally, floating pontoons experience loss in freeboard in the long term. The main reason is due to weight added as a result of modifications in the structural and mechanical elements throughout the service life of the structure. It is prudent to make

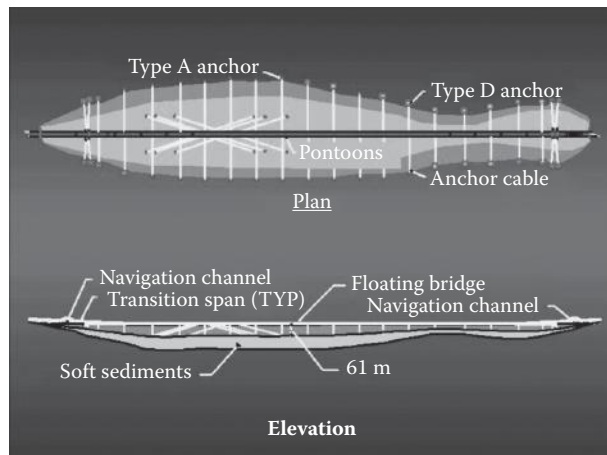


FIGURE 14.14 General layout.

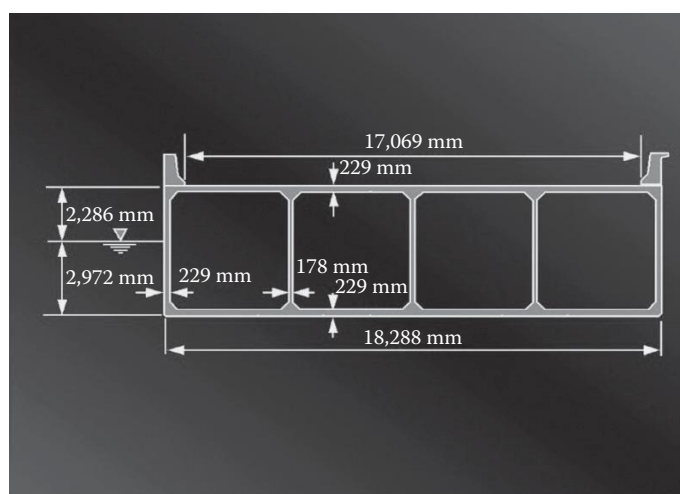


FIGURE 14.15 Typical cross-section.

allowance for this in the design. This can be done by allowing 150–230 mm (6–9 in.) of extra freeboard in a new bridge.

The thicknesses of the walls and slabs should be selected for local and global strength and constructability. The wall thickness should be the minimum needed to provide adequate concrete cover to the reinforcing steel and adequate space for post-tensioning ducts when used. There must also be adequate room for depositing and consolidating concrete. The objective should be to keep the weight of the structure to a minimum, which is essential for cost effective design and the service performance of a floating bridge.

The exterior walls of the pontoons should be designed for wave plus hydrostatic pressures and the potential collision loads. The bottom slab should be designed for wave plus hydrostatic pressures. The interior walls should be designed for hydrostatic pressures due to flooding of a cell to the full height of the wall. The roadway slab should be designed for the live load plus impact in the usual way.

The preliminary design gives the overall cross sectional dimensions and member thicknesses required to meet local demands and construction requirements. The global responses of the floating bridge will be predicted by dynamic analysis.

14.5.2 Dynamic Analysis

The basic approach to dynamic analysis is to solve the equation of motion:

$$M\ddot{X} + C\dot{X} + KX = F(t) \quad (14.4)$$

This equation is familiar to structural engineering in solving most structural dynamic problems of land-based structures. However, in predicting the dynamic response of a floating bridge, the effects of water-structure interaction must be accounted for in the analysis. As a floating bridge responds to the incident waves, the motions (heave, sway, and roll) of the bridge produce hydrodynamic effects generally characterized in terms of added mass and damping coefficients. These hydrodynamic coefficients are frequency-dependent. The equation of motion of a floating structure takes on the general form:

$$[M + A]\ddot{X} + [C_1 + C_2]\dot{X} + [K + k]X = F(t) \quad (14.5)$$

Where X, \dot{X}, \ddot{X} are the generalized displacement, velocity and acceleration at each degree of freedom; M is the mass-inertia matrix of the structure; A is the added mass matrix (frequency dependent); C_1 is the structural damping coefficient; C_2 is the hydrodynamic damping coefficient (frequency dependent); K is the structural stiffness matrix (elastic properties, including effects of mooring lines when used); k is the hydrostatic stiffness (hydrostatic restoring forces); $F(t)$ is the forces acting on the structure.

A substantial amount of experimental data have been obtained for the hydrodynamic coefficients for ships and barges (Frank 1967; Garrison 1984). Based on these experimental data, numerical methods and computer programs have been developed for computing hydrodynamic coefficients of the commonly used cross sectional shapes, such as a rectangular shape. For structural configurations for which no or limited data exist, physical model testing will be necessary to determine the basic sectional added mass, damping and wave excitation loads.

Structural damping is an important source of damping in the structure. It significantly affects the responses. A structural damping coefficient of 2%–5% of critical damping is generally assumed in the analysis. It is recommended that a better assessment of the damping coefficient be made to better represent the materials and structural system used in the final design.

The significant wave height, period and central heading angle may be predicted using the public domain program NARFET developed by the U.S. Army Coastal Engineering Research Center (CERC 1984 and 1989). This program accounts for the effective fetch to a location on the floating structure by a set of radial fetch lines to the point of interest. The Joint North Sea Wave Project (JONSWAP) spectrum

is commonly used to represent the frequency distribution of the wave energy predicted by the program NARFET. This spectrum is considered to represent fetch limited site conditions very well. A spreading function is used to distribute the energy over a range of angles of departure from the major storm heading to the total energy (Mitsuyasu et al. 1975). The spreading function takes the form of an even cosine function, $\cos^{2n} \theta$, where θ is the angle of the incident wave with respect to the central heading angle. Usually $2n$ is 2 or greater. $2n = 2$ is generally used for ocean structures where the structures are relatively small with respect to the open sea. In the case of a floating bridge, the bridge length is very large in comparison to the body of water, resulting in very little energy distributed away from the central heading angle. A larger number of $2n$ will have to be used for a floating bridge. The larger the number of $2n$ the more focused the wave direction near the central heading angle. A $2n$ value of 12–16 have been used in analyzing the floating bridge in Washington State. The value of $2n$ should be selected with care to properly reflect the site condition and the wind and wave directions.

The equation of motion may be solved by the Time Domain (deterministic) Analysis or the Frequency Domain (Probabilistic) Analysis. The time domain approach involves in solving differential equations when the coefficients are constants. The equations become very complex when the coefficients are frequency dependents. This method is tedious and time consuming. The frequency domain approach is very efficient in handling constant and frequency dependent coefficients. The equations are algebraic equations. However, time dependent coefficients are not admissible and nonlinearities will have to be linearized by approximation. For the dynamic analysis of floating bridges subjected to the random nature of environmental forces and the frequency dependent hydrodynamic coefficients, the Frequency Domain Analysis involves only simple and fast calculations.

14.5.3 Frequency Domain Analysis

The frequency domain dynamic analysis is based on the principles of naval architecture and the strip theory developed for use in predicting the response of ships to sea loads (Comstock 1975; Salvesen, Tuck, and Faltinsen 1970). The essence of this approach is the assumption that the flow at one section through the structure does not affect the flow at any other section. Additional assumptions are: (1) the motions are relatively small, (2) the fluid is incompressible and inviscid, and (3) the flow is irrotational. Using the strip theory, the problem of wave-structure interaction can be solved by applying the equation of motion in the frequency domain (Engel and Nachlinger 1982; Hutchison 1984). By Fourier transform, the equation of motion may be expressed in terms of frequencies, ω , as follows:

$$\{-\omega^2[M + A] + i\omega[C_1 + C_2] + [K + k]\} = \{F(\omega)\} \quad (14.6)$$

This equation may be solved as a set of algebraic equations at each frequency and the responses determined. The maximum bending moments, shears, torsion, deflections and rotations can then be predicted using spectral analysis and probability distribution (Marks 1963; Ochi 1973). The basic steps involved in a frequency domain analysis are

1. Compute the physical properties of the bridge—geometry of the bridge elements, section properties, connections between bridge elements, mass-inertia, linearized spring constants, structural damping, etc.
2. Compute hydrodynamic coefficients—frequency dependent added mass and frequency dependent damping.
3. Compute hydrostatic stiffnesses.
4. Calculate wind, wave, and current loads, and other loaded terms.
5. Build a finite element computer model of the bridge (Gray and Hutchison 1986) as a collection of nodes, beam elements and spring elements. The nodes form the joints connecting the beam elements and the spring elements, and each node has six degrees of freedom.

6. Solve the equation of motion in the frequency domain to obtain frequency responses, the magnitudes of which are referred to as Response Amplitude Operators (RAOs).
7. Perform spectral analysis, using the RAOs and the input sea spectrum, to obtain the root mean square (RMS) of responses.
8. Perform probability analysis to obtain the maximum values of the responses with the desired probability of being exceeded.
9. Combine the maximum responses with other loadings, such as wind, current, etc., for final design.

14.6 Fabrication and Construction

Concrete pontoons are generally used for building major floating bridges. The fabrication and construction of the concrete pontoons must follow the best current practices in structural and marine engineering in concrete design, fabrication and construction, with added emphasis on high quality concrete and water tightness. Quality control should be the responsibility of the fabricators/contractors. Final quality assurance and acceptance should be the responsibility of the owners. In addition to these traditional divisions of responsibilities, the construction of a floating bridge necessitates a strong “partnership” arrangement to work together, contracting agencies and contractors, to provide full cooperation and joint training, share knowledge and expertise, share responsibility, and to help each other succeed in building a quality floating bridge. The contractors should have experience in marine construction and engage the services of naval architects or marine engineers to develop plans for monitoring construction activities and identifying flood risks, and prepare contingency plans for mitigating the risks.

Knowledge is power and safety. The construction personnel, including inspectors from the contracting agencies and the contractors, should be trained on the background of the contract requirements and the actions necessary to fully implement the requirements. Their understanding and commitment are necessary for complete and full compliance with contract requirements that bear on personal and bridge safety.

Construction of floating bridges is well established. Many concrete floating bridges have been built successfully using cast-in-place, precast or a combination of cast-in-place and precast methods. Construction techniques are well developed and reported in the literature. Owners of floating bridges have construction specifications and other documents and guidelines for the design and construction of such structures.

Advancement and successful application of self-consolidating concrete (SCC) provide a viable and effective construction method for accelerating the construction of concrete pontoons (Ouchi et al. 2003; Lwin 2005). SCC has many engineering, architectural, economic and environmental benefits. Eliminating the need for vibration reduces the many problems associated with vibration, and improves the overall concrete quality and durability. SCC cuts down on the labor needed, wear and tear on equipment and formwork, and speeds up construction, resulting in cost savings. SCC reduces the noise level in the plants and at the construction sites, resulting in improved working conditions. SCC has the ability to flow into and completely fill intricate and complex forms, and to pass through and bond to congested reinforcement without segregation. The formed surfaces of SCC take on the textures of the forms with little or no defects. The excellent flowability of SCC without vibration makes SCC most suitable for assembly-line production of pontoons for floating bridges. SCC mix design can be automated to deliver SCC at a central point, where SCC can be discharged to components passing through the central point. When placement of SCC is completed, the component can move on, allowing the next component to be cast. For complete pontoon construction, it would be more efficient to move the SCC discharge to the pontoons where they are formed and ready for SCC placement. Innovative and creative use of SCC can accelerate the floating bridge construction through high production and quality with little or no repair of defects.

Floating bridges may be constructed in the dry in graving docks or on slipways built specifically for the purpose. However, construction on a slipway requires more extensive preparation, design and caution. The geometry and strength of the slipway must be consistent with the demand of the construction and launching requirements. Construction of a graving dock utilizes techniques commonly used in

land-based structures. Major floating bridges around the world have been constructed in graving docks (Figure 14.16).

Due to the size of a floating bridge, the bridge is generally built in segments or pontoons compatible with the graving dock dimensions and draft restrictions. The segments or pontoons are floated and towed (Figure 14.17) to an outfitting dock where they are joined and completed in larger sections before towing to the bridge site, where the final assembly is made (Figure 14.18).

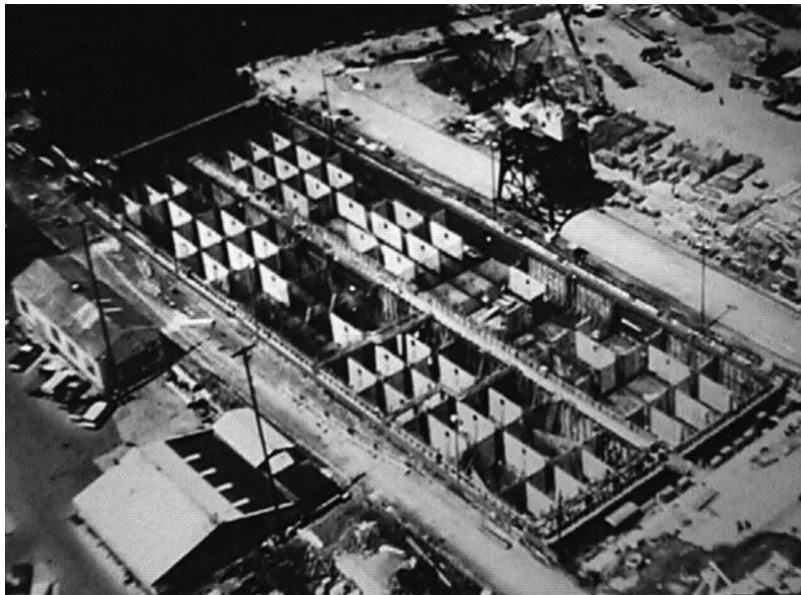


FIGURE 14.16 Construction in a graving dock.



FIGURE 14.17 Towing pontoon



FIGURE 14.18 Final assembly.

It is important to explore the availability of construction facilities and decide on a feasible facility for the project. These actions should be carried out prior to or concurrent with the design of a floating bridge to optimize the design and economy. Some key data that may be collected at this time are

- Length, width, and draft restrictions of the graving dock
- Draft and width restrictions of the waterways leading to the bridge site
- Wind, wave, and current conditions during tow to and installation at the job site

The designers will use the information to design and detail the structural plans and construction specifications accordingly.

14.7 Construction Cost

The construction costs for floating bridges vary significantly from project to project. There are many variables that affect the construction costs. Table 14.4 summarizes construction costs in U.S. dollars for the floating bridges in Washington State to provide a general idea of costs in building concrete floating bridges in the past. These are original bid costs for the floating portion of the bridges. They have not been adjusted for inflation and do not include the costs for the approaches.

14.8 Inspection, Maintenance, and Operation

A floating bridge represents a major investment of resources and a commitment to efficiency and safety to the users of the structure and the waterway. To assure trouble-free and safe performance of the bridge, especially one with a movable span, an inspection, maintenance and operation manual (Manual) should be prepared for the bridge. The main purpose of the Manual is to provide guidelines and procedures for regular inspection, maintenance and operation of the bridge to extend the service life of the structure. Another aspect of the Manual is to clearly define the responsibilities of the personnel assigned to inspect, maintain, and operate the bridge. The Manual must address the specific needs and unique structural, mechanical, hydraulic, electrical, and safety features of the bridge.

TABLE 14.4 Construction Cost of Floating Bridges in Washington State

Name of Bridge	Length, (ft.)	Width of Pontoon, (ft.)	Lanes of Traffic	Cost—Million (Year Bid)
Original Lacey V. Murrow Bridge ^a	1999.8 (6561)	17.9 (58.7)	4	\$3.25 (1938)
Evergreen Point Bridge ^a	2309.8 (7578)	18.3 (60.0)	4	\$10.97 (1960)
Original Hood Canal Bridge ^a	1990.3 (6530)	15.2 (49.9)	2	\$17.67 (1961)
Homer Hadley Bridge	1748.3 (5736)	22.9 (75.1)	5	\$64.89 (1985)
New Lacey V. Murrow Bridge	1999.8 (6561)	18.3 (60.0)	3	\$73.78 (1991)

^a These bridges have movable spans, which increased construction costs.

The development of the Manual should begin at the time the design plans and construction specifications are prepared. This will make sure that the necessary inputs are given to the designers to help with the preparation of the Manual later. The construction specifications should require the contractors to submit documents, such as catalog cuts, schematics, electrical diagrams, and so on, that will be included in the Manual. The Manual should be completed soon after the construction is completed and the bridge is placed into service. The Manual is a dynamic document. Lessons learned and modifications made during the service life of the structure should be incorporated into the Manual on a regular basis.

A training program should be developed for the supervisors and experienced co-workers to impart knowledge to the new or inexperienced workers. The training program should be given regularly and aimed at nurturing a positive environment where workers helping workers understand and diligently apply and update the guidelines and procedures of the Manual.

14.9 Closing Remarks

Floating bridges are cost effective alternatives for crossing large lakes with unusual depth and soft bottom, spanning across picturesque fjords and connecting beautiful islands. For conditions like Lake Washington in Seattle where the lake is over 1610 m wide, 61 m deep and another 61 m of soft bottom, a floating bridge is estimated to cost 3–5 times less than a long span fixed bridge, tube or tunnel.

The bridge engineering community has sound theoretical knowledge, technical expertise and practical skills to build floating bridges to enhance the social and economic activities of the people. However, it takes time to plan, study, design and build floating bridges to form major transportation links in a local or national highway system. There are environmental, social and economic issues to address. In the State of Washington, the first floating bridge was conceived in 1920, but was not built and opened to traffic until 1940. After over 30 years of planning, studies, and overcoming environmental, social and economic issues, Norway finally has the country's first two floating bridges opened to traffic in 1992 and 1994. It is never too early to start the planning process and feasibility studies once interest and a potential site for a floating bridge is identified.

Every floating bridge is unique and has its own set of technical, environmental, social, and economic issues to address during preliminary and final engineering:

- Winds and Waves: predicting accurately the characteristics of winds and waves have been a difficult part of the floating bridge design. Generally there are inadequate data. It is advisable to install instruments in potential bridge sites to collect climatological data as early as possible. Research in the area of wind-wave-structure interactions will assure safe and cost effective structures.
- Earthquake: floating bridges are not directly affected by ground shakings from earthquakes.
- Tsunami and Seiches: these may be of particular significance in building a floating bridge at sites susceptible to these events. The dynamic response of floating bridges to tsunami and seiches must be studied and addressed in the design where deemed necessary.
- Corrosion: materials and details must be carefully selected to reduce corrosion problems to assure long service life with low maintenance.

- Progressive Failure: floating bridges must be designed against progressive failures by dividing the interiors of pontoons into small watertight compartments, by installing instruments for detecting water entry, and by providing the means to discharge the water when necessary.
- Riding Comfort and Convenience: floating bridges must be comfortable to ride on during minor storms. They must have adequate stiffness and stability. They must not be closed to vehicular traffic frequently for storms or marine traffic.
- Public Acceptance: public acceptance is a key part of modern civil and structural engineering. The public must be educated regarding the environmental, social, and economic impacts of proposed projects. Reaching out to the public through community meetings, public hearings, news releases, tours, exhibits, and so on, during the early phase of project development is important to gain support and assure success. Many major public projects have been delayed for years and years because of lack of interaction and understanding.
- Design Criteria: the design criteria must be carefully developed to meet site specific requirements and focused on design excellence and cost effectiveness to provide long term performance and durability. Design excellence and economy come from timely planning, proper selection of materials for durability and strength, and paying attention to design details, constructability, and maintainability. The design team should include professionals with knowledge and experience in engineering, inspection, fabrication, construction, maintenance and operation of floating bridges or marine structures.
- Construction Plan: it is essential to have a good construction plan developed jointly by the contracting agency and the contractor to clearly address qualifications, materials control, quality control, quality assurance, acceptance criteria, post-tensioning techniques, repair techniques, launching and towing requirements, weather conditions, flood control, and surveillance.

Well engineered and maintained floating bridges are efficient, safe, durable and comfortable to ride on. They form important links in major transportation systems in different parts of the world (Figure 14.19).



FIGURE 14.19 Floating bridges on Lake Washington. (Courtesy of Washington State DOT.)

References

- AASHTO. 2002. *Standard Specifications for Highway Bridges*, 17th Edition, American Association of State Highway and Transportation Officials, Washington, D.C.
- AASHTO. 2011. *AASHTO LRFD Movable Highway Bridge Design Specifications*, 2nd Edition, with 2008, 2010 and 2011 Interim Revisions, Association of State Highway and Transportation Officials, Washington, D.C.
- AASHTO. 2012. *AASHTO LRFD Bridge Design Specifications*, Customary US Units, 2012, American Association of State Highway and Transportation Officials, Washington, D.C.
- Andrew, C. E. 1939. "The Lake Washington Pontoon Bridge," *Civil Engineering*, 9(12), 703–706.
- Bachman, H. and Amman, W. 1987. *Vibrations in Structure Induced by Men and Machines*, Structural Engineering Document No. 3e, International Association for Bridge and Structural Engineering, Zurich, Switzerland.
- CERC. 1984. *Shore Protection Manual*, Vol. 1, Coastal Engineering Research Center, Department of the Army. Vicksburg, MS.
- CERC. 1989. *Program NARFET*, Waterways Experiment Station, Corps of Engineers, Coastal Engineering Research Center, Department of the Army, Vicksburg, MS.
- Comstock, J. 1975. *Principles of Naval Architecture*, Society of Naval Architects and Marine Engineers, New York, NY.
- Engel, D. J. and Nachlinger, R. R. 1982. "Frequency domain analysis of dynamic response of floating bridge to waves," *Proceedings of Ocean Structural Dynamics Symposium*, Oregon State University, Corvallis, OR.
- Frank, W. 1967. *Oscillation of Cylinders in or Below the Surface of Deep Fluids*, Report No. 2375, Naval Ships Research and Development Center, Bethesda, MD.
- Garrison, C. J. 1984. "Interaction of oblique waves with an infinite cylinder," *Applied Ocean Research*, 6(1), 4–15.
- Gloyd, C. S. 1988. "Concrete floating bridges," *Concrete International*, 10(5), 17–24.
- Gray, D. L. and Hutchison, B. L. 1986. "A resolution study for computer modeling of floating bridges," *Proceedings of Ocean Structural Dynamics Symposium*, Oregon State University, Corvallis, OR.
- Hetenyi, M. 1979. *Beams on Elastic Foundation*, University of Michigan Press, Ann Arbor, MI.
- Hutchison, B. L. 1984. "Impulse response techniques for floating bridges and breakwaters subject to short-crested seas," *Marine Technology*, 21(3), 270–276.
- Landet, E. 1994. "Planning and construction of floating bridges in Norway," *Proceedings of International Workshop on Floating Structures in Coastal Zone*, Port and Harbour Research Institute, Japan.
- Lwin, M. 2005. "FHWA Effort in Advancing SCC Technology," *Proceedings of Second North American Conference on the Design and Use of Self-Consolidating Concrete*, Chicago, IL.
- Lwin, M. M. 1993. "Floating bridges—solution to a difficult terrain," *Proceedings of the Conference on Transportation Facilities through Difficult Terrain*, Edited by Wu, J. T. H., and Barrett, R. K., Editors, A.A. Balkema, Rotterdam, the Netherlands.
- Lwin, M. M. 1997. "Use of high performance concrete in highway bridges in Washington state," *Proceedings International Symposium on High Performance Concrete*, Prestressed Concrete Institute and Federal Highway Administration, New Orleans, LA.
- Lwin, M. M., Bruesch, A. W., and Evans, C. F. 1995. "High performance concrete for a floating bridge," *Proceedings of the Fourth International Bridge Engineering Conference*, Vol. 1, Federal Highway Administration, Washington, D.C.
- Marks, W. 1963. *The Application of Spectral Analysis and Statistics to Seakeeping*, T&R Bulletin No. 1–24, Society of Naval Architects and Marine Engineers, New York, NY.
- Mitsuyasu, H., Tasai, F., Suhara, T., Mizuno, S., Ohkusu, M., Honda, T., and Rikiishi, K. 1975. "Observations of the directional spectrum of ocean waves using a clover leaf buoy," *J. Phys. Oceanogr.*, 5(4), 750–760.

- Nichols, C. C. 1962. "Construction and performance of Hood Canal floating bridge," *Proceedings of Symposium on Concrete Construction in Aqueous Environment*, ACI Publication SP-8, Detroit, MI.
- Ochi, M. K. 1973. "On prediction of extreme values," *Journal of Ship Research*, 17(1), 29–37.
- Ouchi, M. K., Nakamura, S., Osterberg, T., Hallberg, S. and Lwin, M. 2003. "Applications of self-compacting concrete in Japan, Europe and the United States," *Proceedings of International Symposium on High-Performance Concrete*, Orlando, FL.
- Pegusch, W. 1957. "The Kelowna floating bridge," *The Engineering Journal*, Engineering Institute of Canada, 40(4), 413–421.
- Salvesen, N., Tuck, E. O. and Faltinsen, O. 1970. "Ship motions and sea loads," *Transactions of Society of Naval Architects and Marine Engineers*, 78(6), 1–30.

@Seismicisolation

15

Concrete Decks

15.1	Introduction	573
15.2	Types of Concrete Decks	573
	Cast-in-Place Concrete Deck • Precast Concrete Deck	
15.3	Materials.....	576
	General Requirements • Concrete • Reinforcement • Construction Practices	
15.4	Design Considerations.....	577
	General Requirements • Design Limit States • Analysis Methods	
15.5	Design Example	579
	Bridge Deck Data • Design Requirements • Solution • Calculate Factored Moments—Strength Limit State I • Design for Positive Flexure Design • Design for Negative Flexure • Check Service Limit State—Cracking Control • Determine the Slab Reinforcement Detailing Requirements	
	References.....	588

John Shen
California Department
of Transportation

15.1 Introduction

Bridge decks not only provide the riding surface for traffic, but also support and transfer live loads to the main load-carrying members such as stringer and girders on a bridge superstructure. Bridge decks include cast-in-place (CIP) reinforced concrete, precast concrete deck panel, prestress concrete, timber, filled and unfilled steel grid, and steel orthotropic decks. Selection of bridge deck types depends on locations, spans, traffic, environment, maintenance, aesthetics, and life cycle costs, among other reasons.

This chapter focuses on concrete deck and emphasizes the cast-in-place reinforced concrete deck. A design example of a reinforced concrete bridge deck is provided in accordance with the *AASHTO LRFD Bridge Design Specifications* (AASHTO 2012). For more detailed discussion of the concrete deck, references are made to FHWA (2012) and Barker and Puckett (2007). Steel orthotropic decks are discussed in Chapter 16.

15.2 Types of Concrete Decks

15.2.1 Cast-in-Place Concrete Deck

The CIP concrete deck slab is the predominant deck type in highway bridges in the United States. Figure 15.1 shows a reinforcement layout in a CIP concrete deck on the steel plate girder. Figure 15.2 shows a CIP concrete deck under construction. Figure 15.3 shows a typical CIP concrete deck details. Its main advantages are acceptable skid resistance, the easier field-adjustment of the roadway profile during concrete placement to provide a smooth riding surface, commonly available materials and contractors to do the work. However, CIP slabs have disadvantages including excessive differential shrinkage with



FIGURE 15.1 Reinforcement layout in a cast-in-place concrete deck.



FIGURE 15.2 A cast-in-place concrete deck under construction.

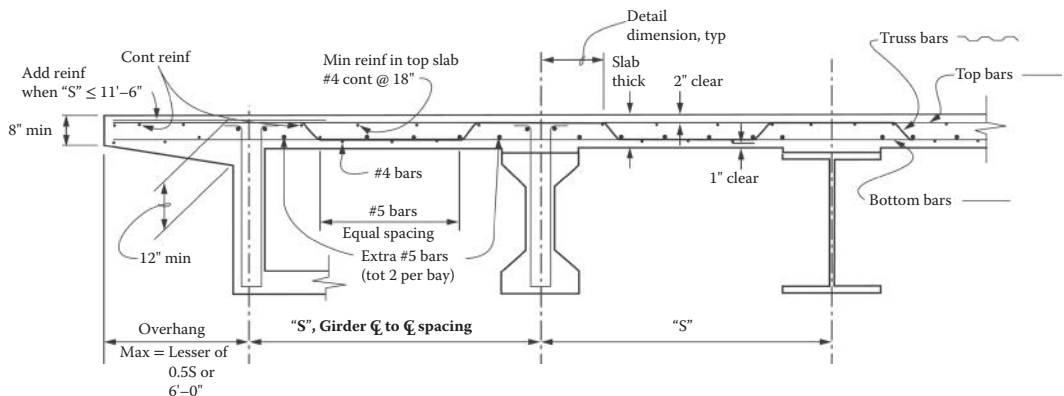


FIGURE 15.3 Typical cast-in-place concrete deck details.

the supporting girders and slow construction, the tendency of the deck rebar to corrode due to deicing salts. In order to develop cost-competitive, fast to construct, and durable alternative systems, recent innovations on CIP decks are focused on developing mixes and curing methods that produce performance characteristics such as freeze-thaw resistance, high abrasion resistance, low stiffness, and low shrinkage, rather than high strength.

15.2.2 Precast Concrete Deck

There are two types of precast concrete decks: full-depth precast panels and stay-in-place (SIP) precast prestressed panels combined with CIP topping.

Figure 15.4 shows full-depth precast concrete deck panels under construction. The full-depth precast panels have the advantages of significant reduction of shrinkage effects and fast construction speed and have been used for deck replacement with high traffic volumes. NCHRP Report 407 (Tardos and Baishya 1998) proposed a full-depth panel system with panels pretensioned in the transverse direction and posttensioned in the longitudinal direction. NCHRP Report 584 (Badie and Tardos 2008) developed two full-depth precast concrete bridge deck panel systems, a transversely pretensioned system and a transversely conventionally reinforced system and proposed guidelines for the design, fabrication, and construction of full-depth precast concrete bridge deck panel systems without the use of posttensioning or overlays and (2) connection details for new deck panel systems.

Figure 15.5 shows a partial depth precast panel or SIP precast prestressed panes combined with CIP topping. The SIP panels act as forms for the topping concrete and also as part of the structural depth of the deck. This system can significantly reduce construction time since field forming is only needed for the exterior girder overhangs. It is cost-competitive with CIP decks for new structures and deck replacement. However, the SIP panel system suffers reflective cracking over the panel-to-panel joints. A modified SIP precast panel system has been developed in NCHRP Report 407 (Tardos and Baishya 1998).



FIGURE 15.4 Full-depth precast concrete deck panels under construction. (Courtesy of FHWA.)

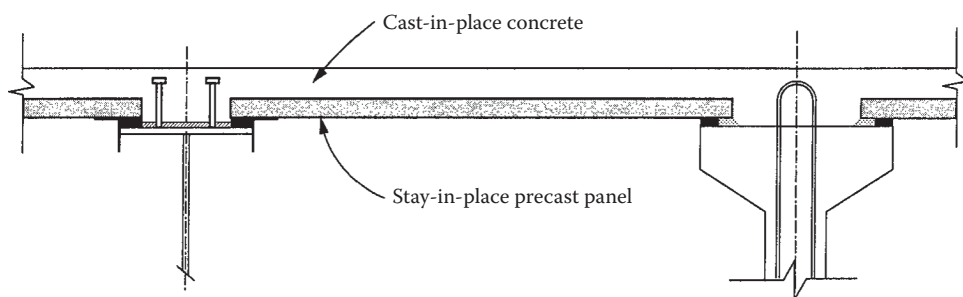


FIGURE 15.5 Typical stay-in-place precast panel with cast-in-place concrete deck.

15.3 Materials

15.3.1 General Requirements

Material characteristics in a bridge deck shall behave to reduce concrete distress and reinforcement corrosion and lead to a long service life with minimum maintenance. Expected concrete deck should behave with the following characteristics (Russell 2004):

- Low chloride permeability
- A top surface that does not deteriorate from freeze thaw or abrasion damage
- Cracking that is limited to fine flexural cracks associated with the structural behavior
- Smooth rideability with adequate skid resistance

NCHRP Synthesis 333 (Russell 2004) recommended that use of the following materials and practices enhances the performance of concrete bridge decks.

15.3.2 Concrete

- Types I, II, and IP cements
- Fly ash up to 35% of the total cementitious materials content
- Silica fume up to 8% of the total cementitious materials content
- Ground-granulated blast furnace slag up to 50% of the total cementitious materials content
- Aggregates with low modulus of elasticity, low coefficient of thermal expansion, and high thermal conductivity
- Largest size aggregate that can be properly placed
- Water-reducing and high-range water-reducing admixtures
- Air-void system with a spacing factor no greater than 0.20 mm (0.008 in.), specific surface area greater than $23.6 \text{ mm}^2/\text{mm}^3$ ($600 \text{ in.}^2/\text{in.}^3$) of air-void volume, and number of air voids per inch of traverse significantly greater than the numerical value of the percentage of air
- Water-cementitious materials ratio in the range of 0.40–0.45
- Concrete compressive strength in the range of 28–41 MPa (4000–6000 psi)
- Concrete permeability per AASHTO Specification T277 in the range of 1500–2500 coulombs

15.3.3 Reinforcement

- Epoxy-coated reinforcement in both layers of deck reinforcement
- Minimum practical transverse bar size and spacing

15.3.4 Construction Practices

- Use moderate concrete temperatures at time of placement
- Use windbreaks and fogging equipment, when necessary, to minimize surface evaporation from fresh concrete
- Provide minimum finishing operations
- Apply wet curing immediately after finishing any portion of the concrete surface and wet cure for at least seven days
- Apply a curing compound after the wet curing period to slow down the shrinkage and enhance the concrete properties
- Use a latex-modified or dense concrete overlay
- Implement a warrant requirement for bridge deck performance
- Gradually develop performance-based specifications

15.4 Design Considerations

15.4.1 General Requirements

- Maintain a minimum structural depth of concrete deck of 7.0 in. and a minimum concrete cover of 2.5 in. (64 mm) $f'_c \geq 4.0$ ksi.
- Use prestressing for depth of slabs less than 1/20 of the design span.
- Place the primary reinforcement in the direction of the skew for the skew angle of the deck less than 25°. Otherwise, place them perpendicular to the main supporting girders.
- Provide shear connectors between concrete decks and supporting beams.
- Provide edge beams at the lines of discontinuity. For the deck supported in the transverse direction and composed with concrete barriers, no additional edge beam is needed.

15.4.2 Design Limit States

Concrete decks must be designed for Strength I limit state (AASHTO 2012) and are usually designed as tension-controlled reinforced concrete components. Strength II limit state of the permit vehicle axle load does not typically control deck design. Concrete decks are also required to meet the requirements for Service I limit state to control excessive deformation and cracking. The deck overhang shall be designed to meet the requirements for Extreme Event II. Concrete decks supported by multi-girder systems are not required to be investigated for the fatigue limit state.

15.4.3 Analysis Methods

15.4.3.1 Approximate Method of Analysis

Approximate method of analysis is traditionally used to design concrete bridge decks (AASHTO 4.6.2.1). The method assumes a concrete deck as transverse slab strips of flexure members supported by the longitudinal girders. The AASHTO specifications (AASHTO 2012) require the maximum positive moment and the maximum negative moment to apply for all positive moment regions and all negative moment regions in the deck slab, respectively. The width of an equivalent interior strip of a concrete deck is provided in Table 15.1 (AASHTO 2012). For deck overhangs, the AASHTO Article 3.6.1.3.4 may apply.

For typical concrete deck supported on different girder arrangements with at least three girders and the distance between the centerlines of the exterior girders not less than 14.0 ft., the maximum live load moments including multiple presence factors and dynamic load allowance based on the equivalent strip method are provided in AASHTO A-4 (AASHTO 2012) and are summarized in Table 15.2.

15.4.3.2 Empirical Method of Analysis

Empirical method of analysis (AASHTO 9.7.2) is a method of concrete deck slab design based on the concept of internal arching action within concrete slabs. In this method, effective length of slab shall be taken as (1) for slabs monolithic with supporting members: the face-to-face distance, and (2) for slabs supported on steel or concrete girders: distance between the webs of girders. Empirical design may be used only if the following conditions are met:

- Cross-frames of diaphragms are used throughout the girders.
- Spacing of intermediate diaphragms between box beams does not exceed 25 ft.
- The deck is composed with supporting steel or concrete girders.
- The deck is fully cast-in-place and water cured, $f'_c \geq 4.0$ ksi.
- Deck of uniform depth ≥ 7.0 in. except for hunched at girder flanges and the distance between extreme layers of reinforcement ≥ 4.0 in.
- Effective length ≤ 13.5 ft., $6.0 \leq$ effective length/design depth ≤ 18.0 .
- Overhang/slab depth ≥ 5.0 ; or overhang/slab depth ≥ 3.0 with slab composites with continuous concrete barrier.

TABLE 15.1 Equivalent Strips of Concrete Decks

Type of Concrete Deck	Direction of Primary Strip Relative to Traffic	Width of Primary Strip (in.)
Cast-in-place	Overhang	$45.0 + 10.0X$
Cast-in-place	Either parallel or perpendicular	$+M: 26.0 + 6.6X$
Cast-in-place with stay-in-place concrete formwork		
Precast, post-tensioned		$-M: 48.0 + 3.0S$

S = spacing of supporting components (ft.).

X = distance from load to point of support (ft.).

+M = positive moment.

-M = negative moment.

TABLE 15.2 Maximum Live Load Moment per Foot Width

Girder Spacing S (ft.)	Positive Moment M_{LL+IM} (kip-ft./ft.)	Negative M_{LL+IM} (kip-ft./ft.)						
		Distance from Centerline of Girder to Design Section for Negative Moment (in.)						
0.0	3.0	6.0	9.0	12.0	18.0	24.0		
4.0	4.68	2.68	2.07	1.74	1.60	1.50	1.34	1.25
4.5	4.63	3.00	2.58	2.10	1.90	1.65	1.32	1.18
5.0	4.65	3.74	3.20	2.66	2.24	1.83	1.26	1.12
5.5	4.71	4.36	3.73	3.11	2.58	2.07	1.30	0.99
6.0	4.83	4.99	4.19	3.50	2.88	2.31	1.39	1.07
6.5	5.00	5.31	4.57	3.84	3.15	2.53	1.50	1.20
7.0	5.21	5.98	5.17	4.36	3.56	2.84	1.63	1.51
7.5	5.44	6.26	5.43	4.61	3.78	3.15	1.88	1.72
8.0	5.69	6.48	5.65	4.81	3.98	3.43	2.49	2.16
8.5	5.99	6.66	5.82	4.98	4.14	3.61	2.96	2.58
9.0	6.29	6.81	5.97	5.13	4.28	3.71	3.31	3.00
9.5	6.59	7.15	6.31	5.46	4.66	4.04	3.68	3.39
10.0	6.89	7.85	6.99	6.13	5.26	4.41	4.09	3.77
10.5	7.15	8.52	7.64	6.77	5.89	5.02	4.48	4.15
11.0	7.46	9.14	8.26	7.38	6.50	5.62	4.86	4.52
11.5	7.74	9.72	8.84	7.96	7.07	7.19	5.52	4.87
12.0	8.01	10.28	9.40	8.51	7.63	6.74	5.56	5.21
12.5	8.28	10.81	9.93	9.04	8.16	7.28	5.97	5.54
13.0	8.54	11.31	10.43	9.55	8.67	7.79	6.38	5.86
13.5	8.78	11.79	10.91	10.03	9.16	8.28	6.79	6.16
14.0	9.02	12.24	11.37	10.50	9.63	8.67	7.18	6.45
14.5	9.25	12.67	11.81	10.94	10.08	9.21	7.57	6.72
15.0	9.47	13.09	12.23	11.37	10.51	9.65	7.94	7.02

15.4.3.3 Refined Methods of Analysis

Refined methods of analysis for concrete deck specified in AASHTO 4.6.3.2 (AASHTO 2012) usually consider flexural and torsional deformation without considering vertical shear deformation. They are more suitable for a more complex deck slab structure, for example, the end zones of skewed girder decks.

15.5 Design Example

15.5.1 Bridge Deck Data

A typical section of a steel-concrete composite plate girder bridge is shown in Figure 15.6.

Concrete: $f'_c = 4000 \text{ psi (27.6 MPa)}$, $E_c = 3625 \text{ ksi (25.0 MPa)}$

Steel Reinforcement: A706 Grade 60

$$f_y = 60 \text{ ksi (414 MPa)}; E_s = 29,000 \text{ ksi (200,000 MPa)}$$

$$n = \frac{E_s}{E_c} = 8$$

Loads: Concrete Barrier weight: $w_{\text{barrier}} = 0.410 \text{ klf}$

3 in. Future wearing surface $w_{\text{fws}} = 0.140 \text{ kcf}$ (AASHTO Table 3.5.1-1)

Reinforced Concrete unit weight $w_{rc} = 0.150 \text{ kcf}$ (AASHTO C3.5.1)

AASHTO HL-93 + dynamic load allowance

15.5.2 Design Requirements

Perform the following design calculations for concrete deck in accordance with the *AASHTO LRFD Bridge Design Specifications*, 2012 Edition.

- Select concrete deck thickness and cover.
- Calculate Unfactored Dead Load Moments.
- Calculate Unfactored Live Load Moments—Equivalent Strip Method.
- Calculate Factored Moments—Strength Limit State I.
- Design for Positive Flexure.
- Design for Negative Flexure.
- Check Service Limit State.
- Determine the Slab Reinforcement Detailing Requirements.

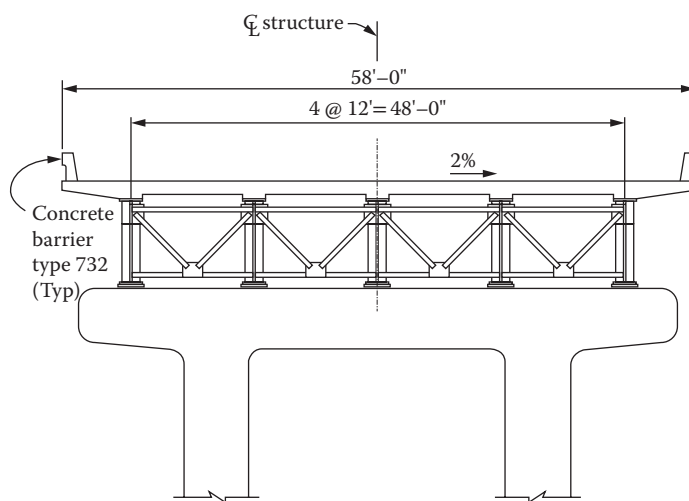


FIGURE 15.6 Typical section of composite plate girder bridge.

15.5.3 Solution

15.5.3.1 Select Concrete Deck Thickness and Cover

Try dec2k slab thickness $t = 9.125$ in. > Minimum deck thickness = 7.0 in.

Depth/Span = $9.125/(144) = 0.064 > 1/20 = 0.05$. No prestressing needed.

Use deck top cover $C_{\text{top}} = 2.0$ in.

Use deck bottom cover $C_{\text{bot}} = 1.0$ in.

15.5.3.2 Calculate Unfactored Dead Load Moments

Dead load for one foot length of concrete deck is calculated as follows:

Deck concrete weight— W_{DC1} —deck concrete weight—

$$W_{\text{DC1}} = (t)(1.0)w_{rc} = \left[\left(\frac{9.125}{12} \right)(1.0) \right](0.15) = 0.114 \text{ kip/ft.}$$

Barrier weight W_{DC2} (concentrate load applied at 7 in. from the edge of deck)

$$W_{\text{DC2}} = (1.0)w_{\text{barrier}} = (1.0)(0.41) = 0.41 \text{ kip}$$

Future wearing surface of 3 in.— W_{DW}

$$W_{\text{DC2}} = (\text{thickness of wearing surface})(1.0)w_{\text{fws}} = \left(\frac{3}{12} \right)(1.0)(0.14) = 0.035 \text{ kip/ft.}$$

The dead load moments for the deck slab can be calculated using a continuous beam as shown in Figure 15.7.

Table 15.3 lists unfactored dead load moments. Only the results for Spans 1 and 2 are shown in the table since the bridge deck is symmetrical the centerline of the bridge.

15.5.3.3 Calculate Unfactored Live Load Moments

From Table 15.2, unfactored live load moments including multiple presence factors and dynamic load allowance are obtained as follows:

For girder spacing $S = 12$ ft., maximum positive live load moments are as

$$M_{\text{LL+IM}} = 8.01 \text{ kip-ft./ft.}$$

For negative flexure, the design sections are located the face of the support for monolithic concrete construction, 1/4 the flange width from the centerline of the support for steel girder bridges, and 1/3 the flange width not exceeding 15 in. from the centerline of the support for precast I-girders or open-box girders (AASHTO 2012, Article 4.6.2.1.6.).

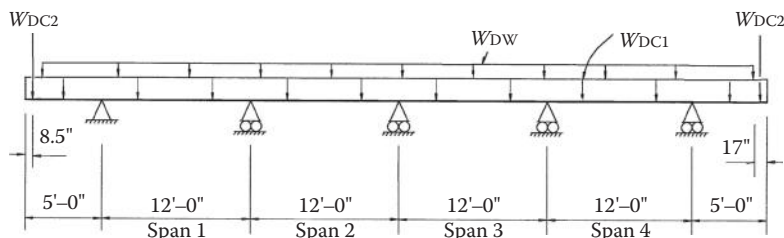
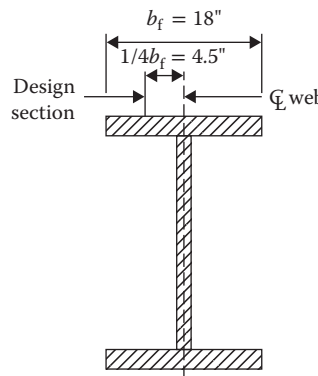


FIGURE 15.7 Concrete deck under unfactored dead loads.

TABLE 15.3 Unfactored Dead Load Moments

Distance from left support X (ft.)	Location X/S	Deck Load DC1 M_{DC1} (kip-ft./ft.)		Barrier Load DC2 M_{DC2} (kip-ft./ft.)		Future Wearing Surface DW M_{DW} (kip-ft./ft.)	
		Span 1	Span 2	Span 1	Span 2	Span 1	Span 2
0.0	0.0	-1.425	-1.352	-1.760	0.496	-0.225	-0.475
1.2	0.1	-0.679	-0.616	-1.534	0.422	-0.023	-0.240
2.4	0.2	-0.097	-0.044	-1.309	0.348	0.128	-0.055
3.6	0.3	0.321	0.365	-1.083	0.273	0.229	0.079
4.8	0.4	0.574	0.608	-0.858	0.199	0.280	0.163
6.0	0.5	0.664	0.688	-0.632	0.125	0.280	0.196
7.2	0.6	0.589	0.604	-0.406	0.051	0.230	0.179
8.4	0.7	0.350	0.355	-0.181	-0.023	0.129	0.112
9.6	0.8	-0.053	-0.058	0.045	-0.097	-0.022	-0.006
10.8	0.9	-0.621	-0.635	0.270	-0.171	-0.223	-0.174
12.0	1.0	-1.352	-1.376	0.496	-0.245	-0.475	-0.393

**FIGURE 15.8** Design section for negative moment.

For this example, assume steel girder flange width = 18 in., the design section is at $\frac{1}{4}(18) = 4.5$ in. from the centerline of steel girder as shown in Figure 15.8. The negative moment can be obtained conservatively as the moment at the centerline of the support or interpolated between moments at 3 in. and 6 in.

$$-M_{LL+IM} = 8.51 + \frac{3-1.5}{3}(9.40 - 8.51) = 8.96 \text{ kip-ft./ft.}$$

15.5.4 Calculate Factored Moments—Strength Limit State I

For Strength Limit State I load combination, factored moment follows:

$$M_u = \eta [\gamma_{DC} (M_{DC1} + M_{DC2}) + \gamma_{DW} M_{DW} + \gamma_{LL} (M_{LL+IM})]$$

$$\eta = \eta_D \eta_R \eta_I \geq 0.95$$

For this example, use $\eta = 0.95$, $\gamma_{DC} = 1.25$, $\gamma_{DW} = 1.50$ and $\gamma_{LL} = 1.75$.

$$M_u = (0.95) [1.25(M_{DC1} + M_{DC2}) + 1.5M_{DW} + 1.75M_{LL+IM}]$$

@Seismicisolation

15.5.4.1 Maximum Positive Factored Moments

From Table 15.3, it is seen that the maximum unfactored positive moments due to the concrete deck slab, barrier, and future wearing surface is located in Span 2 at a distance of 0.5S. The maximum live load positive moment equals 8.01 kip-ft./ft. Therefore, the maximum positive factored moment is

$$M_u = 0.95[(1.25)(0.688 + 0.125) + (1.5)(0.196) + (1.75)(8.01)] = 14.561 \text{ kip-ft./ft.}$$

15.5.4.2 Maximum Negative Factored Moments

From Table 15.3, it is seen that the maximum unfactored negative moments due to the concrete deck slab, barrier and future wearing surface is located Span 1 at the centerline of exterior girder and can be obtained conservatively as the moment at the centerline of the exterior support or interpolated between 0.0S and 0.1S as follows:

$$M_{DC1} = -0.679 - \frac{12-4.5}{12}(1.425 - 0.679) = -1.145 \text{ kip-ft./ft.}$$

$$M_{DC2} = -1.534 - \frac{12-4.5}{12}(1.760 - 1.534) = -1.675 \text{ kip-ft./ft.}$$

$$M_{DW} = -0.023 + \frac{12-4.5}{12}(0.225 - 0.023) = -0.149 \text{ kip-ft./ft.}$$

The maximum factored negative moment is as

$$M_u = 0.95[(1.25)(-1.145 - 1.675) + (1.5)(-0.149) + (1.75)(-8.96)] = -18.457 \text{ kip-ft./ft.}$$

15.5.5 Design for Positive Flexure Design

Try #5 bar size, bar area = 0.31 in.² and bar diameter = 0.625 in.

The effective depth, d_e , = total slab thickness—bottom cover—half bar diameter.

$$d_e = t - C_{bot} - \frac{(\text{bar diameter})}{2} = 9.125 - 1.0 - \frac{(0.625)}{2} = 7.813 \text{ in.}$$

Try #5@8 in., which is less than the maximum spacing $1.5t = 18$ in., $A_s = \frac{12(0.31)}{8} = 0.465 \text{ in.}^2$

For a rectangular section with a width of $b = 12$ in. and depth of $t = 9.125$ in.,
Concrete compression block depth

$$a = \frac{A_s f_y}{0.85 f'_c b} = \frac{(0.465)(60)}{(0.85)(4.0)(12)} = 0.684 \text{ in.}$$

Distance from the extreme compression fiber to the neutral axis

$$c = \frac{a}{\beta_1} = \frac{0.684}{0.85} = 0.801 \text{ in.}$$

Tensile strain of rebar is

$$\varepsilon_t = \frac{d_e - c}{c} (0.003) = \frac{(7.813 - 0.801)}{0.801} (0.003) = 0.026 > 0.005$$

Therefore, the section is tension controlled, resistance factor $\phi = 0.9$.

$$\begin{aligned} M_r &= \phi M_n = \phi A_s f_y \left(d_e - \frac{a}{2} \right) = (0.9)(0.465)(60) \left(7.813 - \frac{0.684}{2} \right) = 187.6 \text{ kip-in./in.} \\ &= 15.63 \text{ kip-ft./ft.} > M_u = 14.56.1 \text{ kip-ft./ft.} \end{aligned}$$

15.5.6 Design for Negative Flexure

Try #5 bar size, bar area = 0.31 in.² and bar diameter = 0.625 in.

The effective depth, d_e , = total slab thickness—top cover—half bar diameter.

$$d_e = t - C_{\text{top}} - \frac{(\text{bar diameter})}{2} = 9.125 - 2.0 - \frac{(0.625)}{2} = 6.813 \text{ in.}$$

$$\text{Try } \#5@5 \text{ in., which is less than maximum spacing } 1.5t = 18 \text{ in., } A_s = \frac{12(0.31)}{5} = 0.744 \text{ in.}^2$$

For a rectangular section with a width of $b = 12$ in. and depth of $t = 9.125$ in.,
Concrete compression block depth

$$a = \frac{A_s f_y}{0.85 f'_c b} = \frac{(0.744)(60)}{(0.85)(4.0)(12)} = 1.094 \text{ in.}$$

Distance from the extreme compression fiber to the neutral axis

$$c = \frac{a}{\beta_1} = \frac{1.094}{0.85} = 1.287$$

Tensile strain of rebar is

$$\varepsilon_t = \frac{d_e - c}{c} (0.003) = \frac{6.813 - 1.287}{1.287} (0.003) = 0.013 > 0.005$$

Therefore, the section is tension controlled, resistance factor $\phi = 0.9$.

$$\begin{aligned} M_r &= \phi M_n = \phi A_s f_y \left(d_e - \frac{a}{2} \right) = (0.9)(0.744)(60) \left(6.813 - \frac{1.094}{2} \right) = 251.74 \text{ kip-in./in.} \\ &= 20.98 \text{ kip-ft./ft.} > |M_u| = 18.457 \text{ kip-ft./ft.} \end{aligned}$$

15.5.7 Check Service Limit State-Cracking Control

Concrete cracking is controlled by the proper distribution of flexure reinforcement at service limit state. AASHTO (2012) requires steel reinforcement spacing s of the layer closest to the tension face to satisfy the following:

$$s \leq \frac{700\gamma_e}{\beta_s f_{ss}} - 2d_c \quad (\text{AASHTO 5.7.3.4-1})$$

in which,

$$\beta_s = 1 + \frac{d_c}{0.7(h - d_c)}$$

where γ_e is 0.75 for Class 2 exposure conditions; d_c is thickness of concrete cover measured from extreme tension fiber to the center of the flexural reinforcement; f_{ss} is tensile stress in steel reinforcement at service limit state and h is overall thickness of the deck.

15.5.7.1 Service I Load Combination

$$M_s = 1.0(M_{DC1} + M_{DC2}) + 1.0M_{DW} + .10M_{LL+IM}$$

Maximum positive moment

$$M_s = 1.0[(1.0)(0.688 + 0.125) + (1.0)(0.196) + (1.0)(8.01)] = 9.019 \text{ kip-ft./ft.}$$

Maximum negative moment

$$M_u = (1.0)[(1.0)(-1.145 - 1.675) + (1.0)(-0.149) + (1.0)(-8.96)] = -11.929 \text{ kip-ft./ft.}$$

15.5.7.2 Positive Flexure Cracking Control

$$d_c = 1.0 + \frac{\text{bar diameter}}{2} = 1.0 + \frac{0.625}{2} = 1.313 \text{ in.}$$

Assume y is the distance of the neutral axis to extreme compression fiber for the transformed rectangular concrete section with, $b = 12$ in.; $d_e = 7.813$ in.; $n = \frac{E_s}{E_c} = 8$, we have

$$\frac{b}{2}y^2 + nA_s y - nA_s d_e = 0$$

$$y = \frac{-B + \sqrt{B^2 - 4AC}}{2A}$$

in which $A = \frac{b}{2}$; $B = nA_s$; $C = -nA_s d_e$.

For bottom reinforcement designed for positive flexure, $A_s = 0.465 \text{ in.}^2$

$$A = \frac{b}{2} = \frac{12}{2} = 6$$

$$B = nA_s = 8(0.465) = 3.72$$

$$C = -nA_s d_e = -(8 \times 0.754 \times 6.75) = -29.064$$

$$y = \frac{-B + \sqrt{B^2 - 4AC}}{2A} = \frac{-3.72 + \sqrt{(3.72)^2 - (4)(6)(-29.064)}}{(2)(6)} = 1.912 \text{ in.}$$

Moment of inertia of cracked for the transformed section I_{cr} , is

$$I_{\text{cr}} = \frac{by^3}{3} + nA_s(d_e - y)^2 = \frac{(12)(1.912)^3}{3} + (8)(0.465)(7.813 - 1.912)^2 = 157.496 \text{ in.}^4$$

Tensile stress, f_{ss} , in the steel reinforcement at service limit state is

$$f_{ss} = \frac{nM_s(d_e - y)}{I_{\text{cr}}} = \frac{(8)(9.019)(12)(7.813 - 1.912)}{213.46} = 32.44 \text{ ksi}$$

$$\beta_s = 1 + \frac{d_c}{0.7(h - d_c)} = 1 + \frac{1.313}{0(0.7)(9.125 - 1.313)} = 1.240$$

$$s = \frac{700\gamma_e}{\beta_s f_{ss}} - 2d_c = \frac{(700)(0.75)}{(1.240)(32.44)} - (2)(1.313) = 10.43 \text{ in.}$$

It is obvious that #5 @ 8 in. meets cracking control requirement.

15.5.7.3 Negative Flexure Cracking Control

$$d_c = 2.5 + \frac{\text{bar diameter}}{2} = 2.5 + \frac{0.625}{2} = 2.813 \text{ in.}$$

Assume y is the distance of the neutral axis to extreme compression fiber for the transformed rectangular concrete section with, $b = 12 \text{ in.}$; $d_e = 6.813 \text{ in.}$; $n = \frac{E_s}{E_c} = 8$, we have

$$\frac{b}{2} y^2 + nA_s y - nA_s d_e = 0$$

$$y = \frac{-B + \sqrt{B^2 - 4AC}}{2A}$$

in which $A = \frac{b}{2}$; $B = nA_s$; $C = -nA_s d_e$.

For top reinforcement designed for negative flexure, $A_s = 0.744 \text{ in.}^2$

$$A = \frac{b}{2} = \frac{12}{2} = 6$$

$$B = nA_s = (8)(0.744) = 5.952$$

$$C = -nA_s d_e = -(8)(0.744)(6.813) = -40.551$$

$$y = \frac{-B + \sqrt{B^2 - 4AC}}{2A} = \frac{-5.952 + \sqrt{(5.952)^2 - (4)(6)(-40.551)^2}}{(2)(6)} = 2.151 \text{ in.}$$

Moment of inertia of cracked for the transformed section I_{cr} , is

$$I_{cr} = \frac{by^3}{3} + nA_s(d_e - y)^2 = \frac{(12)(2.151)^3}{3} + (8)(0.744)(6.813 - 2.151)^2 = 169.17 \text{ in.}^4$$

Tensile stress, f_{ss} , in the steel reinforcement at service limit state is

$$f_{ss} = \frac{nM_s(d_e - y)}{I_{cr}} = \frac{(8)(11.929)(12)(6.813 - 2.151)}{169.17} = 31.561 \text{ ksi}$$

$$\beta_s = 1 + \frac{d_c}{0.7(h - d_c)} = 1 + \frac{2.5}{(0.7)(9.125 - 2.813)} = 1.637$$

$$s = \frac{700\gamma_e}{\beta_s f_{ss}} - 2d_c = \frac{(700)(0.75)}{(1.637)(31.561)} - (2)(2.813) = 4.54 \text{ in.}$$

Try #5@4.5 in. for negative moment in the top reinforcement.

Use #5@9 in. (truss Bar) and #5@9 in. (straight bar) for both top and bottom reinforcement in the transverse direction as shown in Figure 15.9.

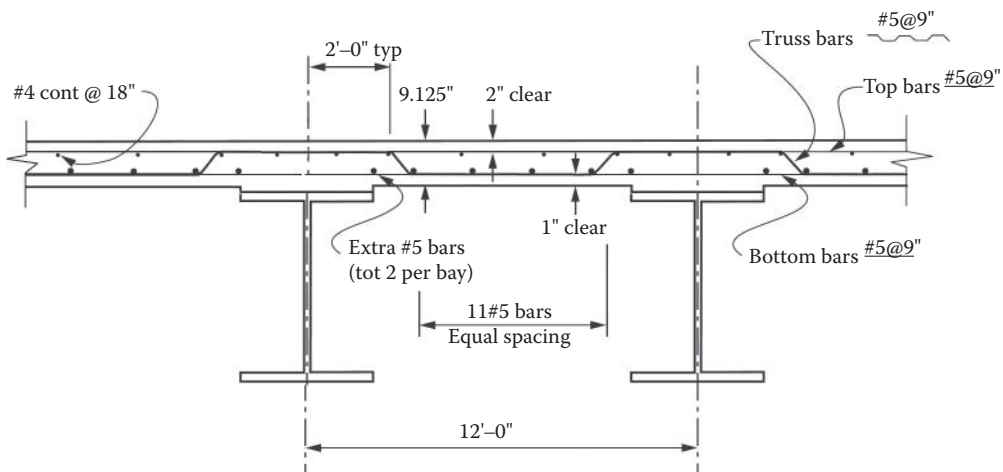


FIGURE 15.9 Bridge deck reinforcement detail.

15.5.8 Determine the Slab Reinforcement Detailing Requirements

15.5.8.1 Top of Slab Shrinkage and Temperature Reinforcement

The top slab distribution reinforcement is for shrinkage and temperature changes near the surface of the exposed concrete slab. AASHTO Article 5.10.8 (AASHTO 2012) requires the area of reinforcement in each direction and each face, A_s , shall meet the following requirements:

$$A_s \geq \frac{1.3bh}{2(b+h)f_y}$$

$$0.11 \leq A_s \leq 0.60$$

where b is the least width of component section; h is least thickness of component section; f_y is specified yield strength of reinforcing bars less than 75 ksi.

Try #4@18 in., bar cross section area = 0.2 in.²,

$$A_s = \frac{12(0.2)}{18} = 0.133 \text{ in.}^2/\text{ft.}$$

$$A_s > \frac{1.3bh}{2(b+h)f_y} = \frac{1.3(12)(9.125)}{2(12+9.125)(60)} = 0.056 \text{ in.}^2/\text{ft.}$$

$$A_s \geq 0.11 \text{ in.}^2/\text{ft.}$$

Using #4@18 in. for longitudinal distribution reinforcement and #5@4.5 in. for Transverse primary reinforcement meets this requirement.

15.5.8.2 Bottom of Slab Distribution Reinforcement

The distribution reinforcement on the bottom of the slab is placed in the perpendicular direction to the primary reinforcement for positive moment and calculated based on whether the primary reinforcement is parallel or perpendicular to traffic (AASHTO 2012). For this example, the primary reinforcement is perpendicular to traffic, AASHTO Article 9.7.3.2 requires that bottom slab distribution reinforcement ratio shall be larger than $220/\sqrt{S} < 67\%$, where S is the effective span length taken as the distance between the flange tips, plus the flange overhang. For steel girder, S is taken as girder spacing of 12 ft. conservatively.

$$\frac{220}{\sqrt{S}} = \frac{220}{\sqrt{12}} = 63.5\% < 67\%$$

$$\text{Bottom primary reinforcement } \#5@4.5 \text{ in. } A_s = \frac{12(0.31)}{4.5} = 0.827 \text{ in.}^2/\text{ft.}$$

Since bottom distribution reinforcement usually placed within the center half of the deck span, total required distribution reinforcement area

$$A_{\text{required}} = 0.635(0.827)(6) = 3.15 \text{ in.}^2$$

Try 11#5 bar, $A_s = (11)(0.31) = 3.41 \text{ in.}^2 > A_{\text{required}} = 3.15 \text{ in.}^2$

Figure 15.9 shows the detailed deck reinforcement for the design example.

References

- AASHTO. 2012. *AASHTO LRFD Bridge Design Specifications*. Customary US Units, 2012, American Association of State Highway and Transportation Officials, Washington, DC.
- Badie, S. S. and Tardos, M. K. 2008. Full-Depth Precast Concrete Bridge Deck Panel Systems, *NCHRP Report 584*. Transportation Research Board, Washington, DC.
- Barker, R. M. and Puckett, J. A. 2007. *Design of Highway Bridges*, 2nd Edition. John Wiley & Sons, Inc., New York, NY.
- FHWA. 2012. *Concrete Deck Design Example Design Step 2*, http://www.fhwa.dot.gov/bridge/lrfd/us_ds2.htm#designstep21_0.
- Russell, H. G. 2004. Concrete Bridge Deck Performance, *NCHRP Synthesis 333*. Transportation Research Board, Washington, DC.
- Tardos, M. K. and Baishya, M. C. 1998. Rapid Replacement of Bridge Decks, *NCHRP Report 407*. Transportation Research Board, Washington, DC.

16

Orthotropic Steel Decks

16.1	Introduction	589
16.2	Conceptual Decisions	590
	Reasons to Select Orthotropic Deck Superstructure • Open Ribs versus Closed Ribs • Economics	
16.3	Applications.....	604
	Re-Decking of Existing Bridges • Movable Bridges • Railroad Bridges • Orthotropic Pedestrian Bridges	
16.4	Design Considerations.....	613
	General • Deck Design • Rib Design • Floorbeam and Girder Design • Bridge Maintenance Issues • Fatigue Repairs • Future Developments	
16.5	Wearing Surface.....	623
	Introduction • Requirements for Orthotropic Steel Deck Wearing Surfaces • Basic Properties of Wearing Surfaces • Laboratory Testing Wearing Surfaces • Wearing Surfaces Systems Used in the United States • Constructing Wearing Surfaces • Maintaining Wearing Surfaces	
	Acknowledgments.....	642
	References.....	642

Alfred Mangus
Bridge Engineer
Sacramento, California

16.1 Introduction

This chapter will summarize the basic design issues of orthotropic steel deck systems. Complete design, fabrication detailing, and the fatigue-resistant details necessary to prepare a set of contract bridge plans for construction is beyond the scope of this chapter. The basic issues of these systems and the key topics and key issues are presented. Comprehensive books in English devoted only to these orthotropic steel deck systems are available as follows: Wolchuk (1963), Troitsky (1987), ICE (1973), Cartledge (1973) and FHWA (2012). The case histories and tables presented in this chapter are different and are complementary to these five books plus Mangus and Sun (2000). The most widely-used codes for orthotropic bridge design are the Eurocode and AASHTO; however, many countries use their own code details, such as the British BS5400 and the German DIN codes, partially due to differences in truck sizes, languages, and political issues. Designs of thermal loads on orthotropic decks and of their wearing surfaces vary between codes and countries (Chatterjee 2003). Japanese researchers have monitored existing orthotropic bridges to create improved design criteria (Matsui et al. 1999). Design loads and bridge details to resist blast-loads, whether due to fuel tanker explosions or terrorism is mainly kept confidential (Son and Astaneh-Asl 2012). Thus it becomes more difficult to compare the many bridge solution details. The concepts are more universal, and are thus featured in this chapter.

16.2 Conceptual Decisions

16.2.1 Reasons to Select Orthotropic Deck Superstructure

The modern orthotropic welded-steel decks were patented by German engineers in 1948 (Sedlacek 1992). They created the word “orthotropic,” which is from orthogonal for “ortho” and anisotropy for “tropic,” which they used in their patents. A design manual, published in 1957, was written in German and was based on the German Bridge Code used at that time. Therefore an orthotropic deck has anisotropic properties at ninety degrees. The shortage of, and the cost of steel after World War II economically forced the adoption of closed-ribs in Europe in the 1950s, with cold-rolled trapezoidal and wine glass shapes appearing in the 1960s. Structural steel is used the most by bridge engineers although other metals such as aluminum, as well as composite (fiberglass) materials can be used. Composites, aluminum, and other light metals are used by the aerospace industry for their flying orthotropic structures.

The typical components of an orthotropic deck bridge system are shown in Figure 16.1.

The density of steel is about three times that of normal concrete. A significant lower-weight superstructure is achieved in orthotropic steel decks for long-span bridges as shown Figure 16.2 because the steel components can be built much thinner than usable concrete bridge components. Nevertheless, the cost of a composite steel-concrete superstructure is normally less than an orthotropic steel superstructure.

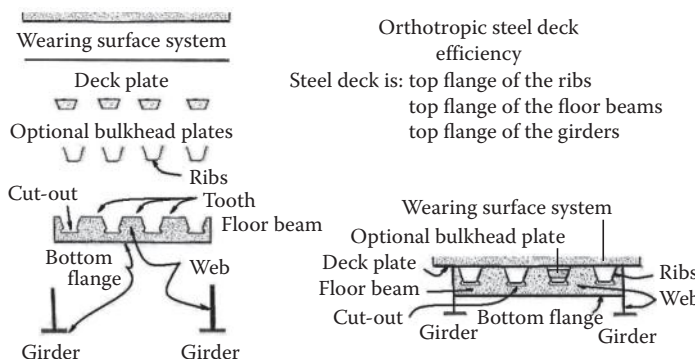


FIGURE 16.1 Components of the orthotropic steel deck system.

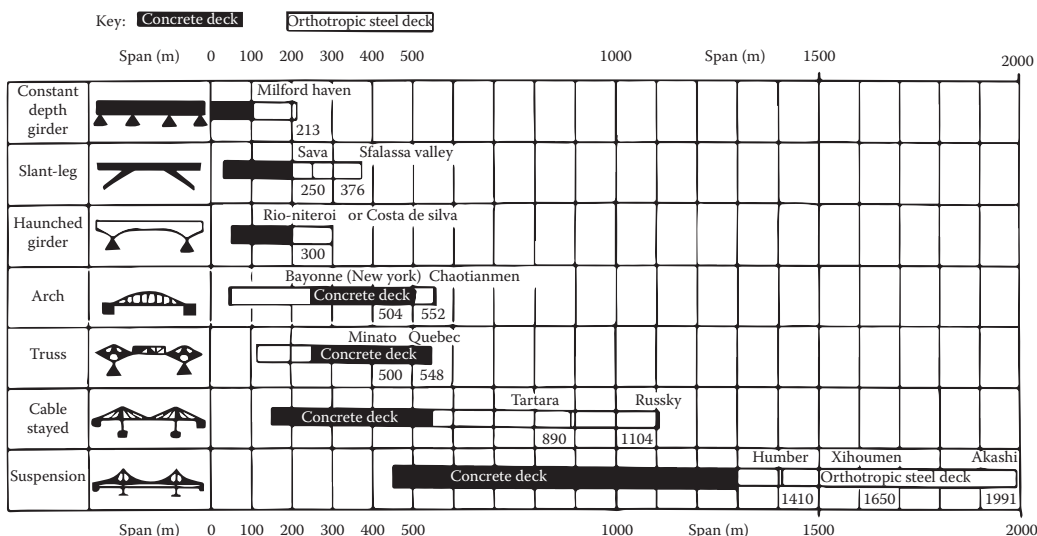


FIGURE 16.2 Orthotropic steel deck bridges dominate long span bridges.

Almost every country has selected orthotropic steel deck superstructures when minimizing the total superstructure dead weight or when thin structural depth is necessary. Due to their very low dead-loads, orthotropic decks are widely utilized (Table 16.1) in the following types of bridge structures:

- Long-span superstructures (world record span types that include suspension, cable-stayed, truss, arch, floating, and movable spans have orthotropic steel deck systems). The world's longest span is steel and has an orthotropic steel deck as shown in Figure 16.2.
- Structures subjected to strong seismic loading (Japan has the most orthotropic bridges of any country, at about 2500, and California (Table 16.2) has the most of any state or province in North America, where only about 100 orthotropic bridges exist; see Table 16.1 [Huang et al, 2009]).
- Structures in cold regions for construction advantages: Russia has about 650 orthotropic bridges, and other examples are found in Korea, northern Europe, Canada, and the cold weather areas of the United States (Mangus 2002; Popov et al. 1998).
- Movable spans are more economical with orthotropic steel decks (Mangus 2000 and 2006; Copelan, Huang, and Mangus 2010).
- Floating superstructures (Mangus 2002).
- Accelerated Bridge Construction (ABC) using larger prefabricated components (Huang et al. 2005, 2006; Murphy 2007, 2008).
- Grade separation bridges where thinner superstructure depth and vertical clearance is critical. The depth of superstructure of haunched HIGHWAY bridges with a span of length, L is approximately for steel orthotropic girders at mid span is equal to $L/60$ and at pier equal to $L/30$; for steel composite girders at mid span equal to $L/45$ and $L/24$; for concrete girders at mid span equal to $L/40$ and at pier equal to $L/20$ (Saul 2005).
- Blast resistance—toughness versus explosions (Son and Astaneh-Asl 2012).
- Temporary panelized bridging systems for emergency situations, temporary detours, or military applications (Amirkian 1970a and 1970b).

TABLE 16.1 Where Orthotropic Deck Bridges Are Utilized

Location	Approximate Number of Bridges	Advantages	Disadvantages
United States	70	Used in high seismic area on west coast and used to renovate existing suspension bridges	Lack of interest by steel industry. Fabrication outside of the United States. Limited code and design information
Canada	35	Used in cold weather	Higher cost in most areas, limited use to long span or remote locations
Mexico	10	Lower cost bridge for long spans	Hot weather more concrete bridges in use
Japan	2500	Used in a high seismic area, especially long span bridges	Older bridges used minimal steel, which resulted in shorter life. Tsunami's can damage coastal bridges
Europe	2500	Used in cold weather, especially long span bridges and movable bridge spans, unique architectural bridges	Higher cost in most areas, limited to when total superstructure weight is critical
Railroad in Europe	1000 +	Thinner superstructure and longer spans	Higher bridge cost
Railroad in North America	10	Thinner superstructure and longer spans	Higher bridge cost

TABLE 16.2 Orthotropic Bridges of California versus Other Orthotropic Bridges

Bridge in Service Name (Year Open to Traffic)	Deck Area (Sq. meters)	Deck Area (Sq. ft)	Bridge Number (by owner)
25th Street POC Pedestrian over Crossing (1953)	115	1,232	35-0048
Dublin I-580/I-680 Test Structure (1965)	1,011	10,880	33-0371G
Ulatis Creek Test Structure (1966)	411	4,420	23-0052R
San Mateo–Hayward (1967)	43,476	468,875	35-0054
18th Street POC Pedestrian over Crossing (1968)	91	976	34-0048
San Diego–Coronado (1969)	10,808	116,568	57-0857
Queensway Twin (1971)	10,256	110,400	53C-0551 L/R
Four—BART Rail (1972)	449	4,840	A-096 A & B
Colusa (1972)	372	4,006	15C-0001
Miller-Sweeney (1973)	722	7,777	33C-0147
Braille Trail Pedestrian (1977)	33	360	N/A
Golden Gate Redecking (1985)	52,583	566,000	N/A
Maritime Off-Ramp (1997)	7,921	85,287	33-0623S
Alfred Zampa at Carquinez (2003)	30,586	329,133	28-0352L
SAS East Span SFOBB (2013)	32,500	349,826	
Total 19 California Bridges	191,434	2,060,580	
Akashi-Kaiyo, Japan (1998)	84,086	905,093	
Millau Viaduct, France (2005)	67,896	730,830	
Total of Korea Bridges (2008)	668,386	7,409,718	Choi (2008)

Source: Data from Mangus, A., *Structure Magazine*, A Joint Publication of NCSEA-CASE-SEI, October 2005, pp. 12–16, 2005a.

Common Superstructures

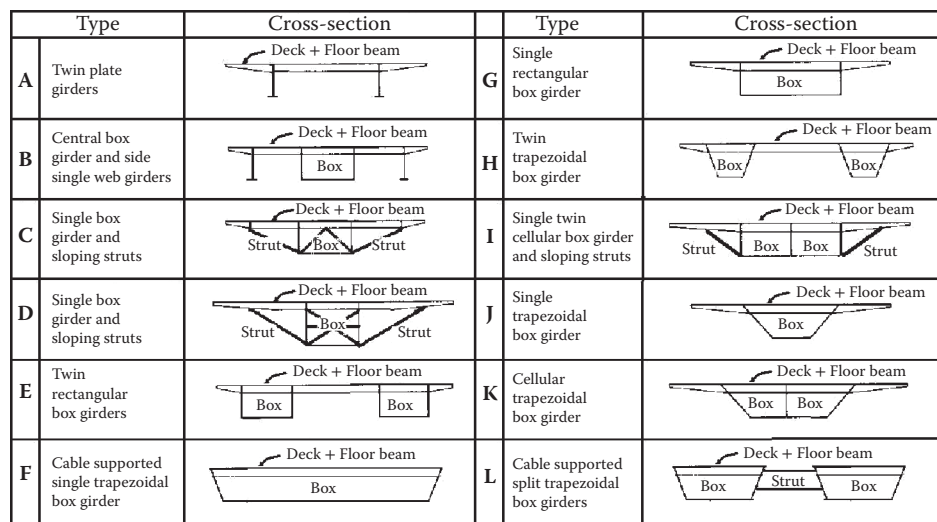
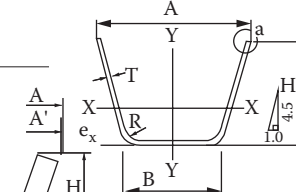
**FIGURE 16.3** Common orthotropic steel deck superstructures using rectangular plates.

Figure 16.3 summarizes common orthotropic deck superstructure types that feature flat-plate steel components. Figure 16.4 provides 44 types of orthotropic deck ribs used in Japanese Bridges. The subject of the superstructure selection process is beyond the scope of this chapter. Aesthetics and lateral loading on the superstructure are other critical issues. The basic issues of aerodynamics are presented in Chapter 22 of *Bridge Engineering Handbook, Second Edition: Fundamentals*, and construction of

Rib Types	Ribs A × H × T	Six Dimensions (mm)									
		t	A	A ¹	B	H	R	Area (cm ²)	Mass (kg/m)	e _x (cm)	I _x (cm ⁴)
18	320 × 240 × 6.0	6	320	319.4	213.3	240	40	40.26	31.6	8.86	2460
22	320 × 260 × 6.0	6	320	319.4	204.4	260	40	42.19	33.1	9.91	3011
26	324.1 × 242 × 8.0	8	324.1	323.3	216.5	242	40	53.90	42.3	8.99	3315
28	324.1 × 262 × 8.0	8	324.1	323.3	207.7	262	40	56.47	44.3	10.03	4055

Trapezoidal Ribs Used as of 1990

Rib Type	Dimension (mm)	Number of Bridges	Rib Type	Dimension (mm)	Number of Bridges		
						Width × Depth × Thick.	Width × Depth × Thick.
1.	280 × 220 × 8	1	23	320 × 260 × 8	5		
2.	300 × 200 × 6	2	24	320 × 270 × 6	1		
3.	300 × 220 × 6	32	25	320 × 300 × 8	1		
4.	300 × 220 × 8	7	26	324.1 × 242 × 8	7		
5.	300 × 224.6 × 7.9	1	27	324.1 × 242 × 15	1		
6.	300 × 240 × 6	1	28	324.1 × 262 × 8	1		
7.	300 × 250 × 8	2	29	325 × 250 × 8	1		
8.	300 × 270 × 6	1	30	327.2 × 274 × 8	1		
9.	300 × 280 × 8	1	31	330 × 250 × 8	2		
10.	300 × 280 × 12	1	32	330 × 250 × 14	1		
11.	304.1 × 222 × 8	1	33	330 × 263 × 6	1		
12.	310 × 250 × 6	1	34	330 × 280 × 8	1		
13.	310 × 250 × 8	1	35	330 × 288 × 8	1		
14.	318 × 258 × 8	1	36	330 × 288 × 10	1		
15.	320 × 200 × 6	7	37	340 × 200 × 9	1		
16.	320 × 200 × 8	1	38	340 × 250 × 8	1		
17.	320 × 230 × 8	1	39	340 × 280 × 8	1		
18.	320 × 240 × 6	96	40	370 × 250 × 8	1		
19.	320 × 240 × 8	15	41*	320 × 240 × 6	8		
20.	320 × 250 × 6	3	42*	320 × 240 × 8	1		
21.	320 × 250 × 8	3	43*	320 × 240 × 6	2		
22.	320 × 260 × 6	37	44*	320 × 260 × 8	1		

RIB CORNER RADIUS R 40 mm

* The width of bottom of trapezoidal ribs value "B" for ribs # 41 to 44 is different than upper table for ribs # 18, 22, 26 and 28.

FIGURE 16.4 Japanese trapezoidal ribs—44 types—survey reprinted and translated. (Adapted from Matsui, S. et al., *Bridges and Roads*, Oct 1998 and Nov 1999. PWRI Public Works Research Institute [in Japanese], 1999.)

components is in Chapters 1 and 2 of *Bridge Engineering Handbook, Second Edition: Construction and Maintenance*. A superstructure may be part concrete and part orthotropic, such as the Normandie Cable-Stayed Bridge in France, and other bridges (Huang and Mangus 2008b).

Figure 16.5 shows a complex, curved orthotropic box-bridge in Japan. The cross-section features a curved section which the architect felt was the best shape for the beautiful harbor setting (Wells 2002; Sueyoshi et al. 1999; Huang and Mangus 2010). The bridge has unique windscreens to protect both vehicles and pedestrians. The curved radius bottom is more efficient in handling the torsional loadings, hence it is greatly admired bridge.

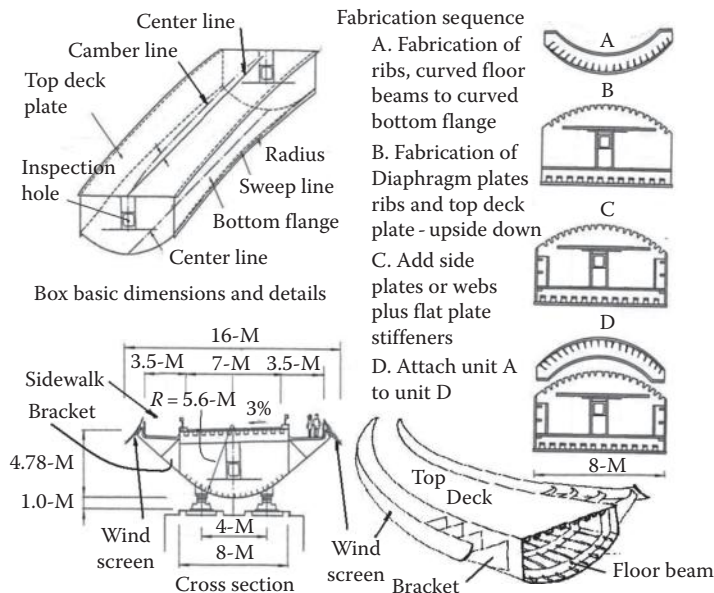


FIGURE 16.5 Complex curved orthotropic steel box—Ushibuka Bridge, Kumamoto, Japan. (From Sueyoshi K. et al. *Report on Fabrication and Erection of Ushibuka Bridge Onhashi*, Yokogawa Bridge Technical Report No. 26, 1997.1 [in Japanese], 1999.)

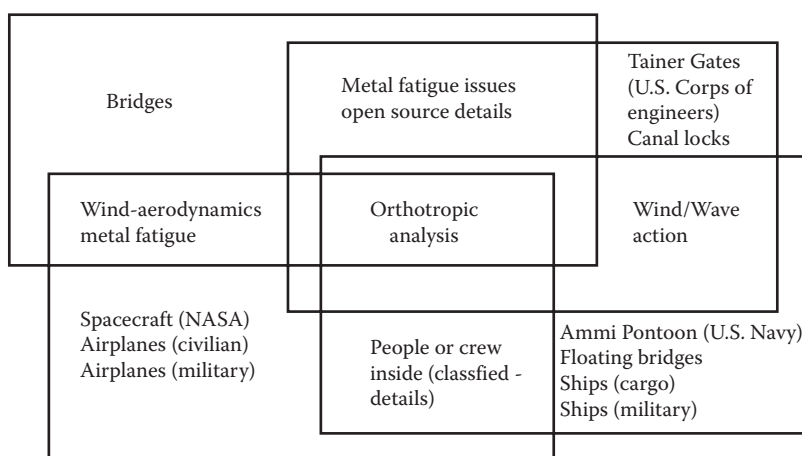


FIGURE 16.6 Graphical representation of interrelationships of objects using orthotropic concepts.

More complex geometries have been used for orthotropic superstructures. Figure 16.6 is a graphic representation of the interrelationship of key objects related to orthotropic steel bridge decks. Table 16.3 summarized major rib fabrication issues. At the center is “orthotropic analysis,” which uses mathematical formulas or equations to analyze an integrated or unified structure comprised of components. The orthotropic analysis by different mathematical methods (Wolchuk 1963; Troitsky 1987) has also been used to analyze concrete and timber deck-systems. Practicable detailing of different types of objects is arranged around the perimeter. The finite-element analysis and wind tunnel analysis originated with the aircraft industries. The Charpy impact-testing originated with welded ship-failure. Welded ship details could be applicable to floating orthotropic bridges.

TABLE 16.3 Comparison of Rib Fabrication Issues

Rib Fabrication Process	Figure	Advantages	Disadvantages	Example
Cut plate	16.10	The cheapest solution. Material such as flat plate in stock.	Extra steel weight and bolts plus fit-up.	Russian
Brake press	16.14, 16.17 and 16.19	Closed ribs are more efficient than open.	Complicated requires an additional machine (length limited by brake press size 3–4 m in length).	Saghticos Parkway
Cold rolled	16.15	Minimizes field splices.	More complicated requires a factory.	Millau Viaduct
Hot-rolled	16.18	Examples include Blub Flat, Split T-Beams and special "U" rib (Figure 16.18) Steel material is where it is the most efficiently used. Unlimited length. Length controlled by shipping issues.	The most complicated and expensive.	Ulatis Creek

A few small bridges were selected to be discussed in this chapter since the owners may be willing to share complete bridge plans and details. Documents describing full details of major bridges are normally very confidential, due to security reasons, to prevent any damage by terrorism. Owners are more likely to share bridge maintenance reports plus complete plan sets and written specifications for smaller bridges with orthotropic steel decks.

Five small orthotropic test bridges were built in the 1960s by American Engineers. Their test reports and research reports are available. Four bridges are still in service: they are Ulatis Creek plus I-580/I-680 in California, Creitz or Creyts Road in Michigan (Mangus and Sun 2000) and Battle Creek in Oregon. Small bridges, using orthotropic steel decks, are used for grade-separation bridges when traffic interruption and/or savings can be achieved in the approach spans or backfill (Roberts et al. 2000). The number of orthotropic bridges in North America is smaller than in most other industrialized countries (Mangus 2005c).

Orthotropic steel deck bridges are a specialty solution because of their high deck-cost for long span bridges. Case history articles explain why a more expensive deck system was selected (Mangus 2001). There are over four million bridges around the world; these include over 5000 orthotropic bridges. A few experts have tried to tabulate the quantity of orthotropic bridges built and create a database (Kolstein 2007; Matsui, Ohta and Nishikawa 1999). Many owners of these bridges do not want to share records to third parties. Many designers never write case histories about their projects for a variety of reasons. Private bridge owners such as an independent toll bridge owner and/or Fortune 500 companies are not required to share details. This is especially true when fatigue and wearing surface failures may embarrass the owners and/or designer of record. The East German Government successfully hid the buckling collapse of a box girder bridge with an orthotropic deck that occurred in the early 1970s (Akesson 2008). Record-span bridges are built with orthotropic steel decks because of the cost savings made by the lower costs of towers, cables, piers, columns, and foundations greatly exceed the higher deck costs. These 5000 bridges exist because they were, and are, a more cost effective solution.

16.2.2 Open Ribs versus Closed Ribs

The selection of open ribs versus closed ribs involves three interrelated major issues: design (steel weight or economy), fabrication, and construction as shown in Figure 16.7. Maintenance issues, such as ease of inspection and the percentage of superstructure exposed to exterior elements are also important. Weight savings in the superstructures are the thriving issue in the utilization of an orthotropic system. Selecting the most efficient system of rib type is the approach to minimize tonnage of steel used in a bridge.

The effective area illustrated to account for buckling is shown as solid black, developed by engineers to demonstrate rib efficiency more clearly, is also shown in Figure 16.7. The length varies with researchers and codes. For most bridges, the ribs are longitudinal connected by welding to the transverse floor

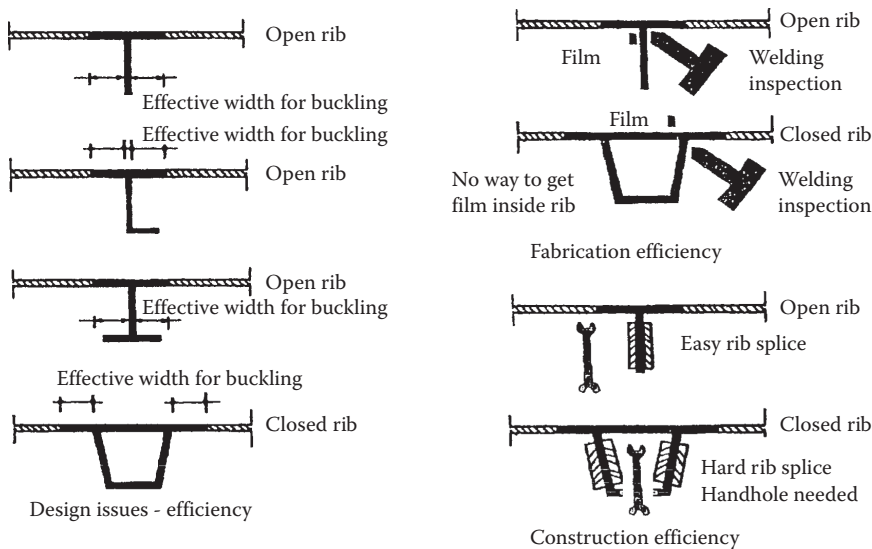


FIGURE 16.7 Selecting a rib system is really based on three issues: design, fabrication, and construction efficiency. (From Mangus, A., *Structure Magazine*, A Joint Publication of NCSEA-CASE-SEI, October 2005, pp. 9–11, 2005b.)

beams. Common details and advantages plus disadvantages are discussed later in this chapter. Code approved details and welds are shown in various codes. Most codes allow designers to use unique design if prepared by a licensed engineer. The oldest orthotropic bridge in the world is only about 60 years old. Thus it is unknown if bridges with orthotropic steel decks will actually last 100-years. Transverse support can be a split hot-rolled beam or w-beam, a small plate girder, a box girder, or a full depth diaphragm plate. The floorbeam is normally orthogonal or transverse to the main span. The deck plate is welded to the web(s) of the transverse floorbeam(s). When full-depth diaphragms are used, access openings are needed for bridge maintenance purposes. The holes also reduce dead-weight and provide a passageway for mechanical and/or electrical utilities.

The deck plate is welded to every component and acts as the top flange for the ribs and for the transverse floor beams, as well as for the longitudinal plate girders or box girders, as shown in Figure 16.1. There are various choices for the ribs, floor beam, and main girders, which can be interchanged resulting in a great variety of orthotropic steel decks and bridge superstructures. A few bridges have the ribs perpendicular to the main girders, which is more common in pedestrian bridges.

However, the retrofit of an historic bridge required the ribs to avoid existing components; the designer felt it was easier to run the ribs in the transverse direction (Zbigniew 2009). A combined railway and highway bascule bridge with an orthotropic steel deck was originally built in the area of the harbor of the city of Valencia, Spain; but due to several urban planning decisions this bridge was mothballed. The original bridge was relocated and recycled to serve in a new function as a swing bridge. The design of the new bridge, completed in July 2007, makes use of the original bridge, using 95% of the steel structure, and 50% of the operating machinery that enabled the movement of the bridge, as well as the span locks that blocked the bridge for its normal use (Calzon and Mendez 2008). The new bridge spans 99.2 m and has an 18-m wide roadway for vehicular traffic, harbor truck traffic, and the Formula 1 Racing cars. The original and the new bridges have massive transverse orthotropic ribs to the main superstructure. The center 10-m widening uses trapezoidal ribs with a depth of 813 mm. The top deck plate is 16 mm and longitudinal girders distribute the loadings effectively.

An open-rib has essentially no torsional capacity. The open-rib types were initially very popular in the pre-computer period because of their simpler mathematical analysis, and easier welding and erection details. A large range of open-rib types have been utilized, as shown in Figure 16.8. The shipbuilding industry utilizes only open ribs.

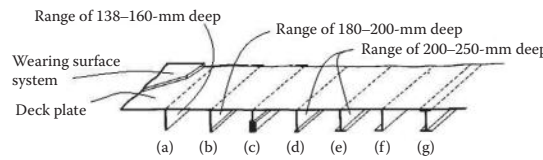


FIGURE 16.8 Popular types of open ribs used in orthotropic steel decks: (a) flat plate; (b) bulb flat—used and design formulas in Britain; (c) special bulb flat rib used on Ben Franklin Bridge redecking; (d) split “I” beam; (e) split W-flange; (f) channel; (g) a wide flange beam.

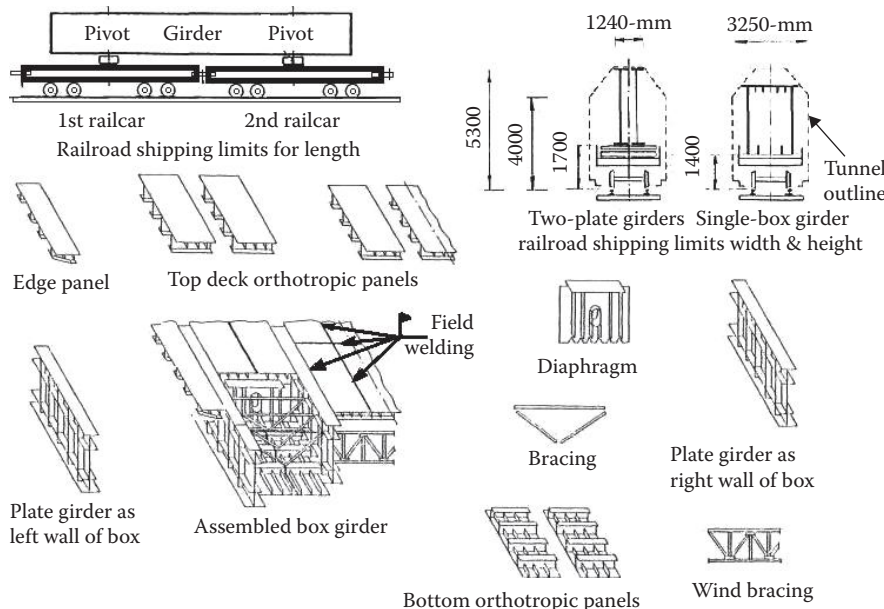


FIGURE 16.9 Exploded view of key components of Russian industrialized open rib orthotropic system.

Russian engineers have industrialized a prefabricated, panelized system of components, as shown in Figure 16.9. The components are shop-fabricated and shipped to the bridge site. This system uses plate girders or box girders for their main supports. About 500 bridges with this system have been built. Russian engineers have made several adjustments to this concept as shown in Figure 16.9. One design group uses “L” elements as box girder walls, and 50% of the bottom flange as a shop-welded component. Figure 16.9 shows the box girder, built from two plate girders, plus a pair of bottom deck panels. The components are rapidly field-bolted, which is an excellent solution for cold regions, and in snowy conditions, as shown in Figure 16.10. The field-welding is minimized for the top deck plate joints in the downward position, which is the easiest position to weld. Sometimes the welders are enclosed in small shelters because of the inclement weather.

Russians have built other solutions, using open ribs including major new bridges (Popov et al. 1998). The dimensions shown in Figure 16.10 for bolting are for a specific project and may be modified as needed for other projects. The open-deck panel has been built as a secondary component where it is connected to plate girders similar to a composite concrete deck. One advantage is that smaller bridges can be erected quickly (see Figure 16.11a).

Twin cable-stayed bridges were designed for a section of the St. Petersburg Ring Road, which crosses the Neva River, the main navigation route of the city. The first bridge was completed in November 2004. The opening of the second was in 2009. It was decided to proceed with the twin structure option over several years because of difficulties with the steel supply for Russian manufacturers (25,000–30,000 tons of structural steel to produce and deliver within 6 months). Figure 16.11b shows a portion of the twin structure cross-section with a distance of 36.4 m between each bridge axis, allowing for four lanes plus two

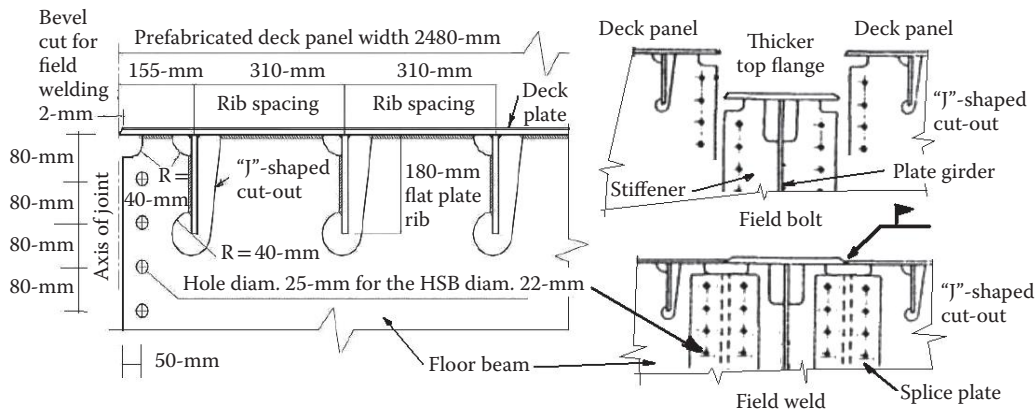


FIGURE 16.10 Industrialized open rib details for the Russian panelized orthotropic system.

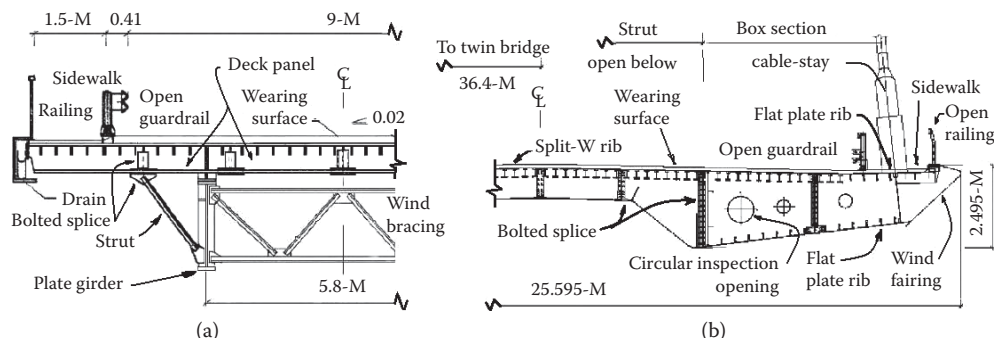


FIGURE 16.11 Russian open rib bridge types small to large. (a) Deck panels on top of girders. (b) Integral deck and ribs.

emergency lanes with a width of 2 m on each bridge deck. The twin pylon structure has a stay-cabled main span of 382-m and two 174-m side spans. The cross-section uses three types of open ribs. Both the deck and the four towers are made of steel. During construction, the deck segments were fabricated by bolting together several elements to create a 24.9 m-wide, 2.4 m-deep and 12 m-long double box girder segment that weighs 120 tons. The design of the bridge was carried out by the Design Institute Giprostroymost in St Petersburg for the Authority for Construction of the St Petersburg Ring Road (Kolyshev 2005).

Skewed bridges can be fabricated easier with straight component ribs, as shown in the Ulati Creek Test Bridge, as shown in Figure 16.12. It was built to test different wearing surface materials for the San Mateo Hayward Bridge (Bouwkamp 1965). Bouwkamp used a finite element computer analysis and verified the analysis by experimental testing (Troitsky 1987). The bridge has been subjected to very heavy traffic and still is fatigued crack free. Thus, it is an acceptable bridge system for other locations.

In 1963, the Oregon DOT was unsure which was the most durable rib-type to utilize for their future bridges. Thus the Battle Creek Test Bridge was designed, in 1965, and was completed in 1967. It is split down the middle, with half-closed ribs and half-open, or flat-plate ribs. The test bridge still does not have any fatigue cracks and has been durable. This bridge is now owned by the City of Salem, Oregon. The bridge is subjected to a limited number of trucks and local car traffic. The bulb flat rib has been used in Britain and Japan because the extra steel at the bottom makes it more efficient than a flat plate. The British has published detailed design equations for a more efficient open rib (Kelly and Braidwood 1999).

Once engineers, fabricators and contractors became familiar with the flat-plate rib system, the switch to the closed-ribs occurred to reduce the dead weight of the superstructure. Engineers from around the world keep trying to find the optimal rib design. Others have tried to find optimization of different

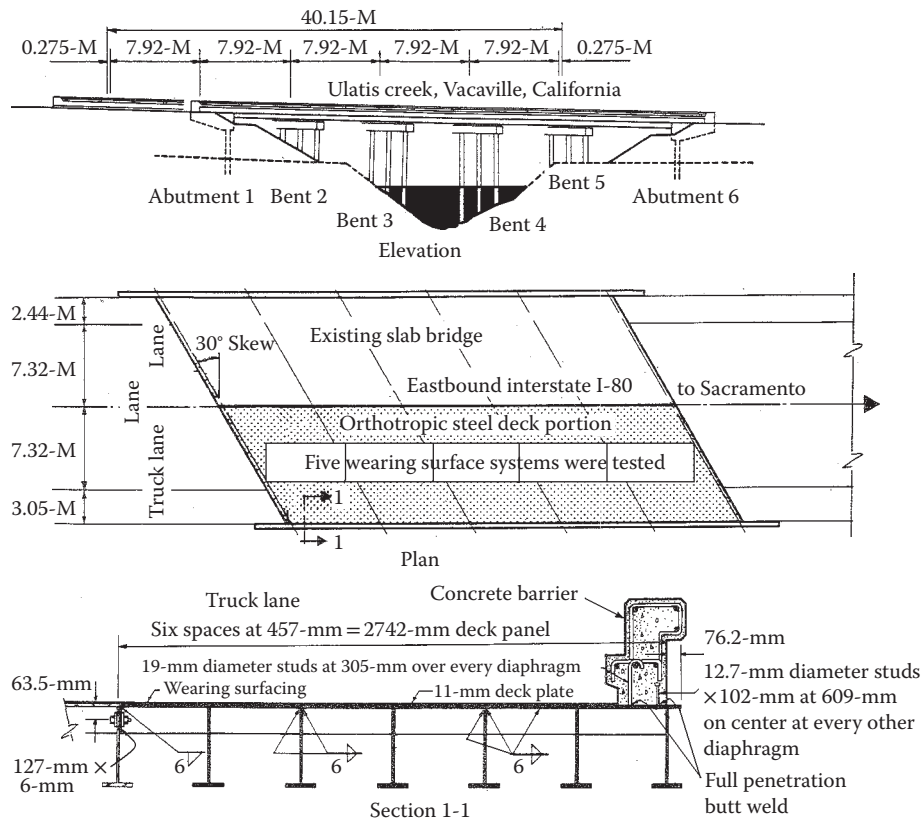


FIGURE 16.12 Skewed open rib Ulatis Creek (test bridge), Vacaville, CA. (From Bouwkamp, J. G., “Behavior of a Skew Steel-Deck Bridge under Static and Dynamic Loads,” California Department of Public Works Contract No. 13365, College of Engineering, University of California, Berkeley, 105 pages [Ulatis Creek Test Bridge], 1965.)

components and/or panelized deck systems. Local buckling issues are described in Section 4.8.1 of the FHWA Manual (FHWA 2012). The lack of understanding of global buckling lead to five box girder bridge collapses in five countries in less than a 5-year period (Akesson 2008). Local buckling could trigger global buckling. In the tension zones, the shape of the rib can be any shape, open or closed, depending on the preference of designers, fabricators or contractors. Maintenance is a consideration, as closed ribs have 50% less rib-surface area to protect from corrosion via painting or galvanizing. A closed-rib is torsionally stiff, and is essentially a miniature box girder. The closed-rib system is more effective for lateral distribution of the individual wheel loads than is the open rib system. Engineers discovered these advantages, as more orthotropic decks were built. Closed ribs are more cost effective for superstructures under large compression loads such as the aerodynamic wing shape used on cable stayed bridges. The structural detailing of bolted splices for closed-ribs requires hand-holes located in the bottom flange of the closed ribs, allowing workers access to install the nut to the bolt. For more detailed discussion on hand-hole geometry, and for case histories for solutions to allow field bolted splicing, reference is made to four comprehensive books (Wolchuk 1963; Troitsky 1987; ICE 1973; Cartledge 1973).

The original closed-rib shapes were patented by the Germans (Sedlacek 1992), and were later adopted in the United States via Bethlehem Steel, Japan, and other countries (ICE 1973). The Canadians utilized the U-shaped rib, while the British used the V-shaped rib. It is readily apparent that a series of miniature box girders, placed side by side, is much more efficient than a series of miniature T-girders, placed side by side. Weight savings has lead designers to switch to the closed ribs, which have a large range of choices. Ribs are usually placed only on the inside faces of the box girders to achieve superior

aesthetics, and to minimize the exterior corrosion surface area that must be painted or protected. Ribs are used as longitudinal interior stiffeners for compression components such as columns, tower struts, and other compression components. The trapezoidal rib system is quite often field welded completely around the superstructure's cross-section to achieve full structural continuity, rather than field bolting. Figure 16.13 shows seven types of closed ribs used in constructing orthotropic deck systems.

A trapezoidal rib can be quickly bent from a piece of steel. A brake press is used to bend the shape in a jig in less than a few minutes (Figure 16.14). Rollers can also be used to form closed ribs. One American steel company, Bethlehem Steel, developed design aid tables for trapezoidal ribs to encourage the utilization of orthotropic deck construction in the United States. Bethlehem Steel had purchased the U.S. patent rights from the German Krupp Steel Company. A code updated version has been included in the new orthotropic bridge manually (FHWA 2012).

This design aid was developed using mainframe computers in 1970, but due to lack of interest in orthotropic decks of bridge engineers this design aid eventually became out of print and was not updated to reflect changes in the AASHTO Bridge Code. A metric version of the table is in the Appendix A of the FHWA Manual (FHWA 2012).

The Brake press is the most common method of creating trapezoidal and other closed-rib shapes. Modern equipment is shown for making the SFOBB SAS ribs in China (Figures 16.14a and b). The trapezoidal ribs for the Bronx-Whitestone Bridge required a mandrel (Figures 16.14c).

The rolling of long orthotropic ribs eliminates some splicing, but the cost of rolling equipment is very expensive (Figure 16.15). German-rolled sheet piling manufacturers were the first to use this process (Sedlacek 1992). The ribs for the Millau Viaduct were rolled by a French Factory, which also manufactures mainly other steel products such as railroad car bodies, but, as needed, produces orthotropic ribs for European bridges. Photography of the manufacturing process is not allowed, but there are some images in textbooks (ICE 1973) of the German equipment. The Eurocode has more criteria requirements for out-of-plumb and straightness requirements than does the U.S. code.

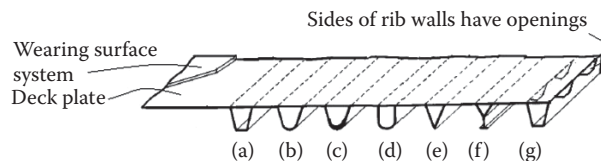


FIGURE 16.13 Seven popular types of closed ribs used in orthotropic (a) trapezoidal rib (b) rounded V shape—used in Canada—see Figure 16.16 (c) hot-roll rib with variable thickness—see figure (d) rounded U shape (e) sharp V shape was used by the British (f) wine glass shape was used by the Germans (g) bi-serrated rib shape or “Ammi” rib. see (Figure 16.20 later in the chapter).

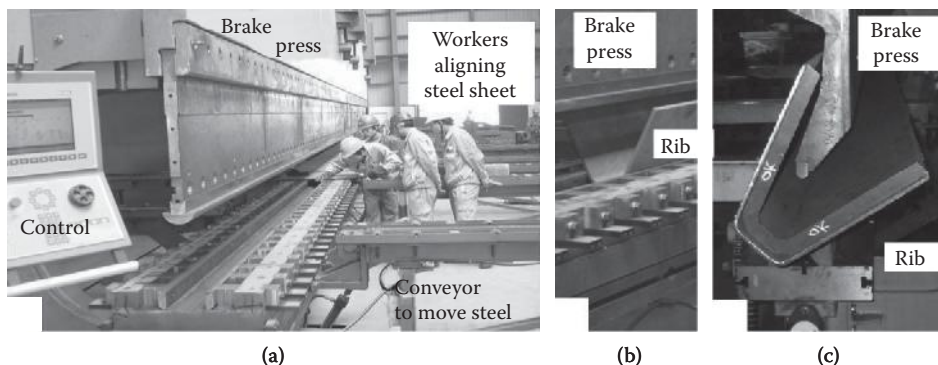


FIGURE 16.14 Examples of state-of-art brake press equipment to make ribs. (Copyright and courtesy of David Mcquaid.)

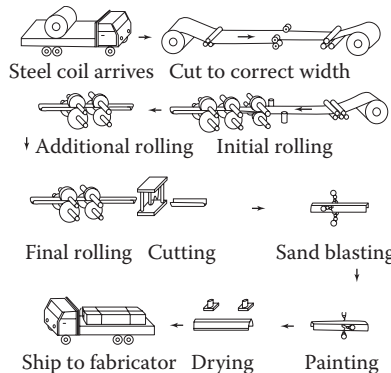


FIGURE 16.15 Cold shaping or cold rolled ribs from coil steel.

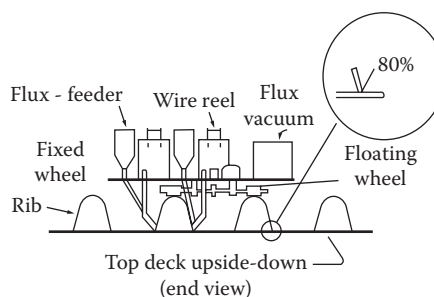


FIGURE 16.16 Welding of ribs.

The U.S. Navy developed the Ammi rib for prefabricated panelized systems for floating ports, and floating panelized bridge systems for rapid installation and deployment (Amirkian 1970a and 1970b). The Ammi rib is the lowest-possible-weight trapezoidal rib, since about 40%–50% of the sides of rib walls have been removed (Figure 16.13g). This saves weight for the floating steel pontoons used on floating bridges and docks. One major disadvantage is that the automatic welding equipment cannot be used to weld the ribs to the deck plate (Figure 16.16). One advantage is that the interior of every rib can be visually inspected to verify that the burn-through of the weld has not occurred (Erzurumlu 1972). The U.S. Navy performed, and paid for the extensive testing of these components with a prototype installed in Vietnam and other locations in the 1960s.

Most trapezoidal ribs, V ribs, and other types of closed ribs, have the rib walls intersecting the deck plate at about a 70° angle. Welding a 70° joint is more difficult than is a 90° joint, as shown in Figure 16.17. Welding experts (Blodgett 1966) developed a rib with a 90° joint plus thicker bottom face. A steel mill would need to hot roll the rib in two thicknesses as shown. The rib would be formed using a brake press. It is unknown if the Blodgett rib was ever utilized. The hot-rolled Tang rib joint, as shown in Figure 16.18 is U shaped and requires a steel mill willing to roll the shape, so it would probably need a very large project, or a government or code-endorsed standard solution to be cost-effective for the steel mill.

The panelized system open rib was studied by U.S. engineers as early as 1961 (Troitsky 1987) and (Mangus and Sun 2000). Bethlehem Steel developed a panelized test bridge at their Sparrows Point Maryland steel mill, across Humphreys Creek, and published a research report very shortly after it was built. Unfortunately they did wait until the bridge had proven to be successful. The Bethlehem Steel components, such as the top deck-plate 3/16 inch (less than 5 mm) were too thin and the ribs were only about 2.5 inches (63.5 mm) deep. Their test bridge had a very short life span of about 10-years before it was torn down due to metal fatigue. Thus the failure of a prestigious company only scared off bridge

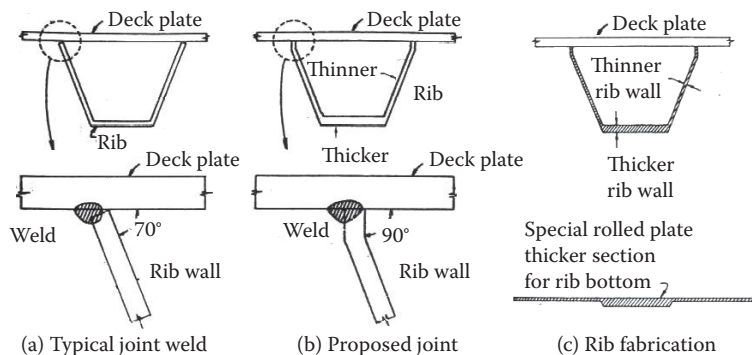


FIGURE 16.17 Brake press ribs with special rolled plate ribs. (From Blodgett, O., *Section 4.11—Orthotropic Bridge Decks of Design of Welded Structures*, The James F. Lincoln Arc Welding Foundation, The Lincoln Electric Company, Cleveland, OH, 1966.)

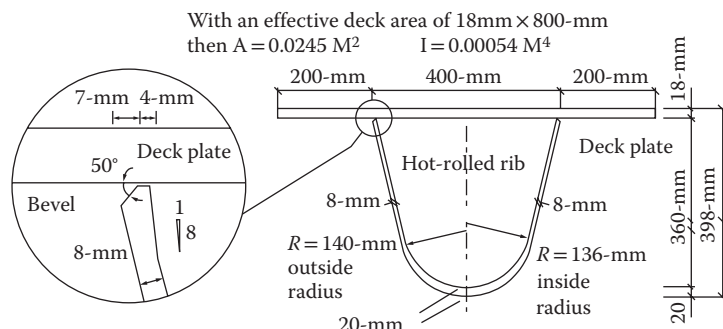


FIGURE 16.18 New hot rolled ribs. (Courtesy of M. C. Tang.)

owners. The Russian panelized system is very simple and does not require inventory. Extra total steel is used but it is a tough and simple system for medium and small bridges. Bethlehem Steel purchased the U.S. rights and promoted the use of the trapezoidal rib shapes patented by Krupp Steel. Bethlehem published design aid booklets for these shapes in the late 1960s (FHWA has reproduced these tables in their manual).

Two other U.S. companies have utilized mass manufacturing techniques. Their products are utilized around the world. The Mettler Toledo truck scales are made in a small factory in Ohio. Ribs are made with a brake press and installed in their welding bed. Pre-cambering of orthotropic decks is needed due to distortions from the welding heat. Thus the technique for mass manufacturing has been in use for decades in this small factory. The Acrow Bridge Company mass manufacturers panelized bridging systems with checkered plate orthotropic steel deck panels. The precast prestressed concrete industry mass manufactures products, but only the Russians have to date industrialized a panelized orthotropic deck system.

A Canadian Company, Structal, promoted the use of a pre-engineered factory-produced orthotropic steel deck system. The first project was the rehabilitation of the existing Congress Avenue Bascule Bridge in Chicago (Vincent 2011).

A custom designed panelized bridge was engineered for the Sagittario Parkway Detour Bridge for a night-launch across an active freeway. The deck panels were field bolted to the vertical plate welded on top of the W36 × 135 steel beams as shown in Figure 16.19. The orthotropic deck panel bridge was torn down after being used as a detour bridge. More details are available in publications (Wolchuk 2004; Mangus and Sun 2000). Figure 16.20 shows the castellated cutting and bending pattern for Ammi trapezoidal ribs.

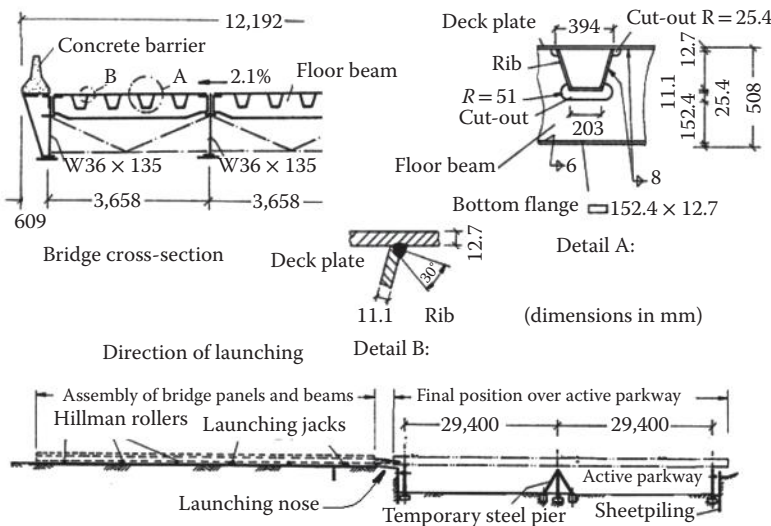


FIGURE 16.19 Sagitics Parkway panelized orthotropic deck Detour Bridge. (From Wolchuk, R. and Baker, G. S., ASCE Seminar on Orthotropic Bridges, Sacramento, CA, 2004.)

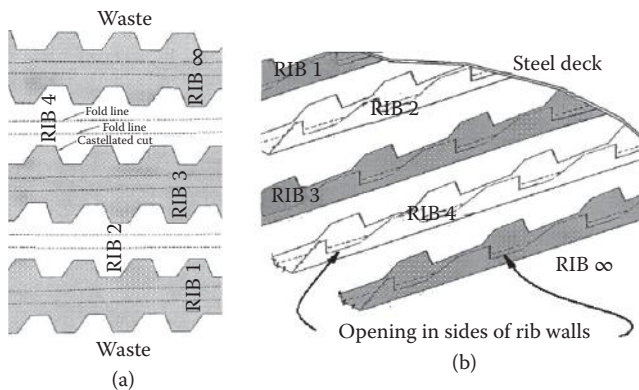


FIGURE 16.20 Castellated cutting and bending pattern for the Ammi trapezoidal rib. (a) Plan view of steel plate, (b) isometric view of deck.

The Federal Highway Administration Orthotropic Bridge Manual (FHWA 2012) provides a rib table to assist engineers in quickly designing orthotropic deck systems, complying with the minimum deck plate thickness; maximum rib span and rib spacing requirements of AASHTO. AASHTO's standardization of ribs has yet to occur, but its implementation has been recommended (Wolchuk 2004; Mangus 2005d). The flat plate industrialized panel system was utilized in Russia. Americanizing the Russian panelized orthotropic deck system in the United States would help to familiarize U.S. owners with orthotropic decks. Extra steel is used in the system but the more complicated partial penetration welding is avoided.

Other countries, bridges designed by local engineers have made orthotropic steel deck bridges even more widely utilized, as both designers and contractors have become familiar with them. Sub-variations on this system, as shown in Figure 16.9 and uniquely-designed orthotropic bridges are engineered and built in Russia. Japanese designs have utilized all types of ribs but there has been no standardization by the Japanese. Experts have tried to tabulate the popularity or all possible rib shapes (Kolstein 2007).

16.2.3 Economics

Orthotropic deck bridges become an economic alternative when the following issues are important: lower gross superstructure weight, thinner or shallower sections, larger-piece erection, cold weather (Mangus 2002; Kolyshov 2005; and Popov 1998) construction and seismic toughness.

Lower superstructure weight is the primary reason for the use of orthotropic decks in long span bridges. There can be a significant superstructure weight reduction achieved from abandoning the usual reinforced concrete deck system and switching to an orthotropic deck system. The weight may be reduced from 18% to 25% for long-span bridges. This is extremely important since the dead-load causes 60%–70% of the stresses in the cables and towers. The cost of the other components becomes smaller, by comparison. Thus the higher orthotropic deck costs are greatly offset in total bridge cost savings.

The mass is also important for bridge responses during an earthquake. The greater the total mass of the bridge, the greater the seismic forces, thus orthotropic bridges have had excellent seismic performance (Huang, Mangus and Copelan 2009). Financial experts calculation the economic losses when a bridge(s) collapse or out of service following an earthquake. Japan has adopted the orthotropic deck system to maintain an operational transportation system after earthquakes. The largest concentration of bridges in the United States are in the Western States with high seismic events. New York City is the next largest concentration with the refurbishment of older suspension bridges with orthotropic deck replacement.

16.3 Applications

Some of the world's most notable, or signature, bridges, as shown in Table 16.4, were built using orthotropic steel decks. All types and ranges of bridges have been built, including simple span bridges and pedestrian bridges. Many other books feature case histories and orthotropic details, which exceed available space in this chapter. The FHWA has been encouraging the use and documentation of accelerated bridge construction (ABC) for all types and sizes of bridges (Mistry and Mangus 2006).

Bridges with orthotropic steel decks can be quickly erected when the entire superstructure is fabricated as a full-width component. The launching of the Millau Viaduct of France was a significant combination of state of the art techniques (Mangus 2005b; OTUA 2004). The original cross section was based on the Normandie Bridge which had a trapezoidal shaped spine girder. The successful low bid contractor redesigned the superstructure. The spine girder was switched to rectangular shaped. The maximum amount of units were factory fabricated. These units were trucked to both sides of the valley. Site assembly using large gantry cranes was used to erect the superstructure. The bridge was simultaneously launched from both sides of the valley. Two of the seven cable-stay towers were first used as temporary launching support devices. The world's largest superstructure also allowed for rolled ribs by a fabricator near Paris. French design techniques are different than AASHTO and use the Eurocode. The world's largest and longest launching process plus complex falsework system were developed and engineered by an American company, Enterpac (ASCE 2004). Table 16.5 lists bridge "ABC" construction techniques.

The Japanese have designed very geometrically complex bridges with orthotropic decks due to very limited land in their urban areas. The "s" shaped 2011 Sakaegawa Cable-Stayed Bridge is based on the successful 1985 "s"-shaped Katsushika-Harp bridge. The Sakaegawa Cable-Stayed Bridge has a hybrid superstructure with a main span of a steel box girder with an orthotropic steel deck over the river and a reinforced concrete box girder for the shorter back-span over the shoreline. The total mass of the shorter concrete span equals the mass of the long orthotropic span.

John Roebling designed a suspension bridge to carry a canal over a river more than 150 years ago in Pennsylvania. Roebling stated that barge weight is not included because it displaces the same amount of water. German engineers selected an orthotropic steel solution to launch a canal bridge or navigable aqueduct or "Water Bridge" that carries river boats and barges across the Elba River (Figure 16.21). The orthotropic steel solution weighed less to move by launching than did a concrete solution. River barges

TABLE 16.4 Icons of Orthotropic Bridges

No.	Country	Name	Type	Reason	Rib Type	Additional References
1	Brazil	Rio Niteroi	Box girder	Accelerated Bridge Construction (ABC)	Closed	Huang, Mangus, and Murphy (2006)
2	Canada	Lions Gate	Suspension	Idea redecking of existing	Closed	Huang and Mangus (2008a)
3	China	Lupu	Arch	Record span	Closed	
4	Denmark	Faro	Cable-stayed	Attractive and cable-stayed erection techniques	Closed	Troitsky (1987)
5	Egypt	El Ferdan Bridge	Double swing truss	Record span—carries railroad traffic across the Suez Canal. Twin spans built adjacent banks of the canal	Closed. With large beams below the tracks	Copelan, Huang, and Mangus (2010)
6	France	Millau Viaduct	Cable-stayed	Record span—Attractive and used to launch	Closed	Mangus (2005b) OTUA (2004)
7	Germany	Fehmarnsund	Network cable-arch	Innovative solution for combined roadway and railroad. Attractive and heavily photographed	Open	Troitsky (1987)
8	Holland	Erasmus	Cable-stayed	Attractive and floating in of large pieces and cable-stayed	Closed. Open on sidewalks	Copelan, Huang and Mangus (2010)
9	Japan	The Akashi-Kaikyo	Suspension	World's longest span	Closed	Huang (2009)
10	Korea	Yeong-Jong	Self anchoring Suspension	Attractive and lifting of large pieces massive floating cranes	Closed	ASCE (2008)
11	Luxembourg	Luxembourg	Slant leg	Attractive and used falsework is selected locations	Closed	Troitsky (1987)
12	Mexico	Chiapas	Box girder	Launched using offshore foundations in deep reservoir	Closed	ASCE (2008)
13	Norway	Nordhordland	Floating	Floated in complete sections of bridge with cable stay	Closed	Mangus (2002)
14	Portugal	Ponte Dom Luiz I	Arch	Saving old bridge by renovation using panelization	Unknown	Huang and Mangus (2008a)

(Continued)

TABLE 16.4 (Continued) Icons of Orthotropic Bridges

No.	Country	Name	Type	Reason	Rib Type	Additional References
15	Rumania	Cernavoda	Arch	Attractive and used shore built and the bridge swung across the river using floats	Closed	
16	Russia	Silver Woods Moscow	Cable-stayed	Attractive symmetrical cable-stayed bridge with restaurant on top of arch pylon. Launching used	Open	Huang and Mangus (2008a)
17	Spain	Gateway to Europe	Double bascule	Attractive and used floating crane to erect as only 2 pieces	Closed. Open on sidewalks	Mangus (2006)
18	Slovakia	Apollo	Arch	Attractive and built on the banks and swung around using floats	Closed	Huang, Mangus, and Murphy (2006)
19	Sweden	Hoga Kosta	Suspension	Attractive and used sections brought in by barge	Closed	Mangus (2002)
20	Taiwan	Kao-Pin His	Cable-stayed	Innovative use of two types of superstructure Steel and concrete (hybrid)	Closed	Huang and Mangus (2008b)
21	Turkey	Bosporus 2	Suspension	Attractive and used brought in by ship	Closed	Copelan, Huang, and Mangus (2010)
22	Ukraine	South Bridge	Cable-stayed	Attractive and used cable-stay erection process. Innovative use of rib (Figure 16.23d)	Open	Mangus (2002)
23	United Kingdom	Severn	Suspension	Pioneered orthotropic wing shaped superstructure	Closed	Troitsky (1987)
24	United States	San Mateo Hayward	Box girder	Attractive and used large pieces lifted by floating crane. Original wearing surface on bridge since 1967	Open	Mangus (2005a)

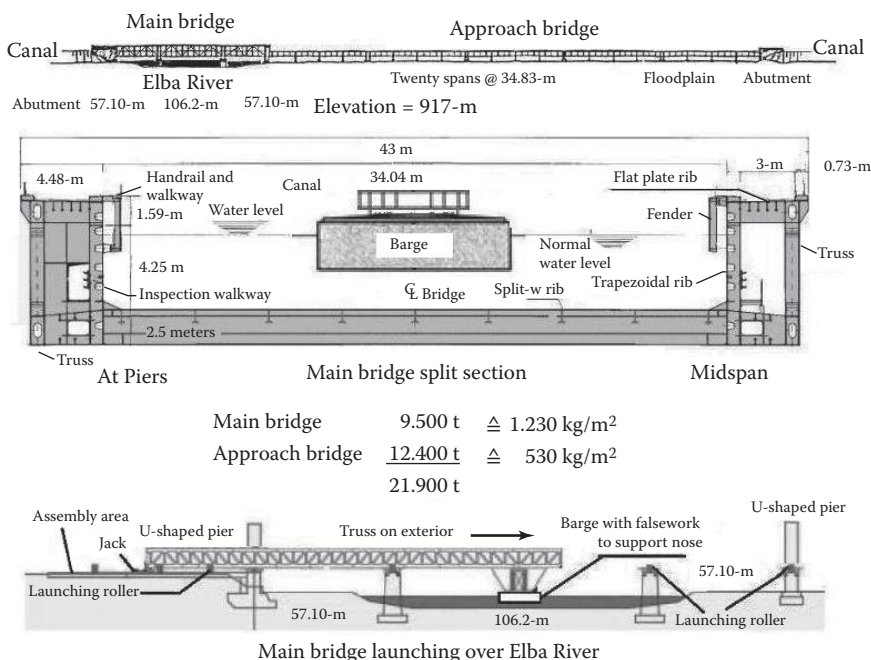
Source: Data from Huang, C. et al., *ICONS Project—An International Discussion* PECG Professional Engineers in California Government at www.orthotropic-bridge.org, 2008.

are more cost-effective than are railroads to transport freight. The filling of the water into the trough-shaped bridge is the critical load on the bridge, producing a load as great as twenty trains (DSD Dillinger et al. 2004; Saul 2005).

A prestressed concrete superstructure becomes more difficult to engineer, due to the complexity of live load combinations from the water filling process creating the continuous canal. The bridge has a

TABLE 16.5 Accelerated Bridge Construction (ABC) Techniques

Erection Process	Example	Advantages	Disadvantages
Lifting from floating crane	Akashi-Kyko	Large piece erection	First bridge erected may pay for 100% of crane cost. Crane may be mothballed with storage costs unless other bridge projects will occur in the future. In the United States the "Jones Act" prevents the use of non-United States floating cranes. Some other countries have similar laws.
Panelizing	Figures 16.9, 16.10, 16.11a, 16.19, and 16.23	Multiple sourcing of components and easier shipping	Smaller pieces
Launching on falsework	Millau Viaduct (ASCE 2004; OTUA 2004)	Area crossed has minimal disturbance	Erection stresses may govern the design
Lifting from the ship	Carquinez (Mangus and Picker 2006)	Only 24 sections to make up the bridge	Complicated requires balanced loading
Cable-stayed	Figure 16.11b	Can be built over active waterways or traffic or deep ravines	Medium sized sections
Launched from the barge	Figure 16.21	Falsework does not have to be in the river	Current of the river may limit solution locations

**FIGURE 16.21** "The Magdeburg Water Bridge" Canal grade separation bridge carrying water plus barges crossing the Elba River with barge traffic near Magdeburg, Germany (opened October 10, 2003).

total length of 917 m with a canal-water width of 34 m and a depth of 4.25 m. The main span portion has a center span of 106.2 m with back spans of 57.10 m. The superstructure utilizes three rib types: flat plate, split w-beam and trapezoidal ribs. The sides of the trough-shaped superstructure are subjected to possible compression (bending and tension too) loads due to ship impact, hence trapezoidal ribs were chosen. The open ribs on the soffit are very deep and hence more cost effective than being trapezoidal ribs.

16.3.1 Re-Decking of Existing Bridges

The re-decking of the superstructure of an existing bridge is a common use for orthotropic steel decks (examples are shown in Table 16.6). Significant weight-savings allow for additional live-load capacity, and sometimes deck widening is possible. Staged construction with deck panels allows the use of the bridge during its renovation.

The use of this renovation solution has spread around the world for both large and small bridges. For example here are some key details of the repair and reconstruction of a historical (120 year-old) steel road bridge built on a historical site in Kłodzko, Poland in the years 1883–1884. This bridge is a simple span through-truss bridge with an effective length of 24 m. It has two stone abutments. The variable depth trusses have a half-parabolic top chord and a horizontal bottom chord. Panelized orthotropic steel deck plates with angle ribs welded perpendicular to the bridge's longitudinal axis support on the original bottom chord. New deck plates were used to restore the sidewalks and steel curbs, enhancing the deck drainage. Cobblestones on a sand base were installed on top of the orthotropic steel deck panels. Thus, the historic requirements were preserved, as well as a maximum use of historic components (Zbigniew 2009).

TABLE 16.6 List of Selected Redecked Bridges Renovated with Orthotropic Steel Deck Panels

Year	Type	Name	Rib Type	Country, Location	Goal	Original Deck
1967	Truss	Cornwall	Closed	Connecticut, U.S.	Ren	Timb
1975	Plate-girder	Lions Gate Approach Spans	Closed	Canada, Vancouver	Ren	Conc
1978	Suspension	George Washington	Closed	U.S., New York City	Ren	Grid
1985	Suspension	Golden Gate	Closed	U.S., San Francisco	Ren	Conc
1986	Suspension	Throgs Neck	Closed	U.S., New York City	Ren	Grid
1987	Suspension	Ben Franklin	Open	U.S., Philadelphia	Ren	Grid
1988	Suspension	Beauharnois	Closed	Canada, Montreal	Ren	Conc
1992	Plate-girder	Sagittos Parkway	Closed	U.S., Long Island, NY	Ren	New
1993	Truss	Champlain	Closed	Canada, Montreal	Ren	Conc
1994	Suspension	Rodenkirchen	Closed	Germany	Wide	Conc
1995	Arch	Theodor-Heuss	Unknown	Germany, Mainz-Wiesbaden	Wide	Conc
1998	Suspension	Williamsburg	Closed	U.S., New York City	Ren	Grid
1999	Suspension	Wakato Ohashi	Open	Japan, Wakato	MT	Conc
1999	Suspension	MacDonald	Closed	Canada	MT	Grid
1999	Truss	Songsu	Closed	Korea	WMT	New
2001	Suspension	Tamar Bridge	Closed	United Kingdom	WMT	Conc
2001	Truss	Mária Valéria	Closed	Hungary	Ren	Conc
2002	Truss	Tornionjoki	Closed	Finland	Ren	Timb
2002	Suspension	Lions Gate Suspension Spans	Closed	Canada, Vancouver	Ren	Conc
2002	Suspension	Triborough	Closed	U.S., New York City	Ren	Grid
2005	Suspension	Bronx Whitestone	Closed	U.S., New York City	Ren	Grid
2005	Steel Arch	Ponte Dom Luiz I	Unknown	Portugal, Porto	Ren	Conc
2005	Concrete Arch	Ohre River	Closed	Czechoslovakia	Ren	Conc
2007	Bascule	Blagoveshchensky	Open	St Petersburg, Russia	Wide	Conc
2008	Steel Truss	Kłodzko	Open	Kłodzko, Poland	Ren	Cobb
2010	Concrete Box	Dalian China	Open	Dalian, China	Ren	Conc
2012	Suspension	Verrazano Narrows	Design	U.S., New York City	Des	Grid
2012	Double Bascule	Congress Avenue	Closed	U.S., Chicago	Ren	Grid

Code for "Goal": Des, design at 70% completion; email, information via email from colleague; MT, more traffic bridge superstructure and piers + foundation the same; Ren, renovated, live loading capacity is increased due to lower weight per square meter deck; WMT, more traffic, bridge superstructure widened, but pier foundations the same; Wide, bridge made physically wider; New, new temporary bridge assembled with panels; www, World Wide Web; Stud, study; Year, year of completion of Redecking, with orthotropic; Code for "Deck" system replaced: Conc, concrete; Grid, steel grid or grating filled with concrete; Timb, timber decking; Cobb for Cobblestone.

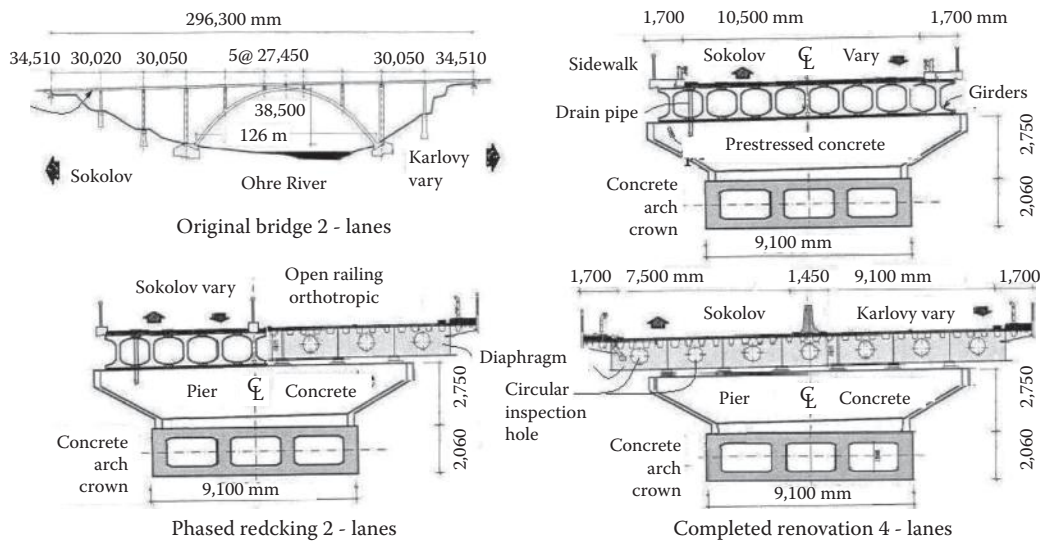


FIGURE 16.22 Staged superstructure replacement of a Czechoslovakian concrete arch bridge.

Engineers are always under pressure to find innovative solutions. The existing concrete arch bridge completed in 1974 spanning the Ohre River in Czechoslovakia was a two-lane bridge with a superstructure which used precast prestressed concrete I-Girders, as shown in Figure 16.22. The superstructure was replaced in stages with an orthotropic steel deck in 1996 (Korbelar 2006). The tremendous weight-savings of this switch allowed for the widening to 4-lanes. The existing arch and its piers were unmodified (Korbelar et al. 2006). Traffic continued during the widening process.

An existing reinforced concrete box girder supported a two-lane bridge in Northeastern Dalian China. Its superstructure was widened on both sides, for symmetry, with an attractively shaped superstructure with an orthotropic steel deck. The wing-shaped panels, with six closed trapezoidal ribs each, were attached transversely with anchor bolts and transverse post-tensioning. Each steel wing has six closed trapezoidal ribs. The tremendous weight savings of this switch allowed for the four-lane live loading. Thus the existing piers and its piers were unmodified (Wang and Zhang 2011).

16.3.2 Movable Bridges

Movable superstructures also utilize orthotropic steel deck systems. A list of selected bridges is shown in Table 16.7. The professional group HMS—Heavy Movable Structures were created to exchange ideas about primarily movable bridges (HMS papers can be downloaded free). Less than twelve movable spans, out of several thousand in North America, have orthotropic steel decks (Mangus 2000 and 2006). Studies for orthotropic steel decks for movable spans have been performed by U.S. engineers but have not been executed, as shown in Table 16.8 and Ecale (1983). The fear of a new, unproven system has delayed the implementation in North America for movable spans (Mangus 2005d). American engineers used steel deck plate bridges in the 1930's but they were not orthotropic plates. The Gateway to Europe Double Bascule Bridge is a unique, very attractive signature bridge located in a Spanish port (Copelan 2010; Mangus 2006). This bridge utilizes an aerodynamic shaped superstructure system with torsional rigidity, and was erected by floating crane in two pieces or two leaves of the double bascule. It is an outstanding example of a modern example of bridge technology and engineering. Orthotropic steel decks are a standard solution for movable bridges in Europe (Saul 2005). At least 200 single leaf bascule spans around 30 meters of them exist in the ports and canals, while some are under construction now. The Krakeroy Bridge in Norway built in 1957 is still in active service (Wolchuk 1963; Troitsky 1987).

TABLE 16.7 List of Selected Movable Span Bridges Using Orthotropic Decks

Year	Type	Name	Main Span (L × W)	Country, Location
1931	Vertical lift	Burlington Bristol*	540 ft × 27 ft	U.S., Burlington, NJ and Bristol, DL
1938	Vertical lift	Harlem River*	320 ft × 72 ft	U.S., New York City
1960	Vertical lift	Guabia	55 m × 18.3 m	Brazil, Porto Alegre
1988	Vertical lift	Danziger	320 ft × 108 ft	U.S., New Orleans
2008	Vertical lift	Gustave-Flaubert	100 m × 27 m	France, Rouen
2013	Vertical lift	Jacques Chaban-Delmas	110 m × 32 m	France, Bordeaux
2006	Articulating ramp	Brainbridge Island Ferry Terminal	109 ft × 23 ft	U.S., Washington
1995	Articulating ramp	Roll-On Roll-Off	2-lane × 10 m	Ireland, Dublin
1995	Articulating ramp	Roll-On Roll-Off	200 ft × 29.5 ft	U.S., Valdez, AK
1968	Floating	U.S. Navy Ammi Pontoons	2-lane × 24 ft	Vietnam, Da Nang
1972	Drop-in	Colusa	105 ft × 38 ft	U.S., Colusa, CA
1973	Single bascule	Miller Sweeney	127 ft × 52 ft	U.S., Oakland, CA
1985	Single bascule	Breydon	30.8 m × 13 m	U.K., Britain, Breydon
1999	Single bascule	Erasmus	52.3 m × 35.8 m	Holland, Rotterdam
1970	Single bascule	Wapole Island	109 ft × 38 ft	Canada, Wapole Island
2011	Single bascule	Teglvaerks	19.6 m × 19.2 m	Copenhagen, Denmark
1933	Double bascule	Portage River	25 m × 15.9 m	U.S., Port Clinton, Ohio (battledeck)
1957	Double bascule	Krakeroy	24 m × 6.5 m	Krakeroy, Norway
1999	Double bascule	Gateway to Europe	109 m × 12 m	Barcelona, Spain
2012	Double bascule	Congress Avenue-Redecking	221.4 ft × 83.6 ft	Chicago, IL
1995	Double swing	Naestved	42 m × 14 m	Denmark, Naestved
2007	Double swing	Formula 1 Racing Circuit	99.5 m × 18 m	Valencia, Spain
2001	Double swing	El Ferdan Railroad	340 m × 12.6 m	Egypt, Suez Canal
2010	Single swing	Samuel Beckett	95 m × 17 m	Dublin, Ireland
2001	Floating swing	Yumeshima-Maishima	1000 ft × 127 ft	Japan, Osaka Aka (Yumemai Bridge of Osaka)

* = riveted non-orthotropic steel plate

TABLE 16.8 Comparison of Deck Options for a 453-ft Span by 55-ft Wide Movable Lift

Deck Type Analyzed and Fully Engineered for Comparison	Lift Span Total Weight (tons)	Advantages	Disadvantages
Orthotropic steel deck	760	Lowest self-weight results in cost savings for towers, foundations, motors, cables, etc.	Lack of current codes, designers required to do their own research and develop their own design software
Exodermic deck (patented system)	1099	Owner does not have to worry about design, which is provided by manufacturer	Patent holder becomes a "sole supplier," which requires a waiver from FHWA
Partially-filled steel grid deck with monolithic overfill	1228	Older historic system where lifespan has been up to 75 years	Has a much higher dead load than orthotropic decks
Lightweight (100 pcf) concrete deck—8 inches thick	1501	Non-proprietary system	Limited number of suppliers of lightweight aggregate Not much dead weight savings

Source: This table is based on one originally created and published by Dr. Thomas A. Fisher of HNTB Corporation (Fisher, T. A., *aper # IBC-98-66 of 15th Annual Internal Bridge Conference and Exhibition*, June 15–17, Pittsburgh, PA, 1998.).

16.3.3 Railroad Bridges

Railroads have been using steel bridges for more than 100 years. There has been no particular advantage in the use of concrete superstructures of railroad bridges. Steel ballast pans have been used for about the same length of time. Reinforced concrete ballast pans are common, but orthotropic steel decks are much more efficient. Thus in Europe (Troitsky 1987; Wolchuk 1997; Wolchuk 1999; Saul 2005; Mangus 2010), the orthotropic steel deck solution has been widely used for all sizes of railroad bridges. The German Federal Railroads have a standard classic two plate girder with an orthotropic steel deck system for their common short-span railroad bridges. Edge plates are used to keep the gravel ballast in place on top of the superstructure (Mangus and Sun 2000).

Four, weathering steel, single track, simple span bridges, as shown in Figure 16.23, were completed for BART, Bay Area Rapid Transit in 1972. Tudor Engineers designed these four bridges located in Berkeley, California. Many railroads prefer weathering steel since maintenance painting is not required. Each bridge supports a single track and has a simple span of 33.53 m. Two parallel bridges cross over Golden Gate Avenue and two parallel bridges cross over the adjacent Chabot Road in Berkeley California. Each deck is divided into ten identical deck panels of about 3.35 m long by 3.35 m width. These essentially square deck panels have six trapezoidal ribs that span the 3.35 m. The 40 identical panels were shop-welded and field-bolted to the transverse floor beams. The unique interlocking system prevents fatigue cracks from spreading. Gravel ballast for rail track on the weathering steel deck is used to make track adjustments to grade. The bridges have no maintenance issues.

Steel box girder railroad bridges using orthotropic efficiency are described in the first edition of The BEH Bridge Engineering Handbook, in Chapter 45, on Steel Bridge Construction written by Durkee and Chapter 66 on Russian Bridges. The Kansas City Southern Railroad Bridge, used steel box girder with an orthotropic steel deck, an award winning bridge, which was designed by Bridgefarmer and Wolchuk. The box girder concept was first used by German Engineers. Two similar Canadian railroad bridges using steel box girders with orthotropic steel decks, were built later using a straightforward rectangular steel box with split w-beam stiffeners for the steel deck (shown in Figure 16.24a). The Design of the Murray and Wolverine River railroad box girder bridges feature unique column designs (Taylor 1984), Durkee performed the erection engineering for launching and wrote a paper describing adjustments made to handle the launching stresses.

A new Russian grade-separation bridge was built for travel to the planned 2014 Winter Olympics site. The flat plate-rib is used but the "J" cutout (Figure 16.11) is not fatigue-resistant as a round cut-out at the base of the flat plate ribs (see Figure 16.24b). Also note the variable depth ballast has greater depths at the perimeters of the ballast pan. These twin box girders are at a slight inclination from the horizontal.

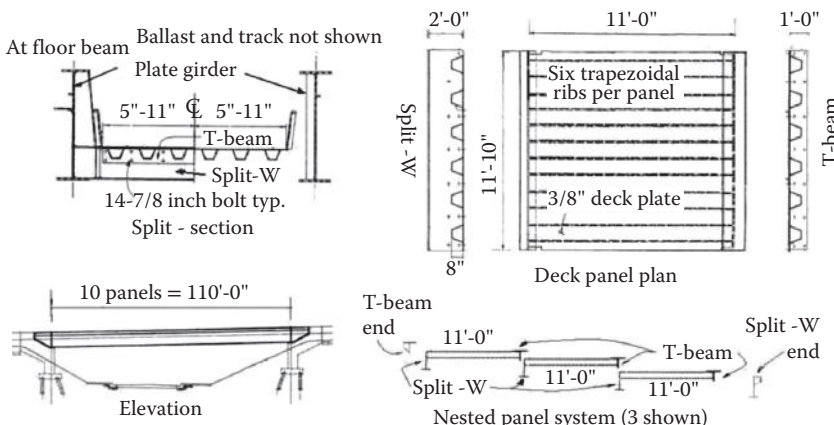


FIGURE 16.23 The four BART bridges in Berkeley, California—nested panel system with closed ribs.

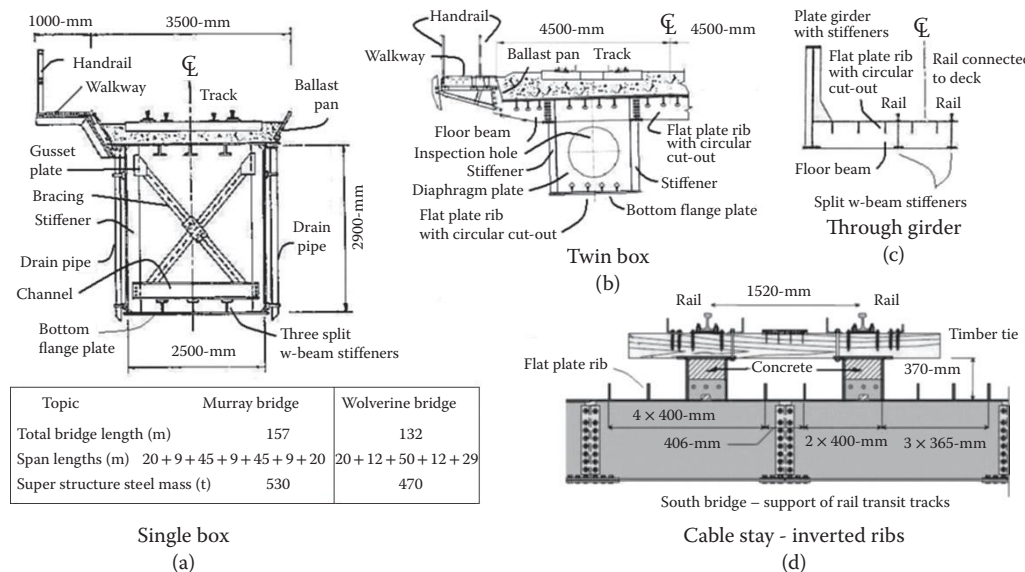


FIGURE 16.24 Canadian, Russian, Czechoslovakian, and Ukrainian open rib orthotropic railroad bridges: (a) single box (b) twin box (c) through girder (d) cable stay, inverted ribs.

Maintenance walkways are bolted, and are not orthotropic. Other types of orthotropic bridges were used on this new railway, built for the games.

There are well over 1000 orthotropic railroad bridges around the world (Wolchuk 1999; Saul 2005). Typical routine grade separation bridges used in Czechoslovakia are shown in Figure 16.24c. The rails are mounted directly to the steel bridge deck, which places a concentrated load on the much-larger ribs (Rotter 2006). Thus a common solution is large split w-beams directly below the rails.

An innovative solution by Korniyiv is on the Ukrainian Bridges (Korniyiv—ASCE 2004). The ribs are positioned on top of the deck with timber ties attached to the orthotropic flat plate ribs (Mangus 2002). Hence another innovative solution (Figure 16.24d).

Much more complex railroad structures, using double swing bridges across the Suez Canal, curved orthotropic truss bridges in Japan and Russia have been engineered and successfully built. Very large truss bridges with orthotropic steel decks carry high-speed rail traffic in Europe and China, such as the Dongping half-through, truss-arch high-speed rail bridge. Cable stayed bridges carrying trolley cars, and light rail traffic exist in Europe (Troitsky 1987). Many bridges in Europe carry combined vehicular and rail traffic. About a dozen arch bridges with orthotropic steel decks, are part of the High Speed Railway lines in Belgium (Van Bogaert- ASCE 2013).

16.3.4 Orthotropic Pedestrian Bridges

Three straight forward pedestrian bridge designs are shown in Figure 16.25a through c. The orthotropic steel deck supported on twin w-beams is the Braille Trial Pedestrian Bridge (Mangus 2001) as shown in Figure 16.25a. A similar larger three span box girder weathering steel bridge with roof crosses Seward Highway for Rabbit Creek Elementary School in Anchorage, Alaska. The 18th Street Bridge was hit by a truck that exceeded the allowable height limits in 1968 (Gilbert 1991) as shown in Figure 16.25b. The original design was similar to the 25th street design utilizing twin plate girders completed in 1953 as shown in Figure 16.25b. Although the orthotropic equations were not used to design it, the steel deck is orthotropic and the deck behaves accordingly. The replacement design used two Vierendeel trusses for the superstructure. Only the damaged steel superstructure was replaced, and the existing abutments were reused. The Vierendeel truss system increased the vertical clearance

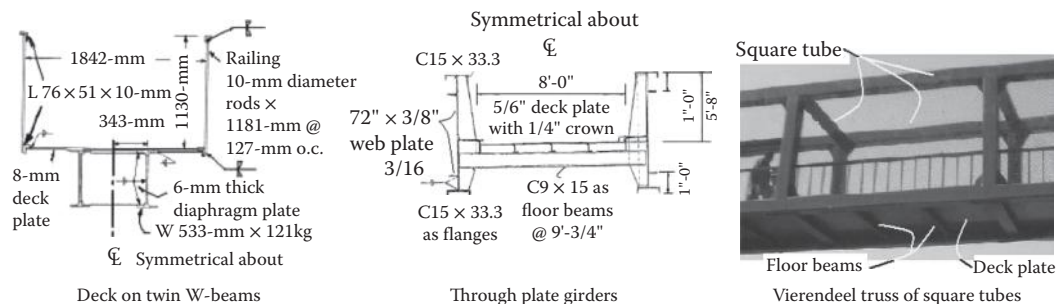


FIGURE 16.25 Three California orthotropic pedestrian bridges built from rectangular components: (a) deck on twin W-beams (b) through plate girders (c) Vierendeel truss of square tubes. (From Mangus, A., *6th Short Medium Span Bridge Conference*, May 20–22, 2001, Vancouver, Canada, CSCE, 2001.)

over this very active freeway and was lifted as a single unit. A similar weathering steel bridge with unbraced top chords and longitudinal trapezoidal ribs was built across Northern Lights Boulevard adjacent to East Anchorage Alaska High School. The Tudor Trail Bridge located in Anchorage Alaska is a curved radial bridge completing a 90° turn. (Nottingham—ASCE 2004; Mangus 2005c). The Bow River Pedestrian Bicycle Peace Bridge in Calgary, Canada by Santiago Calatrava is a recent 2012 project. The span is 126 m with inside dimensions of 3.7 m for pedestrians and 2.5 m for cyclists (Wikipedia 2012). Special pedestrian design loadings are discussed in AASHTO Pedestrian Bridge Code Booklet and CRC Press has a book on footbridge vibration issues. Signature span pedestrian orthotropic bridges have been built in Europe and Asia with orthotropic decks.

16.4 Design Considerations

16.4.1 General

There is insufficient space to go through a design of even a small orthotropic bridge. Thus the basic issues will be summarized. The BSC Balanced Scorecard Management System developed by Kaplan and Norton 1992 is a tool to look at four quadrants of key data simultaneously. These quadrants are related to a central goal. The available sources of knowledge to assist in selecting and designing an orthotropic bridge are shown in Figure 16.26. It is more applicable than a flow chart because the use is simultaneous and not linear. There are over 5000 existing orthotropic bridges and a similar successful bridge probably can be selected to base a new design upon. Bridge maintenance issues in problem designs eliminate their selection in the evolution of bridge technology. They range from short span to world class record span holders. Every year engineers develops variations upon successful orthotropic steel deck solutions. Every bridge built is really a “test bridge,” with successes and failures recorded.

Copying a successful bridge design or use of established standard details, rapidly advances the design of our infrastructure. The Eurocode is more extensive than AASHTO on orthotropic bridge requirements, due to the fact that there about thirty times as many orthotropic bridges built in Europe versus North America.

Each country has its own codes and decision-making process on which details and policies are selected. The design engineer has significant discretion in the selection of details since many of these bridges are unique. For large projects, it is common to have specialized testing of components or details. In contrast with the conventionally designed bridges, where the individual structural elements (stringers, floor beam and main girders) are assumed to perform separately, an orthotropic steel deck superstructure is a complex structural system in which the component members are closely interrelated. The stress in the deck plate is the combination of the effects of the various functions performed by the deck.

An orthotropic steel deck should be considered an integral part of the bridge superstructure; thus the BSC Balanced Scorecard (Figure 16.27) demonstrates the interrelationships of 16 key design issues or choices made by a bridge engineer. The deck plate acts as a common flange of the ribs, the floor beams,

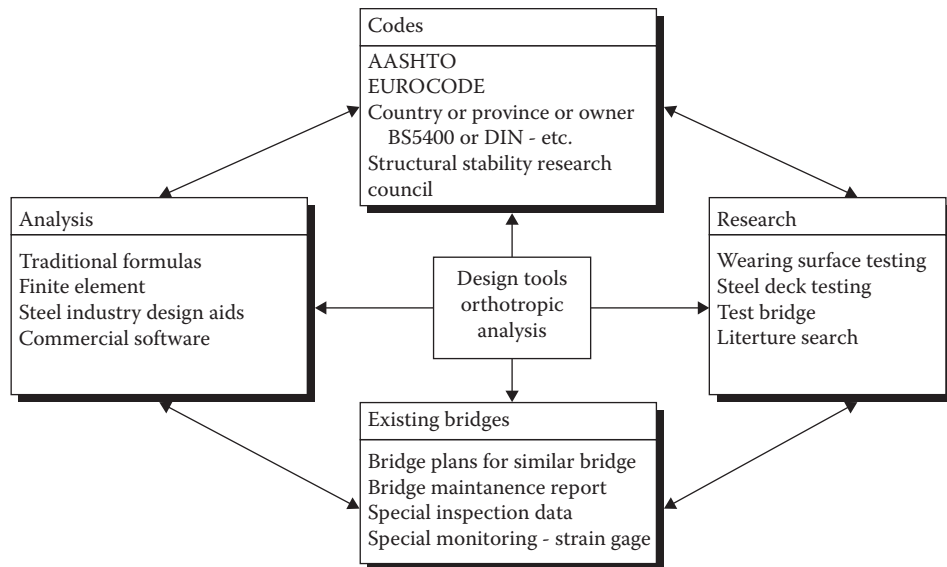


FIGURE 16.26 Balanced scorecard for design tools available for orthotropic analysis -16 possibilities listed.

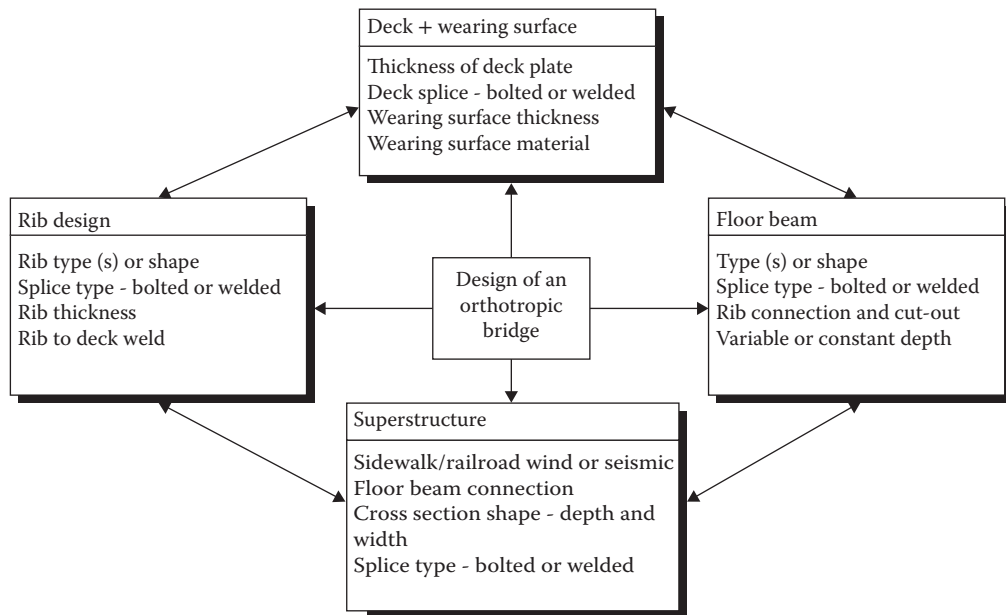


FIGURE 16.27 Balanced scorecard for design of an orthotropic bridge—16 items to monitor simultaneously.

and the main longitudinal components of the bridge. Any structural arrangement in which the deck plate is made to act independently from the main components is undesirable. The effects due to global tension and compression should be considered and combined with local effects.

Diaphragms or cross-frames should be provided at each support and have sufficient stiffness and strength to transmit lateral forces to the bearings and to resist transverse rotation, displacement and distortion. Intermediate diaphragms or cross-frames be provided at locations consistent with the analysis of the girders and should have sufficient stiffness and strength to resist transverse distortions. Access openings are often needed for bridge maintenance staff to inspect the superstructures with enclosed interiors.

16.4.2 Deck Design

The original goal of orthotropic bridges was to use the absolute minimum steel needed with deck plate thickness varying for the deck plate. Today, bridge longevity has become a dominant criterion in design choices. Recommended minimum deck thickness has slowly increased in thickness over the last 50 years. Most codes and experts currently recommend 14 mm as a minimum. The Japanese code now has 16-mm minimum deck plate thickness. The current AASHTO-LFRD (AASHTO 2012) requires that the minimum deck plate thickness, t_p , shall not be less than either 0.5625 inches (14 mm) or 4% of the largest rib spacing. Deck thickness recommended by codes is based on the durability of previously built bridges. This requirement is advisable from the point of view of both constructability and long-term bridge life. Some bridges with light truck traffic, such as the Battle Creek Bridge, still do not have fatigue cracks. The choice of selecting ribs and detailing is an art based upon adopting the systems used for fatigue-crack free bridges with similar live loads.

The steel deck plate's role is to directly support the traffic loads and to transmit the dead and live load reactions to the ribs. The oldest orthotropic bridges are about 60-years old. Owners have requested recent bridges with up to 120 years of useful service life. Thus designs are based on extrapolations of successful bridges currently in service. The deck may experience corrosion if the wearing surface fails. The average life for good wearing surfaces is about 25-years and then they need to be removed and replace surfaces need to be installed. In Belgium, a shorter lifetime of wearing systems is assumed to be 20 years at most, with intermediate renovations, especially for thin systems. This might be because of more congested and heavier traffic, as well as climate conditions (or to thin a deck plate).

An example of a bridge with a wearing surface replacement after 25 years in the United States is the San Diego Coronado Bridge, owned by Caltrans. Caltrans Project EA 11-108254 San Diego-Coronado Bay Bridge New Deck Overlay construction price was \$1,148,460. Quantities for replacement of the wearing surface system are listed in Table 16.9.

San Diego Coronado Bay Bridge Overlay Project was briefly summarized (Bavirisetty 1993):

The decision to replace the existing aged and failing deck for the San Diego Coronado Bridge overlay was made in 1991 [bridge opened to traffic in 1969]. Epoxy Asphalt Concrete [EAC] was the best candidate for the new overlay and seal because of its flexibility, durability, and past performance. Overlay replacement work began in January 1993. Damage due to corrosion was detected in portions of the deck plate when the existing overlay material was removed. It was difficult to determine the amount of section loss during the initial inspection, but it was estimated that the maximum pit depths were 1/8 inch (design plate thickness = 3/8 inch). Deck plate samples were removed from the bridge deck and submitted to an independent laboratory for determination of section losses, which turned out to be 10%, by weight. The Orthotropic deck was analyzed for local effects from wheel loads with two and three dimensional finite element modeling using SAP90 to determine adequacy. The stress levels in all structural elements were within the allowable limits when analyzed by the finite element method. The placement of the overlay was completed in March 1993.

Real world lessons learned from actual bridges can be used to initiate a more detailed parametric study, and/or research test on minimum deck thickness if very long durability is required. At least one expert has published that the deck plate is the least expensive superstructure component (Wolchuk and Baker 2004) as shown in Figure 16.28.

TABLE 16.9 Resurfacing Quantities for San Diego Coronado Bridge

Remove epoxy asphalt concrete surfacing	12,952	Square yards (10,806 square meters)
Epoxy asphalt concrete aggregate	1,330	Ton
Epoxy asphalt concrete surfacing (2 layers)	25,900	Square yards
Epoxy asphalt bond coat and binder	187,280	Pounds
Apply epoxy bond coat (2 layers)	25,900	Square yards
Blast clean and paint undercoat		Lump sum

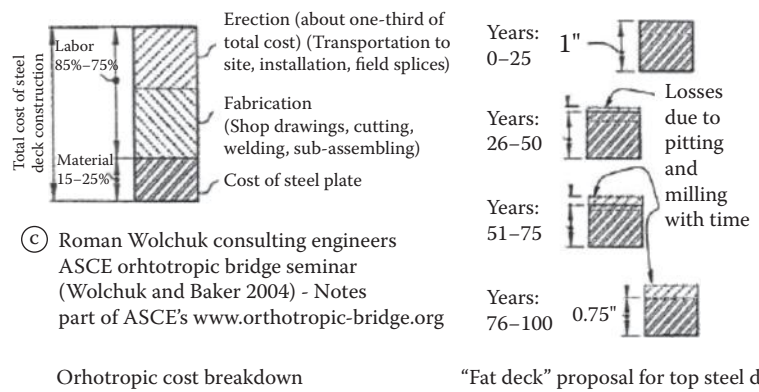


FIGURE 16.28 “Fat Deck” and replacement of wearing surface issue (From Mangus, A., *World Steel Bridge Symposium*, National Steel Bridge Alliance, November 29–December 2, 2005, Orlando, FL. <http://www.steelbridges.org/pages/2005proceedings.html>, 2005d.).

The San Mateo Hayward Bridge, which is still utilizing the original wearing surface that was installed in October 1967, has a deck plate thickness from 5/8 inches to 3/4 inches or about 16–19 mm. The proposal for a “Fat Deck” was first published in 2005 and based in part by AASHTO requirement for milling of grid decks (Mangus 2005d). The current goal of the FHWA is have bridges last 100 years in service. Unfortunately when a wearing surface fails, the replacement surfacing is not always installed in a timely manner. Additional deck steel adds robustness to the deck. The cost of additional sacrificial steel versus the risk of superstructure damage. For example, an 1/4 inch of extra steel to accommodate accidental milling cuts while removing wearing surface of the steel deck and/or corrosion pitting due to cracks in the wearing surface could be added by the bridge designer. The upfront costs of unused deck plate possible could be justified for critical lifeline bridges. Real-world delays from the time between realizing the need for resurfacing to actually starting re-surfacing may allow pitting or rusting to occur in the areas of unprotected deck.

The cost apportionments for orthotropic fabrication were researched and published (Wolchuk and Baker 2004) (Figure 16.28). The logic for the (Mangus 2005d) “Fat Deck” proposal is illustrated in Figure 16.28. For a 100-year bridge, there would be three re-surfacings. The first would occur at year 25; the second re-surfacing occurs at year 50; and the third re-surfacing occurs at year 75. The bridge would be removed at year 100. In an ideal world the deck would be unharmed during any wearing surfacing failure process and any delays in patching or resurfacing. In an ideal world the deck would be unharmed during the resurfacing process. A practicable margin of safety for bridges with 100+ design life would be to add some “fat” to the deck.

The California San Diego-Coronado Bay Bridges with a 3/8 and 5/8 inch or 10-mm and 14-mm deck plate had a 25 year EAC wearing surface life in San Diego (1969–1993) (Table 16.9). The San Mateo Hayward Bridge, with a 5/8 and 3/4 inch thick deck plate has resulted in a 45+ years EAC wearing surface life, October 1967–October 2012. The same engineers designed both bridges. The San Diego Coronado bridge made more efficient use of steel, but the identical wearing surface had a much shorter life span.

The Fremont Bridge has an orthotropic deck with trapezoidal ribs for the upper deck, with a conventional reinforced concrete on steel girders for the lower deck (Huang et al. 2005). This bridge is a tied-arch with a 383-m main span, and was the fourth longest arch in the world upon completion in 1973 (Mangus and Sun 2000). The deck provides lateral stability to the stiffening truss and had an EAC wearing surface. The new replacement wearing surface EAC was added in 2011, so the original lasted about 38-years. An important characteristic of an orthotropic steel deck is its capacity for carrying concentrated loads (Markell-ASCE 2013).

When loads approach the ultimate load the deck plate practically acts as a membrane and can carry on the order of 15–20 times the ultimate load computed in accordance with the ordinary flexural theory. Thus, the bridge deck plate possesses an ample local over-load carrying capacity. However, fatigue is the controlling stress, not the dead low stress. Deck splicing issues are inter-related to the wearing surface

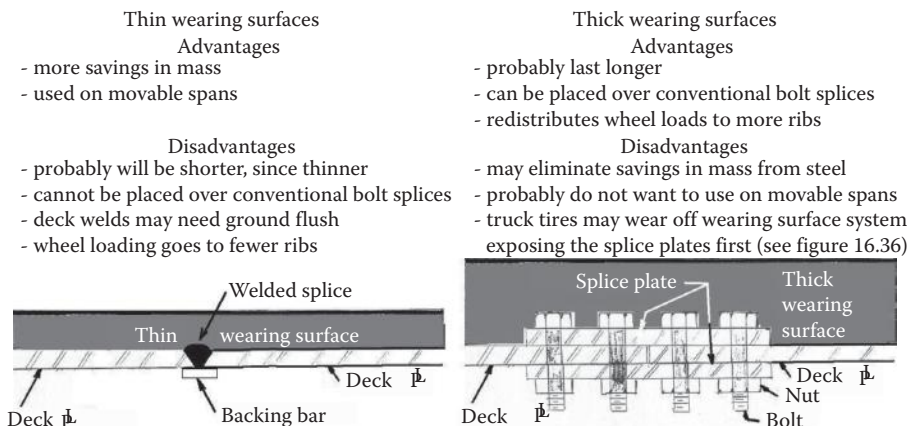


FIGURE 16.29 Thin versus thick wearing surface.

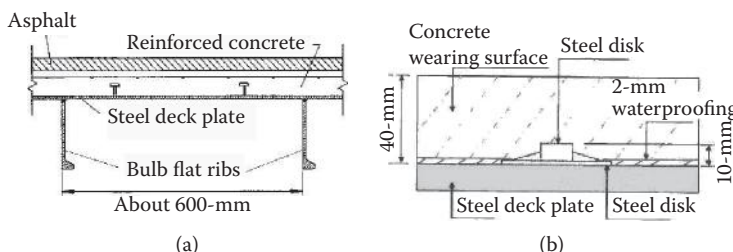


FIGURE 16.30 Composite concrete as wearing surface: (a) Rio Verde, Italy; (b) Japan (From Mangus, A., *World Steel Bridge Symposium*, National Steel Bridge Alliance, November 29–December 2, 2005, Orlando, FL. <http://www.steelbridges.org/pages/2005proceedings.html>, 2005d.)

system selected as shown in Figures 16.29 and 16.30. Thin wearing surfaces require field welded deck splices. Thicker wearing surfaces and composite concrete redistribute local wheel loadings.

16.4.3 Rib Design

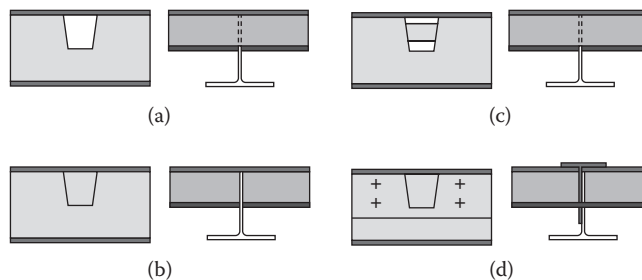
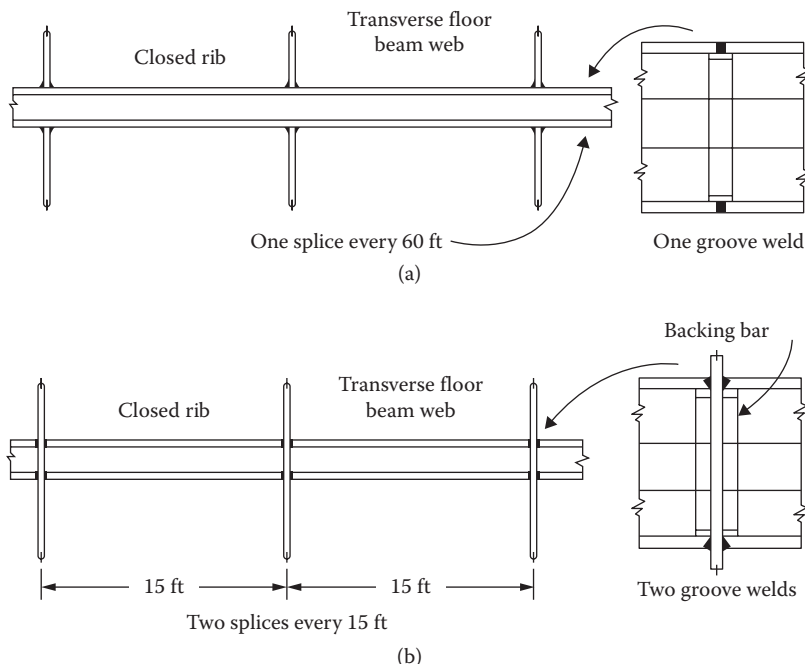
The design of an orthotropic deck system is a complex process and there are quite a few methods utilized. The tabulation is easier using computers because the processes of keeping track of the numerous load combinations are automated. The Eurocode is explained in free internet example by Sanpaolesi and Croce (2005). British code BS5400 is another code in English, which has been explained by (Chatterjee 2003) who assisted in writing the code on orthotropic box girders.

Four common categories of the connection between closed ribs to floorbeam are listed in Table 16.10, and graphically in Figures 16.31 and 16.32. Solution A is the most commonly used. Experts over the last 60 years have discussed, analyzed, and performed physical experiments in university testing facilities to assist designers in selecting the best details. Optimization of orthotropic bridge details has been published and studied. Detailed studies of the best shaped cutouts and every issue have been published. Research continues to produce more durable details. The floorbeam spacing should not exceed 1/3 of the edge-girder spacing to maximize orthotropic efficiency (Sedlacek 1992). Table 6.1 of the FHWA Manual lists recommended limits for components (FHWA 2012).

Figure 16.4 provides statistics on completed Japanese Bridges for rib and floorbeam spacings. Multiple rib types are common in these practicable completed bridges. Flat plate ribs bolt-up quickly and are used in the corners of orthotropic superstructure mainly composed of trapezoidal ribs (Mangus and Picker 2006). Flat ribs can be rolled into radius for curved bridges, such as a Japanese Bridge (Figure 16.5).

TABLE 16.10 Comparison of Rib to Floorbeam Intersections

Deck Type Analyzed and Fully	Advantages	Disadvantages
Rib welded to floorbeam web with cut-out	More complicated fit-up (teeth effect)	Greatly reduces beam web strength (analyzed as teeth)
Rib welded to floorbeam web	The cheapest solution. Floorbeam does not have steel removed	Incorrect alignment of ribs causes problems
Rib welded to floorbeam web. With cut-out plus bulkhead or baffle plate	Assumed to have longer fatigue life	The most complicated and expensive. Fit-up of baffle plate Incorrect alignment of baffle can cause problems
Rib welded to tab plate, which is bolted tab plate	Fatigue crack does not spread to the floorbeam and other panels. BART Railroad Bridge	Extra steel weight and bolts plus fit-up. Nesting requires sequencing of deck panels

**FIGURE 16.31** Conflict between closed rib versus transverse floor: (a) rib goes through beam; (b) beam interrupts ribs; (c) rib goes through beam; (d) BART bridge nested panels field bolted; more shown in Figure 16.23.**FIGURE 16.32** Welding efficiency (From Blodgett, O., Section 4.11—Orthotropic Bridge Decks of Design of Welded Structures, The James F. Lincoln Arc Welding Foundation, The Lincoln Electric Company, Cleveland, OH, 1966.): (a) rib goes through beam and (b) beam interrupts ribs.

Trapezoidal ribs would be placed on tangents as straight ribs (Figure 16.5). The Maritime Off-Ramp Bridge in California used trapezoidal ribs placed on tangents to the curve (Roberts et al. 2000).

16.4.4 Floorbeam and Girder Design

The design of a complete orthotropic deck system is a complex process and there are a few methods that can be utilized. The classic method is to divide the process—in this case the bridge—into four systems to be analyzed in sequence, as shown in Figure 16.34. The deck plate is analyzed as a continuous beam supported by the rib webs with the same spacing as the ribs, and is defined as System 1. The deck plate plus section-properties of the ribs is defined as System 2. System 3 combines the transverse floorbeam with the effective area of the deck plate plus the ribs. System 4 is to analyze the entire superstructure combined with the orthotropic steel deck as one unified element. The balanced scorecard management (BSC) system is closer to reality. All 16 issues are occurring simultaneously. Each component choice or selection affects all the others.

The type of rib affects the net strength of the floor beam. Open ribs remove much less of the floor beam web than the closed rib. The closed rib has been the most popular rib type, so the design issues for this system are featured herein. The removed area of the floor beam web to accommodate an open rib causes complex forces in the remaining portion of the floor beam web (Wolchuk 1999). There are mathematical procedures in the codes to deal with these forces, as shown in Figure 16.33. The Eurocode refers to this as the Vierendeel model which is explained in the FHWA manual (FHWA 2012). Finite element modeling of this area is another technique utilized to determine the stresses and thicknesses of the components. Engineers have researched solutions to make this complex area, bisected with open ribs, have a longer fatigue life, as shown in Figure 16.33.

With today's changes, in the design code is easier when using computers because the process of keeping track of the four integrated systems, as shown in Figure 16.34, is very complex, complicated, as well as time consuming. There is no published complete design example for the Eurocode, for AASHTO, or for the British code BS5400 in English, using a handy method to follow along. The new FHWA Manual has about 37 pages of design examples using Finite Element Techniques (FHWA 2012). This manual can be downloaded from the world wide web for free. The suggested FHWA analysis method is published as a flow chart. The flow chart for the traditional hand methods was part of the 1st edition BEH (Mangus and Sun 2000). Traditional Design examples are in Wolchuk (1963) and Troitsky (1987) and other references in 1st edition (BEH—Mangus and Sun 2000; FHWA 2012).

Three German professors collaborated on a 298-page book devoted to a single design example solution for a two-lane tied arch bridge with an orthotropic steel deck (Muller et al. 2004). A computer model was used to calculate the design forces, but the formatting of the book does allow a practicing engineer

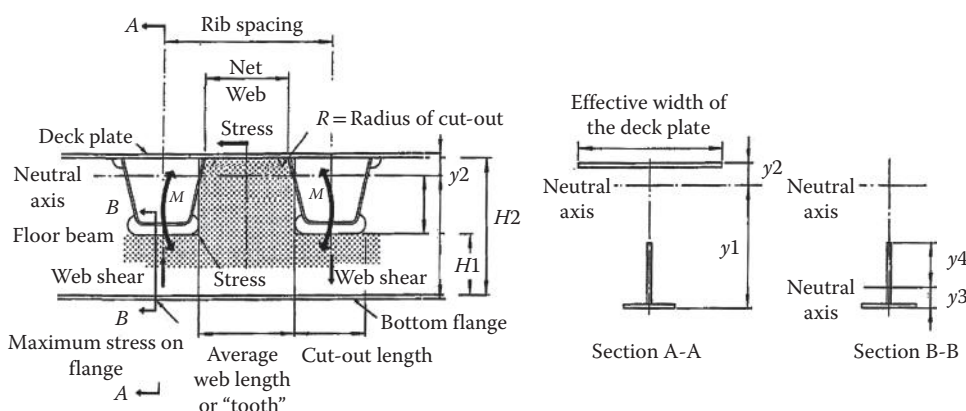


FIGURE 16.33 Analyzing forces at the cut outs at floorbeam becomes complicated. (From Matsui, S. et al., *Bridges and Roads*, Oct 1998 and Nov 1999, PWRI Public Works Research Institute [in Japanese].)

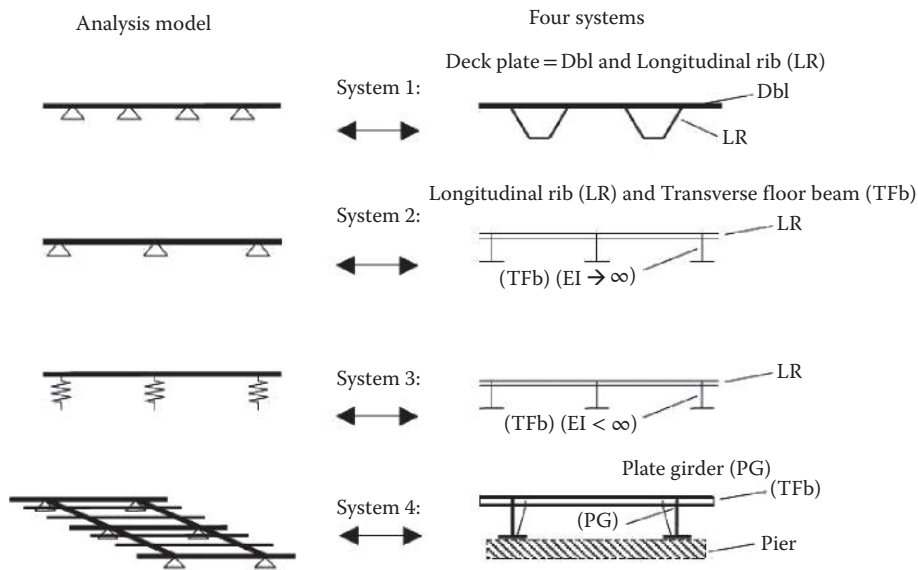


FIGURE 16.34 Four basic integrated orthotropic systems to be analyzed and designed but are integrated.

or student to follow along and check the numbers. All of the key components are designed, including the bearings. Code provisions from either the German DIN code or Eurocode are referenced page by page beside each formula utilized in the design. The layout of the book and the solutions are logical and proceed step by step. The book is in German but the text is limited and mainly code references. MSWord and other software can translate the limited text and vocabulary used in the example problem.

Box-girder design formulas were developed by the British, and were later published in the British BS 5400 code because of a series of five box-girder bridge collapses in five different countries in the late 1960s and early 1970s (Akesson 2008). The Merrison Commission was formed by the British government to create new design procedures (ICE 1973). One participating engineer, Chatterjee, continues to write about the design formulae (Chatterjee 2003). The Stability Research Council has published formulas based on the BS 5400 to analyze buckling loads on diaphragms for box girders (Ziemian 2010). Other ideas for access opening locations and stiffener positions for curved boxes are shown in (Nakai and Yoo 1988; Huang 2010).

The Russian industrialized system, utilized extensively in Russia, has been analyzed hundreds of times, so they have been able to an effective national bridge system. The effective area is reduced for the cross-section of the compression members. This varies with the code and the country. A recent Russian Wolgograd Bridge or Viaduct of 1.25-km total length had a “lock-in-effect” that no matter the wind speed, the bridge vibrated up to 400 mm. Videos of the vibrations were filmed by various Russian citizens and were posted on the Internet. Tuned mass dampers were installed to minimize the vibrations on the 155 m spans crossing a river (Fobo 2012).

Combinations of the stresses are shown in Figure 16.35. Example designs of orthotropic steel decks in the United States are located in two separate references on how to calculate the stresses via the Pelikan-Esslinger method (Wolchuk 1963; Troitsky 1987). These three stresses are calculated from these systems: System I: The local response of the deck plate spanning between the rib walls; System II: The bridge deck response which is comprised of the deck plate, and ribs; System III, the transverse floor beams. The Pelikan-Esslinger assumes that it is a continuous orthotropic plate on flexible supports. System III: The response of the main support element, which is shown as a variable-depth plate girder. The response of the main girder combined the deck plate and longitudinal ribs. System III is assumed to be a large beam spanning between the supports. These three books review the vehicle and lane loadings for older versions of the AASHTO Bridge code. Live load Lane loadings and wind loads are discussed and explained in (Sanpaolese and Croce 2005).

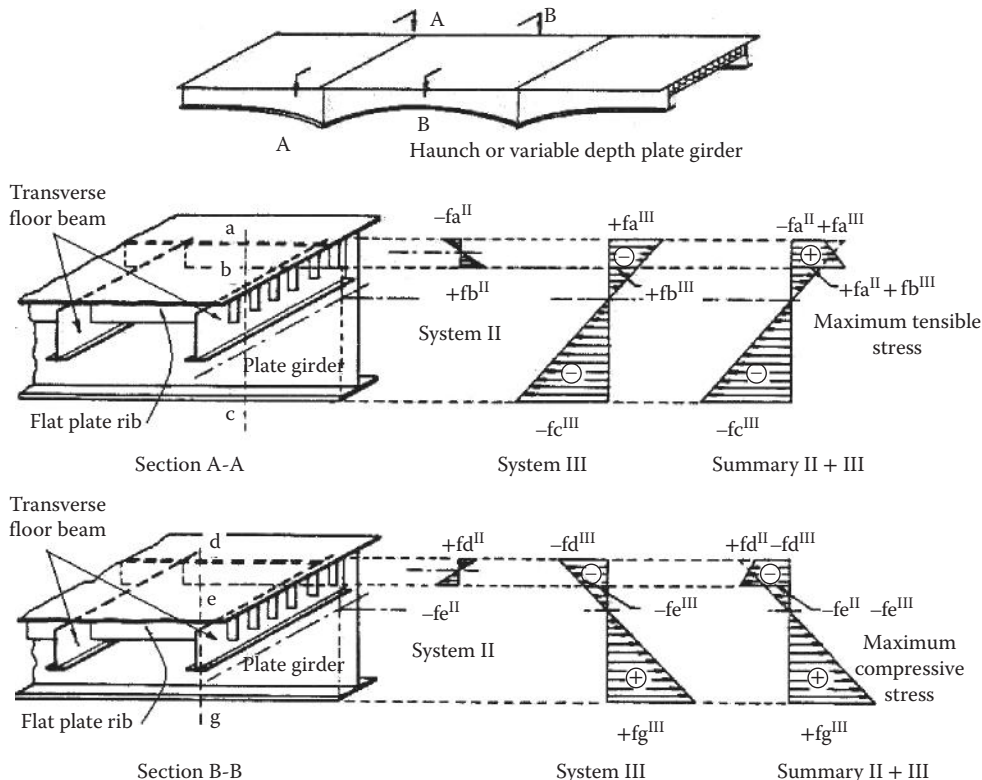


FIGURE 16.35 Orthotropic design requires tracking and superposition of all possible load combinations (After Troitsky, M. S., *Orthotropic Bridges—Theory and Design*, 2nd ed., The James F. Lincoln Arc Welding Foundation, Cleveland, OH, 1987).

Thermal loadings on orthotropic bridges are discussed in Chatterjee (2003) for the British BS5400 code. The Eurocode has similar complex thermal loadings and a simplified method for superstructures with less depth or smaller projects (Sanpaolesi and Croce 2005).

16.4.5 Bridge Maintenance Issues

The AASHTO LFRD (2012) commentary states: “The interior of the closed ribs cannot be inspected and/or repaired. It is essential to hermetically seal them against the ingress of moisture and air.” Atmospheric corrosion of steel requires water and a continuous supply of fresh air. The abrasion will speed up the process.

The three different methods that can be used to protect corrosion for new bridges with orthotropic decks are painted, weathering steel, or dehumidification. Painting is the most common method (Mangus and Sun 2000). Weathering steel was invented by the steel industry to eliminate painting. Corrosion can continue if the rusted layer is abraded.

The Fremont Bridge has an orthotropic deck with trapezoidal ribs for the upper deck. There are no fatigue cracks in the orthotropic steel deck. The original wearing surface lasted about 38-years, thus this is an excellent example of a very successful design without excessive maintenance issues. Figure 16.36 shows common orthotropic bridge maintenance issues with inspection cart and robot.

16.4.6 Fatigue Repairs

Orthotropic deck fatigue repairs and rehabilitation are discussed in Jong 2005, and Chapter 17 of *Bridge Engineering Handbook, Second Edition: Construction and Maintenance*. A composite concrete layer installed on top of the existing steel plate shown in Figure 16.30 is one method for repairs (ASCE 2004, 2008 and 2013).

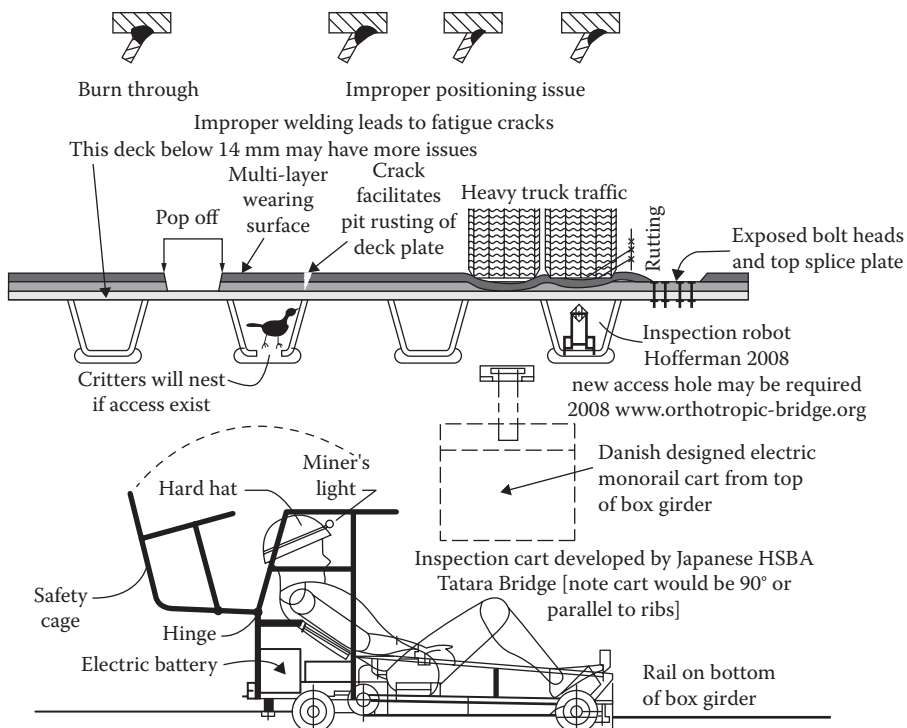


FIGURE 16.36 Common orthotropic bridge maintenance issues with inspection cart and the robot are available to fit inside closed ribs.

16.4.7 Future Developments

The second generation of orthotropic deck bridges will be based on lessons learned from the first group of bridges built. The first generation decks have defined those built without the 14-mm code specified thickness. Technology historians use the evolution because bad ideas become extinct. Solutions less popular or very specialized are side branches of the evolutionary tree. One future goal for orthotropic steel deck cost reduction lies in the standardization of ribs and details by AASHTO or the steel industry. Such standardization has led to the popularization of precast prestressed concrete girders in North America.

A double plate system or sandwich could be an experimental system that evolves into practicable bridges (Bright—ASCE 2008). Another patented system, which looks like an ice-cream sandwich in cross-section. This patented product was developed for ship repairs and consists of two parallel steel plates bonded with a patented resin and is called sandwich plate system (SPS). It can be used to repair an existing deck by adding the resin on top of an existing steel orthotropic deck. The existing wearing surface is removed and the second new plate added (Vincent—ASCE 2008).

The merging and sharing of ideas between industries such as shipbuilding and bridges continues (Figure 16.6). The complexity of floating bridges Chapter 14 and other structures are evolving. A design-build project on San Nicholas Island, California, near Los Angeles was smooth sailing due to the early involvement of AISC-member fabricator Nova Group Inc (Figure 16.37). The floating steel dock was designed for AASHTO HS-44 Loadings and 50-ton crane loadings. Length of the dock was 180-ft and it was floated into position (Pollak and Lewis 2004).

More information is placed on the world wide web every day. Searching for project case histories, studies and videos is another way to get ideas and solutions. Oregon DOT has posted a free to watch YouTube Video on the resurfacing process of the Fremont Bridge. More data and technical videos are

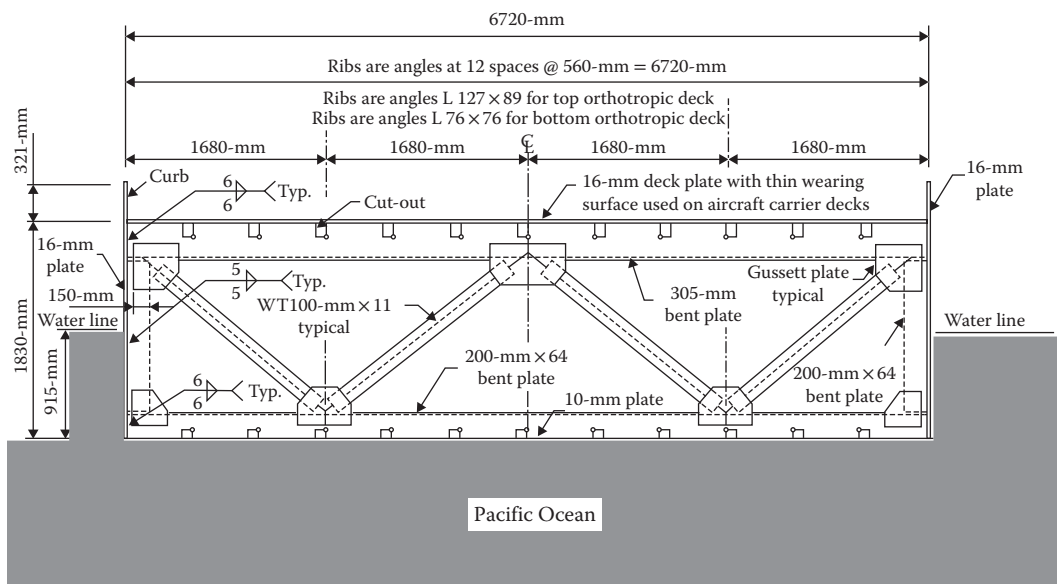


FIGURE 16.37 U.S. Navy floating dock using orthotropic bridge systems by Nova Group Inc + Winzler and Kelly. (From Pollak, B. S. and Lewis, C., *Modern Steel Construction*, October 2004.)

TABLE 16.11 Practicable Search Terms for Orthotropic Steel Deck Bridges Using MSWord Translator and the Internet

Language	Bridge	Orthotropic	Steel	Example Bridge
German	Brücke	orthotropen	Stahl	Erasmus Brücke
Russian	Мост	ортотропных	сталь	Живописный мост
Dutch	Brug	orthotropic	Staal	Erasmusbrug
Spanish	Puente	ortotrópico	acero	Erasmus Puente
Portuguese	Ponte	orthotropic	aço	J K Ponte
Italian	Ponti	ortotropa	acciaio	Il Ponte Di Millau
	Ponte			
French	Pont	orthotrope	Acier	Millau Viaduc
Norwegian	Brua	orthotropic	Stål	Nordhordlandbru

posted with time. Searching in the language of that country will produce more data about bridges built there. Microsoft word and other software have language translators that allow for instant understanding of foreign language references, web sites and downloadable files.

A larger total of published papers have been written in non-English language technical papers than in English about orthotropic steel decks (Table 16.11). Most professional publications have digitized much of their published documents. Obscure references can be downloaded to the desktop. Many organizations such as www.iabse.org are using recorded videos that each engineer can view at their leisure.

16.5 Wearing Surface

16.5.1 Introduction

Without long-life wearing surfaces, orthotropic steel decks (OSD) could not be used for bridges, because driving on wet and wavy steel plates is just not safe. Thus, wearing surfaces are absolute necessities to provide skid-resistant surfaces and smooth rides on orthotropic steel decks. Additionally, they protect

the steel deck from corrosion; have bond-strength to the steel deck to prevent delamination, and resistance to fatigue cracking; and resist deformations such as rutting, shoving, and raveling. A failure of any one of these five properties will destroy the integrity of the wearing surface and then it must be continually patched and repaired, or replaced.

A wearing surface is one of the few items placed on bridges without a code specified factor of safety. A wearing surface is used until it fails at its weakest links such as fatigue cracking, delamination, and loss of skid resistance. A long service-life for wearing surfaces is highly desirable to reduce the costs of replacing worn surfaces numerous times during the service life of the bridge.

Usually OSD are constructed on major and long-span bridges carrying multi-lanes with heavy traffic. These decks will have designed service-lives equal to the designed service-lives of the bridges on which they are constructed. Wearing surfaces should also have long service lives about 25–40 years to minimize traffic interference to repair, patch, and replace the wearing surface. Interfering with traffic every few years to repair cracked or delaminated surfacing, or major closures every 10 or 15 years, to replace worn surfacing on these heavily trafficked bridges, will cause major and costly disruptions to bridge users in addition to the costs of performing the work and supplying the materials.

OSD were developed in Germany in the 1950s, and began to be used in the United States and Canada in the 1960s and 1970s. However, by the 1980s the early enthusiasm for OSD for new bridges had waned, partly because their wearing surfaces began to fail after very short service-lives (Thul 1968).

At that time, bridge engineers had few available wearing surfaces from which to select. Stresses and strains in wearing surfaces were difficult, if not impossible, to calculate at that time; very few field-measurements or tests for stresses, strains, and deflections were made, and no one seemed interested to use such sparse data to design improved wearing surfaces. Sometimes wearing surfaces were installed on bridges just to see if they worked. Because so few OSD were being constructed, there was not a large demand for researching and developing wearing surfacing systems.

In the United States, 30–40 years later, we know a little bit more about wearing surfaces, but our research and development for designing OSD, and the wearing surfacings on them, has lagged because there is no large demand for this technology since only two or three bridges with OSD are built each decade. However, for those few OSD that will be constructed each decade, bridge engineers should treat wearing surfacings as a high performance system to obtain the maximum service life of which the wearing surfacing system is capable (Seim and Manzanarez 2005).

High performance wearing surface systems require the combined technologies of structural analysis, chemists, and materials and testing engineers. The design of high-performance wearing surface systems requires that the engineering team has a good understanding of at least such physical properties as composite moduli, stresses and strains, fatigue resistance, bond stress, rutting, shoving, and skid resistance, and the operating temperature range. If that understanding is weak or not available in the technical literature, the wearing surface system should be laboratory tested to give the engineering team solid, data with which to work.

When a wearing surface begins to deteriorate, the required patching and repairing operations will interfere with traffic and add to the bridge annual maintenance costs. The deterioration will eventually become severe, and the costs of maintaining the wearing surface and the required traffic controls may become so large that wearing-surfacing replacement becomes the only economical solution.

Replacing a wearing surface is a major work project requiring removal of the existing material and constructing a new wearing surface, all of which delays traffic, and often costs millions of dollars. Thus the longer the life of a wearing surface, the less disruption to traffic.

The FHWA Manual for Orthotropic Steel Deck Bridges (FHWA 2012), Chapter 9 is a practicable resource with design aids for wearing surfaces. Table 16.12 gives a good summary of popular wearing surfaces (Wolchuk 2002). Figure 16.38 show typical wearing surfaces used in Germany, Japan, and Netherlands.

TABLE 16.12 Commonly Used Wearing Surface Materials

Type	Description	Application Method	Examples of Use on Orthotropic Decks
A. Thick Pavings (40–80 mm)			
1. Conventional asphalt	Mixes used in highway construction	Conventional paving machines	Throgs Neck Bridge Viaduct (New York)
2. Special bituminous mixes	Mixes using special asphalt or reinforced with fibers	Conventional paving machines	G. Washington Bridge (New York)
3. Poured asphalt	Very hot liquid mix using low penetration grade bitumen	Hand application	Orthotropic decks in Germany and Japan
4. Mastic asphalt	Similar to 3, except for higher bitumen content (12%–17%)	Special paving equipment	Used on most bridges built in the 1980s and 1990s in Europe and Japan (e.g. the Great Belt)
B. Thin Pavings (10–20 mm)			
5. Polymer modified asphalt	Various proprietary formulation	Conventional paving machines	Tried on Poplar St. Bridge, St. Louis
6. Cracked asphalt with admixtures	Proprietary formulation	Conventional paving machines	Several orthotropic decks in Brazil built in 1980s
Polymer Surfacings			
A. Thick Pavings (40–80 mm)			
7. Epoxy asphalt	Epoxy resin + bituminous hardener. Hot mix, thermosetting	Conventional paving machines	San Mateo, Golden Gate (California)
8. Polyurethanes	One-component, setting triggered by moisture	Conventional paving machines	Auckland Harbor Bridge (New Zealand)
B. Thin Pavings (10–20 mm)			
9. Epoxy resins	Epoxy resin + amine hardener. Cold mix	Special dispensing equipment or by hand	Poplar St. Bridge (St. Louis) Macdonald Bridge (Halifax, Canada)
10. Polyurethanes	Three-component compound	Special hand equipments	Erasmus Bridge (Rotterdam, Holland)
11. Methacrylates	Two-component methacrylate compounds providing seamless membranes, topped with thin wearing course	Spraying	Membranes often used as bonding courses under mastic surfacings (Bosphorus Bridge)
12. Polyesters	Polyester resins	Broom and seed or premix and spread	Used on concrete decks, not tried on steel decks

Source: Data from Wolchuk, R., *Structural Engineering International*, 12(2):124–129, May 2000, IABSE, Zurich, Switzerland, 2002.

16.5.2 Requirements for Orthotropic Steel Deck Wearing Surfaces

The main functions of a wearing surface are to provide a skid-resistant and a smooth-riding surface for safety and comfort. The wearing surfacing material must have intrinsic properties in order to maintain these two important functions. For example, if the wearing surface should lose fatigue crack resistance, or if it should delaminate, or should lose its skid resistance due to worn and polished aggregates, wearing surfacing has failed and must be replaced to assure safety to the traveling public, even though replacement will cause considerable disruption to traffic using the bridge.

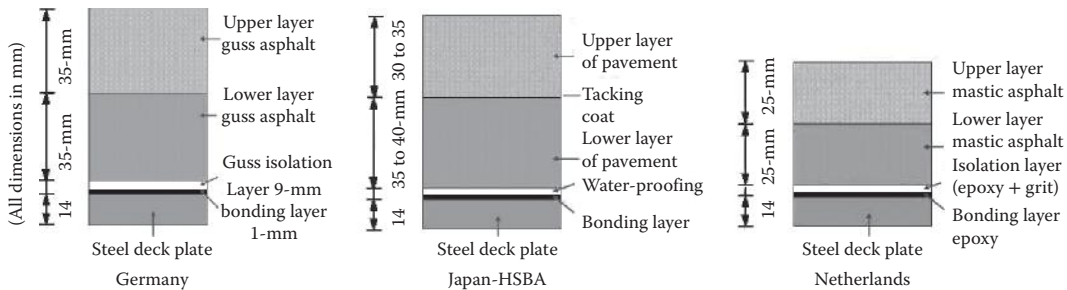


FIGURE 16.38 Standardized orthotropic bridge wearing surface systems.

The wearing surfaces on OSD must be designed and constructed to meet the following physical properties, and to maintain these properties for the service life of the surfacing.

- *Skid Resistance:* Provides a safe, wet skid-resistant surface with polish-resisting aggregates.
- *Ride Quality:* Provides a smooth riding surface for vehicles.
- *Bond Strength:* Has high bond-strength to the steel deck to resist delaminations.
- *Cracking:* Provides resistance against fatigue cracking.
- *Deformation:* Resistance to shoving, rutting, and raveling under high temperature, and resists expansion, contraction, and imposed deformations without cracking and debonding.
- *Watertight:* Impervious to the passage of water through the wearing surfacing.
- *Corrosion Protection:* Provides a corrosion-resisting coating to protect the steel plate by galvanic action.

In addition to these physical properties, other desirable attributes are as follows:

- *Durability:* Be resistant to environmental influences, such as sunlight and solar radiation, oxidation, and temperature changes, and be impervious to de-icing salt, and fuel and oil droppings from traffic, resistant to thermal cracking and deterioration from aging.
- Good Combustion resistance in case of vehicle fire.
- Longer service life of several decades, rather than years.
- Easy-to-repair in case of surface mechanical or fire damage.
- Short setting up time allowing construction equipment access within a day or two after installation.
- Low material and installation costs.
- Installation using existing construction equipment and crews.
- Easy to remove and easy to replace under traffic controls.
- Thick wearing surfaces naturally provide desirable dampening to the deck system to reduce deck vibration and rumbling from trucks.

16.5.3 Basic Properties of Wearing Surfaces

Several paving systems have been used as wearing surfaces for OSD bridges in the United States. These systems can be divided into thermoplastic and thermoset materials, thick or thin layers, with composite action and without composite action.

16.5.3.1 Thermoplastic and Thermoset Materials

This is an important distinction as thermoplastic materials will soften, deform, and melt under heat, whereas thermoset materials will lose moduli but will not deform or melt under heat. Deck temperatures can reach 60–70°C in hot weather and thermoplastic materials under these high temperatures could plastically rut or shove under truck-wheel loading.

16.5.3.1.1 Thermoplastic Materials

Modified asphalts are thermoplastic materials that have been used for OSD with varying degrees of success. Modifiers, such as Ethyl Vinyl Acetate (EVA) and Styrene Butadiene Styrene (SBS), are necessary to strengthen asphalt and to improve adhesion, resistance to rutting, shoving, and fatigue-cracking resistance. They are laid with conventional construction equipment, usually to 50 mm thick, except that some mastics are poured in place up to 75 mm thick. Unmodified asphalts are not recommended for use on the OSD, since the few installations in which these have been used, have shown their service life is too short to be economically feasible.

16.5.3.1.2 Thermoset Materials

Polymer Resins with aggregate embedded in the surfacing; epoxy asphalt; and Portland cement are thermoset materials that have been used for OSD, usually with some success. These materials possess good adhesion with the proper bond coat as well as high stability in hot climates without rutting or shoving. Epoxy asphalt and Portland cement have shown excellent, long-term skid-resistance and resist polishing of the surface aggregates.

The skid-resistance of polymer resins depends upon aggregate embedded in the surface of polymer resins; sometimes skid resistance is lost due to the polishing of the embedded aggregate or the pick-out of the aggregates. Epoxy asphalt has shown excellent resistance to fatigue with some laboratory tests running to over 20 million cycles of fatigue stress. Portland cement should show similar fatigue-resistance, but that has not been demonstrated, as of 2012. Similarly, the fatigue-resistance of polymer resins has not been demonstrated, as of this date.

16.5.3.2 Thin Surfacings and Thick Surfacings

In this chapter, thin systems are arbitrarily selected as 10–24 mm thick; thick systems are 25–75 mm thick. Wearing surfaces thinner than 10 mm should not be used for OSD, because the little thinner than 10 mm that have been used had a service-life of only a short few years. Rarely are wearing surfaces applied to orthotropic steel decks thicker than 75 mm because of the weight of the thick surfacing defeats the use the lightweight of the orthotropic steel deck.

16.5.3.2.1 Thin Wearing Surfaces

Asphalts or modified asphalts are rarely used for thin wearing surfaces, as they have service-lives far too short to be considered as durable wearing surfaces. However, these thin materials may be used for temporary installations during the construction of a permanent-wearing surface system.

Typical installation sequences for thin wearing-surfaces are as follows:

- The steel deck plate is prepared to a Surface Preparation Specification No. 10, "Near-White Blast-Cleaning," of The Society for Protective Coatings.
- First layer is usually a corrosion-protective zinc-rich organic or inorganic paint, applied to the blast-cleaned surface of the steel deck with a thickness from about 3 mils to 6 mils (75–150 µm). The organic, or inorganic paint, protects the steel deck by galvanic action. Water cannot penetrate the zinc-rich paint, so it also acts as a waterproofing layer.
- Second layer is usually a bond-coat to adhere the third layer to the first layer.
- Third layer is usually a slurry of a polymer resin binder with fillers, applied to a minimum thickness of 3/8 inch (10 mm).
- The fourth layer is sprinkling hard aggregate by hand or by mechanical spreaders, on the top of the third layer to provide skid-resistance. After the resin or the blended resin cures, the excess aggregate is broomed off.

Sometimes the corrosion-protection first-layer is omitted, and the bond-coat layer is placed directly on the sandblasted surface of the steel deck. The bond-coat layer may be impervious to water if it is not

damaged, but should it be damaged, or if water does penetrate the adhesion layer for whatever reason, then there is no zinc layer to protect the steel deck from corrosion by galvanic action.

16.5.3.2.2 Thick Wearing Surfaces

Typical installation sequences for thick-wearing surfaces are listed below.

- The steel deck plate is first prepared to the Surface Preparation Specification No. 10, “Near-White Blast Cleaning,” of The Society for Protective Coatings.
- First layer is a corrosion-protective zinc-rich organic or inorganic paint applied to the blast-clean surface of the steel deck with a thickness of about 3–6 mils (75–150 µm). The organic or inorganic paint protects the steel deck by galvanic action. Water cannot penetrate the zinc-rich paint, so it also acts as a waterproofing layer.
- For the second layer, sometimes a waterproofing layer is used, but waterproofing is not explicitly required as the zinc paint acts as a very tough waterproofing layer. If a waterproofing layer is used, it is usually applied about 100–133 mils thick (2.5–3.0 mm). The waterproofing is usually an elastic material, which at this thickness reduces the composite action of the thick wearing surface (see Composite Action section below).
- The second layer is usually a bond-coat to adhere the third layer to the zinc-rich paint. The bond-coat layer varies in thickness from less than 1 mm to 2 mm depending on the type of bond-coat. However, the aggregates in the third layer are pressed into the bond-coat by the actions of compacting the aggregates by rolling; the bond coat is actually only a few mils thick after the aggregate compaction.
- Third layer is a matrix consisting of a binder of modified asphalt or epoxy asphalt and dense-graded aggregates. The dense-graded aggregates and binder develop a concrete matrix that forms an aggregate skeleton with the aggregates in close contact. Sometimes a thin, third layer is applied as a mixture of binder and sand or small aggregates to facilitate removing the fifth layer that has reached the end of its service life.
- The fourth layer is another bond-coat layer to adhere the third layer to the fifth layer.
- The fifth layer is a matrix of the binder and aggregate, usually the same type as the third layer, but it could have a different binder.
- For mastic binders only, a sixth layer is the sprinkling of hard, angular aggregate, by hand or by mechanical spreaders, on the top of the fifth layer; this is pressed into the matrix by rollers to provide skid resistance. Mastics have only small aggregates that float in the binder and are not exposed at the surface to develop skid resistance.

For some proprietary waterproofing systems, the first layer is an application of the waterproofing compound applied directly to the sandblasted and primed steel deck usually with a thickness about 100–130 mils (4–5 µm). Sometimes a fine aggregate is scattered over the waterproofing, before it sets up, to provide a rough surface to improve shear-resistance to the third layer. A bond coat is applied to the waterproofing compound or is applied to the aggregates, if aggregates are used.

16.5.3.3 Composite Action and Non-Composite Action

Composite action between the wearing surfaces and OSD is desirable because it reduces fatigue-stresses both in the steel deck and in the wearing surface. AASHTO LRFD Bridge Design Specification (AASHTO 2012) states that the wearing surface should be regarded as an integral part of the total orthotropic deck system, and the wearing surface should be designed assuming the wearing surface is composite with the deck plate, regardless of whether or not the deck plate is designed on that basis.

The strength of the adhesive bond coat necessary to hold a wearing surface in place and to prevent delamination is often strong enough to achieve composite action. However, the strength of the bond coat may not be adequate to resist the shear stress from composite action added to the shear stresses from braking trucks, particularly on down slopes, and added to the thermal stresses occurring during

the heating and cooling of the wearing surface, relative to the steel deck. Bond-coat strength can reduce over time, so it is prudent engineering to use a material with a bond-strength much larger than that needed for composite action.

16.5.3.3.1 Composite Action for Thin and Thick Wearing Surface Systems

Thin systems also act in composite action, but the reduction in fatigue-stresses in the steel deck and the wearing surface is not as significant as it is for thick systems. Thick systems do lower the fatigue stresses in the steel deck by load distribution and composite action of the wearing surface with the steel deck.

The first way the thick systems achieve lower stresses is by distributing the truck tire footprint over a larger area of the steel deck; AASHTO states a 45-degree distribution of the tire pressure may be assumed to occur in all directions from the surface-contact area to the middle of the deck plate. Thus, the contact-area on the steel deck for a thick system is much larger than the contact area for a thin system.

The second way is that thick systems act compositely with the steel deck, and the composite action reduces the fatigue stress in the steel deck (Gopalaratnam 2009).

Figure 16.39 (FHWA 2012) shows the relative relationship of stresses in steel decks and wearing surfaces as a function of high-modulus wearing surface materials, compared to low-modulus wearing surface materials. Figure 16.39 uses a modular ratio shown by the symbol “ n ” a convenient number that is the ratio between the modulus of steel divided by the modulus of a wearing surface.

$$n = \frac{E_s}{E_{ws}}$$

where E_s is the modulus of steel and E_{ws} is the composite modulus of the wearing surface obtained from testing a composite beam in bending with the wearing surface adhered to the steel plate. The n -value is used to classify wearing surfaces arbitrarily into high-modulus materials with n values below 100, and into low-modulus materials, with n values of 100 and above.

16.5.3.3.2 Sharing Stresses between the Steel Deck and the Wearing Surface

When a loaded truck crosses a selected point on an OSD with a bonded wearing surface system, a moment is produced in the deck; part of that moment at the selected point is resisted by the steel deck

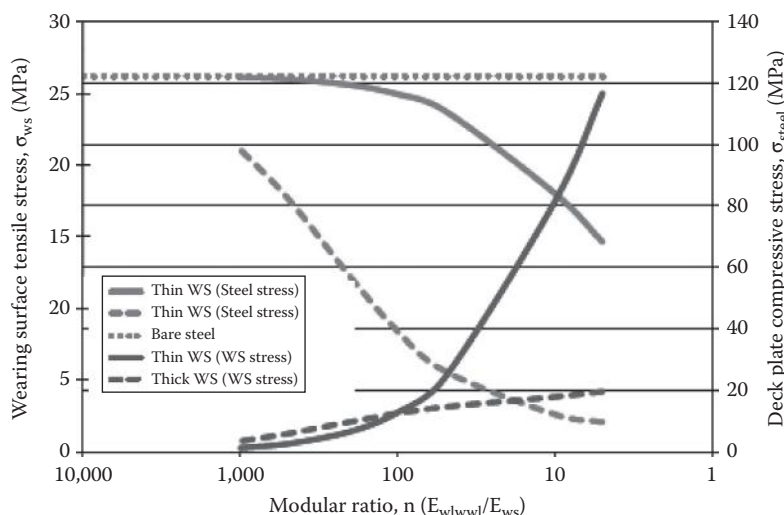


FIGURE 16.39 Stresses in wearing surface systems well bonded to a 14-mm steel deck plate. (From FHWA, *Manual for Design, Construction and Maintenance of Orthotropic Steel Deck Bridges*, HDR Engineering Inc., Performing Organization, Federal Highway Administration, Washington, DC, 2012.)

plate and the remaining part is resisted by the wearing surface. The resisting moment induced into the deck by a loaded truck is shared between the relative stiffness of the two materials in the deck and how well they are bonded together to produce composite action according to the transform area or a Finite Element method of analysis (see Figure 16.39).

A well bonded thick wearing surface system as shown in Figure 16.39 with a high modulus ratio (small “ n ”) will reduce by composite action the fatigue stress in the steel deck from loaded trucks more than will the same-thickness wearing-surface system that has a low modulus ratio (larger “ n ”). This stress difference occurs because the higher modulus material stiffens the steel deck, and thereby reduces the stress in the steel deck more than does the low modulus ratio material.

Conversely, a thick wearing surface system with high modulus ratio will attract larger fatigue stress into the wearing surface, and the larger fatigue stresses will shorten the service life of the wearing surface, unless the wearing surface is specifically designed for the larger fatigue stresses. Should the wearing debonds, then the steel deck plate will carry the loading differently perhaps causing fatigue damage to the steel deck.

16.5.3.3 Isolation and Waterproofing Layers

Laboratory testing of composite beams has shown that a waterproofing or a bonding layer thicker than about a half a millimeter acts similar to an isolation layer and reduces the efficiency of the composite action; the thicker the layer and the lower the stiffness of the waterproofing or bonding layer, the lower the efficiency of the composite action.

16.5.3.4 Linear versus Non-Linear Analyses

Hemeau et al. (1981) discussed the nonlinear action in the cross-section of wearing surfaces when subjected to loading. Since then little research has followed to give bridge engineers a method for incorporating nonlinear action in the analysis of wearing surfaces. However, there are so many variables in the analyses of wearing surfaces and the loading/unloading time from moving trucks, that if any slight nonlinearity does occur, it will not introduce a large error in the analyses. Until further research is published, bridge engineers must use linear analyses of wearing surfaces.

16.5.3.5 Skid Resistance of Thin and Thick Wearing Surfaces

Wearing surfaces, as noted above, must last a long time on the OSD, which means that long-term skid resistance is an important property for any type of wearing surface. Good long-term skid resistance is dependent on the aggregates used in the wearing surface. Aggregates for wearing surfaces should be specified as crushed, hard, and non-polishing, with at least 70% of the aggregate facets showing rough surfaces and the asperities. The aggregate manufacturer should submit certified test results that show the aggregates meet these requirements, or someone, representing the owner of the bridge, should have the aggregates tested in a certified laboratory.

For thin wearing-surfaces, using polymer resins, aggregates are usually exposed on the surface at the time the bridge deck is opened to traffic. For thick wearing-surfaces, it usually takes about a year to wear the binder off and to expose the surfaces of the aggregates. Aggregates with rough surfaces and prominent asperities provide even higher skid resistance.

Numerous fatigue tests of thick wearing surfaces demonstrate that the asperities on aggregates increase the mix resistance to fatigue stresses. It is a worthwhile investment of time and money to select carefully the aggregates to be used in any type of wearing surfacing to obtain long-life skid-resistance and in addition, better fatigue-resistance for thick wearing-surfaces.

16.5.3.4 Temperature Dependency Properties

Figure 16.40 shows the relationship of the composite elastic moduli in terms of the n values and the operating centigrade temperature range, usually between 0°C and 50°C in the United States. Note that the boundary lines are approximate and should not be used for detailed analysis.

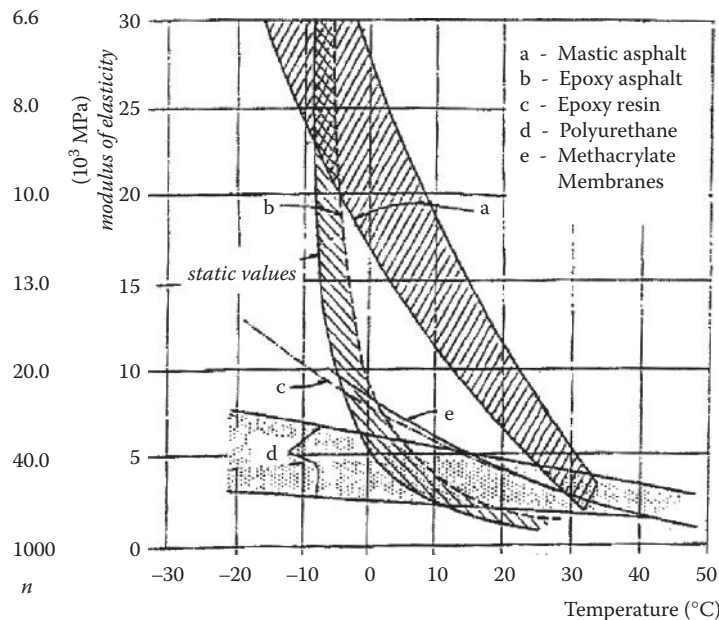


FIGURE 16.40 n Values and elastic moduli of wearing surfaces from tests of composite specimens with surfacing in tension (From Wolchuk, R., *Structural Engineering International*, 12(2):124–129, May 2000, IABSE, Zurich, Switzerland, 2002.)

Figure 16.40 shows the significant changes in moduli of asphalt-based wearing surfaces with temperature changes usually experienced during the normal operation of most bridges. The two important wearing surface materials used predominantly in the United States are mastic asphalt (actually modified asphalt concrete as noted below) and epoxy asphalt (epoxy asphalt concrete). For mastic asphalt, the static n values vary from about 100 to perhaps 10, or an order of magnitude of about 1.0. For epoxy asphalt, the static n values can vary from perhaps 400 to about 40, also an order of magnitude of about 1.0.

Polyurethanes have not been used in the United States as of 2012. Epoxy Resin is rarely applied thicker than about 10 mm and that thickness has little affect in reducing fatigue stresses in the deck system at any operating temperature. Methacrylate Membranes are used as bond coats and for repairing cracks in wearing surfaces; it has been used as a thin wearing surface in Europe. The boundary lines shown in the Figure 16.39 for different materials are approximate and should not be used for the design or analysis of wearing surfaces. Moduli values as a function of temperatures should be obtained from the material supplier, or by laboratory testing.

The moduli increase significantly in lower temperatures, which indicate that asphalts contribute significantly to the stiffness of the deck system in cooler weather; however even at higher temperatures with n values in the 300–400 range can provide up to about 25% reduction of fatigue stress in steel deck systems.

The other variable shown in Figure 16.40 is the dynamic moduli compared to the static moduli as indicated by the spread between the two boundary lines for the two asphalt-based materials. We know little about static moduli and even less about dynamic moduli, unless specifically tested for values dynamic moduli as a function of temperature. As noted above, factors of safety are not applied to wearing surfaces; using the static values of moduli for analysis would provide a conservative factor of safety. Another low-cost factor of safety can easily be added by increasing the thickness of the deck plate 2 mm. The labor cost of the deck is very much fixed regardless of the deck thickness; adding 2 mm of thickness only adds the cost of the extra steel. The increase in the factor of safety increases dramatically for both the wearing surface and the steel deck system.

16.5.4 Laboratory Testing Wearing Surfaces

Figure 16.40 is an important figure to understand the relationships between the moduli of wearing surfaces, the stress in the wearing surface, and the stress in the steel deck. The modulus of the wearing surface used to calculate the modular ratio must be the composite flexure moduli.

This observation brings up a very important difference between the testing of wearing surfaces of asphaltic materials in an asphalt-testing laboratory, and the testing of wearing surfaces of composite steel beams in a structural testing laboratory.

In an asphalt-testing laboratory, all asphalts and asphalt-modified materials are tested as non-composite beams in four-point bending, using constant deflection control. The neutral axis is in the center of the beam, producing both tension and compression strains in the cross-section of the beam. At the start of testing, the stiffness is recorded, and the testing is stopped when the stiffness is reduced to one-half the starting stiffness. The material in the beam specimen is never failed by fatigue cracking.

The AASHTO LRFD Bridge Design Specifications (AASHTO 2012) require that the long-term composite action between deck plate and wearing surface be documented by both static and cyclic load tests.

This requires making laboratory tests on composite beam specimens simulating a small section of the deck and composite wearing surface, although full-scale testing is better but very expensive. There are two fatigue-testing arrangements for testing composite wearing surface test specimens in the United States: a single span, three-point loading using a composite test specimen 100 mm wide and 350 mm long, and a two span, five-point loading using a composite test specimen 150 mm wide and 700 mm long. Both types of test specimens use a steel plate of the same thickness as will be used on the deck of the bridge. The five-point loading test does require a testing machine with a much larger capacity to apply the cyclic loading than for the three-point loading.

Both types of composite test specimens use constant-force loading to replicate the constant force delivered by truck wheels using the bridge. The constant-force is calculated to induce a stress in the steel test specimen, which approximates the calculated stress in the actual steel deck by a loaded truck wheel using Level 2 or Level 3 analyses. The neutral axis is within the upper-half of the steel test plate, placing the full cross-section of the wearing surface material under a varying tension strain from the top surface to the surface in contact with the steel test plate.

16.5.4.1 Testing of Fatigue Resistance of Wearing Surface

Wearing surface is subjected to enormous numbers of truck wheel passages during its service life of decades. It is noted that only major bridges carrying heavy traffic are built with OSD and usually results in about 1/2 million cycles per year. Precision is not needed because there are so many other variable that have not been considered that could affect the number of loaded trucks per year. However, if precision is desired, traffic engineers can make detailed calculations that will determine vehicle traffic, truck traffic, traffic growth per year, and truck weight or other desired data.

The bridge designer or owner can then select a target service life for the wearing surface just as a target service life of the bridge itself is selected at the start of the bridge design process. For a 25-year target, the service life of the wearing surface could be 12,000,000 loaded truck wheels. The selected wearing surface should be capable of carrying this number of fatigue cycles without a major failure of the wearing surface (Seim and Ingham 2004).

These fatigue tests are usually done under laboratory temperature and the test continues until the target number of loading cycles is reached, or the wearing surface fails in fatigue or in bond shear. However, if more sophisticated testings are desired, the specimen can be mounted in an environmental chamber and the temperature varied from high to low temperatures during the testing. The temperatures must be applied to the test specimen in proportion to the yearly temperatures measured at the bridge site. Figure 16.41 shows a Wearing Surface Fatigue Testing Machine with temperature control compartment door open to show vertical loading shaft and roller supports for fatigue test specimen. Figure 16.42 shows Wearing Surface Fatigue Test Specimens 100 mm by 380 mm with 14 mm deck plate,



FIGURE 16.41 Wearing surface fatigue testing machine with environmental chamber. (Courtesy of Charles Seim.)



FIGURE 16.42 Six wearing surface fatigue test rectangular specimens. (Courtesy of Charles Seim.)

and 50 mm of epoxy asphalt concrete after fatigue testing. Plates were welded on at the ends of the specimen rest on roller supports in the Wearing Surface Fatigue Testing Machine.

16.5.4.2 Testing for Composite Action

If the moduli of wearing surfaces as a function of temperature cannot be obtained from the wearing surface manufacture, it can be measured in a testing laboratory. This is done using one or two of the fatigue-test specimen described above, by varying the temperature, as the specimen is loaded in bending both statically and dynamically, as the loading and deflections are recorded.

The moduli can be calculated using the loading and deflection data according to the transform area or a Finite Element method of analysis.

16.5.4.3 Testing the Bond Strength between Steel and the Wearing Surface

The bond coat adheres the wearing surface of the steel deck for the life of the surfacing. If the bond coat fails, shoving and de-bonding happens very quickly. The bond strength is measured in the laboratory using one or two of the fatigue-test specimen described above by coring 50 mm diameter cores into the wearing surface, and by measuring the forces to pull off a series of cores. The bond strength at a low and a high temperature is determined by heating and cooling the test specimens to the temperatures measured at the bridge site.

This test is done in the laboratory and in the field in accordance with ASTM C 1583/C 1583M as modified as noted below in Construction.

16.5.5 Wearing Surfaces Systems Used in the United States

Wearing surface systems used in the United States can be divided into thermoplastic and thermoset materials, as noted above. This section will present thermoplastic materials; thermoset materials will be discussed in the next two sections.

By far the most-used to wear the surface system in the United States has been modified asphalt concretes that use additives to increase the strength and the fatigue resistance of the asphalt. Concretes are so named because the aggregates form a substantial aggregate skeleton that has to be compacted to provide a dense and durable wearing surface system. Pourable mastics have only small aggregates, added as filler, and all of the voids are filled to excess with a stiff asphalt binder. Gussasphalt, which means, “poured asphalt” is available, but has not been used in the United States.

16.5.5.1 Thermoplastic Asphaltic Based Material

The common asphaltic-based materials that have been used for binders in the matrix of wearing surfaces in the United States are as follows:

- Modified asphalt concretes
- Rubberized asphalt concretes
- Pourable asphalt mastics (never used in the United States)
- Modified asphalt stone matrixes

All of these wearing surfaces are thermoplastic and can rut and shove in hot weather. Wearing surfaces using ordinary asphalt binders have a very short service life, and should never be used for OSD. Chip seals, using asphalt binders and unmodified asphalt concretes and should not be used for OSD, as their service life is too short; they can be used for temporary skid-resistance protection during construction stages.

16.5.5.1.1 Modified Asphaltic Concrete

Modified Asphaltic Concrete (often referred to as Mastic Asphalt in the United States) is under-filled voids, asphalt-based mixes with dense graded aggregates, from large aggregate to very fine aggregate, that form an aggregate skeleton within the mix that must be compacted during installation. The binder carries tension stresses and the aggregate skeleton carries compression stresses. The asphalt-binder must be reinforced with additives such as EVA and SBS, that strengthen asphalts, or be blended with stiff and stronger Trinidad Lake Asphalt. The bridge engineer should be cautious in using these blended materials, as the results to date have not always been satisfactory.

Modified asphaltic concrete are usually laid 38 mm thick and placed in one course to 50–63 mm thick and placed in two courses. After the binder wears off the surface, the exposed aggregates usually provide good skid resistance.

The modified asphalt binder is mixed with aggregates in a pugmill or continuous mixer and placed on the deck with ordinary paving machines. The mat needs to be compacted with rollers to form the aggregate skeleton. After compaction, the air voids should be 4% or less to be impermeable to water and increase the resistance to fatigue-cracking. Air voids act as fatigue-crack starters, so a smaller number of air voids is better to enhance the fatigue resistance of this system.

16.5.5.1.2 Rubberized Asphalt Concrete

Rubberized asphalt concrete is similar to modifying asphaltic concrete except that the asphalt binder is blended with a rubberized additive such as styrene butadiene rubber (SBR), crumb rubber modifier (CRM), or proprietary additives of which the formulation is usually kept as a trade secret. The rubberized binder is added to the dense graded aggregates to fill most of the voids. The aggregate skeleton carries the compression stress, and tension stress is carried by the rubberized asphalt binder. After compaction, the air voids should be 4% or less for increased resistance to fatigue cracking. Air voids act as fatigue-crack starters, so a smaller number of air voids enhances the fatigue resistance of this system. After the binder wears off the surface, the exposed aggregates provide good skid resistance.

16.5.5.1.3 Pourable Asphalt Mastic (Developed in Germany as Gussasphalt)

Pourable asphalt mastics are asphaltic binders using very low-penetration asphalt sometimes blended with Trinidad Lake asphalt, with aggregates dispersed within the binder but not sufficient to form an asphalt skeleton. The stiff binder carries both the tension and compression stresses induced into the wearing-surface by composite-action. Gussasphalt is available but has not been used in the United States or Canada.

Pourable asphalt mastic requires special equipment and trained crews to install it, the mix is heated to 210–230°C, much higher temperatures when compared to other types of mixes, and is usually applied in two layers by pouring the hot mixture onto the deck surface. Rollers are not needed to compact the hot-poured mixture as it cools; the mix is usually placed to a total of 60 mm–75 mm thick. The small aggregates do not provide enough aggregate exposure on the running surface of the stiff binder; to provide skid resistance. To provide skid resistance, asphalt-coated aggregates are spread on the top course and are rolled into the mat to lock in the aggregates before the mat cools. This method provides good skid resistance; however, sometimes the aggregates that are not well locked-in begin to ravel off under the action of truck wheels.

16.5.5.1.4 Stone Matrixes

Stone matrixes use larger aggregates that are gap-graded, and the larger aggregates form an aggregate skeleton. Fillers, and sometimes fiber materials, are added to the binder to fill in the voids caused by the gap grading. Stone matrixes are roller-compacted to form the aggregate skeleton. After the binder wears off the surface, the exposed aggregates provide good skid resistance.

The binder carries tension stresses and the aggregate skeleton carries compression stresses. However, the tension stresses between the larger size aggregates are much larger than the tension stresses between the smaller dense graded aggregates used for modified asphalt concretes. The binders used in stone-mastics are not strong enough to resist the larger fatigue stresses between the large aggregates, and they have failed by fatigue, cracking after a service life as short as 5–7 years.

16.5.5.2 Thermoset Polymer Resins, Portland Cement Concrete, and Epoxy Asphalt Concrete

There are predominantly three types of thermoset materials: polymer resins, Portland cement concrete, and epoxy asphalt concrete. This section will discuss these thermoset materials.

16.5.5.2.1 Polymer Resin Based Material

Polymer resins used in the United States and Canada are epoxy and polysulfide epoxy. Polyesters are in the testing stage, but have no service experience in the United States, as of 2012. Outside of the United States, urethanes have been successfully used. Chip seals thinner than 10 mm using resin binders,

should not be used for OSD, as their service life is too short; however, they can be used for temporary skid-resistance protection during construction stages.

Most of these polymer resins are thermoset materials after they cure. Thermoset materials do not melt when heated, as do thermoplastic materials. Heat only lowers the moduli of these thermoset materials. Because they do not melt, wearing-surfaces with thermoset binders usually resist rutting and shoving in hot weather. They can be susceptible to raveling if the aggregates are not well anchored.

Most of these materials are mixed and applied cold, usually about 10 mm thick. These materials do not contain aggregates that form aggregate skeletons; however, sand is often used as an extender to reduce the volume of expensive resin used in the mix. The material depends on the strength of the resin to resist traffic loads and thermal forces.

To provide skid-resistance to the smooth surface of resin, and because most of these resin materials do not have aggregates—or use only sand as an extender in the matrix of the resin, aggregates are spread out on the uncured surface and sink into the matrix, or are pressed into the matrix by rolling. The surfacing is often broomed or power-swept to pick up the un-anchored aggregates before traffic is allowed onto the cured resin surfacing.

A bond coat is used to bond the resin to the waterproofing or to the corrosion-protection material placed on the steel deck. The bond coat must have enough adhesion-strength to provide the full composite action of the resin surfacing; otherwise, the surfacing will fail by delamination. The adhesion layer is the only item within a wearing surface system to which a factor of safety can be applied, as the higher the strength of the adhesion layer, the larger the factor of safety.

Because resins are expensive and make up about 12% or more of the matrix, the resin-based wearing surfaces are usually more costly per unit of thickness (this is needed to clarify the cost difference between 10 mm of T48 and 50 mm of epoxy asphalt) than are asphaltic-based materials. Because resin-based wearing surfaces often are applied to the steel deck by hand methods, the cost of installation can be higher than the cost of the machine-installed asphaltic-based materials; however, mechanical spreaders have been used to distribute these resins to lower the cost of installation.

These thin wearing-surfaces do not have enough thickness or a modulus large enough to reduce appreciably the fatigue stresses in the steel deck. Only a few decks have been surfaced with this material in the United States; their service life is difficult to determine but appears to be about 15 years.

16.5.5.2.2 Portland Cement Concrete

Wearing surfacing using Portland cement concrete has been used occasionally in the United States to strengthen decks that are too thin and that were built back in the 1970s and 1980s. Portland cement concrete is a thermoset material and has a very high modulus (low n value), and the aggregates form an aggregate skeleton. Portland cement concrete is usually placed on the steel deck to thicknesses between 63 mm and 89 mm, and is sometimes reinforced with small steel reinforcing bars, steel mesh, and occasional experiments with steel and carbon fibers.

Because of the very high modulus of the concrete, shear connectors have to be used to transmit the shear at the interface between the concrete and the steel deck. One type of shear connector uses strong epoxy coatings with the embedded aggregate to form a rough surface to resist shear. Another type is using short welded-steel studs with formed heads that help hold the concrete in contact with the deck; the shank provides shear resistance of the concrete. The surface of the concrete must be textured before the cement sets to provide good skid resistance (see Figure 16.30).

The service life of Portland cement concrete wearing surface with shear connectors has not been determined, but the few decks that had been resurfaced with this material seem to be performing well as of 2012.

16.5.5.2.3 Epoxy Asphalt Concrete

Epoxy asphalt concrete is under-filled asphalt-based mixed with dense graded aggregates from large aggregate to very fine aggregate that forms an aggregate skeleton within the mix that must be compacted

during installation. The binder carries tension stresses and the aggregate skeleton carries compression stresses. Epoxy asphalt concrete is usually placed 2 inches thick in two courses; placing it thicker only improves the fatigue resistance by a nominal amount. After the binder wears off the surface, the exposed aggregates provide good skid resistance.

Shell Oil Company developed epoxy asphalt concrete in the 1970s as a thermoset pavement for air-fields; it is impervious to dripping jet fuel, and to gasoline, and oil drips. The epoxy forms cross-linked strands that encapsulate and protect the asphalt from being dissolved. The epoxy asphalt cross-linked strands are ductile and act like rubber reinforcing bars acting in all directions and resisting tensile fatigue-stresses. The epoxy asphalt concrete, being a thermoset material, does not rot or shove under high temperatures, and the high-strength adhesive bond-coat resists delaminations.

Epoxy asphalt concrete was first installed on the San Mateo Bridge in California in 1967; that surfacing is still in service in 2013, but is scheduled to be replaced within the next 5 years. The epoxy asphalt concrete installed on the Golden Gate Bridge in 1985 is also still in service, but is in need of replacement within a few years. Epoxy asphalt concrete was used for the resurfacing of the Fremont Bridge in Oregon in 2011, to replace the original epoxy asphalt concrete placed in 1973 (Markell and Seim, ASCE 2013). Two of these bridges demonstrate that it is possible to achieve a long service life up to 40 years of a properly designed wearing surface. Epoxy asphalt concrete has been used to surface over 35 bridges in China from 2002 to the present (2013).

Regardless of what has been reported in the literature, epoxy asphalt concrete does not set up suddenly; once the epoxy asphalt is mixed and dumped into a haul truck, the setup time is a uniformly controlled, predictable 90 min or so before the truck has to be discharged into the paving machine. However, all the other wearing surface materials have to be discharged from haul trucks or portable mixers before the temperature drops below a preset limit, or before the a preset cure time. Epoxy asphalt concrete is not different from these other materials; otherwise, the Chinese contractors could not have used epoxy asphalt on over 35 bridges in the last 12 years.

Epoxy asphalt concrete is one of the most highly tested wearing surfaces; it was first tested in California and then extensively tested in China over the last 12 years. All of the few failures that have occurred have been thoroughly investigated and were found to be caused by improper installations.

16.5.5.2.4 Importance of Aggregates

After selecting the type of binder for the wearing surface, the next important selection is the aggregate used in the mix, and determining their physical properties of aggregates. The properties and acceptance limits listed in Table 16.13 have been used successfully for many decades on many bridge decks.

The importance of careful aggregate selection is simply that the proper aggregate and gradation will help to obtain the best performance that a binder is capable of providing for a wearing surface. Preferable, aggregates should be crushed for both large and fine aggregates.

TABLE 16.13 Typical Physical Properties of Aggregates

Property	Value	Test Method
Specific gravity (min)	2.5	ASTM C 128
Fractured particles (% min)	80	ASTM 5821
Loss in Los Angeles Rattler (after 100 revolutions) (% max)	10	ASTM C 131
Loss in Los Angeles Rattler (after 500 revolutions) (% max)	25	ASTM C 131
Aggregate absorption		
Fine (% max)	4.5	AASHTO T 84
Coarse (% max)	2.5	AASHTO T 85
Sand equivalent (min)	45	ASTM D 2419

Fatigue testing has demonstrated that the better fatigue performance is gained by using a 1/2- or 3/8-inch aggregate in a dense gradation. Different agencies may use slightly different gradations or sieve sizes; the important objective to obtain a dense gradation. Note that Stone Matrix uses a gap gradation; perhaps that is a partial reason for the demonstrated poor fatigue performance.

For better fatigue performance, aggregates should be hard and crushed particles for both large and fine aggregates with the length-to-width ratio less than three, and preferably with asperities projecting from the rough surfaces. The rough surface and asperities increases the bond area of each aggregate and thereby reducing the tension bond stress, which improves fatigue resistance.

The rough surfaces with asperities improve the resistance to a degree for shoving and rutting. The rough surfaces with asperities also improves skid resistance of the wearing surface as the larger size aggregates are exposed on the top surface; it usually takes about a year for traffic to wear off the binder coating the exposed aggregate, which increases the skid resistance.

16.5.6 Constructing Wearing Surfaces

16.5.6.1 General

The construction phase of wearing surfaces is as important as the selection and design phases because the service life of the wearing surface depends on the proper installation for each layer of the different materials. A poorly constructed wearing surface usually shows some form of failure within the first 3 years. For a wearing surface to perform for the service life of which it is capable, ideally every square meter of every layer has to meet specifications. To achieve this, a detailed set of specifications and plans with quality control procedures for contractors to follow needs to be developed during the design phase.

Constructing a wearing surface on OSD is unfamiliar construction to most contractors, and construction mistakes usually occur near the beginning of the work. Before actual construction of the bridge deck, specifying constructing a test strip off the bridge deck is a helpful tool in the learning process for the contractors, work crews, and the inspection and quality control personnel. A 100-m long test strip is well worth the cost and sufficiently long to demonstrate all of the construction procedures, discovering and correcting construction errors, and proving to the engineer and owner that the construction procedures work, the work crews understand their roles in the construction process, and the quality control methods are capable of detecting construction errors.

The manufacturer of proprietary wearing surfaces will have specifications for mixing, transporting, applying, and quality controls for their specific material. Material suppliers that supply additives, corrosion protection, bond coats, waterproofing materials, and similar materials will have prepared specifications, quality control procedures, and field testing methods for their material. However, these are just bits and pieces of construction items; an overall specification and quality control procedures is required to tie everything together into a construction package.

16.5.6.2 Construction Procedures for Asphalt-Based Wearing Surfaces

The following overview of construction procedures is for asphalt-based wearing surfaces including epoxy asphalt concrete, but excluding pourable mastics and stone matrix. Polymer resins and Portland cement have not been used too frequently or too successful in the United States and is outside the scope of this chapter.

The first item of construction is designing the wearing surface mix of binder and aggregates. Perhaps the best method to do this is the Marshall Stability Method that started as ASTM D 1559, which was withdrawn and replaced with the current ASTM D 6927. The Marshall Stability tests a series of mixes with different binder contents in a hockey-puck size specimen at 140°F, which is a temperature that wearing surfaces can achieve on a hot day.

The primary reason for using the Marshall Salability tests is that the series of mixes are tested in tension, as the mix will be subjected to tension with each passage on a truck wheel. This test provides

values of stability, density, flow, air voids, and more all in one single test for four different percent binder contents. In addition to providing these physical properties, the purpose of using the Marshall tests is to select a binder content that will provide a long life-wearing surface. Marshall Testing Machine as shown in Figure 16.43, according to ASTM D 6927, shows the load cell measuring the force on the round jaws that squashes the 104 mm (4 in) diameter Marshall Test specimens (Figure 16.44). The ram applies the forced thrusts upward from the enclosed box and also supports the reaction posts. The molded specimens with distortions or cracks are tested, and specimens without damage were improperly molded and should be discarded.



FIGURE 16.43 Marshall testing machine. (Courtesy of Charles Seim.)

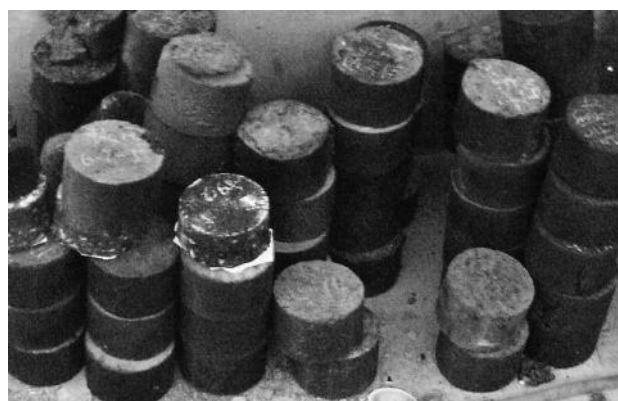


FIGURE 16.44 Over forty Marshall test 104 mm diameter specimens. (Courtesy of Charles Seim.)

Perhaps the most important property to determine in these series of tests is the air voids content. Fatigue testing experience has shown that fatigue resistance reduces drastically above an air void content of 3.5%–4% binder content. In addition, air voids above those values are more permeable to the admission of water. The air voids cannot be set too low because it is difficult to compact the mat to achieve air voids in the 1%–2% range, unless the binder content is set too high, which reduces the stability value. Perhaps the optimum selection would be a binder content that produces air voids in the 2.5%–3% range, which allows about 1%–1.5% margin before reaching the 4% maximum air void content.

The next important material selection is the bond coat between the first mat layer and the corrosion protection layer, and used between the first mat layer and a second mat layer.

The bond coat pull off test is made in both the laboratory and in the field to determine the pull off strength. This test is done in accordance with ASTM C 1583/C 1583M with the following modifications to the selected section numbers:

1. Scope—Add to Section 1.1.2: The overlay material may be asphalt concrete and the substrate may be steel plate.
4. Summary of Test Method—Add to Section 4.1: This test may be performed on asphalt concrete surfacing on a steel plate substrate.
4. Add the following: The test specimen is formed by drilling a nearly full-depth core into and perpendicular to the surface of the asphalt concrete overlay and leaving the intact core attached to the steel plate. A steel disk is bonded to the top surface of the test specimen.
5. Significance and Use—Add to Section 5.1: This test method determines the tensile strength of the bond coat to the steel plate substrate.
10. Preparation of Test Specimen—Add to Section 10.1: For epoxy asphalt concrete overlay, drill to within 0.2 in plus 0.1 in minus 0.1 in of the steel plate substrate after first determining the thickness of the epoxy asphalt overlay.
13. Precision and Bias—Does not apply to asphalt concrete overlay and steel plate substrate tests.

Many other tests are required depending on the materials selected for the wearing surface and beyond the scope of this chapter. Suffice to state that wearing surfaces are a high performing material and must be designed, constructed, and tested under quality control procedures to ensure that high performance is obtained. Figure 16.45 shows paving “train” of equipment for constructing a wearing surface. From left to right, haul truck is dumping material into hopper of side loader, side loader is transferring material into the hopper of the paving machine that is applying the material uniformly onto the steel deck, and the rollers that are compacting the material to very low air voids.



FIGURE 16.45 Paving train of equipment for constructing a wearing surface. (Courtesy of Charles Seim.)

16.5.7 Maintaining Wearing Surfaces

16.5.7.1 General

Well-designed and constructed wearing surface should require little maintenance except for occasionally sweeping the deck and keeping the deck drains open; as these wearing surfaces nears the end of its service life, maintenance effort will increase. By that time, the wearing surface has reached about 90%–95% of its service life, and should be scheduled for replacement as soon as possible; thus spending the money saved on repairs to help pay for the replacement costs.

Sometimes during the service life of well-designed and well-constructed wearing surfaces, cracks, potholes, and delamination mysteriously do appear, and damage occurring from various means. These distressed areas should be repaired as soon as possible after they are found to preserve the integrity and service life of the wearing surface.

There is little published information on the repairs of distressed wearing surfaces. Some suppliers of proprietary wearing surface material have methods of repairing their product. Probably most of the repairs that have been made to wear surfaces were done by maintenance people using their ingenuity and trial and error to make effective repairs.

16.5.7.2 Maintenance Procedures for Asphalt-Based Wearing Surfaces

Maintaining wearing surfaces is more art than engineering. The following overviews are commenting as to what are some of the distresses that can occur and some suggestions for methods that can be tried for maintaining wearing surfaces.

The primary distresses are usually fatigue cracking and delaminations. Sometimes a vehicle catches on fire on the bridge deck and damages the wearing surface. Vehicular accidents can gouge out pieces of the wearing surface and heavy loads can tumble off trucks.

1. Cracks: Cracks regardless of wherever they are long or short should be sealed at the first opportunity after detection. Asphalt has been used to fill cracks but apparently does not work as well as low viscosity polymeric materials such as methacrylate or low viscosity epoxies. Note that methacrylate has to be handled very carefully as a safety precaution. The cracks should be carefully blown out with dry compressed air before applying the crack sealer.
2. Bubbles: Bubbles usually occur right after the wearing surfaces is placed and is usually caused by water dripping off the rollers during the compaction operation. The easiest way is to prevent bubbles from occurring during the paving operation. However, if they do occur and the wearing surface material is still uncured and flexible, puncturing the center of the bubble and compressing the area back into place by rolling with small roller may work. If this does not work, the area could be treated as a small delamination or diamond sawed out and replaced.
3. Small delaminations: Small delaminations are difficult to find until they suddenly pop up. Before they pop up, delaminations can be detected by chain dragging, acoustic hammers, and other devices developed for detecting delaminations on bridge decks. Once detected, small delaminations can be repaired by first drilling access holes over the area of the delamination. Then inject low viscosity methacrylate, epoxy, or similar material until the material emerges from the drilled hole to show full filling of the delamination void.
4. Large delaminations: Large delaminations are usually detected when pieces of the wearing surface are dislodged. The most feasible repair is by diamond seen cutting the wearing surface around the delamination area and replace the removed material. However, the problem is what to use to fill and bond the removed material. Ideally, the original wearing surface materials should be used but that may not be possible either to obtain the material or to install in the same manner as the original. Some manufacturers of proprietary wearing surface may have material that they recommend for repairing their wearing surface. Asphalt has been used quite frequently because it is readily

available, but usually only lasts a year or two before requiring replacement. There are proprietary rubber-based concretes that seem to work well for a time if well bonded to the steel deck.

5. Fire damage: Fire damage can be repaired similar to the repair for large delamination areas.
6. Gouged areas: Gouged out areas are just super-wide cracks that allow the repaired material to be placed in the gouged area without injection. The materials used for repairing large delaminations can be used, but should be securely bonded to the bottom and sides of the gouge.

Acknowledgments

The writing of this chapter was based on years emails and papers written by orthotropic bridge colleagues, over 300 individuals including Dr. Lian Duan, who united in the creation of the 2004, 2008, and 2013 www.orthotropic-bridge.org events and proceedings. Section 16.5 Wearing Surface Systems was written by Mr. Charles Seim who has many decades of designing wearing surface. Special thanks to Mr. Craig Copelan, Mr. Carl Huang, Professor Hans De Backer, Dr. Brian Kozy, Mr. David McQuaid, Dr. Vadim Seliverstov and Mr. Roman Wolchuk for prepublication peer review of material and for years of sharing ideas and papers on orthotropic bridges.

References

- Akesson, B. 2008. *Understanding Bridge Collapses*, Taylor & Francis, London, UK, 266 pages.
- Amirkian, A. 1970a. "Welded Steel Pontoon of Novel Rib Framing Serves as Multipurpose Harbor Facility," *Modern Welded Structures*, Volume III, James F. Lincoln Arc Welding, Cleveland, OH, pp. I-30-I-35.
- Amirkian, A. 1970b. "Welded-Steel Pontoon Bridge Keeps Military Road Open," *Modern Welded Structures*, Volume III, James F. Lincoln Arc Welding, Cleveland, OH, pp. I-36-I-38.
- ASCE. 2004. *Proceedings of Orthotropic Bridge Conference*, August 23–27, www.orthotropic-bridge.org, ASCE Capital Branch, Sacramento, CA.
- ASCE. 2008. *Proceedings of 2nd International Orthotropic Bridge Conference*, August 25–29, www.orthotropic-bridge.org, ASCE Sacramento Section, Sacramento, CA.
- ASCE. 2013. *Proceedings of 3rd Orthotropic Bridge Conference*, June 24–30, www.orthotropic-bridge.org, ASCE Capital Branch, Sacramento, CA.
- Bavirisetty, R. 1993. San Diego Coronado Bay Bridge Overlay Project (Orthotropic Deck), *Structure Notes*, California Department of Transportation, Sacramento, CA.
- Blodgett, O. 1966. *Section 4.11—Orthotropic Bridge Decks of Design of Welded Structures*, The James F. Lincoln Arc Welding Foundation, The Lincoln Electric Company, Cleveland, OH.
- Bouwkamp, J. G. 1965. "Behavior of a Skew Steel-Deck Bridge Under Static and Dynamic Loads," California Department of Public Works Contract No. 13365, College of Engineering, University of California Berkeley, 105 pages (Ubatis Creek Test Bridge).
- Calzon, J. M. and Mendez, G. L. A. 2008. "Swing Bridge for the Formula 1 Race Course on Valencia Harbour, Spain," *Structural Engineering International*, IABSE 18(4):332–336. Zurich, Switzerland.
- Cartledge, P., Ed. 1973. *Proceedings of the International Conference on Steel Box Girder Bridges*, The Institution of Civil Engineers, Thomas Telford Publishing London, UK.
- Chatterjee, S. 2003. *The Design of Modern Steel Bridges* (2nd edition), BSP Professional Books of Blackwell Scientific Publications, London, UK.
- Copelan, C., Huang, C. and Mangus, A. 2010. "Icons of Movable Steel Orthotropic Bridges," ASCE-SEI www.asce.org, May 2010 Orlando, ASCE www.asce.org.
- DSD Dillinger Stahibau GmbH, and Bilfinger-Berger. 2004. Canal Bridge over the Elbe River, 20 pp, (In German).
- Ecale, H. and Lu, T.-H., 1983. "New Chicago-Type Bascule Bridge," *Journal of Structural Engineering*, 109(10): 2340–2354, October, ASCE: www.asce.org.

- Erzurumlu, H. T. 1972. "Fatigue of Orthotropic Steel Decks," *Journal of the Structural Division*, 98(ST4), 813–883.
- Eurocode 1993-2. *Design of steel structures Part 2: Steel Bridges*, European Committee for Standardisation, Brussels, Belgium.
- FHWA. 2012. *Manual for Design, Construction and Maintenance of Orthotropic Steel Deck Bridges*, HDR Engineering Inc., Performing Organization, Federal Highway Administration, Washington, DC.
- Fisher, T. A. 1998. "Chelsea Street Bridge Replacement," *Paper # IBC-98-66 of 15th Annual Internal Bridge Conference and Exhibition*, June 15–17, Pittsburgh, PA.
- Fobo, W. 2012. "Last Dance," *Wolga Bridge, Bridge Design & Engineer*, 67:58–59 (Second Quarter 2012).
- Gilbert, C. 1991. "Vierendeel Bridges," *Structure Spans by Division of Engineer Services*, October 1991, Caltrans, California Department of Transportation, Sacramento, CA, www.dot.ca.gov.
- Gopalaratnam, V. S. 2009. "Stresses and Composite Action of the Wearing Surface in Orthotropic Steel Bridge Decks," *Report*, University of Missouri, Columbia, MO.
- Hemeau, G., Puch, C. and Ajour, A-M. 1981. "Bridge deck surfacings on metal floors-2-fatigue behavior under negative bending moment," *Bulletin de Liaison des Laboratoires des Ponts et Chaussees*, Laboratoire Central des Ponts et Chausees, Paris (in French).
- Huang, C., Mangus, A. and Copelan, C. 2009. "The Excellent Seismic Performance of Steel Orthotropic Bridges," ASCE-ATC, www.asce.org, December 2009, San Francisco, CA.
- Huang, C. and Mangus, A. 2008a. "An International Perspective: Widening Existing Bridges with Orthotropic Steel Deck Panels," *Structural Engineering International*, IABSE 18(4):381–389, Zurich, Switzerland.
- Huang, C. and Mangus, A. 2008b. "An International Perspective: Existing Bridges with Hybrid Superstructure Orthotropic Deck with Prestressed Concrete," *Accelerated Bridge Construction—Highway for Life Conference*, March 19–21, Baltimore, MA. <http://www.fhwa.dot.gov/bridge/accelerated/index.cfm>.
- Huang, C., Mangus, A. and Murphy, J. 2005. "Accelerated Bridge Construction Techniques for Large Steel Orthotropic Deck Bridges," *FHWA ABC Symposium* December 15–16, 2005, at the Sheraton Hotel and Marina in San Diego, CA.
- Huang, C., Mangus, A. and Murphy, J. 2006. "Easy as 'ABC,'" *Structure Magazine*, A Joint Publication of NCSEA-CASE-SEI, October 2006, pp. 11–15.
- Huang, C. and Mangus, A. 2010. "Curved Orthotropic Bridges, an ABC Solution" *ABC Conference*, FHWA, Orlando, Florida.
- Huang, C., Mangus, A. Murphy, J. and Socha, M. 2008. "Twenty Four Icons of Orthotropic Steel Deck Bridge Engineering," *ICONS Project—An International Discussion PECG Professional Engineers in California Government* at www.orthotropic-bridge.org.
- ICE. 1973. *Steel Box Girder Bridges, Proceedings of the International Conference*, The Institution of Civil Engineers, Thomas Telford Publishing, London, UK, Feb 13–14, 1973.
- Kelly, R. B. and Braidwood, L. T. 1999. "A Comparison of Theory and Practice in Plate Stiffener Behaviour under Axial Loading," *Current and Future Trends in Bridge Design, Construction and Maintenance*, Thomas Telford, pp. 131–142.
- Kolstein, M. K. 2007. *Fatigue Classification of Welded Joints in Orthotropic Steel Bridge Decks*, Technical University of the Delft, 484 pages (ISBN-13:978-90-9021933-2).
- Kolyshev, I. 2005. "Detailed Design of the Neva River Twin Cable-Stayed Orthotropic Bridge," *Symposium BRÜCKENBAU in Leipzig, Germany*, February 2005.
- Korbelar, J., Schindler, J., Kroupar, M., Ryjacek and Korbelarova, J. 2006. "The Bridge over Ohre River by Loket," *Sixth International Symposium on Ocelove Mosty Steel Bridges Prague Czechoslovakia*, pp. 167–172, May 31–June 2, 2006.
- Mangus, A. 2000. "Existing Movable Bridges with Orthotropic Steel Decks," *HMS Eighth Biennial Movable Bridge Symposium Proceedings*, November 8–10, 2000, HMS Heavy Movable Structures Inc., Middletown, NJ.

- Mangus, A. 2001. "Short Span Orthotropic Deck Bridges," *6th Short Medium Span Bridge Conference*, May 20–22, 2001, Vancouver, Canada, CSCE.
- Mangus, A. 2002. "Orthotropic Deck Bridges Constructed in Cold Regions," Anchorage, AK, Merrill, K. S., Eds., *Proceedings of the 11th Cold Regions Engineering Conference*, May 20–22, 2002, ASCE, Reston, VA, www.asce.org.
- Mangus, A. 2005a. "California's Orthotropic Bridges, 1965–2005. 40 Years of Evolution," *Structure Magazine*, A Joint Publication of NCSEA-CASE-SEI, October 2005, pp. 12–16.
- Mangus, A. 2005b. "Millau Viaduct Orthotropic Bridge," *Structure Magazine*, A Joint Publication of NCSEA-CASE-SEI, October 2005, pp. 9–11, www.structuremag.org/OldArchives/2005/.../Orthotropics-Oct-05.pdf.
- Mangus, A. 2005c. "A Fresh Look at Orthotropic Technology," *Public Roads* (electronic edition). The U.S. Department of Transportation, Federal Highway Administration, www.tfhrc.gov, March/April 2005, Washington, DC, pp. 38–45.
- Mangus, A. 2005d. "The Next Generation Orthotropic Steel Deck Bridges," *World Steel Bridge Symposium*, National Steel Bridge Alliance, November 29–December 2, 2005, Orlando, FL. <http://www.steelbridges.org/pages/2005proceedings.html>.
- Mangus, A. 2006. "Even more Existing Movable Bridges with Orthotropic Steel Decks," *HMS 11th Biennial Movable Bridge Symposium Proceedings*, November 8–10, 2006, HMS Heavy Movable Structures Inc., Middletown, NJ, www.heavymovablestructures.org.
- Mangus, A., Copelan, C. and Huang, C. 2010, "What's up with orthotropic bridges?", Railroad Track and Structures, August 2010, pp. 55–60.
- Mangus, A. and Picker, S. 2006. "Alfred Zampa Memorial Bridge," *Steel Tips # 95*, The Structural Steel Educational Council, June 2006, 50 pages, <http://www.steeltips.org/>.
- Mangus, A. and Sun, S. 2000. "Chapter 14 Orthotropic Deck Bridges," *Bridge Engineering Handbook*, Chen, W. F. and Duan, L. Eds., CRC Press, Boca Raton, FL. <http://www.crcpress.com/>.
- Matsui, S., Ohta, K. and Nishikawa, K. 1999. *Orthotropic Steel Decks* appears in "Bridges and Roads" Oct 1998 and Nov 1999. PWRI Public Works Research Institute (in Japanese).
- Mistry, V. and Mangus, A. 2006. "Get In, Stay In, Get Out, Stay Out," *Public Roads*, 70(3), United States Department of Transportation, November/December.
- Muller, M., Bauer, T. and Uth, H.-J. 2004, *Steel toad bridges built according to DIN Codes (Strassenbrücken in Stahlbauweise nach DIN-Fachbericht)*, Bauwerk, Berlin, 298 pages (in German).
- Murphy, J. P. 2007. "Early California Accelerated Bridge Construction," *Steel Tips, # 98*, The Structural Steel Educational Council, June 2007, 25 pages, <http://www.steeltips.org/>.
- Murphy, J. P. 2008. "Cost Effective Bridge Fabrication," *Steel Tips, # 101*, The Structural Steel Educational Council, April 2008, 23 pages, <http://www.steeltips.org/>.
- Nakai, H. and Yoo, C. H. 1988. *Analysis and Design of Curved Steel Bridges*, McGraw-Hill Book Company, New York, NY, 673 pages.
- OTUA. 2004. *Proceedings Steel Bridge 2004*, Steel Bridges Extend Structural Limits, Millau, France, June 23–25, 2004. Office Technique pour l'Utilisation de l'Acier (OTUA), Paris, France.
- Pollak, B. S. and Lewis, C. 2004. "Fabrication Afloat," *Modern Steel Construction*, October 2004 pp, www.modernsteel.com/Uploads/Issues/October_2004/30734_nova.pdf, accessed Sept. 16, 2013.
- Popov, O. A., Monov, B. N., Kornoukhov, G. P. and Seliverstov, V. A. 1998. Standard Structural Solutions in Steel Bridges, *Journal of Constructional Steel Research*, 46:1–3, Paper No. 51.
- Roberts, J., Marquez, T., Huang, C., Mangus, A., Williams, J. and Benoit, M. 2000. "California's First Curved Orthotropic Bridge," *Structural Engineering International*, 10(2):124–127, May 2000, IABSE, Zurich, Switzerland.
- Rotter, T., Studnicka, J. 2006. "Ocelove Mosty" (Steel Bridges). *Czech Technical University, Prague (Ceska Technika—nakladatelstvi CVUT)*, Czech Republic., 166 pages.

- Sanpaolesi, L. and Croce, P. 2005. "Handbook 4 Design of Bridges: Guide to Basis Design Related to Eurocode Supplemented by Practical Examples," Leonardo Da Vinci Pilot Project CZ/02/B/F/PP-134007, 174 pages.
- Saul, R. 2005. *Double Deck Steel Bridges*, Stuttgart: Arcelor, <http://www.lap-consult.com/pdf>.
- Sedlacek, G. 1992. "Orthotropic Plate Bridge Decks," In *Constructional Steel Design, An International Guide*, Dowling, P. J., Harding, J. E., Bjorhovde, R. (Eds.). Elsevier Applied Science: London, 1992, p. 950 (Chapter 2.10, www.Elsevier.com).
- Seim, C. and Ingham, T. 2004. "Influence of Wearing Surfacing on Performance of Orthotropic Steel Plate Decks," *Transportation Research Record No. 1892*, pp. 98–106.
- Seim, C. and Manzanarez, R. 2005. "Performance Based Surfacing for the Orthotropic Deck of the New San Francisco-Oakland Bay Bridge," *Proceedings of www.orthotropic-bridge.org* for August 25–2005, ASCE Capital Branch of Sacramento, CA, 875 pages.
- Son, J. and Astaneh-Asl, A. 2012. "Blast Resistance of Steel Orthotropic Bridge Decks," *ASCE Journal of Bridge Engineering*, July–August, pp. 589–598.
- Sueyoshi, A., Kitano, K. and Takahashi, K et al. 1999. *Report on Fabrication and Erection of Ushibuka Bridge Onhashi*, Yokogawa Bridge Technical Report No. 26, 1997.1 (in Japanese).
- Tang, M.-C. 2011. "A New Concept of Orthotropic Steel Bridge Deck," *Structure and Infrastructure Engineering*, 7(7–8):587–595.
- Taylor, G. W. 1984. "Design of the Murray and Wolverine River Rail Bridges," *Canadian Journal of Civil Engineering*, 11:703–708.
- Thul, H. and Reinitzhuber, F. K. 1968. *Asphaltic Wearing Surfaces*, International Association of Bridge and Structural Engineers, Zurich Switerland.
- Troitsky, M. S. 1987. *Orthotropic Bridges—Theory and Design*, 2nd ed., The James F. Lincoln Arc Welding Foundation, Cleveland, OH.
- Vincent, R. B. 2011. "New Orthotropic Bridge Deck Designed for Multiple Longitudinal Girder Bridges," *BridgeLife 2011: Bridge Safety and Longevity Conference & Expo*, Ottawa, Ontario, April 14, 2011.
- Wang, Q. and Zhang, Z. 2011. Orthotropic Steel Cantilever Widening Method of Concrete Box Girder, *Structural Engineering International*, pp. 228–232 (2nd Quarter).
- Wells, M. 2002. *30 Bridges*, Watson Guptill Publications, NY, New York. 191 pages.
- Wikipedia. 2013. Peace Bridge (Calgary), [http://en.wikipedia.org/wiki/Peace_Bridge_\(Calgary\)](http://en.wikipedia.org/wiki/Peace_Bridge_(Calgary)), accessed on Sept. 16, 2013.
- Wolchuk, R. 1963. *Design Manual for Orthotropic Steel Plate Deck Bridges*, American Institute of Steel Construction, Chicago, IL.
- Wolchuk, R. 1997. "Steel-Plate—Deck Bridges and Steel Box Girder Bridges," *Structural Engineering Handbook* (4th edition), Gaylord, E. H., Gaylord, C. N. and Stallmeyer, J. E., Eds. McGraw-Hill Book Company, New York, NY, 1997 (Chapter 19).
- Wolchuk, R. 1999. "Steel Orthotropic Decks—Developments in the 1990's," *Transportation Research Board Annual Meeting*, Washington, DC.
- Wolchuk, R. 2002. "Structural Behavior of Surfacings on Steel Orthotropic Decks and Considerations for Practical Design," *Structural Engineering International*, 12(2):124–129, May 2000, IABSE, Zurich, Switzerland.
- Wolchuk, R. and Baker, G. S. 2004. *ASCE Seminar on Orthotropic Bridges*, Sacramento, CA.
- Zbigniew, M. 2009. "Restoration of Service Value to Historical Steel Road Truss Bridge in Klodzko," *Poland Transportation Research Board Annual Meeting 88th Annual Meeting*, 2009, Paper #09-1915, Washington, DC, 22 pages.
- Ziemian, R. D. 2010. *Guide to Stability Design Criteria for Metal Structures* (6th edition), Structural Stability Research Council, 1078 pages, John Wiley & Sons, New York, NY.

@Seismicisolation

17

Approach Slabs

17.1	Introduction	647
17.2	Structural Design Considerations.....	647
17.3	Definitions of the Bump and the Bump Tolerance.....	648
Definition of the Bump • Bump Tolerances		
17.4	Mechanisms Causing the Formation of the “Bump”	649
Consolidation Settlement of Foundation Soil • Poor Compaction and Consolidation of Backfill Material • Poor Drainage and Soil Erosion • Types of Bridge Abutments • Traffic Volume • Age of the Approach Slab • Approach Slab Design • Skewness of the Bridge • Seasonal Temperature Variations		
17.5	Mitigation Techniques for Distressed Approach Slabs.....	659
Drainage Method • Replacement Method • Mud/Slab Jacking • Grouting • Other Methods		
17.6	Mitigation Techniques for New Approach Slabs	667
Improvement of Embankment Foundation Soil • New Foundation Technologies • Improvement of Approach Embankment/Backfill Material • Design of Bridge Foundation Systems • Effective Drainage and Erosion Control Methods		
17.7	Summary.....	671
	References.....	672

Anand J. Puppala
*University of Texas,
Arlington*

Bhaskar C. S.
Chittoori
Boise State University

Sireesh Saride
*Indian Institute of
Technology, Hyderabad*

17.1 Introduction

This chapter presents comprehensive information collected from available literature addressing the problem of the differential settlement at the bridge approach. General structural design considerations are presented in Section 17.1. In the second and third sections, general information on the definitions of the bridge approach and the bump at the end of the bridge and the tolerance of the bump are given. Thereafter, in the third section, the mechanisms causing the formation of the bump such as consolidation of foundation soil, poor compaction of the backfill material, poor water drainage and soil erosion close to the bridge abutments, types of bridge abutments, traffic volume passing over the bridge decks, age of the approach slab, the design of the approach slab, skewness of the bridge and seasonal temperature variations are mentioned and reviewed in detail. The fourth section presents maintenance measures normally employed by highway agencies to alleviate distressed approach slabs. Subsequently, a brief summary of the techniques used to mitigate the bump at the end of the bridge of the new bridge is presented.

17.2 Structural Design Considerations

The bridge approach slab is a part of a bridge that rests on the abutment at one end and on the embankment or a sleeper slab on the other end (Wahls, 1990). The slabs are designed to provide a smooth transition between the bridge deck and the roadway pavement and to minimize the effect of differential

settlements between the bridge abutment founded on the shafts or piles and the embankment fill (White et al., 2005).

There are two types of approach types used by highway agencies. Some agencies use a bituminous approach pavement because it can be maintained easily by overlay type rehabilitation. However, the use of bituminous approaches with Portland concrete roadways is still not highly preferred by the DOTs (Wahls, 1990).

Other agencies use a reinforced concrete slab because they believe the rigid approach slab is successful in preventing the bridge approach settlement (Wahls, 1990). In this case, one end of the slab is connected to the main structure by two methods. The first option connects the slab directly to the bridge deck by extending the main reinforcement from the bridge deck to the approach slab. The second option connects the approach slab to the abutment by using a dowel/tie bar (White et al., 2005).

Based on a survey of over 131 bridges in Texas by James et al. (1991), it was found that the bridges with a flexible pavement had a smoother transition than those with a rigid pavement. However, Pierce et al. (2001) reported that the approach slab with asphalt overlays tend to increase the surface roughness. According to the TxDOT Bridge Manual (2001), the use of approach slabs is only an option and districts have had success with and without their use. However, if the approach slab is constructed by the non-integral bridge system, the use of a dowel/tie bar must be implemented between the slab and the abutment (Hoppe, 1999).

James et al. (1991) stated that the roughness or IRI values of the approach slab are influenced by the longitudinal pavement movements resulting from temperature cycles. They also mentioned that the approach pavement settlement/roughness can be attributed to impact loads due to poor design and constructed expansion joints. White et al. (2005) stated that the performance of the approach slabs depends on these following factors: approach slab dimensions, steel reinforcement, use of a sleeper slab, and type of connection between the approach slab and the bridge.

Most of the reinforced concrete approach slabs used in the United States have lengths varying from 20 to 40 ft. (6–16 m) (Wahls, 1990). According to an extensive survey of different state agencies conducted by Hoppe (1999), typical approach slab dimensions for the various states surveyed are collected and summarized. From this study, it is seen that most approach slab dimensions vary between 15 ft. and 30 ft. (5–10 m) in length and 9–17 in. (23–43 cm) in thickness.

17.3 Definitions of the Bump and the Bump Tolerance

17.3.1 Definition of the Bump

Generally, roadways and embankments are built on subgrade foundations and compacted fill materials respectively, which undergo load-induced compression and settlements with time. In contrast, the bridges typically need to rest on deep foundations such as pile, pier or other types of deep foundation systems resting on a firm foundation material such as bedrock. Therefore, by resting on a firm foundation, the total settlement of the bridge is usually much smaller than the total settlement of the roadway or adjacent embankment. As a result, a considerable differential settlement occurs in the area between the bridge and roadway interfaces, and a noticeable bump can develop at the bridge ends.

The “bump” can affect drivers, varying from feeling uncomfortable to being hazardous to their lives (Hopkins, 1969; Ardani, 1987). To eliminate the effects of the bump, the approach slab must be built to provide a smooth grade transition between these two structures (bridge and roadway). Another function of the approach slab is to keep the magnitude of differential settlement within a control limit (Mahmood, 1990; Hoppe, 1999). However, in practice, it is found that the approach slabs also exceed differential settlements (Mahmood, 1990; Hoppe, 1999). In such cases, the approach slab moves the differential settlement problem at the end of the bridge to the end of the slab connecting with the roadway. Hence, the “bump” or “approach settlement” can be defined as the differential settlement or heave of the approach slab with reference to the bridge abutment structure.

17.3.2 Bump Tolerances

The differential settlement near the bridge approach is a common problem that plagues several bridges in the state of Texas (Jayawickrama et al., 2005). One of the major maintenance problems is to establish a standard of severity levels of the bump that require remedial measures so that it is easy to determine when repairs should be initiated.

Walkinshaw (1978) suggested that bridges with a differential settlement of 2.5 in. (63 mm) or greater needs to be repaired. Bozozuk (1978) stated that settlement bumps could be allowed up to 3.9 in. (100 mm) in the vertical direction and 2.0 in. (50 mm) in the horizontal direction. Several researchers define the allowable bumps in terms of gradients as a function of the length of the approach slab. Wahls (1990) and Stark et al. (1995) suggested an allowable settlement gradient as 1/200 of the approach slab length. This critical gradient was also referred by Long et al. (1998), and was used by the Illinois DOT for initiating maintenance operations.

Das et al. (1990) used the international roughness index (IRI) to describe the riding quality. The IRI is defined as the accumulations of undulations of a given segment length and is usually reported in m/km or mm/m. The IRI values at the bridge approaches of 3.9 (mm/m) or less indicates a very good riding quality. On the other hand, if the IRI value is equal to 10 or greater, then the approach leading to the bridge is considered as a very poor riding quality. Albajar et al. (2005) established a vertical settlement in the transition zone of 1.6 in. (4 cm) as a threshold value to initiate maintenance procedures on bridge approach areas. In Australia, a differential settlement or change in grade of 0.3% both in the transverse and the longitudinal direction and a residual settlement of 100 mm (for a 40-year design period) are considered as limiting values for bridge approach settlement problems (Hsi and Martin, 2005; Hsi, 2007).

17.4 Mechanisms Causing the Formation of the “Bump”

Bridge approach settlement and the formation of the bump is a common problem that uses significant resources for maintenance, and creates a negative perception of the bridge owners in the minds of transportation users. From thorough studies compiled from the existing and on-going research studies on the bridge approach settlement, the causes of the problem can be varied and are still too complex to identify them easily. However, the primary sources of the problem can be broadly divided into four categories: material properties of the foundation and embankment; design criteria for bridge foundation, abutment and deck; construction supervision of the structures; and maintenance criteria. It should be noted that not all the factors contribute to the formation of the bump concurrently.

There have been many studies employed across the states in the United States to study the causes of the problem and the methodologies to solve it (Hopkins, 1969, 1985; Stewart, 1985; Greimann et al., 1987; Laguros et al., 1990; Kramer and Sajer, 1991; Ha et al., 2002; Jayawickrama et al., 2005; White et al., 2005, 2007; Chen and Cai, 2011). White et al. (2005) define the term “bridge approach” not just in terms of the approach slab alone, but in terms of a larger area, covering from the bridge structure (abutment) to a distance of about 100 ft. (30.5 m) away from the abutment. This definition includes the backfill and embankment areas under and beyond the approach slab as significant contributors to the settlements in the bridge approach region.

Many factors are reported in the literatures that explain the mechanisms causing the formation of bumps on the bridge transition (Hopkins, 1969; Stewart, 1985; Kramer and Sajer, 1991). According to Hopkins (1969), the factors causing differential settlement of the bridge approaches are listed as

- a. Type and compressibility of the soil or fill material used in the embankment and foundation
- b. Thickness of the compressible foundation soil layer
- c. Height of the embankment
- d. Type of abutment

In the following, three studies by Briaud et al. (1997), Seo (2003), and White et al. (2007) listed factors that contribute to bumps. Briaud et al. (1997) summarized various factors that contributed to the formation of bumps/settlements at the approach slabs in Figure 17.1. These factors were grouped and ranked in the following order in which they contribute to the soil movements: fill on compressible foundation, approach slab too short, poor fill material, compressible fill, high deep embankment, poor drainage, soil erosion, and poor joint design and maintenance.

Seo (2003) performed a circular track test involving the approach slab, which was repeatedly loaded by a vehicle model. Seo (2003) listed the following observations:

1. Number of cycles of loading over the approach slab is proportional to the increase in the bump.
2. Shorter approach slabs result in higher displacements of the slab.
3. More highly compacted stiffer soils result in less deflection of the slab.
4. The velocity of vehicles has an influence on the increase in magnitude of the bump.
5. The weight of vehicles relates to the degree of the settlement.

A recent study conducted by White et al. (2007) summarized the following factors as contributors to differential settlements of the approach slab:

1. Backfill materials under poorly performing approach slabs are often loose and under compacted.
2. The foundation soil or embankment fill settles.
3. Many bridge approach elevation profiles have slopes higher than 1/200, which is considered a maximum acceptable gradient for bridge approaches.
4. Voids develop under bridge approaches within 1 year of construction, indicating insufficiently compacted and erodible backfill material.

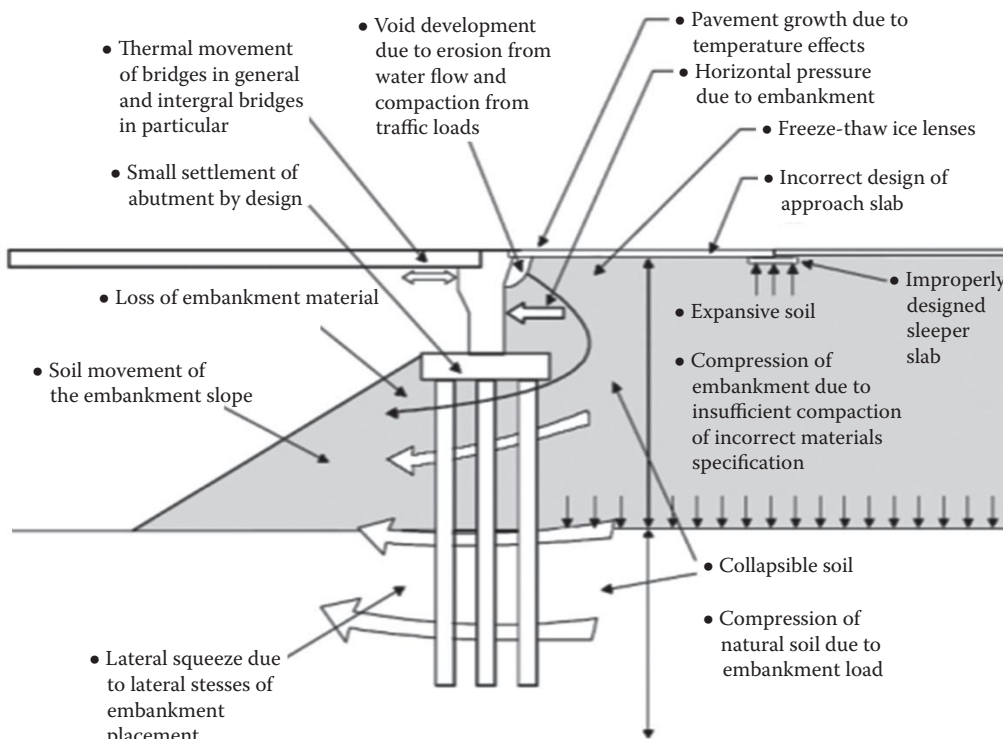


FIGURE 17.1 Schematic of different origins that lead to the formation of a bump at the end of the bridge. (From Briaud, J. L. et al., *Transportation Research Board*, National Research Council, Washington, D.C., 1997.)

5. Inadequate drainage is a major bridge approach problem. Many abutment subdrains are dry with no evidence of water, are blocked with soil and debris, or have collapsed.
6. Many expansion joints are not sufficiently filled, allowing water to flow into the underlying fill materials.

This chapter presents the following major factors that caused approach bumps by summarizing the above studies as well as a review of other investigations that addressed this bump problem:

1. Consolidation settlement of foundation soil
2. Poor compaction and consolidation of backfill material
3. Poor drainage and soil erosion
4. Types of bridge abutments
5. Traffic volume
6. Age of the approach slab
7. Approach slab design
8. Skewness of the bridge
9. Seasonal temperature variations

Salient details of these factors are presented in the following subsections.

17.4.1 Consolidation Settlement of Foundation Soil

Consolidation of foundation soil under an approach embankment is regarded as one of the most important contributing factors to bridge approach settlements (Hopkins, 1969; Wahls, 1990; Dupont and Allen, 2002). It usually occurs because of dynamic traffic loads applied at the embankment surface and static load due to the embankment weight itself (Dupont and Allen, 2002). Foundation problems usually are more severe in cohesive soils than in non-cohesive soils. Cohesive soils, such as soft or high plasticity clays, represent a more critical situation due to their time-dependent consolidation behavior. In addition, cohesive soils are more susceptible to lateral or permanent plastic deformation, which can exacerbate the approach settlement problem.

Typically, settlement of soils can be divided into three different phases (Hopkins, 1969): initial, primary, and secondary consolidations, which are explained in the following sections.

17.4.1.1 Initial Consolidation

The initial settlement is the short-term deformation of the foundation when a load is applied to a soil mass. This type of settlement does not contribute to the formation of bumps, because it usually occurs before the construction of the approach structure (Hopkins, 1969).

17.4.1.2 Primary Consolidation

Primary settlement is the main factor that contributes to the total settlement of soils. The gradual escape of water due to the compression of the loaded soil is believed to be the reason for this type of settlement. This primary settlement lasts from a few months for granular soils, for a period of up to 10 years for some types of clay (Hopkins, 1973). This significant difference is attributed to the small void ratio and high permeability of granular soils.

17.4.1.3 Secondary Consolidation

This phase occurs as a result of changes in void ratio of the loaded soil after dissipation of excess pore pressure (Hopkins, 1969). In this case, particles and water in the soil mass readjust in a plastic way under a constant applied stress. In the case of very soft, highly plastic or organic clays, secondary consolidation can be as large as the primary consolidation, while in granular soils, it is negligible (Hopkins, 1969).

17.4.2 Poor Compaction and Consolidation of Backfill Material

The approach settlements can be induced by low quality materials (such as locally available soft, cohesive expansive soils and soils sensitive to freeze-thaw) in terms of bigger “bumps.” In general, cohesive soils are more difficult to compact to their optimum moisture content and density than coarser or granular fill materials (Hopkins, 1973).

Poor compaction control of the embankment material is found to be a factor, resulting in low density and highly deformable embankment mass (Lenke, 2006). Poor compaction can also be attributed to limited access or difficulty in access within the confined working space behind the bridge abutment (Wahls, 1990). Many highway agencies require only granular fills that can be better compacted and are able to reach their maximum consolidation in less time than more cohesive soils (Wahls, 1990; Lenke, 2006). The TxDOT Bridge Design Manual (2001) notes that either improper backfill materials used for mechanically stabilized earth (MSE) or the inadequate compaction of the backfill materials in the embankment are the contributing factors to the backfill failure.

In addition to compression of the backfill material, lateral stability and shear strength are of great importance to the overall stability against the approach settlement. In the case of the foundation soil, lateral confining forces are significant, while on the embankment fills, the confinement effects are much less pronounced (Wahls, 1990). Hence, slope design, material selection and loads applied to the backfill need to be carefully evaluated to anticipate or minimize the final settlement (Wahls, 1990).

17.4.3 Poor Drainage and Soil Erosion

Several researchers reported the importance of the surface and subsurface drainage and soil erosion near the bridge abutment and embankment interface. Wahls (1990), Jayawikrama et al. (2005), Mekkawy et al. (2005), White et al. (2005), and Abu-Hejleh et al. (2006) identified the drainage system of the abutment and embankment as one of the most important factors that affect approach settlement. The dysfunctional, damaged or blocked drainage systems cause erosion in the abutment and slope, increasing soil erosion and void development. The dysfunctional drainage systems may be caused by either incorrect construction or improper design. It was observed that incorrect placement of the drainage pipes, such as outlet flow line higher than an inlet flow line on a newly constructed bridge, can impair the drainage system. Briaud et al. (1997) explains how the poor joints between the pavement and the abutment structure can lead to soil erosion of the embankment and abutment backfill.

Jayawikrama et al. (2005) noted that the erosion of soil on the abutment face and poor drainage material can induce serious approach settlement problems. The intrusion of surface water (rain) through weak expansion joints (openings) between the approach slab and bridge abutments can erode backfill material and further amplify the problem of approach slab settlements. Based on the detailed study of a few TxDOT bridges, they noted that these joint openings resulted from poor construction practices such as poor compaction of backfill material near the abutments, poor construction of joint sealants and poor surface and subsurface drainage systems.

In addition, the expansion joints should transfer traffic loads, prevent surface water from entering into the abutment, and allow pavement expansion without damaging the abutment structure (Wolde-Tinsae et al., 1987). Based on a comprehensive research study performed by White et al. (2005) on many bridges in Iowa, most of the expansion joints of the bridges inspected were not sufficiently filled, allowing water to flow into the underlying fill materials. On the other hand, cracks were often encountered next to closed joints in bridge approaches because of the crushing and cracking of neighboring concrete, allowing for leakage of water as well.

Similar observations were made by Mekkawy et al. (2005), which are discussed here. Based on field investigations in different states, Mekkawy et al. (2005) reported that inadequate drainage and subsequent severe soil erosion contributed to settlement problems about 40% of the bridge approach slabs that were surveyed by them. Moisture flow into the backfill, coupled with poor drainage conditions,

can cause failure of embankment, backfill and bridge abutments either by excessive settlement or by soil strength failure. Typically, water can seep into the embankment fill material via faulty joints and cracked concrete pavement sections. The leaked water can soften the embankment fill and can cause internal erosion as the fines typically wash out from the fill material. Without approach slabs, water leakage will immediately induce settlement; with approach slabs, voids beneath the slab will form, amplifying the erosion by compression of the soil.

The erodability of soils is based on their grain size distribution. Some soil gradation guidelines can be found in soils that are erosion resistant and those that are prone to erosion (Briaud et al., 1997; Hoppe, 1999). A gradation band of material in the sand to silt size materials is a bad choice for embankments and backfill unless additional preventive actions, such as providing appropriate drainage design or erosion control systems, are taken (Briaud et al., 1997).

17.4.4 Types of Bridge Abutments

Abutments are characterized as integral (movable) or non-integral (conventional or stub) types (Greimann et al., 1987). In the integral type, the bridge superstructure is monolithically connected to the abutment, and the abutment is allowed to move laterally along with the bridge deck slab; while in the non-integral type, the bridge superstructure is independent of the abutment, and the longitudinal movements of the bridge deck are taken care of by roller/pin-bearing plates (Greimann et al., 1987). The advantages of integral bridge abutments are reduced construction and maintenance costs, minimum number of piles required to support the foundation and enhanced seismic stability (Greimann et al., 1987; Hoppe and Gomez, 1996). To avoid the use of the bearings and to reduce potential maintenance problems (such as frequent repair of bearings, expansion joint sealants) associated with non-integral bridge abutments, the use of integral bridge abutments has been increased since the 1960s (Horvath, 2000; Kunin and Alampalli, 2000). The following sections describe the advantages and disadvantages of both types of abutments.

17.4.4.1 Integral Abutments

Figure 17.2 shows an integral abutment bridge. The approach slab system of an integral bridge consists of the backfill, the approach fill, and the soil foundation. If an approach slab and a sleeper slab are used, they are also considered in the system. Integral abutment bridges are designed to carry the primary

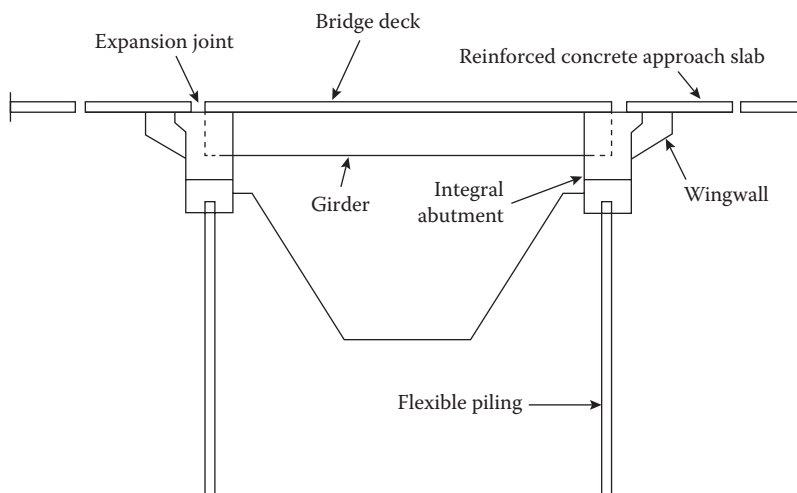


FIGURE 17.2 A simplified cross section of an integral abutment bridge. (From Greimann, L. F. et al., *Final Report Iowa DOT Project HR 273*, ERI Project 1780, ISU-ERI-Ames-88060, Ames, IA, 1987.)

loads (dead and live loads) and also the secondary loads coming from creep, shrinkage, thermal gradients and differential settlements. Integral abutments are rigidly connected to the bridge superstructure including beams and decks without expansion joints.

Even though integral abutments present structural advantages over non-integral abutments, they also introduce thermal movements in the approach system that can aggravate the bump problem on the approach system (Schaefer and Koch, 1992; White et al., 2005). Hence, special attention has to be paid in this type of abutment for the lateral loads imposed on the foundation piles due to horizontal movements induced by temperature cycles (Wahls, 1990).

17.4.4.2 Non-Integral Abutments

A non-integral abutment is shown in Figure 17.3. In this case, superstructure is supported on bearing connections that allow longitudinal movements of the superstructure without transferring lateral loads to the abutment. The non-integral bridge abutment is separated from the bridge beams and deck by a mechanical joint that allows for the thermal expansion and contraction of the bridge (Nassif, 2002).

Three major types of non-integral abutment: Closed or U-type, Spill-through or Cantilever, and Stub or Shelf abutments are usually used (Hopkins and Deen, 1970; Timmerman, 1976; Wahls, 1990; TxDOT Bridge Design Manual, 2001).

17.4.4.3 Closed Abutment or U-Type

A typical closed abutment or U-type is shown in Figure 17.4a. The U-type abutments have two side walls and a front wall resting on spread footings below natural ground (TxDOT Bridge Design Manual, 2001). For this type of abutment, the side walls are long enough to keep the embankment from encroaching on the bridge opening. In addition, the taller the abutment is, the longer the sidewalls will be. The compaction of the embankment fill is rather difficult in these abutments because of the confined space near the abutment and due to the wall, which is extended over the whole height of the abutment (TxDOT Bridge Design Manual, 2001). These abutments are also subjected to higher lateral earth pressures than other types.

17.4.4.4 Spill-Through or Cantilever Abutment

A spill-through abutment is shown in Figure 17.4b. A spill-through abutment is supported on the columns and hence, the compaction of the backfill material between the columns and near the abutment is

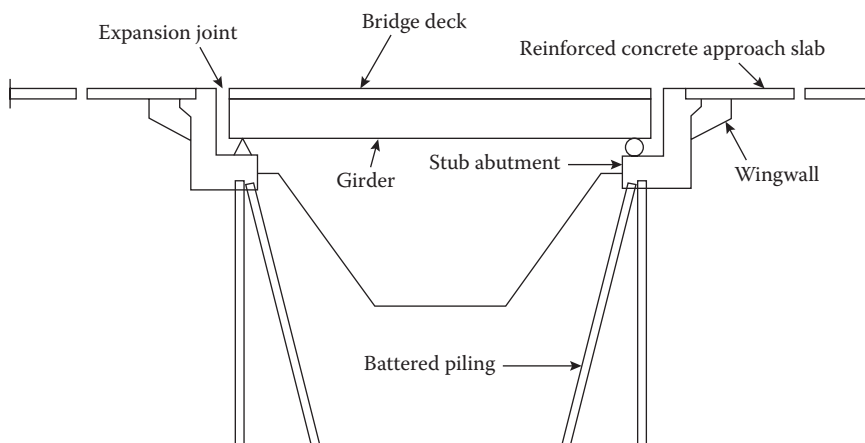


FIGURE 17.3 A simplified cross section of a non-integral abutment bridge. (From Greimann, L. F. et al., *Final Report Iowa DOT Project HR 273*, ERI Project 1780, ISU-ERI-Ames-88060, Ames, IA, 1987.)

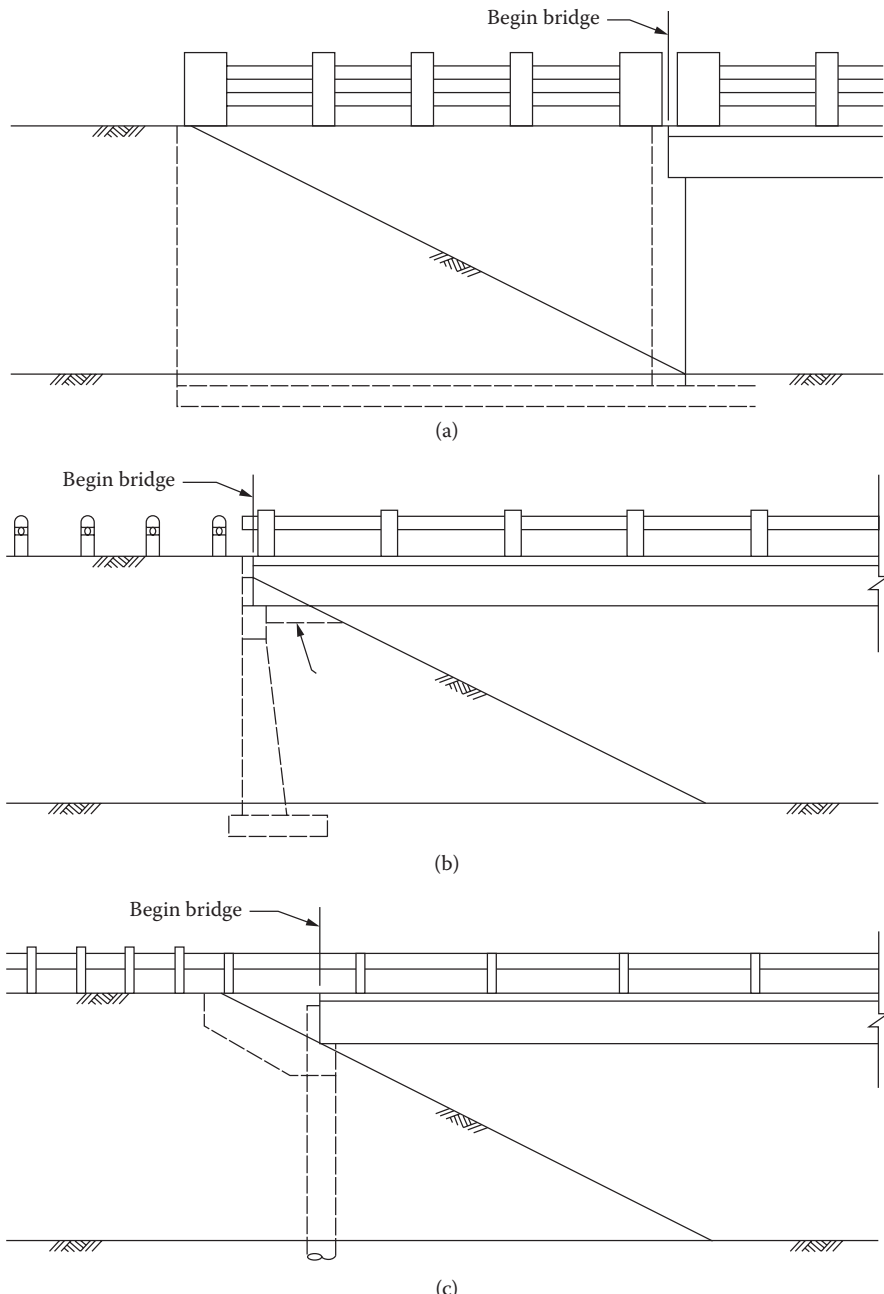


FIGURE 17.4 Non-integral abutment types: (a) U-type; (b) cantilever type; and (c) stub type. (From Texas Department of Transportation (TxDOT), *Bridge Design Manual*. Texas Department of Transportation, December, 2001.)

very difficult. Cantilever type abutments have variable width rectangular columns supported on spread footings below natural ground (TxDOT Bridge Design Manual, 2001). The fill is built around the columns and allowed to spill through, on a reasonable slope, into the bridge openings. A great number of these types of abutments have been constructed in Texas, and they have performed well in the past (TxDOT Bridge Design Manual, 2001). However, this type of abutment presents detailing and construction problems, as well as higher construction costs.

17.4.4.5 Stub or Shelf Abutment

A stub type abutment is shown in Figure 17.4c. A stub abutment is constructed after the embankment, so its height is directly affected by the embankment height. The compaction of the backfill material is relatively easier, compared with the closed type except for the soil behind the abutment (TxDOT Bridge Design Manual, 2001).

Although more economical, stub abutments have maintenance problems. The “bump at the beginning of the bridge,” caused by fill settlement is particularly noticed on stub type abutments (TxDOT Bridge Design Manual, 2001).

From the past experiences with these non-integral abutment bridges, TxDOT officials attribute the approach settlements to the poor construction practices due to inaccessibility to compact the backfill/embankment fill near the vicinity of the abutment leading to the aggressive approach settlements (Jayawikrama et al., 2005).

17.4.5 Traffic Volume

Heavy truck traffic has been found in some studies to be a major factor contributing to the severity of this bump, along with the age of the bridge and approach, especially in the late 1970s or early 1980s (Wong and Small, 1994; Lenke, 2006). High-volume traffic has been found as a compelling reason for including approach slabs in the construction of both conventional and integral bridges. Lenke (2006) noted that “the bump” was found to increase with vehicle velocity, vehicle weight, especially heavy truck traffic, and number of cycles of repetitive loading, in terms of average daily traffic (ADT). On the other hand, Bakeer et al. (2005) have concluded that factors such as speed limit and traffic count have no distinguishable impact on the performance of the approach slabs.

17.4.6 Age of the Approach Slab

The age of the approach slab is an important factor in the performance of different elements of bridge structures, especially at the expansion joints next to the approach slab, which could negatively affect the backfill performance in terms of controlling settlements underneath the slab (Laguros et al., 1990; Bakeer et al., 2005). Another factor known as alkali-silica reactivity (ASR) formed under the concrete approach slabs is known to induce expansion stresses. These stresses can potentially lead to slab expansion and distress in the approach slabs, approach joints, and vertical uplift of the slabs and pavement preceding the slabs (Lenke, 2006).

Bakeer et al. (2005) studied the influence of approach age by investigating a number of approach slabs built in the 1960s, 1970s, 1980s, and 1990s. Based on the condition ratings, the newer pile- and soil-supported approach slabs were generally in better condition than the older ones. The IRI ratings showed that pile-supported approach slabs built in the 1980s performed better than those built in the 1990s and that the approach slabs built in the 1990s performed better than those built in the 1970s.

Laguros et al. (1990) reported that the flexibility of the approach pavements has a considerable influence as well. They observed greater differential settlement in flexible pavements than rigid pavements during initial stages following construction (short term performance), while both pavement types performed similarly over the long term.

17.4.7 Approach Slab Design

The purpose of the approach slab is to minimize the effects of differential settlement between the bridge abutment and the embankment fill, to provide a smooth transition between the roadway pavement and the bridge, to prevent voids that might occur under the slab and to provide a better seal against water percolation and erosion of the backfill material (Burke, 1987). However, a rough transition can occasionally develop with time in bridge approaches due to differential settlements between the abutment and roadway. This can be attributed to the different support systems of the two structures connected by

the approach slab. The approach slab and the roadway are typically constructed over an earth embankment or natural soil subgrade, whereas the bridge abutment is usually supported on piles.

Insufficient length of approach slabs can create differential settlements at the bridge end due to high traffic-induced excessive destruction in the approach slab (Briaud et al., 1997). Based on an extensive survey performed by Hoppe (1999) in 39 states, approach slab lengths varied from 10 to 40 ft. and thicknesses ranged from 8 to 17 in. Some studies based on the IRI ratings, report that 80 foot-long slabs performed the best, and no significant difference was found when compared to 100 foot-long slabs (Bakeer et al., 2005).

The rigidity of the approach slab is also a major contributing factor. Dunn et al. (1983) compared the performance of various approach slab pavements in Wisconsin and reported that 76% of the flexible approaches rated poor, 56% of the non-reinforced approaches rated fair, and 93% of the reinforced concrete approaches rated good. All these ratings were based on the performance of the approach slab in controlling the differential settlements.

17.4.8 Skewness of the Bridge

Skew angle also has a significant effect on the formation of approach settlements and the overall bridge performance. Skewed integral bridges tend to rotate under the influence of cyclic changes in earth pressures on the abutment (Hoppe and Gomez, 1996).

Nassif (2002) conducted a finite element study to understand the influence of skewness of bridge approaches and transition slabs on their behavior. It was found that the skew angle of the approach slab resulted in an uneven distribution of the axial load, so that only one side of the axles actually had contact with the approach slab. Figure 17.5 shows that for the same loading conditions, the tensile axial stresses on skewed approach slabs are found to be 20%–40% higher than the same on straight approach slabs. In addition, the pinned connection at the edge of the approach slabs, which connects them with the bridge abutment, prevented any displacement taking place along this edge, thus providing more strength to the elements of this region (Nassif, 2002).

Additionally, higher rates of settlements at the bridge exit were considered to be accountable to the effect of the skew angle of the approach slab as well as improper compaction conditions in hard-to-reach soil areas close to the abutments (Nassif, 2002).

17.4.9 Seasonal Temperature Variations

The seasonal temperature changes between summer and winter contribute to differential settlement between bridge and approach slab, especially for bridges with integral abutments (Schaefer and Koch, 1992; Arsoy et al., 1999; Horvath, 2005; White et al., 2005). This temperature change causes cyclical

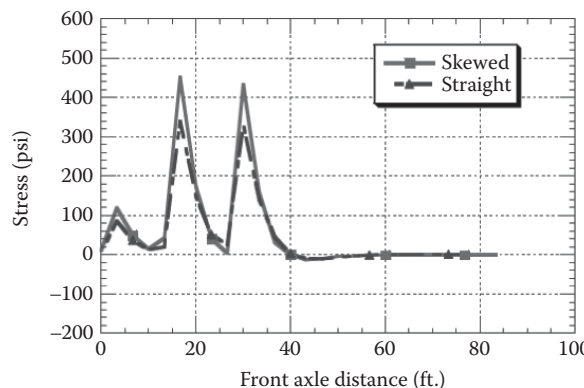


FIGURE 17.5 Variation of tensile axial stress with front axle distance for skewed and straight approach slabs. (From Nassif, H., Rep. No. FHWA-NJ-2002-007, Department of Civil and Environmental Engineering, Center for Advanced Infrastructure & Transportation [CAIT], Rutgers, NJ, 2002.)

horizontal displacements on the abutment backfill soil, which can create soil displacement behind the abutment, leading to void development under the approach slab (White et al., 2005). As a result, the infiltration of water under the slab and therefore erosion and loss of backfill material may accelerate.

Due to seasonal temperature changes, abutments move inward or outward with respect to the soil that they retain. During winter, the abutments move away (outward) from the retained earth due to contraction of the bridge structure, while in summer, they move towards (inward) the retained soil due to thermal expansion of the bridge structure (Arsoy et al., 1999; Horvath, 2005). At the end of each thermal cycle, abutments have a net displacement inward and outward from the soil which is usually retained (see Figure 17.6). This is attributed to the displacement of an “active soil wedge,” which moves downward and toward the abutment during winter, but cannot fully recover due to the inelastic behavior of the soil during the summer abutment movement. This phenomenon was noted in all types of embankment materials (Horvath, 2005). Besides, these horizontal displacements are observed to be greater at the top of the abutment and hence the problem is aggravated when the superstructure is mainly constructed with concrete (Horvath, 2005). Figure 17.7 shows how the expansion-contraction movements of the bridge with the seasonal temperature change will lead to the creation of voids below the approach slab.

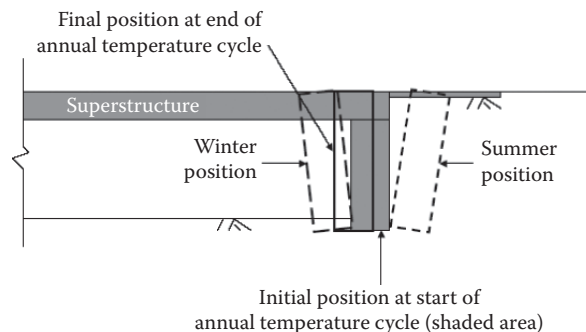


FIGURE 17.6 Thermally induced IAB abutment displacements. (From Horvath, J. S., *IAJB 2005—The 2005 FHWA Conference on Integral Abutment and Jointless Bridges*, 16–18 March, Baltimore, MD, 2005.)

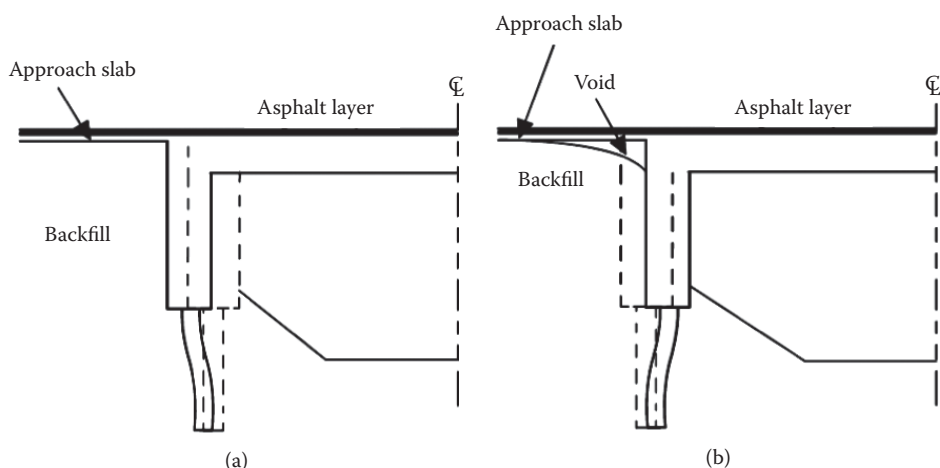


FIGURE 17.7 Movement of bridge structure: (a) expansion of bridge and (b) contraction of bridge. (From Arsoy, S., Barker, R. M., and Duncan, J. M., “The Behavior of Integral Abutment Bridges.” Rep. No. VTRC 00-CR3, Virginia Transportation Research Council, Charlottesville, VA, 1999.)

The temperature effect on the bridge-abutment interaction also creates pavement growth due to friction between the pavement and its subbase (Burke, 1993). After the pavement expands, it does not contract to its original length because of this friction. This residual expansion accumulates after repeated temperature cycles, resulting in pavement growth that can be rapid and incremental at pressure relief joints (Burke, 1993). The pressure generated will transmit to the bridge in terms of longitudinal compressive force and, therefore, should be considered by engineers when designing the pressure relief joints.

James et al. (1991), through a numerical study, documented a case of severe abutment damage for a bridge without pressure relief joints. This numerical stress analysis indicated that the damage was caused by the longitudinal growth of continuous reinforced concrete pavement, causing excessive longitudinal pressures on the abutments.

The cycle of climatic change, especially the temperature change, also can cause certain irreversible damage to the pavement or bridge approach slabs in terms of ice lenses due to frost action. Here, ice lenses are derived from freezing and thawing of moisture in a material (in this case soil) and the structures that are in contact with each other (UFC, 2004). The existence of freezing temperatures and presence of water on the pavement, either from precipitation or from other sources such as ground water movement in liquid or vapor forms under the slabs, can cause frost heave in pavements. This phenomenon causes the pavement rising because of ice crystal formation in frost-susceptible subgrade or subbase that can affect the durability of concrete. The frost-induced heave is not a serious problem in pavements in dry weather states such as Texas.

As noted by the above sections, bump or differential settlements are induced by several factors, either by individual mechanisms or by combination mechanisms. In the following sub-sections, different maintenance measures required for approach slabs are discussed.

17.5 Mitigation Techniques for Distressed Approach Slabs

Several soil stabilization techniques have been developed to stabilize the fill under the approach slab. These techniques are intended to smooth the approaches by raising the sleeper slab and approaches, especially if an application of an asphalt overlay is not feasible (Abu-Hejleh et al., 2006). The most important techniques are pressure grouting under the slab, slab-jacking or mud-jacking technique, the Urethane method, and compaction or high pressure grouting. Most of these techniques are often used as remedial measures after problems are detected. However, the same could be applied even in new bridge constructions. A brief overview of these methods is presented below.

17.5.1 Drainage Method

A periodic cleanup and maintenance schedule is required for all drainage structures on the bridge and the bridge approach system to insure proper removal of water away from the structure and to minimize runoff infiltration into underlying fill layers (Lenke, 2006). Most frequently, maintenance of drainage structures and joints is lacking and must be improved in order to take full advantage of these design features (Lenke, 2006; Wu et al., 2006).

White, et al. (2005) performed a review of several drainage designs implemented by various State Agencies to compare different state-of-practices in the United States and these results are presented in Table 17.1. As per this study the most common practices were; porous backfill around a perforated drain pipe; geotextiles wrapped around the porous fill; and vertical geo-composite drainage system. White et al. (2005) also conducted a comprehensive study in a case of lack of maintenance of drainage structures, such as clogged or blocked drains; animal interaction; and deterioration of joint fillers, gutters and channels. The study showed that many problems occurred due to the lack of maintenance, resulting in numerous and costly repair operations. White et al. (2005) also pointed out some potential causes of bridge approach

TABLE 17.1 Drainage Method Used by Various States

State	Porous Fill	Geotextile	Geocomposite Drainage System
Iowa	X	-	-
California	X	X	X
Colorado	-	X	X
Indiana	X	X	-
Louisiana	X	X	X
Missouri	-	X	X
Nebraska	-	X	X
New Jersey	X	X	X
New York	-	-	X
North Carolina	X	X	-
Oklahoma	X	X	-
Oregon	X	X	-
Tennessee	X	X	-
Texas	X	X	-
Washington	X	-	-
Wisconsin	X	X	-

Source: Data from White, D. et al., CTRE Project 02-118, Iowa State University, Ames, IA, 2005.

settlement discovered during the maintenance activities. For example, they mentioned that the loose and not properly compacted backfill materials can cause poorly performing approach slabs. Coring operations revealed that voids are highest near the bridge abutment and decreased with distance with void sizes ranging from 0.5 to 12 in. Snake cameras used at sub-drain outlets demonstrated that most of the investigated subdrains were not functioning properly. The subdrains were either dry, with no evidence of water, or blocked with soil fines and debris or had collapsed. Some of these problems are attributed to erosion-induced movements in the fill material from moisture infiltration. This signifies the need for constant maintenance of joints and drains so that infiltration into the soil layers will be low. Along with the maintenance, reconstruction or rehabilitation of distressed approach slabs is very necessary.

Lenke (2006) suggested that to prevent stress buildup at the expansion joints between the bridge structure, the approach slab, and the pavement system, a good maintenance by cleaning and replacement (when necessary) is required. Such stresses cannot only cause damage to the deck and the abutment, but can also cause distortions of the approach slab.

17.5.2 Replacement Method

Highly deteriorated approach slabs due to the formation of a bump are mostly replaced with the new approach slabs. This process is the most expensive and often results in frequent closure of lanes, traffic congestion, and so on. A new research project has been initiated by the California Department of Transportation (Chen and Chai, 2010) to examine different replacement alternatives for deteriorated approach slabs. In this project, prefabricated fiber reinforced polymer (FRP) decks as well as FRP grid forms and rebars were investigated as replacement options. Full scale approach slabs were tested under simulated wheel loads. The performance of the approach slabs was also examined under simulated washout conditions. Figure 17.8 shows the test schematic.

17.5.3 Mud/Slab Jacking

Mud/slab jacking is a quick and economical technique of raising a settled slab section to a desired elevation by pressure injecting cement grout or mud-cement mixtures under the slabs (EM 1110-2-3506, January 20, 1984). According to EM 1110-2-3506, slab jacking is used to improve the riding qualities of the surface of



FIGURE 17.8 Simulated approach slab deflection by UC Davis research team (<http://cee.engr.ucdavis.edu/faculty/chai/Research/ApproachSlab/ApproachSlab.html>).

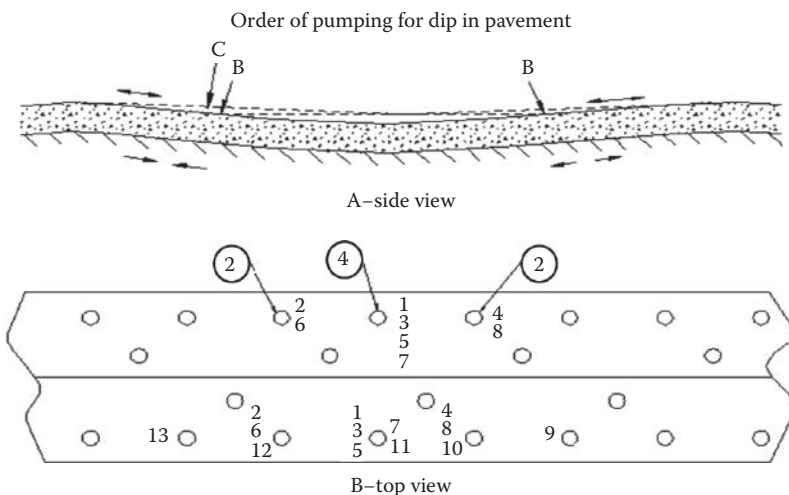


FIGURE 17.9 Mud-jacking injection sequences. (From Bowders, J. et al., *Project Rep. No. R199-029*, Missouri Department of Transportation, Jefferson, MO, 2002.)

the pavement, prevent impact loading over the irregularities by fast-moving traffic, correct faulty drainage, prevent pumping at transverse joints, lift or level other structures, and prevent additional settlement.

In this method, the mud grout is prepared using the topsoil which is free from roots, rocks and debris mixed with cement and enough water to produce a thick grout. This grout is injected to fill the void spaces underneath the approach slab through grout holes made through the approach slabs (Bowders et al., 2002). The injection is performed in a systematic manner to avoid cracks on the approach slab as shown in Figure 17.9. Precautionary measures need to be taken near to side retaining walls and abutment walls (Luna et al., 2004).

Even though this technique has been successfully adopted by several states including Kentucky, Missouri, Minnesota, North Dakota, Oklahoma, Oregon, and Texas for lifting the settled approach slabs, the mud/slab jacking can be quite expensive. Mud jacking may also cause drainage systems next to the abutment to become clogged, and is difficult sometimes to control the placement of the material (Dupont and Allen, 2002). Other difficulties, including the limited spread of grout into voids, large access holes which must be filled and lack of sufficient procedural process made this technique as uneconomical (Soltesz, 2002). Abu al-Eis and LaBarca (2007) reported that the cost of this technique was between \$40 and \$60 per one square yard of pavement used based on two test sections constructed in Columbia and Dane counties in Wisconsin.

17.5.4 Grouting

17.5.4.1 Pressure Grouting under the Slab

The presence of voids beneath the approach slab can lead to instability, cracking, sinking and pounding problems (Abu-Hejleh et al., 2006). In order to mitigate the problem, pressure grouting is commonly used for bridge approach maintenance practice as a preventive measure (White et al., 2005, 2007). Pressure grouting under the slab is used to fill the voids beneath the approach slab through injection of flowable grout, without raising the slab (Abu-Hejleh et al., 2006).

According to White et al. (2007), undersealing the approach slab by pressure grouting normally has two operations within the first year after completion of approach pavement construction. The first operation is done within the first 2–6 months, while the second one is employed within 6 months after the first undersealing. The grout mix design consists of Type 1 Portland cement and Class C fly ash at a ratio of 1:3. Water is also added to the grouting material to achieve the specified fluidity (Buss, 1989). Moreover, in order to avoid the lifting of the approach slab, grout injection pressures are kept to less than 35 kPa (White et al., 2007).

Abu-Hejleh et al. (2006) stated that the construction techniques of this method are to drill 1 7/8" holes through the concrete or asphalt approach slabs using a rectangular spacing. The depth is determined by the ease of driving the stinger or outlet tube, which is pounded into the hole (Abu-Hejleh et al., 2006). A fence post pounder is used to hammer the stinger and extension pieces into the soil (Abu-Hejleh et al., 2006). As the stinger is pounded down, the operator can determine if the soil is loose or soft and if there are voids under the slab.

Although grouting under the approach slab is commonly used for bridge approach settlement as a mitigation method, White et al. (2007) stated that the grouting is not a long term solution for this problem. The grouting does not prevent further settlement or loss of backfill material due to erosion (White et al., 2005, 2007).

17.5.4.2 Compaction or High Pressure Grouting

Compaction grouting is a method for improving the soil by densifying loose and liquefaction soils and resulting in increasing the soil strength (Miller and Roykroft, 2004). The compaction grouting is a physical process, involving pressure-displacement of soils with stiff, low-mobility sand-cement grout (Strauss et al., 2004).

According to the ASCE Grouting Committee (1980), the grout generally does not enter the soil pores but remains as a homogenous mass that gives controlled displacement to compact loose soils, gives controlled displacement for lifting of structures, or both.

The compaction grouting can be used to stabilize both shallow and deep seated soft layers (Abu-Hejleh et al., 2006). Section 211 of the CDOT Standard Specifications (Miller and Roykroft, 2004) stipulates that the grouting must be low slump and low mobility, with a high internal friction angle. When the technique is used in weak or loose soils, the grout typically forms a coherent “bulb” at the tip of the injection pipe; thus, the surrounding soil is compacted and/or densified. For relatively free draining soils including gravel, sands, and coarse silts, the method has proven to be effective (Abu-Hejleh et al., 2006).

17.5.4.3 Urethane Injection Technique

The Urethane injection technique was first developed in 1975 in Finland to lift and underseal concrete pavements and was subsequently adopted in several U.S. states to lift concrete pavements (Abu al-Eis and LaBarca, 2007). In this process, a resin manufactured from high density polyurethane is injected through grout holes (5/8 in. diameter) made through the approach slab to lift, fill the voids and to underseal the slab (Abu al-Eis and LaBarca, 2007). The injected resin will gain 90% of its maximum compressive strength (minimum compressive strength is 40 psi) within 15 min. Once the voids are filled, the grout holes are filled with inexpensive grout material. Elevated levels are taken before and after the process to ensure the required lifting is achieved (Abu al-Eis and LaBarca, 2007).

As reported by Abu al-Eis and LaBarca (2007), the Louisiana Department of Transportation successfully adopted this technique for two different bridge approaches and observed that the international roughness index (IRI) values were reduced by 33% to 57% after monitoring for 4 years. This method involves the precise liquid injection of high-density polyurethane plastic through small (5/8") holes drilled in the sagging concrete slab (Abu al-Eis and LaBarca, 2007). Once it is applied, the material expands to lift and stabilize the slab, while filling voids in the underlying soil and undersealing the existing concrete (Concrete Stabilize Technology Inc.; <http://www.stableconcrete.com/uretek.html>). Based on the manufacturer-provided information, this technology is simple and rapid. It can lead to a permanent solution and also can resist erosion and compression over a time period.

Brewer et al. (1994) first evaluated the Urethane injection technique to raise bridge approach slabs in Oklahoma. They reported that three out of six test slabs were cracked during or after the injection and, in one case, the PCC slab broke in half during the injection. The Michigan Department of Transportation reported that this technique provided a temporary increase in base stability and improvement in ride quality for 1 year (Opland and Barnhart, 1995). Soltesz (2002) noticed that the Urethane treatment was successful even after 2 years where the injection holes were properly sealed. The Oregon Department of Transportation researchers reported that the Urethane material was able to penetrate holes with diameters as small as 1/8 in., which was an added advantage of this technique, to fill the minor pores of the subbase and lift the pavement slabs (Soltesz, 2002).

Abu al-Eis and LaBarca (2007) reported that the cost of this technique was between \$6 to \$7 per pound of foam used, which was calculated based on two test sections constructed in Columbia and Dane counties in Wisconsin. They summarized the cost comparison of this technique with other slab lifting methods (as shown in Table 17.2) and concluded that this technique is expensive when compared to other methods if calculated based on direct costs. They also reported that this technique is very fast, and traffic lanes can be opened immediately after the treatment. The amount of urethane resin used in each project is also questionable, as this quantity is directly used in the cost analysis. Considering this fact, TXDOT amended its Special Specification 3043-001, which requires a Special Provision for determining the quantity of polymer resin used for "Raising and Undersealing Concrete Slabs." Regarding the Special Specification 3043-001, the quantity of the resin utilized will be calculated by one of the following methods:

1. Payment will be made according to the actual quantity of polymer resin used in the work by using certified scales to weigh each holding tank with components before and after each day's work.
2. Payment will be made according to the actual quantity of polymer resin used in the work, which will be determined by measuring the depth of polymer resin in the holding tanks before and after each day's work. A Professional Engineer and a site engineer must approve the calculation method, which is based on the certified measured volume of each tank and the unit weight of each component.

Several districts in Texas use this method as a remediation method, and based on the present research contacts, these methods are deemed effective. Figure 17.10 shows the schematic and a photographic view of the bridge site with the void developed under the approach slab. The cause of the problem was identified as the erosion of the granular backfill material under the approach slab.

TABLE 17.2 Cost Comparisons for Four Slab Faulting Repair Methods

Location	Method	Total Cost	Cost per yd ²	Days to Complete
I-30 (80 yd ²)	URETEK	\$19,440	\$243	0.75
	Slab replacement	\$34,000	\$425	3
	HMA overlay	\$3,630	\$45	1
	Mud-jacking	\$3,000	\$38	1
USH 14 (53.4 yd ²)	URETEK	\$6,260	\$117	0.5
	Slab replacement	\$22,670	\$425	3
	HMA overlay	\$3,375	\$63	1
	Mud-jacking	\$3,000	\$56	1

Figure 17.11 depicts the position of the approach slab during and after the injection process. During and immediately after the injection process, researchers observed a few minor hairline cracks on the approach slab as shown in Figure 17.12. The minor cracks on the surface of the approach slab during this injection operation are relatively common and will not lead to further distress of the approach slab. The post-performance of this method is very crucial to address the expansion of the hairline cracks and movements of repairing approach slabs. A simple field monitoring study, including elevation surveys and visual inspection of these minor cracks, would reveal the effectiveness of this technique.

As per the discussions with TxDOT engineers in Houston, the process was quite effective. Several Houston sites that were visited were repaired utilizing this injection method 10 years ago, and they are

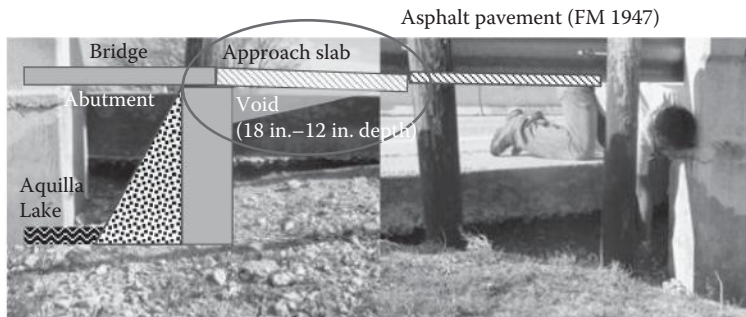


FIGURE 17.10 Schematic of the approach slab with developed void under the bridge at FM 1947 Hill County, TX.



FIGURE 17.11 Position of approach slab during and after the urethane injection process.



FIGURE 17.12 Hairline crack observed on the approach slab during the urethane injection.

still functioning adequately. The work reported in the Houston District was instrumental in the development of the TxDOT Special Specification for the use of the urethane injection method for lifting the distressed approach slabs.

17.5.4.4 Flowable Fill

Flowable fill or controlled low-strength material is defined by the ACI Committee 229 as a self-compacting, cementitious material used primarily as a backfill in lieu of compacted fill. The flowable fill has other common names, such as unshrinkable fill, controlled density fill, flowable mortar, flowable fill, plastic soil-cement and soil-cement slurry (Du et al., 2006). This controlled low-strength filling material is made of cement, fly ash, water, sand, and typically an air-entraining admixture (NCHRP, 597). A significant requisite property of flowable fill is the self-leveling ability, which allows it to flow; no compaction is needed to fill voids and hard-to-reach zones (Abu-Hejleh et al., 2006). Therefore, the flowable fill is commonly used in the backfill applications, utility bedding, void fill and bridge approaches (Du et al., 2006).

A primary purpose of using flowable fill is as a backfill behind the abutment. CDOT has used the flowable fill backfill behind the abutment wall in an effort to reduce the approach settlements since 1992 (Abu-Hejleh et al., 2006). The other new applications for the flowable fill are for use as a subbase under bridge approaches and as repair work of the approaches (Du et al., 2006). Historically, the application of using flowable fill as a subbase was first employed in Ohio by ODOT (Brewer, 1992).

In Iowa, the flowable fill is a favorable backfill used as a placement under the existing bridge, around or within box culverts or culvert pipes, and in open trenches (Smadi, 2001). Smadi (2001) also cited that the advantages of flowable mortar are not only due to its fluidity, but also due to its durability, requiring less frequent maintenance. Moreover, the flowable mortar is also easily excavated. Therefore, the maintenance work, if required, can be done effortlessly (Smadi, 2001). Figure 17.13 shows details of flowable mortar used under a roadway pavement.

In Texas, the flowable fill was used for the first time for repairing severe settlements of bridge approaches at the intersection of I-35 and O'Conner Drive in San Antonio in 2002 by TxDOT (Folliard et al., 2008; Du et al., 2006). For this practice, TxDOT used a specialized mixture using flowable fill, which consisted

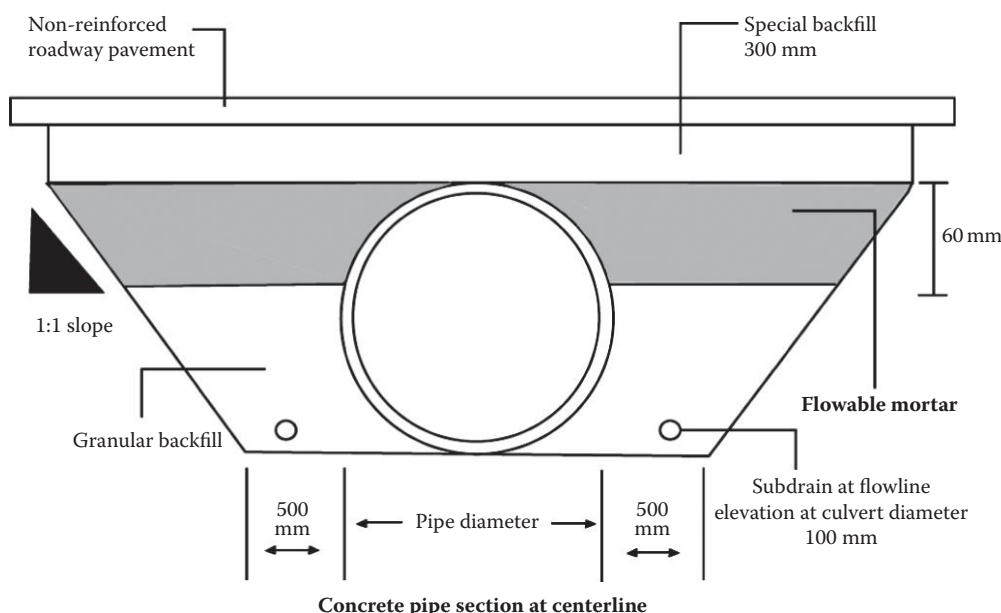


FIGURE 17.13 The flowable mortar used under a roadway pavement. (From Smadi, O., http://www.ctre.iastate.edu/PUBS/tech_news/2001/julaug/flowable_mortar.pdf, 2001.)

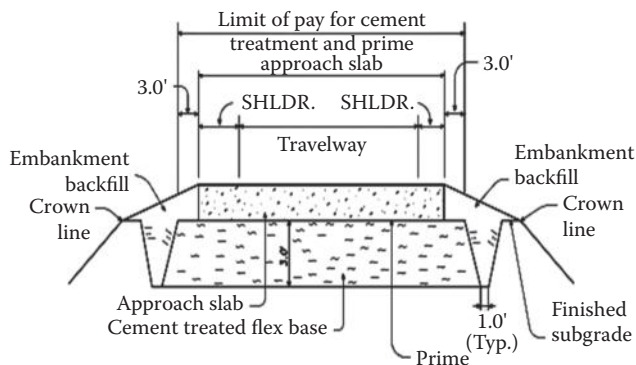


FIGURE 17.14 The flowable fill used as a base material. (From Du, L., Arellano et al., *ACI Material Journal*, September–October, 2006.)

of sand, flyash and water; no cement. The compressive strength of cored samples indicated that the long-term strength and rigidity of the flowable fill were strong enough to serve this purpose (Folliard et al., 2008). After the mixture proportions were adjusted to have adequate flowability for the application, the flowable fill was very successful in repairing the approaches (Du et al., 2006). Recently, the flowable fill was used in the Fort Worth District in place of a flexible base beneath the approach slab. The 3 ft. deep flex base is prepared with Type 1 cement (2.4% by weight) as a base material, as shown in Figure 17.14.

17.5.5 Other Methods

Several other techniques are also available to mitigate the settlement problem of the approach slab and are discussed in the following.

17.5.5.1 Precambering

If the approach pavement settlement cannot be controlled economically, a pre-cambered roadway approach may be applied (Tadros and Benak, 1989). Hoppe (1999) recommended implementing pre-cambering of bridge approaches for up to a 1/125 longitudinal gradient. The pre-cambering is used to accommodate the differential settlement that will inevitably occur between a structure constructed on deep foundations and adjoining earthworks.

Briaud et al. (1997) recommended pre-cambering with gradient values of less than 1/200 of the approach slab length to compensate for the anticipated post-construction settlements. The pre-cambered design utilizes a paving notch that supports a concrete slab. The notch must be effectively hinged, which allows the concrete slab to move radially (see Figure 17.15). The flexible pavement over the slab will absorb some movement below it, but not to a great extent (Briaud et al., 1997). The pre-cambered approach system also requires an accurate assessment of the settlement potential (if possible). The pre-cambered approach design could be specified in situations where time is not available for more conventional settlement remediation, such as preloading, wick drains, and others (Luna, 2004).

Wong and Small (1994) conducted laboratory tests to investigate the effects of constructing approach slabs with an angle from the horizontal on reducing the bump at the end of the bridge. It was found that horizontal slabs suffered a rapid change in surface deformation with the formation of obvious bumps, while pre-cambering the slabs with angles of 5° to 10° provided a smoother transition.

17.5.5.2 Lightweight Fill Materials

The lightweight materials such as Expanded Polystyrene (EPS) Geofoam and Expanded Clay Shale (ECS) (Saride et al., 2010) can be used either as a construction embankment fill material for new bridge approach embankments or can be used as a fill material during the repair of distressed approach slabs.

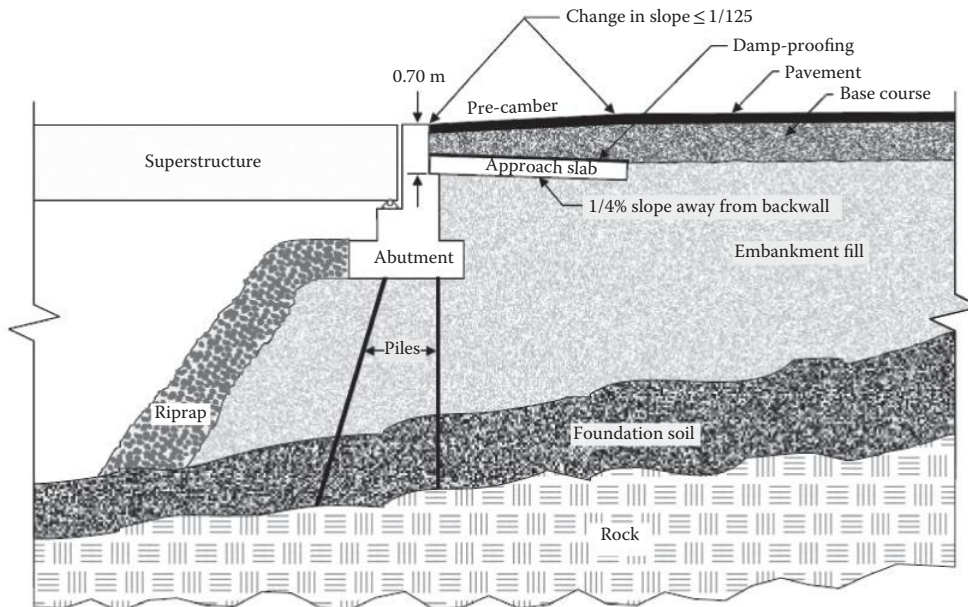


FIGURE 17.15 Pre-cambered approach design. (From Hoppe, E. J., Rep. No. VTRC 00-R4, Virginia Transportation Research Council, Charlottesville, VA, 1999.)

17.5.5.3 Expanded Polystyrene (EPS) Geofoam

Expanded Polystyrene (EPS) Geofoam is a lightweight material made of rigid foam plastic that has been used as fill material around the world for more than 30 years. This material is approximately 100 times lighter than conventional soils and at least 20–30 times lighter than any other lightweight fill alternatives. The added advantages of EPS Geofoam, including reduced loads on underlying subgrade, increased construction speed, and reduced lateral stresses on retaining structures, has increased the adoptability of this material to many highway construction projects. More than 20 state DOTs including Minnesota, New York, Massachusetts, and Utah adopted the EPS Geofoam to mitigate the differential settlement at the bridge abutments, slope stability, and alternate construction on fill for approach embankments. They reported high success in terms of ease and speed of construction and reduced total project costs.

Lightweight EPS Geofoam was used as an alternate fill material at the Kaneohe Interchange in Oahu, Hawaii while encountering a 6 m thick layer of very soft organic soil during construction. 17,000 m³ of EPS Geofoam was used to support a 21 m high embankment construction (Mimura and Kimura, 1995). They reported the efficiency of the material in reducing the pre- and post-construction settlements.

17.6 Mitigation Techniques for New Approach Slabs

The following techniques can be adopted for mitigating potential settlements expected in new bridges:

- Improvement of foundation soil
- New foundation technologies
- Improvement of backfill material
- Effective drainage and erosion control methods

A comprehensive summary of the above methods can be found in Puppala et al. (2012).

TABLE 17.3 Summary of Ground Improvement Methods Based on Soil Type

Technique	Cohesionless Soils	Cohesive Soils
Excavation and replacement	ρ	α
Preloading w or w/o surcharge	α	α
Dynamic compaction	α	α
Grouting	α	α
Wick drains	ρ	α
Compaction piles	α	ρ
Gravel columns	α	ρ
Lime treatment	ρ	α
Stone columns	ρ	α
Soil reinforcement	α	α
Geopier	α	α

17.6.1 Improvement of Embankment Foundation Soil

The behavior of foundation soil beneath the embankment fill is one of the most important factors in the better performance of bridges (Wahls, 1990). Generally, if the foundation soil is a granular material type, such as sand, gravel, and rock, which do not undergo long-term settlements, then the differential settlement between the bridge structure and the roadway embankment can be negligible. On the other hand, if the approach embankments are constructed on cohesive soils such as normal or under consolidated clays, then those soils can undergo large settlements either from primary and/or secondary consolidation settlements. These settlements will subsequently lead to the settlement of embankment structures and the formation of the bumps or approach settlement problems leading to poor performance of the bridge approaches. Several attempts have been made by many researchers both from the U.S. and abroad to mitigate these unequal settlements arising from highly compressible embankment fills (Wahls, 1990; Dupont and Allen, 2002; White et al., 2005; Abu-Hejleh et al., 2006; Hsi, 2008). Table 17.3 summarizes these ground improvement techniques, not limited to one, for each foundation soil in a chronological order of their importance and the level of settlement problem. Most of the combined techniques are chosen for a particular field situation. For example, preloading with the installation of wick drains will lead to faster consolidation settlement of weak soft foundation soils. These techniques are again divided into three subcategories such as mechanical, hydraulic, and reinforcement techniques based on the function of each stabilization technique (Table 17.4).

17.6.2 New Foundation Technologies

17.6.2.1 Geopiers

Geopiers, sometimes referred to as short aggregate piers, are constructed by drilling the soft ground and ramming selected aggregate into the cavity in lifts, using a beveled tamper (Lien and Fox, 2001). The basic concept in this technique is to push/tamp the aggregate vertically as well as laterally against the soft soil to improve the stiffness against compressibility between the piers. These short piers can also allow radial drainage, due to their open-graded stone aggregate structure, to accelerate the time dependent consolidation process and also to relieve excess pore water pressures generated in the soft soil (Lien and Fox, 2001).

17.6.2.2 Deep Soil Mixing (DSM)

Deep Soil Mixing (DSM) technology was pioneered in Japan in the late 1970s, and over many years, has gained popularity in the United States in the field of ground improvement (Barron et al., 2006;

TABLE 17.4 Summary of Ground Improvement Techniques Based on the Function

Embankment on Soft Foundation Soil Improvement Techniques		
Mechanical	Hydraulic	Reinforcement
Excavation and replacement	Sand drains	<p>Columns</p> <p>Stone and lime columns</p> <p>Geopiers</p> <p>Concrete injected columns</p> <p>Deep soil mixing columns</p>
Preloading and surcharge	Prefabricated drains	<p>Deep foundations</p> <p>In-situ: Compacted piles</p> <p>CFA piles</p> <p>Driven piles: Timber and concrete piles</p>
Dynamic compaction	Surcharge loading	<p>Geosynthetics</p> <p>Geotextiles/geogrids</p> <p>Geocells</p>

Puppala et al., 2004; Cai et al., 2009). DSM is a process to improve the soil by injecting grout through augers that mix in with the soil forming in-place soil-cement columns (Barron et al., 2006). Recently, the cement binder has been replaced with many other cementitious compounds such as lime, flyash, or a combination of any two compounds. Hence, in a broader sense, the DSM technique is an in-situ mixing of stabilizers such as quicklime, cement, lime-cement, or ashes with soft and/or expansive soils to form deep columns to modify weak subgrade soils (Porbaha, 1998, 2000).

17.6.2.3 Concrete Injected Columns

Concrete injected columns (CICs) are an innovative technique where a soil displacement pile mechanism is used to create in-situ concrete columns without reinforcement (Hsi, 2007, 2008). CICs are installed by inserting a displacement tool (auger) into the soft soil and then rotating and pushing the tool. Upon reaching the final depth, concrete is pumped through the hollow stem of the tool during extraction. Inserting reinforced casing into the CICs is optional, and the depth to which the reinforcement casing can be installed is limited (Hsi, 2008). Typically these columns are prepared with a 19.7 in. (500 mm) diameter and the length of these columns can be extended to reach a stiff strata or shallow bed rock. This technique is widely used to reinforce the very soft-to-soft-foundation soils (Hsi, 2007). CICs were recently adopted to control the excessive long-term settlements of approach embankments constructed on estuarine and marine soft clays along an upgrade to the Brunswick Heads—Yelgun Pacific Highway in Australia.

17.6.2.4 Continuous Flight Auger Cast Piles (CFA)

Continuous Flight Auger Cast Piles (CFA) are installed by rotating a continuous-flight hollow shaft auger into the soil to reach a specified depth. High strength cement grout, sand, or concrete is pumped under pressure through the hollow shaft as the auger is slowly withdrawn. If this process uses pressure grouting, these CFA piles are sometimes termed as auger pressure grouted (APG) piles. The resulting grout column hardens and forms an auger cast pile (Neely, 1991; Brown et al., 2007). Reinforcing, when required, must be installed while the cement grout is still fluid, or in the case of full length single reinforcing bars, through the hollow shaft of the auger prior to the withdrawal and grouting process (Neely, 1991; Brown et al., 2007).

17.6.3 Improvement of Approach Embankment/Backfill Material

The bridge approach embankment has two functions: first, to support the highway pavement system, and second, to connect the main road with the bridge deck. Most of the approach embankments are normally constructed by conventional compaction procedures using materials from nearby roadway excavation or a convenient borrow pit close to the bridge site. This implies that the serviceability of the embankment, in the aspects of slope stability, settlement, consolidation, or bearing capacity issues, depends on the geotechnical properties of the fill materials (Wahls, 1990). In addition, since the embankment must provide a good transition between the roadway and the bridge, the standards for design and construction considerations, both in materials' quality requirements and compaction specifications, must be specified in order to limit the settlement magnitude within a small acceptable degree (Wahls, 1990).

Generally, the materials for embankment construction should have the following properties (White et al., 2005): easily compacted, not time-dependent, not sensitive to moisture, provides good drainage, erosion resistant, shear resistant. Dupont and Allen (2002) cited that the most successful method for constructing the approach embankments is to select high quality fill material, with the majority of them being a coarse granular material with high internal frictional characteristics.

Mechanically Stabilized Earth (MSE) walls have been rapidly developed and widely used since the 1970s (Wahls, 1990). The MSE method is a mitigation technique that involves the mechanical stabilization of soil with the assistance of tied-back walls. In this technique, footing of the bridge is directly supported by backfill; therefore, a reinforcement system in the upper layer of the embankment where the backfill is most affected by the transferred load from the superstructure must be carefully designed (Wahls, 1990). On the contrary, the facing element of the wall does not have to be designed for the loading since the transferred load from the bridge in the MSE scheme does not act on the MSE wall (Wahls, 1990).

Geosynthetic Reinforced Soil (GRS) is recommended as a method to achieve a backfill compaction at the optimal moisture content, especially for a coarse-grained backfill material (Abu-Hejleh et al., 2006). The GRS is a geosynthetic-reinforced soil structure constructed either vertically or horizontally in order to minimize the uneven settlements between the bridge and its approach. Abu-Hejleh et al. (2006) discovered that with the use of GRS, the monitored movements of the bridge structure were smaller than those anticipated in the design or allowed by performance requirements. In addition, they also stated that with the use of GRS systems, post-construction movements can be reduced substantially, thus the bump problem at the bridge transition is minimized.

Another concept for reducing the vertical loading or stress from the embankment as it exerts itself on the foundation subsoil is the use of lightweight material as an embankment fill material. The reduction of embankment weight or load increases the stabilities of the embankment and also reduces the compression of the underlying foundation soil. As a result, the settlement potential of the embankment will be decreased. The lightweight fills such as lightweight aggregate, expanded polystyrene, lightweight concrete, or others can be used to achieve this benefit (Luna et al., 2004; Dupont and Allen, 2002; Mahmood, 1990). Based on the surveys conducted by Hoppe (1999) approximately 27% of responding DOTs have already experimented with the use of non-soil materials behind bridge abutments.

17.6.4 Design of Bridge Foundation Systems

The bridge foundation is considered a major factor in bridge structure design. Bridges can be supported either by shallow or deep foundation systems (Wahls, 1990). In both cases, the foundations should be able to carry the loads from the above superstructures and the traffic volumes, but also limit the horizontal and vertical movement of the abutment to acceptable levels (Wahls, 1990). The selection of a safe and economical foundation system requires consideration of structural loads, environmental factors, subsurface conditions, bedrock types and depths, performance criteria, construction methods, and economics (ODOT, 2005).

Spread footings, driven piles, and drilled shafts are generally used as bridge foundations. According to Wahls (1990), the spread footing has its advantage over the deep foundation because of its inexpensive cost. However, the uncertainties in the performance prediction and the potential for scouring make shallow foundations an unattractive choice for a bridge foundation system. Moreover, since the compaction of backfill near the abutment is difficult to achieve, the possibilities of loads from the superstructure and traffic volume stressing the poorly compacted backfill and contributing to the settlement of bridge approaches can be high (Wahls, 1990).

For those reasons, the deep foundations, including driven piles or drilled shafts, are preferred to support the bridges. The deep pile foundations have been demonstrated to be the most efficient means of transferring heavy loads from superstructures to substructures and bearing materials without significant distress from excessive settlement (Abu-Hejleh et al., 2006). Hopkins (1985) cited that the settlement of the bridge abutment resting on pile foundations is usually negligible. However, due to the fact that the bridges supported by pile foundations do not usually settle as much as the approach embankments, the differential settlement between these two adjacent structures can lead to the bump problems at the bridge approach. Hopkins and Deen (1970) stated that the differential settlement between the abutment and the approach slab is usually high for pile support abutments.

17.6.5 Effective Drainage and Erosion Control Methods

According to Mekkawy et al. (2005) and White et al. (2005), insufficient drainage is another problem often attributed to the settlements near the bridge abutments. Water collected on the bridge pavement can flow into the underlying fill materials due to ineffective seals at the joints between the bridge approach slab and the abutments, and this infiltrated water can erode the backfill material. The material erosion can cause void development under the bridge abutments, resulting in the eventual settlements of the bridge approach slabs. Hence, the design of bridge approaches has to be incorporated with an efficient drainage system, such as providing drainage inlets at the end of a bridge deck to collect surface water before getting to the approach slab (Abu-Hejleh et al., 2006).

Also, additional surface or internal drainage to keep water off the slopes is recommended for correcting the superficial erosion of embankments (Wahls, 1990). Keeping the water away from the soil is a simple and a significant factor in reducing the settlement of the soil. Construction costs added to incorporate a good drainage system are not high when compared to the expensive maintenance costs that they might experience during the service life of the bridge (Dupont and Allen, 2002). Hence, all efforts should be made to design the bridge embankments with effective seals and good drainage conditions in and around the bridge structures.

Some of the recommendations reported in the literature to improve drainage conditions include the use of a large diameter surface drain and gutter system in the shoulder of the approach slab and use of a geo-composite vertical drainage system around the embankments with both drainage systems having the potential to increase the drainage capacity (White et al., 2005). This study also recommended the use of porous backfill material or limiting the percentage of fine particles in the fill material to reduce material plasticity and enhance drainage properties.

17.7 Summary

This chapter presented a thorough review for settlement at the bridge approach. The definition of the settlement of the bridge approach problem is first presented, followed by the magnitude of the bump tolerance. Afterward, major mechanisms causing the bump problem are introduced. The primary sources of the problem broadly divided into four categories are the material properties of the foundation and embankment, design criteria for bridge foundation, abutment and deck, construction supervision of the structures, and maintenance criteria.

The maintenance measures for distressed approach slabs are normally used as remedial measures after problems are detected. The most important techniques in this category are pressure grouting under the slab, slab-jacking or mud-jacking technique, the Urethane method, and compaction or high pressure grouting. It can be noted that many of these measures could also be applied for the improvement of backfill material in new bridge constructions. Various methods for new bridge approach slab design and soil improvements are also summarized in the chapter. More details on these methods can be found in Puppala et al. (2012).

References

- Abu al-Eis, K. and LaBarca, I. K. 2007. "Evaluation of the URETEK Method of Pavement Lifting." *Report No. WI-02-07*, Wisconsin Department of Transportation, Division of Transportation Systems Development, Madison, WI.
- Abu-Hejleh, N., Hanneman, D., White, D. J., and Ksouri, I. 2006. "Flow fill and MSE Bridge Approaches: Performance, Cost and Recommendations for Improvements." *Report No. CDOT-DTD-R-2006-2*. Colorado Department of Transportation, Denver, CO.
- Albajar, L., Gascón, C., Hernando, A., and Pacheco, J. 2005. "Transition Works of Step-Embankment. Approach to the State of the Art and Spanish Experiences", Technical Association of Roads, Ministry of Development, Madrid, Spain (In Spanish).
- Ardani, A. 1987. "Bridge Approach Settlement." *Report No. CDOT-DTP-R-87-06*, Colorado Department of Highways, Denver, CO.
- Arsoy, S., Barker, R. M., and Duncan, J. M. 1999. "The Behavior of Integral Abutment Bridges." *Report No. VTRC 00-CR3*, Virginia Transportation Research Council, Charlottesville, VA.
- ASCE Grouting Committee. 1980. "Preliminary Glossary of Terms Relating to Grouting." *ASCE Journal of Geotechnical Division*, 106(GT7), 803–815.
- Bakeer, M., Shutt, M., Zhong, J., Das, S., and Morvant, M. 2005. "Performance of Pile-Supported Bridge Approach Slabs." *Journal of Bridge Engineering*, 10(2), 228–237.
- Barron, R. F., Wright, J., Kramer, C., Andrew, W. H., Fung, H., and Liu, C. 2006. "Cement Deep Soil Mixing Remediation of Sunset North Basin Dam." *Proceedings of Dam Safety 2006*, Association of Dam Safety Officials.
- Bowders, J., Loehr, E., Luna, R., and Petry, T. M. 2002. "Determination and Prioritization of MoDOT Geotechnical Related Problems with Emphasis on Effectiveness of Designs for Bridge Approach Slabs and Pavement Edge Drains." *Project Report No. R199-029*, Missouri Department of Transportation, Jefferson, MO.
- Bozozuk, M. 1978. "Bridge Foundations Move." *Transportation Research Record* 678: Tolerable Movements of Bridge Foundations, Sand Drains, K-Test, Slopes, and Culverts, Transportation Research Board, National Research Council, Washington, D.C., pp. 17–21.
- Brewer, W. E. 1992. "The Design and Construction of Small Span Bridges and Culvert Using Controlled Low Strength Material (CLSM)." *FHWA/OH-93/014*, Ohio Department of Transportation, Columbus, p. 129.
- Brewer, W. B., Hayes, C. J., and Sawyer, S. 1994. "URETEK Construction Report." *Construction Report Number OK 94(03)*, Oklahoma Department of Transportation, Oklahoma City, OK.
- Briaud, J. L., James, R. W., and Hoffman, S. B. 1997. "NCHRP Synthesis 234: Settlement of Bridge Approaches (the bump at the end of the bridge)." *Transportation Research Board*, National Research Council, Washington, D.C., p. 75.
- Brown, D. A., Steve, D. D., Thompson, W. R., and Lazarte, C. A. 2007. "Design and Construction of Continuous Flight Auger (CFA) Piles." *Geotechnical Engineering Circular No. 8*, Federal Highway Administration, Washington, D.C.
- Burke, M. P. 1987. "Bridge Approach Pavements, Integral Bridges, and Cycle-Control Joints." *Transportation Research Record* 1113, TRB, National Research Council, Washington D.C., pp. 54–65.
- Burke, M.P. 1993. "Integral bridges: attributes and limitations." *Transportation Research Record*, 1393, 1–8, Transportation Research Board, 75th Annual Meeting, Washington, DC.

- Buss, W. E. 1989. "Iowa Flowable Mortar Saves Bridges and Culverts." *Transportation Research Record* 1234, TRB, National Research Council, Washington, D.C., pp. 30–34.
- Cai, G., Liu, S., Puppala, A. J., Tong, L. Y., Du, G. Y., and Fei, J. 2009. "Evaluation of Stabilization Effect of "T" Shaped Deep Mixing Column from SCPTU data." *Proceedings of the International Symposium on Ground Improvement Technologies and Case Histories (ISGI09)*, Singapore, December, 2009.
- Chen, Y. T. and Chai, Y. H. 2010. "Evaluation of Structural Performance of Bridge Approach Slabs." Report to Caltrans under Contract Number 59A0485. Sacramento, CA: California Department of Transportation, Engineering Services Center.
- Chen, Y. T. and Chai, Y. H. 2011. "Experimental Study on the Performance of Approach Slabs under Deteriorating Soil Washout Conditions," *Journal of Bridge Engineering*, 16, p. 624.
- Das, S. C., Bakeer, R., Zhong, J., and Schutt, M. 1990. "Assessment of Mitigation Embankment Settlement with Pile Supported Approach Slabs." Louisiana Transportation and Research Center, Baton Rouge, LA.
- Du, L., Arellano, M., Folliard, K. J., Nazarian, S., and Trejo, D. 2006. "Rapid-Setting CLSM for Bridge Approach Repair: A Case Study." *ACI Material Journal*, September–October, 312–318.
- Dunn, K. H., Anderson, G. H., Rodes, T. H., and Zieher, J. J. 1983. "Performance Evaluation of Bridge Approaches." Wisconsin Department of Transportation.
- Dupont, B. and Allen, D. 2002. "Movements and Settlements of Highway Bridge Approaches." *Report No. KTC-02-18/SPR-220-00-1F*, Kentucky Transportation Center Report, Lexington, KY.
- Folliard, K. J., Du, L., Trejo, D., Halmen, C., Sabol, S., and Leshchinsky, D. 2008. "Development of a Recommended Practice for Use of Controlled Low-strength Material in Highway Construction." *Report No. NCHRP 597*, Transportation Research Board, Washington, D.C.
- Greimann, L. F., Abendroth, R. E., Johnson, D. E., and Ebner, P. B. 1987. "Pile Design and Tests for Integral Abutment Bridges." *Final Report Iowa DOT Project HR 273*, ERI Project 1780, ISU-ERI-Ames-88060, Ames, IA.
- Ha, H., Seo, J., and Briaud, J.-L. 2002. "Investigation of Settlement at Bridge Approach Slab Expansion Joint: Survey and Site Investigations." *Report No. FHWA/TX-03/4147-1*, Texas Transportation Institute, Texas A & M University, College Station, TX.
- Hopkins, T. C. 1973. "Settlement of Highway Bridge Approaches and Embankment Foundations." *Report No. KYHPR-64-17; HPR-1(8)*, Kentucky Transportation Center, Lexington, Kentucky, p. 40.
- Hopkins, T. C. 1969. "Settlement of Highway Bridge Approaches and Embankment Foundations." *Report No. KYHPR-64-17; HPR-1(4)*, Kentucky Transportation Center, Lexington, KT.
- Hopkins, T. C. 1985. "Long-Term Movements of Highway Bridge Approach Embankments and Pavements." University of Kentucky, Transportation Research Program.
- Hopkins, T. C. and Deen, R. C. 1970. "The Bump at the End of the Bridge." *Highway Research Record No. 302*, Highway Research Board, National Research Council, Washington, D.C., pp. 72–75.
- Hoppe, E. J. 1999. "Guidelines for the Use, Design, and Construction of Bridge Approach Slabs." *Report No. VTRC 00-R4*, Virginia Transportation Research Council, Charlottesville, VA.
- Hoppe, E. J. and Gomez, J. P. 1996. "Field Study of an Integral Backwall Bridge." *Report No. VTRC 97-R7*, Virginia Transportation Research Council, Charlottesville, VA.
- Horvath, J. S. 2000. "Integral Abutment Bridges: Problem and Innovative Solutions Using EPS Geofoam and Other Geosynthetics." *Research Report No. CE/GE-00-2*, Manhattan College, Bronx, New York.
- Horvath, J. S. 2005. "Integral-Abutment Bridges: Geotechnical Problems and Solutions Using Geosynthetics and Ground Improvement." *IAJB 2005—The 2005 FHWA Conference on Integral Abutment and Jointless Bridges*, 16–18 March, Baltimore, MD.
- Hsi, J. and Martin, J. 2005. "Soft Ground Treatment and Performance, Yelgun to Chinderah Freeway, New South Wales, Australia." In *Ground Improvement-Case Histories*, Elsevier Geo-Engineering Book Series, Volume 3, 563–599.
- Hsi, J. P. 2007. "Managing Difficult Ground-Case Studies." *Proceedings of First Sri Lankan Geotechnical Society International Conference on Soil and Rock Engineering*, Colombo.
- Hsi, J. P. 2008. "Bridge Approach Embankments Supported on Concrete Injected Columns." *Proceedings of the Challenge of Sustainability in the Geoenvironment*, ASCE, Geocongress 08, New Orleans, LA.

- James, R. W., Zhang, H., and Zollinger, D. G. 1991. "Observations of Severe Abutment Backwall Damage." *Transportation Research Record* 1319, Transportation Research Board, pp. 55–61.
- Jayawickrama, P., Nash, P., Leaverton, M., and Mishra, D. 2005. "Water Intrusion in Base/Subgrade Materials at Bridge Ends." *TxDOT Report, FHWA/TX-06-0-5096-1*, Texas Tech University, Lubbock, TX.
- Kramer, S. L. and Sajer, P. 1991. "Bridge Approach Slab Effectiveness." *Final Report*, Washington State Department of Transportation, Olympia, WA.
- Kunin, J. and Alampalli, S. 2000. "Integral Abutment Bridges: Current Practice in United States and Canada." *ASCE Journal of Performance of Constructed Facilities*, 14(3), 104–111.
- Laguros, J. G., Zaman, M. M., and Mahmood, I. U. 1990. "Evaluation of Causes of Excessive Settlements of Pavements Behind Bridge Abutments and their Remedies; Phase II. (Executive Summary)." *Report No. FHWA/OK 89 (07)*, Oklahoma Department of Transportation.
- Lenke, L. R. 2006. "Settlement Issues-Bridge Approach Slabs." *Report No. NM04MNT-02*, New Mexico Department of Transportation.
- Lien, B. H. and Fox, N. S. 2001. "Case Histories of Geopier® Soil Reinforcement for Transportation Applications." *Proceedings of Asian Institute of Technology Conference*, Bangkok, Thailand.
- Long, J. H., Olson, S. M., and Stark, T. D. 1998. "Differential Movement at Embankment/Bridge Structure Interface in Illinois." *Transportation Research Record No. 1633*, Transportation Research Board, Washington, D.C., pp. 53–60.
- Luna R., Jonathan, L. R., and Andrew, J. W. 2004. "Evaluation of Bridge Approach Slabs, Performance and Design." *Report No. RDT 04-010*, Department of Civil, Architectural and Environmental Engineering, University of Missouri, Rolla.
- Mahmood, I. U. 1990. "Evaluation of Causes of Bridge Approach Settlement and Development of Settlement Prediction Models." *PhD Thesis*, University of Oklahoma, Norman, OK.
- Mekkawy, M., White, D. J., Souleiman, M. T., and Sritharan, S. 2005. "Simple Design Alternatives to Improve Drainage and Reduce Erosion at Bridge Abutments." *Proceedings of the 2005 Mid-Continent Transportation Research Symposium*, Ames, IA.
- Miller, E. A. and Roykroft, G. A. 2004. "Compaction Grouting Test Program for Liquefaction Control." *Journal of Geotechnical and Geoenvironmental Engineering*, ASCE, 130(4), 355–361.
- Mimura, C. S. and Kimura, S. A. 1995. "A Light-Weight Solution." *Proceedings Geosynthetics'95*, Nashville, Tennessee, Vol. 1, pp. 39–51.
- Nassif, H. 2002. "Finite Element Modeling of Bridge Approach and Transition Slabs." *Report No. FHWA-NJ-2002-007*, Department of Civil and Environmental Engineering, Center for Advanced Infrastructure & Transportation (CAIT), Rutgers, NJ.
- Neely, W. J. 1991. "Bearing Capacity of Auger-Cast Piles in Sand." *Journal of Geotechnical Engineering*, 117(2), 331–345.
- ODOT. 2005. "Bridge Foundation Design Practices and Procedures." *Bridge Engineering Section*, Oregon Department of Transportation, p. 20.
- Opland, W. H. and Barnhart, V. T. 1995. "Evaluation of the URETEK Method for Pavement Undersealing." *Research Report No. R-1340*, Michigan Department of Transportation in Cooperation with the U.S. Department of Transportation.
- Pierce, C. E., Baus, R. L., Harries, K. A., and Yang, W. 2001. "Investigation into Improvement of Bridge Approaches in South Carolina." *Summary Report, Rep. No. FHWA-SC-01-02*, South Carolina Department of Transportation, Columbia, SC.
- Porbaha, A. 1998. "State of the Art in Deep Mixing Technology, Part I: Basic Concepts and Overview of Technology." *Ground Improvement*, 2(2), 8–92.
- Porbaha, A. 2000. "State of the Art in Deep Mixing Technology: Design Considerations." *Ground Improvement*, 4(3), 111–125.
- Puppala, A. J., Porbaha, A., Bhadriraju, V., and Wattanasanthicharoen, E. 2004. "In Situ Test Protocols for Quality Assessments of Deep Mixing Columns." *Geo-Trans 2004*, ASCE Geotechnical Special Publication No. 126, Los Angeles, 2004, pp. 1429–1438.

- Puppala, A. J., Saride, S., Archeewa, E., Hoyos, L. R., and Nazarian, S. 2012. "Technical Report on Recommendations for Design, Construction and Maintenance of Bridge Approach Slabs." *TxDOT Report, FHWA/TX-09/0-6022-2*, University of Texas at Arlington, Arlington, TX.
- Saride, S., Puppala, A. J. and Willammee, R. 2010. "Use of Lightweight Expanded Clay and Shale (ECS) as a Fill Material to Control Approach Embankment Settlements." *ASCE Journal of Materials*, 22(6), 607–617.
- Schaefer, V. R. and Koch, J. C. 1992. "Void Development Under Bridge Approaches," *Report No. SD90-03*, South Dakota Department of Transportation.
- Seo, J. 2003. "The Bump at the End of the Bridge: An Investigation." *Dissertation Submitted in Partial Fulfillment of the Requirements for the Degree of the Doctor of Philosophy*, Texas, A & M University, College Station, TX.
- Smadi, O. 2001. "The Strength of Flowable Mortar." http://www.ctre.iastate.edu/PUBS/tech_news/2001/julaug/flowable_mortar.pdf.
- Soltesz, S. 2002. "Injected Polyurethane Slab Jacking." *Final Report, Report No. FHWA-OR-RD-02-19*, Oregon Department of Transportation Research Group.
- Stark, T. D., Olson, S. M., and Long, J. H. 1995. "Differential Movement at the Embankment/Structure Interface Mitigation and Rehabilitation." *Report No. IABH1*, FY 93, Illinois Department of Transportation, Springfield, IL.
- Stewart, C. F. 1985. *Highway Structure Approaches*. California Department of Transportation, Sacramento, CA.
- Strauss, J., Dahnke, D., and Nonamaker, F. 2004. "Compaction Grouting to Mitigate Settlement Beneath Approach Fills, California State Route 73 at Laguna Canyon Road." *Geotechnical Engineering for Transportation Project*, ASCE, pp. 1876–1883.
- Tadros, M. K. and Benak, J. V. 1989. "Bridge Abutment and Approach Slab Settlement (Phase I Final Report)." University of Nebraska, Lincoln.
- Texas Department of Transportation (TxDOT). 2001. *Bridge Design Manual*. Texas Department of Transportation, December.
- Timmerman, D. H. 1976. "An Evaluation of Bridge Approach Design and Construction Techniques." *Final Report, Report No. OHIODOT-03-77*, Ohio Department of Transportation.
- Unified Facilities Criteria (UFC). 2004. "Pavement Design for Roads, Streets, Walk, and Open Storage Area." *Report No. UFC 3-250-01FA*, US Army Corps of Engineers.
- Wahls, H. E. 1990. *NCHRP Synthesis of Highway Practice No. 159: Design and Construction of Bridge Approaches*. Transportation Research Board, National Research Council, Washington, D.C.
- Walkinshaw, J. L. 1978. "Survey of Bridge Movements in the Western United States." *Transportation Research Record 678: Tolerable Movements of Bridge Foundations, Sand Drains, K-Test, Slopes, and Culverts*, Transportation Research Board, National Research Council, Washington, D.C., pp. 6–12.
- White, D., Mohamed, M., Sritharan, S., and Suleiman, M. 2007. "Underlying Causes for Settlement of Bridge Approach Pavement Systems." *Journal of Performance of Constructed Facilities*, ASCE, 21(4) 273–282.
- White, D., Sritharan, S., Suleiman, M., Mohamed M., and Sudhar, C. 2005. "Identification of the Best Practices for Design, Construction, and Repair of Bridge Approaches." *CTRE. Project 02-118*, Iowa State University, Ames, IA.
- Wolde-Tinsae, A. M., Aggour, S. M., and Chini, S. A. 1987. "Structural and Soil Provisions for Approaches to Bridges." *Interim Report AW087-321-046*, Maryland Department of Transportation.
- Wong, H. K. W. and Small, J. C. 1994. "Effect of Orientation of Bridge Slabs on Pavement Deformation." *Journal of Transportation Engineering*, 120(4), 590–602.
- Wu, J. T. H., Lee, K. Z. Z., Helwany, B. S., and Ketchart, K. 2006. "Design and Construction Guidelines for Geosynthetic-Reinforced Soil Bridge Abutments with a Flexible Facing." *Proceedings of NCHRP Report 556*. Transportation Research Board, Washington, D.C.

@Seismicisolation

18

Expansion Joints

18.1	Introduction	677
18.2	General Design Criteria.....	678
18.3	Jointless Bridges	679
18.4	Small Movement Range Joints..... Sliding Steel Plate Joints • Elastomeric Compression Seal Joints • Bonded Preformed Seal Joints • Asphaltic Plug Joints • Poured Sealant Joints • Design Example 1: Elastomeric Compression Seal	679
18.5	Medium Movement Range Joints..... Bolt-Down Panel Joints • Elastomeric Strip Seal Joints • Steel Finger Joints • Design Example 2: Elastomeric Strip Seal	689
18.6	Large Movement Range Joints	694
18.7	Modular Expansion Joints • Design Example 3: Modular Expansion Joint System Installation Considerations..... Thermal Effects • Design Example 4: Finger Joint Installation Procedure	699
18.8	Summary..... References.....	702

Ralph J. Dornsife

*Washington State
Department of Transportation*

18.1 Introduction

Expansion joint systems are integrated, yet often overlooked, components designed to accommodate repeated cycles of movement. Properly functioning bridge expansion joint systems accommodate these movements without imposing significant secondary stresses on the superstructure. Sealed expansion joint systems also provide barriers preventing runoff water and deicing chemicals from passing through the joint onto bearing and substructure elements below the bridge deck. Water and deicing chemicals have a detrimental impact on overall structural performance by accelerating degradation of bridge deck, bearing, and substructure elements. In extreme cases, this degradation has resulted in premature, catastrophic structural failure. In fulfilling their functions, expansion joints must provide a reasonably smooth ride for motorists.

Perhaps because expansion joints are generally designed and installed last, they are often relegated to peripheral status by designers, builders, and inspectors. As a result of their geometric configuration and the presence of multiple axle vehicles, expansion joint elements are generally subjected to a significantly larger number of loadings than other structural members. Impact, a consequence of bridge discontinuity inherent at a joint, exacerbates loading. Unfortunately, specific expansion joint systems are often selected based upon their initial cost with minimal consideration for long-term performance, durability, and maintainability. Consequently, a plethora of bridge maintenance problems plagues them.

In striving to improve existing and develop new expansion joint systems, manufacturers present engineers with a multitudinous array of options. In selecting a particular system, the designer must carefully assess specific requirements. The magnitude and direction of movement, type of structure, traffic

volumes, climatic conditions, skew angles, initial and life cycle costs, and past performance of various systems must all be considered. For classification in the ensuing discussion, expansion joint systems will be grouped into three broad categories depending upon the total movement range accommodated. Small movement range joints encompass all systems capable of accommodating total motion ranges of up to about 1.75 in. (45 mm). Medium movement range joints include systems accommodating total motion ranges between about 1.75 in. (45 mm) and about 5 in. (127 mm). Large movement range joints accommodate total motion ranges in excess of about 5 in. (127 mm). These delineated ranges are somewhat arbitrary in that some systems can accommodate movement ranges overlapping these broad categories.

18.2 General Design Criteria

Expansion joints must accommodate movements produced by concrete shrinkage and creep, post-tensioning shortening, thermal variations, dead and live loads, wind and seismic loads, and structure settlements. Concrete shrinkage, post-tensioning shortening, and uniform thermal variation are generally taken into account explicitly in design calculations. Thermal gradients, most commonly produced by unequal solar heating of the superstructure, cause curvature effects. These effects are much more difficult to quantify and are commonly neglected for all but complex or very deep superstructures. Because of uncertainties in predicting, and the increased costs associated with accommodating large displacements, seismic movements have generally not been explicitly included in calculations.

Expansion joints should be designed to accommodate all shrinkage occurring after their installation. For unrestrained concrete, ultimate shrinkage strain after installation, β , may be estimated as 0.0002 (WSDOT 2011). More detailed estimations can be used, which include the effect of ambient relative humidity and volume-to-surface ratios (AASHTO 2012). Shrinkage shortening of the bridge deck, Δ_{shrink} , is calculated as

$$\Delta_{\text{shrink}} = \beta(\mu)(L_{\text{trib}}) \quad (18.1)$$

where

L_{trib} = tributary length of structure subject to shrinkage; ft.

β = ultimate shrinkage strain after expansion joint installation; estimated as 0.0002 in lieu of more refined calculations

μ = factor accounting for restraining effect imposed by structural elements installed before slab is cast (WSDOT 2011)

= 0.0 for steel girders, 0.5 for precast prestressed concrete girders, 0.8 for concrete box girders and T-beams, 1.0 for flat slabs

Uniform thermal displacements are calculated using the maximum and minimum anticipated bridge deck temperatures. These extreme values are functions of the structure's geographic location and the bridge type. Uniform thermal movement is calculated as

$$\Delta_{\text{temp}} = \alpha(L_{\text{trib}})(\delta T) \quad (18.2)$$

where

α = Coefficient of thermal expansion; 0.000006 in./in./°F for concrete and 0.0000065 in./in./°F for steel

L_{trib} = tributary length of structure subject to thermal variation; ft.

δT = temperature variation; °F

Because the AASHTO LRFD specifications stipulate that the expansion joint design be based upon strength limit state load combinations, the load factor on uniform thermal displacement, TU, specified in LRFD Table 3.4.1-1, is applicable (AASHTO 2012). As noted in LRFD Article 3.4.1, the larger of the two load factors, 1.2, is used for deformations. It is presumed here that the load factor of 1.2 was correlated with the

thermal ranges specified in LRFD Article 3.12.1 for the purpose of calculating uniform thermal displacements. Some transportation agencies have established conservatively wider thermal ranges for calculating bridge movements. In such situations, a reduced value of the load factor applied to TU may be justified.

Any other predictable movements following expansion joint installation, such as concrete post-tensioning shortening and creep, should also be included in the design calculations.

18.3 Jointless Bridges

Bridge designers have employed superstructure continuously in an effort to avoid some of the maintenance problems associated with expansion joints (Burke 1989). This evolution from simple span construction was facilitated by the development of the moment distribution procedure (Cross 1932). In recent years, some transportation agencies have extended this strategy by developing jointless bridge designs. Jointless bridges are characterized by continuous spans built integrally with their abutments. In many instances, approach slabs are tied to the superstructure slab or to the abutments. The resulting designs are termed integral or semi-integral depending upon the degree of continuity developed among superstructure, substructure, and approach slab elements. Design methods and details for jointless bridges vary considerably (Burke 1989; Steiger 1991). Many transportation agencies have empirically established maximum lengths for jointless bridges (Steiger 1991).

Jointless bridges should not be considered a panacea for addressing expansion joint maintenance issues. As superstructure movements are restrained in jointless bridges, secondary stresses are induced in superstructure and substructure elements. Stresses may also be induced in approach slabs. If they are inadequately addressed during design, these stresses can damage structural elements and adjacent pavement. Damaged structural elements, slabs, and pavements are accompanied by increased probability of moisture infiltration, further exacerbating deterioration. Long-term performance and durability will determine how extensively the jointless bridge concept is applied to future construction.

18.4 Small Movement Range Joints

Many different systems exist for accommodating movement ranges under about 1.75 in. (45 mm). These include, but are not limited to, steel sliding plates, elastomeric compression seals, preformed closed cell foam, epoxy-bonded cellular neoprene seals, asphaltic plug joints, bolt-down elastomeric panels, and poured sealants. In this section, several of these systems will be discussed with an emphasis on design procedures and past performance.

18.4.1 Sliding Steel Plate Joints

Sliding steel plate joints, depicted in Figure 18.1, have been used extensively in the past for expansion joints in both concrete and timber bridge decks. Two overlapping steel plates are attached to the bridge

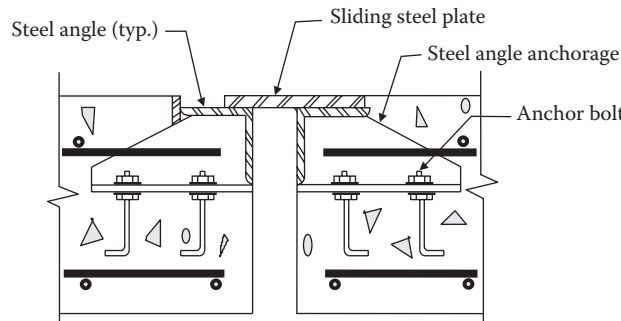


FIGURE 18.1 Sliding steel plate joint (cross section).



FIGURE 18.2 Sliding steel plate joint application.

deck, one on each side of the expansion joint opening. They are generally installed so that the top surfaces of the plates are flush with the top of the bridge deck. The plates are generally bolted to timber deck panels or embedded with steel anchorages into a concrete deck. Steel plate widths are sized to accommodate anticipated total movements. Plate thicknesses are determined by structural requirements.

Standard sliding steel plate joints do not generally provide an effective seal against intrusion of water and deicing chemicals into the joint and onto substructure elements. As a result of plate corrosion and debris collection, the sliding steel plates often bind up, impeding free movement of the superstructure. Repeated impact and weathering tend to loosen or break anchorages to the bridge deck. With the exception of sidewalk applications, sliding plate systems are rarely specified for new bridge construction today. Nevertheless, sliding plate systems still exist on many older bridges. These systems can be replaced with newer systems providing increased resistance against water and debris infiltration. In situations where the integrity of the deck anchorage has not been compromised, sliding plates can be retrofitted with poured sealants or elastomeric strip seals.

Figure 18.2 shows two variations of sliding steel plate joint applications. In the foreground is a typical sliding steel plate joint. In the background is a sliding steel plate joint that has been modified to accommodate an asphalt overlay by welding steel riser bars to the tops of the horizontal steel plates. In this photograph, the original bridge (background) was widened (foreground). Prior to the widening, the original bridge received an asphalt overlay.

18.4.2 Elastomeric Compression Seal Joints

Elastomeric compression seals, depicted in Figure 18.3, are continuous preformed elastomeric shapes, typically with extruded internal web systems, installed within an expansion joint gap to effectively seal the joint against water and debris infiltration. Compression seals are held in place by mobilizing

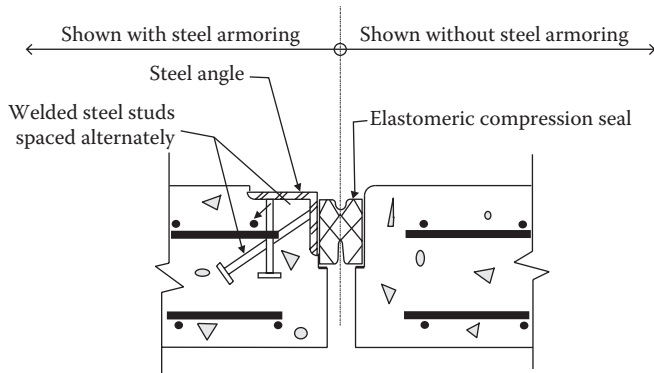


FIGURE 18.3 Elastomeric compression seal joint (cross section).



FIGURE 18.4 Elastomeric compression seal application.

friction against adjacent vertical joint faces. Hence, design philosophy requires that they be sized and installed to always be in a state of compression. Compression seals may be installed against smooth concrete faces or against steel armoring. When the compression seal is installed directly against concrete, polymer concrete nosing material is often used to provide added impact resistance. Combination lubricant/adhesive is typically used to install the seal in its compressed state. A typical compression seal expansion joint is shown in Figure 18.4.

Because elastomeric compression seals are held in place by friction, their performance is extremely dependent upon the close correlation of constructed joint width and design joint width. If the joint opening is constructed too wide, the mobilized friction force will be insufficient to prevent the compression

seal from slipping out of the joint at wider expansion gap widths. Relaxation of the elastomer and debris accumulation atop the seal contribute to seal slippage. To minimize slippage and maximize compression seal performance, the expansion gap may be formed narrower than the design width, then sawcut immediately prior to compression seal installation. The sawcut width is calculated based upon ambient bridge deck temperature and the degree of slab shrinkage that has already occurred. As an alternative to sawcutting, block outs can be formed on each side of the joint during bridge deck casting. Prior to compression seal installation, concrete is cast into the block outs, often with steel armoring, to form an expanded gap width compatible with ambient temperature.

In design calculations, the maximum and minimum compressed widths of the seal are generally set at 85% and 40% of the uncompressed seal width (WSDOT 2011). These widths are measured perpendicular to the axis of the joint. Thus, ignoring deck shrinkage effects, it may be assumed that the width of the seal in the middle of the historical temperature range is about 62% of its uncompressed width. For skewed joints, bridge deck movement must be separated into components perpendicular to and parallel to the joint axis. Shear displacement of the compression seal should be limited to a specified percentage of its uncompressed width, usually set at about 22% (WSDOT 2011). Additionally, the expansion gap width should be set so that the compression seal can be installed over a reasonably wide range of construction temperatures. Manufacturers' catalogues generally specify the minimum expansion gap widths into which specific size compression seals can be installed. The expansion gap width should be specified on the contract drawings as a function of the bridge deck temperature.

Design relationships can be stated as follows:

$$\Delta_{\text{temp-normal}} = \Delta_{\text{temp}} \cos \theta \quad [\text{thermal movement normal to joint}] \quad (18.3)$$

$$\Delta_{\text{temp-parallel}} = \Delta_{\text{temp}} \sin \theta \quad [\text{thermal movement parallel to joint}] \quad (18.4)$$

$$\Delta_{\text{shrink-normal}} = \Delta_{\text{shrink}} \cos \theta \quad [\text{shrinkage movement normal to joint}] \quad (18.5)$$

$$\Delta_{\text{shrink-parallel}} = \Delta_{\text{shrink}} \sin \theta \quad [\text{shrinkage movement parallel to joint}] \quad (18.6)$$

$$W_{\min} = W_{\text{midrange}} - \left[\frac{T_{\max} - T_{\text{install}}}{T_{\max} - T_{\min}} \right] \Delta_{\text{temp-normal}} > 0.4W \quad (18.7)$$

$$W_{\max} = W_{\text{midrange}} + \left[\frac{T_{\text{install}} - T_{\min}}{T_{\max} - T_{\min}} \right] \Delta_{\text{temp-normal}} + \Delta_{\text{shrink-normal}} < 0.85W \quad (18.8)$$

where θ = skew angle of expansion joint, measured with respect to a line perpendicular to the bridge longitudinal axis; degrees, W = uncompressed width of compression seal; in., W_{midrange} = expansion gap at the midrange of temperature extremes; in., T_{install} = bridge deck temperature at time of installation; °F, W_{\min} , W_{\max} = minimum and maximum expansion gap widths; in., T_{\min} , T_{\max} = minimum and maximum bridge deck temperatures; °F.

Multiplying (18.7) by -1.0, adding to (18.8), and rearranging yields:

$$W > \frac{\Delta_{\text{temp-normal}} + \Delta_{\text{shrink-normal}}}{0.45} \quad (18.9)$$

Similarly,

$$W > \frac{\Delta_{\text{temp-parallel}} + \Delta_{\text{shrink-parallel}}}{0.22} \quad (18.10)$$

Now, assuming $W_{\text{midrange}} = 0.62W$,

$$W_{\max} = 0.62W + \left[\frac{T_{\text{midrange}} - T_{\min}}{T_{\max} - T_{\min}} \right] \Delta_{\text{temp-normal}} + \Delta_{\text{shrink-normal}} < 0.85W \quad (18.11)$$

which, upon rearranging, yields:

$$W > \frac{0.5\Delta_{\text{temp-normal}} + \Delta_{\text{shrink-normal}}}{0.23} \quad (18.12)$$

Equations 18.9, 18.10, and 18.12 are used to calculate the required compression seal size. Next, expansion gap widths at various construction temperatures can be evaluated.

18.4.3 Bonded Preformed Seal Joints

A variety of field glued preformed proprietary joint seals are marketed. These systems are designed to accommodate expansion and contraction by resisting both compression and tension. The performance of these systems is highly dependent upon the durability of the concrete headers on each side of the joint seal. Cracking or spalling of the headers adversely affect a glued seal's performance and lead to premature failure. Advanced elastomeric concretes exhibit significantly improved performance under impact loading. They perform well as expansion joint headers, greatly improving the performance of both compression seals and glued preformed proprietary joint seals.

Closed-cell foam is one type of field glued joint seal. Evazote, an impermeable, resilient, preformed, ultraviolet resistant, flexible foam material is one proprietary example. It is a cross-linked, ethylene vinyl acetate, low density polyethylene copolymer, nitrogen blown resilient, nonextrudable foam material. Closed-cell foam is bonded in a compressed state to adjacent concrete surfaces using a two-component epoxy adhesive. Grooves are formed in the bonded faces of the material to enhance bonding. The material is typically oversized for the joint opening and cut to the length required.

Another type of glued preformed seal joint system is manufactured using flexible cellular neoprene expanded rubber produced by a relatively dense skin layer at its exterior surface to enhance durability. The sides of these seals are typically serrated to enhance bonding to substrate concrete using a two-component epoxy adhesive.

A variation of the glued preformed seal joint system consists of a voided neoprene shape similar in appearance to a compression seal. The sides of these seals are generally serrated to enhance bonding to concrete with a two-component epoxy adhesive. Complete adhesion of the epoxy to the seal and substrate surfaces is achieved by air inflation of the seal during the installation process. Once bonded, the seal can resist tension and compression.

Figure 18.5 shows three preformed proprietary seals that are used for field glued expansion joint applications. From left to right are closed-cell foam material, a preformed cellular neoprene seal, and an inflatable voided neoprene seal.

18.4.4 Asphaltic Plug Joints

Asphaltic plug joints comprise liquid polymer binder and graded aggregates compacted in preformed block outs as depicted in Figure 18.6. The compacted composite material is referred to as polymer modified asphalt (PMA). These joints have been used to accommodate movement ranges up to 2 in. (51 mm). This expansion joint system was originally developed in Europe and can be adapted for use with concrete or asphalt bridge deck surfaces. The PMA is installed in multiple lifts within a block out to center over the expansion joint opening with the top of the PMA flush with the roadway surface. A steel plate retains the PMA at the bottom of the block out during installation. The polymer binder material is



FIGURE 18.5 Bonded preformed seals.

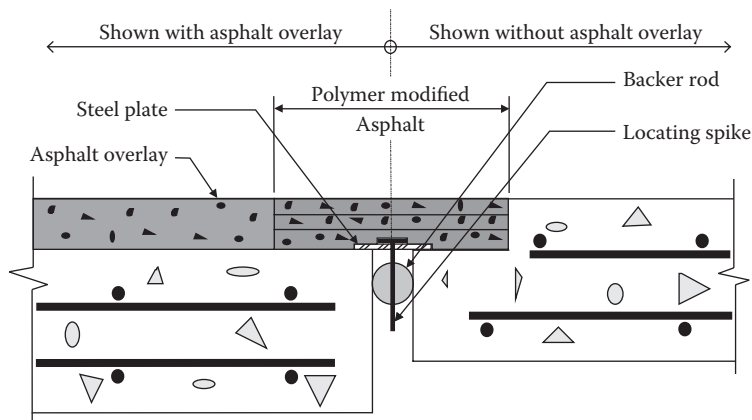


FIGURE 18.6 Asphaltic plug joint (cross section).

generally installed in heated form. Aggregate gradation, binder properties, and construction quality are critical to asphaltic plug joint performance.

The asphaltic plug joint is designed to provide a smooth, seamless roadway surface. It is relatively quick and easy to install, fairly inexpensive, and relatively easy to repair. It is not as susceptible to snow plow damage as other expansion joint systems, and can be cold milled and/or built up for roadway resurfacing. Given these factors, it is a particularly attractive alternative for rural applications with low traffic demands.

As with other expansion joint systems, asphaltic plug joints have their own set of disadvantages, which must be considered in the selection of appropriate expansion joint systems. The performance of asphaltic plug joints in the United States has been somewhat erratic (Bramel et al. 1996). The material properties of PMA vary with temperature. Asphaltic plug joints have demonstrated a proclivity to soften and creep at warmer temperatures, exhibiting wheel rutting and migration of PMA out of the block outs under high traffic volumes. At warmer temperatures and lower traffic volumes, they tend to heave as joints are compressed. In very cold temperatures, the PMA can become brittle and crack at the plug joint-to-pavement interface, making the joint susceptible to water infiltration. Figure 18.7 shows a failed asphaltic plug joint application.



FIGURE 18.7 Failed asphaltic plug joint application.

Some of the performance problems exhibited by asphaltic plug joints can be attributed to inadequate blockout preparation or the use of incompatible binder materials. In other instances, unsatisfactory performance is a result of applying the system to inappropriate applications. Research has been performed to investigate these issues and develop objective design guidelines, material specifications, and installation procedures to improve performance (Bramel et al. 1999).

Anecdotal observations indicate that asphaltic plug joint installations have higher success rates when they are installed near the center of the temperature range to which they will be subjected (Kazakavich, V., Personal Communication, March 2, 2012, Schenectady, NY). Experience has also shown that installations exhibit better cold weather performance after an adequately long warm weather curing period, indicating the preferability of installing asphaltic plug joints during the late spring or early summer seasons (Dolan, C.W., Personal Communication, March 2, 2012, University of Wyoming—College of Engineering and Applied Science—Civil and Architectural Engineering, Laramie, WY).

As with all expansion joint systems, designers must understand the limitations of asphaltic plug joints. These joints were not designed for, and should not be used in, accommodating differential vertical displacements, as may occur at longitudinal joints. Because of the PMA creep susceptibility, asphaltic plug joints should not be used where the roadway is subject to significant traffic acceleration and braking. Examples include freeway off ramps and roadway sections in the vicinity of traffic signals. Asphaltic plug joints have also performed poorly in highly skewed applications and in applications subjected to large rotations. Maintaining the minimum block at depth specified by the manufacturer is particularly critical to successful performance. In spite of these limitations, asphaltic plug joints do offer advantages not inherent in other expansion joint systems. However, they should not be considered as maintenance-free, long-term solutions to accommodate movement.

Ongoing research in Europe has developed an advanced polyurethane variation of the asphaltic plug joint (Gallai 2011). The aim of this research has been to combine the advantages of existing asphaltic plug joints with new less temperature sensitive materials to achieve an increase in movement capability and working temperature range. The developers of this new system assert that the two-component advanced polyurethane incorporated into the new plug joint does not exhibit the same adverse temperature dependent characteristics as bituminous polymer used in standard asphaltic plug joints and can accommodate movements of up to 4 in. (102 mm). The researchers report that trial installations in Austria, the United Kingdom, and Italy have performed well for over two years (Gallai 2011).

18.4.5 Poured Sealant Joints

Durable low-modulus sealants, poured cold to provide watertight expansion joint seals as depicted in Figure 18.8, have been used in new construction and in rehabilitation projects. Properties and application procedures vary between products. Most silicone sealants possess good elastic performance over a wide range of temperatures while demonstrating high levels of resistance to ultraviolet and ozone degradation. Rapid-curing sealants are ideal candidates for rehabilitation in situations where significant traffic disruption from extended traffic lane closure is unacceptable. Other desirable sealant properties include self-leveling and self-bonding capabilities. Installation procedures vary among different products, with some products requiring specialized equipment for mixing individual components. Designers must assess the design and construction requirements, weighing desirable properties against material costs for alternative sealants. Figure 18.9 shows a typical poured sealant expansion joint application.

Most sealants can be installed against either concrete or steel. Particularly in rehabilitation projects, it is extremely critical that the concrete or steel substrates be thoroughly cleaned before the sealant is placed. Some manufacturers require application of specific primers onto substrate surfaces prior to sealant placement to enhance bonding. Debonding of sealant from substrate concrete or steel, compromising the integrity of the watertight seal, have previously plagued poured sealant joints. More recently developed sealants have demonstrated very favorable performance and versatility of use in bridge rehabilitation. Continuing improvements in durability can be expected to extend their range of future application.

Poured sealant joints should be designed based upon the manufacturers' recommendations. Maximum and minimum working widths of the poured sealant joint are generally recommended as a percentage of the sealant joint width at installation. A minimum recess is typically required between the top of the roadway surface and the top of the sealant. This recess is critical in preventing tires from contacting and debonding the sealant from its substrate material.

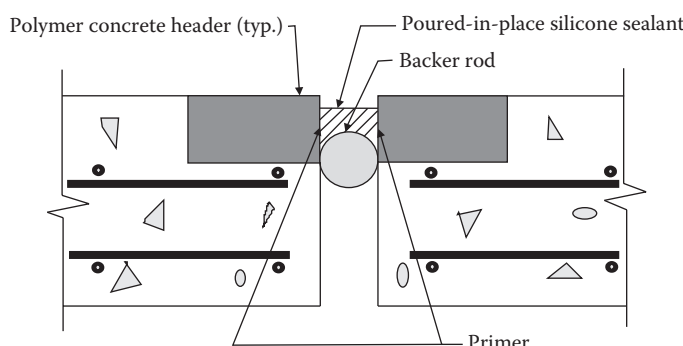


FIGURE 18.8 Poured sealant joint (cross section).



FIGURE 18.9 Poured sealant application.

18.4.6 Design Example 1: Elastomeric Compression Seal

Given:

A reinforced concrete box girder bridge has an overall length of 300 ft. (61 m). A compression seal expansion joint at each abutment will accommodate half of the total bridge movement. These expansion joints are skewed 20°. Superstructure temperature range shall be determined using Procedure A as defined in Article 3.12 of the *AASHTO LRFD Bridge Design Specifications*, 6th Edition (AASHTO 2012). A moderate climate is assumed.

Requirements:

Elastomeric compression seal sizes and construction gap widths at 40°F (4.4°C), 65°F (18.3°C), and 80°F (26.7°C).

Solution:

Step 1: Determine the appropriate temperature range for the bridge.

AASHTO LRFD Article 3.12.2 allows the use of either Procedure A or Procedure B for determining the design thermal movement associated with a uniform temperature change for a concrete deck bridge supported on concrete girders. LRFD Table 3.12.2.1-1 identifies the temperature range for a concrete girder bridge located in a moderate climate as being 10°F (-12.2°C) to 80°F (26.7°C). A moderate climate is defined as one in which there are less than 14 days per year in which the average temperature is less than 32°F.

Step 2: Calculate temperature and shrinkage movements.

The expansion joint design is based upon the strength limit state, which applies a load factor of 1.2 on uniform thermal displacements. For the purpose of calculating design movements, the 1.2 load factor will be applied to the temperature range determined from LRFD Table 3.12.2.1-1, with minimum and maximum temperatures adjusted accordingly.

$$T_{\text{range}} = 1.2(80 - 10) = 84^{\circ}\text{F}$$

$$T_{\text{min}} = 10 - \frac{(84 - (80 - 10))}{2} = 3^{\circ}\text{F}$$

$$T_{\text{max}} = 80 + \frac{(84 - (80 - 10))}{2} = 87^{\circ}\text{F}$$

$$T_{\text{midrange}} = \frac{3 + 87}{2} = 45^{\circ}\text{F}$$

$$\Delta_{\text{temp}} = (\frac{1}{2})(0.000006)(87 - 3)(300)(12) = 0.91 \text{ in.}$$

$$\Delta_{\text{shrink}} = (\frac{1}{2})(0.0002)(0.8)(300)(12) = 0.29 \text{ in.}$$

$$\Delta_{\text{temp}} + \Delta_{\text{shrink}} = 0.91 + 0.29 = 1.20 \text{ in.}$$

$$\Delta_{\text{temp-normal}} + \Delta_{\text{shrink-normal}} = (1.20)(\cos 20^{\circ}) = 1.13 \text{ in.}$$

$$\Delta_{\text{temp-parallel}} + \Delta_{\text{shrink-parallel}} = (1.20)(\sin 20^{\circ}) = 0.41 \text{ in.}$$

Step 3: Determine required compression seal width from Equations 18.9, 18.10, and 18.12.

$$W > \frac{1.13}{0.45} = 2.51 \text{ in.}$$

$$W > \frac{0.41}{0.22} = 1.86 \text{ in.}$$

$$W > \frac{[0.5(0.91) + 0.29]\cos(20^{\circ})}{0.23} = 3.04 \text{ in.}$$

→ Use 3 in. (76 mm) compression seal

Step 4: Evaluate construction gap widths for various temperatures for a 3 in. compression seal.

$$\text{Construction width at } 45^{\circ}\text{F} = (0.62)(3) = 1.86 \text{ in.}$$

$$\text{Construction width at } 40^{\circ}\text{F} = 1.86 + \frac{(45 - 40)}{(87 - 3)}(0.91)(\cos 20^{\circ}) = 1.91 \text{ in.}$$

$$\text{Construction width at } 65^{\circ}\text{F} = 1.86 - \left(\frac{65-45}{87-3} \right) (0.91)(\cos 20^{\circ}) = 1.66 \text{ in.}$$

$$\text{Construction width at } 80^{\circ}\text{F} = 1.86 - \left(\frac{80-45}{87-3} \right) (0.91)(\cos 20^{\circ}) = 1.50 \text{ in.}$$

Conclusion:

Use 3 in. (76 mm) elastomeric compression seals. Construction gap widths for installation temperatures of 40°F, 65°F, and 80°F are 1.91 in. (49 mm), 1.66 in. (42 mm), and 1.50 in. (38 mm), respectively.

18.5 Medium Movement Range Joints

Medium movement range expansion joints accommodate movement ranges from about 1.75 in. (45 mm) to about 5 in. (127 mm) and include sliding steel plate systems, bolt-down panel joints (elastomeric expansion dams), strip seal joints, and steel finger joints. Sliding steel plate systems were previously discussed under small motion range joints.

18.5.1 Bolt-Down Panel Joints

Bolt-down panel joints, also referred to as elastomeric expansion dams, consist of monolithically molded elastomeric panels reinforced with steel plates as depicted in Figure 18.10. They are bolted into block outs formed in the concrete bridge deck on each side of an expansion joint gap. Manufacturers fabricate bolt-down panels in varying widths roughly proportional to the total allowable movement range. Expansion is accompanied by uniform stress and strain across the width of the panel joint between anchor bolt rows. Unfortunately, the bolts and nuts connecting bolt-down panels to bridge decks have historically been prone to loosening and breaking under high speed traffic. The resulting loose panels and hardware in the roadway present hazards to vehicular traffic, particularly motorcycles. Consequently, to mitigate liability, some transportation agencies have phased out their use of bolt-down panel joints. With the increased use of cast-in-place and adhesive anchors in lieu of expansion anchors, bolt-down panel joints have exhibited improved performance and experienced some resurgence in recent years (Kazakavich, V., Personal Communication, March 2, 2012, Schenectady, NY). A typical bolt-down panel expansion joint application is shown in Figure 18.11.

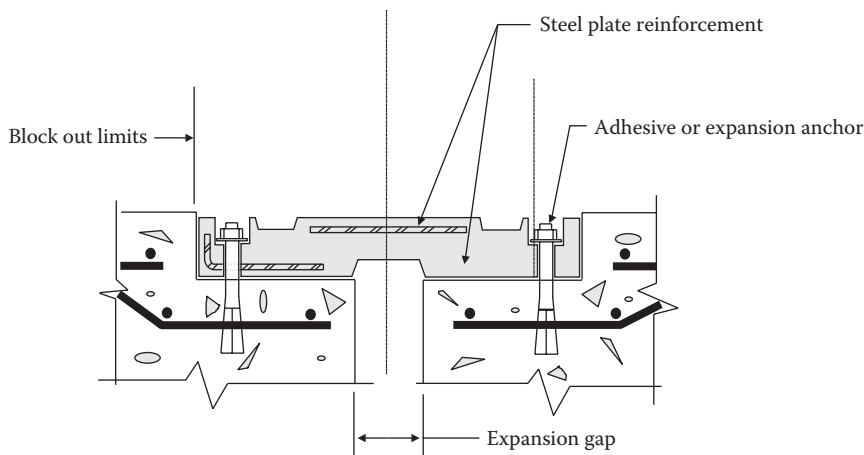


FIGURE 18.10 Bolt-down panel joint (cross section).



FIGURE 18.11 Bolt-down panel application.

18.5.2 Elastomeric Strip Seal Joints

An elastomeric strip seal expansion joint system, depicted in Figure 18.12, consists of a preformed elastomeric gland mechanically locked onto metallic edge rails embedded into concrete on each side of an expansion joint gap. Movement is accommodated by unfolding of the elastomeric gland. Steel studs or reinforcing bars are generally welded to the edge rails to facilitate bonding with the concrete in forming block outs. In some instances, the edge rails are welded or bolted in place. Edge rails provide armoring for the adjacent bridge deck concrete. Properly installed strip seals have demonstrated exceptionally good performance. Damaged or worn glands can be replaced with minimal traffic disruptions. The elastomeric glands exhibit a proclivity for accumulating debris. In some instances, this debris can resist joint movement and result in premature gland failure. A typical elastomeric strip seal expansion joint application is shown in Figure 18.13.

The preformed silicone joint sealing system is a variation of the conventionally armored elastomeric strip seal expansion joint system (Watson 2011). This system uses a preformed silicone joint sealing gland that is bonded to vertical concrete or steel joint faces using a single component silicone-based adhesive. The constituent silicone elements of this system have exhibited good resistance against weathering and other types of environmental exposure.

18.5.3 Steel Finger Joints

Steel finger joints, depicted in Figure 18.14, have been used to accommodate medium and large movement ranges. These joints are generally fabricated from steel plate and are installed in cantilever or prop cantilever configurations. The steel fingers must be designed to support traffic loads with sufficient stiffness to preclude excessive vibration. In addition to longitudinal movement, they must also accommodate any

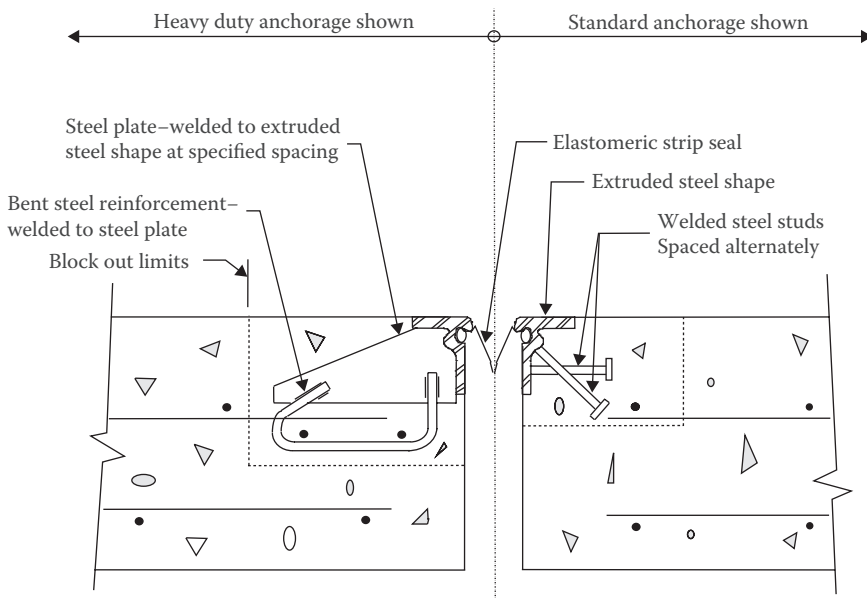


FIGURE 18.12 Elastomeric strip seal joint (cross section).



FIGURE 18.13 Elastomeric strip seal application.

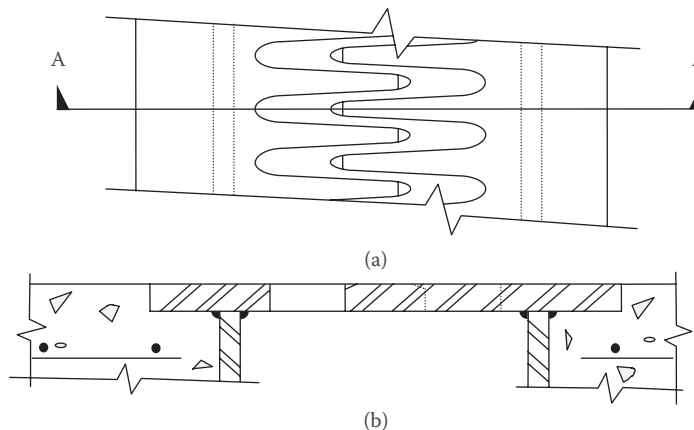


FIGURE 18.14 Steel finger joint. (a) Plan view. (b) Section A-A.

rotation or differential vertical deflection across the joint. To minimize the potential for damage from snowplow blade impact, steel fingers may be fabricated with a slight downward taper toward the joint centerline. Generally, steel finger joints do not provide a seal against water intrusion to substructure elements. Elastomeric or metallic troughs can be installed beneath the steel finger joint assembly to catch and redirect water and debris runoff. However, unless regularly maintained, these troughs clog with debris and become ineffective (Burke 1989). Two steel finger joint applications are shown in Figure 18.15.

Steel finger joints may be fabricated and installed in full roadway width segments, partial roadway width segments, or shorter modular segments. Robust anchorage of the steel finger joint segments to the bridge superstructure is critical in achieving satisfactory longevity of the overall finger joint system. The most common failures of older steel finger joints are related to anchorage. Impact loading, moisture penetration, and corrosion make these anchorages particularly susceptible to fatigue. Some companies are now marketing standardized steel finger joint panels of shorter modular lengths. Some of these proprietary systems incorporate post-tensioned anchorages for improved durability. In some situations, failed steel finger joint systems cannot be replaced with more modern watertight systems because of spatial limitations or other considerations. In these instances, standardized finger joint panel systems can be installed as replacements. The shorter modular panel segments allow construction to be staged more easily to accommodate traffic demands during construction.

Steel finger joints can present particular hazards to bicyclist and pedestrians. In these situations, the finger joint assemblies can be modified with cover plates to minimize these hazards. A non-skid surfaces further minimizes any hazard.

18.5.4 Design Example 2: Elastomeric Strip Seal

Given:

A steel plate girder bridge located in east central Indiana has a total length of 600 ft. (183 m). It is symmetrical and has a strip seal expansion joint at each end. These expansion joints are skewed 15°. Superstructure temperature range shall be determined using Procedure B as defined in Article 3.12 of the *AASHTO LRFD Bridge Design Specifications*, 6th Edition (AASHTO 2012).

Assume an approximate installation temperature of 65°F (18.3°C).

Requirements:

Type A and Type B elastomeric strip seal sizes and construction gap widths at 40°F (4.4°C), 65°F (18.3°C), and 80°F (26.7°C). Type A strip seals have a $\frac{1}{2}$ in. (13 mm) gap at full closure. Type B strip seals are able to fully close, leaving no gap.

@Seismicisolation

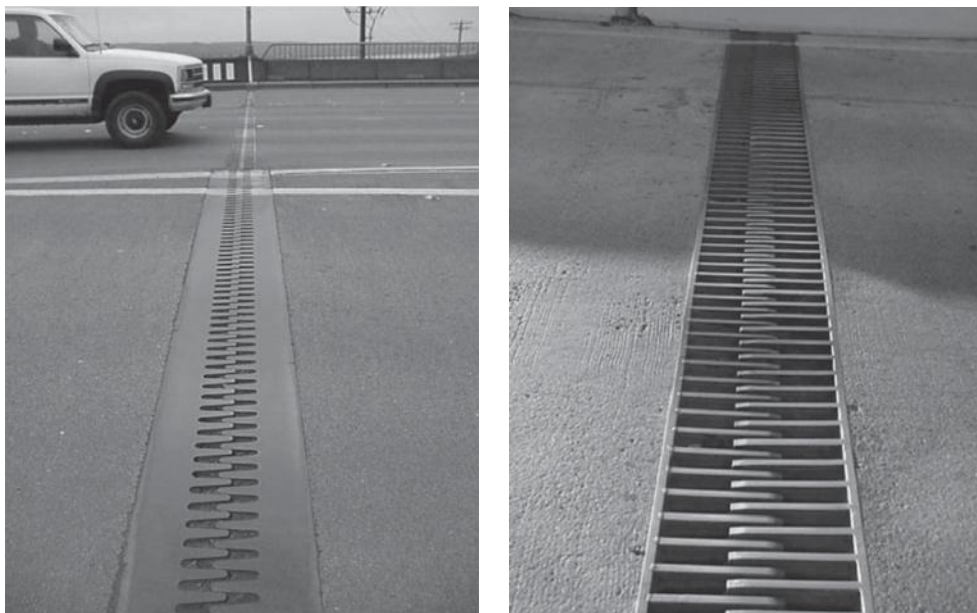


FIGURE 18.15 Steel finger joint applications.

Solution:

Step 1: Determine the appropriate temperature range for the bridge.

AASHTO LRFD Article 3.12.2 allows the use of either Procedure A or Procedure B for determining the design thermal movement associated with a uniform temperature change for a concrete deck bridge having steel girders. AASHTO LRFD Figures 3.12.2.2-3 and 3.12.2.2-4 identify the maximum and minimum design temperature for a steel girder bridge located in an east central Indiana as being 115°F (46.1°C) and -10°F (-23.3°C), respectively.

Step 2: Calculate temperature and shrinkage movement.

The expansion joint design is based upon the strength limit state, which applies a load factor of 1.2 on uniform thermal displacements. For the purpose of calculating design movements, the 1.2 load factor will be applied to the temperature range determined from LRFD Figures 3.12.2.2-3 and 3.12.2.2-4, with minimum and maximum temperatures adjusted accordingly.

$$T_{\text{range}} = 1.2(115 + 10) = 150^{\circ}\text{F}$$

$$T_{\text{min}} = -10 - \frac{(150 - (115 + 10))}{2} = -22.5^{\circ}\text{F}$$

$$T_{\text{max}} = 115 + \frac{(150 - (115 + 10))}{2} = 127.5^{\circ}\text{F}$$

$$T_{\text{midrange}} = \frac{-22.5 + 127.5}{2} = 52.5^{\circ}\text{F}$$

$$\Delta_{\text{temp}} = (\frac{1}{2})(0.0000065)(150)(600)(12) = 3.51 \text{ in.}$$

$$\Delta_{\text{shrink}} = 0.0 \quad (\text{no shrinkage}, \mu = 0.0 \text{ for steel bridge})$$

$$\Delta_{\text{temp}} + \Delta_{\text{shrink}} = 3.51 + 0 = 3.51 \text{ in.}$$

$$\Delta_{\text{temp-normal-closing}} = \left(\frac{127.5 - 65}{127.5 + 22.5} \right) (3.51)(\cos 15^\circ) = 1.41 \text{ in.}$$

$$\Delta_{\text{temp-normal-opening}} = \left(\frac{65 + 22.5}{127.5 + 22.5} \right) (3.51)(\cos 15^\circ) = 1.98 \text{ in.}$$

Step 3: Determine required strip seal size. Assume a minimum construction gap width of 1.50 in. at 65°F in order to assure that the seal can be replaced at that temperature in the future.

Type A: Construction gap width of 1.50 in. at 65°F will not accommodate 1.41 in. closing and still allow a 0.50 in. gap at full closure. Therefore, construction gap width at 65°F must be at least 1.41 in. + 0.50 in. = 1.91 in. → Use 2 in.

Size required = $2.00 + 1.98 - 0.50 = 3.48 \text{ in.} < 4.00 \rightarrow \text{Use 4 in. (100 mm) strip seal}$

Type B: Construction width of 1.50 in. at 65°F is adequate.

Size required = $1.50 + 1.98 = 3.48 \text{ in.} < 4.00 \rightarrow \text{Use 4 in. (100 mm) strip seal}$

Step 4: Evaluate construction gap widths for various temperatures for a 4 in. strip seal.

Type A: Required construction gap width at 65°F = $0.50 + 1.41 = 1.91 \text{ in.} \rightarrow \text{Use 2 in.}$

$$\text{Construction gap width at } 40^\circ\text{F} = 2.00 + \left(\frac{65 - 40}{65 + 22.5} \right) (1.98) = 2.57 \text{ in.}$$

$$\text{Construction gap width at } 80^\circ\text{F} = 2.00 - \left(\frac{80 - 65}{127.5 - 65} \right) (1.41) = 1.66 \text{ in.}$$

Type B: Construction width of 1.50 in. at 65°F is adequate.

$$\text{Construction gap width at } 40^\circ\text{F} = 1.50 + \left(\frac{65 - 40}{65 + 22.5} \right) (1.98) = 2.07 \text{ in.}$$

$$\text{Construction gap width at } 80^\circ\text{F} = 1.50 - \left(\frac{80 - 65}{127.5 - 65} \right) (1.41) = 1.16 \text{ in.}$$

Conclusion:

Use 4 in. (100 mm) elastomeric strip seals. Construction gap widths for Type A strip seals at installation temperatures of 40°F (4.4°C), 65°F (18.3°C), and 80°F (26.7°C) are 2.57 in. (65 mm), 2.00 in. (51 mm), and 1.66 in. (42 mm), respectively. Construction gap widths for Type B strip seals at installation temperatures of 40°F, 65°F, and 80°F are 2.07 in. (53 mm), 1.50 in. (38 mm), and 1.16 in. (30 mm), respectively.

18.6 Large Movement Range Joints

Large movement range joints accommodate more than 5 in. (127 mm) of total movement and include bolt-down panel joints (elastomeric expansion dams), steel finger joints, and modular expansion joints. Bolt-down panel and steel finger joints were previously discussed as medium movement range joints.

18.6.1 Modular Expansion Joints

Modular expansion joints (MEJ), depicted in Figure 18.16, are more complex structural systems designed to provide watertight wheel load transfer across wide expansion joint openings. These systems were developed in Europe and introduced in the United States in the 1960s (Kaczinski et al. 1996). They have been used to accommodate the movements of over 7 ft. (2.1 m). MEJs are generally shipped to the construction site for installation in a fully assembled configuration. A typical MEJ application is shown in Figure 18.17.

Early generation MEJs were designed to accommodate movement in one primary direction. In response to the need to accommodate more complex movements, manufacturers have developed proprietary enhancements to standard MEJs, allowing them to articulate in multiple directions and to accommodate multi-axes rotations. These enhanced MEJs have been used to accommodate complex movements ranging from seismic response to floating bridge transition span movements (Dornsince and Kaczinski 2011). The increased acceptance and use of seismic isolation to mitigate seismic hazards for new and existing bridges has resulted in an increased need to accommodate complex movements between superstructure and substructure elements. In response to this need, manufacturers have further improved MEJ systems and dynamically tested them under laboratory simulated seismic displacement and velocity demands.

MEJs comprise a series of center beams supported atop support bars. The center beams are oriented parallel to the joint axis while the support bars span across the joint opening. MEJs can be classified as either single support bar systems or multiple support bar systems. In multiple support bar systems, each center beam is supported by a separate support bar at each support box location. Figure 18.16 depicts a multiple support bar system. In the more complex single support bar system, one support bar supports all center beams at each support box location. This design concept requires that each center beam be free to translate along the longitudinal axis of the support bar as the joint opens and closes. This is accomplished by attaching steel yokes to the underside of the center beams. The support bar passes through the openings

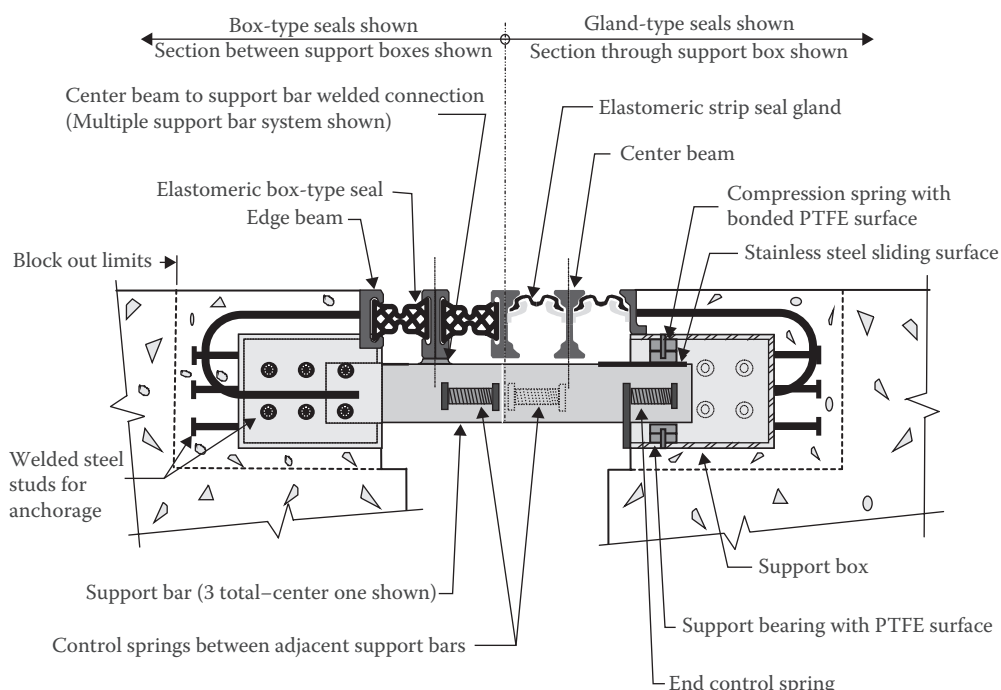


FIGURE 18.16 Modular expansion joint (multiple support bar system; cross section).

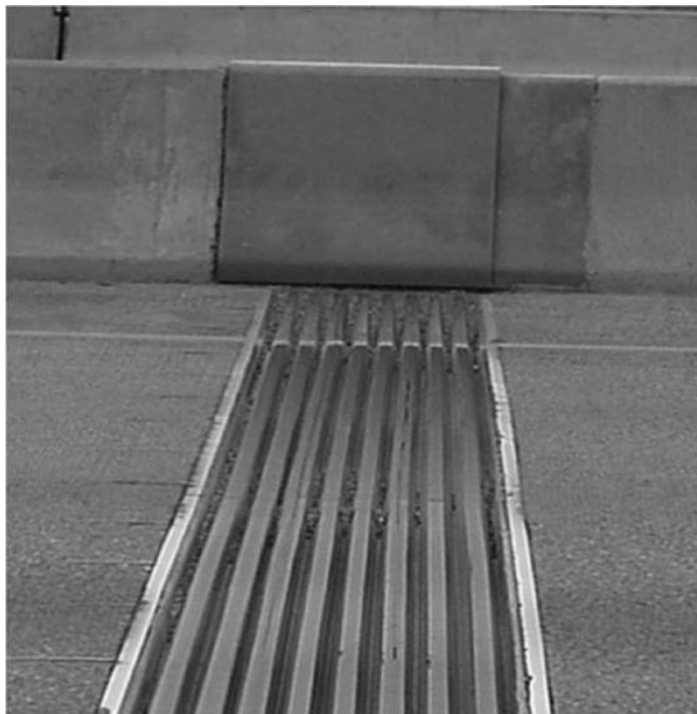


FIGURE 18.17 Modular expansion joint and cover plate application.

in the yokes. Elastomeric springs and sliding bearing surfaces between the underside of each center beam and the top of the support bar and between the bottom of the support bar and the bottom of the yoke support each center beam and permit it to translate along the longitudinal axis of the support bar.

The support bars are, in turn, supported on sliding bearings mounted within support boxes. PTFE (PolyTetraFluoroEthylene) or other proprietary low friction material-to-stainless steel interfaces between elastomeric support bearings and support bars facilitate movement of the support bars as the expansion gap opens and closes. Control springs between adjacent support bars and between support bars and support boxes of multiple support bar MEJs are designed to maintain equal distances between center beams as the expansion gap varies. The support boxes are embedded in bridge deck concrete on each side of the expansion joint. Elastomeric strip seals or elastomeric box type seals attach to adjacent center beams, providing resistance to water and debris intrusion.

The highly repetitive nature of axle loads predisposes MEJ components and connections to high fatigue susceptibility, particularly at center beam-to-support bar connections. Bolted connections have generally performed poorly. Welded connections are preferred, but must be carefully designed, fatigue tested, fabricated, and inspected to assure satisfactory performance and durability. Lack of understanding of the dynamic response of these systems, connection detail complexity, and the competitive nature of the marketplace have exacerbated fatigue susceptibility. Fortunately, research has developed fatigue resistant structural design specifications in addition to minimum performance standards, performance and acceptance test methods, and installation guidelines for MEJs (Kaczinski et al. 1996; Dexter et al. 1997).

As mentioned earlier, modular expansion joints may need to be shipped and installed in two or more segments in order to accommodate projected staging requirements or shipping length restrictions. The center beams are the elements that must be field spliced. These field connections may be either welded, bolted, or a combination of both. Center beam field splices have historically been weak links in the durable performance of MEJs because of their high fatigue susceptibility and tendency to initiate progressive system failures. The reduced level of quality control achievable in the field vis-à-vis a shop

operation contributes to this susceptibility. Mitigating measures include reducing support box spacing, using bolted shear-type connections, and careful detailing, control, and inspection over any field welding operations.

Total movement demands establish MEJ size. Because today's fatigue resistant MEJ systems, unlike other simpler and less expensive expansion joints, are expected to provide durability for the full life of the structure without the need for replacement, some transportation agencies apply a nominal safety factor on the calculated movement range. The safety factor also permits some latitude in anchoring a very large MEJ at its appropriate gap setting.

Presently available systems permit 3 in. (76 mm) of movement per strip seal element; hence the total movement rating provided will be a multiple of 3 in. (76 mm). To minimize impact and wear on bearing elements, the maximum gap between adjacent center beams is limited, typically, to about 3.5 in. (89 mm) (Van Lund 1991). To facilitate installation within concrete block outs, contract drawings should specify the distance face-to-face from edge beams as a function of superstructure temperature at the time of installation.

Design relationships can be expressed as

$$n = \frac{MR}{mr} \quad (18.13)$$

$$G_{\min} = (n-1)(w) + ng \quad (18.14)$$

$$G_{\max} = G_{\min} + MR \quad (18.15)$$

where

MR = total movement rating of the MEJ system; in.

mr = movement rating per strip seal element; in.

n = number of seals

$n - 1$ = number of center beams

w = width of each center beam; in.

g = minimum gap per strip seal element at full closure; in.

G_{\min} = minimum distance face-to-face of edge beams; in.

G_{\max} = maximum distance face-to-face of edge beams; in.

Structural design of MEJs is generally performed by the manufacturer. Project specifications should require that the manufacturer submit structural calculations, detailed fabrication drawings, and applicable fatigue test results for approval. All elements and connections must be designed and detailed to resist fatigue stresses imposed by repetitive vertical and horizontal wheel loadings. Additionally, MEJs should be detailed to provide access for inspection and periodic maintenance, including replacement of seals, control springs, and bearing components.

18.6.2 Design Example 3: Modular Expansion Joint System

Given:

Two cast-in-place post-tensioned concrete box girder bridge frames meet at an intermediate pier where they are free to translate longitudinally. Skew angle is 0°. The transportation agency owning this bridge has established its own historical temperature range for evaluating superstructure uniform thermal displacements. That temperature range is conservative relative to the procedures delineated in AASHTO LRFD Article 3.12.2, thus a strength limit load factor of 1.0 on uniform thermal movement is justified. Superstructure ambient temperatures are deemed to range from 5°F (-15°C) to 120°F (48.9°C). A MEJ will be installed 60 days after post-tensioning operations have been completed. Specified creep

is 150% of elastic shortening. Assume that 50% of shrinkage has already occurred at installation time. The transportation agency has an internal policy of sizing MEJ for 115% of the calculated movement demand. The following longitudinal movements were calculated for each of the two frames:

Movement	Frame A in. (mm)	Frame B in. (mm)
Shrinkage	1.18 (30)	0.59 (15)
Elastic Shortening	1.42 (36)	0.79 (20)
Creep (1.5 × Elastic Shortening)	2.13 (54)	1.18 (30)
Temperature Fall (65°F to 5°F)	2.99 (76)	1.50 (38)
Temperature Rise (65°F to 120°F)	2.60 (66)	1.30 (33)

Requirements:

MEJ size required to accommodate the total calculated movements and the installation gaps measured face-to-face of edge beams, G_{install} , at 40°F (4.4°C), 65°F (18.3°C), and 80°F (26.7°C).

Solution:

Step 1: Determine MEJ size.

$$\text{Total opening movement (Frame A)} = (0.5)(1.18) + 2.13 + 2.99 = 5.71 \text{ in.}$$

$$\text{Total opening movement (Frame B)} = (0.5)(0.59) + 1.18 + 1.50 = 2.99 \text{ in.}$$

$$\text{Total opening movement (Both Frames)} = 5.71 + 2.99 = 8.70 \text{ in.}$$

$$\text{Total closing movement (Both Frames)} = 2.60 + 1.30 = 3.90 \text{ in.}$$

Determine size of MEJ, including a 15% allowance:

$$1.15(8.70 + 3.90) = 14.49 \text{ in.}$$

→ Use 15 in. (381 mm) movement rating MEJ

Step 2: Evaluate installation gaps measured face-to-face of edge beams at 40°F, 65°F, and 80°F.

$$MR = 15 \text{ in. (MEJ movement range)}$$

$$mr = 3 \text{ in. (maximum movement rating per strip seal element)}$$

$$n = 15/3 = 5 \text{ strip seal elements}$$

$$n - 1 = 4 \text{ center beams}$$

$$w = 2.5 \text{ in. (center beam top flange width)}$$

$$g = 0 \text{ in.}$$

$$G_{\min} = (n-1)(w) + ng = (4)(2.5) + (5)(0) = 10 \text{ in.}$$

$$G_{\max} = G_{\min} + MR = 10 + 15 = 25 \text{ in.}$$

Recognizing that shrinkage and creep effects will cause the joint to permanently open with time, the installation strategy will be to set the joint as closely as possible to being fully closed if it experiences the maximum temperature extreme immediately following installation.

$$G_{65F} = G_{\min} + 1.15(\text{Total closing movement}) = 10 + 1.15(3.90) = 14.48 \text{ in.}$$

→ Use 14.5 in.

$$G_{40F} = 14.5 + \left(\frac{65-40}{65-5} \right) (2.99 + 1.50) = 16.37 \text{ in.}$$

$$G_{80F} = 14.5 - \left(\frac{80-65}{120-65} \right) (2.60 + 1.30) = 13.44 \text{ in.}$$

Check spacing between center beams at minimum temperature:

$$G_{5F} = 15 + 8.70 = 23.70 \text{ in.}$$

$$\text{Maximum spacing} = \frac{23.70 - (4)(2.5)}{5} = 2.74 \text{ in.} < 3.5 \text{ in.} \quad \text{O.K.}$$

Check spacing between center beams at 65°F for seal replacement:

$$\text{Spacing} = \frac{15 - (4)(2.5)}{5} = 1.00 \text{ in.} < 1.5 \text{ in.}$$

Therefore, center beams must be mechanically jacked in order to replace strip seal elements.

Conclusion:

Use a MEJ with a 15 in. (381 mm) movement rating. Installation gaps measured face-to-face of edge beams at installation temperatures of 40°F (4.4°C), 65°F (18.3°C), and 80°F (26.7°C) are 16.37 in. (416 mm), 14.5 in. (368 mm), and 13.44 in. (341 mm), respectively.

18.7 Installation Considerations

Proper installation of an expansion joint system is a critical element of assuring its long-term performance and durability. Proper installation requires an understanding of how a structure and its expansion joints respond to thermal effects during the installation process. Particularly for a more complex proprietary expansion joint system, it also requires an intimate understanding of the critical aspects of the installation process as they relate to the performance of the system. For example, it is extremely critical that good concrete consolidation be achieved underneath modular expansion joint support boxes.

It is highly advisable that the contract specifications require a qualified installation technician be present at the job site in order to assure proper installation of more complex expansion joint systems. The specifications should preferably stipulate that the technician is a full-time employee of the manufacturer of the expansion joint system in order to assure that the technician is adequately trained and knowledgeable.

For less complex expansion joint systems, provision shall be included to assure that a contractor's crew is adequately trained in the nuances of installation prior to performing its first installation of that system. For example, installation of a rapid-cure silicone sealant expansion joint system requires adequate knowledge and training in joint surface preparation, primer application, and sealant installation and curing requirements.

18.7.1 Thermal Effects

Bridge expansion joints are constantly moving in response to a number of different phenomena. The most significant of these phenomena is uniform variation in structure temperature with time. Fixed dimensions identified on contract drawings are generally associated with a *mean* or *construction* temperature. A contractor is required to adjust his concrete forms accordingly when the structure is built at other temperatures. Similarly, a steel fabricator is required to adjust his dimensions commensurately when fabricating at other temperatures.

Likewise, expansion joint gaps vary with changes in bridge superstructure temperature. For expansion joint hardware installed in preformed blockouts that are subsequently filled with concrete, this requires some accommodation during the hardware setting process. Specifically, a strip seal, steel finger, or the modular expansion joint system must be anchored in blockouts at a gap setting corresponding to the temperature of the superstructure at the time of anchorage. A compression seal installed in a sawcut gap requires similar accommodation. The gap must be sawcut to an opening width that corresponds to the temperature of the superstructure at the time of sawcutting. The temperature—gap setting relationship is best communicated to the contractor by including a temperature versus gap setting table in the contract drawings.

Structures are subject to several modes of heat transfer: radiation, convection, and conduction. Each mode affects the thermal response of a structure differently. Variations in ambient air temperature produce uniform thermal variation in the superstructure with concomitant lengthening or shortening if unrestrained. Solar radiation imposed upon a bridge deck produces thermal gradient effects in the superstructure. The overall thermal response of a superstructure lags changes in ambient air temperature in accordance with thermodynamic principles. More massive concrete bridges respond more slowly than steel bridges composed of thinner, more heat conductive, elements. The slower response attenuates both diurnal and seasonal temperature extremes of the superstructure relative to ambient air temperature. Objective evaluation of the superstructure's temperature at any time must take these factors into consideration.

Installation of a larger expansion joint system requires a well-thought out logical procedure for temporarily supporting the system and anchoring it at the appropriate gap setting. The procedure must include reasonably accurate evaluation of the superstructure temperature and recognition that the superstructure is constantly moving under varying temperature. The latter point is important because the anchorage and concrete placement sequence may take several hours to complete. The installation process must assure that any temporary restraints against opening or closing of the expansion joint system are promptly removed once concrete begins to set up. Otherwise, the restraint will damage or tear out the anchorages from the concrete.

18.7.2 Design Example 4: Finger Joint Installation Procedure

Given:

An existing steel finger expansion joint system has reached the end of its serviceable life and needs to be replaced. Spatial constraints associated with the existing steel truss structure and concrete approach span preclude replacement of the existing system with a watertight modular expansion joint system. A proprietary steel finger joint system composed of modular segments is selected to accommodate traffic staging requirements. This system incorporates post-tensioned anchorages of the finger joint panels for enhanced durability. A single row of vertical bolts anchor the panels on each side of the joint. The contract drawings include a temperature versus gap setting table showing the horizontal distance between the two rows of bolts to be 1'-9" @ 40°F (533 mm @ 4.4°C), 1'-7½" @ 64°F (489 mm @ 17.8°C), and 1'-6" @ 80°F (457 mm @ 26.7°C).

Requirements:

Develop a logical procedure for installing the finger joint panels at the appropriate expansion gap setting. The procedure shall include a rational approach to measure the temperature of the superstructure for the purpose of locating the finger joint panels, for temporarily supporting the finger joint panels prior to concrete placement, and for the timely removal of any temporary restraint devices.

Solution:

Exposure to direct sunlight and varying ambient air temperature makes it difficult, if not impossible, to approximate average superstructure temperature based upon ambient air temperature. The bridge deck surface temperature on a sunny afternoon, as opposed to a very cloudy overcast day, is not representative of the average superstructure temperature. After several hours of relatively stable nighttime temperature conditions, ambient air temperature best approximates bridge superstructure temperature. With this in mind, take an air temperature reading within one-half hour (before or after) sunrise. The stepwise procedure for installing the steel finger joint panels is as follows:

Step 1: Measure the air temperature reading at sunrise as 52°F (11.1°C). Interpolate from the temperature versus gap setting table to determine that the appropriate distance between the two bolt rows at 52°F (11.1°C) is 1'-8 $\frac{1}{8}$ " (511 mm).

Step 2: Immediately paint, or otherwise mark, two fine parallel lines along the axis of the expansion joint. One line is approximately centered at the bottom of the concrete blockout on the approach span side of the expansion joint. The second line is on the inside bottom of the stay-in-place steel form on the truss span side of the expansion joint, separated horizontally from the first line by 1'-8 $\frac{1}{8}$ ". The stay-in-place steel form serves as the bottom and sides of a reinforced concrete beam supporting the finger joint panels. These two painted lines establish the location of the two rows of anchor bolts. Henceforth, the distance between these two lines will vary as the bridge expands and contracts throughout the day.

Step 3: Place temporary support beams atop the bridge deck with both sides of the finger joint segments bolted underneath. The temporary support beams span fully across the expansion joint blockouts perpendicular to the axis of the expansion joint. Anchor the support beams to the top of the concrete deck on the approach span side of the expansion joint using temporary expansion anchors. (The temporary support beams remain free to slide relative to the top of the bridge deck on the steel truss span side of the expansion joint.)

Step 4: Adjust the finger joint segments on the approach span side of the expansion joint so that their anchor bolts line up vertically with the painted line at the bottom of the concrete blockout.

Step 5: Place concrete in the formed blockout underneath the finger joint segments on the approach span side of the expansion joint.

Step 6: After concrete has set, loosen and remove bolted attachment of the steel finger joint segments to the temporary support beams on the approach span side of the expansion joint.

Step 7: Remove the temporary expansion anchors anchoring the temporary support beams to the approach span side of the expansion joint.

Step 8: Anchor the support beams to the top of the concrete deck on the steel truss span side of the expansion joint using temporary expansion anchors. (The temporary support beams are now free to slide relative to the top of the bridge deck on the approach span side of the expansion joint.)

Step 9: Adjust the finger joint segments on the steel truss span side of the expansion joint so that their anchor bolts line up vertically with the painted line on the inside bottom of the stay-in-place steel form.

Step 10: Place concrete in the blockout underneath the finger joint segments on the steel truss span side of the expansion joint. Note: It is important that adequate time be provided between the two concrete pours to allow the first concrete pour to set, to permit the temporary support beam expansion anchors to be removed and reset, and to reposition all finger joint segments on the steel truss span side of the bridge.

Step 11: After concrete in the second blockout has set, loosen and remove bolted attachment of the steel finger joint segments to the temporary support beams on the steel truss span side of the expansion joint.

Step 12: Remove the temporary expansion anchors anchoring the temporary support beams to the steel truss span side of the expansion joint.

Step 13: Remove all temporary support beams and hardware. Fill all expansion anchor holes in the bridge deck with approved grout.

18.8 Summary

A wide range of different expansion joint systems is available for accommodating bridge superstructure movements. Appropriate selection and design procedures, quality fabrication, competent installation practices, careful inspection, and routine maintenance all contribute to enhancing the long-term performance and durability of expansion joint installations. Expansion joint components and connections experience severe loading under harsh environmental conditions. An adequately designed system must be properly manufactured, installed, and maintained to assure adequate performance under these conditions. The importance of quality control cannot be overemphasized. Contract drawings and specifications must explicitly state all design, material, fabrication, installation, and quality control requirements. Structural calculations and detailed fabrication drawings should be submitted to the bridge designer for careful review and approval prior to fabrication. A qualified installation technician employed by the expansion joint system manufacturer should be present during installation to assure that all the manufacturer's installation recommendations are being followed.

Research and experience continues to improve expansion joint system technology (Stoyle 1991; Atkinson 1996). It is vitally important that design engineers keep abreast of new technological developments. Interdisciplinary and inter-agency communication plays a vital role in the exchange of important information. Maintenance personnel can furnish valuable feedback to designers for implementation in future designs. Designers can provide valuable guidance to maintenance personnel with the goal of increasing service life. Manufacturers furnish designers and maintenance crews with guidelines and limitations for successfully designing and maintaining their products. In turn, designers and maintenance personnel provide feedback to manufacturers on the performance of their products and how they might be improved. Communication among disciplines is paramount to improving the long term performance and durability of expansion joint systems.

References

- AASHTO. 2012. *AASHTO LRFD Bridge Design Specifications*, Customary U.S. Units, 2012, American Association of State Highway and Transportation Officials, Washington, DC.
- Atkinson, B. 1996. *Fourth World Congress on Joint Sealants and Bearing Systems for Concrete Structures*, American Concrete Institute, Farmington Hills, MI.
- Bramel, B.K., C.W. Dolan, J.A. Puckett, and K. Ksaibati. 1999. *Asphalt Plug Joints: Characterization and Specification*, FHWA-WY-99/03F, University of Wyoming, Laramie, WY.
- Bramel, B.K., J.A. Puckett, K. Ksaibati, and C.W. Dolan. 1996. "Asphalt plug joint usage and perceptions in the United States," *Draft Paper Prepared for the Annual Meeting of the Transportation Research Board*, National Research Council, Washington, DC.
- Burke, M.P., Jr. 1989. "Bridge deck joints," *NCHRP Report 141*, Transportation Research Board, National Research Council, Washington, DC.
- Cross, H. 1932. "Analysis of continuous frames by distributing fixed-end moments," *Transactions*, ASCE, 96(1), 1–10.
- Dexter, R.J., R.J. Connor, and M.R. Kaczinski. 1997. "Fatigue design of modular bridge expansion joints," *NCHRP Report 402*, Transportation Research Board, National Research Council. Washington, DC.
- Dornsife, R.J., and M.R. Kaczinski. 2011. "Homer M. Hadley bridge large modular expansion joint replacement," *Seventh World Congress on Joints, Bearings, and Seismic Systems for Concrete Structures*, American Concrete Institute, Farmington Hills, MI.

- Gallai, G. 2011. "A new flexible plug joint—polyflex advanced PU," *Seventh World Congress on Joints, Bearings, and Seismic Systems for Concrete Structures*, American Concrete Institute, Farmington Hills, MI.
- Kaczinski, M.R., R.J. Dexter, and R.J. Connor. 1996. "Fatigue design and testing of modular bridge expansion joints," *Fourth World Congress on Joint Sealants and Bearing Systems for Concrete Structures*, ed. Atkinson, B., American Concrete Institute, Farmington Hills, MI, 97.
- Steiger, D.J. 1991. "Field evaluation and study of jointless bridges," *Third World Congress on Joint Sealing and Bearing Systems for Concrete Structures*, ed. Stoyle, J.E., American Concrete Institute, Farmington Hills, MI, 227.
- Stoyle, J.E. 1991. *Third World Congress on Joint Sealing and Bearing Systems for Concrete Structures*, American Concrete Institute, Farmington Hills, MI.
- Van Lund, J.A. 1991. "Bridge deck joints in Washington State," *Third World Congress on Joint Sealing and Bearing Systems for Concrete Structures*, ed. Stoyle, J.E., American Concrete Institute, Farmington Hills, MI, 371.
- Watson, E.S. 2011. "High performance joint sealing system for the 21st century," *Seventh World Congress on Joints, Bearings, and Seismic Systems for Concrete Structures*, American Concrete Institute, Farmington Hills, MI.
- WSDOT. 2011. "Bearings and expansion joints," *Bridge Design Manual (LRFD)*, Washington State Department of Transportation, Olympia, WA.

@Seismicisolation

19

Railings

19.1	Introduction	705
19.2	Vehicle Railings..... Background • History and Philosophy of Bridge Railing Design • Stakeholders for Bridge Railing Design • Full-Scale Crash Test • Prototype Railing Design Guidelines	705
19.3	Other Types of Railings..... Bicycle and Pedestrian Railings	714
	References.....	715

Lijia Zhang
*California High-Speed
Rail Authority*

19.1 Introduction

Railings are provided along the edges of a bridge to protect vehicles, bicyclists, and pedestrians. Based on functionalities, bridge railings may be classified as: pedestrian railings, bicycle railings, traffic railings, and combination railings as shown in Figure 19.1.

Though the design methodology for pedestrian and bicycle railing remain almost unchanged in the United States since the 1930s, the changes in vehicle railing design have been significant starting from 1970s. In this chapter, discussions will be mainly concentrated on vehicle railings and a brief summary of geometry and live load requirements for bicycle and pedestrian railing will then follow.

19.2 Vehicle Railings

19.2.1 Background

Railings connecting to the bridge deck are bridge items in the construction contract. Bridge engineers are usually responsible for designing and managing the construction. However, functionally, bridge railing belongs to longitudinal barrier—a roadway item. The longitudinal barrier together with crush crushing and break away or yielding support for sign and luminaries makes up Roadside Hardware. Roadside Hardware in turn is a major subject of the Federal Highway Administration (FHWA) Safety Program. As such, the development of the design criteria and methodology has been driven by forces from bridge, roadway engineering disciplines as well as highway safety. The bridge engineers and researchers have their focus mainly on the structural strength and people from the other two areas are concerned more of occupants' safety and the safety of nearby traffic. Since the 1960s, with the increasing consciousness of highway safety by researchers, engineers, the public, and lawmakers, huge driving forces and impetus have been pushing people in the roadway engineering discipline to develop more reliable roadside hardware that adopts the state-of-the-art technology and correctly reflect the up to date vehicle fleet. In this safety consciousness movement, roadway engineers have taken the lead and the beneficiary to the bridge railing can be considered as a by-product.

On the other side, the bridge engineers were not as active in upgrading railings until the late 1980s. Part of the reason could be that the railings were traditionally not considered as structurally significant



FIGURE 19.1 Typical bridge railings.

members. They are not critical links of the main load path to carry dead load, live load and other code specified loads to the ground. Failure of railings seldom impairs the overall structural integrity of the bridge. From the first edition issued in 1928 to the eighth edition issued in 1961, AASHTO Standard Specification For Highway Bridges (AASHTO 1928, 1961) only requested that railings be provided on the both edges of the bridge and then specified geometry requirements. No method of calculation was provided or suggested. Only in the fourth edition issued in 1941 did the bridge code specify 100 lb/ft vehicle impact load. Starting from the 1964 interim of the ninth edition, the specifications provided railing configuration in a drawing that not only provided the geometrical information of the railings but also the way to distribute the vehicle impact load. The impact load was specified as 10 kip for the first time. The 13th edition of AASHTO Standard Specification (AASHTO 1977), for the first time allowed the passing of full-scale impact tests as an alternative to the accepting criteria for bridge railings. The testing procedure and performance evaluation criteria would follow the guidelines from NCHRP Report 153 (Bronstad and Michie 1974), a product of roadway discipline. The philosophy of treating full-scale testing as an alternative accepting criterion for railing design carried on all the way until the AASHTO 17th edition of the *Standard Specifications* (AASHTO 2002). However, starting in 1994, AASHTO published *LRFD Bridge Design Specifications* as an alternative to the legacy AASHTO Standard Specifications for Highway Bridge. The two codes went shoulder by shoulder until 2004. The LRFD specifications changed the optional full-scale test to mandatory railing approval and acceptance criteria. The design specifications became guidelines to the prototype design that helps to make it crash-worthy. This change was driven dramatically by the pressures from roadway discipline as well as the federal government and the public.

Vehicle crashing is a very complicated non-linear, large deformation, and dynamic problem. The movements of the vehicle and the occupants belong to a problem of even more complicated multi-rigid (or flexible) body dynamics, which is beyond conventional structure engineers' scope of studies. Roadway engineers as the lead to the development of the design criteria and methodology in this

area naturally turned to the tools widely used in the auto industry—full-scale crash testing. Starting from the first one-page guideline on crash testing issued in 1962 in NCHRP Report 350 (Ross et al. 1993) published in 1993 and until AASHTO Manual for Assessing Safety Hardware (MASH) in 2009 (AASHTO 2009), instead of searching for analytical or numerical solution of the problem, focus was put on how to standardize and update test vehicles and testing procedures to best reflect the most current vehicle fleet and the “worst possibility.” The experience and lessons learned from the crash testing data then becomes the guidelines to design the testing prototype.

19.2.2 History and Philosophy of Bridge Railing Design

Before the 1960s, an errant vehicle was considered the result of “the nut behind the wheel.” Increasing highway safety consciousness and knowledge gained by researchers, engineers, the public and lawmakers formed high demand to improve the design of the vehicle itself, roadway geometry, as well as roadside hardware, which include longitudinal barriers. With the combined efforts, the fatality rate, measured in fatalities per 100 million vehicle-miles of travel (100 MVMT) in the United States had dropped to 1.5 in 1999 from 5.5 in 1966. This achievement was partially attributable to the improvement of roadside safety hardware design and installation. Roadside safety hardware, among other things, includes longitudinal barriers. Functionally, bridge railings are one type of longitudinal barriers. Roadway engineers and researchers often address the bridge railings on the way to develop the design and testing guidelines for longitudinal barriers. Two concepts gradually surfaced regarding longitudinal barrier designs during this highway safety movement: The first is that the longitudinal barrier designs should be crash tested. The second is that the longitudinal barrier performance needs differ greatly from site to site over highway network. NCHRP Report 153 (Bronstad and Michie 1974) “Recommendation Procedure for Vehicle Crash Testing of Highway Appurtenances” updated the one-page first-testing criteria HRCS (1962), “Proposed Full-Scale Testing Procedures for Guardrails.” Highway Research Correlation Services Circular 482 published in 1962. NCHRP published Report 230 (Michie 1980) “Recommended Procedures for the Safety Performance Evaluation of Highway Safety Appurtenances” incorporated new procedures and updated evaluation procedures. NCHRP Report 350 (Ross et al. 1993) “Recommended Procedures for the Safety Performance Evaluation of Highway Features” introduced six test levels the first time. These NCHRP publications not only specified and standardized testing vehicles and procedures but also the performance evaluation criteria and procedures. However, NCHRP Report 350 failed to address how to apply those test levels to the barriers and railings at different locations with different traffic conditions. Bridge engineers and researchers filled the gap through NCHRP Project 22-02(03), Multiple Service Level Highway Bridge Railings—later published as NCHRP Report 239 (Bronstad and Michie 1981), AASHTO Guide Specifications for Bridge Railings (AASHTO 1989) and AASHTO LRFD *Bridge Design Specifications* (AASHTO 1994, 2012).

19.2.3 Stakeholders for Bridge Railing Design

Technically bridge and roadway disciplines are interacting with each other to push forward the railing design criteria. In the meantime, there are other stakeholders who have led, funded, coordinated the progress, and enforced the guidelines and criteria. It is beneficial to clarify the roles and relationships among those stakeholders in order to better understand why it has to take multiple steps and has to deal with different agencies and stakeholders to get a new railing type designed, tested, and approved.

19.2.3.1 NCHRP

By the late 1950s, many states were researching similar highway problems in uncoordinated efforts, a situation noted with concern by the predecessor organizations to AASHTO and FHWA. Together, these organizations developed the idea of funding highway research by pooling state funds in a cooperative effort to address critical highway problems common to many states. The National Academy

of Sciences (NAS) was approached to administer the new National Cooperative Highway Research Program (NCHRP) within its Highway Research Board, now the Transportation Research Board (TRB). NCHRP has played a major role in standardizing the crash test procedures and performance evaluation criteria by publishing a series of reports mentioned in the previous section. There are still several ongoing NCHRP projects addressing longitudinal barrier and bridge railing issue waiting to be published soon.

19.2.3.2 AASHTO

The American Association of State Highway Officials (AASHO, now AASHTO) was founded in 1914 to give the states a common voice with which to advocate national programs for road improvement. The state DOTs, working through AASHTO, develop design standards through a series of committees and task forces. The AASHTO Standing Committee on Research (SCOR) solicits research problems and recommends annual programs of NCHRP for consideration. Candidate problems go to SCOR and AASHTO's Research Advisory Committee (RAC)—a committee of state DOT research managers—for rating and selection for funding. Research findings are published by NCHRP, frequently in the form of manuals, recommended standards, or guidelines, some of which are adopted by AASHTO or member DOTs as standards, specifications, and guidelines. A standard is a detailed, formally ratified and fixed technology, format, or method that enables the performance of a particular task or activity. It's like a menu of items provided for user to choose from. A specification is similar to a standard but more flexible. It either prescribes steps or requirements to follow, or provides criteria to meet. Guidelines are non-mandatory suggestions. The NCHRP Project 12-33 was later adopted as the first edition of *AASHTO LRFD Bridge Design Specifications*, which for the first time required a full scale test of railings as a mandatory accepting criterion.

19.2.3.3 FHWA

U.S. law requires that design standards for projects on the National Highway System (NHS) must be approved by the Secretary of the U.S. Department of Transportation in cooperation with the state highway departments. The Secretary has delegated this authority to the Federal Highway Administrator. FHWA, as a non-voting member of AASHTO, contributes to the development of the design standards and sponsors research efforts. Following development of the design standards, FHWA uses a formal rulemaking process to adopt those it considers suitable for application on the NHS. FHWA also issues memos to address policies and to clarify confusions. FHWA enforces its policy by setting up the federal fund reimbursement procedures and requirements. Although Bridge railings, functionally classified as longitudinal barriers, are a roadway item, bridge engineer are responsible for their design and construction. A crash test, if requested, should be set up in a way to allow most existing railings to pass. The proposed cost/benefit model and performance level (PL) concept to set up the full scale test in a way most existing railings will pass the PL-2 test and more expensive railings will have to pass the PL-3 test and railings in remote areas and areas with low average daily traffic (ADT) can be designed with less expensive railings to meet the PL-1 test. To coordinate the two forces and clarify the confusion FHWA first issued a policy memorandum on August 28, 1986 to request all bridge railings used on federal-aid projects meet full-scale crash-test criteria. FHWA subsequently issued memorandums on August 13, 1990 and May 30, 1997. In the 1997 memorandum, FHWA clarified confusion and established equivalency ratings that related to different criteria that were developed at different times and by people from both roadway and bridge sides. These criteria contributed by the roadway side included NCHRP Report 230 (Michie 1980) and NCHRP Report 350 (Ross et al. 1993) with six test levels. Those contributed by the bridge side included NCHRP 239 (Bronstad and Michie 1981), "Multiple-Service-Level Highway Bridge Railing Selection Procedures" with four multiple-service-level (MSL-1 to MSL-4) and AASHTO Guide Specifications for Bridge Railings (AASHTO 1989) with three performance levels (PL-1 to PL-3). These FHWA memorandums were enforced by federal fund reimbursement procedure for federal-aid projects.

19.2.3.4 State DOTs

Members of AASHTO include the department of transportations of 50 states, the District of Columbia, and Puerto Rico. The state DOTs receive federal funding to supplement of their own state funding to deliver projects. They also develop policy, standards, and guidelines for other local agencies that receive funding directly from the federal government to use for delivering projects. Because of the long durations of the design, testing, and approval process for bridge railings and high cost, bridge railings used in a particular project are chosen from a pool of pre-approved standard railings instead of being specially designed for the projects. State DOTs and manufacturers are making efforts to develop new railings and FHWA is responsible for evaluating and approving the railings to be used in the NHS based on their full-scale test performance. For large projects, such as the San Francisco Oakland Bay Bridge East Span Self-Anchored Suspension Bridge, the project-specific railings were designed to meet the unique bridge structure and aesthetic needs, but the project schedule was also carefully arranged to allow time for railing testing and FHWA approval.

19.2.3.5 Task Force 13

Task Force 13 (TF-13) is a Task Force under the Subcommittee on New Highway Materials and Technologies of AASHTO-AGC-ARTBA Joint Committee, which was first established between AASHTO and the Associated General Contractors of America (AGC) in 1921 and then merged with the American Road and Transportation Builders Association (ARTBA) in 1972. The TF-13 has nine subcommittees and Subcommittee #3—Bridge Railing and Transition Hardware is to aid, oversee, and participate in the preparation and maintenance of an online inventory of crashworthy bridge railing and approach guardrail transition systems. This web utility, the so-called online guide to bridge railings, provides a content management system for bridge railing systems submitted to, reviewed by, and approved by AASHTO-ARTBA-AGC Task Force 13. It will allow full viewing, submission, management, and reporting services to its users and the general public. The systems shown in the guide have been submitted to the Task Force. The approval status indicates whether the system has been reviewed or approved by the Task Force. These guides provide a clear and concise compilation of crash-tested bridge railing and transition systems for use by researchers, bridge and roadway engineers in public transportation agencies, consulting engineers, and hardware manufacturers. A system eventually has to receive an acceptance letter from FHWA before it can be used in the project on the NHS.

19.2.4 Full-Scale Crash Test

The important role of the full-scale crash test was first realized in the early 1960s. Until the latest AASHTO *LRFD Bridge Design Specifications*, 6th Edition (AASHTO 2012), full-scale crash testing had been specified as the accepting criteria for any new developed bridge railing types. The railing design guidelines provided in the specifications to the contrary only play the secondary roles as aiding tools to help prepare crash-worthy prototype railings ready for crash test use. A number of different agencies in the United States were conducting such tests, and there was a need for more uniformity in the procedure and evaluation criteria used. The first standardized testing procedure was the one-page document Highway Research Correlation Services Circular 482 published in 1962. The testing procedures have been updated over the years in response to an improved understanding of safety performance, a changing vehicle fleet, and the need for adding a broader range of roadside hardwares (or appurtenances). These changes can be summarized in the following areas:

1. Vehicle mass

Only 1,800-lb passenger vehicles and 4,500-lb pickup trucks were procedured to test in the beginning.

When the MASH published in 2009 and *AASHTO LRFD Bridge Design Specifications*, 6th Edition published in 2012, the mass of passenger vehicles changed to 2,500 lb and the mass of the pickup vehicles has been changed to 5,000 lb. In addition, 18,000-lb single trucks, 30,000-lb buses, 80,000-lb tractor trailer trucks and 80,000-lb tanker trucks have been added to the test

TABLE 19.1 Railing Testing Parameters

Test Level	Test Vehicle Designation and Type	Test Vehicle Weight (lb)	Test Conditions	
			Speed (Mph)	Impact Angle (°)
1	1100C (passenger car)	2,420	31	25
	2270P (pickup truck)	5,000	31	25
2	1100C (passenger car)	2,420	44	25
	2270P (pickup truck)	5,000	44	25
3	1100C (passenger car)	2,420	62	25
	2270P (pickup truck)	5,000	62	25
4	1100C (passenger car)	2,420	62	25
	2270P (pickup truck)	5,000	62	25
	10000S (single-unit truck)	22,000	56	15
5	1100C (passenger car)	2,420	62	25
	2270P (pickup truck)	5,000	62	25
	36000V (tractor-van trailer)	79,300	50	15
6	1100C (passenger car)	2,420	62	25
	2270P (pickup truck)	5,000	62	25
	36000V (tractor-tank trailer)	79,300	50	15

procedures. Corresponding to the changes in mass, the vehicle configurations, such as height of center of gravity (CG) and the height of impact points, are also changed accordingly.

2. Impact angle and speed

The first recommended procedures for performing full-scale crash tests, published in 1962, specified a 4,000-lb test vehicle, two impact angles (7° and 25°), and an impact velocity of 60 mph. The MASH published in 2009 adopted a philosophy of “worst practical conditions”: the impact speed and angle combination represent approximately the 92.5 percentile of real-world crashes. The matrix of the speed and angle combinations for different test levels and vehicles are summarized in Table 19.1.

3. Performance criteria

NCHRP Report 153, published in 1974, specified the maximum vehicle acceleration of 5 and 10 g of lateral and longitudinal direction respectively. However, the MASH, published in 2009, specified the maximum occupant ride-down acceleration to 20.49 g in both directions. This relaxed restriction reflects the improvement of vehicle safety design and the enforcement of laws requiring the use of safety devices (safety belts and air bags).

19.2.4.1 Test Levels

With the ever increasing types of vehicles tested in the procedures, the concept of test level is introduced. Such a concept was first brought to attention from the bridge engineering discipline. Bridge engineers had long been using 10 kips static load specified in the AASHTO Standard Specifications for Highway Bridge to design bridge railings. Unlike their roadway engineering counterparts, bridge engineers in general were satisfied with the existing rail design specifications. They first proposed an idea to develop a set of testing procedures and a parameter that most of existing railings designed with the current standard will pass the test, while developing a higher performance level test procedure for future railings and a lower service level testing procedure. This concept was developed in the NCHRP project 22-02(02) & 22-02(03) from 1976 to 1981 and later published as NCHRP Report 239. This concept, together with NCHRP 230—the most updated crash test procedures, was first adopted by AASHTO and was published as the AASHTO guideline for bridge railing design in 1989, an alternative to the existing railing design standards. In turn, the next update of the test procedure, NCHRP 350 introduced a multi-level system

TABLE 19.2 Performance Evaluation Criteria from MASH

Evaluation Factors	Evaluation Criteria
Structural adequacy	Test article should contain and redirect the vehicle or bring the vehicle to a controlled stop; the vehicle should not penetrate, underride, or override the installation although controlled lateral deflection of the test article is acceptable.
Occupant risk	<p>Detached elements, fragments, or other debris from the test railing should not penetrate or show potential for penetrating the occupant compartment, or present undue hazard to other traffic, pedestrians, or personnel in a work zone.</p> <p>Deformation of, or intrusions into, the occupant compartment should not exceed the limits set forth.</p> <p>The vehicle should remain upright during and after a collision. The maximum roll and pitch angles are not to exceed 75°.</p> <p>It is preferable, although not essential, that the vehicle remain upright during and after collision. (For heavy trucks only)</p> <p>Occupant impact velocities (OIV).</p> <p>Longitudinal/Transverse preferable 30 ft/s maximum 40 ft/s.</p> <p>The occupant rides down acceleration.</p> <p>Longitudinal/Transverse preferable 15.0 G maximum 20.49 G.</p>

as well. However, instead of focusing on the railing performance, NCHRP 350 directly created six test levels as listed in Table 19.1. For the first three levels, only 2,500-lb passenger vehicles and 5,000-lb pickup trucks are used in the test. For test level 4 to 6, in addition to those two vehicles, each will add an additional 22,000-lb single unit truck, 80,000-lb tract trailer truck and 80,000-lb tanker truck respectively. Though NCHRP 350 does not provide directions on how to choose different test levels, this six test level category finally received consensus among the bridge and roadway sides.

19.2.4.2 Evaluation Criteria

Bridge railings shall be designed to perform successfully in two aspects. Firstly, railings shall not fail after impact so they can still contain a vehicle that would otherwise fall under the bridge, causing fatal damage to the occupants and traffic and pedestrians underneath as well. Secondly, the railings shall not cause fatal injury to the occupants by excessive deceleration of a vehicle, the vehicle turning over, spinning around, exiting at a steep angle and running into traffic in the adjacent lanes, or by the vehicle snagged by extruding parts or hit by flying broken pieces. The first railing performance aspect is a problem of structural strength. Though it is a non-linear dynamic problem, the solution can be obtained by analytical or numerical modeling with calibrating and justification of experimental testing. However, for the second performance aspects, there is yet an alternative solution to full-scale testing. Considering that full-scale testing is not avoidable anyway, it naturally becomes an important tool for structure-strength design of bridge railings. Table 19.2 lists performance evaluation criteria extracted from MASH.

19.2.5 Prototype Railing Design Guidelines

The design guidelines follow the same consideration of the performance evaluation criteria:

- Structure adequacy
- Occupant risk
- Post impact vehicular response

19.2.5.1 Yield Line Theory

Allowable stress design methods with a 10 kips lateral impact load have long been used for bridge railing design until the most recent update of the AASHTO *Standard Specifications for Highway Bridges*, 17th edition in 2002 (AASHTO 2002). The yield line theory method was first introduced to railing design

by Hirsch (1978) and was adopted in the first edition of *AASHTO LRFD Bridge Design Specifications* (AASHTO 1994) in 1994. Essentially, Hirsch's idea is a particular application of a more general development of yield line theory in reinforced concrete structure, which was first introduced by Ingerslev in 1923 to solve a simply supported rectangular slab. Thanks to Johansen's work in 1943 (translated by the concrete association in 1962), this method and application became more widespread.

Both the allowable stress method and the yield line theory are based on two fundamental laws of physics of solid mechanics: equilibrium and compatibility. Equilibrium means any portion of a system has to be in a state of equilibrium under the action of the combined external load and internal forces. The compatibility means the deformation between any two adjacent points is small and continuous without creating gaps or overlap. The allowable stress method achieves the compatibility goal by meeting the hook's law, whereas the yield line theory finds its way to compatibility by looking for a set of yield lines. For both methods, the equilibrium can be expressed as either differential equations or equations of virtual work done. Figure 19.2 shows the yield line pattern assumed by Hirsch. The actual length of L_c will be the one resulting in the minimum internal work. With L_c resolved, F_t can be derived from the equation of external work from vehicle impact and the internal works generated at the yield lines (moment times rotation angle along the yield lines).

M_b = moment capacity of beam at top of wall, k-ft

M_c = flexural resistance of wall about horizontal axis, k-ft/ft

M_w = flexural resistance of wall about vertical axis, k-ft/ft

L_t = length of distribution of impact force, ft

H = wall height, ft

Internal Work:

The internal work comes with two parts, work done on the beam (AD' and D'C) and work done with the slab (AB, DB, and BC). For the top beam, the total rotations are 4θ as show in Figure 19.3.

For internal work on the slab, Hirsch did not calculate the slab rotation strictly along the axis of rotation, which is δ , but distribute the rotation into vertical and horizontal component with rotation angles of φ and θ , respectively.

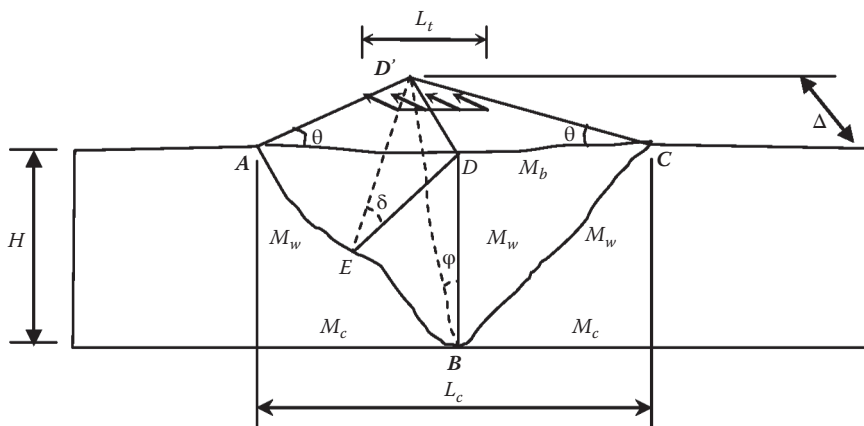


FIGURE 19.2 Yield line patten.



FIGURE 19.3 Internal work diagram.

The slab and beam can be separated into two parts. For the beam see Figure 19.2:

$$\text{Internal Work Done (Top Beam)} = 4M_b\theta = \frac{4M_b\Delta}{L_c/2} = \frac{8M_b\Delta}{L_c} \quad (19.1)$$

$$\text{where } \theta = \frac{\Delta}{L_c/2} = \frac{2\Delta}{L_c}$$

$$\begin{aligned} \text{Internal Work Done (Slab Vertical Component)} &= (M_w\theta + M_w\theta + 2M_w\theta)H \\ &= 4HM_w\theta \\ &= 4HM_w\Delta(L_c/2) \\ &= 8M_w\Delta H/L_c \end{aligned} \quad (19.2)$$

$$\begin{aligned} \text{Internal Work Done (Slab Vertical Component)} &= (L_c/2)M_c\phi + (L_c/2)M_c\phi \\ &= L_cM_c\phi \\ &= L_cM_c(\Delta/H) \\ &= M_c\Delta L_c/H \end{aligned} \quad (19.3)$$

External Work Done (Figure 19.4):

External work done is F_t times the shaded area. For simplicity, ignore the triangle area and only take the square area xL_t ,

where $x = \Delta(L_c - L_t/2)/L_c$

$$\text{External Work Done} = (F_t L_t) x = F_t \Delta L_t (L_c - L_t/2)/L_c \quad (19.4)$$

Equal the external work to internal work:

$$F_t \Delta L_t (L_c - L_t/2)/L_c = 4M_b\Delta(L_c/2) + 8M_w\Delta H/L_c + M_c\Delta L_c/H \quad (19.5)$$

Solve for $F_t L_t (= R_w)$

$$R_w = F_t L_t = \frac{8M_b}{(L_c - L_t/2)} + \frac{8M_w H}{(L_c - L_t/2)} + \frac{M_c \Delta L_c^2}{H(L_c - L_t/2)} \quad (19.6)$$

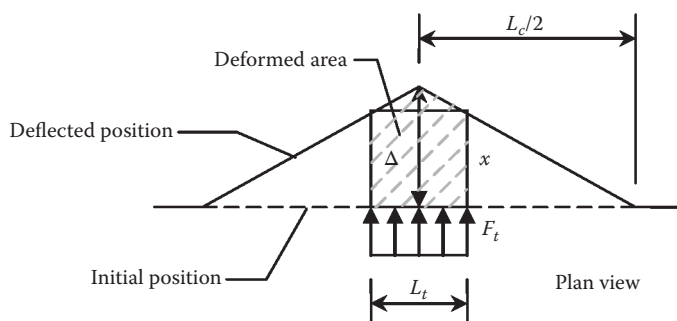


FIGURE 19.4 External work diagram.

$$R_w = \frac{8M_b}{(L_c - L_t/2)} + \frac{8M_w H}{(L_c - L_t/2)} + \frac{M_c \Delta L_c^2}{H(L_c - L_t/2)} \quad (19.7)$$

The next step is to find L_c .

L_c is the cracking length, which will result in the minimum internal work done. Solution of L_c can be found by taking directive of $d(R_w)/dL_c = 0$

$$\frac{d(R_w)}{d(L_c)} = L_c^2 - L_t L_c - \frac{H(8M_b + 8M_w H)}{M_c} \quad (19.8)$$

Solve the equation for L_c .

$$L_c = \frac{L_t}{2} + \sqrt{\left(\frac{L_t}{2}\right)^2 + \frac{8H(M_b + M_w H)}{M_c}} \quad (19.9)$$

19.2.5.2 Geometry and Shape

Crash testing provides a practical way to check the performance of bridge railings. However, the specified crash tests are designed for ideal conditions, or the so-called “worst practical conditions.” A railing passing the crash tests does not mean it will perform safely in complex real-world conditions. Besides the mandatory crash testing requirement, the *AASHTO LRFD Bridge Design Specifications* also provide mandatory descriptive criteria for railing geometry and shape requirements as follows:

1. Traffic railings shall be at least 27.0 in. for TL-3, 32.0 in. for TL-4, 42.0 in. for TL-5, and 90.0 in. in height for TL-6.
2. The bottom 3.0-in. lip of the safety shape shall not be increased for future overlay considerations.

19.3 Other Types of Railings

19.3.1 Bicycle and Pedestrian Railings

Bicycles and pedestrians travel at low speeds. The impact loads are small and crash testing is not required for railings protecting them. As shown in Figures 19.5 and 19.6, and Table 19.3, the design methodology for these railings has remained unchanged for years:

1. Specify the railing heights, maximum openings horizontal rail and vertical post spacing.
2. Specify a uniformly distributed load and a concentrated load.

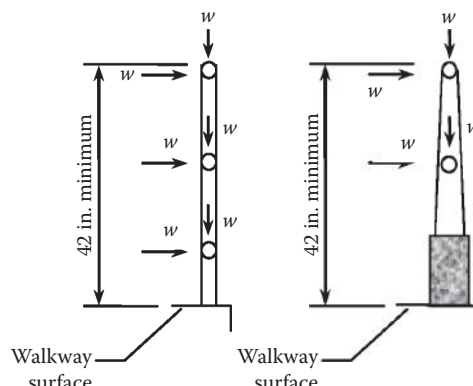


FIGURE 19.5 Pedestrian railings and loads.

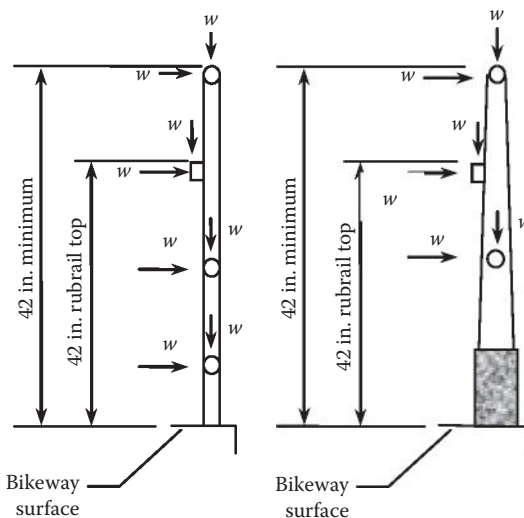


FIGURE 19.6 Bicycle railings and loads.

TABLE 19.3 Design Considerations of Pedestrian and Bicycle Railings

Design Considerations	Pedestrian Railings	Bicycle Railings
Height (min)	42 in.	Same
Rail clear open	6 in. below 27 in. and 8 in. above 27 in.	Same
Horizontal rail open	6 in.	Same
LL (distributed load)	$W = 0.050 \text{ klf}$ (acting in transverse and vertical direction simultaneously)	Same for rail height less than 54 in.
LL (concentrated load)	$P = 0.20 \text{ kips}$ (acting simultaneously with the above loads at any points)	Same for rail height less than 54 in.

References

- AASHTO. 1928. *Standard Specifications for Highway Bridges*, American Association of State Highway Officials, Washington, DC.
- AASHTO. 1961. *Standard Specifications for Highway Bridges*, 8th Edition. American Association of State Highway and Transportation Officials, Washington, DC.
- AASHTO. 1977. *Standard Specifications for Highway Bridges*, 13th Edition. American Association of State Highway and Transportation Officials, Washington, DC.
- AASHTO. 1989. *Guide Specifications for Bridge Railings*, American Association of State Highway and Transportation Officials, Washington, DC.
- AASHTO. 1994. *AASHTO LRFD Bridge Design Specifications*, 1st Edition. American Association of State Highway and Transportation Officials, Washington, DC.
- AASHTO. 2002. *Standard Specifications for Highway Bridges*, 17th Edition. American Association of State Highway and Transportation Officials, Washington, DC.
- AASHTO. 2009. *Manual for Assessing Safety Hardware*, American Association of State Highway and Transportation Officials, Washington, DC.
- AASHTO. 2012. *AASHTO LRFD Bridge Design Specifications*, Customary U.S. Units 2012, American Association of State Highway and Transportation Officials, Washington, DC.
- Bronstad, M. E. and Michie, J. D. 1974. "Recommended Procedures for Vehicle Crash Testing of Highway Appurtenances," *NCHRP Report 153*. Transportation Research Board, Washington, DC.

- Bronstad, M. E. and Michie, J. D. 1981. "Multiple-Service-Level Highway Bridge Railing Selection Procedures," *NCHRP Report 239*. Transportation Research Board, Washington, DC.
- Hirsch, T. J. 1978. "Analytical Evaluation of Texas Bridge Rails to Contain Buses and Trucks," *Report FHWA/TX78-230-2*. Texas Transportation Institute, Austin, TX.
- HRCS. 1962. "Proposed Full-Scale Testing Procedures for Guardrails," *Highway Research Correlation Services Circular 482*. Highway Research Correlation Services, Washington, DC.
- Michie, J. D. 1980. "Recommended procedures for Safety Performance Evaluation of Highway Safety Appurtenances," *NCHRP Report 230*. Transportation Research Board, Washington, DC.
- Ross, H. E., Sicking, D. K., Zimmer, R. A. and Michie, J. D. 1993. "Recommended Procedures for the Safety Performance Evaluation of Highway Features," *NCHRP Report 350*. Transportation Research Board, Washington, DC.

Bridge Engineering Handbook

SECOND EDITION

SUPERSTRUCTURE DESIGN

Over 140 experts, 14 countries, and 89 chapters are represented in the second edition of the **Bridge Engineering Handbook**. This extensive collection highlights bridge engineering specimens from around the world, contains detailed information on bridge engineering, and thoroughly explains the concepts and practical applications surrounding the subject.

Published in five books: **Fundamentals**, **Superstructure Design**, **Substructure Design**, **Seismic Design**, and **Construction and Maintenance**, this new edition provides numerous worked-out examples that give readers step-by-step design procedures, includes contributions by leading experts from around the world in their respective areas of bridge engineering, contains 26 completely new chapters, and updates most other chapters. It offers design concepts, specifications, and practice, as well as the various types of bridges. The text includes over 2,500 tables, charts, illustrations, and photos. The book covers new, innovative and traditional methods and practices; explores rehabilitation, retrofit, and maintenance; and examines seismic design and building materials.

The second book, **Superstructure Design**, contains 19 chapters, and covers information on how to design all types of bridges.

What's New in the Second Edition:

- Includes two new chapters: **Extradosed Bridges** and **Stress Ribbon Pedestrian Bridges**
- Updates the **Prestressed Concrete Girder Bridges** chapter and rewrites it as two chapters: **Precast/Pretensioned Concrete Girder Bridges** and **Cast-In-Place Post-Tensioned Prestressed Concrete Girder Bridges**
- Expands the chapter on **Bridge Decks and Approach Slabs** and divides it into two chapters: **Concrete Decks** and **Approach Slabs**
- Rewrites seven chapters: **Segmental Concrete Bridges**, **Composite Steel I-Girder Bridges**, **Composite Steel Box Girder Bridges**, **Arch Bridges**, **Cable-Stayed Bridges**, **Orthotropic Steel Decks**, and **Railings**

This text is an ideal reference for practicing bridge engineers and consultants (design, construction, maintenance), and can also be used as a reference for students in bridge engineering courses.

K12397

ISBN: 978-1-4398-5221-7

90000

